

# **Synthesis and Properties of a Series of 1,1,*n,n*- Tetramethyl[*n*](2,11)teropyrenophanes**

by

Kiran Sagar Unikela

A thesis submitted to the  
School of Graduate Studies  
in partial fulfilment of the requirements  
for the degree of Doctor of Philosophy

Department of Chemistry

Memorial University

October 2014

St. John's

Newfoundland

*Dedicated to my parents*

Peddiraju Unikela

Bhanumathi Unikela

*and*

In memory of

Late Prof. *G. Sundararajan*

## Abstract

The work described in this thesis revolves around the 1,1,*n*-tetramethyl[*n*](2,11)teropyrenophanes, which are a series of [*n*]cyclophanes with a severely bent, board-shaped polynuclear aromatic hydrocarbons (PAH).

The thesis is divided into seven Chapters. The first Chapter contains an overview of the seminal work on [*n*]cyclophanes of the first two members of the “capped rylene” series of PAHs: benzene and pyrene. Three different general strategies for the synthesis of [*n*]cyclophanes are discussed and this leads in to a discussion of some selected syntheses of [*n*]paracyclophanes and [*n*](2,7)pyrenophanes. The chemical, structural, spectroscopic and photophysical properties of these benzene and pyrene-derived cyclophanes are discussed with emphasis on the changes that occur with changes in the structure of the aromatic system. Chapter 1 concludes with a brief introduction to [*n*]cyclophanes of the fourth member of the capped rylene series of PAHs: teropyrene.

The focus of the work described in Chapter 2 is the synthesis of 1,1,*n*-tetramethyl[*n*](2,11)teropyrenophane (*n* = 6 and 7) using a double-McMurry strategy. While the synthesis of 1,1,7,7-tetramethyl[7](2,11)teropyrenophane was successful, the synthesis of the lower homologue 1,1,6,6-tetramethyl[6](2,11)teropyrenophane was not. The conformational behaviour of [*n*.2]pyrenophanes was also studied by <sup>1</sup>H NMR spectroscopy and this provided a conformation-based rationale for the failure of the synthesis of 1,1,6,6-tetramethyl[6](2,11)teropyrenophane.

Chapter 3 contains details of the synthesis of 1,1,*n*-tetramethyl[*n*](2,11)teropyrenophanes (*n* = 7-9) using a Wurtz / McMurry strategy, which proved to be more

general than the double McMurry strategy. The three teropyrenophanes were obtained in *ca.* 10 milligram quantities. Trends in the spectroscopic properties that accompany changes in the structure of the teropyrene system are discussed. A violation of Kasha's rule was observed when the teropyrenophanes were irradiated at 260 nm.

The work described in the fourth Chapter concentrates on the development of gram-scale syntheses of 1,1,*n,n*-tetramethyl[*n*](2,11)teropyrenophanes (*n* = 7–10) using the Wurtz / McMurry strategy. Several major modifications to the original synthetic pathway had to be made to enable the first several steps to be performed comfortably on tens of grams of material. Solubility problems severely limited the amount of material that could be produced at a late stage of the synthetic pathways leading to the even-numbered members of the series (*n* = 8, 10). Ultimately, only 1,1,9,9-tetramethyl[9](2,11)teropyrenophane was synthesized on a multi-gram scale. In the final step in the synthesis, a valence isomerization / dehydrogenation (VID) reaction, the teropyrenophane was observed to become unstable under the conditions of its formation at *n* = 8. The synthesis of 1,1,10,10-tetramethyl[10](2,11)teropyrenophane was achieved for the first time, but only on a few hundred milligram scale.

In Chapter 5, the results of an investigation of the electrophilic aromatic bromination of the 1,1,*n,n*-tetramethyl[*n*](2,11)teropyrenophanes (*n* = 7–10) are presented. Being the most abundant cyclophane, most of the work was performed on 1,1,9,9-tetramethyl[9](2,11)teropyrenophane. Reaction of this compound with varying amounts of bromine revealed that bromination occurs most rapidly at the symmetry-related 4, 9, 13 and 18 positions (teropyrene numbering) and that the 4,9,13,18-tetrabromide could be formed exclusively. Subsequent bromination occurs selectively on



the symmetry-related 6, 7, 15 and 16 positions (teropyrene numbering), but considerably more slowly. Only mixtures of penta-, hexa-, hepta and octabromides could be formed. Bromination reactions of the higher and lower homologues ( $n = 7, 8$  and  $10$ ) revealed that the reactivity of the teropyrene system increased with the degree of bend. Crystal structures of some tetra-, hexa-, hepta- and octa-brominated products were obtained.

The goal of the work described in Chapter 6 is to use 1,1,9,9-tetramethyl[9](2,11)teropyrenophane as a starting material for the synthesis of warped nanographenophanes. A bromination, Suzuki-Miyaura, cyclodehydrogenation sequence was unsuccessful, as was a C–H arylation / cyclodehydrogenation approach. Itami's recently-developed *K*-region-selective annulative  $\pi$ -extension (APEX) reaction proved to be successful, affording a giant [ $n$ ]cyclophane with a C<sub>84</sub> PAH. Attempted bay-region Diels-Alder reactions and some cursory host-guest chemistry of teropyrenophanes are also discussed.

In Chapter 7 a synthetic approach toward a planar model compound, 2,11-di-*t*-butylteropyrene, is described. The synthesis could not be completed owing to solubility problems at the end of the synthetic pathway.

## **Acknowledgements**

Firstly, I would like to convey my sincere gratitude to my supervisor Dr. Graham J. Bodwell for providing me with a wonderful project (which I have thoroughly enjoyed) and guiding me for these many years with relentless enthusiasm, valuable guidance and with excellence patience. I truly admired and influenced by his pursuit of perfection, attention to details and intellect.

I would like to thank my co-supervisor Dr. Dave Thompson and supervisory committee members Dr. Sunil V. Pansare and Dr. Travis Fridgen for their helpful criticisms whenever required. I would also like to extend my thanks to Dr. Zhao, Dr. Georghiou and Dr. Lucas for their wonderful discussions and support.

I am always in debt to Dr. Venkata Ramana and Dr. Koteswar Rao who really helped in getting this PhD position and standing by me at all times. I am grateful to Dr. S. Chandrasekharan, Dr. B. Rajakumar and Dr. Manivannan for their innumerable support under tough times which really changed my life.

I should also mention all Bod group members whom I am associated with Kerry-Lynn (particularly), Penchal, Anh Thu, Yixi Yng, Salah, Marc, Tiff, Joseph, David, Curtis and Terry. Special thanks to the teropyrenophane team members Václav, Josh, Kaitlin, Jayothi, Landon and Franziska for their valuable contributions for this project. My best wishes to Parisa who accepted to continue this project.

I would like to sincerely thank Prof. Itami, Nagoya University, for giving me the opportunity of doing fruitful collaborative research in his laboratory. I also would like to thank his secretary Rika Kato and his group members for their wonderful help during my

stay. I would also like to thank Prof. Shawn Collins and Anne-Catherine, University of Montréal for a very short collaboration.

I extend my sincerest gratitude to Arvind family, Saraswathy family and Fizza family for their unconditional love and support during my stay in St. John's. I would like to thank Arvind, Ramesh, Fizza, Priya, Niveditha and Chithran for being my wonderful roommates and showering me their love and affection. Also, I have to mention Penchal, Rajender, Karimulla, Arvind W., Gopi, Suresh, Rajinikanth, Kaivalya, Rakesh, Sridhar, Ranjith, Saravana, Hemanth, Guru moorthy, Amarendar, Gopinathan and many others who formed a wonderful community and always keeping me fresh and energetic with their support.

I would like to thank my best friends Karunakar, Srinu Babu, Gopal and Raheem and my dearest sister Jhansi who always shared my burdens and took care of my parents in the absence of me. My sincere gratitude to my wife and best friend Dr. Tanuja who always worried about my future more than myself. Despite of not being with me, she always supported me at her best.

The services of C-CART and CREAT are greatly acknowledged. Specifically, the assistance of Dr. Louise Dawe (X-ray crystallography), Dr. Celine Schneider (NMR), Linda Winsor (HRMS), Dr. Brent Myron and Tim Strange (UV-Vis and fluorescence), Julie Collins (IR).

Finally, I would like to extend my thanks to MUN organic group, staff and students of Chemistry Department, School of Graduate Studies for the financial support and Memorial University of Newfoundland.

# Contents

Dedication	ii
Abstract	iii
Acknowledgements	vi
Contents	viii
List of Figures	xvii
List of Tables	xxvi
List of Schemes	xxviii
List of Abbreviations	xxxiii
General experimental details	xxxix

## Chapter 1

<b>Introduction to <math>[n]</math>paracyclophanes</b>	<b>1</b>
1.1 Cyclophane chemistry .....	1
1.1.1 Scope of cyclophane chemistry.....	1
1.2 The rylenes and capped rylenes.....	3
1.3 The $[n]$ paracyclophanes .....	5
1.3.1 Synthesis.....	6
1.3.1.1 Synthesis of $[n]$ paracyclophanes using the ring closure approach (Strategy 1).....	7
1.3.1.2 Synthesis of $[n]$ paracyclophanes using the ring contraction approach (Strategy 2).....	8
1.3.1.3 Synthesis of $[n]$ paracyclophanes using an arene-forming	

approach (Strategy 3).....	10
1.3.2 Consequences of bending an aromatic system.....	16
1.3.2.1 Deformation angles (bend angles) .....	16
1.3.2.2 Strain energy ( <i>SE</i> ) in the [ <i>n</i> ]paracyclophanes.....	19
1.3.2.3 Aromaticity of [ <i>n</i> ]paracyclophanes .....	20
1.3.2.3.1 Chemical reactivity of small cyclphanes.....	21
1.3.2.3.2 Spectroscopic properties .....	22
1.3.2.4 Conformational behaviour of the aliphatic chain.....	24
1.4 The [ <i>n</i> ](2,7)Pyrenophanes.....	25
1.4.1 Synthetic strategy and interesting considerations.....	26
1.4.2 Important aspects of the [ <i>n</i> ](2,7)pyrenophanes.....	31
1.4.2.1 Quantification of the non-planarity of pyrene system.....	31
1.4.2.2 Aromaticity and strain .....	32
1.4.2.3 Chemical reactivity and spectroscopic properties.....	34
1.5 Peropyrenophanes.....	38
1.6 [ <i>n</i> ](2,11)Teropyrenophanes.....	39
1.7 Conclusions.....	41
1.8 References.....	41

## Chapter 2

<b>Synthesis of Teropyrenophanes Using a Double-McMurry Strategy</b>	<b>48</b>
2.1 Introduction.....	48
2.1.1 Reported synthesis of teropyrenophane <b>103c</b> .....	48
2.1.2 Key features of the synthesis of teropyrenophane <b>103c</b> .....	50
2.2 Results and discussion.....	51
2.2.1 Synthesis of [7](2,11)teropyrenophane <b>103b</b> using a double- McMurry strategy.....	51
2.2.2 Crystal structure of [7](2,11)teropyrenophane <b>103b</b> .....	53
2.3 Attempted synthesis of [6](2,11)teropyrenophane <b>103a</b> using a double-McMurry strategy.....	57
2.4 <sup>1</sup> H NMR spectra and conformational behaviour of the [n.2](7,1)pyrenophanes.....	58
2.5 Conclusions.....	68
2.5 Experimental Section.....	68
2.6 References.....	77
APPENDIX 1.....	80

## Chapter 3

<b>Synthesis of a Series of 1,1,<i>n</i>,<i>n</i>-Tetramethyl[n](2,11)teropyrenophanes Using a Wurtz / McMurry Strategy</b>	<b>101</b>
---	------------

3.1	Introduction.....	101
3.2	Synthesis of tetramethyl[ <i>n</i> ](2,11)teropyrenophanes <b>103b-d</b> .....	103
3.2.1	Crystal structure of compound <b>103d</b> .....	106
3.2.2	NMR spectra of teropyrenophanes <b>103b-d</b> .....	109
3.2.3	Absorbtion and emission spectroscopy of teropyrenophanes <b>103b-d</b> .....	112
3.3	Violation of Kasha's rule.....	114
3.4	Conclusions.....	116
3.5	Experimental section.....	116
3.6	References.....	116

## Chapter 4

### Synthesis of 1,1,*n,n*-Tetramethyl[*n*](2,11)teropyrenophanes on the Multigram

<b>Scale</b>	<b>119</b>
4.1 Introduction.....	119
4.2 Results and Discussion.....	121
4.2.1 Grignard reaction.....	122
4.2.2 Chlorination.....	123
4.2.2.1 GCMS analysis of crude dichloride.....	124
4.2.3 Issues/concerns with Friedel-Crafts alkylation.....	125
4.2.3.1 Attempts to improve the Friedel-Crafts alkylation reaction.....	129

4.2.3.1.1 Attempted alkylation using Lewis acids.....	130
4.2.3.1.2 Attempted alkylation using Brønsted acids.....	130
4.2.3.1.3 Attempts to alkylate 1- and 2-substituted pyrenes.....	131
4.2.3.2 <i>In-situ</i> chlorination / Friedel-Crafts alkylation reaction.....	135
4.2.4 Rieche formylation of di(2-pyrenyl)alkanes.....	138
4.2.5 Reduction of the dialdehydes <b>97b-e</b> .....	139
4.2.6 Problems associated with bromination reaction.....	140
4.2.7 Bromination / Wurtz coupling reaction.....	141
4.2.7.1 <i>In-situ</i> bromination / Wurtz coupling reaction.....	142
4.2.7.2 <i>In-situ</i> iodination / Wurtz coupling reaction.....	142
4.2.7.3 Solubility problems with the even-tethered cyclophanes.....	145
4.2.7.4 Conformational mobility of cyclophanes.....	147
4.2.8 Problems associated with Rieche formylation.....	148
4.2.8.1 Modification to the Rieche formylation reaction.....	149
4.2.8.2 Structure assignment of <b>108d</b> , <b>138d</b> and <b>139d</b> using 1-D and 2-D NMR spectroscopy.....	152
4.2.8.3 Alternative unsuccessful attempts to formylate <b>107d</b> .....	156
4.2.9 McMurry reactions of cyclophanedialdehydes <b>108b-d</b> .....	157
4.2.9.1 Identification of compounds <b>144c</b> and <b>144b</b> .....	157



4.2.9.2 McMurry reaction of cyclophanedialdehyde <b>108e</b> .....	158
4.2.9.2.1 Crystal structure of <b>145e</b> .....	161
4.2.9.2.2 Identification and crystal structure of cyclophane <b>147</b> ....	163
4.2.10 VID reaction leading to <b>103d</b> .....	170
4.2.10.1 Problems associated with VID reaction.....	172
4.2.10.2 DDQ as a chlorinating reagent.....	173
4.2.10.3 Modified conditions for the synthesis of <b>103d</b> .....	177
4.2.10.4 Screening of reaction conditions for the conversion of <b>109c</b> to <b>103c</b> .....	178
4.2.10.5 Issues during the VID reaction of <b>109b</b> to <b>103b</b> .....	186
4.2.10.6 VID reaction of <b>109e</b> to <b>103e</b> .....	187
4.2.10.6.1 Crystal structure of [10](2,11)teropyrenophane.....	188
4.3 Conclusions.....	192
4.4 Experimental section.....	193
4.5 References.....	254
APPENDIX 2.....	259
 <b>Chapter 5</b>	
<b>Bromination of the 1,1,<i>n,n</i>-Tetramethyl[<i>n</i>](2,11)teropyrenophanes</b>	<b>420</b>

5.1	Introduction.....	420
5.1.1	Bromination chemistry of pyrene.....	423
5.2	Results and discussion.....	430
5.2.1	Bromination of Cyclophanemonoene <b>109d</b> .....	430
5.2.2	Structure determination of dibromoteropyrenophane <b>212</b> .....	434
5.2.3	Interesting points about dibromoteropyrenophane <b>213</b> .....	436
5.2.4	Treatment of <b>109d</b> with excess Br <sub>2</sub> .....	438
5.3	Bromination chemistry of teropyrenophane <b>103d</b> .....	441
5.3.1	Crystal structures of <b>223</b> , <b>224</b> and <b>225</b> .....	451
5.3.1.1	X-Ray structure of tetrabromo[9](2,11)teropyrenophane ( <b>223</b> ).....	451
5.3.1.2	X-Ray structure of hexabromo[9](2,11)teropyrenophane <b>224A</b> .....	453
5.3.1.3	X-Ray structure of heptabromo[9](2,11)teropyrenophane <b>225</b> .....	455
5.4	Bromination of 1,1,7,7-tetramethyl[7](2,11)teropyrenophane ( <b>103b</b> ), 1,1,8,8-tetramethyl[8](2,11)teropyrenophane ( <b>103c</b> ) and 1,1,10,10-tetramethyl[10](2,11)teropyrenophane ( <b>103e</b> ).....	457
5.4.1	X-Ray structure of octabromo[8](2,11)teropyrenophane <b>241</b> .....	460
5.5	Conclusion.....	463
5.6	Experimental section.....	464
5.7	References.....	468

APPENDIX 3.....	473
 <b>Chapter 6</b>	
<b>Chemistry of 1,1,<i>n,n</i>,-Tetramethyl[<i>n</i>](2,11)teropyrenophanes</b>	<b>518</b>
6.1 Introduction.....	518
6.2 Results and discussion.....	520
6.2.1 Suzuki coupling of teropyrenophane <b>103d</b> .....	520
6.2.2 Attempted cyclodehydrogenation reaction of compound <b>256</b> .....	523
6.2.3 Coupling chemistry by C-H activation of aryl systems.....	524
6.2.3.1 Attempted coupling chemistry by C-H activation of <b>103d</b> .....	526
6.2.4 One-shot <i>K</i> -region-selective annulative $\pi$ -extension (APEX) reaction.....	528
6.2.4.1 1:4 APEX reaction of teropyrenophane <b>103d</b> .....	530
6.2.4.2 Structural characteristics of the cyclophane <b>287</b> .....	541
6.2.4.3 Absorption and emission properties of cyclophane <b>287</b> .....	542
6.2.5 Bay region Diels-Alder chemistry of [9](2,11)teropyrenophane <b>103d</b> .....	543
6.2.6 Host guest chemistry of [ <i>n</i> ](2,11)teropyrenophanes.....	546
6.5 Conclusions.....	549
6.6 Experimental Section.....	550
6.7 References.....	553
APPENDIX 4.....	556

## Chapter 7

<b>Attempted synthesis of the model compound (2,7-di-<i>t</i>-butylteropyrene)</b>	<b>563</b>
7.1 Introduction.....	563
7.2 Attempted synthesis of compound <b>318</b> using a double-Wurtz coupling strategy....	564
7.2.1 Absorption and emission spectra of compound <b>14</b> .....	567
7.2.2 Absorption and emission spectra of compound <b>15</b> .....	570
7.03 Plausible alternatives of synthesizing a teropyrene system.....	573
7.04 Conclusions.....	575
7.05 Experimental Section.....	577
7.06 References.....	584
APPENDIX 5.....	586

## List of Figures

<b>Figure 1.01</b> [2.2]Paracyclophane.....	1
<b>Figure 1.02</b> Cyclophanes with various bridging positions.....	2
<b>Figure 1.03</b> Some examples of cyclophanes.....	3
<b>Figure 1.04</b> The rylenes, the capped rylenes and some capped rylene-derived [n]cyclophanes.....	4
<b>Figure 1.05</b> Representation of the deformation angles in a [n]paracyclophane.....	16
<b>Figure 1.06</b> Calculated conformational structures for [n]paracyclophanes ( $n = 5-10$ ) ....	25
<b>Figure 1.07</b> A series of [n](2,7)pyrenophanes (left) and 1,n-dioxa[x](2,7)pyrenophanes (right).....	30
<b>Figure 1.08</b> Left) the parameters bend angles ( $\theta$ , $\alpha$ ), and bowl depth ( $h$ ); right) numbering of the pyrene system.....	32
<b>Figure 1.09</b> Definition of the total bend angle ( $\theta_{\text{tot}}$ ), other bend angles $\theta_1$ , $\theta_2$ , $\theta_3$ and distance between the two terminal carbons ( $d_1$ ).....	40
<b>Figure 2.01</b> X-ray crystal structure of compound <b>103b</b> ; 30% probability displacement ellipsoids.....	54
<b>Figure 2.02</b> Chain-like arrangement of molecules parallel to the b-axis (coincident with a 2-fold screw axis). i = 1-x, -1/2 + y, 1/2-z; ii = x, -1 + y, z; iii = 1-x, 1/2+y, 1/2-z. 30% probability ellipsoids, hydrogen atoms and minor solvent disorder removed for clarity...	55

<b>Figure 2.03</b> Rotation of Figure 2.02 to view down the b-axis. 30% probability ellipsoids, hydrogen atoms and minor solvent disorder removed for clarity.....	56
<b>Figure 2.04</b> Short intermolecular contacts between molecules, running parallel to the a-axis, represented by dashed lines. i = -1/2+x, 1.5-y, 1-z; ii = -1+x, y, z; iii = 1/2 +x, 1.5-y, 1-z; iv = 1+x, y, z. 30% probability ellipsoids, hydrogen atoms and minor solvent disorder removed for clarity. Short contacts: C3-C15 <sup>i</sup> = 3.393(5) Å and C5-C17 <sup>i</sup> = 3.338(5) Å.....	56
<b>Figure 2.05</b> The <sup>1</sup> H NMR spectra of dialkylpyrene <b>96a</b> and [n.2](7,1)pyrenophane <b>99a</b> .....	59
<b>Figure 2.06</b> Shielding of H <sub>b</sub> protons in <i>all-anti</i> conformations of <b>96a</b> using Newman projections.....	60
<b>Figure 2.07</b> <i>Anti</i> - and <i>syn</i> - conformations of cyclophane <b>99a</b> .....	61
<b>Figure 2.08</b> VT-NMR spectrum of <b>99a</b> . Coalescence of both methyl singlets was observed at <i>T</i> <sub>c</sub> = 318.....	62
<b>Figure 2.09</b> Exchange of the environment of methyl groups by ring flip.....	63
<b>Figure 2.10</b> The <sup>1</sup> H NMR spectra of dialkylpyrene <b>96b</b> and [7.2](7,1)pyrenophane <b>99b</b> .....	64
<b>Figure 2.11</b> Equilibrium mixture of <i>syn</i> - and <i>anti</i> - <b>99b</b> .....	65

<b>Figure 2.12</b> VT-NMR spectrum of <b>99b</b> . Coalescence of both methyl singlets was observed at $T_c = 238$ .....	67
<b>Figure 2.13</b> Equilibrium mixture of <i>syn</i> -, <i>syn'</i> - and <i>anti</i> -, <i>anti'</i> - <b>99b</b> .....	67
<b>Figure 3.01</b> X-ray crystal structure of <b>103d</b> , 50% probability displacement ellipsoids.....	106
<b>Figure 3.02</b> Partial packing diagram with 30% probability ellipsoids. H-atoms and lattice solvent molecules omitted for clarity. Molecules pack with inversion related, pairwise, facing alkyl chains. Mean plane separation for C40-C46 and C40 <sup>i</sup> -C46 <sup>i</sup> is 4.024(3) Å offset by 0.405(10) Å. i = ½-x, 1-y, z-1/2; ii = ½+x, y, 3/2-z; iii = ½-x, ½+y, z; iv = ½+x, ½-y, 1-z.....	107
<b>Figure 3.03</b> Bend angles, strain energies (SE), and aromatic proton resonances for <b>103b</b> ( $n=7$ ), <b>103c</b> ( $n=8$ ) and <b>103d</b> ( $n=9$ ).....	108
<b>Figure 3.04</b> <sup>1</sup> H NMR spectra of [ <i>n</i> ](2,11)teropyrenophanes <b>103b</b> , <b>103c</b> and <b>103d</b> .....	110
<b>Figure 3.05</b> Aliphatic proton resonances for <b>103b</b> , <b>103c</b> and <b>103d</b> .....	111
<b>Figure 3.06</b> Normalized absorption and emission spectra for teropyrenophanes <b>103b</b> ( $2.34 \times 10^{-8}$ M in MeCN), <b>103c</b> ( $1.99 \times 10^{-8}$ M in MeCN), and <b>103d</b> ( $1.90 \times 10^{-8}$ M in MeCN). $\lambda_{exc} = 350$ nm, 360 nm and 365 nm respectively.....	113
<b>Figure 3.07</b> Absorption, emission and excitation spectra of <b>103b-d</b> .....	115
<b>Figure 4.01</b> Structures of superphane ( <b>110</b> ), buckminsterfullerene (C <sub>60</sub> ) ( <b>111</b> ), corannulene ( <b>112</b> ) and the [ <i>n</i> ]cycloparaphenylenes (CPP) ( <b>113</b> ).....	120

<b>Figure 4.02</b>	Reported strategies for synthesizing teropyrenophanes <b>103b-d</b> .....	121
<b>Figure 4.03</b>	GCMS trace of the product obtained from the chlorination of <b>94b</b> under the originally reported conditions.....	124
<b>Figure 4.04</b>	Products of the chlorination reaction evidenced by GCMS.....	125
<b>Figure 4.05</b>	Stacked $^{13}\text{C}$ NMR spectra showing the lowest field signals.....	127
<b>Figure 4.06</b>	Different types of low-field quaternary carbon atoms in byproducts <b>116c</b> , <b>117c</b> and <b>118c</b> .....	128
<b>Figure 4.07</b>	a) Introduction of a temporary group at the 2 position of pyrene b) introduction of a permanent group at the 1 position of pyrene.....	132
<b>Figure 4.08</b>	Top) MALDI-TOF MS analysis of the poorly-soluble white precipitate obtained from the reaction leading to <b>107e</b> . Bottom) MALDI-TOF MS analysis of the soluble <b>107e</b> .....	146
<b>Figure 4.09</b>	Predicted sites of enhanced rates of electrophilic aromatic substitution of a 1,7-dialkylpyrene.....	149
<b>Figure 4.10</b>	NOESY spectrum of dialdehyde <b>108d</b> .....	153
<b>Figure 4.11</b>	Three regio-isomers <b>108d</b> , <b>138d</b> and <b>139d</b> .....	154
<b>Figure 4.12</b>	NOESY spectrum of dialdehyde <b>138d</b> .....	155
<b>Figure 4.13</b>	Crystal structure of <b>145e</b> .....	161
<b>Figure 4.14</b>	$^1\text{H}$ NMR spectrum of <b>147</b> .....	163
<b>Figure 4.15</b>	Experimental and calculated $^1\text{H}$ NMR data of compound <b>147</b> .....	164



<b>Figure 4.16</b> Crystal structure of <b>147</b> represented by 50% probability ellipsoids.....	166
<b>Figure 4.17</b> Packed unit cell for <b>147</b> .....	167
<b>Figure 4.18</b> C-H... $\pi$ interactions for <b>147</b> . Symmetry operations: (i) = x, y, z; (ii) = x, 1-y, $\frac{1}{2}+z$ ; (iv) x, 2-y, z-1/2. Cg1, Cg2, Cg3 and Cg4 refer to ring centroids. 50% displacement ellipsoids.....	167
<b>Figure 4.19</b> Highly unusual polyoxa-bridged pyrenophanes <b>148e</b> , <b>149e</b> and <b>150e</b> .....	169
<b>Figure 4.20</b> Top) APCI(+)-LC-MS spectrum; bottom) APPI-LC-MS spectrum.....	169
<b>Figure 4.21</b> Stacked spectra (aromatic region) of <b>109b-e</b> .....	171
<b>Figure 4.22</b> Absorption spectra of cyclophanes <b>109b-e</b> .....	171
<b>Figure 4.23</b> Possible byproducts of the VID reaction of <b>109c</b> in the presence of $\text{Cl}_2\text{CHCOOH}$ .....	184
<b>Figure 4.24</b> X-ray crystal structure of <b>103e</b> ; 30% probability displacement ellipsoids.....	189
<b>Figure 4.25</b> A single solvent channel, illustrating the disordered hexane molecules (each are modeled at $\frac{1}{2}$ -occupancy in the asymmetric unit, and represented in blue for emphasis). Symmetry operations: (i) = x,y,z; (ii) = $\frac{3}{2}-x$ , y-1/2, z; (iii) $\frac{3}{2}-x$ , $\frac{1}{2}+y$ , z; (iv) x, 1+y, z.....	190
<b>Figure 4.26</b> Packed unit cell showing hexane solvent channels threaded through the <b>103e</b> molecules, running parallel to the b-axis.....	190

<b>Figure 4.27</b> Close pair-wise $\pi$ - $\pi$ contacts in <b>103e</b> . Symmetry operations: (i) = x, y, z; (ii) = 1-x, 1-y, 1-z; (iii)= 1-x, $\frac{1}{2}$ +y, $\frac{1}{2}$ -z; (iv) = x, $\frac{3}{2}$ -y, z-1/2; (v) = 1-x, y-1/2, $\frac{3}{2}$ -z; (vi) = x, $\frac{1}{2}$ -y, $\frac{1}{2}$ +z.....	191
<b>Figure 4.28</b> Strain energy (SE) in teropyrenophanes <b>103a-f</b> .....	192
<b>Figure 5.01</b> Arm-chair, zig-zag and chiral CNTs.....	421
<b>Figure 5.02</b> Segments of armchair and zig-zag CNTs and fullerenes.....	422
<b>Figure 5.03</b> Various brominated peropyrenes.....	430
<b>Figure 5.04</b> Four possible $C_2$ -symmetric isomers of dibromo compound.....	434
<b>Figure 5.05</b> Structure determination of 12,21-dibromo-1,1,9,9-tetramethylteropyrenophane.....	435
<b>Figure 5.06</b> Possible structures for the hexabrominated product.....	439
<b>Figure 5.07</b> Possible structures for the heptabromo compound.....	440
<b>Figure 5.08</b> Left) Bar chart showing the results of the bromination of <b>103d</b> at rt. Right) Bar chart showing the results of the bromination of <b>103d</b> at 35 °C.....	445
<b>Figure 5.09</b> Left) distribution of various brominated products at rt using 0.0–10.0 equiv., 20.0 equiv. of bromine (in dichloromethane) and neat bromine. Right) at 35 °C using 6.0–10.0 equiv. and 20.0 equiv. of bromine (in dichloromethane).....	445
<b>Figure 5.10.</b> Two possible heptabromo isomers <b>225</b> and <b>225A</b> .....	447
<b>Figure 5.11</b> $^1\text{H}$ NMR chemical shifts of brominated teropyrenophanes.....	450

<b>Figure 5.12</b> Asymmetric unit of <b>223</b> with the symmetry expanded hexane molecule, represented with 50% probability ellipsoids. (a) and (b) are rotated by 90° to each other.....	452
<b>Figure 5.13</b> Close $\pi$ - $\pi$ contacts in <b>223</b> . H-atoms omitted for clarity. Symmetry operations $i = -x, 1-y, 1-z$ ; $ii = 1-x, 1-y, 1-z$ ; $iii = 1+x, y, z$ .....	452
<b>Figure 5.14</b> Close methyl $C_{sp^3}$ -H $\cdots\pi$ contacts in <b>223</b> . H-atoms omitted for clarity. Symmetry operations $iv = x, -1-y, z$ ; $v = x, 1+y, z$ .....	453
<b>Figure 5.15</b> The asymmetric unit of <b>224A</b> . H-atoms and minor Br disorder components omitted for clarity. Solvent molecules represented as capped sticks. All other atoms represented as 50% probability ellipsoids.....	454
<b>Figure 5.16</b> Molecule C from <b>224A</b> ; (a) includes both major and minor occupancy Br atoms while (b) has omitted both the minor occupancy Br(7) and Br(8) as well as the H-atoms.....	454
<b>Figure 5.17</b> 50% probability ellipsoids showing (a) the asymmetric unit of <b>225</b> , including the symmetry expanded half-occupancy <i>n</i> -hexane molecule and (b) the bromine atom labelling to show the location of the partial occupancy Br(3), Br(4), Br(5) and Br(6) atoms, with H atoms omitted for clarity.....	456
<b>Figure 5.18</b> Packed unit cell showing the inversion relationship and close contacts between <b>225</b> and the <i>n</i> -hexane molecules present in the lattice. H atoms omitted for clarity. $i = 1-x, 1-y, 1-z$ .....	456

<b>Figure 5.19</b> Packing diagram showing close $\pi$ - $\pi$ contacts in <b>225</b> . H atoms omitted for clarity. ii = 1-x, -y, 1-z; iii = 1-x, 1-y, -z.....	457
<b>Figure 5.20</b> 50% probability displacement ellipsoids for <b>241</b> showing (a) the minor disorder components for both bromine atoms and the alkyl chain (with H-atoms and lattice solvent omitted for clarity) and (b) the asymmetric unit of <b>241</b> with minor disorder components omitted for clarity, and lattice solvent included to show close association with the main molecule.....	461
<b>Figure 5.21</b> Partially packed unit cell showing the rotation by $45^\circ$ and close contacts between <b>241</b> and the <i>n</i> -hexane molecules present in the lattice, running parallel to the <i>c</i> -axis. H-atoms omitted for clarity. i = $\frac{1}{2}$ -x, y, $\frac{1}{2}$ -z; ii = $\frac{1}{2}$ -x, y, $\frac{3}{2}$ -z.....	461
<b>Figure 5.22</b> The inverse pairwise association of molecules in <b>241</b> via $\pi$ - $\pi$ interactions. H-atoms, lattice solvent and minor disorder components omitted for clarity. iii = -x, 1-y, 1-z.....	462
<b>Figure 6.01</b> Few possible products of 1:4 APEX reaction during optimization.....	525
<b>Figure 6.02</b> A few possible products of the 1:4 APEX reaction of <b>103d</b> with <b>274</b> .....	534
<b>Figure 6.03</b> Calculated structure of cyclophane <b>287</b> .....	542
<b>Figure 6.04</b> Normalized absorption and emission spectra of cyclophane <b>287</b> ; recorded in ( $6.5 \times 10^{-5}$ M) acetonitrile solutions.....	543
<b>Figure 6.05</b> A Vögtle belt <b>171</b> .....	544
<b>Figure 6.06</b> Inclusion complexes of <b>103b-d</b> with TCNQ, <b>304</b> .....	547
<b>Figure 6.07</b> $^1\text{H}$ NMR spectra of 2:1 solutions of <b>304</b> : <b>103b-d</b> in $\text{CDCl}_3$ .....	547
<b>Figure 6.08</b> $^1\text{H}$ NMR spectra of 2:1 solutions of <b>304</b> : <b>103b-d</b> in $\text{DMSO}-d_6$ .....	548

<b>Figure 7.01</b>	Absorption and emission spectra of compound <b>14</b> .....	568
<b>Figure 7.02</b>	Absorption and emission spectra of compound <b>15</b> .....	571
<b>Figure 7.03</b>	Solid state $^{13}\text{C}$ NMR spectra of compounds <b>15</b> and <b>17</b> .....	572

## List of Tables

<b>Table 1.01</b> Bend angles ( $\alpha$ , $\beta$ ), strain energies ( $SE$ ) and aromatic stabilization energies (ASE) of $[n]$ paracyclophanes <b>2a-2h</b> ( $n = 3-10$ ) .....	18
<b>Table 1.02</b> Ultraviolet spectral data of $[n]$ paracyclophanes <b>2b-h</b> .....	23
<b>Table 1.03</b> NMR data for the shielded protons of $[n]$ paracyclophanes.....	23
<b>Table 1.04</b> The experimental and calculated bend angles ( $\theta$ ) of pyrenophanes <b>24b-e</b> and <b>83b-g</b> .....	32
<b>Table 1.05</b> Calculated HOMA, NICS and $\Delta ASE$ values for pyrenophanes <b>83b-g</b> and <b>24a-g</b> .....	33
<b>Table 1.06</b> $^1H$ NMR shifts of pyrenophanes <b>24b-d</b> and <b>83b-g</b> .....	37
<b>Table 1.07</b> Ultraviolet spectral data of <b>24b-d</b> , <b>83b-g</b> and <b>20</b> .....	38
<b>Table 2.01</b> Comparison of $\Delta\delta$ values for each $H_X$ between <b>96a</b> and <b>99a</b> .....	61
<b>Table 2.02</b> Comparison of $\Delta\delta$ values for each $H_X$ between <b>96b</b> and <b>99b</b> .....	65
<b>Table 3.01</b> $^{13}C$ NMR resonances for compounds <b>103b</b> , <b>103c</b> and <b>103d</b> .....	112
<b>Table 3.02</b> $\lambda_{max}$ of the two additional emission bands.....	115
<b>Table 4.01</b> <i>In-situ</i> halogenation-Wurtz coupling reaction.....	143
<b>Table 4.02</b> Rieche formylations of <b>107d</b> .....	150
<b>Table 4.03</b> Results of preliminary experiments on the scale-up of the VID reaction of <b>109d</b> .....	171

<b>Table 4.04</b>	VID reaction conditions of cyclophanemonoene <b>109d</b> .....	177
<b>Table 4.05</b>	Optimization of the VID reaction of cyclophanemonoene <b>109c</b> .....	180
<b>Table 4.06</b>	Optimization of the VID reaction conditions of cyclophanemonoene <b>109c</b> .....	186
<b>Table 5.01</b>	Reactions of cyclophanemonoene <b>109d</b> with bromine.....	432
<b>Table 5.02</b>	Distribution of the product mixture (in terms of mole fractions) during the reaction of teropyrenophane <b>103d</b> with varying equiv. of Br <sub>2</sub> .....	443
<b>Table 5.03</b>	<sup>1</sup> H NMR data of bromocompounds <b>226-225</b> .....	449
<b>Table 5.04</b>	Bromination of teropyrenophanes <b>103b</b> , <b>103c</b> and <b>103d</b> .....	459
<b>Table 5.05</b>	List of the experiments performed by increasing 0.5 equiv. of Br <sub>2</sub> .....	457
<b>Table 6.01</b>	Attempted Suzuki coupling reactions.....	521
<b>Table 6.02</b>	Optimization of the 1:4 APEX reaction conditions.....	533
<b>Table 6.03</b>	Other oxidizing agents screened for the 1:4 APEX.....	535
<b>Table 6.04</b>	Optimization of the 1:4 APEX reaction conditions.....	537
<b>Table 6.05</b>	Optimization of 1:4 APEX reaction.....	539

## List of Schemes

<b>Scheme 1.01</b>	Three general synthetic strategies for the synthesis of [n]paracyclophanes.....	7
<b>Scheme 1.02</b>	Top) synthesis of [12]- and [10]paracyclophane ( <b>2h</b> and <b>2j</b> ); bottom) failure of Wurtz coupling to generate [8]paracyclophane ( <b>2f</b> ).....	8
<b>Scheme 1.03</b>	A recent approach to the synthesis of [10]paracyclophane <b>2h</b> .....	9
<b>Scheme 1.04</b>	Synthesis of cyclophanes <b>36</b> and <b>37</b> .....	10
<b>Scheme 1.05</b>	Synthesis of [9]paracyclophane <b>2g</b> .....	11
<b>Scheme 1.06</b>	Synthesis of [7]- and [8]paracyclophanes <b>2e</b> and <b>2f</b> .....	12
<b>Scheme 1.07</b>	Synthesis of [6]paracyclophane <b>2d</b> .....	13
<b>Scheme 1.08</b>	Photochemical equilibrium between compounds <b>49b</b> and <b>2c</b> .....	14
<b>Scheme 1.09</b>	Transient formation of <b>2b</b> from its Dewar isomer <b>49b</b> .....	15
<b>Scheme 1.10</b>	<i>In-situ</i> generation of [4]paracyclophane <b>57</b> .....	15
<b>Scheme 1.11</b>	Reactions of strained [n]paracyclophanes.....	21
<b>Scheme 1.12</b>	General strategy for the synthesis of [n](2,11)pyrenophanes.....	27
<b>Scheme 1.13</b>	The more favoured <i>anti</i> -configuration of [2.2]metacyclophanes .....	27
<b>Scheme 1.14</b>	A valence isomerization/dehydrogenation (VID) reaction.....	28
<b>Scheme 1.15</b>	Synthesis of 1, <i>n</i> -dioxan[n](2,7)pyrenophanes ( <i>n</i> = 7-12) <b>83b-g</b> .....	30
<b>Scheme 1.16</b>	Reduction of [n](2,7)pyrenophanes <b>24b-e</b> with Li metal.....	35



<b>Scheme 1.17</b> Bromination reactions of pyrenophane <b>83e</b> and diene <b>87</b> .....	36
<b>Scheme 1.18</b> General strategy for the synthesis of $[n](2,11)$ teropyrenophanes <b>25</b> .....	39
<b>Scheme 2.01</b> Synthesis of 1,1,8,8-tetramethyl[8](2,11)teropyrenophane <b>103c</b> using a double-McMurry strategy.....	49
<b>Scheme 2.02</b> Synthesis of teropyrenophanes <b>103b</b> and <b>103a</b> .....	52
<b>Scheme 3.01</b> Strategies for the synthesis of $[n](2,11)$ teropyrenophanes.....	101
<b>Scheme 3.02</b> Failure of <i>anti</i> - <b>101a</b> to generate <b>101a</b> during a McMurry reaction .....	102
<b>Scheme 3.03</b> Synthesis of teropyrenophanes <b>103b-c</b> and attempted synthesis of <b>103b</b> .....	104
<b>Scheme 4.01</b> Synthesis of diols <b>94b-e</b> .....	122
<b>Scheme 4.02</b> Previous synthesis of dichlorides <b>95b-d</b> .....	123
<b>Scheme 4.03</b> Friedel-Crafts alkylation of <b>95b-d</b> .....	125
<b>Scheme 4.04</b> Formation of byproducts <b>116c-120c</b> during Friedel-Crafts alkylation using original conditions.....	127
<b>Scheme 4.05</b> <i>t</i> -Butylation of pyrene ( <b>20</b> ).....	130
<b>Scheme 4.06</b> Attempted lithiation of pyrene ( <b>20</b> ).....	132
<b>Scheme 4.07</b> Attempted alkylation of substituted pyrenes.....	133
<b>Scheme 4.08</b> Attempted alkylations of protected pyrenes.....	135
<b>Scheme 4.09</b> Modified conditions for the Friedel-Crafts alkylation.....	137

<b>Scheme 4.10</b> Rieche formylation.....	139
<b>Scheme 4-11</b> Reduciton of dialdehydes <b>97b-e</b> .....	140
<b>Scheme 4.12</b> Previous conditions for the Wurtz coupling.....	141
<b>Scheme 4.13</b> <i>In-situ</i> iodination / Wurtz coupling of diols <b>134b-e</b> .....	144
<b>Scheme 4.14</b> Previous conditions for the Rieche formylation reaction of cyclophane <b>107d</b> .....	148
<b>Scheme 4.15</b> Synthesis of dialdehydes <b>108b-e</b> using modified Rieche formylation conditions.....	151
<b>Scheme 4.16</b> Attempted reactions for the generation of cyclophane dialdehyde <b>108d</b> .....	156
<b>Scheme 4.17</b> McMurry reaction of cyclophane dialdehydes <b>108b-c</b> .....	159
<b>Scheme 4.18</b> McMurry reaction of dialdehyde <b>108e</b> .....	160
<b>Scheme 4.19</b> Plausible synthetic strategy for the formation of cyclophane <b>147</b> .....	165
<b>Scheme 4.20</b> Reaction of methylated aromatic solvents with DDQ.....	173
<b>Scheme 4.21</b> Unexpected chlorination of teropyrenophane <b>103d</b> .....	175
<b>Scheme 4.22</b> Byproducts formed in the presence of CF <sub>3</sub> CO <sub>2</sub> H.....	182
<b>Scheme 4.23</b> Mechanism for the formation of compound <b>160c</b> .....	183
<b>Scheme 4.24</b> Conversion of <b>109b</b> to <b>103b</b> .....	187
<b>Scheme 4.25</b> VID reaction of <b>109e</b> to <b>103e</b> .....	188

<b>Scheme 5.01</b> Bromination of pyrene.....	424
<b>Scheme 5.02</b> Bromination chemistry of pyrene.....	425
<b>Scheme 5.03</b> Bromination chemistry of pyrene.....	426
<b>Scheme 5.04</b> Bromination of 1,6-dibutylpyrene ( <b>193</b> ).....	427
<b>Scheme 5.05</b> Selected bromination reaction of substituted pyrenes.....	428
<b>Scheme 5.06</b> Bromination of pyrenediketone <b>202</b> .....	429
<b>Scheme 5.07</b> Bromination of layered metacyclophanes.....	431
<b>Scheme 5.08</b> Bromination of <i>anti</i> -8-methoxy[2]metacyclo[2](1,3)pyrenophane <b>219</b> ....	437
<b>Scheme 5.09</b> Reaction of <b>109d</b> with excess bromine.....	438
<b>Scheme 6.01</b> A strategy for the synthesis of a nano graphene sheet.....	519
<b>Scheme 6.02</b> Suzuki coupling of tetrabromoterypyrenophane <b>223</b> .....	523
<b>Scheme 6.03</b> An unsuccessful attempt of a ten-fold cyclodehydrogenation reaction....	524
<b>Scheme 6.04</b> Coupling of pyrene <b>20</b> and phenylboroxine <b>265</b> using direct C-H activation.....	525
<b>Scheme 6.05</b> Direct C-H arylation of [9](2,11)teropyrenophane <b>103d</b> . The regio- chemistry of the products <b>266-273</b> was assigned based the bromination reaction and is purely tentative. Each of these compounds could be a mix of regioisomers.....	526
<b>Scheme 6.06</b> 1:1 APEX and 1:2 APEX reactions.....	529
<b>Scheme 6.07</b> Attempted Diels-Alder reaction of the bay regions.....	545

<b>Scheme 7.01</b> Two previously explored and failed approaches to model compound <b>318</b> ; top) a double-McMurry strategy; bottom) a Wurtz / McMurry strategy.....	564
<b>Scheme 7.02</b> Attempted synthesis of model compound <b>318</b> .....	566
<b>Scheme 7.03</b> Attempted aromatization of cyclophanemonoene <b>315</b> .....	569
<b>Scheme 7.04</b> Misumi's synthesis of teropyrene <b>22</b> .....	573
<b>Scheme 7.05</b> Introduction of large alkyl group to improve the solubility of teropyrene system.....	574
<b>Scheme 7.06</b> A plausible strategy for generating the teropyrene system.....	574

## List of Abbreviations

PAH	polycyclic aromatic hydrocarbon
NMR	nuclear magnetic resonance
UV-vis	ultraviolet-visible
kcal	kilocalorie
mol	mole
ASE	aromatic stabilization energy
HMPA	hexamethylphosphoramide
THF	tetrahydrofuran
rt	room temperature
TMSCl	trimethylsilyl chloride
equiv.	equiv.
Pd/C	palladium/charcoal
conc.	concentrated
TFA	trifluoroacetic acid
DDQ	2,3-dichloro-5,6-dicyano-1,4-benzoquinone
<i>m</i> -CPBA	<i>meta</i> -chloroperbenzoic acid
°C	degree centigrade

nm	nanometer
STO-3G	slater type orbital-3 Gaussian
MINDO	modified intermediate neglect of diatomic overlap
B3LYP	Becke-3-Lee-Yang Parr
<i>SE</i>	strain energy
VID	valence isomerization / dehydrogenation
DBU	1,8-diazabicycloundec-7-ene
AM1	Austin model one
DFT	density functional theory
MM	molecular mechanics
HOMA	harmonic oscillator model of aromaticity
NICS	nucleus-independent chemical shift
NBS	<i>N</i> -bromosuccinimide
SWCNT	single-walled carbon nanotube
h	hour
py	pyridine
mg	milligram
<sup>1</sup> H NMR	proton nuclear magnetic resonance
$\delta$	chemical shift

ppm	parts per million
COSY	correlation spectroscopy
HMQC	heteronuclear multiple quantum coherence
<i>cf.</i>	confero (I compare, <i>Latin</i> )
$\Delta\delta$	difference in chemical shift
VT-NMR	variable temperature nuclear magnetic resonance
K	Kelvin
$T_c$	coalescence temperature
$\Delta\nu_o$	difference in frequency at $T_c$
$G^\ddagger$	free energy of activation
mL	milliliter
g	gram
L	liter
min	minutes
$R_f$	retention factor
m.p.	melting point
MHz	megahertz
br d	broad doublet

$J$	coupling constant
br s	broad singlet
LC-MS	liquid chromatography mass spectrometry
HRMS	high resolution mass spectrometry
APPI	atmospheric pressure photoionization
$m/z$	mass to charge ratio
cm	centimeter
s	singlet
d	doublet
m	multiplet
q	quintet
CI	chemical ionization
calcd	calculated
rel. int.	relative intensity
EI	electron impact
CPP	cycloparaphenylene
$\lambda_{\text{exe}}$	excitation wavelength
HPLC	high pressure liquid chromatography
GCMS	gas chromatography mass spectroscopy



LiTMP	lithium 2,2,6,6-tetramethylpiperidide
tlc	thin layer chromatography
TIPSCl	triisopropylsilyl chloride
DMAP	4-(dimethylamino)pyridine
Bz	benzoyl
<i>ca.</i>	circa
S <sub>N</sub> 2	substitution nucleophilic bimolecular
PMHS	polymethylhydrosiloxane
MALDI-TOF	matrix-assisted laser desorption/ionization - time of flight
1-D	one dimensional
2-D	two dimensional
EWG	electron withdrawing group
ACS	American Chemical Society
NOESY	nuclear Overhauser effect spectroscopy
DMF	<i>N,N</i> -dimethylformamide
MW	microwave
<i>m</i> -	meta
<i>p</i> -	para
W	Watt

$pK_a$	acid dissociation constant at logarithmic scale
$\theta_{\text{tot}}$	total bend
DCE	1,2-dichloroethane
APEX	annulative $\pi$ -extension
TCNQ	7,7,8,8-tetracyano-1,4-quinodimethane
CT	charge transfer

## General experimental details

Reactions involving moisture sensitive catalysts and reagents were carried out under an inert atmosphere of nitrogen gas using standard techniques. Commercially available starting materials and reagents were used for the reactions without further purification. Either ACS grade or drum grade dichloromethane and tetrahydrofuran were used for all the reactions except for the McMurry reaction, where the drum THF was distilled over sodium and benzophenone.  $^1\text{H}$  and  $^{13}\text{C}$  NMR spectra were recorded from  $\text{CDCl}_3$  solutions at 300 MHz (75 MHz for  $^{13}\text{C}$ ) on a Bruker AVANCE III multinuclear spectrometer with a BBFO probe or at 500 MHz (125 MHz for  $^{13}\text{C}$ ) on a Bruker AVANCE spectrometer. All NMR spectra were referenced to  $\text{CDCl}_3$  ( $\delta_{\text{H}} = 0.00$  ppm) and  $\text{CDCl}_3$  ( $\delta_{\text{H}} = 7.26$  ppm).  $^1\text{H}$  NMR data are presented as follows: chemical shift ( $\delta$ , ppm), multiplicity (s = singlet, br s = broad singlet, d = doublet, br d = broad doublet, t = triplet, q = quartet dd = doublet of doublet, m = multiplet, br m = broad multiplet, quin=quintet), coupling constants ( $J$  in Hz). Solid state NMR spectra recorded at 600 MHz (175 MHz for  $^{13}\text{C}$ ) on a Bruker AVANCE II high resolution spectrometer. Low resolution mass spectrometric (LC-MS) data were obtained using an Agilent 1100 series LC/MSD instrument, Agilent 1100 series LC/MSD (trap) or an Agilent 6200 series Accurate-Mass-Time-of-Flight instrument respectively. High resolution mass spectroscopic data were obtained using a Waters Micromass<sup>®</sup> GCT Premier<sup>TM</sup> instrument or an Agilent 6200 series Accurate-Mass-Time-of-Flight instrument respectively. Mass spectrometric (MS) data were as follows: ionization mode,  $m/z$  (relative intensity), assignment (when appropriate), calculated mass and found mass for

the given formula. High pressure liquid chromatography (HPLC) was performed using an Agilent 1100 series LC/MSD instrument interfaced to an ion trap mass analyzer. Gas chromatography (GCMS) was performed on an Agilent 6890N system interfaced to a single quadrupole 5937 inert MSD. Matrix-assisted laser desorption/ionization-time of flight (MALDI-TOF) spectra were recorded using the Applied biosystems/MDS SCIEX 4800 series. UV-Vis Absorption spectra recorded on an Agilent HP8453A UV-visible absorbance spectrophotometer. Fluorescence spectra were recorded on a 6000 series PTI QuantaMaster spectrofluorometer. Melting points were recorded using Mettler automatic digital melting point apparatus. Microwave reactions performed on a CEM discoverer SP microwave synthesizer equipped with explorer-12 hybrid. Silica column chromatography was conducted using Zeochem Zeoprep 60 Eco40-63  $\mu\text{m}$  silica gel. Thin layer chromatography (tlc) was performed using commercially pre-coated plastic-backed POLYGRAM® SILG/UV254 silica gel plates (layer thickness 200  $\mu\text{m}$ ). Column dimensions are recorded as height  $\times$  diameter. Solvents were removed under reduced pressure. Developed plates were visualized using UV light at 254 and 365 nm and phosphomolibdic acid stain. All glassware was oven dried at 150  $^{\circ}\text{C}$  and cooled under an inert atmosphere of nitrogen unless otherwise noted.

Single crystal structures were collected at Department of Chemistry X-Ray Facility, Western University. Data was collected on a Bruker APEX-II CCD diffractometer. The crystal was kept at 110(2) K during data collection. Using Olex2, the structures were solved with the ShelXT structure solution program using

Direct Methods and refined with the ShelXL refinement package using Least Squares minimisation.

Samples for crystallographic analysis at the synchrotron were submitted through the SCrALS (Service Crystallography at Advanced Light Source) program. Crystallographic data were collected at Beamline 11.3.1 at the Advanced Light Source (ALS), Lawrence Berkeley National Laboratory. The ALS is supported by the U.S. Department of Energy, Office of Energy Sciences Materials Sciences Division, under contract DE-AC02-05CH11231. Intensity data were collected at 150K on a D8 goniostat equipped with a Bruker APEXII CCD detector at Beamline 11.3.1 at the Advanced Light Source (Lawrence Berkeley National Laboratory) using synchrotron radiation tuned to  $\lambda=0.77490\text{\AA}$ . For data collection frames were measured for a duration of 1-s at  $0.3^\circ$  intervals of  $\omega$  with a maximum resolution of  $\sim 0.60\text{\AA}$ . The data frames were collected using the program APEX2 and processed using the program SAINT routine within APEX2. The data were corrected for absorption and beam corrections based on the multi-scan technique as implemented in SADABS. Using Olex2, the structure was solved with the ShelXD structure solution program using Dual Space and refined with the ShelXL refinement package using Least Squares minimisation.

## Chapter 1. Introduction to $[n]$ Cyclophanes

### 1.1 Cyclophane Chemistry

Landmark events in cyclophane chemistry were the discovery of [2.2]paracyclophane (**1**) (Figure 1.01) by Brown and Farthing<sup>1</sup> in 1949 and its rational synthesis by Cram in 1951.<sup>2</sup> Thereafter, cyclophanes quickly developed into a distinct class of compounds due to their unusual structures (especially nonplanar aromatic systems) and interesting chemical and physical properties. A large body of literature on cyclophanes has been published, among which can be found a number of reviews, monographs and books.<sup>3</sup>

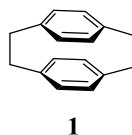


**Figure 1.01** [2.2]paracyclophane.

#### 1.1.1 Scope of cyclophane chemistry

Simply stated, cyclophanes contain one or more aromatic systems (*e.g.* benzene) that are bridged by one or more aliphatic chains at non-adjacent positions. For benzene, only two bridging motifs are available, namely *para*- (1,4) or *meta*- (1,3) (Figure 1.02). The *ortho*- (1,2) bridging motif is equivalent to ring fusion, so “orthocyclophanes” are usually excluded from discussions about cyclophane chemistry. The unlimited scope of cyclophane structures comes into focus when one considers that a cyclophane can have any number and any type of aromatic rings and as many bridges as allowed by the

aromatic systems. The bridges can be of any length and can vary in the atom type and degree of unsaturation. A detailed discussion of structural diversity in cyclophanes has recently been published.<sup>4</sup>

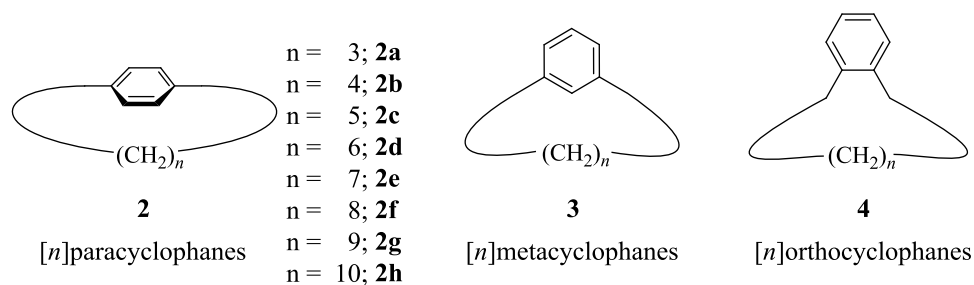


**Figure 1.02** Cyclophanes with various bridging positions.

To briefly illustrate the structural diversity, some examples of cyclophanes are shown in Figure 1.03.<sup>5</sup> In accord with the great structural diversity in cyclophanes, they have attracted interest for a wide range of reasons, including their unusual structures, synthetic challenge, strain and its consequences, nonplanar aromatics, unusual chemical behaviour, unusual physical properties, fundamental phenomena such as aromaticity, host-guest chemistry, through-space interactions, conformational behaviour and chirality.

The focus of this particular thesis is on a set of cyclophanes consisting of only one aromatic system and one bridge, which make them members of the simplest class of cyclophanes, the  $[n]$ cyclophanes. This type of cyclophane is especially interesting because variation of the value of  $n$  (the number of atoms in the bridge) directly affects the degree of distortion from planarity in the aromatic system. As such, incremental changes in structure in a particular aromatic system can be correlated with the resulting changes in chemical and physical properties. Therefore the  $[n]$ cyclophane approach to systemati-

cally distorting aromatic systems provides a tremendous opportunity to learn. It can conceivably be applied to virtually any aromatic system, but has only ever been done (over a wide range of distortion) for benzene and pyrene (see below).

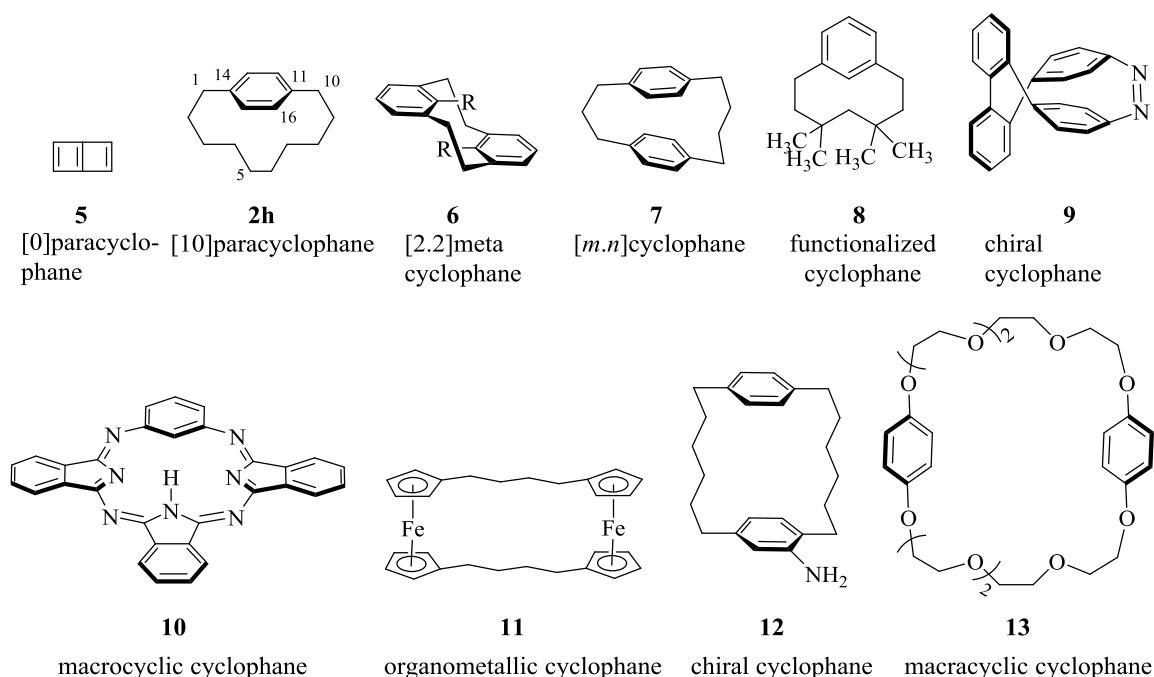


**Figure 1.03** Selected examples of cyclophanes.

## 1.2 The rylenes and capped rylenes

Polycyclic aromatic hydrocarbons (PAH)s are a very important and widely-studied class of compounds.<sup>6</sup> With the emergence of graphene as a new material,<sup>7</sup> there is considerable current interest in the synthesis and characterization of graphene segments, or “nanographenes”.<sup>8</sup> PAH-based nanoribbons (**14**) are one type of nanoribbon, which can be viewed as being derived from either of two series of compounds. The first of these is the rylenes,<sup>9</sup> which start with naphthalene (**15**) and progress to perylene (**16**), terrylene (**17**), quaterrylene (**18**) and beyond through the successive



addition of naphthalene ( $C_{10}$ ) units (Figure 1.04). The other series, which does not appear to have been given a name, starts with benzene (**19**) and progresses to pyrene (**20**),

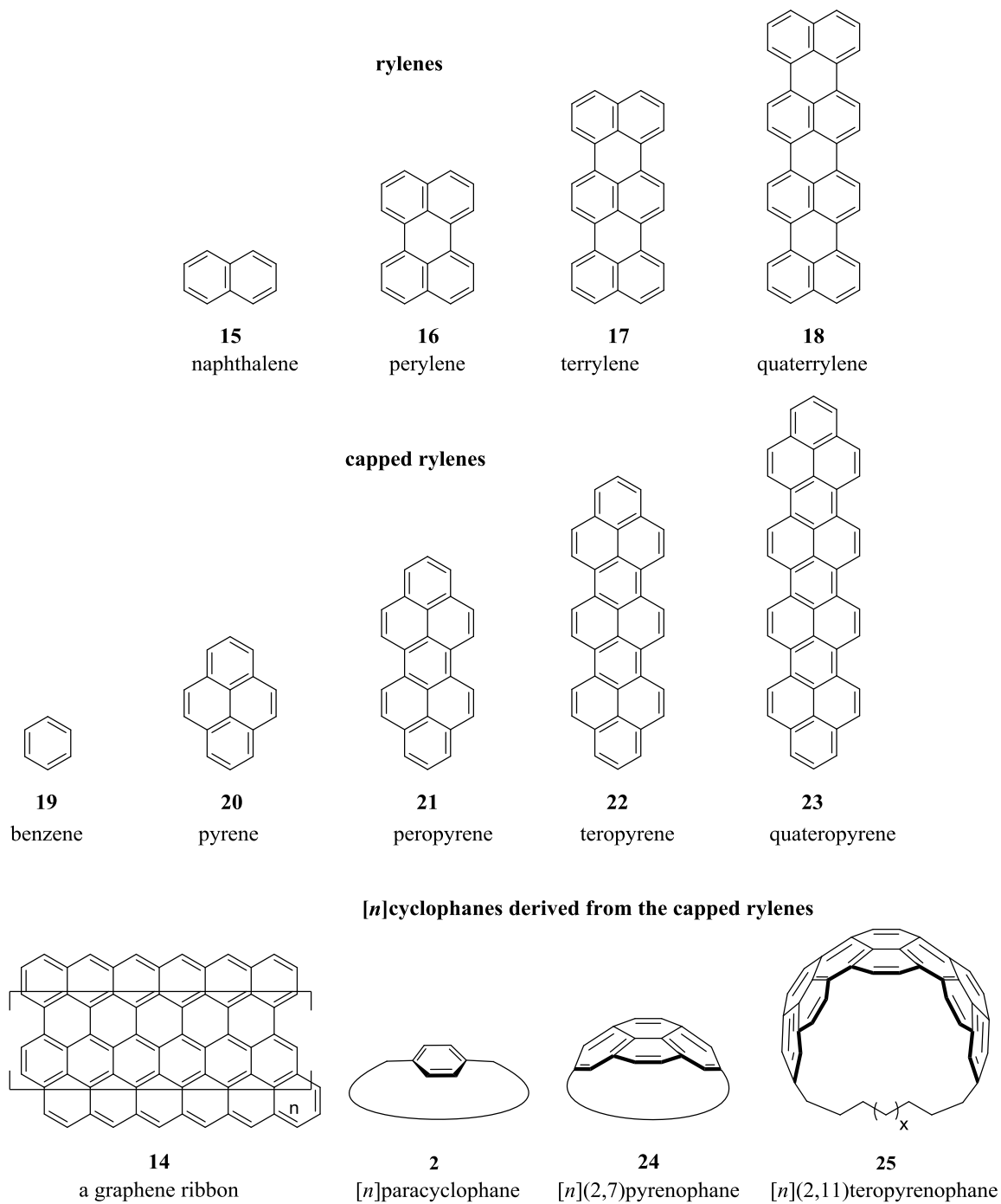


**Figure 1.04** Rylenes, capped rylenes and some capped rylene-derived [n]cyclophanes.

peropyrene (**21**), teropyrene (**22**), quateropyrene (**23**) and beyond through the successive addition of C<sub>10</sub> units. The latter series can be viewed as capped rylenes. From a ring fusion perspective, both series are extended by the fusion of a phenalene unit. From the [n]cyclophane perspective, the capped rylenes are more interesting because bridging of the two most remote positions affords a series of nicely symmetric [n]cyclophanes in which the PAH is bent in an end-to-end fashion.

### 1.3 The [n]paracyclophanes

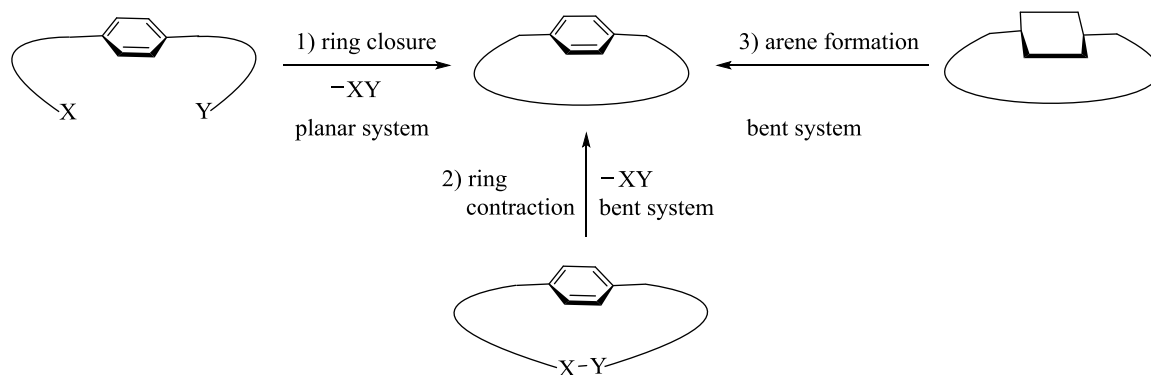
Benzene is the archetypal aromatic molecule and is by far the most commonly employed aromatic system in cyclophanes. The [n]paracyclophanes (**2**) are the simplest cyclophanes with the (1,4) bridging motif and they have attracted interest for more than six decades.<sup>3</sup> Initial work on this family of compounds was reported by Cram and Allinger in 1954.<sup>10</sup> Paracyclophanes (or derivatives thereof) with  $n = 4$ –16 have been synthesized. The smallest isolable member of the series is [6]paracyclophane. [5]Paracyclophane is in equilibrium with its Dewar benzene valence isomer and [4]paracyclophane has been trapped only below  $-196\text{ }^{\circ}\text{C}$ . Interestingly, the highly unstable butadiene **5** can be viewed as [0]paracyclophane, but this compound has not been isolated. Various chemical and physical properties of the [n]paracyclophanes have been studied both experimentally and theoretically. The benzene ring in the [n]paracyclophanes with  $n > 10$  is essentially planar due to the sufficiently long bridge length. Accordingly, their chemical (electrophilic aromatic substitution reactions) and spectroscopic (NMR, UV-vis, *etc.*) properties closely resemble those of 1,4-dialkylbenzenes. On the

other hand, the chemical and physical properties of the  $[n]$ paracyclophanes with  $n \leq 10$  deviate increasingly from “normal” as the value of  $n$  becomes smaller (see below).

### 1.3.1 Synthesis

To date, no single strategy has been employed to synthesize a long series of  $[n]$ paracyclophanes. Instead, a variety of strategies has been employed, each of which has been used to synthesize only one or two members of the homologous series. In general terms, three different types of approaches have been used to synthesize  $[n]$ paracyclophanes: (1) macrocyclic ring closure, (2) ring contraction or (3) arene formation (Scheme 1.01). The first of these three approaches involves bond formation in the bridge to generate the cyclophane. This is an entropically challenging process for unstrained  $[n]$ paracyclophanes ( $n > 10$ ) and both enthalpically and entropically challenging for strained  $[n]$ paracyclophanes ( $n < 10$ ). As a result, this approach has never been successfully applied to any  $[n]$ paracyclophane with  $n < 10$ . The second approach involves the application of ring-contraction reaction to an existing  $[n]$ paracyclophane. This approach has been successfully applied to  $[n]$ paracyclophanes as small as  $n = 6$ . Presumably, the increase in strain that comes with further ring-contraction is too much of an energetic disincentive for the chemistry to succeed. The third approach is the most powerful one. It involves the synthesis of a bridged “pre-aromatic” system and the conversion of the “pre-arene” into a benzene ring. The big advantage of this method is that the formation of a benzene ring is accompanied by *ca.* 30 kcal/mol of aromatic stabilization energy (ASE),<sup>11</sup> which offsets developing strain during cyclophane formation. This approach

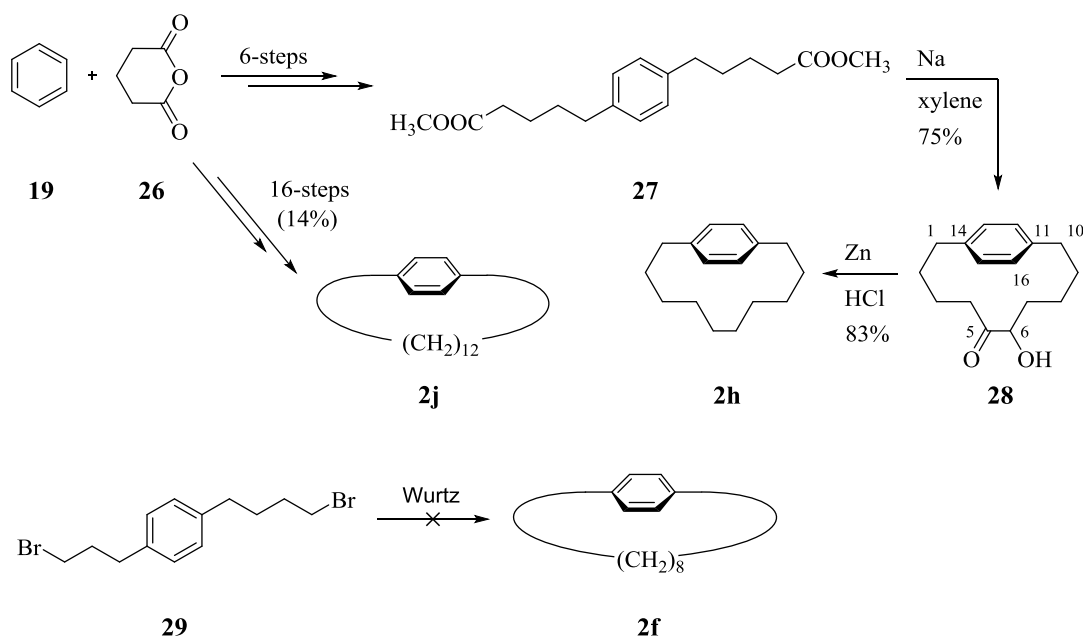
has been used for the smallest and most strained  $[n]$ paracyclophanes. For each of these general strategies, some very interesting and creative chemistry has been employed, a selection of which is illustrated in the following sections.



**Scheme 1.01** Three general synthetic strategies for the synthesis of  $[n]$ paracyclophanes.

### 1.3.1.1 Synthesis of $[n]$ paracyclophanes using the ring closure approach (Strategy 1)

The parent [10]paracyclophane (**2h**) was synthesized by Cram *et al.* using an intramolecular acyloin condensation as the key cyclophane-forming reaction (Scheme 1.02, top).<sup>12</sup> The synthesis started from benzene (**19**) and glutaric anhydride (**26**) and led to key intermediate **27** in 6 steps. Intramolecular acyloin condensation afforded [10]paracyclophane derivative **28** in 75% yield. Complete reduction of the functional groups on the bridge afforded **2h** in 26% overall yield for the 8-step synthesis. The synthesis of [12]paracyclophane (**2j**) was achieved using the same approach in 16 steps with 14% overall yield.<sup>13</sup> On the other hand, attempts to synthesize the lower homologue [8]paracyclophane (**2f**) using intramolecular Wurtz coupling of dibromide **29** failed (Scheme 1.02, bottom).

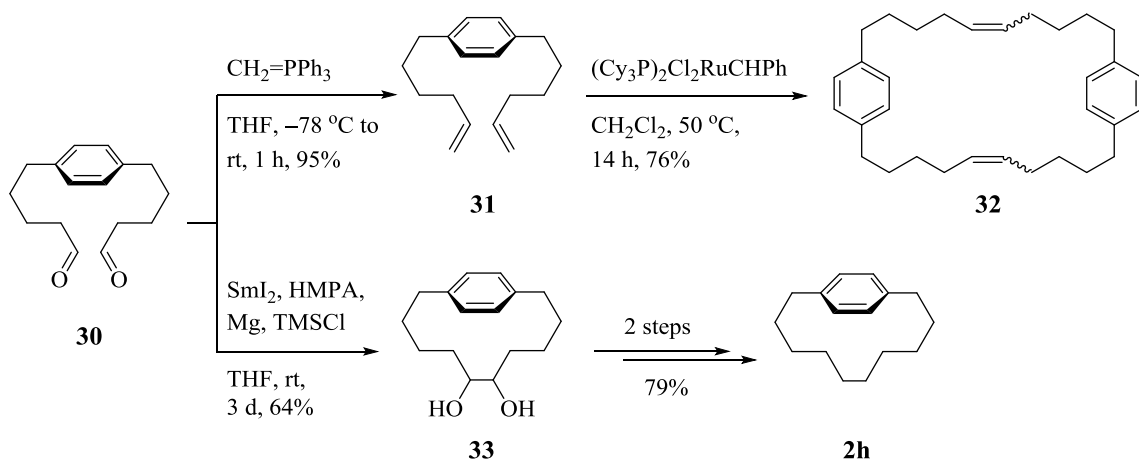


**Scheme 1.02** Top) synthesis of [12]- and [10]paracyclophane (**2h** and **2j**); bottom) failure of Wurtz coupling to generate [8]paracyclophane (**2f**).

More recently, an attempt to synthesize [10]paracyclophane (**2h**) using ring-closing metathesis (RCM) of diene **31** failed, giving only macrocycle **32** (Scheme 1.03).<sup>14</sup> On the other hand, SmI<sub>2</sub>-mediated pinacol coupling of dialdehyde **30** afforded [10]paracyclophane-5,6-diol (**33**) in four steps (52% overall yield), which could be converted into **2h** in two steps in 79% yield (Scheme 1.03).

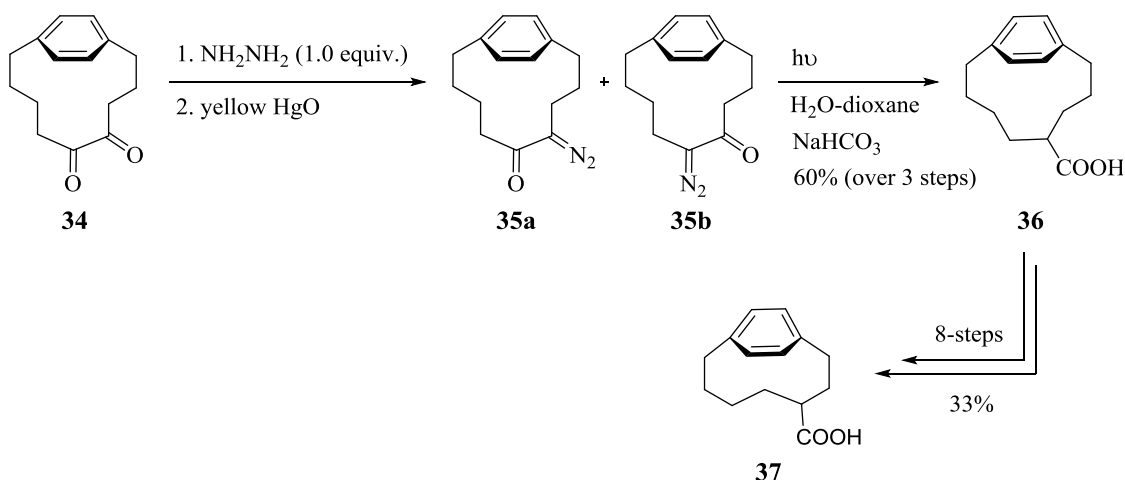
### 1.3.1.2 Synthesis of [*n*]paracyclophanes using the ring contraction approach (Strategy 2)

The ring contraction approach typically delivers bridge-substituted cyclophanes, which must be synthetically manipulated to give the corresponding parent (unsubstituted)



**Scheme 1.03** A recent approach to the synthesis of [10]paracyclophane **2h**.

[*n*]paracyclophanes. Allinger *et al.* used the ring contraction approach in the synthesis of [8]- and [7]paracyclophanes and it proved to be quite laborious work.<sup>15</sup> [9]Paracyclophane-4,5-dione (**34**) was synthesized according to Strategy 1 by an 8-step sequence. Reaction of diketone **34** with 1.0 equiv. of 95% hydrazine yielded a mixture of regioisomeric monohydrazones, which was immediately oxidized using mercuric oxide to afford the isomeric azonium compounds **35a** and **35b** (Scheme 1.04). This isomer mixture underwent Wolff rearrangement (ring contraction) upon irradiation in the presence of water to afford [8]paracyclophane-4-carboxylic acid (**36**). Carboxylic acid **36** was subsequently converted to its lower homologue **37** in another 8 steps using a similar ring contraction strategy (Scheme 1.04).<sup>16</sup> No further attempts to synthesize the next lower homologue of **37** using the ring contraction approach have been reported, which suggests that either that the lower limit for this strategy was reached or the length of the synthetic sequence precluded further study.



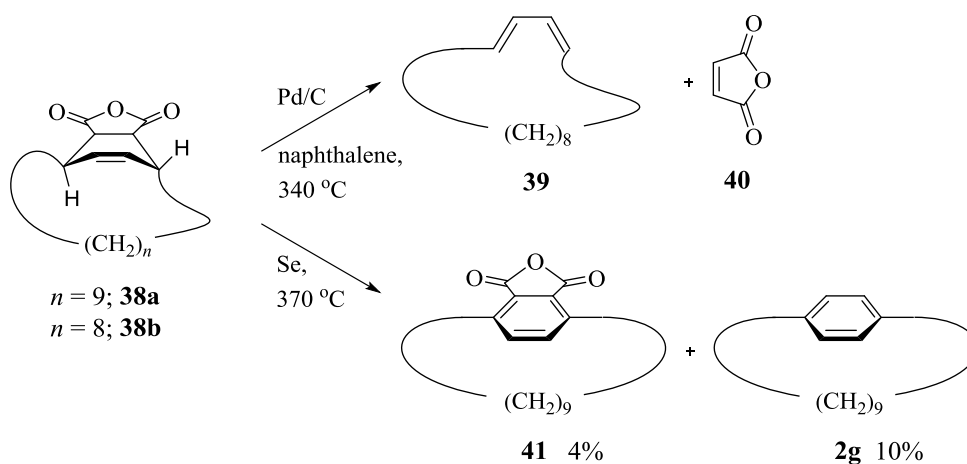
**Scheme 1.04** Synthesis of cyclophanes **36** and **37**.

### 1.3.1.3 Synthesis of $[n]$ paracyclophanes using an arene-forming approach (Strategy 3)

As described earlier, this approach begins with an intact bridging unit followed by the generation of an aromatic system (usually nonplanar) from some sort of a non-aromatic precursor (a "pre-arene"). In most cases, the pre-arene has a kinked structure, which can accommodate a relatively short bridge without an appreciable amount of strain. The final step of the synthesis is always the arene-forming reaction, during which the interplay between developing strain and developing aromaticity is a key factor in determining the success or failure of the reaction.

Bartlett *et al.* synthesized a partially unsaturated cyclophane precursor **38a**, which contains an intact 9-atom bridge.<sup>17</sup> Probably, the *trans*-relationship of the substituents on the cyclohexene system (the pre-arene) imposes some strain in the molecule. Attempted dehydrogenation of **38a** using Pd/C in boiling naphthalene failed to afford the anhydride

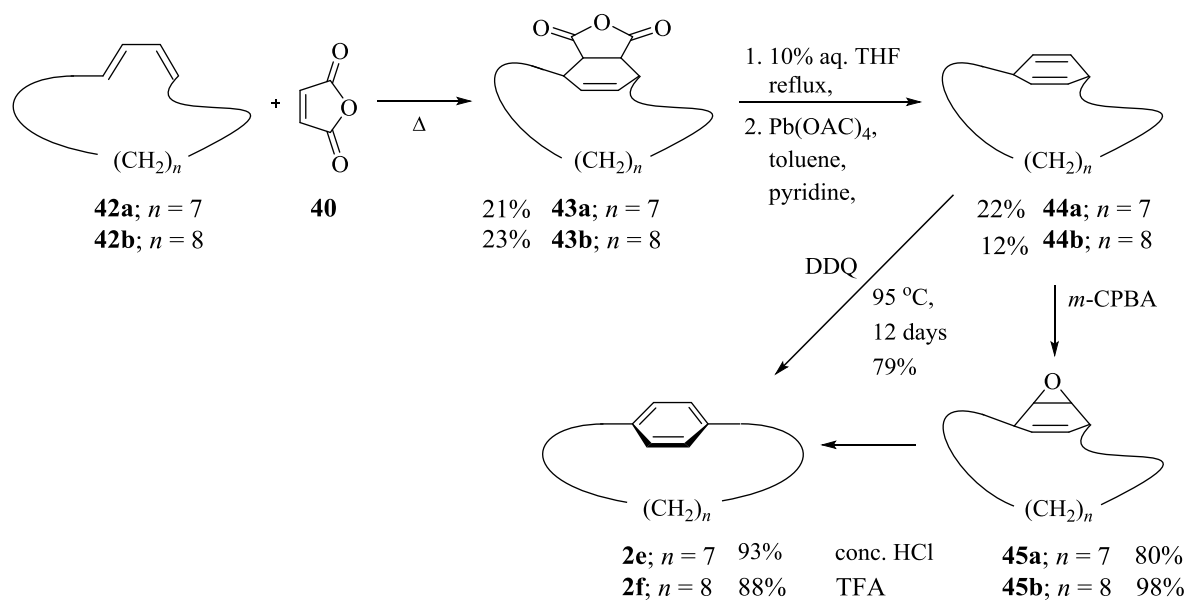
derivative of [9]paracyclophane **41** instead, only starting material recovered. Under similar reactions conditions the lower homologue **38b** ( $n = 8$ ) produced cyclic diene **39** instead of the **2g** *via* retro-Diels-Alder reaction (Scheme 1.05). The desired transformation was ultimately accomplished in 4% yield using selenium at 370 °C. Under these conditions, the parent [9]paracyclophane **2g** was also formed in 10% yield.



**Scheme 1.05** Synthesis of [9]paracyclophane **2g**.

Following the unsuccessful attempt to synthesize **2e** using dehydrogenation, other methodology was exploited for the formation of lower homologues with  $n \leq 8$ . Addition of maleic anhydride **40** to (*E,Z*)-diene **42a** resulted in the Diels-Alder adduct **43a** in 21% yield (Scheme 1.06).<sup>18</sup> This compound was then converted to 1,4-diene **44a** in two steps (hydrolysis and decarboxylation) in 22% yield. Epoxidation of **44a** followed by treatment of the resulting epoxide **45a** with conc. HCl afforded cyclophane **2e** in 93% yield. This strategy was also powerful enough to produce the higher homologue **2f** ( $n = 8$ ) in 88% yield during the aromatization step using TFA (see Scheme 1.06). Alternatively, heating **44a** in the presence of DDQ for 12 days produced **2e** in 79% yield.

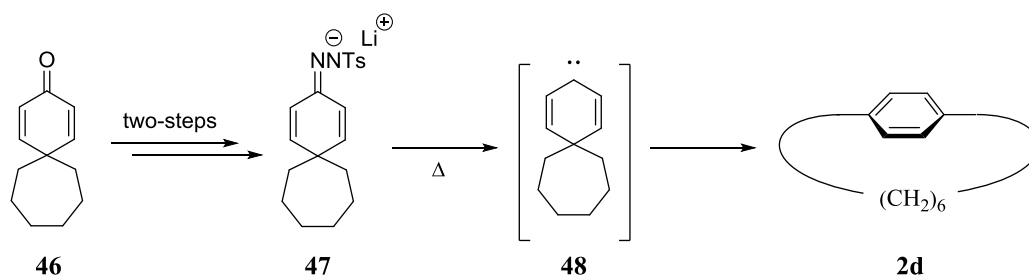




**Scheme 1.06** Synthesis of [7]- and [8]paracyclophanes **2e** and **2f**.

In order to synthesize the next smaller cyclophane **2d**, another clever and concise synthetic pathway was utilized.<sup>19</sup> Spirocyclic ketone **46** was converted to the lithium salt of its tosylhydrazone **47** in two steps. Flash vacuum pyrolysis of **47** afforded **2d** in 5-10% yield (Scheme 1.07). This reaction presumably proceeded through carbene intermediate **48**, which then rearranged to form [6]paracyclophane **2d**. The highly energetic nature of carbene **48** and the formation of a benzene ring presumably work together to favour the formation of **2d**, which is the smallest [*n*]paracyclophane that has been isolated at room temperature.

Interestingly, for [*n*]paracyclophanes with  $n \leq 6$  the Dewar benzene valence isomer comes into the picture. Normally, a Dewar benzene is substantially less stable than its Kekulé valence isomer due to strain energy and the absence of aromatic stabilization energy. For these reasons, bridged Dewar benzenes have been used as

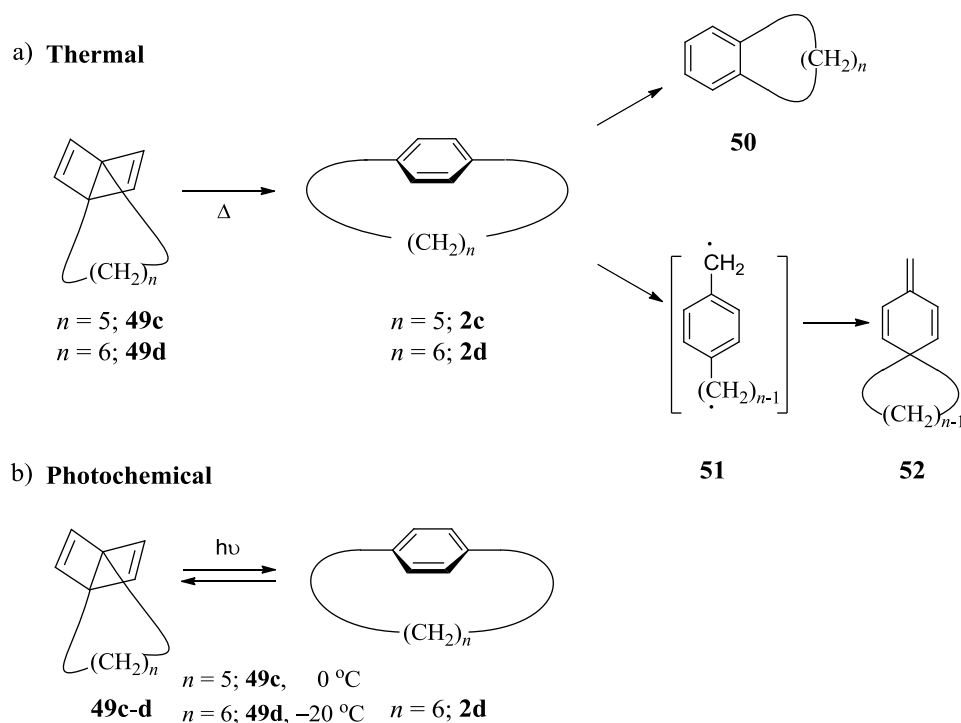


**Scheme 1.07** Synthesis of [6]paracyclophane **2d**.

[*n*]paracyclophane precursors, especially for the synthesis of the more highly strained [*n*]paracyclophanes. As the value of *n* becomes smaller, the strain energy in the [*n*]paracyclophanes goes up, which means that the energy difference between the Dewar and Kekulé isomers becomes progressively smaller. For *n* = 6, the strain in the cyclophane is enough to bring the Dewar isomer into play. When **49d** was heated at 50–90 °C it cleanly isomerised to **2d** (Scheme 1.08a).<sup>20</sup> In contrast, Dewar isomer **49c** shows exceptional stability in solution, even at 150 °C.<sup>21</sup> Upon flash-vacuum thermolysis at temperatures above 280 °C, **2c** was not formed, but rather rearranged products **50**, **52** and polymeric material (Scheme 1.08a).<sup>22</sup> It was postulated that formation of these byproducts involves the intermediacy of [5]paracyclophane (**2c**).

A much milder method for the conversion of a Dewar benzene to its Kekulé isomer is photochemical irradiation, which can be conducted at much lower temperatures (below 0 °C). This can allow unstable products to survive for some time under the conditions of their formation and thus enable their observation. For example, Dewar benzene **49d** was cleanly converted to **2d** by photochemical irradiation with a low pressure mercury lamp below 0 °C (Scheme 1.08b).<sup>20</sup> Interestingly, this photochemical

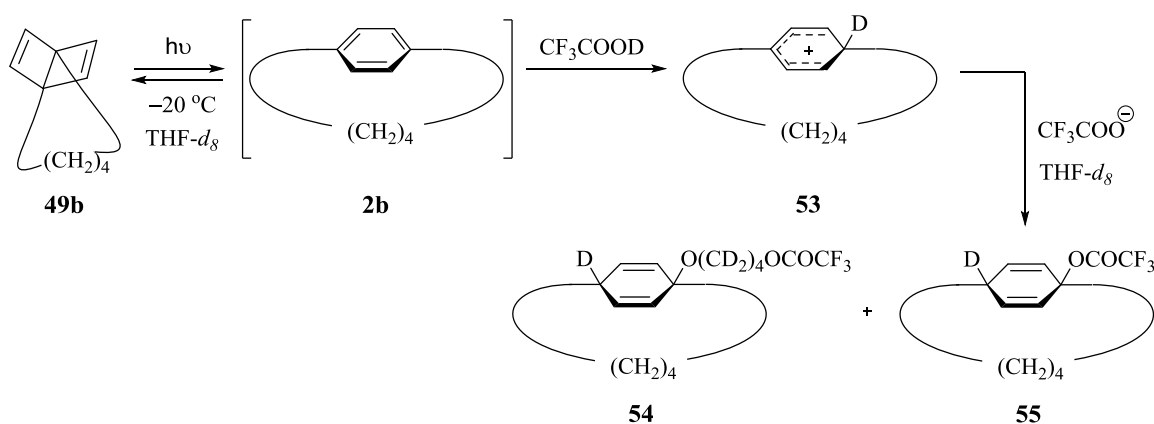
reaction was found to be completely reversible as **49d** was formed quantitatively upon photochemical irradiation of **2d**. Subsequently, [5]paracyclophane (**2c**) was also observed to have a photochemical equilibrium with its Dewar isomer **49c** (7:93) respectively when irradiated with a low pressure mercury lamp at  $-20\text{ }^{\circ}\text{C}$  for 45 min (Scheme 1.08b).<sup>23</sup> Prolonged irradiation of the reaction mixture resulted in either decomposition of **2c** and the formation of insoluble colourless polymeric material. [5]Paracyclophane (**2c**) was found to be stable only below  $-20\text{ }^{\circ}\text{C}$  in solution and polymerize above  $0\text{ }^{\circ}\text{C}$ .



**Scheme 1.08** Photochemical equilibrium between compounds **49b** and **2c**.

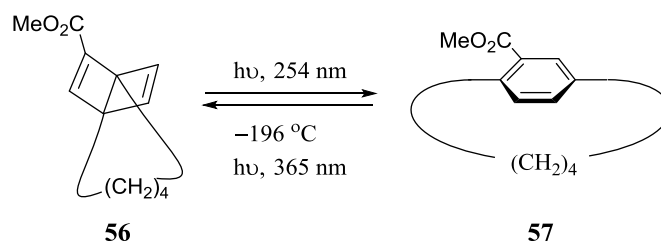
Since **2c** is only stable up to  $-20\text{ }^{\circ}\text{C}$ , it is easy to predict that the more strained lower homologue **2b** ( $n = 4$ ) will readily decompose at this temperature and below. No

evidence for the formation of **2b** was observed when its Dewar isomer **49b** was irradiated in THF-*d*<sub>8</sub> at −50 °C and only polymerization products were observed.<sup>24</sup> Instead, when compound **49b** was irradiated at −60 °C in THF-*d*<sub>8</sub> in the presence of CF<sub>3</sub>COOD (under which **49b** is stable for hours) two new 1,4-addition products **54** and **55** were observed instead of polymerization (Scheme 1.09). Formation of these products can be explained by the intermediacy of cyclophane **2b** and bridgehead-protonated carbocation **53**.



**Scheme 1.09** Transient formation of **2b** from its Dewar isomer **49b**.

Tsuji *et al.* were able to generate a stable enough [4]paracyclophane derivative by introducing an electron withdrawing group (Scheme 1.10).<sup>25</sup> Irradiation of bridged Dewar benzene **56** at 254 nm at −196 °C resulted in the formation of [4]paracyclophane



**Scheme 1.10** *In-situ* generation of [4]paracyclophane **57**.

(**57**), as evidenced by changes in the UV-Vis spectrum of the reaction mixture. Subsequent irradiation at 365 nm converted the cyclophane **57** back to **56**. The cyclophane **57** was highly unstable and decomposed in solutions even below  $-130\text{ }^{\circ}\text{C}$ .

### 1.3.2 Consequences of bending an aromatic system

When an aromatic system in a cyclophane is forced to adopt a nonplanar conformation, it is important to be able to not only quantify the nature and degree of distortion from planarity, but also the changes in properties, including strain energy, aromaticity, spectroscopic properties, *etc.* These issues are briefly discussed in the following Sections.

#### 1.3.2.1 Deformation angles (bend angles)

In the [*n*]paracyclophanes, the benzene ring is bent in an end-to-end fashion such that the benzene ring adopts a boat-like conformation. The degree of distortion from planarity in the benzene system is usually quantified by the parameters  $\alpha$  and  $\beta$ . The former is defined as the smallest angle formed between the planes C2-C1-C6 and C2-C3-C5-C6, *i.e.* an envelope flap angle (Figure 1.05, left). The latter is defined as the smallest angle formed by the plane C2-C1-C6 and the line formed by C1-C7 (bridgehead-benzylic carbon atoms). In many cases, the overall bend in the cyclophane has been quantified by the sum of both these parameters ( $\alpha + \beta$ ).

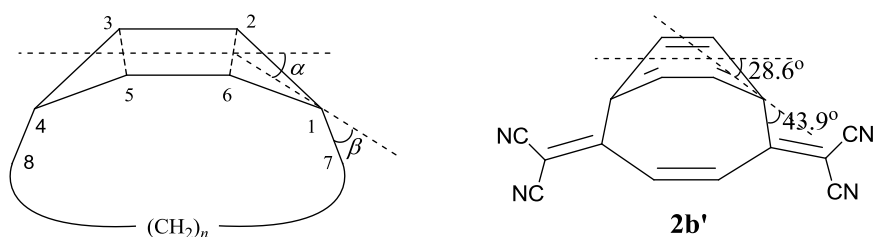


**Figure 1.05** Representation of the deformation angles in a  $[n]$ paracyclophane.

As mentioned earlier, the deformation angle of the benzene ring ( $\alpha$ ) increases with the reduction in the bridging methylene units. The calculated  $\alpha$  values<sup>26</sup> using STO-3G, MINDO/3 and double zeta basis sets (which are in good agreement with the experimental values) for  $[n]$ paracyclophanes **2a-2h** ( $n = 3-10$ ) are given in Table 1.01 along with the experimental values obtained from the crystal structures of the 8-carboxy[6]paracyclophane (**58**),<sup>27</sup> 3-carboxy[7]paracyclophane (**37**)<sup>28</sup> and 4-carboxy[8]paracyclophane (**36**),<sup>15b</sup> which are the derivatives of **2d**, **2e** and **2f** respectively (Table 1.01). The calculated  $\alpha$  and  $\beta$  values for a tetracyano derivative of [4]paracyclophane **2b'** at B3LYP/6-31+G\* level are 28.6° and 43.9° respectively,<sup>25</sup> which gives a total deviation of 72.5° ( $\alpha + \beta$ ) (Figure 1.05, right).

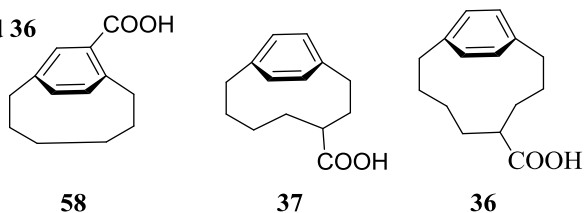
**Table 1.01** Bend angles ( $\alpha$ ,  $\beta$ ), strain energies ( $SE$ ) and aromatic stabilization energies (ASE) of  $[n]$ paracyclophanes **2a-2h** ( $n = 3-10$ ).

parameter	<b>2a</b> ( $n = 3$ )	<b>2b</b> ( $n = 4$ )	<b>2c</b> ( $n = 5$ )	<b>2d</b> ( $n = 6$ )	<b>2e</b> ( $n = 7$ )	<b>2f</b> ( $n = 8$ )	<b>2g</b> ( $n = 9$ )	<b>2h</b> ( $n = 10$ )
bend angles (in degrees)								
$\alpha$ STO-3G		39.5 <sup>b</sup>	22.4	17.2	12.7	8.4	4.6	3.3
MINDO/3	39.1	33.3	27.8	22.6	18.4	14.5	11.0	8.6
double zeta			23.7	18.6	14.2			
exp. <sup>a</sup>				20.9, 20.1	18.3, 15.2	9.0, 9.2		
$\beta$ exp. <sup>a</sup>				19.2, 18.1	5.7, 7.8	14.2, 15.2		
Dewar benzene								
$\alpha$ MNDO/3	79.3	79.4	79.3	79.4	79.3	79.3	79.1	79.3
$SE_{\text{ring}}$ (kcal/mol)								
STO-3G		111.8 <sup>b</sup>	76.0	38.4	19.4	8.1	2.3	1.6
MINDO/3	113.2	81.8	56.4	36.0	23.5	16.1	9.9	7.0
$SE_{\text{bridge}}$ (kcal/mol)								
MINDO/3	8.8	8.9	9.8	9.3	9.3	9.8	10.3	11.8
Dewar benzene								
$SE_{\text{ring}}$ (kcal/mol)								
MNDO	13.0	5.9	5.9	7.6	7.5	7.8	7.8	9.8
MINDO/3	12.8	7.2	7.5	9.1	9.4	9.8	9.8	10.4
$SE_{\text{bridge}}$ (kcal/mol)								
MINDO/3	8.6	6.6	7.4	11.0	14.2	16.9	21.6	19.4
ASE (kcal/mol) <sup>c</sup>								
B3LYP/6-31G*	5.1	15.1	20.0	26.7	31.9	33.0		

<sup>a</sup>crystal data obtained from compounds **58**, **37** and **36**

<sup>b</sup>reference 26c

<sup>c</sup>reference 26b



### 1.3.2.2 Strain energy ( $SE$ ) in the $[n]$ paracyclophanes

In the  $[n]$ paracyclophanes ( $n \leq 10$ ), it is not possible for all of the carbon atoms (both  $sp^2$  and  $sp^3$ ) to adopt ideal geometries, so strain energy ( $SE$ ) comes into picture. The total strain energy  $SE_{\text{tot}}$  can be defined as "*the difference between the heats of formation of the (strained) molecule and a fictitious unstrained molecule*" (Equation 1).<sup>26a</sup>

$$SE_{\text{tot}} = \Delta H_{f,\text{strained}}^0 - \Delta H_{f,\text{unstrained}}^0 \quad \text{eqn. 1}$$

As in any strained system, the strain is distributed around the whole molecule in a way that minimizes the total strain. This being the case, the total strain energy ( $SE_{\text{tot}}$ ) in the  $[n]$ paracyclophanes can be represented as,  $SE_{\text{tot}} = SE_{\text{ring}} + SE_{\text{bridge}}$ , where  $SE_{\text{ring}}$  is the energy required to bend the aromatic ring and  $SE_{\text{bridge}}$  is the amount of energy required to stretch the bridging alkyl chain from its ideal geometry. The STO-3G and/or MINDO/3-calculated strain energies<sup>26a,c</sup> of the aromatic ring ( $SE_{\text{ring}}$ ) and the oligomethylene chains ( $SE_{\text{bridge}}$ ) for the  $[n]$ paracyclophanes ( $n = 3-10$ ) are presented in Table 1.01. As expected, an increase in the  $SE_{\text{ring}}$  was calculated as the chain gets shorter. For smaller cyclophanes ( $n \leq 6$ ),  $SE_{\text{ring}}$  is predominant whereas,  $SE_{\text{bridge}}$  is comparable with  $SE_{\text{ring}}$  when  $n \geq 7$ . For example, the  $SE_{\text{tot}}$  calculated for [4]paracyclophane using STO-3G basis set was found to be 125.9 kcal/mol, out of which 111.8 kcal/mol energy (89%) was due to the  $SE_{\text{ring}}$ .  $SE_{\text{bridge}}$  contributes only 14.1 kcal/mol (11%). On the other hand, the strain energies of the Dewar benzene systems ( $SE_{\text{ring}}$ ) in the corresponding bridged Dewar benzenes ( $n = 3-10$ ) are small (7.2–12.8 kcal/mol) and more or less independent of the bridge length (the same kind of scenario was observed in the case of bend angle,  $\alpha$ ). This explains why the



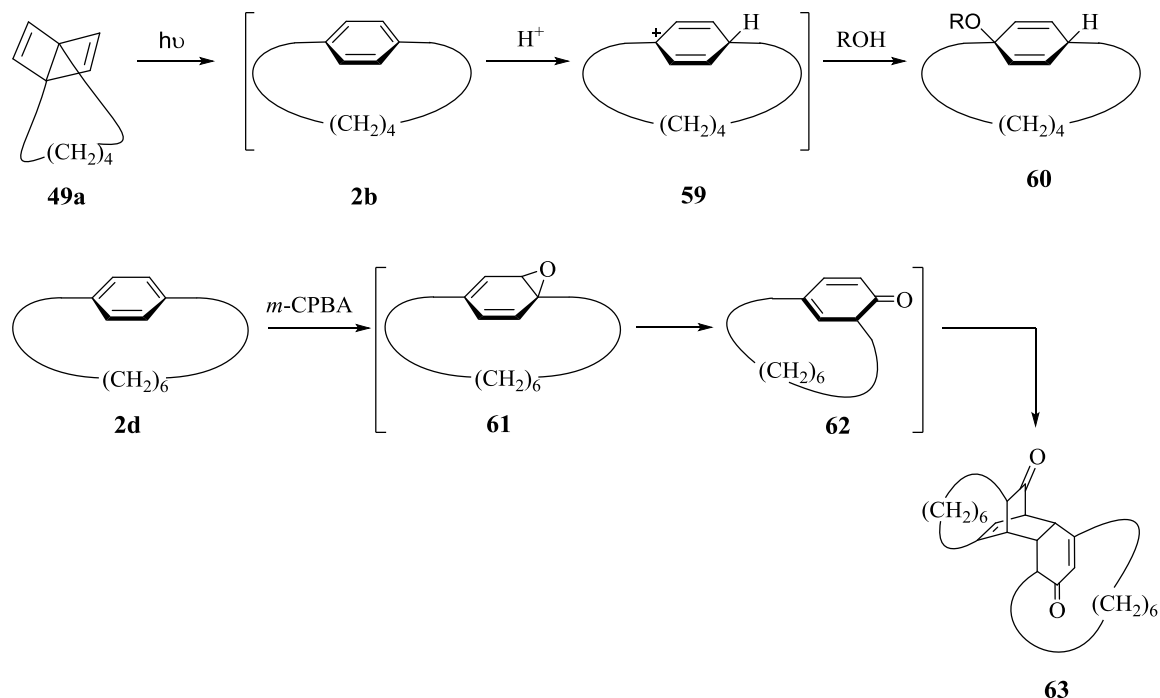
Dewar benzene becomes the preferred isomer for the cyclophanes with  $n \leq 6$ .

### 1.3.2.3 Aromaticity of $[n]$ paracyclophanes

As cyclophane chemistry developed, the aromaticity of nonplanar aromatic systems was viewed in different ways by researchers from different disciplines and remained as a subject of discussion for many years. The statement of Schaefer III *et al.* in 1987 about aromaticity capture the essence of this discussion at that time.<sup>29</sup> *"Synthetic organic chemists often define an aromatic compound as one which is exceptionally stable and which participates more readily in electrophilic aromatic substitution reactions than addition reactions. In contrast, UV spectroscopists frequently note an aromatic compound by the bathochromic shift from conjugated dienes. NMR spectroscopists typically view an aromatic compound as one in which the aromatic proton signals are shifted to low field due to the ring current, and, as in the case of many cyclophanes, protons inside the cone of the ring are shifted to high field. It is also clear that from recent articles on aromaticity and aromatic compounds that even today a universal definition of aromaticity does not exist"*. Nowadays, much of the chemical community appears to be comfortable with the notion that the concept of aromaticity becomes increasingly complicated and nebulous the closer it is examined and that various criteria (reactivity, structural, magnetic, energetic, spectroscopic) can be used to evaluate it, sometimes with different conclusions. Indeed, the small  $[n]$ paracyclophanes ( $n \leq 6$ ) play a key role in illustrating this point, whereby conclusions based on their chemical reactivity can be at odds with those drawn from their physical properties.

### 1.3.2.3.1 Chemical reactivity of small cyclophanes

The  $SE_{\text{ring}}$  in smaller  $[n]$ paracyclophanes ( $n \leq 6$ ) exceeds the aromatic stabilization energy of benzene (*ca.* 30 kcal/mol), so the benefit of strain relief can more than compensate for the loss of aromaticity. As such, these cyclophanes are highly reactive when compared to the larger cyclophanes ( $n \geq 7$ ) and react in ways that normal aromatic compounds do not, *e.g.* polymerization, rearrangement or 1,4-addition of alcohols, acids, halogens, dienophiles, *etc.* at bridgeheads (Schemes 1.08, 1.09 and 1.11).<sup>30,24a,c,27</sup> The increasing preference for the Dewar benzene isomer as the value of  $n$  becomes smaller can also be explained in terms of strain relief being a more important consideration, but the observed reactivity still don't really answer the question as to whether the benzene



**Scheme 1.11** Reactions of strained  $[n]$ paracyclophanes.

ring has lost its aromaticity. Computationally, it appears as though the aromatic stabilization of the benzene ring decreases as it becomes more bent (ASE = 5.1, 15.1 and 20.0 kcal/mol for [5]- (**2c**), [4]- (**2b**) and [3]paracyclophane (**2a**), respectively), but it does not vanish, even in the most extremely distorted system **2a**.

#### 1.3.2.3.2 Spectroscopic properties

The bent aromatic systems are best characterized by both UV-vis and  $^1\text{H}$  NMR spectroscopic techniques. The UV-vis spectra for the unstrained cyclophanes ( $n \geq 10$ ) are similar to those of non-bridged aromatic compounds. On the other hand, the UV-vis spectra of the strained cyclophanes ( $n < 10$ ) show a gradual bathochromic shift in their longest wavelength band as the value of  $n$  becomes smaller (Table 1.02).<sup>28,23</sup> At the same time, the fine structure of the spectrum is steadily lost. The consistent trend in the bathochromic shift and benzene-like spectra suggest the cyclophanes **2c** and **2b** are still aromatic. Surely one can argue that this indicates a steady loss of aromaticity.

The  $^1\text{H}$  NMR chemical shifts of the most shielded protons of the bridging unit (the central methylene units, which lie directly under the benzene system) and the distorted benzene ring are presented in (Table 1.03).<sup>28,23</sup> Clearly, one can observe the increasing upfield shift of the most shielded bridging protons with the reduction in the number of methylene units (in the parent cyclophanes **2h**, **2g**, **2c** and **2b**). This extra shielding effect is attributed to the ring current that is exerted by the benzene system. In the case of substituted cyclophanes **36** and **37** the most shielded methylene protons are shifted by up to 2.0 ppm when compared to the normal methylene unit ( $\delta$  1.4 ppm). This phenomenal

shift is probably due to the combination of ring current and the presence of as electron withdrawing groups. On the other hand, the aromatic protons move consistently to higher

**Table 1.02** UV-Vis spectral data of [n]paracyclophanes **2b-h**.

[n]paracyclophane	$\lambda_{\text{max}}$ (nm) (experimental)			
<i>p</i> -diethylbenzene	193	193	214	265
<b>2h</b> ; ( <i>n</i> = 10)			223	268
<b>2g</b> ; ( <i>n</i> = 9)			224	271
<b>2f</b> ; ( <i>n</i> = 8)	200	205	230	275
<b>2e</b> ; ( <i>n</i> = 7)	196	207	237	284
<b>2d</b> ; ( <i>n</i> = 6)		212	253	296
<b>2c</b> ; ( <i>n</i> = 5)			280	330
<b>2b</b> ; ( <i>n</i> = 4)			260	340

**Table 1.03** NMR data for the shielded protons of [n]paracyclophanes.

[n]paracyclophane	shielded Hs (ppm) (multiplicity, no. of Hs)	aromatic Hs; ppm (multiplicity, no. of Hs)
<b>2h</b>	+0.51 (m, 4H)	7.04 (s, 4H)
<b>2g</b>	+0.40 (m, 4H)	7.00 (s, 4H)
<b>36</b>	−0.25 (m, 1H)	7.15 (m, 4H)
<b>37</b>	−1.40 (dd, 1H)	7.15 (d, 4H)
<b>2d</b>	+0.33 (m, 4H)	7.17 (s, 4H)
<b>2c</b>	+0.01 (m, 1H)	7.44-7.43 (m, 4H)
<b>2b</b>	+5.85 (s, 2H)	7.97 (S, 2H)

field with an increase in the bend of the aromatic system, which may be indicative of diminished ring current and/or increasing vinylic character (Table 1.03).

#### 1.3.2.4 Conformational behaviour of the aliphatic chain

So far, much chemistry has been discussed about various aspects of the bent benzene ring in [*n*]paracyclophanes. Another interesting aspect of cyclophanes is their structure that arises due to different conformations in the bridge (Figure 1.06). Bridging the benzene ring at the 1 and 4 positions not only reduces the symmetry of the benzene system as it deviates from its planarity (planar benzene;  $D_{6h}$  symmetry), but also restricts the freedom of the aliphatic chain as it is stretched. Allinger and Carballeira independently calculated the *SEs* using molecular mechanics (MM) for all the conformations listed in (see Table in Figure 1.06).<sup>31</sup> Even though the absolute numbers for the *SEs* from the two sets of calculations varied significantly in most cases, they agreed that cyclophanes with odd-numbered bridges prefer either  $C_s$  or  $C_2$  symmetry and cyclophanes with even-numbered bridges prefer  $C_2$  symmetry. These preferences presumably have their origin in the minimization of torsional strain (maximization of staggering) in the bridge.

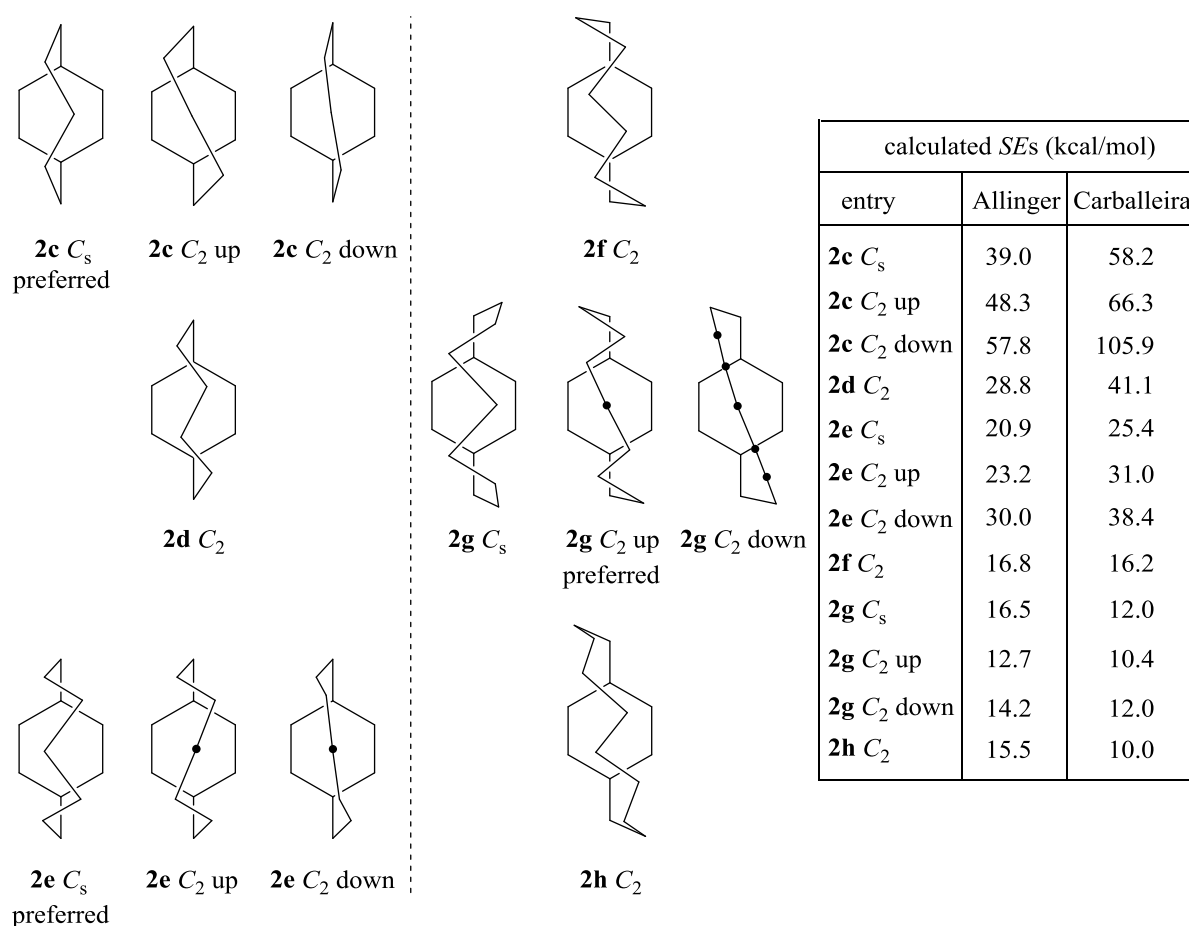


**Figure 1.06** Calculated conformational structures for  $[n]$ paracyclophanes ( $n = 5-10$ ).

## 1.4 The $[n](2,7)$ Pyrenophanes

After benzene (**19**), the next member in the series of capped rylenes (Figure 1.04) is pyrene (**20**). The (2,7) bridging motif in pyrene is analogous to the (1,4), or *para*, motif in benzene, not only because the bonds emanating from these positions are colinear, but also because the presence of the bridge imparts bend over the full length of the aromatic system. At the same time, the move from benzene to pyrene brings a much more interesting aromatic system into play. Pyrene is probably the most well-studied PAH, due primarily to its photochemical and photophysical properties.<sup>32</sup> It forms intramolecular

excimers in solution, has a high fluorescence quantum yield ( $\phi = 0.65$ ) and a long excited state half-life (410 ns). The corresponding monomer and excimer fluorescence bands are also very well-separated. The fluorescence behaviour is very sensitive to its microenvironment and this has led many researchers to use the pyrene system as a fluorescent probe. In fact, pyrene has been described as being the “*gold standard as a molecular probe for microenvironments*”.<sup>33</sup>

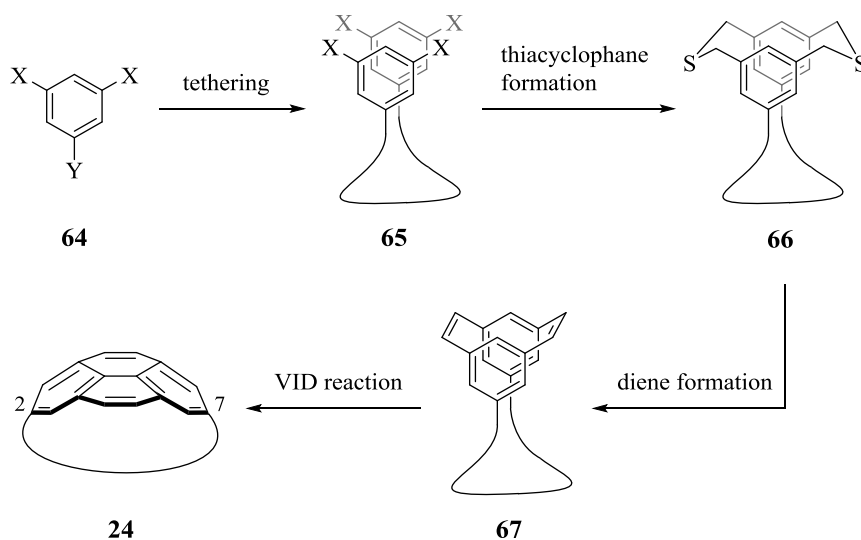
Over the past two decades, the Bodwell group has reported the synthesis of several  $[n](2,7)$ pyrenophanes and their chemical, physical and spectral properties have been studied in detail.<sup>36,38,39,41-45</sup> Unlike the benzene-containing  $[n]$ paracyclophanes, a common synthetic strategy (Strategy 3, Scheme 1.01) was employed for all of them.

#### 1.4.1 Synthetic strategy and interesting considerations

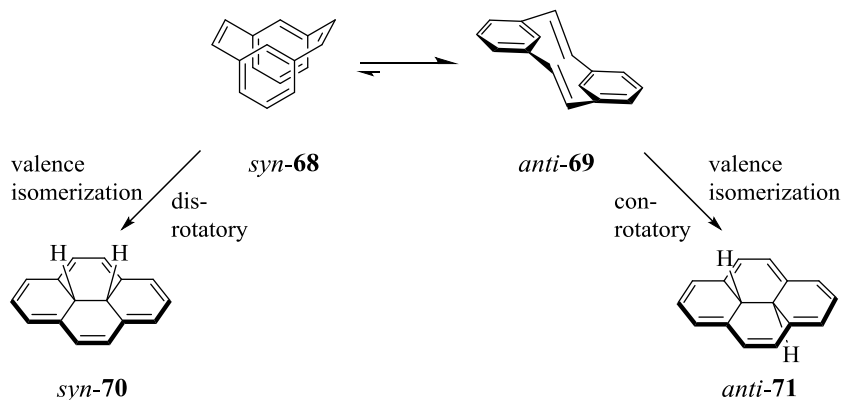
The general strategy used for the synthesis of  $[n](2,7)$ pyrenophanes **24** is outlined in Scheme 1.12. Tethering of an appropriately functionalized benzene **64** generates functionalized diarylalkanes **65**, which are then converted into dithia $[n.3.3]$ cylophanes **66**. The essentially unstrained dithiacyclophanes are then converted into the corresponding  $[n.2.2]$ metacyclophanedienes **67**, which are the direct precursors to the  $[n](2,7)$ pyrenophanes (**24**).

The face-to-face orientation of the two benzene rings (*syn*-conformation) in dienes **67** is enforced by the long bridge. Without the long bridge, the  $[2.2]$ metacyclophane system strongly prefers the *anti*-conformation. The conformation has important consequences on the oxidative bond formation between the two internal carbons of the

diene **67** that generates the pyrene system and furnishes the desired  $[n](2,7)$ pyrenophanes **24**. This transformation is known as the valence isomerization / dehydrogenation (VID) reaction.<sup>34</sup> The valence isomerization is a  $6\pi$  electrocyclic ring closure that affords a



**Scheme 1.12** General strategy for the synthesis of  $[n](2,11)$ pyrenophanes.

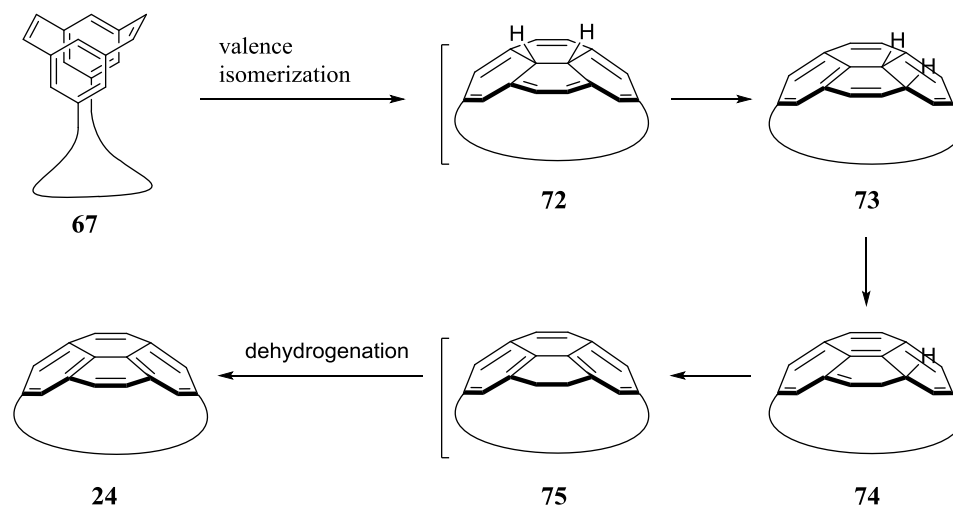


**Scheme 1.13** The more favoured *anti*-configuration of  $[2.2]$ metacyclophanes.

10b,10c-dihydropyrene. For *anti*- $[2.2]$ metacyclophanediene **69**, this leads to *trans*-**71** by way of an antarafacial conrotatory process, which is thermally forbidden / photochemi-



cally allowed by the rules of conservation of orbital symmetry (Scheme 1.13).<sup>35</sup> In contrast, the valence isomerization in the *syn*-[2.2]metacyclophanediene **68** is a suprafacial disrotatory process, which affords *cis*-**68** via a thermally allowed / photochemically forbidden pathway. By the same token, the  $[n.2.2]$ cyclophanedienes **67** valence isomerize to afford *cis*-dihydropyrenophanes **72**. In some cases (1,*n*-dioxan[*n*](2,7)pyrenophanes with low strain), the dihydropyrenophanes **72** have isomerized to dihydropyrenophanes **75**, presumably through a series of [1,5]-H shifts (Scheme 1.14).<sup>36</sup> Whatever the case, dehydrogenation (either with or without an added oxidant such as DDQ) leads to the formation of the required  $[n](2,7)$ pyrenophanes **24**.

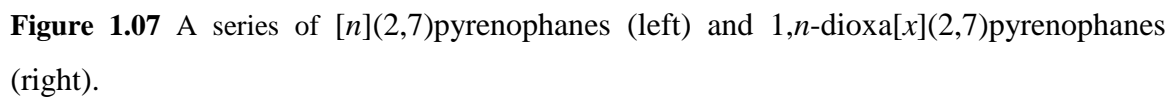
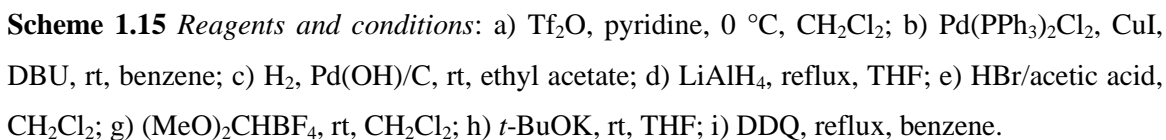


**Scheme 1.14** A valence isomerization/dehydrogenation (VID) reaction.

*cis*-10b,10c-Dihydropyrene (**72**) is naturally saucer-shaped due to the eclipsed ethano unit in the centre of the molecule. As a result, even relatively short bridges can still be accommodated without much strain. Thus, the dehydrogenation of the dihydropyrenophanes **72** to afford the  $[n](2,7)$ pyrenophanes (**24**) is where the majority of

the strain is thought to build up. However, the pyrene system is forming at the same time. The conversion of a [14]annulene in *cis*-dihydropyrenophanes **72** (ASE = 20.9 kcal/mol)<sup>37</sup> into a pyrene system (ASE = 74.6 ± 1 kcal/mol)<sup>38</sup> means that there is a large amount of ASE working in favour of the reaction. Studies by Bodwell, Cyranski and Schleyer have shown that the ASE of pyrene drops off only weakly as the pyrene system is bent. Thus, the dehydrogenation step of the VID reaction still has a lot of power when called upon to synthesize highly strained  $[n](2,7)$ pyrenophanes (**24**).

To illustrate the general approach to the  $[n](2,7)$ pyrenophanes (**24**), the synthesis of [7](2,7)pyrenophane (**24a**) is shown in Scheme 1.15. The synthesis commenced with 5-hydroxyisophthalic acid **76**, which was esterified and triflated to set up the tethering event: a Sonagashira reaction with 1,6-heptadiyne to afford compound **77**. The alkynes in **77** were hydrogenated and this was followed by a four-fold reduction and bromination of the resulting tetrol to afford tetrabromide **79**. Dithiacyclophane formation was then achieved using Na<sub>2</sub>S/Al<sub>2</sub>O<sub>3</sub><sup>39</sup> to afford **80**. Dithiacyclophane **80** was converted into metacyclophanediene **82** using a well-established four-step sequence consisting of *S*-methylation, thia-Stevens rearrangement, *S*-methylation and Hofmann elimination.<sup>40</sup> Treatment of metacyclophanediene **82** with DDQ brought about VID reaction to give the desired [7](2,7)pyrenophane **24b**. Using this general strategy, two different series of pyrenophanes,  $[n](2,7)$ pyrenophanes ( $n = 7-10$ )<sup>41</sup> **24b-e** and 1,*n*-dioxan[*n*](2,7)pyrenophanes ( $n = 7-12$ )<sup>36,42</sup> **83b-g** were synthesized (Figure 1.07).



### 1.4.2 Important aspects of the [n](2,7)pyrenophanes

The Bodwell group's work on the two series of pyrenophanes enabled the investigation of some fundamental questions 1) to what extent can the pyrene system be bent? 2) how much strain can a pyrene system take? 3) what happens to the aromaticity of the pyrene system as it is bent, and 4) how do the chemical and physical properties of the pyrene system change as it is bent increasingly out of planarity?

#### 1.4.2.1 Quantification of the non-planarity of pyrene system

In order to quantify the bend in the pyrenophanes, an angle  $\theta$  was introduced. It is defined as the smallest angle formed between the two terminal planes C1-C2-C3 and C6-C7-C8 (Figure 1.08).<sup>41,42</sup> Later, two other parameters were also used to quantify the in the pyrene system – the bend angle ( $\alpha$ ) and the bowl depth ( $h$ ). Both of these parameters correlate very well with  $\theta$ . Experimental (X-ray analysis) and calculated (AM1) values of  $\theta$  were obtained for both series of pyrenophanes (Table 1.04). In all but one case, the low level (semiempirical) calculations consistently overestimated the value of  $\theta$  by 4-8°. Density functional theory (DFT) calculations would likely provide closer agreement between theory and experiment, but such work has not been done for these compounds. Compound **83b** stands as the current record holder for highest measured  $\theta$  value for an isolated pyrenophane ( $\theta = 109.2^\circ$ ). This means that the pyrene system is slightly more bent than the pyrene system that maps onto the equator of  $D_{5h}$  C<sub>70</sub> ( $\theta = 108.0^\circ$ ). Clearly, the VID methodology is very powerful.

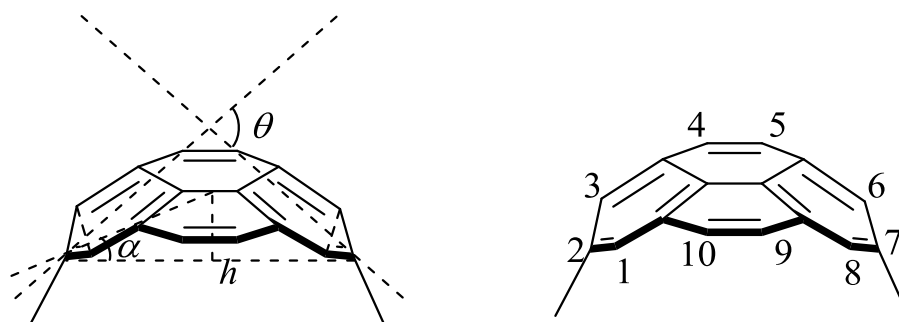


**Figure 1.08** Left) the parameters bend angles ( $\theta$ ,  $\alpha$ ), and bowl depth ( $h$ ); right) numbering of the pyrene system.

**Table 1.04** The experimental and calculated bend angles ( $\theta$ ) of pyrenophanes **24b-e** and **83b-g**.

entry	compound	$\theta_{\text{x-ray}} (^{\circ})$	$\theta_{\text{AM1-calc}} (^{\circ})$
1	$-\text{O}(\text{CH}_2)_5\text{O}-$ ( <b>83b</b> )	109.2	113.3
2	$-(\text{CH}_2)_7-$ ( <b>24b</b> )	-	104.6
3	$-\text{O}(\text{CH}_2)_6\text{O}-$ ( <b>83c</b> )	87.8	94.9
4	$-(\text{CH}_2)_8-$ ( <b>24c</b> )	80.8	87.0
5	$-\text{O}(\text{CH}_2)_7\text{O}-$ ( <b>83d</b> )	72.9	77.8
6	$-(\text{CH}_2)_9-$ ( <b>24d</b> )	62.4	70.3
7	$-\text{O}(\text{CH}_2)_8\text{O}-$ ( <b>83e</b> )	57.7	61.2
8	$-(\text{CH}_2)_{10}-$ ( <b>24e</b> )	46.4	54.4
9	$-\text{O}(\text{CH}_2)_9\text{O}-$ ( <b>83f</b> )	39.9	42.2
10	$-\text{O}(\text{CH}_2)_{10}\text{O}-$ ( <b>83g</b> )	34.6	33.1

### 1.4.2.2 Aromaticity and strain

As discussed earlier, there are various ways to describe aromaticity and several methods have been developed to measure or quantify it. The aromaticity of the pyrenophanes was

measured using three different indices: 1) the harmonic oscillator model of aromaticity (HOMA), which is geometry-based, 2) the nucleus-independent chemical shift (NICS), which is magnetism-based and 3) the aromatic stabilization energy (ASE),<sup>42a,43</sup> which is energy-based (Table 1.05). For the 1,*n*-dioxan[*n*](2,7)pyrenophanes **83b-g** and [8](2,7)-pyrenophane **24c**, HOMA and NICS indicate that very little of the aromaticity present in

**Table 1.05** Calculated HOMA, NICS and  $\Delta$ ASE values for pyrenophanes **83b-g** and **24a-g**.

entry	compound	HOMA (%) <sup>a</sup>	NICS (%) <sup>a</sup>	$\Delta$ ASE (kcal/mol)	$SE_{\text{pyrene}}$ (kcal/mol) <sup>b</sup>	$SE_{\text{bridge}}$ (kcal/mol) <sup>c</sup>
1	–O(CH <sub>2</sub> ) <sub>5</sub> O– ( <b>83b</b> )	0.305 (64)	–3.77 (81)			
2	–O(CH <sub>2</sub> ) <sub>6</sub> O– ( <b>83c</b> )	0.392 (82)	–4.20 (90)			
3	–O(CH <sub>2</sub> ) <sub>7</sub> O– ( <b>83d</b> )	0.451 (94)	–4.47 (96)			
4	–O(CH <sub>2</sub> ) <sub>8</sub> O– ( <b>83e</b> )	0.399 (83)	–4.69 (101)			
5	–O(CH <sub>2</sub> ) <sub>9</sub> O– ( <b>83f</b> )	0.422 (88)	–4.89 (106)			
6	–O(CH <sub>2</sub> ) <sub>10</sub> O– ( <b>83g</b> )	0.441 (92)	–4.82 (104)			
7	–(CH <sub>2</sub> ) <sub>6</sub> – ( <b>24a</b> )			–15.8	50.2	33.9
8	–(CH <sub>2</sub> ) <sub>7</sub> – ( <b>24b</b> )			–12.1	35.5	28.4
9	–(CH <sub>2</sub> ) <sub>8</sub> – ( <b>24c</b> )	0.373 (78)	–4.25 (92)	–10.6	22.1	26.7
10	–(CH <sub>2</sub> ) <sub>9</sub> – ( <b>24d</b> )			–7.5	13.9	20.0
11	–(CH <sub>2</sub> ) <sub>10</sub> – ( <b>24e</b> )			–6.2	6.4	16.1
12	–(CH <sub>2</sub> ) <sub>11</sub> – ( <b>24f</b> )			–3.4	3.2	17.1
13	–(CH <sub>2</sub> ) <sub>12</sub> – ( <b>24g</b> )			–3.1	0.0	14.5
14	pyrene ( <b>20</b> )	0.479	–4.63	0.0		

<sup>a</sup>values in paranthesis represents the % of aromatic character retained in the bent pyrene with respect to the planar pyrene (**20**)

planar pyrene (**20**) is lost as the pyrene system becomes increasingly bent. The loss becomes more significant at the upper end of the series, but even the most bent pyrene system **83b** retains 64% of its aromatic character according to HOMA, or 81% according to NICS. For the  $[n](2,11)$ pyrenophanes **24a-g**, the  $\Delta$ ASE calculated is also in agreement with the above results and shows only 16% loss of the ASE for the smallest member that could be isolated, **24b**. This number was arrived at using an ASE for pyrene of 77.8 kcal/mol. Later work put the ASE for pyrene at 74.6 kcal/mol but this does not meaningfully change the calculated loss of ASE in **24b** (15.6% vs. 16.2%).

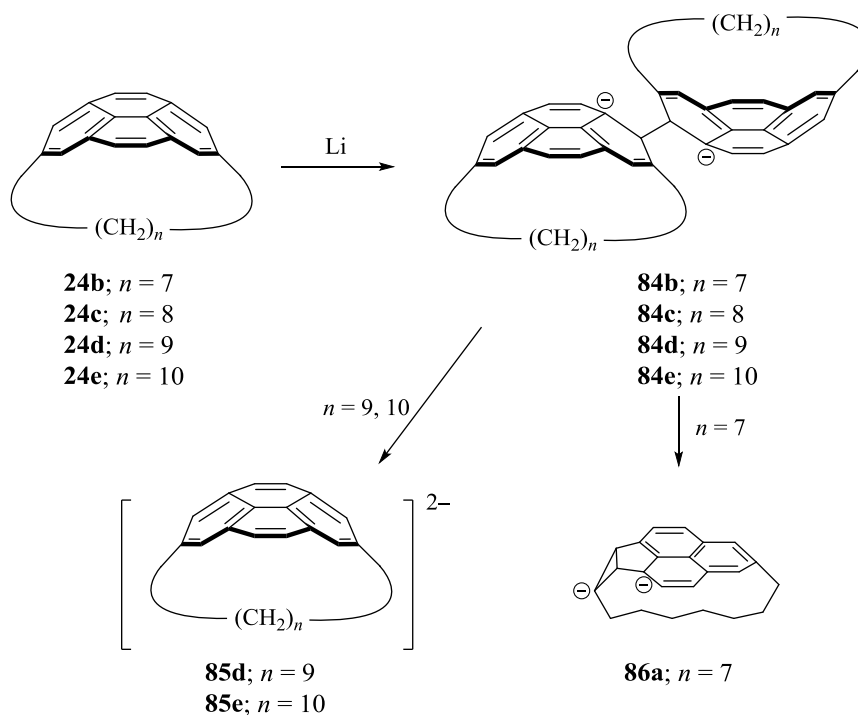
The strain energies of both the bent pyrene system ( $SE_{\text{pyrene}}$ ) and the bridge ( $SE_{\text{bridge}}$ ) were calculated (Table 1.05)<sup>43</sup> for the  $[n](2,7)$ pyrenophanes **24a-g** and it was found that the strain in the pyrene system ( $SE_{\text{pyrene}}$ ) spans a much larger range of values (50.2 kcal/mol) than the strain in the bridging unit ( $SE_{\text{bridge}}$ ) (19.4 kcal/mol). That having been said, the strain in the bridge is spread over successively fewer C atoms. The  $SE_{\text{pyrene}}$  in moving from **24g** (0.0 kcal/mol) to **24a** (50.2 kcal/mol) is three times larger than that of the decrease in the ASE (15.8 kcal/mol), which indicates that strain relief may be a more important factor than diminished aromaticity when it comes to reactivity.

### 1.4.2.3 Chemical reactivity and spectroscopic properties

When the  $[n](2,7)$ pyrenophanes **24b-e** were subjected to reduction using lithium metal, all of them formed dimers **84b-e** resulting from coupling of a radical anion.<sup>44,41b</sup> Depending on the length of the bridging system, different reactivity was observed upon further exposure to lithium metal. While the larger pyrenophanes (**24d-e**) formed

antiaromatic dianions **85d-e**, the next smaller member **24c** didn't react, presumably because the more strained antiaromatic system was just too unfavourable. Surprisingly, the smallest member of the series **24b** underwent a further rearrangement reaction giving bicyclo[3.1.0] compound **86b**. A higher amount of strain relief was likely the driving force for this remarkable escape from strained antiaromaticity (Scheme 1.16).

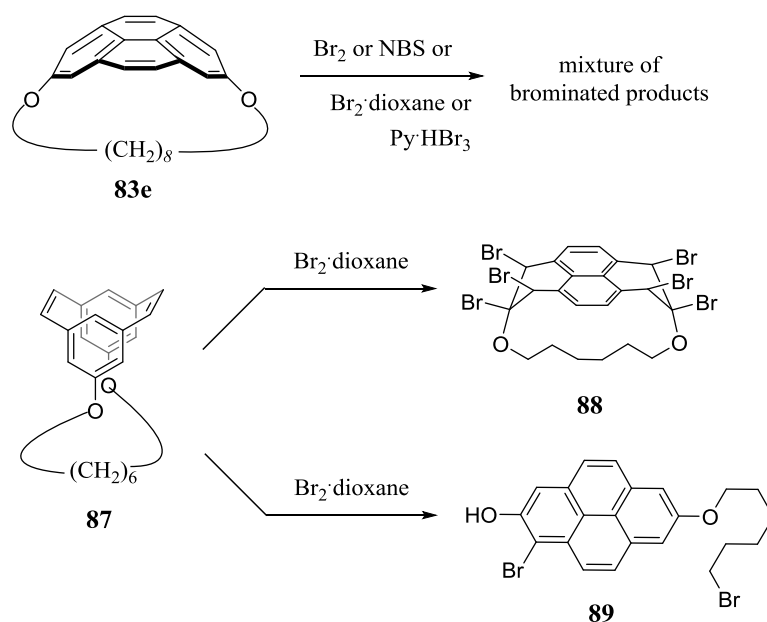
Attempted bromination of 1,8-dioxo[8](2,7)pyrenophane **83e** using  $\text{Br}_2$ ,<sup>41a</sup>  $\text{Br}_2$ -dioxane complex, pyridinium perbromide or NBS resulted in the formation of a mixture of inseparable brominated products (Scheme 1.17). Instead, bromination of the cyclophane-diene **87** using  $\text{Br}_2$ -dioxane complex at 0 °C resulted in the formation of the very unusual hexabromide **88**. On the other hand, performing the same reaction at -78 °C cleaved the bridge to afford **89**. No attempted bromination reactions of the  $[n](2,7)$ -



**Scheme 1.16** Reduction of  $[n](2,7)$ pyrenophanes **24b-e** with Li metal.



pyrenophanes have been reported.

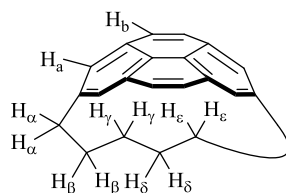


**Scheme 1.17** Bromination reactions of pyrenophane **83e** and diene **87**.

The  $^1\text{H}$  NMR spectroscopic data for the pyrenophanes **24b-d** and **83b-g** are presented in Table 1.06.<sup>45</sup> Clear relationships between the bend in the pyrene system and the chemical shifts of both the aromatic and the bridge protons were observed. As the bridge becomes shorter, the benzylic protons ( $\text{H}_\alpha$ ), the homobenzylic protons ( $\text{H}_\beta$ ) and bis(homobenzylic)protons ( $\text{H}_\gamma$ ) all move upfield, as was observed in  $[n]$ paracyclophanes (Sec. 1.3.2.2.2). On the other hand, the aromatic protons ( $\text{H}_a$  and  $\text{H}_b$ ) also move upfield with increasing bend in the pyrene system. Surprisingly, this is the converse of what was observed for the benzene ring protons in the  $[n]$ paracyclophanes.

The absorption spectra of the pyrenophanes also follow the trends that resemble those observed for the  $[n]$ paracyclophanes (Sec. 1.3.2.2.2).<sup>45</sup> The absorption spectrum of

**Table 1.06**  $^1\text{H}$  NMR shifts of pyrenophanes **24b-d** and **83b-g**.

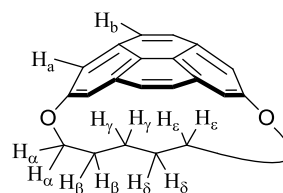


**24b**;  $n = 7$

**24c**;  $n = 8$

**24d**;  $n = 9$

**24e**;  $n = 10$



**83a**;  $n = 5$

**83b**;  $n = 6$

**83c**;  $n = 7$

**83d**;  $n = 8$

**83e**;  $n = 9$

**83f**;  $n = 10$

compound	$\delta\text{H}_a$	$\delta\text{H}_b$	$\delta\text{H}_\alpha$	$\delta\text{H}_\beta$	$\delta\text{H}_\gamma$	$\delta\text{H}_\delta$	$\delta\text{H}_\epsilon$
<b>24b</b>	7.34	7.67	2.30	0.45	-1.38	-1.38	
<b>24c</b>	7.59	7.84	2.59	0.88	-0.69	-1.45	
<b>24d</b>	7.75	7.91	2.84	1.10	0.05	-0.94	-2.08
<b>83a</b>	7.22	7.72	3.31	-0.04	-2.10		
<b>83b</b>	7.44	7.84	3.59	0.10	-1.46		
<b>83c</b>	7.64	7.91	3.76	0.71	-1.89	-0.73	
<b>83d</b>	7.72	7.92	4.02	0.93	-1.17	-0.67	
<b>83e</b>	7.83	7.98	4.19	1.22	-0.27	-0.64	-1.04
<b>83f</b>	7.85	7.96	4.31	1.41	-0.14	-0.14	-0.63

the planar pyrene **20** contains four types of absorption bands; a strong  $\beta'$  band (242 nm), a strong  $\beta$  band (273 nm), a series of three  $p$  bands (306, 320 and 336 nm) and very weak  $\alpha$  bands (352–372 nm), which are difficult to observe. The absorption data of  $[n](2,7)$ pyrenophanes **24b-d** and 1, $n$ -dioxo- $[x](2,7)$ pyrenophanes **83b-g** are presented in

Table 1.07. The  $\beta'$  bands are red-shifted by 15-38 nm when compared to pyrene and this was gradually increased with increasing bend in the pyrene system. On the other hand, the same kind of trend was not observed with the two other types of bands ( $\beta$  and  $p$  bands). The  $\beta$  bands are red-shifted by just 6-15 nm and the  $p$  bands move negligibly.

**Table 1.07** Ultraviolet spectral data of **24b-d**, **83b-g** and **20**.

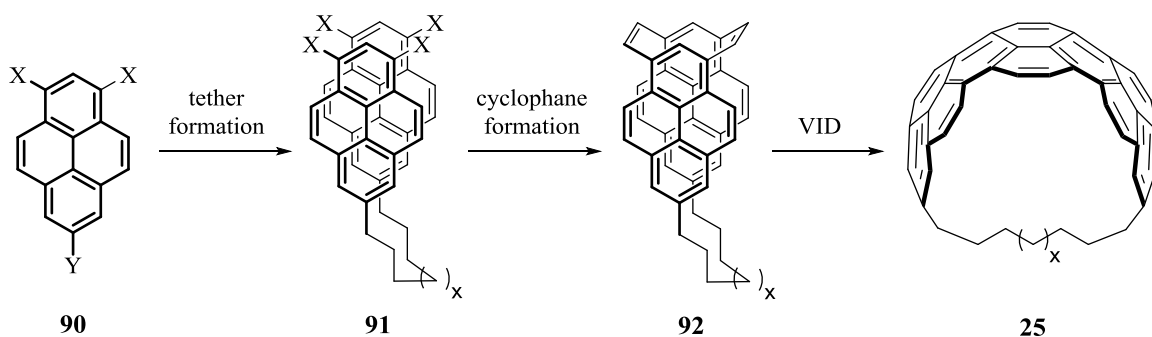
Absorption bands	$\beta'$	$\beta$	$p$		
[ <i>n</i> ](2,7)pyrenophane	$\lambda_{\max}$ (nm)	$\lambda_{\max}$ (nm)	$\lambda_{\max}$ (nm)		
<b>24b</b>	277	-	309	323	338
<b>24c</b>	267	287	311	324	339
<b>24d</b>	261	284	309	323	338
<b>83b</b>	280	-	-	318	334
<b>83c</b>	270	-	309	322	337
<b>83d</b>	263	282	309	322	337
<b>83e</b>	259	280	310	323	339
<b>83f</b>	257	280	310	323	339
<b>83g</b>	257	279	309	323	338
<b>20</b>	242	273	306	320	336

## 1.5 Peropyrenophanes

After pyrene (**20**), the next member of the capped rylene series is peropyrene (**21**).<sup>46</sup> Bridging the two most remote positions gives rise to the [*n*](2,9)peropyrenophanes, none of which have been synthesized.

## 1.6 $[n](2,11)$ Teropyrenophanes

The next member of the capped rylene series is teropyrene (**22**) and the  $[n](2,11)$ -teropyrenophanes (**25**) are the  $[n]$ cyclophanes that involve bridging of the two most remote sites. In order to build these larger aromatic systems, a strategy resembling the one used for the  $[n](2,7)$ pyrenophanes could be considered. The main difference would be the use of a 1,3,7-trisubstituted pyrene (**90**) instead of a 1,3,5-trisubstituted benzene as the initial aromatic building block (Scheme 1.18). Tethering two appropriately functionalized pyrene units of **90** would result in **91**, which would then lead to pyrenophanediene **92** (Scheme 1.17). Application of the powerful VID reaction, would generate the corresponding  $[n](2,11)$ teropyrenophanes **25**.



**Scheme 1.18** General strategy for the synthesis of  $[n](2,11)$ teropyrenophanes **25**.

A modified version of this idea was recently taken forward and the synthesis of the first member of the series, 1,1,8,8-tetramethyl[8](2,11)teropyrenophane **25c** ( $x=2$ )<sup>47</sup> was achieved by the Bodwell group. Details of the synthesis are discussed in Chapter 2. The remainder of the thesis deals with the synthesis of some higher and lower

homologues of **25** and investigations of their structural, spectroscopic and chemical properties.

The extent of the end-to-end bend in the teropyrene systems can be quantified in an analogous fashion to the  $[n](2,7)$ pyrenophanes (Section 1.4.1.1), *i.e.* the smallest angle formed between the two terminal planes of three carbon atoms in the teropyrene system (Figure 1.09). Three pyrene systems are embedded in the teropyrene systems and individual  $\theta$  values ( $\theta_1$ ,  $\theta_2$ ,  $\theta_3$ ) can be measured for each of them, thereby providing a means to quantify local deviations from planarity. Another parameter, the distance between the two bridgehead carbon atoms ( $d_1$ ) is also worth including since the bent teropyrene systems can be viewed as the segments of single-walled carbon nanotubes (SWCNT), in which diameter is an important parameter.

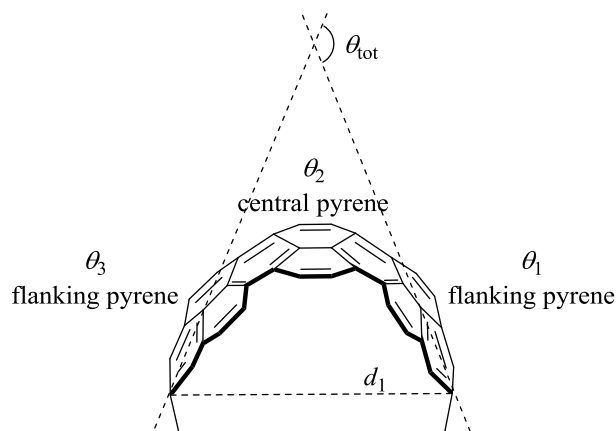


**Figure 1.09** Definition of the total bend angle ( $\theta_{tot}$ ), other bend angles  $\theta_1$ ,  $\theta_2$ ,  $\theta_3$  and distance between the two terminal carbons ( $d_1$ ).

## 1.7 Conclusions

In this chapter, the capped rylene series of PAHs was introduced (benzene (**19**), pyrene (**20**), peropyrene (**21**), teropyrene (**22**), quateropyrene (**23**)) and the chemistry and properties of some of their  $[n]$ cyclophanes was examined. Bridging the two most remote positions of each of these PAHs gives rise to a series of cyclophanes ( $[n]$ paracyclophanes,  $[n](2,7)$ pyrenophanes,  $[n](2,9)$ peropyrenophanes,  $[n](2,11)$ teropyrenophanes, *etc.*), in which bend is imparted over the full length of the aromatic systems. A great deal of work has been done on the  $[n]$ paracyclophanes and much has been learned from studying them. Considerably less work has been done on the  $[n](2,7)$ pyrenophanes, but the results of this work have also proved to be interesting and instructive. No work has been done on the  $[n](2,9)$ peropyrenophanes and, at the outset of this work, the surface had just been scratched in the case of the  $[n](2,11)$ teropyrenophanes.

## 1.8 References

1. C. J. Brown and A. C. Farthing, *Nature*, 1949, **164**, 915–916.
2. D. J. Cram and H. Steinberg, *J. Am. Chem. Soc.*, 1951, **73**, 5961–5704.
3. a) R. Gleiter and H. Hopf (Eds): *Modern Cyclophane Chemistry*, Wiley-VCH Verlag GmbH & Co. KGaA, 2004; b) F. Bickelhaupt, *Pure and Applied Chem.*, 1990, **62**, 373–382; c) For the most recent of collection of reviews on cyclophanes (Special issue on cyclophanes), see: *Isr. J. chem.*, 2012, **52**, 1–192.
4. P. G. Ghasemabadi, T. G. Yao and G. J. Bodwell, *Chem. Soc. Rev.*, 2015, **44**, 6494–6518.

5. a) F. Vögtle, *Cyclophane Chemistry: Synthesis, Structures and Reactions*, Wiley: Chichester, 1993; b) P. M. Keehn, S. M. Rosenfeld, *Cyclophanes*, Academic Press: New York, 1983; c) F. Diederich, *Cyclophanes*, The Royal Society of Chemistry: London, 1991; d) D. J. Cram, J. M. Cram, *Container Molecules and their Guests*, The Royal Society of Chemistry: London, 1994.
6. R. G. Harvey, *Polycyclic aromatic hydrocarbons*, Wiley-VCH: New York, 1997.
7. K. S. Novoselov, A. K. Geim, S. V. Morozov, D. Jiang, Y. Zhang, S. V. Dubonos, I. V. Grigorieva and A. A. Firsov, *Science*, 2004, **306**, 666–669.
8. a) For the most recent of collection of reviews on nanographene segments, see: *Top. curr. chem.*, 2014, **349**, 1–248; b) M. Treier, C. A. Pignedoli, T. Laino, R. Rieger, K. Müllen, D. Passerone and R. Fasel, *Nature Chem.*, 2011, **3**, 61–67. c) J. Cao, Y-M. Liu, X. Jing, J. Yin, J. Li, B. Xu, Y-Z. Tan, and N. Zheng, *J. Am. Chem. Soc.*, 2015, **137**, 10914–10917; d) K. A. Simonov, N. A. Vinogradov, A. S. Vinogradov, A. V. Generalov, E. M. Zagrebina, G. I. Svirskiy, A. A. Cafolla, T. Carpy, J. P. Cunniffe, T. Taketsugu, A. Lyalin, N. Mårtensson, and A. B. Preobrajenski, *ACS Nano*, 2015, **9**, 8997–9017.
9. M. Rumi, G. Zerbi and K. Müllen, *J. Chem. Phys.*, 1998, **108**, 8662–8670.
10. D. J. Cram, N. L. Allinger and H. Steinberg, *J. Am. Chem. Soc.*, 1954, **76**, 2743–2752.
11. T. M. Krygowski and M. K. Cyrański, *Chem. Rev.*, 2001, **101**, 1385–1419.
12. D. J. Cram and H. U. Daeniker, *J. Am. Chem. Soc.*, 1954, **76**, 2743–2752.

13. D. J. Cram, N. L. Allinger and H. Steinberg, *J. Am. Chem. Soc.*, 1954, **76**, 6132–6141.
14. T. Ueda, N. Kanomata, and H. Machida, *Org. Lett.*, 2005, **7**, 2365–2368.
15. a) N. L. Allinger, L. A. Freiberg, R. B. Hermann and M. A. Miller, *J. Am. Chem. Soc.*, 1963, **85**, 1171–1176; b) M. G. Newton, T. J. Walter and N. L. Allinger, *J. Am. Chem. Soc.*, 1973, **95**, 5652–5658.
16. N. L. Allinger and T. J. Walter, *J. Am. Chem. Soc.*, 1972, **94**, 9267–9268.
17. M. F. Bartlett, S. K. Figdor and K. Wiesner, *Can. J. chem.*, 1952, **30**, 291–294.
18. P. G. Gassman, T. F. Bailey and R. C. Hoye, *J. Org. Chem.*, 1980, **45**, 2923–2924.
19. a) V. V. Kane, A. D. Wolf and M. Jones Jr., *J. Am. Chem. Soc.*, 1974, **96**, 2643–2644; b) A. D. Wolf, V. V. Kane, R. H. Levin and M. Jones Jr., *J. Am. Chem. Soc.*, 1973, **95**, 1680.
20. S. L. Kammula, L. D. Iroff, M. Jones, Jr., J. W. van Swatcn, W. H. de Wolf, F. Bickelhaupt, Y. Tobe, K. Kakiuchi and Y. Odaira, *J. Am. Chem. Soc.*, 1985, **107**, 3716–3717.
21. F. Bickelhaupt and W.H. de Wolf, *Red. Trav. Chim. Pays-Bas*, 1988, **107**, 459–478.
22. J. W. van Swatcn, I. J. Landheer, W. H. de Wolf and F. Bickelhaupt, *Tett. Lett.*, 1975, **16**, 4499–4502.



23. L. W. Jenneskens, F. J. J. de Kanter, P. A. Kraakman, L. A. M. Turcknburg, W. E. Koolhaas, W. H. de Wolf, F. Bickelhaupt, Y. Tobe, K. Kakiuchi and Y. Odaira, *J. Am. Chem. Soc.*, 1985, **107**, 3716–3717.
24. a) T. Tsuji and S. Nishida, *J. Chem. Soc. Chem. Commun.*, 1987, 1189–1190; b) T. Tsuji and S. Nishida, *J. Am. Chem. Soc.*, 1988, **110**, 2157–2164; c) T. Tsuji, S. Nishida, M. Okuyama and E. Osawa, *J. Am. Chem. Soc.*, 1995, **117**, 9804–9803.
25. T. Tsuji, M. Okuyama, M. Ohkita, H. Kawai and T. Suzuki, *J. Am. Chem. Soc.*, 2003, **125**, 951–961.
26. a) F. Bockisch, J. C. Rayez, D. Liotard and B. Duguay, *J. Comput. Chem.*, 1992, **13**, 1047–1056; b) M. Elango, R. Parthasarathi, V. Subramanian and P. K. Chattaraj, *J. Mol. Struct. theochem.*, 2007, **820**, 1–6; c) L. W. Jenneskens, J. N. Louwen, W. H. D. Wolf and F. Bickelhaupt, *J. Phys. Org. Chem.*, 1990, **3**, 295–300.
27. Y. Tobe, K. I. Ueda, K. Kakiuchi, Y. Kai and N. Kasai, *Tetrahedron*, 1986, **42**, 1851–1858.
28. N. L. Allinger, T. J. Walter and M. G. Newton, *J. Am. chem. Soc.*, 1974, **96**, 4588–4596.
29. J. E. Rice, T. J. Lee, R. B. Remington, W. D. Allen, D. A. Clabo, Jr. and H. F. Schaefer III, *J. Am. Chem. Soc.*, 1987, **109**, 2902–2909.
30. a) T. Tsuji and S. Nishida, *J. Am. Chem. Soc.*, 1989, **111**, 368–369; b) Y. Tobe, A. Takemura, M. Jimbo, T. Takahashi, K. Kobiro, K. Kakiuchi, *J. Am. Chem. Soc.*,

- 1992, **114**, 3479–3491.
31. a) L. Carballeria, J. Casado, E. González and M. A. Ríos, *J. Chem. Phys.* 1982, **77**, 5655–5663; b) N. L. Allinger, J. T. Sprague and T. Liljefors, *J. Am. Chem. Soc.*, 1974, **96**, 5100–5104.
  32. a) T. Förster and K. Z. Kasper, *Elektrochem.* 1955, **59**, 976–980; b) J. B. Birks, *Photophysics of Aromatic Molecules*, Wiley-Interscience: London, 1970; c) F. M. Winnik, *Chem. Rev.*, 1994, **94**, 587–614; d) I. B. Berlman, *Handbook of Fluorescence Spectra of Aromatic Molecules*, Academic Press: New York, 1971; d) S. Karupannan and J.-C. Chambron, *Chem. – Asian J.*, 2011, **6**, 964–984.
  33. a) K. Kalyanasundaram and J. K. Thomas, *J. Am. Chem. Soc.*, 1977, **99**, 2309–2044; b) V. I. Vullev, H. Jiang and G. Jones II, in *Advanced Concepts in Fluorescence Sensing. Part B: Macromolecular Sensing*, Eds: C. D. Goddes and J. R. Lakowicz, Springer: New York, 2005, ch. 7, pp. 211–239.
  34. R. H. Mitchell and V. Boekelheide, *J. Am. Chem. Soc.*, 1970, **92**, 3510–3512.
  35. R. B. Woodward and R. Hoffmann, *Angew. Chem. Int. Ed.*, 1969, **8**, 781–853.
  36. G. J. Bodwell, J. N. Bridson, M. Cyrański, J.W. J. Kennedy, T. M. Krygowski, M. R. Mannion and D. O. Miller, *J. Org. Chem.* 2003, **68**, 2089–2098.
  37. C. S. Wannere and P. v. R. Schleyer, *Org. Lett.*, **5**, 865–868.
  38. J. Wu, M. K. Cyrański, M. A. Dobrowolski, B. L. Merner, G. J. Bodwell, Y. Mo and P. v. R. Schleyer, *Mol. Phys.*, 2009, **107**, 1177–1186.
  39. G. J. Bodwell, T. J. Houghton, H. E. Koury and B. Yarlagadda, *Synlett*, 1995,

751–752.

40. R. H. Mitchell, T. R. Ward and Y. Wang, *Heterocycles*, 2001, **54**, 249–257.
41. a) G. J. Bodwell, J. J. Flemming, M. R. Mannion and D. O. Miller, *J. Org. Chem.* 2000, **65**, 5360–5370; b) I. Aprahamian, G. J. Bodwell, J. J. Fleming, G. P. Manning, M. R. Mannion, B. L. Merner, T. Sheradsky, R. J. Vermeij and M. Rabinovitz, *J. Am. Chem. Soc.*, 2004, **126**, 6765–6775.
42. a) G. J. Bodwell, J. N. Bridson, M. K. Cyrański, J. W. J. Kennedy, T. M. Krygowski, M. R. Mannion and D. O. Miller, *J. Org. Chem.*, 2003, **68**, 2089–2098; b) G. J. Bodwell, J. N. Bridson, T. J. Houghton, J. W. J. Kennedy and M. R. Mannion, *Chem. – Eur. J.*, 1999, **5**, 1823–1827; c) G. J. Bodwell, J. N. Bridson, T. J. Houghton, J. W. J. Kennedy and M. R. Mannion, *Angew. Chem. Int. Ed.*, 1996, **35**, 1320–1321.
43. M. A. Dobrowolski, M. K. Cyrański, B. L. Merner, G. J. Bodwell, J. I. Wu and P. v. R. Schleyer, *J. Org. Chem.*, 2008, **73**, 8001–8009.
44. a) I. Aprahamian, G. J. Bodwell, J. J. Fleming, G. P. Manning, M. R. Mannion, T. Sheradsky, R. J. Vermeij and M. Rabinovitz, *J. Am. Chem. Soc.*, 2003, **125**, 1720–1721; b) I. Aprahamian, G. J. Bodwell, J. J. Fleming, G. P. Manning, M. R. Mannion, T. Sheradsky, R. J. Vermeij and M. Rabinovitz, *Angew. Chem. Int. Ed.*, 2003, **42**, 2547–2550.
45. M. R. Mannion and G. J. Bodwell, PhD thesis, 1999.

46. a) S. Pogodin and I. Agranat, *Org. Lett.*, 1999, **1**, 1387–1390; b) V. M. Nichols, M. T. Rodriguez, G. B. Piland, F. Tham, V. N. Nesterov, W. J. Youngblood and C. J. Bardeen, *J. Phys. Chem., C*, 2013, **177**, 16802–16810.
47. B. L. Merner, L. N. Dawe and G. J. Bodwell, *Angew. Chem. Int. Ed.*, 2009, **48**, 5487–5491.

## Chapter 2: Synthesis of Teropyrenophanes Using a Double-McMurry Strategy

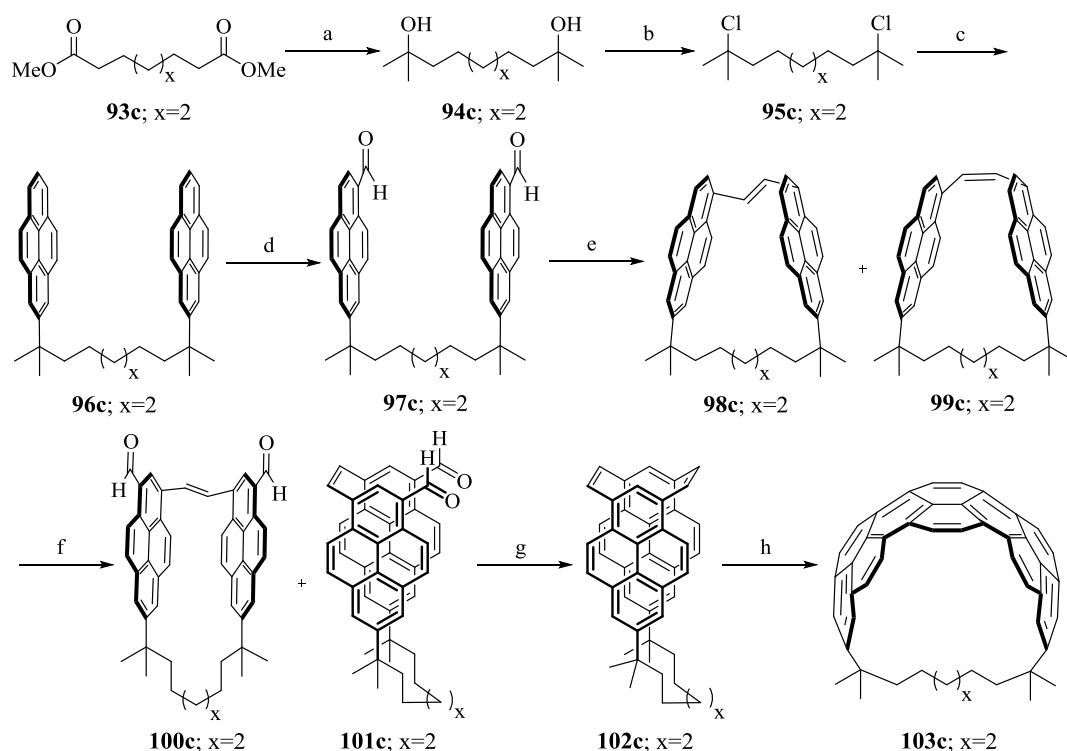
### 2.1 Introduction

In Chapter 1, the general strategy for the double-McMurry approach to teropyrenophanes was introduced. Earlier, this strategy was successfully applied to the synthesis of 1,1,8,8-tetramethyl[8](2,11)teropyrenophane **103c** by former Bodwell group member, Brad Merner.<sup>1</sup> By varying the length of the bridge, it would be possible to gain access to a series of cyclophanes with increasingly distorted teropyrene systems. This would be very useful because it would allow for the investigation of how the chemical and physical properties of the teropyrene system change with incremental changes in the degree of distortion from planarity (*cf.* the  $[n](2,7)$ pyrenophanes).<sup>2</sup> Accordingly, plans for the synthesis of higher and lower homologs of **103c** using the double-McMurry strategy were put in place. Before going into the results of this work, it would be instructive to consider the details of the synthesis of compound **103c** and the conclusions drawn therefrom.

#### 2.1.1 Reported synthesis of teropyrenophane **103c**

The synthesis of **103c** commenced with a two-fold Grignard reaction of diester **93c** to produce diol **94c** (86%), which was treated with concentrated HCl to afford dichloride **95c** (91%) (Scheme 2.01). Friedel-Crafts alkylation of pyrene with **95c** yielded dipyrenylalkane **96c** (54%). As expected, complete regioselectivity for the 2 positions of the pyrene systems was observed.<sup>3</sup> Hydrocarbon **96c** was then subjected to

Rieche formylation to provide dialdehyde **97c** (88%), again with complete regioselectivity. Intramolecular McMurry reaction of **97c** resulted in reductive coupling of the two aldehyde groups to produce a chromatographically inseparable mixture of *E* and *Z* isomers **98c** and **99c**. This mixture was subjected to another Rieche formylation reaction to produce a chromatographically separable 1:5 mixture of cyclophanedialdehydes (*E*)-**100c** (11%) and (*Z*)-**101c** (55%). The geometry of the *E*-configured alkene in (*E*)-**100c** prevents the two aldehyde groups from coming close to one another, so it is not suitable



**Scheme 2.01** Synthesis of 1,1,8,8-tetramethyl[8](2,11)teropyrenophane **103c** using a double-McMurry strategy. *Reagents and conditions*: a) MeMgBr, THF, 0 °C to reflux, 17 h, 86%; b) 12 M HCl (aq), rt, 2 h, 91%; c) pyrene, AlCl<sub>3</sub>, CH<sub>2</sub>Cl<sub>2</sub>, 0 °C to rt, 1 h, 54%; d) Cl<sub>2</sub>CHOCH<sub>3</sub>, TiCl<sub>4</sub>, CH<sub>2</sub>Cl<sub>2</sub>, 0 °C to rt, 2 h, 88%; e) TiCl<sub>4</sub>, Zn, pyridine, THF, 0 °C to reflux, 5 h; f) Cl<sub>2</sub>CHOCH<sub>3</sub>, TiCl<sub>4</sub>, CH<sub>2</sub>Cl<sub>2</sub>, 0 °C to rt, 2 h, 11% (*E*)-**100c**, 57% (*Z*)-**101c**; g) TiCl<sub>4</sub>, Zn, pyridine, THF, 0 °C to reflux, 4 h, 41%; h) DDQ, *m*-xylene, 145 °C, 48 h, 95%.

for a subsequent intramolecular McMurry reaction. The converse is true for the major isomer (Z)-**101c**, which successfully underwent intramolecular McMurry reaction to produce cyclophanediene **102c** (41%). Subjection of **102c** to a VID reaction then delivered the target cyclophane **103c** (95%).

### 2.1.2 Key features of the synthesis of teropyrenophane **103c**

The C<sub>36</sub> teropyrene system in compound **103c** has the largest end-to-end bend (167.0°) ever reported for a PAH. It structurally resembles about half of the *D*<sub>8h</sub>-symmetric Vögtle belt and, as such, can be viewed as a sizeable segment of an armchair (8,8) SWCNT. The synthesis of teropyrenophane **103c** is noteworthy for several reasons. It is only 8 steps in length (10% overall yield), which is several steps shorter than all of the syntheses of the [*n*](2,7)pyrenophanes and higher yielding than most of them.<sup>2</sup> The use of a McMurry reaction to generate a [2.2]metacyclophane system was the first time that this had been accomplished in anything better than 4% yield.<sup>4</sup> The teropyrene system in **103c** is (after the parent compound **22**<sup>5</sup>) only the second example known in the literature. Unlike the planar teropyrene (**22**), teropyrenophane **103c** has good solubility in common organic solvents, which means that opportunities exist to explore the chemistry of the teropyrene system. The ability of the VID reaction<sup>6</sup> to afford a nearly semicircular PAH gives hope to the possibility of generating more extended non-planar aromatic systems, including full belts.<sup>7</sup>

After the successful synthesis of teropyrenophane **103c** using the double-McMurry strategy, Merner turned his attention to higher and lower members of the series.

The synthesis of the next higher homologue [9](2,11)teropyrenophane failed at the stage of the first McMurry reaction because it exclusively afforded the *E*-isomer of the newly-formed double bond, which is incapable of undergoing the next reductive coupling reaction in an intramolecular fashion.<sup>8</sup> Therefore, the upper limit for the synthesis of teropyrenophanes using the double-McMurry approach is **103c**. Merner did not complete the synthesis of teropyrenophane **103b** using the double-McMurry strategy. Thus, to probe the lower limit of the synthetic strategy, work aimed at the synthesis of teropyrenophanes **103a-b** was the initial focus of the present work.

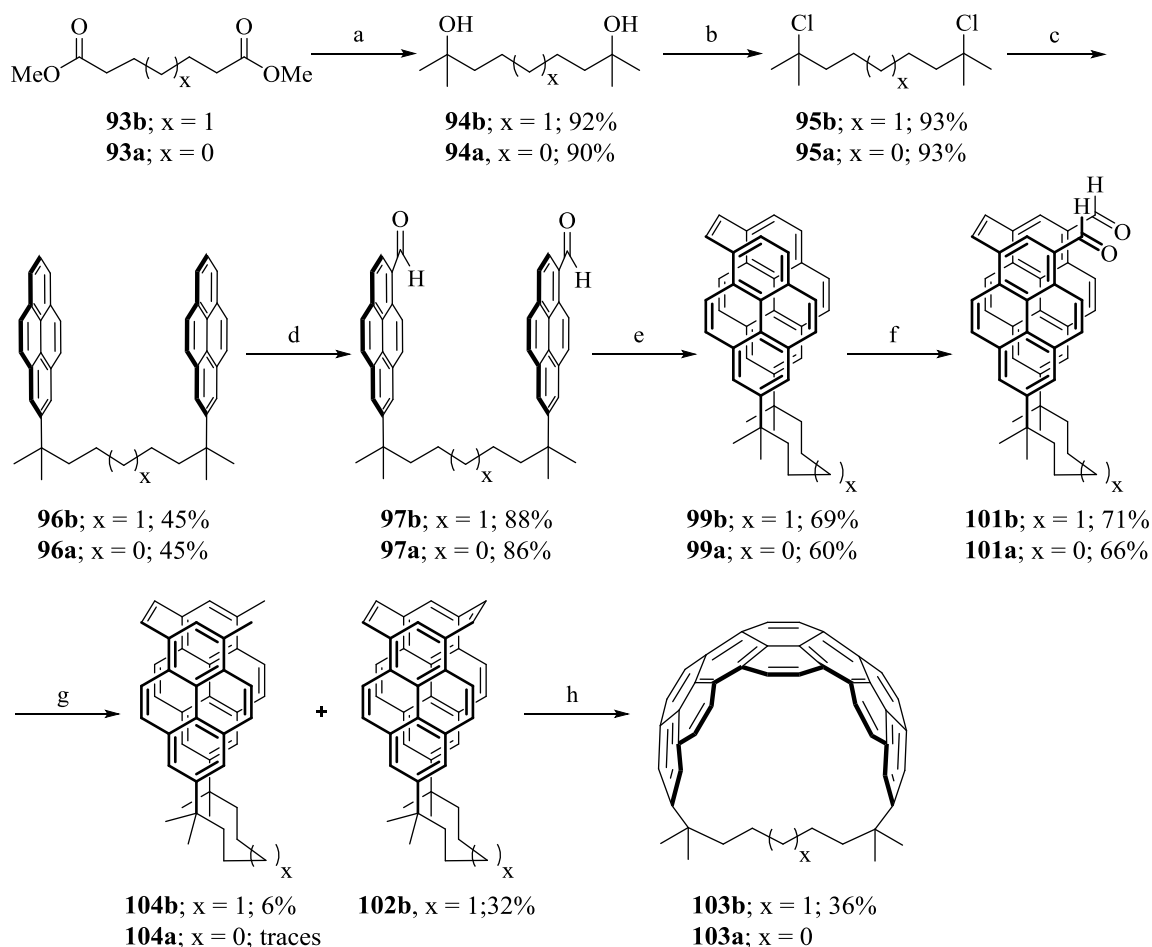
## 2.2 Results and discussion

### 2.2.1 Synthesis of [7](2,11)teropyrenophane **103b** using a double-McMurry strategy

The synthesis of [7](2,11)teropyrenophane **103b** proceeded in a similar way to that of [8](2,11)teropyrenophane **103c** (Scheme 2.02). Dimethyl pimelate **93b** was subjected to a two-fold Grignard reaction to afford diol **94b** (92%), which was then treated with concentrated HCl to yield dichloride **95b** (93%). Compound **95b** was then reacted with pyrene (**20**) under Friedel-Crafts alkylation conditions to generate dipyrenylalkane **96b** (45%). As before, complete selectivity for the 2 position of both pyrene systems was observed. Hydrocarbon **96b** underwent a fully regioselective Rieche formylation that installed one formyl group on each pyrene unit of **96b** to give dialdehyde **98b** (88%). The first alkene bridge between the two pyrene systems was constructed using an intramolecular McMurry coupling of compound **98b**, which afforded cyclophane **99b** (69%). In contrast to the case of **97c**, the alkene formation was completely



stereoselective and gave only the *Z*-isomer. It is quite striking that going from **97d** to **97b** (removal of two methylene units from the bridge) resulted in a total reversal of the stereochemical outcome of the McMurry reaction from *E* to *Z*. Rieche formylation of



**Scheme 2.02** Synthesis of teropyrenophanes **103b** and **103a**. *Reagents and conditions*: a) MeMgBr, THF, 0 °C to reflux, 17 h; b) 12 M HCl (aq), rt, 2 h; c) pyrene, AlCl<sub>3</sub>, CH<sub>2</sub>Cl<sub>2</sub>, 0 °C to rt, 1 h; d) Cl<sub>2</sub>CHOCH<sub>3</sub>, TiCl<sub>4</sub>, CH<sub>2</sub>Cl<sub>2</sub>, rt, 2 h; e) TiCl<sub>4</sub>, Zn, pyridine, THF, 0 °C to reflux, 5 h; f) Cl<sub>2</sub>CHOCH<sub>3</sub>, TiCl<sub>4</sub>, CH<sub>2</sub>Cl<sub>2</sub>, 0 °C to rt, 2 h; g) TiCl<sub>4</sub>, Zn, pyridine, THF, 0 °C to reflux, 4–24 h; h) DDQ (20 equiv.), *m*-xylene, 125 °C, 30 h.

(*Z*)-**99b** introduced two aldehydes groups to provide compound **101b** (71%) and a second intramolecular McMurry reaction led to the formation of the second alkene bridge in cyclophanediene **102b** (32%).

Dimethyl compound **104b** (6%), which arose from complete reduction of both the aldehyde groups was also isolated. No such reduction product was observed in the first McMurry reaction (**97b** to **99b**), so the formation of **104b** in the second McMurry is most likely a consequence of greater strain in [7.2.2]cyclophanediene **102b** than in [7.2]cyclophane **99b**. Although it was not reported in the open literature, a reduction product analogous to **104b** was obtained (in low yield) from the McMurry reaction of **101c**.<sup>8</sup> VID reaction of cyclophanediene **102b** was conducted in the presence of 20 equiv. of DDQ in *m*-xylene to produce teropyrenophane **103b** in 36% yield. A small amount of starting material (5-10%) was always recovered from this reaction. The much lower yield of **103b** than that of **103c** (95%) is almost certainly a consequence of the greater strain in the smaller teropyrenophane **103b**. Irrespective of this, the synthesis of compound **103b** was achieved for the first time in a 2% overall yield over 8 steps from dimethyl pimelate **93b**.

## 2.2.2 Crystal structure of [7](2,11)teropyrenophane **103b**

Small crystals of **103b**<sup>f</sup> were grown over a period of several weeks from a –15 °C solution in 2% ethyl acetate / hexanes. Due to the very small size of the crystals, synchrotron radiation was needed to collect a dataset from which a solution could be

---

<sup>f</sup> Crystallographic data were collected at the Advanced Light Source (ALS), Lawrence Berkeley National Laboratory. Refinement and solution were performed by Dr. Louise N. Dawe, Chemistry Department, Wilfrid Laurier University.

obtained (Figure 2.01). The end-to-end bend angle ( $\theta_{\text{tot}}$ ) for the teropyrene system in **103b** is  $177.9^\circ$ , which is in excellent agreement with the calculated value (B3LYP/cc-pVTZ)\*\* of  $178.7^\circ$  and just shy of the  $180^\circ$  angle that corresponds to half a turn. As in

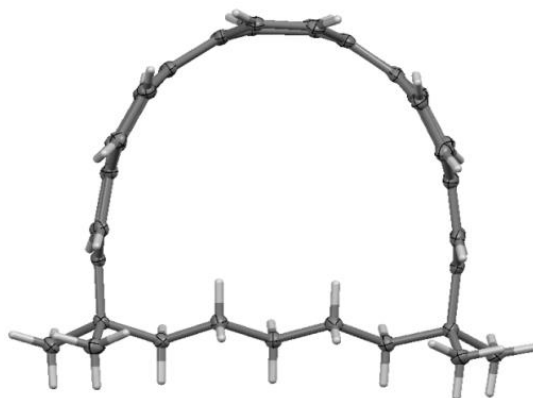


**Figure 2.01** X-ray crystal structure of compound **103b**; 30% probability displacement ellipsoids.

the case of **103c**, the shape of the bent teropyrene system is semielliptical rather than semicircular. In other words, there is much more bend in the central part of the teropyrene system than there is at the ends. To quantify this, the middle pyrene subunit in the teropyrene framework has a bend angle ( $\theta_2$ ) of  $102.3^\circ$ , whereas the two terminal pyrene subunits have bend angles ( $\theta_1$  and  $\theta_3$ ) of  $72.6^\circ$  and  $73.6^\circ$ , respectively. Of course, all of these values are a few degrees larger than the corresponding values in **103c**. The distance between the bridgehead carbons in **103b** ( $d_1 = 8.08 \text{ \AA}$ ) is substantially shorter than the corresponding distance in **103c** ( $d_1 = 9.10 \text{ \AA}$ ). The aromatic bond lengths are not significantly different from those of **103c** and the same is true for the bridging C–C bond lengths. On the other hand, some of the bond angles in the bridge unit are enlarged.

---

\*\* Calculations were performed by Dr. Christopher Rowley, Memorial University of Newfoundland.

Specifically, the C–C–C angles at the homobenzylic positions are 118.6° and 117.7°. By comparison, the largest bond angle in the bridge of **103c** is 118.2° and the largest angle in 1,7-dioxo[7](2,7)pyrenophane (**83b**) is 117.6°. <sup>2b</sup>

In the crystal, molecules of **103b** are arranged in an alternating up-down fashion along a two-fold screw axis that is parallel to the *b* axis (Figure 2.02). This creates columns with small channels, which are filled with disordered solvent molecules (Figure 2.03). Adjacent columns are rotated by about 90° with respect to one another such that each teropyrene system has a close  $\pi$ - $\pi$  contact with two other teropyrene systems (3.338(5) Å – 3.393(5) Å (Figure 2.04).

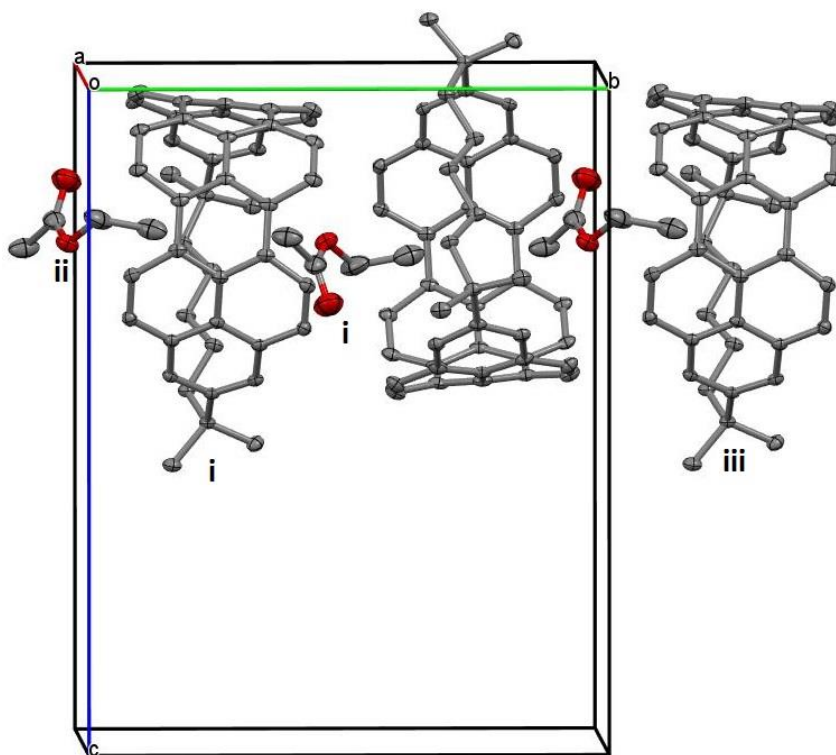


**Figure 2.02** Chain-like arrangement of molecules parallel to the *b*-axis (coincident with a 2-fold screw axis). i = 1-*x*, -1/2 + *y*, 1/2-*z*; ii = *x*, -1 + *y*, *z*; iii = 1-*x*, 1/2+*y*, 1/2-*z*. 30% probability ellipsoids, hydrogen atoms and minor solvent disorder removed for clarity.

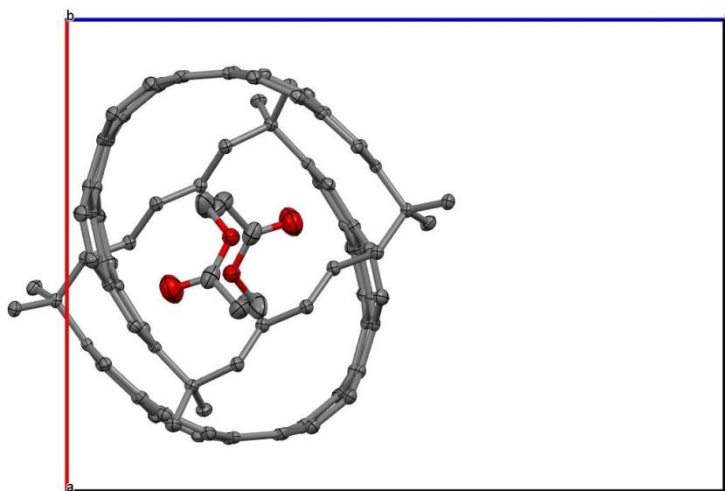


**Figure 2.03** Rotation of Figure 2.02 to view down the b-axis. 30% probability ellipsoids, hydrogen atoms and minor solvent disorder removed for clarity.

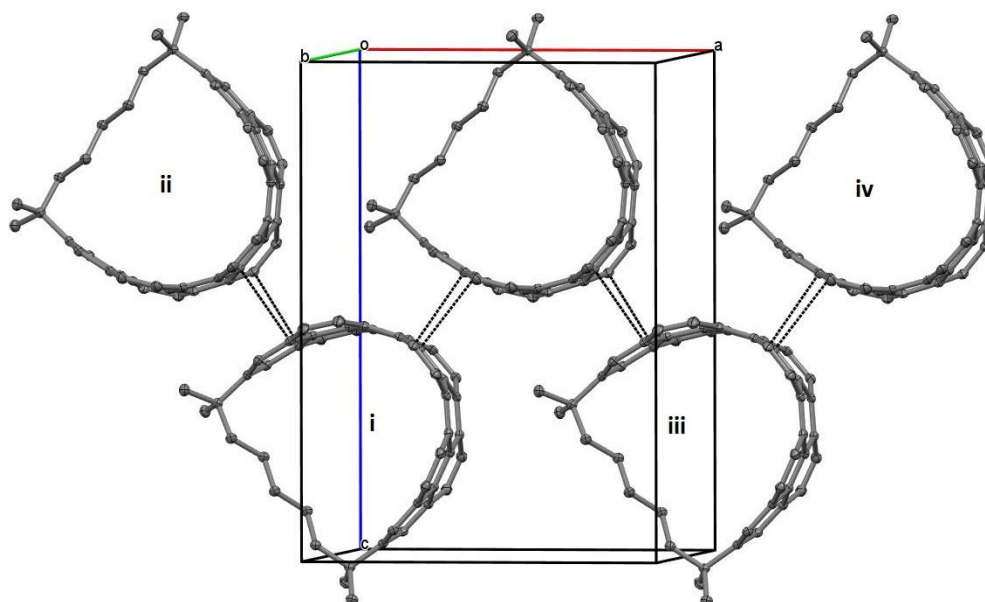


**Figure 2.04** Short intermolecular contacts between molecules, running parallel to the a-axis, represented by dashed lines.  $i = -1/2+x, 1.5-y, 1-z$ ;  $ii = -1+x, y, z$ ;  $iii = 1/2 +x, 1.5-y, 1-z$ ;  $iv = 1+x, y, z$ . 30% probability ellipsoids, hydrogen atoms and minor solvent disorder removed for clarity. Short contacts:  $C3-C15^i = 3.393(5) \text{ \AA}$  and  $C5-C17^i = 3.338(5) \text{ \AA}$ .

### 2.3 Attempted synthesis of [6](2,11)teropyrenophane **103a** using a double-McMurry strategy

The attempted synthesis of [6](2,11)teropyrenophane according to the previously successful double-McMurry approach began smoothly. Grignard reaction of dimethyl adipate **93a** produced diol **94a** (90%) (Scheme 2.02). Treatment of **94a** with concentrated HCl generated dichloride **95a** (93%), which was immediately subjected to Friedel-Crafts alkylation to form dipyrenylalkane **96a** (25%). Compound **96a** underwent Rieche formylation to afford dialdehyde **97a** (86%) and this was followed by an intramolecular McMurry reaction to generate [6.2]cyclophaneene **99a** (60%). With just a six-atom bridge connecting the two pyrene systems, it was expected that only the *Z*-isomer would form and this was indeed the case. Subjection of **99a** to another Rieche formylation reaction led to the formation of dialdehyde **101a** (66%). When compound **101a** was subjected to a second McMurry reaction, the consumption of the starting material was observed to be much slower than for **101b**. After 4 h of reaction (the time it took for **101b** to be fully consumed) essentially no consumption of the starting material appeared to have occurred (tlc analysis). Upon continuing the reaction for a further 20 h, the dark black-brown colour of the reaction mixture that is characteristic of (if not essential for) a successful reaction faded to yellow. The majority of the starting material still appeared to be present (tlc analysis), but several small new spots had appeared. During one unsuccessful attempt to recover the starting material in pure form using column chromatography, a small quantity (2 mg) of the undesired dimethyl compound **104a** was recovered and characterized using just  $^1\text{H}$  NMR spectroscopy. A few further attempts to

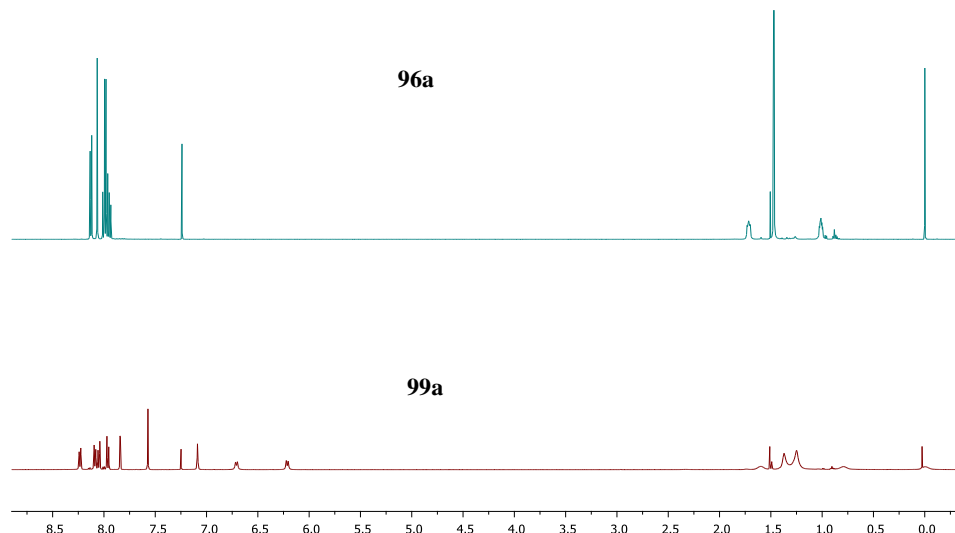
synthesize **102a** were kept to 4 h and were consistently unsuccessful, showing negligible formation of **102a** or **104a**. At the same time, attempts to recover the starting material in pure form were not successful due to unidentified minor products with similar  $R_f$  values.

The low reactivity of the aldehyde groups in **101a** is somewhat puzzling because there does not appear to be a significant difference in their environment compared to those in **101b**. There also does not appear to be a significant difference in strain between the product **102a** and its higher homolog **102b** according to the analysis of simple molecular models. Calculated structures might be useful here. Whatever the reason(s) for the failure of this reaction, the pathway to **103b** came to an end at this point. Hence [7](2,11)-teropyrenophane **103b** seems to be the lower limit for the formation of teropyrenophanes using this approach. Therefore, the scope of the double-McMurry strategy is limited to the synthesis of just [7]- and [8]teropyrenophanes **103b** and **103c**.

## 2.4 $^1\text{H}$ NMR spectra and conformational behaviour of the $[n.2](7,1)$ pyrenophanes

Two of the most interesting consequences that arise from incorporating an aromatic system into a cyclophane are the emergence of conformational processes and unusual features in the  $^1\text{H}$  NMR spectrum.<sup>9</sup> These two issues are often related. In this regard, several features of the  $^1\text{H}$  NMR spectra of the  $[n.2](7,1)$ pyrenophanes **99a** and **99b** stood out when compared to those of the dipyrenylalkanes **96a-b**, some of which indicated that conformational processes were occurring.

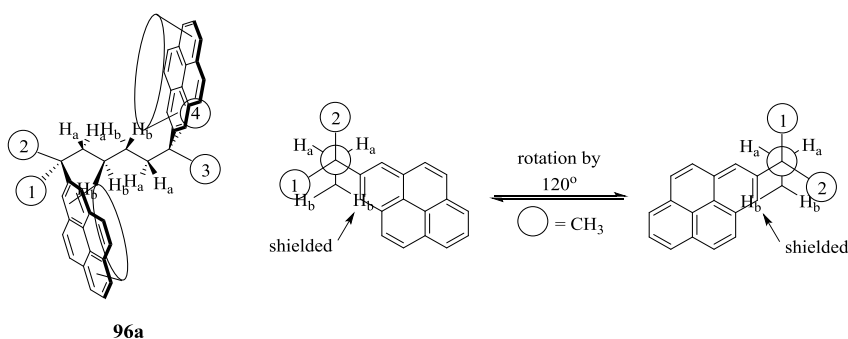
The aromatic region of the  $^1\text{H}$  NMR spectrum of dipyrenylalkane **96a** contains sharp, well-resolved signals ranging from  $\delta$  8.13 to  $\delta$  7.93 (Figure 2.05), which are typical



**Figure 2.05** The  $^1\text{H}$  NMR spectra of dialkylpyrene **96a** and  $[n.2](7,1)$ pyrenophane **99a**.

of simple pyrene systems. In the aliphatic region, two signals at  $\delta$  1.70 and  $\delta$  1.01 are present for the bridging unit. The latter signal, which was shown to be due to the central bridge protons  $\text{H}_b$  using COSY and HMQC experiments, is at significantly higher field than that of the methylene protons in hexanes ( $\delta$  1.27). The high field shift of the  $\text{H}_b$  protons can be explained as being a consequence of the magnetic anisotropy of pyrene systems. Thus, when **96a** adopts an *all-anti* conformation *that includes a methyl group at each end of the chain* (the alternate conformation in which the pyrene group is *anti* to the carbon chain is presumably of higher energy due to the presence of gauche interactions between both methyl groups and an  $\text{H}_b$  (*cf.* 1,3-diaxial interactions)), then the pyrene systems are situated such that one of the nearby  $\text{H}_b$  protons lies within their shielding zones (Figure 2.06). A simple C–C bond rotation, which presumably does not have a very high energy barrier, places the other  $\text{H}_b$  proton in the shielding zone. Thus, on the NMR timescale, the signal for  $\text{H}_b$  appears as a symmetric high-field multiplet.





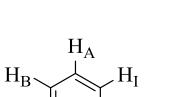
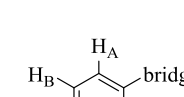
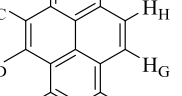
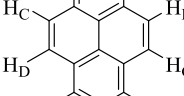
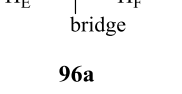
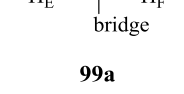



**Figure 2.06** Shielding of  $H_b$  protons in *all-anti* conformations of **96a** using Newman projections.

In moving to cyclophane **96a**, the aromatic signals of the pyrene systems spread out considerably to span a range of  $\delta$  8.25 to  $\delta$  6.23. All proton signals were assigned unambiguously using  $^1\text{H}$ ,  $^1\text{H}$ -COSY and NOESY experiments. What immediately stands out is that the protons on one side of the pyrene systems ( $H_F$ ,  $H_G$  and  $H_H$ ) are much more high field shifted than those of the other side ( $H_A$ ,  $H_B$ ,  $H_C$ ,  $H_D$  and  $H_E$ ). The change in chemical shift ( $\Delta\delta$ ) in going from **96a** to **99a** for the former set of protons ranges from  $-0.96$  to  $-1.77$  ppm, whereas the latter set has  $\Delta\delta$  values ranging from  $0.12$  to  $-0.20$  (Table 2.01).

The  $\Delta\delta$  data suggest that **99a** adopts a solution phase structure in which  $H_F$ ,  $H_G$  and  $H_H$  are within the shielding zone of the opposite pyrene system (and  $H_A$ ,  $H_B$ ,  $H_C$ ,  $H_D$  and  $H_E$  are not). The gas phase structure of **99a** was calculated at the B3LYP/6-31G\* level of theory<sup>††</sup> and two low-energy conformations were identified, *syn-99a* and  $C_2$ -symmetric *anti-99a* (Figure 2.07). The former was calculated to be 2.65 kcal/mol higher in energy than the former. In *syn-99a*, the two very gently bent pyrene systems were

<sup>††</sup> Calculations were performed by Dr. Yuming Zhao, Memorial University of Newfoundland.

	96a	99a	$\Delta\delta$
	7.96	8.10	-0.15
	8.15	8.25	0.12
	8.02 or 7.99	8.06	0.16 or 0.18
	7.99 or 8.02	7.97	-0.01 or -0.03
	8.08	7.86	-0.20
	8.08	7.10	-0.96
	7.99 or 8.02	6.23	-1.75 or -1.77
	8.02 or 7.99	6.72	-1.26 or -1.28
	8.15		

2.65

61

In the aliphatic region of the  $^1\text{H}$  NMR spectrum of **99a**, two broad singlets ( $\delta$  1.38, 1.26) and three broad multiplets ( $\delta$  1.60, 0.81,  $-0.04$ ) are observed (Figure 2.08).  $^1\text{H}$ ,  $^1\text{H}$ -COSY and HSQC experiments revealed the presence of a fourth broad multiplet underneath one of the singlets ( $\delta$  1.26). The broadness of the peaks indicated that a conformational process is near coalescence, so a VT-NMR experiment was performed (Figure 2.08). The methyl groups appeared as sharp singlets at 258 K and the fourth broad multiplet became clearly visible. Upon warming, the methyl groups became progressively broader and eventually coalesced at  $T_c = 318$  K. With  $\Delta\nu_0 = 61.3$  Hz, the free energy of activation for the conformational process was calculated to be  $\Delta G^\ddagger = 14.5$

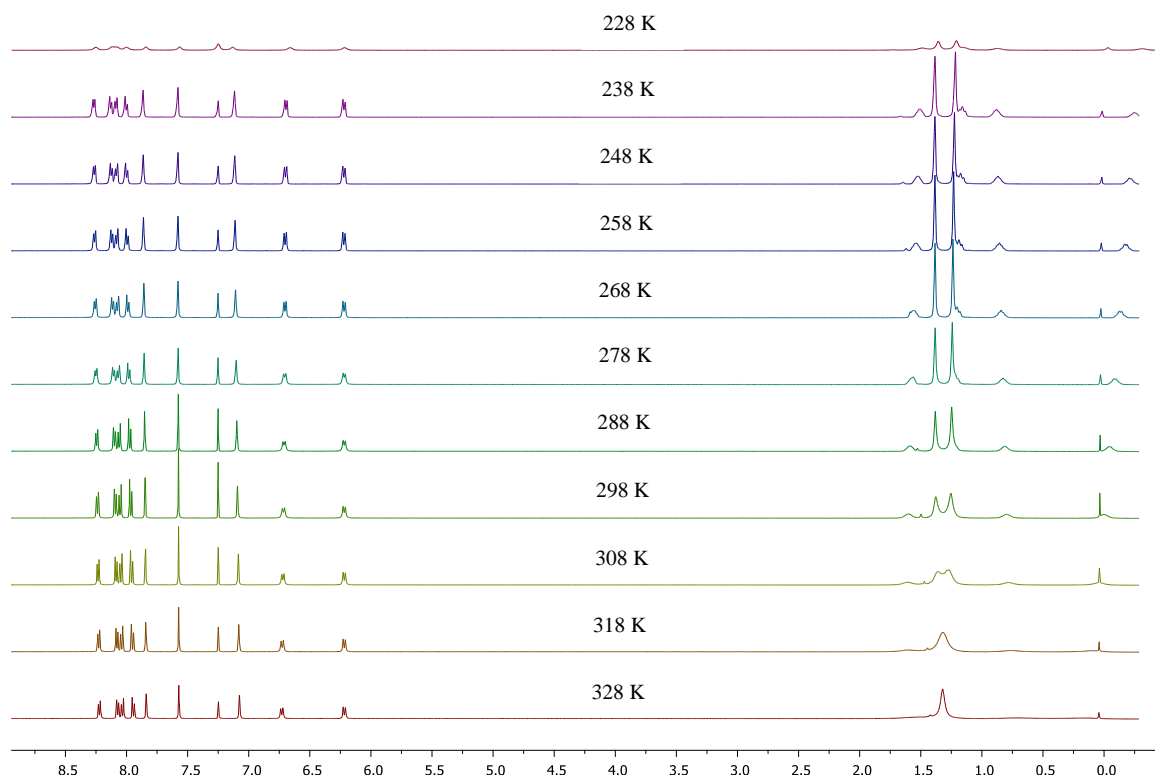


**Figure 2.08** VT-NMR spectrum of **99a**. Coalescence of both methyl singlets was observed at  $T_c = 318$ .

kcal/mol.<sup>10</sup> The four broad multiplets also broadened with warming and were barely discernible from the baseline at the coalescence temperature of the singlets.

In the calculated structure of **99a**, the two methyl groups are in different environments (one pointing to the inner edge of the adjacent pyrene system (black ball) and one pointing to the outer edge (red ball)) and the coalescence of their signals means that the observed conformational process exchanges their environments. The only process that achieves such an exchange is an *anti-anti'* ring flip of the two pyrene systems (Figure 2.09).

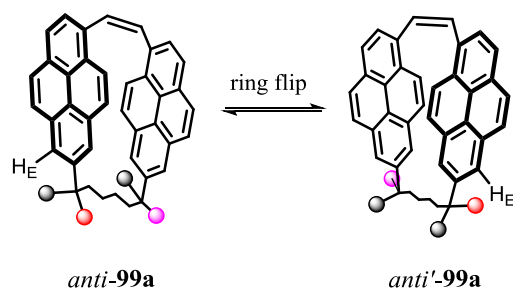


**Figure 2.09** Exchange of the environment of methyl groups by ring flip.

A further conformational process is available to both the *syn* and *anti* conformers of **99a**, *i.e.* a bridge flip. This is a rather complicated process and, based on the observation of four multiplets for the bridge protons at 238 K, certainly has a low-energy barrier. A detailed experimental and computational study of this process in **99a** and its higher homologs **99b-c** is underway.<sup>††</sup>

In moving to the next higher homolog **99b**, the situation changes. The starting point (dipyrenylalkane **96b**) is essentially the same as before, *i.e.* the <sup>1</sup>H NMR spectrum

<sup>††</sup> Collaboration with Prof. T. Dudding, Brock University.

of **96b** closely resembles that of **96a**. Sharp, well-resolved signals appear in the range of  $\delta$  8.11 to  $\delta$  7.94 (Figure 2.10). Upon going from **96b** to **99b**, the aromatic signals spread out as they did in going from **96a** to **99a**, but not nearly as much as they did for **99a** (Table 2.02). The  $\Delta\delta$  values for **99b** range from 0.03 to 0.70 ppm, the largest values (by far) being observed for H<sub>E</sub> or H<sub>F</sub> ( $\Delta\delta$  = 0.29-0.30 ppm) and H<sub>G</sub> ( $\Delta\delta$  = 0.67-0.70 ppm). This is consistent with a solution phase preference for the *syn* conformation (*syn*-**99b**) over the *anti* conformation (*anti*-**99b**) (Figure 2.10). More specifically, a splayed face-to-face orientation of the two pyrene systems in *syn*-**99b**, would place H<sub>F</sub> and H<sub>G</sub> closer to the shielding zones of the opposing aromatic systems than the other aromatic protons.

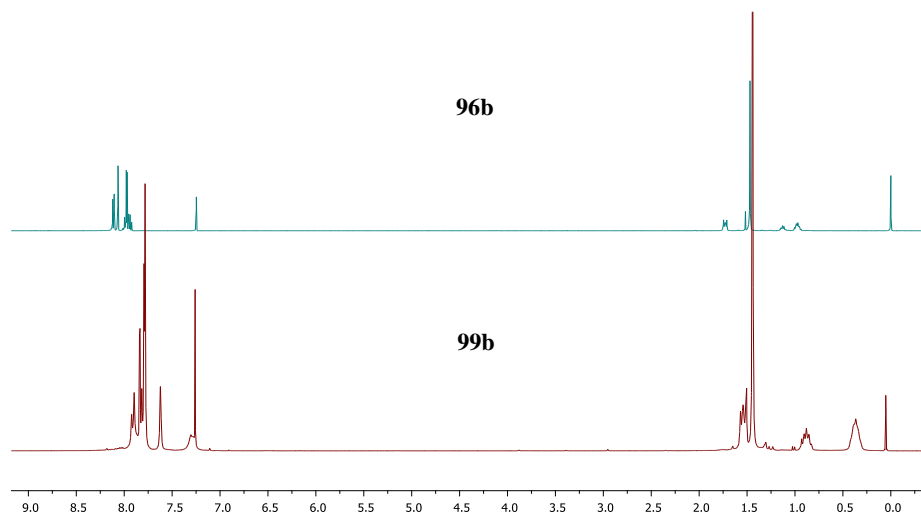


**Figure 2.10** The <sup>1</sup>H NMR spectra of dialkylpyrene **96b** and [7.2](7,1)pyrenophane **99b**.

The change in conformational preference in going from **99a** and **99b** is fully consistent with known conformational preferences in small cyclophanes.<sup>10</sup> In the case of **99a** and **99b**, the most appropriate comparison is with metacyclophanes because the bonds emanating from 1 and 7 positions in pyrene form an angle of 120°, as do those of the 1

**Table 2.02** Comparison of  $\Delta\delta$  values for each  $H_X$  between **96b** and **99b**.

	<b>96b</b>	<b>99b</b>	$\Delta\delta$
$H_A$	7.95	7.92	0.03
$H_B$	8.12	7.89	0.23
$H_C$	8.00 or 7.97	7.83 or 7.79	0.17 or 0.18
$H_D$	7.97 or 8.00	7.79 or 7.83	0.18 or 0.17
$H_E$	8.08	7.79 or 7.78	0.29 or 0.30
$H_F$	8.08	7.79 or 7.78	0.29 or 0.30
$H_G$	8.00 or 7.97	7.30	0.70 or 0.67
$H_H$	7.97 or 8.00	7.62	0.35 or 0.38
$H_I$	8.12		

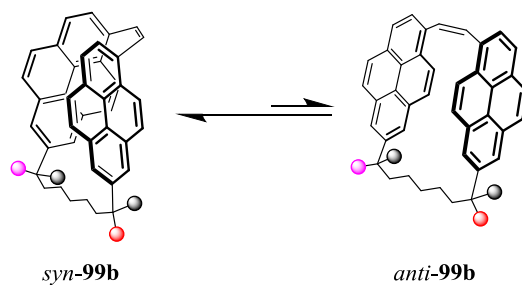
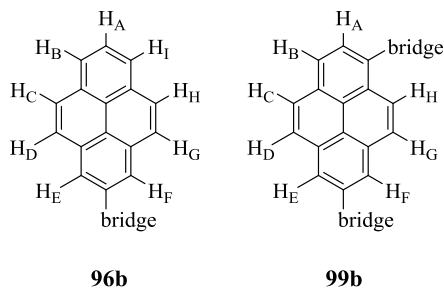


**Figure 2.11** Equilibrium mixture of *syn*- and *anti-99b*.

and 3 positions in benzene. In the  $[n.n]$ metacyclopentadienes, even-numbered bridges tend to favour the *anti* conformation ([2.2]metacyclopentadiene is exclusively *anti*)<sup>10</sup> and odd-numbered bridges tend to favour the *syn* conformation ([3.3]metacyclopentadiene is exclusively *syn*).

In the room temperature  $^1\text{H}$  NMR spectrum of **99b**, the methyl protons are observed as a sharp singlet at  $\delta$  1.43, which suggests that a *syn-syn'* ring flip that

exchanges the environments of the two different methyl groups occurs rapidly at room temperature. Upon cooling, the methyl signal becomes broad and eventually splits into two signals at 228 K (Figure 2.12). With  $\Delta\nu_0 = 15.7$  Hz and  $T_c = 238$  K, the energy barrier for the ring flip was calculated to be  $\Delta G^\ddagger = 12.6$  kcal/mol.<sup>r</sup> It seems reasonable that the value for **99b** is lower than that for **99a** because the long bridge in **99b** is longer than that in **99a**. Interestingly, signals corresponding to *anti*-**99b** (e.g.  $\delta$  8.40 (H<sub>B</sub>),  $\delta$  7.36 (H<sub>F</sub>),  $\delta$  7.02 (H<sub>H</sub>) and  $\delta$  6.63 (H<sub>G</sub>)) can be seen in the 218 K spectrum. A detailed study of the conformational behaviour of **99b** is underway.

Overall, it would appear that the [*n*.2](7,1)pyrenophanes undergo a linked set of ring flipping processes that connect the *syn*, *anti*, *syn*' and *anti*' conformations (Figure 2.13). As alluded to earlier, flipping of the long bridge adds considerable complexity, but this can be ignored for the time being since it appears to be a low-energy process. If the bridge flipping is ignored, then it is evident that the *anti* and *anti*' conformers are enantiomers, whereas the *syn* and *syn*' conformers are degenerate.

The next higher homolog **99c** was obtained as an inseparable mixture of *E* and *Z* isomers, which precluded the investigation of the conformational behaviour of either isomer. Based on what was observed for **99a** and **99b**, it would be expected that (*Z*)-**99c** would show a preference for the *anti* conformation and have a lower barrier to inversion than **99a** and **99b**.

---

<sup>r</sup> The  $\Delta\nu_0$  was calculated for the two newly appeared methyl singlets at  $T_c = 238$  K correspond to an intermediate spectrum. Therefore, the  $\Delta G^\ddagger = 12.6$  kcal/mol represents the maximum energy barrier.

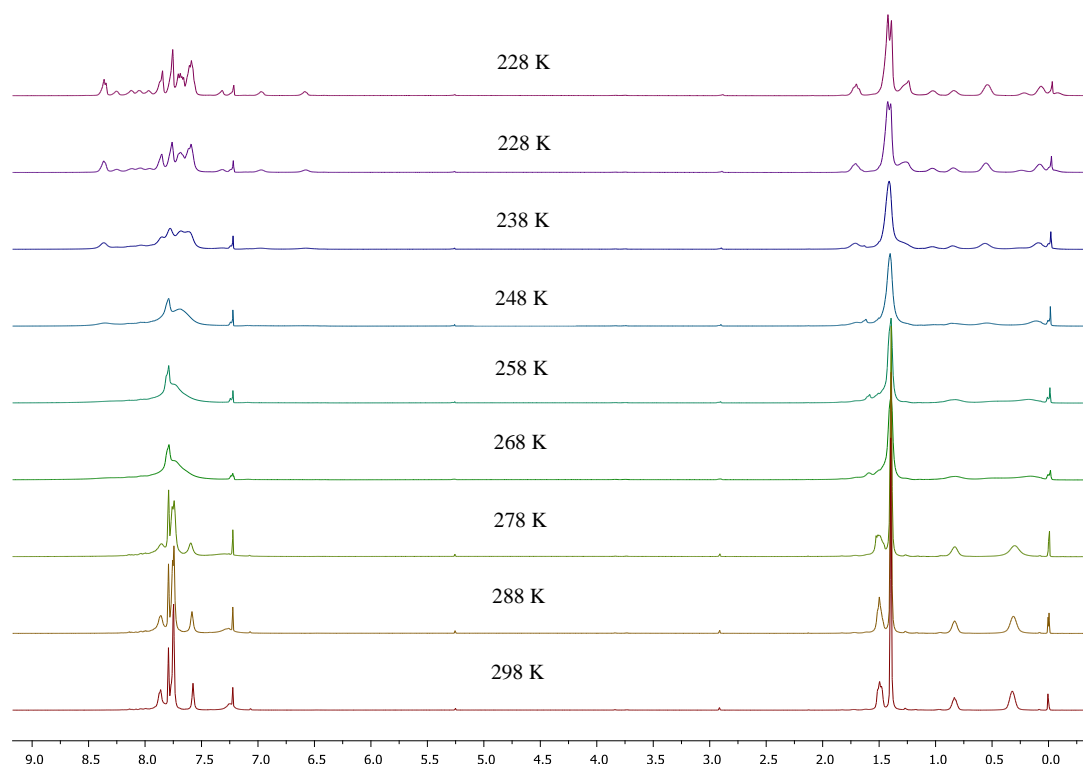


**Figure 2.12** VT-NMR spectrum of **99b**. Coalescence of both methyl singlets was observed at  $T_c = 238$ .

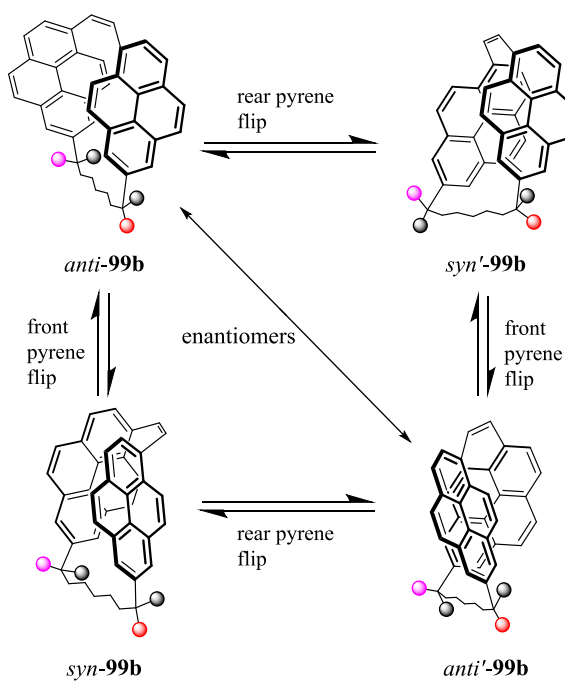


**Figure 2.13** Equilibrium mixture of *syn*-, *syn'*- and *anti*-, *anti'*-**99b**.

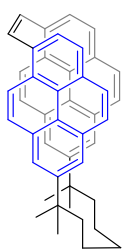


## 2.5 Conclusions

The synthesis of 1,1,7,7-tetramethyl[7](2,11)teropyrenophane (**103b**) has been achieved in a 2% overall yield over 8 steps using a strategy in which the two key ethenylene bridging units in the teropyrenophane precursor **102b** were assembled using two iterative Rieche formylation / McMurry coupling sequences. On the other hand, the formation of the next lower homologue **102a** was unsuccessful due to the failure of the McMurry reaction that was to have generated the second ethenylene bridge. The conformational behaviour of the dipyrenylalkanes **96a-b** and [n.2](7,1)pyrenophanes **99a-b** was investigated using  $^1\text{H}$  NMR experiments. From this work, it can be inferred that the failure of **101a** to afford **102a** was due to the preference of **101a** for an *anti* conformation in which the two formyl groups are too far away from one another to react.

## 2.6 Experimental Section

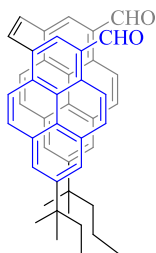
### (Z)-1,1,7,7-Tetramethyl[7.2](7,1)pyrenophane (**99b**)



Titanium(IV) chloride (3.87 g, 20.1 mmol) was added slowly to a stirred slurry of zinc dust (2.70 g, 40.9 mmol) in anhydrous THF (75 mL) at room temperature under nitrogen atmosphere and the resulting brownish black slurry was heated at reflux for 1 h, during which time a dark black colour persisted (the loss of this colour indicates that the McMurry reaction will fail completely). Pyridine (2.72 mL, 34.3 mmol) was added by a syringe and the reaction was continued to heat at reflux for further 10 min. 2,8-Bis(6-formylpyren-2-yl)-2,8-dimethylnonane (**97b**)

(1.47 g, 2.4 mmol) in THF (125 mL) was then added slowly over 10 min to the refluxing dark black solution and the reaction was continued to reflux over a period of 4 h. The hot reaction mixture was then poured into chloroform (200 mL) and the resulting greenish black solution was concentrated under reduced pressure. The residue obtained was adsorbed onto silica gel and subjected to a column chromatography (25 × 4.5 cm, 6% dichloromethane / hexanes) to afford (Z)-1,1,7,7-tetramethyl[7,2](7,1)pyrenophane (**99b**) as a yellow solid (965 mg, 69%):  $R_f$  = 0.33 (10% dichloromethane / hexanes); m.p. 277.0–278.0 °C,  $^1\text{H}$  NMR (300 MHz,  $\text{CDCl}_3$ )  $\delta$  7.91 (br d,  $J=7.8$  Hz, 4H), 7.85–7.74 (br m, 10H), 7.62 (br s, 2H), 7.36–7.26 (br m, 2H), 1.60–1.48 (br m, 4H), 1.44 (s, 12H), 0.87 (p,  $J=7.9$  Hz, 2H) 0.40–0.25 (m, 4H);  $^{13}\text{C}$  NMR (75 MHz,  $\text{CDCl}_3$ )  $\delta$  146.24, 133.44, 133.09, 130.62, 130.15, 129.95, 127.82, 127.18, 126.97, 126.83, 125.88, 125.66, 124.26, 123.83, 122.51, 122.50, 122.40, 45.48, 38.35, 30.99, 29.30, 25.67; LC-MS (CI-(+))  $m/z$  (rel. int.) 584 (4), 583 (6), 582 (36), 581 ( $[\text{M}+\text{H}]^+$ , 100); HRMS (APPI) calcd for  $\text{C}_{45}\text{H}_{40}$  ( $[\text{M}]^+$ ) 580.3130, found 580.3109.

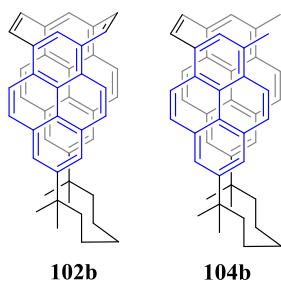
**(Z)-12,22-Diformyl-1,1,7,7-tetramethyl[7.2](7,1)pyrenophane (101b)**



To a stirred mixture of (Z)-**99b** (0.51 g, 0.9 mmol) and  $\alpha,\alpha$ -dichloromethyl methyl ether (0.47 mL, 5.3 mmol) in dichloromethane (60 mL) at 0 °C was added titanium(IV) chloride (0.58 mL, 5.3 mmol). The ice bath was removed and the resulting dark purple solution was stirred at room temperature for 2 h. The reaction mixture was poured into ice-cold water (200 mL) and the organic layer was separated. The aqueous layer was extracted with dichloromethane (3 × 30 mL) and the combined organic layers were washed with brine (100 mL) and dried

over anhydrous sodium sulfate. The organic layers were concentrated under reduced pressure and the obtained residue was subjected to column chromatography (18 × 4.5 cm, dichloromethane) to afford (Z)-12,22-diformyl-1,1,7,7-tetramethyl[7.2](7,1)pyrenophane (**101b**) as a bright yellow solid (400 mg, 71%):  $R_f$  = 0.31 (dichloromethane); m.p. > 300 °C,  $^1\text{H}$  NMR (300 MHz,  $\text{CDCl}_3$ )  $\delta$  10.59 (s, 2H), 9.11 (br d,  $J=9.2$  Hz, 2H), 8.16 (br s, 2H), 7.99 (d,  $J=9.3$  Hz, 2H), 7.93 (d,  $J=1.7$  Hz, 4H), 7.80 (s, 2H), 7.70 (br s, 2H), 7.44 (br s, 2H), 1.53–1.43 (m, 4H), 0.90–0.60 (m, 2H), 0.30 (br s, 4H);  $^{13}\text{C}$  NMR (75 MHz,  $\text{CDCl}_3$ )  $\delta$  192.89, 147.31, 132.32, 132.22, 132.12, 130.66, 129.94, 129.79, 129.69, 129.35, 126.34, 125.16, 124.60, 124.53, 124.32, 122.41, 121.81, 45.26, 38.40, 30.79, 28.00, 25.53; LC-MS (CI-(+))  $m/z$  (rel. int.) 639 (7), 638 (50), 637 ( $[\text{M}]^+$ , 100); HRMS (APPI) calcd for  $\text{C}_{47}\text{H}_{40}\text{O}_2$  ( $[\text{M}]^+$ ) 636.3028, found 630.3018.

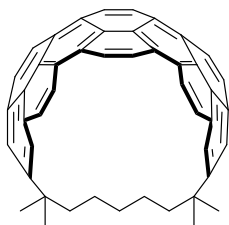
**1,1,7,7-Tetramethyl[7.2.2](2,6,8)pyrenophane (102b) and (Z)-12,22-dimethyl-1,1,7,7-tetramethyl[7.2](7,1)pyrenophane (104b)**



Titanium(IV) chloride (1.37 g, 7.3 mmol) was added slowly to a stirred slurry of zinc dust (0.95 g, 15.2 mmol) in anhydrous THF (40 mL) at room temperature under nitrogen atmosphere and the resulting brownish black slurry was heated at reflux for 1 h, during which time a dark black colour persisted (the loss of this colour indicates that the McMurry reaction will fail completely). Pyridine (0.96 mL, 12.0 mmol) was added by a syringe and the reaction was continued to reflux for further 10 min. The dialdehyde **101b** (540 mg, 0.8 mmol) was dissolved in anhydrous THF (80 mL) and added slowly to the black mixture. The reaction mixture was continued to reflux for a further 4 h. The

hot reaction mixture was poured into chloroform (100 mL) and the resulting greenish black solution was concentrated under reduced pressure. The residue obtained was adsorbed onto silica gel and subjected to a column chromatography (25 × 4.5 cm, 6% dichloromethane / hexanes) to first afford **104b** (15 mg, 3%) as a pale yellow solid:  $R_f$  = 0.52 (20% dichloromethane / hexanes); m.p. 243.0–246.0 °C;  $^1\text{H}$  NMR (300 MHz,  $\text{CDCl}_3$ )  $\delta$  8.00 (d,  $J$ =9.1 Hz, 2H), 7.84 (d,  $J$ =9.1 Hz, 2H), 7.80 (d,  $J$ =1.6 Hz, 2H), 7.75–7.65 (br m, 6H), 7.53 (s, 2H), 7.17–7.05 (m, 2H), 2.85 (s, 2H), 1.53–1.45 (m, 4H), 1.40 (s, 12H), 0.90–0.75 (m, 2H), 0.45–0.20 (m, 4H);  $^{13}\text{C}$  NMR (75 MHz,  $\text{CDCl}_3$ )  $\delta$  146.19, 133.19, 132.95, 130.96, 130.60, 129.14, 128.35, 127.06, 125.90, 125.04, 124.74, 123.30, 122.86, 122.48, 122.40, 45.70, 38.44, 31.11, 29.95, 29.38, 25.76, 22.94, 19.80, 14.37; LC-MS (CI-(+))  $m/z$  (rel. int.) 611 (10), 610 (48), 609 ( $[\text{M}]^+$ , 100); HRMS (EI+) calcd for  $\text{C}_{47}\text{H}_{44}$  ( $[\text{M}]^+$ ) 608.3443, found 608.3434. 1,1,7,7-Tetramethyl[7.2.2](2,6,8)-pyrenophane (**102b**) as a yellow solid (165 mg, 32%):  $R_f$  = 0.48 (20% dichloromethane / hexanes); m.p. > 300 °C,  $^1\text{H}$  NMR (300 MHz,  $\text{CDCl}_3$ )  $\delta$  8.11 (s, 4H), 8.04 (s, 2H), 7.64 (d,  $J$ =9.1 Hz, 4H), 7.56 (s, 4H), 7.48 (d,  $J$ =9.1 Hz, 4H), 1.40–1.36 (m, 4H), 1.36 (s, 12H), 0.70–0.60 (m, 2H), 0.15–0.04 (m, 4H);  $^{13}\text{C}$  NMR (75 MHz,  $\text{CDCl}_3$ )  $\delta$  145.57, 137.46, 137.30, 129.88, 128.77, 128.23, 126.21, 123.45, 122.68, 122.37, 122.81, 46.22, 38.29, 30.94, 29.75, 28.46, 26.54; LC-MS (CI-(+))  $m/z$  (rel. int.) 608 (2), 607 (12), 606 (56), 605 ( $[\text{M}]^+$ , 100); HRMS (APPI) calcd for  $\text{C}_{47}\text{H}_{40}$  ( $[\text{M}]^+$ ) 604.3130, found 604.3116.

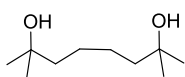
### 1,1,7,7-Tetramethyl[7](2,11)teropyrenophane (**103b**)



1,1,7,7-tetramethyl[7.2.2](7,1,3)pyrenophane (**102b**) (15 mg, 0.03 mmol) in *m*-xylene (3 mL) was heated at 125 °C and DDQ (67 mg, 0.3 mmol) was added in equal portions (1.0 equiv. at each time) and at regular intervals (2 h). The dark red reaction mixture was

continued to stir over a period of 30 h and the hot solvent was evaporated using a stream of nitrogen. The obtained residue was subjected to a column chromatography (36 × 3 cm; 5% ethyl acetate / hexanes) to afford 1,1,7,7-tetramethyl[7](2,11)teropyrenophane (**103b**) (5.3 mg, 36%) as a reddish brown solid:  $R_f$  = 0.29 (10% ethyl acetate / hexanes); m.p. >300 °C;  $^1\text{H}$  NMR (500 MHz,  $\text{CDCl}_3$ )  $\delta$  8.45 (s, 4H), 8.25 (d,  $J$ =9.5 Hz, 4H), 7.61 (d,  $J$ =9.5 Hz, 4H), 7.28 (s, 4H), 1.28 (s, 12H), 0.80–0.71 (m, 4H), 0.10–0.00 (m, 2H), (–1.10)–(–1.20) (m, 4H);  $^{13}\text{C}$  NMR (125 MHz,  $\text{CDCl}_3$ )  $\delta$  144.50, 128.75, 128.41, 127.89, 126.97, 126.03, 125.44, 124.89, 124.18, 123.54, 123.18, 47.74, 38.23, 31.18, 28.42, 24.27; LCMS (APCI(+))  $m/z$  (rel. int.) 605 (11), 604 (51), 603 ( $[\text{M}+\text{H}]^+$ , 100); HRMS (EI(+)) calculated for  $\text{C}_{47}\text{H}_{38}$  ( $[\text{M}]^+$ ) 602.2974, found 602.2961.

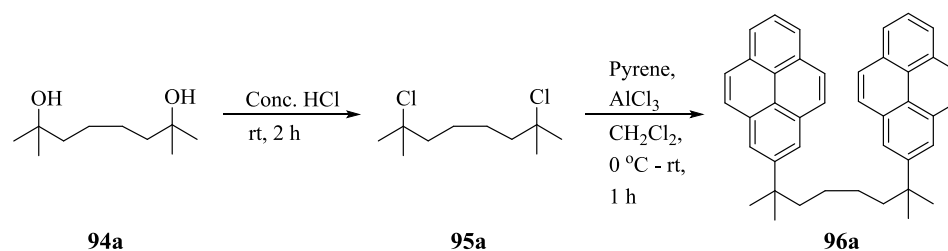
### 2,7-Dimethyl-2,7-octanediol (**94a**)



A solution of dimethyl adipate (**93a**) (15.32 g, 87.2 mmol) in THF (150 mL) was added dropwise over a period of 1.5 h to a stirred 0 °C solution of methylmagnesium bromide (3.0 M, 129 mL, 287 mmol). After the addition was complete, the reaction mixture was heated at reflux for 17 h and the resulting white cake was cooled to 0 °C. The reaction mixture was neutralized by the slow addition of saturated ammonium chloride solution (200 mL) with vigorous stirring. As much of the THF as possible was removed under reduced pressure and the resulting turbid aqueous

mixture was diluted with water (250 mL) and extracted with dichloromethane ( $3 \times 200$  mL). The combined organic layers were dried over  $\text{Na}_2\text{SO}_4$ , filtered and concentrated to afford 2,7-dimethyl-2,7-octanediol (**94a**) (13.50 g, 90%) as a white powder:  $R_f = 0.19$  (50% ethyl acetate / hexanes); m.p. 63.2–64.0 °C;  $^1\text{H}$  NMR (300 MHz,  $\text{CDCl}_3$ )  $\delta$  1.51–1.45 (m, 4H), 1.43–1.30 (m, 4H), 1.21 (s, 12H);  $^{13}\text{C}$  NMR (75 MHz,  $\text{CDCl}_3$ )  $\delta$  70.99, 43.92, 29.25, 24.88; LCMS (CI(-))  $m/z$  173  $[\text{M}-\text{H}]^-$ ; HRMS data could not be obtained.

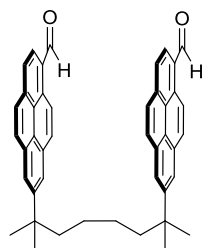
### Synthesis of 2,7-bis(2-pyrenyl)-2,7-dimethyloctane (**96a**)



A mixture of 2,7-dimethyl-2,7-octanediol (**94a**) (10.30 g, 59.1 mmol) and concentrated aqueous HCl solution (200 mL) was stirred at room temperature for 2 h. The reaction mixture was then poured into ice water (600 mL) and extracted with dichloromethane ( $3 \times 100$  mL). The combined organic layers were washed with a saturated solution of sodium bicarbonate ( $2 \times 100$  mL), washed with brine (150 mL), dried over anhydrous  $\text{Na}_2\text{SO}_4$ , filtered and concentrated under reduced pressure to afford 2,7-dichloro-2,7-dimethyloctane (**95a**) (11.61 g, 93%) as a colourless oil, which was used subsequently without further purification:  $R_f = 0.24$  (hexanes);  $^1\text{H}$  NMR (300 MHz,  $\text{CDCl}_3$ )  $\delta$  1.80–1.71 (m, 4H), 1.57 (s, 12H), 1.55–1.46 (m, 4H);  $^{13}\text{C}$  NMR (75 MHz,  $\text{CDCl}_3$ )  $\delta$  71.06, 45.92, 32.46, 25.19; LCMS (CI(+))  $m/z$  (rel. int.) 211  $[\text{M}+\text{H}]^+$ ; no HRMS data

could be obtained for this compound. Dichloride (**95a**) (5.40 g, 24.3 mmol) was dissolved in dichloromethane (500 mL) and pyrene (23.90 g, 118 mmol) was added. The solution was cooled to 0 °C and AlCl<sub>3</sub> (6.93 g, 52.1 mmol) was added. The resulting mixture was continued to stir at room temperature over a period of 1 h and then poured into ice-cold water (200 mL). The layers were separated and the aqueous layer was extracted with dichloromethane (2 × 100 mL). The combined organic layers were washed with brine (200 mL), dried over Na<sub>2</sub>SO<sub>4</sub>, filtered and concentrated under reduced pressure. The yellow residue was subjected to a column chromatography (30 × 4.5 cm; hexanes, then 7% dichloromethane / hexanes) to afford **96a** as an off-white solid (8.08 g, 45%): *R*<sub>f</sub> = 0.22 (15% dichloromethane / hexanes); m.p. 91.0–92.5 °C; <sup>1</sup>H NMR (500 MHz, CDCl<sub>3</sub>) δ 8.13 (d, *J*=7.6 Hz, 4H), 8.06 (s, 4H), 7.98 (dd, *J*=16.0, 8.9 Hz, 8H), 7.94 (dd, *J*=7.8, 7.7 Hz, 4H), 1.74–1.68 (m, 4H), 1.47 (s, 12H), 1.16–1.10 (q, *J*=4.5 Hz, 4H); <sup>13</sup>C NMR (125 MHz, CDCl<sub>3</sub>) δ 147.55, 130.94, 130.85, 127.58, 127.12, 125.45, 124.67, 124.58, 122.81, 122.76, 45.14, 38.18, 29.46, 25.60; LCMS (CI-(+)) *m/z* (rel. int.) 545 (4), 544, (53), 543 ([M+H]<sup>+</sup>, 100); HRMS (EI+) calculated for C<sub>42</sub>H<sub>38</sub> ([M]<sup>+</sup>) 542.2974, found 542.2993.

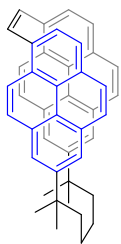
### 2,7-Bis(6-formylpyren-2-yl)-2,7-dimethyloctane (**97a**)



2,7-Bis(2-pyrenyl)-2,7-dimethylnonane (**96a**) (800 mg, 1.6 mmol) was dissolved in dichloromethane (40 mL) and α,α-dichloromethyl methyl ether (0.63 mL, 7.1 mmol), titanium(IV) chloride (0.78 mL, 7.1 mmol) were added at 0 °C and the resulting dark purple solution was continued to stir at room temperature for 2 h. The reaction mixture was poured into ice-cold water (100 mL) and the organic layer was separated. The aqueous layer was extracted with

dichloromethane (2 × 30 mL) and the combined organic layers were washed with brine (50 mL). The solvents was concentrated under reduced pressure and the resulting brown residue was subjected to a column chromatography (10 × 3 cm; dichloromethane) to afford **97a** as a bright yellow solid (760 mg, 86%):  $R_f$  = 0.07 (dichloromethane); m.p. 199.3–200.4 °C;  $^1\text{H}$  NMR (500 MHz,  $\text{CDCl}_3$ )  $\delta$  10.62 (s, 2H), 9.17 (d,  $J$ =9.2 Hz, 2H), 8.20 (d,  $J$ =7.9 Hz, 2H), 8.14 (d,  $J$ =1.5 Hz, 2H), 8.12 (d,  $J$ =1.5 Hz, 2H), 8.07 (d,  $J$ =9.2 Hz, 2H), 8.00 (d,  $J$ =8.9 Hz, 2H), 7.99 (d,  $J$ =7.9 Hz, 2H), 7.85 (d,  $J$ =8.9 Hz, 2H), 1.78–1.69 (m, 4H), 1.50 (s, 12H), 1.10–0.98 (m, 4H);  $^{13}\text{C}$  NMR (125 MHz,  $\text{CDCl}_3$ )  $\delta$  193.01, 148.42, 135.24, 130.94, 130.93, 130.86, 130.76, 130.75, 130.23, 127.19, 126.99, 124.96, 124.65, 124.41, 124.26, 122.80, 122.21, 45.33, 38.41, 29.52, 25.80; LCMS (CI-(+))  $m/z$  (rel. int.) 602 (2), 601 (12), 600 (48), 599 ( $[\text{M}+\text{H}]^+$ , 100); HRMS (APPI) calcd for  $\text{C}_{44}\text{H}_{38}\text{O}_2$  ( $[\text{M}]^+$ ) 598.2872, found 598.2876.

**(Z)-1,1,6,6-Tetramethyl[6,2](7.1)pyrenophane (99a)**

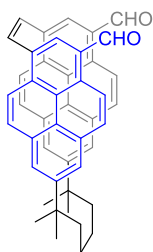


Titanium(IV) chloride (0.55 mL, 5.0 mmol) was added slowly to a stirred slurry of zinc dust (660 mg, 9.9 mmol) in anhydrous THF (35 mL) at room temperature under nitrogen atmosphere and the resulting brownish black slurry was heated at reflux for 1 h, during which time a dark black colour persisted (the loss of this colour indicates that the McMurry reaction will fail completely). Pyridine (0.68 mL, 8.4 mmol) was added by syringe and stirring was continued at reflux for a further 10 min. 2,7-Bis(6-formylpyren-2-yl)-2,7-dimethyloctane (**97a**) (350 mg, 0.6 mmol) in THF (65 mL) was then added slowly over 10 min and the reaction mixture was heated at reflux for a further 4 h. The hot reaction mixture was poured into chloroform



(100 mL) and the solvents were removed under reduced pressure. The residue was adsorbed onto silica gel and subjected to column chromatography (20×3.5 cm, 10% chloroform/hexanes) to afford (Z)-1,1,6,6-tetramethyl[6.2](7,1)pyrenophane (**99a**) as a yellow solid (200 mg, 60%):  $R_f$ =0.28 (15% chloroform/hexanes); m.p. 254.6–255.5 °C,  $^1\text{H}$  NMR (500 MHz,  $\text{CDCl}_3$ )  $\delta$  8.24 (d,  $J$ =7.9 Hz, 2H), 8.10 (d,  $J$ =7.9 Hz, 2H), 8.06 (d,  $J$ =8.8 Hz, 2H), 7.97 (d,  $J$ =8.8 Hz, 2H), 7.85 (d,  $J$ =1.8 Hz, 2H), 7.58 (s, 2H), 7.10 (d,  $J$ =1.8 Hz, 2H), 6.72 (d,  $J$ =9.2 Hz, 2H), 6.22 (d,  $J$ =9.2 Hz, 2H), 1.60 (br s, 2H), 1.38 (br s, 6H), 1.26 (br s, 8H), 0.81 (br s, 2H) –0.01 (br s, 2H);  $^{13}\text{C}$  NMR (75 MHz,  $\text{CDCl}_3$ )  $\delta$  146.44, 133.32, 131.27, 130.68, 130.37, 130.05, 128.00, 127.78, 127.26, 126.93, 125.23, 125.09, 124.58, 124.44, 122.77, 122.31, 122.12, 46.02, 38.26, 30.88, 27.85, 26.35; LCMS (CI-(+))  $m/z$  (rel. int.) 570 (3), 569 (13), 568 (48), 567 ( $[\text{M}+\text{H}]^+$ , 100); HRMS (APPI) calcd for  $\text{C}_{44}\text{H}_{38}$  ( $[\text{M}]^+$ ) 566.2974, found 566.2945.

**(Z)-12,22-Diformyl-1,1,7,7-tetramethyl[7.2](7,1)pyrenophane (101a)**



To a stirred 0 °C solution of (Z)-**99a** (80 mg, 0.14 mmol) and  $\alpha,\alpha$ -dichloromethyl methyl ether (0.03 mL, 0.4 mmol) in dichloromethane (7 mL) was added titanium(IV) chloride (0.04 mL, 0.4 mmol). The ice bath was removed and the reaction mixture was stirred at room temperature for 2 h. The reaction mixture was poured into ice-cold water (20 mL) and the organic layer was separated. The aqueous layer was extracted with dichloromethane (2×15 mL) and the combined organic layers were washed with brine (20 mL) and dried over  $\text{Na}_2\text{SO}_4$ . The solvent was removed under reduced pressure and the residue was subjected to column chromatography (10.0×2.5 cm, dichloromethane) to afford (Z)-**101a** as a bright

yellow solid (58 mg, 66%):  $R_f=0.30$  (dichloromethane); m.p.  $>300\text{ }^{\circ}\text{C}$ ,  $^1\text{H}$  NMR (500 MHz,  $\text{CDCl}_3$ )  $\delta$  10.88 (s, 2H), 9.41 (br d,  $J=9.2\text{ Hz}$ , 2H), 8.54 (br s, 2H), 8.19 (d,  $J=9.2\text{ Hz}$ , 2H), 7.96 (s, 2H), 7.66 (s, 2H), 7.15 (br s, 2H), 7.12 (br d,  $J=8.0\text{ Hz}$ , 2H), 6.34 (br d,  $J=8.3\text{ Hz}$ , 2H), 1.66 (br s, 2H), 1.35 (br s, 6H), 1.25 (br s, 8H), 0.71 (br s, 2H), 0.07 (br s, 2H);  $^{13}\text{C}$  NMR (125 MHz,  $\text{CDCl}_3$ )  $\delta$  193.14, 147.37, 132.37, 132.37, 131.32, 130.97, 129.99, 129.53, 129.44, 128.35, 126.82, 124.64, 124.62, 124.52, 124.00, 122.39, 121.39, 45.58, 38.05, 29.95, 28.00, 26.14; LC-MS (CI-(+))  $m/z$  (rel. int.) 625 (18), 624 (35), 623 ( $[\text{M}]^+$ ), 100); HRMS (APPI) calcd for  $\text{C}_{46}\text{H}_{38}\text{O}_2$  ( $[\text{M}]^+$ ) 622.2872, found 622.2876.

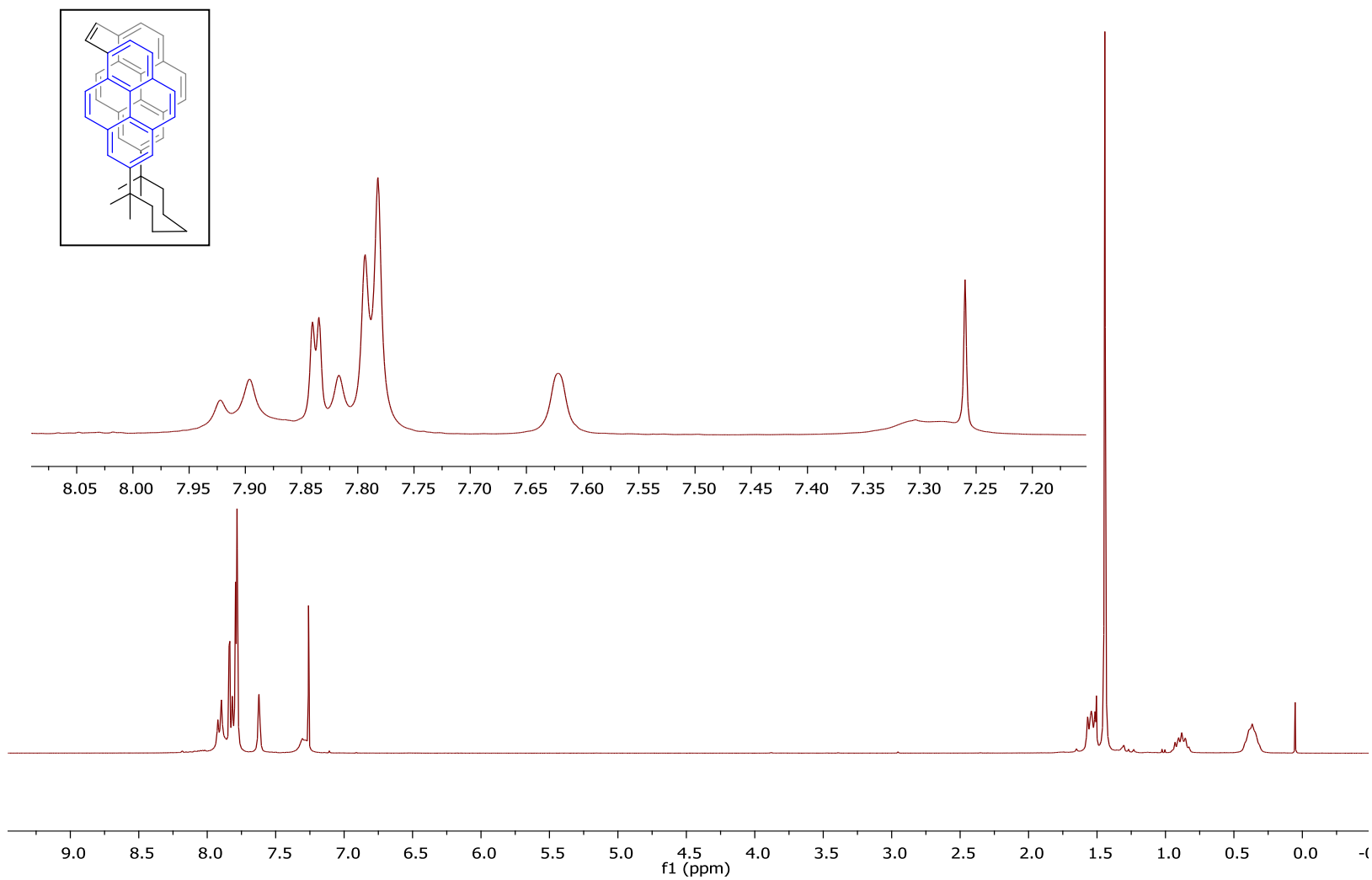
## 2.7 References

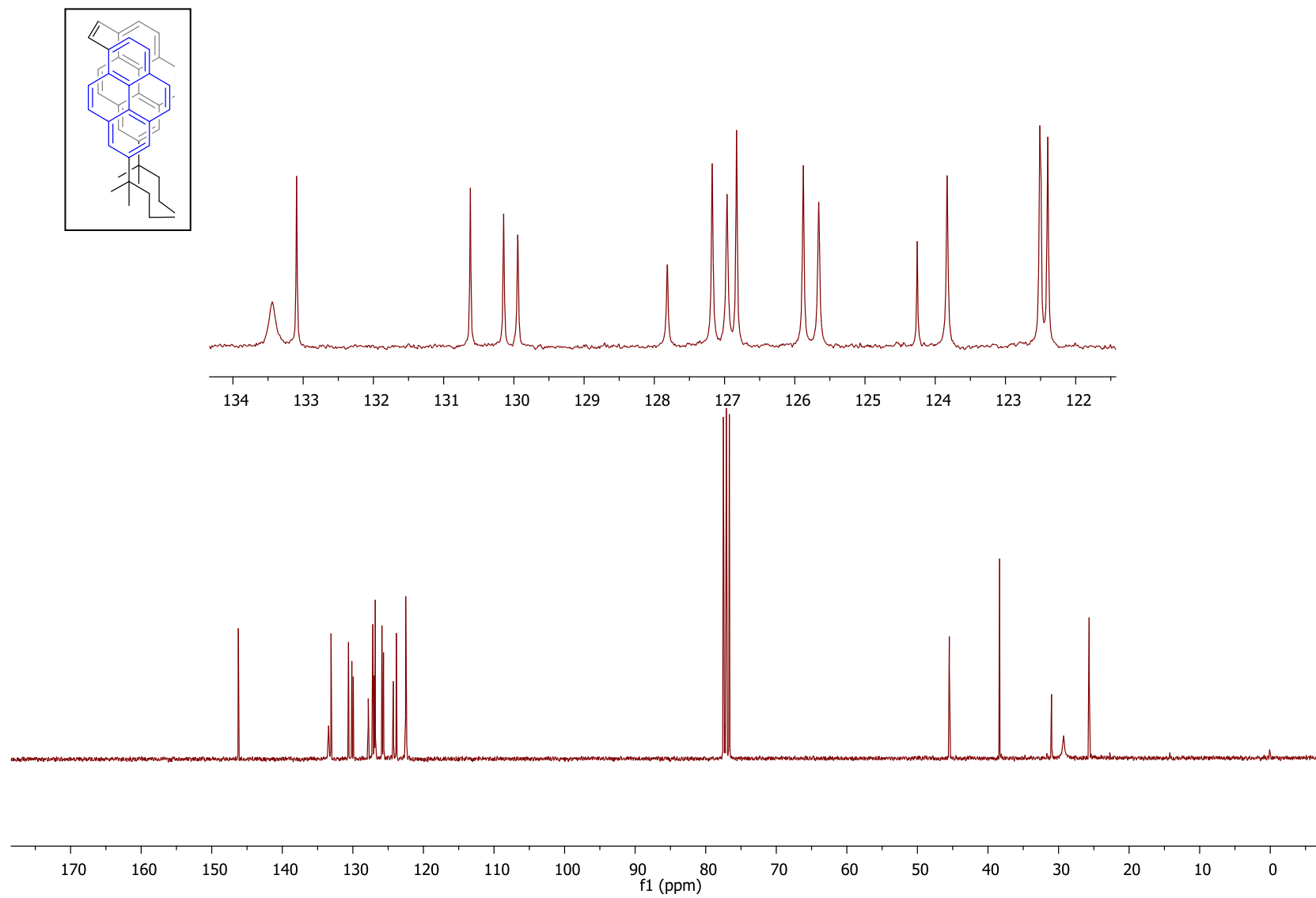
1. B. L. Merner, L. N. Dawe and G. J. Bodwell, *Angew. Chem. Int. Ed.*, 2009, **48**, 5487–5491.
2. a) G. J. Bodwell, J. N. Bridson, T. J. Houghton, J. W. J. Kennedy and M. R. Mannion, *Angew. Chem., Int. Ed. Engl.*, 1996, **35**, 1320–1321. b) G. J. Bodwell, J. N. Bridson, T. J. Houghton, J. W. J. Kennedy and M. R. Mannion, *Chem. Eur. J.*, 1999, **5**, 1823–1827. c) G. J. Bodwell, J. N. Bridson, M. K. Cyrański, J. W. J. Kennedy, T. M. Krygowski, M. R. Mannion and D. O. Miller, *J. Org. Chem.*, 2003, **68**, 2089–2098. d) G. J. Bodwell, J. J. Fleming, M. R. Mannion and D. O. Miller, *J. Org. Chem.*, 2000, **65**, 5360–5370. e) I. Aprahamian, G. J. Bodwell, J. J. Fleming, G. P. Manning, M. R. Mannion, B. L. Merner, T. Sheradsky, R. J. Vermeij and M. Rabinovitz, *J. Am. Chem. Soc.*, 2004, **126**, 6765–6775. f) G. J.

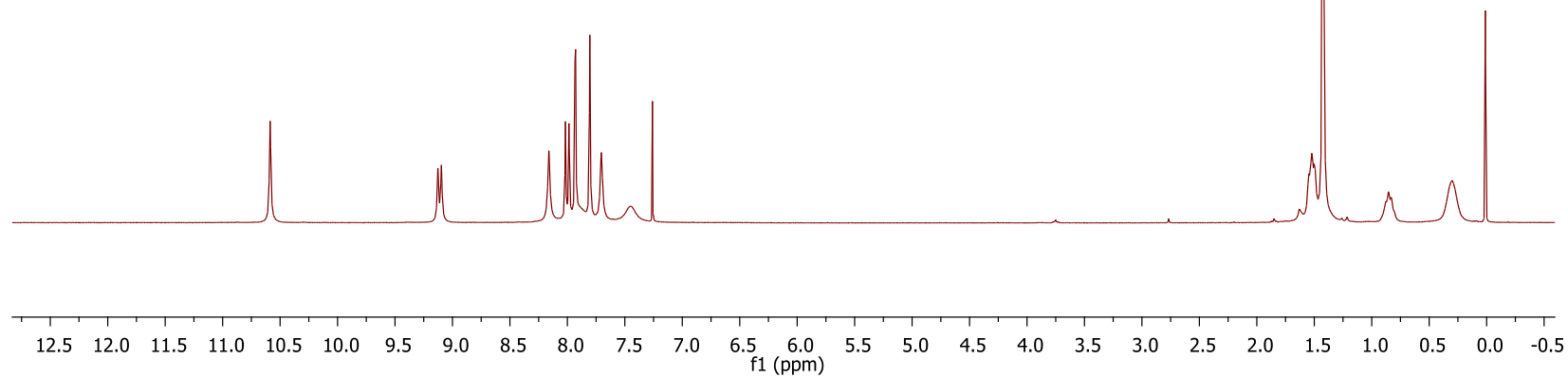
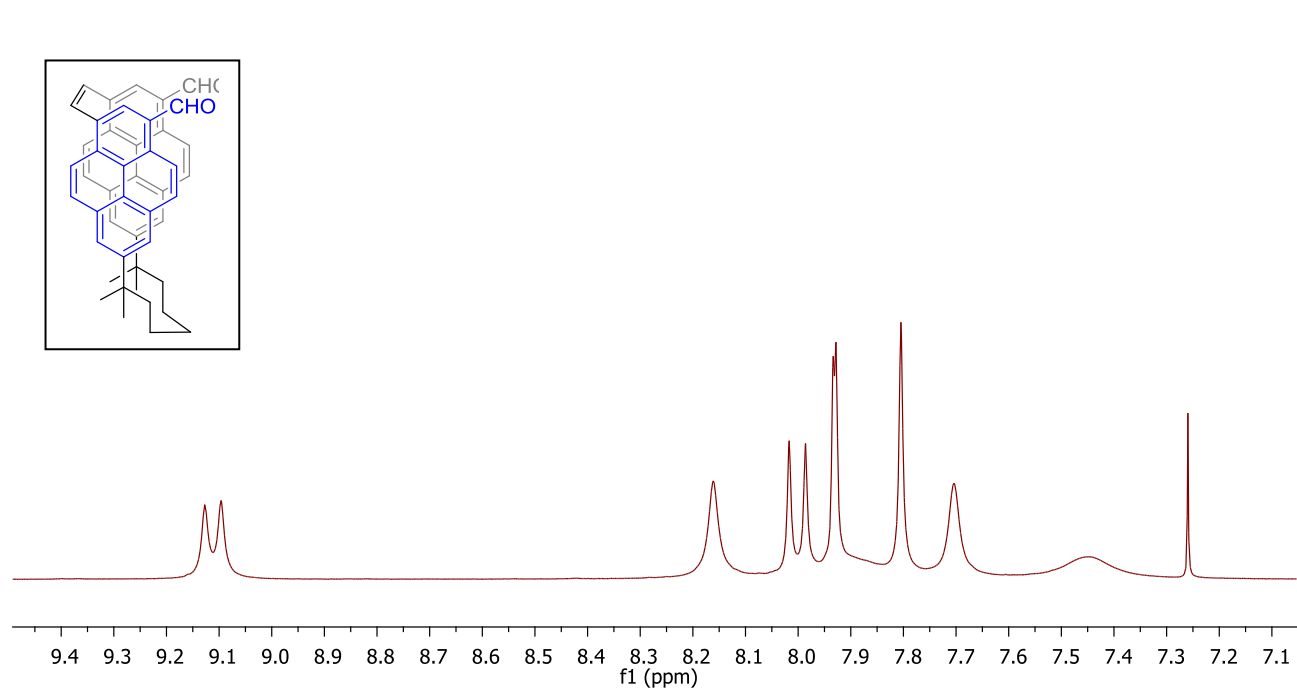
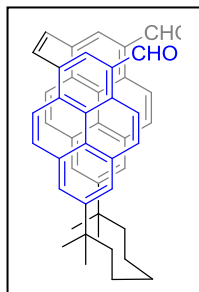
- Bodwell, R. J. Vermeij and D. O. Miller, *Org. Lett.*, 2001, **3**, 2093–2096. g) B. Zhang, G. P. Manning, M. A. Dobrowolski, M. K. Cyrański and G. J. Bodwell, *Org. Lett.*, 2008, **10**, 273–276. h) P. R. Nandaluru, L. N. Dawe, P. Dongare, C. M. Kraml, R. A. Pascal Jr., D. W. Thompson and G. J. Bodwell, *Chem. Commun.*, 2012, **48**, 7744–7749.
3. Y. Miura, E. Yamano, A. Tanaka, J. Yamauchi, *J. Org. Chem.* 1994, **59**, 3294–3300.
  4. G. J. Bodwell and P. R. Nandaluru, *Isr. J. Chem.*, 2012, **52**, 105–138.
  5. T. Umemoto, T. Kawashima, Y. Sakata and S. Misumi, *Tetrahedron Lett.*, 1975, **16**, 1005–1006.
  6. R. H. Mitchell, V. Boekelheide, *J. Am. Chem. Soc.*, 1970, **92**, 3510–3512.
  7. T. Yao, H. Yu, R. J. Vermeij, G. J. Bodwell, *Pure Appl. Chem.*, 2008, **80**, 533–546.
  8. B. L. Merner and G. J. Bodwell, unpolished results.
  9. a) M. Inouye, K. Fujimoto, M. Furusyo and H. Nakazumi, *J. Am. Chem. Soc.*, 1999, **121**, 1452–1458. b) G. J. Bodwell, J. J. Fleming and D. O. Miller, *Tetrahedron*, 2001, **57**, 3577–3585. c) H. Hayashi, *J. Chem. Res.*, 2004, 599–601. d) A. Tsuge, M. Otsuka, T. Moriguchi and K. Sakata, *Org. Biomol. Chem.* 2005, **3**, 3590–3593. e) A. Paudel, *J. Chem. Res.*, 2008, 731–734. f) D. Franz, S. T. Robbins, R. T. Boéré and P. W. Dibble, *J. Org. Chem.*, 2009, **74**, 7544–7547. g) Y. Yang, M. R. Mannion, L. N. Dawe, C. M. Kraml, R. A. Pascal Jr. and G. J.

- Bodwell, *J. Org. chem.*, 2012, **77**, 57–67. h) M. D. Halling, K. S. Unikela, G. J. Bodwell, D. M. Grant and R. J. Pugmire, *J. Phys. Chem. A*, 2012, **116**, 5193–5198.
10. R. H. Mitchell, Eds: P. Keehn and S. Rosenfeld, *Nuclear Magnetic Resonance Properties and Conformational Behaviour of Cyclophanes, Chapter 4*; Academic press, 1983, 239–310.

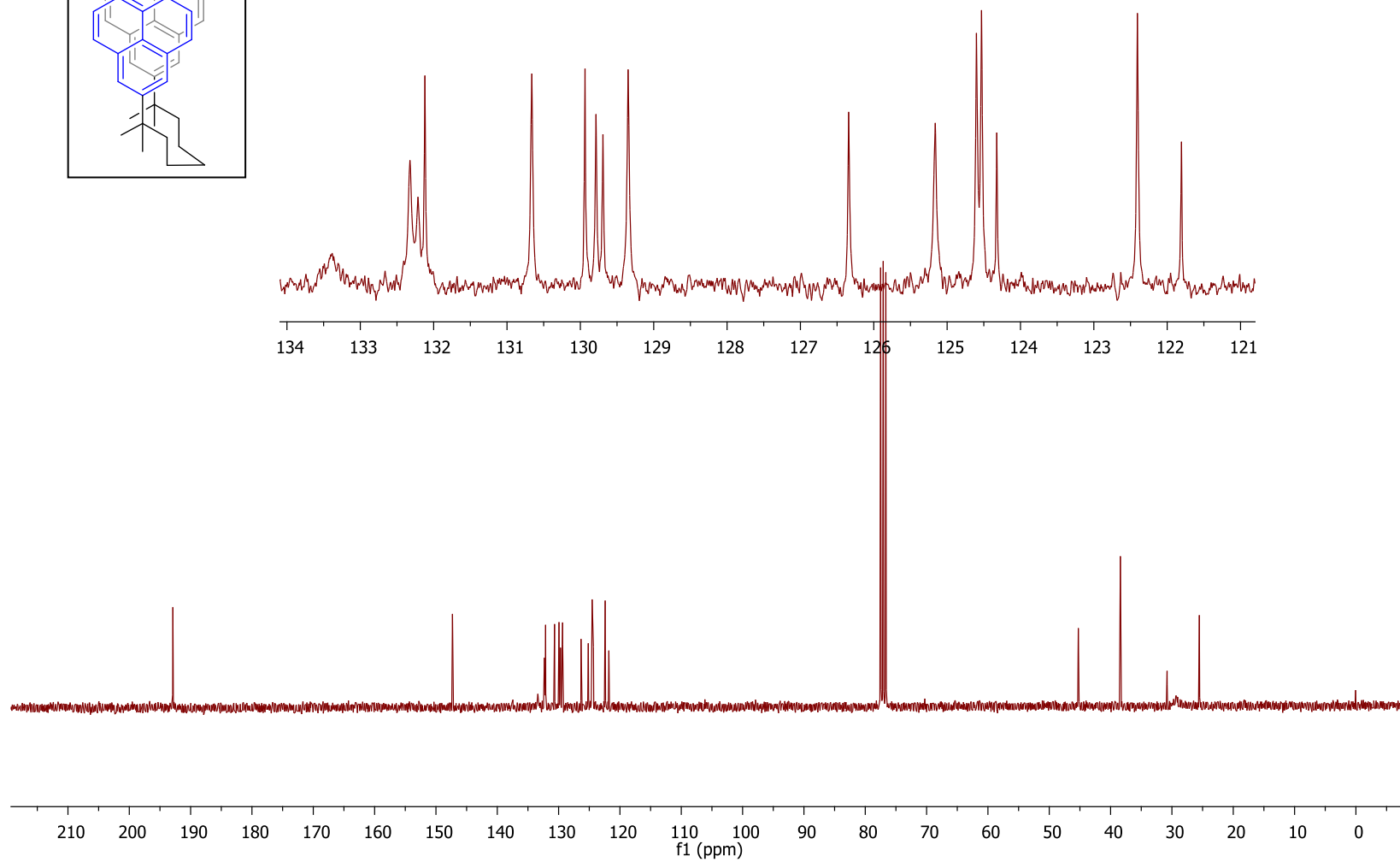
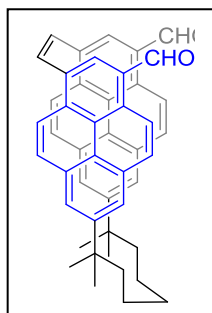
# APPENDIX 1

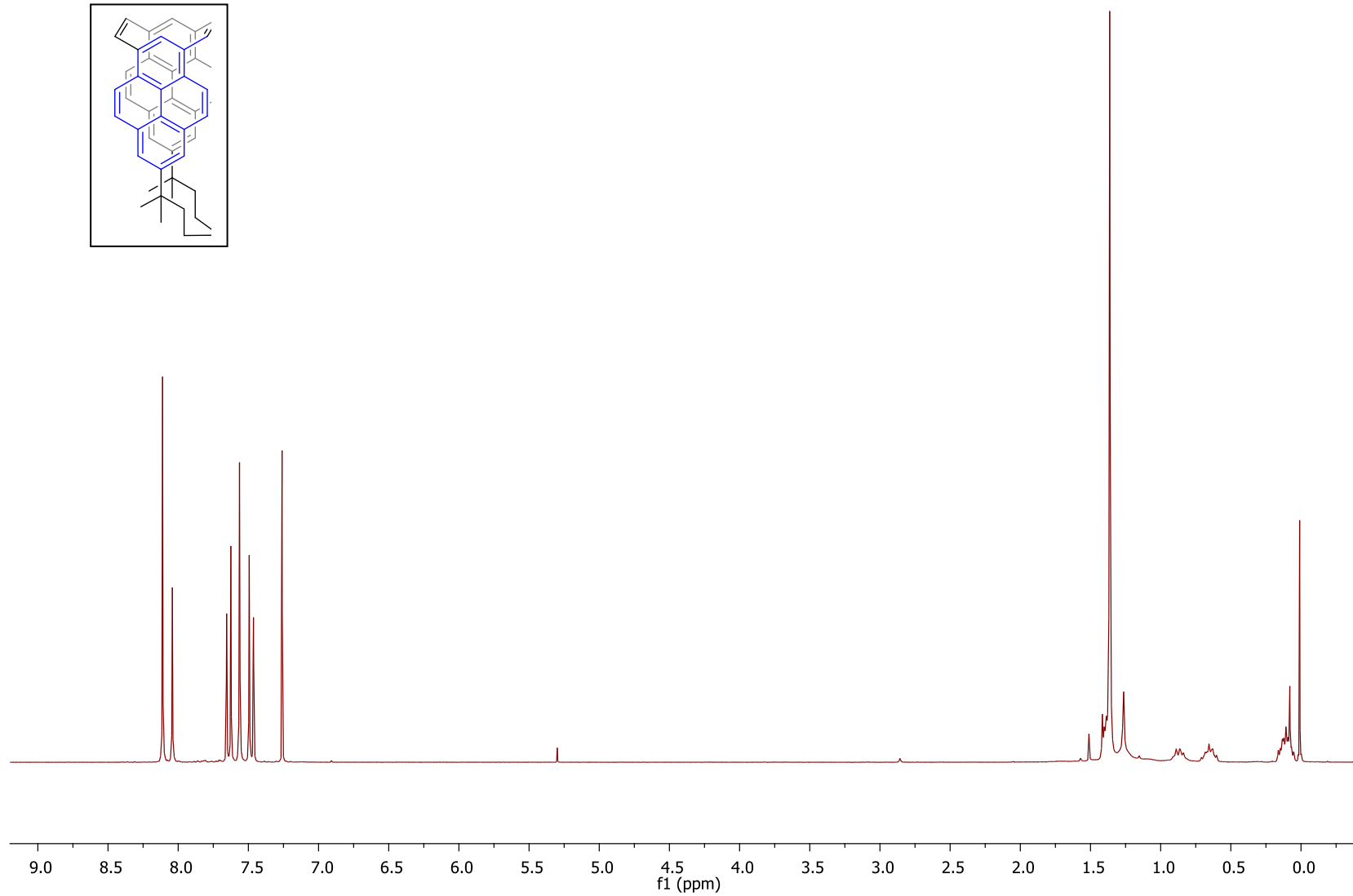
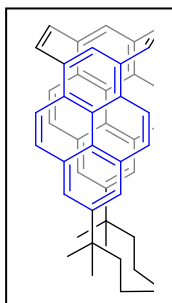


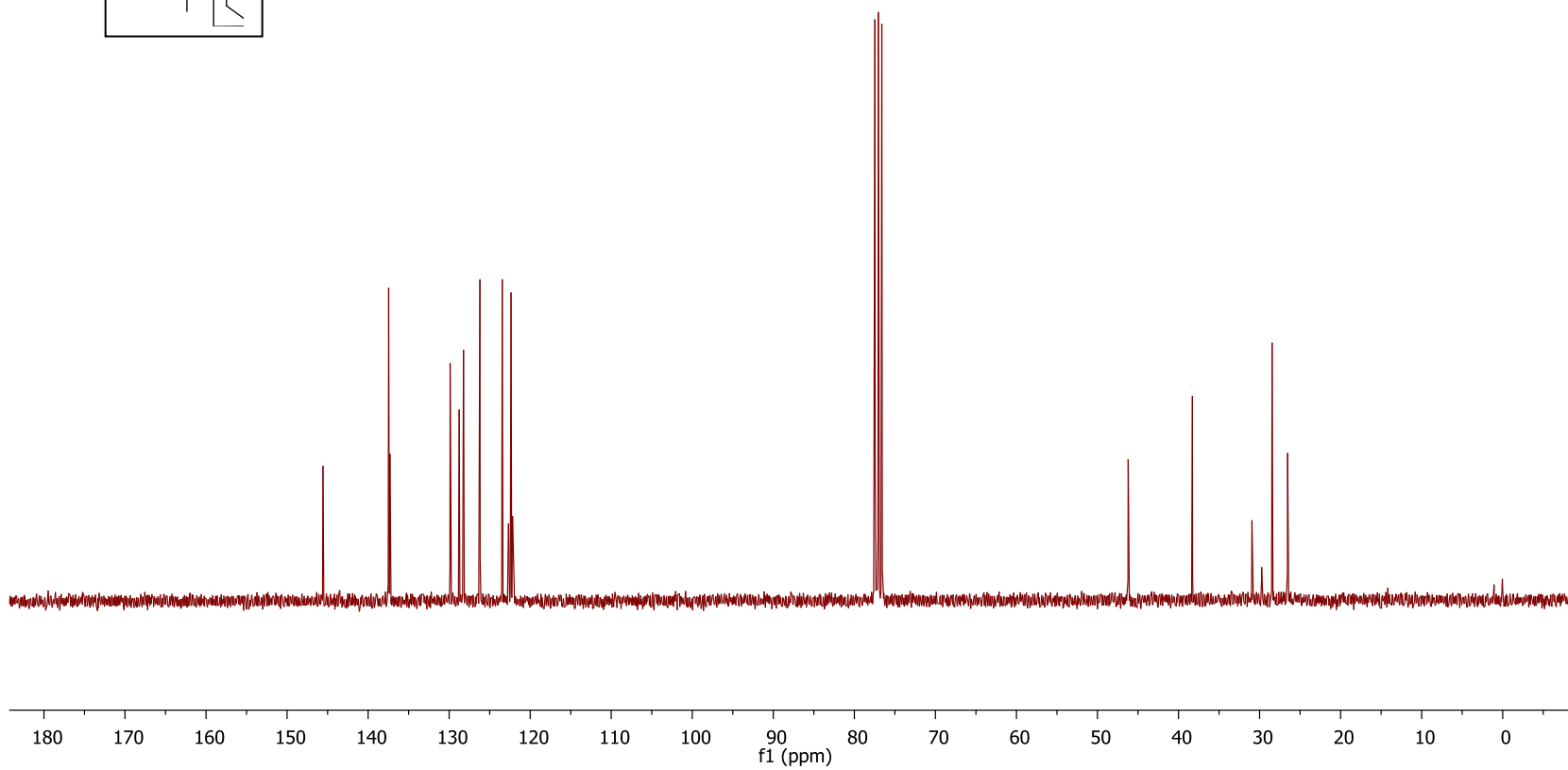
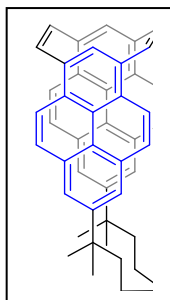


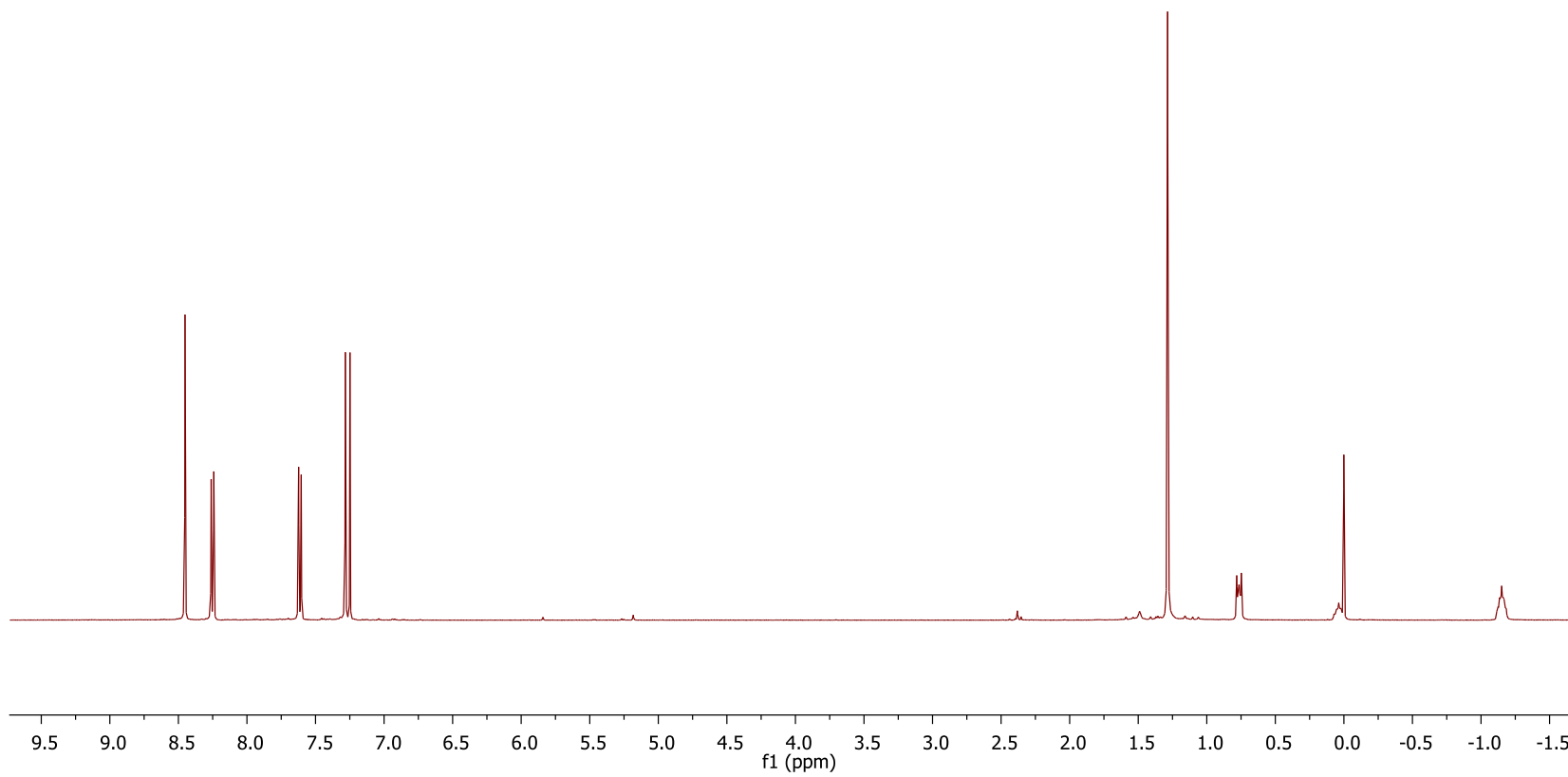
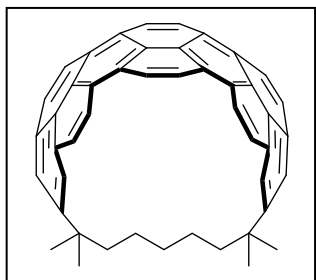


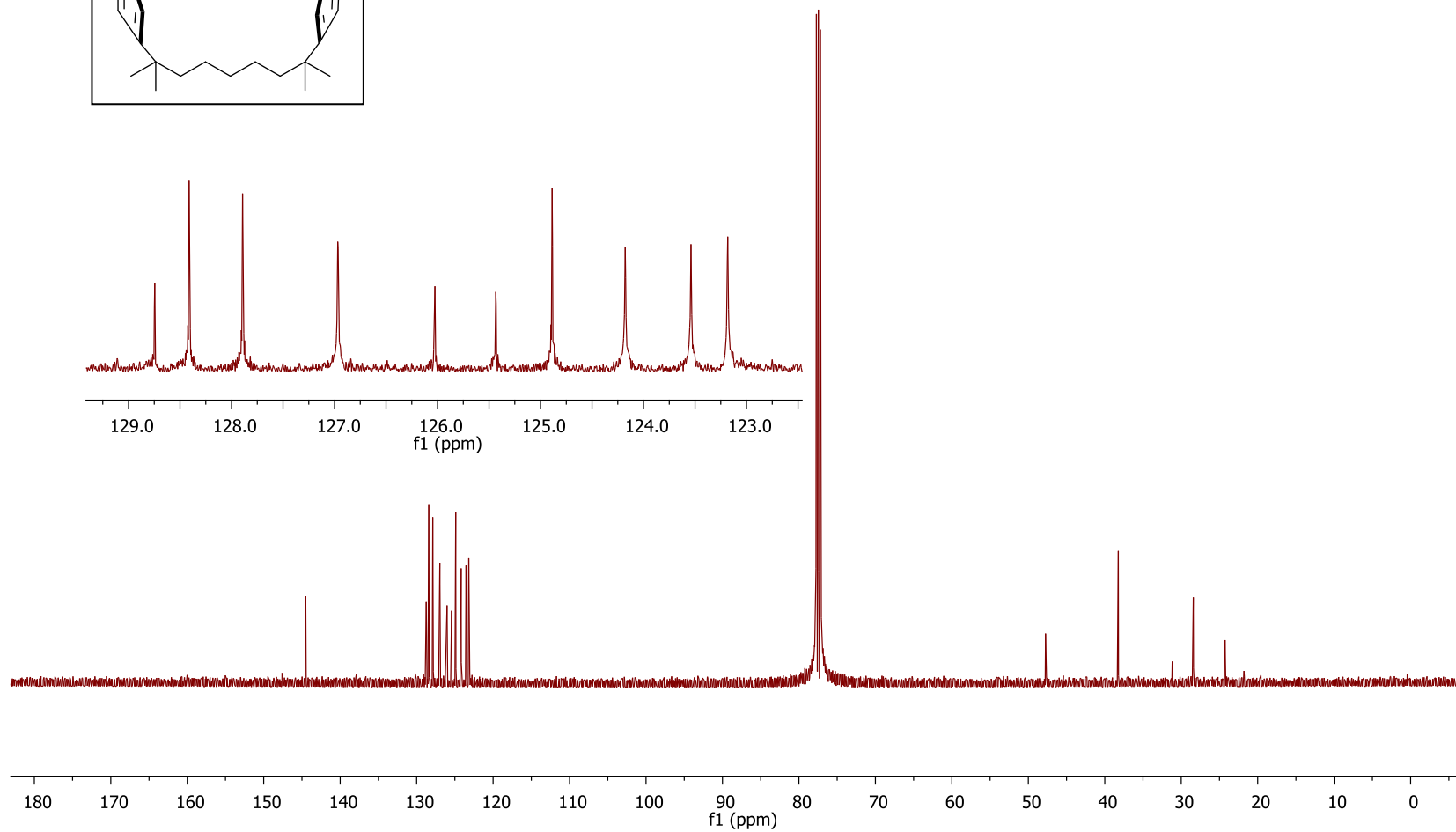
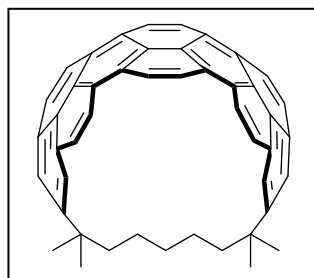


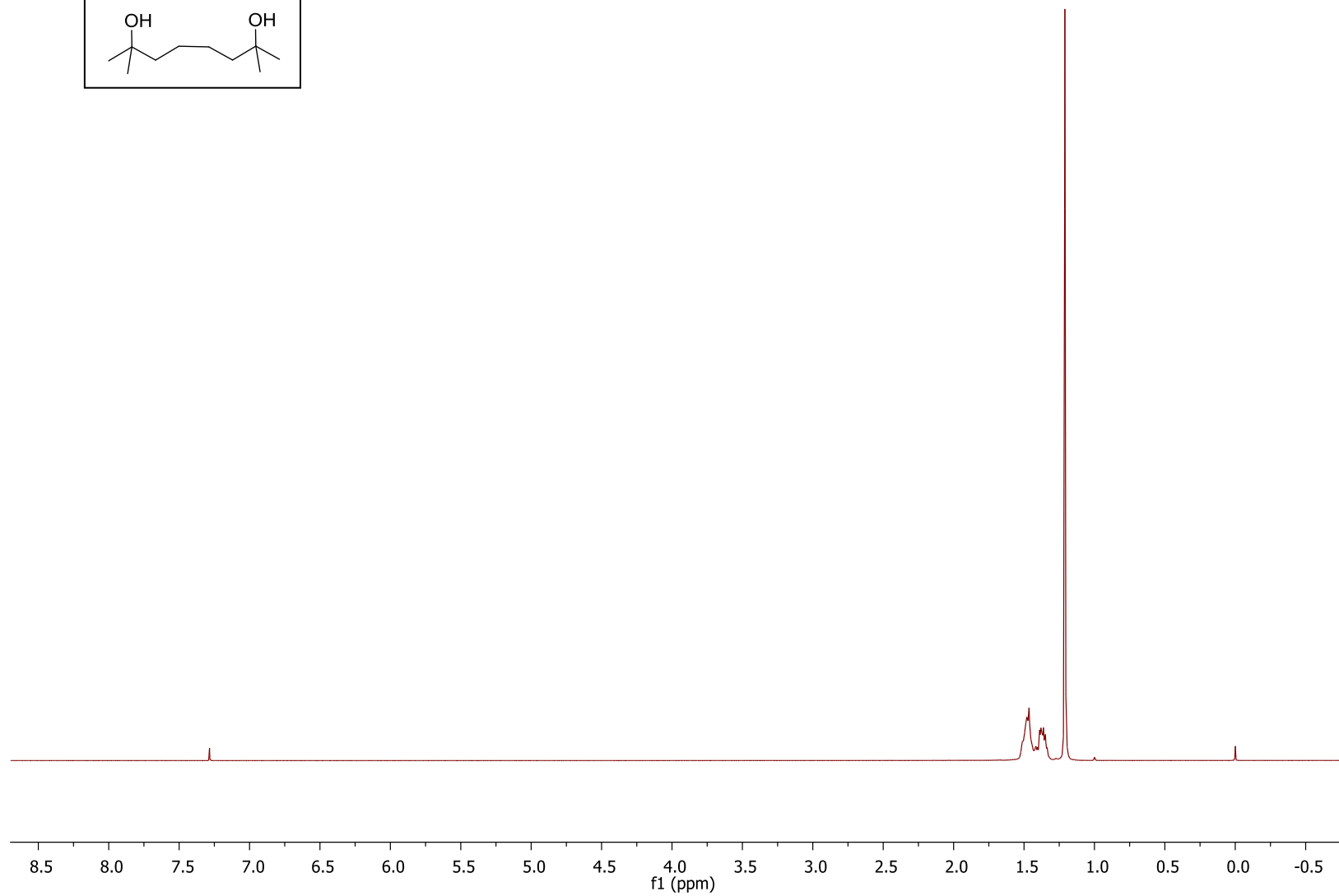
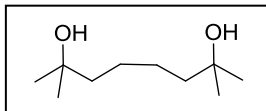


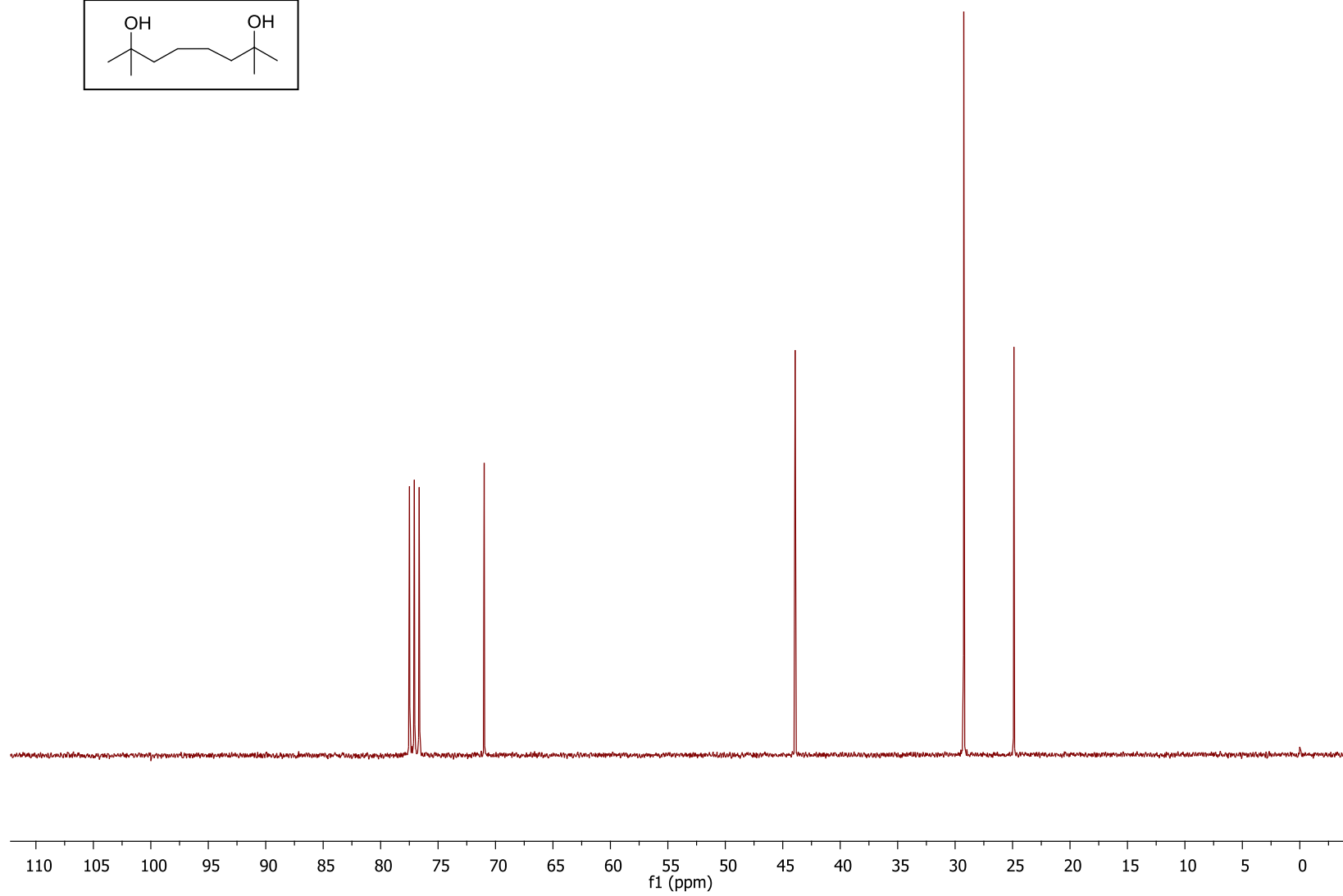
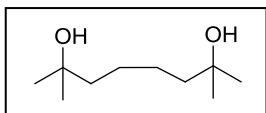


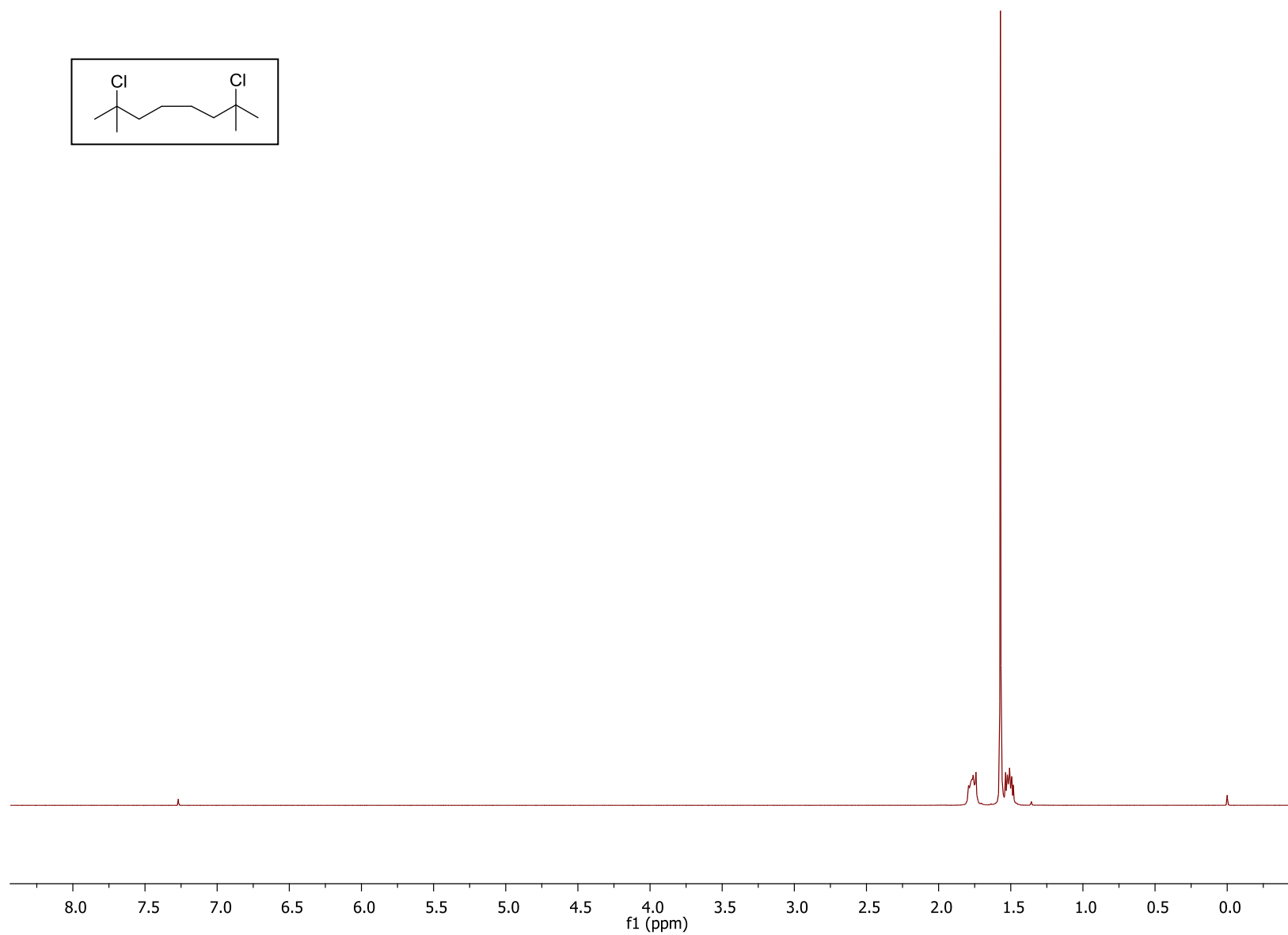
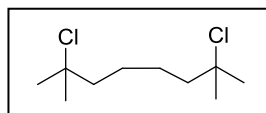




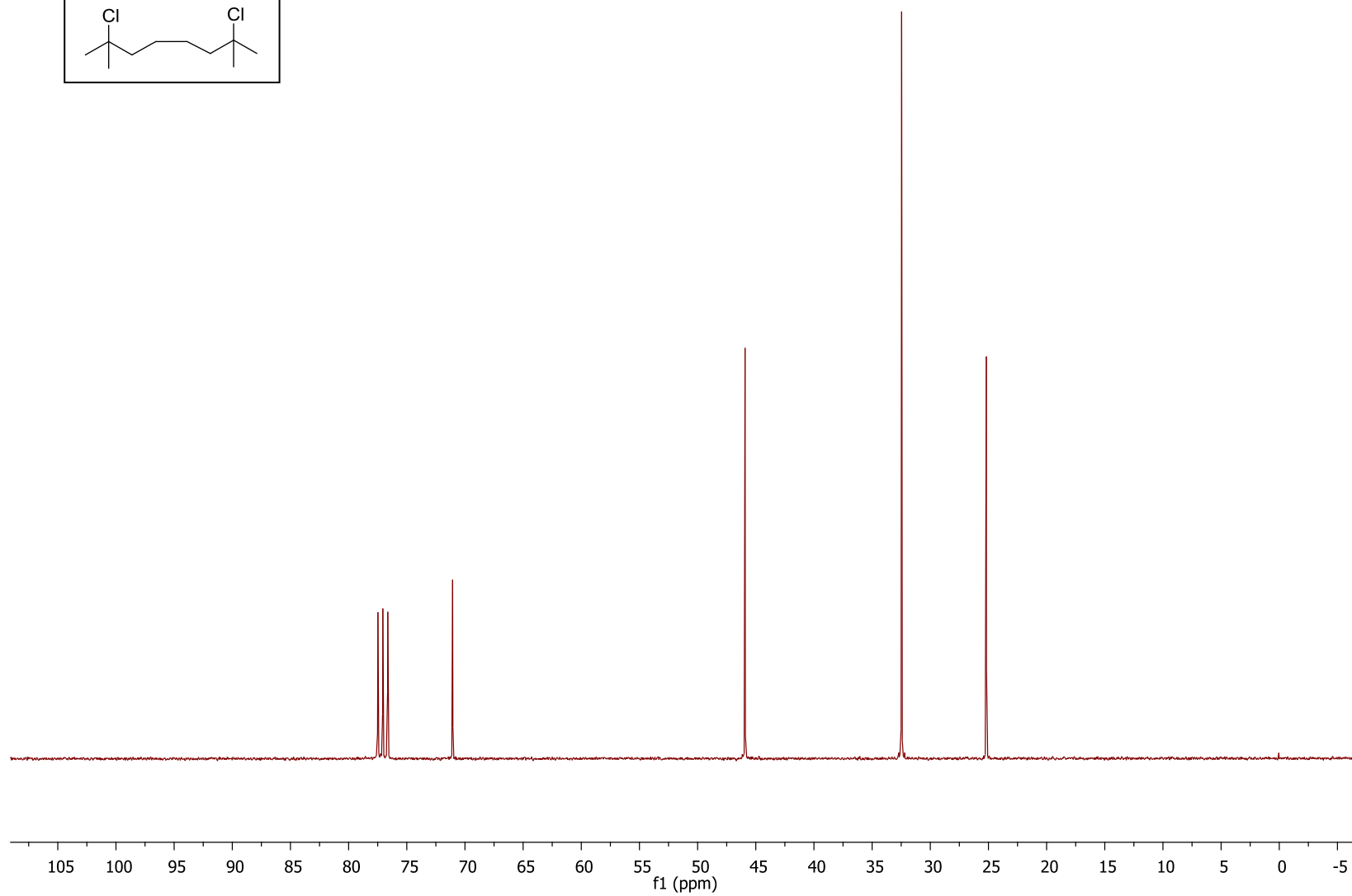
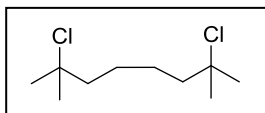


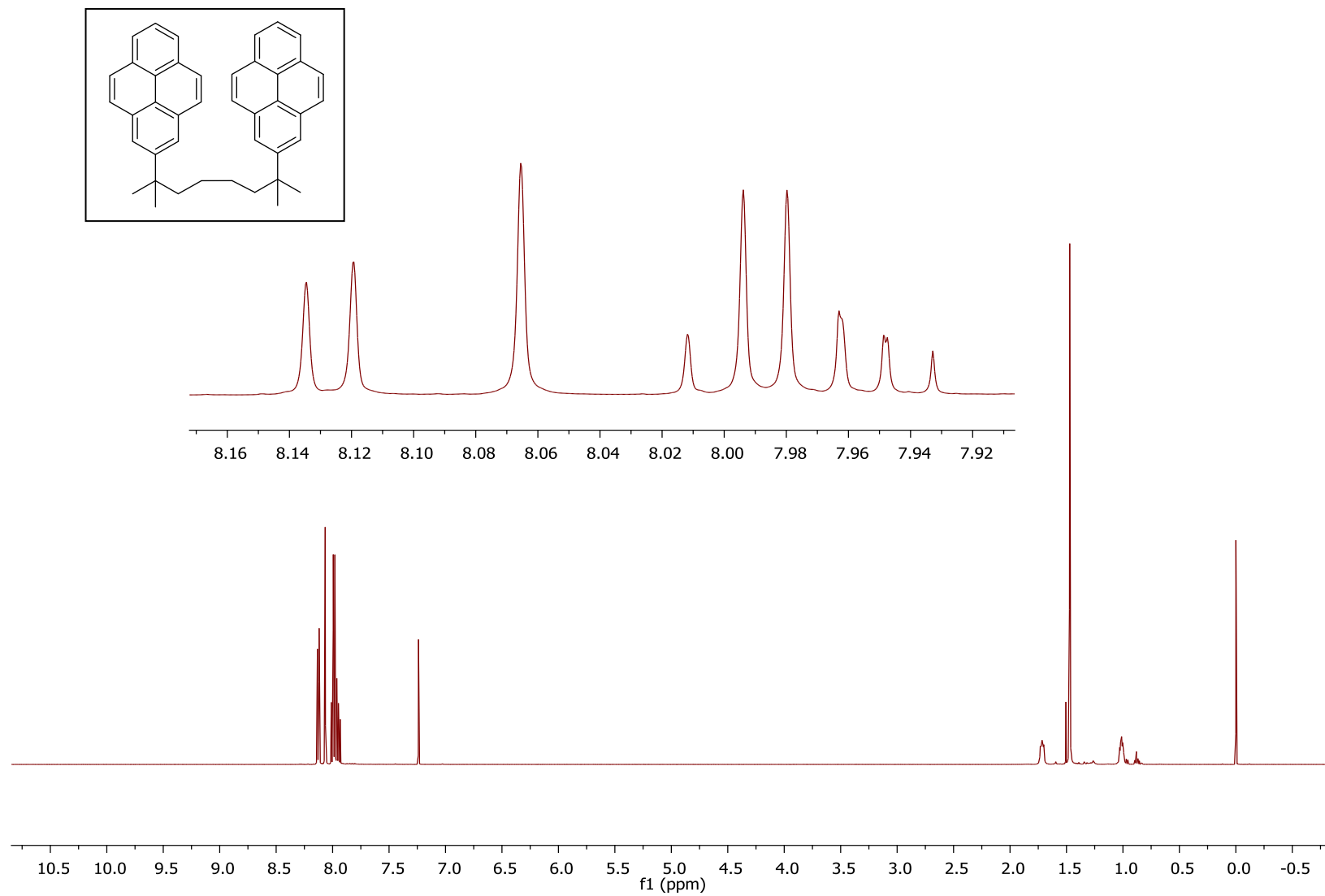


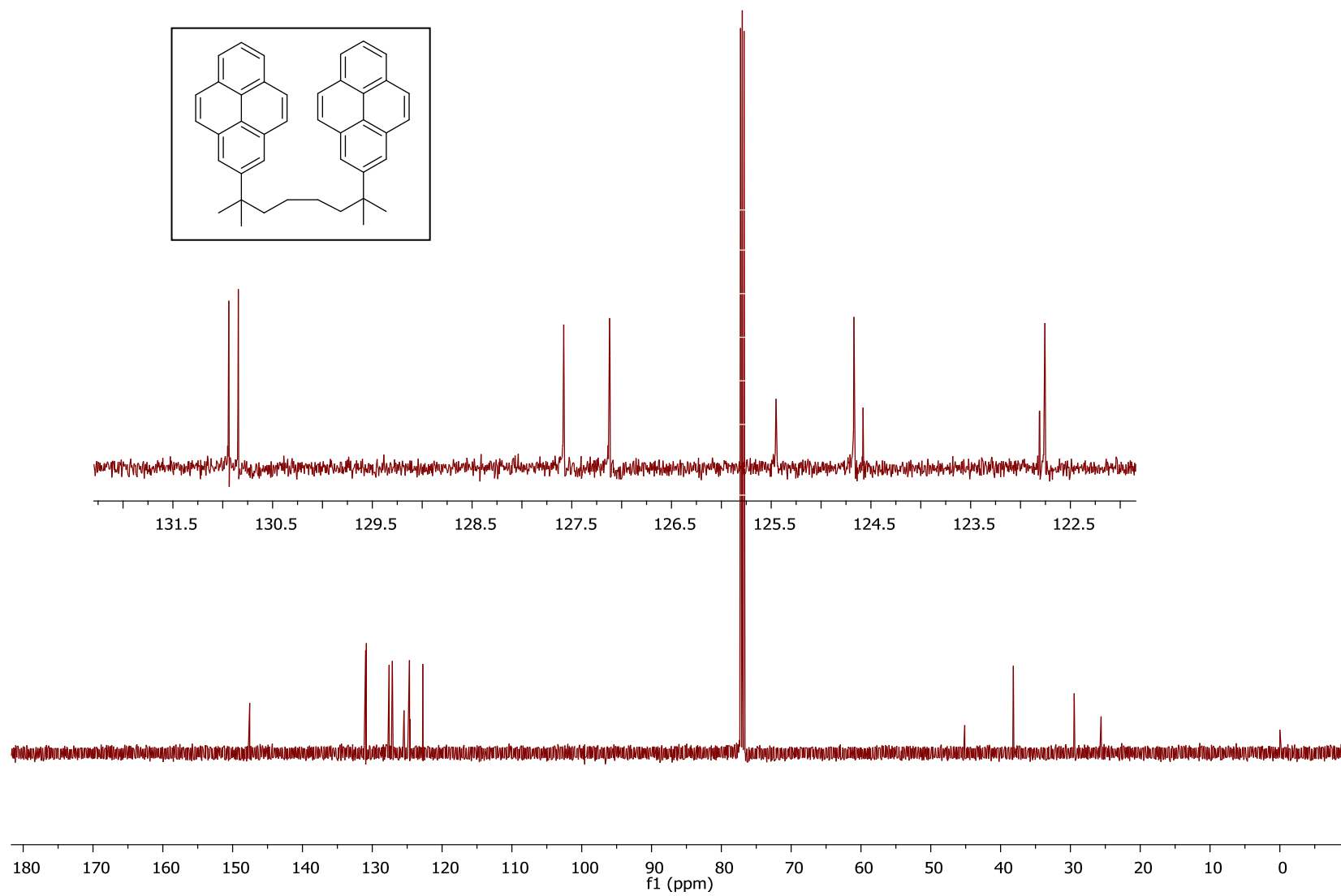


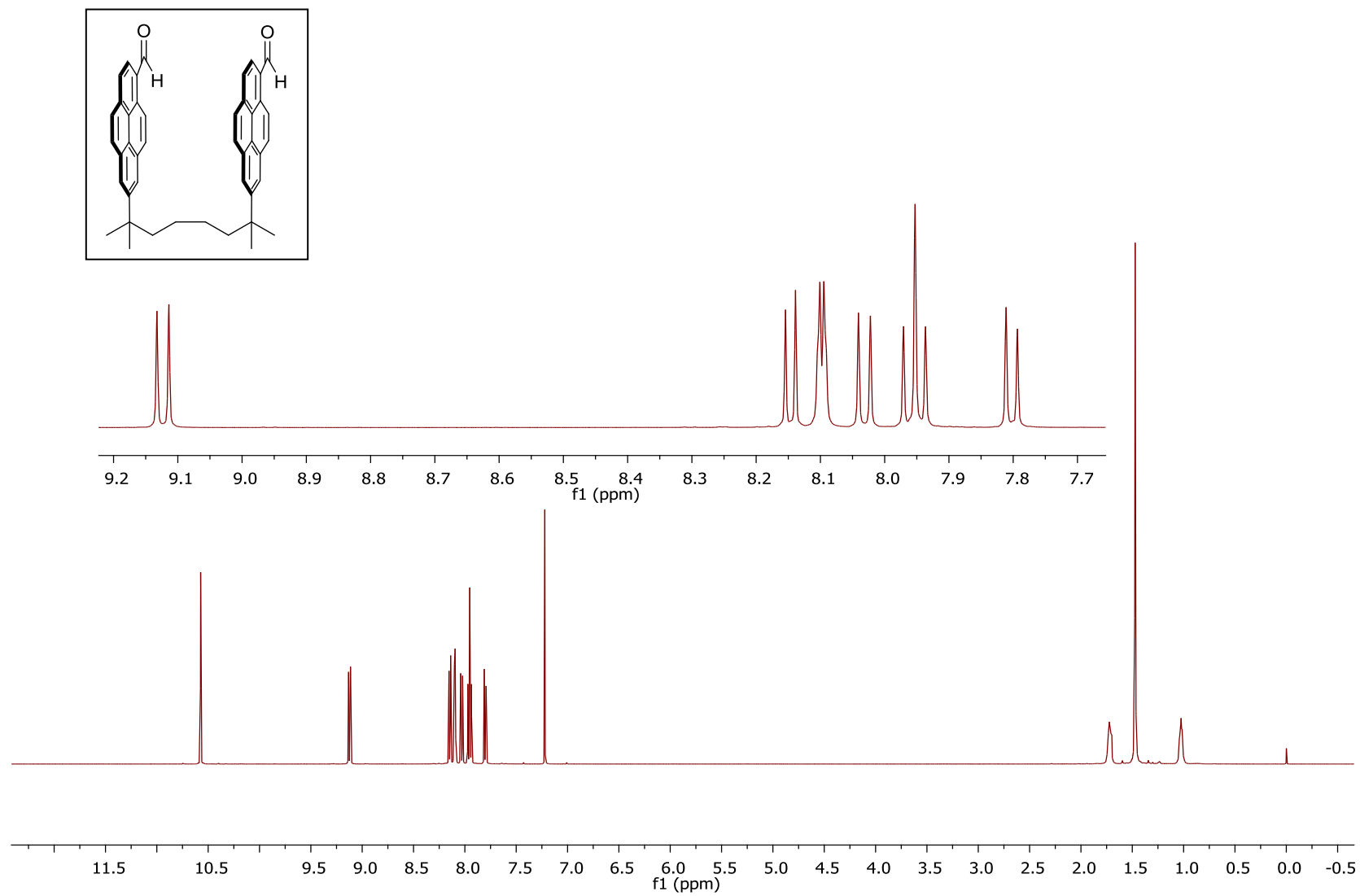


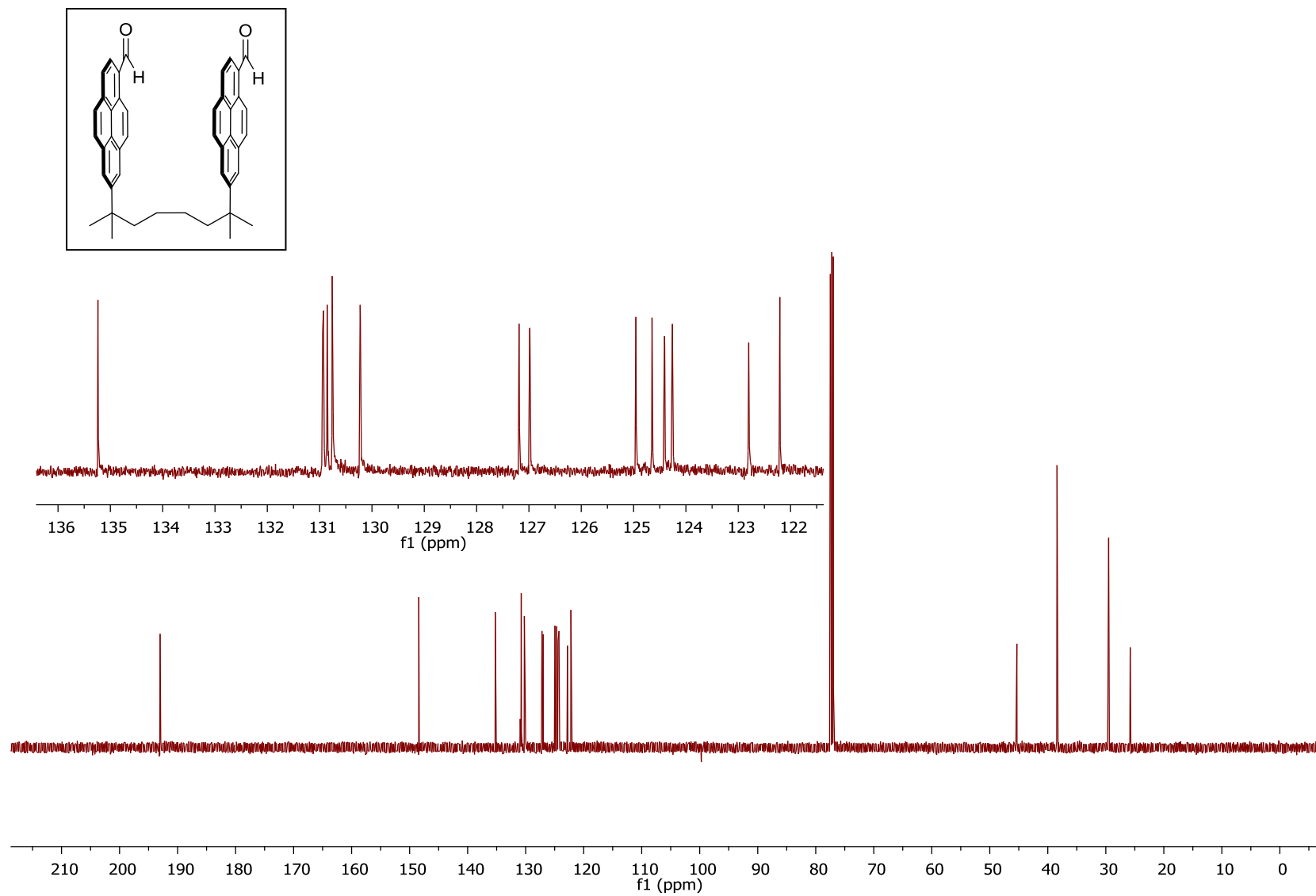


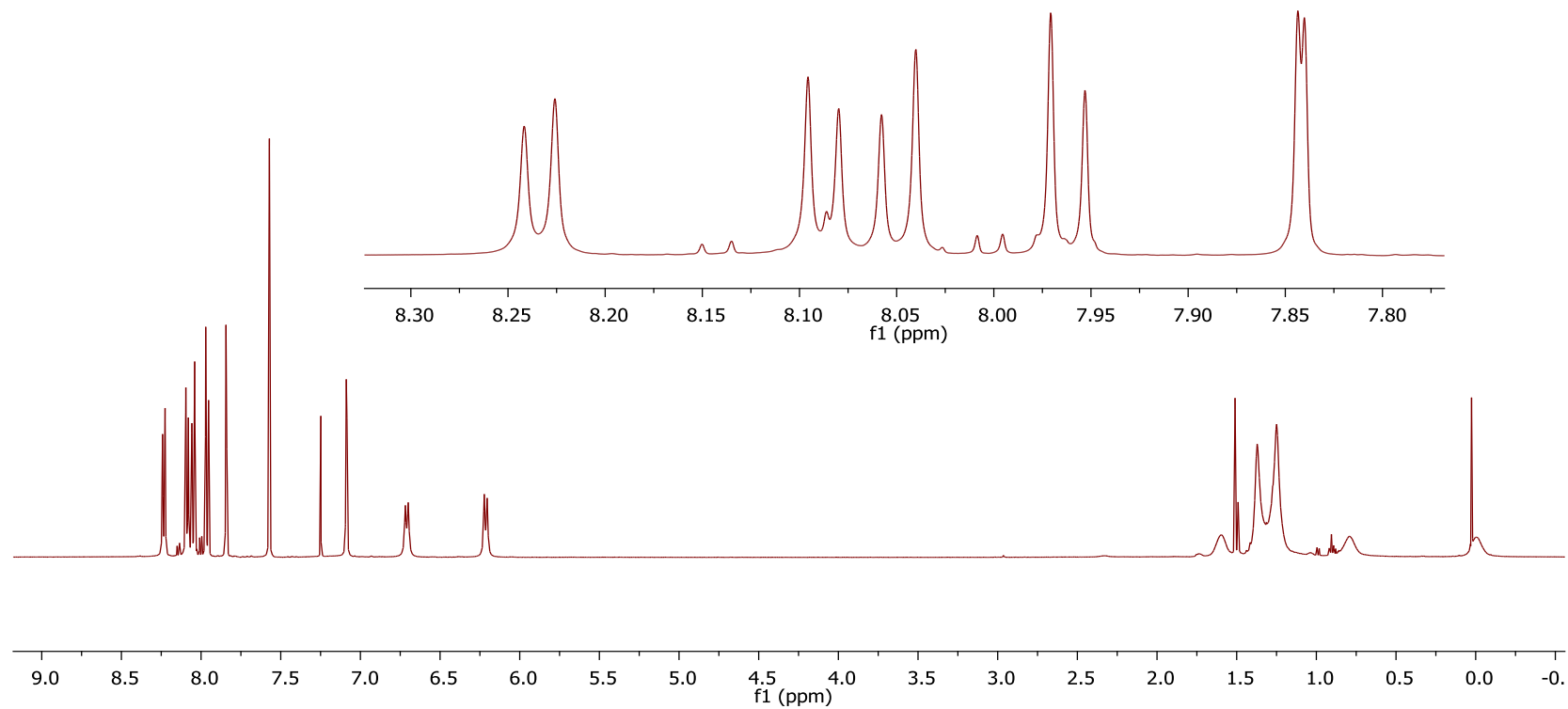
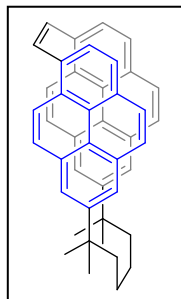


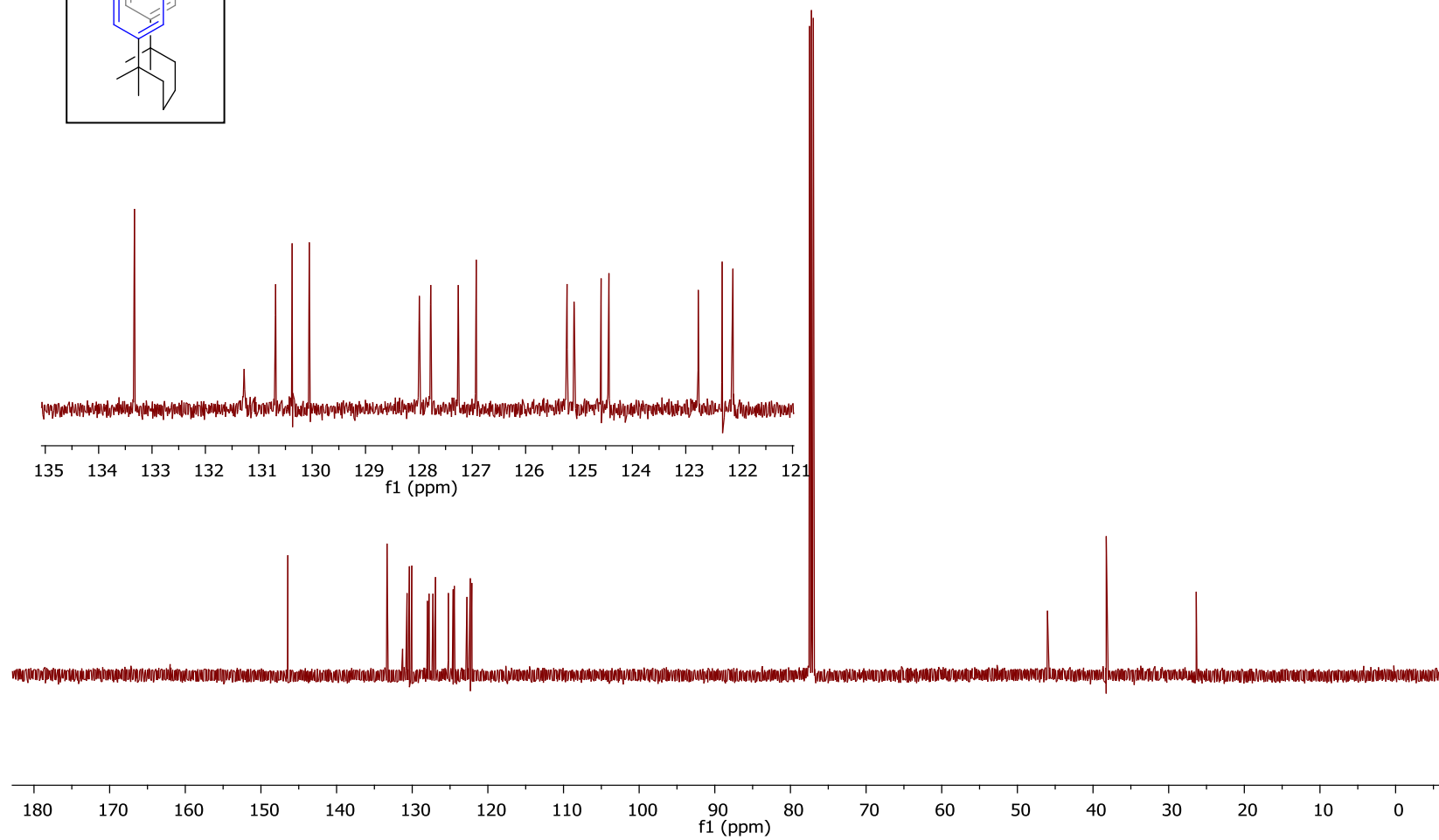
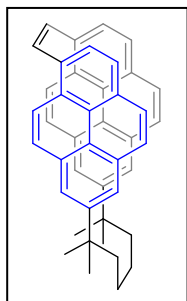


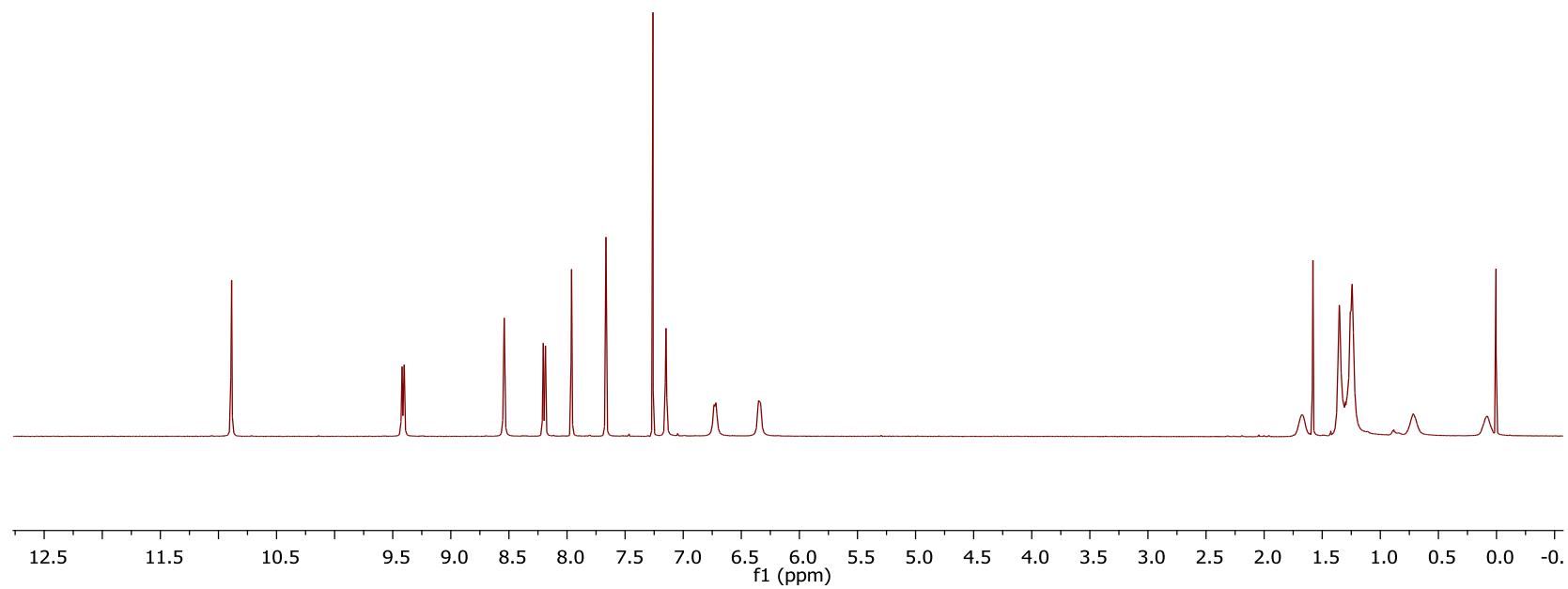
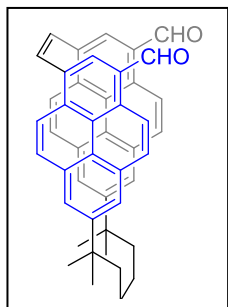




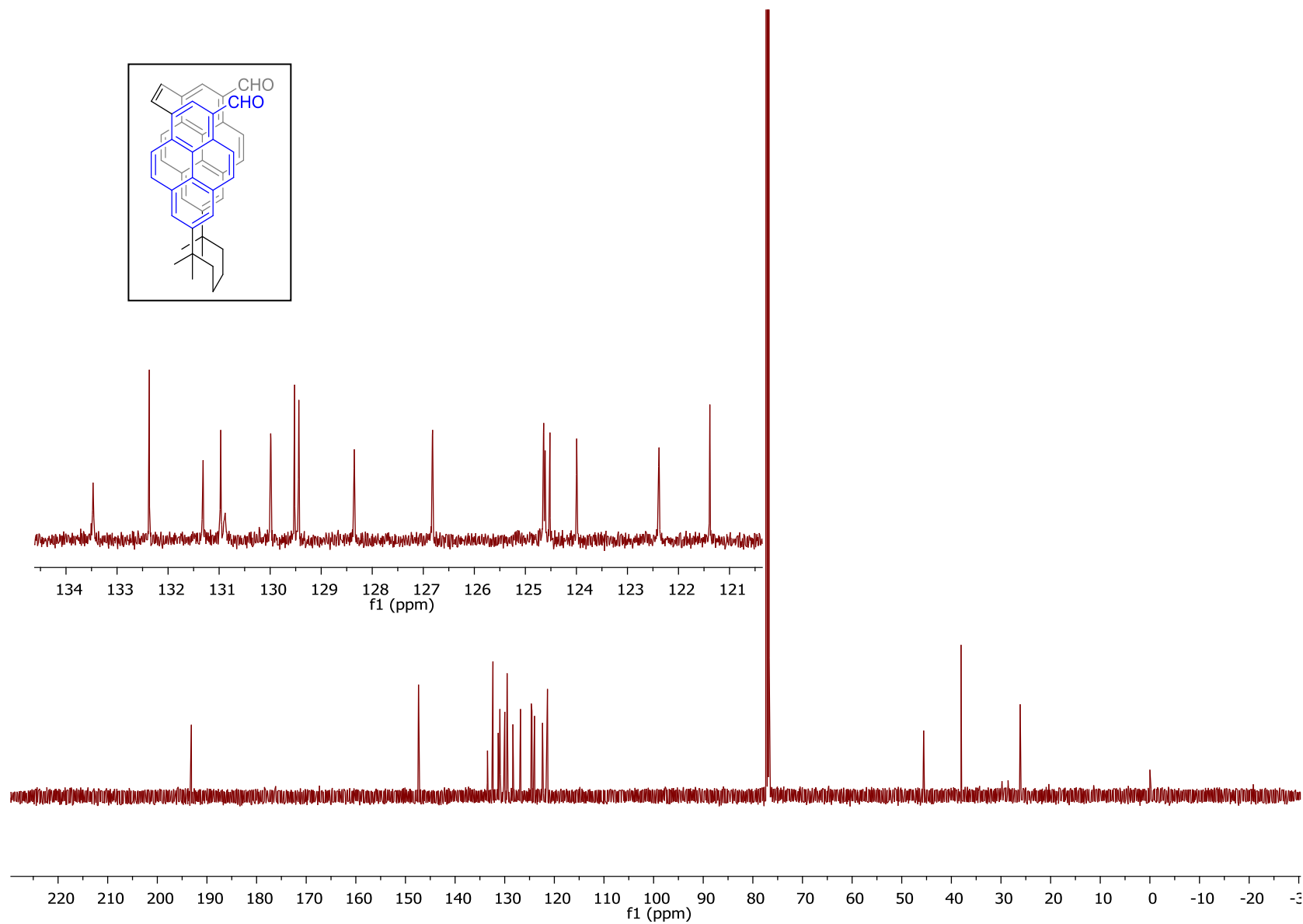
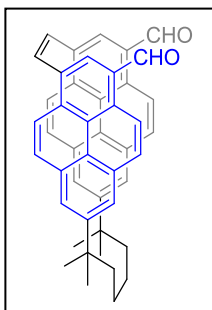










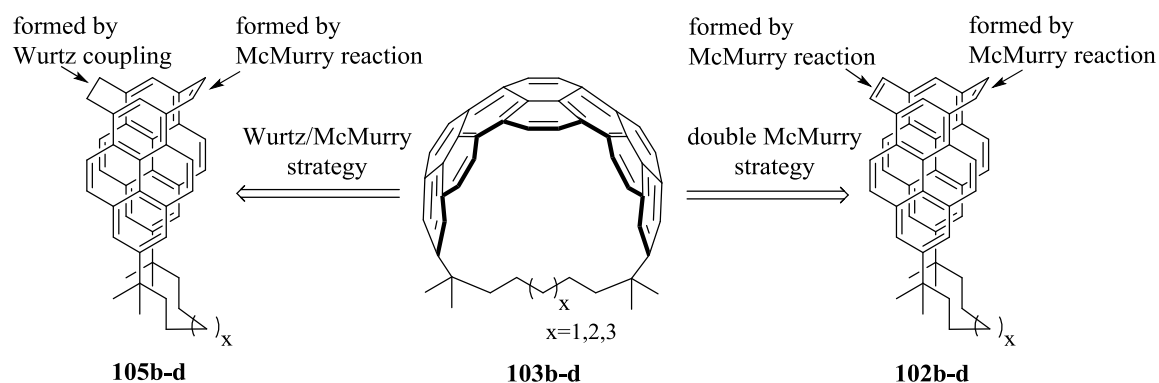


## Chapter 3: Synthesis of a Series of 1,1,*n,n*-Tetramethyl[*n*](2,11)teropyrenophanes

### Using a Wurtz / McMurry Strategy

#### 3.1 Introduction

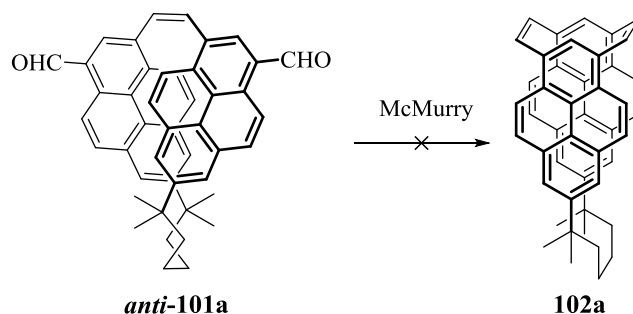
In order to learn how incremental changes in the degree of bend in the teropyrene system affects its physical and chemical properties, the synthesis of a series of [*n*](2,11)-teropyrenophanes was targeted. A previous graduate student (Brad Merner) in the Bodwell group developed a double-McMurry strategy for this purpose and successfully synthesized the first teropyrenophane, 1,1,8,8-tetramethyl[8](2,11)teropyrenophane (**103c**) (Scheme 3.01).<sup>1</sup> This approach turned out to be unsuitable for the synthesis of the next higher homologue **103d**, as only the *trans*-configured olefin was formed in the first bridge-forming reaction.<sup>2</sup> As described in Chapter 2, the synthesis of the next lower



**Scheme 3.01** Strategies for the synthesis of [*n*](2,11)teropyrenophanes.

homologue, **103b**, was achieved using the double-McMurry strategy, but work aimed at the synthesis of **103a** failed at the stage of the second McMurry reaction due (presumably) to the *anti*-conformation of dialdehyde **101a** (Scheme 3.02). Thus, the double-

McMurry strategy is limited to just teropyrenophanes **103b** and **103c**, which is too narrow a range of compounds to start making meaningful connections between changes in structure and changes in properties.



**Scheme 3.02** Failure of *anti-101a* to generate **101a** during a McMurry reaction.

To avoid the “upper limit” problem of the double bond geometry, the replacement of the first McMurry reaction with one that installs a C–C single bond instead of a C=C double bond was identified as a potential solution. Wurtz-type coupling, which has been used successfully in the synthesis of [2.2]metacyclophanes,<sup>3</sup> was therefore investigated as a means to construct the first two-carbon bridge (Scheme 3.01). An unchanged formylation / McMurry reaction sequence was envisaged to install the second two-atom (unsaturated) bridge. A major concern with the proposed modification of the synthetic strategy was whether or not the resulting cyclophanemonoenes **105b-d** would be suitable substrates for the key teropyrene-forming reaction. The presence of just one double bond in the [2.2]metacyclophane sub-unit is cause for optimism because there is still a 6 $\pi$ -electron system available for the occurrence of a valence isomerization reaction.<sup>4</sup> On the other hand, there does not appear to be any precedent for pyrene formation from a [2.2]metacyclophanemonoene. Pyrene formation from **105b-d** also requires more

extensive dehydrogenation than from the corresponding dienes **102b-d** (Chapter 2), but this was expected to be less of a challenge than the key C–C bond formation.

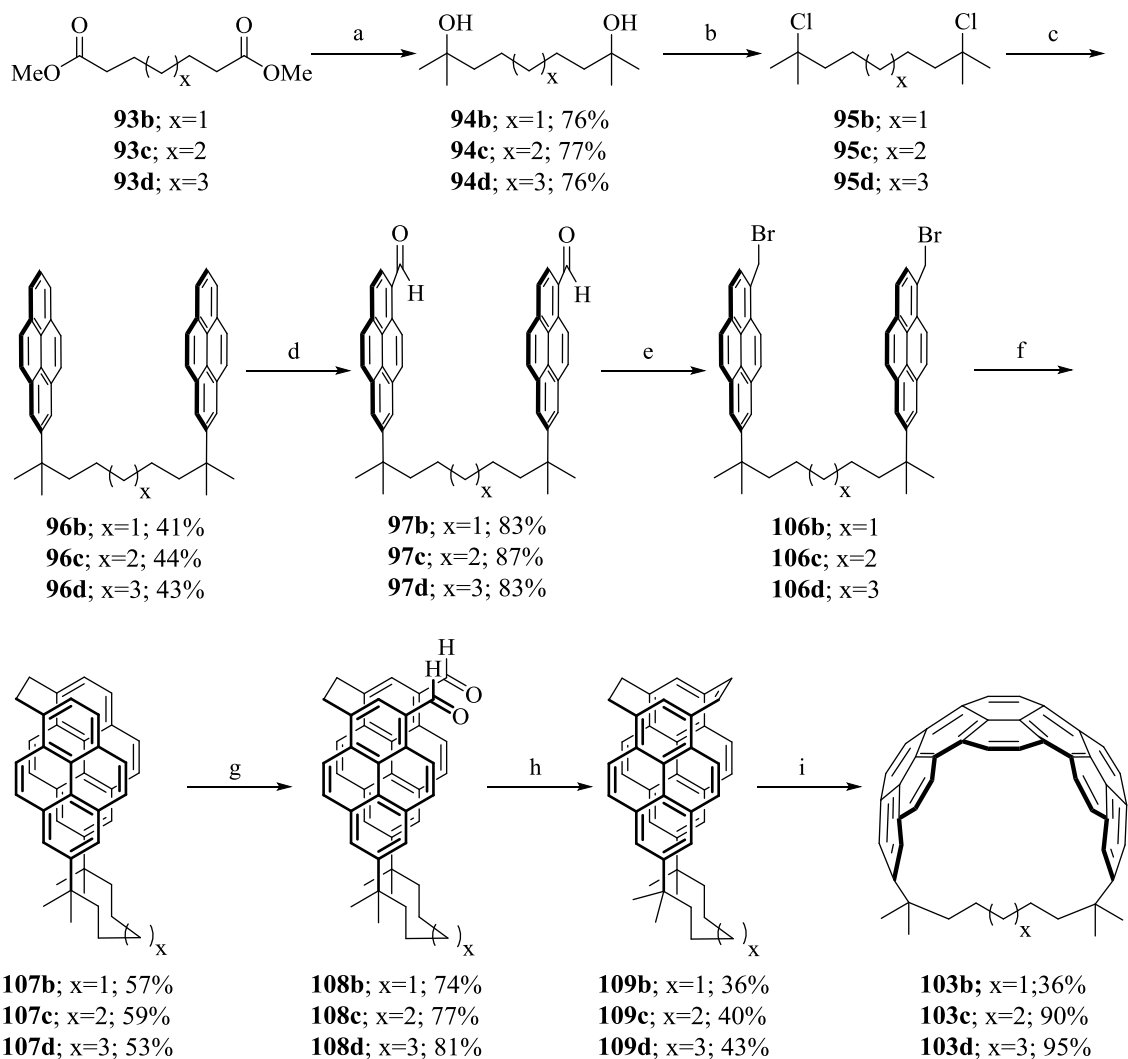
### 3.2 Synthesis of tetramethyl[*n*](2,11)teropyrenophanes **103b-d**

The synthesis of a homologous series of 1,1,*n,n*-tetramethyl[*n*](2,11)teropyrenophanes **103b-d** according to the modified strategy commenced as per the original double-McMurry strategy. Grignard reaction of three commercially available diesters, dimethyl pimelate (**93b**), dimethyl suberate (**93c**), and dimethyl azelate (**93d**) with methylmagnesium bromide produced tertiary diols **94b-d**, which were reacted in crude form with conc. HCl to afford dichlorides **95b-d** in nearly identical yields (76-77%) for the two-step sequence (Scheme 3.03). Two pyrene systems were tethered using Friedel-Crafts alkylation reactions of pyrene with **95b-d**, which gave dipyrenylalkanes **96b-d** (41-44%).

Regioselective formylation of **96b-d** afforded dialdehydes **97b-d** (83-87%). At this point, the synthetic pathway moved in a new direction. Reduction of the dialdehydes **97b-d** with sodium borohydride, followed by bromination of the resulting alcohols with phosphorous tribromide furnished dibromides **106b-d**, which were required for the planned Wurtz-type coupling reactions. Treatment of **106b-d** with *n*-butyllithium at –15 °C gratifyingly gave the desired [*n*.2](7,1)pyrenophanes **107b-d** (53-59%, over 3-steps). The yields are a little lower than those of the first McMurry reactions in the double-McMurry approach, but are perfectly acceptable nonetheless.

Rieche formylation of **107b-d** occurred with complete regioselectivity to afford

dialdehydes **108b-d** (74-81%), which were subjected to intramolecular McMurry reactions to afford the [n.2.2](7,1,3)pyrenophanes **109b-d** (36-43%). The yields of these McMurry reactions are very close to those of the second McMurry reactions in the



**Scheme 3.03** Synthesis of teropyrenophanes **103b-c** and attempted synthesis of **103b**; *Reaction conditions*: a) MeMgBr, THF, 0 °C to reflux, 17 h; b) 12 M HCl (aq), rt, 2 h; c) pyrene, AlCl<sub>3</sub>, CH<sub>2</sub>Cl<sub>2</sub>, 0 °C to rt, 1 h; d) Cl<sub>2</sub>CHOCH<sub>3</sub>, TiCl<sub>4</sub>, CH<sub>2</sub>Cl<sub>2</sub>, 0 °C to rt, 2 h; e) i. NaBH<sub>4</sub>, THF, rt, 12 h ii. PBr<sub>3</sub>, 0 °C, CH<sub>2</sub>Cl<sub>2</sub>, 1 h; f) *n*-BuLi, THF, -15 °C, 30 min; g) Cl<sub>2</sub>CHOCH<sub>3</sub>, TiCl<sub>4</sub>, CH<sub>2</sub>Cl<sub>2</sub>, 0 °C to rt, 2 h; h) TiCl<sub>4</sub>, Zn, pyridine, THF, 0 °C to reflux, 4 h; i) DDQ, *m*-xylene, 125–145 °C, 30–48 h.

double-McMurry strategy. The successful synthesis of **109d** is important because it demonstrates that the presence of a saturated 2-atom bridge can indeed provide entry to direct precursors to larger teropyrenophanes. It is also worth noting that the success of these McMurry reactions adds to the very small (but growing) set of examples of its use in generating a [2.2]metacyclophane system.<sup>3a,5</sup>

Any concerns regarding the performance of the VID reaction<sup>6</sup> on a cyclophane-monoene system were quickly extinguished upon treatment of **109b-d** with DDQ in *m*-xylene, which brought about the formation of the (2,11)teropyrenophane targets **103b-d**. The only products isolated from the VID reactions of **109b-d** were the desired teropyrenophanes. No intermediate tetrahydro- or dihydroteropyrenophanes were observed (tlc, LCMS, <sup>1</sup>H NMR analysis), which confirmed that the more extensive dehydrogenation involved in these reactions was not an issue. Whereas the conversions of **109c** to **103c** and **109d** to **103d** were high-yielding, the reaction of **109b** to give the most strained homologue **103b** (36%, 50% borsm) was considerably more sluggish and required a larger excess of DDQ (20 equiv. instead of 4 equiv.). Full consumption of **109b** could not be accomplished, but this was not problematic due to the pronounced difference in *R<sub>f</sub>* values between **109b** (0.60, 10% ethyl acetate / hexanes) and **103b** (0.27, 10% ethyl acetate / hexanes) on silica gel. Remarkably, the *R<sub>f</sub>* values of the two compounds were virtually identical using several other solvent systems, *e.g.* 15% CH<sub>2</sub>Cl<sub>2</sub> / hexanes (**109b**: 0.18; **103**: 0.17).

### 3.2.1 Crystal structure of compound **103d**

Crystals suitable for X-ray crystallographic analysis of **103d** were grown from ethanol. The determination of the crystal structure of **103d**<sup>†</sup> (Figure 3.01) completed the set of crystal structures for **103b-d**, the crystal structure of **103c** having been reported previously,<sup>1</sup> and that of **103b** having been presented in Chapter 2. Calculated structures (B3YLP/cc-pVTZ) for all three teropyrenophanes were also obtained<sup>§</sup> and were found to be in very good agreement with the experimental structures.

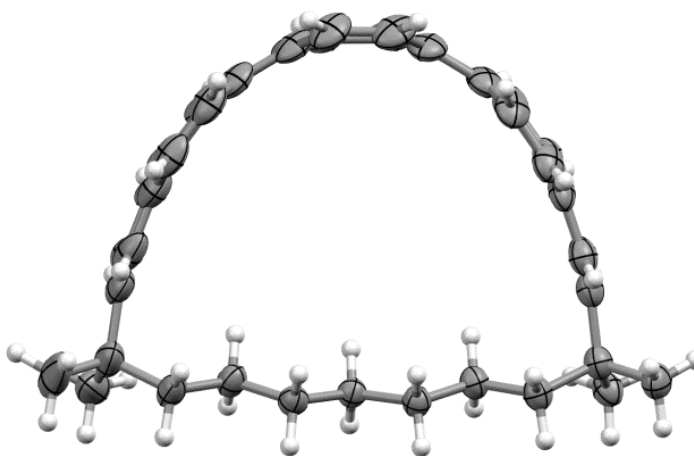


**Figure 3.01** X-ray crystal structure of **103d**, 50% probability displacement ellipsoids.

Unlike **103b** and **103c**, teropyrenophane **103d** does not exhibit any interesting packing features, such as close C–H $\cdots\pi$  contacts,  $\pi$ – $\pi$  contacts or channels (Figure 3.02).

Three pyrene subunits can be identified on the teropyrene systems of **103b**, **103c**

<sup>†</sup> Data collection and solution of the crystal structure were performed by Dr. Louise Dawe, Memorial University. Current affiliation: Wilfrid Laurier University.

<sup>§</sup> Calculations were performed by Dr. Christopher Rowley, Memorial University of Newfoundland.

and **103d**, one at each end of the teropyrene system (flanking pyrene subunits) and one in the middle (central pyrene subunit) (Figure 3.03). The degree of bend in each of them

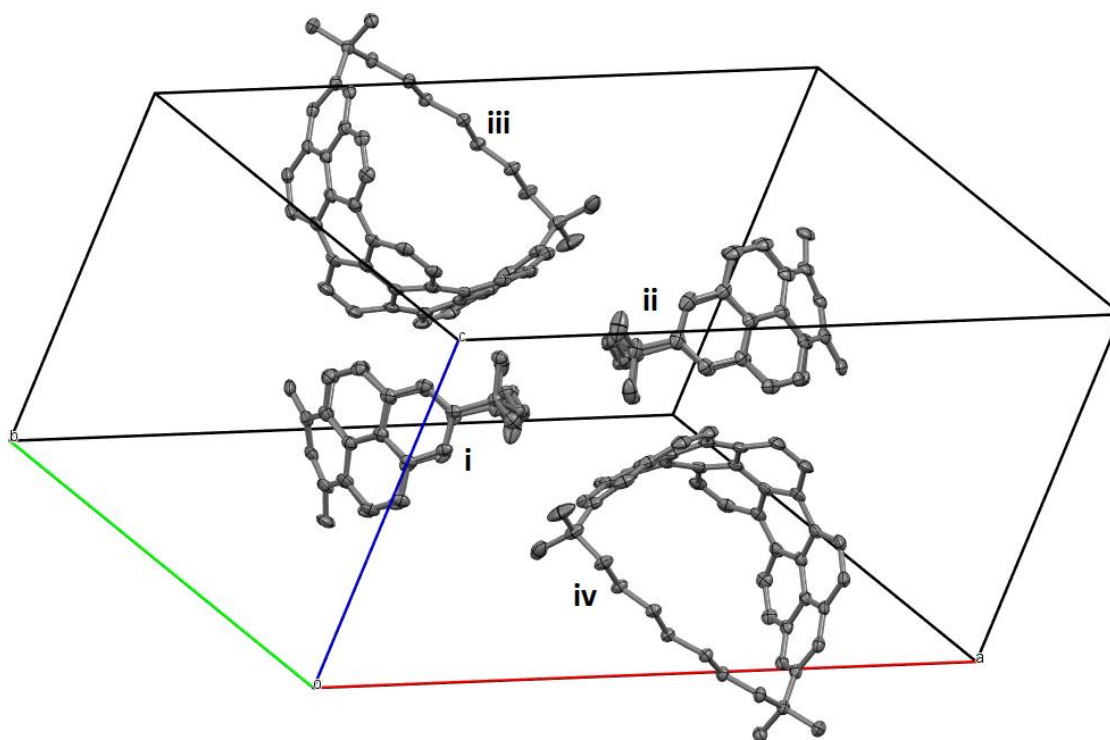


**Figure 3.02** Partial packing diagram with 30% probability ellipsoids. H-atoms and lattice solvent molecules omitted for clarity. Molecules pack with inversion related, pairwise, facing alkyl chains. Mean plane separation for C40-C46 and C40<sup>i</sup>-C46<sup>i</sup> is 4.024(3) Å off-set by 0.405(10) Å. i =  $\frac{1}{2}-x, 1-y, z-1/2$ ; ii =  $\frac{1}{2}+x, y, 3/2-z$ ; iii =  $\frac{1}{2}-x, \frac{1}{2}+y, z$ ; iv =  $\frac{1}{2}+x, \frac{1}{2}-y, 1-z$ .

can be quantified using the bend angle  $\theta$ ,<sup>7</sup> which has been used previously for numerous pyrenophanes. In the case of all three teropyrenophanes (**103b-d**), the bend angle for the central pyrene subunit ( $\theta_2$ ), is considerably larger than those of the two flanking pyrene subunits ( $\theta_1$  and  $\theta_3$ ). The greater bend of the central pyrene system means that the teropyrene systems have semi-elliptical profiles rather than semicircular. The B3YLP/cc-



pVTZ calculated values for  $\theta_1$  and  $\theta_3$  are all greater than the measured ones, while the calculated values for  $\theta_2$  are all smaller than the measured ones. It is interesting to note that the agreement between calculated and experimental values becomes better as the teropyrenophane becomes smaller.

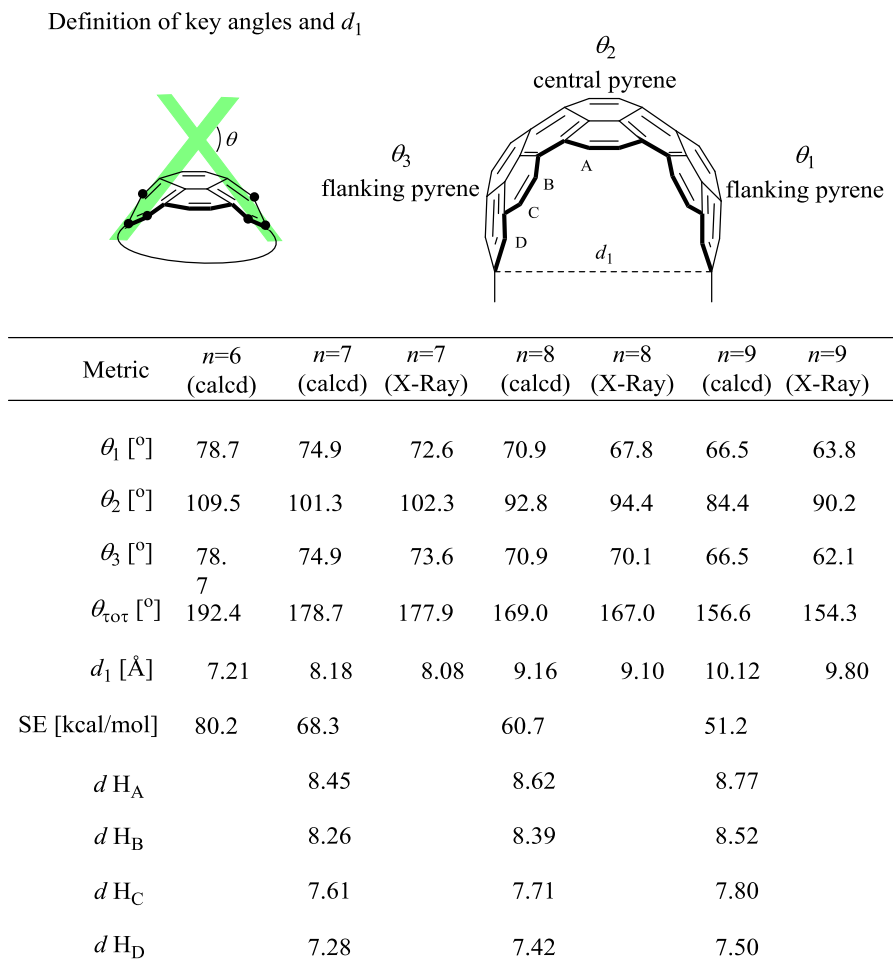


**Figure 3.03** Bend angles, strain energies ( $SE$ ), and aromatic proton resonances for **103b** ( $n=7$ ), **103c** ( $n=8$ ) and **103d** ( $n=9$ ).

Overall, the calculated end-to-end bend ( $\theta_{\text{tot}}$ ) in the teropyrene systems (**103b**: 178.7°, **103c**: 169.0°, **103d**: 156.6°) is very close to the experimental values (**103b**:

177.8°, **103c**: 167.0°, **103d**: 154.3°) and the agreement between the calculated and experimental values again becomes closer as the cyclophane becomes smaller. Shortening the bridge by another carbon atom (to  $n=6$ ) is predicted to bring the bend in the teropyrene system well past 180° ( $\theta_{\text{tot}} = 192.4^\circ$ ). Whether or not the VID methodology is powerful enough to deliver this considerably more strained system (SE = 80.2 kcal/mol for **103a**, SE = 68.3 kcal/mol for **103b**) using either the double-McMurry strategy (Chapter 2) or the Wurtz/McMurry strategy (see above) has yet to be investigated. A different approach to a teropyrene with a bend of  $>180^\circ$  would be the replacement of one of the carbon atoms in the bridge of **103b** with an oxygen atom. This tactic has been demonstrated to increase the  $\theta$  value of  $[n](2,7)$ pyrenophanes by *ca.* 4° per replacement.<sup>8</sup>

As the bridge of the teropyrenophanes becomes shorter, so does the distance between the bridgehead carbon atoms ( $d_1$ , Figure 3.03). Interestingly, the experimental value of  $d_1$  for **103b** (8.08 Å) is same as the reported distance across [6]CPP (8.08 Å).<sup>9</sup>

### 3.2.2 NMR spectra of teropyrenophanes 103b-d

As observed in the  $[n](2,7)$ pyrenophanes,<sup>8,10</sup> the chemical shifts of the aryl protons of **103b-d** all move to higher field with increasing distortion of the aromatic system from planarity. In going from **103d** to **103b**, a shift ( $\Delta\delta$ ) of  $-0.32$  to  $-0.19$  ppm is observed. The largest shift is seen for H<sub>A</sub>, which is located where the greatest deviation from planarity occurs (Figure 3.04). Various factors might contribute to the observed

upfield shifts, including diminished aromaticity and/or ring current,<sup>11</sup> and changes in the hybridization of the skeletal carbon atoms.<sup>10</sup>

In the aliphatic region, all of the bridge protons are observed at higher field than the methylene protons of hexanes ( $\delta$  1.26), as would be expected for protons that lie

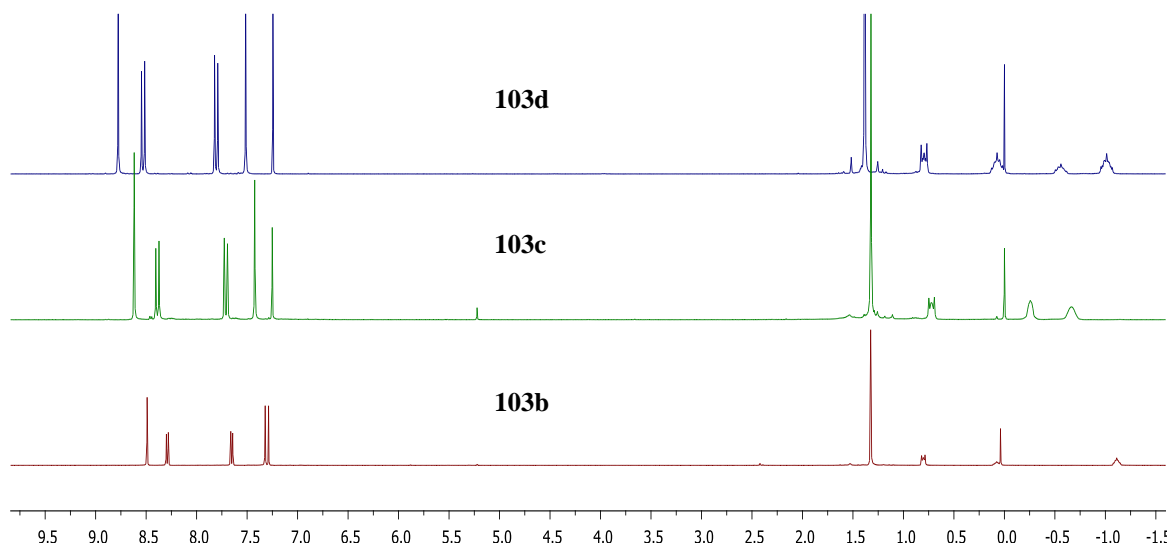


**Figure 3.04**  $^1\text{H}$  NMR spectra of  $[n](2,11)$ teropyrenophanes **103b**, **103c** and **103d**.

underneath an aromatic system, *i.e.* within its shielding zone. The homobenzylic protons ( $\text{H}_a$ ) of **103b-d** appear at slightly higher field than the methylene protons of hexane ( $\delta$  1.26) and at roughly the same chemical shift ( $\delta$  0.73 to 0.81) (Figure 3.05). The remaining bridge protons ( $\text{H}_b$ ,  $\text{H}_c$  and  $\text{H}_d$ ) are scattered at substantially higher field ( $\delta$  0.09 to  $-1.14$ ). The highest field signal is due to  $\text{H}_c$  of **103b** ( $\delta -1.14$ ). Unlike the aromatic protons, no clear trends are apparent, which is not surprising because the bridge protons of one compound lie under a differently shaped teropyrene system and in

different regions of their shielding zone than those of another. Nevertheless, the beginnings of an odd/even trend are suggested by the similarity of the chemical shifts for **103b** and **103d**:  $\delta(\text{H}_b) = -1.14$  and  $-1.12$ , respectively;  $\delta(\text{H}_c) = 0.04$  and  $0.09$ , respectively. Of course, more data (more teropyrenophanes) would be needed to validate the existence of such a trend.

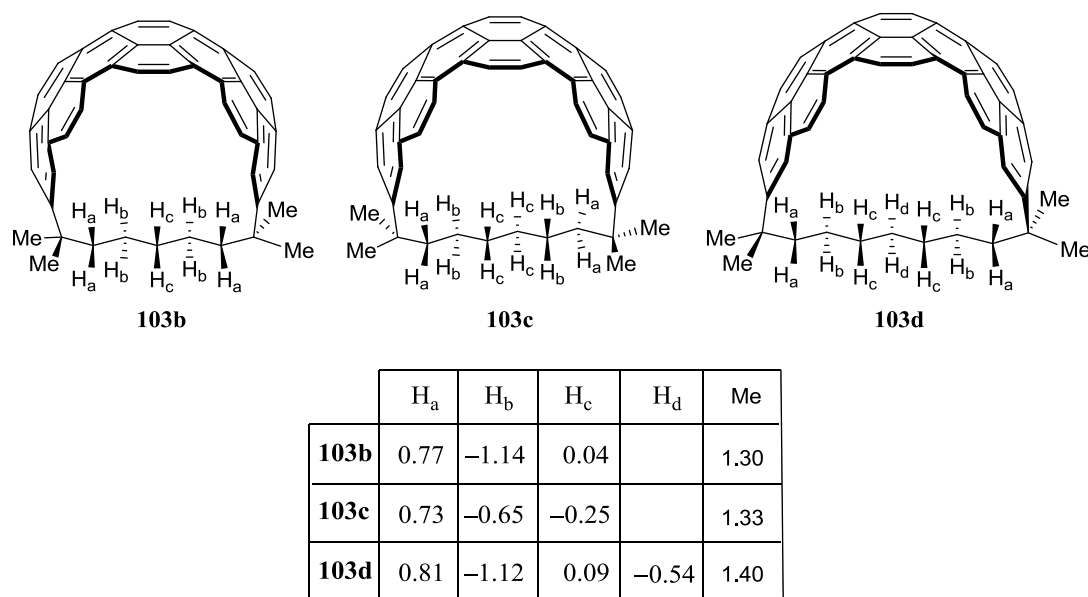
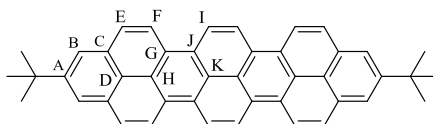


**Figure 3.05** Aliphatic proton resonances for **103b**, **103c** and **103d**.

The  $^{13}\text{C}$  NMR data of **103b-d** are very similar to one another (Table 3.01). For the aromatic carbon atoms, the chemical shifts of aromatic protons do not show any major changes as the teropyrene system becomes more distorted. The largest change in going from **103d** to **103b** is the chemical shift of  $\text{C}_F$ , which moves from  $\delta$  123.15 to 123.90 ( $\Delta\delta = 0.75$  ppm). In the aliphatic region, there are also no clear trends. The signals for the

benzylic carbon atoms ( $\delta$  47.33-47.46), C<sub>Quat</sub> ( $\delta$  38.10-37.95) and C<sub>Me</sub> (28.14-27.20) are shown little variation.

**Table 3.01**  $^{13}\text{C}$  NMR resonances for compounds **103b**, **103c** and **103d**.



C <sub>x</sub>	C <sub>7</sub>	C <sub>8</sub>	C <sub>9</sub>
C <sub>A</sub>	144.22	144.92	144.93
C <sub>B</sub>	122.90	123.26	123.27
C <sub>C</sub>	128.13/127.61/124.61	128.14/127.03/124.14	128.71/126.72/123.93
C <sub>D</sub>	128.47/125.75/125.16	127.33/125.50/124.73	126.52/125.24/124.49
C <sub>E</sub>	126.69	126.95	127.20
C <sub>F</sub>	123.90	123.26	123.15
C <sub>G</sub>	128.13/127.61/124.61	128.14/127.03/124.14	128.71/126.72/123.93
C <sub>H</sub>	128.47/125.75/125.16	127.33/125.50/124.73	126.52/125.24/124.49
C <sub>I</sub>	123.26	122.89	122.78
C <sub>J</sub>	128.13/127.61/124.61	128.14/127.03/124.14	128.71/126.72/123.93
C <sub>K</sub>	128.47/125.75/125.16	127.33/125.50/124.73	126.52/125.24/124.49
C <sub>Me</sub>	28.14	27.20	27.49
C <sub>Quat</sub>	37.95	38.10	38.09
C <sub>a</sub>	47.46	47.34	47.33
C <sub>b</sub>	23.99	23.53	24.67
C <sub>c</sub>	30.90	29.35	30.23
C <sub>d</sub>	–	–	30.67

### 3.2.3 Absorbtion and emission spectroscopy of teropyrenophanes 103b-d

The absorption spectra of **103b-d** each consist of three sets of bands, in the ranges of 220-280 nm, 280-380 nm and 380-520 nm. The longest wavelength absorption

maxima are observed at 484, 489, and 494 nm for **103b**, **103c** and **103d** respectively (Figure 3-06). The emission spectra for all three teropyrenophanes show two closely overlapping fluorescence bands:  $\lambda_{\text{max}}$  (**103b**) = 503 and 516 nm,  $\lambda_{\text{max}}$  (**103c**) = 505 and 526 nm and

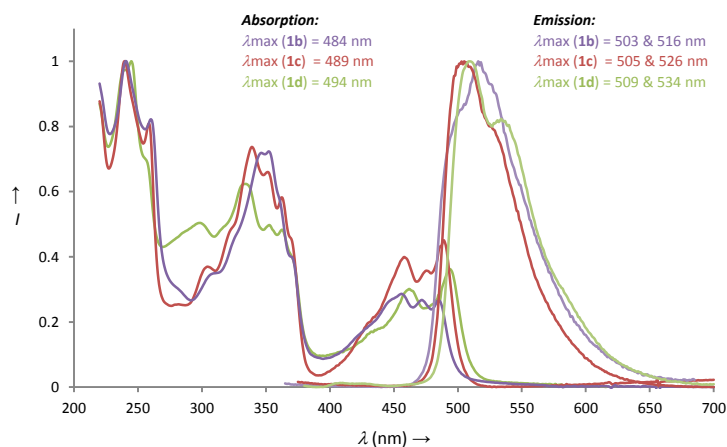


**Figure 3.06** Normalized absorption and emission spectra for teropyrenophanes **103b** ( $2.34 \times 10^{-8}$  M in MeCN), **103c** ( $1.99 \times 10^{-8}$  M in MeCN), and **103d** ( $1.90 \times 10^{-8}$  M in MeCN).  $\lambda_{\text{exc}}$  = 350 nm, 360 nm and 365 nm respectively.

526 nm,  $\lambda_{\text{max}}$  (**103d**) = 509 and 534 nm (Figure 3.06). The longest wavelength absorption ( $\lambda_{\text{max}}$ ) for the parent (planar) teropyrene in 1,2,4-trichlorobenzene has been reported to be 537 nm,<sup>12</sup> which is consistent with the observed trend in **103b-d**. Time-dependent DFT calculations<sup>¶</sup> (B3YLP/cc-pVDZ) of the electronic absorption spectrum of teropyrene ( $\lambda_{\text{max}}$  = 534 nm) and teropyrenophanes **103b**, **103c** and **103d** ( $\lambda_{\text{max}}$  = 500, 507, and 513 nm, respectively) are in good agreement with the experimentally determined values, and also support a blue shift with increasing bend in the teropyrene system. The blue shift with increasing bend in the  $\pi$ -system is consistent with what is observed for the 1,*n*-

<sup>¶</sup> Calculations were performed by Dr. Christopher Rowley, Memorial University of Newfoundland.

dioxa[*n*](2,7)pyrenophanes,<sup>8</sup> but opposite to what is observed for the [*n*]cycloparaphenylenes.<sup>13</sup> It would thus appear that the  $\pi$ -system needs to be wrapped around on itself before the relationship between  $\lambda_{\text{max}}$  and bend reverses.

### 3.3 Violation of Kasha's rule

A remarkable observation was made when the teropyrenophanes **103b-d** were irradiated at 260 nm. Two additional bands were observed (Table 3.02). As such these compounds violate Kasha's rule, which state that "*when light is shined on a molecule, the molecule will only emit light (fluorescence or phosphorescence) from its lowest energy excited state*".<sup>14</sup> The violation of Kasha's rule is rare.<sup>15</sup> To confirm that the violation of Kasha's rule is genuine, the purity of the samples was shown to be >99.9% by HPLC and the emission spectra of the direct precursors to **103b-d** were measured (and found to be inconsistent with the observed emissions). The most convincing evidence was provided by recording excitation spectra, whereby the detector is fixed on the S<sub>1</sub> emission and the excitation wavelength is scanned from 260 nm up to  $\lambda_{\text{max}}$  of the S<sub>1</sub> emission. A system that obeys Kasha's rule will have an excitation spectrum that overlays the absorption spectrum whereas, a system that violates Kasha's rule will have an excitation spectrum that is below the absorbance spectrum (Figure 3.07). This indicates that energy is leaving the system by an avenue other than S<sub>1</sub>. In the case of **103b-d**, the excitation spectra are well below the absorption spectra until the long wavelength absorption wavelength band is reached, at which point only excitation to S<sub>1</sub> is occurring. This surprising result is being investigated in detail in collaboration with the Thompson group at Memorial

university of Newfoundland. The working hypothesis for the violation of Kasha's rule is that the rigidity of the  $\pi$ -system inhibits vibronic coupling between the excited states, which slow the rate of internal conversion (relaxation of all the excited states to  $S_1$ ) and thus makes fluorescence a competitive process.

**Table 3.02**  $\lambda_{\text{max}}$  of the two additional emission bands.

sample		103b	103c	103d
$\lambda_{\text{em}}$	$S_3 \longrightarrow S_0$	315	315	314
	$S_2 \longrightarrow S_0$	445	425 450	405 425

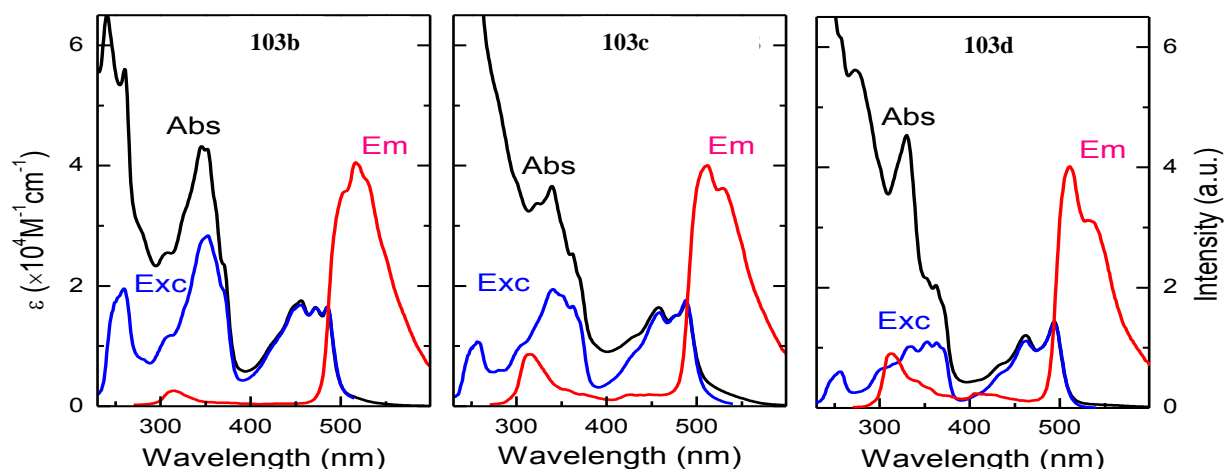


**Figure 3.07** Absorption, emission and excitation spectra of **103b-d**. Absorption, emission with  $\lambda_{\text{exc}}$  at 270 nm and emission excitation scan with  $\lambda_{\text{mon}}$  at 550 nm of **103b**, **103c** and **103d** in acetonitrile at room temperature. The excitation spectra were normalized to the same intensity at low energy side as the absorption spectra. The normalized emission spectra were scaled by a factor of 3 to reveal the  $S_2$  and  $S_3$  emitting states.



### 3.4 Conclusions

The synthesis of a homologous series of 1,1,*n,n*-tetramethyl[*n*](2,11)teropyrenophanes has been achieved using a new iterative bridge formation sequence that directly assembles the ethano (Wurtz-type coupling) and ethylene (McMurry reaction) bridging units in the teropyrenophane precursors **109b-d**. This modified strategy has enabled the synthesis of one new teropyrenophane (**103d**), which was inaccessible using the original double-McMurry strategy. It was also demonstrated that cyclophanemonoenes are viable substrates for the key teropyrene-forming (VID) reaction.

### 3.5 Experimental section

The experimental procedures and characterization data for all of the compounds described in this Chapter appear in the experimental section of Chapter 4 (Multi gram scale synthesis of [*n*](2,11)teropyrenophanes).

### 3.6 References

1. B. L. Merner, L. N. Dawe and G. J. Bodwell, *Angew. Chem. Int. Ed.* 2009, **48**, 5487–5491.
2. B. L. Merner and G. J. Bodwell, unpublished results.
3. a) T. Yamato, S. Miyamoto, T. Saisyo, T. Manabe and K. Okuyama, *J. Chem. Res. (S)*, 2003, 63–65; b) A. Tsuge, H. Nago, S. Mataka and M. Tashiro *J. Chem.*

- Soc Perkin Trans. I*, 1992, 1179–1185; c) R. Paioni and W. Jenny, *Helv. Chim. Acta*, 1969, **52**, 2041–2054.
4. a) D. R. Arnold, V. Y. Abraitys, D. McLeod Jr., *Can. J. Chem.* 1971, **49**, 923–935; b) T. H. Koch and D. A. Brown, *J. Org. Chem.*, 1971, **36**, 1934–1937; c) N. C. Baird, A. M. Draper and P. D. Mayo, *Can. J. Chem.* 1988, **66**, 1579–1588.
  5. For a review on olefin-forming reactions in the synthesis of cyclophanes, see: G. J. Bodwell and P. R. Nandaluru, *Isr. J. Chem.*, 2012, **52**, 105–138.
  6. a) R. H. Mitchell, V. Boekelheide, *J. Am. Chem. Soc.*, 1970, **92**, 3510–3512; b) M. A. Petrukhina, L. T. Scott, *Fragments of Fullerenes and Carbon Nanotubes*, Wiley: New Jersey, 2011.
  7. G. J. Bodwell, J. J. Fleming and D. O. Miller, *Tetrahedron*, 2001, **57**, 3577–3585.
  8. G. J. Bodwell, J. N. Bridson, M. K. Cyrański, J. W. J. Kennedy, T. M. Krygowski, M. R. Mannion and D. O. Miller, *J. Org. Chem.*, 2003, **68**, 2089–2098.
  9. J. Xia and R. Jasti, *Angew. Chem. Int. Ed.* 2012, **51**, 2474–2476.
  10. G. J. Bodwell, J. J. Fleming, M. R. Mannion and D. O. Miller, *J. Org. Chem.*, 2000, **65**, 5360–5370.
  11. M. R. Mannion and G. J. Bodwell, unpublished results.
  12. T. Umemoto, T. Kawashima, Y. Sakata and S. Misumi, *Tetrahedron Lett.*, 1975, **16**, 1005–1006.

13. a) R. Jasti, J. Bhattacharjee, J. B. Neaton and C. R. Bertozzi, *J. Am. Chem. Soc.*, 2008, **130**, 17646–17647; b) C. Camacho, T. A. Niehaus, K. Itami and S. Irle, *Chem. Sci.*, 2013, **4**, 187–195; c) T. Nishihara, Y. Segawa, K. Itami and Y. Kanemitsu, *J. Phys. Chem. Lett.*, 2012, **3**, 3125–3128; d) Y. Segawa, A. Fukazawa, S. Matsuura, H. Omachi, S. Yamaguchi, S. Irle and K. Itami, *Org. Biomol. Chem.*, 2012, **10**, 5979–5984.
14. a) M. Kasha, *Discuss. Faraday Soc.*, 1950, **9**, 14–19; b) H. Ghosh, *Chem. Phys. Lett.*, 2006, **426**, 431–435.
15. a) P. Klán and J. Wirz, *Photochemistry of Organic Compounds*, Wiley, 2009, Ch. 2, 40–41; b) M. A. Loi, J. Gao, F. Cordella, P. Blondeau, E. Menna, B. Bártová, C. Hébert, S. Lazar, G. A. Botton, M. Milko and C. A-. Draxl, *Adv. Mater.*, 2010, **22**, 1635–1639; c) K. Yanagi and H. Kataura, *Nat. Photonics*, 2010, **4**, 200–201.

## Chapter 4: Synthesis of 1,1,*n,n*-Tetramethyl[*n*](2,11)teropyrenophanes on the Multigram Scale

### 4.1 Introduction

The design and efficient synthesis of  $\pi$ -electronic systems has grown remarkably in recent years because of the very broad range of conceivable structures and intriguing properties that may lead to applications in the field of materials science.<sup>1</sup> The first synthesis of a new designed  $\pi$ -system can be very challenging, triumphantly delivering only a few milligrams of the target compound. In some cases, e.g. superphane (**110**) (Figure 4.01),<sup>2</sup> the original synthesis (syntheses) ends up never being repeated/improved, but lives on as a classic piece of synthetic work in textbooks.<sup>3</sup> The lack of material limits the extent to which the molecule can be studied, let alone be used as a starting material for more elaborate systems or to be incorporated into other interesting systems. In other cases, further generations of synthetic routes are developed and a molecule moves from being novel to being an abundant building block, e.g. buckminsterfullerene (C<sub>60</sub>) (**111**), corannulene (**112**) and the cycloparaphenylenes (CPP) (**113**) (Figure 4.01). The original report of C<sub>60</sub> (**111**) by Kroto, Smalley and Curl<sup>4</sup> produced only minute quantities of the new carbon allotrope. Currently, C<sub>60</sub> is being produced commercially on a metric ton scale.<sup>5</sup> The first report of corannulene by Barth and Lawton<sup>6</sup> claimed a 0.4% overall yield from a 17-step synthesis. Later, more efficient syntheses were developed (9-12 steps), which improved the overall yield to up to 85%.<sup>7</sup> Much more recently, a kilogram-scale synthesis of corannulene (**112**) was disclosed.<sup>8</sup> In the same vein, Bertozzi *et al.*<sup>9</sup> reported the first synthesis of CPPs ([9]- (**113b**, x=4), [12]- (**113d**, x=7) and [18]CPP

(**113e**,  $x=13$ ) with just a few milligrams of each compound. A few years later, Jasti *et al.*<sup>10</sup> came up with a gram-scale synthesis of [8]- (**113a**,  $x=3$ ) and [10]CPP (**113c**,  $x=5$ ). The ability to produce tons, kilograms and grams, respectively, of these fascinating molecules has enabled the investigation of their physical and chemical properties as well as their use for further elaboration in ways that reflect the scale of their availability.

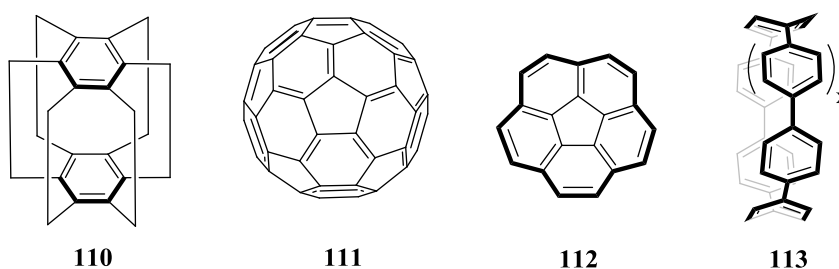


**Figure 4.01** Structures of superphane (**110**), buckminsterfullerene (C<sub>60</sub>) (**111**), corannulene (**112**) and the [n]cycloparaphenylenes (CPP) (**113**).

The Bodwell group recently reported two synthetic approaches to a small series of 1,1,*n,n*-tetramethyl[*n*](2,11)teropyrenophanes, **103b-d**.<sup>11</sup> The two routes are similar, as they differ only in the method used for the installation of the first two-carbon bridge in triply bridged pyrenophanes **102** and **109**, which serve as direct synthetic precursors to the teropyrenophanes (Figure 4.02). These cyclophanes feature a very bent 36-carbon polycyclic aromatic system (teropyrene), a cavity and good solubility in common organic solvents (unlike the parent teropyrene,<sup>12</sup> which has extremely low solubility). The original synthetic routes delivered 5-20 mg of the teropyrenophanes, which allowed for the determination of their crystal structures and the measurement of various physical and spectroscopic properties. However, very little material was available to investigate their chemical behaviour. As with C<sub>60</sub>, corannulene and the CPPs, the exploration of the

covalent and supramolecular chemistry of the teropyrenophanes and their use as starting points for the synthesis of larger (even much larger) and freely soluble non-planar graphene segments would require access to multigram quantities of the teropyrenophanes. Therefore, this Chapter deals with a modified synthetic approach of **103b-d** on the multi-gram scale. The synthesis of the larger teropyrenophane **103e** ( $x=4$ ) is also described.

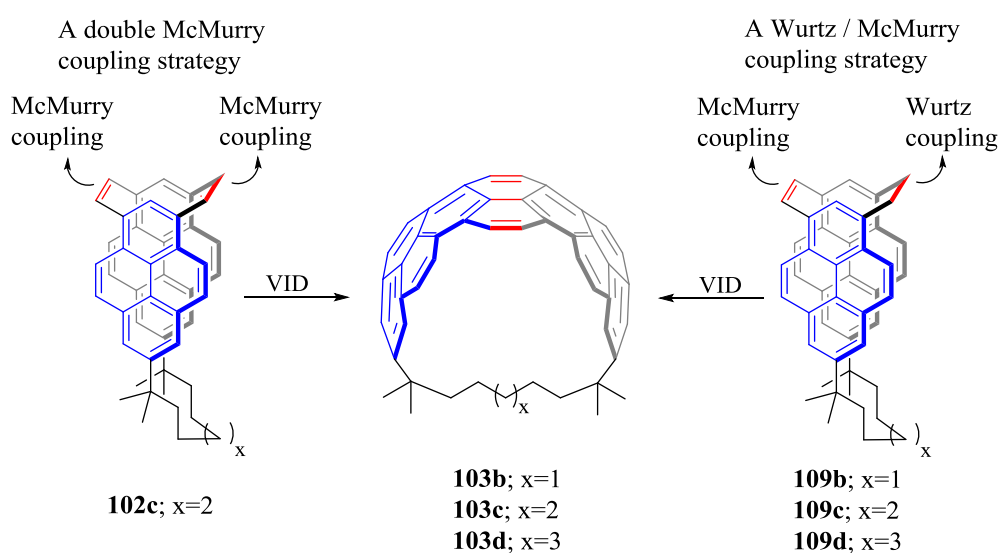


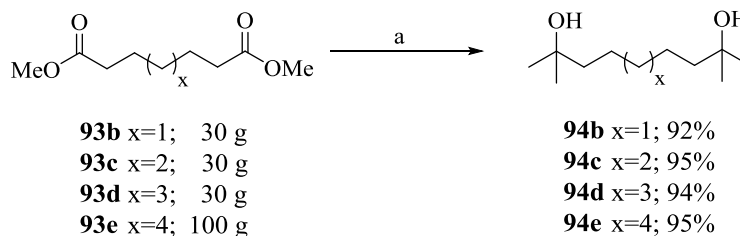
**Figure 4.02** Reported strategies for synthesizing teropyrenophanes **103b-d**.

## 4.2 Results and Discussion

Initial work aimed at the synthesis of synthetically useful amounts of the teropyrenophanes simply involved attempted scale-up of the existing Wurtz / McMurry route. Unfortunately, this proved to be problematic from the very start. Therefore, careful attention had to be paid to each reaction step (for at least one member of the homologous series leading to **103b-e**).

### 4.2.1 Grignard reaction

The first step of the existing routes, Grignard reactions between diesters **93b-e** and methylmagnesium bromide, had always been restricted to a 10 g scale. The reason for this was the large exotherm during the addition of diesters **93b-e** to the solution of the Grignard reagent. To circumvent this problem and allow for larger scale reactions, the commercially available solution of the Grignard reagent (3.0 M in hexanes) was diluted (*ca.* 1:1) with THF. For the addition, very vigorous magnetic stirring was used and the reaction vessel was cooled on a *ca.*  $-15^{\circ}\text{C}$  salt/ice bath. During the initial stages of the addition, the rate of addition was kept very slow (1 drop per second) and once the reaction mixture became turbid, the rate of addition could be increased to (5 drops per second). *It is extremely important that the initial rate of reaction be kept very slow to avoid a violent exotherm.* When roughly 75% of the addition was complete, the reaction mixture became too thick to stir and it remained this way until the addition was complete. At this point, the reaction mixture was heated at reflux for 17-24 h and a solid white cake formed.



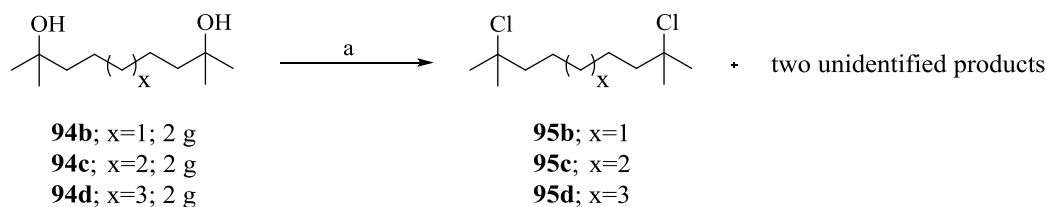
**Scheme 4.01** Synthesis of diols **94b-e**; *Reagents and conditions*: a) (i) MeMgBr (3.0 M in Et<sub>2</sub>O), THF,  $-15^{\circ}\text{C}$ –reflux, 17-24 h; (ii) saturated aqueous NH<sub>4</sub>Cl.

Using this procedure, the Grignard reactions could be conveniently performed on

as much as a 100 g scale of the diester (Scheme 4.01). Diols **94b-e** were obtained in 90-95% yield, which is slightly better than the previously reported method. It was also found that replacing the expensive dry THF with drum THF did not affect the yields of the products, but slightly more Grignard reagent (5.0–5.5 equiv. vs. 4.5 equiv.) was required to obtain equivalent yields.

#### 4.2.2 Chlorination

The second step in the synthesis was the conversion of diols **94b-e** into the corresponding dichlorides **95b-e**. This proved to be even more challenging to scale up than the Grignard reactions, starting with the discovery that the reaction was not as clean as it had originally thought to be. Using the original conditions for the chlorination of **94b-d** (conc. HCl, 2 g scale), the reactions proceeded as previously described and the  $^1\text{H}$  and  $^{13}\text{C}$  NMR spectra of the products (appendix 4.6) were consistent with dichlorides **95b-d** (Scheme 4.02). However, careful examination of the tlc plates indicated that two minor products were present in addition to the major product. For example, chlorination of **94d** gave a product that showed spots with  $R_f$  values (hexanes) of 0.24 (major), 0.28 and 0.32. No separation could be achieved using column chromatography. The spot with the  $R_f$  value of 0.24 was subsequently shown to be dichloride **95d** (*vide infra*).



**Scheme 4.02** Previous synthesis of **95b-d**; *Reagents and conditions*: a) conc. HCl, rt, 3 h.



#### 4.2.2.1 GCMS analysis of crude dichloride

GCMS (EI(+)) analysis of the product obtained from the chlorination of **94d** provided useful information about the identity of the other two products. Three major sets of peaks were present, every individual peak of which showed  $m/z = 180$  (Figure 4.03). The first set contained three peaks (retention time = 6.20, 6.26, 6.31 min), which were assigned as a mixture of three isomeric dienes **115d** ( $[M]^+ = 180$ ) (Figure 4.04). The second set consisted of two peaks (retention time = 7.20, 7.24 min) and were assigned as a mixture of two isomeric chloroalkenes **114d** ( $[M-HCl]^+ = 180$ ). Finally, the single peak with a retention time of 8.15 min was attributed to the required dichloride **95d** ( $[M-2HCl]^+ = 180$ ). The loss of HCl from **115d** and **114d** during MS analysis (EI(+)) is not surprising considering that the chlorides are tertiary. It is reasonable to assume that similar product mixtures were obtained from the chlorination of the other diols, **94b** and **94c**.

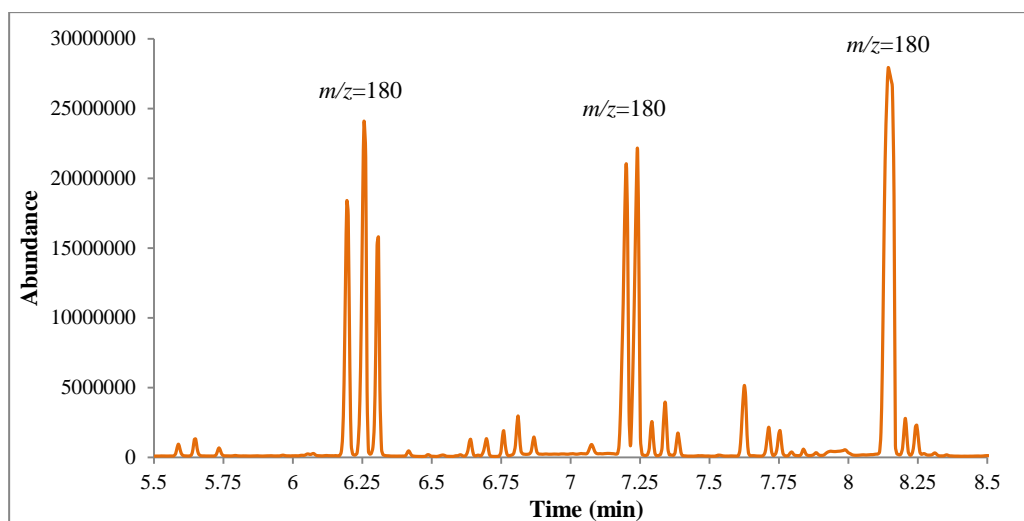


**Figure 4.03** GCMS trace of the product obtained from the chlorination of **94b** under the originally reported conditions.

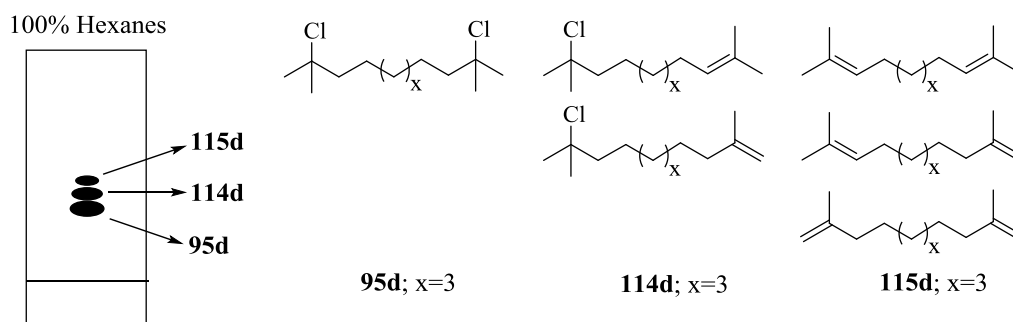
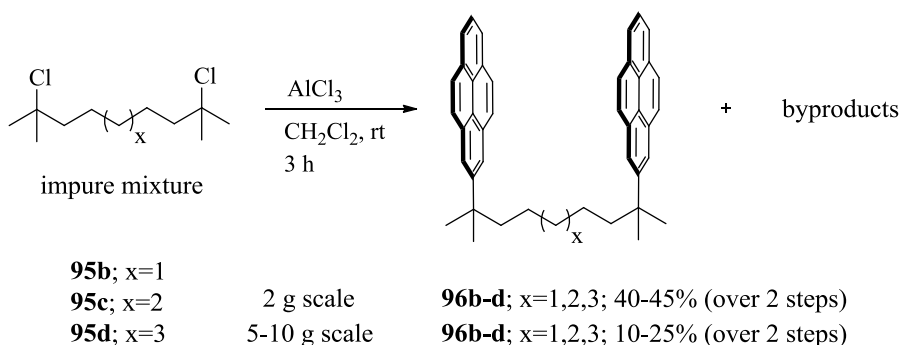


**Figure 4.04** Products of the chlorination reaction evidenced by GCMS.

#### 4.2.3 Issues/concerns with Friedel-Crafts alkylation

In the original synthetic pathway, the (impure) dichlorides obtained from column chromatography were used directly in the subsequent Friedel-Crafts alkylation reactions of pyrene to afford di(2-pyrenyl)alkanes **96b-d** (Scheme 4.03). Practically, these reactions were limited to a *ca.* 2 g scale for two reasons.



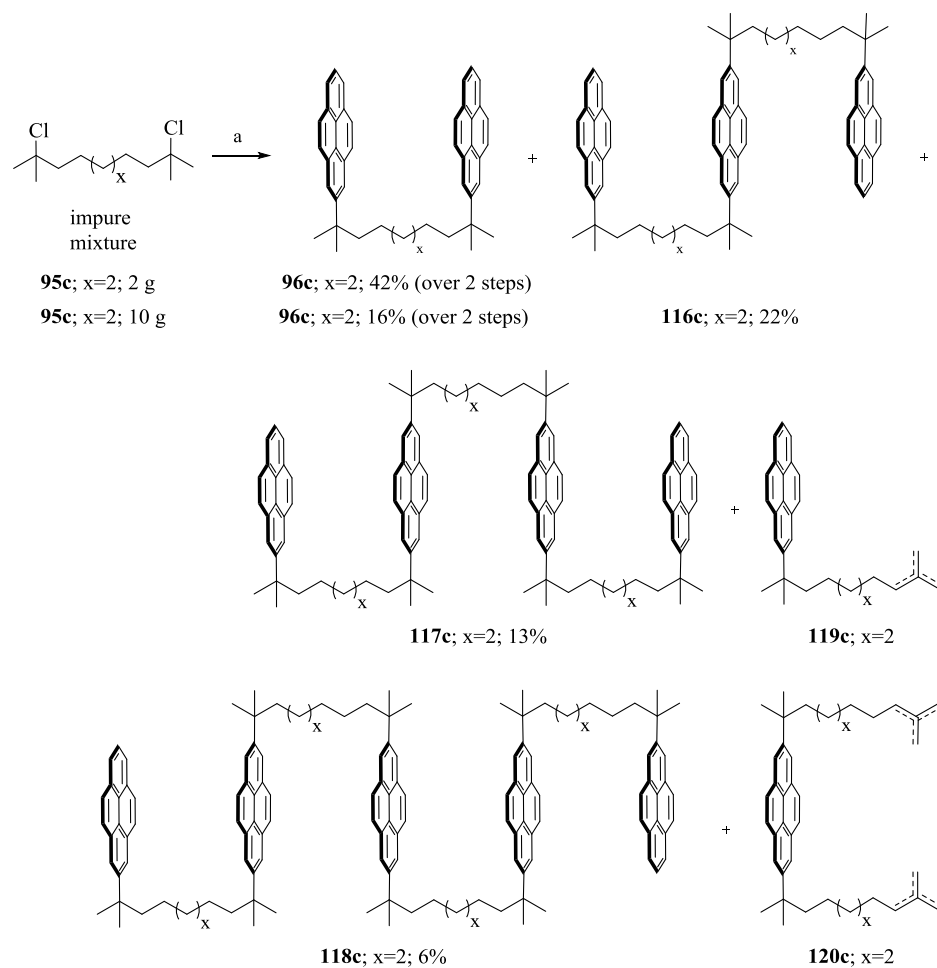
**Scheme 4.03** Friedel-Crafts alkylation of **95b-d**.

First, the largest column available for column chromatography (during the initial stages of this work) needed to be filled to capacity to fully separate the excess of pyrene (*ca.* 7 g) from the various reaction products, which have similar  $R_f$  values. The excess of

pyrene (5.0 equiv. are used in the reactions) is necessary to minimize the participation of the desired products **96b-d** in subsequent Friedel-Crafts alkylation reactions. This problem was ultimately solved by having larger columns constructed in house. Unfortunately, a second problem arose when the scale of the Friedel-Crafts alkylation reactions was increased to 5 or 10 g, *i.e.* the yields of **96b-d** dropped significantly from the 40-45% levels that were obtained previously on a 2 g scale<sup>11a</sup> to just 10-25% (Scheme 4.03).

In all of the Friedel-Crafts alkylations using dichlorides **95b-d**, tlc analysis (15% dichloromethane / hexanes) was essentially the same: numerous compounds with  $R_f$  values ranging from 0.05 to 0.53 were present. Pyrene was among the fastest moving compounds ( $R_f = 0.50$ ) and the desired bis(2-pyrenyl)alkanes **96b-d** were in the middle of the pack ( $R_f \approx 0.22$ ). The Friedel-Crafts alkylation of pyrene with (impure) dichloride **95c** was selected for the identification of as many byproducts as possible. Repeated column chromatography of the product mixture resulted in the isolation of three of the slower-eluting byproducts in pure form along with the intended product **96c** (Scheme 4.04).

The close similarity of the  $^1\text{H}$  NMR and  $^{13}\text{C}$  NMR spectra of these compounds was used to assign the structures of these compounds as the linear oligomers **116c** ( $R_f = 0.15$ ), **117c** ( $R_f = 0.10$ ) and **118c** ( $R_f = 0.05$ ). A key feature of the  $^{13}\text{C}$  NMR spectra was the signals near  $\delta$  147, which correspond to the quaternary pyrene carbon atoms to which the alkyl chains are attached (Figure 4.05).



**Scheme 4.04** Reagents and conditions: a) pyrene (5.0 equiv.), AlCl<sub>3</sub>, CH<sub>2</sub>Cl<sub>2</sub>, rt, 4 h.

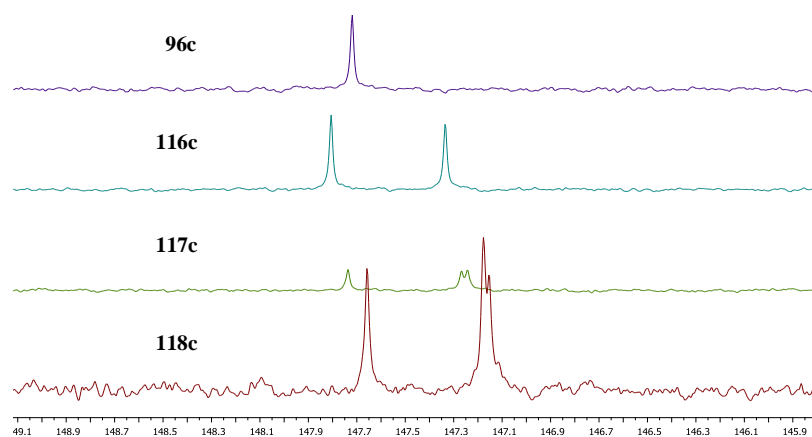


**Figure 4.05** Stacked <sup>13</sup>C NMR spectra showing the quaternary pyrenyl carbon signals.

For **96c**, there is only one such carbon atom ( $\delta$  147.72), whereas there are two for **116c** ( $\delta$  147.81, 147.33) and three for **117c** ( $\delta$  147.74, 147.28, 147.24). Only three of the four expected signals for **118c** were observed ( $\delta$  147.66, 147.18, 147.15), but the signal at  $\delta$  147.18 has the appearance of two overlapping signals (Figure 4.05). The consistent appearance of new signals at the higher end of the range (*ca.*  $\delta$  147.2) suggests that the lowest field signal for **116c**, **117c** and **118c** is attributable to the terminal pyrene systems (blue dots in Figure 4.06).

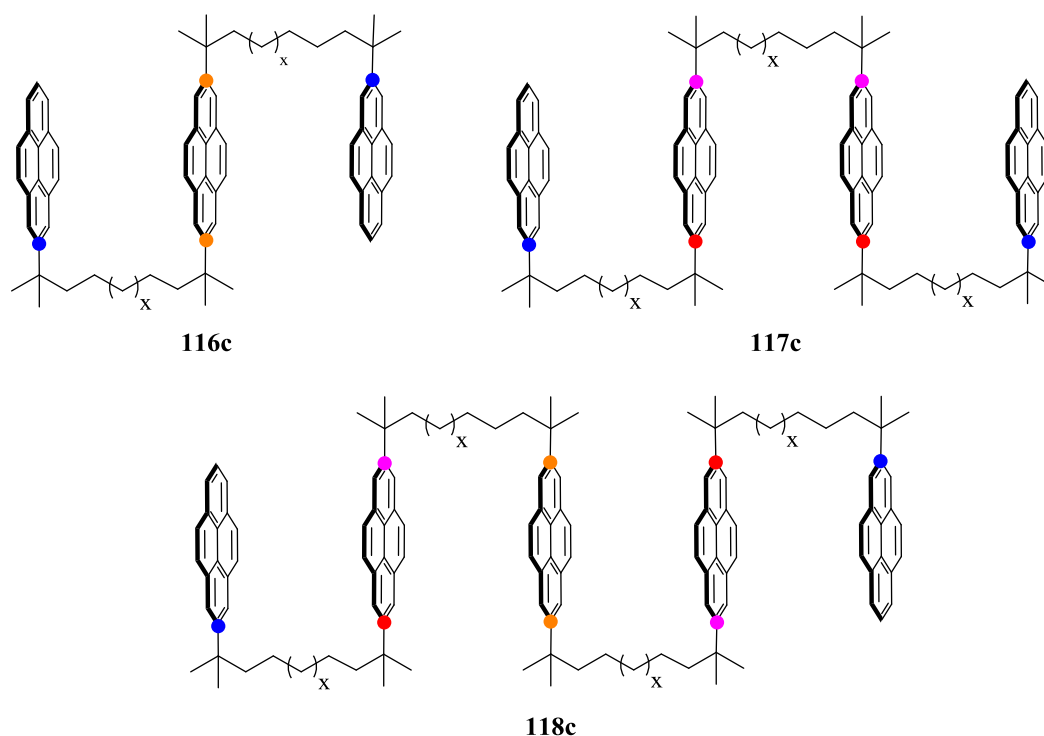


**Figure 4.06** Different types of low-field quaternary carbon atoms in byproducts **116c**, **117c** and **118c**.

LC-MS (APCI(+)) analysis of compound **96c** showed a molecular ion ( $[M+1]^+$   $m/z = 571$ ) and an intense fragment signal ( $m/z = 369$ ), which corresponds to the loss of

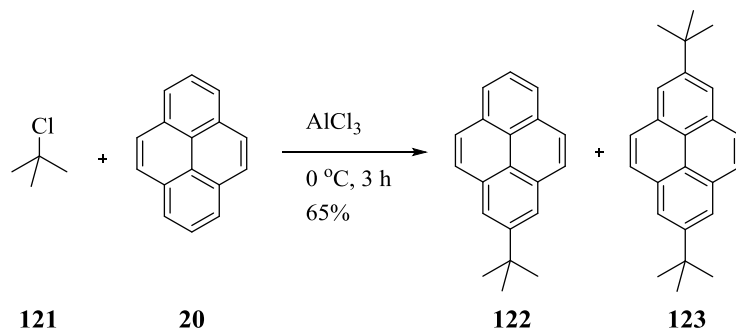
pyrene. The next higher oligomer **116c** showed a molecular ion ( $[M+1]^+$   $m/z = 939$ ) and two major fragment peaks ( $m/z = 737$  and  $369$ ), which correspond to the loss of pyrene and the loss of **96c**, respectively. A small peak corresponding to the molecular ion of **96c** was also observed, which corresponds to the loss of pyrene and an alkyl chain from **116c**. The higher oligomers **117c** and **118c** showed very weak molecular ions, along with peaks corresponding to the losses of various numbers of pyrene units (202 mass units) and alkyl chains (166 mass units), especially  $m/z = 939$ ,  $737$ ,  $571$  and  $369$ ).

A mixture of two faster-eluting byproducts was also isolated, neither of which could be obtained in pure form after multiple attempts to separate them. LC-MS (APCI(+)) analysis suggested these products could be **119c** ( $m/z = 369$ ) and **120c** ( $m/z = 535$ ), which would arise from Friedel-Crafts alkylation of pyrene with one and two equiv. of chloroalkene mixture **114c**, respectively. Since it appears as though **114c** is capable of alkylating pyrene, it is a little surprising that no products arising from the alkylation of **96c**, **116c**, **117c** or **118c** with **114c** were isolated. It may simply be that such products were formed, but could not be isolated.

#### 4.2.3.1 Attempts to improve the Friedel-Craft's alkylation reaction

The major problems with the large-scale Friedel-Crafts alkylations were 1) the overalkylation and 2) the quality of the dichlorides **95b-d**. With regard to the former issue, it is well-documented in the literature that the Friedel-Crafts alkylations tend to bring about poly-alkylation and can be very difficult to restrict to monoalkylation.<sup>13</sup> A case in point is the *t*-butylation of pyrene.<sup>14</sup> Di-*t*-butylation is easily accomplished, but

mono-*t*-butylation requires laborious separation of pyrene, 2-*t*-butylpyrene (**122**) and 2,7-di-*t*-butylpyrene (**123**) (Scheme 4.05).



**Scheme 4.05** *t*-Butylation of pyrene (**20**).

#### 4.2.3.1.1 Attempted alkylation using Lewis acids

It has been reported that pyrene can be monoalkylated exclusively using  $\text{AlBr}_3$ ,<sup>15</sup> but there does not appear to be any report of this work having been successfully repeated. Nevertheless, it was decided to investigate the effect of the Lewis acid on the outcome of the Friedel-Crafts alkylation involving **95d**. Initially, the strong Lewis acid  $\text{AlCl}_3$  was replaced with a series of milder Lewis acids:  $\text{FeCl}_3$ ,  $\text{InCl}_3$ ,  $\text{WCl}_4$ ,  $\text{CeCl}_3$  and  $\text{BF}_3 \cdot \text{OEt}_2$ . Only in case of  $\text{FeCl}_3$  was there any indication of the formation of a small amount of **96d** (tlc analysis) after 12 h at room temperature. The same results were obtained when the reactions were performed at 80 °C for 1 h under microwave irradiation.

#### 4.2.3.1.2 Attempted alkylation using Brønsted acids

It is well-documented that *t*-butylation reactions can be carried out using tertiary alcohols.<sup>16</sup> Harvey *et al.*<sup>17</sup> investigated *t*-butylation of pyrene using TFA as a Brønsted

acid under reflux conditions which produced only 2,7-di-*t*-butylpyrene (**123**) (8.6% yield) as the only product. Therefore, the reaction of pyrene with diol **94d** in the presence of various Brønsted acids was investigated. Only trace amounts of **96d** were observed (tlc analysis) when the reactions were conducted at 100 °C for 1 h under microwave irradiation using either 60% H<sub>2</sub>SO<sub>4</sub>, HBF<sub>4</sub>–diethylether complex (50-55 wt%) or TFA as the solvent. No reaction was observed when H<sub>3</sub>PO<sub>4</sub>, TFA/H<sub>2</sub>SO<sub>4</sub> (1:1) were used as solvents under the same conditions. When pyrene was added at room temperature to a mixture of conc. H<sub>2</sub>SO<sub>4</sub> and **94d** in dichloromethane, the reaction mixture instantaneously became deep purple, but no product formation was observed (tlc analysis). The colour may simply be due to protonated pyrene.<sup>18</sup> Encouragingly, 99% TfOH in CH<sub>2</sub>Cl<sub>2</sub> produced the desired product at room temperature in 30% yield on a 20 mg scale of **94d**, but the yield dropped to 10% when the reaction scale was increased to 500 mg. Finally, the use of AlCl<sub>3</sub> led to the formation of only trace amounts of **96d** (tlc analysis).

#### 4.2.3.1.3 Attempts to alkylate 1- and 2-substituted pyrenes

Having had no success in finding a better Lewis or Brønsted acid to solve the dialkylation problem, an alternative strategy was investigated. This involved the introduction of a substituent at one end of the pyrene system followed by selective alkylation at the other end. Two approaches are conceivable under this scenario. First, introduction of a removable substituent (protecting group) at the 2 position of pyrene would completely rule out dialkylation (Figure 4.07a), but this would require the selective monofunctionalization of pyrene. The protection group would also need to withstand the



strongly Lewis acidic conditions of the Friedel-Crafts alkylation. Woolsey *et al.*<sup>19</sup> reported the completely selective introduction of a trimethylsilyl group at C2 by the

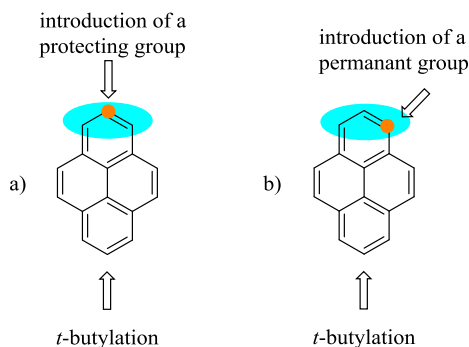
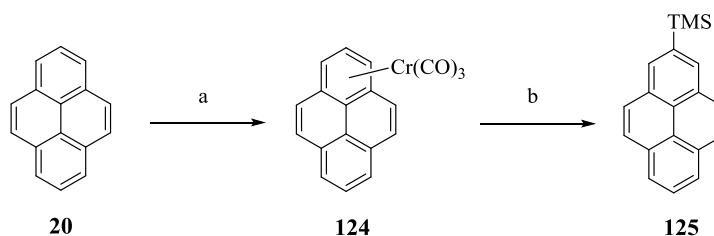


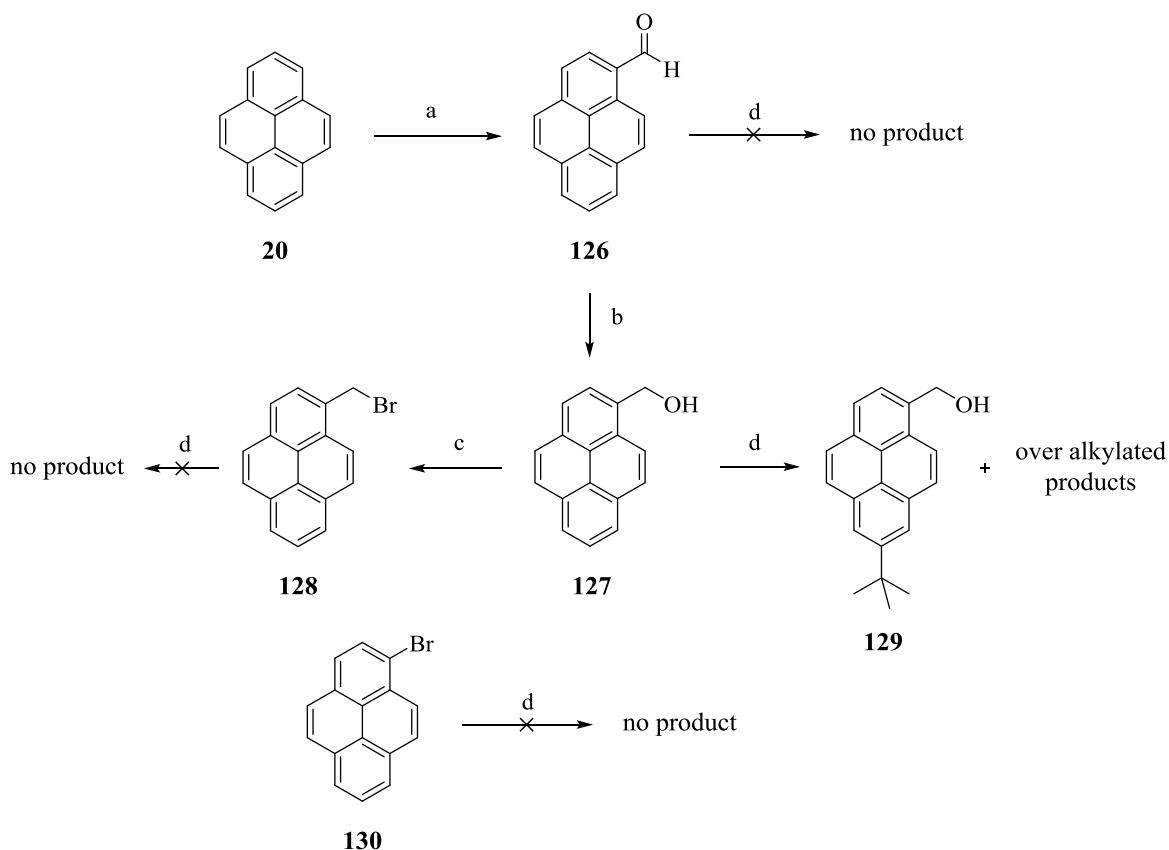
**Figure 4.07** a) Introduction of a temporary group at the 2 position of pyrene b) introduction of a permanent group at the 1 position of pyrene.

deprotonation of (pyrene)tricarbonylCr(0) **124** using LiTMP in the presence of TMSCl (Scheme 4.06). However, this chemistry was not pursued because it was conducted in a glove box on a 1.2 g scale and did not appear to be amenable to large-scale work (on both practical and economical grounds). A cursory attempt to lithiate uncomplexed pyrene was made (*t*-BuLi at  $-78\text{ }^{\circ}\text{C}$  followed by the addition of TMSCl), but this unsurprisingly resulted in the formation of a complex mixture of products (tlc analysis).



**Scheme 4.06** Attempted lithiation of pyrene (**20**); *Reagents and conditions*: a)  $(\text{NH}_3)_3\text{Cr}(\text{CO})_3$ ,  $\text{BF}_3 \cdot \text{OEt}_2$ ,  $\text{Et}_2\text{O}$ ,  $0\text{ }^{\circ}\text{C}$ –rt, 4 days, 58%; b) (i) LiTMP, TMSCl, THF,  $-78\text{ }^{\circ}\text{C}$ , 1 h; (ii) 0.2 N “Ce(IV) solution”, 98%.

The second approach involved the introduction of a permanent substituent at the 1 position of pyrene, *i.e.* one that can be used for subsequent bridge formation (Figure 4.07b). While the 2 position is still available for Friedel-Crafts alkylation, the presence of a substituent at the 1 position should provide enough steric bulk to disfavour it. Various substituents can be introduced at the 1 position of pyrene using electrophilic aromatic substitution and through further synthetic manipulation, so this approach was investigated further. 1-Formylpyrene **126** (obtained in 88% yield from the Rieche formylation of pyrene (**20**)) was reacted with *t*-butyl chloride in the presence of AlCl<sub>3</sub>, but no product



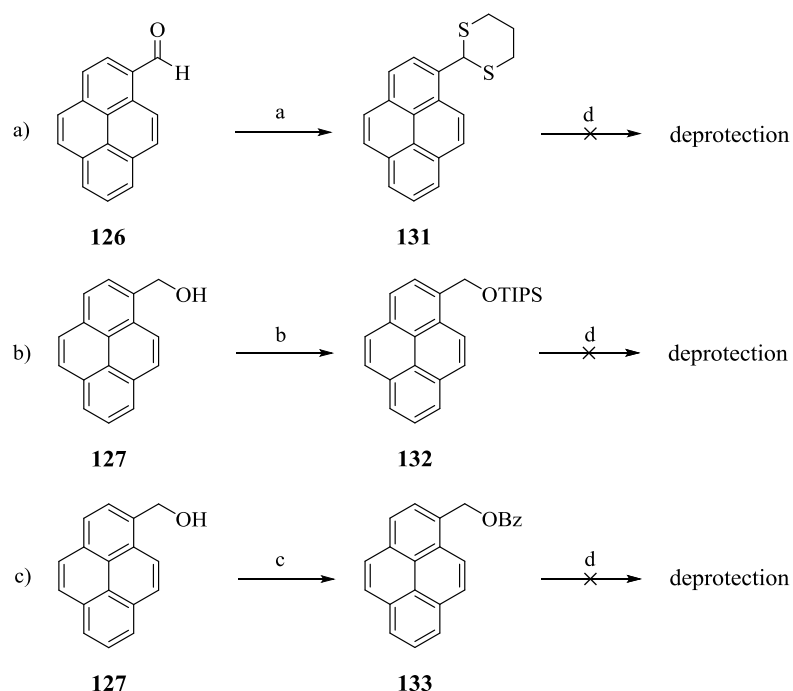
**Scheme 4.07** Attempted alkylation of substituted pyrenes; *Reagents and conditions*: a) Cl<sub>2</sub>CHOCH<sub>3</sub>, TiCl<sub>4</sub>, CH<sub>2</sub>Cl<sub>2</sub>, rt, 30 min, 88%; b) NaBH<sub>4</sub>, THF, rt, 2 h, 95%; c) PBr<sub>3</sub>, CH<sub>2</sub>Cl<sub>2</sub>, rt, 1 h, 90%; d) *t*-BuCl, AlCl<sub>3</sub>, CH<sub>2</sub>Cl<sub>2</sub>, rt, 30 min.

formation was observed (tlc analysis) (Scheme 4.07). The lack of reactivity may be due to the coordination of  $\text{AlCl}_3$  to the formyl group, which rendered the pyrene system strongly electron deficient. Reduction of aldehyde **126** with  $\text{NaBH}_4$  afforded 1-(hydroxymethyl)pyrene (**127**) (95%), which was then subjected to Friedel-Crafts *t*-butylation. The formation of numerous products was observed (by TLC). A similar result was obtained with 1-(bromomethyl)pyrene (**128**), which was obtained in 90% yield from the reaction of **127** with  $\text{PBr}_3$ . The formation of benzylic carbocations from **127** and **128** may be the reason for the failure of these reactions. Friedel-Crafts *t*-butylation of 1-bromopyrene (**130**) was moderately successful, but the yield could not be improved beyond 19%, even with an excess of *t*-butyl chloride.

1,3-Dithanes are typically stable to  $\text{AlCl}_3$  at  $0\text{ }^\circ\text{C}$ ,<sup>20</sup> so the protection of 1-formylpyrene **126** was carried out. Reaction of **126** with 1,3-propanedithiol in the presence of  $\text{Mg}(\text{HSO}_4)_2$ <sup>21</sup> produced 2-(1-pyrenyl)-1,3-dithane (**131**) quantitatively (Scheme 4.08a). This compound exhibited very low solubility and could only be characterized by LC-MS and HRMS. The synthesis of this compound using different reaction conditions was subsequently reported by another group, who was able to obtain more extensive characterization data.<sup>22</sup> Regardless, dithiane **131** was instantaneously deprotected when subjected to Friedel-Crafts *t*-butylation. The greater stability of the 1-pyrenylmethyl carbocation (compared to the parent benzyl carbocation)<sup>23</sup> may again be responsible for the rapid deprotection.

Protection of 1-(hydroxymethyl)pyrene (**127**) was also investigated. Reaction of **127** with TIPSCl and benzoyl chloride in the presence of appropriate bases afforded the

corresponding protected products **132** (99%) and **133** (99%), respectively (Scheme 4.08b and 4.08c). Neither of these compounds had been previously reported at the time of their synthesis, but compound **133** was reported subsequently using the same reaction conditions.<sup>24</sup> Both these products were deprotected instantaneously upon attempted *t*-butylation. Evidently, even large protecting groups such as TIPS cannot prevent carbocation formation, assuming that this is indeed the problem.



**Scheme 4.08** Attempted alkylations of protected pyrenes; *Reagents and conditions*: a) 1,3-propanedithiol,  $\text{Mg}(\text{HSO}_4)_2$ ,  $\text{CH}_3\text{CN}$ , 20 °C, 5 min, 99%; b) TIPSCl, imidazole,  $\text{CH}_2\text{Cl}_2$ , 20 °C, 4 h, 99%; c) BzCl, DMAP,  $\text{Et}_3\text{N}$ ,  $\text{CH}_2\text{Cl}_2$ , 20 °C, 30 min, 99%; d) *t*-BuCl,  $\text{AlCl}_3$ ,  $\text{CH}_2\text{Cl}_2$ , rt, 2 min.

#### 4.2.3.2 *In-situ* chlorination / Friedel-Crafts alkylation reaction

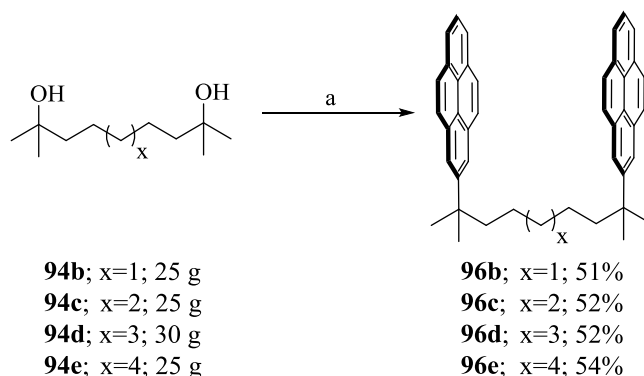
Having had little success in addressing the problem of overalkylation, attention was turned to the problem of the quality of the dichlorides **95b-d**, which were found to be

contaminated with varying amounts of elimination products **115b-d** and **116b-d** on the small scale (up to 2 g). Upon closely monitoring (tlc analysis) several chlorination reactions from the beginning of the reaction all the way to the isolation of the product, it was consistently observed that **95b-d**, **115b-d** and **116b-d** were all present from the early stages of the reaction to the point at which the starting material had been fully consumed (*ca.* 3 h). Over the course of the reaction, the distribution of **95b-d:115b-d:116b-d** was observed to be heavily weighted toward **95b-d**. Chloroalkenes **115b-d** were always more abundant than dienes **116b-d**. The relative amounts of **95b-d:115b-d:116b-d** did not appear to change significantly during the 3 h reaction, but if the reactions were allowed to proceed for longer periods of time, the spots for **115b-d** and **116b-d** clearly grew in intensity. The spots for **115b-d** and **116b-d** never became more intense than those of **95b-d**, which suggests that an equilibrium had been reached (see the chromatogram in Figure 4.04).

As the chlorination reactions were worked up, the proportions of **115b-d** and **116b-d** gradually increased. This process tended to occur more rapidly as the scale of the reaction increased, which may explain why higher purity dichlorides were obtained on smaller scales. The purity of the dichlorides was also found to decrease slowly (over a period of several days) when samples were left to stand in closed containers. As such, freshly-prepared dichlorides are obviously preferable.

In an attempt to minimize the proportions of the byproducts, conc. HCl (37% aqueous solution) was replaced with HCl gas (generated from the dropwise addition of conc. HCl to conc. H<sub>2</sub>SO<sub>4</sub>), which was bubbled into a solution of diol **94d** in dry

dichloromethane. Tlc analysis indicated that **94d** was consumed in about 4-5 h and, more importantly, **95d** appeared to be the only product. No trace of **115d** or **116d** was observed. To avoid giving **95d** the opportunity to suffer elimination during workup, the HCl stream was removed and the reaction mixture was first purged with nitrogen gas (to remove excess HCl) and then used immediately for a Friedel-Crafts alkylation of pyrene. Thus the addition of pyrene (5 equiv.) and AlCl<sub>3</sub> to the crude solution of **95d** led to the formation of di(2-pyrenyl)alkane **96d** in 38% yield on a 2 g scale. Gratifyingly, a 42% yield of **96d** was obtained when the reaction was performed on a 10 g scale. Tlc analysis of the Friedel-Crafts alkylation reaction showed no significant spots corresponding to **120d** and **121d** (being between pyrene (**20**) and **96d**), but spots corresponding to **117d**, **118d** and **119d** were still present. To minimize oligomer formation, the number of equiv. of pyrene (**20**) was raised from 5.0 to 10.0. This improved the yield of **96d** to 53% on a 10 g scale. With a much improved procedure in hand, the diols **94b-e** were then converted to the corresponding di(2-pyrenyl)alkanes **96b-e** on a 25-30 g scale with



**Scheme 4.09** Modified conditions for the Friedel-Crafts alkylation; *Reagents and conditions*: a) 1. HCl (gas), 4-5 h, 2. N<sub>2</sub> (gas), 20 min, 3. pyrene, AlCl<sub>3</sub>, CH<sub>2</sub>Cl<sub>2</sub>, rt, 1 h.

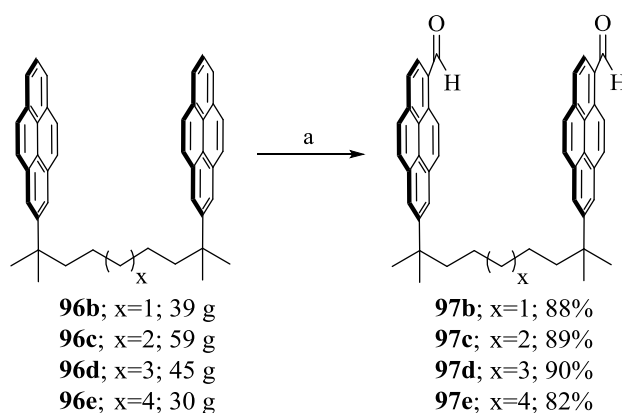
no reduction in yield (51-54%) (Scheme 4.09). It was therefore possible to produce 35-40 g of **96b-e** in a single synthetic operation. It was then found that replacing ACS grade  $\text{CH}_2\text{Cl}_2$  with drum grade  $\text{CH}_2\text{Cl}_2$  had no detrimental effect on the yield.

The use of 10 equiv. of pyrene on such a large scale means that a very large column ( $70 \times 12.5$  cm) was required for the isolation of **96b-e**. This limited the scale of the reaction to 30 g. Both the solvent (8% chloroform / hexanes) and the recovered pyrene (*ca.* 240 g) could be reused. In fact, the purity and appearance of the recovered pyrene was superior to the commercial material. Interestingly, the odd-tethered compounds **96b** and **96d** were obtained as fluffy solids and were found to be more soluble in  $\text{CH}_2\text{Cl}_2$  than the even-tethered compounds **96c** and **96e**, which were obtained as powders or crystalline solids. Indeed, the chromatography of **96c** is more difficult due to its lower solubility in  $\text{CH}_2\text{Cl}_2$ .

#### 4.2.4 Rieche formylation of di(2-pyrenyl)alkanes

The third step of the modified route to the teropyrenophanes was the Rieche formylation of tethered bis(2-pyrenyl)alkanes **96b-e**, which proved to be much easier to scale up than the previous step. Only minor changes to the original protocol were required. On a 500 mg scale, 2.5 equiv. of both  $\text{TiCl}_4$  and  $\text{Cl}_2\text{CHOCH}_3$  were used to convert **96b-e** to the corresponding dialdehydes **97b-e**. On a multi gram scale, the use of these amounts of reagents resulted in incomplete reactions with low product yields (40-45%). When 5.0 equiv. of  $\text{TiCl}_4$  and  $\text{Cl}_2\text{CHOCH}_3$  were employed, quantitative conversion was observed (tlc analysis). The temperature was also changed from 0 °C to

room temperature because full conversion could be achieved after about 30 minutes (*cf.* incomplete conversion after several hours at 0 °C). With these modifications, the Rieche formylations could be performed conveniently on a 30-59 g scale to produce the corresponding dialdehydes **23b-e** in yields (82-90%) very similar to those obtained on a small scale (84-88%) (Scheme 4.10).



**Scheme 4.10** Rieche formylation; *Reagents and conditions*: a)  $\text{Cl}_2\text{CHOCH}_3$ ,  $\text{TiCl}_4$ ,  $\text{CH}_2\text{Cl}_2$ , rt, 2 h.

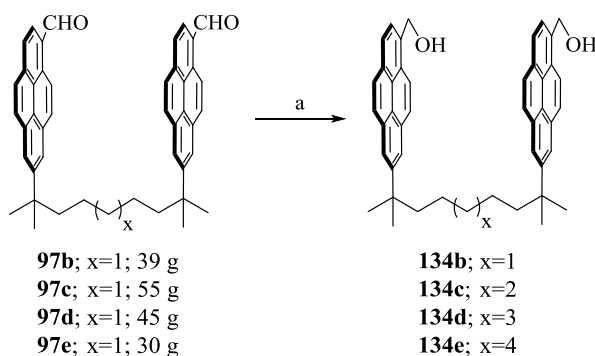
As in the previous step, it was found that the Rieche formylations could be performed using drum grade  $\text{CH}_2\text{Cl}_2$ , but this sometimes required the addition of 0.5-1.0 additional equiv. of both  $\text{TiCl}_4$  and  $\text{Cl}_2\text{CHOCH}_3$  if the reaction had not gone to completion (tlc analysis) after 30 minutes. All of the dialdehydes **97b-e** exhibited good solubility in  $\text{CH}_2\text{Cl}_2$ , THF and ethyl acetate.

#### 4.2.5 Reduction of the dialdehydes **97b-e**

The next step in the synthetic pathway was the reduction of dialdehydes **97b-e** with  $\text{NaBH}_4$ , which proceeded efficiently to afford diols **134b-e** on a 30-55 g scale



(Scheme 4.11). The only modification to the small-scale procedures was the use of drum THF (*cf.* distilled THF) and a 10-fold increase in concentration. The recovered THF could be reused without any detrimental effect on the reaction. The diols **134b-e** exhibited good solubility in CH<sub>2</sub>Cl<sub>2</sub>, THF and ethyl acetate. Attempted purification by column chromatography and crystallization resulted in substantial losses of material. Since, <sup>1</sup>H NMR analysis of the crude products indicated that they are of >90% purity, they were used without purification in the following step.



**Scheme 4-11** Reduction of dialdehydes **97b-e**; *Reagents and conditions*: a) NaBH<sub>4</sub>, THF, rt, 2 h.

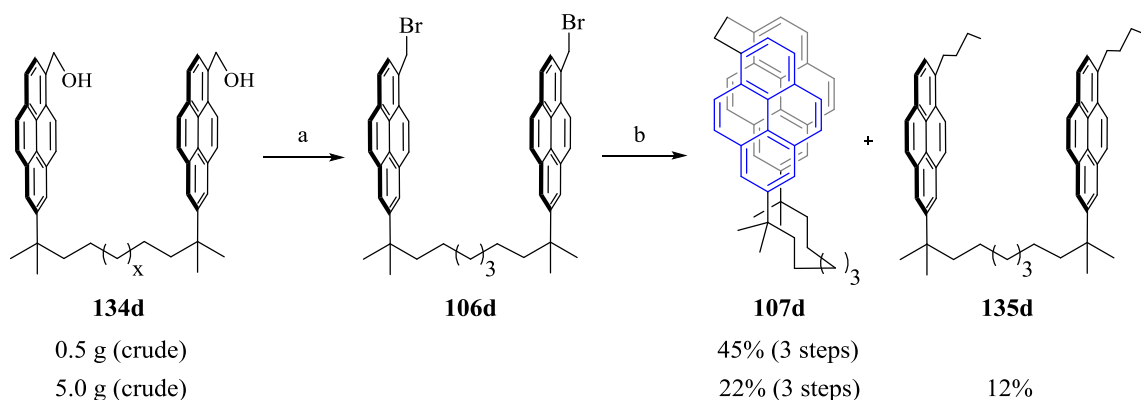
#### 4.2.6 Problems associated with bromination reaction

In the original Wurtz-McMurry pathway, the next step was the bromination of diols **134b-d** to produce dibromides **106b-d**. These dibromides were always isolated using an aqueous workup followed by column chromatography. During initial attempts to increase the scale of the bromination of diol **134d**, it was found that hydrolysis of the resulting dibromide **106d** (to give back diol **134d**) during both workup and (to a greater extent) column chromatography on silica gel became increasingly prevalent as the scale of the reaction increased. On a 10 g scale, only 42% of **106d** was obtained. The stability

of the 1-pyrenylmethyl cation is most likely the cause for the ease with which **106d** undergoes hydrolysis.

#### 4.2.7 Bromination / Wurtz coupling reaction

Since the majority of the hydrolysis appeared to occur during chromatography, it was decided to omit the chromatography and use the crude dibromide **106d** in the subsequent intramolecular Wurtz coupling reaction leading to [n.2]pyrenophane **107d** (Scheme 4.12). When this reaction was performed on a 500 mg scale, cyclophane **107d** was obtained in a respectable 45% combined yield over three steps (reduction, bromination and Wurtz coupling). However, the yield for the three-step sequence dropped to 22% when the scale was increased to 5 g. Several byproducts were formed (tlc analysis) and the most abundant one was isolated in pure form.  $^1\text{H}$  NMR and  $^{13}\text{C}$  NMR as well as MS analysis were used to identify it as **135d** (12%), the product of twofold  $\text{S}_{\text{N}}2$  reaction of **135d** with *n*-BuLi.



**Scheme 4.12** Previous conditions for the Wurtz coupling; *Reagents and conditions*: a)  $\text{PBr}_3$ ,  $\text{CH}_2\text{Cl}_2$ ,  $0\text{ }^\circ\text{C}$ –rt, 1 h; b) *n*-BuLi, THF,  $-15\text{ }^\circ\text{C}$ , 10 min.

#### 4.2.7.1 *In-situ* bromination / Wurtz coupling reaction

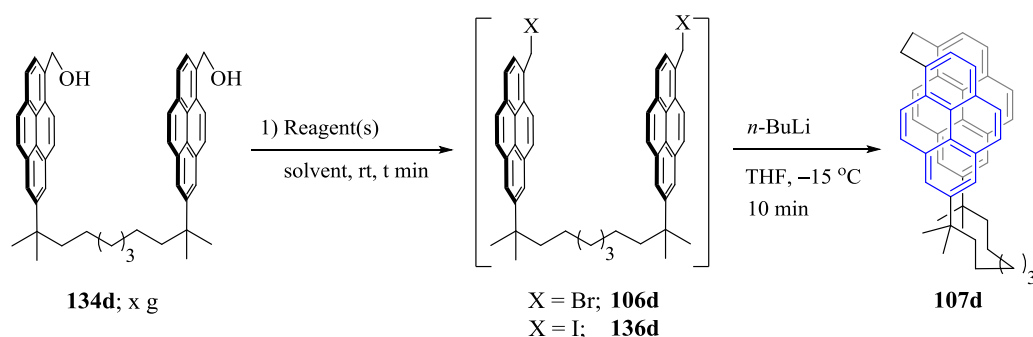
To avoid both the aqueous workup and the column chromatography, a further modification to the procedure was made. Treatment of diol **134d** (50 mg) with  $\text{PBr}_3$  as before generated dibromide **106d** (essentially one spot by tlc analysis) and the solvent was removed under reduced pressure. The residue was immediately redissolved in anhydrous THF and the solution was cooled to 0 °C. At this point, it was envisaged that the addition of *n*-BuLi would bring about the desired Wurtz coupling, either following or parallel to reactions between *n*-BuLi and the phosphorus-containing species that were still present. Cyclophane **107d** was indeed formed, but it was part of a complex mixture of products (tlc analysis) and it could be isolated in only 10% yield (from diol **134d**) (Table 4.01, Entry 1).

#### 4.2.7.2 *In-situ* iodination / Wurtz coupling reaction

Wurtz couplings are known to work better for alkyl iodides than the corresponding alkyl bromides,<sup>25</sup> so the possibility of replacing dibromide **107d** with diiodide **136d** was investigated. Attempted conversion of diol **134d** (50 mg) into diiodide **136d** using the Appel reaction ( $\text{PPh}_3/\text{I}_2/\text{DMAP}$ ) gave a mixture of products (tlc analysis). Not surprisingly, addition of *n*-BuLi to this mixture gave an even more complex mixture. Cyclophane **107d** may have been present, but no attempt was made to isolate it (Table 4.01, Entry 2).

Das *et al.*<sup>26</sup> reported the iodination of benzylic alcohols using PMHS/ $\text{I}_2$  in  $\text{CHCl}_3$ . Applying these conditions to diol **134d** (200 mg) resulted in clean conversion to diiodide

**Table 4.01** *In-situ* halogenation-Wurtz coupling reaction.

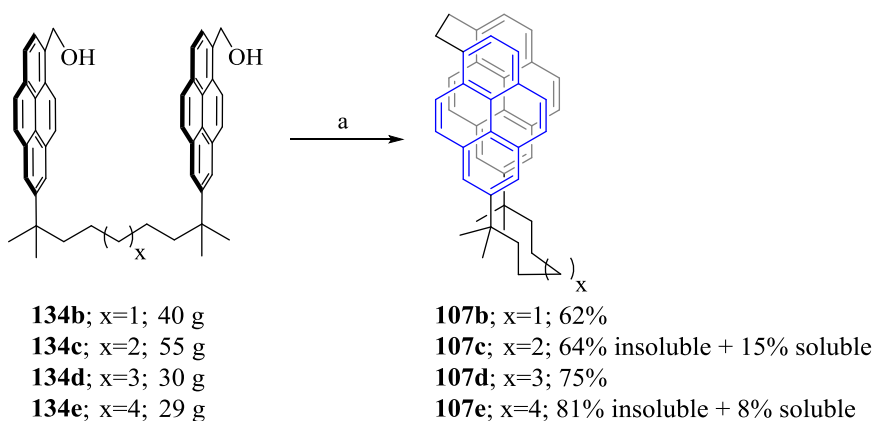


entry	<b>134d</b> (g)	reagent(s)/solvent	t (min)	<i>n</i> -BuLi (equiv.)	<b>107d</b> (%)
1	0.05	PBr <sub>3</sub> /CH <sub>2</sub> Cl <sub>2</sub>	120	1 - 8	10
2	0.05	I <sub>2</sub> /PPh <sub>3</sub> /DMAP/CHCl <sub>3</sub>	120	1 - 30	mixture
3	0.20	I <sub>2</sub> /PMHS/CHCl <sub>3</sub>	20	6.2	61
4	0.20	I <sub>2</sub> /PMHS/THF	20	6.2	61
5	2.00	I <sub>2</sub> /PMHS/THF	40	6.2	61
6	8.90	I <sub>2</sub> /PMHS/THF	90	6.2	66
7	30.00	I <sub>2</sub> /PMHS/THF	180	6.2	75

**136d** in 20 min at room temperature (tlc analysis). The CHCl<sub>3</sub> was removed under reduced pressure and the residue was dissolved in dry THF. Addition of 4-5 equiv. of *n*-BuLi at 0 °C did not result in the formation of any trace of **107d**, presumably because it was reacting with residual PHMS, I<sub>2</sub> and any byproducts from the iodination reaction (tlc analysis). Further addition of *n*-BuLi (up to a total of 6.5 equiv.) was accompanied by the emergence of a very strong spot corresponding to **107d**. The desired cyclophane **107d** was then isolated in 61% yield (Table 4.01, Entry 3).

To avoid having to change solvents during the iodination / Wurtz coupling protocol, the iodination step was then conducted using dry THF as the solvent. The formation of diiodide **136d** was as quick and as clean as when the reaction was performed in  $\text{CHCl}_3$  (tlc analysis). Once the diiodide formation was complete, the reaction mixture was diluted *ca.* tenfold with THF (to promote intramolecular Wurtz coupling) and *n*-BuLi was added slowly at  $-15\text{ }^\circ\text{C}$ . As before, compound **107d** was isolated in 61% yield (three steps from **134d**) (Table 4.01, Entry 4). At the same time, the amount of **135d** that formed decreased significantly (tlc analysis). Most gratifyingly, an *increase* in yield was observed as the reaction scale was increased to 2 g (61%), 9 g (66%) and then 30 g (75%) (Table 4.01, Entries 5 to 7). For the 30 g scale reaction, the concentration was increased (*ca.* two-fold) and it was found that drum THF could be used with no effect on the yield. An additional 0.5-1.0 equiv. of *n*-BuLi (tlc analysis) was, however, required to complete the reaction.

With a reliable large-scale procedure in hand, the other diols **134b**, **134c** and **134e**



**Scheme 4.13** *In-situ* iodination / Wurtz coupling of diols **134b-e**; *Reagents and conditions*: a) (i)  $\text{I}_2/\text{PMHS}$ , THF, rt, 20 min; (ii) *n*-BuLi, THF,  $-15\text{ }^\circ\text{C}$ , 10 min.

were then subjected to the iodination / Wurtz coupling sequence. The reaction of **134b** proceeded smoothly on a 40 g scale and cyclophane **107b** was obtained in 62% yield (Scheme 4.13). On the other hand, a solubility problem arose with the reactions of **134c** and **134e** (even-numbered tethers).

#### 4.2.7.3 Solubility problems with the even-tethered cyclophanes

In the well-behaved reactions leading to **107b** and **107d** (odd-numbered bridge lengths), the turbid brown solutions of the diiodides became clear pale yellow from the first sign of cyclophane formation to the completion of the reactions. In contrast, the reactions leading to **107c** (55 g scale) and **107e** (29 g scale) (even-numbered bridge lengths) (Scheme 4.12) exhibited the precipitation of an off-white solid very shortly after the point where the reaction mixture became pale yellow and the first traces of cyclophane formation were observed (tlc analysis). As the addition of *n*-BuLi proceeded, the amount of off-white precipitate increased. For the reaction leading to **107c**, the off-white precipitate was isolated by filtration and its mass corresponded to a 64% yield of **107c** and/or higher oligomers. Cyclophane **107c** (15%) was isolated from the filtrate as a fluffy white solid, which exhibited good solubility in common organic solvents. The white precipitate was found to be very poorly soluble in the same solvents.

In the case of **107e**, the problem was even more pronounced. An 81% yield of the white precipitate was obtained along with only 8% of **107e**. Again, the fluffy white product obtained from the filtrate was found to be soluble in common organic solvents, whereas the white precipitate was not. Curiously, MALDI-TOF MS analysis of both the

poorly soluble white precipitate (Figure 4.08 top) and the nicely soluble fluffy white solid (Figure 4.08 below) showed essentially a single peak at  $m/z = 624$ , which corresponds to

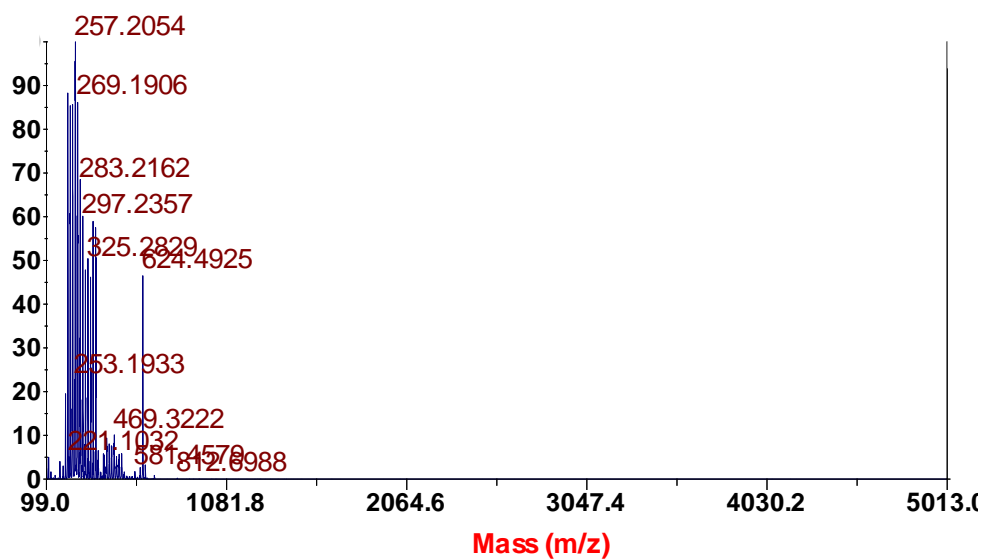
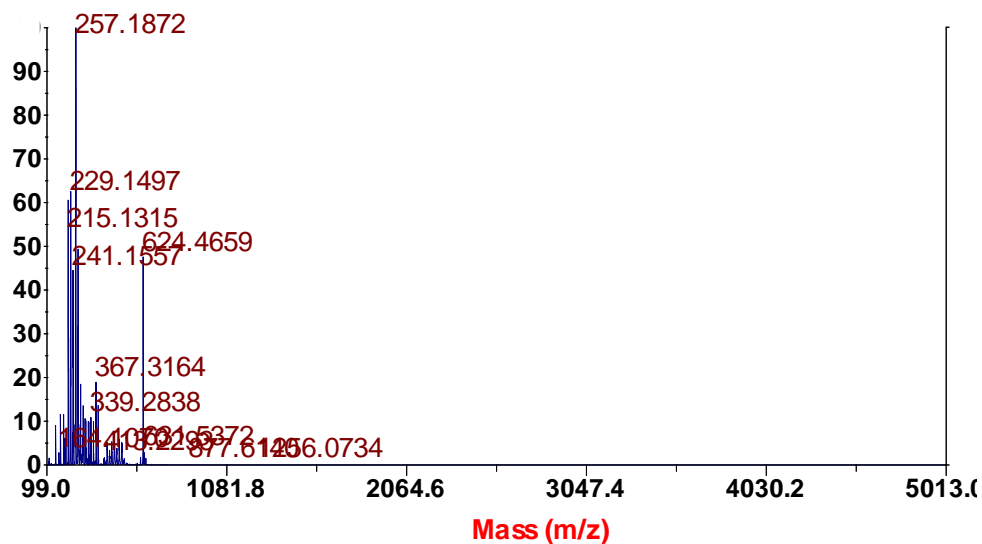


**Figure 4.08** Top) MALDI-TOF MS analysis of the poorly-soluble white precipitate obtained from the reaction leading to **107e**. Bottom) MALDI-TOF MS analysis of the soluble **107e**.

**107e**. In both cases, only the faintest traces of a peak corresponding to a cyclic dimer ( $m/z = 1248$ ) were observed.

The possibility that two forms of the same compound were obtained was briefly investigated by solid-state NMR. The  $^1\text{H}$  and  $^{13}\text{C}$  spectra of the poorly-soluble material both contained sharp peaks, whereas those of the more soluble material appeared to be significantly broadened versions of the same spectrum (appendix 4.6). This may be indicative of greater crystallinity in the poorly-soluble material. More detailed analysis of the poorly-soluble materials would be needed to state with certainty that they are indeed **107c** and **107e**, but based on the available information, it does seem likely that they are. Regardless of their nature, it was still possible to isolate a few grams of **107c** and **107e**, which could be used for further synthetic elaboration. Interestingly, on a 0.5 g scale at the original concentration, this problem did not come into play and the cyclophanes **107c** and **107e** could be isolated in 61% and 60% yields, respectively.

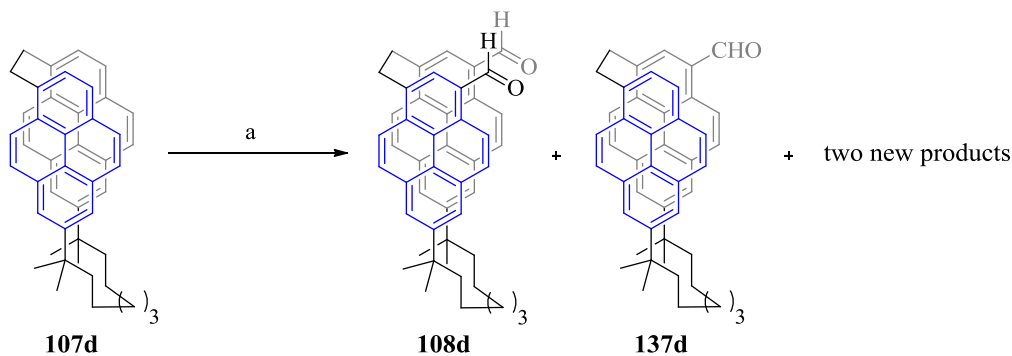
#### 4.2.7.4 Conformational mobility of cyclophanes

Like the cyclophanemonoenes **99a-b** (Chapter 2.1.1), cyclophanes **107b-d** were observed to be conformationally mobile ( $^1\text{H}$  NMR analysis). At the time of writing this thesis, the analysis of the conformational behavior was incomplete, but it seems reasonable to expect that a *syn-anti* interconversion is taking place (*cf.* **99a-b**). Based on the appearance of the room temperature  $^1\text{H}$  NMR spectra of **107b-d**, it is clear that the energy barrier for the process being observed increases at the length of the long bridge becomes shorter.



#### 4.2.8 Problems associated with Rieche formylation

The next step in the synthesis of teropyrenophanes **103d-b** was the Rieche formylation of  $[n.2](7,1)$ pyrenophanes **107b-d**. As before, the system with the 9-membered bridge (**107d**) was selected for scale-up work. In the original synthesis of **103d**, Rieche formylation of **107d** on a 50 mg scale afforded the corresponding dialdehyde **108d** ( $R_f = 0.12$ ;  $\text{CH}_2\text{Cl}_2$ ) in 75% yield (Table 4.02, Entry 1). When the reaction scale was increased to 250 mg (Table 4.02, Entry 2), the yield of **108d** (30%) dropped significantly. Unlike the Rieche formylations leading to **97b-d** (Scheme 4.09), this formylation was sluggish and did not go to completion. The crude reaction mixture contained the intermediate monoaldehyde **137d** ( $R_f = 0.40$ ;  $\text{CH}_2\text{Cl}_2$ ) as well as two previously unobserved products ( $R_f = 0.24$  and  $0.33$ ) (Scheme 4.14).



**Scheme 4.14** Previous conditions for the Rieche formylation reaction of cyclophane **107d**; *Reagents and conditions*: a)  $\text{TiCl}_4$ ,  $\text{Cl}_2\text{CHOCH}_3$ ,  $\text{CH}_2\text{Cl}_2$ ,  $0\text{ }^\circ\text{C}$ –rt, 3 h.

HRMS analysis of the two new products showed a single peak at  $m/z = 666.3511$ , which suggested they might be regioisomers of **108d** (calc. for  $m/z = 666.3511$ ). The positions of the aldehyde groups could not be determined at this stage by  $^1\text{H}$  NMR

experiments due to overlapping peaks and broadness arising from conformational processes. All attempts to grow crystals failed. Based simply on the combined directing effects of the two alkyl groups in a 1,7-dialkylpyrene (Figure 4.09), the initial working hypothesis was that the structures of the two byproducts were **138d** and **139d**. These assignments were supported by 1-D and 2-D NMR experiments (Section 4.2.8.2 below) and, in the case of **139d**, by a crystal structure of a byproduct from a later stage of the synthesis (Section 4.2.9.2 below).

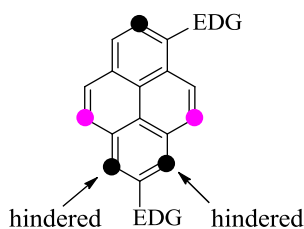


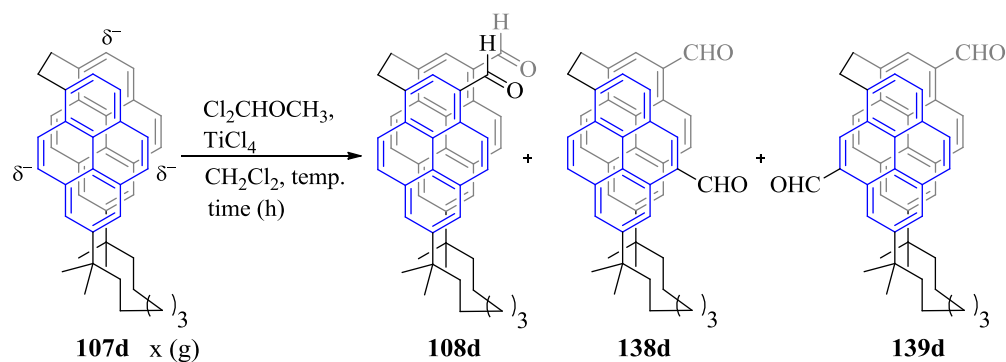
**Figure 4.09** Predicted sites of enhanced rates of electrophilic aromatic substitution of a 1,7-dialkylpyrene.

To force the formylation of **107d** to completion, 6.0 equiv. of both  $\text{TiCl}_4$  and  $\text{CHCl}_2\text{OCH}_3$  were employed (Table 4.02, Entry 3) and the yield of **108d** improved to 63% (250 mg scale). Under the same conditions, the yield of **108d** was found to drop significantly with increasing temperature (Table 4.02, Entries 4 to 6) or with an increase in the scale of reaction up to 4.5 g (Table 4.02, Entries 7 to 8).

#### 4.2.8.1 Modification to the Rieche formylation reaction

The order of addition of the reagents ( $\text{TiCl}_4$  and  $\text{Cl}_2\text{CHOCH}_3$ ) to **107d** was then changed. Instead of the direct addition of  $\text{Cl}_2\text{CHOCH}_3$  and then  $\text{TiCl}_4$  to a solution of

**Table 4.02** Rieche formylations of **107d**.

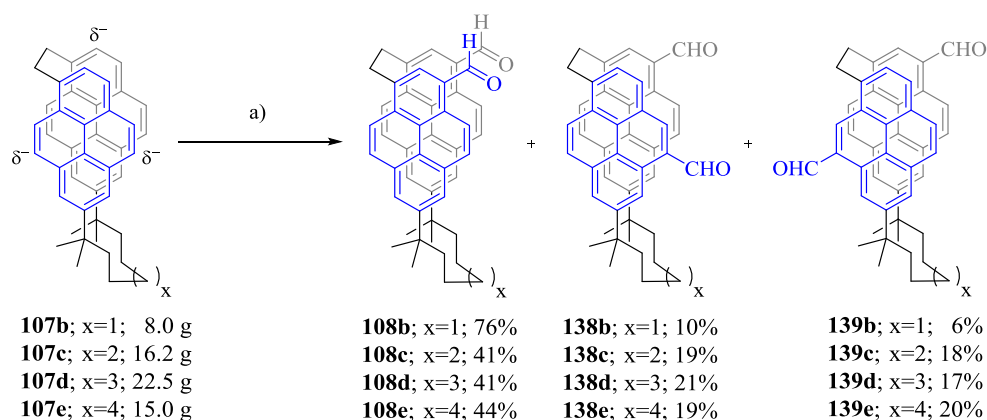


entry	<b>107d</b> (g)	TiCl <sub>4</sub> (equiv.)	Cl <sub>2</sub> CHOCH <sub>3</sub> (equiv.)	t (h)	temp (°C)	<b>108d</b> (%)	<b>138d</b> (%)	<b>139d</b> (%)
1	0.05	2.5	2.5	2	0	75		
2	0.25	2.5	2.5	2	0	30	20	18
3	0.25	6.0	6.0	2	0	63		
4	0.25	6.0	6.0	2	0-rt	54		
5	0.25	6.0	6.0	2	rt	47		
6	0.25	6.0	6.0	2	40	38		
7	0.96	6.0	6.0	2	0	32		
8	4.50	6.0	6.0	2	0	16		
9	0.50	6.0	6.0	17	0-rt	50		
10	0.50	15.0	15.0	17	0-rt	58		
11	1.10	15.0	15.0	17	0-rt	40		
12	5.00	15.0	15.0	17	0-rt	45	19	16

cyclophane **107d** in CH<sub>2</sub>Cl<sub>2</sub> at 0 °C, a freshly-prepared mixture of the two reagents in CH<sub>2</sub>Cl<sub>2</sub> at 0 °C was added dropwise to a 0 °C solution of **107d** (500 mg scale) in CH<sub>2</sub>Cl<sub>2</sub>. The resulting reaction mixture was stirred at room temperature for a period of 17 h, which improved the yield of **108d** to 50% (Table 4.02, Entry 9). Increasing the number of

equiv. of  $\text{TiCl}_4$  and  $\text{Cl}_2\text{CHOCH}_3$  to 15 resulted in an increase in the yield to 58% (Table 4.02, Entry 10). Only a moderate reduction in yields was observed upon increasing the scale of the reaction to 5 g (Table 4.02, Entries 10 to 12). On a 5 g scale, significant amounts of the two regioisomers **138d** (19%) and **139d** (16%) still formed (Table 4.02, Entry 2 and Entry 12).

With optimized conditions in hand, all of the cyclophanes **107b-e** were converted to the corresponding dialdehydes **108b-e** on 8-25 g scales (Scheme 4.15). The smallest member of the series **107b** behaved differently than the other members of the series. Whereas the yields of **108c-e** (41-44%), **138c-e** (19-21%) and **139c-e** (17-20%) were quite consistent, the formylation of **107b** afforded the desired dialdehyde **108b** in much better yield (76%) and the undesired regioisomers **138b** and **139b** in significantly reduced yield (10% and 6%, respectively). Initially, dry  $\text{CH}_2\text{Cl}_2$  was used for the formylation reactions, but it was subsequently found that ACS grade or even drum grade  $\text{CH}_2\text{Cl}_2$



**Scheme 4.15** Synthesis of dialdehydes **108b-e** using modified Rieche formylation conditions;  
*Reagents and conditions:*  $\text{TiCl}_4$ ,  $\text{Cl}_2\text{CHOCH}_3$ ,  $\text{CH}_2\text{Cl}_2$ , 0 °C–rt, 17 h.

could be used with no appreciable effect on the yield. All of the yellow dialdehydes **108b-d**, **138b-d** and **139b-d** are nicely soluble in CH<sub>2</sub>Cl<sub>2</sub>. Interestingly, when the poorly-soluble samples of cyclophanes **108b** and **108d** were subjected to the optimized Rieche formylation conditions, poorly-soluble yellow products were produced. The identity of these products was not determined.

#### 4.2.8.2 Structural assignment of **108d**, **138d** and **139d** using 1-D and 2-D NMR spectroscopy

A suite of 1-D and 2-D NMR experiments was used to assign the structures of dialdehydes **108d**, **138d** and **139d**. The <sup>1</sup>H NMR spectrum of **108d** is quite straightforward as the molecule has symmetry (a mirror plane in the *syn* conformation and a C<sub>2</sub> axis in the *anti* conformation) that renders the two halves of the molecule equivalent. The aldehyde signal appears at  $\delta$  10.81 and in the NOESY spectrum it shows a cross peak to a singlet at  $\delta$  8.43, which can be assigned as H<sub>a</sub>, and a cross peak to a doublet at  $\delta$  9.24, which can be assigned as H<sub>c</sub> (Figure 4.10). The very low-field chemical shift of this proton is consistent with its *peri* relationship to the aldehyde group. The doublet at  $\delta$  9.24 is part of a well-resolved AX system at  $\delta$  9.24 and  $\delta$  8.11 ( $J$  = 9.2 Hz), which means that the doublet at  $\delta$  8.11 can be assigned to H<sub>d</sub>. In the NOESY spectrum, the doublet at  $\delta$  8.11 shows a cross peak to the doublet at  $\delta$  8.01, which can be assigned as H<sub>e</sub>. The doublet at  $\delta$  8.01 is part of a well-resolved AB system at  $\delta$  8.01 and  $\delta$  7.70 ( $J$  = 1.8 Hz), which means that the doublet at  $\delta$  7.70 can be assigned to H<sub>f</sub>. In the NOESY spectrum, the doublet at  $\delta$  7.70 shows a cross peak to one of the very broad

signals at  $\delta$  7.19-7.04, which can be assigned as  $H_g$ . The two broad signals at  $\delta$  7.19-7.04 are coupled to one another ( $^1H, ^1H$ -COSY), which means that they are attributable to  $H_g$  and  $H_h$ . In the NOESY spectrum, these broad signals at  $\delta$  7.19-7.04 shows a cross peak to the singlet at  $\delta$  3.99, which can be assigned as  $H_i$ .

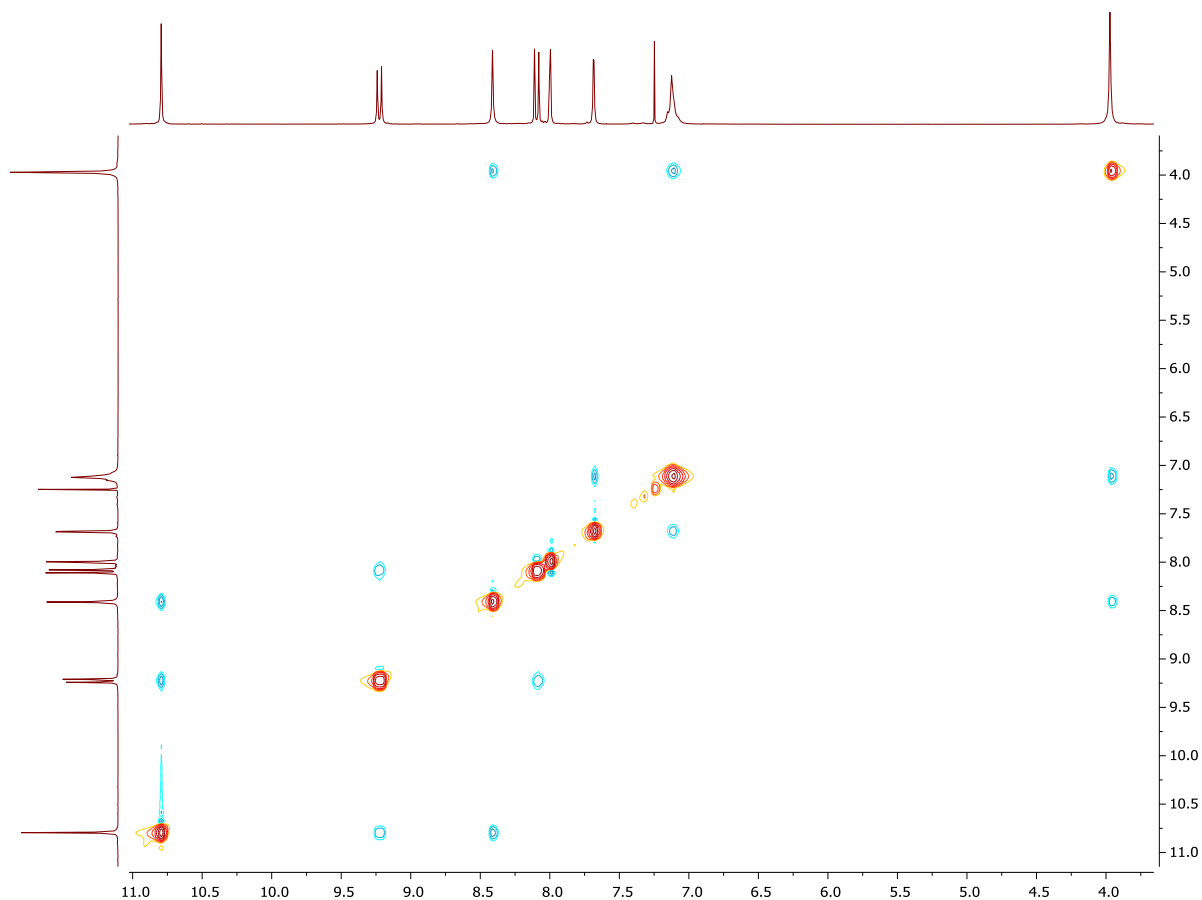


**Figure 4.10** NOESY spectrum of dialdehyde **108d**.

The  $^1H$  NMR spectrum of the fastest-moving byproduct contains two aldehyde signals at  $\delta$  10.78 and  $\delta$  10.39, which immediately points to a structure with lower ( $C_1$ ) symmetry. Using the approach described above for the assignment of **108d** (starting with

the aldehyde signal at  $\delta$  10.81), it could be determined that one of the pyrene systems bears the formyl group at the same position as the pyrene systems in **108d** (Figure 4.11). Where unambiguous assignments could be made, the chemical shifts for the protons of this ring are very close to those of the corresponding protons of **108d** ( $\Delta\delta < 0.1$  ppm). To determine the position of the formyl group on the other pyrene system, a NOESY cross peak (Figure 4.12) between the formyl signal at  $\delta$  10.36 and the doublet at  $\delta$  9.44 ( $J = 1.7$  Hz) narrowed it down to being *peri* to either  $H_n$  or  $H_o$ , i.e. the structure of the byproduct is (in line with the initial expectations) either **138d** or **139d**. A cross peak to a singlet at  $\delta$  8.30 was also observed, which therefore corresponds to either  $H_i$  in **138d** or  $H_q$  in **139d**. The singlet at  $\delta$  8.30 exhibits a cross peak to the doublet at  $\delta$  8.08 (which is coincident with a doublet due to  $H_d$  of the other pyrene system). This cross peak is inconsistent with  $H_q$  in **139d**, but fits with  $H_k$  in **138d**. Furthermore, the signal at  $\delta$  8.08 is coupled to the doublet at  $\delta$  7.88 ( $J = 7.8$  Hz), which in turn shows a NOESY cross peak to the broad singlet at  $\delta$  3.91 due to the ethano bridge protons. Thus the structure of the byproduct was confidently assigned as **138d**.

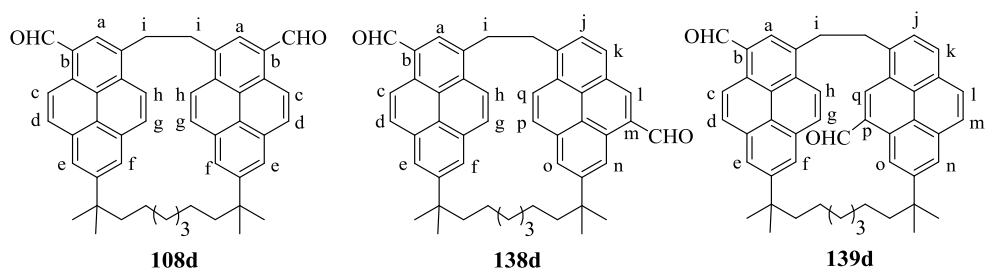


**Figure 4.11** Three regio-isomers **108d**, **138d** and **139d**.

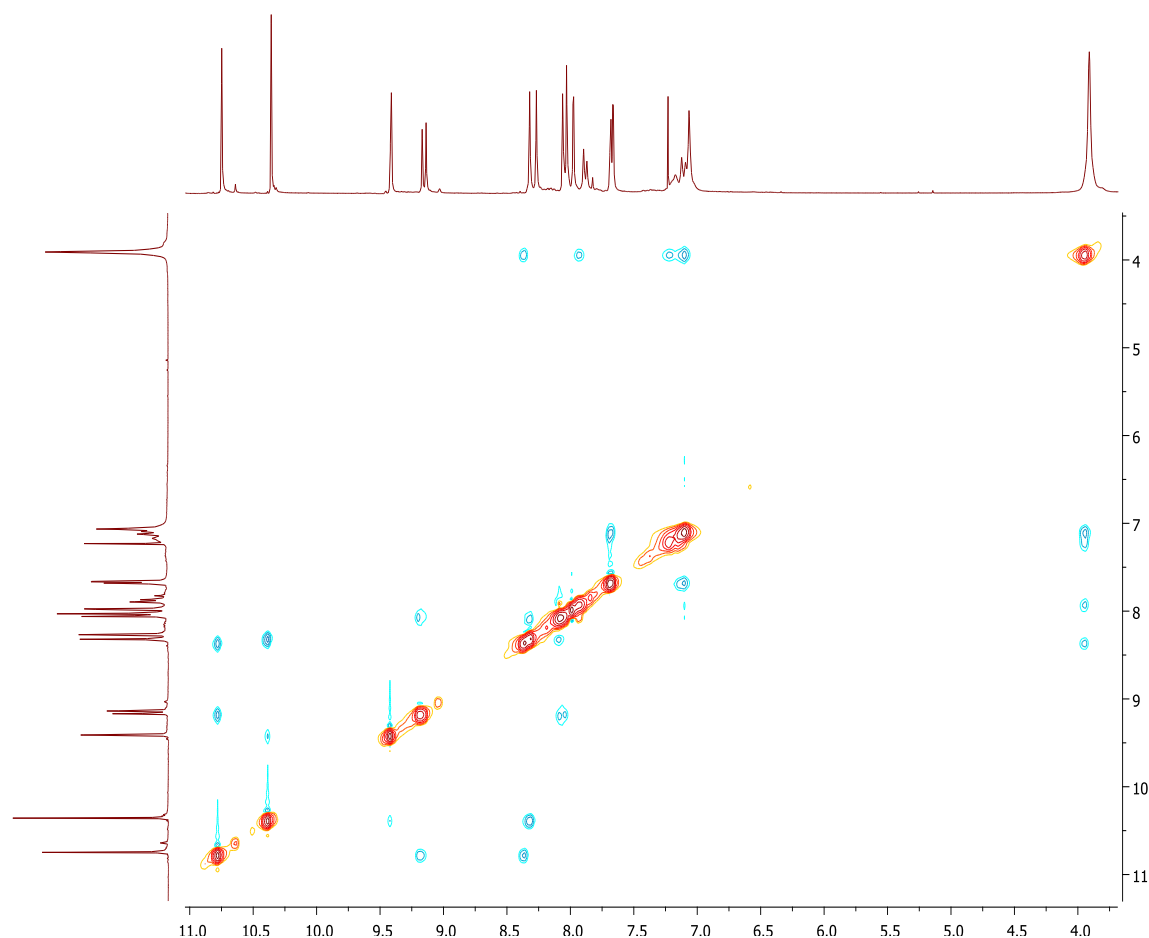


**Figure 4.12** NOESY spectrum of dialdehyde **138d**.

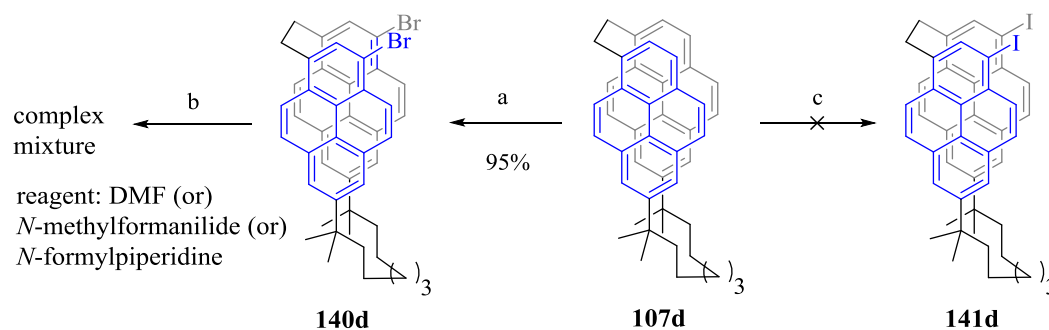
Most of the signals in  $^1\text{H}$  NMR spectrum of the second dialdehyde byproduct from the formylation of **139d** were broad, presumably due to a conformational process near coalescence. As such, an NMR-based structural assignment at ambient temperature was not possible. Interestingly, several peaks appeared to be twinned with similar peaks of roughly one third of the intensity, which suggests the presence of more than one conformer. Whatever the case, no concrete conclusions about the structure of this compound could be drawn using NMR. Ultimately, the structure of this compound was



assigned as **139d** by analogy to **139e**, which has a very similar  $^1\text{H}$  NMR spectrum. The structure of **139e** was determined later (see Section 4.2.9.2) by inference from a crystal structure of a byproduct from a subsequent McMurry reaction. The structures of **138b-c** and **138e** were assigned on the basis of the similarity of their  $^1\text{H}$  NMR spectra to that of **138d**.

#### 4.2.8.3 Alternative unsuccessful attempts to formylate **107d**

In an attempt to avoid the formation of regioisomeric byproducts, other methods of formylating cyclophane **107d** were explored. Bromination of cyclophane **107d** using  $\text{Fe}/\text{Br}_2$  afforded dibromide **140d** in 95% yield and with complete regioselectivity (Scheme 4.16). However, all attempts to lithiate **140d** and formylate the resulting dianion with DMF, *N*-methylformanilide and *N*-formylpiperidine resulted in the formation of complex mixtures of products from which no pure compound could be isolated. An attempt to synthesize diiodide **141d** was unsuccessful, which concluded work on the formylations of **107b-e**.



**Scheme 4.16** Attempted reactions for the generation of cyclophane dialdehyde **108d**; *Reagents and conditions*: a)  $\text{Br}_2$ ,  $\text{Fe}$ ,  $\text{CH}_2\text{Cl}_2$ ,  $15\text{--}20^\circ\text{C}$ , 1 h; b) 1. *n*-BuLi, 30 min, THF,  $-78^\circ\text{C}$ , 2. reagent,  $-78^\circ\text{C}$ , 4 h; c)  $\text{I}_2$ ,  $\text{Hg}(\text{OAc})_2$ ,  $\text{CH}_2\text{Cl}_2$ , rt, 15 h.

#### 4.2.9 McMurry reactions of cyclophanedialdehydes **108b-d**

The scale-up of the intramolecular McMurry reactions of cyclophanedialdehydes **108b-d** to afford [n.2.2](7,1,3)pyrenophanes **109b-d** was accomplished on a 6-12 g scale without changing the existing conditions and the products were obtained with moderate, but acceptable, reductions in yields (30-32%, *cf.* 36-44% previously) (Scheme 4.16). The formation of **109e** will be discussed separately in the following Section. As in the previously reported small-scale reactions, fully reduced compounds **142b-d** were observed as byproducts (tlc analysis). Compounds **142b** (5%) and **142d** (4%) were isolated and characterized, whereas **142c** was not isolated in pure form.

##### 4.2.9.1 Identification of compounds **144c** and **144b**

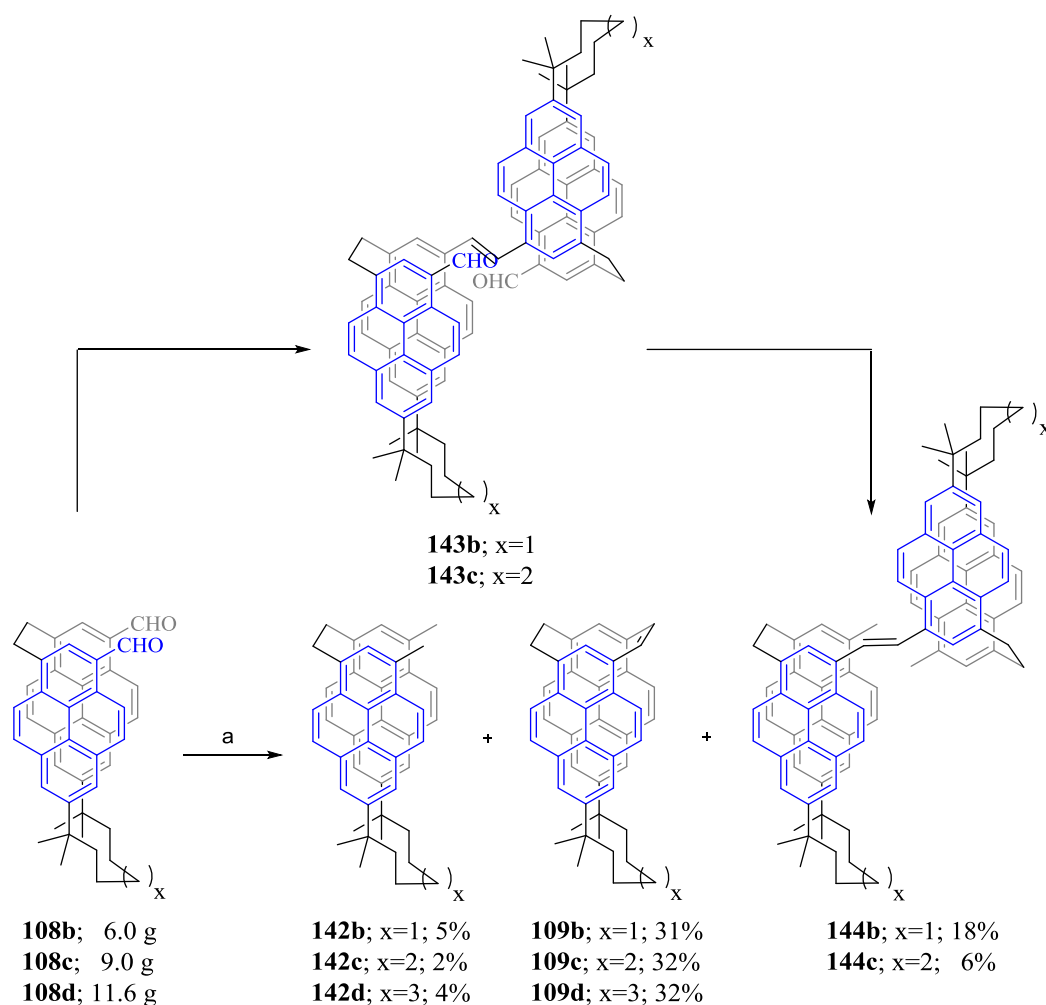
A common feature of the McMurry reactions (both at this stage and earlier in the synthesis) is the presence of numerous bright green fluorescent spots below the product spot (tlc analysis). The two fastest-moving of these spots are the most prominent. All previous attempts to identify these two narrowly-separated products were unsuccessful, due mainly to separation and solubility problems. Gratifyingly, in the case of the large-scale reaction leading to **109c**, the fastest-moving spot could be isolated in pure form and it was found to be soluble enough for characterization. APCI(+)-LC-MS analysis showed a base peak ( $[M+1]^+$ ) at  $m/z = 1245$  and APPI-HRMS analysis showed it to be at  $m/z = 1244.7199$ , which corresponds exactly to  $C_{96}H_{92}$  (calc. 1244.7199). The total of 96 carbon atoms suggested that two molecules of **108c** were joined to form the byproduct,

which can be easily explained by an intermolecular McMurry reaction to give dialdehyde **143c** (Scheme 4.17). In the  $^1\text{H}$  NMR spectrum, the majority of the peaks were broad, which is consistent with conformational mobility. The presence of broad singlets at  $\delta$  4.05 (8H) and  $\delta$  3.13 (6H) pointed towards the complete reduction of the two formyl groups in **143c** to methyl groups to afford **144c**. Whatever the configuration of the newly-formed alkene, the two remaining formyl groups are not close to one another. As such, it is not surprising that reduction occurs at this point.

In the case of the large-scale McMurry reaction of **108b**, a partial separation of the prominent byproducts was achieved ( $R_f = 0.33$  and  $0.32$ , 30% dichloromethane / hexanes), but their relatively poor solubility caused problems with their characterization (especially NMR). The first one to elute was the purest (tlc analysis), and was assigned as **144b** on the basis of its APCI(+)-LC-MS ( $m/z = 1217$ ,  $[\text{M}+1]^+$ ), APPI-HRMS ( $m/z = 1216.6808$ , calc. for  $\text{C}_{94}\text{H}_{88}$  (calc. 1216.6886) and  $^1\text{H}$  NMR ( $\delta$  4.05 (br s, 8H) and  $\delta$  3.13 (br s, 6H)) spectra. The second (less pure and less soluble) compound showed virtually identical characteristics, but it is difficult to tell whether or not these arise from contamination from the first byproduct. As such, the structure of the second byproduct (the complementary double bond isomer of **144b**?) could not be assigned.

#### 4.2.9.2 McMurry reaction of cyclophanedialdehyde **108e**

When cyclophanedialdehyde **142e** was subjected to McMurry reaction under the reaction conditions used for other members of the series, two major spots were observed by tlc ( $R_f = 0.45$  and  $0.36$ , 30% dichloromethane / hexanes) ahead of the usual two

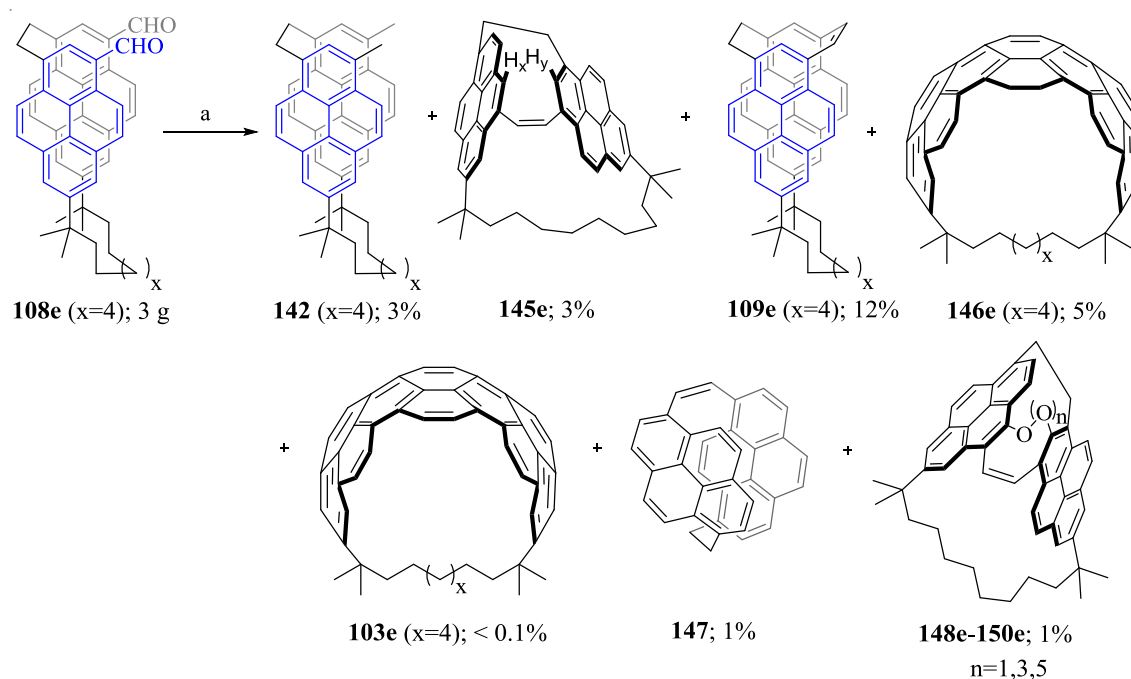


**Scheme 4.17** McMurry reaction of cyclophanedialdehydes **108b-c**; *Reagents and conditions*: a)  $\text{TiCl}_4$ , Zn, pyridine, THF, reflux, 4 h.

narrowly-separated bright green fluorescent spots and several other fainter ones below them. The leading spot was isolated and the brown solid was determined to be mainly **142e** (12%) by APCI(+)-LC-MS and  $^1\text{H}$  NMR analysis (Scheme 4.18). The identity of the contaminant that was presumably responsible for the colour could not be determined.

APCI(+)-LC-MS analysis of the second spot (yellow solid) showed a peak at  $m/z = 649$ , which corresponds to  $[\text{M}+1]^+$  for the required cyclophanemonoene **109e**, but the

complexity of the  $^1\text{H}$  NMR spectrum clearly indicated the presence of more than one product. Further tlc experiments revealed that what had been initially interpreted as a single spot was in fact at least three very narrowly separated spots ( $R_f = 0.36\text{--}0.38$ , eluent). This compound mixture was then subjected to *ca.* 15 further column chromatographic separations, which led to the isolation of five compounds with varying levels of purity. The first compound to be eluted (*ca.* 95% purity,  $^1\text{H}$  NMR analysis) had the same mass as the desired cyclophane **109e** (APCI(+)-LC-MS:  $m/z = 647$ ), but the complexity of the  $^1\text{H}$  NMR spectrum showed it to be a less symmetrical isomer. The presence of three AB systems with  $J = 8.9\text{--}9.3$  Hz indicated the presence of three unsubstituted K regions, which immediately suggested that the product may be the result of intramolecular McMurry coupling of dialdehyde **138e** or **139e**.



**Scheme 4.18** McMurry reaction of dialdehyde **108e**.

#### 4.2.9.2.1 Crystal structure of **145e**

Crystals suitable for X-ray crystallographic analysis of **145e** were obtained from dichloromethane / hexanes (Figure 4.13).<sup>‡</sup> Solution of the crystal structure revealed that the product was **145e**, which is the product of intramolecular McMurry coupling of dialdehyde **138e**. The angle between the best planes of the two pyrene systems is 51.29°, which appears to place the “internal” protons H<sub>x</sub> and H<sub>y</sub> (Scheme 4.18; **145e**) in the deshielding regions of the opposite aromatic systems. This is consistent with the observation that the signals for these two protons are observed at relatively low field ( $\delta$  8.62 and 8.59, unassigned). One of the bridge protons is also observed at unusually low field ( $\delta$  4.60), but it is not clear from the examination of models which one this might be. A final unusual feature of the <sup>1</sup>H NMR spectrum is that the alkene signals appear as an AB system at very low field ( $\delta$  8.20 and 8.03, unassigned,  $J = 10.8$  Hz). The origin of the low field shifts is unclear.

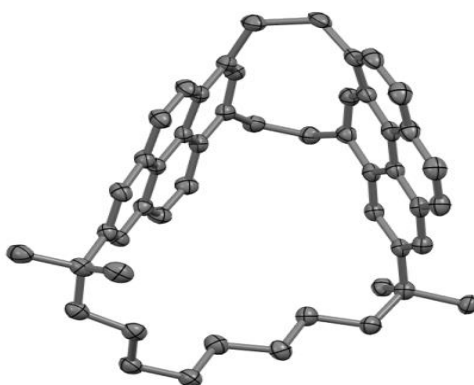


**Figure 4.13** Crystal structure of a single molecule in **145e**, with 50% probability ellipsoids. H-atoms, minor disorder components and solvent molecules omitted for clarity.

<sup>‡</sup> Data collection was performed by Dr. Paul Boyle, Chemistry Department, Western University, on Bruker APEX-II CCD diffractometer. Refinement and solution were performed by Dr. Louise N. Dawe, Chemistry Department, Wilfrid Laurier University.

The second compound to elute was found to be dihydroteropyrenophane **146e**, which was isolated as a *ca.* 80:20 mixture of **146e**:**145e** (Scheme 4.18). APCI(+)-LC-MS analysis of the orange solid showed strong peaks at  $m/z = 647$  and  $649$ , which is consistent with a mixture of **145e** and **146e**. The major peaks in the  $^1\text{H}$  NMR spectrum clearly pointed toward **146e**. The aromatic region consists of two K-region AX systems ( $J = 9.3\text{--}9.5$  Hz), a singlet and an AB system ( $J = 1.7$  Hz). Key signals in the aliphatic region contain are AA'BB'' system for the ethano unit and two 6H singlets for the two different types of methyl groups. The isolation of a dihydroteropyrenophane from a McMurry reaction had not been observed before. It would seem that cyclophanemonoene **109e** was generated as expected, but underwent valence isomerization and partial dehydrogenation under the conditions of its formation (THF, reflux). The lower level of strain in the [10](2,11)teropyrenophane framework compared to its lower homologs presumably allows for the central bond formation to occur in cyclophane **109e**, but the fact that this occurred under reductive conditions (VID reactions are typically performed under oxidative conditions) and at relatively low temperature (compared to  $>120$  °C) was somewhat surprising but not unprecedented<sup>27</sup>. The third compound to elute was teropyrenophane **103e**, but it was only observed (APCI(+)-LC-MS and  $^1\text{H}$  NMR analysis) as a minor component (*ca.* 0.1%) of a very small quantity of a mixture with **146e**.

The fourth compound to elute was the desired cyclophanemonoene **109e**, which was isolated in pure form in 12% yield. The  $^1\text{H}$  NMR spectrum closely resembled to

those of **109b-d**. For the sake of comparison (with **145e**), the internal proton of this compound is observed at  $\delta$  8.11.

#### 4.2.9.2.2 Identification and crystal structure of cyclophane **147**

The fifth and final compound to elute from the cluster of compounds was isolated in *ca.* 90% purity ( $^1\text{H}$  NMR analysis) and immediately provided some surprises. APCI(+)-LC-MS analysis showed a strong peak at  $m/z = 455$ , which corresponds to  $[\text{M}+1]^+$  of a [2.2]pyrenophanemonoene *without a long bridge*.  $^1\text{H}$  and  $^{13}\text{C}$  NMR analysis confirmed the absence of the long bridge. The  $^{13}\text{C}$  NMR spectrum contained 34 signals in the range of 119-136 ppm, which is consistent with two differently substituted pyrene systems ( $2 \times 16\text{C}$ ) and an alkene (2C). The aliphatic region showed just two signals for an ethano bridge. In the  $^1\text{H}$  NMR spectrum, the aromatic signals spanned a very broad range ( $\delta$  8.3-4.6) (Figure 4.14), which suggested that some of the aromatic protons sit

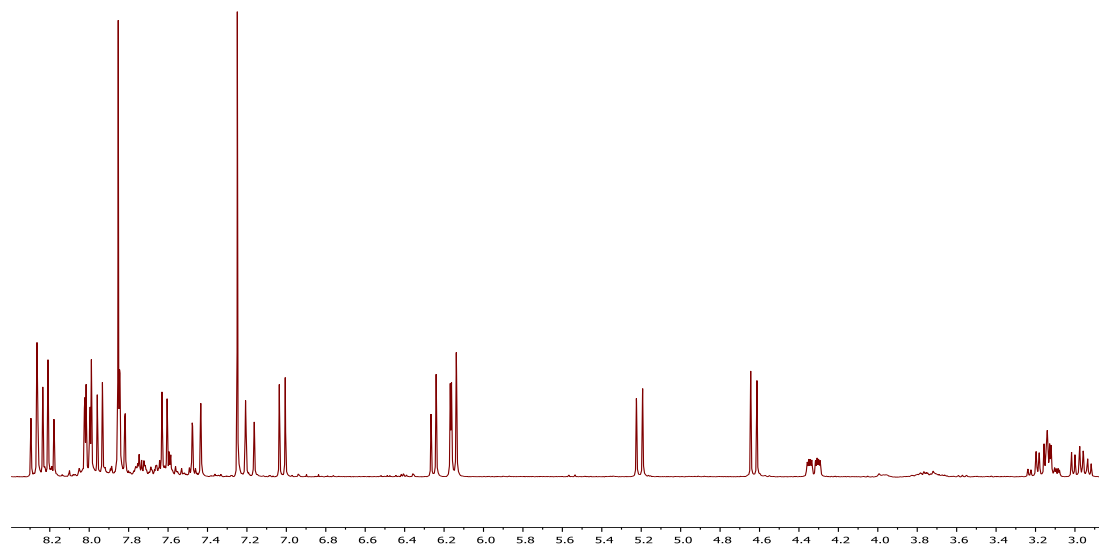


**Figure 4.14**  $^1\text{H}$  NMR spectrum of **147** (300 MHz,  $\text{CDCl}_3$ ).



deep within the shielding zone of the opposite pyrene system.

The absence of any ABC spin systems ruled out the possibility that the compound was the result of loss of the long bridge from either **109e** or **145e**. The observation of four AB systems with  $J = 7.7$ - $8.0$  Hz indicated that the two pyrene systems are 1,6 or 1,8 disubstituted. This being the case, then four *K*-region AB systems ( $J \approx 9.2$  Hz) should be observed. In fact, three are observed along with a 2H singlet, which could be an accidentally degenerate AB system. The structure of the compound was assigned as **147**, in which one ring is 1,6-disubstituted and the other is 1,8-disubstituted. If both rings have the same substitution pattern, then the molecule would be too symmetrical for the observed spectra. The structure of **147** was calculated<sup>§</sup> at the B3LYP/6-31-G(d) level of theory. The predicted  $^1\text{H}$  NMR shifts agree quite well with the observed chemical shifts ( $\Delta\delta = 0.01$ - $0.60$  ppm), especially the high-field-shifted signals for  $\text{H}_a$ ,  $\text{H}_b$ ,  $\text{H}_c$  and  $\text{H}_d$  on the 1,6-disubstituted pyrene system and  $\text{H}_o$  and  $\text{H}_p$  on the 1,8-disubstituted pyrene system (Figure 4.15).

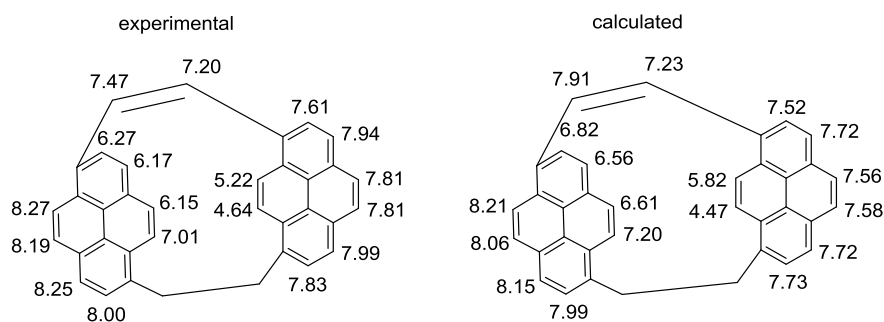
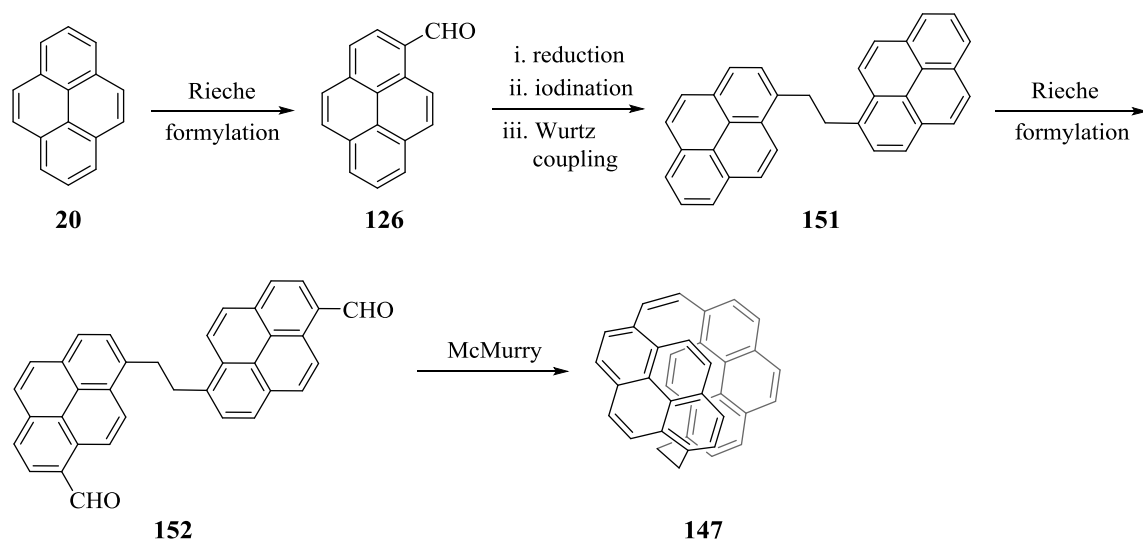


**Figure 4.15** Experimental and calculated  $^1\text{H}$  NMR data of compound **147**.

<sup>§</sup> Calculations were performed by Prof. Yuming Zhao, Chemistry Department, Memorial University.

It is more likely that **147** is the product of reactions of impurities rather than a product of the McMurry reaction of **108e** (or **138e** or **139e**). One possibility is that the incomplete removal of pyrene from the Friedel-Crafts alkylation reaction would result in the formation of pyrene-1-carboxaldehyde (**126**) in the first Rieche formylation (Scheme 4.19). If carried through the reduction, iodination and Wurtz coupling sequence, this would give rise to dipyren-1-ylethane **151**, formylation of which might afford dialdehyde **152** (among other isomers). Intramolecular McMurry reaction of **152** would afford **147**. Perhaps other [2.2]pyrenophanemonoenes were formed (from regioisomers of **152**), but none were isolated. It would be interesting to synthesize **147** and investigate both the formylation and subsequent McMurry reactions as a way to access **147** and related [2.2]pyrenophanes.



**Scheme 4.19** Plausible synthetic strategy for the formation of cyclophane **147**.

Crystals suitable for the X-ray crystallographic studies were obtained in dichloromethane / hexanes (Figure 4.16). The structure of the compound was confirmed as **147** which contains 1,6- and 1,8-disubstituted pyrene systems. For the less distorted C3-C18 pyrene the bend angle (taken as the angle formed between the planes containing atoms [C3, C4 and C18] and atoms [C11, C12 and C13]) was  $9.8^\circ$ , while for the C21-C36 pyrene system the bend angle (taken as the angle formed between the planes containing atoms [C21, C22 and C34] and atoms [C27, C28 and C29]) was  $44.5^\circ$ . The space group is centrosymmetric. Adjacent molecules in the packed unit cell have the opposite configuration and every second molecule is superimposable, but adjacent molecules are not (Figure 4.17). Furthermore, the close supramolecular C-H $\cdots$  $\pi$  interactions between the molecules lead to a chain-like arrangement (Figure 4.18).

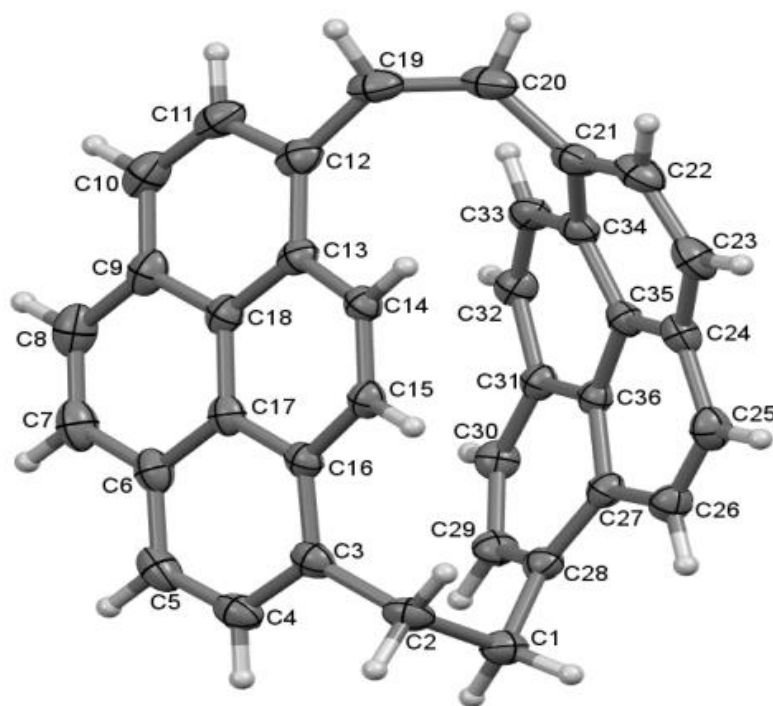


**Figure 4.16** Crystal structure of **147** represented by 50% probability ellipsoids.

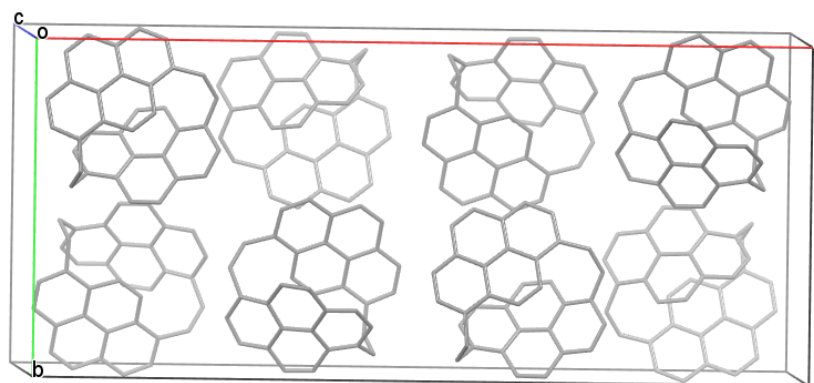


**Figure 4.17** Packed unit cell for **147**.

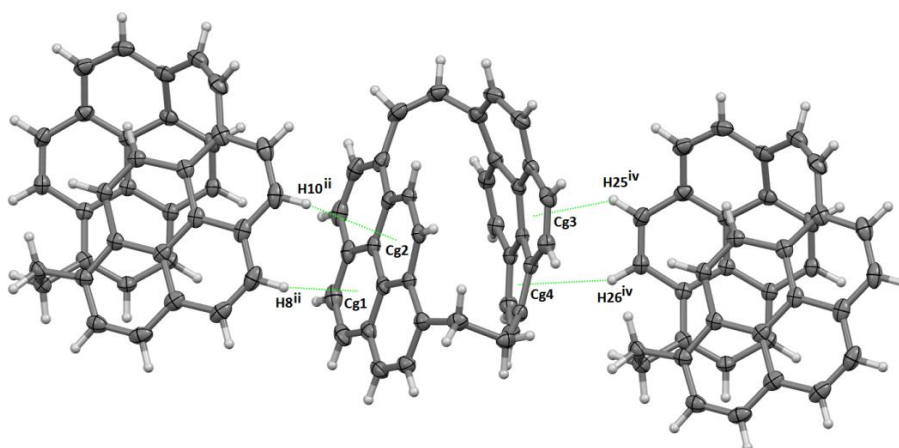


**Figure 4.18** C-H $\cdots\pi$  interactions for **147**. Symmetry operations: (i) =  $x, y, z$ ; (ii) =  $x, 1-y, \frac{1}{2}+z$ ; (iv)  $x, 2-y, z-1/2$ . Cg1, Cg2, Cg3 and Cg4 refer to ring centroids. 50% displacement ellipsoids.

A further compound was isolated from the column chromatography of the product obtained from the McMurry reaction of dialdehyde **108e**. It eluted considerably more slowly ( $R_f = 0.12$  (10% dichloromethane / hexanes)) than the cluster of compounds described above ( $R_f = 0.36$ - $0.38$ ). The aromatic region of the  $^1\text{H}$  NMR spectrum is spread out from  $\delta$  8.3 to 5.5 ppm and contains three *K*-region AB/AX systems ( $J = 8.9$ - $9.4$  Hz), two meta-coupled AB systems ( $J = 1.6$ - $1.9$  Hz), an AB system with  $J = 10.1$  Hz (likely an

alkene) and an AX system ( $J = 7.1$  Hz). The latter spin system manifests itself as two unusually high field doublets at  $\delta$  6.81 and 5.53. From this information, it appears as though the compound has two differently substituted pyrene systems, one of which has K-region substitution and the other of which does not (*cf.* **145e**). However, there are only 14 proton signals in the aromatic region, two of which most likely come from an alkene bridge. This leaves just 12 signals from the pyrene systems, which means that there is an additional substituent per pyrene system. The absence of any singlets in the aromatic region means that the additional substituents must be at the positions *ortho* to the alkene bridge. The  $^{13}\text{C}$  NMR spectrum contains two signals at  $\delta$  153.85 and 151.51, which is consistent with an *O*-substituted aromatic system (*cf.*  $\delta$  151-157 for the 1,*n*-dioxan[*n*](2,7)-pyrenophanes).<sup>28</sup> At this point, the highly unusual peroxy-bridge pyrenophane **148e** (Figure 4.19) was arrived at as a tentative structure. The corresponding diol was not considered due to the absence of OH signals in the  $^1\text{H}$  NMR spectrum and in consistency with the mass spectral data (see below).

MS analysis of the compound provided ambiguous results. The  $[\text{M}+1]^+$  peak for **148e** would be expected at  $m/z = 679$ . The APCI(+)-LC-MS spectrum of the compound showed a progression of peaks separated by 16 mass units, *i.e.*  $m/z$  (%) = 663 (2), 679 (11), 695 (8), 711 (100), 727 (100), 743 (7) (Figure 4.20top). Thus, the peak at  $m/z = 679$  is present, but relatively weak. By far the most intense peak was observed at  $m/z = 711$ , which corresponds to two additional O atoms. This would be consistent with the utterly bizarre structure **149e**,<sup>29</sup> which would not have been expected to form under the reaction conditions or survive multiple chromatographic separations. APPI-LC-MS showed the

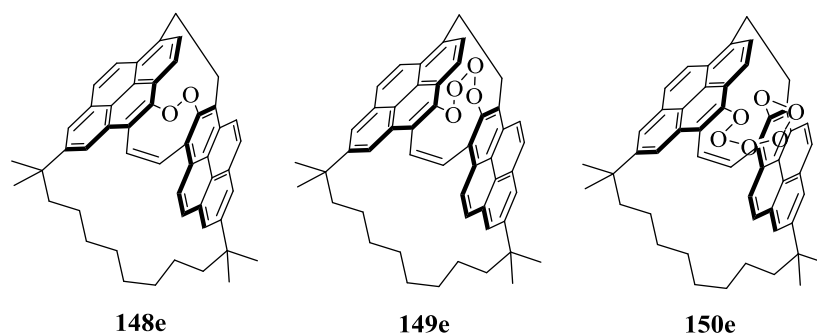


**Figure 4.19** Highly unusual polyoxa-bridged pyrenophanes **148e**, **149e** and **150e**.

same progression of peaks, but with different relative intensities:  $m/z = 663$  (2), 679 (19), 695 (2), 711 (49), 727 (11), 743 (100) (Figure 4.20 bottom). The base peak at  $m/z = 743$  corresponds to the ridiculous structure **150e**. APPI-HRMS analysis of the peaks at  $m/z =$

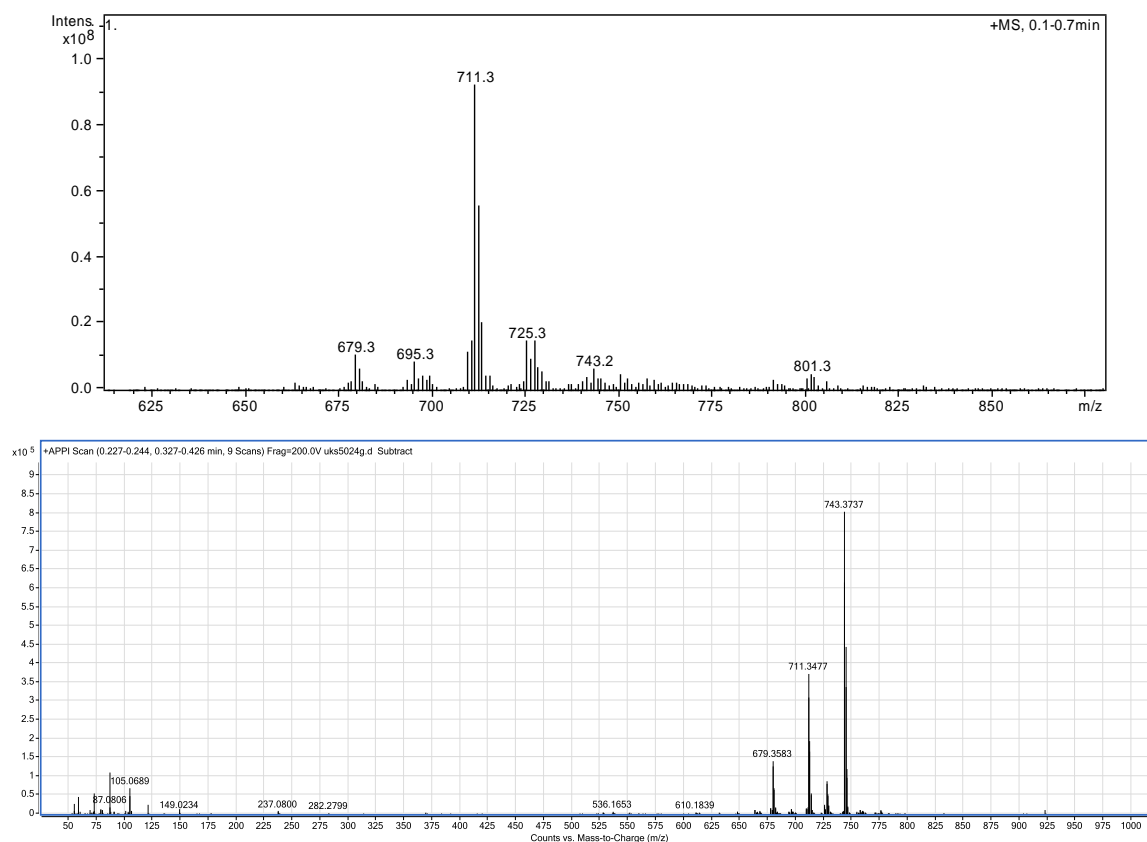


**Figure 4.20** Top) APCI(+)-LC-MS spectrum; bottom) APPI-LC-MS spectrum.

679 and  $m/z = 711$  match very well with the molecular formulae corresponding to protonated **148e** ( $C_{50}H_{47}O_2$ ,  $m/z = 679.3589$ , calc. 679.3581) and **149e** ( $C_{50}H_{47}O_4$ ,  $m/z = 711.3484$ , calc. 711.3472), respectively, but the peak at  $m/z = 743$  does not match **150e** ( $C_{50}H_{47}O_6$ ) within 20 ppm. As unappealing as the polyoxa bridged structures **148e**, **149e** and **150e** seem, no better structures that fit the spectroscopic data could be identified. Extensive examination of molecular models did not result in the identification of a structure that would fit the spectroscopic data, especially the high field AX system at  $\delta$  6.81 and 5.53 ( $J = 7.1$  Hz). Crystals suitable for X-ray crystallographic analysis could not be obtained. Thus, the identity of this compound remains unclear.

Returning to the series of  $[n.2.2](7,1,3)$ cyclophanemonoenes **109b-e**, the  $^1H$  NMR spectra are very similar, the only noteworthy difference being the change in the chemical shift of the internal protons through the series. This proton moves to higher field as the long bridge becomes shorter: **109b** ( $\delta$  7.62), **109c** ( $\delta$  7.65), **109d** ( $\delta$  7.81), **109e** ( $\delta$  8.05) (Figure 4.21). This may be related to a decrease in the bite angle between the two pyrene systems as the long bridge becomes shorter. The absorption spectra of the four cyclophanes are also very similar, but show a steady decrease in the intensity of the longest-wavelength feature (Figure 4.22).

#### 4.2.10 VID reaction leading to 103d

With all of the  $[n.2.2](7,1,3)$ pyrenophanes **109b-e** in hand, work aimed at the scale up of the final step of the synthesis (VID reaction to afford teropyrenophanes **109b-e**) was initiated. Since **109d** was the most abundant cyclophanemonoene, it was used for

preliminary scale-up work. The original small-scale synthesis of **103d** was performed on a 15 mg scale and delivered **103d** in 76% yield (Table 4.03, Entry 1). Directly scaling up this reaction to an 80 mg scale resulted in a substantial drop in yield to 45% (Table 4.03, Entry 2). A further drop in the yield (to 21%) was observed when the scale of the reaction was increased to 500 mg (Table 4.03, Entry 3).

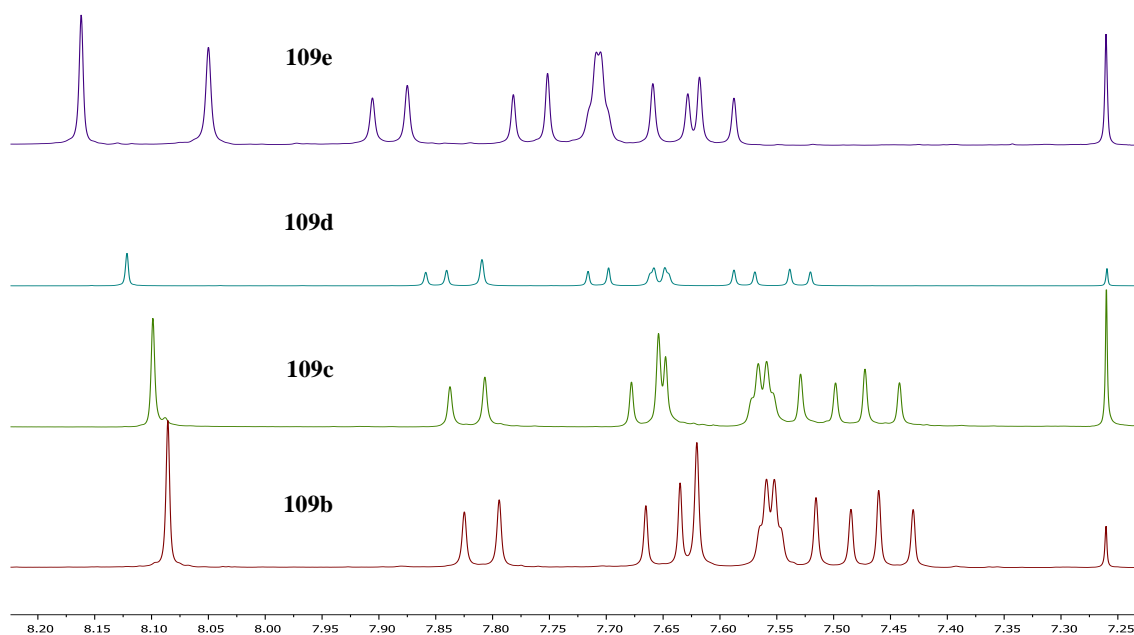


**Figure 4.21** Stacked  $^1\text{H}$  NMR spectra (aromatic region) of **109b-e** (300 MHz,  $\text{CDCl}_3$ ).

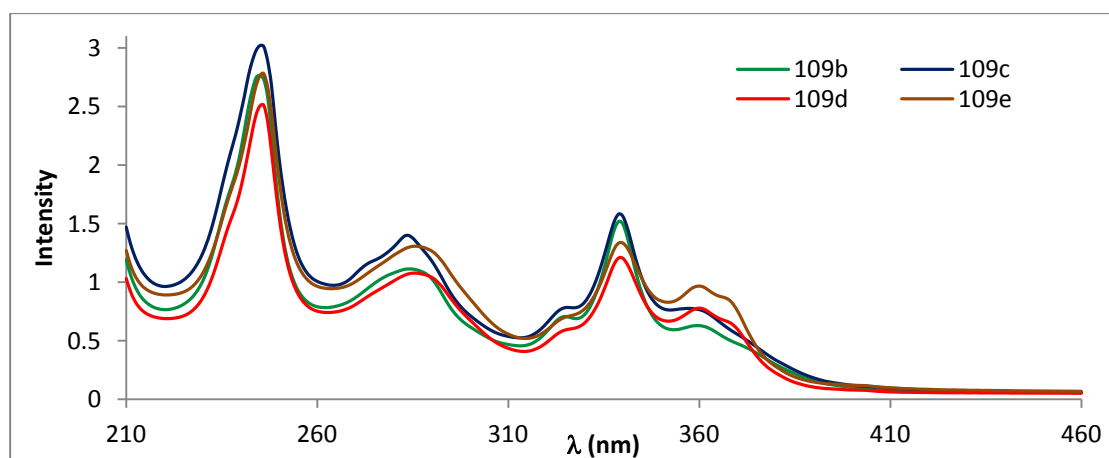
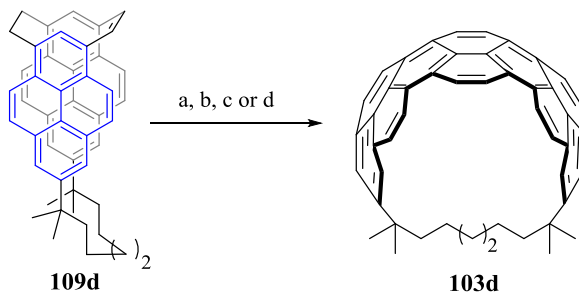


**Figure 4.22** Absorption spectra of cyclophanes **109b-e**.



**Table 4.03** Results of preliminary experiments on the scale-up of the VID reaction of **109d**.



entry	<b>109d</b> (mg)	conditions*	t (h)	DDQ (equiv.)	<b>103d</b> (%)
1	15	a	24	10	76
2	80	a	36	10	45
3	500	a	36	10	21
4	100	b	48	10	-
5	40	c	36	4	18
6	40	d	1	4	77
7	300	d	1	4	20

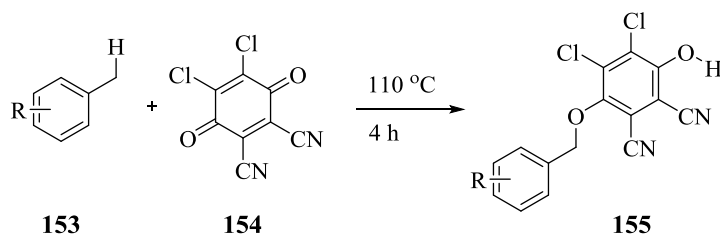
- \*a. DDQ, *m*-xylene, 130 °C
- b. DDQ, *p*-xylene, reflux
- c. DDQ, benzene, reflux
- d. DDQ, benzene, MW, 130 °C, 250 Watt

#### 4.2.10.1 Problems associated with VID reaction

At this point, it was clear that significant changes to the reaction would be required. A major drawback of the existing reaction was the need for a high-boiling solvent (*m*-xylene), which was not easily removed upon completion of the reaction. On the small scale, *m*-xylene was normally removed by blowing nitrogen gas over the still hot solution. Not only is this impractical on the large scale, but it also produces a highly concentrated hot reaction mixture, which may have a detrimental effect on the yield. In

an attempt to avoid the hot removal of the solvent, *p*-xylene was used as the solvent. The intention was to freeze the *p*-xylene (m.p. = 13.2 °C) upon completion of the reaction and extract the product with another solvent such as ethyl acetate. Unfortunately, the reaction did not show any meaningful progress after 48 h at 125 °C. (Table 4.03, Entry 4).

A second major problem was the large amount of DDQ (10 equiv.) that was required and the need to add in multiple portions (as a freshly-prepared solution) at regular intervals until the starting material was consumed (tlc analysis). Insight into why the reaction needed to be conducted in this fashion came from a recent paper by Batista *et al.*,<sup>30</sup> who reported that DDQ inserts into the benzylic C–H bond of methylated aromatic solvents such as toluene at temperatures greater than 110 °C (Scheme 4.20).

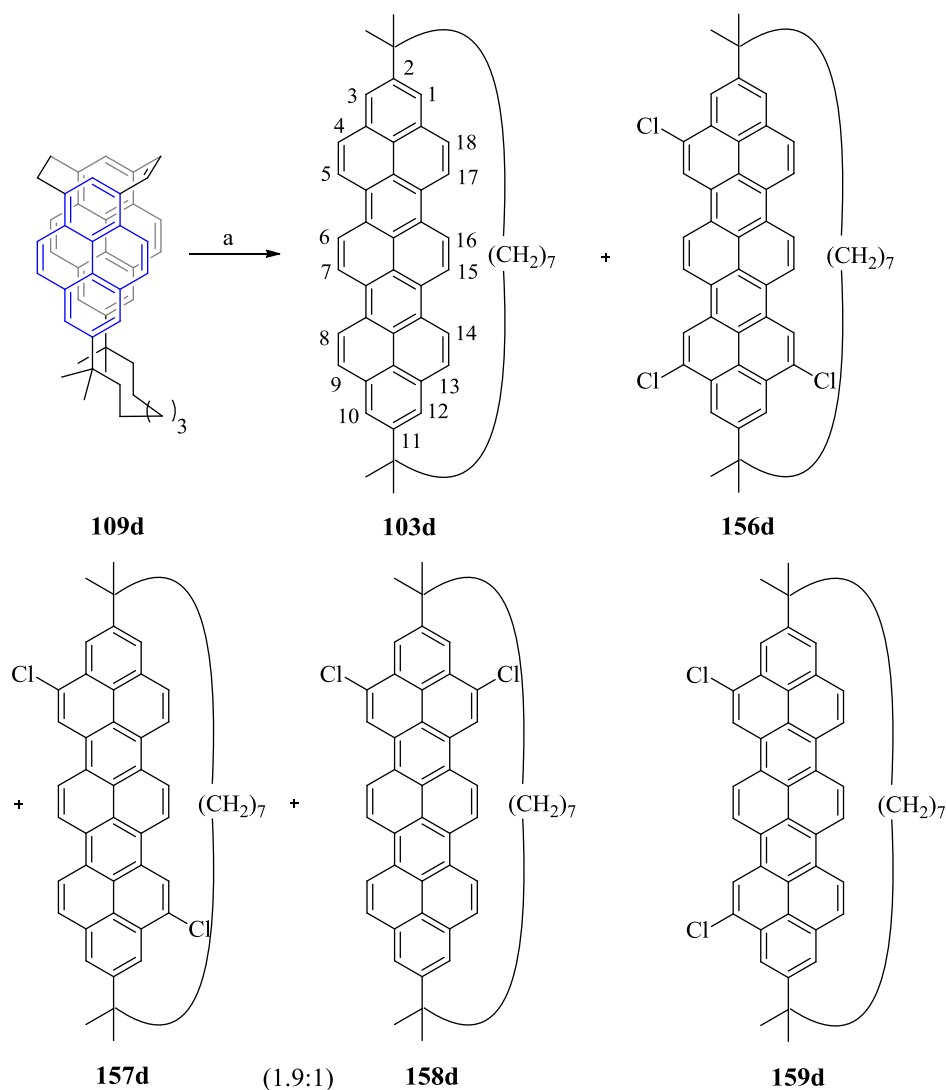


**Scheme 4.20** Reaction of methylated aromatic solvents with DDQ.

#### 4.2.10.2 DDQ as a chlorinating reagent

To avoid reaction between DDQ and the *m*-xylene, the use of chlorobenzene (b.p. = 131 °C) was considered, but ultimately not pursued because of anticipated problems with solvent removal on the large scale. Instead, benzene was investigated, despite its much lower boiling point (80 °C). In fact, benzene was initially used in the seminal report of the synthesis of **103c**, but the reaction was found to be sluggish.<sup>31</sup> Considering

that **103d** is less strained than **103c**, it was hoped that **103d** would form more easily. However, this was not the case. The use of benzene at reflux with 4.0 equiv. of DDQ afforded **103d** in just 18% yield after 36 h (Table 4.03, Entry 5). On the other hand, microwave irradiation of **109d** (40 mg scale) in benzene in the presence and DDQ (4.0 equiv.) produced **103d** in 77% yield (Table 4.03, Entry 6). Disappointingly, scaling this reaction up to a 300 mg scale resulted in a drastic drop in the yield of **103d** to 20% (Table 4.03, Entry 7). At the same time, tlc analysis showed the presence of two new spots that eluted faster ( $R_f$  (10% ethyl acetate / hexanes) = 0.45 and 0.42) than **103d** ( $R_f$  (10% ethyl acetate / hexanes) = 0.40). Isolation of the fastest moving spot afforded trichloroteropyrenophane **156d** in 27% yield (Scheme 4.21). APCI(+)-LC-MS analysis showed a base peak at  $m/z = 733$ , which corresponds to  $[M+1]^+$  for  $C_{39}H_{40}^{35}Cl_3$ . The predicted isotopic pattern for this molecular formula closely resembles the observed pattern in the range  $m/z = 733$ -738. APPI-HRMS analysis also showed a match with this formula (found 733.2162, calc. 733.2164). The aromatic region of the  $^1H$  NMR spectrum contained a total of thirteen protons, which is consistent with trisubstitution of the teropyrene system. Not all of the peaks could be assigned due to some overlap, but the observed signals were consistent with trichloride **156c**. The assignment of the regiochemistry was made in an analogous fashion to the corresponding tribromide, the details of which are presented in Chapter 5. Briefly, the low-field chemical shifts of H-3 ( $\delta$  7.95), H-10 ( $\delta$  8.01), H-12 ( $\delta$  8.01) compared to that of H-1 ( $\delta$  7.60) and the corresponding protons in **103d** ( $\delta$  7.53) are diagnostic for substitution at the 4, 9 and 13 positions of the teropyrene system. The observation of four methyl singlets ( $\delta$  1.45, 1.44,



**Scheme 4.21** Reagents and conditions: a) DDQ, benzene, microwave, 250 W, 120 °C, 1 h.

1.43, 1.39) is also consistent with this structure.

The second spot to be eluted was found to be a *ca.* 1.9:1 mixture of dichlorides **157d** and **158d**. APCI(+)-LC-MS analysis showed a base peak at  $m/z = 699$ , which corresponds to  $[M+1]^+$  for  $C_{39}H_{41}^{35}Cl_2$ . The predicted isotopic pattern for this molecular formula closely resembles the observed pattern in the range  $m/z = 699$ -703. APPI-HRMS

analysis also showed a match with this formula (found 699.2548, calc. 699.2537). The regiochemistry was easily assigned from the  $^1\text{H}$  NMR spectrum of the mixture. The major component **157d** exhibited an AB system ( $\delta$  7.87 and 7.52,  $J = 1.6$  Hz) for H-3/H-12 (low-field shifted) and H-1/H-10 (normal chemical shift), respectively. The isomeric dichloride **159d** would also be expected to exhibit this type of AB system, but the absence of three singlets elsewhere in the aromatic region ruled out this isomer. The minor component was identified as **158d** by virtue of the two singlets ( $\delta$  7.93 and 7.47) for H-1/H-3 (low-field shifted) and H-10/H-12 (normal chemical shift), respectively.

The observation of chlorination of the teropyrene system was very surprising because the source of the chlorine atoms could only have been DDQ or the corresponding hydroquinone. Upon consultation of the literature, very few reported examples of DDQ acting as a chlorinating agent were found,<sup>32</sup> most of which involve 2-arylpyridines and 2-arylpyrimidines under Pd catalysis. There does not appear to be any example of uncatalysed ring chlorination of an aromatic system using DDQ. As such, the extent of chlorination of **103d** is remarkable. Other intriguing aspects of this reaction are the selectivity for the 4,9,13,18 positions of the teropyrene system, the absence of dichloride isomer **159d** and the absence of a monochloride. Although no further work was done on this very unusual chlorination reaction, it certainly deserves further investigation. The results of bromination reactions of **103d** are presented in Chapter 5.

### 4.2.10.3 Modified conditions for the synthesis of **103d**

Rathore *et al.* reported the use of DDQ in 9:1 CH<sub>2</sub>Cl<sub>2</sub> / CH<sub>3</sub>SO<sub>3</sub>H at 0 °C and converted the *ortho*-diphenylbenzene system into triphenylene.<sup>33</sup> The conversion was complete in 5 min with only 2.0 equiv. of DDQ. Applying these conditions to **109d** resulted in the formation of **103d** in a very low yield (5%) (Table 4.04, Entry 1). An important note here is that the starting material **109d** was completely consumed. This contrasts all previous reactions, in which traces of **109d** were always observed by tlc analysis. Using Rathore's conditions no significant mobile spots other than **103d** were observed on tlc, which suggested that **103d** reacted further under the conditions of its

**Table 4.04** VID reaction conditions of cyclophanemonoene **109d**.

$  \begin{array}{c}  \text{CH}_3\text{SO}_3\text{H} \\  \text{DDQ (2.2 equiv.)} \\  \text{109d} \xrightarrow{\text{CH}_2\text{Cl}_2, \text{ t min}} \text{103d} \\  \text{temp}  \end{array}  $					
entry	109d (mg)	CH <sub>3</sub> SO <sub>3</sub> H (equiv.)	t (min)	temp (°C)	103d (%)
1	0.01	9:1 CH <sub>2</sub> Cl <sub>2</sub> / CH <sub>3</sub> SO <sub>3</sub> H	2	0	5
2	0.01	9.5:0.5 CH <sub>2</sub> Cl <sub>2</sub> / CH <sub>3</sub> SO <sub>3</sub> H	2	0	12
3	0.01	1	120	40	75
4	0.01	2	8	rt	88
5	0.10	2	10	rt	88
6	0.50	2	10	rt	88
7	1.04	2	10	rt	85
8	2.20	2	10	rt	83

formation. Since Rathore's conditions were designed to facilitate intramolecular Scholl reaction, it might be that **103d** underwent intermolecular Scholl reactions.

To minimize the postulated self-Scholl reaction of **103d**, the proportion of  $\text{CH}_3\text{SO}_3\text{H}$  in the solvent mixture was reduced by half (to 95:5, but still *ca.* 500 equiv. with respect to **109d**) (Table 4.04, Entry 2). The yield of **103d** improved to 12%, but was still very poor. A new green fluorescent spot running roughly half way between **103d** and baseline was also observed by tlc. The amount of  $\text{CH}_3\text{SO}_3\text{H}$  was then drastically reduced to 1.0 equiv. The reaction did show some small signs of progress at room temperature (tlc analysis), but was very sluggish. When the reaction was conducted at 40 °C for 2 h, **103d** was obtained in 75% yield (Table 4.04, Entry 3). With 2.0 equiv. of  $\text{CH}_3\text{SO}_3\text{H}$ , the reaction was completed at room temperature after 8 min and **103d** was isolated in 88% yield (Table 4.04, Entry 4). An important observation was that the spot for **103d** diminished rapidly if the reaction was not stopped as soon as **109d** had been fully consumed (tlc analysis). Up to this point, the reactions had been conducted on a 10 mg scale. Most gratifyingly, progressively increasing the scale of the reaction up to 2.2 g resulted in only a very slight reduction in yield (83%) (Table 4.04, Entries 5-8). In total, 3.84 g of teropyrenophane **103d** was synthesized using these conditions, 1.85 g of which was produced in a single experiment.

#### 4.2.10.4 Screening of reaction conditions for the conversion of **109c** to **103c**

With the optimized conditions in hand (DDQ (2.2 equiv.),  $\text{CH}_3\text{SO}_3\text{H}$  (2.0 equiv.),  $\text{CH}_2\text{Cl}_2$ , rt, 8-30 min depending on the scale), attention was turned to the conversion of

**109c** to **103c**. On a 5 mg scale, the starting material **109c** was fully consumed in 5 min, but the yield of **103c** was only 5% (Table 4.05, Entry 1). Tlc analysis showed the presence of minor amounts of some other mobile compounds, but their identity could not be determined at that time. This disappointing result hinted to that **103c** is more reactive than the less strained **103d** in the presence of DDQ and an acid. Accordingly, the amount of  $\text{CH}_3\text{SO}_3\text{H}$  was reduced to 1.5 equiv. (Table 4.05, Entry 2). The yield of **103c** improved to 22% and the same set of byproduct spots was observed by tlc (Table 4.05, Entry 2). Upon further reducing the amount of  $\text{CH}_3\text{SO}_3\text{H}$  to 1.0 equiv., the starting material **109c** was not completely consumed after 2 h of stirring and it was clear by tlc analysis that the product spot was decreasing in size. Performing the reaction at 40 °C afforded the product in 52% yield (Table 4.05, Entry 3). When 0.5 equiv. of  $\text{CH}_3\text{SO}_3\text{H}$  was used, only the starting material and product were observed after 2.5 h at 40 °C. Unlike all of the previous reactions, no byproduct spots were observed by tlc. Compound **103b** was obtained in 38% yield and the unreacted starting material was recovered (Table 4.05, Entry 4). Repeating this reaction at 70 °C (in  $\text{CHCl}_3$ ) marginally improved the yield of **103c** (44%), but the byproduct spots were again observed by tlc (Table 4.05, Entry 5).

In an attempt to disfavour the follow-on reactions of **103c**, the replacement of  $\text{CH}_3\text{SO}_3\text{H}$  ( $\text{p}K_{\text{a}} = -1.9$ )<sup>34</sup> with other (weaker) acids was investigated. Starting with  $\text{CF}_3\text{COOH}$  ( $\text{p}K_{\text{a}} = 0.2$ )<sup>35</sup> a series of experiments was performed keeping the amount of DDQ at 3.0 equiv. On a 5 mg scale, the reaction was sluggish when 2.2 equiv. of TFA was used and **103c** was isolated in 5% yield after a 4 h reaction (Table 4.05, Entry 6). Increasing the amount of  $\text{CF}_3\text{COOH}$  to 4.5 and then 7.5 equiv. improved the yield of **103c**



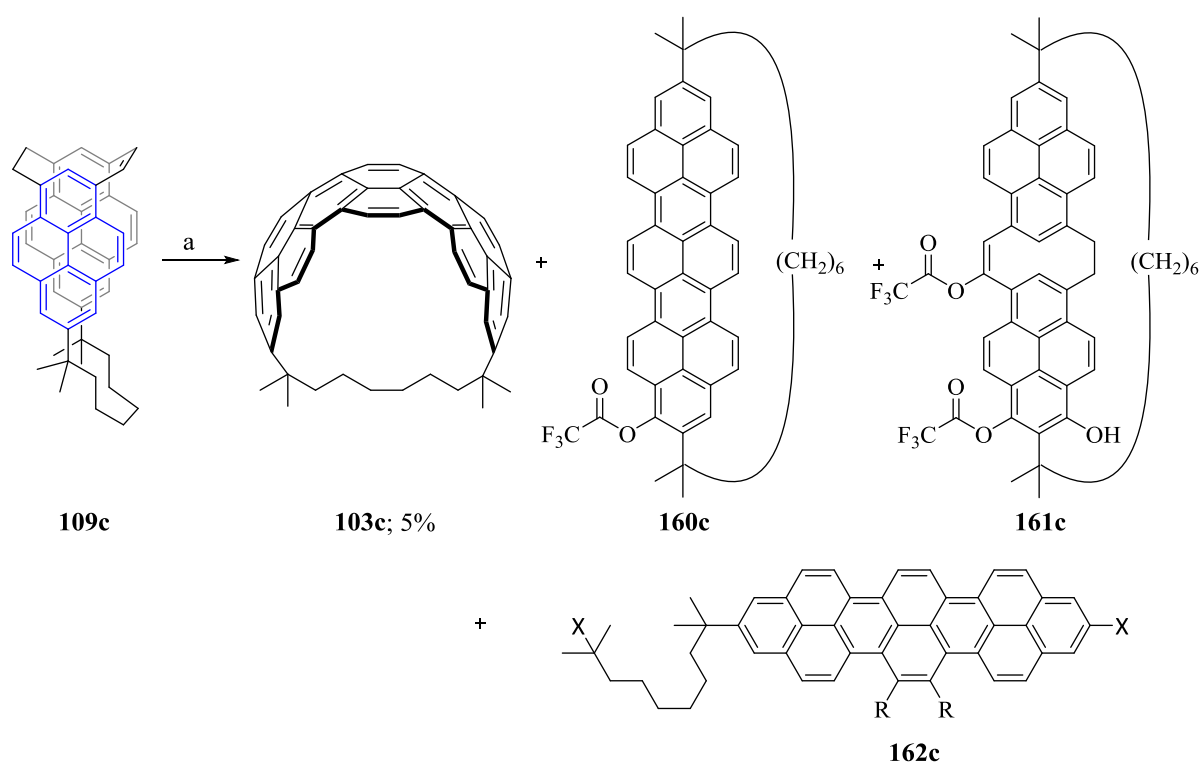
**Table 4.05** Optimization of the VID reaction of cyclophanemonoene **109c**.

$\text{109c} \xrightarrow[\text{solvent, t h}]{\text{acid DDQ (3.0 equiv.)}} \text{103c} + \text{unidentified products}$ temperature						
entry	109c (mg)	acid (equiv.)	solvent	t (h)	temp (°C)	103c (%)
1	5	CH <sub>3</sub> SO <sub>3</sub> H (2.0)	CH <sub>2</sub> Cl <sub>2</sub>	0.1	rt	5
2	50	CH <sub>3</sub> SO <sub>3</sub> H (1.5)	CH <sub>2</sub> Cl <sub>2</sub>	0.1	rt	22
3	50	CH <sub>3</sub> SO <sub>3</sub> H (1.0)	CH <sub>2</sub> Cl <sub>2</sub>	0.15	40	52
4	50	CH <sub>3</sub> SO <sub>3</sub> H (0.5)	CH <sub>2</sub> Cl <sub>2</sub>	2.5	40	38
5	50	CH <sub>3</sub> SO <sub>3</sub> H (0.5)	CHCl <sub>3</sub>	2.5	70	44
6	5	CF <sub>3</sub> CO <sub>2</sub> H (2.2)	CH <sub>2</sub> Cl <sub>2</sub>	4.0	rt	5
7	5	CF <sub>3</sub> CO <sub>2</sub> H (4.5)	CH <sub>2</sub> Cl <sub>2</sub>	1.5	rt	30
8	5	CF <sub>3</sub> CO <sub>2</sub> H (7.5)	CH <sub>2</sub> Cl <sub>2</sub>	0.5	rt	60
9	10	CF <sub>3</sub> CO <sub>2</sub> H (7.5)	CH <sub>2</sub> Cl <sub>2</sub>	0.5	rt	30
10	10	CF <sub>3</sub> CO <sub>2</sub> H (15.0)	CH <sub>2</sub> Cl <sub>2</sub>	0.1	rt	53
11	10	CF <sub>3</sub> CO <sub>2</sub> H (35.0)	CH <sub>2</sub> Cl <sub>2</sub>	0.1	rt	8
12	50	CF <sub>3</sub> CO <sub>2</sub> H (15.0)	CH <sub>2</sub> Cl <sub>2</sub>	0.1	0	21
13	50	CF <sub>3</sub> CO <sub>2</sub> H (15.0)	CH <sub>2</sub> Cl <sub>2</sub>	0.2	-30	15
14	50	CF <sub>3</sub> CO <sub>2</sub> H (15.0)	toluene	48.0	rt	-
15	50	CF <sub>3</sub> CO <sub>2</sub> H (15.0)	ethyl acetate	96.0	rt	-
16	10	CHCl <sub>2</sub> CO <sub>2</sub> H (15.0)	CH <sub>2</sub> Cl <sub>2</sub>	24.0	rt	5
17	10	CHCl <sub>2</sub> CO <sub>2</sub> H (30.0)	CH <sub>2</sub> Cl <sub>2</sub>	16.0	rt	10
18	10	CHCl <sub>2</sub> CO <sub>2</sub> H (45.0)	CH <sub>2</sub> Cl <sub>2</sub>	16.0	rt	16
19	100	CHCl <sub>2</sub> CO <sub>2</sub> H (0.5 mL)	CH <sub>2</sub> Cl <sub>2</sub> (9.5 mL)	1.0	rt	29
20	10	CH <sub>3</sub> CO <sub>2</sub> H (15.0)	CH <sub>2</sub> Cl <sub>2</sub>	24.0	rt	trace
21	10	CH <sub>3</sub> CO <sub>2</sub> H (0.5 mL)	CH <sub>2</sub> Cl <sub>2</sub> (0.5 mL)	12.0	50	10
22	10	CH <sub>3</sub> CO <sub>2</sub> H (0.5 mL)	-	48.0	50	-
23	10	<i>p</i> -TsOH (1.0)	CH <sub>2</sub> Cl <sub>2</sub>	12.0	rt	trace

to 30% and 60%, respectively (Table 4.05, Entries 7-8). However, the yield of **103c** dropped back to 30% when the reaction scale was increased to 50 mg (Table 4.05, Entry 9). The yield improved to 53% when the amount of CF<sub>3</sub>COOH was increased to 15 equiv. (Table 4.05, Entry 10), but then fell sharply to 8% when 35 equiv. were employed (Table 4.5, Entry 11). With 15 equiv. of CF<sub>3</sub>COOH, lowering the temperature of the reaction to 0 °C and to –30 °C resulted in a steady decrease in yield to 21% and 15%, respectively (Table 4.05, Entries 12-13). Curiously, the use of toluene or ethyl acetate as the solvent resulted in no reaction (Table 4.05, Entries 14-15).

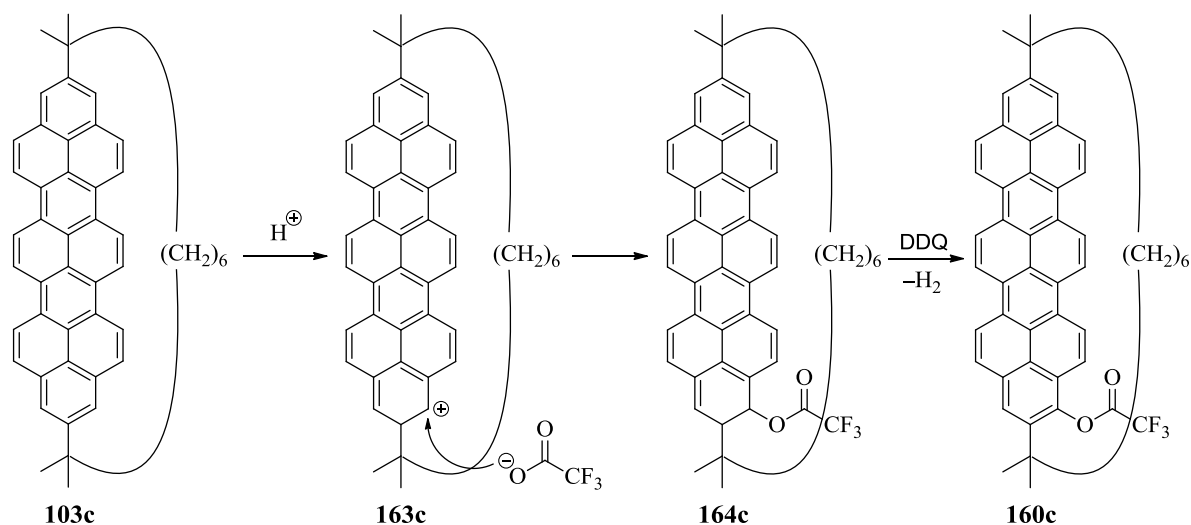
From the reactions described in Table 4.05, Entries 8-13, three common byproducts were observed all of which eluted more slowly than **103c** ( $R_f = 0.33$ , 10% ethyl acetate / hexanes). These byproducts were isolated by column chromatography. APCI(+)-LC-MS analysis of the first byproduct to elute ( $R_f = 0.28$ ) showed a base peak at  $m/z = 729.3$ , which corresponds to  $[M+1]^+$  of a trifluoroacetoxy substituted derivative of **103c**. To confirm the (unexpected) presence of a trifluoroacetoxy group, the <sup>19</sup>F NMR spectrum was recorded and a singlet at  $\delta -74.22$  was indeed observed. This chemical shift is typical for a trifluoroacetate group (*cf.* CF<sub>3</sub>CO<sub>2</sub>H,  $\delta -76.55$ ).<sup>36</sup> The aromatic region of the <sup>1</sup>H NMR spectrum contains six *K*-region AB/AX systems ( $J = 9.4$ - $10.1$  Hz), a *meta*-coupled AB system ( $J = 1.7$  Hz) and singlet. The only point of substitution of **103c** that would give such a collection of signals is the position adjacent to the bridge. Thus the structure of the byproduct was assigned with reasonable confidence as **160c** (Scheme 4.22). The yield of **160c** could then be calculated as 9%. The amount of material (*ca.* 1 mg) was insufficient for the acquisition of meaningful two-dimensional spectra, so the

structural assignment could not be made with complete confidence. The trifluoroacetoxy group obviously comes from  $\text{CF}_3\text{CO}_2\text{H}$  and a possible mechanism is protonation at the bridgehead carbon atom to give cation **163c**, followed by addition of trifluoroacetate anion to give **164c** and dehydrogenation would then lead to **160c** (Scheme 4.23). Multiple other sites of protonation of **109c** in a similar fashion could then also lead to **161c** (Scheme 4.22).



**Scheme 4.22** Byproducts formed in the presence of  $\text{CF}_3\text{CO}_2\text{H}$ ; *Reagents and conditions*: a)  $\text{CF}_3\text{CO}_2\text{H}$ , DDQ,  $\text{CH}_2\text{Cl}_2$ , 6 min, rt.

APCI(+)-LC-MS analysis of the second byproduct to elute ( $R_f = 0.12$ ) showed a base peak at  $m/z = 861$ , which was eventually found to match with a derivative of the starting cyclophanemonoene **109c** that bears two trifluoroacetoxy groups and one OH



**Scheme 4.23** Mechanism for the formation of compound **160c**.

group. The compound exhibited green fluorescence similar to **103c**. The relatively clean  $^1\text{H}$  NMR spectrum shows several features that are consistent with this structure, including a set of multiplets at  $\delta$  3.85-3.10 saturated bridging unit (ethano bridge), a singlet at  $\delta$  5.68 (phenolic OH) and a sharp high-field singlet at  $\delta$  3.94 (vinyl ether). A low-field doublet ( $J = 1.9$  Hz) at  $\delta$  8.18 is indicative of a pair of *meta*-coupled protons and singlets at  $\delta$  7.56 and 7.21 are consistent with two different internal protons. Based on these observations, one possible structure is **161c**, but numerous other possibilities exist. The OH group presumably comes from the hydrolysis of a trifluoroacetoxy group.

The third byproduct to elute ( $R_f = 0.03$ ) exhibited a base peak in its APCI(+)-LC-MS spectrum at  $m/z = 647$ , which has not yet been matched with any reasonable structure. The aromatic region of the  $^1\text{H}$  NMR spectrum ranges from  $\delta$  9.1 to 7.4 ppm and is well-resolved. Five *K*-region AB/AX spin systems are present ( $J = 9.5$ -10.1 Hz) as well as two *meta*-coupled AB systems ( $J = 1.7$ -2.0 Hz). Not much information could be obtained

from the aliphatic region due to relatively strong signals for “grease”. It may be that the byproduct is a di-substituted compound, such as **162c** (Scheme 4.22). A conclusive structural assignment could not be made.

The conversion of **109c** into teropyrenophane **103c** was also achieved using DDQ in conjunction with even weaker acids, but the results were not as good as with  $\text{CF}_3\text{CO}_2\text{H}$ . Teropyrenophane **103c** was obtained in 5%, 10%, 16% and 29% yield when 15, 30, 45 and >500 equiv. of dichloroacetic acid ( $\text{p}K_{\text{a}} = 1.29$ )<sup>37</sup> were used (Table 4.05, Entries 16-19). Two common byproduct from all of these reactions were collected. The first one showed a strong peak at  $m/z = 747$  in its APCI(+)-LC-MS spectrum, which corresponds (including the isotopic pattern) to a dichloroacetoxy-substituted derivative of **109c** (*e.g.* **65c**) (Figure 4.23). The  $^1\text{H}$  NMR spectrum was poorly resolved and provided little useful information.

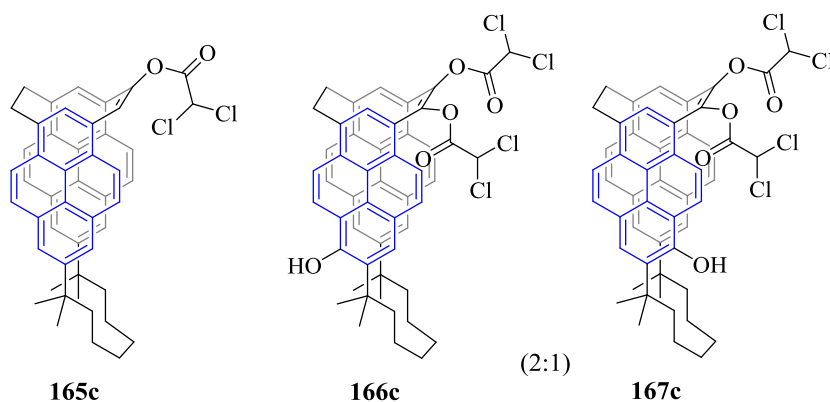


**Figure 4.23** Possible byproducts of the VID reaction of **109c** in the presence of  $\text{Cl}_2\text{CHCOOH}$ .

APCI(+)-LC-MS analysis of the second byproduct to elute ( $R_{\text{f}} = 0.12$ ) showed a base peak at  $m/z = 891$ , which fits a derivative of the starting cyclophanemone **109c**

bearing two dichloroacetoxy groups and one OH group (*cf.* **166c**). The  $^1\text{H}$  NMR spectrum is well-resolved and indicates the presence of two isomers in a *ca.* 2:1 ratio. The spectra of the two isomers are similar. The major difference between them and that of **165c** is the presence of two  $-\text{CHCl}_2$  singlets ( $\delta$  6.12 and 6.06 for the major isomer;  $\delta$  6.10 and 6.09 for the minor isomer) and the absence of vinyl ether singlets. Two possible structures are **166c** and **167c**.

Conversion to **103c** was observed even in the presence of acetic acid ( $\text{p}K_{\text{a}} = 4.76$ ).<sup>38</sup> Teropyrenophane **103c** was isolated in 10% yield when 1:1  $\text{CH}_2\text{Cl}_2$ : $\text{CH}_3\text{COOH}$  was used at rt. Also, **109c** was recovered in 78% yield. Tlc analysis showed only spots corresponding to **109c** and **103c** (Table 4.05, Entry 21). Cyclophanemonoene **109c** was found to have very poor solubility in pure acetic acid and hence no conversion to **103c** was observed (Table 4.05, Entry 22). Surprisingly, when the stronger acid *p*-TsOH was used, only trace amounts of **103c** were observed and **109c** was recovered in 76% yield (Table 4.05, Entry 23).

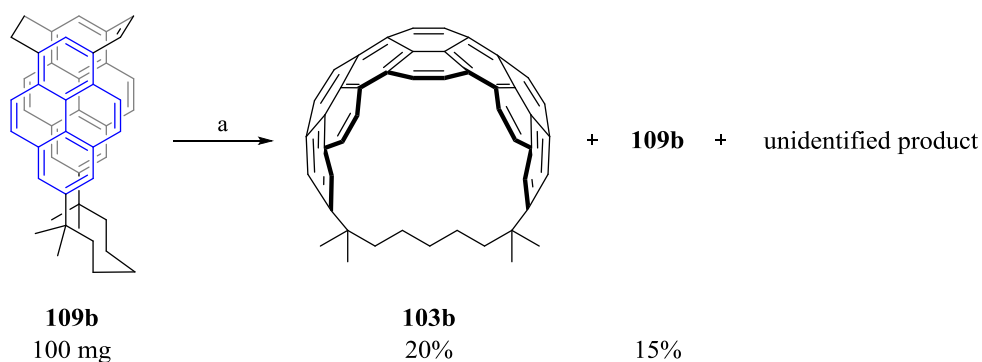
So far, the best result observed to generate **1c** was when 15.0 equiv. of TFA was used (Table 4.05, Entry 10). Therefore by fixing these reaction conditions, the oxidizing agent DDQ was replaced with other oxidizing agents such as *o*-chloranil, *p*-chloranil and benzoquinone (Table 4.06, Entries 1-4). Only *p*-chloranil showed good activity with TFA and formed **1b** in 55% yield after 96 h (Table 4.06, Entry 1). No increase in the conversion was observed even after heating the reaction at 40 °C for 3 days (Table 4.06, Entry 2). Therefore, at this stage DDQ still appears to be the best among the oxidizing agents tested. Further research of exploring the scale-up of **1c** is currently in progress.

**Table 4.06** Optimization of the VID reaction conditions of cyclophanemonoene **109c**.

$\text{109c} \xrightarrow[\text{CH}_2\text{Cl}_2, \text{ t h}]{\text{CF}_3\text{CO}_2\text{H} \text{ oxidant (2.2 equiv.)}} \text{103c}$ <p style="text-align: center;">temp</p>					
entry	109c (mg)	oxidant	t (h)	temp (°C)	103c (%)
1	0.01	<i>o</i> -chloranil	96	rt	55
2	0.01	<i>o</i> -chloranil	72	72	55
3	0.01	<i>p</i> -chloranil	48		complex mixture
4	0.01	1,4-benzoquinone	96		-

#### 4.2.10.5 Issues during the VID reaction of 109b to 103b

The scale-up of cyclophanemonoene **109b** was also examined using DDQ / CH<sub>3</sub>SO<sub>3</sub>H (1.0 equiv.) at 40 °C for 2 h (the best conditions for the conversion of **109c** to **103c**). Only 20% of **103b** was isolated along with some unreacted starting material **109b** (15%) (Scheme 4.24). Cyclophane **109b** was not completely consumed, even after increasing the amount of CH<sub>3</sub>SO<sub>3</sub>H from 1.0 equiv. to 3.5 equiv. As with **103c**, it was evident from the tlc analysis that, the teropyrenophane **103b** was reactive under the conditions of its formation. A green fluorescent byproduct spot, which was observed below the product spot, was also observed to grow initially and then diminish in size after a certain point in the reaction (tlc analysis). The identification of superior conditions for the conversion of **109b** to **103b** has not yet been accomplished, but based on the experience with **103c**, it seems likely that further work will achieve this goal.



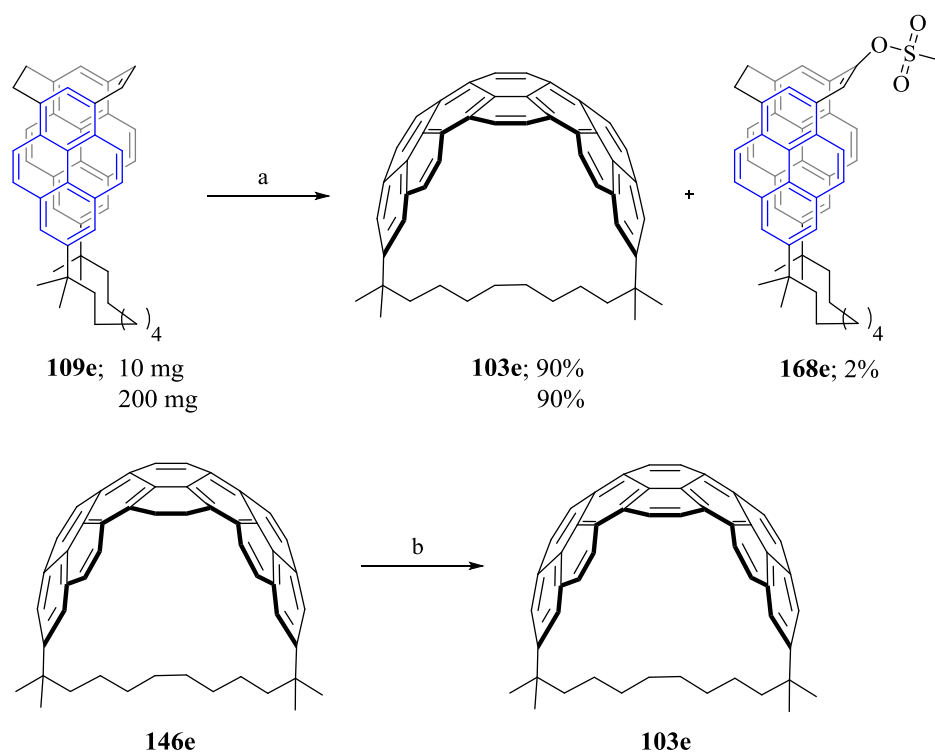
**Scheme 4.24** Conversion of **109b** to **103b**; *Reagents and conditions*: a. DDQ (2.2 equiv.),  $\text{CH}_3\text{SO}_3\text{H}$  (1.0–3.5 equiv.),  $\text{CH}_2\text{Cl}_2$ , 30 min, 40 °C.

#### 4.2.10.6 VID reaction of **109e** to **103e**

When cyclophanemonoene **109e** was subjected to reaction with 6.0 equiv. of  $\text{CH}_3\text{SO}_3\text{H}$  and 3.0 equiv. of DDQ, teropyrenophane **103e** was obtained in 90% yield on a 10 mg scale. The same yield was observed for **103e** (90%) when the reaction was repeated on a 200 mg scale of **109e** (Scheme 4.25). A small amount of byproduct **168e** (2%) was also isolated. The structure of **168e** was determined by NMR and MS experiments along the lines of those described earlier. Dihydroteropyrenophane **146e** that was obtained during the McMurry reaction of **108e** was also conveniently converted to **103e** using 3.0 equiv. of  $\text{CH}_3\text{SO}_3\text{H}$  and 1.5 equiv. of DDQ (Scheme 4.25).

Considering how nicely the reaction leading to **103d** could be scaled up, there is cause for optimism that the reaction leading to **103e** will also behave in this way.





**Scheme 4.25** *Reagents and conditions:* a)  $\text{CH}_3\text{SO}_3\text{H}$  (6.0 equiv.), DDQ (3.0 equiv.),  $\text{CH}_2\text{Cl}_2$ , 40 min, rt; b)  $\text{CH}_3\text{SO}_3\text{H}$  (3.0 equiv.), DDQ (1.5 equiv.),  $\text{CH}_2\text{Cl}_2$ , 30 min, rt.

#### 4.2.10.6.1 Crystal structure of [10](2,11)teropyrenophane

Crystals suitable for the X-ray crystallographic studies of **103e** were obtained from an ethyl acetate / hexanes solution (Figure 4.24). Determination of the crystal structure of **103e**<sup>◇</sup> added a new member to the set of crystals structures **103b-d**. The end-to-end bend angle ( $\theta_{\text{tot}}$ ) for the teropyrene system in **103e** is  $145.2^\circ$  (whereas the  $\theta_{\text{tot}}$  for **103b** =  $177.9^\circ$ , **103c** =  $169.0^\circ$  and **103d** =  $154.3^\circ$ ). As expected, in moving from **103b** to **103e**,  $\theta_{\text{tot}}$  decreases by steps of *ca.*  $10^\circ$  ( $10.9^\circ$ ,  $12.7^\circ$  and  $9.1^\circ$ ). As seen in the other

<sup>◇</sup> Data collection was performed by Dr. Paul Boyle, Chemistry Department, Western University, on a Bruker APEX-II CCD diffractometer. Refinement and solution were performed by Dr. Louise N. Dawe, Chemistry Department, Wilfrid Laurier University.

teropyrenophanes **103b-d**, the bend angle of the central pyrene system ( $\theta_2 = 75.6^\circ$ ) in **103e** is larger than those of the two flanking pyrene systems ( $\theta_1 = 56.7^\circ$  and  $\theta_3 = 50.7^\circ$ ) but the differences are smaller. Nevertheless, the teropyrene system has an elliptical profile rather than a semi-circular one.



**Figure 4.24** X-ray crystal structure of **103e**; 30% probability displacement ellipsoids.

In the crystal, molecules of **103b** are arranged (similar to **103b**) in an alternating up-down fashion along a two-fold screw axis that is parallel to the *b* axis (Figure 4.25). This creates columns with small channels, which are filled with solvent molecules (Figure 4.26). Adjacent columns are rotated by about  $90^\circ$  with respect to one another such that the centroid-to-centroid separations for the planes defined by C19, C21, C24 and C26 and its symmetry related (1-*x*, 1-*y*, 1-*z*) equivalent is 3.717 Å (Figure 4.27).

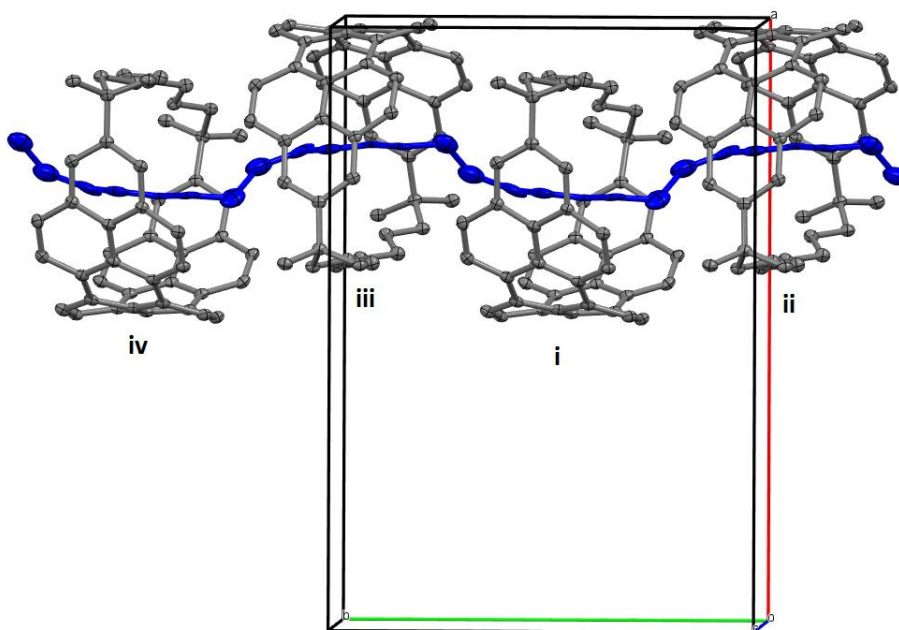


**Figure 4.25** A single solvent channel, illustrating the disordered hexane molecules (each are modeled at  $\frac{1}{2}$ -occupancy in the asymmetric unit, and represented in blue for emphasis). Symmetry operations: (i) =  $x, y, z$ ; (ii) =  $3/2-x, y-1/2, z$ ; (iii)  $3/2-x, \frac{1}{2}+y, z$ ; (iv)  $x, 1+y, z$ .

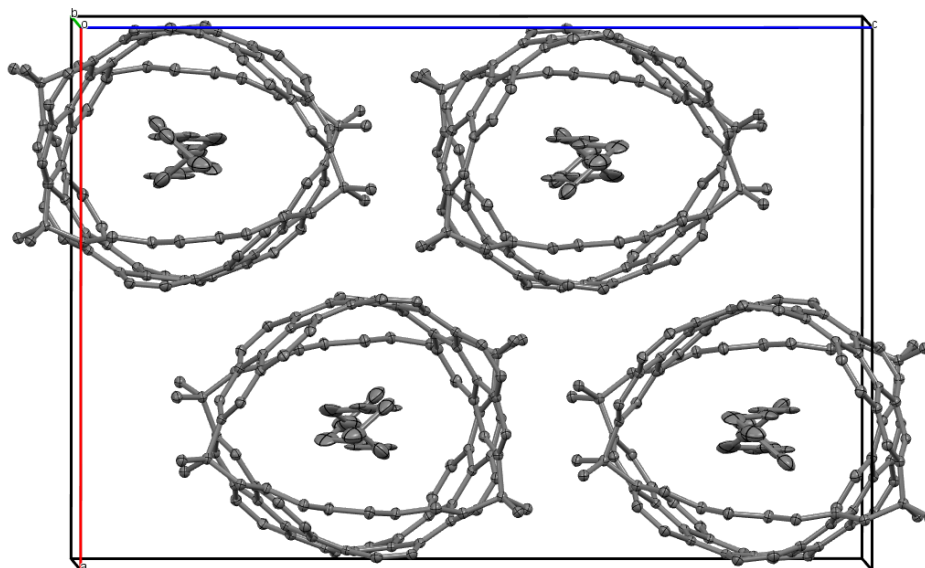


**Figure 4.26** Packed unit cell showing hexane solvent channels threaded through the **103e** molecules, running parallel to the b-axis.

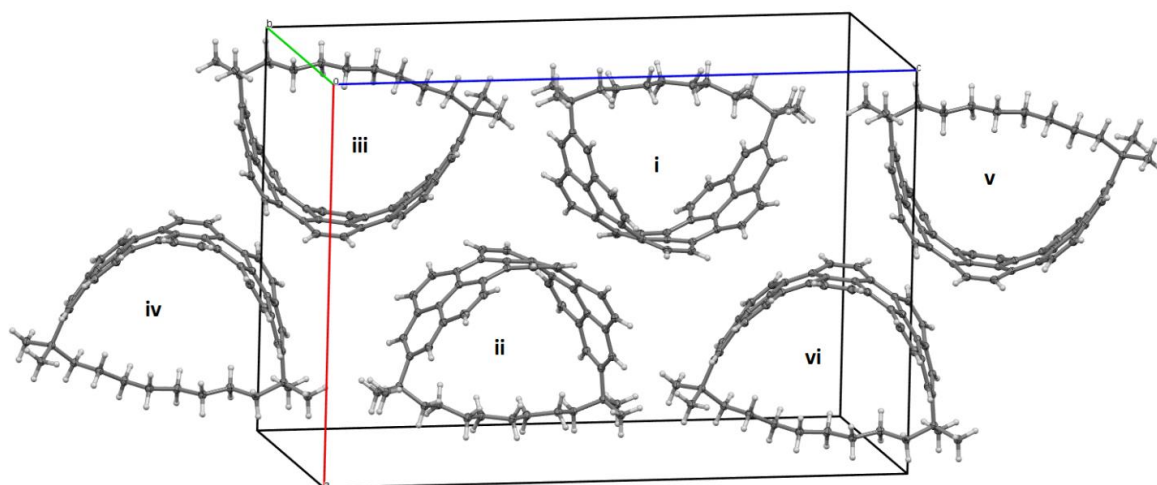


**Figure 4.27** Close pair-wise  $\pi$ - $\pi$  contacts in **103e**. Symmetry operations: (i) =  $x, y, z$ ; (ii) =  $1-x, 1-y, 1-z$ ; (iii) =  $1-x, \frac{1}{2}+y, \frac{1}{2}-z$ ; (iv) =  $x, \frac{3}{2}-y, z-\frac{1}{2}$ ; (v) =  $1-x, y-\frac{1}{2}, \frac{3}{2}-z$ ; (vi) =  $x, \frac{1}{2}-y, \frac{1}{2}+z$ .

With regard to strain energy (*SE*), the structures of teropyrenophanes **103a-f** were calculated at the B3LYP/cc-pVTZ level of theory (Figure 4.28). *SEs* were estimated by B3LYP/cc-pVTZ level of theory. Interestingly, the amount of *SE* in the bridge remains more or less constant (3-5 kcal/mol) as the bridge becomes shorter. However, the amount of *SE* per methylene group does increase steadily. The teropyrenophane **103f** is calculated to have 37.5 kcal/mol of *SE* and it increases quite steadily in ~9 kcal/mol increments with each removal of a  $\text{CH}_2$  group up to 80.2 kcal/mol for **103a**. Considering that [5]CPP was calculated to have 119 kcal/mol of *SE*, the total *SE* of 80 kcal/mol in **103a** gives some hope that this compound will eventually be synthesized.

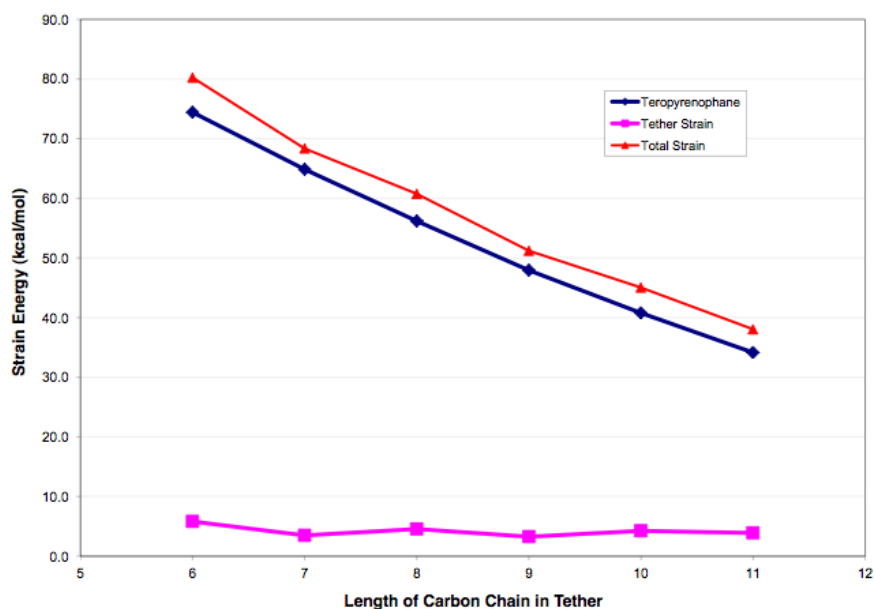


**Figure 4.28** Strain energy (*SE*) in teropyrenophanes **103a-f**.

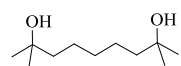
### 4.3 Conclusions

A variety of problems were encountered during the scale up of the synthesis of a series of  $[n](2,11)$ teropyrenophanes **103a-e**. Consequently many modifications to the existing Wurtz / McMurry strategy had to be made. The most important developments were 1) the development of an *in-situ* chlorination / Friedel-Crafts reaction leading to **96b-e** on a 35-40 g scale and 2) the development of an *in-situ* iodination / Wurtz coupling reaction leading to **107b-e** on a 2-25 g scale. The greatest challenges were faced during the conversion of **109b-e** to teropyrenophanes **103b-e**. Each reaction behaved differently and specific reaction conditions for each reaction needed to be found. Ultimately, **103b** was synthesized on up to 20 mg scale and the overall yield of **103b** was 1.2%. Teropyrenophane **103c** was synthesized on up to 26 mg scale and the overall yield of **103c** was 0.5%. The most well-behaved series was the one with the 9-atom bridge, i.e.

leading to teropyrenophane **103d**. This cyclophane was synthesized on up to 1.85 g scale and the overall yield of **1d** was 3.6%. Finally, the synthesis of **103e** was achieved for the first time. It was obtained in 1.6% overall yield over 8 steps.

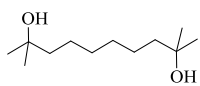
## 4.4 Experimental section

### 2,8-Dimethyl-2,8-nonanediol (**94b**)



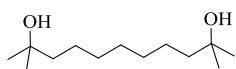
A solution of dimethyl pimelate (**93b**) (30.15 g, 158 mmol) in THF (150 mL) was added dropwise over a period of 1.5 h to a stirred  $-15\text{ }^{\circ}\text{C}$  solution of methylmagnesium bromide (3.0 M, 175.5 mL, 795 mmol) in THF (175 mL). After the addition was complete, the reaction mixture was heated at reflux for 17 h and the resulting white cake was cooled to  $0\text{ }^{\circ}\text{C}$ . The white cake was neutralized by the slow addition (caution: highly exothermic!) of saturated ammonium chloride solution (400 mL) with vigorous stirring. As much of the THF as possible was removed under reduced pressure and the resulting white turbid aqueous mixture was diluted with water (500 mL) and extracted with dichloromethane ( $3 \times 500\text{ mL}$ ). The combined organic layers were dried over  $\text{Na}_2\text{SO}_4$ , filtered and concentrated to afford **94b** (27.61 g, 92%) as a white powder:  $R_f = 0.19$  (50% ethyl acetate / hexanes); m.p.  $71.3\text{--}72.1\text{ }^{\circ}\text{C}$ ;  $^1\text{H}$  NMR (300 MHz,  $\text{CDCl}_3$ )  $\delta$  2.03 (s, 2H), 1.50–1.27 (m, 10H), 1.98 (s, 10H);  $^{13}\text{C}$  NMR (75 MHz,  $\text{CDCl}_3$ )  $\delta$  70.89, 43.85, 30.62, 29.14, 24.25; LCMS (CI(-))  $m/z$  187  $[\text{M}-\text{H}]^-$ ; HRMS (EI(+)) calculated for  $\text{C}_{11}\text{H}_{25}\text{O}_2$  ( $[\text{M}+\text{H}]^+$ ) 189.1855, found 189.1849.

### 2,9-Dimethyl-2,9-decanediol (**94c**)



A solution of dimethyl suberate (**93c**) (30.02 g, 148 mmol) in THF (150 mL) was added dropwise over a period of 1.5 h to a stirred 0 °C solution of methylmagnesium bromide (3.0 M, 165.2 mL, 742 mmol) in THF (175 mL). After the addition was complete, the reaction mixture was heated at reflux for 17 h and the resulting white cake was cooled to 0 °C. The white cake was neutralized by the slow addition (caution: highly exothermic!) of saturated ammonium chloride solution (400 mL) with vigorous stirring. As much as the THF as possible was removed under reduced pressure and the resulting white turbid aqueous mixture was diluted with water (500 mL) and extracted with dichloromethane (3 × 500 mL). The combined organic layers were dried over Na<sub>2</sub>SO<sub>4</sub>, filtered and concentrated to afford **94c** (28.52 g, 95%) as a white powder: *R*<sub>f</sub> = 0.26 (50% ethyl acetate / hexanes); m.p. 89.6–91.0 °C; <sup>1</sup>H NMR (500 MHz, CDCl<sub>3</sub>) δ 1.50–1.47 (m, 4H) 1.39–1.33 (m, 8H), 1.23 (s, 12H); <sup>13</sup>C NMR (125 MHz, CDCl<sub>3</sub>) δ 71.29, 44.32, 30.52, 29.55, 29.53, 24.66; LCMS (CI(–)) *m/z* 201 [M–H, 100]<sup>–</sup>; HRMS (EI(+)) calculated for C<sub>12</sub>H<sub>27</sub>O<sub>2</sub> ([M+H]<sup>+</sup>) 203.2011, found 203.2011.

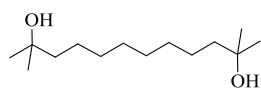
### 2,10-Dimethyl-2,10-undecanediol (**94d**)



A solution of dimethyl azelate (**93d**) (30.05 g, 139 mmol) in THF (150 mL) was added dropwise over a period of 1.5 h to a stirred 0 °C solution of methylmagnesium bromide (3.0 M, 154.3 mL, 693 mmol) in THF (175 mL). After the addition was complete, the reaction mixture was heated at reflux for 17 h and

the resulting white cake was cooled to 0 °C. The white cake was then neutralized by the slow addition (caution: highly exothermic!) of saturated ammonium chloride solution (400 mL) with vigorous stirring. As much of the THF as possible was removed under reduced pressure and the resulting white turbid aqueous mixture was diluted with water (500 mL) and extracted with dichloromethane (3 × 500 mL). The combined organic layers were dried over Na<sub>2</sub>SO<sub>4</sub>, filtered and concentrated to afford **94d** (28.20 g, 94%) as a white powder: *R*<sub>f</sub> = 0.28 (50% ethyl acetate / hexanes); m.p. 55.0–56.2 °C; <sup>1</sup>H NMR (500 MHz, CDCl<sub>3</sub>) δ 1.48–1.42 (m, 4H), 1.40–1.25 (m, 10H) 1.20 (s, 12H); <sup>13</sup>C NMR (125 MHz, CDCl<sub>3</sub>) δ 71.07, 43.98, 30.14, 29.63, 29.25, 24.35; LCMS (CI(–)) *m/z* 216 (25) 215 [M–H]<sup>–</sup>; HRMS (EI(+)) calculated for C<sub>13</sub>H<sub>29</sub>O<sub>2</sub> ([M+H]<sup>+</sup>) 217.2168, found 217.2160.

### 2,11-Dimethyl-2,11-dodecanediol (**94e**)

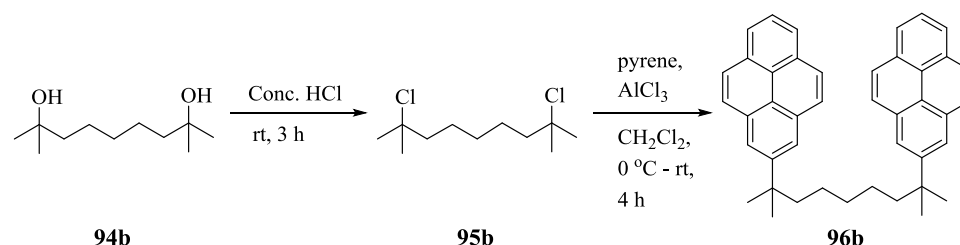


A solution of dimethyl sebacate (**93e**) (100.18 g, 435 mmol) in THF (500 mL) was added dropwise over a period of 1.5 h to a stirred 0 °C solution of methylmagnesium bromide (3.0 M, 480.5 mL, 217 mol) in THF (500 mL). After the addition was complete, the reaction mixture was heated at reflux for 17 h and the resulting white cake was cooled to 0 °C. The white cake was then neutralized by the slow addition (highly exothermic) of saturated ammonium chloride solution (1.2 L) with vigorous stirring. As much of the THF as possible was removed under reduced pressure and the resulting white turbid aqueous mixture was diluted with water (1.5 L) and extracted with dichloromethane (3 × 800 mL). The combined organic layers were dried over Na<sub>2</sub>SO<sub>4</sub>, filtered and concentrated to afford **94e** (94.98 g, 95%) as



a white powder:  $R_f$  = 0.33 (50% ethyl acetate / hexanes); m.p. 53.5–54.5 °C;  $^1\text{H}$  NMR (300 MHz,  $\text{CDCl}_3$ )  $\delta$  1.51–1.40 (m, 4H) 1.41–1.25 (m, 12H) 1.20 (s, 12H);  $^{13}\text{C}$  NMR (75 MHz,  $\text{CDCl}_3$ )  $\delta$  71.05, 43.99, 30.18, 29.60, 29.22, 24.35; LCMS data could not be obtained; HRMS data could not be obtained.

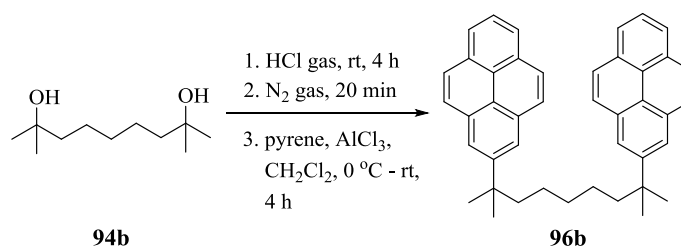
### Two-step synthesis of 2,8-bis(2-pyrenyl)-2,8-dimethylnonane (**96b**)



2,8-Dimethyl-2,8-nonanediol (**94b**) (10.28 g, 54.8 mmol) in concentrated HCl (200 mL) was stirred at room temperature over a period of 2 h. The reaction mixture was then slowly poured into ice water (600 mL) and extracted with dichloromethane ( $3 \times 100$  mL). The combined organic layers were carefully washed with a saturated solution of sodium bicarbonate ( $2 \times 100$  mL), washed with brine (150 mL), dried over  $\text{Na}_2\text{SO}_4$ , filtered and concentrated under reduced pressure to afford 2,8-dichloro-2,8-dimethylnonane (**95b**) (11.12 g, 93%) as a light yellow oil, which was used subsequently without purification:  $R_f$  = 0.24 (hexanes);  $^1\text{H}$  NMR (500 MHz,  $\text{CDCl}_3$ )  $\delta$  1.77–1.71 (m, 4H), 1.57 (s, 12H), 1.33 (m, 2H);  $^{13}\text{C}$  NMR (75 MHz,  $\text{CDCl}_3$ )  $\delta$  71.14, 45.99, 32.45, 29.77, 25.03; LCMS (CI-(+))  $m/z$  (rel. int.) 225  $[\text{M}+\text{H}]^+$ ; no HRMS data could be obtained for this compound. Dichloride **95b** (10.08 g, 44.2 mmol) was dissolved in dichloromethane (1 L) and the solution was cooled to 0 °C. Pyrene (44.90 g, 222 mmol) and  $\text{AlCl}_3$  (14.81 g, 111 mmol) were subsequently added and the resulting dark brown solution was continued to stir at

room temperature over a period of 4 h. The solution was then slowly poured (exothermic) into ice-cold water (200 mL) and the layers were separated. The aqueous layer was extracted with dichloromethane (2 × 200 mL). The combined organic layers were washed with brine (350 mL), dried over Na<sub>2</sub>SO<sub>4</sub>, filtered and concentrated under reduced pressure. The yellow residue obtained was subjected to column chromatography (8 × 30 cm; hexanes, then 7% dichloromethane / hexanes) to afford **96b** as an off-white solid (5.68 g, 23%): *R*<sub>f</sub> = 0.22 (15% dichloromethane / hexanes); m.p. 114.1–115.7 °C; <sup>1</sup>H NMR (500 MHz, CDCl<sub>3</sub>) δ 8.11 (d, *J*=7.6 Hz, 4H), 8.06 (s, 4H), 7.98 (d, *J*=8.9 Hz, 4H), 7.96 (d, *J*=8.7 Hz, 4H), 7.94 (t, *J*=7.7 Hz, 2H), 1.74–1.72 (m, 4H), 1.47 (s, 12H), 1.16–1.10 (m, 2H), 1.00–0.93 (m, 4H); <sup>13</sup>C NMR (75 MHz, CDCl<sub>3</sub>) δ 147.65, 130.98, 130.89, 127.62, 127.18, 125.49, 124.72, 124.63, 122.85, 122.80, 45.21, 38.24, 31.03, 29.54, 24.83; LCMS (CI(+)) *m/z* (rel. int.) 559 (12), 558, (47) 557 ([M+H]<sup>+</sup>, 100); HRMS (APPI) calculated for C<sub>43</sub>H<sub>41</sub> ([M+H]<sup>+</sup>) 557.3188, found 557.3167.

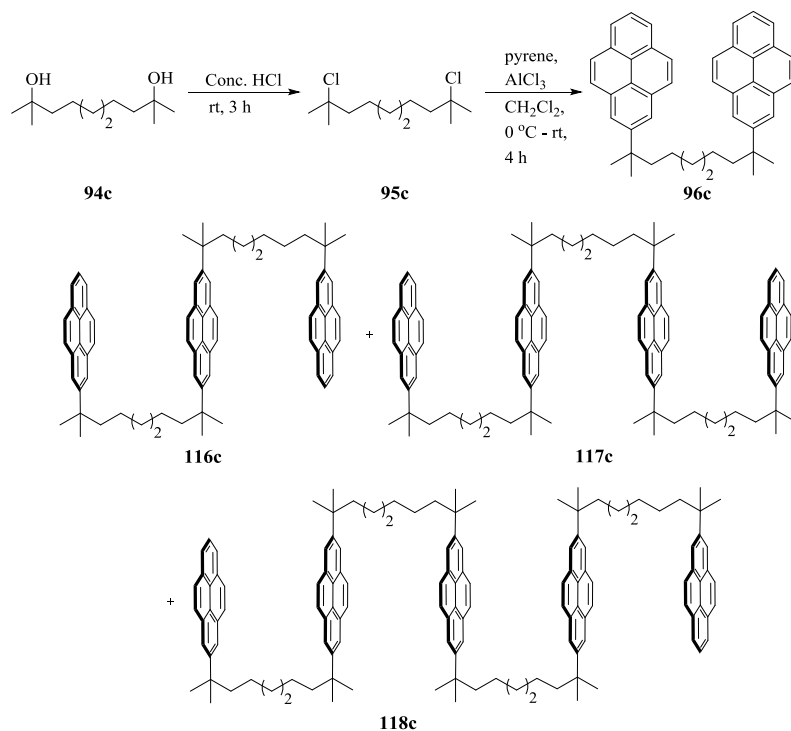
#### Modified synthesis of 2,8-bis(2-pyrenyl)-2,8-dimethylnonane (**96b**)



The crude diol **94b** (25.01 g, 124 mmol) was dissolved in dichloromethane (2.50 L) and HCl gas (generated by the dropwise addition of concentrated HCl into 98% sulfuric acid) was purged into the solution for a period of *ca.* 4 h (purging should be continued until the complete conversion of **114b** and **115b** into **95b**; monitored by tlc analysis using a PMA

stain). Nitrogen was purged into the reaction mixture for 20 min to remove the excess HCl. The solution was then cooled to 0 °C followed by the addition of pyrene (250.12 g, 1240 mmol) and aluminium chloride (41.20 g, 309 mmol). The ice bath was removed and the resulting dark brown mixture was stirred at room temperature for 1 h. The reaction mixture was poured slowly (exothermic) into ice-cold water (1.5 L) and the layers were separated. The aqueous layer was washed with dichloromethane (2 × 200 mL) and the combined organic layers were washed with brine solution (1 × 500 mL). Organic layer was dried over sodium sulfate and solvents were removed under reduced pressure. The yellow residue obtained was subjected to column chromatography (12.5 × 33 cm; 7% chloroform / hexanes) to afford **96b** as an off-white solid (35.38 g, 51%).

**Two-step synthesis of 2,9-bis(2-pyrenyl)-2,9-dimethyldecane (96c) and the byproducts 116c, 117c and 118c**

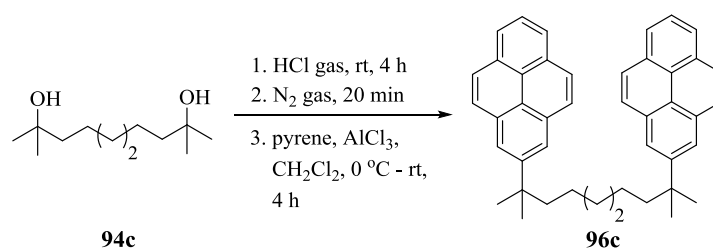


2,9-Dimethyl-2,9-decanediol (**94c**) (10.16 g, 49.2 mmol) in concentrated HCl (200 mL) was stirred at room temperature over a period of 2 h. The reaction mixture was poured slowly (exothermic) into ice-cold water (600 mL) and extracted with dichloromethane (3 × 100 mL). The combined organic layers were washed with a saturated solution of sodium bicarbonate (2 × 100 mL), washed with brine (150 mL), dried over Na<sub>2</sub>SO<sub>4</sub>, filtered and concentrated under reduced pressure to afford 2,9-dichloro-2,9-dimethyldecane (**95c**) (11.23 g, 95%) as a light yellow oil, which was used subsequently without purification: *R*<sub>f</sub> = 0.24 (hexanes); <sup>1</sup>H NMR (500 MHz, CDCl<sub>3</sub>) δ 1.75–1.71 (m, 4H), 1.56 (s, 12H), 1.51–1.43 (m, 4H), 1.38–1.30 (m, 4H); <sup>13</sup>C NMR (75 MHz, CDCl<sub>3</sub>) δ 71.19, 46.05, 32.44, 29.60, 25.05; LCMS (CI-(+)) *m/z* (rel. int.) 239 [M+H]<sup>+</sup>; no HRMS data could be obtained for this compound. Dichloride **95c** (10.21 g, 41.4 mmol) was dissolved in dichloromethane (1 L) and pyrene (42.35 g, 209 mmol) was added. The solution was cooled to 0 °C and AlCl<sub>3</sub> (13.93 g, 105 mmol) was added. The resulting dark brown mixture was stirred at room temperature for 4 h and then slowly poured (exothermic) into ice-cold water (200 mL). The layers were separated and the aqueous layer was extracted with dichloromethane (2 × 200 mL). The combined organic layers were washed with brine solution (350 mL), dried over Na<sub>2</sub>SO<sub>4</sub>, filtered and concentrated under reduced pressure. The yellow residue obtained was subjected to column chromatography (8 × 30 cm; hexanes, then 7% dichloromethane / hexanes) to first afford **96c** (5.52 g, 20%) as an off-white solid: *R*<sub>f</sub> = 0.22 (15% dichloromethane / hexanes); m.p. 152.0–153.9 °C; <sup>1</sup>H NMR (300 MHz, CDCl<sub>3</sub>) δ 8.11 (d, *J*=7.6 Hz, 4H), 8.07 (s, 12H), 8.00 (d, *J*=9.0 Hz, 4H), 7.97 (d, *J*=9.0 Hz, 4H), 7.93 (dd, *J*=8.1, 6.0 Hz, 2H), 1.76–1.70

(m, 4H), 1.45 (s, 12H), 1.11-1.03 (m, 4H), 1.03-0.91 (m, 4H);  $^{13}\text{C}$  NMR (75 MHz,  $\text{CDCl}_3$ )  $\delta$  141.72, 131.00, 127.66, 127.19, 125.51, 124.73, 124.66, 122.88, 122.82, 45.12, 38.24, 30.14, 29.78, 29.54, 24.81; LCMS (CI-(+))  $m/z$  (rel. int.) 573 (10), 572, (36) 557 ( $[\text{M}+\text{H}]^+$ , 100); HRMS (APPI) calculated for  $\text{C}_{44}\text{H}_{43}$  ( $[\text{M}+\text{H}]^+$ ) 571.3347, found 571.3332. Compound **116c**: Off-white solid (3.39 g, 22%):  $R_f$  = 0.15 (15% dichloromethane / hexanes); m.p. 181.0–182.0 °C;  $^1\text{H}$  NMR (300 MHz,  $\text{CDCl}_3$ )  $\delta$  8.19 (d,  $J=7.5$  Hz, 4H), 8.17 (d,  $J=7.4$  Hz, 8H), 8.08 (br s, 8H), 8.06 (d,  $J=7.9$  Hz, 4H), 8.00 (dd,  $J=8.1$ , 7.1 Hz, 2H), 1.90–1.75 (m, 8H), 1.57 (s, 12H), 1.56 (s, 12H), 1.25–0.98 (m, 16H);  $^{13}\text{C}$  NMR (75 MHz,  $\text{CDCl}_3$ )  $\delta$  147.81, 147.33, 131.09, 131.04, 130.85, 127.76, 127.53, 127.29, 125.59, 124.83, 124.76, 123.00, 122.96, 122.92, 122.69, 45.27, 38.31, 30.25, 29.64, 24.92; LCMS (CI-(+))  $m/z$  (rel. int.) 943 (1), 942 (17), 941 (2.9), 940 (78), 939 ( $[\text{M}+\text{H}]^+$ , 100); HRMS (APPI) calculated for  $\text{C}_{72}\text{H}_{75}$  ( $[\text{M}+\text{H}]^+$ ) 939.5848, found 939.5825. Compound **117c**: off-white solid (3.85 g, 13%):  $R_f$  = 0.10 (15% dichloromethane / hexanes); m.p. 181.0–182.0 °C;  $^1\text{H}$  NMR (300 MHz,  $\text{CDCl}_3$ )  $\delta$  8.14 (d,  $J=7.6$  Hz, 4H), 8.11 (s, 4H), 8.09–8.04 (m, 8H), 8.02 (s, 8H), 7.97 (s, 8H), 7.96–7.92 (m, 2H), 1.76–1.65 (m, 12H), 1.49 (s, 36H), 1.13–0.85 (m, 24H);  $^{13}\text{C}$  NMR (75 MHz,  $\text{CDCl}_3$ )  $\delta$  147.73, 147.26, 147.24, 131.01, 130.94, 130.74, 127.68, 127.43, 127.20, 125.52, 124.74, 124.67, 122.90, 122.84, 122.59, 45.18, 38.24, 30.16, 29.55, 24.83; LCMS (CI-(+))  $m/z$  (rel. int.) 1306 (37), 1307 (76), 1308 (90), 1309 ( $[\text{M}+\text{H}]^+$ , 100), 1310 (75); HRMS data could not be obtained. Compound **118c**: off-white solid (2.37 g, 6%):  $R_f$  = 0.05 (15% dichloromethane / hexanes); m.p. 217.9–219.4 °C;  $^1\text{H}$  NMR (300 MHz,  $\text{CDCl}_3$ )  $\delta$  8.11 (d,  $J=7.6$  Hz, 4H), 8.07 (s, 4H), 8.05–8.01 (m, 12H), 8.01–7.95 (m, 8H),

7.93 (s, 12H), 7.91–7.86 (m, 2H), 1.79–1.65 (m, 16H), 1.44 (s, 48H), 1.15–0.78 (m, 32H);  $^{13}\text{C}$  NMR (75 MHz,  $\text{CDCl}_3$ )  $\delta$  147.66, 147.17, 147.15, 130.93, 130.84, 130.64, 127.59, 127.33, 125.43, 124.65, 124.58, 122.80, 122.75, 122.50, 45.09, 38.15, 30.07, 29.70, 29.46, 24.73; LCMS (CI-(+))  $m/z$  (rel. int.) 1676 ( $[\text{M}+\text{H}]^+$ , 100); HRMS data could not be obtained.

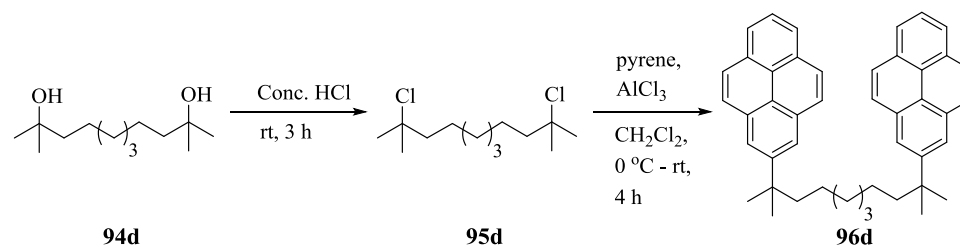
### Modified synthesis of 2,9-bis(2-pyrenyl)-2,9-dimethyldecane (**96c**)



The crude compound **94c** (25.20 g, 123 mmol) was dissolved in dichloromethane (2.5 L) and HCl gas (generated by the dropwise addition of concentrated HCl into 98% sulfuric acid) was purged into the solution over a period of *ca.* 4 h (purging should be continued until the complete conversion of **114c** and **115c** into **95c**; monitored by tlc analysis using a PMA stain). Nitrogen was purged into the reaction mixture for 20 min to remove the excess HCl. The solution was then cooled to  $0\text{ }^\circ\text{C}$  followed by the addition of pyrene (250.02 g, 1230 mmol) and aluminium chloride (41.23 g, 309 mmol). The ice bath was removed and the resulted dark brown solution was stirred at room temperature for 1 h. The solution was then slowly poured (exothermic) into ice-cold water (1.5 L) and the resulting layers were separated. The aqueous layer was washed with dichloromethane ( $2 \times 200\text{ mL}$ ) and the combined organic layers were washed with brine solution ( $1 \times 500\text{ mL}$ ). Organic layer was dried over sodium sulfate and solvents were removed under

reduced pressure. The yellow residue obtained was subjected to column chromatography (12.5 × 30 cm; 7% chloroform / hexanes) to afford **96c** as an off-white solid (36.92 g, 52% yield).

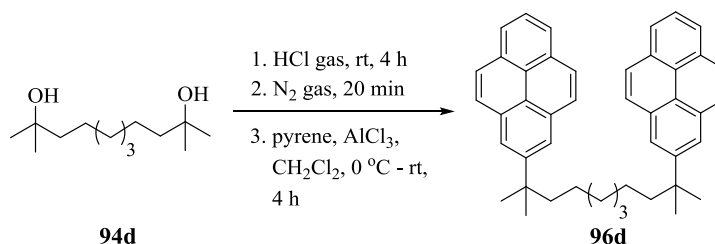
### Two-step synthesis of 2,10-bis(2-pyrenyl)-2,10-dimethylundecane (**96d**)



2,10-Dimethyl-2,10-undecanediol (**94d**) (10.11 g, 46.1 mmol) in concentrated HCl (200 mL) was stirred at room temperature over a period of 2 h. The reaction mixture was then slowly poured (exothermic) into ice-cold water (600 mL) and extracted with dichloromethane (3 × 100 mL). The combined organic layers were washed with a saturated solution of sodium bicarbonate (2 × 100 mL), washed with brine (150 mL), dried over Na<sub>2</sub>SO<sub>4</sub>, filtered and concentrated under reduced pressure to afford 2,10-dichloro-2,10-dimethylundecane (**95d**) (10.53 g, 90%) as a light yellow oil, which was used subsequently without purification: *R*<sub>f</sub> = 0.24 (hexanes); <sup>1</sup>H NMR (500 MHz, CDCl<sub>3</sub>) δ 1.75–1.71 (m, 4H), 1.56 (s, 12H), 1.51–1.43 (m, 4H), 1.35–1.28 (m, 6H); <sup>13</sup>C NMR (75 MHz, CDCl<sub>3</sub>) δ 77.13, 46.09, 32.45, 29.66, 29.43, 25.11; LCMS (CI-(+)) *m/z* (rel. int.) 253 [M+H]<sup>+</sup>; no HRMS data could be obtained for this compound. Dichloride **95d** (10.50 g, 39.2 mmol) was dissolved in dichloromethane (1 L) and pyrene (40.02 g, 197 mmol) was added. The solution was cooled to 0 °C and AlCl<sub>3</sub> (13.10 g, 99.7 mmol) was added. The deep brown solution was stirred at room temperature for 4 h and then poured into ice-

cold water (200 mL). The layers were separated and the aqueous layer was extracted with dichloromethane (2 × 200 mL). The combined organic layers were washed with brine (350 mL), dried over Na<sub>2</sub>SO<sub>4</sub>, filtered and concentrated under reduced pressure. The yellow residue obtained was subjected to column chromatography (8 × 30 cm; hexanes then 7% dichloromethane / hexanes) to afford **96d** as an off-white solid (5.50 g, 20%): *R*<sub>f</sub> = 0.22 (15% dichloromethane / hexanes); m.p. 163.0–164.0 °C; <sup>1</sup>H NMR (300 MHz, CDCl<sub>3</sub>) δ 8.15–8.04 (m, 8H), 8.00 (s, 12H), 7.98–7.89 (m, 4H), 1.78–1.71 (m, 4H), 1.51–1.46 (m, 12H), 1.06–0.98 (m, 6H), 0.86–0.84 (m, 4H); <sup>13</sup>C NMR (75 MHz, CDCl<sub>3</sub>) δ 147.86, 131.09, 127.80, 127.34, 125.64, 124.88, 124.81, 123.05, 122.97, 45.32, 38.40, 30.46, 29.72, 29.53, 24.99; LCMS (CI-(+)) *m/z* (rel. int.) 589 (0.7), 588 (4), 587 (15), 586 (48), 585 ([M+H]<sup>+</sup>, 100); HRMS (EI-(+)) calculated for C<sub>45</sub>H<sub>44</sub> ([M]<sup>+</sup>) 584.3443, found 584.3417.

#### Modified synthesis of 2,10-bis(2-pyrenyl)-2,10-dimethylundecane (**96d**)

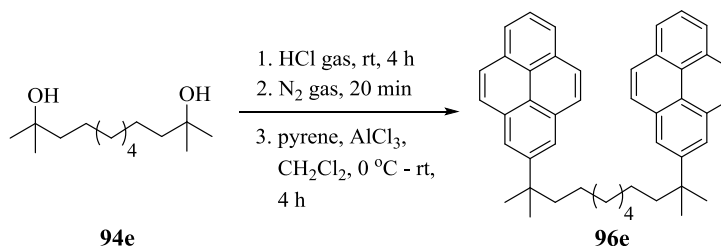


The crude compound **94d** (30.31 g, 140 mmol) was dissolved in dichloromethane (2.50 L) and HCl gas (generated by the dropwise addition of concentrated HCl into 98% sulfuric acid) was purged into the solution over a period of *ca.* 4 h (purging should be continued until the complete conversion of **114d** and **115d** into **95d**; monitored by tlc analysis using a PMA stain). Nitrogen gas was purged into the solution for 20 min to



remove the excess HCl. The solution was then cooled to 0 °C followed by the addition of pyrene (280.25 g, 1391 mmol) and aluminium chloride (46.22 g, 348 mmol). The resulting deep brown solution was stirred at room temperature for 1 h and then slowly (exothermic) poured into ice-cold water (1.5 L). The layers were separated and the aqueous layer was washed with dichloromethane (2 × 200 mL). The combined organic layers were washed with brine (1 × 500 mL), dried over anhydrous sodium sulfate, filtered and the solvents were removed under reduced pressure. The yellow residue was subjected to column chromatography (12.5 × 35 cm; 7% chloroform / hexanes) to afford **96d** as an off-white solid (42.10 g, 52%).

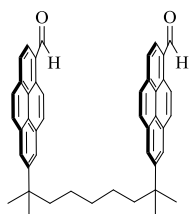
#### Modified synthesis of 2,11-bis(2-pyrenyl)-2,11-dimethyldodecane (**96e**)



The crude compound **94e** (25.25 g, 110 mmol) was dissolved in dichloromethane (2.2 L) and HCl gas (generated by the dropwise addition of concentrated HCl into 98% sulfuric acid) was purged through the solution over a period of *ca.* 4 h (purging should be continued until the complete conversion of **114e** and **115e** into **95e**; monitored by tlc analysis using a PMA stain). Nitrogen gas was then purged into the solution for 20 min to remove the excess HCl. The solution was then cooled to 0 °C followed by the addition of pyrene (219.01 g, 1080 mmol) and aluminium chloride (32.03 g, 239 mmol). The resulting deep brown solution was stirred for 1 h and then slowly (exothermic) poured

into the ice-cold water (1.5 L). The layers were separated and the aqueous layer was washed with dichloromethane (2 × 200 mL). The combined organic layers were washed with brine (1 × 500 mL), dried over anhydrous sodium sulfate, filtered and the solvents were concentrated under reduced pressure. The yellow residue obtained was subjected to column chromatography (12.5 × 30 cm; 7% chloroform / hexanes) to afford **96e** as an off-white solid (35.12 g, 54%):  $R_f$  = 0.22 (15% dichloromethane / hexanes); m.p. 129.5–131.3 °C;  $^1\text{H}$  NMR (300 MHz,  $\text{CDCl}_3$ )  $\delta$  8.12–8.16 (m, 8H), 8.00 (s, 8H), 7.92 (dd,  $J$  = 8.1, 7.1 Hz, 2H), 1.78–1.72 (m, 4H), 1.49 (s, 12H), 1.15–0.93 (m, 12H);  $^{13}\text{C}$  NMR (75 MHz,  $\text{CDCl}_3$ )  $\delta$  147.77, 131.01, 130.94, 127.67, 127.21, 125.53, 124.75, 124.67, 122.89, 122.86, 45.21, 38.28, 30.35, 29.60, 29.51, 24.87; LCMS (CI-(+))  $m/z$  (rel. int.) 601 (13), 600 (43), 599 ( $[\text{M}+\text{H}]^+$ , 100); HRMS (APPI) calculated for  $\text{C}_{46}\text{H}_{47}$  ( $[\text{M}+\text{H}]^+$ ) 599.3660, found 598.3735.

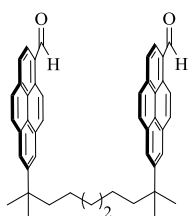
### 2,8-Bis(6-formylpyren-2-yl)-2,8-dimethylnonane (**97b**)



2,8-Bis(2-pyrenyl)-2,8-dimethylnonane (**96b**) (39.60 g, 71 mmol) was dissolved in dichloromethane (2.50 L) and  $\alpha,\alpha$ -dichloromethylmethyl ether (36.71 g, 320 mmol), titanium(IV) chloride (60.70 g, 320 mmol) were added. The resulting deep purple solution was stirred at room temperature for 2 h and then slowly poured (exothermic) into ice-cold water (1.5 L). The layers were separated and the aqueous layer was extracted with dichloromethane (2 × 200 mL). The combined organic layers were washed with brine (500 mL) and the solvents were removed under reduced pressure. The brown residue obtained was subjected to column chromatography (12.5 × 10 cm; dichloromethane) to afford **97b** as a yellow solid (38.44

g, 88%):  $R_f$  = 0.07 (dichloromethane); m.p. 201.4–203.0 °C;  $^1\text{H}$  NMR (300 MHz,  $\text{CDCl}_3$ )  $\delta$  10.48 (s, 2H), 9.04 (d,  $J$ =9.2 Hz, 2H), 8.09–8.07 (m, 4H), 7.99 (d,  $J$ =9.3 Hz, 2H), 7.98 (d,  $J$ =7.9 Hz, 2H), 7.93 (d,  $J$ =8.8 Hz, 2H), 7.81 (d,  $J$ =7.9 Hz, 2H), 7.73 (d,  $J$ =8.8 Hz, 2H), 1.76–1.73 (m, 4H), 1.48 (s, 12H), 1.19–1.16 (m, 2H), 1.01–1.16 (m, 4H);  $^{13}\text{C}$  NMR (75 MHz,  $\text{CDCl}_3$ )  $\delta$  192.73, 148.17, 134.84, 130.58, 130.55, 130.52, 130.48, 130.35, 129.94, 126.79, 126.72, 124.67, 124.36, 124.00, 123.88, 122.53, 121.89, 45.20, 38.23, 30.96, 29.34, 25.00; LCMS (CI(+))  $m/z$  (rel. int.) 615 (13), 614 (51), 613 ( $[\text{M}+\text{H}]^+$ , 100); HRMS (APPI) calculated for  $\text{C}_{45}\text{H}_{41}\text{O}_2$  ( $[\text{M}+\text{H}]^+$ ) 613.3088, found 613.3077.

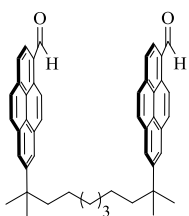
### 2,9-Bis(6-formylpyren-2-yl)-2,9-dimethyldecane (**97c**)



2,9-Bis(2-pyrenyl)-2,9-dimethylnonane (**96c**) (59.11 g, 103 mmol) was dissolved in dichloromethane (2.5 L) and  $\alpha,\alpha$ -dichloromethylmethyl ether (53.60 g, 466 mmol), titanium(IV) chloride (88.41 g, 466 mmol) were added. The resulting deep purple solution was stirred at room temperature for 2 h and then slowly poured (exothermic) into ice-cold water (1.5 L). The layers were separated and the aqueous layer was washed with dichloromethane ( $2 \times 200$  mL). The combined organic layers were washed with brine (500 mL) and the solvents were removed under reduced pressure. The brown residue obtained was subjected to column chromatography ( $12.5 \times 13$  cm; dichloromethane) to afford **97c** as a yellow solid (57.68 g, 89%):  $R_f$  = 0.17 (dichloromethane); m.p. 203.7–205.0 °C;  $^1\text{H}$  NMR (500 MHz,  $\text{CDCl}_3$ )  $\delta$  10.74 (s, 2H), 9.35 (d,  $J$ =9.2 Hz, 2H), 8.37 (d,  $J$ =7.9 Hz, 2H), 8.22 (d,  $J$ =9.3 Hz, 2H), 8.20 (d,  $J$ =1.7 Hz, 2H), 8.18 (d,  $J$ =1.7 Hz, 2H), 8.18 (d,  $J$ =7.9 Hz, 2H), 8.13 (d,  $J$ =8.9 Hz, 2H), 8.01 (d,  $J$ =8.9 Hz, 2H), 1.76–1.73 (m, 4H), 1.48 (s, 12H), 1.13–1.09 (m, 4H),

1.01–0.94 (m, 4H);  $^{13}\text{C}$  NMR (75 MHz,  $\text{CDCl}_3$ )  $\delta$  193.02, 148.47, 135.21, 130.95, 130.92, 130.83, 130.71, 130.69, 130.16, 127.13, 126.90, 124.88, 124.57, 124.39, 123.19, 122.76, 122.13, 44.99, 38.28, 30.09, 29.47, 24.77; LCMS (CI-(+))  $m/z$  (rel. int.) 630 (6), 629 (21), 628 (63), 627 ( $[\text{M}+\text{H}]^+$ , 100); HRMS (APPI) calculated for  $\text{C}_{46}\text{H}_{43}\text{O}_2$  ( $[\text{M}+\text{H}]^+$ ) 627.3245, found 627.3233.

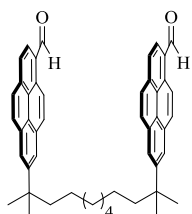
### 2,10-Bis(6-formylpyren-2-yl)-2,10-dimethylundecane (**97d**)



2,10-Bis(2-pyrenyl)-2,10-dimethylundecane (**96d**) (45.23 g, 77.5 mmol) was dissolved in dichloromethane (2.5 L) and  $\alpha,\alpha$ -dichloromethylmethyl ether (39.81 g, 346 mmol), titanium(IV) chloride (65.80 g, 346 mmol) were added. The resulting deep purple solution was stirred at room temperature for 2 h and then slowly poured (exothermic) into ice-cold water (1.5 L). The layers were separated and the aqueous layer was washed with dichloromethane ( $2 \times 200$  mL). The combined organic layers were washed with brine (500 mL) and the solvents were removed under reduced pressure. The brown residue obtained was subjected to column chromatography ( $12.5 \times 15$  cm; dichloromethane) to afford **97c** as a yellow solid (44.37 g, 90%):  $R_f$  = 0.21 (dichloromethane); m.p. 206.2–207.5  $^\circ\text{C}$ ;  $^1\text{H}$  NMR (500 MHz,  $\text{CDCl}_3$ )  $\delta$  10.74 (s, 2H), 9.36 (d,  $J=9.3$  Hz, 2H), 8.37 (d,  $J=7.9$  Hz, 2H), 8.23 (d,  $J=9.3$  Hz, 2H), 8.22 (d,  $J=1.7$  Hz, 2H), 8.20 (d,  $J=1.7$  Hz, 2H), 8.19 (d,  $J=7.9$  Hz, 2H), 8.15 (d,  $J=8.9$  Hz, 2H), 8.02 (d,  $J=8.9$  Hz, 2H), 1.77–1.74 (m, 4H), 1.50 (s, 12H), 1.10–0.90 (m, 10H), 1.01–0.94 (m, 4H);  $^{13}\text{C}$  NMR (75 MHz,  $\text{CDCl}_3$ )  $\delta$  193.13, 148.56, 135.35, 131.12, 131.06, 130.94, 130.85, 130.72, 130.21, 127.35, 126.94, 124.93, 124.62, 124.56, 124.29, 122.85, 122.22, 45.03, 38.28, 30.18, 29.41, 29.28, 24.76; LCMS (CI-(+))  $m/z$  (rel. int.)

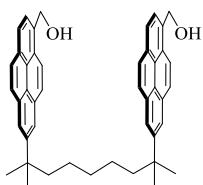
644 (3), 643 (14), 642 (53), 641 ( $[M+H]^+$ , 100); HRMS (EI-(+)) calculated for  $C_{47}H_{44}O_2$  ( $[M]^+$ ) 640.3341, found 640.3315.

**2,11-Bis(6-formylpyren-2-yl)-2,11-dimethyldodecane (97e)**



2,11-Bis(2-pyrenyl)-2,11-dimethyldodecane (**96e**) (29.61 g, 49.4 mmol) was dissolved in dichloromethane (1.5 L) and  $\alpha,\alpha$ -dichloromethylmethyl ether (25.62 g, 222 mmol), titanium(IV) chloride (42.20 g, 222 mmol) were added. The resulting deep purple solution was stirred at room temperature for 2 h and then slowly poured (exothermic) into ice-cold water (1.5 L). The layers were separated and the aqueous layer was washed with dichloromethane ( $2 \times 200$  mL). The combined organic layers were washed with brine (500 mL) and the solvents were removed under reduced pressure. The brown residue obtained was subjected to column chromatography ( $12.5 \times 14$  cm; dichloromethane) to afford **97e** as a yellow solid (26.72 g, 82%);  $R_f = 0.28$  (dichloromethane); m.p. 208-7–210.0 °C;  $^1H$  NMR (500 MHz,  $CDCl_3$ )  $\delta$  10.74 (s, 2H), 9.36 (d,  $J=9.3$  Hz, 2H), 8.37 (d,  $J=7.9$  Hz, 2H), 8.23 (d,  $J=9.3$  Hz, 2H), 8.22 (d,  $J=1.7$  Hz, 2H), 8.20 (d,  $J=1.7$  Hz, 2H), 8.19 (d,  $J=7.9$  Hz, 2H), 8.15 (d,  $J=8.9$  Hz, 2H), 8.02 (d,  $J=8.9$  Hz, 2H), 1.77–1.74 (m, 4H), 1.50 (s, 12H), 1.10–0.90 (m, 10H), 1.01–0.94 (m, 4H);  $^{13}C$  NMR (75 MHz,  $CDCl_3$ )  $\delta$  193.18, 148.61, 135.37, 131.15, 131.09, 130.97, 130.87, 130.76, 130.24, 127.25, 126.97, 124.98, 124.67, 124.57, 124.31, 122.87, 122.24, 45.06, 38.32, 30.25, 29.48, 29.42, 24.81; LCMS (CI-(+))  $m/z$  (rel. int.) 658 (2), 657 (10), 656 (50), 655 ( $[M+H]^+$ , 100); HRMS (EI-(+)) calculated for  $C_{48}H_{46}O_2$  ( $[M+H]^+$ ) 654.3498, found 654.3496.

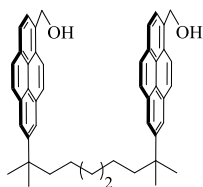
### 2,8-Bis[6-(hydroxymethyl)pyren-2-yl]-2,8-dimethylnonane (**134b**)



2,8-Bis(6-formylpyren-2-yl)-2,8-dimethylnonane (**97b**) (38.50 g, 62.8 mmol) was dissolved in THF (700 mL) and sodium borohydride (9.36 g, 253 mmol) was slowly added (exothermic). The reaction mixture was stirred at room temperature for 2 h and then cooled to 0 °C. The reaction mixture was neutralized using 5.0 M aqueous HCl and as much THF as possible was removed under reduced pressure. The crude residue was dissolved in dichloromethane (500 mL). The organic solution was subsequently washed with water (2 × 300 mL), brine (300 mL), dried over Na<sub>2</sub>SO<sub>4</sub>, filtered and concentrated under reduced pressure to afford **134b** as a fluffy white solid (37.14 g, 96%): *R*<sub>f</sub> = 0.12 (50% ethyl acetate / hexanes); m.p. 98.7 °C; <sup>1</sup>H NMR (500 MHz, CDCl<sub>3</sub>) δ 8.19 (d, *J*=9.2 Hz, 2H), 8.08 (d, *J*=7.9 Hz, 2H), 8.07 (d, *J*=1.7 Hz, 2H), 8.05 (d, *J*=1.7 Hz, 2H), 7.98 (d, *J*=7.8 Hz, 2H), 7.94 (d, *J*=9.0 Hz, 2H), 7.94 (s, 6H), 5.33 (s, 4H), 1.96 (br s, 2H), 1.70–1.76 (m, 4H), 1.48 (s, 12H), 1.19–1.11 (quin, 2H), 0.93–1.13 (m, 4H); <sup>13</sup>C NMR (125 MHz, CDCl<sub>3</sub>) δ 147.92, 133.76, 131.25, 131.20, 130.71, 128.74, 128.24, 127.84, 127.33, 125.84, 125.03, 124.63, 123.33, 123.22, 123.10, 122.92, 63.99, 45.20, 38.42, 29.73, 24.92, 14.45; LCMS (CI-(+)) *m/z* (rel. int.) 597 (12), 596 (51), 595 ([M–OH]<sup>+</sup>, 100); HRMS (EI-(+)) calculated for C<sub>44</sub>H<sub>45</sub>O<sub>2</sub> ([M]<sup>+</sup>) 616.3341, found 616.3334. Compound **134b** was taken to the next step without further purification.

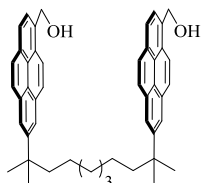
### 2,9-Bis[6-(hydroxymethyl)pyren-2-yl]-2,9-dimethyldecane (**134c**)

2,9-Bis(6-formylpyren-2-yl)-2,9-dimethyldecane (**97c**) (39.12 g, 62.2 mmol) was



dissolved in THF (400 mL) and sodium borohydride (9.30 g, 249 mmol) was slowly added (exothermic). The reaction mixture was stirred at room temperature for 2 h and then cooled to 0 °C. The reaction mixture was neutralized using 5.0 M aqueous HCl and as much THF as possible was removed under reduced pressure. The crude residue was dissolved in dichloromethane (500 mL). The organic solution was subsequently washed with water (2 × 300 mL), brine (300 mL), dried over Na<sub>2</sub>SO<sub>4</sub>, filtered and concentrated under reduced pressure to afford **134c** as a fluffy light brown solid (37.30 g, 95%): *R*<sub>f</sub> = 0.15 (50% ethyl acetate / hexanes); m.p. 93.3 °C; <sup>1</sup>H NMR (300 MHz, CDCl<sub>3</sub>) δ 8.23 (d, *J*=9.2 Hz, 2H), 8.07 (s, 2H), 8.05 (d, *J*=7.6 Hz, 2H), 8.00 (d, *J*=9.2 Hz, 2H), 7.95 (s, 4H), 7.94 (d, *J*=7.8 Hz, 2H), 5.32 (s, 4H), 2.00 (br s, 2H), 1.76–1.71 (m, 4H), 1.46 (s, 12H), 1.12–0.90 (m, 8H), <sup>13</sup>C NMR (75 MHz, CDCl<sub>3</sub>) δ 147.77 133.53, 131.05, 130.97, 130.50, 128.55, 128.08, 127.65, 127.11, 125.63, 124.85, 124.43, 123.13, 123.03, 122.90, 122.73, 63.81, 44.98, 38.15, 30.01, 29.46, 24.67; LCMS (CI-(+)) *m/z* (rel. int.) 615 (15), 614 (50), 613 ([M–OH]<sup>+</sup>, 100); HRMS (EI-(+)) calculated for C<sub>46</sub>H<sub>46</sub>O<sub>2</sub> ([M]<sup>+</sup>) 630.3498, found 630.3496. Compound **134c** was taken to the next step without further purification.

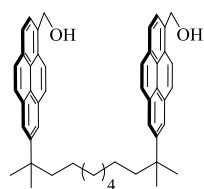
#### 2,10-Bis[6-(hydroxymethyl)pyren-2-yl]-2,10-dimethylundecane (**134d**)



2,10-Bis(6-formylpyren-2-yl)-2,10-dimethylundecane (**97d**) (45.01 g, 70.3 mmol) was dissolved in THF (700 mL) and sodium borohydride (10.50 g, 281 mmol) was slowly added (exothermic). The reaction mixture was stirred at room temperature over a period of 2 h and then cooled to 0 °C. The reaction mixture was neutralized using 5.0 M aqueous HCl and as much THF as

possible was removed under reduced pressure. The crude residue obtained was dissolved in dichloromethane (500 mL). The organic solution was subsequently washed with water (2 × 300 mL), brine (300 mL), dried over Na<sub>2</sub>SO<sub>4</sub>, filtered and concentrated under reduced pressure to afford **134d** as a fluffy light brown solid (37.30 g, 95%): *R*<sub>f</sub> = 0.18 (50% ethyl acetate / hexanes); m.p. 86.9 °C; <sup>1</sup>H NMR (300 MHz, CDCl<sub>3</sub>) δ 8.15 (d, *J*=9.2 Hz, 2H), 8.07 (s, 4H), 7.97 (d, *J*=7.7 Hz, 2H), 7.96 (d, *J*=9.2 Hz, 2H), 7.91 (dd, *J*=18.5, 9.0 Hz, 4H), 7.85 (d, *J*=7.7 Hz, 2H), 5.22 (s, 4H), 2.12 (br s, 2H), 1.76–1.71 (m, 4H), 1.48 (s, 12H), 1.20–0.90 (m, 10H), <sup>13</sup>C NMR (75 MHz, CDCl<sub>3</sub>) δ 147.75 133.47, 130.94, 130.47, 128.43, 128.00, 127.58, 127.08, 125.51, 124.76, 124.37, 123.08, 122.98, 122.86, 122.68, 63.64, 45.00, 38.15, 30.11, 29.44, 29.19, 24.70; LCMS (CI-(+)) *m/z* (rel. int.) 630 (3), 629 (14), 628 (50), 627 ([M–OH]<sup>+</sup>, 100); HRMS (EI-(+)) calculated for C<sub>47</sub>H<sub>48</sub>O<sub>2</sub> ([M]<sup>+</sup>) 644.3654, found 644.3710. Compound **134d** was used to the next step without further purification.

#### 2,11-Bis[6-(hydroxymethyl)pyren-2-yl]-2,11-dimethyldecane (**134e**)

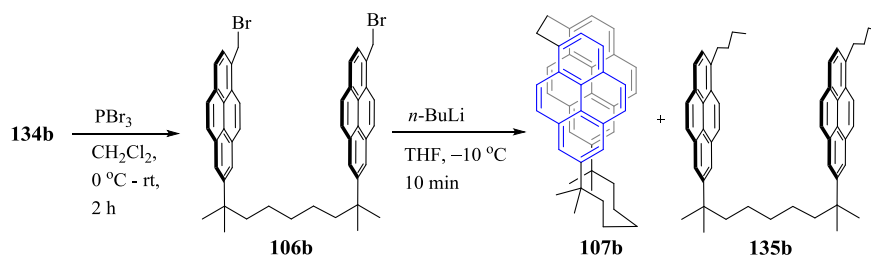


2,11-Bis(6-formylpyren-2-yl)-2,11-dimethyldodecane (**97e**) (30.01 g, 46 mmol) was dissolved in THF (300 mL) and sodium borohydride (6.93 g, 183 mmol) was added slowly. The reaction mixture was stirred at room temperature for 2 h and then cooled to 0 °C. The cooled reaction mixture was neutralized using 5.0 M aqueous HCl and as much THF as possible was removed under reduced pressure. The crude residue obtained was dissolved in dichloromethane (500 mL). The organic solution was subsequently washed with water (2 × 300 mL), brine (300 mL), dried over Na<sub>2</sub>SO<sub>4</sub>, filtered and concentrated to afford **134e** as a fluffy light brown (29.02



g, 96%):  $R_f$  = 0.28 (50% ethyl acetate / hexanes); m.p. 79.6 °C;  $^1\text{H}$  NMR (300 MHz,  $\text{CDCl}_3$ )  $\delta$  8.15 (d,  $J$ =9.2 Hz, 2H), 8.07 (s, 4H), 7.95 (d,  $J$ =9.2 Hz, 2H), 7.95 (d,  $J$ =7.8 Hz, 2H), 7.92 (d,  $J$ =9.1 Hz, 2H), 7.87 (d,  $J$ =9.0 Hz, 2H), 7.81 (d,  $J$ =7.8 Hz, 2H), 5.20 (s, 4H), 2.26 (br s, 1H), 1.82–1.71 (m, 4H), 1.48 (s, 12H), 1.12–0.90 (m, 4H);  $^{13}\text{C}$  NMR (75 MHz,  $\text{CDCl}_3$ )  $\delta$  147.87, 133.58, 131.11, 131.03, 130.57, 128.60, 128.16, 127.72, 127.17, 125.68, 124.90, 124.49, 123.21, 123.11, 122.95, 122.80, 63.86, 45.12, 38.24, 30.29, 29.55, 29.40, 24.79; LCMS (CI(+))  $m/z$  (rel. int.) 644 (3), 643 (13), 642 (50), 641 ( $[\text{M}-\text{OH}]^+$ , 100); HRMS (EI(+)) calculated for  $\text{C}_{48}\text{H}_{50}\text{O}_2$  ( $[\text{M}]^+$ ) 658.3811, found 658.3806. Compound **134e** was used to the next step without further purification.

### Two-step synthesis of 1,1,7,7-tetramethyl[7.2](7,1)pyrenophane (**107b**)

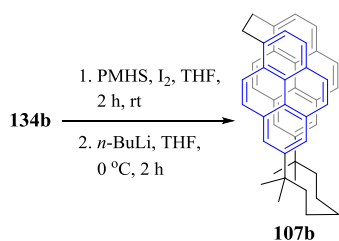


Diol **134b** (0.51 mg, 0.82 mmol) was dissolved in dichloromethane (30 mL) and the solution was cooled to 0 °C. Phosphorous tribromide (0.33 mg, 1.21 mmol) was added and the reaction mixture was stirred at 0 °C for 1 h. The reaction mixture was poured into ice-cold water and the resulting layers were separated. The aqueous layer was washed with dichloromethane ( $2 \times 10$  mL) and the combined organic layers were washed with brine (25 mL), dried over  $\text{Na}_2\text{SO}_4$ , filtered and concentrated under reduced pressure to afford **106b** (0.52 g, 85%) as a pale yellow solid:  $R_f$  = 0.65 (20% ethyl acetate / hexanes);

m.p. 235.0–236.2 °C;  $^1\text{H}$  NMR (500 MHz,  $\text{CDCl}_3$ )  $\delta$  8.28 (d,  $J=9.2$  Hz, 2H), 8.11 (d,  $J=9.2$  Hz, 2H), 8.13–8.09 (m, 4H), 8.04 (d,  $J=7.8$  Hz, 2H), 7.96 (dd,  $J=16.0, 8.8$  Hz, 4H), 7.96 (d,  $J=7.8$  Hz, 2H), 5.22 (s, 4H), 1.75–1.71 (m, 4H), 1.48 (s, 12H), 1.13 (q,  $J=\text{xx}$  Hz, 4H), 0.98–0.93 (m, 4H);  $^{13}\text{C}$  NMR data could not be obtained; LCMS (CI-(+))  $m/z$  (rel. int.) 667 (12), 666 (53), 665 ( $[\text{M}(^{81}\text{Br})-\text{Br}$ , 98), 663 ( $[\text{M}(^{79}\text{Br})-\text{Br}$ , 100); HRMS data could not be obtained. Dibromide **106b** (0.52 g, 0.70 mmol) was dissolved in anhydrous THF (200 mL) and the solution was cooled to 0 °C under nitrogen atmosphere. *n*-BuLi (1.50 M, 0.47 mL, 0.70 mmol) was added dropwise over a period of 20 min at the same temperature. The reaction mixture was then quenched with ice-cold water (50 mL) and as much of the THF as possible was removed under reduced pressure. The resulting aqueous layer was taken into dichloromethane (30 mL) and the layers were separated. The aqueous layer was extracted with dichloromethane ( $2 \times 20$  mL) and the combined organic layers were washed with brine (25 mL). The organic layer was dried over  $\text{Na}_2\text{SO}_4$ , filtered and concentrated under reduced pressure. The pale yellow residue obtained was subjected to column chromatography ( $4.5 \times 18$  cm; 12% dichloromethane / hexanes) to afford pyrenophane **107b** (0.18 g, 45%) as a fluffy white solid:  $R_f = 0.40$  (25% dichloromethane / hexanes); m.p. 206.0–207.3 °C;  $^1\text{H}$  NMR (500 MHz,  $\text{CDCl}_3$ )  $\delta$  8.15 (dd,  $J=58.4, 7.4$  Hz, 4H), 7.96 (dd,  $J=54.4, 8.8$  Hz, 4H), 7.8439 (d,  $J=0.5$  Hz, 4H), 3.85 (s, 4H), 1.45–1.24 (m, 16H), 0.80 (quin,  $J=7.5$  Hz, 2H), 0.71–0.40 (br s, 2H), 0.40–0.09 (br s, 2H);  $^{13}\text{C}$  NMR (75 MHz,  $\text{CDCl}_3$ )  $\delta$  145.98, 136.61, 130.67, 129.89, 129.83, 129.66, 127.52, 126.97, 126.93, 125.11, 124.94, 124.53, 122.83, 122.35, 122.12, 122.05, 45.61, 38.21, 36.55, 30.22, 29.49, 28.18, 25.54; LCMS (CI-(+))  $m/z$  (rel. int.) 586

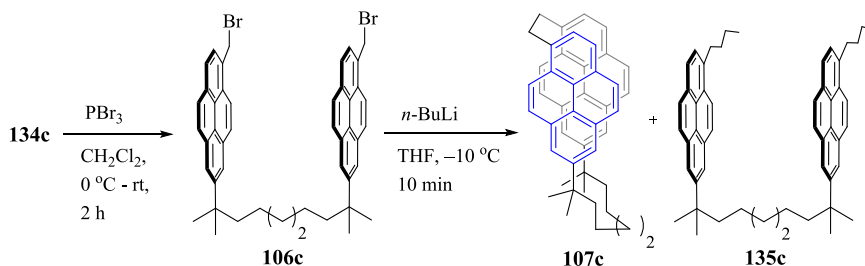
(3), 585 (14), 584 (53), 583 ( $[M+H]^+$ , 100); HRMS (APPI) calculated for  $C_{45}H_{43}$  ( $[M+H]^+$ ) 583.3347, found 583.3329.

#### Modified synthesis of 1,1,7,7-tetramethyl[7.2](7,1)pyrenophane (**107b**)



Diol **134b** (39.71 g, 64.4 mmol) was dissolved in THF (300 mL) and polymethylhydrosiloxane (11.60 g, 193 mmol), iodine (34.30 g, 135 mmol) were added under nitrogen atmosphere. The reaction mixture was stirred at room temperature until the starting material was completely consumed (*ca.* 1 h, monitored by TLC). Then, the reaction mixture was further diluted with THF (1.8 L) and was cooled to 0 °C. *n*-BuLi (1.50 M, 232 mL, 135 mmol) was added through cannula over a period of 2.5 h during which the brown solution turned pale yellow. As much of the THF as possible was then removed under reduced pressure and the resulting residue was taken into dichloromethane (700 mL). The solution was cooled to 0 °C, quenched with ice-cold water (500 mL) and the layers were separated. The aqueous layer was extracted with dichloromethane (2 × 200 mL) and the combined organic layers were washed with brine (350 mL). The organic layer was dried over  $Na_2SO_4$ , filtered and concentrated under reduced pressure to obtain a yellow residue which was subjected to column chromatography (12.5 × 30 cm; 12% chloroform / hexanes) to afford **107b** (23.25 g, 62%) as a fluffy white solid.

**Two-step synthesis of 1,1,8,8-tetramethyl[8.2](7,1)pyrenophane (107c) and 2,9-bis[6-(1-pentyl)pyrene-2-yl]-2,9-dimethyldecane (135c)**

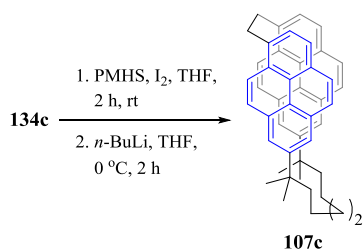


Diol **134c** (0.50 mg, 0.79 mmol) was dissolved in dichloromethane (30 mL) and phosphorous tribromide (0.32 g, 1.21 mmol) was added. The reaction mixture was stirred at  $0\text{ }^\circ\text{C}$  for 1 h and then poured into ice-cold water. The layers were separated and the aqueous layer was extracted with dichloromethane ( $2 \times 10\text{ mL}$ ). The combined organic layers were washed with brine (25 mL), dried over  $\text{Na}_2\text{SO}_4$ , filtered and concentrated under reduced pressure to afford **106c** (0.52 g, 88%) as a pale yellow solid:  $R_f = 0.65$  (20% ethyl acetate / hexanes); m.p.  $211.7\text{--}213.3\text{ }^\circ\text{C}$ ;  $^1\text{H}$  NMR (300 MHz,  $\text{CDCl}_3$ )  $\delta$  8.30 (d,  $J=9.2\text{ Hz}$ , 2H), 8.14 (d,  $J=9.2\text{ Hz}$ , 2H), 8.13 (d,  $J=1.6\text{ Hz}$ , 2H), 8.10 (d,  $J=1.6\text{ Hz}$ , 2H), 8.04 (d,  $J=7.8\text{ Hz}$ , 2H), 7.97 (dd,  $J=14.2, 9.0\text{ Hz}$ , 4H), 7.94 (d,  $J=7.8\text{ Hz}$ , 2H), 5.22 (s, 4H), 1.77–1.70 (m, 4H), 1.46 (s, 12H), 1.14–0.83 (m, 8H);  $^{13}\text{C}$  NMR (75 MHz,  $\text{CDCl}_3$ )  $\delta$  148.15, 131.81, 131.00, 130.56, 130.36, 128.91, 128.49, 128.30, 127.36, 127.12, 125.07, 124.63, 123.51, 123.49, 122.83, 122.67, 45.05, 38.23, 32.36, 30.08, 29.47, 24.76; LCMS (CI(+))  $m/z$  (rel. int.) 679 (12), 678 (41), 677 ( $[\text{M}(^{81}\text{Br})\text{--Br}]$ , 98), 675 ( $[\text{M}(^{79}\text{Br})\text{--Br}]$ , 100); HRMS (EI(+)) calculated for  $\text{C}_{46}\text{H}_{44}\text{Br}_2$  ( $[\text{M}]^+$ ) 754.1801, found 754.1804. Compound **106c** (0.52 g, 0.69 mmol) was dissolved in anhydrous THF (200 mL) and the solution was cooled to  $0\text{ }^\circ\text{C}$  under nitrogen atmosphere. To this solution  $n\text{-BuLi}$  (1.50 M,

0.46 mL, 0.69 mmol) was added dropwise over a period of 15 min. The reaction mixture was quenched with water (20 mL) and as much of the THF as possible was removed under reduced pressure. The resulting aqueous layer was taken into dichloromethane (40 mL) and the layers were separated. The aqueous layer was extracted with dichloromethane (2 × 15 mL) and the combined organic layers were washed with brine (25 mL). The organic layer was dried over Na<sub>2</sub>SO<sub>4</sub>, filtered and concentrated under reduced pressure to obtain a yellow residue which was subjected to column chromatography (3.5 × 20 cm; 10% dichloromethane / hexanes) to first afford compound **135c** (55 mg, 12%) as an off-white solid: *R*<sub>f</sub> = 0.57 (25% dichloromethane / hexanes); m.p. 129.0–130.2 °C; <sup>1</sup>H NMR (300 MHz, CDCl<sub>3</sub>) δ 8.20 (d, *J*=9.2 Hz, 2H), 8.08–7.97 (m, 8H), 7.92 (dd, *J*=13.0, 9.0 Hz, 4H), 7.80 (d, *J*=7.8 Hz, 2H), 3.28 (t, *J*=7.6 Hz, 4H), 1.82 (quin, *J*=7.4 Hz, 4H), 1.45 (s, 12H), 1.44–1.30 (m, 8H), 1.13–0.92 (br m, 8H), 0.89 (t, *J*=7.0 Hz, 6H); <sup>13</sup>C NMR (75 MHz, CDCl<sub>3</sub>) δ 147.54, 137.14, 131.26, 130.74, 129.56, 128.47, 127.34, 126.90, 126.74, 125.08, 124.57, 123.39, 123.30, 122.68, 122.47, 45.13, 38.19, 33.60, 32.06, 31.69, 30.18, 29.51, 24.84, 27.73, 14.17; LCMS (CI-(+)) *m/z* (rel. int.) 713 (14), 712 (40), 711 ([M+H]<sup>+</sup>, 100); HRMS (APPI) calculated for C<sub>54</sub>H<sub>63</sub> ([M+H]<sup>+</sup>) 711.4912, found 711.4894. Pyrenophane **107c** (0.17 g, 41%) as a white powder: *R*<sub>f</sub> = 0.38 (25% dichloromethane / hexanes); m.p. 259.9–260.8 °C; <sup>1</sup>H NMR (500 MHz, CDCl<sub>3</sub>) δ 8.11 (br d, *J*=6.1 Hz, 2H), 8.00 (br d, *J*=6.9 Hz, 2H), 7.92 (d, *J*=8.6 Hz, 2H), 7.85–7.77 (m, 4H), 7.30 (s, 2H), 6.70–6.35 (br m, 4H), 3.78 (s, 4H), 1.70–1.40 (br m, 4H), 1.40–1.20 (br m, 12H), 1.15–0.85 (br s, 4H), 0.60–0.30 (br s, 2H), 0.30–0.09 (br s, 2H); <sup>13</sup>C NMR (75 MHz, CDCl<sub>3</sub>) δ 145.94, 136.44, 130.91, 129.87, 129.78, 129.64,

127.46, 127.02, 126.83, 125.39, 124.88, 124.51, 122.70, 122.39, 122.21, 121.90, 46.29, 37.95, 36.46, 31.26, 30.33, 27.93, 24.06; LCMS (CI-(+))  $m/z$  (rel. int.) 600 (2), 599 (12), 598 (33), 597 ( $[M+H]^+$ , 100); HRMS (APPI) calculated for  $C_{46}H_{45}$  ( $[M+H]^+$ ) 597.3503, found 597.3485.

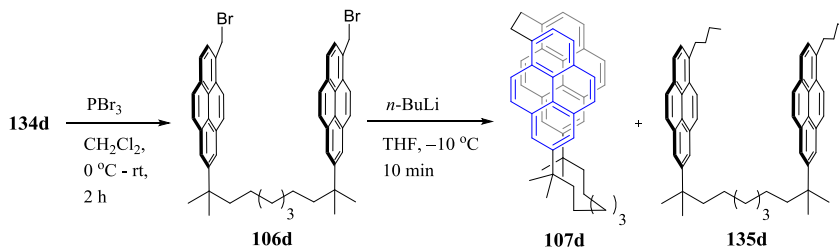
### Modified synthesis of 1,1,8,8-tetramethyl[8.2](7,1)pyrenophane (**107c**)



Diol **134c** (55.12 g, 87.1 mmol) was dissolved in THF (450 mL) and polymethylhydrosiloxane (15.71 g, 262 mmol), iodine (46.30 g, 183 mmol) were added under nitrogen atmosphere. The reaction mixture was stirred at room temperature until the starting material was completely consumed (*ca.* 1 h, monitored by TLC). The resulting mixture was further diluted with THF (2.00 L) and was cooled to 0 °C.  $n$ -BuLi (1.50 M, 232 mL, 135 mmol) was added through cannula over a period of 2 h during which the brown solution turned pale yellow in colour and an insoluble pale yellow solid was simultaneously precipitated out of the solution. As much of THF as possible was then removed under reduced pressure and the residue was taken into dichloromethane (1 L), cooled to 0 °C, quenched with ice-cold water (100 mL). The insoluble solid was filtered using a Buchner funnel and the residue was dried under vacuum to afford **107c** (33.30 g, 64%) as a pale yellow powder. The filtrate was washed with water (500 mL) and the organic layer was separated. The aqueous layer was extracted with dichloromethane (1  $\times$  200 mL). The combined organic layers were washed with brine (350 mL), dried over  $Na_2SO_4$ , filtered and concentrated to obtain a yellow

residue which was subjected to column chromatography (8.5 × 20 cm; 15% chloroform / hexanes) to afford compound **107c** (7.80 g, 15%) as an off-white solid.

**Two-step synthesis of 1,1,9,9-tetramethyl[9.2](7,1)pyrenophane (107d) and 2,10-bis[6-(1-pentyl)pyrene-2-yl]-2,10-dimethylundecane (135d)**



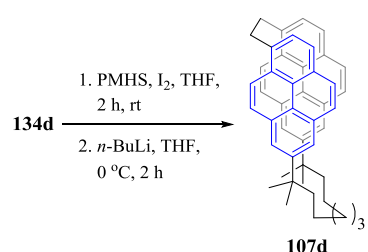
Diol **134d** (0.51 mg, 0.80 mmol) was dissolved in dichloromethane (30 mL), phosphorous tribromide (0.31 mg, 1.19 mmol) was added and the reaction mixture was stirred at 0 °C for 1 h. The reaction mixture was quenched with ice-cold water and the layers were separated. The aqueous layer was washed with dichloromethane (2 × 10 mL) and the combined organic layers were washed with brine (25 mL), dried over Na<sub>2</sub>SO<sub>4</sub>, filtered, concentrated under reduced pressure to afford **106d** (0.51 g, 86%) as a pale yellow solid:  $R_f$  = 0.65 (20% ethyl acetate / hexanes); m.p. 163.4–165.3 °C; <sup>1</sup>H NMR (500 MHz, CDCl<sub>3</sub>) δ 8.30 (d,  $J$ =9.2 Hz, 2H), 8.14 (d,  $J$ =9.2 Hz, 2H), 8.14 (d,  $J$ =1.7 Hz, 2H), 8.12 (d,  $J$ =1.7 Hz, 2H), 8.02 (d,  $J$ =7.8 Hz, 2H), 7.80 (d, 9.0 Hz, 2H), 7.94 (d,  $J$ =9.0 Hz, 2H), 7.92 (d,  $J$ =7.8 Hz, 2H), 5.20 (s, 4H), 1.77–1.70 (m, 4H), 1.46 (s, 12H), 1.14–0.83 (m, 8H); <sup>13</sup>C NMR (75 MHz, CDCl<sub>3</sub>) δ 148.35, 131.98, 131.18, 130.74, 130.52, 129.08, 128.66, 128.47, 127.52, 127.29, 125.24, 124.80, 123.70, 123.67, 123.01, 122.84, 45.28, 38.43, 32.54, 30.40, 29.68, 29.49, 24.97; LCMS (CI(+))  $m/z$  (rel. int.) 693 (12), 692 (44), 691 ([M(<sup>81</sup>Br)–Br, 100), 690 (46), 689 ([M(<sup>79</sup>Br)–Br], 92); HRMS (EI(+)) calculated for

$\text{C}_{47}\text{H}_{46}\text{Br}_2$  ( $[\text{M}]^+$ ) 768.1966, found 768.1961. Compound **106d** (0.51 g, 0.69 mmol) was dissolved in dry THF and the solution was cooled to 0 °C under a stream of nitrogen atmosphere. *n*-BuLi (1.50 M, 0.44 mL, 0.69 mmol) was added dropwise over a period of 15 min. The reaction mixture was quenched with ice-cold water (20 mL) and as much THF as possible was removed under reduced pressure. The pale yellow residue was taken into dichloromethane and the layers were separated. The aqueous layer was extracted with dichloromethane ( $2 \times 15$  mL) and the combined organic layers were washed with brine (25 mL), dried over  $\text{Na}_2\text{SO}_4$ , filtered, concentrated under reduced pressure to obtain a yellow residue which was subjected to column chromatography ( $3.5 \times 20$  cm; 10% dichloromethane / hexanes) to first afford **27d** (0.06 g, 12%); off-white solid:  $R_f = 0.57$  (25% dichloromethane / hexanes); m.p. 98.6 °C;  $^1\text{H}$  NMR (300 MHz,  $\text{CDCl}_3$ )  $\delta$  8.17 (d,  $J=9.2$  Hz, 2H), 8.08–7.94 (m, 8H), 7.89 (s, 4H), 7.72 (d,  $J=7.8$  Hz, 2H), 3.23 (t,  $J=7.6$  Hz, 4H), 1.90–1.65 (m, 8H), 1.43 (s, 12H), 1.44–1.30 (m, 8H), 1.13–0.92 (br m, 8H), 0.87 (t,  $J=7.0$  Hz, 6H);  $^{13}\text{C}$  NMR (75 MHz,  $\text{CDCl}_3$ )  $\delta$  147.64, 137.21, 131.40, 130.88, 129.67, 128.58, 127.47, 126.99, 126.86, 125.20, 124.69, 123.49, 123.45, 122.78, 122.58, 45.28, 38.29, 33.69, 32.15, 31.77, 29.68, 24.96, 22.93, 27.90, 22.84, 14.36; LCMS (CI-(+))  $m/z$  (rel. int.) 728 (2), 727 (20), 726 (48) 725 ( $[\text{M}+\text{H}]^+$ , 100); HRMS (APPI) calculated for  $\text{C}_{55}\text{H}_{65}$  ( $[\text{M}+\text{H}]^+$ ) 725.5068, found 725.5050. Pyrenophane **107d** (0.18 g, 45%) as a fluffy white solid:  $R_f = 0.38$  (25% dichloromethane / hexanes); m.p. 163.2–165.0 °C;  $^1\text{H}$  NMR (500 MHz,  $\text{CDCl}_3$ )  $\delta$  8.05 (dd,  $J=42.0, 7.8$  Hz, 4H), 7.90 (d,  $J=8.8$  Hz, 2H), 7.87–7.80 (m, 4H), 7.60 (s, 2H), 7.14 (br d,  $J=7.3$  Hz, 2H), 7.03 (d,  $J=9.1$  Hz, 2H), 3.93 (s, 4H), 1.61–1.54 (m, 4H), 1.38 (s, 12H), 0.90–0.80 (m, 6H), 0.72–0.60



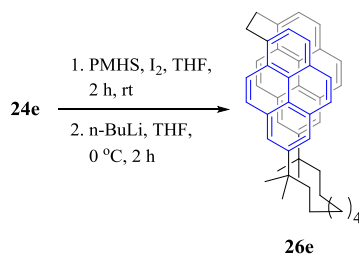
(m, 4H);  $^{13}\text{C}$  NMR (75 MHz,  $\text{CDCl}_3$ )  $\delta$  146.36, 135.93, 130.70, 130.09, 129.41, 129.37, 127.48, 127.01, 126.64, 126.09, 124.56, 124.52, 122.98, 122.66, 122.28, 122.17, 45.33, 38.06, 34.40, 29.79, 29.42, 29.10, 24.80; LCMS (CI-(+))  $m/z$  (rel. int.) 615 (3), 614 (17), 613 (46), 611 ( $[\text{M}+\text{H}]^+$ , 100); HRMS (EI-(+)) calculated for  $\text{C}_{47}\text{H}_4$  ( $[\text{M}]^+$ ) 610.3600, found 610.3595.

### Modified synthesis of 1,1,9,9-tetramethyl[9.2](7,1)pyrenophane (**107d**)



Diol **134d** (30.00 g, 46.9 mmol) was dissolved in THF (300 mL) and polymethylhydrosiloxane (8.41 g, 140 mmol), iodine (24.80 g, 97.8 mmol) were added under nitrogen atmosphere. The reaction mixture was stirred at room temperature until the starting material was completely consumed (*ca.* 1 h, monitored by TLC). The reaction mixture was further diluted with THF (1.5 L) and was cooled to  $0\text{ }^\circ\text{C}$ .  $n\text{-BuLi}$  (1.50 M, 163 mL, 302 mmol) was added through cannula over a period of 2 h during which the brown solution turned pale yellow. As much of the THF as possible was removed under reduced pressure and the resulting residue was taken into dichloromethane (500 mL). The solution was cooled to  $0\text{ }^\circ\text{C}$ , quenched with ice-cold water (500 mL) and the organic layer was separated. The aqueous layer was extracted with dichloromethane ( $2 \times 200\text{ mL}$ ) and the combined organic layers were washed with brine (350 mL), dried over  $\text{Na}_2\text{SO}_4$ , filtered and concentrated. The yellow residue obtained was subjected to column chromatography ( $12.5 \times 20\text{ cm}$ ; 8% chloroform / hexanes) to afford compound **107d** (21.35 g, 75%) as a fluffy white solid.

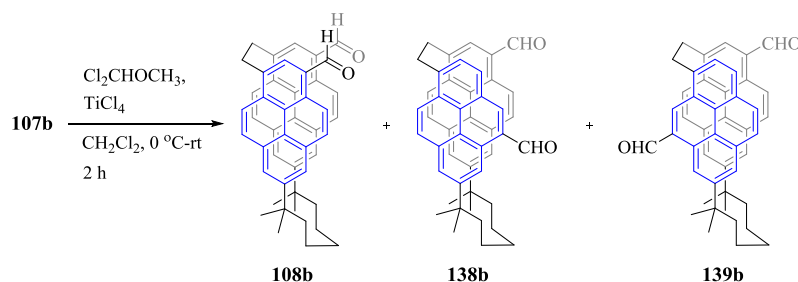
### Modified synthesis of 1,1,10,10-tetramethyl[10.2](7,1)pyrenophane (**107e**)



Diol **134e** (29.02 g, 44.1 mmol) was dissolved in THF (300 mL) and polymethylhydrosiloxane (33.60 g, 132 mmol), iodine (22.89 g, 90.2 mmol) were added under nitrogen atmosphere. The reaction mixture was stirred at room temperature until the starting material was completely consumed (*ca.* 1 h, observed by TLC). The reaction mixture was further diluted with THF (1.60 L) and was cooled to 0 °C. *n*-BuLi (1.50 M, 177 mL, 266 mmol) was added through cannula over a period of 2 h during which the brown solution turned pale yellow and an insoluble pale yellow solid was simultaneously started to precipitate out of the solution. Once the addition was completed, as much of the THF as possible was removed under reduced pressure and the resulted residue was taken into dichloromethane (1 L). The residue was cooled to 0 °C and quenched with ice-cold water (100 mL). The insoluble solid was filtered using a Buchner funnel and dried to afford **107e** (21.45 g, 78%): MALDI-TOF (reflector-EI(+)) (rel. int.) ([M]<sup>+</sup>) 624.4659; The filtrate was taken into water (500 mL) and the organic layer was separated. The aqueous layer was extracted with dichloromethane (1 × 200 mL) and the combined organic layers were washed with brine (350 mL), dried over Na<sub>2</sub>SO<sub>4</sub>, filtered and concentrated. The yellow residue obtained was subjected to column chromatography (12.5 × 20 cm; 12% chloroform / hexanes) to afford compound **107e** (2.75 g, 10%) as a white powder: *R*<sub>f</sub> = 0.40 (25% dichloromethane / hexanes); m.p. 219.5–220.3 °C; <sup>1</sup>H NMR (300 MHz, CDCl<sub>3</sub>) δ 8.15 (dd, *J*=18.1, 7.9 Hz, 4H), 7.91 (d, *J*=1.6 Hz, 2H), 7.86 (dd, *J*=17.3, 8.9 Hz, 4H), 7.63 (d, *J*=1.6 Hz, 2H), 7.33 (br d, *J*=8.9

Hz, 2H), 7.21 (br d,  $J=9.3$  Hz, 2H), 7.40 (s, 4H), 1.64–1.58 (m, 4H), 1.40 (s, 12H), 1.04–0.95 (m, 4H), 0.89–0.80 (m, 4H), 0.73–0.56 (m, 4H);  $^{13}\text{C}$  NMR (75 MHz,  $\text{CDCl}_3$ )  $\delta$  146.40, 135.82, 130.99, 130.10, 129.42, 127.56, 127.20, 126.75, 126.66, 124.60, 124.56, 122.94, 122.85, 122.53, 122.35 45.70, 38.09, 35.18, 30.21, 29.80, 29.24, 24.80; LCMS (CI(+))  $m/z$  (rel. int.) 627 (18), 626 (68), 625 ( $[\text{M}+\text{H}]^+$ , 100); HRMS (EI(+)) calculated for  $\text{C}_{48}\text{H}_{48}$  ( $[\text{M}]^+$ ) 624.3756, found 624.3756; MALDI-TOF (reflector-EI(+)) (rel. int.) ( $[\text{M}]^+$ ) 624.492.

### Synthesis of 12,22-diformyl-1,1,7,7-tetramethyl[7.2](7,1)pyrenophane (**108b**)



Pyrenophane **107b** (0.25 g, 0.43 mmol) was dissolved in dichloromethane (25 mL) and the solution was cooled to  $0\text{ }^\circ\text{C}$  under nitrogen atmosphere. Titanium(IV) chloride (0.20 g, 1.1 mmol) and dichloromethylmethyl ether (0.12 g, 1.1 mmol) were added accordingly and the resulting deep purple solution was stirred at room temperature for 2 h. The reaction mixture was then slowly poured (exothermic) into ice-cold water (50 mL) and the organic layer was separated. The aqueous layer was extracted with dichloromethane ( $2 \times 20$  mL) and the combined organic layers were washed with brine ( $1 \times 30$  mL), dried over  $\text{Na}_2\text{SO}_4$ , filtered and concentrated. The yellow residue obtained was subjected to column chromatography ( $3.5 \times 8$  cm; dichloromethane) to first afford 10,22-diformyl-

1,1,7,7-tetramethyl[7.2](7,1)pyrenophane (**138b**) (0.06 g, 18%) as a yellow solid:  $R_f$  = 0.24 (dichloromethane); m.p. 225.8–227.3 °C;  $^1\text{H}$  NMR (300 MHz,  $\text{CDCl}_3$ )  $\delta$  10.81 (s, 1H), 10.41 (s, 1H), 9.32 (d,  $J$ =1.7 Hz, 1H), 9.27–9.15 (m, 1H), 8.45–8.30 (m, 2H), 8.25–8.16 (m, 1H), 8.10–7.95 (m, 2H), 7.93–7.85 (m, 2H), 7.38–7.25 (m, 2H), 6.59–6.18 (br m, 4H), 3.76 (br s, 4H) 1.54–1.12 (br m, 16H), 0.81–0.66 (m, 2H), 0.52–0.06 (br m, 4H);  $^{13}\text{C}$  NMR (75 MHz,  $\text{CDCl}_3$ )  $\delta$  194.00, 193.03, 147.75, 147.04, 141.71, 134.14, 132.39, 130.64, 130.32, 129.83, 129.57, 129.51, 129.46, 129.42, 128.25, 127.93, 127.73, 127.31, 127.08, 126.61, 126.23, 125.79, 124.42, 124.18, 124.15, 123.56, 123.30, 122.60, 122.24, 122.05, 121.54, 120.98, 45.41, 38.58, 38.27, 38.25, 38.21, 30.02, 29.02, 25.44; LCMS (CI-(+))  $m/z$  (rel. int.) 642 (5), 641 (20), 640 (62), 639 ( $[\text{M}+\text{H}]^+$ , 100); HRMS (APPI) calculated for  $\text{C}_{47}\text{H}_{43}\text{O}_2$  ( $[\text{M}+\text{H}]^+$ ) 639.3245, found 639.3234. 10,22-Diformyl-1,1,7,7-tetramethyl[7.2](7,1)pyrenophane (**139b**): yellow solid (0.05 g, 16%):  $R_f$  = 0.21 (dichloromethane); m.p. 242.5–244.0 °C;  $^1\text{H}$  NMR (300 MHz,  $\text{CDCl}_3$ )  $\delta$  10.84 (s, 1H), 10.43 (s, 1H), 9.34 (d,  $J$ =1.7 Hz, 1H), 9.24 (d,  $J$ =9.2 Hz, 1H), 8.42 (br s, 1H), 8.40 (br s, 1H), 8.24 (br d,  $J$ =7.8 Hz, 1H), 8.11–8.00 (m, 2H), 7.92 (d,  $J$ =1.7 Hz, 1H), 7.34 (br s, 1H), 7.31 (br s, 1H), 6.68–6.20 (br m, 4H), 3.79 (br s, 4H), 1.59–1.12 (br m, 16H), 0.90–0.79 (m, 2H), 0.70–0.08 (br m, 4H);  $^{13}\text{C}$  NMR (75 MHz,  $\text{CDCl}_3$ )  $\delta$  194.00, 193.04, 194.78, 147.06, 141.71, 132.43, 130.68, 130.34, 129.85, 129.66, 129.60, 129.53, 129.44, 128.28, 127.96, 127.77, 127.33, 127.11, 126.63, 126.26, 125.83, 124.46, 124.20, 124.16, 123.31, 122.63, 122.26, 122.06, 121.74, 121.57, 120.99, 45.42, 45.37, 38.59, 38.27, 36.37, 30.02, 29.75, 29.01, 28.93, 25.44; LCMS (CI-(+))  $m/z$  (rel. int.) 641 (15), 640 (56), 639 ( $[\text{M}+\text{H}]^+$ , 100); HRMS (APPI) calculated for  $\text{C}_{47}\text{H}_{43}\text{O}_2$  ( $[\text{M}+\text{H}]^+$ ) 639.3245, found

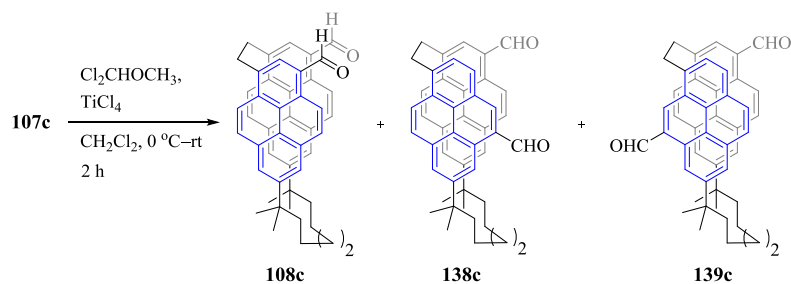
639.3242. Compound **108b** (0.08 g, 24%) as a yellow solid:  $R_f = 0.14$  (dichloromethane); m.p.  $>300\text{ }^{\circ}\text{C}$ ;  $^1\text{H}$  NMR (300 MHz,  $\text{CDCl}_3$ )  $\delta$  10.87 (s, 2H), 9.29 (d,  $J=9.0$  Hz, 2H), 8.47 (s, 2H), 8.11 (d,  $J=9.3$  Hz, 2H), 7.94 (d,  $J=1.6$  Hz, 2H), 7.34 (s, 2H), 6.56 (br d,  $J=8.2$  Hz, 2H), 6.50–6.31 (br s, 2H), 3.83 (br s, 4H), 1.50–1.35 (br m, 16H), 0.78 (quin,  $J=7.4$  Hz, 2H), 0.59–0.37 (br s, 2H), 0.37–0.10 (br s, 2H);  $^{13}\text{C}$  NMR (75 MHz,  $\text{CDCl}_3$ )  $\delta$  193.04, 146.94, 135.71, 134.14, 132.48, 130.32, 129.82, 129.56, 129.37, 128.47, 127.15, 124.42, 124.17, 124.12, 122.20, 122.08, 121.52, 45.33, 38.22, 36.04, 29.94, 29.16, 25.36; LCMS (CI-(+))  $m/z$  (rel. int.) 642 (2), 641 (17), 640 (54), 639 ( $[\text{M}+\text{H}]^+$ , 100); HRMS (APPI) calculated for  $\text{C}_{47}\text{H}_{43}\text{O}_2$  ( $[\text{M}+\text{H}]^+$ ) 639.3245, found 639.3234;

**Modified synthesis of 12,22-diformyl-1,1,7,7-tetramethyl[7.2](7,1)pyrenophane (108b)**

Pyrenophane **107b** (8.02 g, 18.76 mmol) was dissolved in dichloromethane (300 mL) and the solution was cooled to  $0\text{ }^{\circ}\text{C}$  under nitrogen atmosphere. In a separate round bottomed flask, a pre-complex was formed by the addition of titanium(IV) chloride (39.21 g, 206 mmol) to dichloromethylmethyl ether (23.70 g, 206 mmol) in dichloromethane (500 mL) at  $0\text{ }^{\circ}\text{C}$  under nitrogen atmosphere. This complex was transferred to the pyrenophane solution using a cannula over a period of 2 h at  $0\text{ }^{\circ}\text{C}$  while stirring. The ice-bath was removed and the resulting deep purple solution was continued to stir at room temperature for 17 h. The reaction mixture was cooled to  $0\text{ }^{\circ}\text{C}$  and quenched by the slow addition of ice-cold water (600 mL). The organic layer was separated and the aqueous layer was extracted with dichloromethane ( $1 \times 200\text{ mL}$ ). The combined organic layers were washed with brine (500 mL), dried over  $\text{Na}_2\text{SO}_4$ , filtered and concentrated. The yellow residue

obtained was subjected to column chromatography ( $8.5 \times 10$  cm, dichloromethane) to afford dialdehydes **138b** (0.88 g, 10%), **139b** (0.53 g, 6%) and **108b** (6.70 g, 76%) as yellow solids respectively.

### Synthesis of 13,23-diformyl-1,1,8,8-tetramethyl[8.2](7,1)pyrenophane (**108c**)



Pyrenophane (**107c**) (0.25 g, 0.42 mmol) was dissolved in dichloromethane (25 mL) and the solution was cooled to  $0\text{ }^\circ\text{C}$  under nitrogen atmosphere. Titanium(IV) chloride (0.20 g, 1.1 mmol) and dichloromethylmethyl ether (0.12 g, 1.1 mmol) were added respectively and the resulting deep purple solution was stirred at room temperature for 2 h. The solution was then poured into ice-cold water (50 mL) and the organic layer was separated. The aqueous layer was extracted with dichloromethane ( $2 \times 20$  mL) and the combined organic layers were washed with brine ( $1 \times 30$  mL), dried over  $\text{Na}_2\text{SO}_4$ , filtered and concentrated. The yellow residue obtained was subjected to column chromatography ( $3.5 \times 8$  cm; dichloromethane) to first afford 11,23-diformyl-1,1,8,8-tetramethyl[8.2](7,1)-pyrenophane (**138c**); yellow solid (36 mg, 13%);  $R_f = 0.38$  (dichloromethane); m.p.  $208.4\text{--}210.6\text{ }^\circ\text{C}$ ;  $^1\text{H}$  NMR (300 MHz,  $\text{CDCl}_3$ )  $\delta$  10.89 (s, 1H), 10.45 (s, 1H), 9.34 (d,  $J=1.7$  Hz, 1H), 9.25 (br d,  $J=9.1$  Hz, 1H), 8.49 (br s, 1H), 8.42 (br s, 1H), 8.35–8.22 (br m, 1H), 8.19–8.09 (br m, 1H), 8.06 (d,  $J=9.3$  Hz, 1H), 7.93 (d,  $J=1.6$  Hz, 1H) 7.41 (br s,

1H), 7.37 (br s, 1H), 6.72–6.30 (br m, 4H), 3.85 (br s, 4H), 1.82–1.63 (br m, 4H), 1.63–1.20 (br m, 12H), 1.20–0.80 (br m, 4H), 0.70–0.40 (br s, 2H), 0.30–0.05 (br s, 2H); <sup>13</sup>C NMR (75 MHz, CDCl<sub>3</sub>) δ 193.98, 193.06, 147.82, 147.05, 141.78, 140.10, 135.39, 134.22, 132.27, 130.62, 130.26, 130.07, 129.71, 129.43, 129.28, 128.57, 127.93, 127.79, 127.28, 127.08, 126.82, 126.50, 125.76, 124.39, 124.30, 123.90, 123.08, 122.58, 122.02, 121.56, 121.50, 121.00, 45.71, 38.29, 37.99, 31.72, 29.74, 27.56, 23.62; LCMS (CI-(+)) *m/z* (rel. int.) 656 (4), 655 (12), 654 (50), 653 ([M+H]<sup>+</sup>, 100); HRMS (APPI) calculated for C<sub>48</sub>H<sub>45</sub>O<sub>2</sub> ([M+H]<sup>+</sup>) 653.3401, found 653.3391. 11,23-Diformyl-1,1,8,8-tetramethyl-[8.2](7,1)pyrenophane (**139c**): yellow solid (30 mg, 10%); *R*<sub>f</sub> = 0.37 (dichloromethane); m.p. 230.0–232.6 °C; <sup>1</sup>H NMR (300 MHz, CDCl<sub>3</sub>) δ 10.87 (s, 1H), 10.43 (s, 1H), 9.33 (d, *J*=1.6 Hz, 1H), 9.23 (br d, *J*=9.0 Hz, 1H), 8.46 (br s, 1H), 8.39 (br s, 1H), 8.32–8.18 (br m, 1H), 8.14–8.09 (br m, 1H), 8.04 (d, *J*=9.3 Hz, 1H), 7.92 (d, *J*=1.4 Hz, 1H) 7.41 (br s, 1H), 7.37 (br s, 1H), 6.72–6.30 (br m, 4H), 3.85 (br s, 4H), 1.82–1.63 (br m, 4H), 1.63–1.20 (br m, 12H), 1.20–0.80 (br m, 4H), 0.70–0.40 (br s, 2H), 0.30–0.05 (br s, 2H); <sup>13</sup>C NMR (75 MHz, CDCl<sub>3</sub>) δ 194.00, 193.07, 147.80, 147.03, 141.79, 140.11, 135.42, 134.19, 132.25, 130.58, 130.24, 130.06, 129.68, 129.41, 129.27, 128.54, 127.90, 127.76, 127.26, 127.04, 126.80, 126.48, 125.72, 124.39, 124.35, 124.29, 123.89, 123.06, 122.56, 122.01, 121.53, 121.49, 120.99, 45.71, 38.29, 37.99, 35.89, 31.71, 29.75, 27.60, 23.65; LCMS (CI-(+)) *m/z* (rel. int.) 656 (3), 655 (16), 654 (47), 653 ([M+H]<sup>+</sup>, 100); HRMS (APPI) calculated for C<sub>48</sub>H<sub>45</sub>O<sub>2</sub> ([M+H]<sup>+</sup>) 653.3401, found 653.3400. Compound **108c** (55 mg, 20%) as a yellow solid: *R*<sub>f</sub> = 0.19 (dichloromethane); m.p. >300 °C; <sup>1</sup>H NMR (500 MHz, CDCl<sub>3</sub>) δ 10.79 (br s, 2H), 9.17 (d, *J*=8.7 Hz, 2H), 8.34 (br s, 2H), 7.98 (d,

$J=9.2$  Hz, 2H), 7.87 (d,  $J=1.5$  Hz, 2H), 7.33 (br s, 2H), 6.60 (br s, 2H), 6.37 (br s, 2H), 3.71 (br s, 4H), 1.69–1.59 (br m, 2H), 1.51–1.40 (br m, 2H), 1.35 (br s, 6H), 1.28 (br s, 6H), 1.14–1.01 (br s, 2H), 1.01–0.88 (br s, 2H), 0.55–0.40 (br s, 2H), 0.19–0.05 (br s, 2H);  $^{13}\text{C}$  NMR (75 MHz,  $\text{CDCl}_3$ )  $\delta$  193.10, 146.94, 135.34, 134.11, 132.30, 130.21, 130.00, 129.62, 129.24, 128.70, 127.06, 124.28, 124.22, 123.93, 122.02, 121.90, 121.46, 45.65, 37.97, 35.82, 31.74, 29.71, 27.60, 23.59; LCMS (CI-(+))  $m/z$  (rel. int.) 655 (23), 654 (66), 653 ( $[\text{M}+\text{H}]^+$ , 100); HRMS (APPI) calculated for  $\text{C}_{48}\text{H}_{45}\text{O}_2$  ( $[\text{M}+\text{H}]^+$ ) 653.3401, found 653.3396.

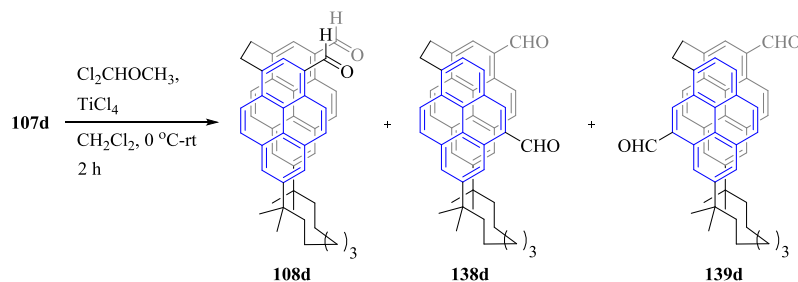
#### **Modified synthesis of 11,23-diformyl-1,1,8,8-tetramethyl[8.2](7,1)pyrenophane (108c)**

Pyrenophane (**107c**) (16.3 g, 27.3 mmol) was dissolved in dichloromethane (500 mL) and the solution was cooled to 0 °C under nitrogen atmosphere. In a separate round bottomed flask, a pre-complex was formed by the addition of titanium(IV) chloride (77.60 g, 409 mmol) to dichloromethylmethyl ether (46.94 g, 409 mmol) in dichloromethane (1 L) at 0 °C under nitrogen atmosphere. This complex was transferred to the pyrenophane solution using a cannula over a period of 3 h at 0 °C while stirring. The resulting deep purple solution was continued to stir at room temperature for 17 h. The solution was then cooled to 0 °C and was quenched by the slow addition of ice-cold water (1 L). The organic layer was separated and the aqueous layer was extracted with dichloromethane (1  $\times$  300 mL). The combined organic layers were washed with brine (700 mL), dried over  $\text{Na}_2\text{SO}_4$ , filtered and concentrated. The yellow residue obtained was subjected to column chromatography (12.5  $\times$  10 cm, dichloromethane) to first afford dialdehyde **138c** (3.41 g,



19%). Compound **139c** (3.25 g, 18%) was eluted as the next product which was followed by the required dialdehyde **108c** (7.29 g, 41%) as a yellow solid.

### Synthesis of 14,24-diformyl-1,1,9,9-tetramethyl[9.2](7,1)pyrenophane (**108d**)



Pyrenophane (**107d**) (0.25 g, 0.4 mmol) was dissolved in dichloromethane (25 mL) and the solution was cooled at  $0\text{ }^\circ\text{C}$  under nitrogen atmosphere. Titanium(IV) chloride (0.20 g, 1.0 mmol) and dichloromethylmethyl ether (0.12 g, 1.0 mmol) were added respectively and the resulting deep purple solution was stirred at room temperature for 2 h. The solution was then slowly poured into ice-cold water (50 mL) and the organic layer was separated. The aqueous layer was extracted with dichloromethane ( $2 \times 20\text{ mL}$ ) and the combined organic layers were washed with brine ( $1 \times 30\text{ mL}$ ), dried over  $\text{Na}_2\text{SO}_4$ , filtered and concentrated. The yellow residue obtained was subjected to column chromatography ( $3.5 \times 8\text{ cm}$ ; dichloromethane) to first afford 12,24-diformyl-1,1,9,9-tetramethyl[9.2](7,1)pyrenophane (**138d**) as a yellow solid (27 mg, 10%):  $R_f = 0.33$  (dichloromethane); m.p.  $185.2\text{--}187.0\text{ }^\circ\text{C}$ ;  $^1\text{H NMR}$  (300 MHz,  $\text{CDCl}_3$ )  $\delta$  10.75 (s, 1H), 10.36 (s, 1H), 9.41 (d,  $J=1.7\text{ Hz}$ , 1H), 9.15 (d,  $J=9.3\text{ Hz}$ , 1H), 8.32 (s, 1H), 8.27 (s, 1H), 8.04 (d,  $J=9.3\text{ Hz}$ , 1H), 7.97 (d,  $J=1.6\text{ Hz}$ , 1H), 7.96 (dd,  $J=48.0, 7.8\text{ Hz}$ , 2H), 7.68 (d,  $J=1.4\text{ Hz}$ , 1H), 7.66 (d,  $J=1.6\text{ Hz}$ , 1H), 7.23–6.97 (br m, 4H), 3.91 (br s, 4H), 1.66–1.50 (br m, 4H), 1.43 (s, 6H),

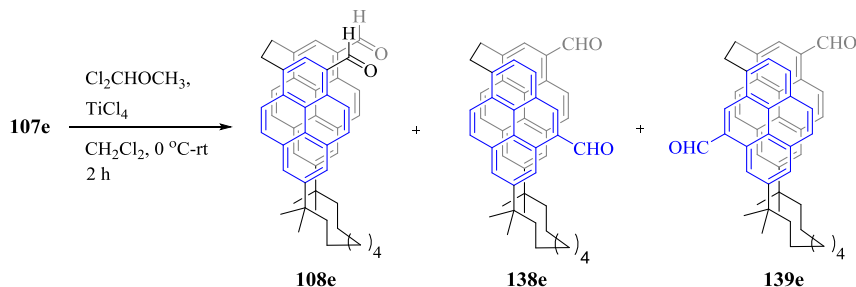
1.38 (s, 6H), 1.00–0.75 (br m, 6H), 0.75–0.60 (br m, 4H);  $^{13}\text{C}$  NMR (75 MHz,  $\text{CDCl}_3$ )  $\delta$  193.82, 192.81, 148.22, 147.45, 141.80, 139.20, 134.86, 133.81, 132.25, 130.51, 130.05, 129.97, 129.80, 129.68, 129.39, 129.23, 127.93, 127.59, 127.27, 126.86, 126.73, 126.60, 125.91, 124.47, 124.33, 124.23, 123.54, 123.01, 122.40, 122.10, 121.89, 121.14, 45.19, 44.83, 38.46, 38.15, 35.25, 34.69, 29.65, 29.42, 29.02, 28.90, 24.76, 24.73; LCMS (CI-(+))  $m/z$  (rel. int.) 670 (6), 669 (20), 668 (52), 667 ( $[\text{M}+\text{H}]^+$ , 100); HRMS (EI-(+)) calculated for  $\text{C}_{49}\text{H}_{46}\text{O}_2$  ( $[\text{M}]^+$ ) 666.3489, found 666.3524. 12,24-Diformyl-1,1,9,9-tetramethyl[9.2](7,1)pyrenophane (**139d**): yellow solid (26 mg, 10%):  $R_f$  = 0.24 (dichloromethane); m.p. 220.0–222.0 °C;  $^1\text{H}$  NMR (300 MHz,  $\text{CDCl}_3$ )  $\delta$  10.81 (s, 1H), 10.64 (s, 1H), 9.25–8.90 (m, 2H), 8.45–7.82 (m, 7H), 7.78 (br s, 2H), 7.45–7.22 (br m, 2H), 6.70–6.25 (br m, 1H), 3.84 (br s, 4H), 1.75–1.50 (br m, 4H), 1.43 (s, 6H), 1.36 (s, 6H), 0.95–0.76 (br m, 6H), 0.76–0.43 (br m, 4H);  $^{13}\text{C}$  NMR (75 MHz,  $\text{CDCl}_3$ )  $\delta$  193.06, 192.84, 192.38, 148.32, 147.65, 146.92, 137.83, 133.61, 131.83, 130.58, 130.40, 130.00, 129.87, 129.64, 129.32, 128.32, 127.70, 127.55, 127.36, 126.67, 126.27, 125.78, 124.71, 124.48, 123.60, 122.94, 122.31, 121.88, 121.77, 121.04, 45.57, 38.52, 38.26, 37.99, 35.04, 29.58, 29.23, 28.79, 24.71; LCMS (CI-(+))  $m/z$  (rel. int.) 670 (3), 669 (16), 668 (55), 667 ( $[\text{M}+\text{H}]^+$ , 100); HRMS (EI-(+)) calculated for  $\text{C}_{49}\text{H}_{46}\text{O}_2$  ( $[\text{M}]^+$ ) 666.3489, found 666.3521. Compound **108d** (46 mg, 17%), yellow solid:  $R_f$  = 0.12 (dichloromethane); m.p. 290.9–292.5 °C;  $^1\text{H}$  NMR (500 MHz,  $\text{CDCl}_3$ )  $\delta$  10.68 (s, 2H), 9.11 (d,  $J=9.2$  Hz, 2H), 8.22 (s, 2H), 7.99 (d,  $J=9.3$  Hz, 2H), 7.93 (d,  $J=1.8$  Hz, 2H), 7.61 (s, 2H), 7.07–6.97 (br m, 2H), 6.97–6.85 (br s, 2H), 3.79 (s, 4H), 1.56–1.50 (m, 4H), 1.38 (s, 12H), 0.82–0.80 (m, 6H), 0.61–0.50 (m, 4H);  $^{13}\text{C}$  NMR (75 MHz,  $\text{CDCl}_3$ )  $\delta$  192.97, 147.48,

135.07, 133.82, 132.49, 130.16, 130.05, 129.75, 129.52, 129.41, 126.88, 124.56, 124.49, 124.33, 122.39, 122.28, 121.94, 45.34, 38.28, 35.08, 29.75, 29.45, 28.99, 24.80, 23.59; LCMS (CI-(+))  $m/z$  (rel. int.) 670 (3), 669 (14), 668 (53), 667 ( $[M+H]^+$ , 100); HRMS (EI-(+)) calculated for  $C_{49}H_{46}O_2$  ( $[M]^+$ ) 666.3498, found 666.3511.

**Modified synthesis of 14,24-diformyl-1,1,9,9-tetramethyl[9.2](7,1)pyrenophane (108d)**

Pyrenophane (**107d**) (22.50 g, 37 mmol) was dissolved in dichloromethane (500 mL) and the solution was cooled to 0 °C under nitrogen atmosphere. In a separate round bottomed flask, a pre-complex was formed by the addition of titanium(IV) chloride (104.20 g, 553 mmol) to dichloromethylmethyl ether (63.45 g, 555 mmol) in dichloromethane (1 L) at 0 °C under nitrogen atmosphere. This complex was transferred to the pyrenophane solution using a cannula over a period of 3 h at 0 °C while the reaction mixture was stirring. The resulting deep purple solution was continued to stir at room temperature for 17 h. The solution was then cooled to 0 °C and was quenched by the slow addition of ice-cold water (1 L). The organic layer was separated and the aqueous layer was extracted with dichloromethane (1 × 300 mL). The combined organic layers were washed with brine (700 mL), dried over  $Na_2SO_4$ , filtered and concentrated. The yellow residue obtained was subjected to column chromatography (12.5 × 10 cm, dichloromethane) to afford dialdehyde **138d** (5.22 g, 21%), **139d** (4.26 g, 17%) and **108d** (10.10 g, 41%) as yellow solids.

**Modified synthesis of 15,25-diformyl-1,1,10,10-tetramethyl[10.2](7,1)pyrenophane (107e)**

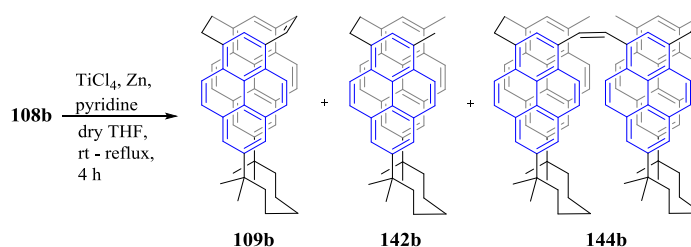


Pyrenophane (**107e**) (15.30 g, 24.5 mmol) was dissolved in dichloromethane (500 mL) and the solution was cooled to  $0\text{ }^\circ\text{C}$  under nitrogen atmosphere. In a separate round bottomed flask, a pre-complex was formed by the addition of titanium(IV) chloride (69.74 g, 368 mmol) to dichloromethylmethyl ether (42.26 g, 368 mmol) in dichloromethane (1 L) at  $0\text{ }^\circ\text{C}$  under nitrogen atmosphere. This resulting complex was slowly transferred to the pyrenophane solution using a cannula over a period of 3 h at  $0\text{ }^\circ\text{C}$  while the reaction mixture was stirring. The resulting deep purple solution was continued to stir at room temperature for 17 h. The solution was then cooled to  $0\text{ }^\circ\text{C}$  and quenched by the slow addition of ice-cold water (1 L). The organic layer was separated and the aqueous layer was extracted with dichloromethane ( $1 \times 300\text{ mL}$ ). The combined organic layers were washed with brine (700 mL), dried over  $\text{Na}_2\text{SO}_4$ , filtered and concentrated to obtain a yellow residue which was subjected to column chromatography ( $12.5 \times 10\text{ cm}$ , dichloromethane) to first afford 13,25-diformyl-1,1,10,10-tetramethyl-[10.2](10,1)pyrenophane (**138e**) as a yellow solid (3.20 g, 19%):  $R_f = 0.19$  (dichloromethane); m.p.  $175.9\text{--}176.9\text{ }^\circ\text{C}$ ;  $^1\text{H NMR}$  (300 MHz,  $\text{CDCl}_3$ )  $\delta$  10.75 (s, 1H),

10.35 (s, 1H), 9.46 (d,  $J=1.7$  Hz, 1H), 9.13 (d,  $J=9.3$  Hz, 1H), 8.34 (br s, 1H), 8.26 (br s, 1H), 8.08–7.97 (m, 3H), 7.93–7.80 (br m, 1H), 7.75–7.66 (m, 2H), 7.45–7.23 (br m, 4H), 3.95 (br s, 4H), 1.71–1.62 (br m, 4H), 1.45 (s, 6H), 1.41 (s, 6H), 1.00 (br s, 4H), 0.83 (br s, 4H) 0.64 (br s, 4H);  $^{13}\text{C}$  NMR (75 MHz,  $\text{CDCl}_3$ )  $\delta$  193.89, 192.85, 148.29, 147.45, 142.08, 139.38, 134.78, 133.84, 132.20, 130.56, 130.30, 130.10, 129.93, 129.89, 129.75, 129.50, 129.27, 128.00, 127.91, 127.64, 127.04, 126.84, 126.73, 126.01, 124.61, 124.58, 124.33, 123.57, 123.22, 122.37, 122.23, 122.14, 121.87, 121.53, 45.39, 45.15, 38.48, 38.15, 35.08, 34.45, 30.02, 29.98, 29.88, 29.86, 29.76, 29.05, 28.97, 24.70, 24.61; LCMS (CI-(+))  $m/z$  (rel. int.) 684 (5), 683 (20), 682 (52), 681 ( $[\text{M}+\text{H}]^+$ , 100); HRMS (EI-(+)) calculated for  $\text{C}_{50}\text{H}_{48}\text{O}_2$  ( $[\text{M}]^+$ ) 680.3658, found 680.3658. 13,25-Diformyl-1,1,10,10-tetramethyl[10.2](10,1)pyrenophane (**139e**) (3.36 g, 20%); yellow solid:  $R_f$  = 0.19 (dichloromethane); m.p. 199.2–200.4 °C;  $^1\text{H}$  NMR (300 MHz,  $\text{CDCl}_3$ )  $\delta$  10.84 (br s, 1H), 10.51 (br s, 1H), 9.25 (s, 1H), 9.06 (d,  $J=1.6$  Hz, 1H), 8.93 (d,  $J=9.2$  Hz, 1H), 8.50–7.85 (m, 6H), 7.85–7.45 (m, 4H), 3.90 (br s, 4H), 1.70–1.50 (br m, 4H), 1.47 (s, 6H), 1.38 (s, 6H), 1.07–0.50 (br m, 10H),  $^{13}\text{C}$  NMR (75 MHz,  $\text{CDCl}_3$ )  $\delta$  193.03, 192.46, 148.27, 147.66, 137.63, 133.58, 131.93, 130.84, 130.49, 130.33, 130.25, 130.06, 129.75, 129.63, 129.31, 128.24, 127.68, 127.59, 127.43, 126.33, 125.83, 124.95, 124.61, 124.54, 124.03, 123.11, 122.29, 121.15, 121.95, 120.86, 45.55, 38.39, 38.25, 35.10, 30.02, 29.98, 29.00, 28.67, 24.51, 24.38; LCMS (CI-(+))  $m/z$  (rel. int.) 684 (6), 683 (18), 682 (51), 681 ( $[\text{M}+\text{H}]^+$ , 100); HRMS (EI-(+)) calculated for  $\text{C}_{50}\text{H}_{48}\text{O}_2$  ( $[\text{M}]^+$ ) 680.3654, found 680.3641. Compound **108e** (7.33 g, 44%) as a yellow solid:  $R_f$  = 0.33 (dichloromethane); m.p. 254.0–256.0 °C;  $^1\text{H}$  NMR (300 MHz,  $\text{CDCl}_3$ )  $\delta$  10.75 (br s, 2H), 9.16 (br d,  $J=8.9$

Hz, 2H), 8.37 (br s, 2H), 8.12–7.95 (br m, 4H), 7.72 (s, 2H), 7.30 (br s, 2H), 3.97 (br s, 4H), 1.68–1.50 (m, 4H), 1.42 (s, 12H), 0.98 (br s, 4H), 0.82 (br s, 4H) 0.61 (br s, 4H);  $^{13}\text{C}$  NMR (75 MHz,  $\text{CDCl}_3$ )  $\delta$  192.93, 147.45, 134.90, 133.80, 132.40, 130.24, 130.19, 130.10, 129.73, 129.47, 126.79, 124.60, 124.52, 122.27, 122.13, 45.46, 38.16, 34.69, 30.01, 29.04, 24.69; LCMS (CI(+))  $m/z$  (rel. int.) 684 (5), 683 (15), 682 (54), 681 ( $[\text{M}+\text{H}]^+$ , 100); HRMS (EI(+)) calculated for  $\text{C}_{50}\text{H}_{48}\text{O}_2$  ( $[\text{M}]^+$ ) 680.3654, found 680.3650.

### Synthesis of 1,1,7,7-tetramethyl[7.2.2](7,1,3)pyrenophane-18-monoene (109b)

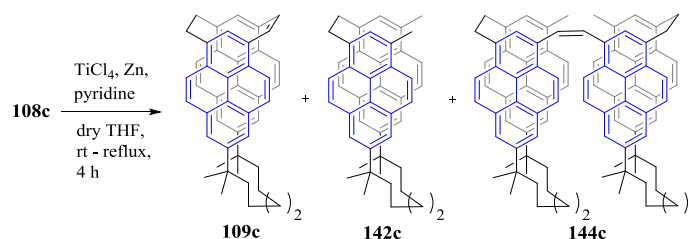


Titanium(IV) chloride (15.06 g, 78.8 mmol) was added to a stirred slurry of zinc dust (10.46 g, 159 mmol) in anhydrous THF (500 mL) at room temperature under nitrogen atmosphere. The resulting brownish black slurry was heated to reflux for 1 h during which a dark black colour persisted (the loss of this colour indicates that the McMurry reaction will fail completely). Pyridine (10.55 mL, 131 mmol) was added and the reaction mixture was continued to reflux for further 10 min. The dialdehyde **108b** (6.10 g, 9.4 mmol) was dissolved in anhydrous THF (600 mL) and slowly added to the black solution. After the addition was completed the reaction mixture was continued to reflux for a further 3 h. The hot reaction mixture was poured into chloroform and the solvents were removed under reduced pressure. The resulting residue was subjected to column

chromatography (8 × 20 cm, 10% dichloromethane / hexanes) to first afford 12,22-dimethyl-1,1,7,7-tetramethyl[7.2](7,1)pyrenophane (**142b**) (0.22 g, 4%) as a pale yellow solid:  $R_f$  = 0.45 (10% dichloromethane / hexanes); m.p. >300 °C;  $^1\text{H}$  NMR (300 MHz,  $\text{CDCl}_3$ )  $\delta$  8.22–8.16 (m, 2H), 8.03–7.92 (m, 4H), 7.88–7.76 (m, 2H), 7.28–7.25 (m, 1H), 6.60–6.30 (4H), 3.80 (s, 4H), 3.07 (s, 6H), 1.65–1.30 (m, 18H), 0.90–0.70 (m, 4H);  $^{13}\text{C}$  NMR (75 MHz,  $\text{CDCl}_3$ )  $\delta$  145.83, 136.35, 131.79, 131.19, 130.56, 130.29, 129.63, 128.52, 127.82, 127.44, 126.64, 125.90, 124.99, 124.85, 124.23, 123.20, 123.13, 122.62, 122.01, 121.84, 45.60, 38.16, 36.45, 30.18, 29.78, 25.53, 19.99; LCMS (CI-(+))  $m/z$  (rel. int.) 613 (12), 612 (42) 611 ( $[\text{M}+\text{H}]^+$ , 100); HRMS (APPI) calculated for  $\text{C}_{47}\text{H}_{47}$  ( $[\text{M}+\text{H}]^+$ ) 611.3660, found 611.3636. Monoene **109b** (1.75 g, 31%) as a white solid:  $R_f$  = 0.38 (10% dichloromethane / hexanes); m.p. >300 °C;  $^1\text{H}$  NMR (300 MHz,  $\text{CDCl}_3$ )  $\delta$  8.05 (s, 2H), 7.99 (d,  $J=9.2$  Hz, 2H), 7.61 (d,  $J=9.0$  Hz, 2H), 7.59 (s, 2H), 7.54–7.50 (m, 2H), 7.47 (d,  $J=9.2$  Hz, 2H), 7.41 (d,  $J=9.1$  Hz, 2H), 4.35–4.13 (m, 2H), 3.78–3.58 (m, 2H), 1.42–1.39 (m, 4H), 1.33 (s, 12 H), 0.72 (d,  $J=7.7$  Hz, 2H), 0.35–0.15 (m, 4H);  $^{13}\text{C}$  NMR (75 MHz,  $\text{CDCl}_3$ )  $\delta$  145.47, 137.52, 135.98, 129.99, 129.88, 128.11, 127.87, 126.13, 125.60, 123.84, 123.48, 122.27, 122.11, 122.06, 121.86, 45.96, 38.29, 30.86, 30.28, 28.62, 28.54, 26.38; LCMS (CI-(+))  $m/z$  (rel. int.) 610 (3), 609 (19), 608 (40), 607 ( $[\text{M}+\text{H}]^+$ , 100); HRMS (APPI) calculated for  $\text{C}_{47}\text{H}_{43}$  ( $[\text{M}+\text{H}]^+$ ) 607.3347, found 607.3335. Compound **144b** (0.44 g, 4%) as a green yellow solid:  $R_f$  = 0.33 (10% dichloromethane / hexanes); m.p. >300 °C;  $^1\text{H}$  NMR: poor solubility; LCMS (CI-(+))  $m/z$  (rel. int.) 1221 (4), 1220 (16), 1219 (42) 1218 (100), 1217 ( $[\text{M}+\text{H}]^+$ , 100); HRMS (APPI) calculated for  $\text{C}_{94}\text{H}_{89}$  ( $[\text{M}+\text{H}]^+$ ) 1217.6946, found 1217.6868. Compound **144'b** (0.39 g,

3%) as a green yellow solid:  $R_f = 0.32$  (10% dichloromethane / hexanes); m.p. > 300 °C;  $^1\text{H}$  NMR could not be obtained due to poor solubility; LCMS (CI-(+))  $m/z$  (rel. int.) 1221 (3), 1220 (16), 1219 (42) 1218 (95), 1217 ( $[\text{M}+\text{H}]^+$ , 100); HRMS (APPI) calculated for  $\text{C}_{94}\text{H}_{89}$  ( $[\text{M}+\text{H}]^+$ ) 1216.6946, found 1216.6876.

### Synthesis of 1,1,8,8-tetramethyl[8.2.2](8,1,3)pyrenophane-19-monoene (109c)



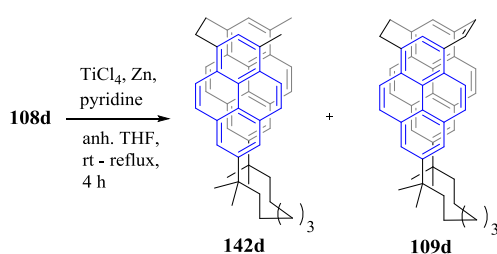
Titanium(IV) chloride (48.01 g, 247 mmol) was slowly added to a stirred slurry of zinc (32.60 g, 495 mmol) in anhydrous THF (1.00 L) at room temperature under nitrogen atmosphere. The resulting brownish black slurry was heated to reflux for 1 h, during which time a dark black colour persisted (the loss of this colour indicates that the McMurry reaction will fail completely). Pyridine (32.92 mL, 407 mmol) was added by syringe and the reaction was continued to reflux for further 10 min. The dialdehyde **108c** (19.01 g, 29 mmol) was dissolved in anhydrous THF (1.00 L) and slowly added to the black solution. After the addition was completed the reaction mixture was continued to reflux for a further 3 h. The hot reaction mixture was poured into chloroform (1 L) and the solvents were removed under reduced pressure. The resulting slurry was subjected to column chromatography (12.5 × 16 cm, 7% chloroform / hexanes) to afford monoene **109b** (5.80 g, 32%) as a white solid:  $R_f = 0.33$  (30% dichloromethane / hexanes); m.p. >300 °C;  $^1\text{H}$  NMR (300 MHz,  $\text{CDCl}_3$ )  $\delta$  8.07 (s, 2H), 7.80 (d,  $J=9.2$  Hz,



2H), 7.64 (d,  $J=9.0$  Hz, 2H), 7.63 (s, 2H), 7.57–7.52 (m, 2H), 7.48 (d,  $J=9.2$  Hz, 2H), 7.43 (d,  $J=9.1$  Hz, 2H), 4.35–4.15 (m, 2H), 3.80–3.61 (m, 2H), 1.55–1.43 (m, 4H), 1.32 (s, 6 H), 1.31 (s, 6H), 1.14–0.85 (m, 4H), 0.35–0.15 (m, 4H);  $^{13}\text{C}$  NMR (75 MHz,  $\text{CDCl}_3$ )  $\delta$  145.16, 137.48, 135.77, 129.89, 129.86, 128.06, 127.79, 126.09, 125.57, 123.75, 123.43, 122.24, 122.04, 121.91, 121.73, 46.30, 37.76, 30.46, 30.40, 30.31, 29.58, 29.50, 24.28; LCMS (CI-(+))  $m/z$  (rel. int.) 623 (31), 622 (49), 621 ( $[\text{M}+\text{H}]^+$ , 100); HRMS (EI-(+)) calculated for  $\text{C}_{48}\text{H}_{44}$  ( $[\text{M}]^+$ ) 620.3443, found 620.3440. Compound **144b** (1.80 g, 5%) as a green yellow solid:  $R_f$  = 0.34 (30% dichloromethane / hexanes); m.p. >300 °C;  $^1\text{H}$  NMR (300 MHz,  $\text{CDCl}_3$ )  $\delta$  8.84–8.63 (m, 6H), 8.23 (d,  $J=9.1$  Hz, 2H), 8.13–8.28 (m, 4H), 7.97 (d,  $J=9.2$  Hz, 2H), 7.92 (d,  $J=1.4$  Hz, 2H), 7.88 (d,  $J=1.4$  Hz, 2H), 7.39 (s, 4H), 6.90–6.60 (m, 8H), 4.05 (br s, 8H), 3.13 (s, 6H), 1.71–1.52 (br s, 8H), 1.52–1.38 (br m, 24 H), 1.25–1.06 (br s, 8H), 0.55–0.07 (br m, 8H);  $^{13}\text{C}$  NMR (75 MHz,  $\text{CDCl}_3$ )  $\delta$  146.13, 145.84, 136.14, 136.10, 132.12, 131.92, 130.81, 130.70, 130.25, 130.10, 130.00, 129.96, 129.61, 128.73, 128.02, 127.32, 127.27, 127.22, 126.56, 125.47, 125.24, 124.92, 124.69, 123.22, 123.04, 122.77, 122.65, 122.40, 122.03, 121.98, 46.30, 38.41, 37.94, 31.24, 30.25, 24.02, 20.38; LCMS (CI-(+))  $m/z$  (rel. int.) 1248 (23), 1247 (35), 1246 (71), 1245 ( $[\text{M}+\text{H}]^+$ , 100); HRMS (APPI) calculated for  $\text{C}_{96}\text{H}_{93}$  ( $[\text{M}+\text{H}]^+$ ) 1244.7259, found 1244.7259.

### Synthesis of 1,1,9,9-Tetramethyl[9.2.2](9,1,3)pyrenophane-20-monoene (109d)

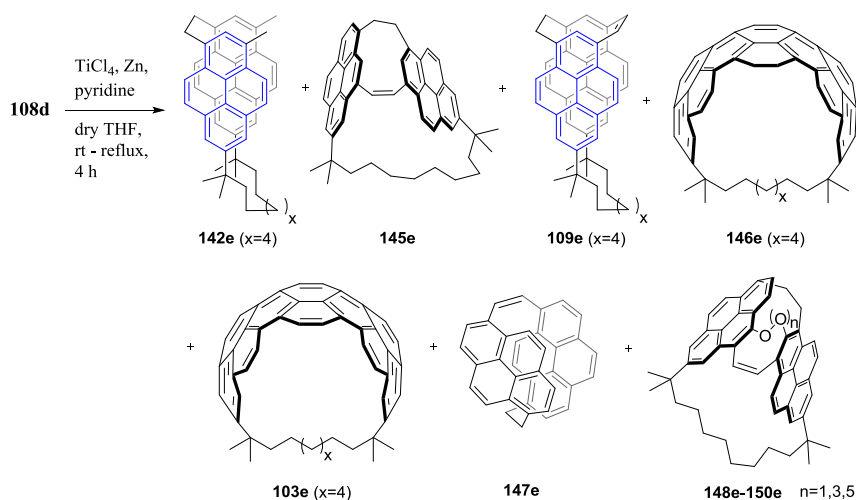
Titanium(IV) chloride (28.16 g, 148 mmol) was added slowly to a stirred slurry of zinc (19.56 g, 297 mmol) in anhydrous THF (1 L) at room temperature under nitrogen atmosphere. The resulting brownish black slurry was heated to reflux for 1 h during



which time a dark black colour persisted (the loss of this colour indicates that the McMurry reaction will fail completely). Pyridine (19.70 mL, 244 mmol) was added and the reaction was continued to reflux for further 10 min. The dialdehyde **108d** (11.64 g, 17.5 mmol) was dissolved in anhydrous THF (1.20 L) and slowly added to the black mixture. After the addition was completed the reaction mixture was continued to reflux for a further 3 h. The hot reaction mixture was poured into chloroform (1 L) and the solvents were removed under reduced pressure. The resulting slurry was subjected to column chromatography (12.5 × 12 cm, 7% dichloromethane / hexanes) to first afford 14,24-dimethyl-1,1,9,9-tetramethyl[9.2](9,1)pyrenophane (**142d**) (0.56 g, 5%) as a yellow brown solid:  $R_f$  = 0.47 (30% dichloromethane / hexanes); m.p. > 300 °C;  $^1\text{H}$  NMR (500 MHz,  $\text{CDCl}_3$ )  $\delta$  8.10 (d,  $J$ =9.1 Hz, 2H), 7.95 (d,  $J$ =9.1 Hz, 2H), 7.91 (d,  $J$ =1.8 Hz, 2H), 7.14 (br d,  $J$ =9.2 Hz, 1H), 7.00 (d,  $J$ =9.2 Hz, 2H), 3.90 (s, 4H), 2.95 (s, 4H), 1.59–1.53 (m, 4H), 1.39 (s, 12H), 0.91–0.83 (m, 6H), 0.84–0.62 (m, 4H);  $^{13}\text{C}$  NMR (75 MHz,  $\text{CDCl}_3$ )  $\delta$  146.47, 135.97, 131.68, 130.80, 130.70, 129.85, 128.30, 127.82, 126.59, 125.43, 125.07, 123.49, 123.44, 123.12, 122.44, 122.15, 45.56, 38.26, 35.59, 30.00, 29.94, 29.66, 29.38, 25.04, 20.03; LCMS (CI(+))  $m/z$  (rel. int.) 641 (11), 640 (47) 639 ( $[\text{M}+\text{H}]^+$ , 100); HRMS (APPI) calculated for  $\text{C}_{49}\text{H}_{51}$  ( $[\text{M}+\text{H}]^+$ ) 639.3973, found 639.3959. Monoene **109d** (3.58 g, 32%) as an off-white solid:  $R_f$  = 0.33 (30% dichloromethane / hexanes); m.p. > 300 °C;  $^1\text{H}$  NMR (500 MHz,  $\text{CDCl}_3$ )  $\delta$  8.07 (s, 2H), 7.85 (d,  $J$ =9.2 Hz, 2H), 7.81 (s, 2H), 7.70 (d,  $J$ =9.0 Hz, 2H), 7.67–7.63 (m, 4H), 7.57 (d,

$J=9.2$  Hz, 2H), 7.52 (d,  $J=9.0$  Hz, 2H), 4.33–4.20 (m, 2H), 3.83–3.70 (m, 2H), 1.50 (t,  $J=8.1$  Hz, 4H), 1.31 (s, 6 H), 1.31 (s, 6H), 0.94–0.85 (m, 4H), 0.85–0.75 (m, 2H), 0.72–0.58 (m, 4H);  $^{13}\text{C}$  NMR (75 MHz,  $\text{CDCl}_3$ )  $\delta$  146.02, 137.34, 135.70, 130.16, 130.14, 129.37, 129.29, 128.20, 127.78, 126.45, 125.97, 123.73, 123.57, 122.64, 122.28, 122.15, 122.11, 45.91, 38.12, 30.60, 30.15, 29.36, 29.25, 28.66, 24.94; LCMS (CI-(+))  $m/z$  (rel. int.) 638 (2), 637 (13), 636 (52), 635 ( $[\text{M}+\text{H}]^+$ , 100); HRMS (APPI) calculated for  $\text{C}_{49}\text{H}_{47}$  ( $[\text{M}+\text{H}]^+$ ) 635.3660, found 635.3649.

### Synthesis of 1,1,10,10-tetramethyl[10.2.2](10,1,3)pyrenophane-21-monoene (109e)



Titanium(IV) chloride (19.30 g, 102 mmol) was added slowly to a stirred slurry of zinc dust (4.93 g, 75 mmol) in anhydrous THF (400 mL) at room temperature under nitrogen atmosphere. The resulting brownish black slurry was heated at reflux for 1 h, during which time a dark black colour was persisted (the loss of this colour indicates that the McMurry reaction will fail completely). Pyridine (5.20 mL, 62 mmol) was added and the reaction mixture was continued to reflux for a further 10 min. The dialdehyde **108e** (3.01

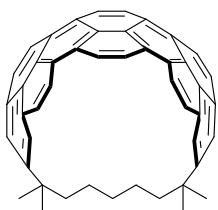
g, 4.4 mmol) was dissolved in anhydrous THF (500 mL) and added slowly to the black mixture. After the addition was completed the black reaction mixture was continued to reflux for 3 h. The hot reaction mixture was poured into chloroform (500 mL) and the solvents were removed under reduced pressure. The resulting residue was taken into dichloromethane (500 mL) and was washed with ice-cold water. The layers were separated and the aqueous layer was washed with dichloromethane ( $2 \times 100$  mL). The combined organic layers were washed with brine (300 mL), dried over  $\text{Na}_2\text{SO}_4$ , filtered and concentrated to obtain a yellow residue which was subjected to column chromatography ( $8 \times 25$  cm, 10% chloroform / hexanes) to first afford 15,25-dimethyl-1,1,10,10-tetramethyl[10.2](10,1)pyrenophane (**142e**) (80 mg, 3%) as a white solid:  $R_f = 0.45$  (30% dichloromethane / hexanes); m.p.  $> 300$  °C;  $^1\text{H}$  NMR (300 MHz,  $\text{CDCl}_3$ )  $\delta$  8.08 (d,  $J=9.2$  Hz, 2H), 8.00–7.53 (m, 9H), 7.26–7.24 (br m, 1H), 7.14 (d,  $J=9.2$  Hz, 2H), 3.93 (s, 4H), 2.93 (s, 4H), 1.59–1.53 (m, 4H), 1.41 (s, 12H), 1.20–0.50 (m, 12H);  $^{13}\text{C}$  NMR (75 MHz,  $\text{CDCl}_3$ )  $\delta$  146.16, 135.49, 131.35, 130.73, 130.36, 129.61, 128.01, 127.47, 126.27, 125.75, 124.81, 123.35, 123.27, 123.03, 122.95, 122.20, 122.16, 45.66, 37.96, 30.15, 29.70, 29.14, 24.72, 22.69, 19.17; LCMS (CI(+))  $m/z$  (rel. int.) 656 (3), 655 (13), 654 (54), 653 ( $[\text{M}+\text{H}]^+$ , 100); HRMS (APPI) calculated for  $\text{C}_{50}\text{H}_{53}$  ( $[\text{M}+\text{H}]^+$ ) 653.4129, found 653.4127. Compound **145d** (74 mg, 3%) as a brown solid:  $R_f = 0.38$  (30% dichloromethane / hexanes); m.p. 190.1–192.0.  $^1\text{H}$  NMR (300 MHz,  $\text{CDCl}_3$ )  $\delta$  8.60 (d,  $J=8.6$  Hz, 2H), 8.20 (d,  $J=10.8$  Hz, 1H), 8.03 (d,  $J=10.8$  Hz, 1H), 7.87 (d,  $J=9.2$  Hz, 1H), 7.84 (d,  $J=1.8$  Hz, 1H), 7.78–7.69 (m, 4H), 7.68 (d,  $J=1.6$  Hz, 1H), 7.65 (d,  $J=1.6$  Hz, 1H), 7.58 (dd,  $J=11.4, 8.9$  Hz, 2H), 7.54 (d,  $J=9.3$  Hz, 1H), 7.47 (d,  $J=9.2$  Hz, 1H),

4.66–4.51 (m, 1H), 3.87–3.61 (m, 3H), 2.18–3.69 (m, 1H), 1.61–1.20 (m, 4H), 1.59 (s, 3H), 1.43 (s, 3H), 1.39 (s, 3H), 1.22 (s, 3H), 1.20–0.90 (m, 4H), 0.90–0.70 (m, 2H), 0.70–0.40 (m, 4H), 0.40–0.03 (m, 1H);  $^{13}\text{C}$  NMR (75 MHz,  $\text{CDCl}_3$ )  $\delta$  146.23, 146.02, 136.25, 136.10, 134.79, 134.04, 130.97, 130.71, 130.61, 130.54, 130.03, 129.27, 129.19, 128.86, 128.69, 128.33, 127.70, 127.22, 126.87, 126.46, 126.33, 126.30, 125.75, 124.31, 124.03, 123.63, 123.53, 122.84, 122.39, 122.35, 122.16, 122.02, 121.88, 46.53, 42.10, 38.28, 38.12, 35.44, 32.72, 30.94, 30.86, 30.62, 28.84, 28.28, 27.97, 22.56, 26.26, 25.32, 21.87; LCMS (CI(+))  $m/z$  (rel. int.) 651 (10), 650 (36), 649 ( $[\text{M}+\text{H}]^+$ , 100); HRMS (APPI) calculated for  $\text{C}_{50}\text{H}_{49}$  ( $[\text{M}+\text{H}]^+$ ) 649.3816, found 649.3813. Monoene **109d** (320 mg, 12%) as a brown crystalline solid:  $R_f$  = 0.36 (30% dichloromethane / hexanes); m.p. > 300 °C;  $^1\text{H}$  NMR (300 MHz,  $\text{CDCl}_3$ )  $\delta$  8.12 (s, 2H), 8.00 (s, 2H), 7.84 (d,  $J$ =9.2 Hz, 2H), 7.72 (d,  $J$ =9.0 Hz, 2H), 7.69–7.63 (m, 4H), 7.60 (d,  $J$ =9.2 Hz, 2H), 7.56 (d,  $J$ =9.1 Hz, 2H), 4.28–4.10 (m, 2H), 3.88–3.70 (m, 2H), 1.60–1.45 (m, 4H), 1.36 (s, 6 H), 1.35 (s, 6H), 1.03–0.94 (m, 4H), 0.86–0.77 (m, 4H), 0.70–0.50 (m, 4H);  $^{13}\text{C}$  NMR (75 MHz,  $\text{CDCl}_3$ )  $\delta$  145.67, 136.77, 135.16, 130.23, 130.17, 128.30, 128.15, 128.05, 127.41, 126.61, 126.19, 123.39, 122.86, 122.44, 122.25, 122.00, 46.20, 37.97, 30.62, 30.11, 29.48, 29.45, 25.22; LCMS (CI(+))  $m/z$  (rel. int.) 652 (4), 651 (19), 650 (48), 649 ( $[\text{M}+\text{H}]^+$ , 100); HRMS (APPI) calculated for  $\text{C}_{50}\text{H}_{49}$  ( $[\text{M}+\text{H}]^+$ ) 649.3816, found 649.3806. 1,1,10,10-Tetramethyl[10](2,11)-6,7-dihydroteropyrenophane **146e** (55 mg, 2%) as a brown solid:  $R_f$  = 0.36 (10% dichloromethane / hexanes); m.p. > 300 °C;  $^1\text{H}$  NMR (300 MHz,  $\text{CDCl}_3$ )  $\delta$  8.61 (s, 2H), 8.48 (d,  $J$ =9.3 Hz, 2H), 8.11 (d,  $J$ =9.5 Hz, 2H), 7.84 (d,  $J$ =9.3 Hz, 1H), 7.71 (d,  $J$ =9.5 Hz, 2H), 7.67–7.62 (m, 4H), 4.13–3.85 (m, 4H),

1.46 (s, 6H), 1.42 (s, 6H), 1.15–0.85 (m, 4H), 0.25–0.03 (br m, 8H), (–0.20)–(–0.45) (br s, 4H);  $^{13}\text{C}$  NMR (75 MHz,  $\text{CDCl}_3$ )  $\delta$  145.25, 129.89, 129.75, 129.58, 127.43, 126.93, 126.75, 126.50, 126.22, 124.90, 124.74, 123.02, 122.99, 123.50, 122.10, 47.36, 38.31, 30.49, 30.20, 27.73, 27.52, 25.50, 24.36; LCMS (CI-(+))  $m/z$  (rel. int.) 648 (48), 647 ( $[\text{M}+\text{H}]^+$ , 100); HRMS (APPI) calculated for  $\text{C}_{50}\text{H}_{53}$  ( $[\text{M}+\text{H}]^+$ ) 647.3660, found 647.3643. Compound **147e** (25 mg, 1%) as a brown solid:  $R_f$  = 0.36 (10% dichloromethane / hexanes); m.p. could not be obtained;  $^1\text{H}$  NMR (300 MHz,  $\text{CDCl}_3$ )  $\delta$  8.27 (d,  $J=9.2$  Hz, 1H), 8.24 (d,  $J=8.0$  Hz, 1H), 8.19 (d,  $J=9.1$  Hz, 1H), 8.01 (d,  $J=7.9$  Hz, 1H), 8.01 (d,  $J=7.9$  Hz, 1H), 8.00 (d,  $J=8.0$  Hz, 1H), 7.94 (d,  $J=7.9$  Hz, 1H), 7.85 (s, 2H), 7.83 (d,  $J=8.0$  Hz, 1H), 7.83 (d,  $J=8.0$  Hz, 1H), 7.62 (d,  $J=7.9$  Hz, 1H), 7.45 (d,  $J=13.2$  Hz, 1H), 7.18 (d,  $J=13.2$  Hz, 1H), 7.02 (d,  $J=9.0$  Hz, 1H), 6.25 (d,  $J=7.7$  Hz, 1H), 6.15 (d,  $J=9.0$  Hz, 1H), 6.14 (d,  $J=7.7$  Hz, 1H), 5.21 (d,  $J=9.5$  Hz, 1H), 4.63 (d,  $J=9.5$  Hz, 1H), 4.35–4.29 (m, 1H), 3.25–3.06 (m, 2H), 3.03–2.90 (m, 1H);  $^{13}\text{C}$  NMR (75 MHz,  $\text{CDCl}_3$ )  $\delta$  135.01, 134.22, 133.04, 133.04, 132.09, 130.79, 130.12, 129.28, 129.05, 128.88, 128.84, 128.45, 128.30, 128.21, 128.03, 127.70, 127.17, 127.01, 126.78, 126.56, 126.23, 126.20, 125.89, 125.15, 124.97, 124.92, 124.50, 124.20, 124.17, 124.02, 123.61, 121.99, 121.73, 119.63, 37.64, 31.64; LCMS (CI-(+))  $m/z$  (rel. int.) 457 (6), 456 (42), 455 ( $[\text{M}+\text{H}]^+$ , 100); HRMS (APPI) calculated for  $\text{C}_{36}\text{H}_{23}$  ( $[\text{M}+\text{H}]^+$ ) 455.1782, found 455.1851. Compounds **148e-150e** (26 mg, 1%) as a brown solid:  $R_f$  = 0.12 (10% dichloromethane / hexanes); m.p. >300 °C;  $^1\text{H}$  NMR (300 MHz,  $\text{CDCl}_3$ )  $\delta$  8.32 (d,  $J=9.4$  Hz, 1H), 7.96 (d,  $J=9.3$  Hz, 1H), 7.93 (d,  $J=1.6$  Hz, 1H), 7.92 (d,  $J=9.3$  Hz, 1H), 7.88 (d,  $J=1.6$  Hz, 1H), 7.81 (d,  $J=9.3$  Hz, 1H), 7.69 (d,  $J=10.1$  Hz, 1H), 7.67 (d,  $J=8.9$  Hz, 1H), 7.44 (d,  $J=10.1$  Hz, 1H),

7.25 (d,  $J=8.9$  Hz, 1H), 7.20 (d,  $J=1.9$  Hz, 1H), 6.94 (d,  $J=1.8$  Hz, 1H), 6.81 (d,  $J=7.0$  Hz, 1H), 5.53 (d,  $J=7.2$  Hz, 1H), 3.80–3.65 (m, 1H), 3.47–3.28 (m, 1H), 3.11–2.87 (m, 2H), 1.58 (s, 3H), 1.50 (s, 3H), 1.47–1.40 (m, 4H), 1.25 (s, 12H), 1.19–1.00 (m, 2H), 0.72–0.55 (m, 2H), 0.55–0.37 (m, 4H), 0.37–0.23 (m, 2H), 0.00–(–0.40) (m, 4H);  $^{13}\text{C}$  NMR (75 MHz,  $\text{CDCl}_3$ )  $\delta$  153.86, 151.51, 145.89, 145.60, 145.16, 131.85, 128.19, 127.26, 124.80, 123.76, 123.67, 123.36, 122.92, 122.81, 122.11, 121.96, 119.23, 111.11, 46.80, 45.59, 38.26, 37.28, 31.70, 31.39, 31.03, 30.91, 30.84, 30.44, 29.71, 25.05, 14.12; LCMS (CI-(+))  $m/z$  (rel. int.) 713 (22), 712 (60), 711 ( $[\text{M}+\text{H}]^+$ , 100); HRMS (APPI) molecular formula unknown, found 743.3736 ( $[\text{M}+\text{H}]^+$ ).

#### Previous synthesis of 1,1,7,7-tetramethyl[7](2,11)teropyrenophane (**103b**)

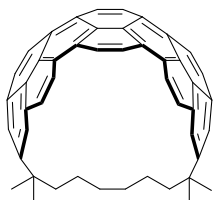


Cyclophanemonoene (**109b**) (0.015 g, 0.03 mmol) in *m*-xylene (3.0 mL) was heated at 125 °C and DDQ (67 mg, 0.3 mmol) was added in equal portions (1.0 equiv. at each time) and at regular intervals (2 h).

Over all, the reaction mixture was stirred for 36 h and the hot solvent was evaporated using a stream of nitrogen. The residue was subjected to column chromatography (36 cm  $\times$  3 cm; 5% ethyl acetate / hexanes) to afford teropyrenophane **103b** (5.3 mg, 36%) as a brown solid:  $R_f$  = 0.29 (10% ethyl acetate / hexanes); m.p. > 300 °C;  $^1\text{H}$  NMR (500 MHz,  $\text{CDCl}_3$ )  $\delta$  8.45 (s, 4H), 8.25 (d,  $J=9.5$  Hz, 4H), 7.61 (d,  $J=9.5$  Hz, 4H), 7.28 (s, 4H), 1.28 (s, 12H), 0.80–0.71 (m, 4H), 0.10–0.00 (m, 2H), (–1.10)–(–1.20) (m, 4H);  $^{13}\text{C}$  NMR (75 MHz,  $\text{CDCl}_3$ )  $\delta$  144.50, 128.75, 128.41, 127.89, 126.97, 126.03, 125.44, 124.89, 124.18, 123.54, 123.18, 47.74, 38.23, 31.18, 28.42, 24.27; LCMS (CI-(+))  $m/z$  (rel. int.) 605 (11),

604 (51), 603 ( $[M+H]^+$ , 100); HRMS (EI-(+)) calculated for  $C_{47}H_{38}$  ( $[M]^+$ ) 602.2974, found 602.2961.

#### Previous synthesis of 1,1,8,8-Tetramethyl[8](2,11)teropyrenophane (**103c**)



Cyclophanemonoene (**109c**) (0.01 g, 0.02 mmol) in *m*-xylene (2 mL) was heated at 125 °C and DDQ (41 mg, 0.2 mmol) was added in equal portions (1.0 equiv. at each time) at regular intervals (2 h). The reaction mixture was stirred for 24 h. The hot solvent was evaporated using a stream of nitrogen and the resulting residue was subjected to column chromatography (36 cm × 3 cm; 4% ethyl acetate / hexanes) to first afford teropyrenophane **103c** (7.4 mg, 75%) as a brown solid:  $R_f$  = 0.33 (10% ethyl acetate / hexanes); m.p. > 300 °C;  $^1H$  NMR (500 MHz,  $CDCl_3$ )  $\delta$  8.62 (s, 4H), 8.39 (d,  $J$ =9.5 Hz, 4H), 7.71 (d,  $J$ =9.5 Hz, 4H), 7.42 (s, 4H), 1.32 (s, 12H), 0.74–0.68 (m, 4H), –0.21–0.31 (m, 4H), (–0.60)–(–0.72) (m, 4H);  $^{13}C$  NMR (75 MHz,  $CDCl_3$ )  $\delta$  144.92, 128.14, 127.33, 127.02, 126.95, 125.50, 124.73, 124.14, 123.26, 122.88, 123.18, 47.74, 38.23, 31.18, 28.42, 24.27; LCMS (CI-(+))  $m/z$  (rel. int.) 619 (11), 618 (46), 617 ( $[M+H]^+$ , 100); HRMS (EI-(+)) calculated for  $C_{48}H_{40}$  ( $[M]^+$ ) 616.3130, found 616.3134;

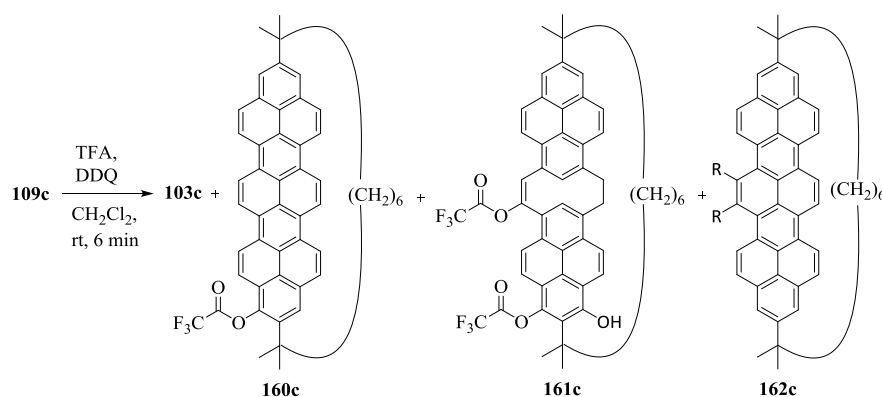
#### Modified synthesis of 1,1,8,8-tetramethyl[8](2,11)teropyrenophane (**103c**)

Cyclophanemonoene (**109c**) (0.05 g, 0.08 mmol) was dissolved in dichloromethane (5.0 mL) and DDQ (55 mg, 0.24 mmol) was added. Methanesulfonic acid (0.005 mL, 0.08 mmol) in dichloromethane (4.0 mL) was added at once to this solution and the reaction mixture was stirred at 40 °C for 10 min. The reaction mixture was quenched by 2.5 M



aqueous NaOH (4.0 mL) and the organic layer was separated. The aqueous layer was extracted with dichloromethane (3 × 5 mL) and the combined organic layer was washed with brine solution (15 mL), dried over Na<sub>2</sub>SO<sub>4</sub>, filtered and concentrated. The solid residue obtained was subjected to column chromatography (8.5 cm × 10 cm; 2% ethyl acetate / hexanes) to afford teropyrenophane **103c** (25 mg, 52%) as a reddish brown solid.

#### Modified synthesis of 1,1,8,8-Tetramethyl[8](2,11)teropyrenophane (**103c**)

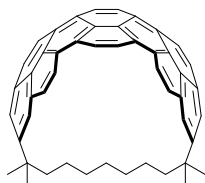


Cyclophanemonoene **109c** (0.05 g, 0.08 mmol) was dissolved in dichloromethane (5.0 mL) and DDQ (0.055 g, 0.24 mmol) was added. Trifluoroacetic acid (0.09 mL, 1.2 mmol) in dichloromethane (4.0 mL) was added to this solution and the reaction mixture was stirred at room temperature for 6 min. The reaction mixture was poured into ice-cold water (10 mL) and the organic layer was separated. The aqueous layer was extracted with dichloromethane (3 × 5 mL) and the combined organic layer was washed with brine solution (15 mL), dried over Na<sub>2</sub>SO<sub>4</sub>, filtered and concentrated. The solid residue obtained was subjected to column chromatography (8.5 cm × 10 cm; 2% ethyl acetate / hexanes) to first afford teropyrenophane (**103c**) (26 mg, 53%) as a reddish brown solid (for complete characterization see below); compound **160c**: (1.0 mg, 9%) as a brown

solid:  $R_f$  = 0.28 (10% ethyl acetate / hexanes);  $^1\text{H}$  NMR (300 MHz,  $\text{CDCl}_3$ )  $\delta$  8.69 (d,  $J$ =10.0 Hz, 1H), 8.67 (d,  $J$ =10.0 Hz, 1H), 8.63 (s, 1H), 8.62 (d,  $J$ =10.1 Hz, 1H), 8.49 (d,  $J$ =9.8 Hz, 1H), 8.44 (d,  $J$ =9.4 Hz, 1H), 8.41 (d,  $J$ =8.8 Hz, 1H), 8.38 (d,  $J$ =9.5 Hz, 1H), 7.75 (d,  $J$ =9.8 Hz, 1H), 7.72 (d,  $J$ =9.6 Hz, 1H), 7.71 (d,  $J$ =9.5 Hz, 1H), 7.49 (d,  $J$ =1.6 Hz, 1H), 7.44 (s, 1H), 7.40 (d,  $J$ =1.6 Hz, 1H), 7.35 (d,  $J$ =9.8 Hz, 1H), 2.37–2.22 (m, 2H), 2.08–1.93 (m, 4H), 1.44 (s, 3H), 1.39 (s, 3H), 1.21 (s, 6H), (–0.05)–(–0.18) (m, 2H), (–0.33)–(–0.65) (m, 2H), (–1.06)–(–1.28) (m, 2H);  $^{19}\text{F}$  NMR (282 MHz,  $\text{CDCl}_3$ )  $\delta$  –74.22; LCMS (CI-(+))  $m/z$  (rel. int.) 731 (17), 730 (54), 729 ( $[\text{M}+\text{H}]^+$ , 100); HRMS data could not be obtained for this compound. Compound **161c**: (1.0 mg) as a brown solid:  $R_f$  = 0.12 (10% ethyl acetate / hexanes);  $^1\text{H}$  NMR (300 MHz,  $\text{CDCl}_3$ )  $\delta$  8.69 (d,  $J$ =1.9 Hz, 1H), 7.98–7.75 (m, 8H), 7.59 (d,  $J$ =8.8 Hz, 1H), 7.58 (d,  $J$ =9.9 Hz, 1H), 7.56 (d,  $J$ =1.8 Hz, 1H), 7.20 (s, 1H), 7.01 (d,  $J$ =9.9 Hz, 1H), 5.68 (s, 1H), 3.88–3.54 (m, 2H), 3.52–3.37 (m, 1H), 3.37–3.10 (m, 1H), 1.53 (s, 3H), 1.51 (s, 3H), 1.27 (s, 3H), 1.20 (m, 3H), 0.70–0.25 (m, 6H), (–0.05)–(–0.55) (m, 6H); LCMS (CI-(+))  $m/z$  (rel. int.) 863 (13), 862 (46), 861 ( $[\text{M}+\text{H}]^+$ , 100); HRMS data could not be obtained for this compound. Compound **162c**: (1.0 mg) as a green solid:  $R_f$  = 0.03 (10% ethyl acetate / hexanes);  $^1\text{H}$  NMR (300 MHz,  $\text{CDCl}_3$ )  $\delta$  9.08 (d,  $J$ =10.1 Hz, 1H), 8.90 (d,  $J$ =9.9 Hz, 1H), 8.77 (d,  $J$ =10.1 Hz, 1H), 8.56 (d,  $J$ =9.4 Hz, 1H), 8.55 (d,  $J$ =9.9 Hz, 1H), 8.50 (d,  $J$ =9.5 Hz, 1H), 8.20 (d,  $J$ =9.4 Hz, 1H), 7.92 (d,  $J$ =9.4 Hz, 1H), 7.90 (d,  $J$ =9.5 Hz, 1H), 7.79 (d,  $J$ =2.0 Hz, 1H), 7.63 (d,  $J$ =1.7 Hz, 1H), 7.59 (d,  $J$ =1.7 Hz, 1H), 7.50 (d,  $J$ =9.5 Hz, 1H), 7.42 (d,  $J$ =2.0 Hz, 1H), 2.40–2.24 (m, 2H), 2.15–1.90 (m, 1H), 1.75–1.51 (m, 2H), 1.43 (s, 3H), 1.34 (s, 3H), 1.28 (s, 3H), 1.17 (s, 3H), 0.76–0.63 (m, 2H), (–0.05)–(–0.75) (m, 2H); LCMS (CI-(+))  $m/z$  (rel. int.)

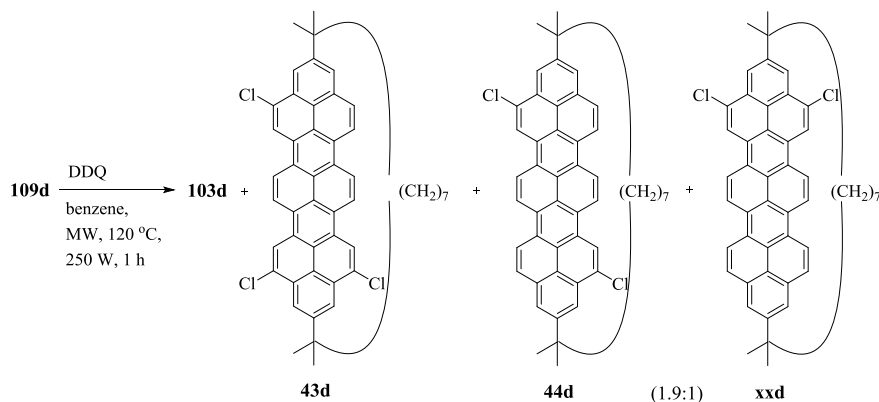
649 (14), 648 (43), 647 ( $[M+H]^+$ , 100); HRMS data could not be obtained for this compound.

#### Previous synthesis of 1,1,9,9-tetramethyl[9](2,11)teropyrenophane (**103d**)



Cyclophanemonoene **109d** (0.50 g, 0.8 mmol) in *m*-xylene (10 mL) was heated at 125 °C and DDQ (1.74 g, 7.7 mmol) was added in equal portions (1.0 equiv. each) at regular intervals (2 h) for 24 h while the reaction was stirring. The hot solvent was evaporated using a stream of nitrogen and the resulting solid residue was subjected to column chromatography (4.5 cm × 20 cm; 2% ethyl acetate / hexanes) to afford teropyrenophane **103d** (105 mg, 21%) as a reddish brown solid:  $R_f$  = 0.40 (10% ethyl acetate / hexanes); m.p. > 300 °C;  $^1\text{H}$  NMR (300 MHz,  $\text{CDCl}_3$ )  $\delta$  8.78 (s, 4H), 8.53 (d,  $J$ =9.5 Hz, 4H), 7.81 (d,  $J$ =9.5 Hz, 4H), 7.51 (s, 4H), 1.38 (s, 12H), 0.83–0.76 (m, 4H), 0.02–0.00 (m, 4H), (–0.48)–(–0.53) (m, 2H), (–0.80)–(–1.20) (m, 4H);  $^{13}\text{C}$  NMR (125 MHz,  $\text{CDCl}_3$ )  $\delta$  144.94, 129.11, 127.60, 127.12, 126.92, 125.64, 124.90, 124.33, 123.67, 123.55, 123.18, 47.35, 38.11, 30.24, 29.71, 27.50, 24.68; LCMS (APCI-(+))  $m/z$  (rel. int.) 633 (12), 632 (44), 631 ( $[M+H]^+$ , 100); HRMS (APPI) calculated for  $\text{C}_{49}\text{H}_{43}$  ( $[M+H]^+$ ) 631.3347, found 631.3349.

## Synthesis of 1,1,9,9-tetramethyl[9](2,11)teropyrenophane (**103d**) under microwave conditions



Cyclophanemonoene **109d** (100 mg, 0.16 mmol) was taken in benzene (10 mL) and DDQ (175 mg, 0.63 mmol) was added. The reaction mixture was heated to 120 °C under microwave conditions (250 W) for a period of 1 h. Benzene was removed under reduced pressure and the solid residue obtained was subjected to column chromatography (3.5 cm  $\times$  22 cm; 2% ethyl acetate / hexanes) to first afford teropyrenophane **103d** (20 mg, 20%) as a reddish brown solid; 1,1,9,9-tetramethyl-4,9,18-trichloro[9](2,11)teropyrenophane **156d**: (32 mg, 27%) as an orange crystalline solid:  $R_f$  = 0.45 (10% ethyl acetate / hexanes); m.p. > 300 °C;  $^1\text{H}$  NMR (300 MHz,  $\text{CDCl}_3$ )  $\delta$  8.80 (d,  $J$ =10.0 Hz, 1H), 8.75 (d,  $J$ =10.0 Hz, 1H), 8.72 (s, 1H), 8.71 (d,  $J$ =10.0 Hz, 1H), 8.62 (s, 2H), 8.60 (d,  $J$ =10.0 Hz, 1H), 8.54 (d,  $J$ =9.4 Hz, 1H), 8.01 (s, 2H), 7.95 (d,  $J$ =1.6 Hz, 1H), 7.84 (d,  $J$ =9.4 Hz, 1H), 7.60 (d,  $J$ =1.6 Hz, 1H), 1.45 (s, 3H), 1.44 (s, 3H), 1.43 (s, 3H), 0.90–0.80 (m, 4H), 0.20–0.02 (m, 4H), (–0.39)–(–0.60) (m, 2H), (–0.86)–(–1.20) (m, 4H);  $^{13}\text{C}$  NMR (75 MHz,  $\text{CDCl}_3$ )  $\delta$  147.26, 146.32, 132.22, 131.74, 131.60, 128.65, 127.54, 127.05, 126.90, 126.78, 126.74, 126.64, 126.39, 126.32, 126.30, 126.14, 125.67, 125.06, 124.64, 124.05,

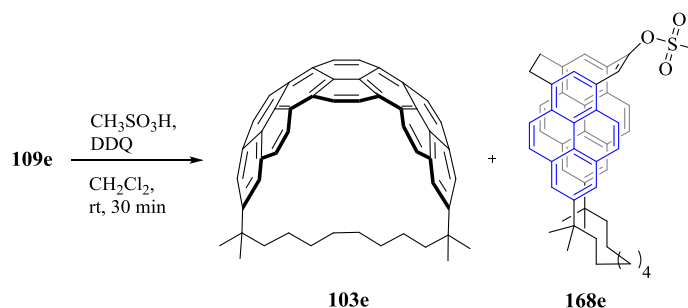
124.06, 123.65, 123.45, 123.33, 123.12, 123.00, 122.80, 122.71, 122.70, 122.62, 122.50, 121.81, 121.77, 120.86, 47.31, 38.64, 38.41, 30.70, 30.18, 29.73, 27.65, 27.26, 24.72; LCMS (CI-(+))  $m/z$  (rel. int.) 739 (8), 738 (10), 737 (31), 736 (42), 735 (96), 734 (43), 733 ( $[M+H]^+$ , 100); HRMS (APPI) calculated for  $C_{49}H_{40}Cl_3$  ( $[M+H]^+$ ) 733.2177, found 733.2864; 1,1,9,9-tetramethyl-4,13-dichloro[9](2,11)teropyrenophane **157d** and 1,1,9,9-tetramethyl-4,18-dichloro[9](2,11)teropyrenophane **158d**: (46 mg, 42%) as a dark brown crystalline solid:  $R_f$  = 0.42 (10% ethyl acetate / hexanes); m.p. > 300 °C;  $^1H$  NMR (300 MHz,  $CDCl_3$ )  $\delta$  8.74 (d,  $J=9.9$  Hz, 2H), 8.71 (d,  $J=9.9$  Hz, 2H), 8.64 (d,  $J=9.9$  Hz, 2H), 8.61 (d,  $J=9.9$  Hz, 2H), 8.54 (s, 4H), 8.45 (d,  $J=9.4$  Hz, 2H), 7.92 (s, 2H), 7.86 (d,  $J=1.6$  Hz, 2H), 7.77 (d,  $J=9.4$  Hz, 2H), 7.75 (d,  $J=9.4$  Hz, 2H), 7.51 (d,  $J=1.6$  Hz, 2H), 7.46 (s, 2H), 1.36 (s, 6H), 1.35 (s, 6H), 1.32 (s, 6H), 1.31 (s, 6H), 0.85–0.65 (m, 8H), 0.10–(–0.05) (m, 8H), (–0.50)–(–0.68) (m, 4H), (–0.98)–(–1.18) (m, 8H);  $^{13}C$  NMR (75 MHz,  $CDCl_3$ )  $\delta$  146.06, 145.12, 144.22, 130.81, 130.33, 127.70, 127.67, 126.75, 126.31, 126.20, 125.77, 125.65, 125.60, 125.47, 125.03, 124.65, 123.46, 123.17, 123.08, 122.75, 122.68, 122.61, 122.56, 122.03, 121.99, 121.86, 121.80, 121.64, 121.17, 120.60, 119.65, 46.28, 37.56, 37.33, 37.11, 29.64, 29.15, 28.68, 26.42, 23.66; LCMS (CI-(+))  $m/z$  (rel. int.) 704 (6), 703 (20), 702 (37), 701 (78), 700 (63), 699 ( $[M+H]^+$ , 100); HRMS (APPI) calculated for  $C_{49}H_{41}Cl_2$  ( $[M+H]^+$ ) 699.2567, found 699.2517.

### Modified synthesis of 1,1,9,9-tetramethyl[9](2,11)teropyrenophane **103d**

Cyclophanemonoene **109d** (2.10 g, 3.31 mmol) was dissolved in dichloromethane (300 mL) and DDQ (2.02 g, 7.28 mmol) was added. Methanesulfonic acid (0.43 mL, 6.62 mmol) in dichloromethane (200 mL) was added at once to this solution and the reaction

mixture was stirred at room temperature for 10 min. The reaction mixture was quenched with 2.50 M aqueous NaOH (200 mL) and the organic layer was separated. The aqueous layer was extracted with dichloromethane ( $2 \times 100$  mL) and the combined organic layer was washed with brine solution (300 mL), dried over Na<sub>2</sub>SO<sub>4</sub>, filtered and concentrated. The solid was subjected to column chromatography (8.5 cm  $\times$  10 cm; 2% ethyl acetate / hexanes) to obtain 1,1,9,9-tetramethyl[9](2,11)teropyrenophane **103d** (1.85 g, 83%) as an orange red solid.

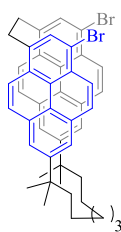
#### Preparation of 1,1,10,10-Tetramethyl[10](2,11)teropyrenophane **103e**



Cyclophanemonoene **109e** (0.025 mg, 0.04 mmol) was dissolved in dichloromethane (3.0 mL) and DDQ (0.019 mg, 0.08 mmol) was added. Methanesulfonic acid (5.0  $\mu$ L, 0.08 mmol) in dichloromethane (2.0 mL) was added at once to this solution and the reaction mixture was stirred at room temperature for 35 min. The reaction mixture was quenched with 2.50 M aqueous NaOH (10 mL) and the organic layer was separated. The aqueous layer was extracted with dichloromethane ( $2 \times 10$  mL) and the combined organic layer was washed with brine solution (10 mL), dried over Na<sub>2</sub>SO<sub>4</sub>, filtered and concentrated. The resulting solid residue was subjected to column chromatography (2.5 cm  $\times$  15 cm; 2% ethyl acetate / hexanes) to first afford teropyrenophane **103e** (22 mg, 90%) as an

orange red solid:  $R_f = 0.45$  (10% ethyl acetate / hexanes); m.p.  $>300\text{ }^{\circ}\text{C}$ ;  $^1\text{H}$  NMR (300 MHz,  $\text{CDCl}_3$ )  $\delta$  8.90 (s, 4H), 8.64 (d,  $J=9.5\text{ Hz}$ , 4H), 7.88 (d,  $J=9.5\text{ Hz}$ , 4H), 7.62 (s, 4H), 1.41 (s, 12H), 0.91–0.75 (m, 8H),  $-0.04$  (br s, 4H),  $(-0.40)$ – $(-0.52)$  (br m, 4H);  $^{13}\text{C}$  NMR (75 MHz,  $\text{CDCl}_3$ )  $\delta$  145.45, 129.08, 127.44, 126.82, 125.88, 125.00, 124.67, 123.73, 123.47, 123.15, 122.73, 47.33, 38.32, 30.24, 29.97, 29.73, 27.45, 24.14; LCMS (CI-(+))  $m/z$  (rel. int.) 648 (6), 647 (18), 646 (38), 645 ( $[\text{M}+\text{H}]^+$ , 100); HRMS (APPI) calculated for  $\text{C}_{50}\text{H}_{45}$  ( $[\text{M}+\text{H}]^+$ ) 645.3503, found 645.3502. Compound **168e**; (2.0 mg, 0.5%) as a brown solid:  $R_f = 0.05$  (10% ethyl acetate / hexanes);  $^1\text{H}$  NMR (300 MHz,  $\text{CDCl}_3$ )  $\delta$  8.96 (d,  $J=10.0\text{ Hz}$ , 1H), 8.95 (d,  $J=10.0\text{ Hz}$ , 1H), 8.89 (d,  $J=9.9\text{ Hz}$ , 1H), 8.84 (d,  $J=10.0\text{ Hz}$ , 1H), 8.67 (d,  $J=1.5\text{ Hz}$ , 1H), 8.66 (s, 1H), 8.64 (d,  $J=1.5\text{ Hz}$ , 1H), 8.64 (d,  $J=9.7\text{ Hz}$ , 1H), 7.92 (d,  $J=9.4\text{ Hz}$ , 1H), 7.91 (d,  $J=9.4\text{ Hz}$ , 1H), 7.90 (d,  $J=1.5\text{ Hz}$ , 1H), 7.88 (d,  $J=9.5\text{ Hz}$ , 1H), 7.70 (d,  $J=1.5\text{ Hz}$ , 1H), 7.64 (s, 2H), 5.45–5.28 (m, 2H), 5.21–5.05 (m, 1H), 4.34–4.00 (m, 1H), 3.25 (s, 3H), 2.38–2.25 (m, 2H), 2.11–1.96 (m, 4H), 1.42 (s, 12H),  $-0.04$  (br s, 6H),  $(-0.46)$ – $(-0.61)$  (br s, 4H); LCMS (CI-(+))  $m/z$  (rel. int.) 742 (4), 741 (20), 740 (51), 739 ( $[\text{M}+\text{H}]^+$ , 100); HRMS (APPI) calculated for  $\text{C}_{51}\text{H}_{47}\text{O}_3\text{S}$  ( $[\text{M}+\text{H}]^+$ ) 739.3228, found 738.3222.

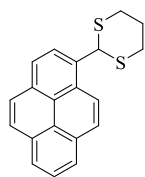
### Synthesis of 14,24-dibromo-1,1,9,9-tetramethyl[9.2](7,1)pyrenophane (**140d**)



Cyclophane **107d** (200 mg, 0.3 mmol) was dissolved in dichloromethane (3.0 mL) and Fe filings (4.7 mg, 0.1 mmol) were added. To this slurry, bromine (126 mg, 0.79 mmol) was added and the reaction mixture was continued to stir at  $15\text{--}20\text{ }^{\circ}\text{C}$  over a period of 1 h. The solution was quenched using saturated sodium thiosulphate solution (1.0 mL) and was poured into ice-cold water (3.0 mL). The

organic layer was separated and the aqueous layer was washed with dichloromethane (3 × 3.0 mL). The combined organic layers were washed with brine, dried over anhydrous sodium sulphate and were concentrated under reduced pressure to afford dibromo compound **104d** (240 mg, 95%) as a pale yellow solid:  $R_f$  = 0.45 (30% dichloromethane / hexanes);  $^1\text{H}$  NMR (300 MHz,  $\text{CDCl}_3$ )  $\delta$  8.32 (d,  $J$ =8.6 Hz, 4H), 8.30 (s, 2H), 7.99 (d,  $J$ =9.2 Hz, 4H), 7.93 (d,  $J$ =1.7 Hz, 2H), 7.64 (d,  $J$ =1.7 Hz, 2H), 7.15–7.05 (m, 4H), 1.64–1.55 (br m, 4H), 1.39 (s, 12H), 0.95 (br m, 6H), 0.72–0.57 (br m, 4H);  $^{13}\text{C}$  NMR (75 MHz,  $\text{CDCl}_3$ )  $\delta$  147.33, 136.62, 131.35, 130.62, 130.23, 129.00, 128.43, 128.05, 126.62, 125.86, 125.56, 123.22, 122.95, 122.64, 122.04, 119.53, 45.36, 38.16, 34.98, 29.69, 29.36, 28.98, 24.75; LCMS and HRMS data could not be obtained.

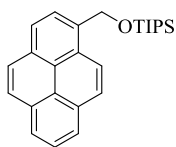
### Synthesis of 2-(pyrene-1-yl)-1,3-dithiane **131**



Aldehyde **126** (100 mg, 0.4 mmol) was suspended in acetonitrile (5.0 mL) and 1,3-propanedithiol (52 mg, 0.5 mmol) was added. To this  $\text{Mg}(\text{HSO}_4)_2$  (19 mg, 0.1 mmol) was added and the resulting pale yellow suspension was stirred at room temperature for 5 min. Dichloromethane (10 mL) was added and the solution was washed with saturated  $\text{NaHCO}_3$ , dried over anhydrous sodium sulfate and concentrated under reduced pressure to afford dithiane **131** (139 mg, 99%) as an off-white solid:  $R_f$  = 0.43 (20% ethyl acetate / hexanes); LCMS (CI-(+))  $m/z$  (rel. int.) 323 (10), 322 (22), 321 ( $[\text{M}+\text{H}]^+$ , 100); HRMS (EI-(+)) calculated for  $\text{C}_{20}\text{H}_{16}\text{S}_2$  ( $[\text{M}]^+$ ) 320.0693, found 320.0711.

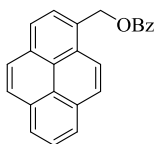


### Synthesis of 1-(triisopropyloxymethyl)pyrene **132**



1-(Hydroxymethyl)pyrene **127** (20 mg, 0.10 mmol) was dissolved in dichloromethane (5.0 mL) and TIPSCl (23 mg, 0.10 mmol) was added under a stream of nitrogen atmosphere. To this solution imidazole (15 mg, 0.2 mmol). The reaction mixture was stirred at room temperature for 4 h and then poured into ice-cold water (15 mL). The organic layer was separated and the aqueous layer was extracted with dichloromethane (3 × 5 mL) and the combined organic layers were washed with brine solution (15 mL). The organic layer was dried over anhydrous sodium sulfate and was concentrated under reduced pressure. The residue obtained was subjected to column chromatography (2.5 cm × 6 cm; 4% ethyl acetate / hexanes) to afford compound **132** (33 mg, 99%) as an off-white solid:  $R_f$  = 0.69 (20% ethyl acetate / hexanes);  $^1\text{H}$  NMR (300 MHz,  $\text{CDCl}_3$ )  $\delta$  8.90 (d,  $J$ =9.2 Hz, 1H), 8.17 (d,  $J$ =7.9 Hz, 1H), 8.14–8.07 (m, 3H), 8.04 (d,  $J$ =9.2 Hz, 1H), 7.96 (dd,  $J$ =12.1, 9.0 Hz, 2H), 7.90 (d,  $J$ =7.6 Hz, 1H), 5.66 (s, 2H), 1.34–1.20 (m, 3H), 1.18 (s, 12H), 1.13 (s, 6H);  $^{13}\text{C}$  NMR (75 MHz,  $\text{CDCl}_3$ )  $\delta$  134.87, 131.43, 130.90, 130.57, 127.79, 127.64, 127.37, 126.93, 125.84, 125.10, 125.06, 124.96, 124.83, 124.78, 124.47, 122.89, 63.85, 18.27, 12.28; LCMS (CI(+))  $m/z$  (rel. int.) 390 (6), 389 (37), 388 (81), 387 ( $[\text{M}-\text{H}]^+$ , 100); HRMS (EI(+)) calculated for  $\text{C}_{26}\text{H}_{32}\text{OSi}$  ( $[\text{M}]^+$ ) 388.2222, found 388.2231.

### Synthesis of 1-(benzoyloxymethyl)pyrene **133**



1-(Hydroxymethyl)pyrene **127** (60 mg, 0.3 mmol) was dissolved in dichloromethane (5.0 mL) and benzoyl chloride (55 mg, 0.4 mmol) was added under a stream of nitrogen atmosphere. To this solution DMAP (6.3 mg, 0.1

mmol) and triethylamine (52 mg, 0.5 mmol) were added. The reaction mixture was stirred at room temperature for 30 min and then poured into ice-cold water (15 mL). The organic layer was separated and the aqueous layer was extracted with dichloromethane (3 × 5 mL) and the combined organic layers were washed with brine solution (15 mL). The organic layer was dried over anhydrous sodium sulfate and was concentrated under reduced pressure. The residue obtained was subjected to column chromatography (2.5 cm × 6 cm; 8% ethyl acetate / hexanes) to afford compound **133** (85 mg, 99%) as an off-white solid:  $R_f$  = 0.66 (40% ethyl acetate / hexanes); m.p. 131.8–132.4 °C;  $^1\text{H}$  NMR (300 MHz,  $\text{CDCl}_3$ )  $\delta$  8.45 (d,  $J$ =9.2 Hz, 1H), 8.22–8.10 (m, 4H), 8.10–7.97 (m, 4H), 7.69–7.61 (m, 1H), 7.54–7.46 (m, 2H), 7.42–7.33 (m, 2H), 6.06 (s, 2H);  $^{13}\text{C}$  NMR (75 MHz,  $\text{CDCl}_3$ )  $\delta$  166.62, 134.57, 133.09, 131.82, 131.24, 130.73, 130.61, 130.15, 129.79, 129.70, 128.92, 128.42, 128.30, 127.88, 127.79, 127.41, 126.13, 125.57, 125.50, 124.94, 124.67, 122.99, 65.37; LCMS (CI-(+))  $m/z$  (rel. int.) 337 (28), 636 ( $[\text{M}]^+$ , 100); HRMS (EI-(+)) calculated for  $\text{C}_{24}\text{H}_{16}\text{O}_2$  ( $[\text{M}]^+$ ) 336.1150, found 336.1187.

## 4.5 References

1. a) M. A. Petrukhina, L. T. Scott (eds.), *Fragments of Fullerenes and Carbon Nanotubes*, Wiley-VCH: New Jersey, 2011; b) R. P. Sijbesma, R. J. M. Nolte, *Top. Curr. Chem.* 1995, **175**, 25–56; c) R. A. Pascal, Jr. *Chem. Rev.* 2006, **106**, 4809–4819; d) V. M. Tsefrikas, L. T. Scott, *Chem. Rev.* 2006, **106**, 4868–4884; e) A. Jorio, M. S. Dresselhaus, G. Dresselhaus (eds.), *Carbon Nanotubes: Advanced Topics in the Synthesis, Structure, Properties and Applications*, Springer: Heidelberg, 2008; f) A. Hirsch, M. Brettreich, *Fullerenes: Chemistry and Reactions*, Wiley-VCH, New York, 2005; g) J. E. Anthony, *Angew. Chem.* 2008, **120**, 460–492; *Angew. Chem. Int. Ed.* 2008, **47**, 452–483; h) R. H. Crabtree, *The Organometallic Chemistry of the Transition Metals. 4th ed.*, Wiley, New York, 1992; i) M. S. Arnold, A. A. Green, J. F. Hulvat, S. I. Stup and M. C. Hersam, *Nature Nanotech.* 2006, **1**, 60–65; j) Y. Kato, Y. Niidome and N. Nakashima, *Angew. Chem.* 2009, **121**, 5543–5546; *Angew. Chem. Int. Ed.* 2009, **48**, 5435–5438; H. Omachi, Y. Segawa and K. Itami, *Acc. Chem. Res.* 2012, **45**, 1378–1389. T. Yao, H. Yu, R. J. Vermeiji and G. J. Bodwell, *Pure Appl. Chem.* 2008, **80**, 533–546; T. Kawase and H. Kurata, *Chem. Rev.* 2006, **106**, 5250–5273.
2. a) Y. Kine, M. Brown and V. Boekelheide, *J. Am. Chem. Soc.*, 1979, **101**, 3126–3127; b) Y. Sekine and V. Boekelheide, *J. Am. Chem. Soc.*, 1981, **103**, 1777–1785; W. D. Rohrbach, R. Sheley, V. Boekelheide, *Tetrahedron*, 1984, **40**, 4823–4828.

3. H. Hopf, *Classics in Hydrocarbon Chemistry: Synthesis, Concepts, Perspectives*, Wiley-VCH: Weinheim, 2000.
4. H. W. Kroto, J. R. Heath, S. C. O'Brien, R. F. Curl and R. E. Smalley, *Nature*, 1985, **318**, 162–163.
5. H. Murayama, S. Tomonoh, J. M. Alford and M. E. Karpuk, *Fullerenes, nanotubes and carbon nanostructures*, 2004, **12**, 1–9.
6. W. E. Barth and R. G. Lawton, *J. Am. Chem. Soc.*, 1971, **93**, 1730–1745.
7. a) L. T. Scott, M. M. Hashemi, D. T. Meyer and H. B. Warren, *J. Am. Chem. Soc.*, 1991, **113**, 7082–7084; b) L. T. Scott, P.-C. Cheng, M. M. Hashemi, M. S. Bratcher, D. T. Meyer and H. B. Warren, *J. Am. Chem. Soc.*, 1997, **119**, 10963–10968; c) A. Sygula and P. W. Rabideau, *J. Am. Chem. Soc.*, 2000, **122**, 6323–6324; d) T. J. Seiders, E. L. Elliot, G. H. Grube and J. S. Siegel, *J. Am. Chem. Soc.*, 1999, **121**, 7804–7813.
8. A. M. Butterfield, B. Gilomen and J. S. Seigel, *Org. Process Res. Dev.*, 2012, **16**, 664–676.
9. R. Jasti, J. Bhattacharjee, J. B. Neaton and C. R. Bertozzi, *J. Am. Chem. Soc.*, 2008, **130**, 17646–17647.
10. J. Xia, J. W. Bacon and R. Jasti, *Chem. Sci.*, 2012, **3**, 3018–3021.
11. a) B. L. Merner, L. N. Dawe and G. J. Bodwell, *Angew. Chem. Int. Ed.*, 2009, **48**, 5487–5491; b) B. L. Merner, K. S. Unikela, L. N. Dawe, D. W. Thompson and G.

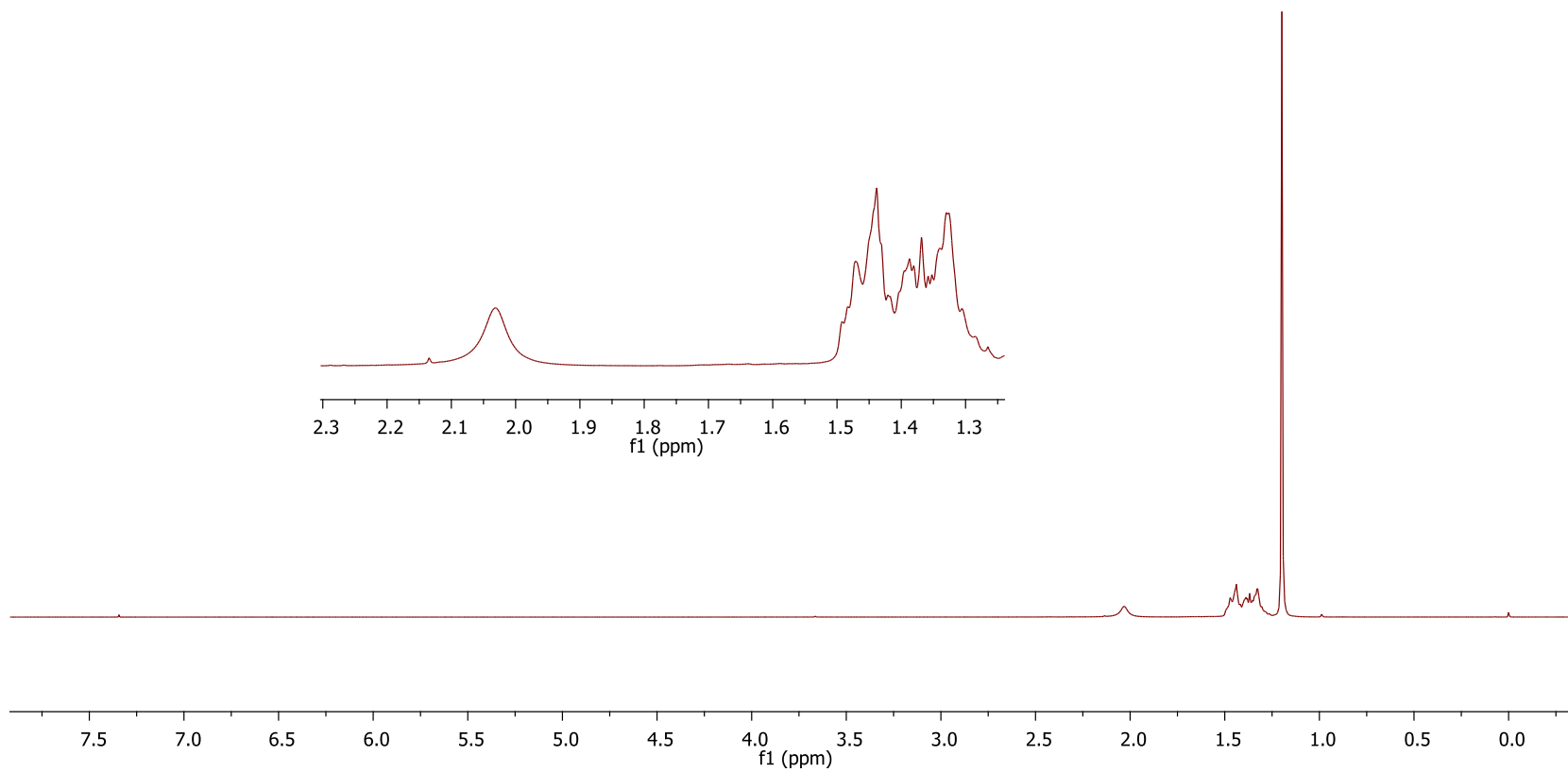
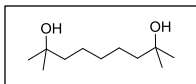
- J. Bodwell, *Chem. Commun.*, 2013, **49**, 5930–5932.
12. T. Umemoto, T. Kawashima, Y. Sakata and S. Misumi, *Tetrahedron Lett.*, 1975, **16**, 1005–1006.
  13. R. M. Roberts and A. A. Khalaf, *Friedel-Crafts Alkylation Chemistry: A Century of Discovery*, M. Dekker: New York, c1984.
  14. Y. Miura, E. Yamano, A. Tanaka and J. Yamauchi, *J. Org. Chem.* 1994, **59**, 3294–3300.
  15. L. Rodenburg, *recl. trav. chim. pays-bas (1920)*, 1986, **105**, 156–161.
  16. a) J. F. Norris and B. M. Sturgis, *J. Am. Chem. Soc.*, 1939, **61**, 1413–1417; b) X. Wang, F. B. Mallory, C. W. Mallory, H. R. Odhner and P. A. Beckmann, *J. Chem. Phys.*, 2014, **140**, 194304/1–194304/15.
  17. J. Pataki, M. Konieczny and R. g. Harvey, *J. Org. Chem.*, 1982, **47**, 1133–1136.
  18. F. –X. Hardy, O. Gause, C. A. Rice and J. P. Maier, *Astrophys. J. Lett.* , 2013, **778**, L30/1–L30/3.
  19. J. A. Morley and N. F. Woolsey, *J. Org. Chem.*, 1992, **57**, 6487–6495.
  20. J. F. W. McOmie (Ed.), *Protective Groups in Organic Chemistry*, Plenum Press: London, 1973.
  21. H. R. Shaterian, A. Hosseini, M. Ghashang and F. Khorami, *Phosphorous, sulfur silicon Relat. Elem.*, 2008, **183**, 2490–2501.

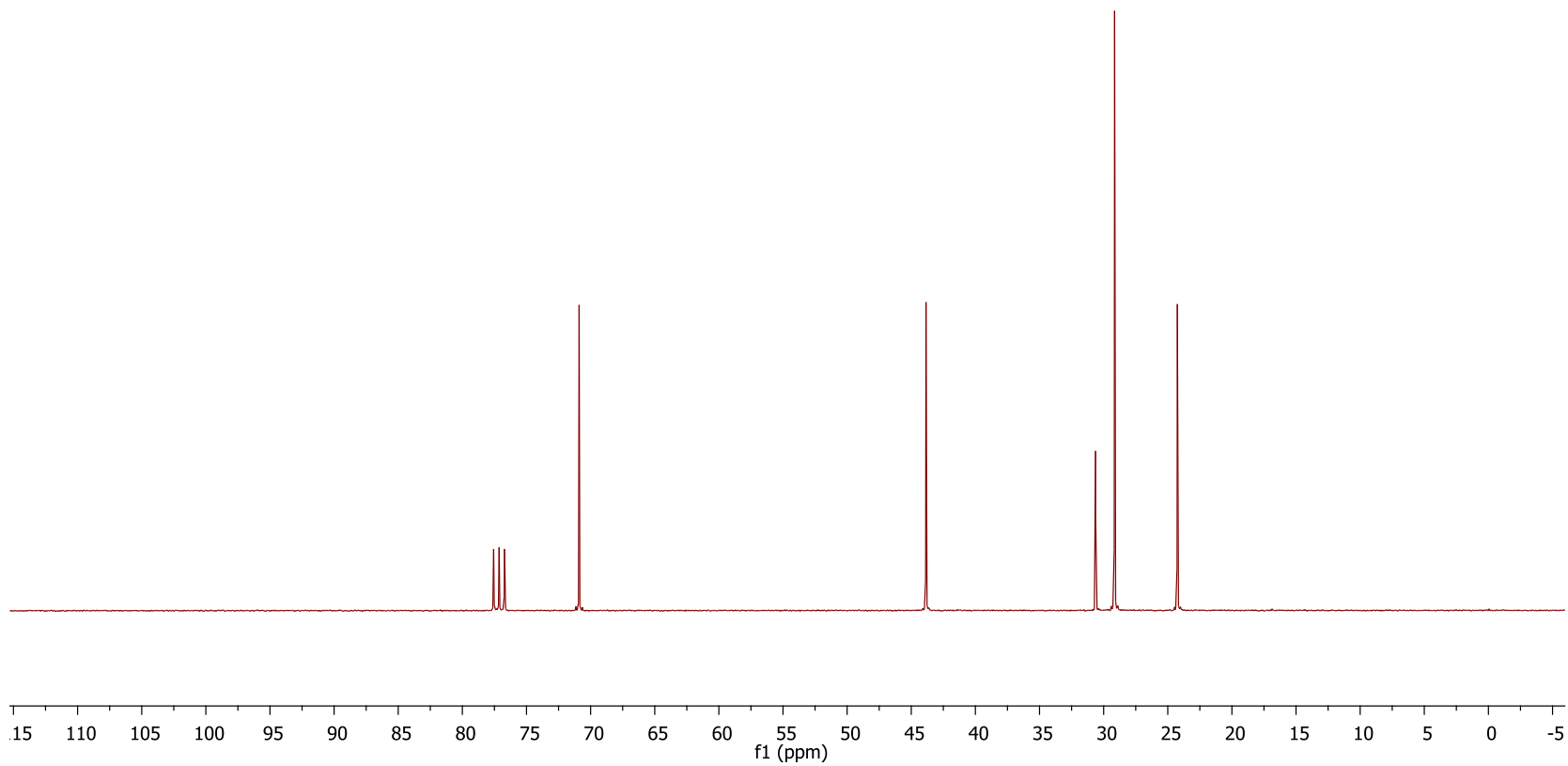
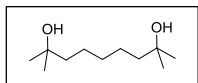
22. J. Hwang, M. G. Choi, J. Bae and S. -K. Chang, *Org. Biomol. Chem.*, 2011, **9**, 7011–7015.
23. K. K. Laali and P. E. Hansen, *J. Org. Chem.*, 1997, **62**, 5804–5810.
24. A. T. Haedler, H. Misslitz, C. Buehlmeier, R. Q. Albuquerque, A. Köhler and H.-W. Schmidt, *ChemPhysChem*, 2013, **14**, 1818–1829.
25. a) S. Nunomoto, Y. Kawakami and Y. Yamashita, *Bulletin Chem. Soc. Jap.*, 1981, **54**, 2831–2832; b) J. W. H. Oldham and A. R. Ubbelohde, *J. chem. Soc.* 1938, 201–206.
26. B. Das, H. Holla, Y. Srinivas, N. Chowdhury and B. P. Bandgar, *Tetrahedron Lett.*, 2007, **48**, 3201–3204.
27. P. R. Nandaluru, P. Dongare, C. M. Kraml, R. A. Pascal Jr., L. N. Dawe, D. W. Thompson and G. J. Bodwell, *Chem. Commun.*, 2012, **48**, 7747–7749.
28. G. J. Bodwell, J. N. Bridson, M. K. Cyranski, J. S. W. Kennedy, T. M. Krygowski, M. R. Mannion and D. O. Miller, *J. Org. Chem.* 2003, **68**, 2089–2098.
29. B. Quintero, M. C. Cabeza, M. I. Martínez, P. Gutiérrez, and P. J. Martínez, *Can. J. Chem.*, 2003, **81**, 832–839.
30. V. S. Batista, R. H. Crabtree, S. J. Konezny, O. R. Luca and J. M. Praetorius, *New J. Chem.*, 2012, **36**, 1141–1144.
31. B. L Merner and G. J. Bodwell, unpublished results.

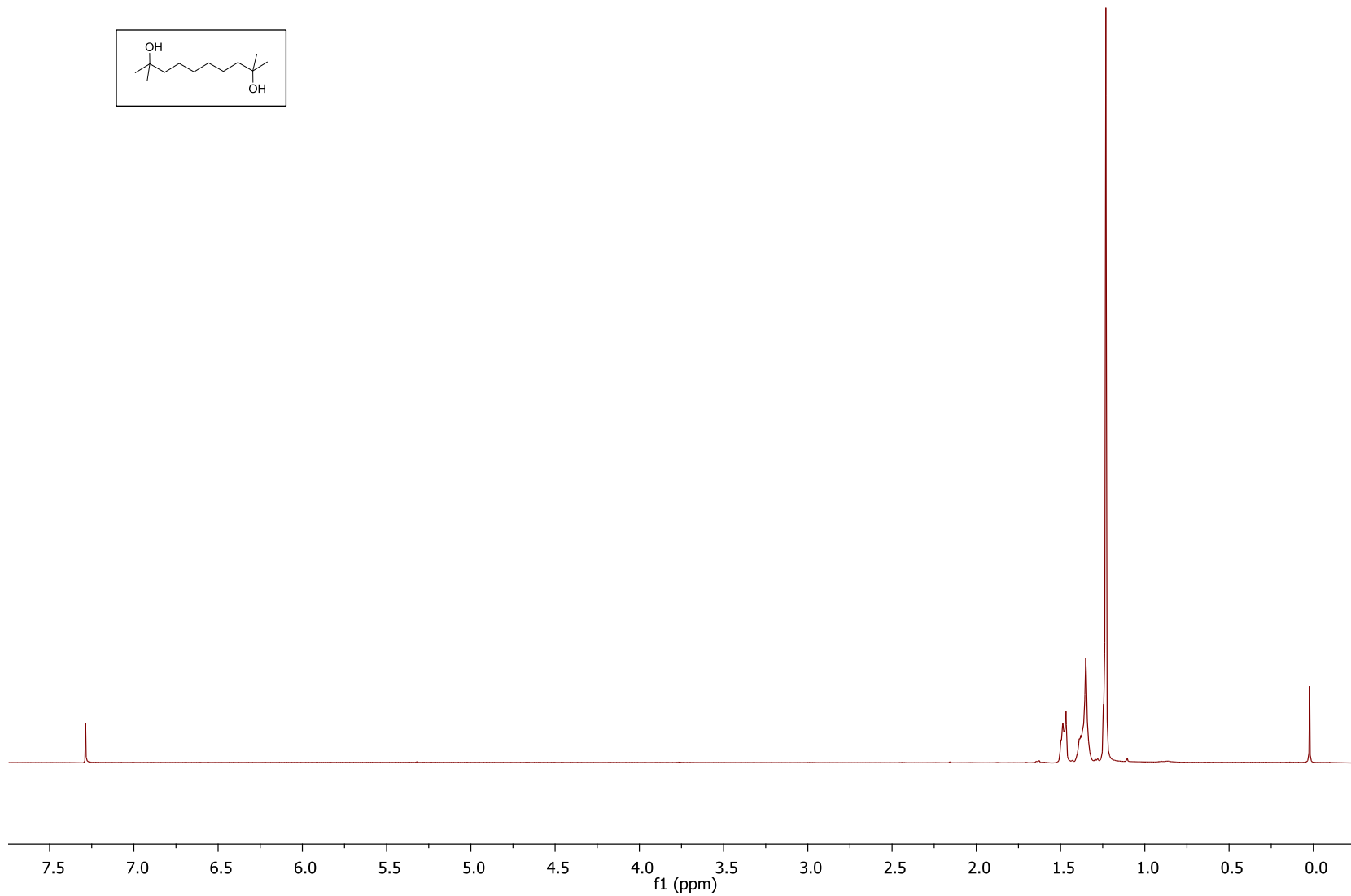
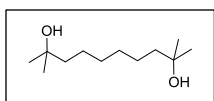
32. a) P. V. P. Pragnacharyulu and E. Abushanab, *Tetrahedron Lett.*, 1997, **38**, 3683–3686; b) Q. Zhang, F. Yang and Y. Wu, *Org. Chem. Front.*, 2014, **1**, 694–697; c) L. Minuti, A. Taticchi, A. Marrocchi, D. Lanari, E. Gacs-Baitz and A. Gomory, *Tetrahedron Lett.*, 2005, **46**, 949–950.
33. L. Zhai, R. Shukla and R. Rathore, *Org. Lett.*, 2009, **11**, 3474–3477.
34. a) J. P. Guthrie, *Can. J. Chem.*, 1978, **56**, 2342–2354; b) A. Albert and E. P. Serjeant, *Ionization Constants of Acids and Bases*, Methuen: London, 1962.
35. S. Przeszlakowski and R. Kocjan, *Chromatographia*, 1979, **12**, 587–594.
36. C. H. Dungan and J. R. V. Wazer, *Compilation of Reported F19 NMR Chemical Shifts, 1951 to Mid-1967*, Wiley-Interscience: London, 1970.
37. D. D. Perrin, B. Dempsey and E. P. Serjeant, *pKa Prediction for Organic Acids and Bases*, Springer: Netherlands, 1981.
38. P. J. Evans, E. R. Darji and R. Jasti, *Nature Chem.*, 2014, **6**, 404–408.

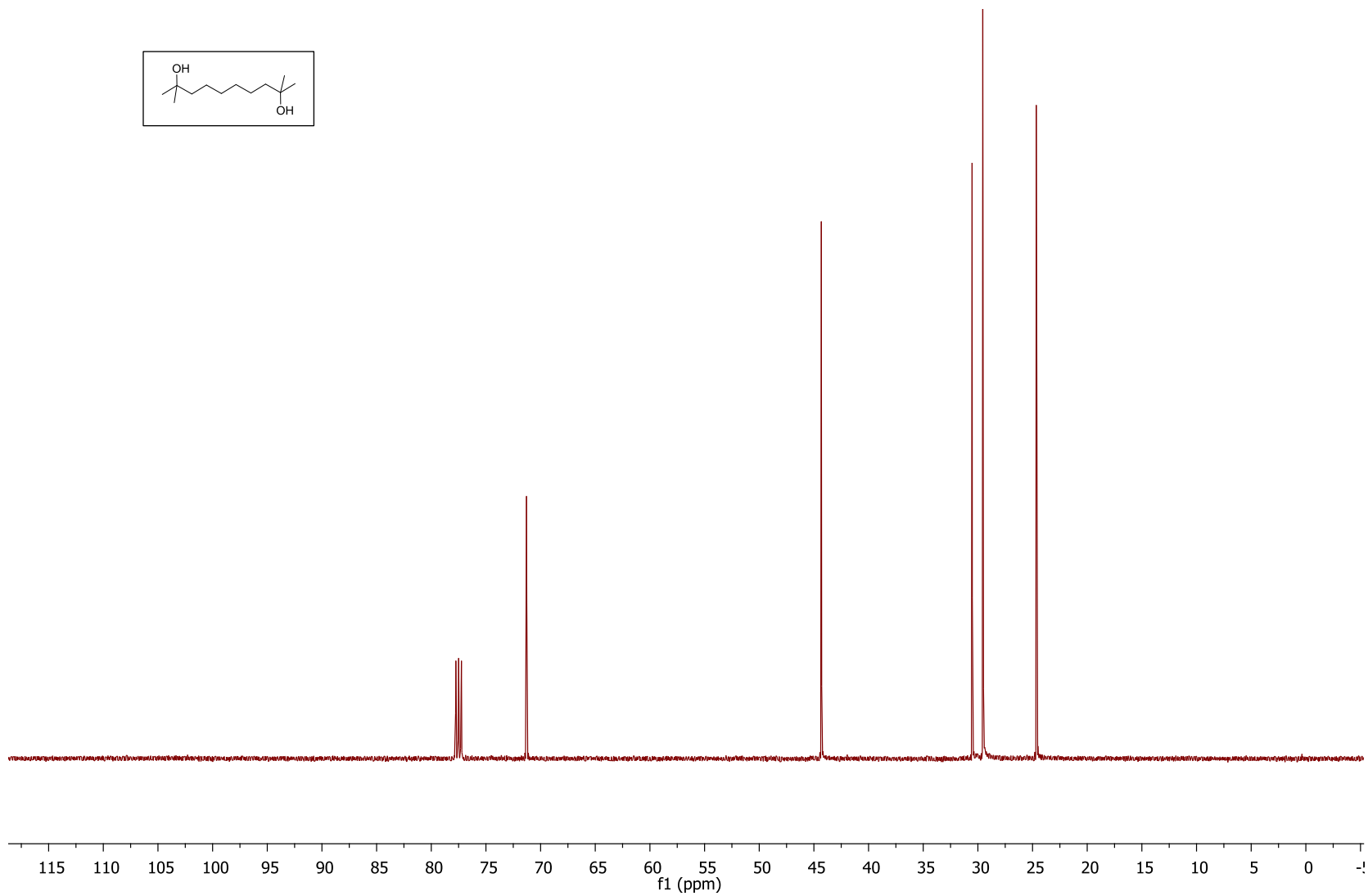
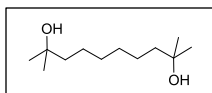
# APPENDIX 2

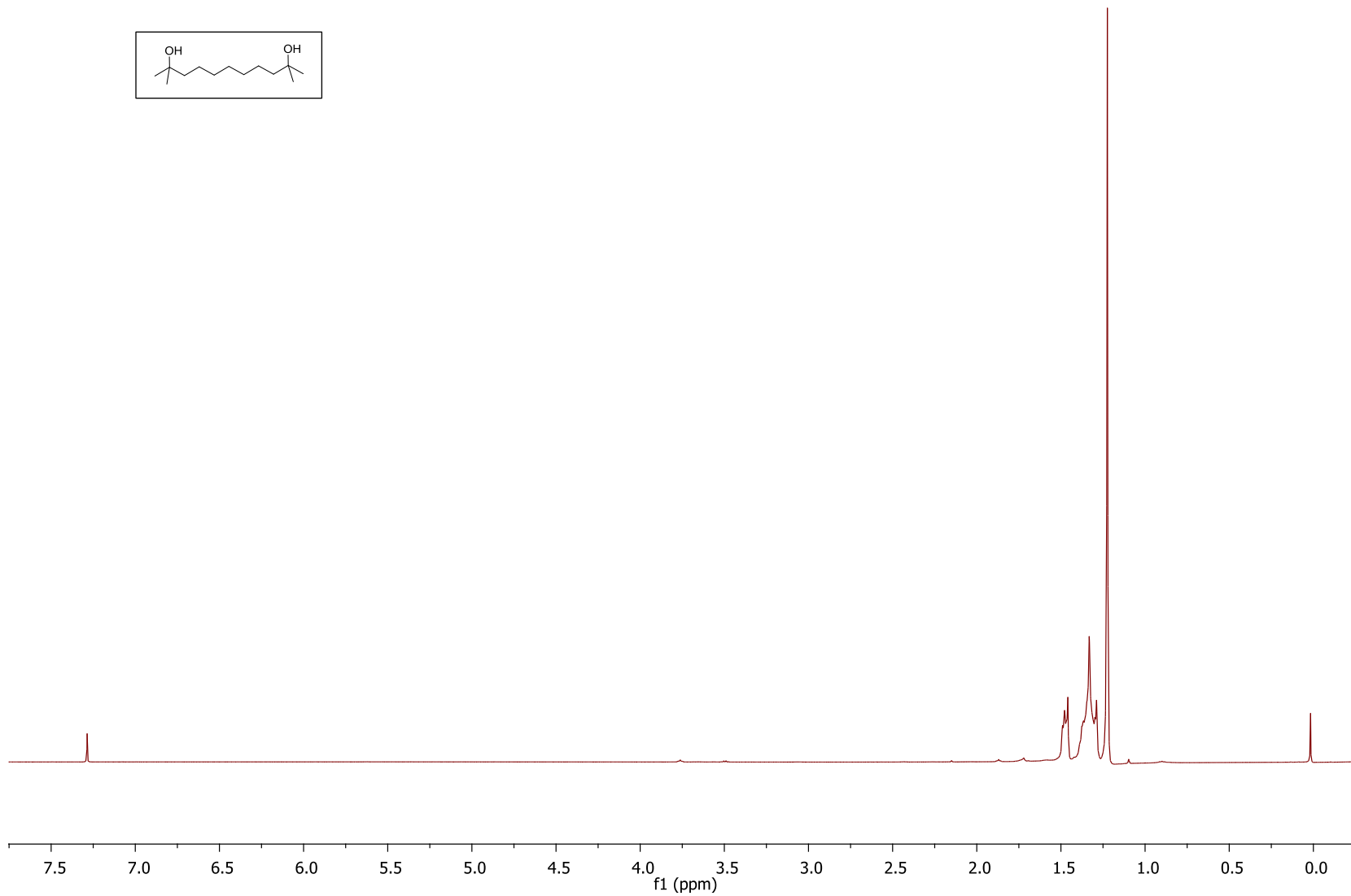
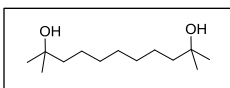


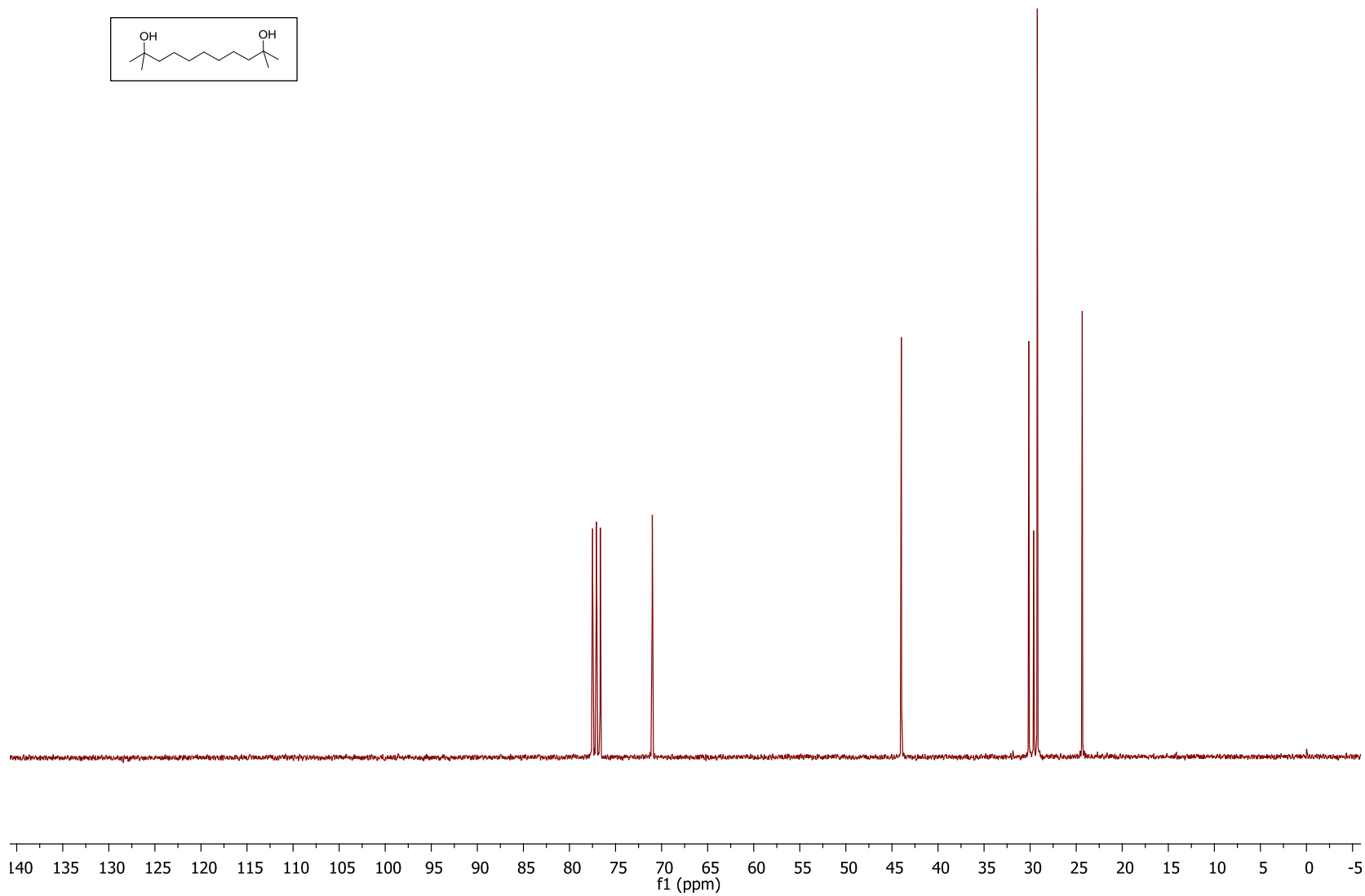
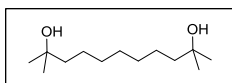


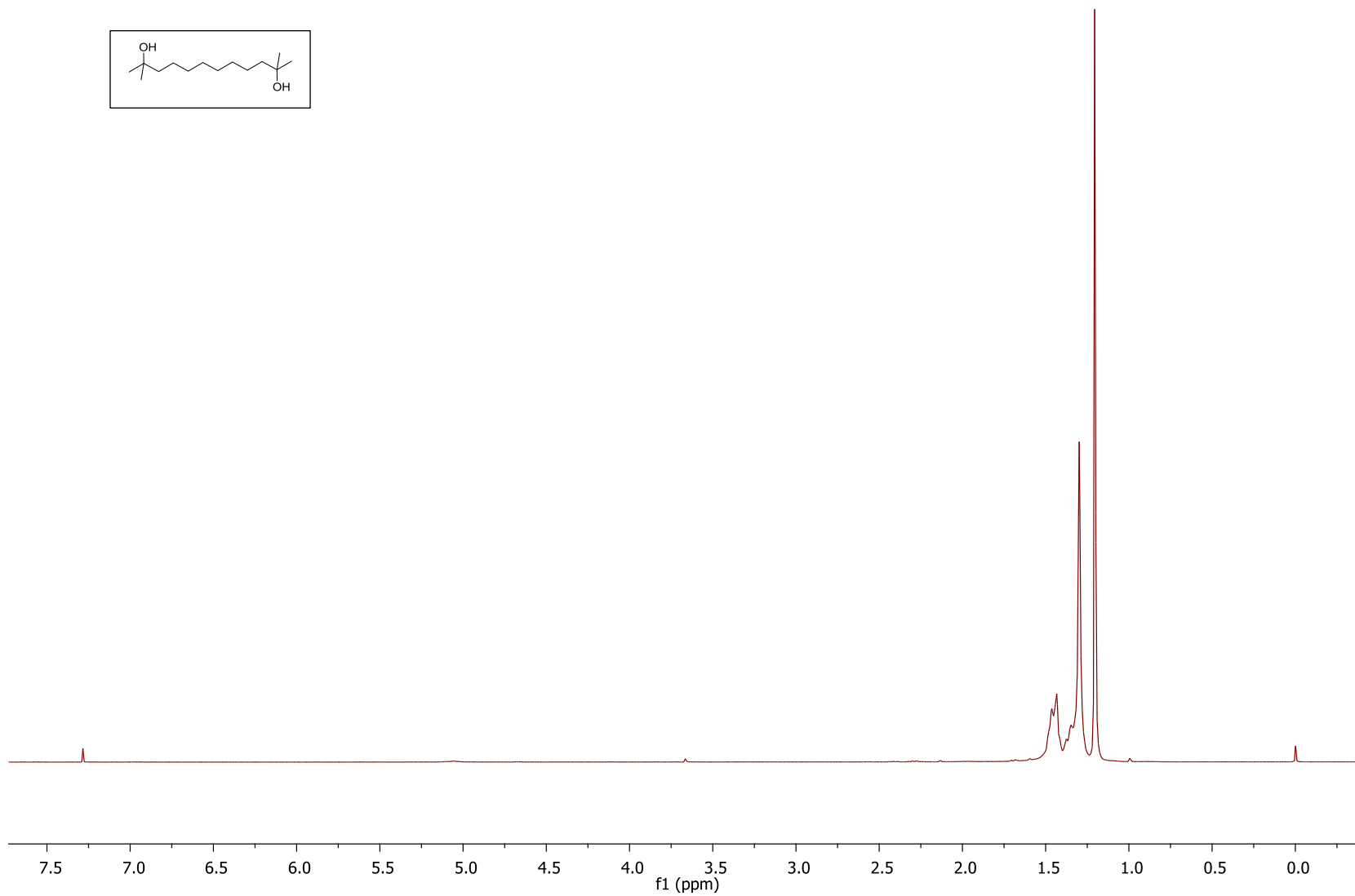
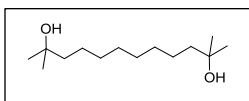


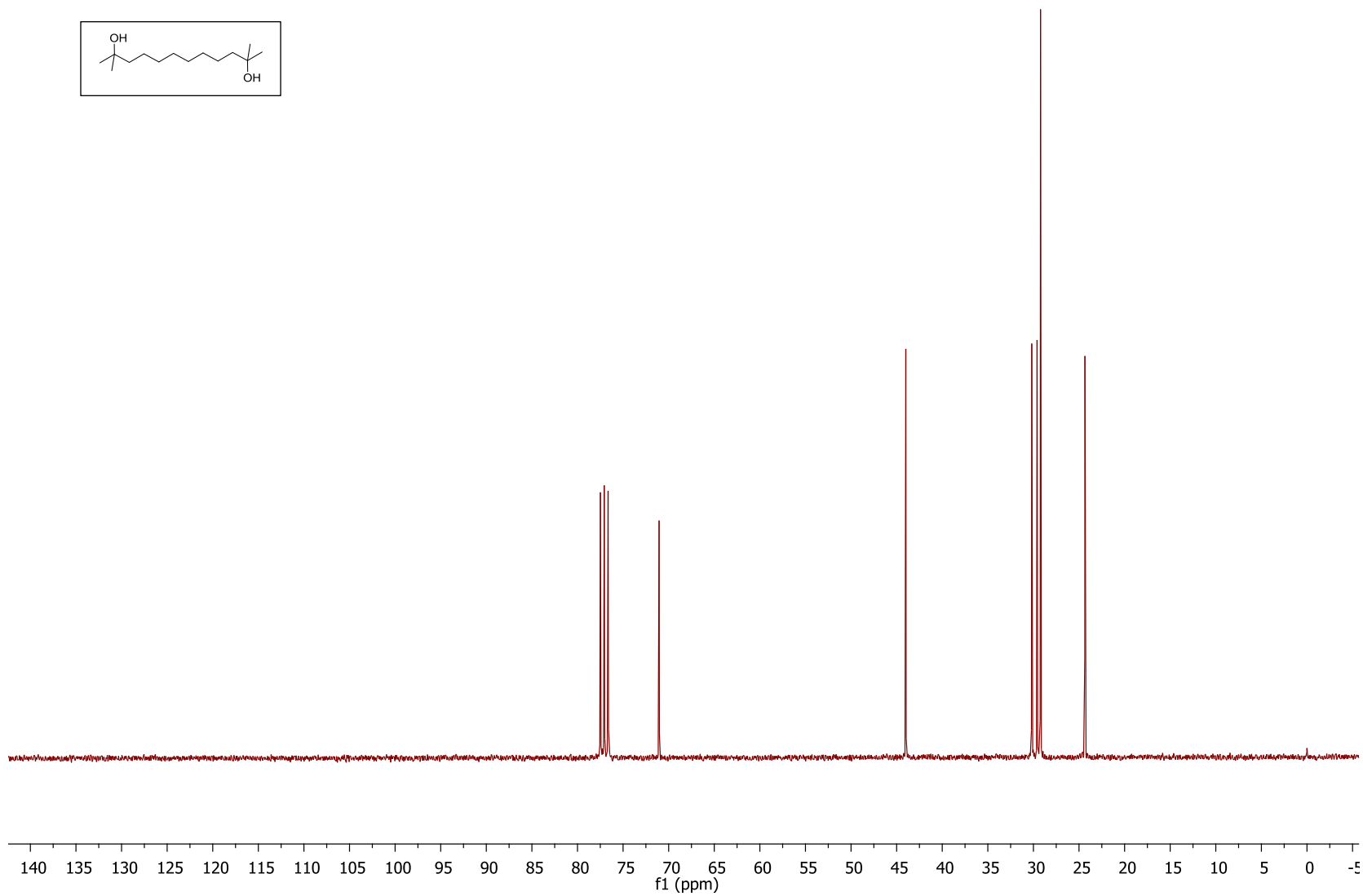
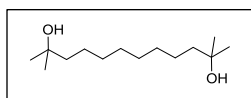




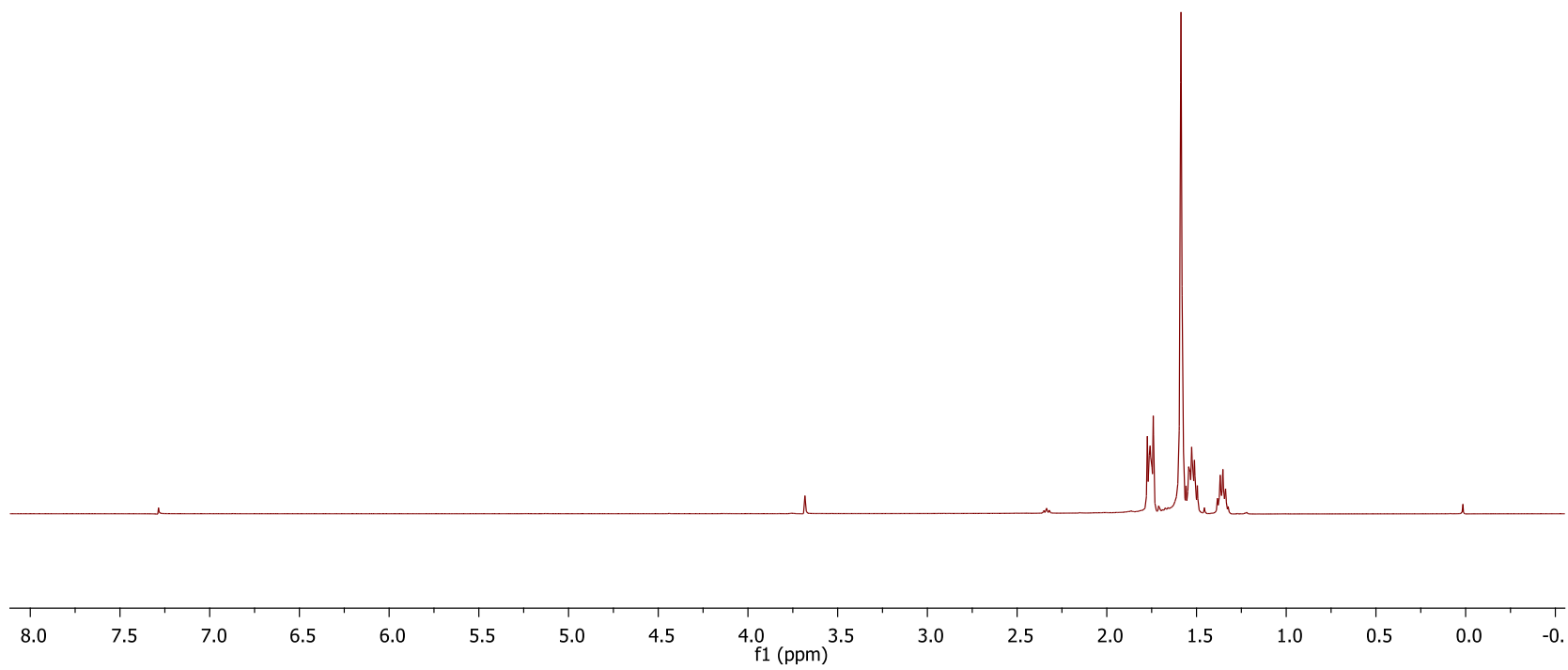
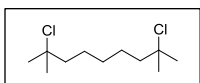


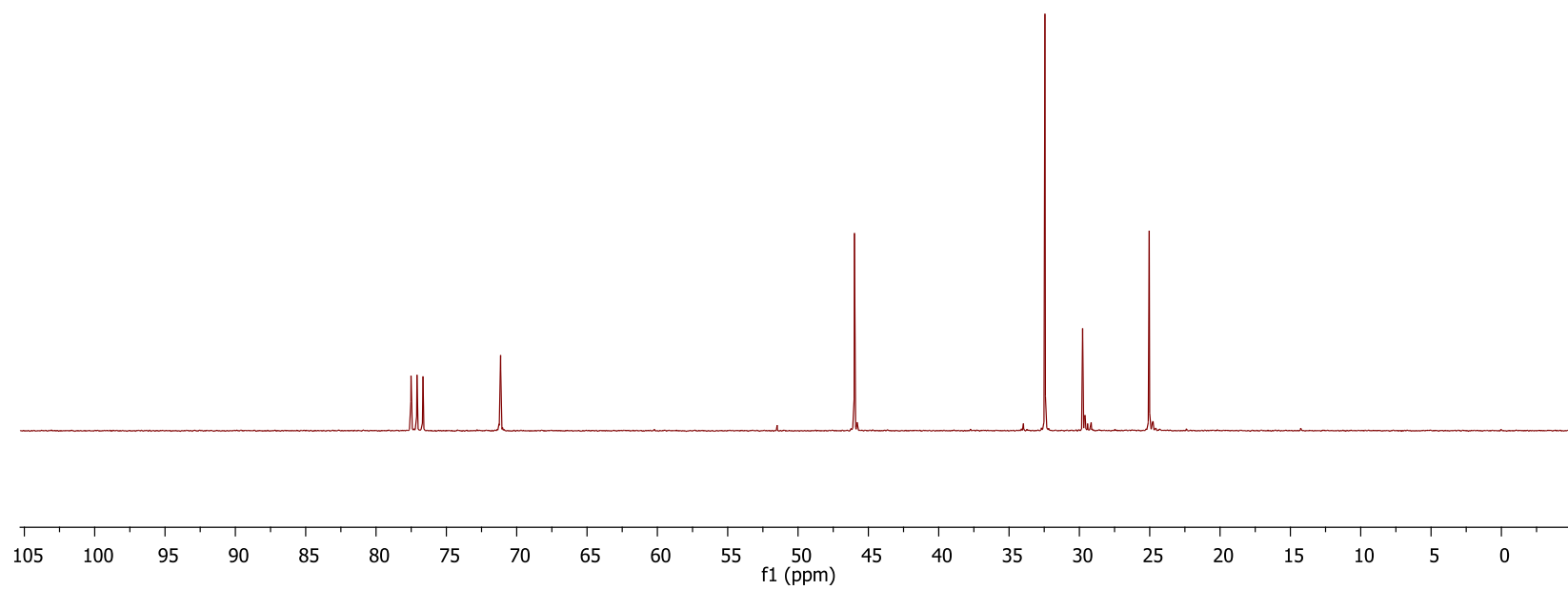
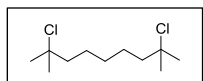


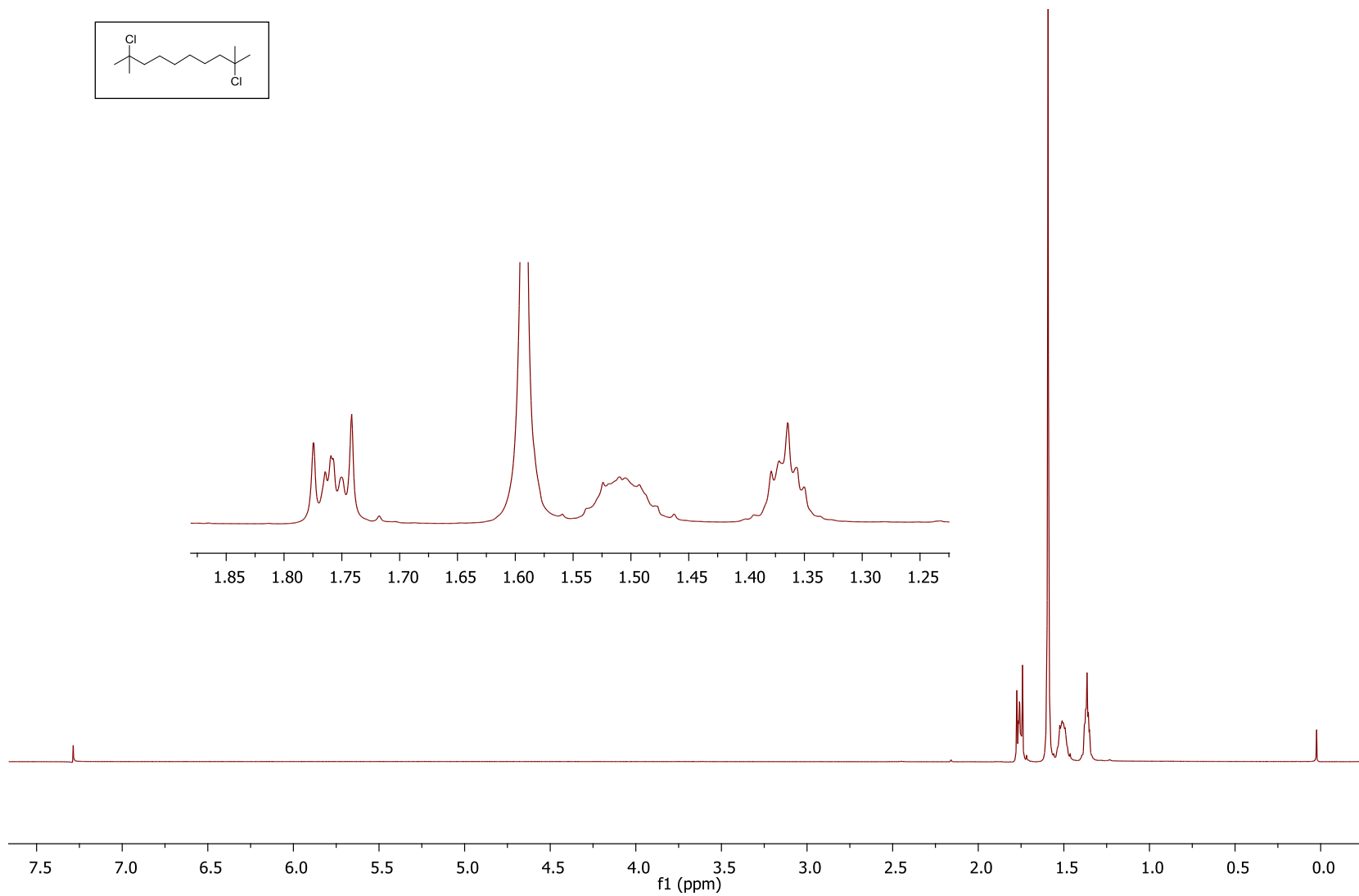
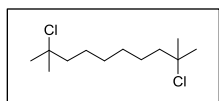


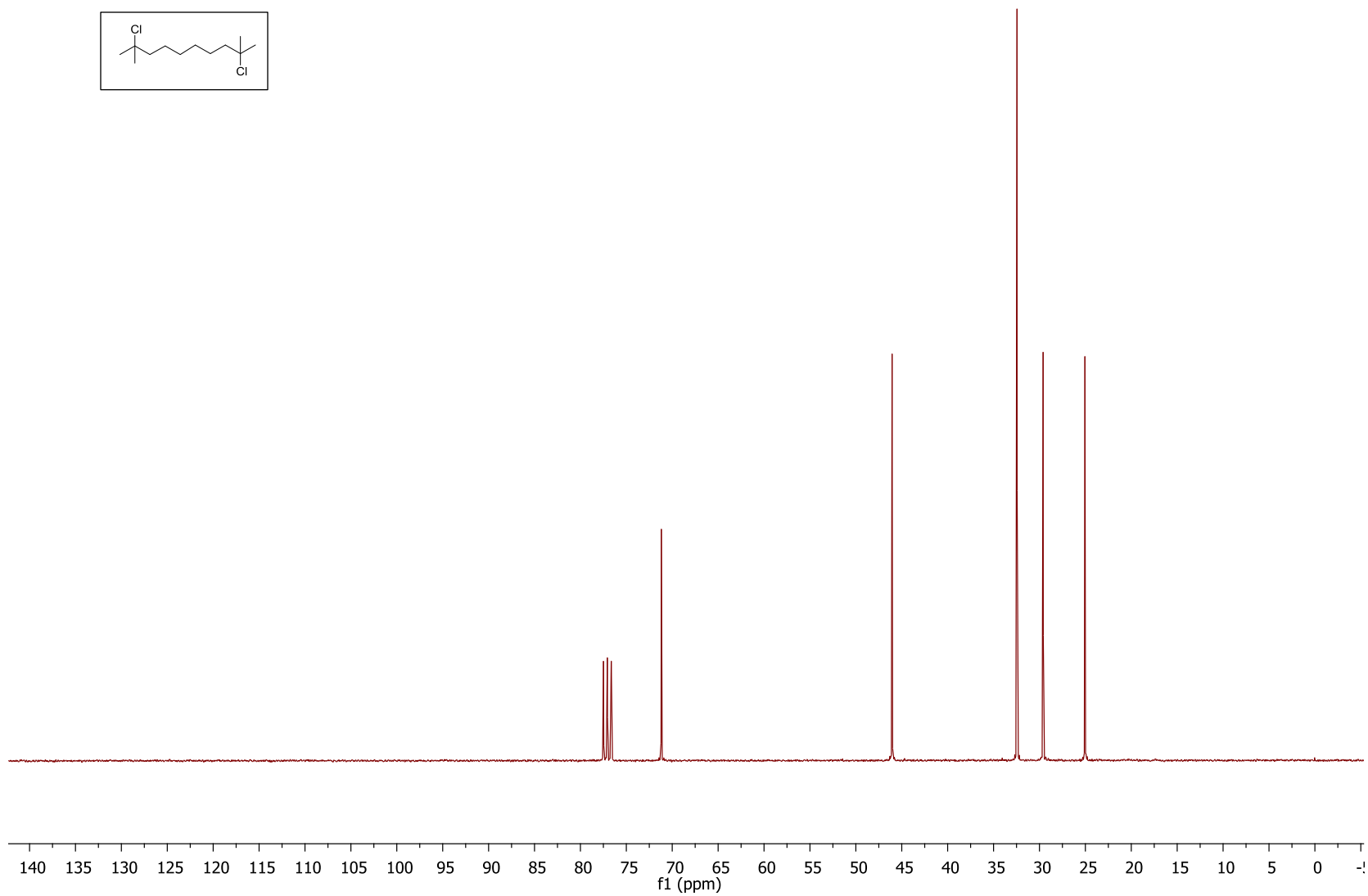
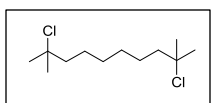


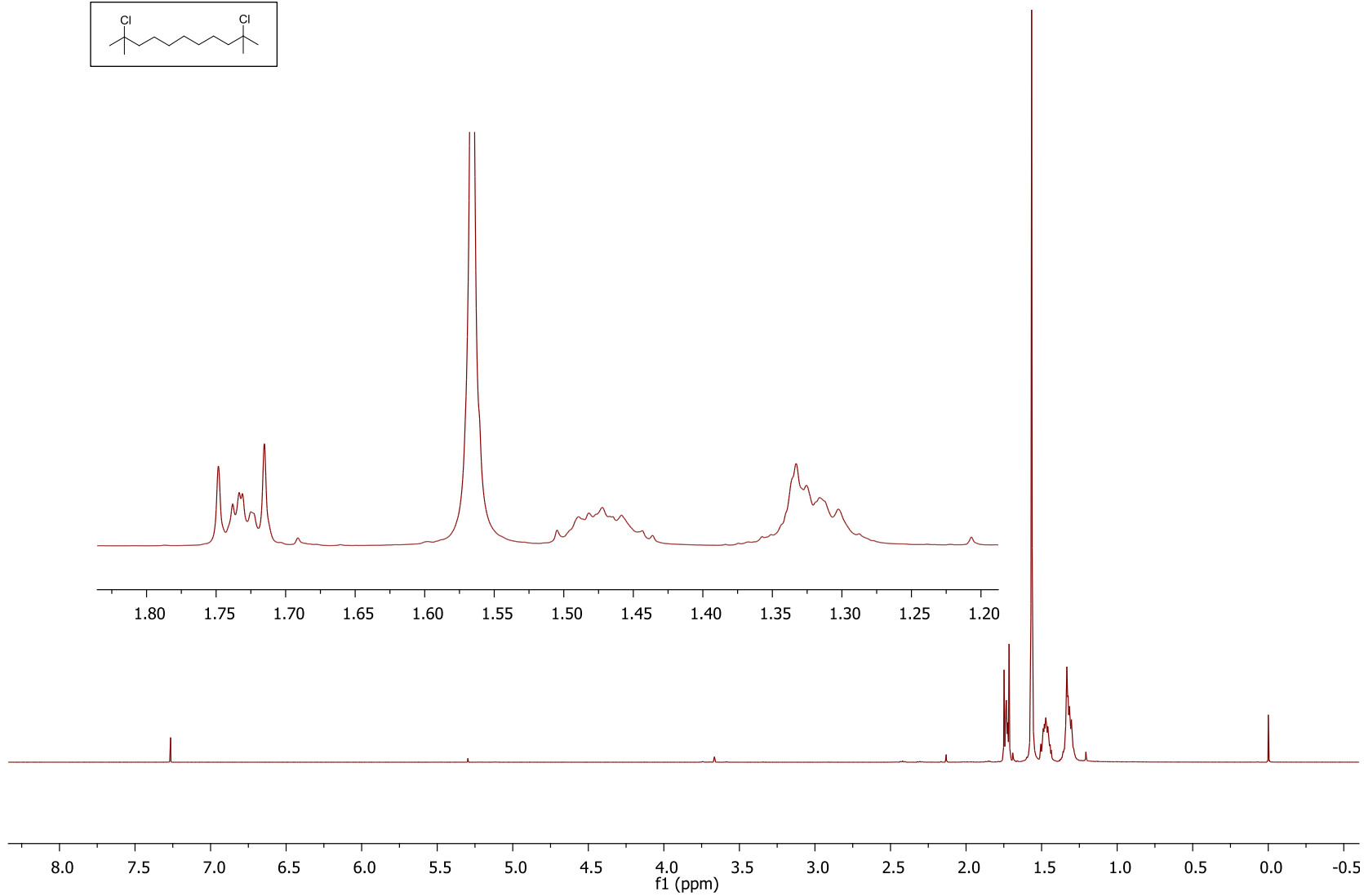
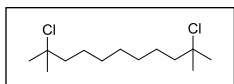


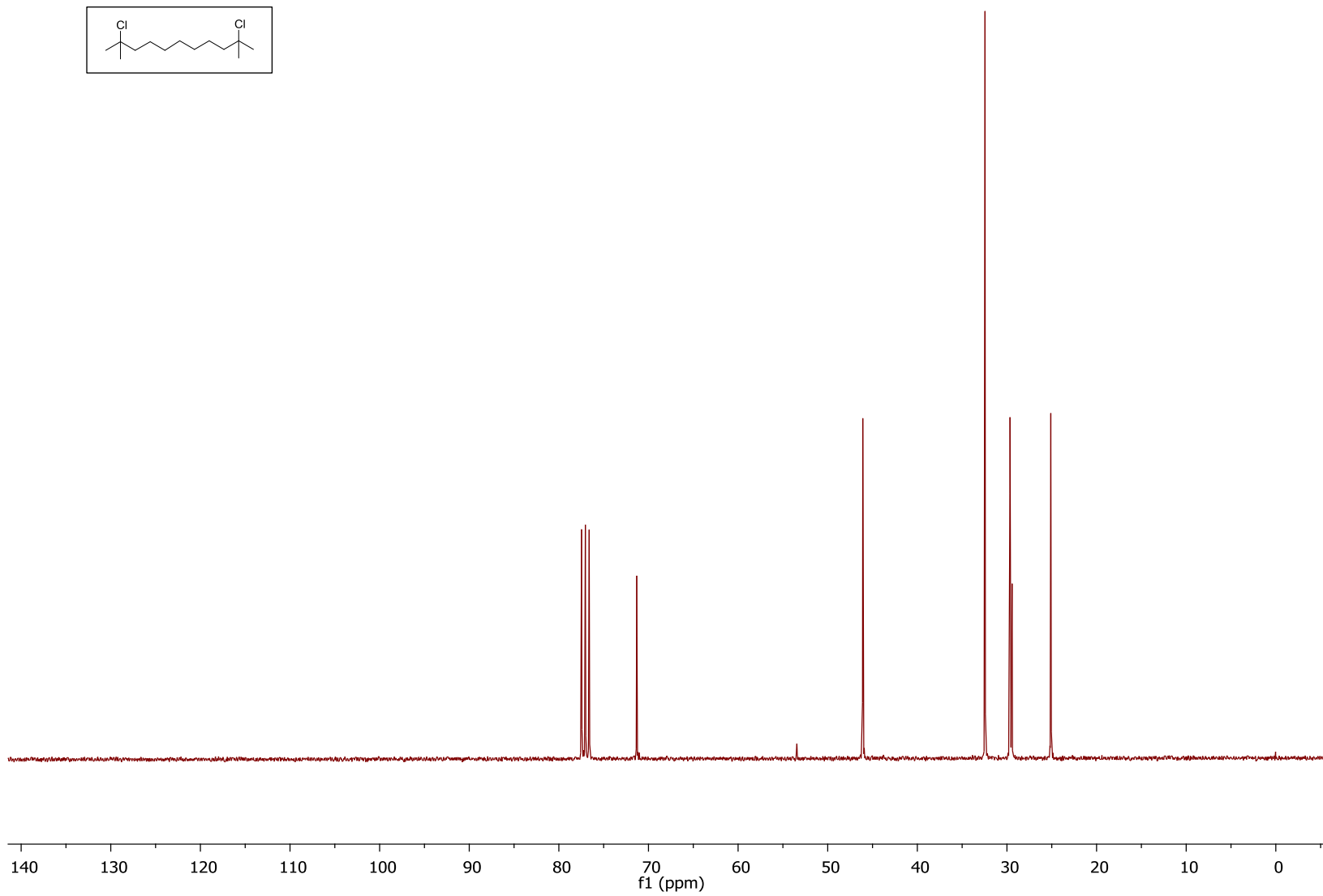
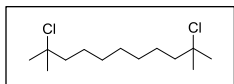


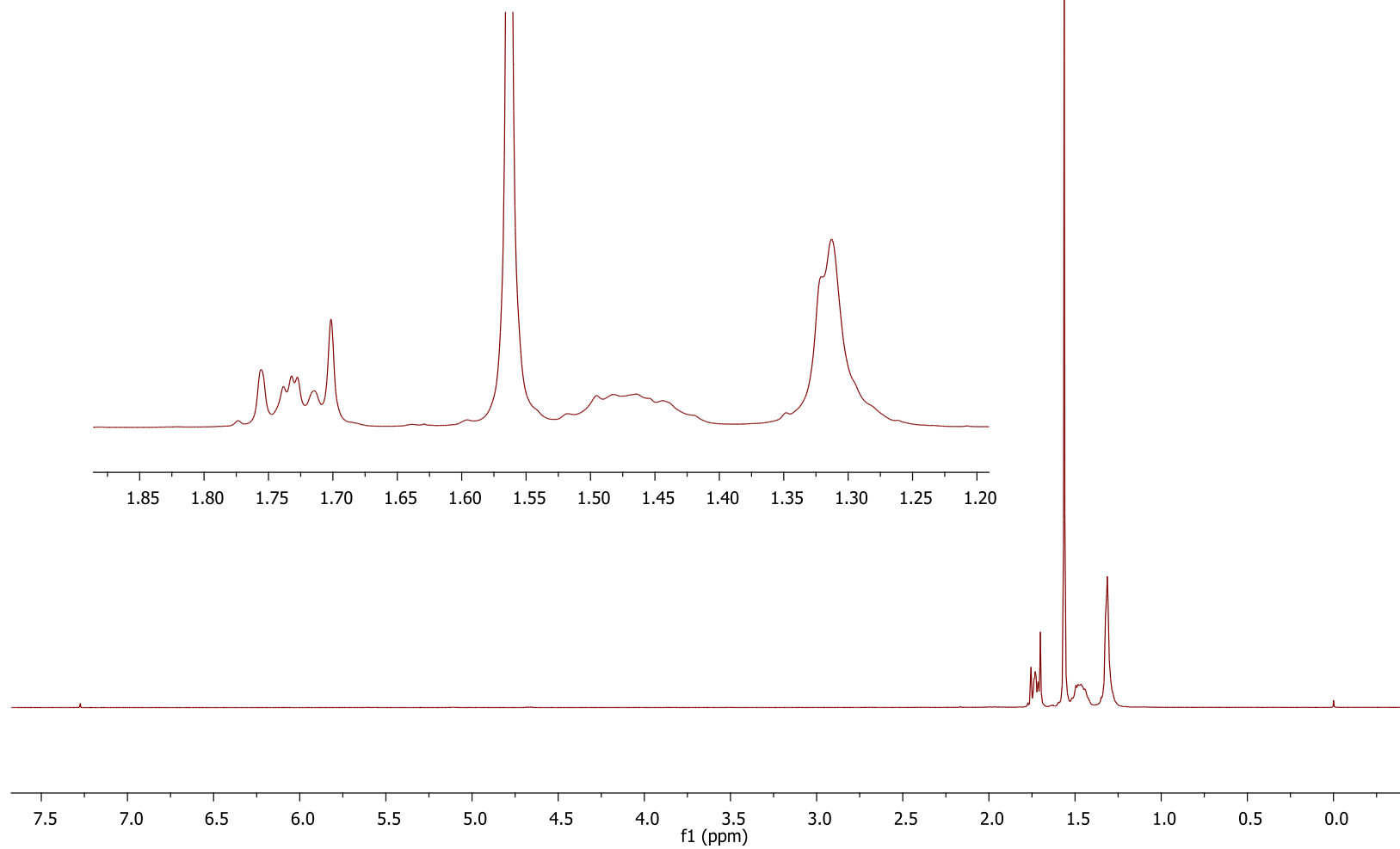
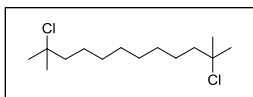


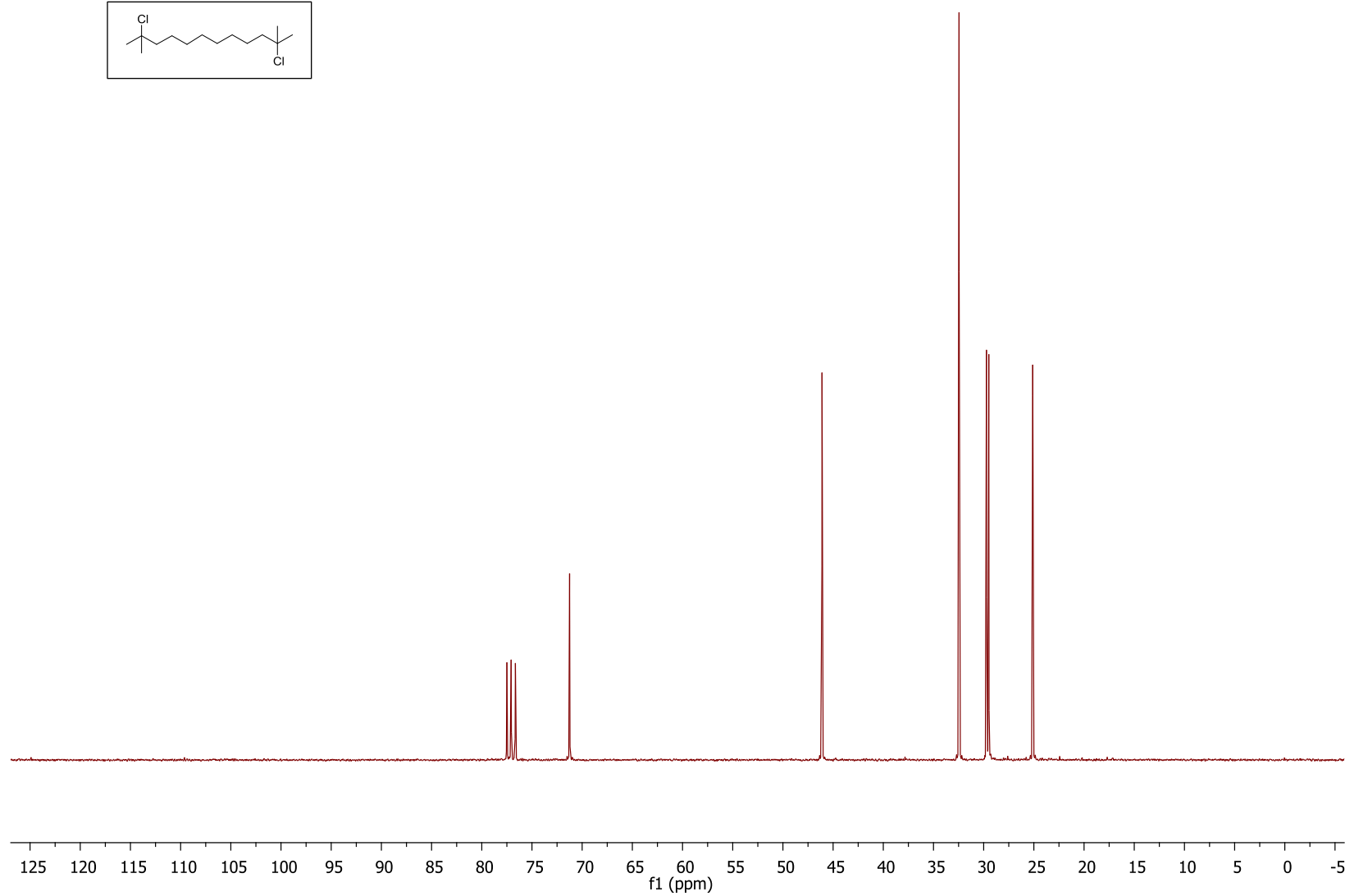
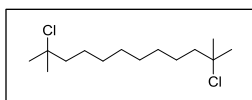




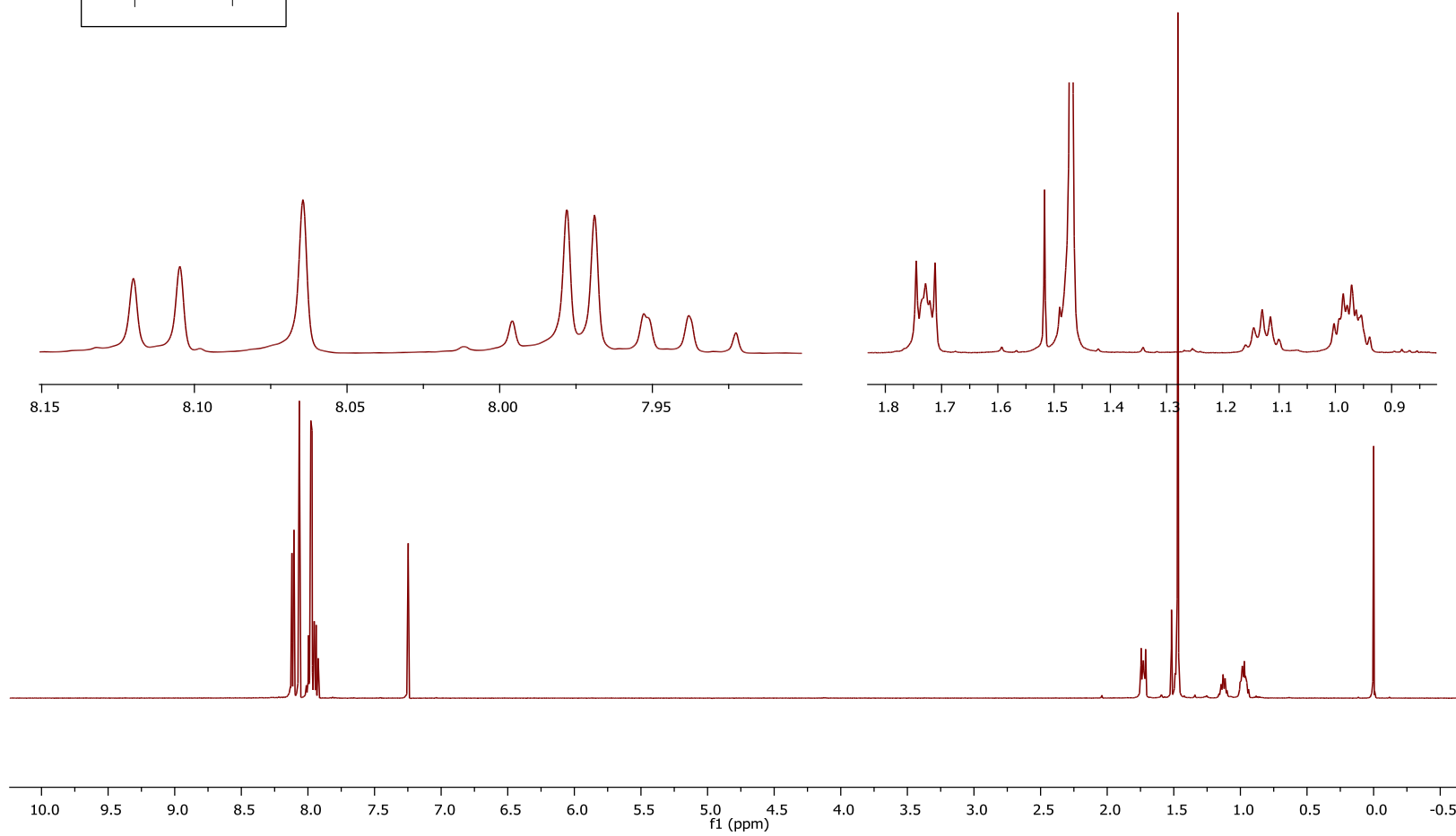
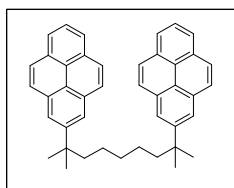


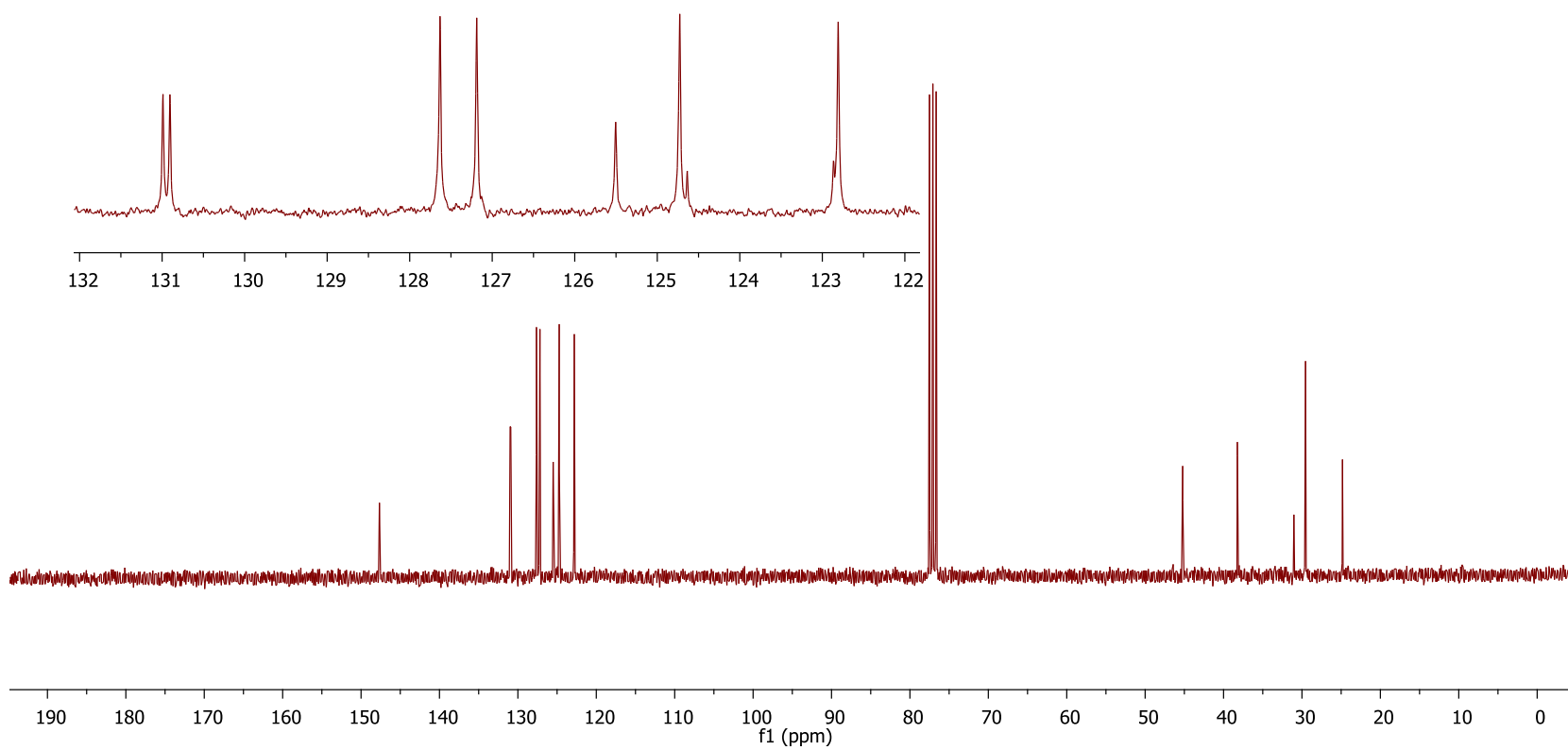
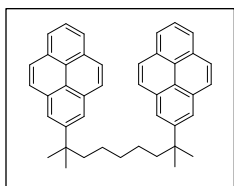


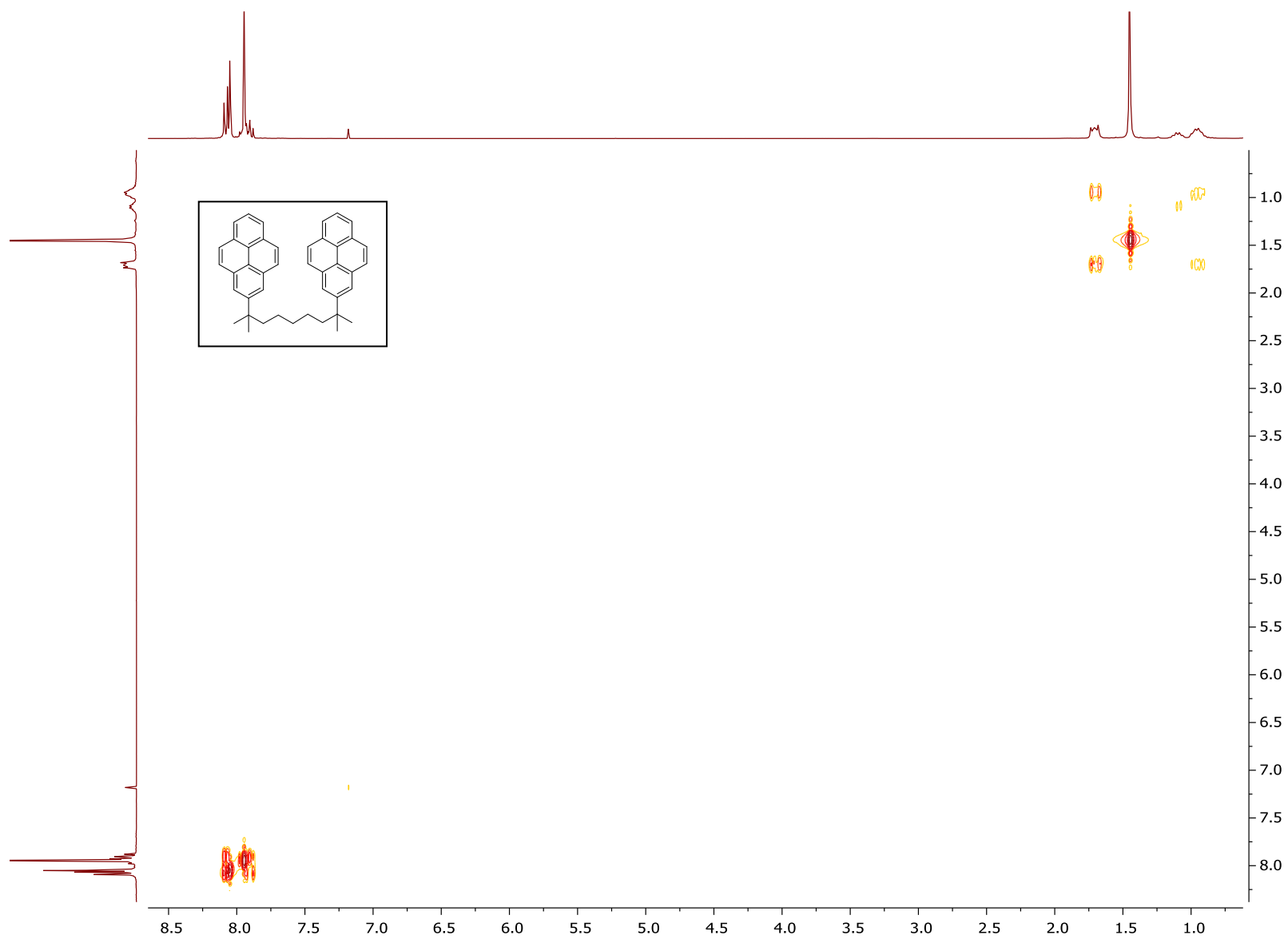


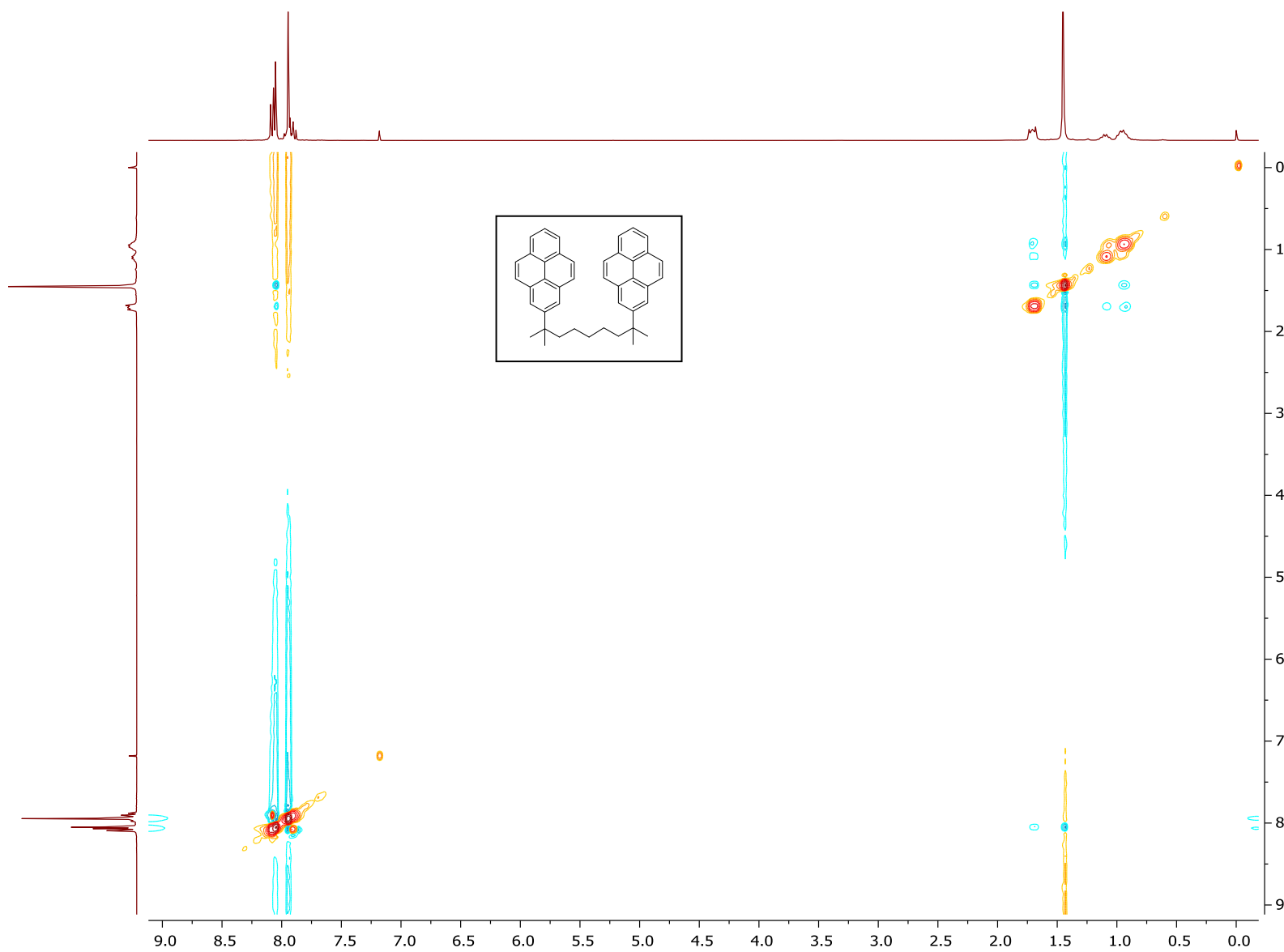


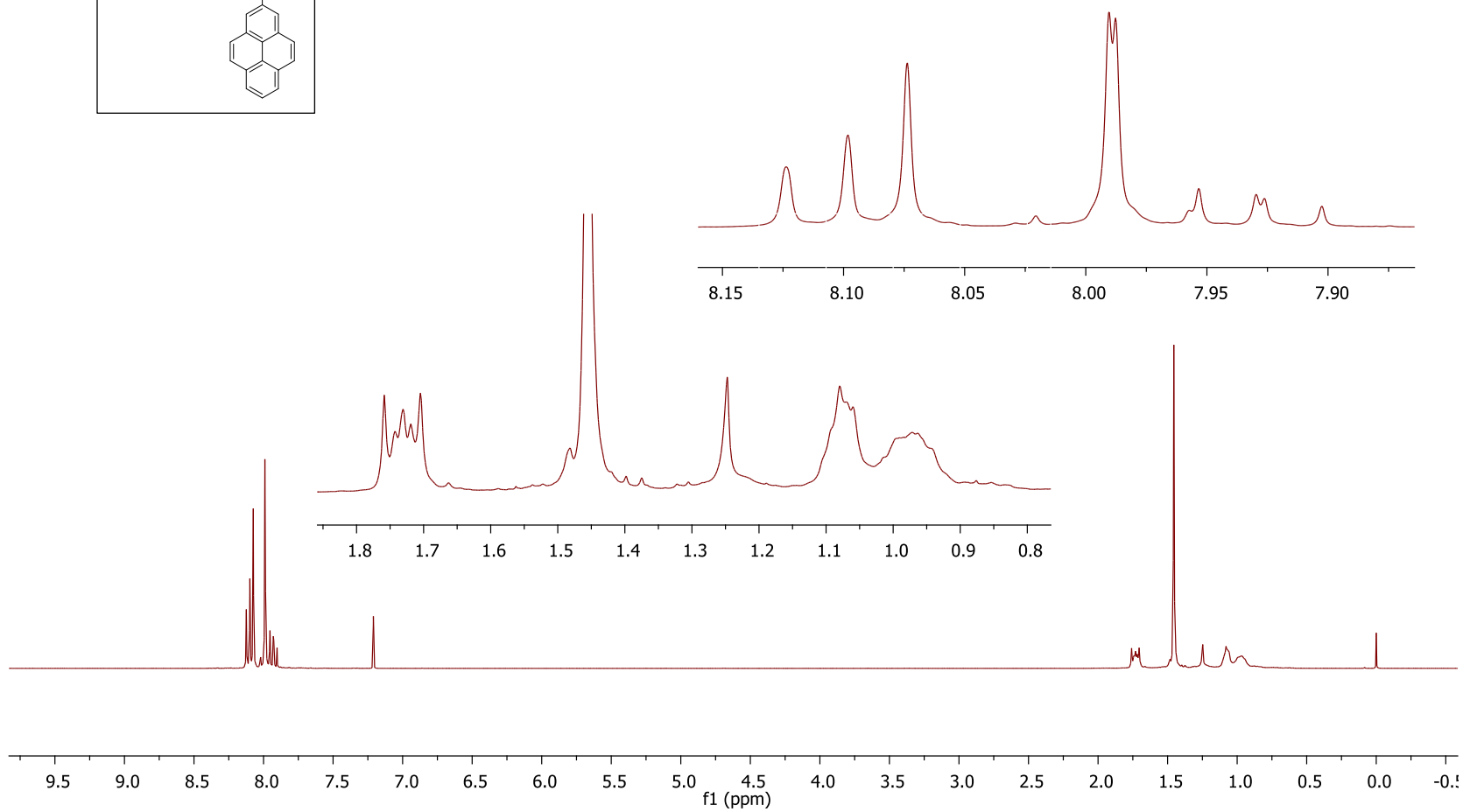
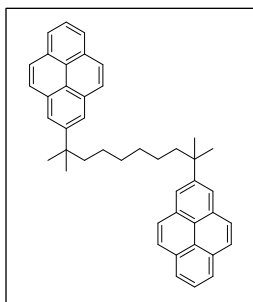


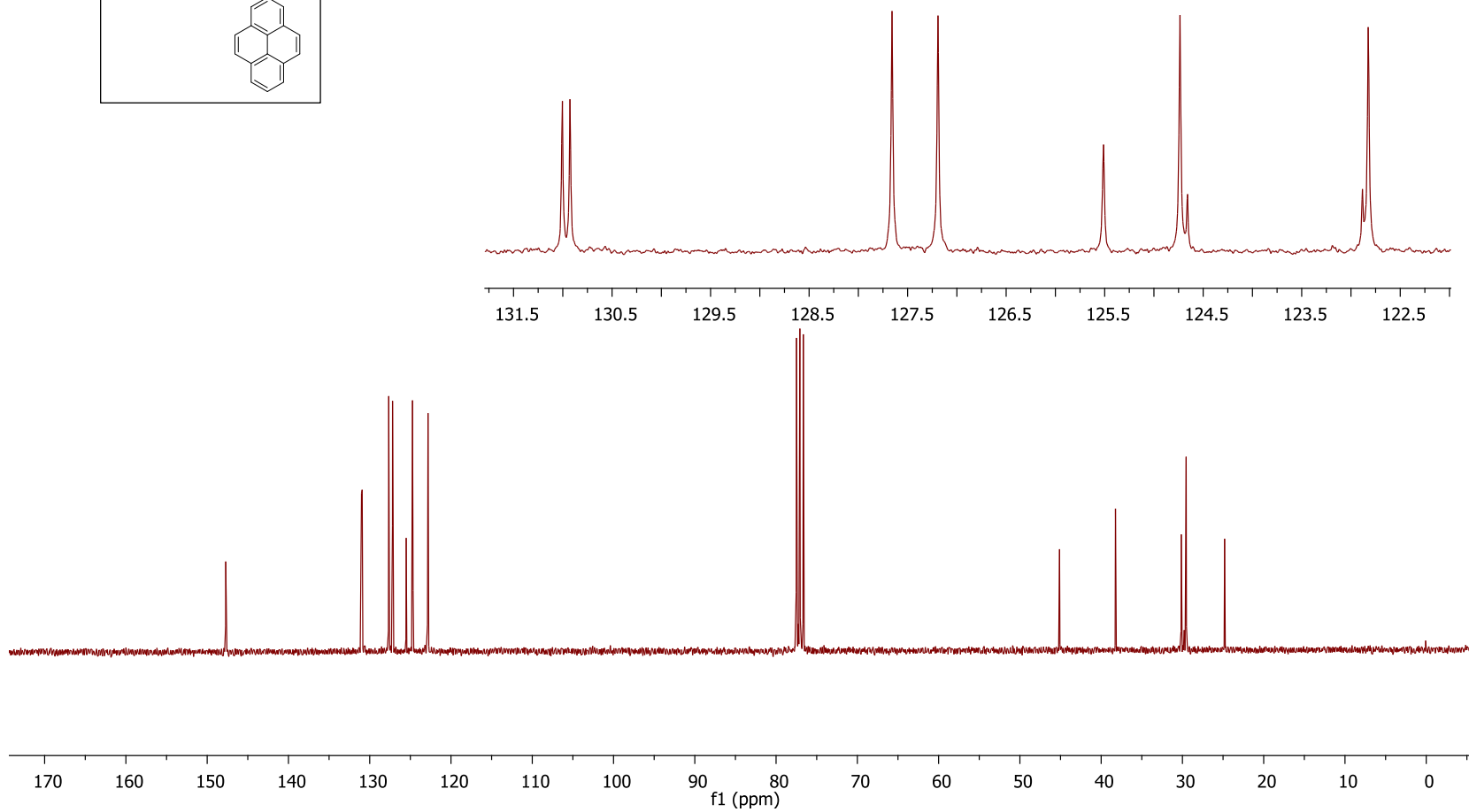
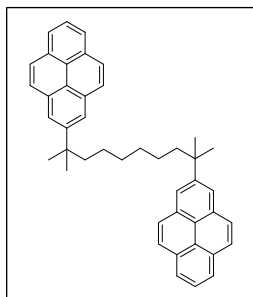


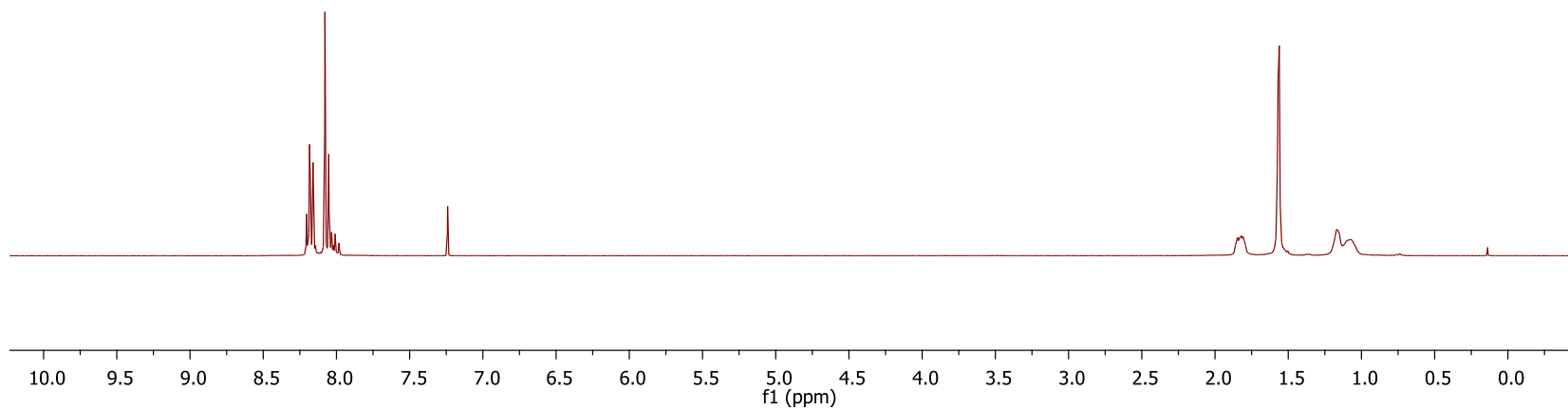
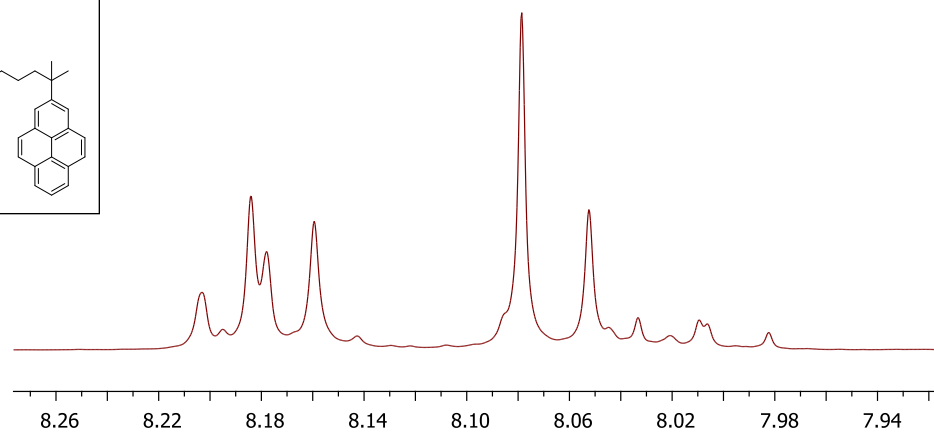
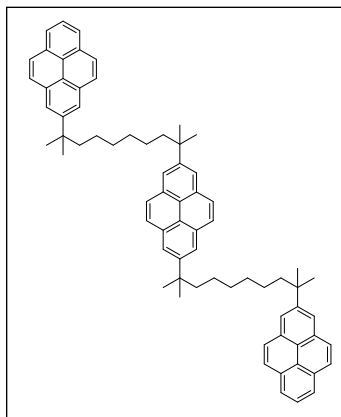


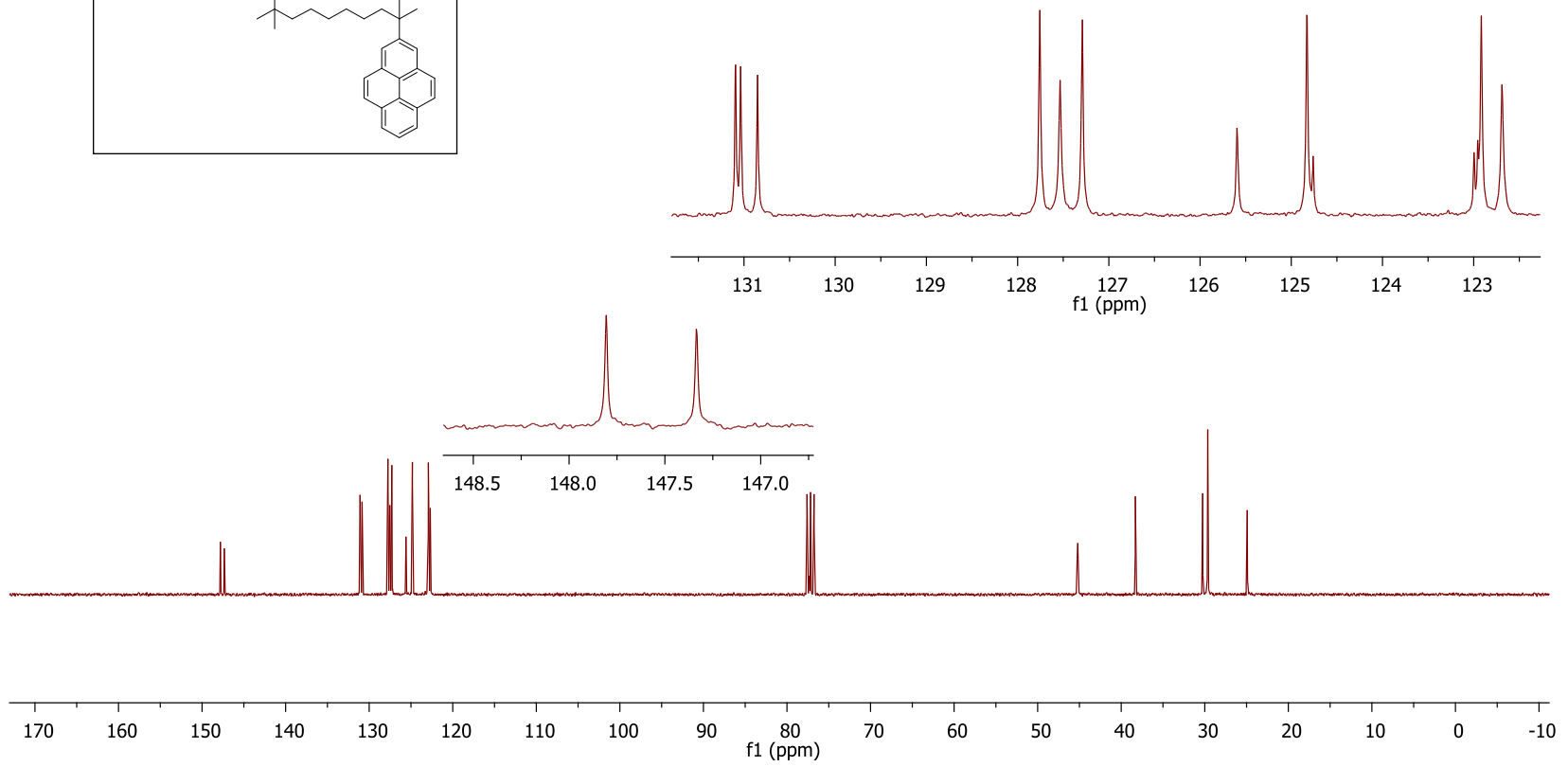




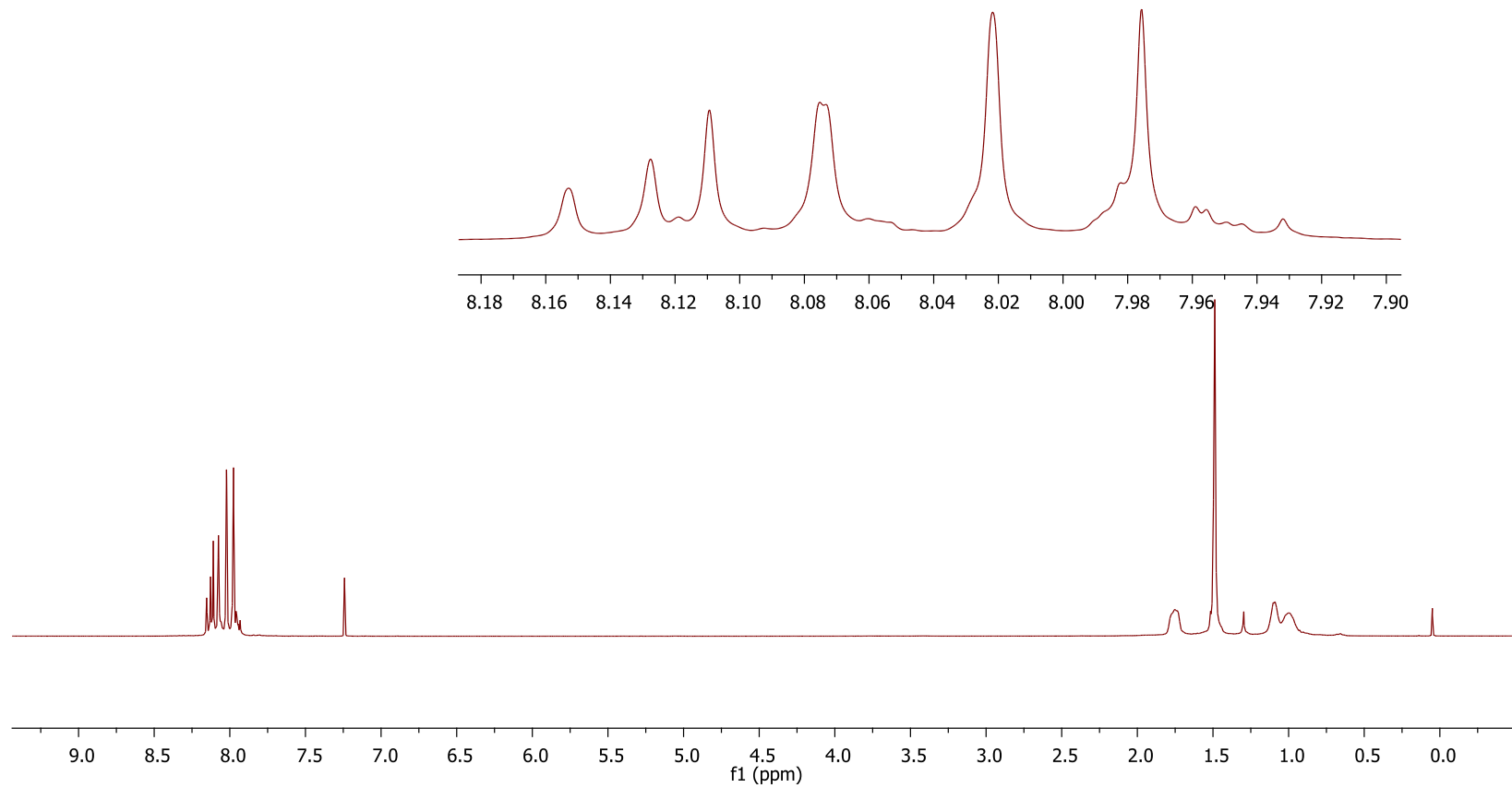
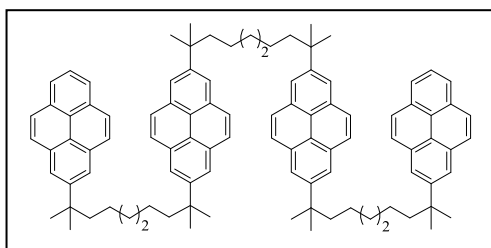


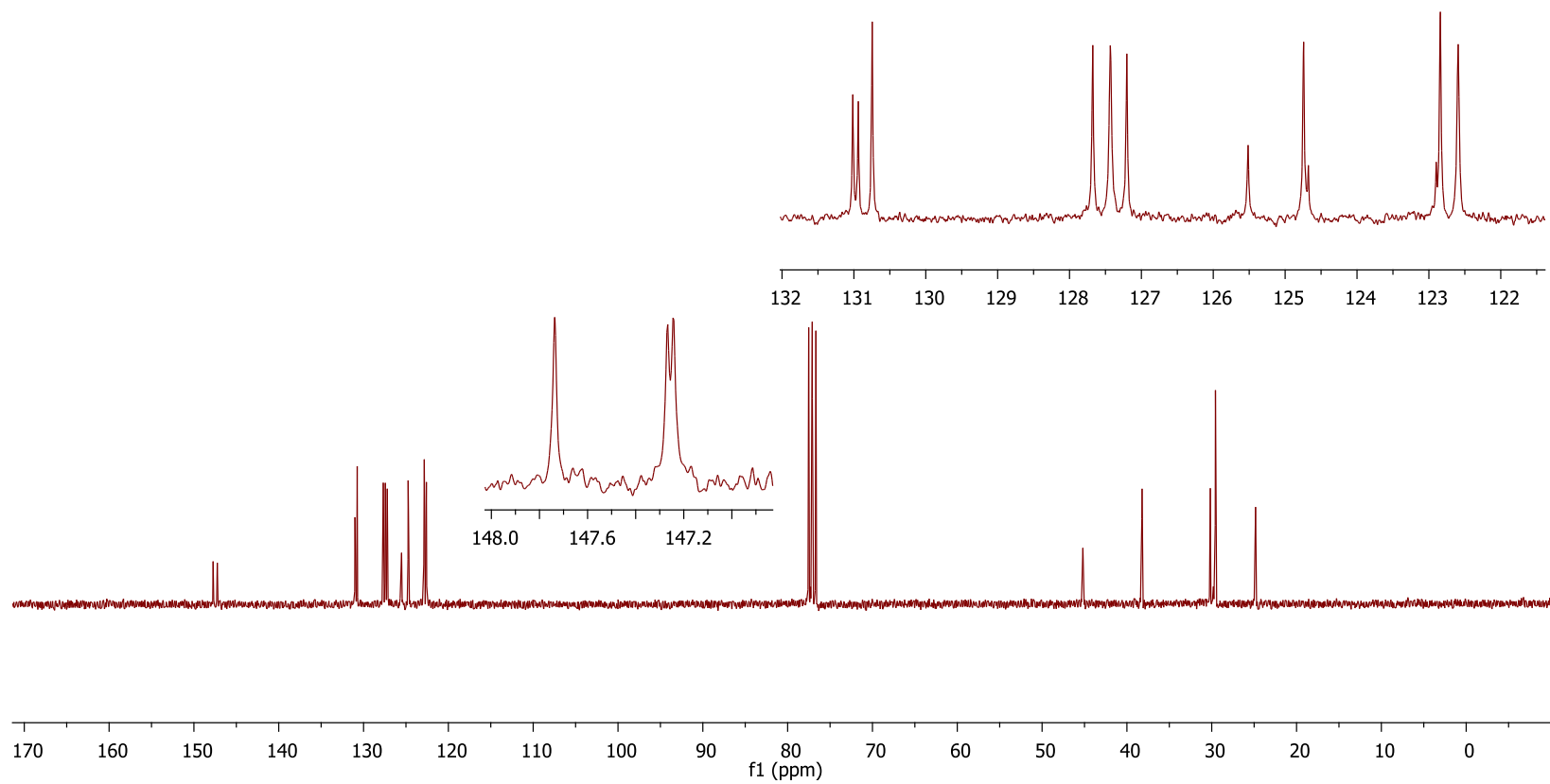
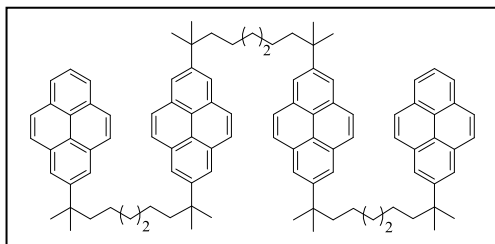


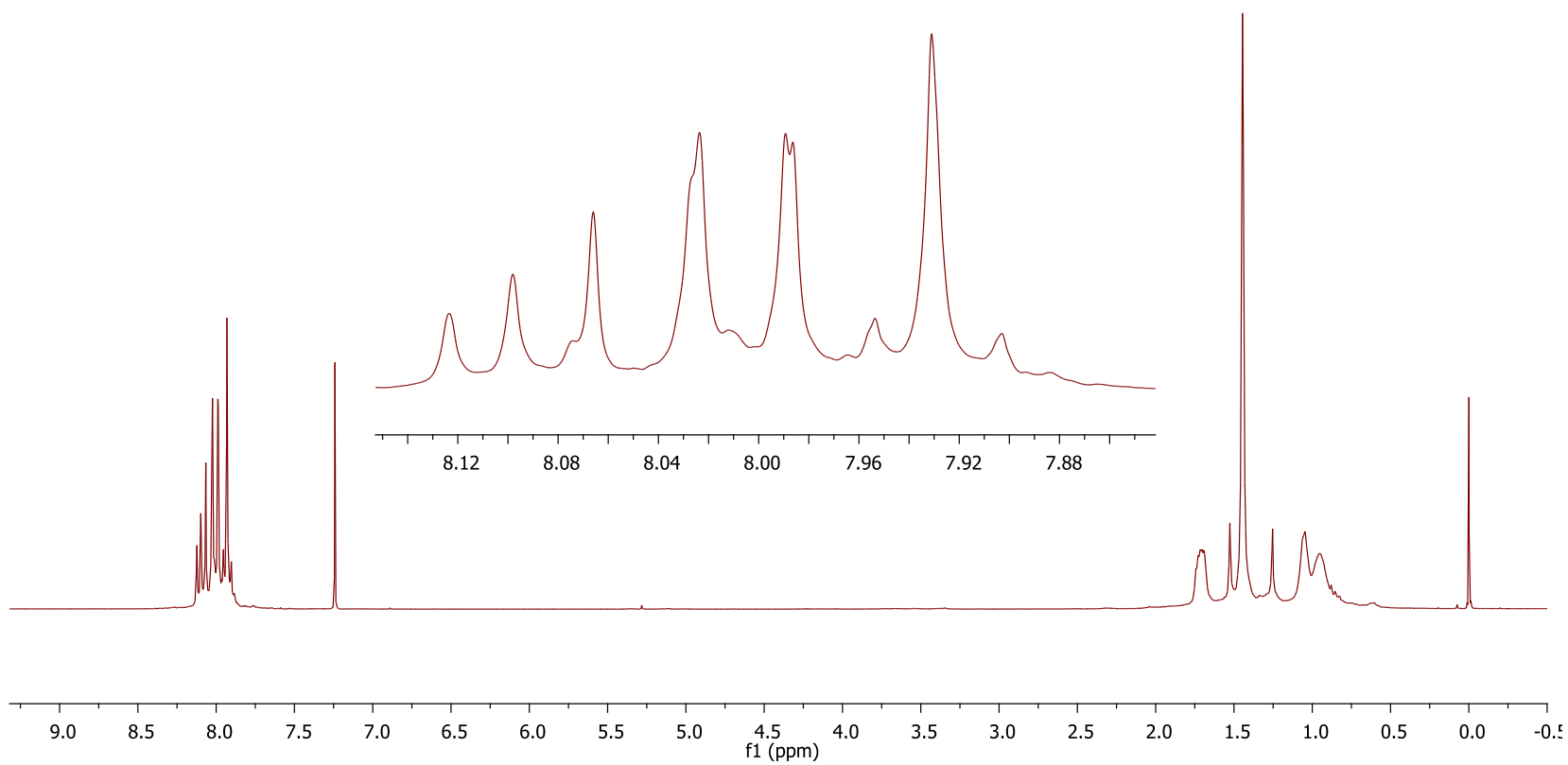
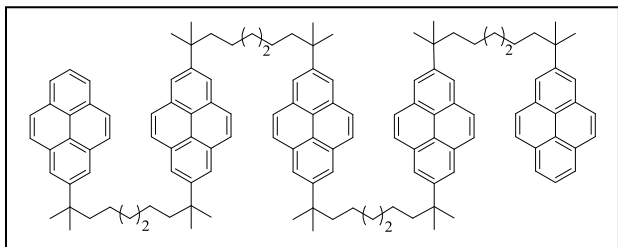


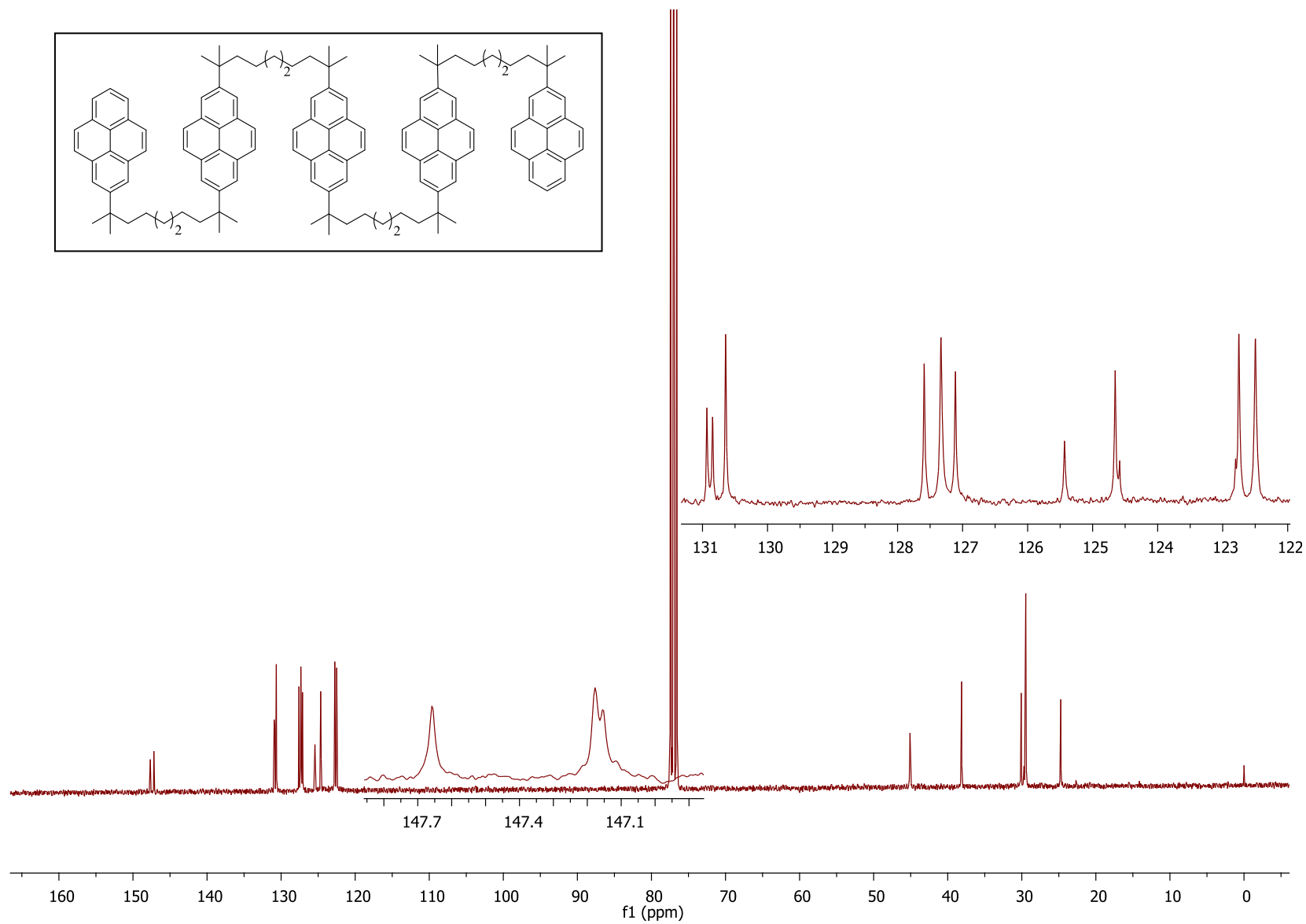
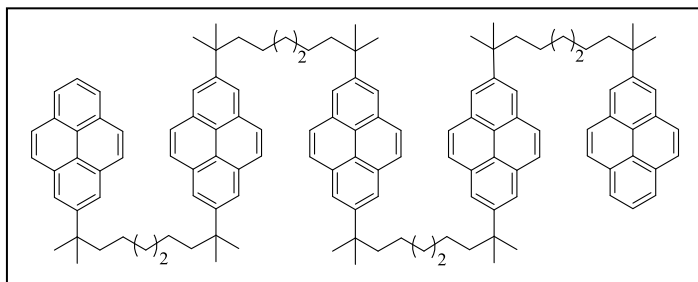


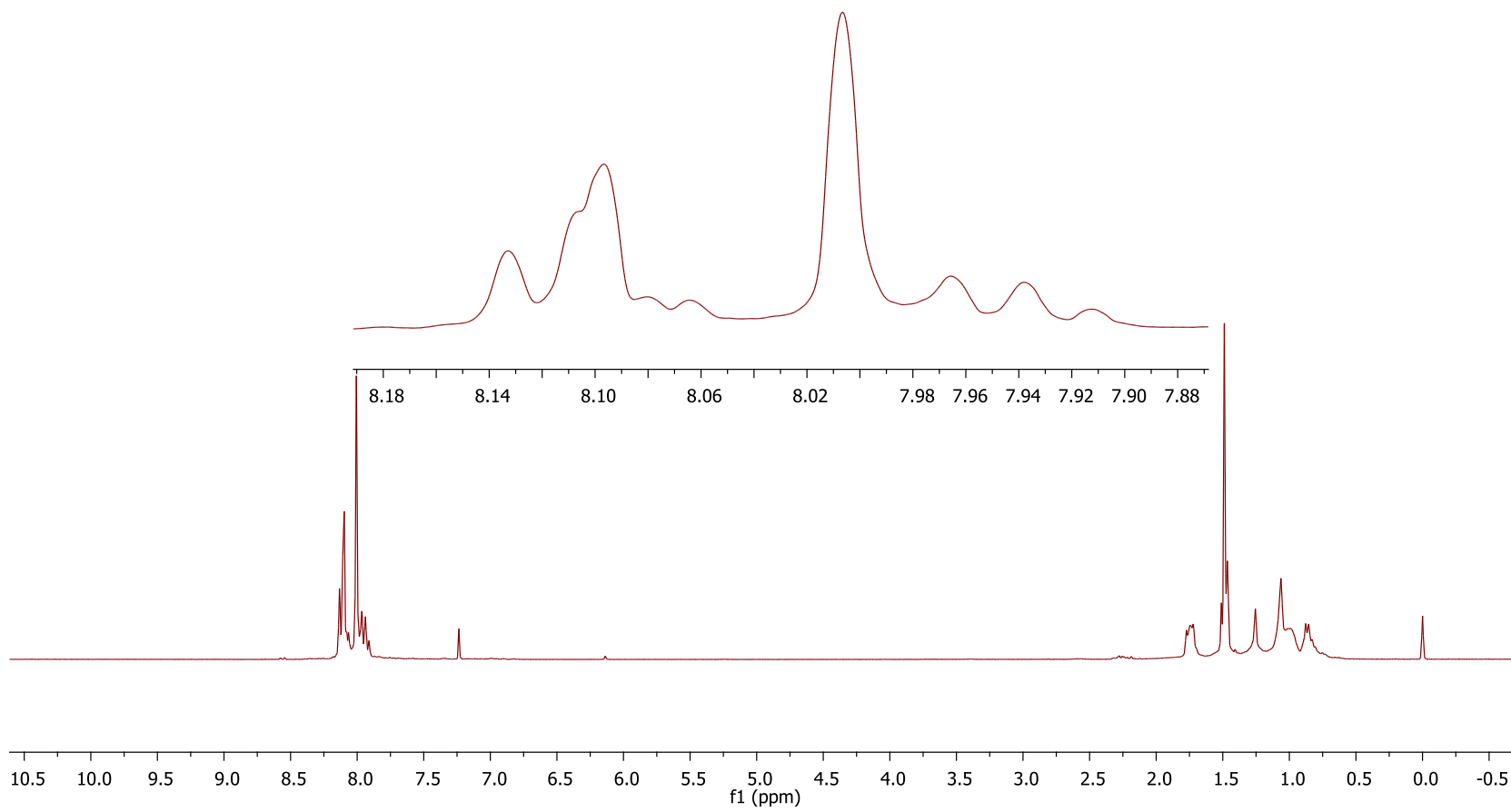
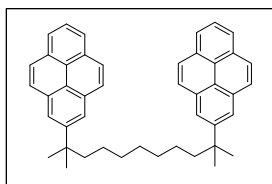


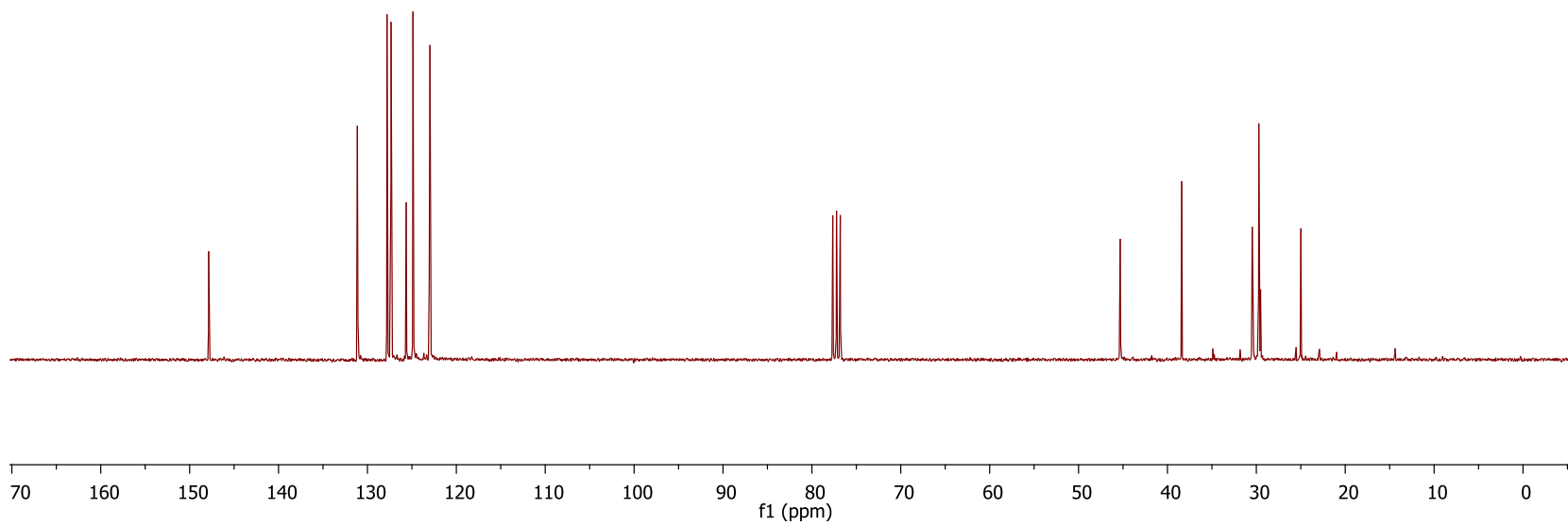
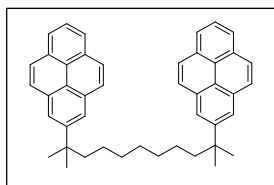


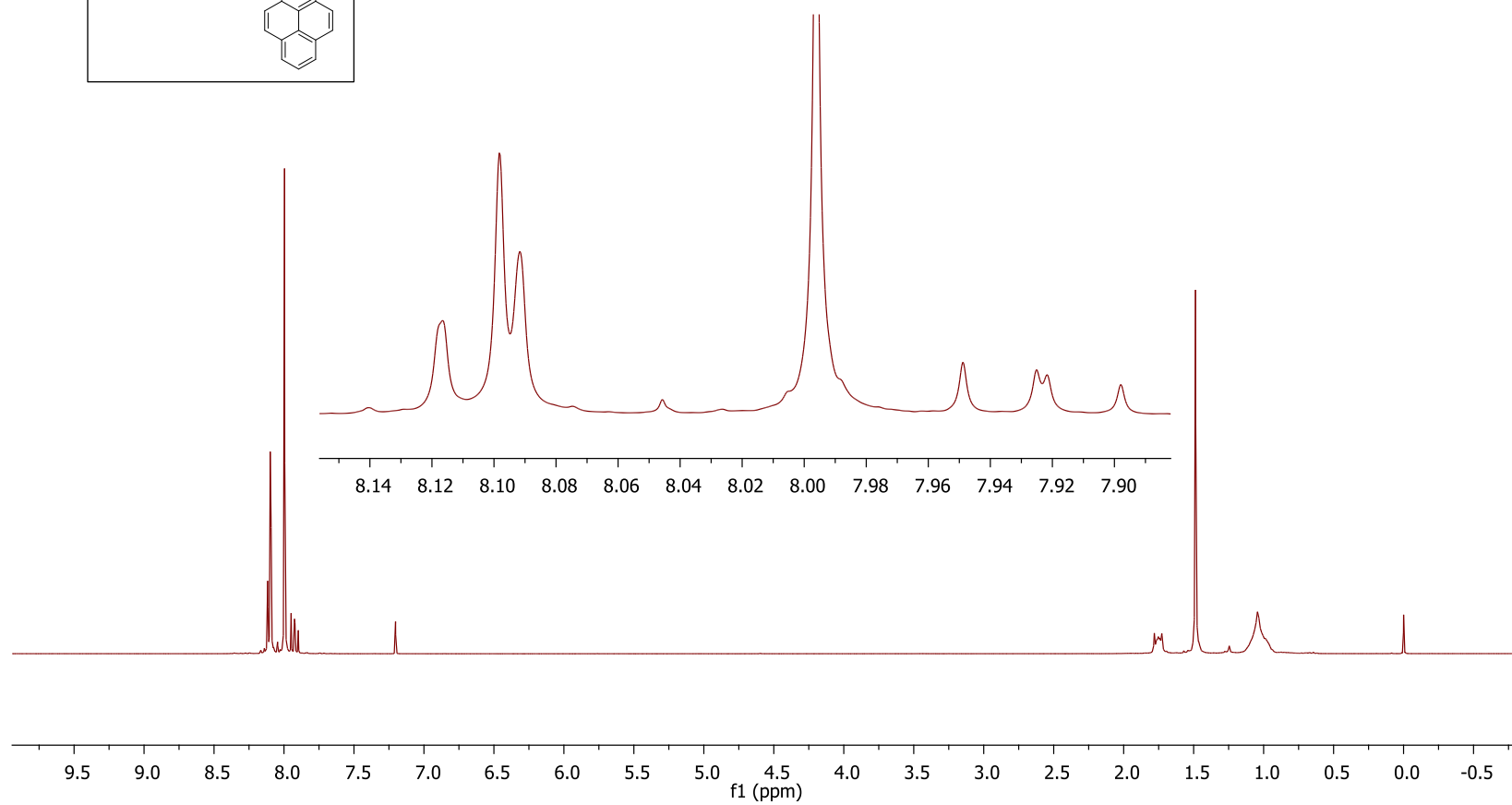
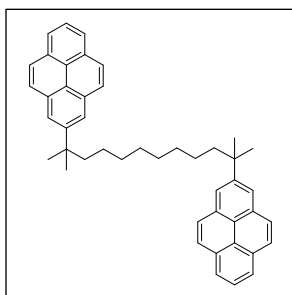


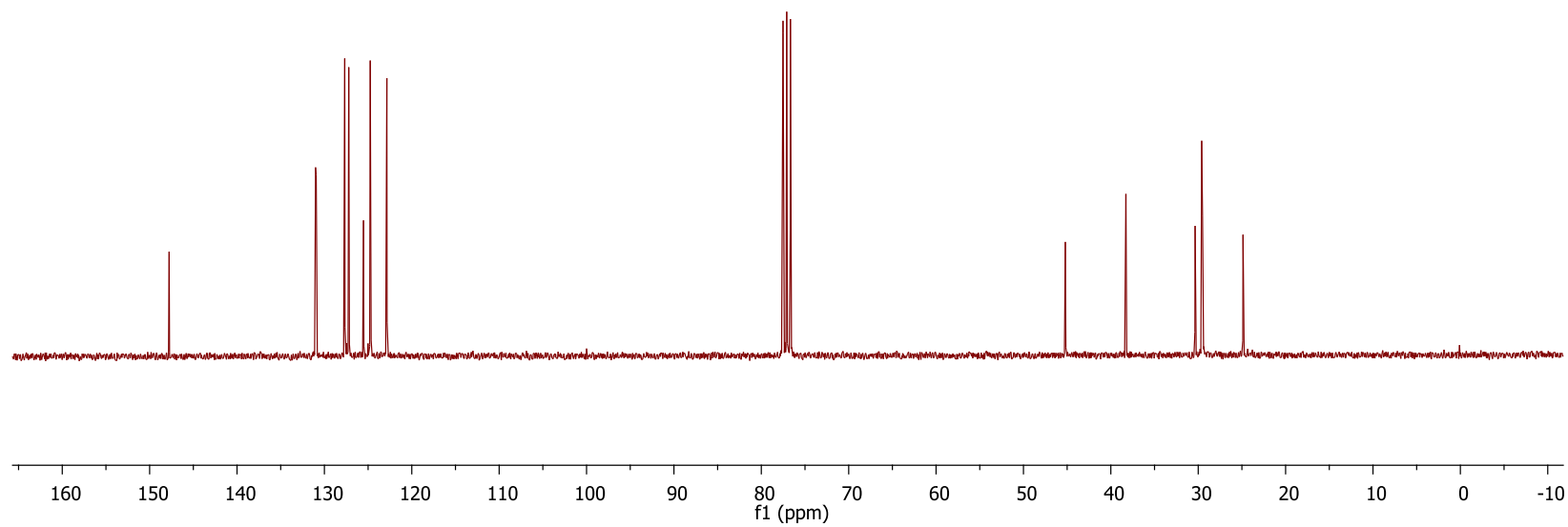
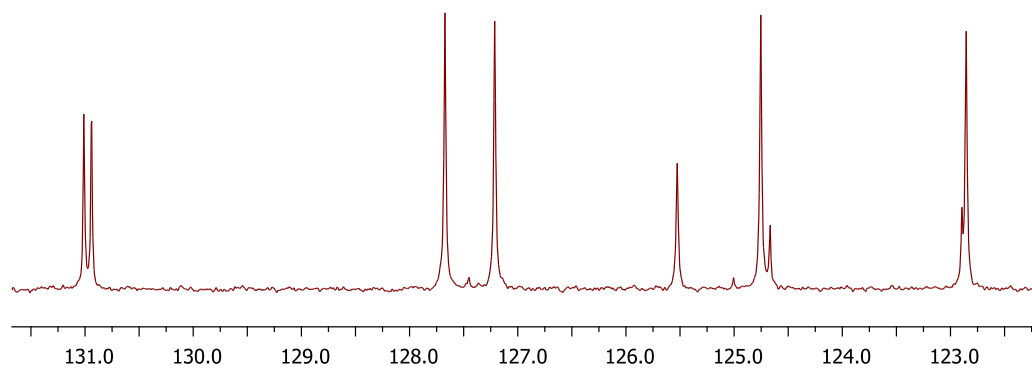
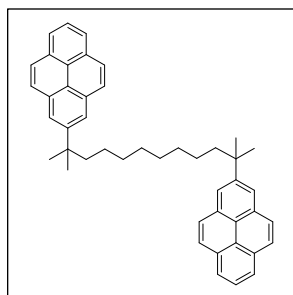




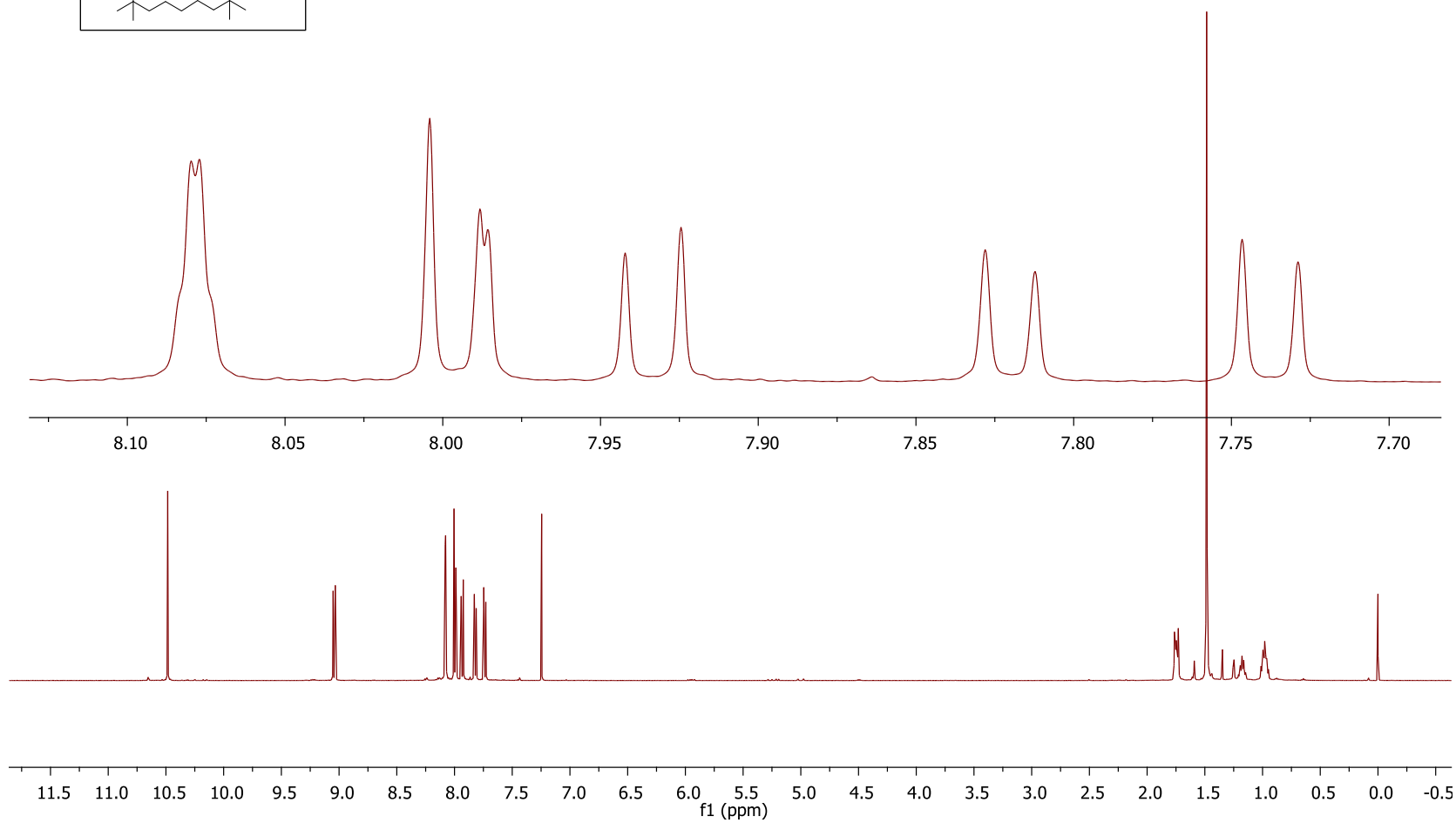
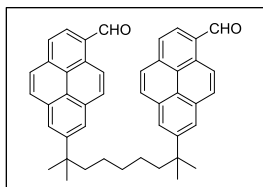


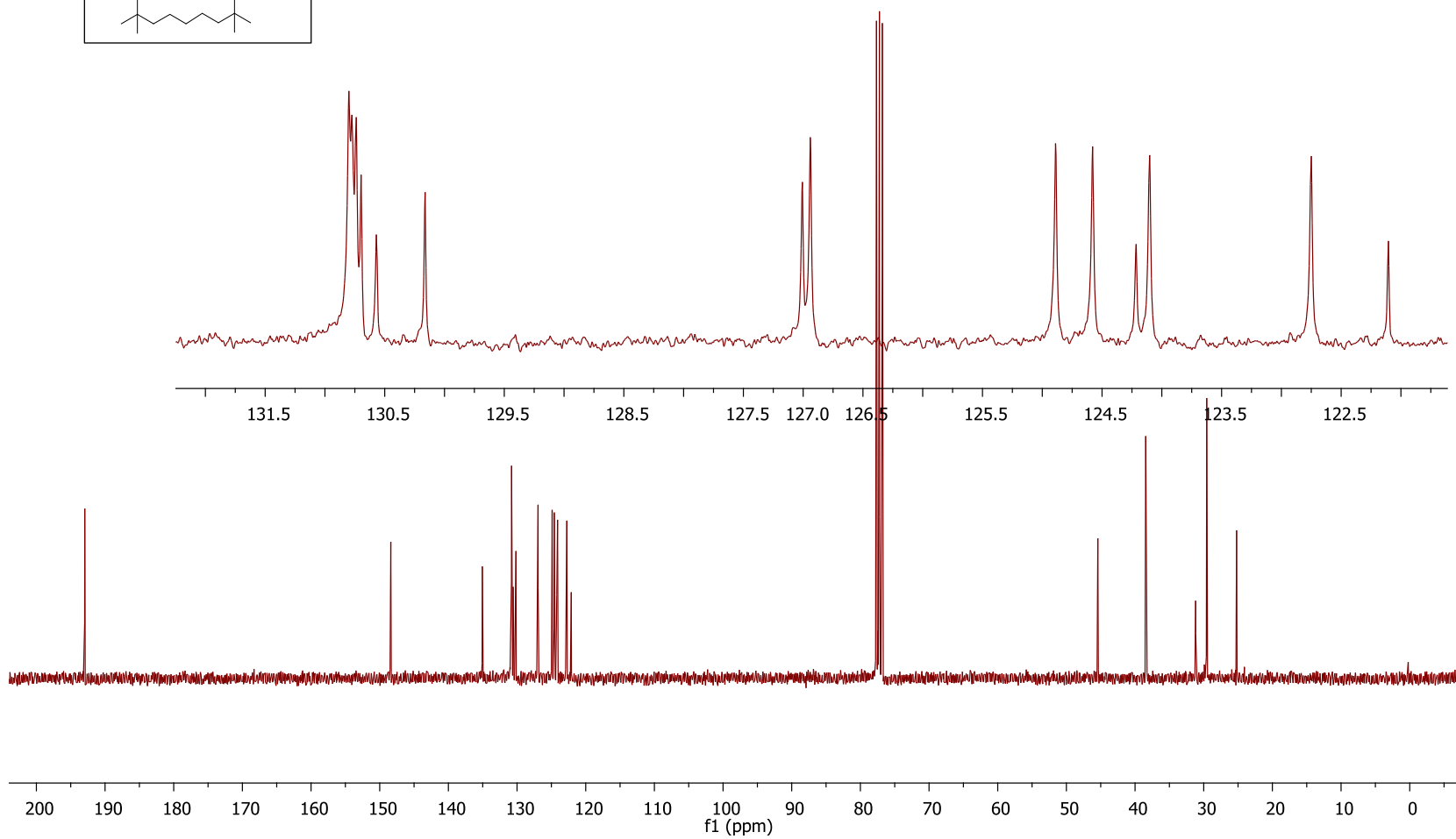
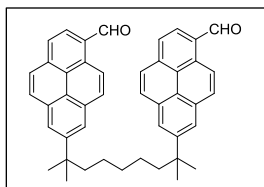


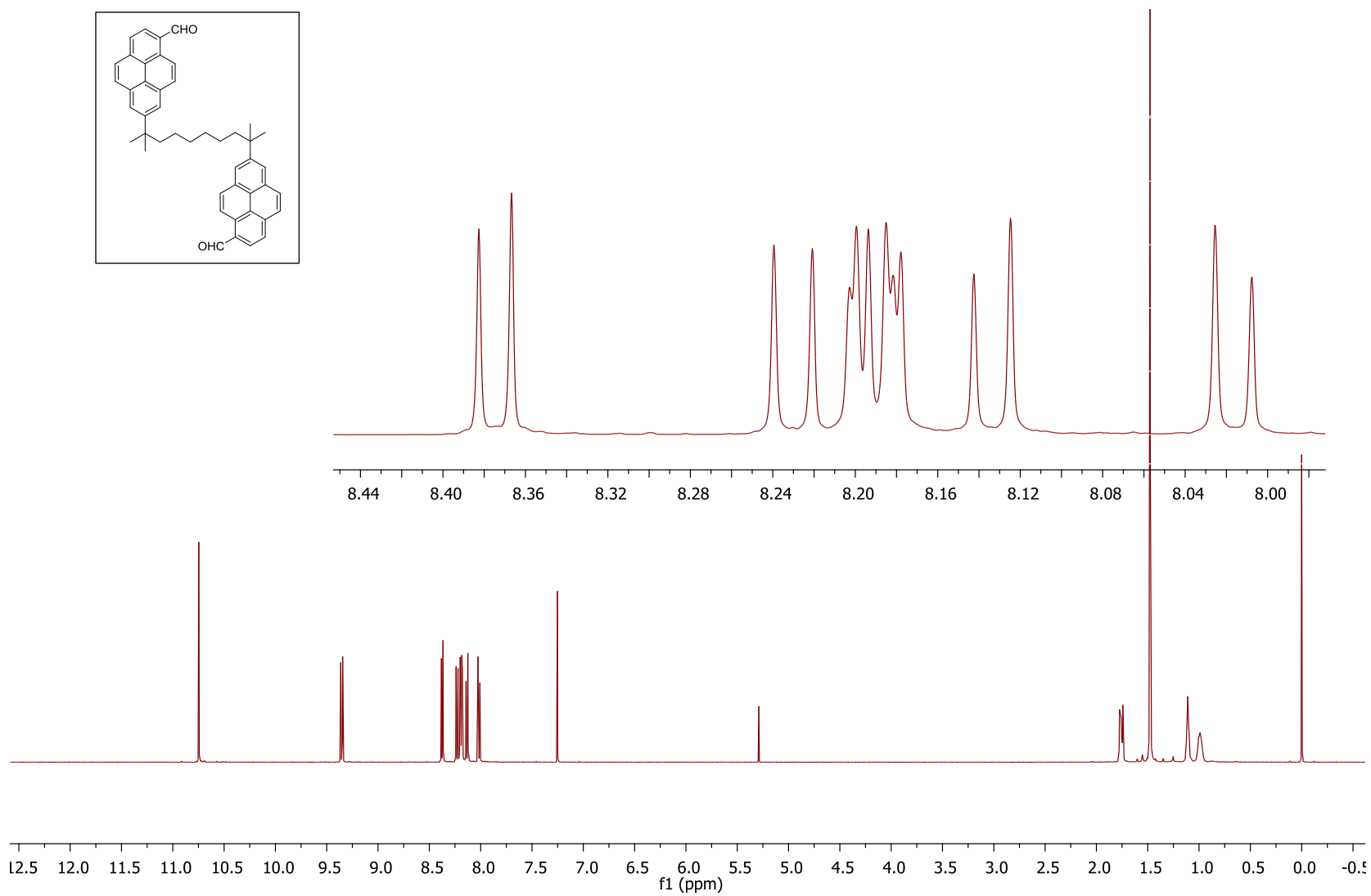
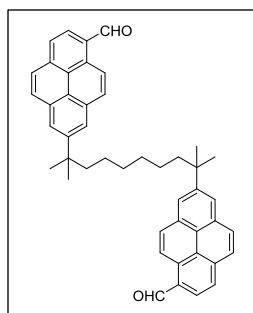


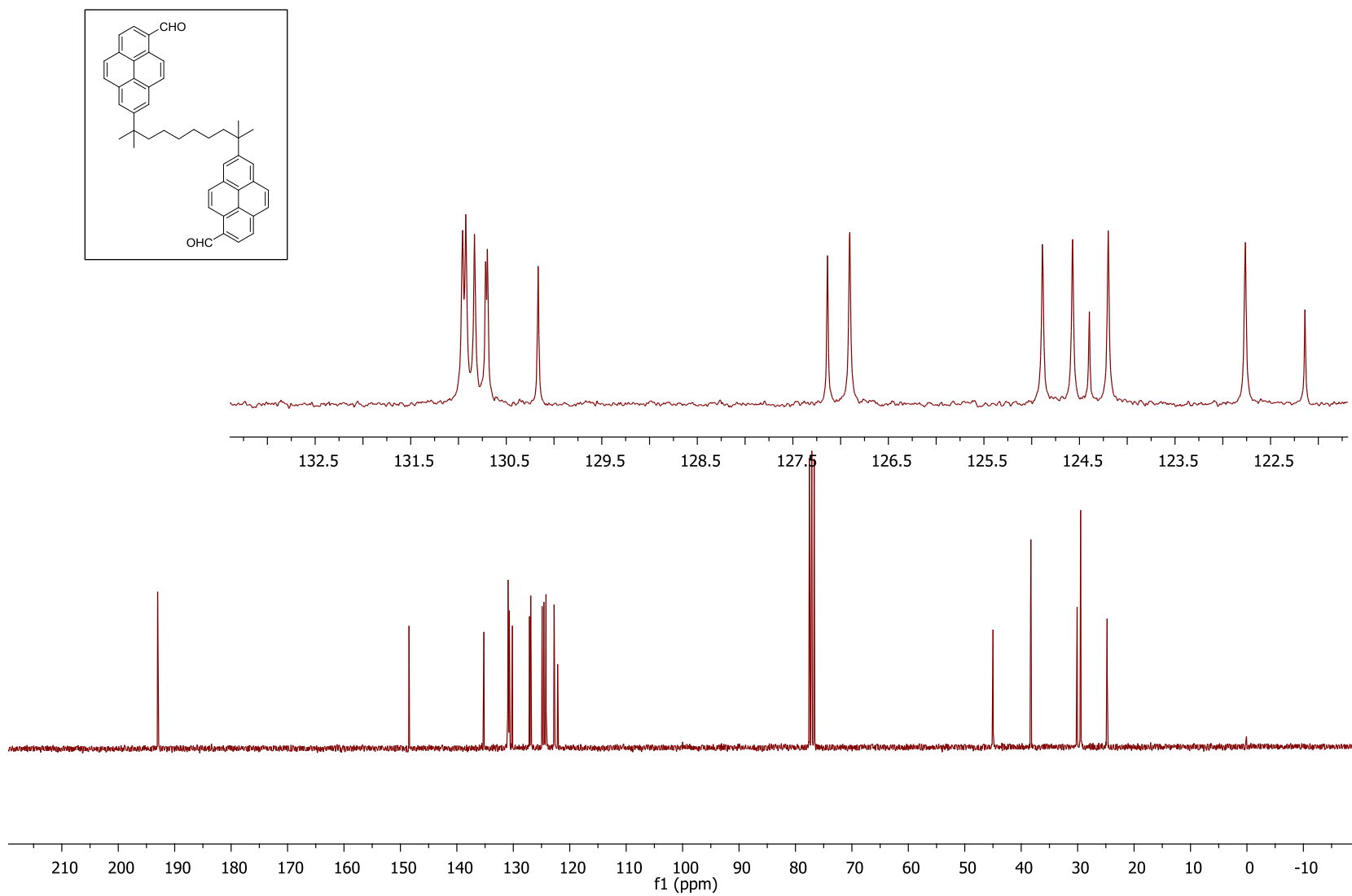


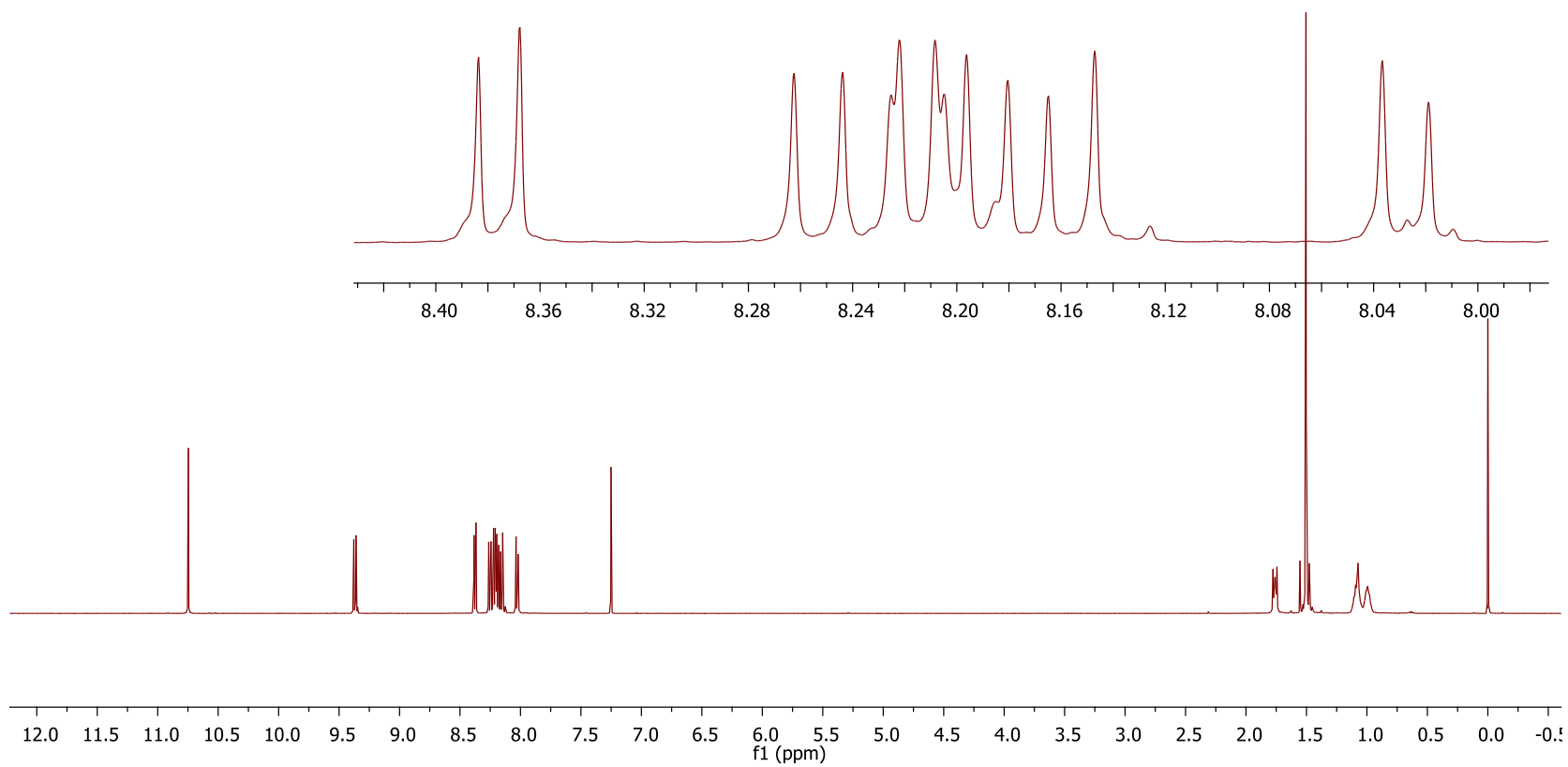
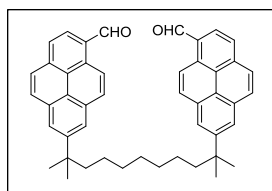


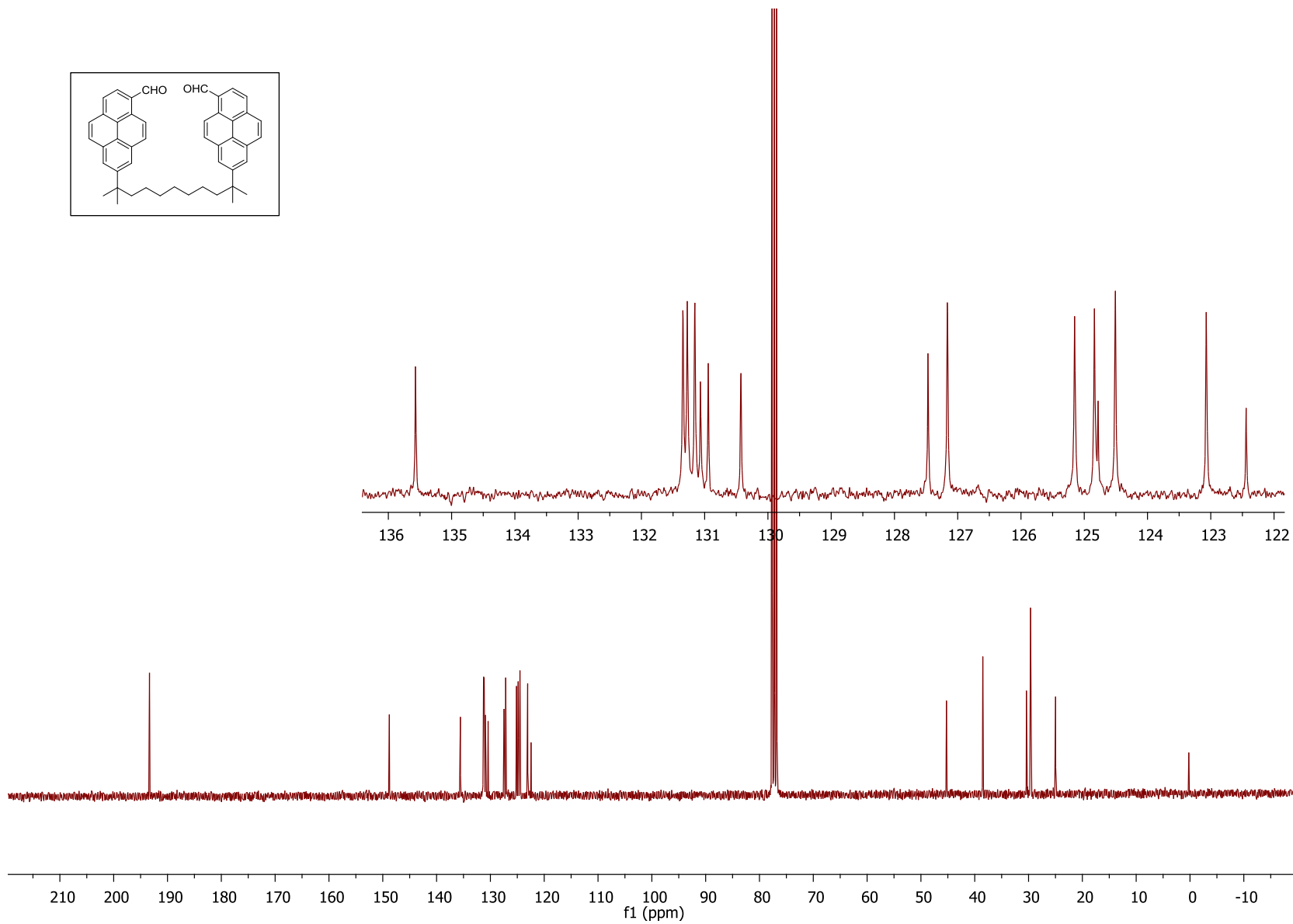
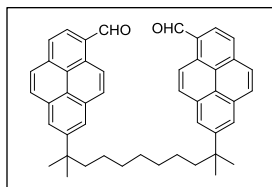


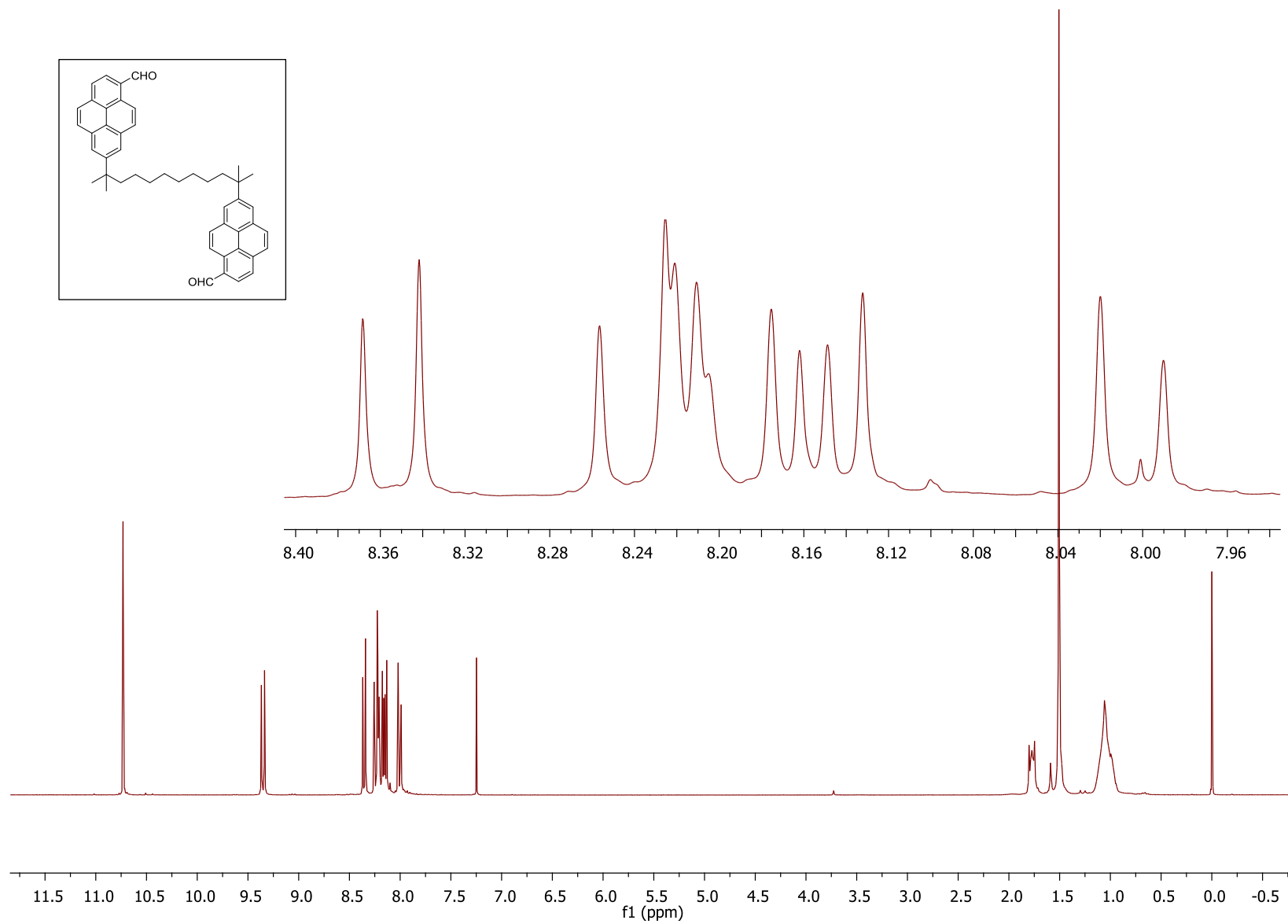
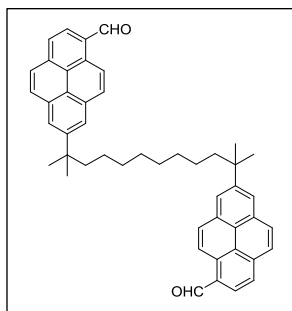


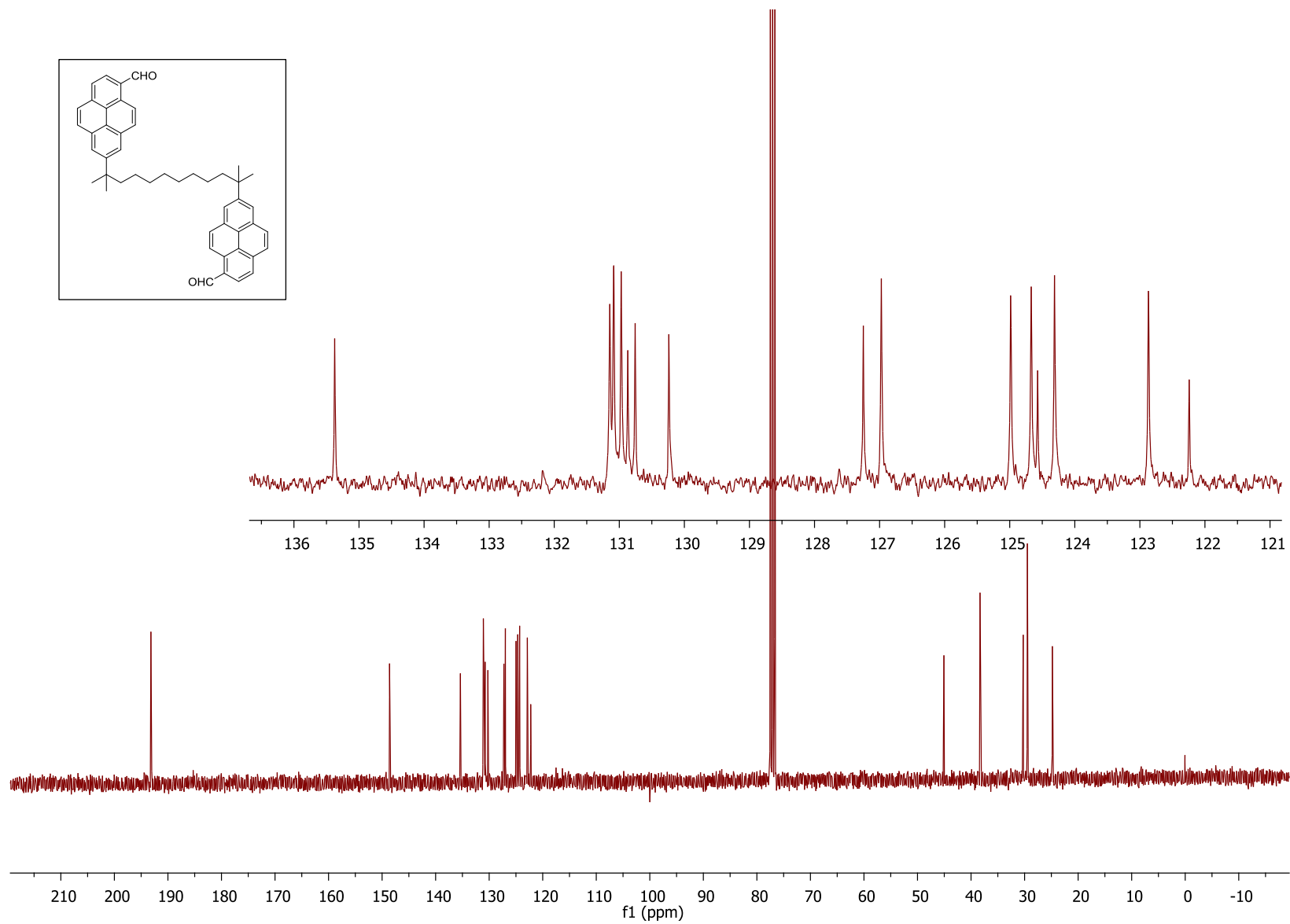
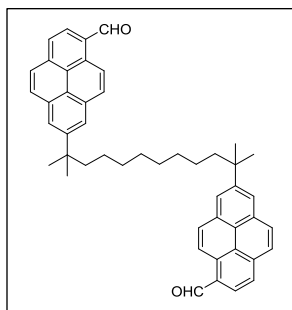




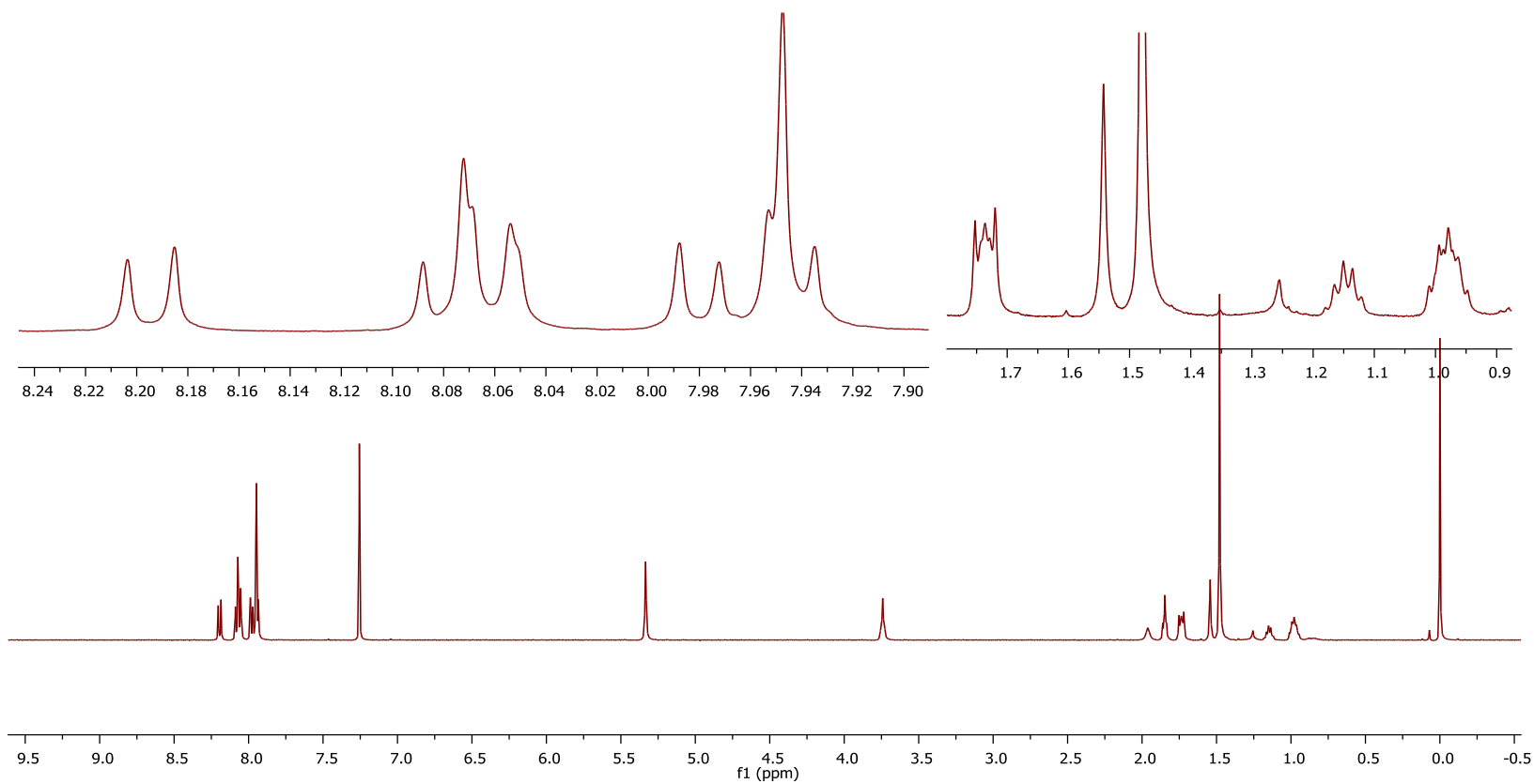
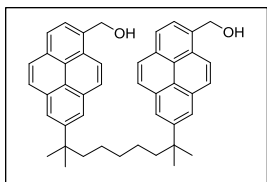


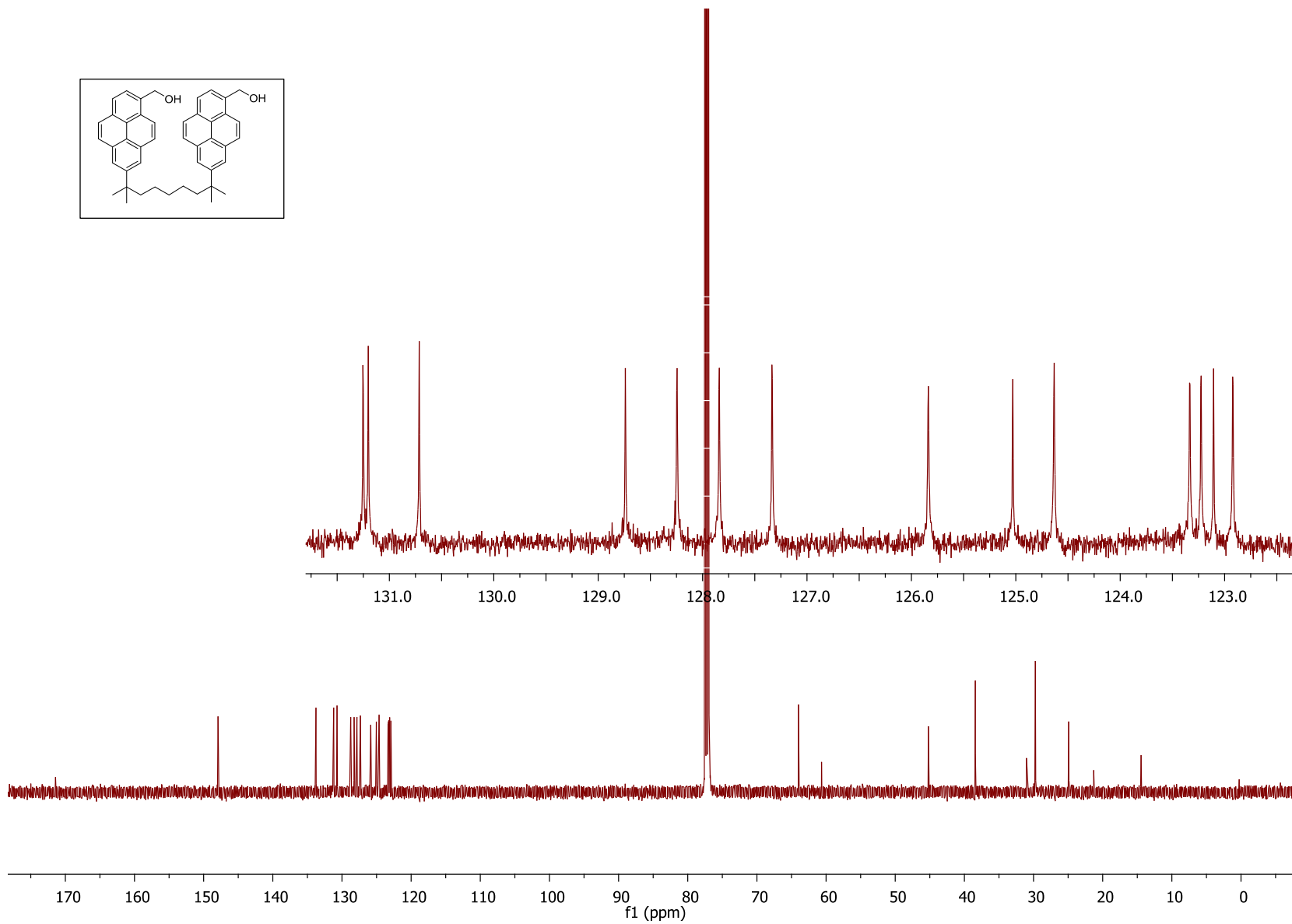
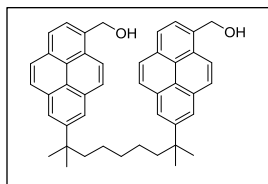


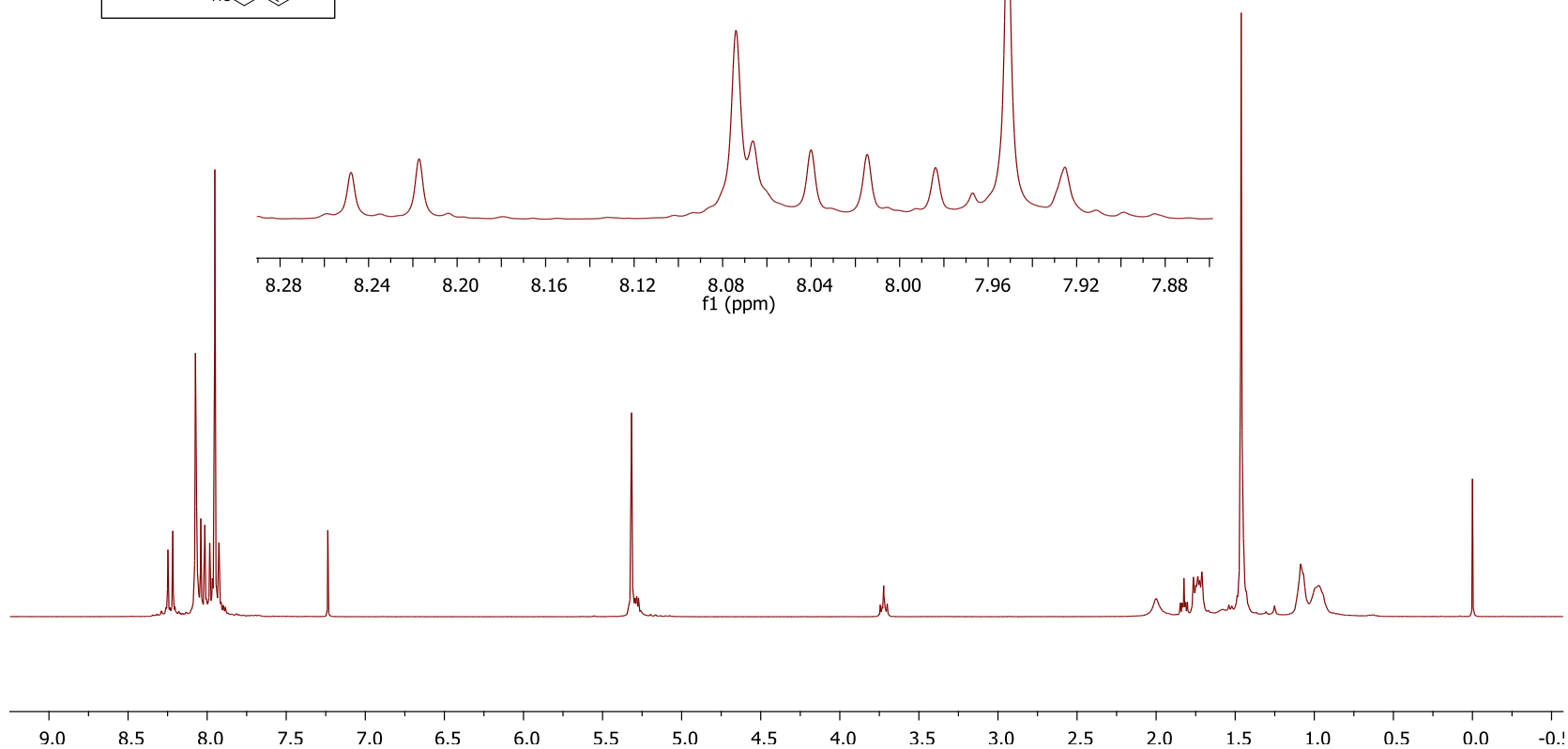


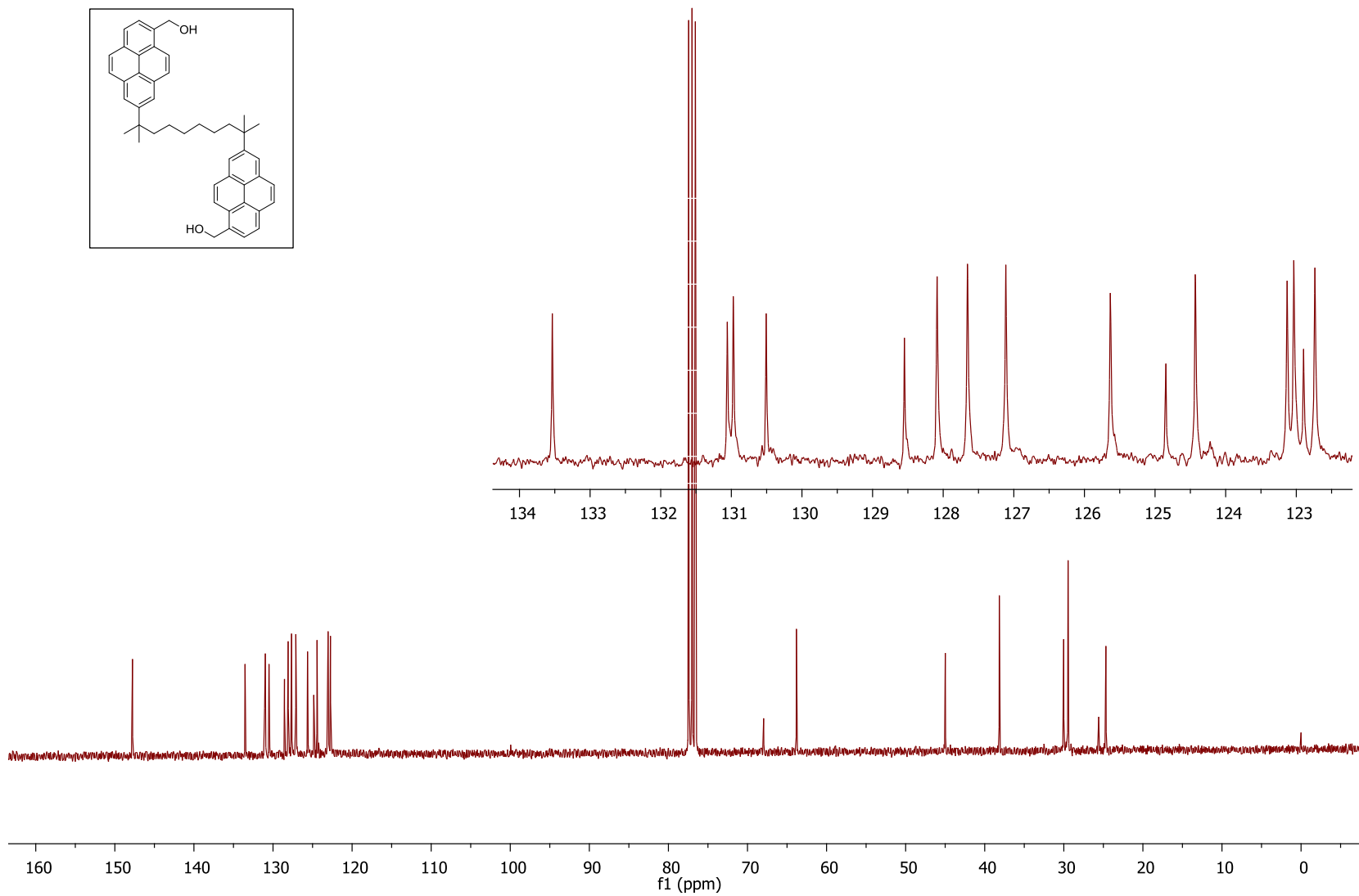


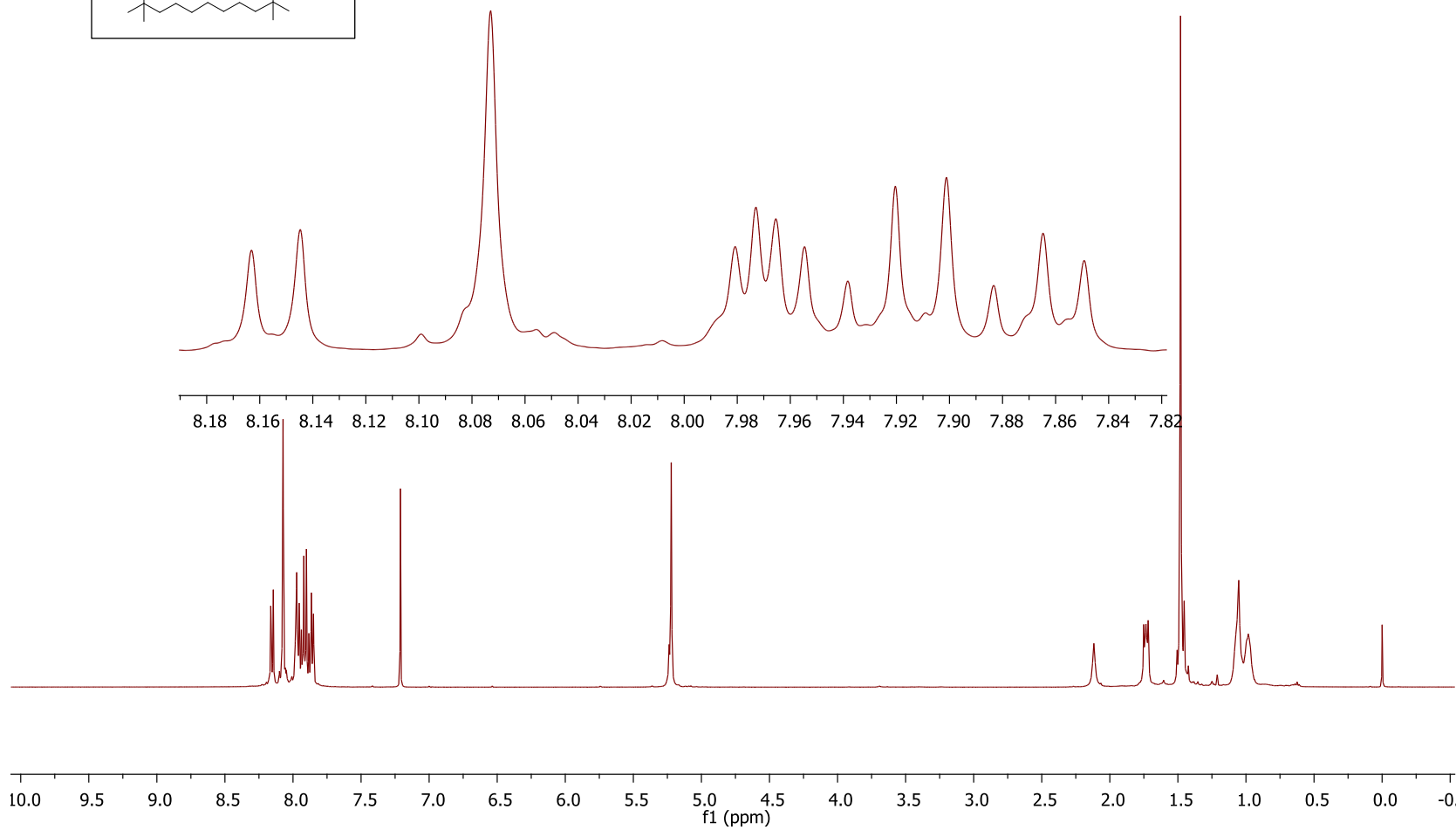
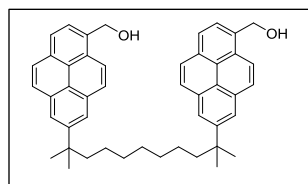


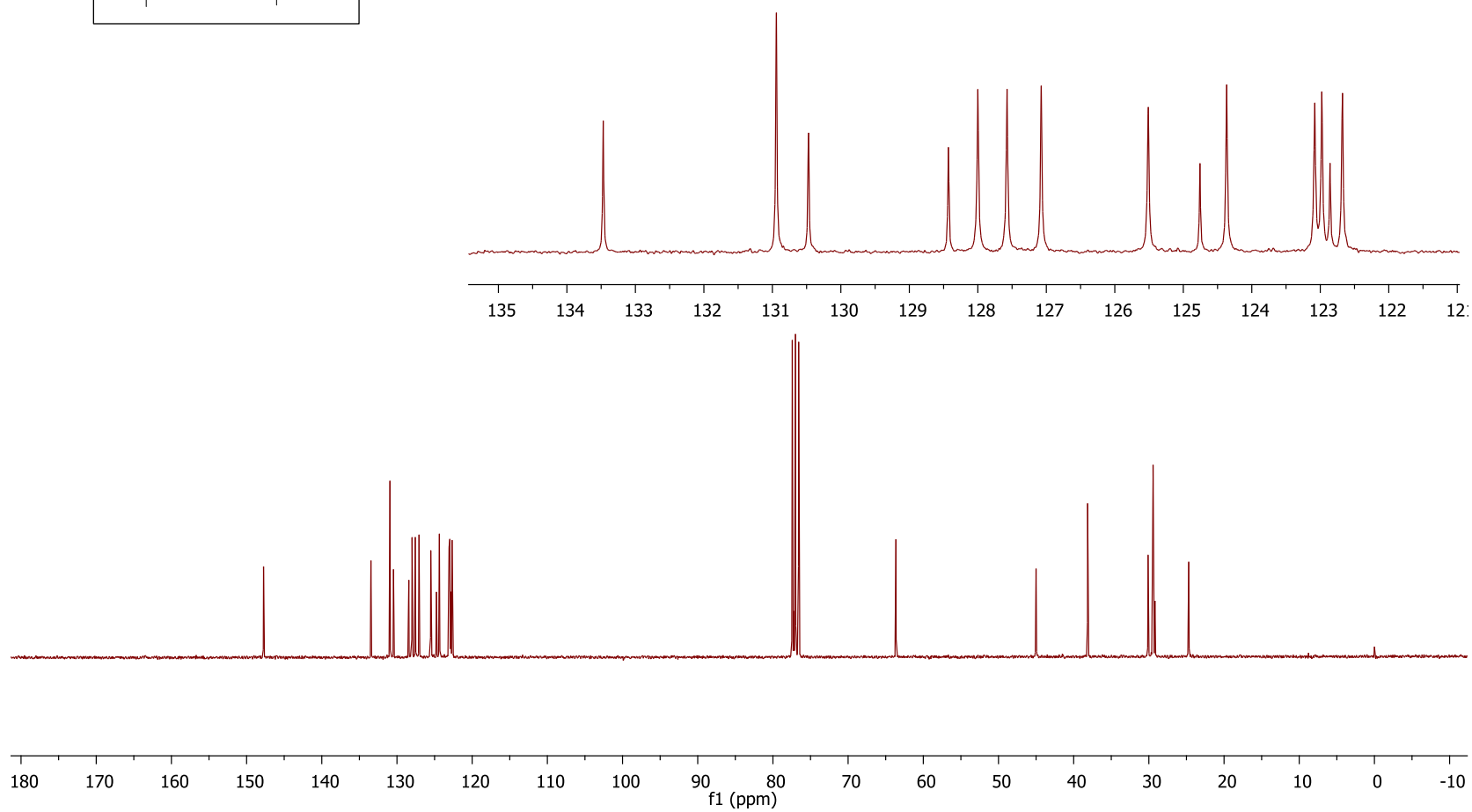
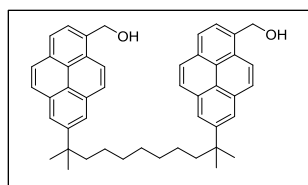


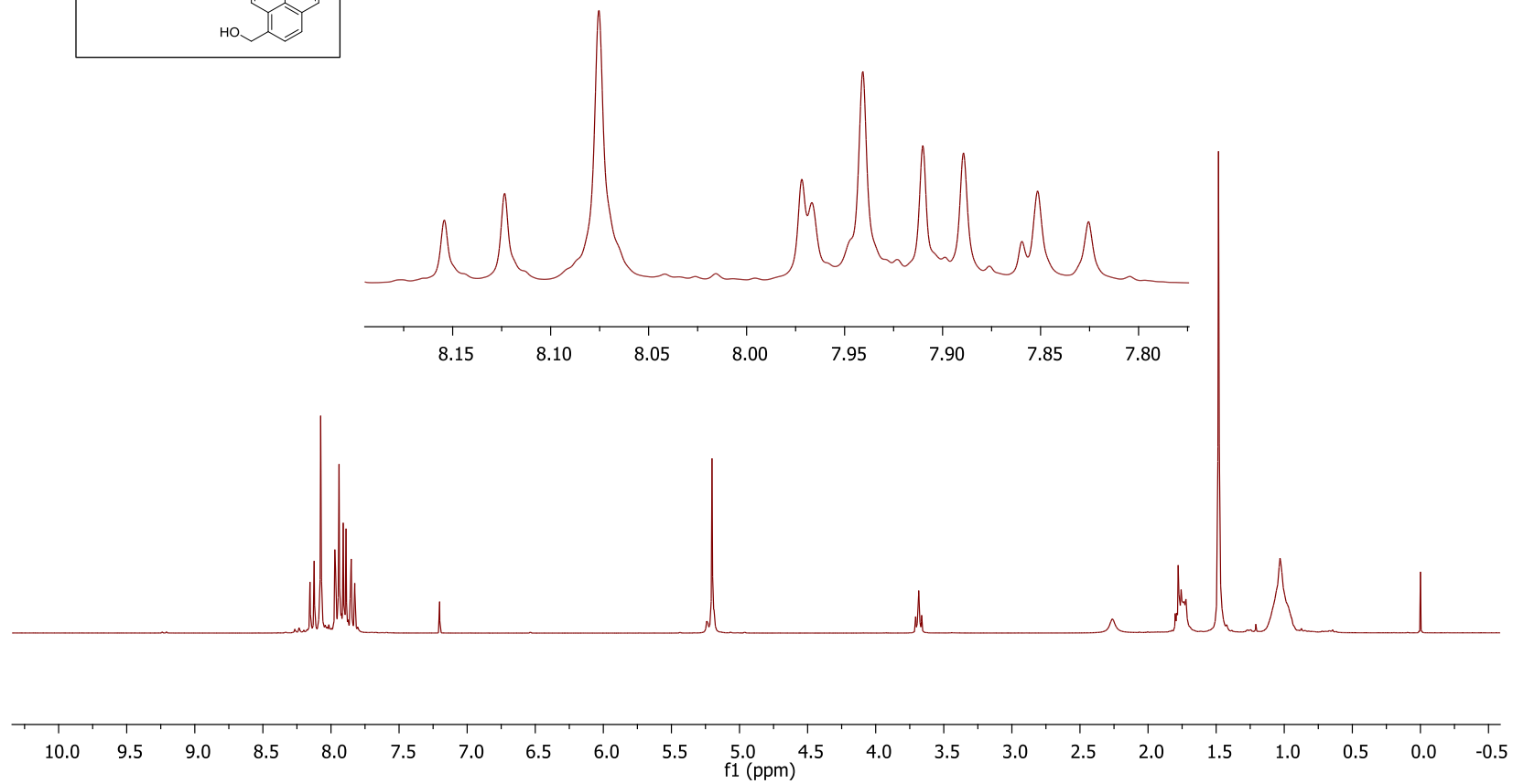
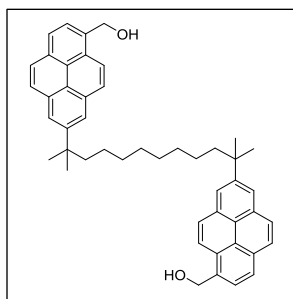


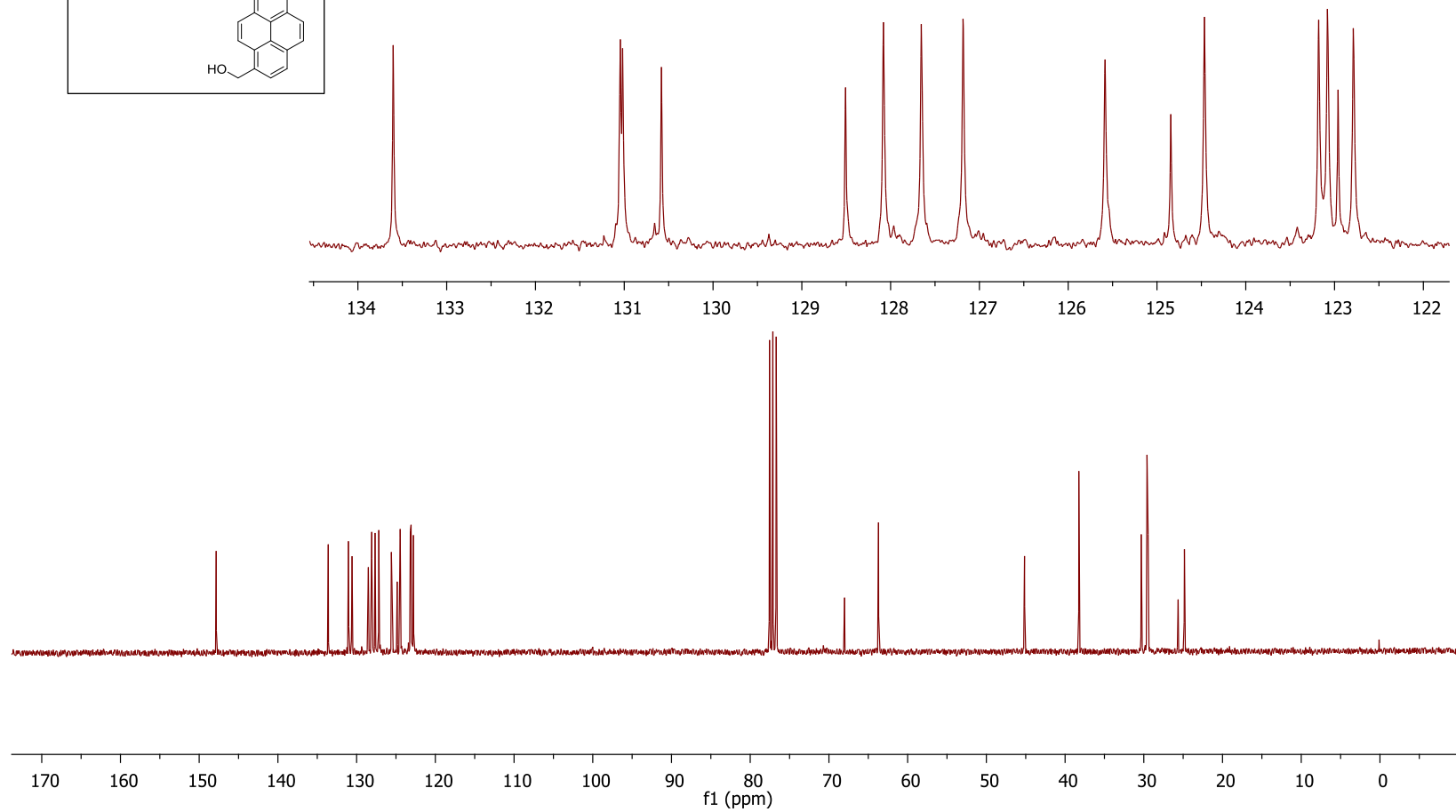
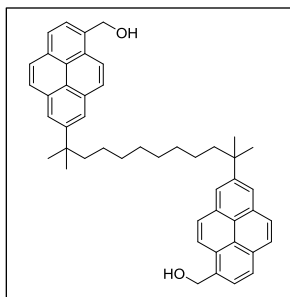




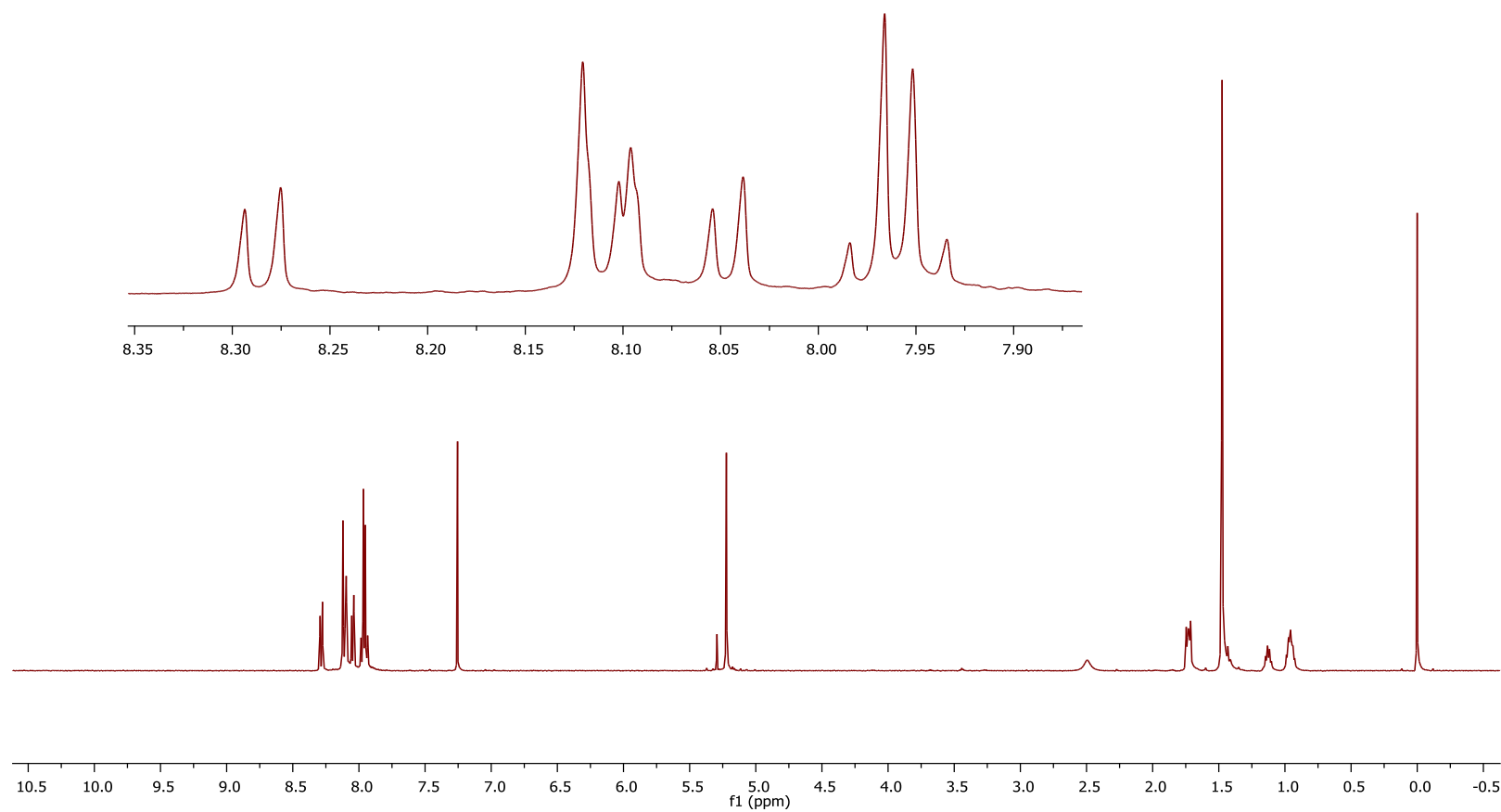
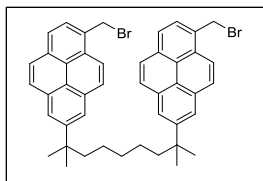


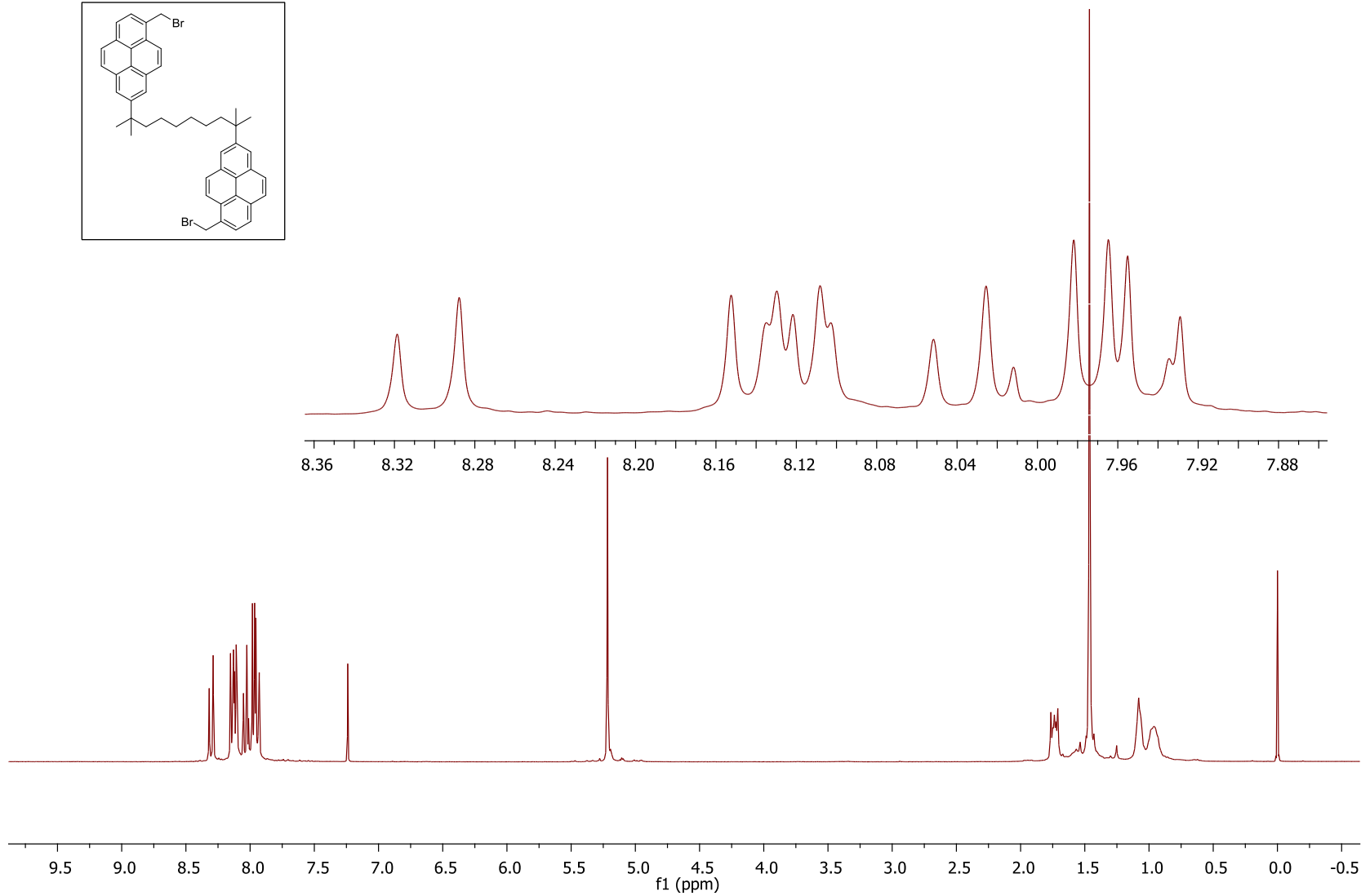
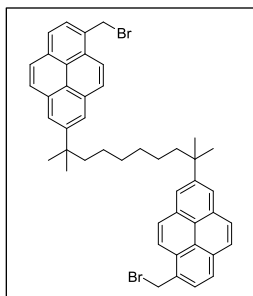


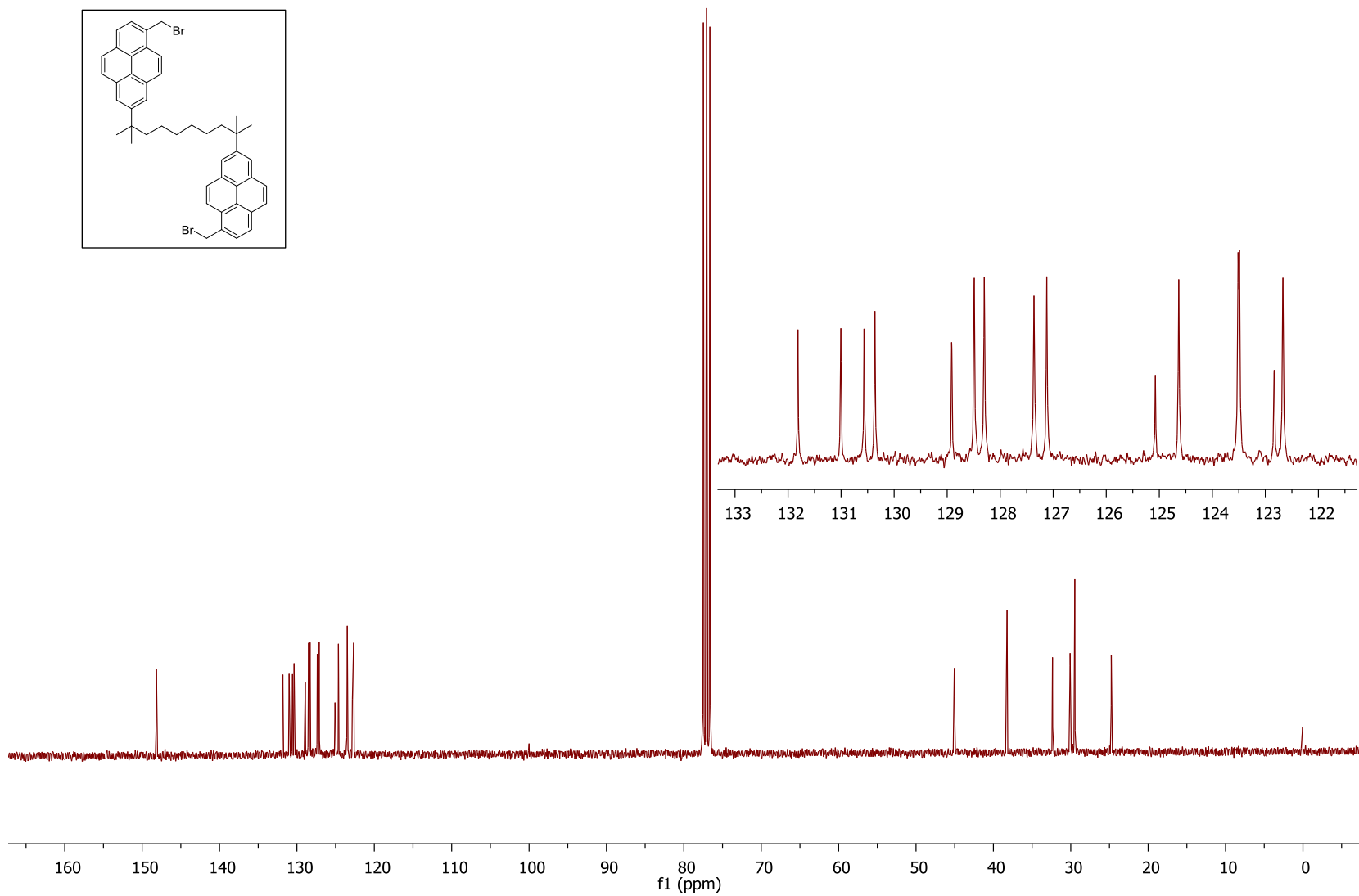


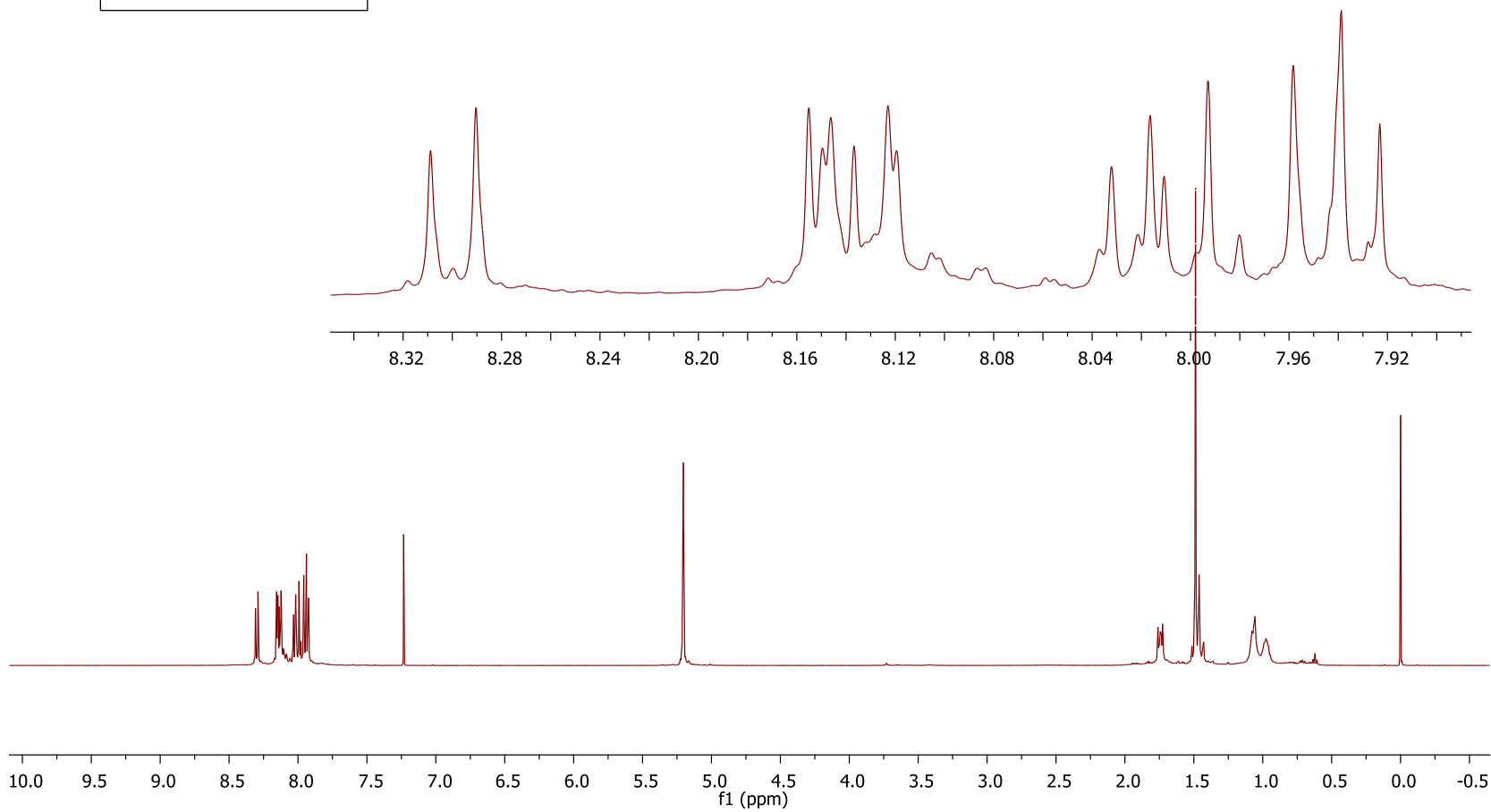
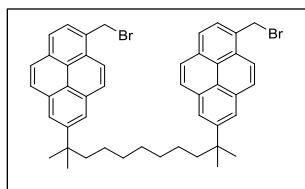


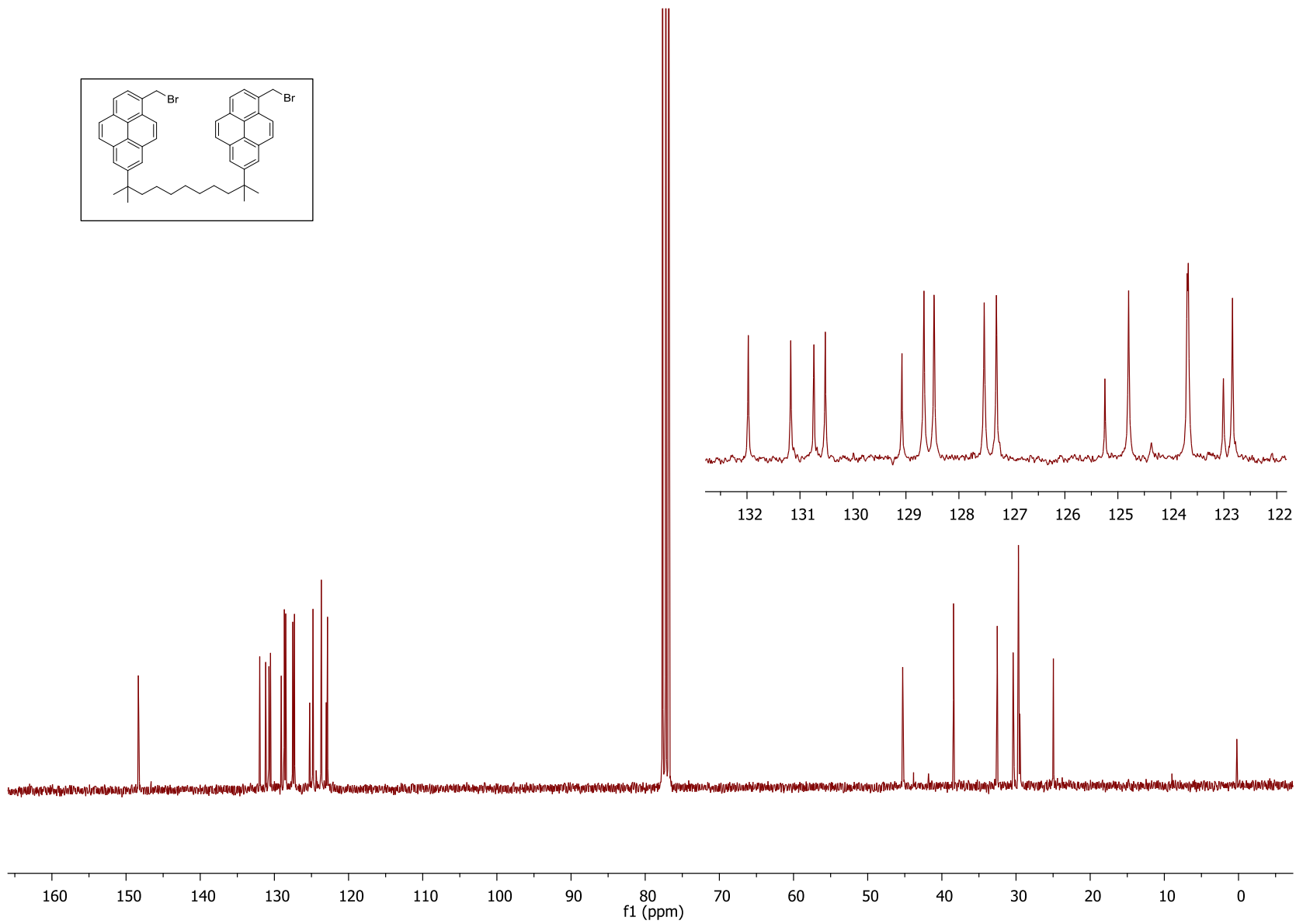


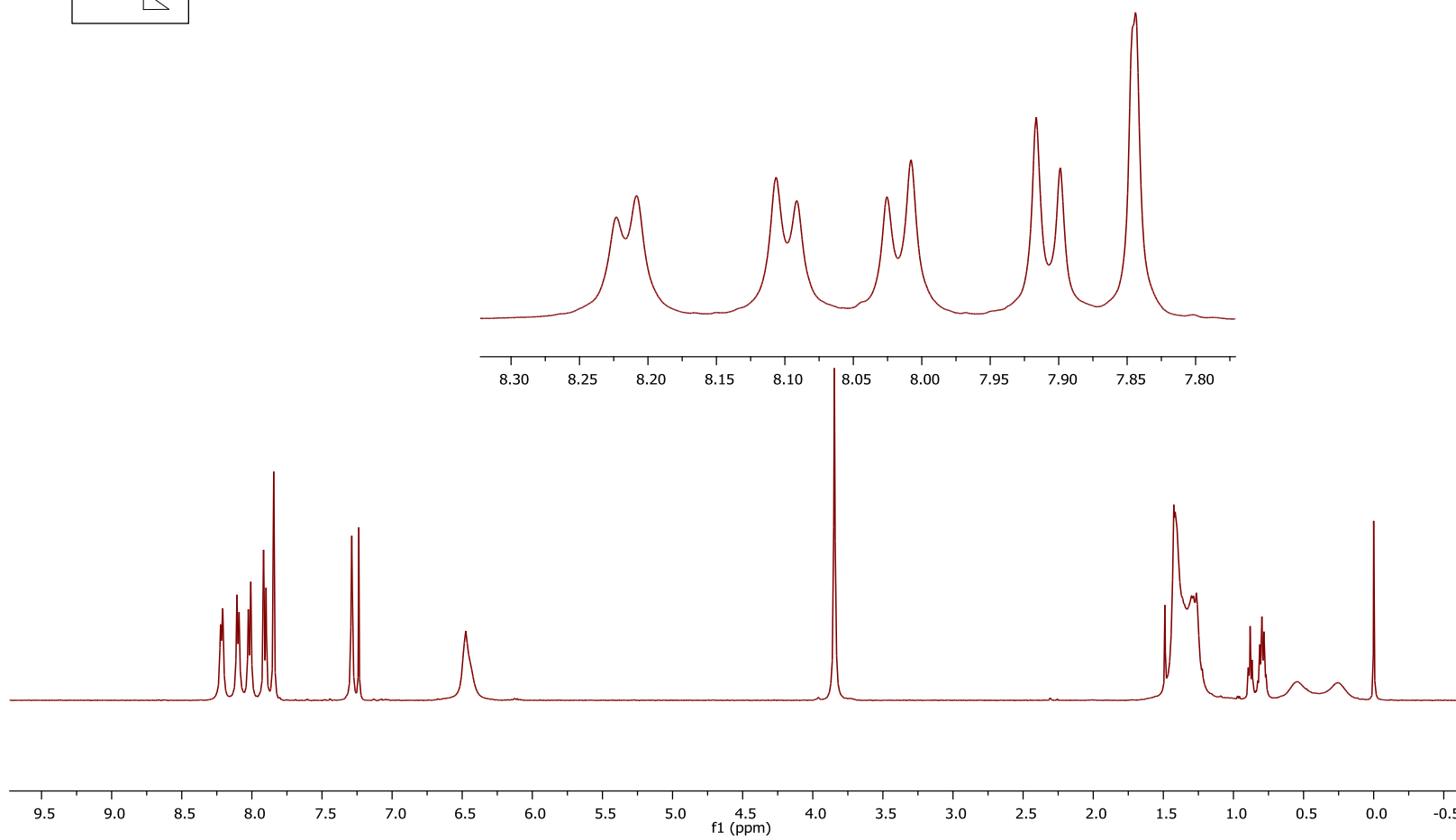
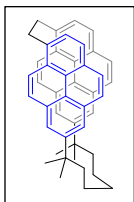


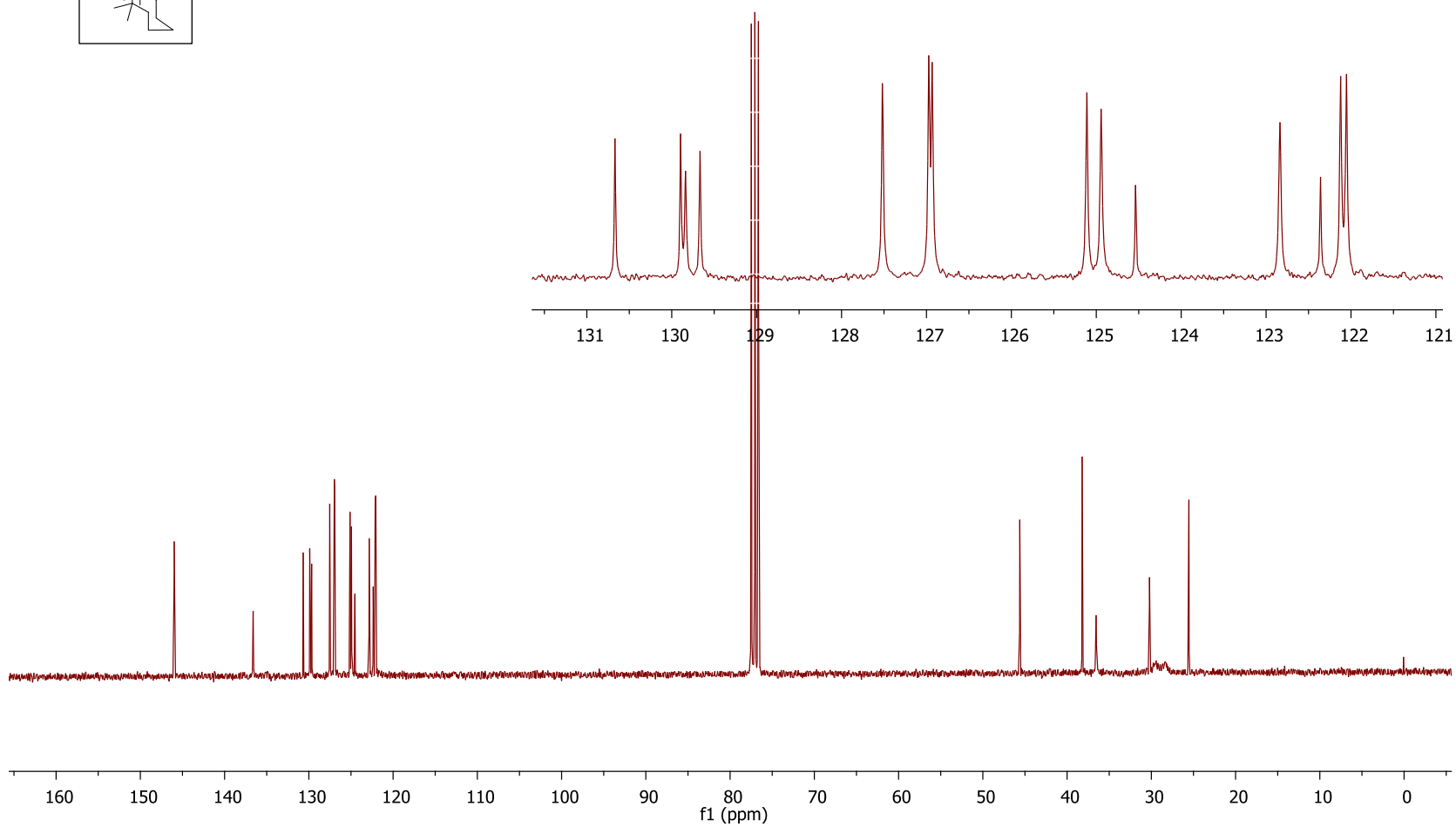
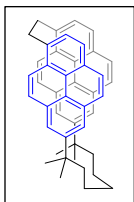


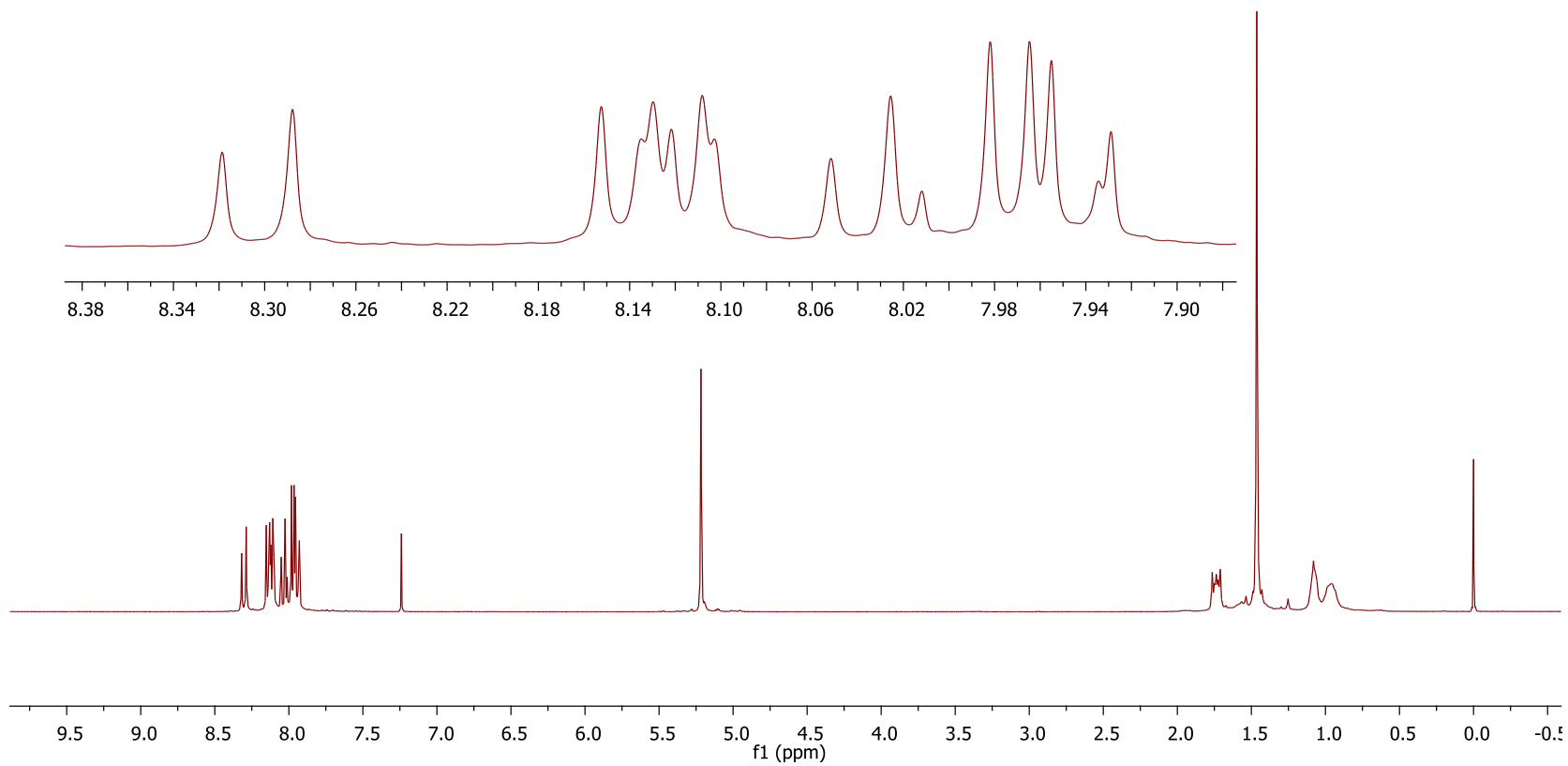
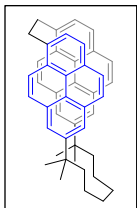




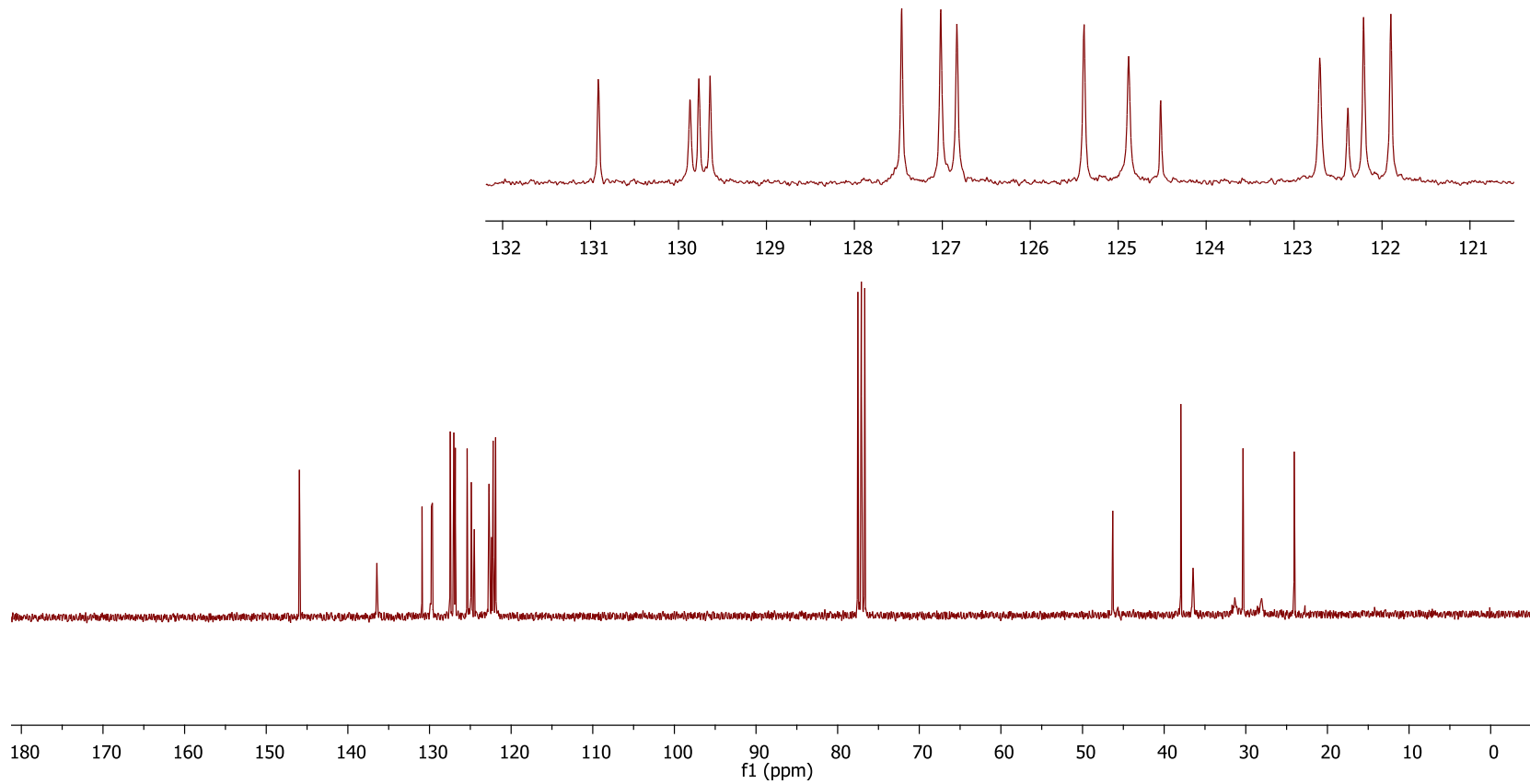
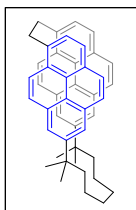


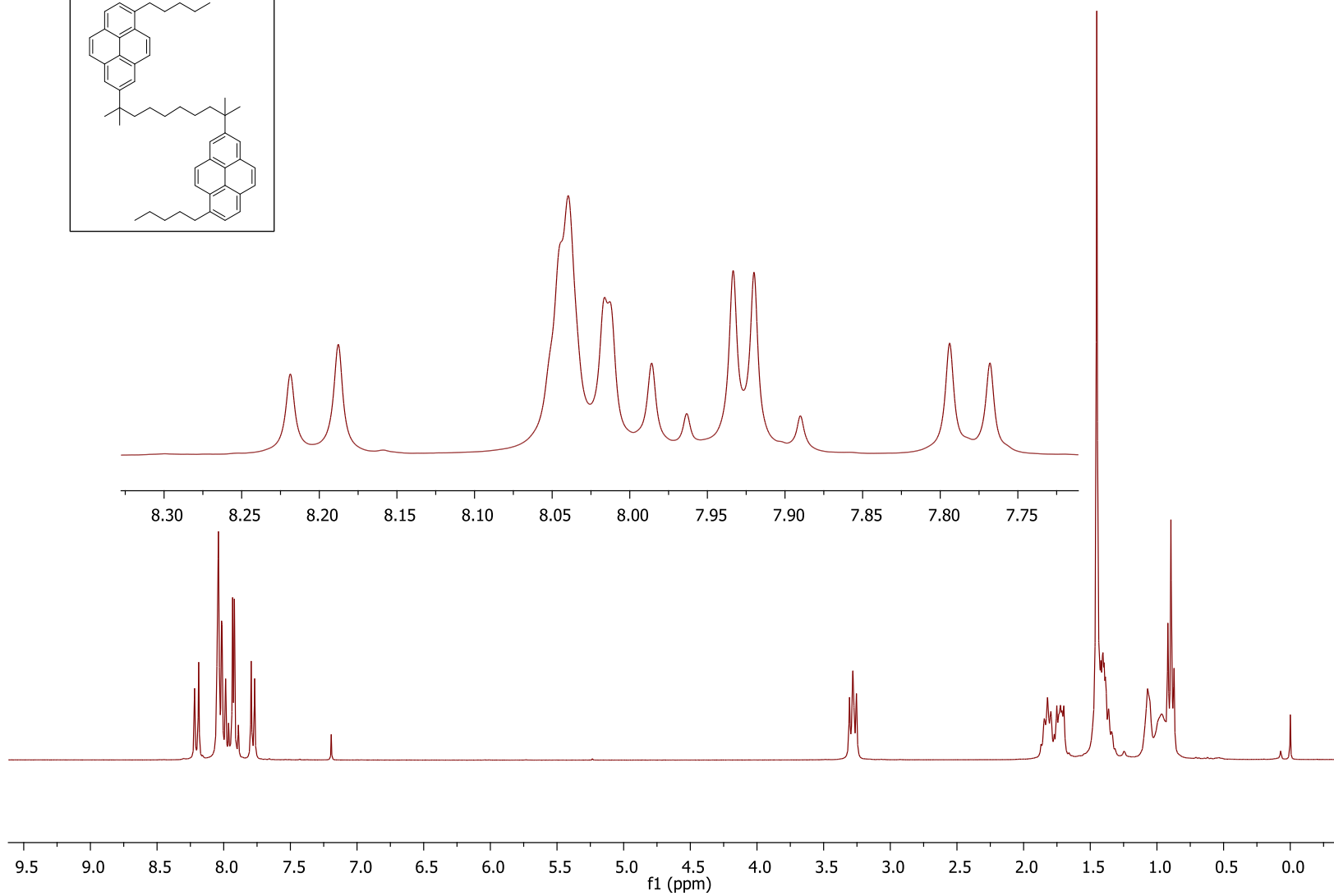
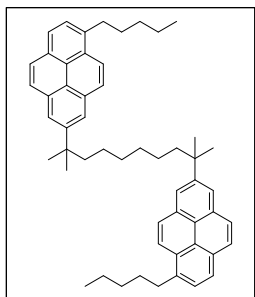


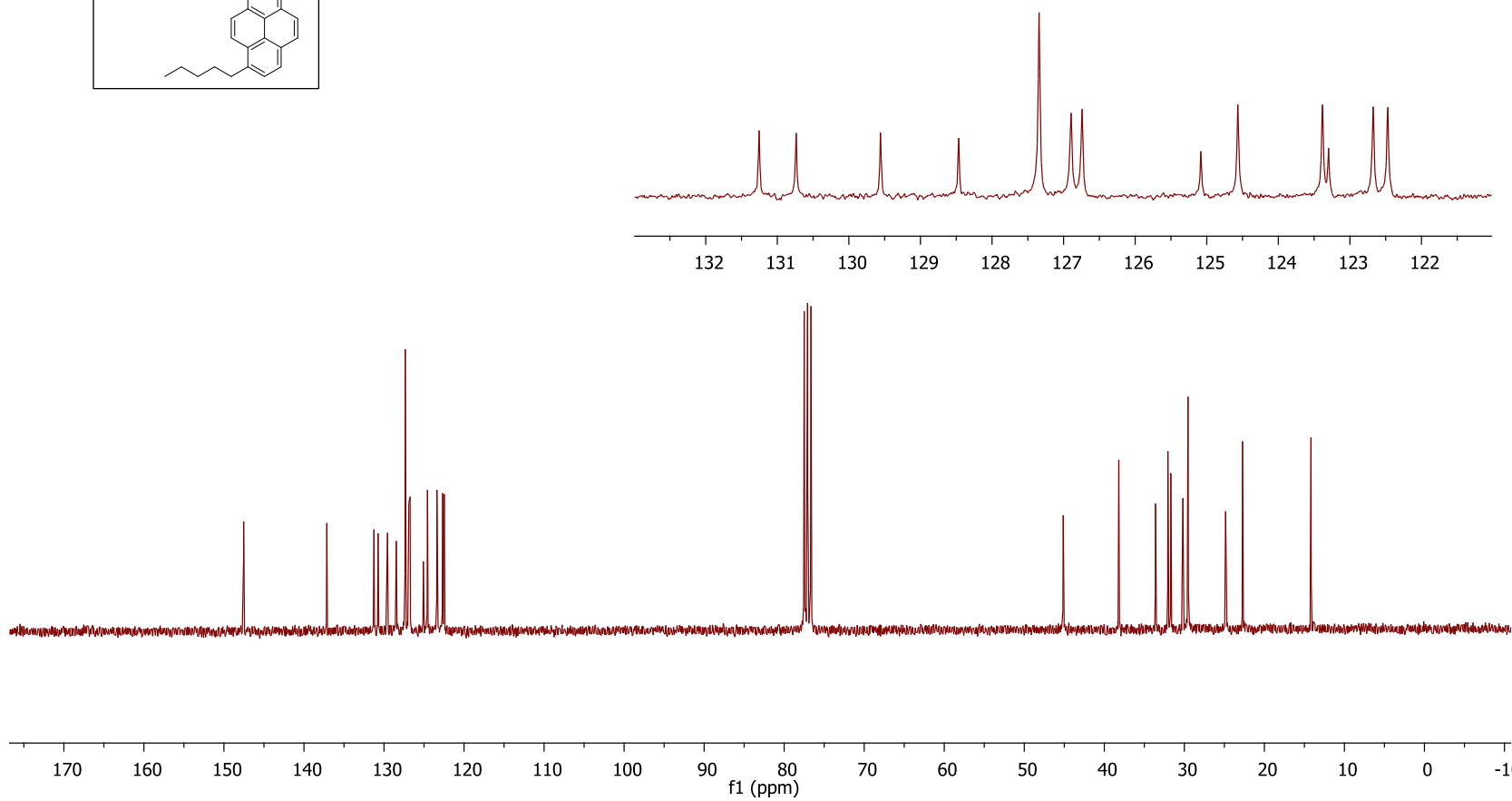
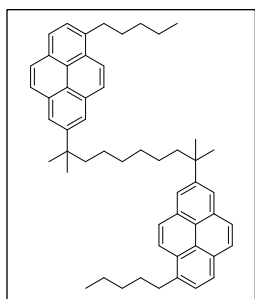


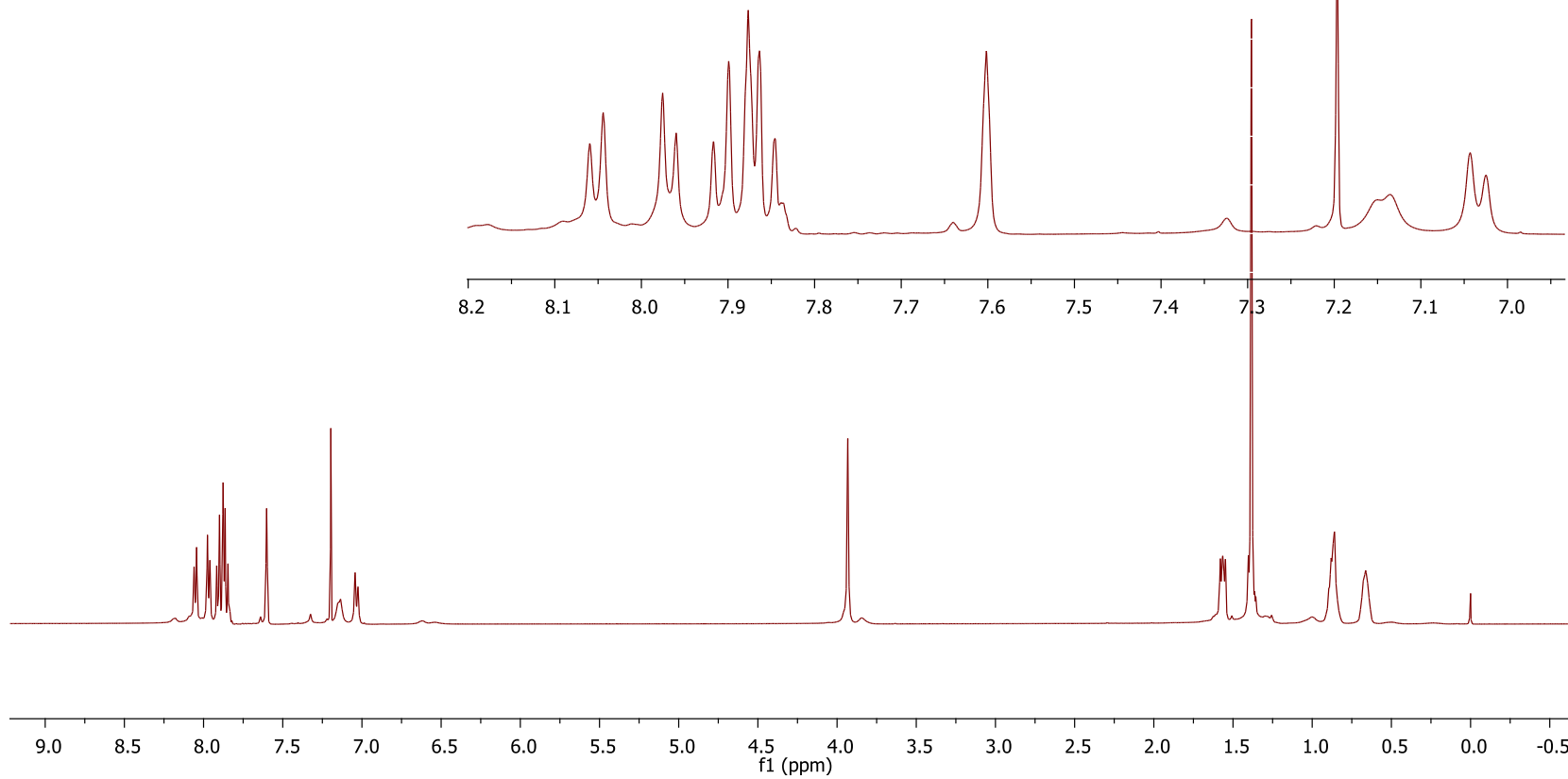
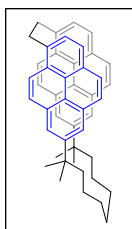


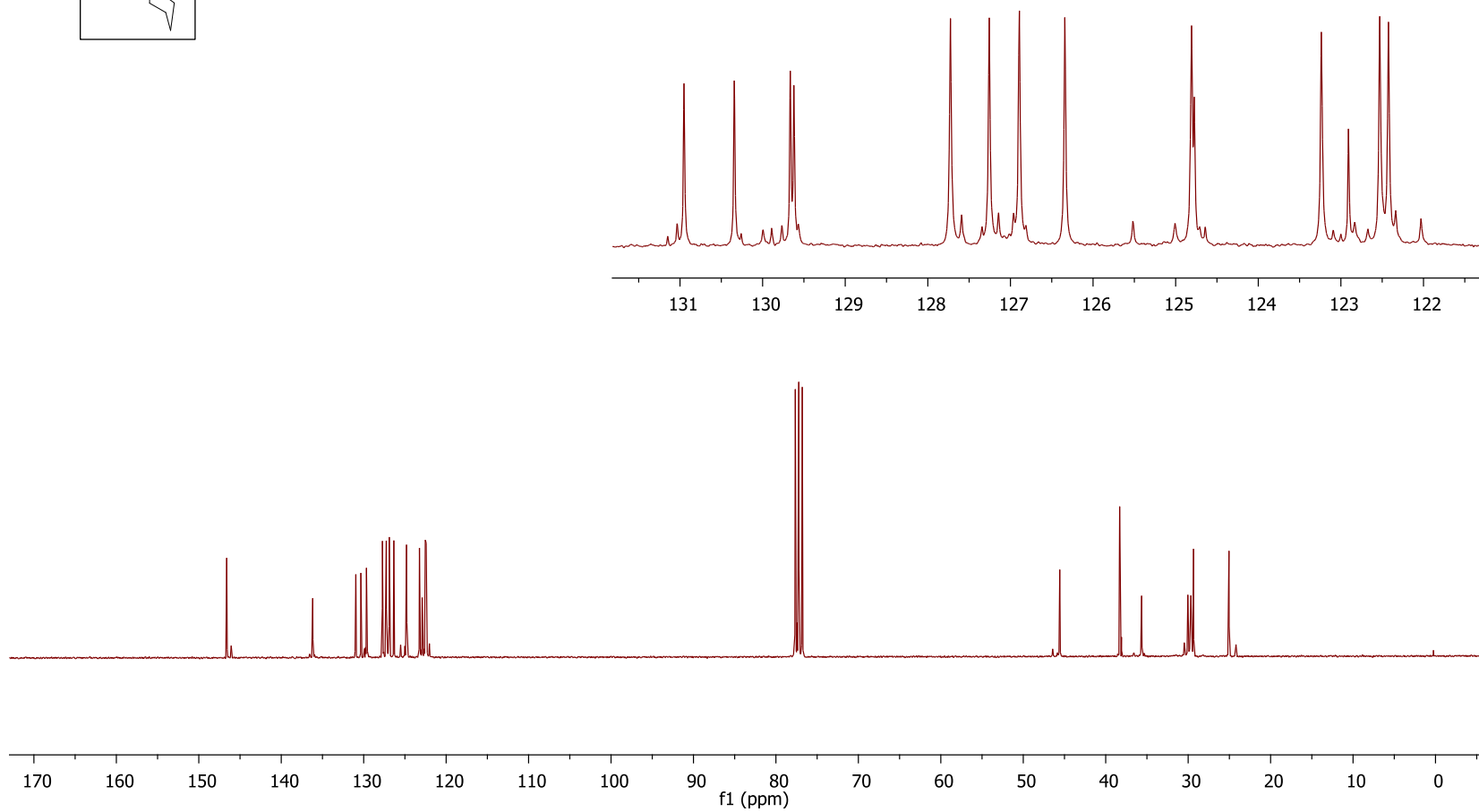
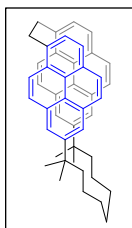


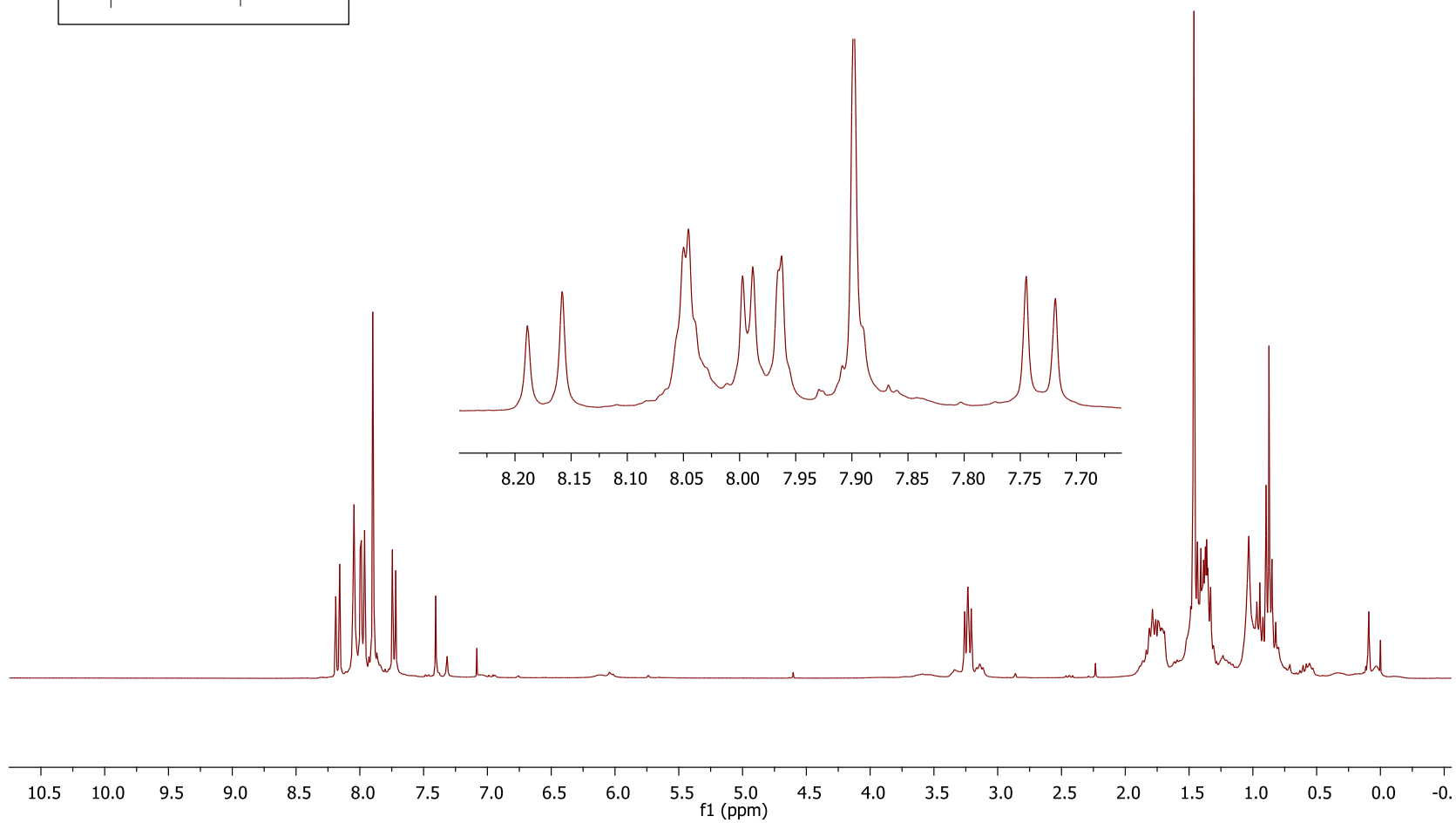
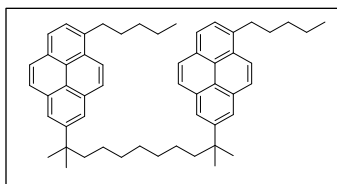


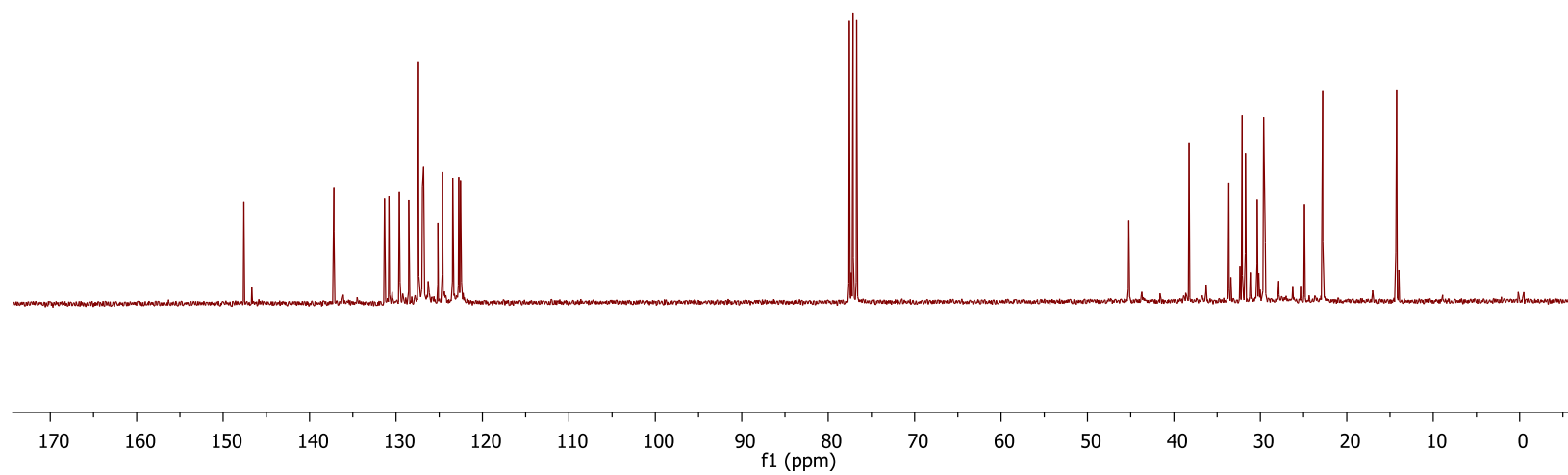
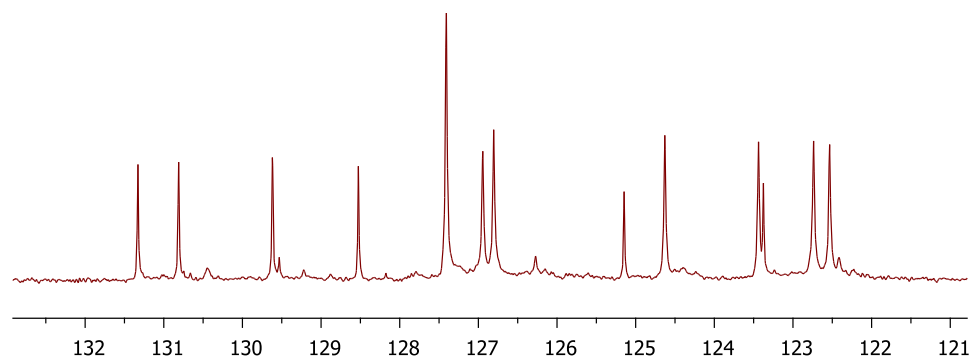
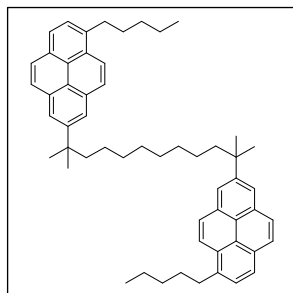


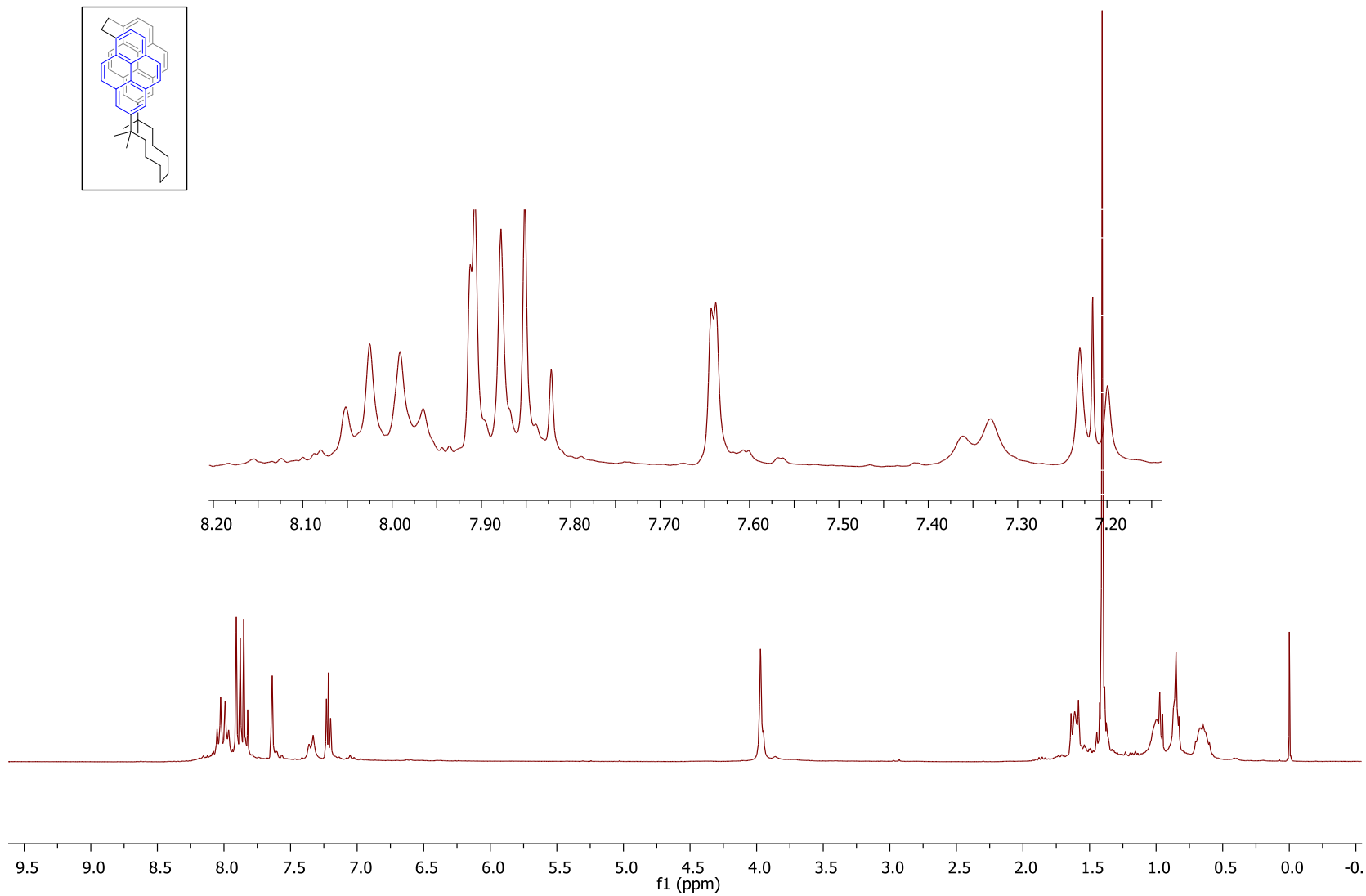
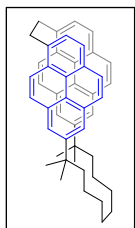




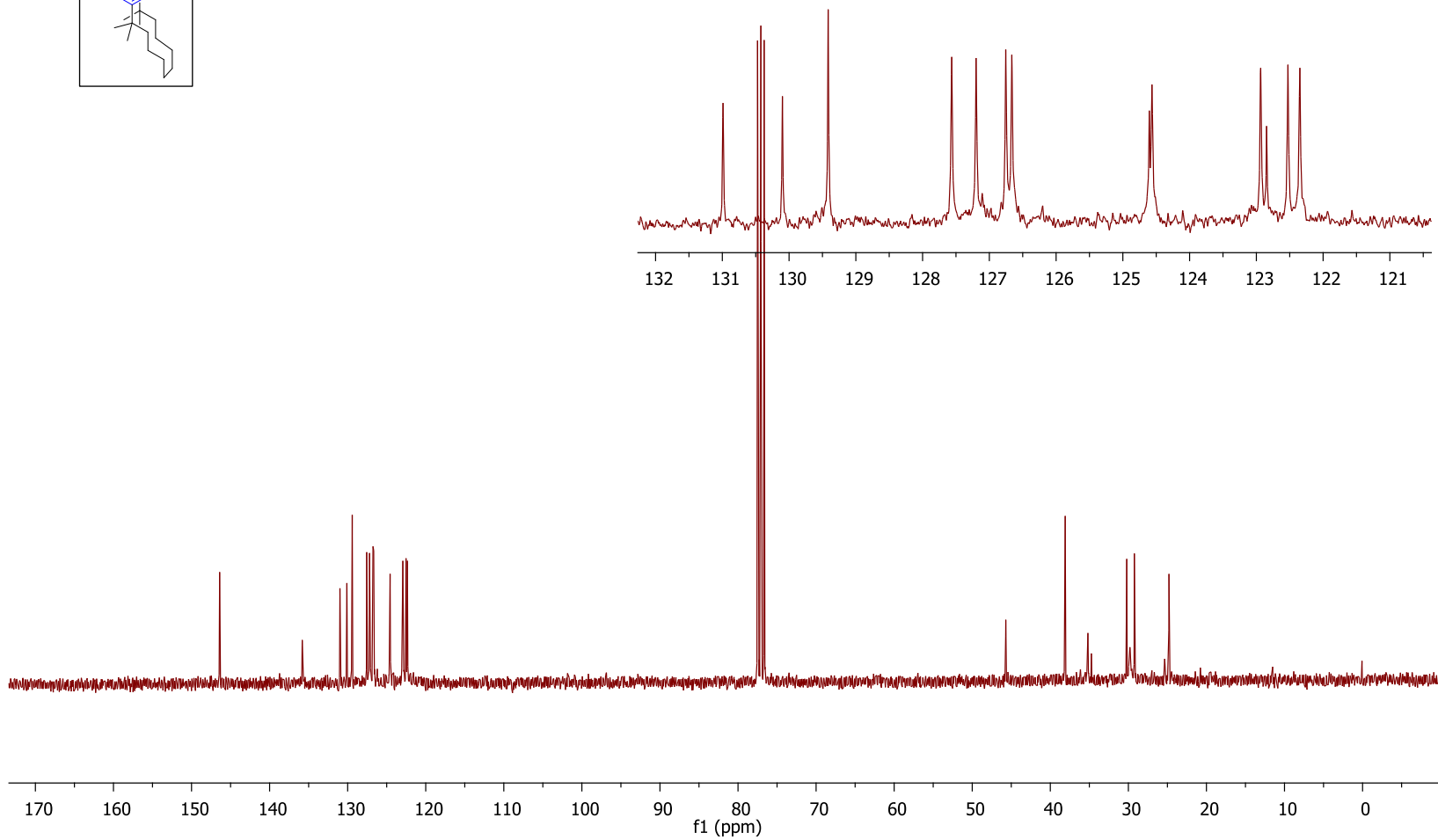


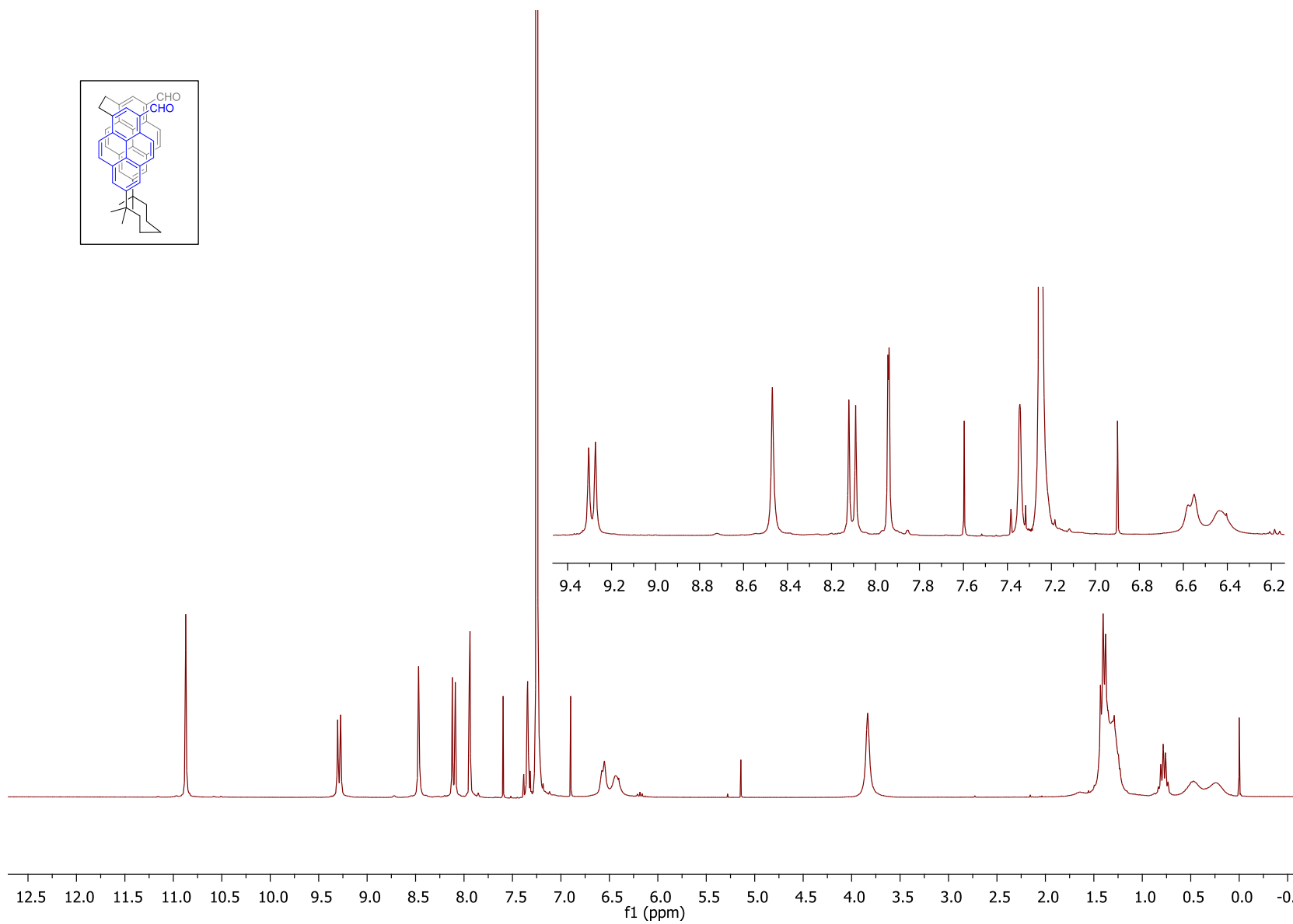
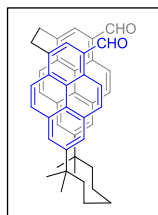


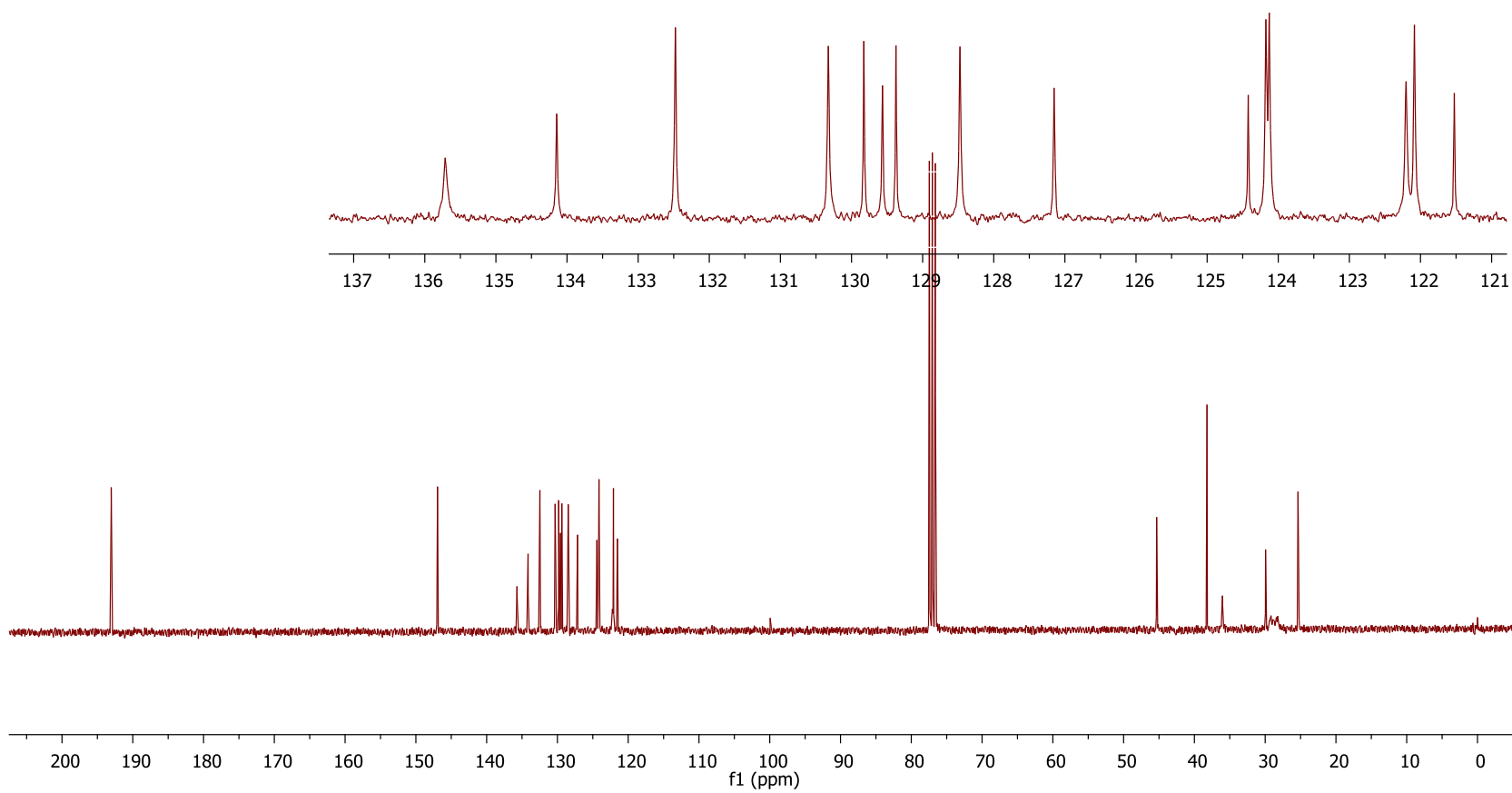
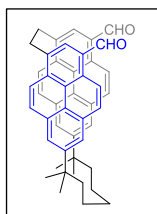


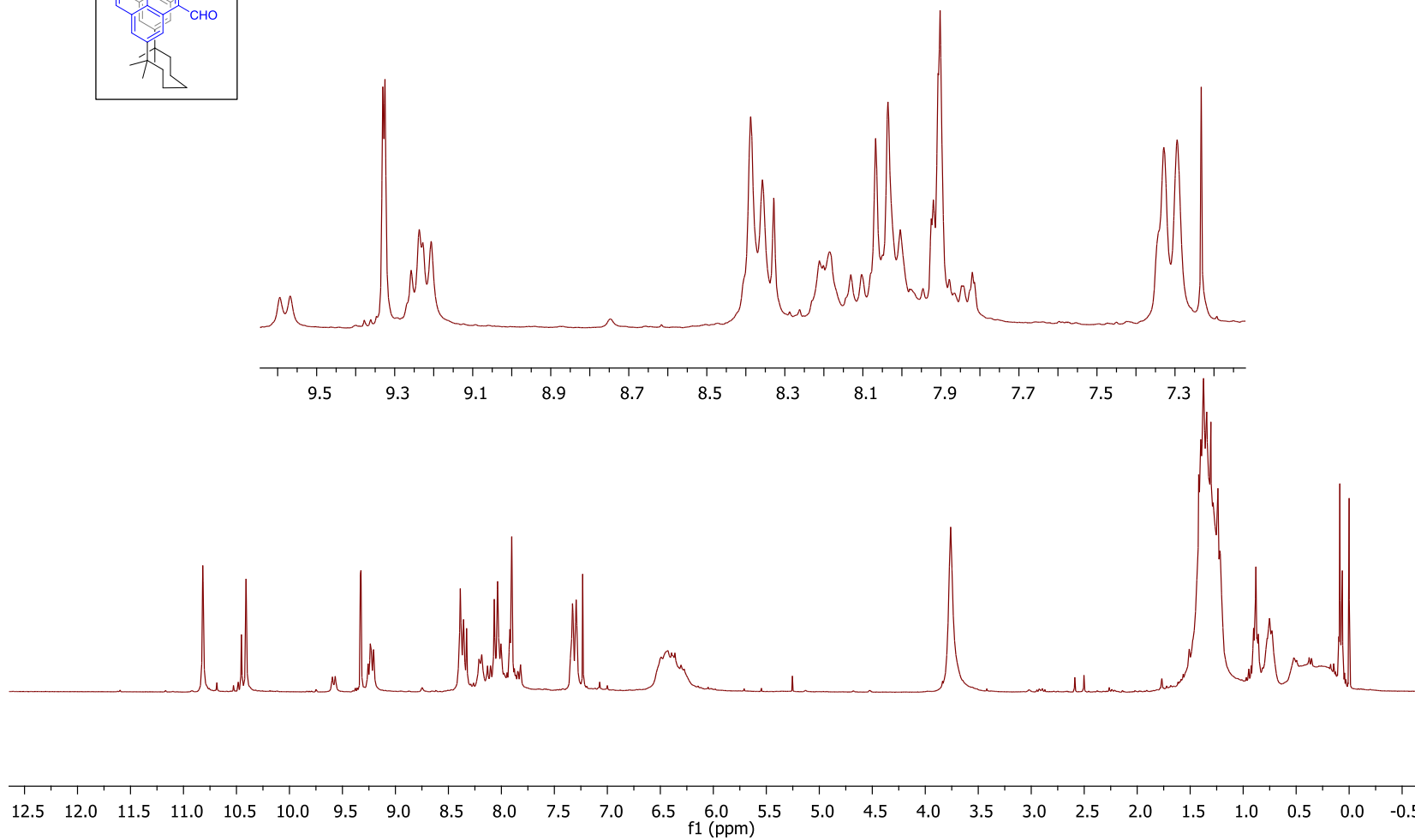
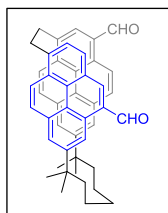


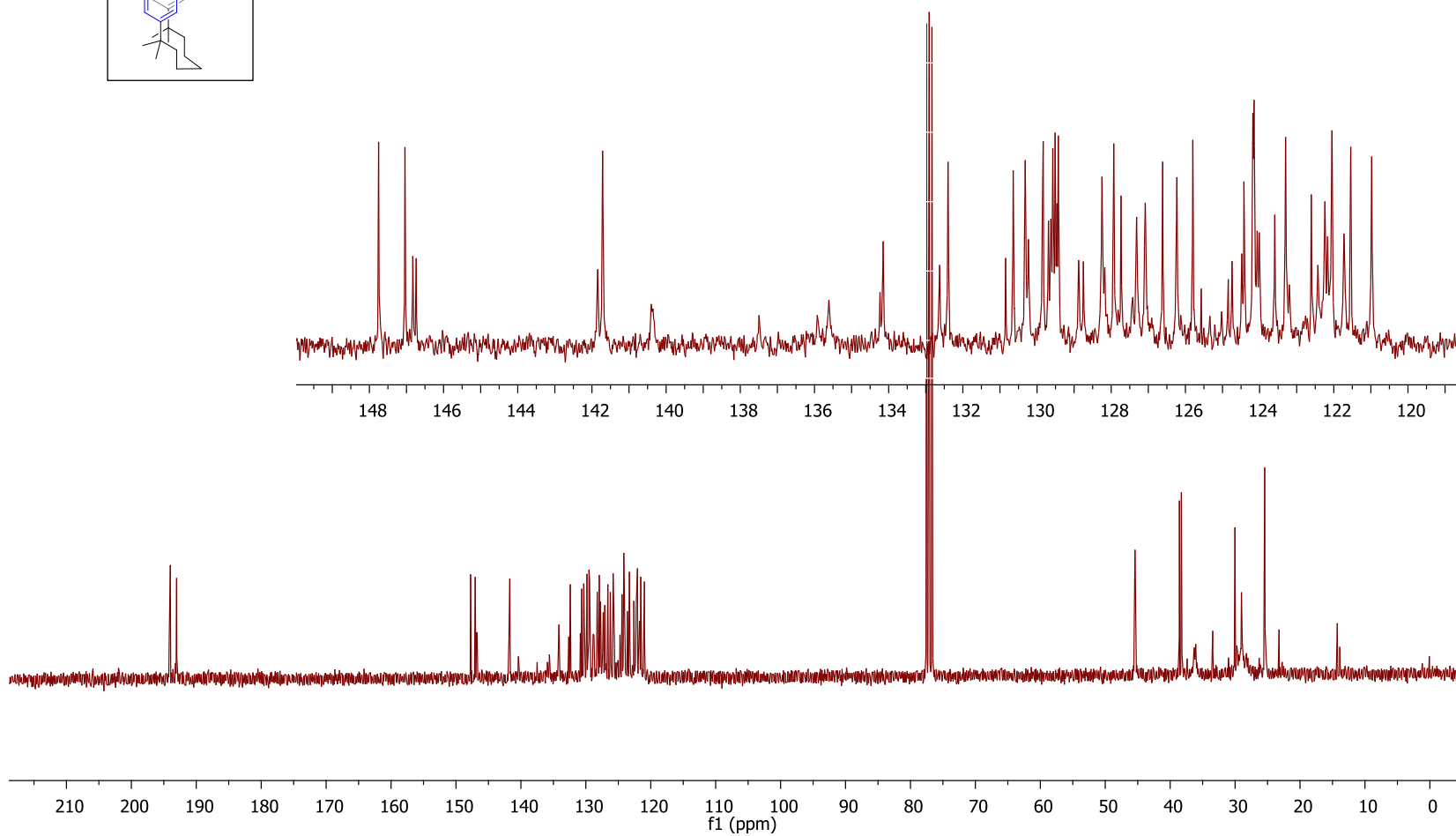
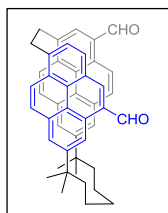


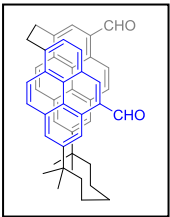


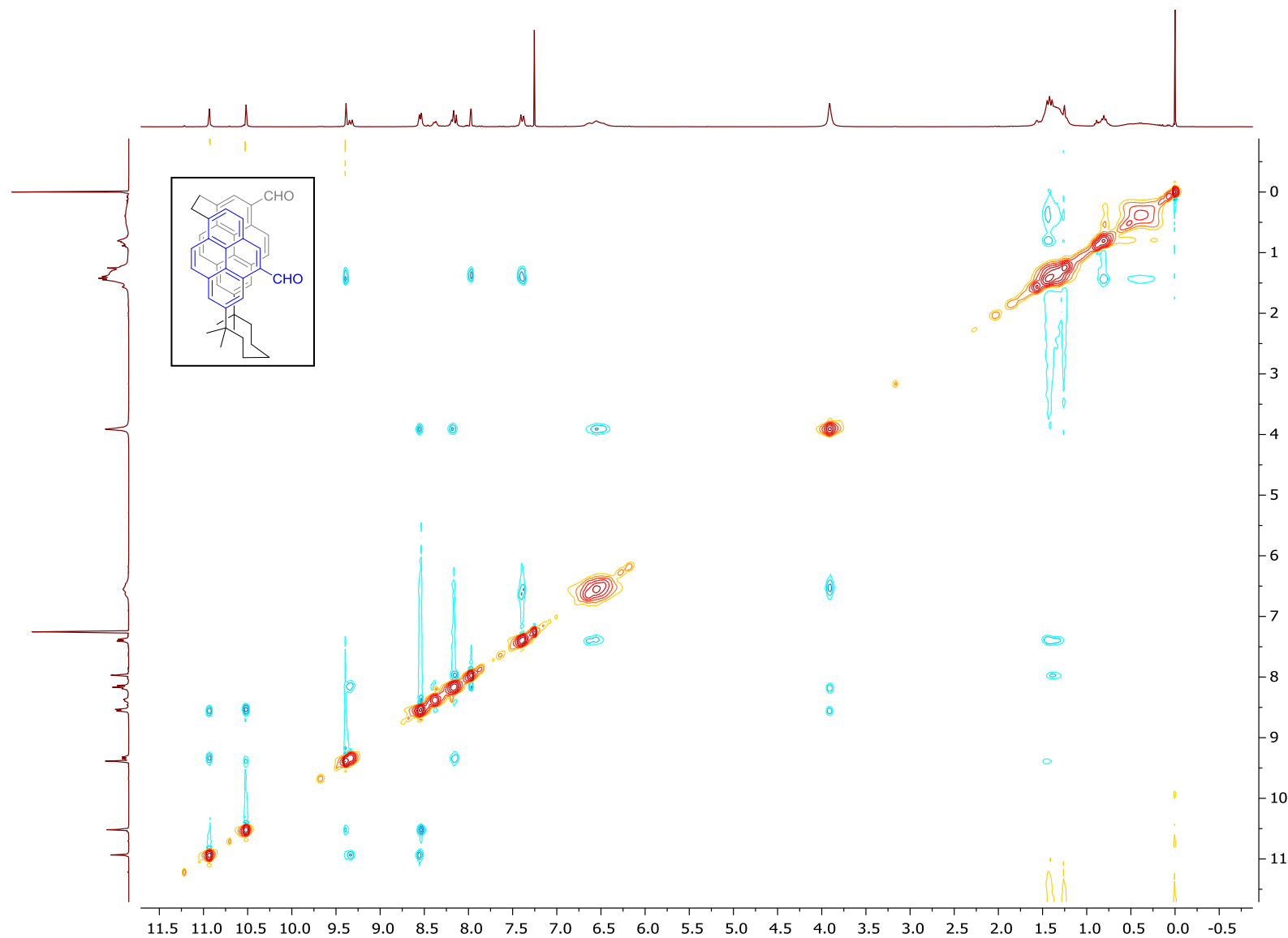


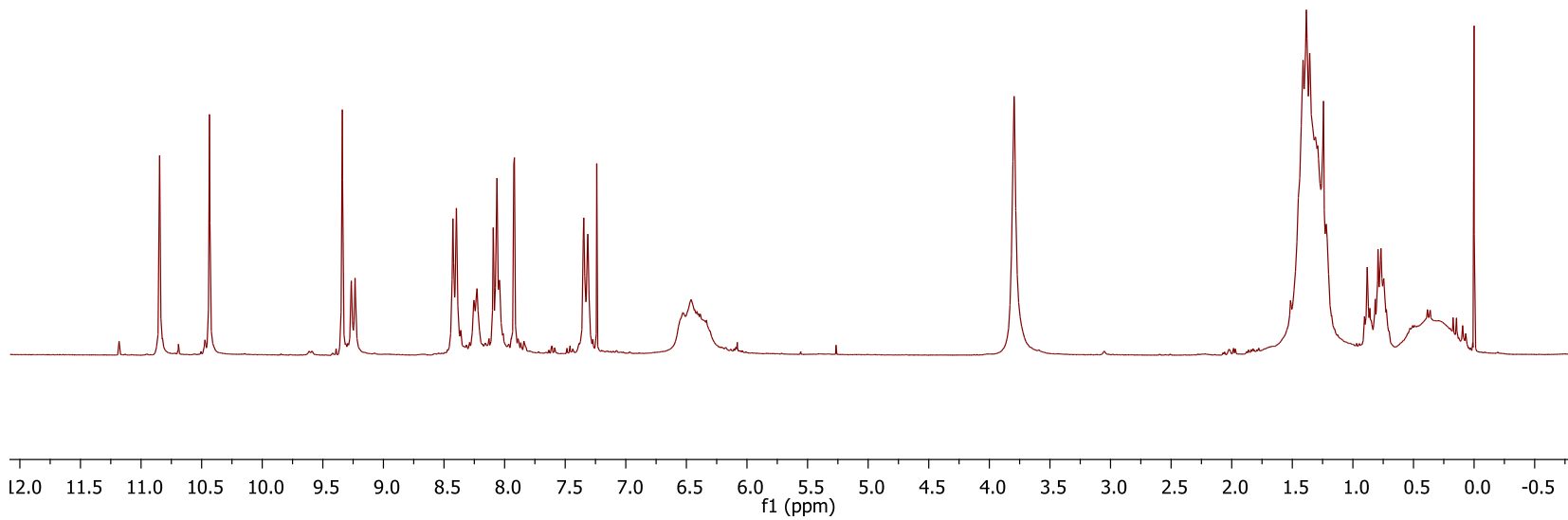
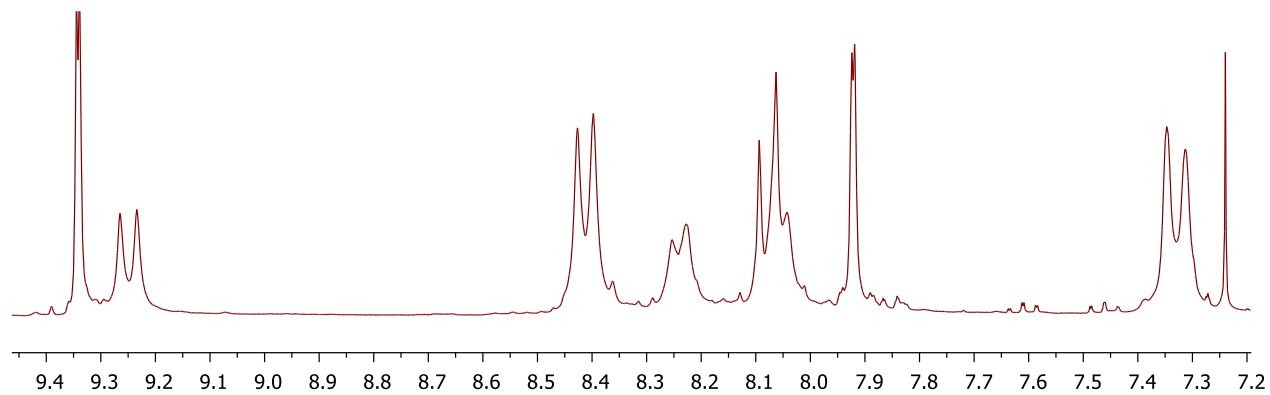
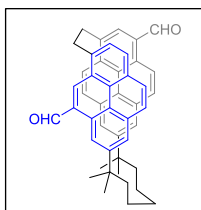




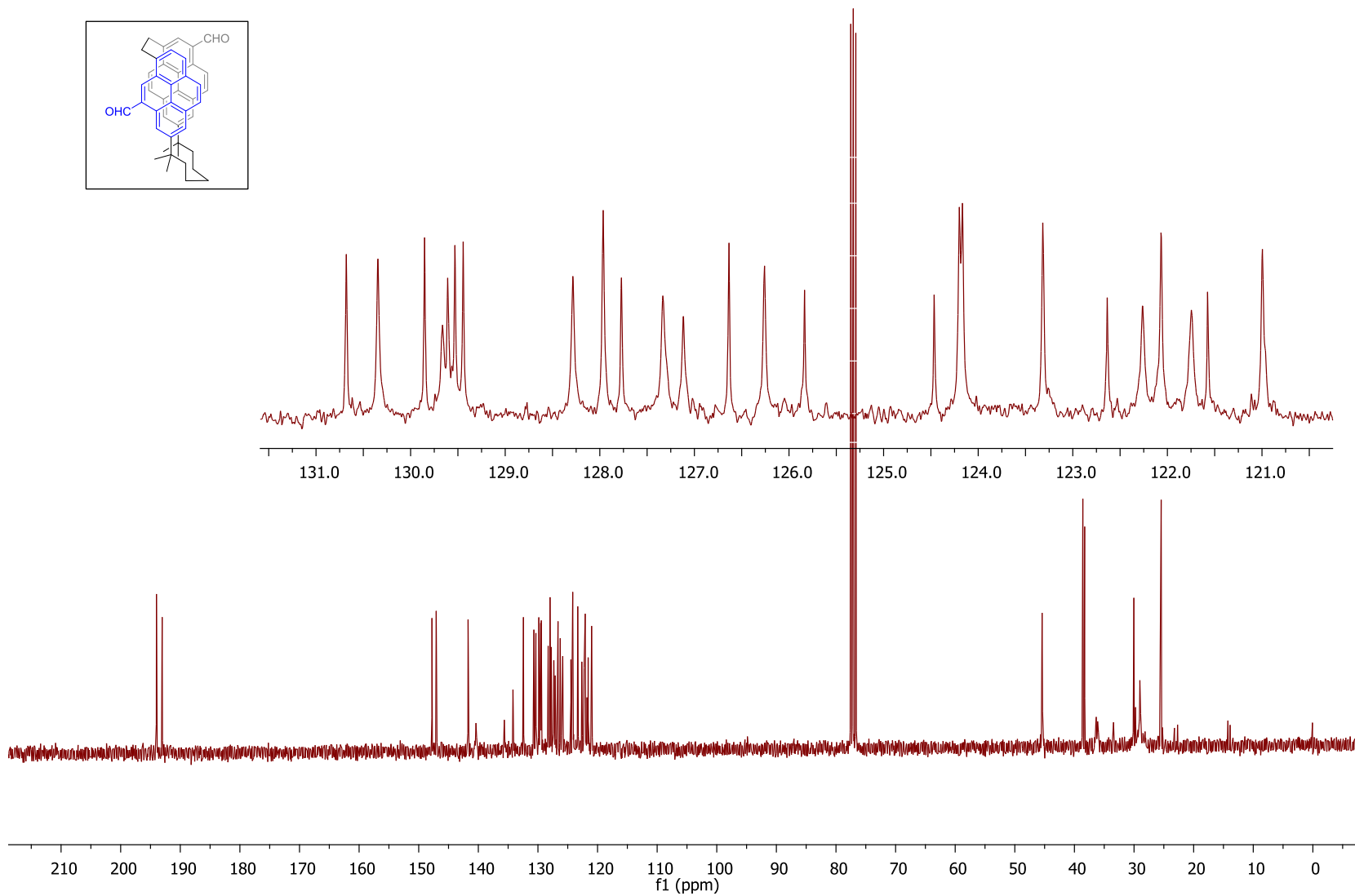
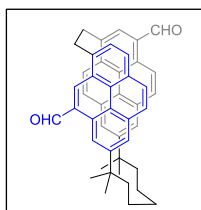


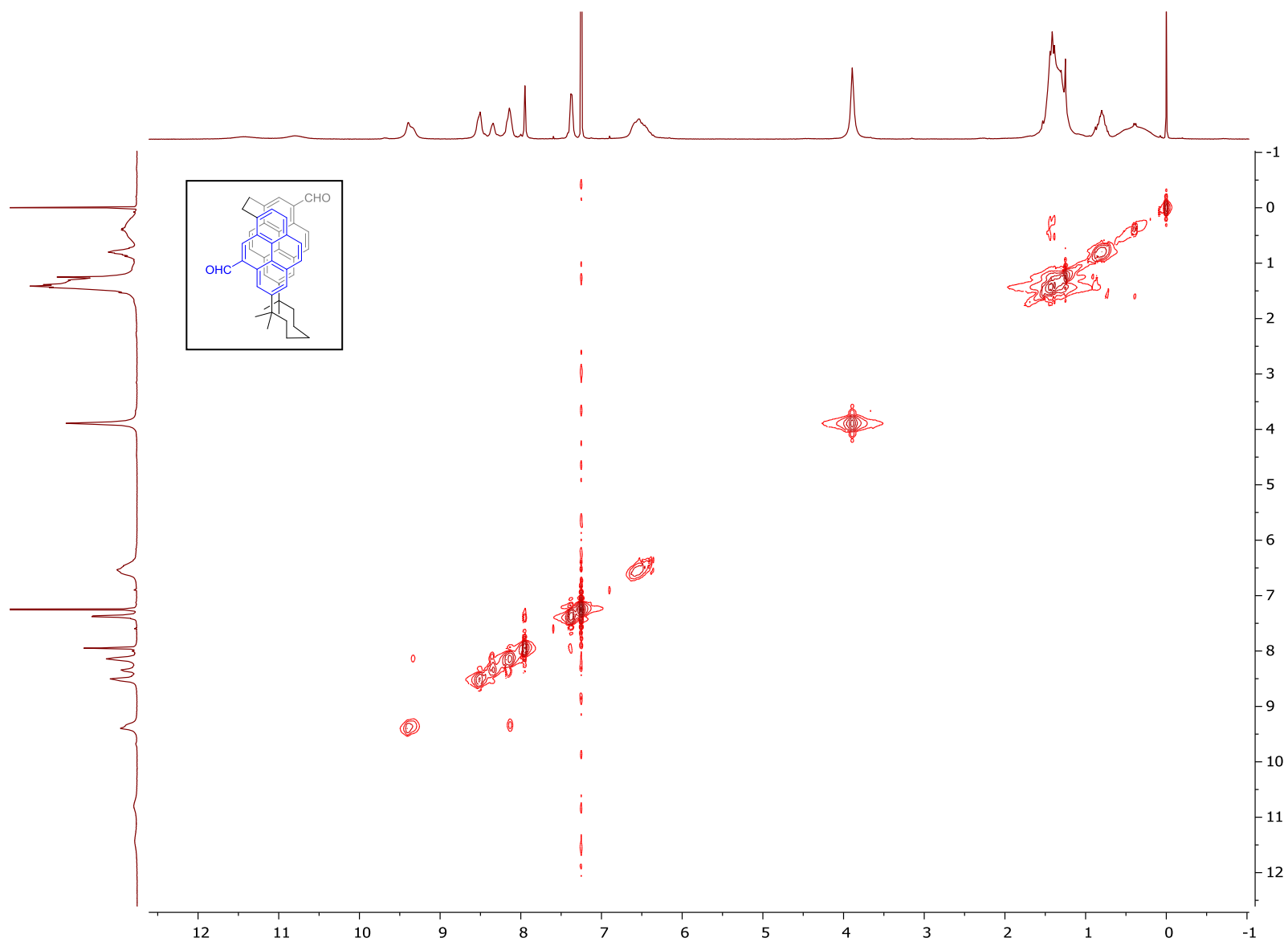


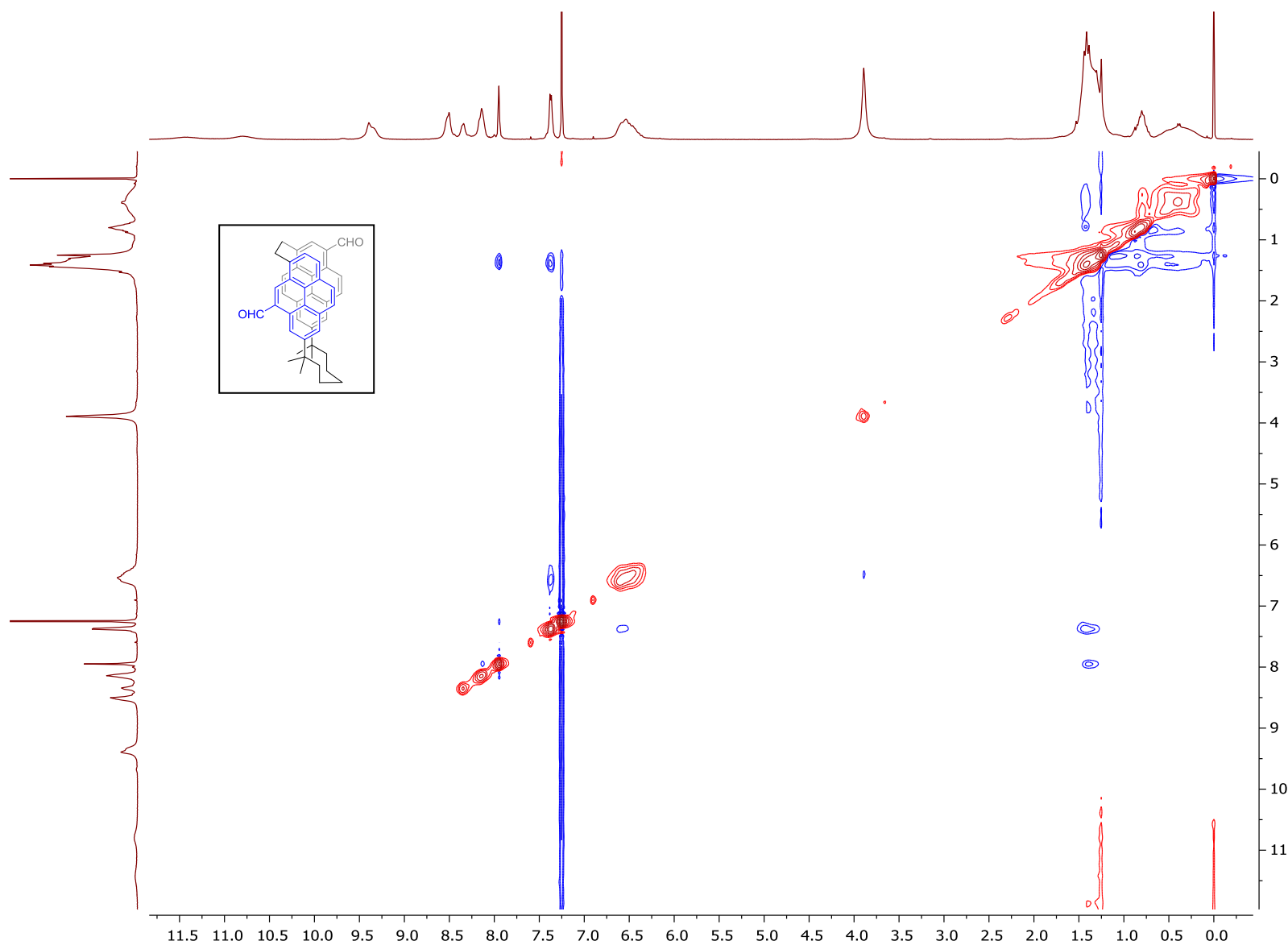


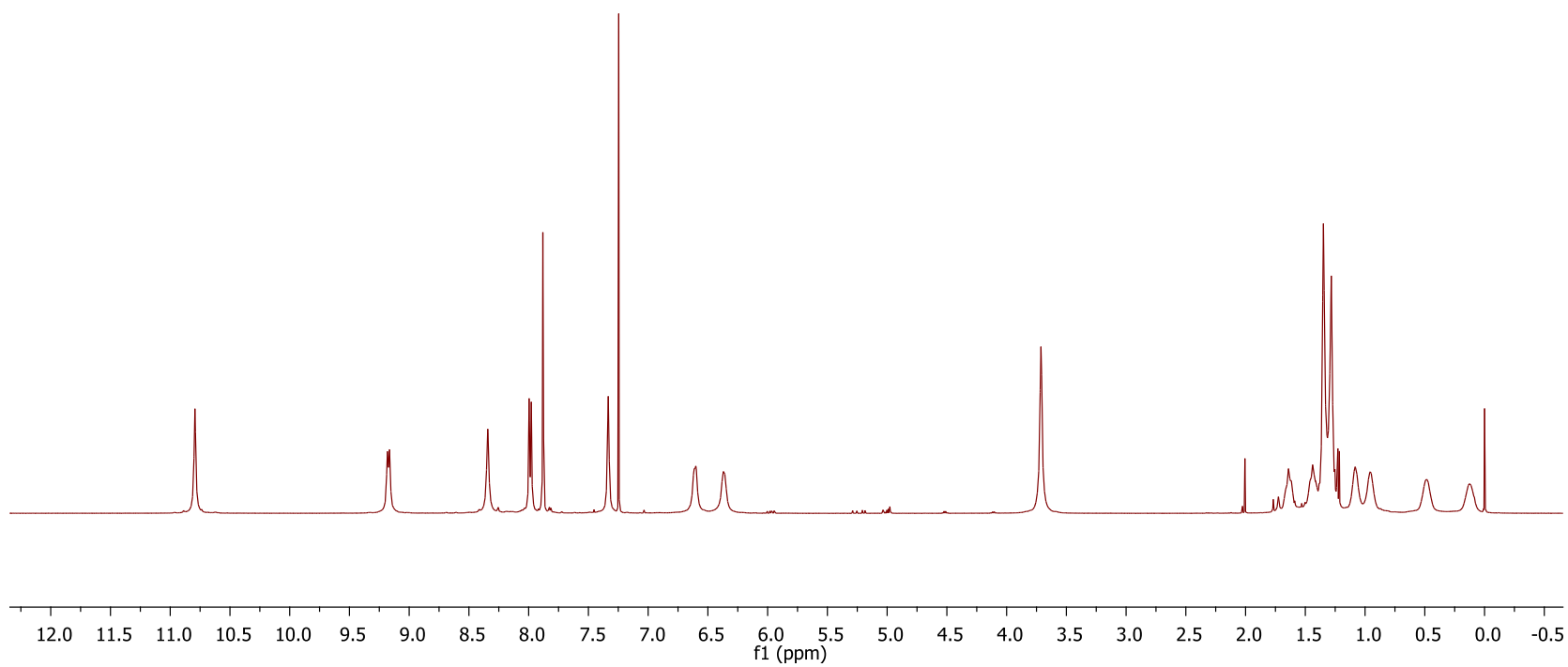
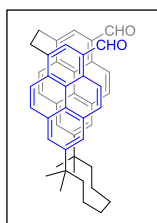


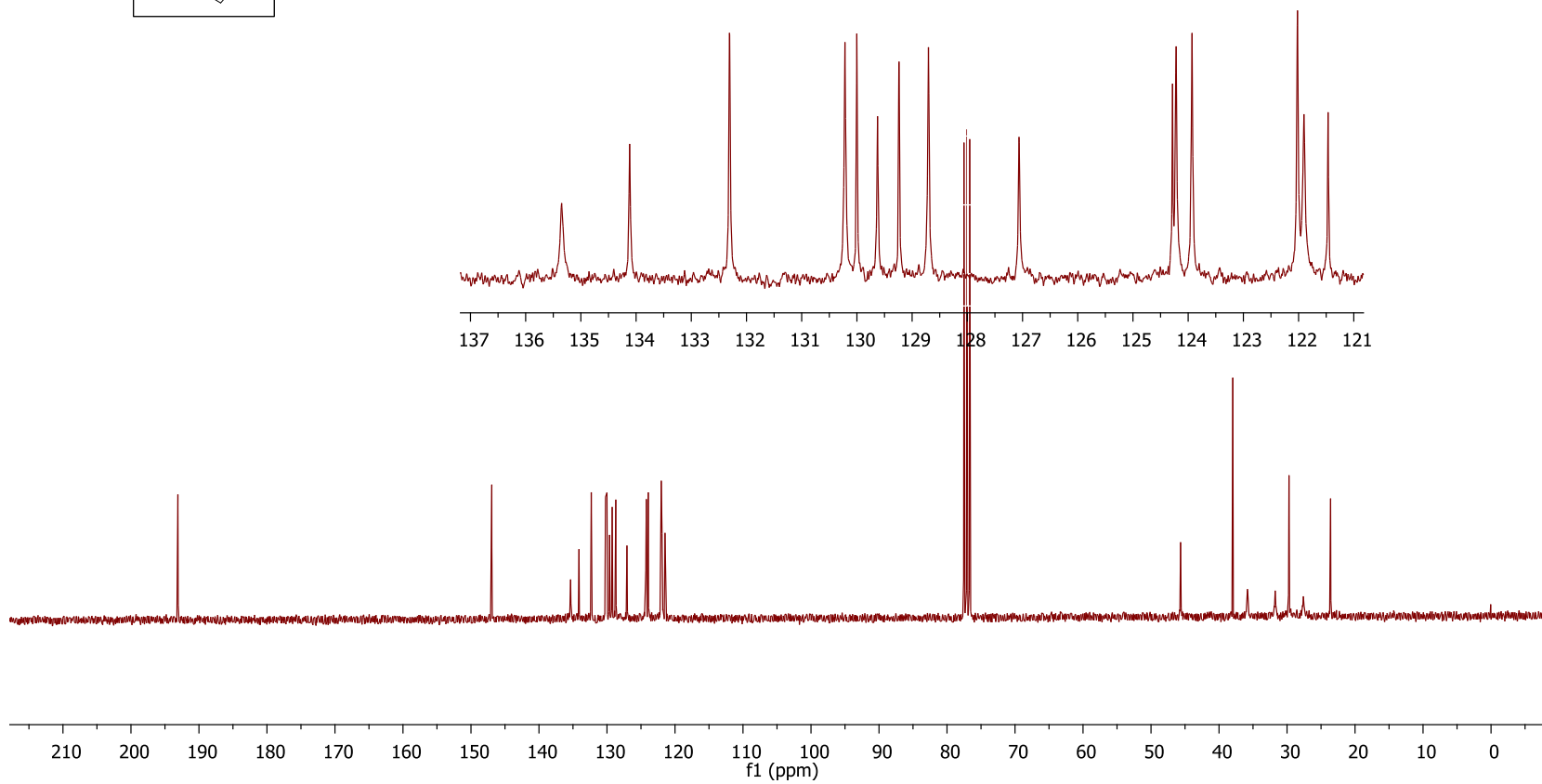
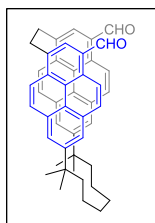


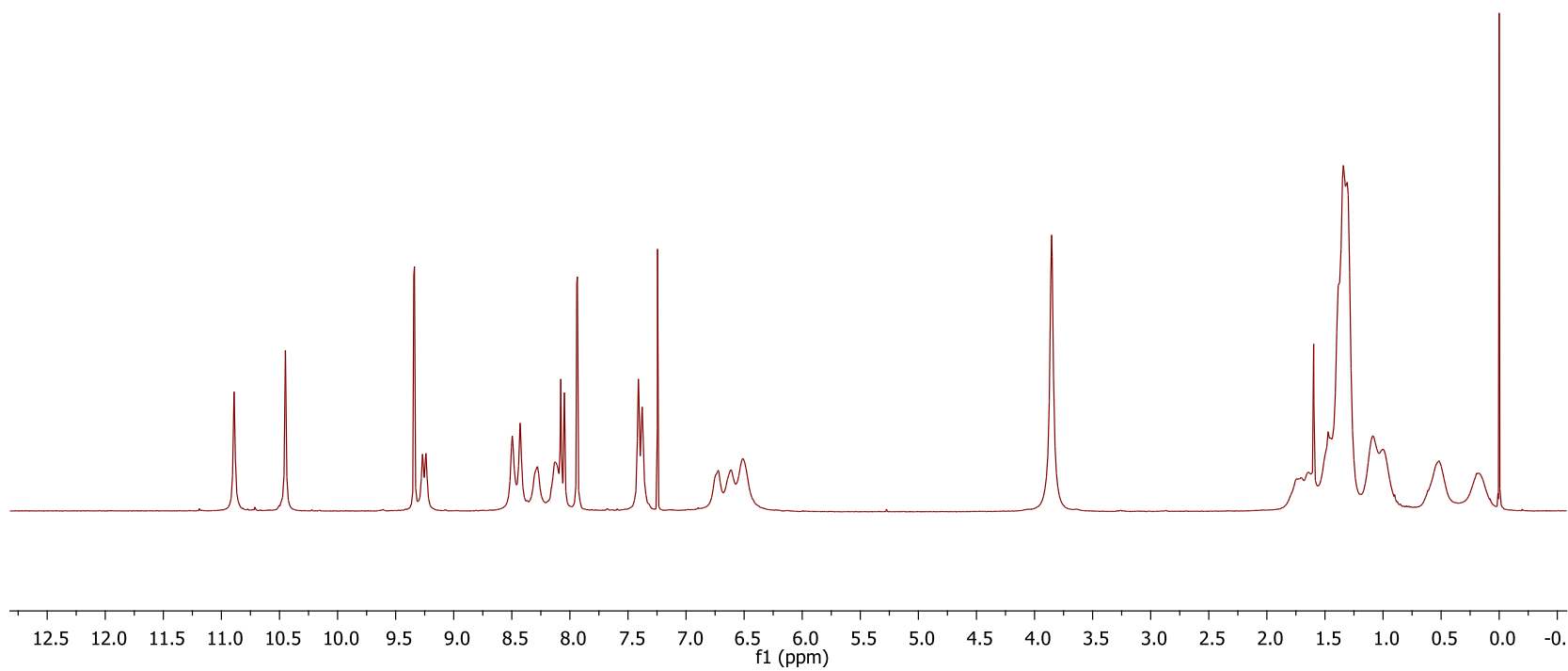
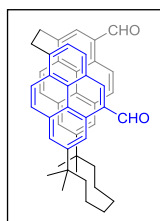


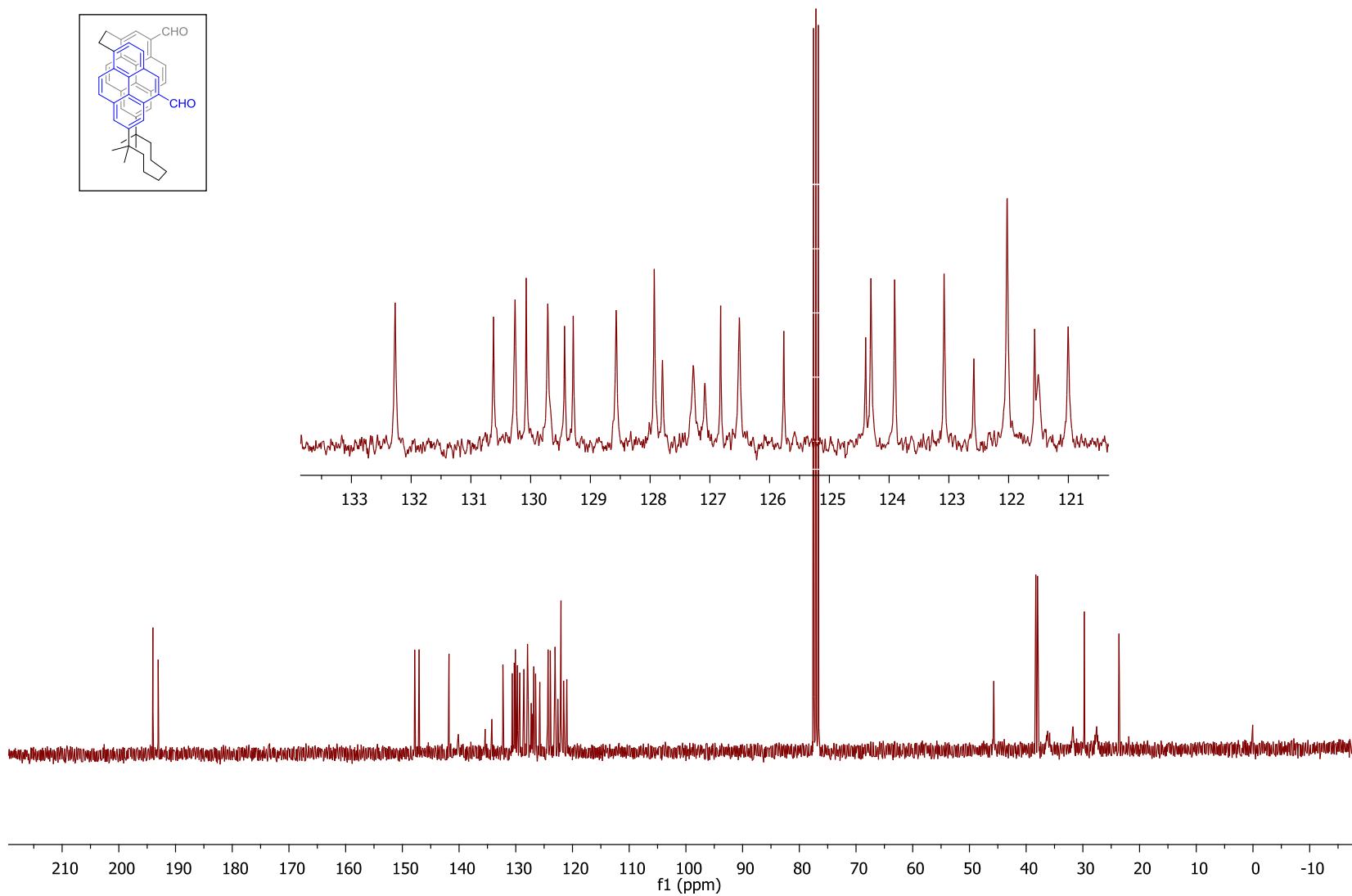
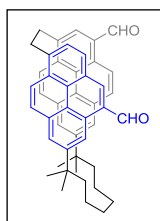


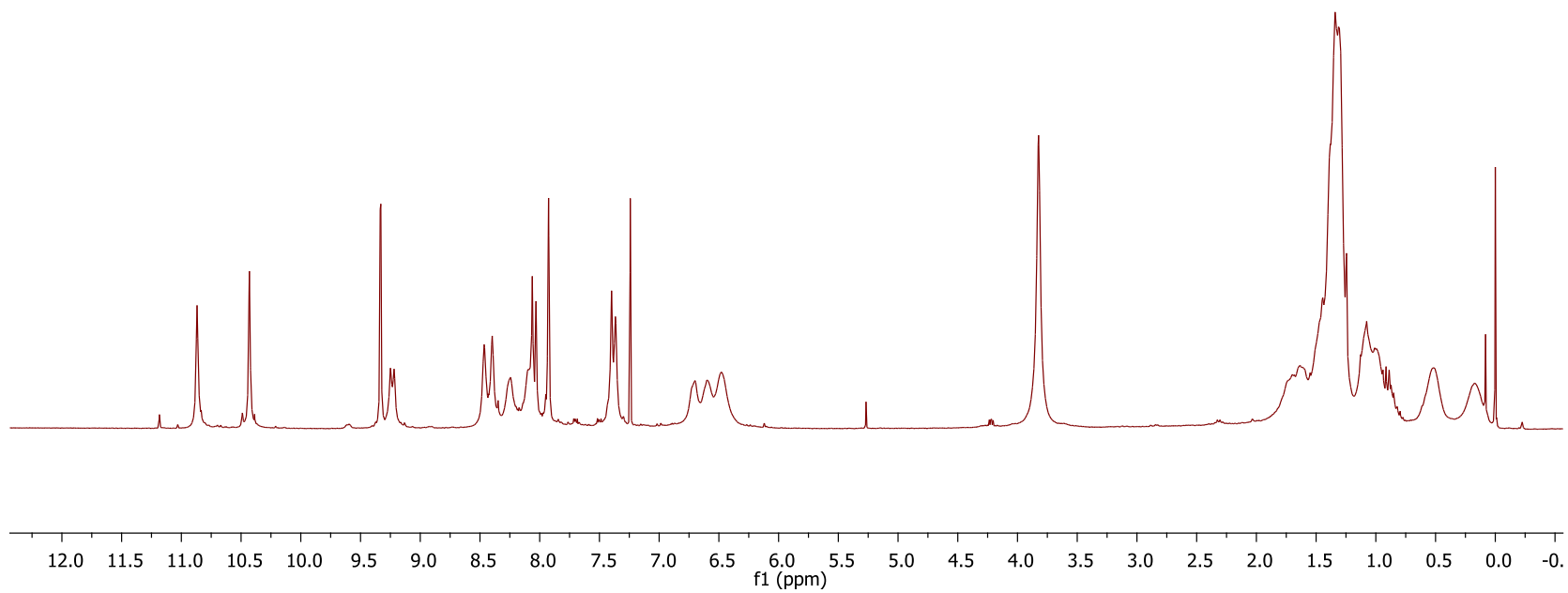
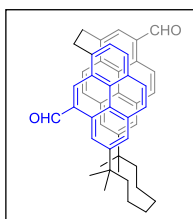




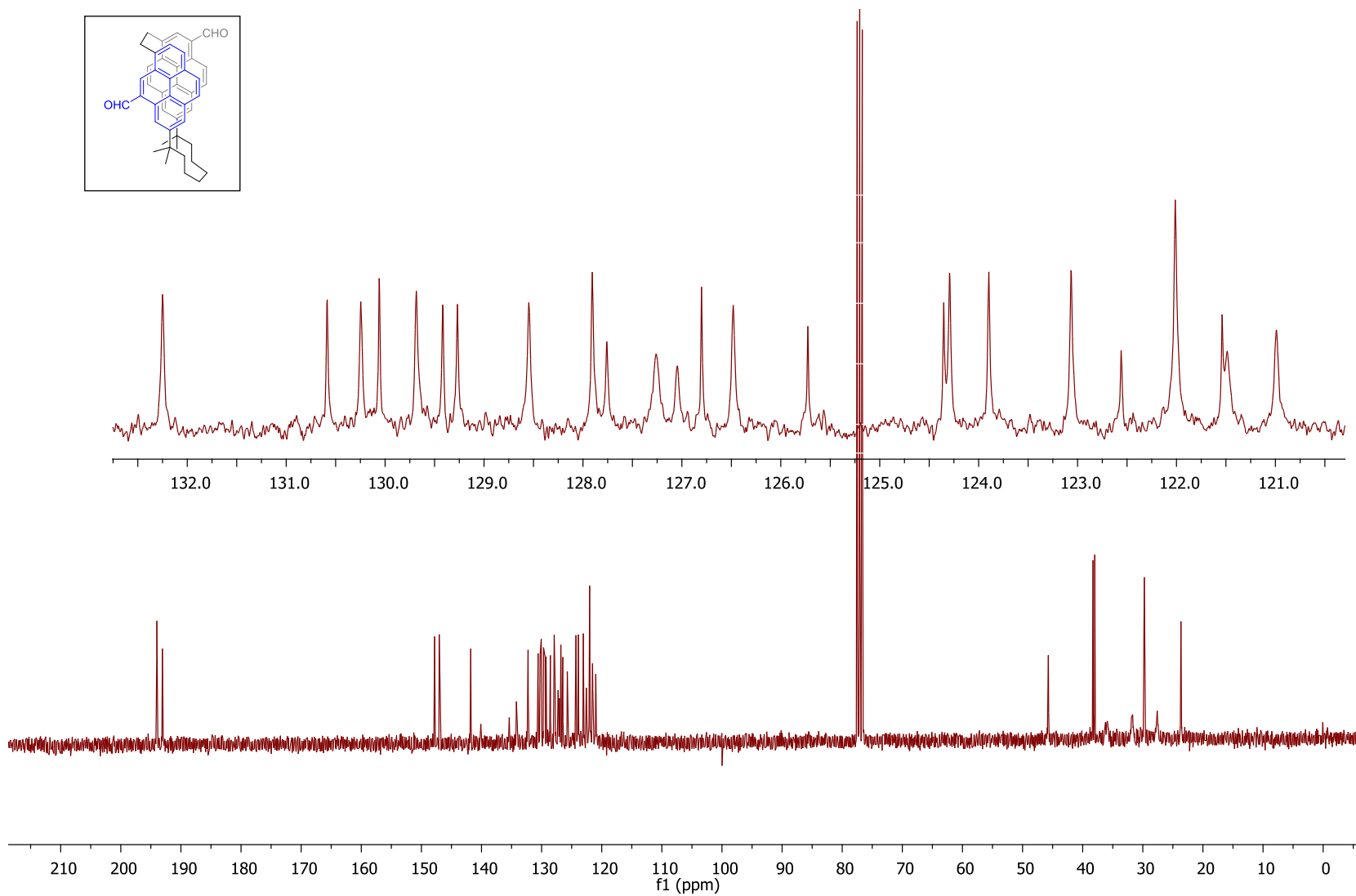
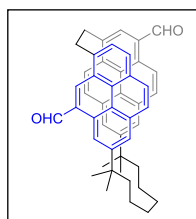


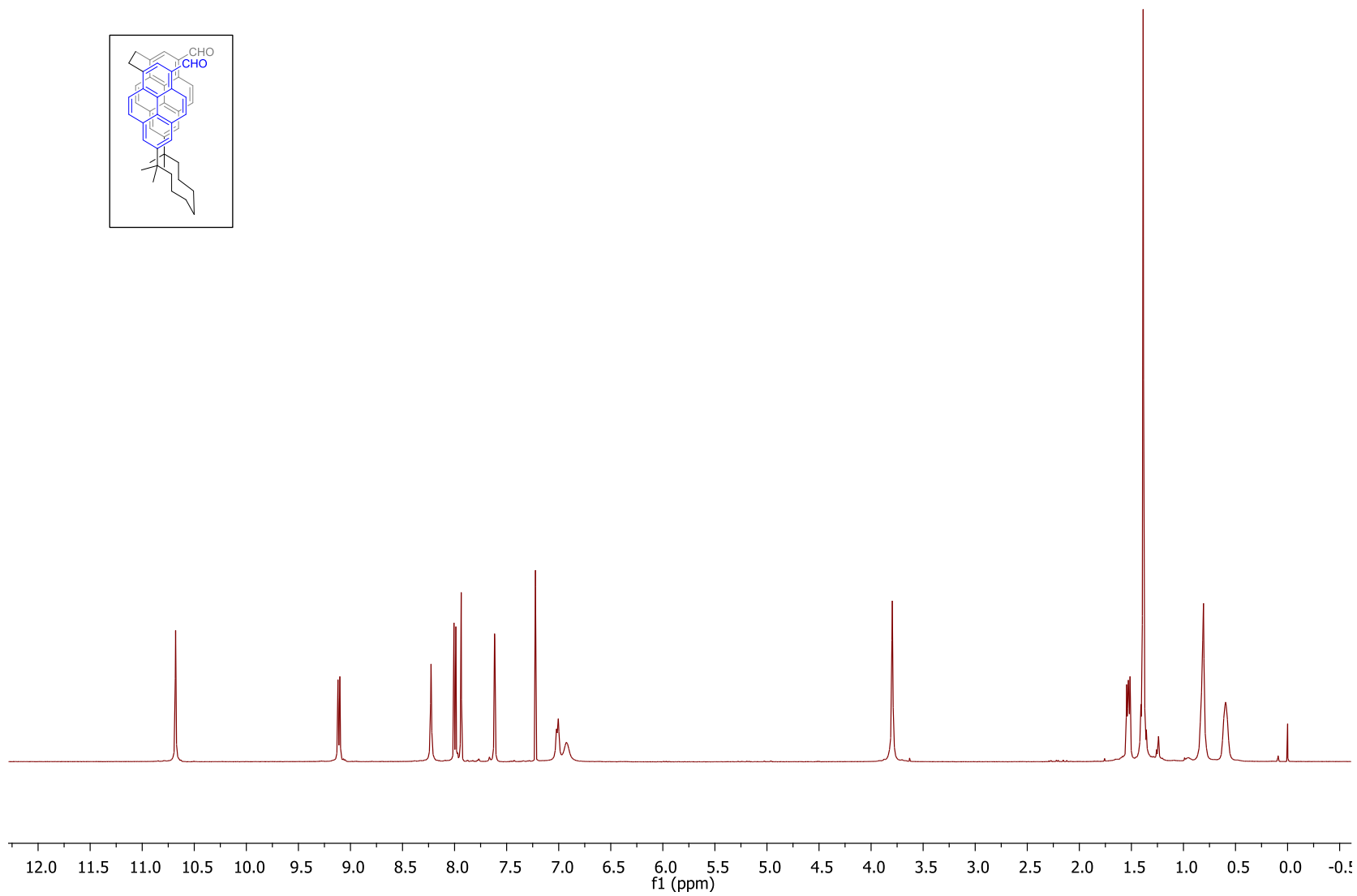
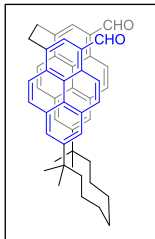


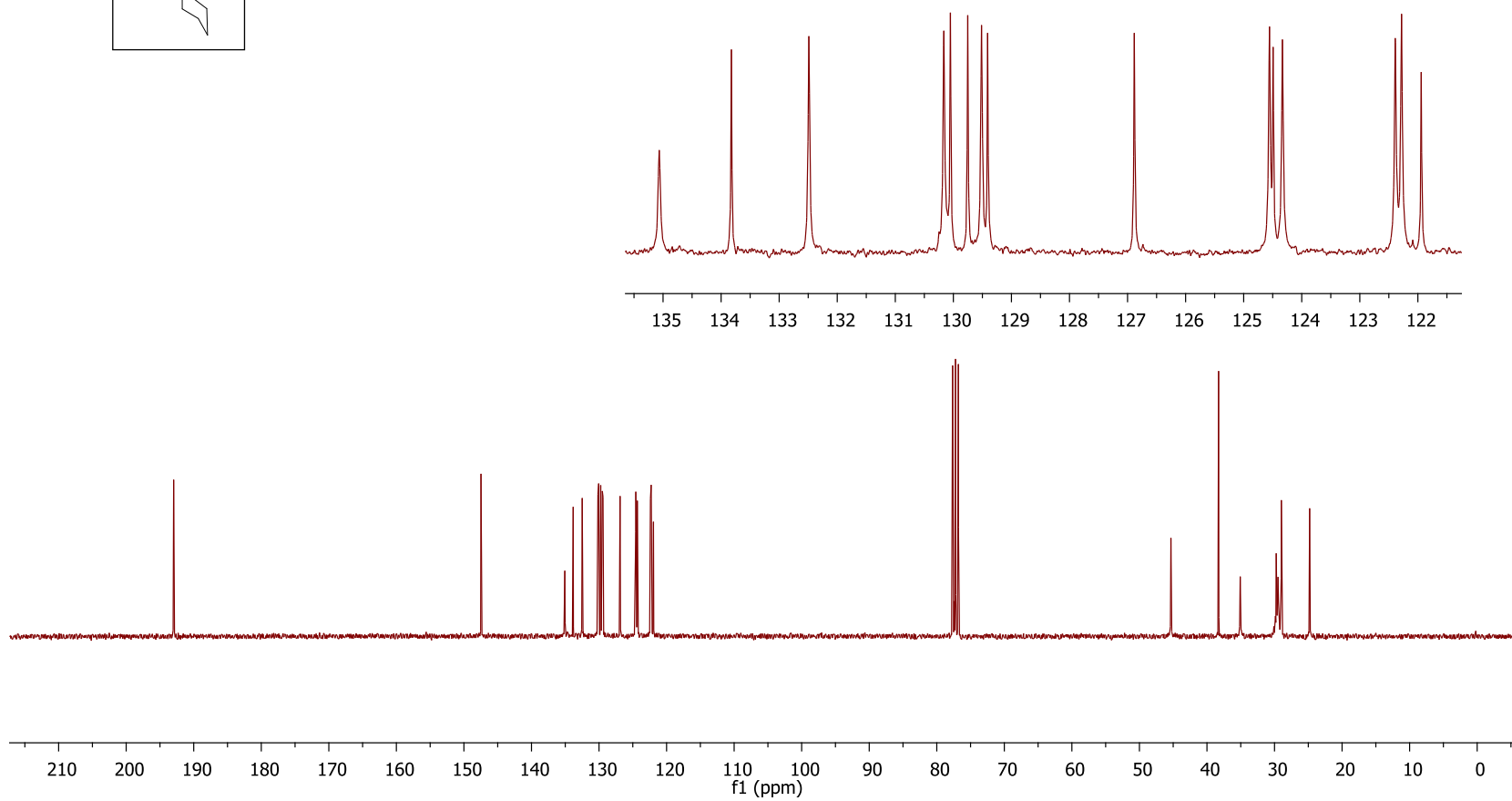
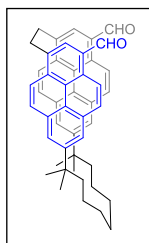


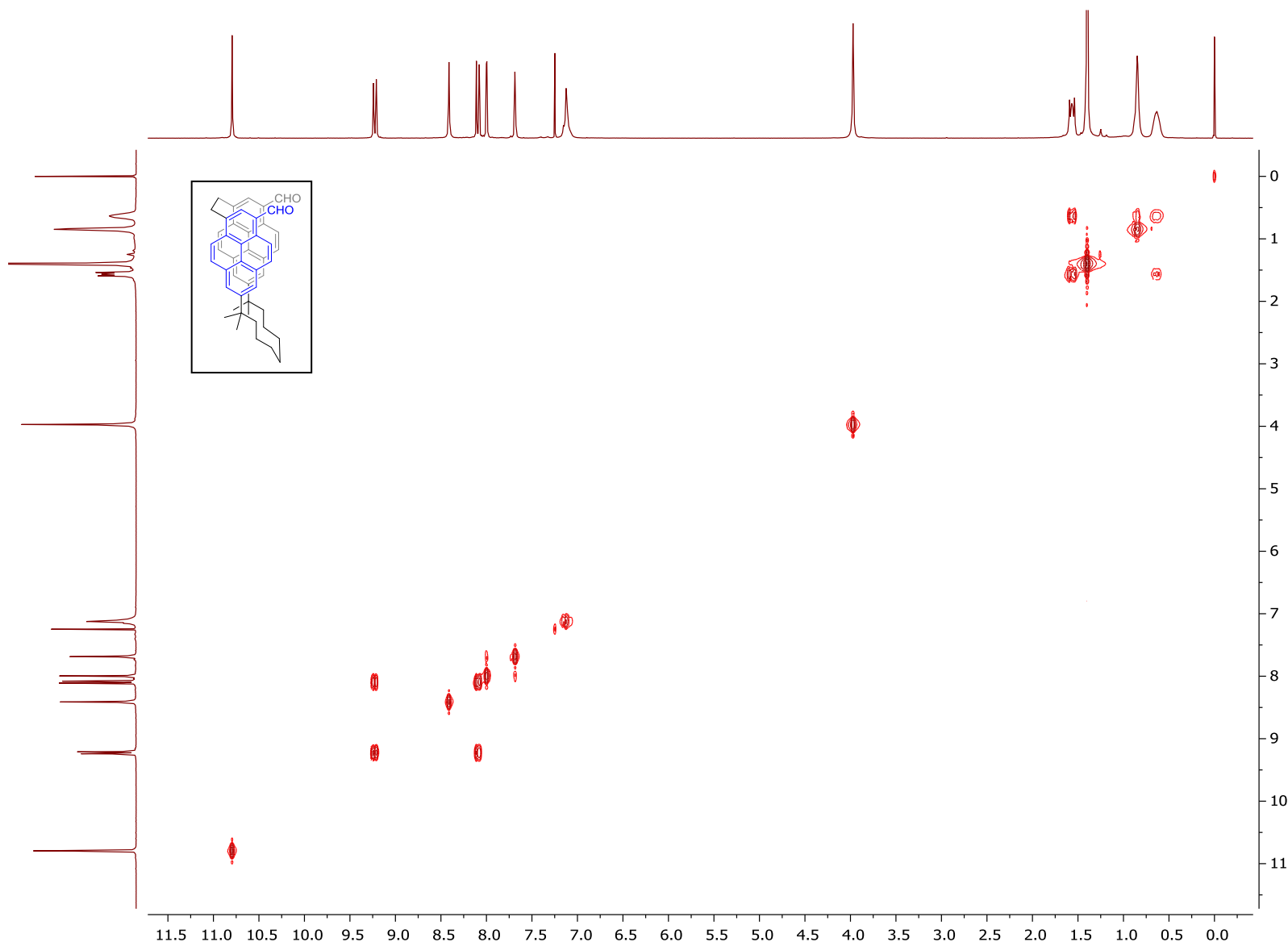


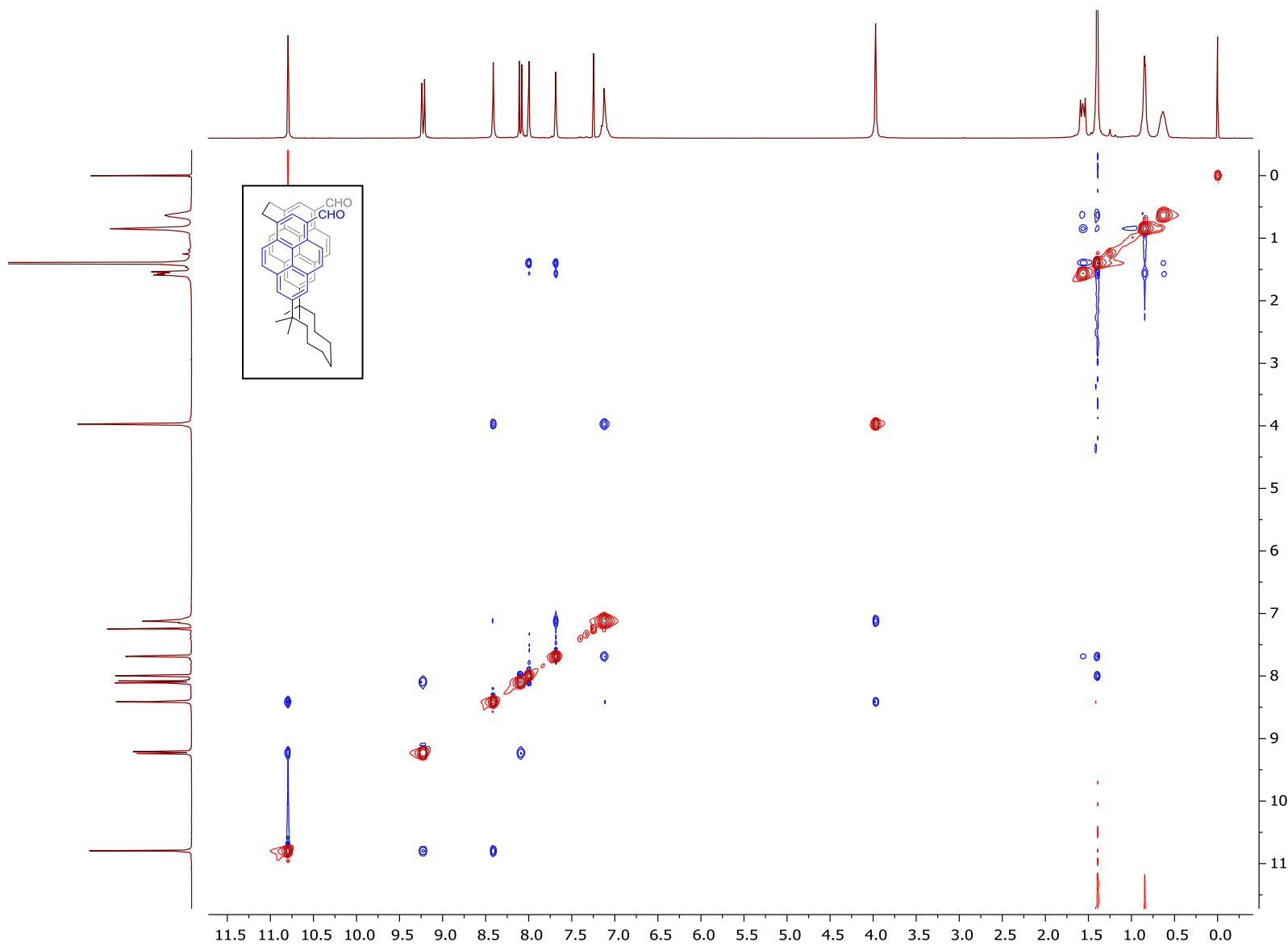


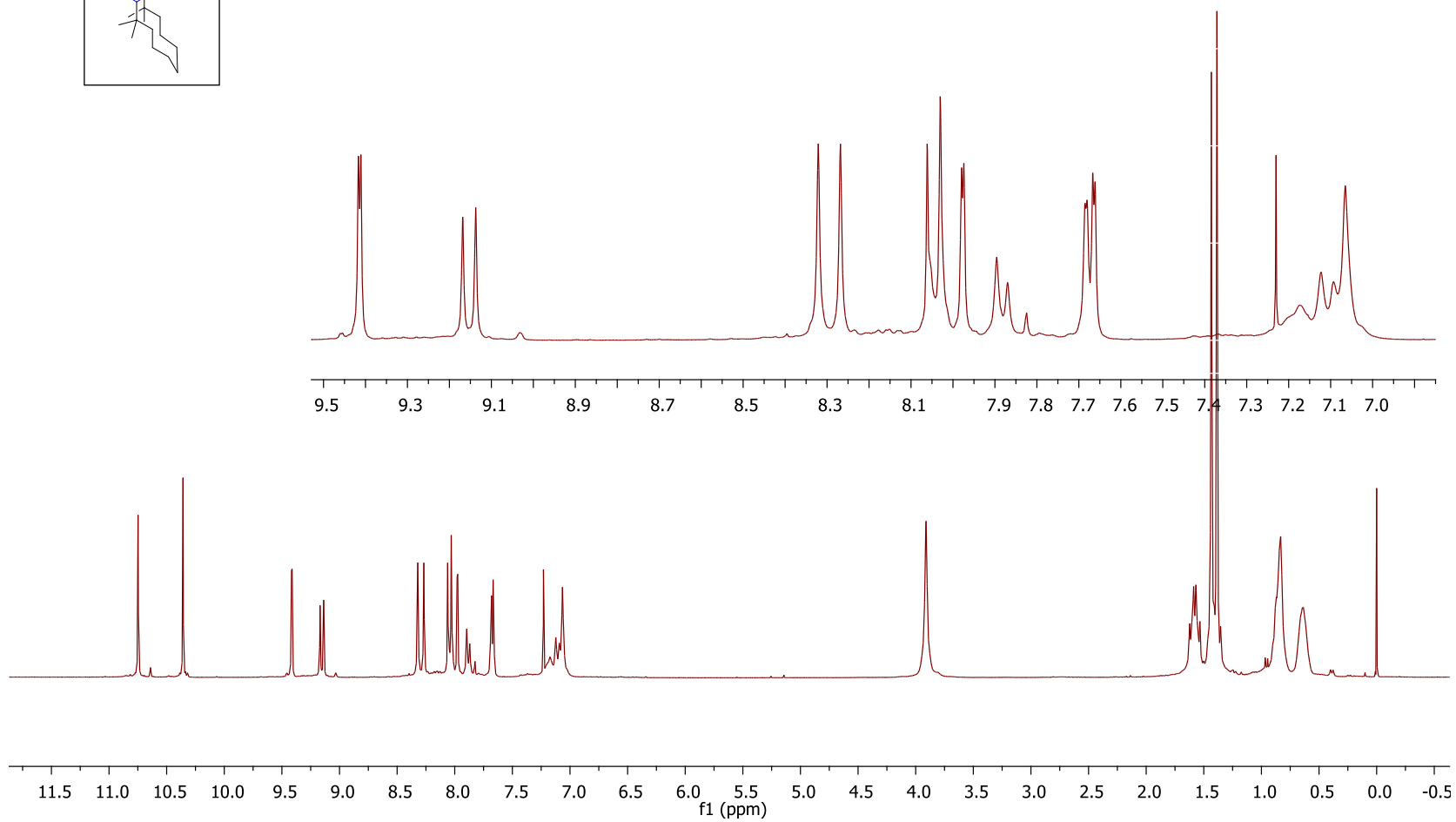
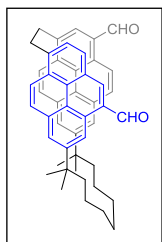


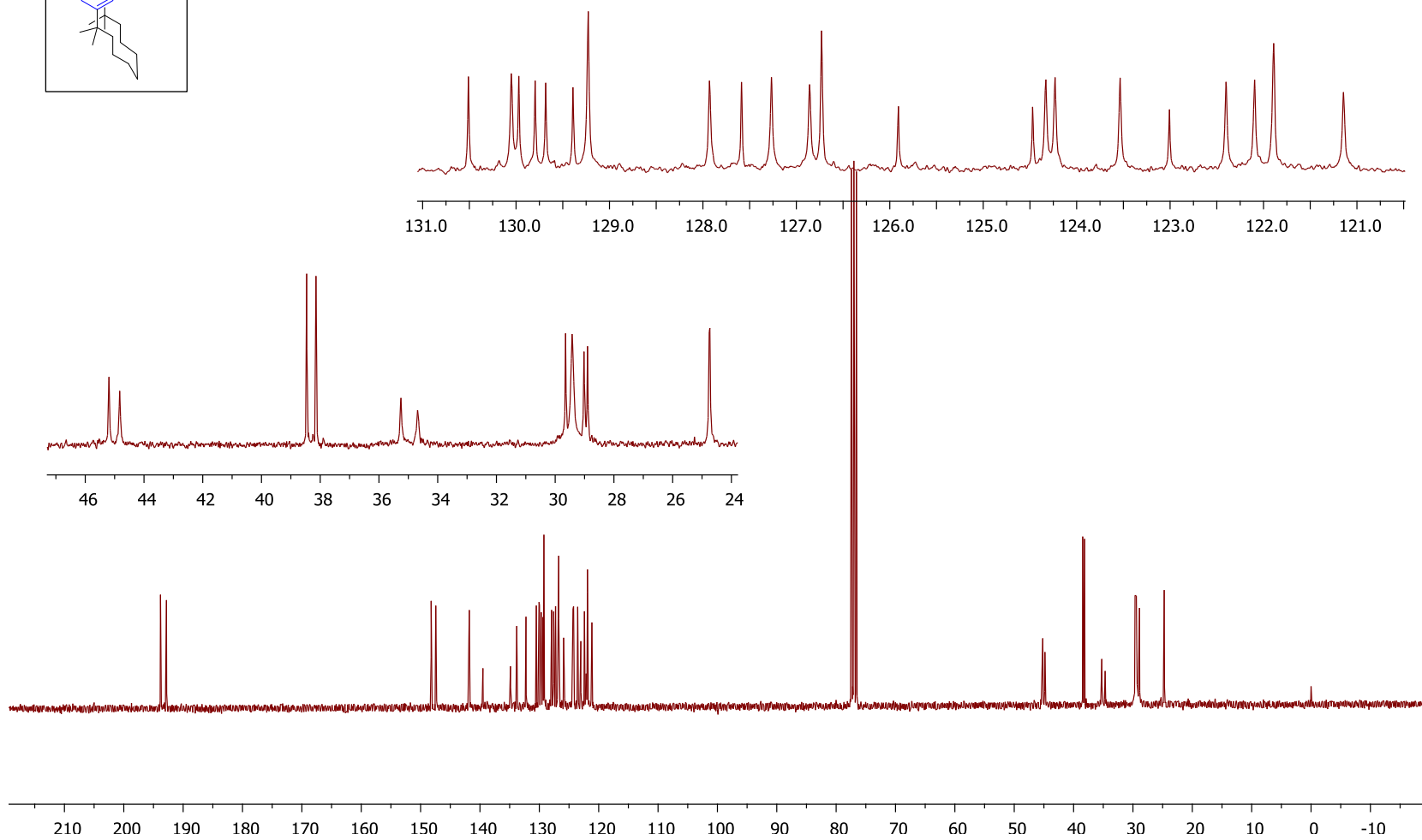
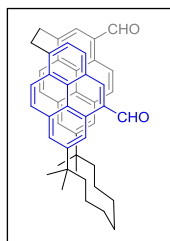






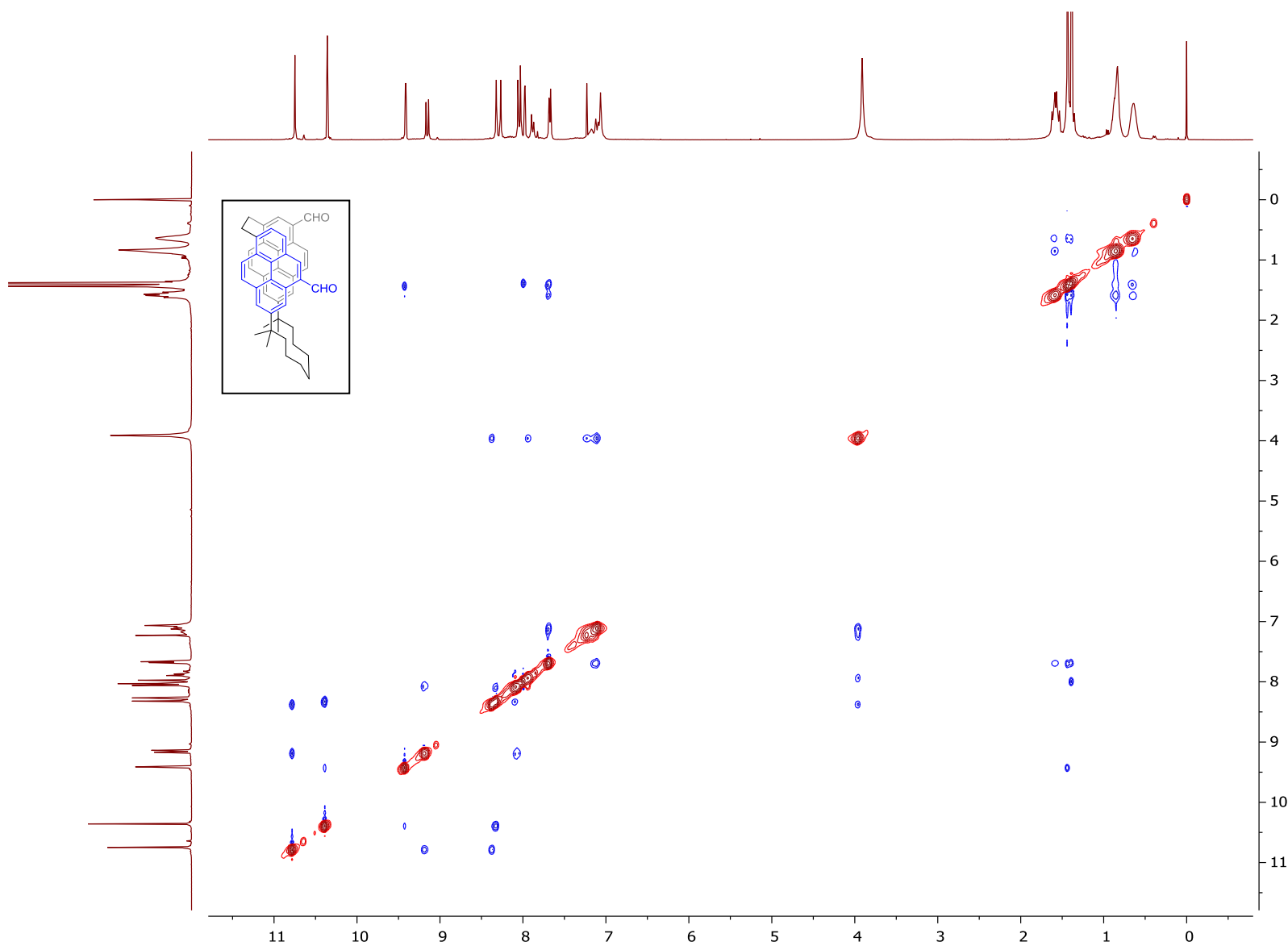


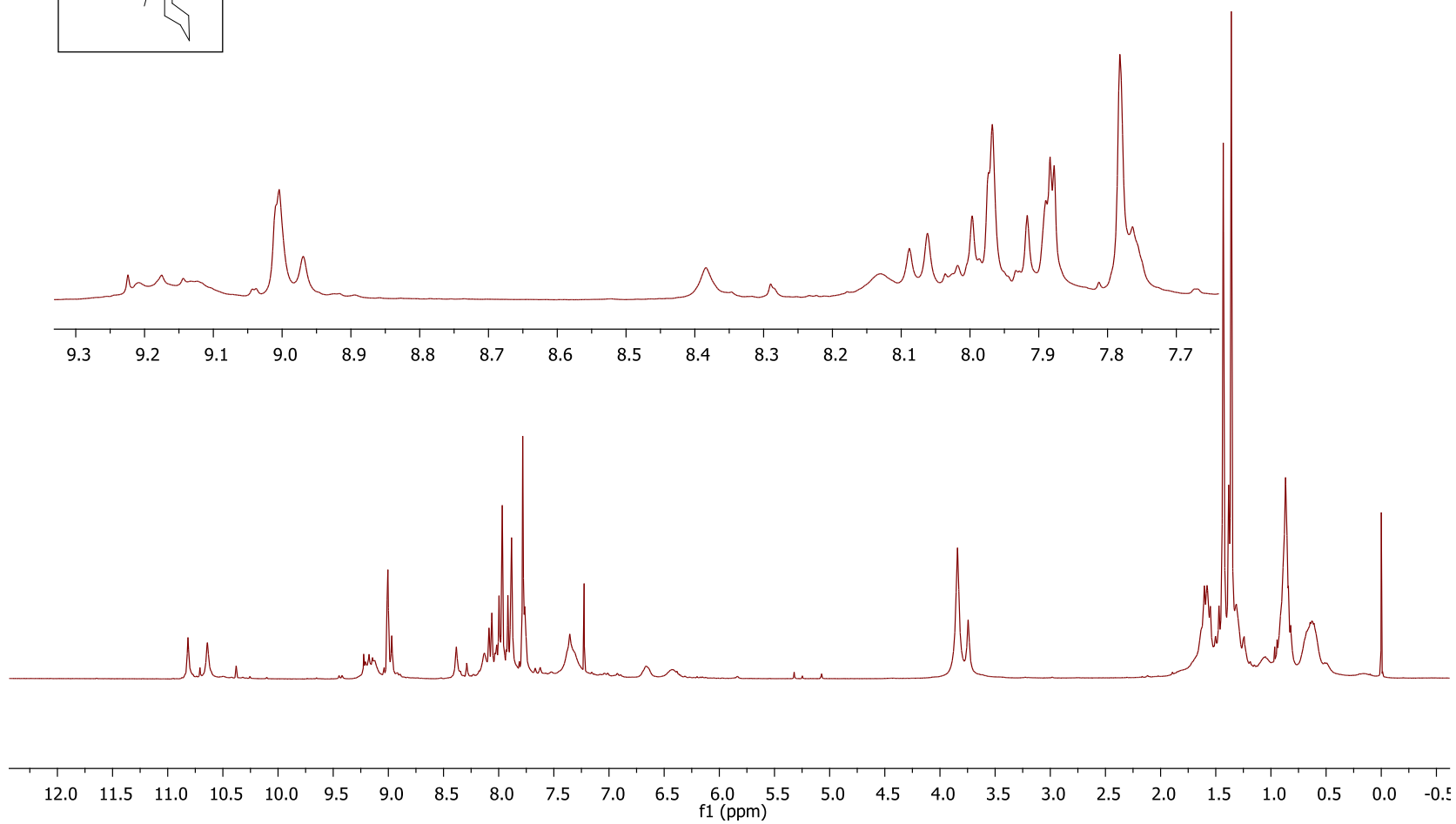
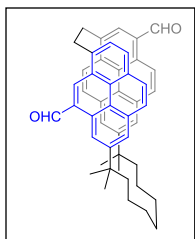


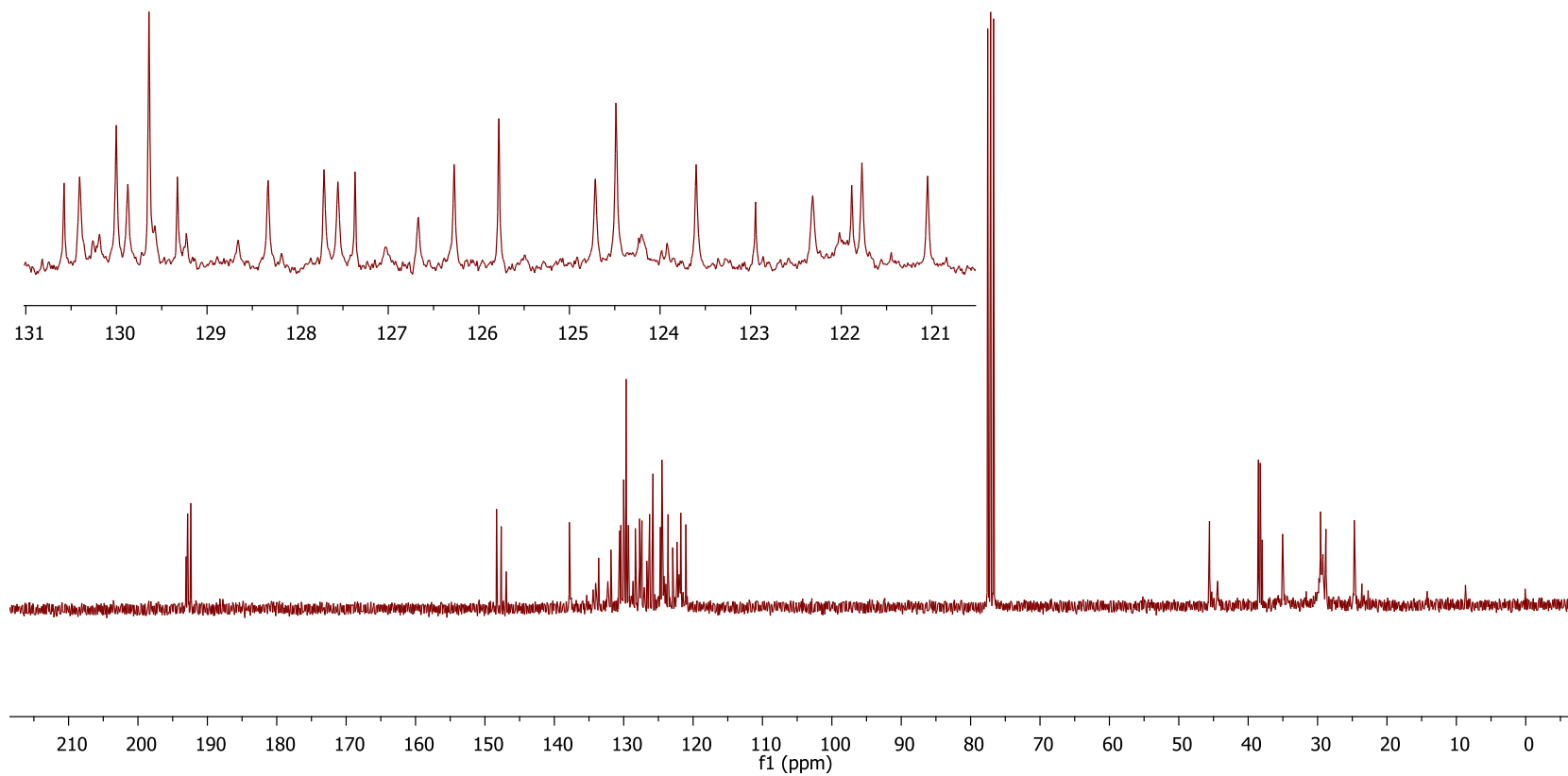
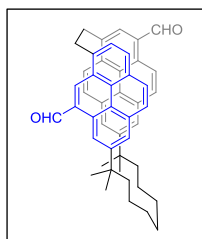


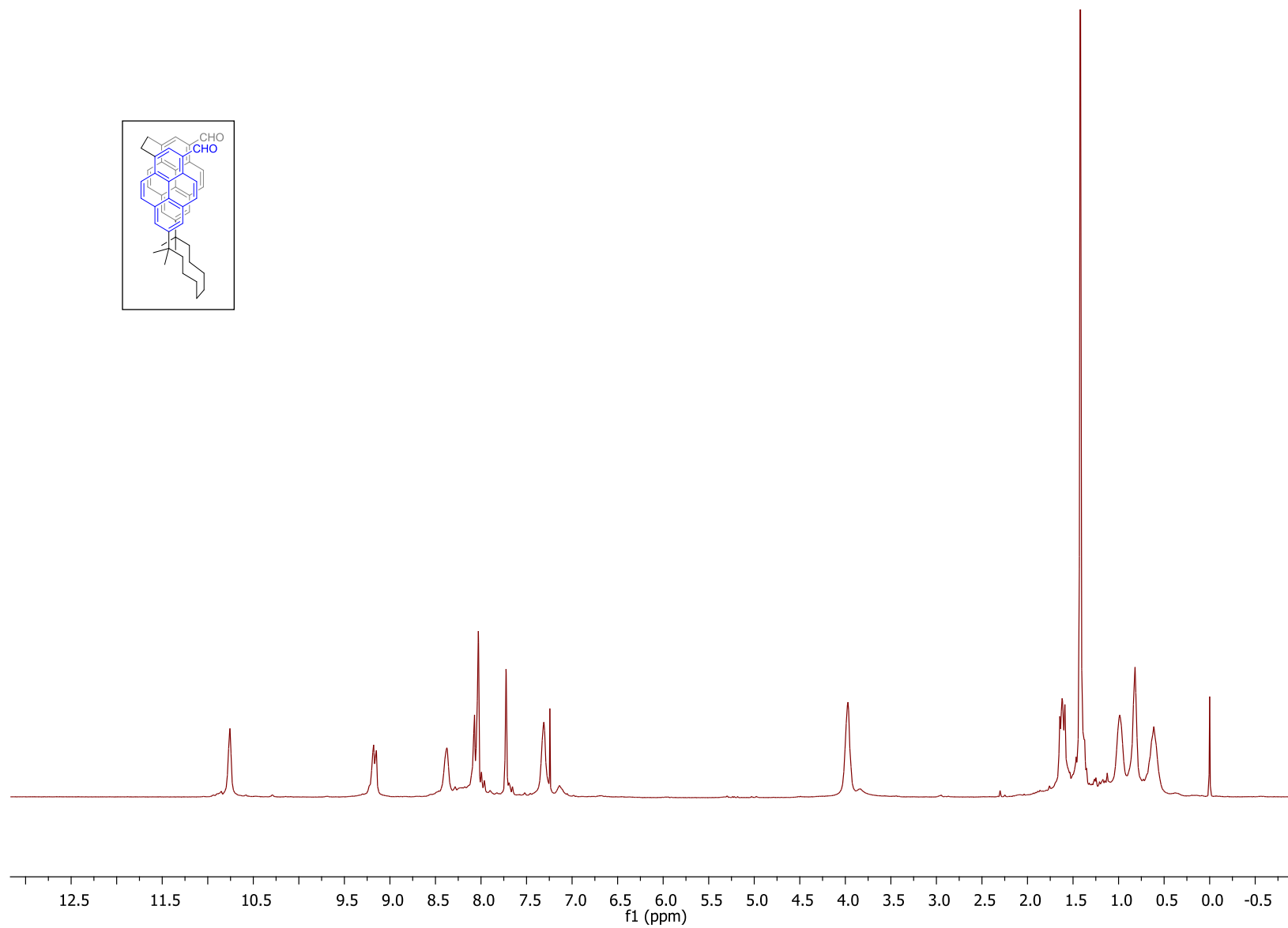
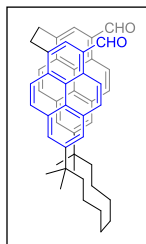


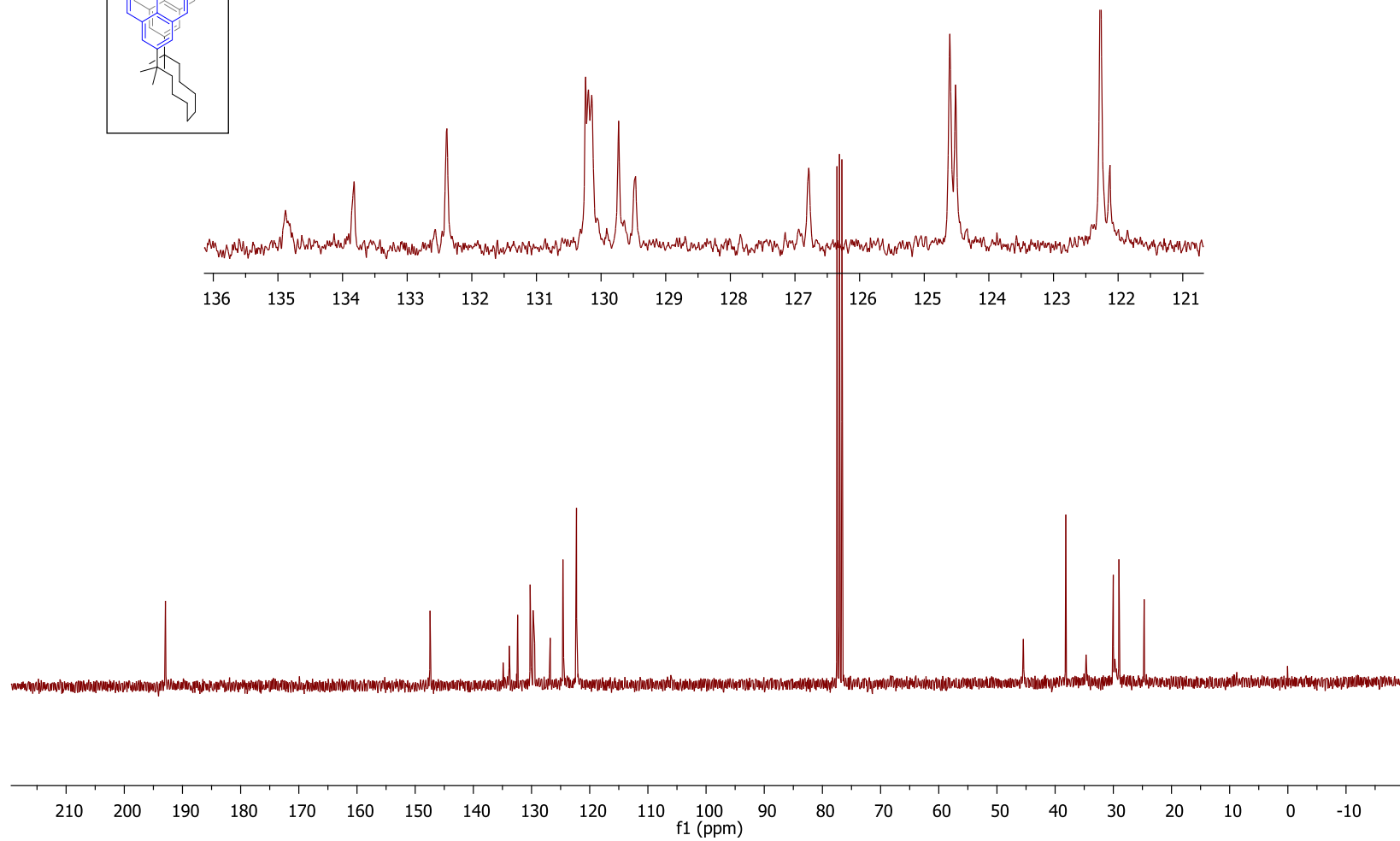
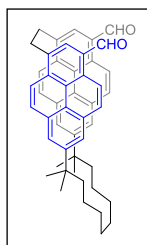


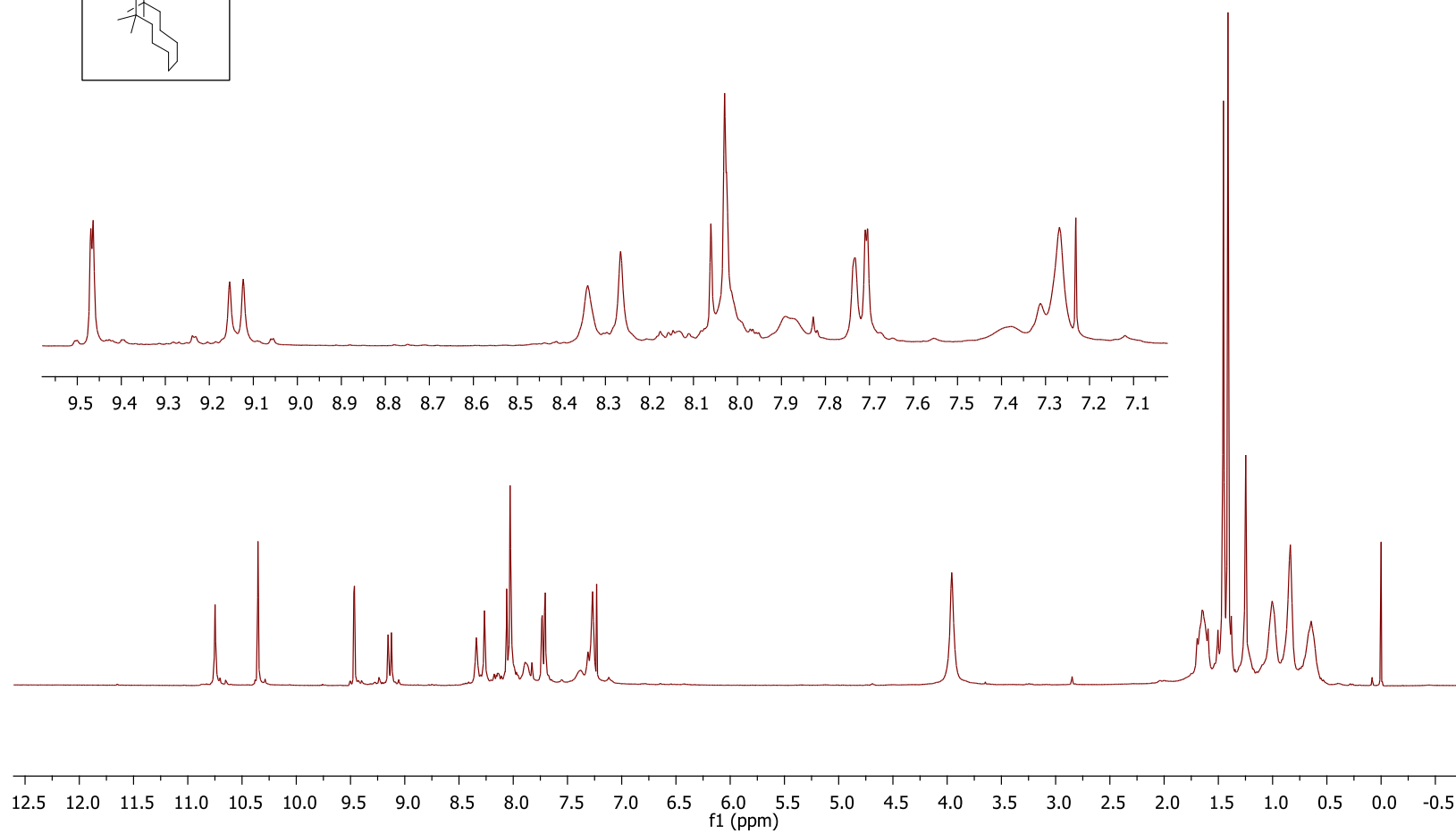
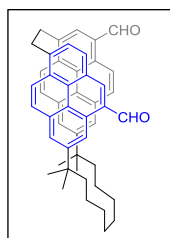


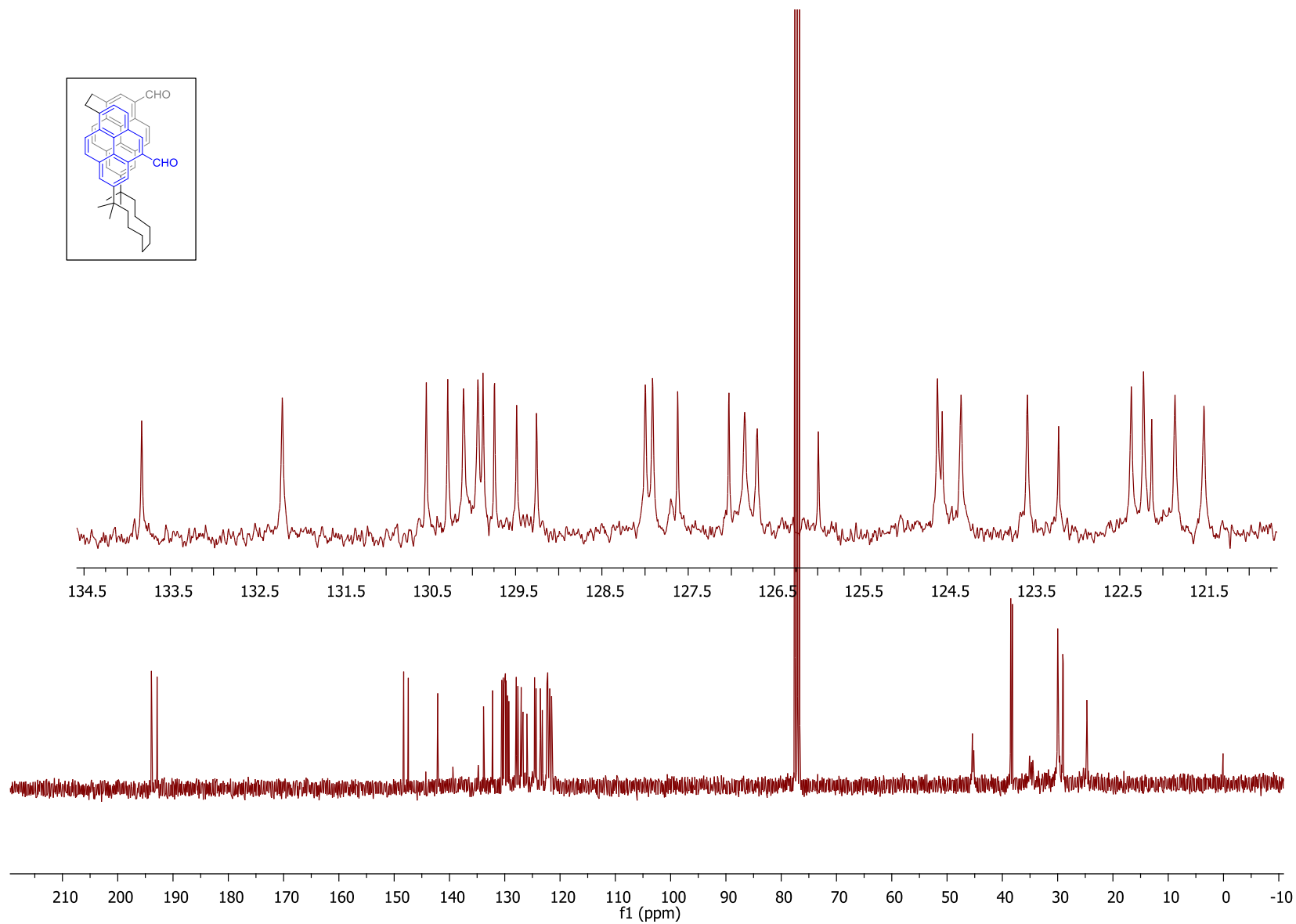
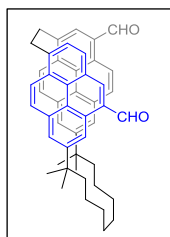


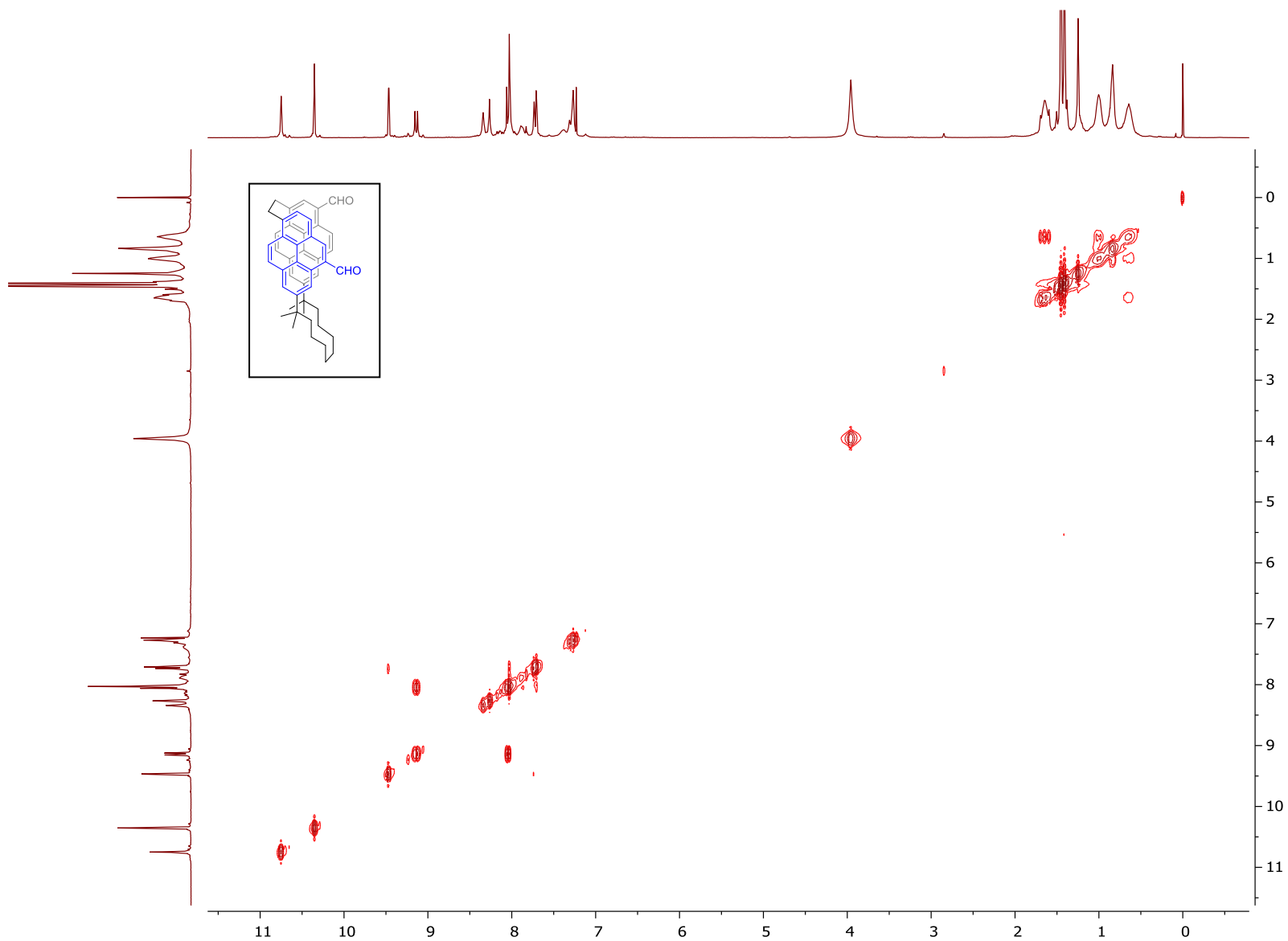




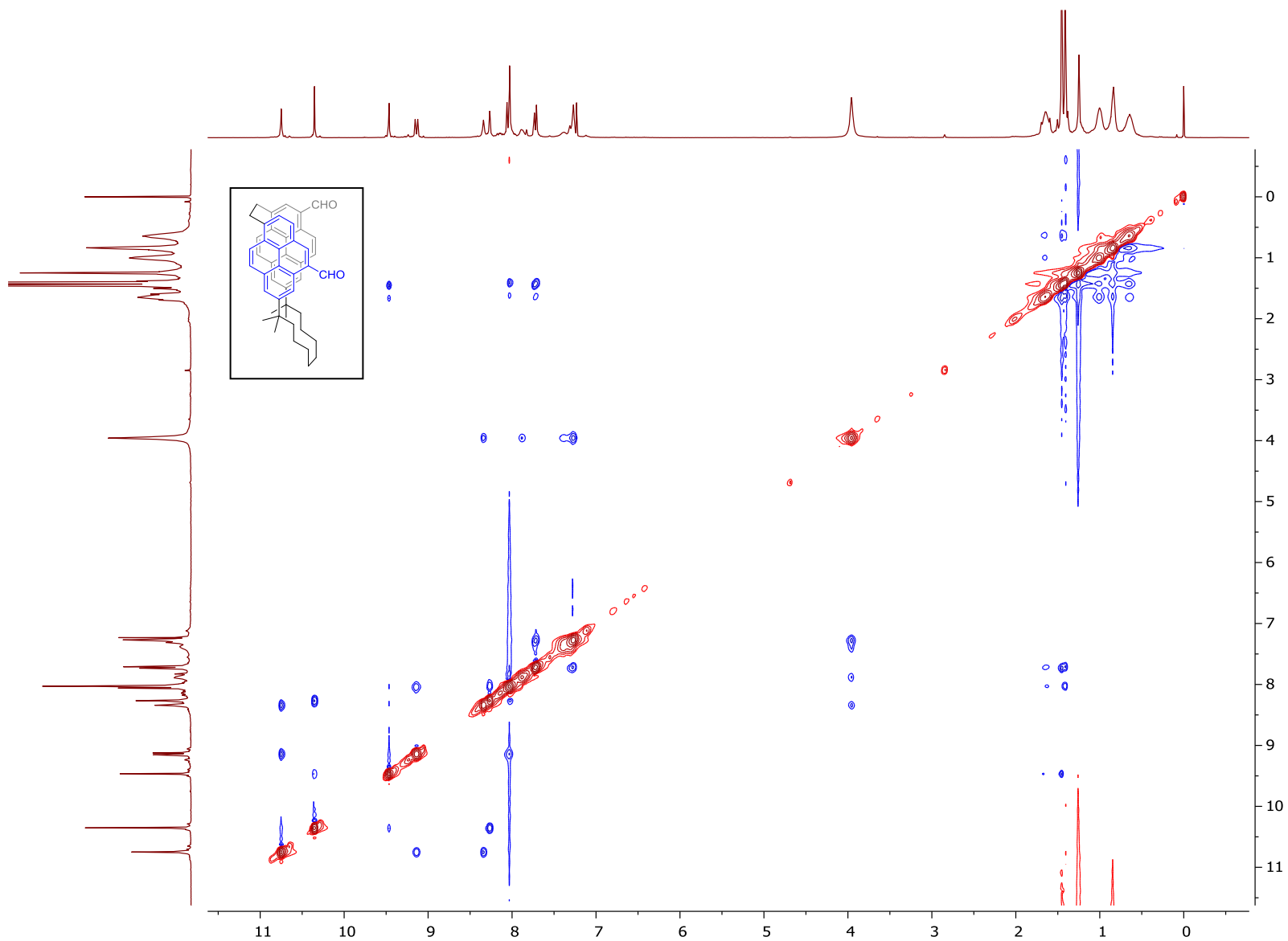


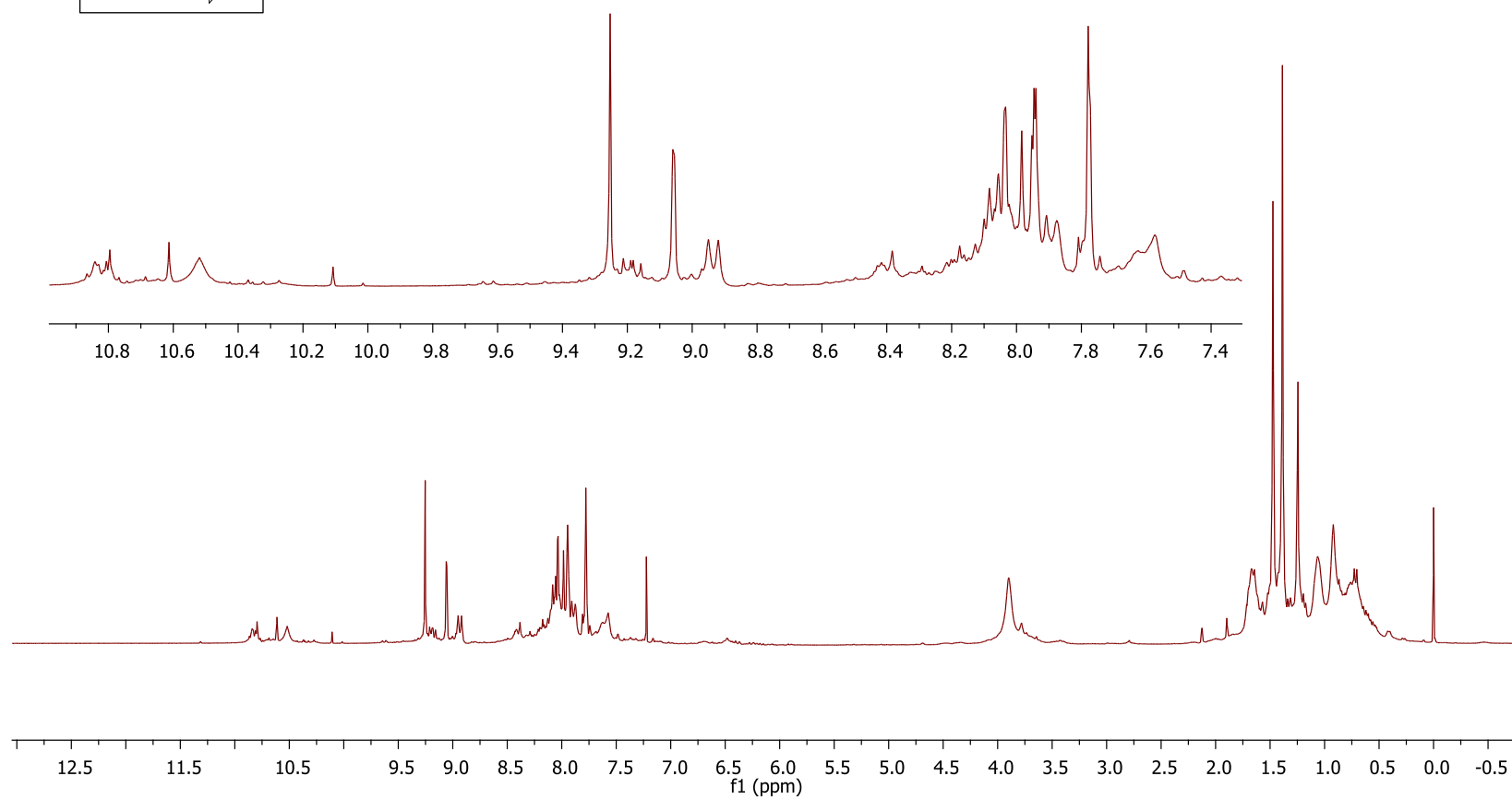
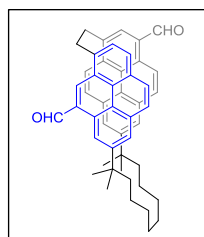


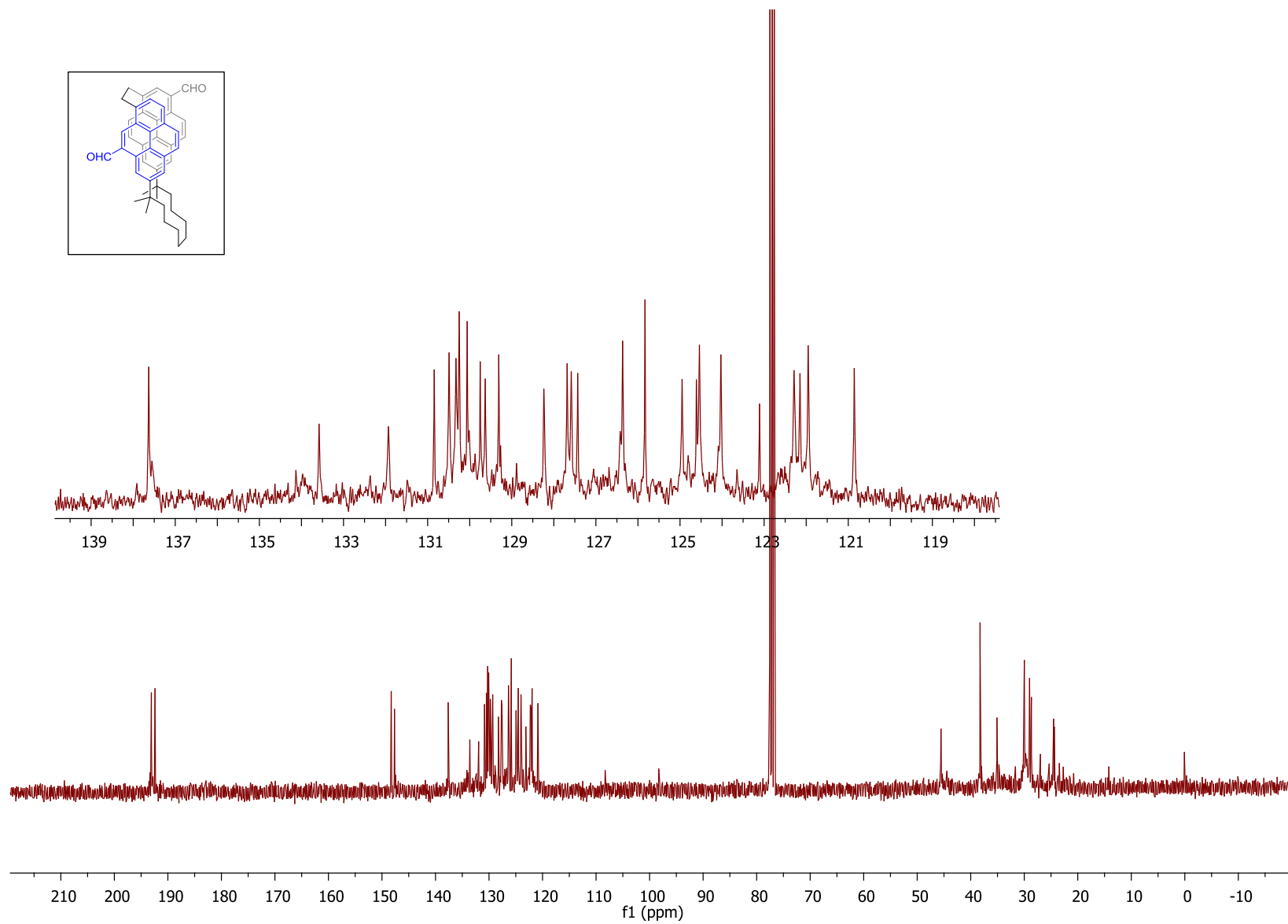
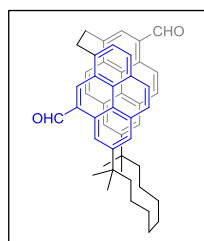


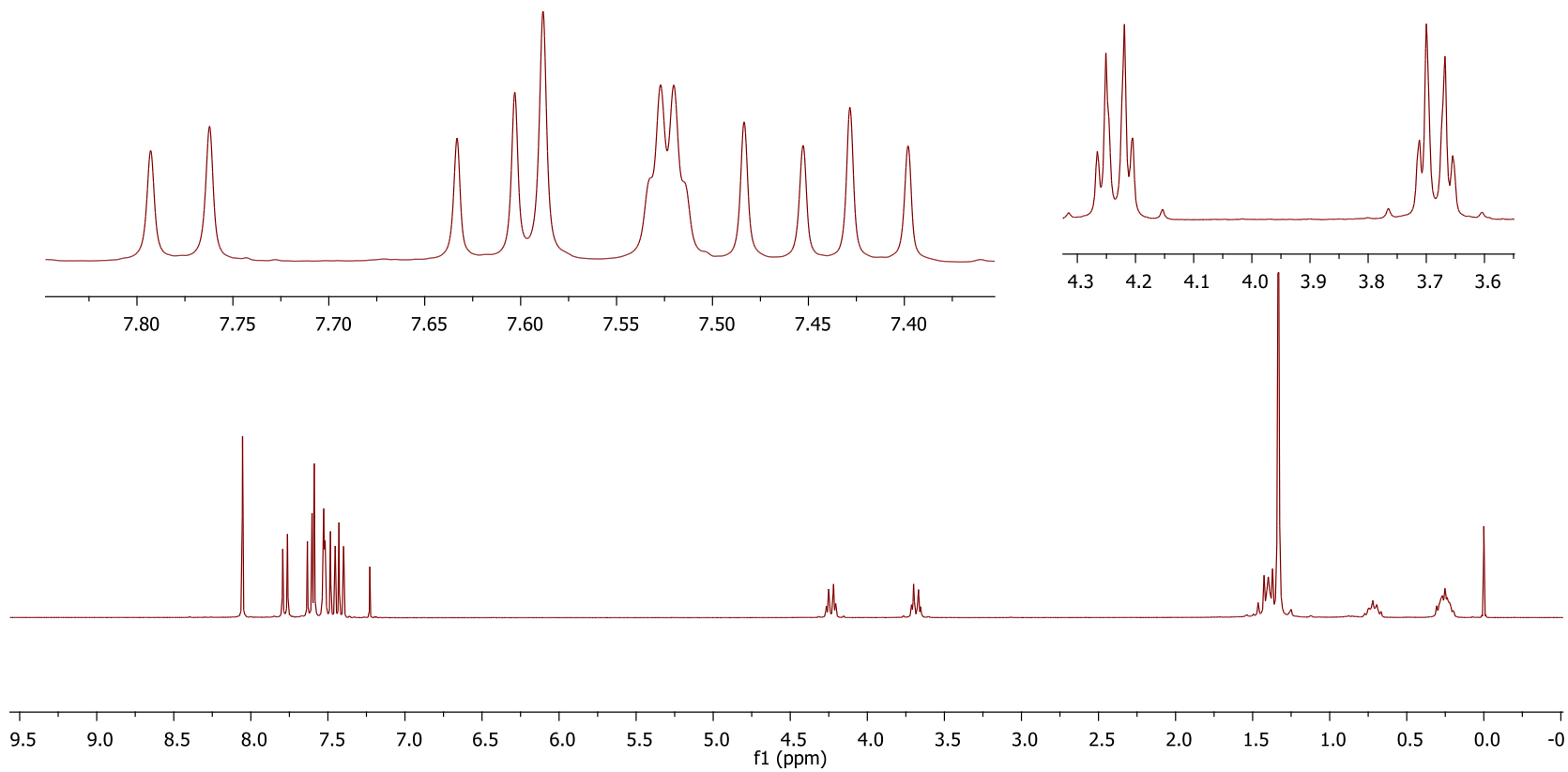
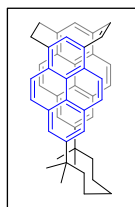


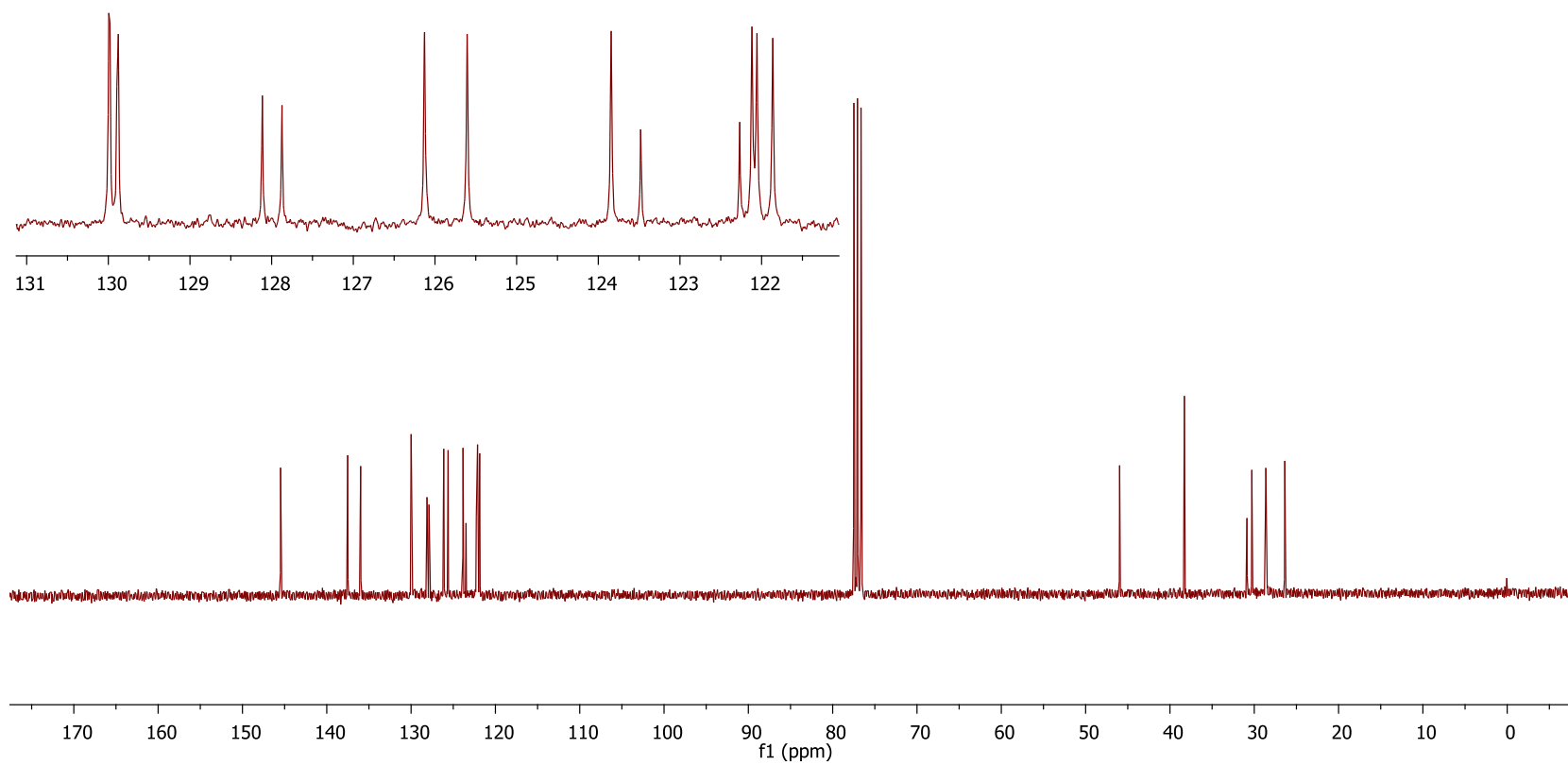
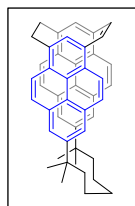


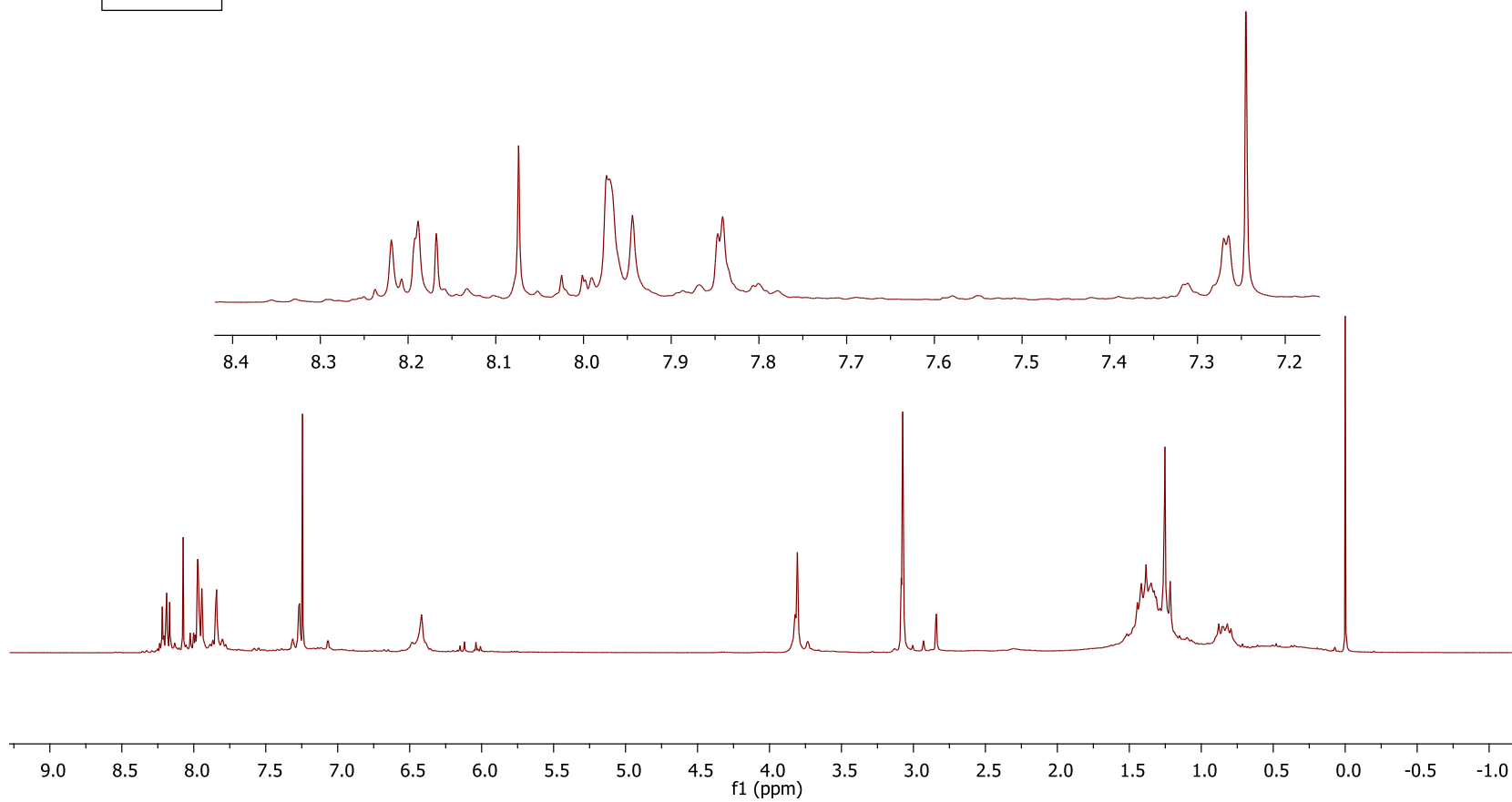
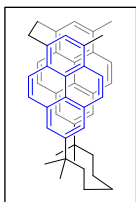


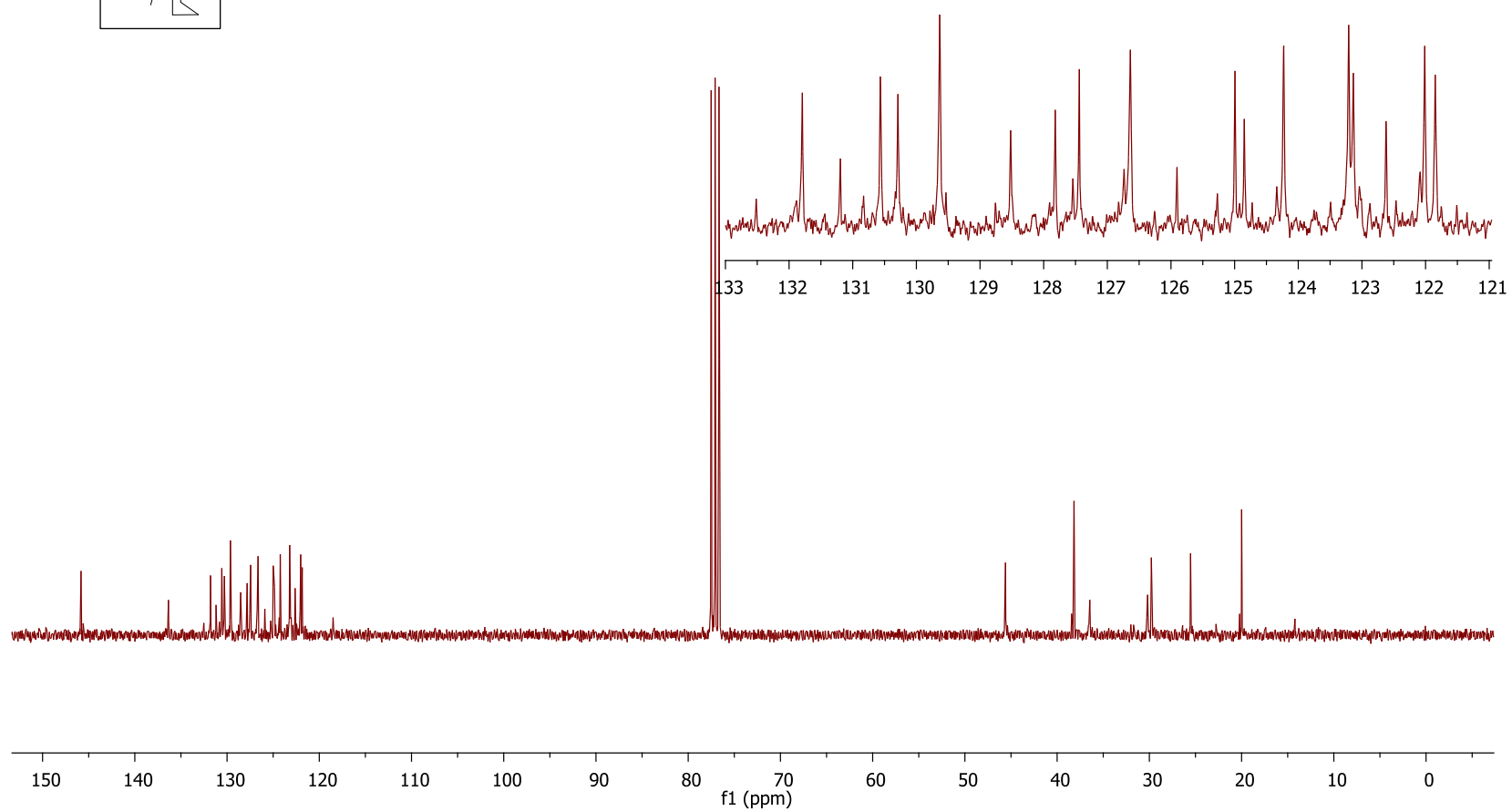
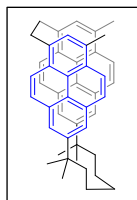


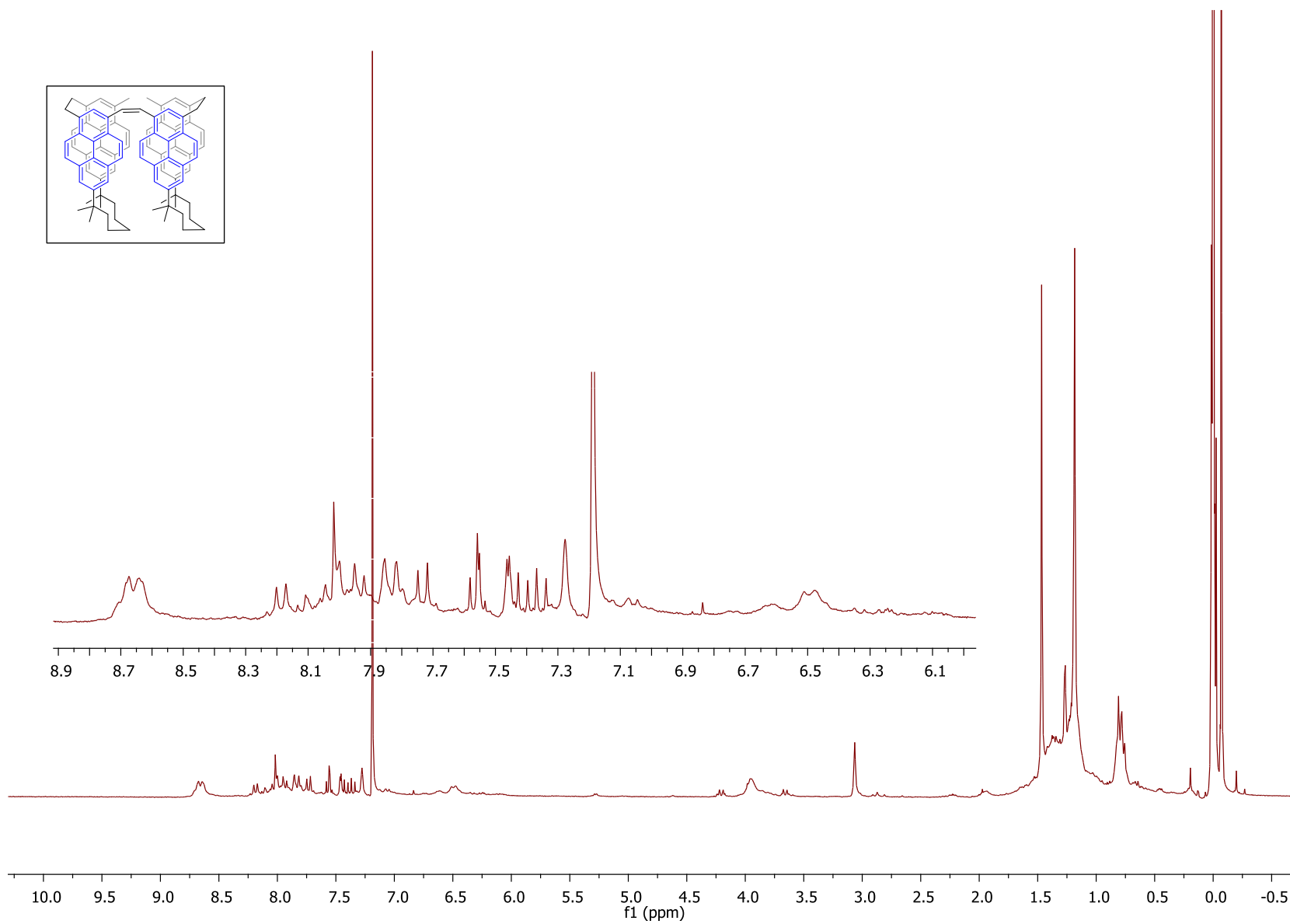




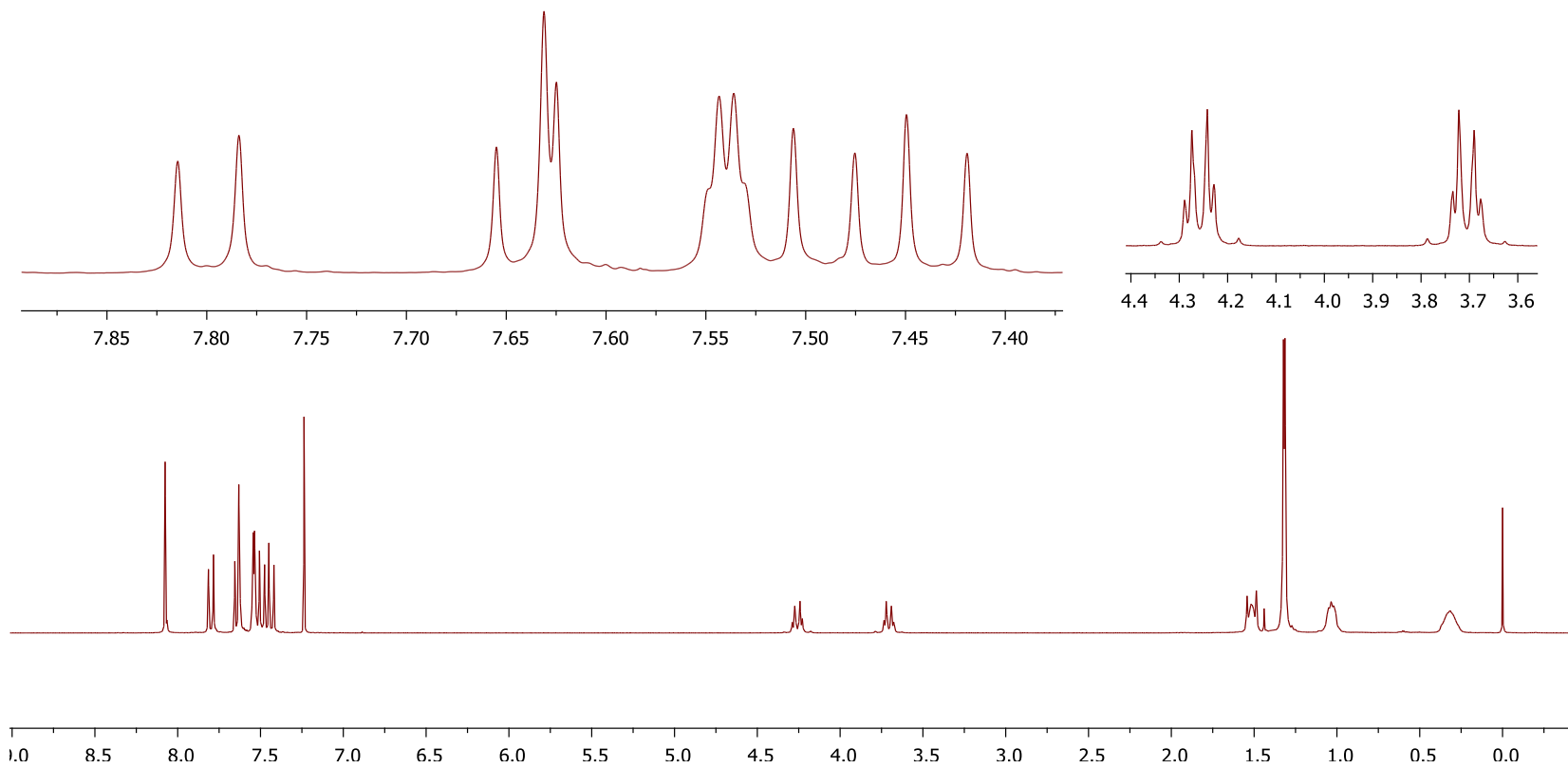
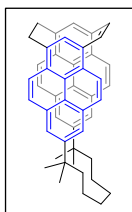


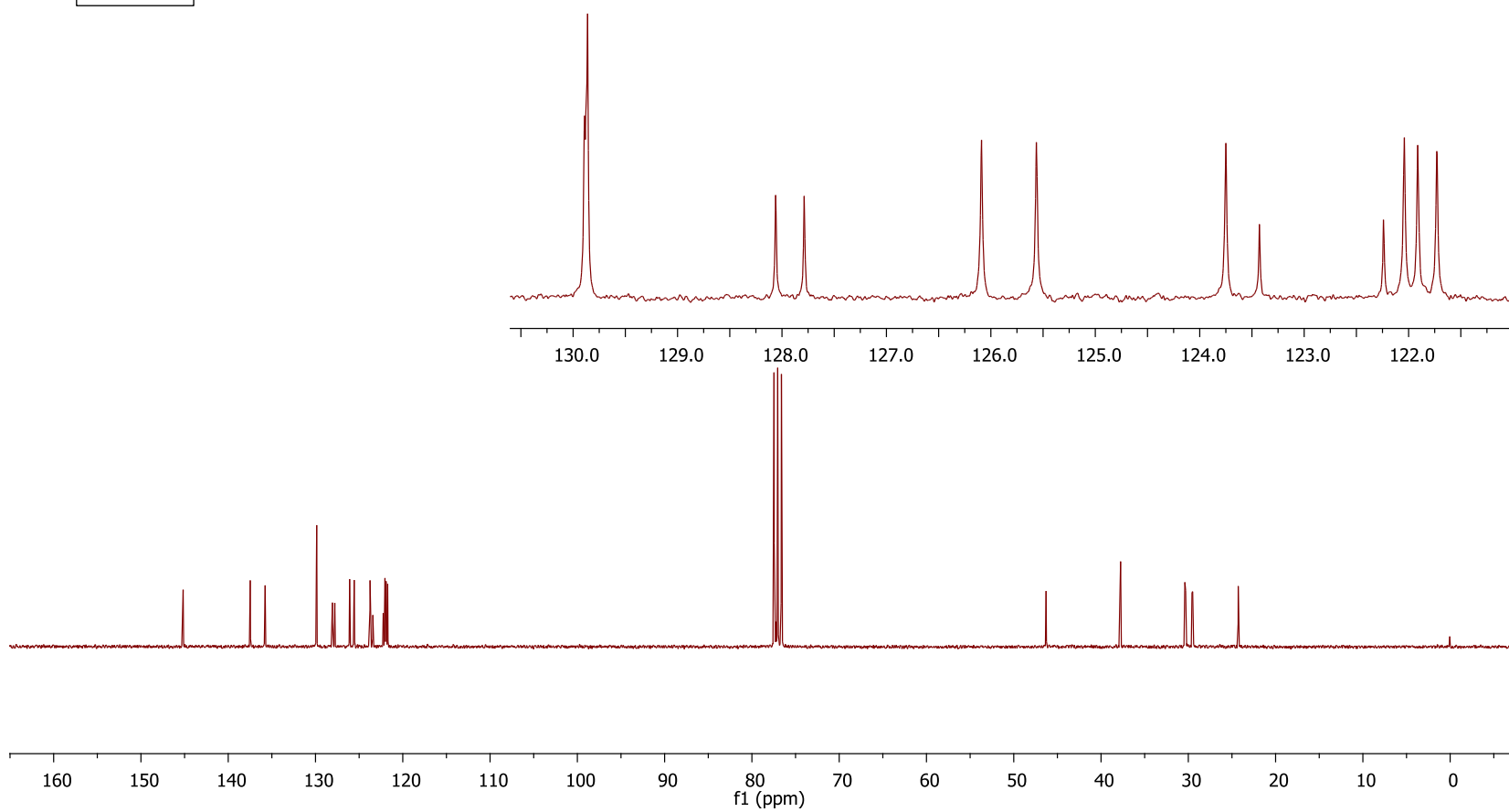
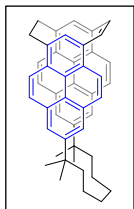


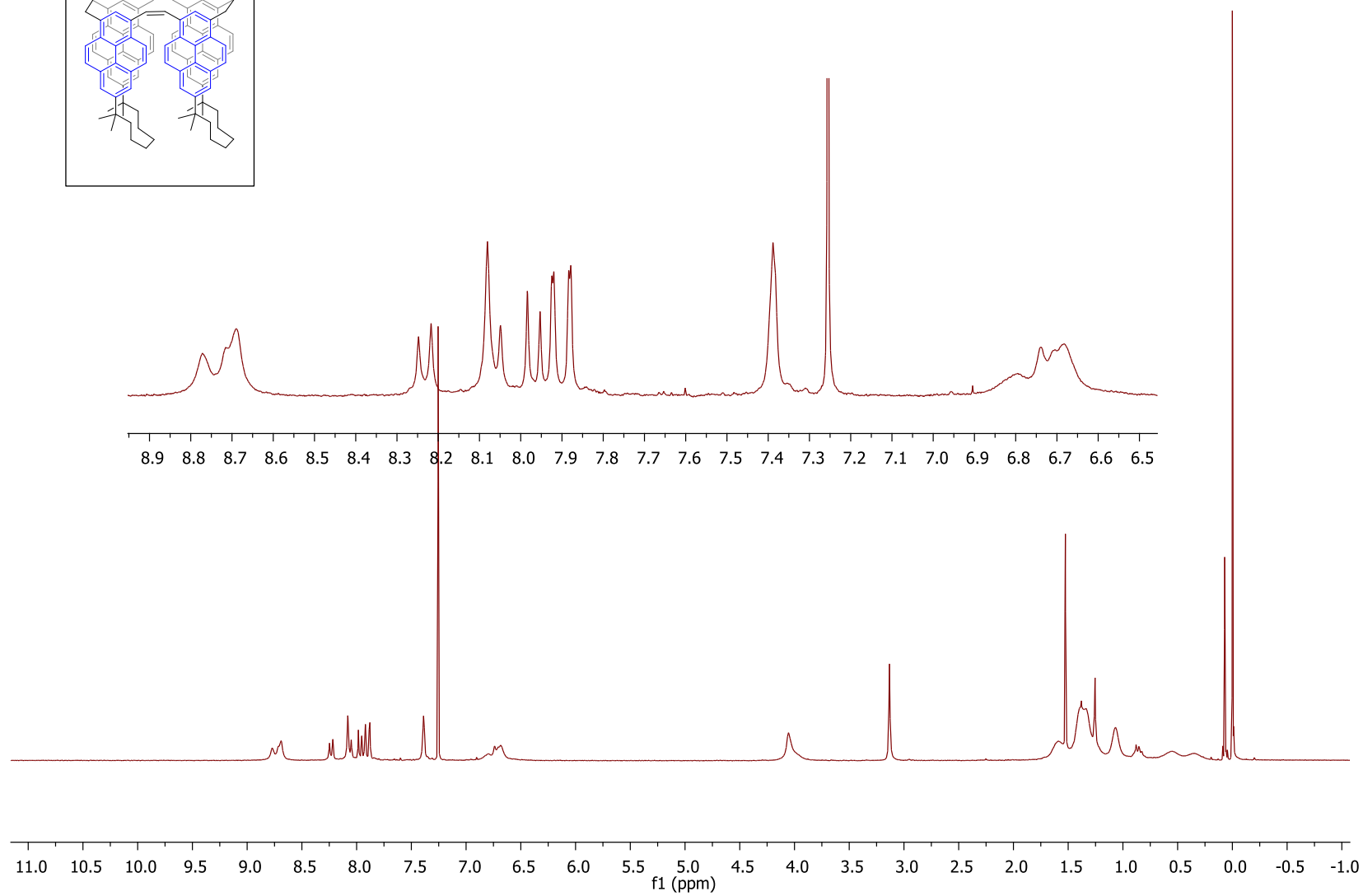
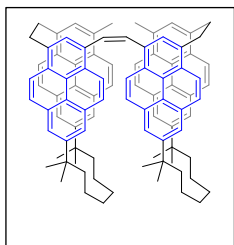


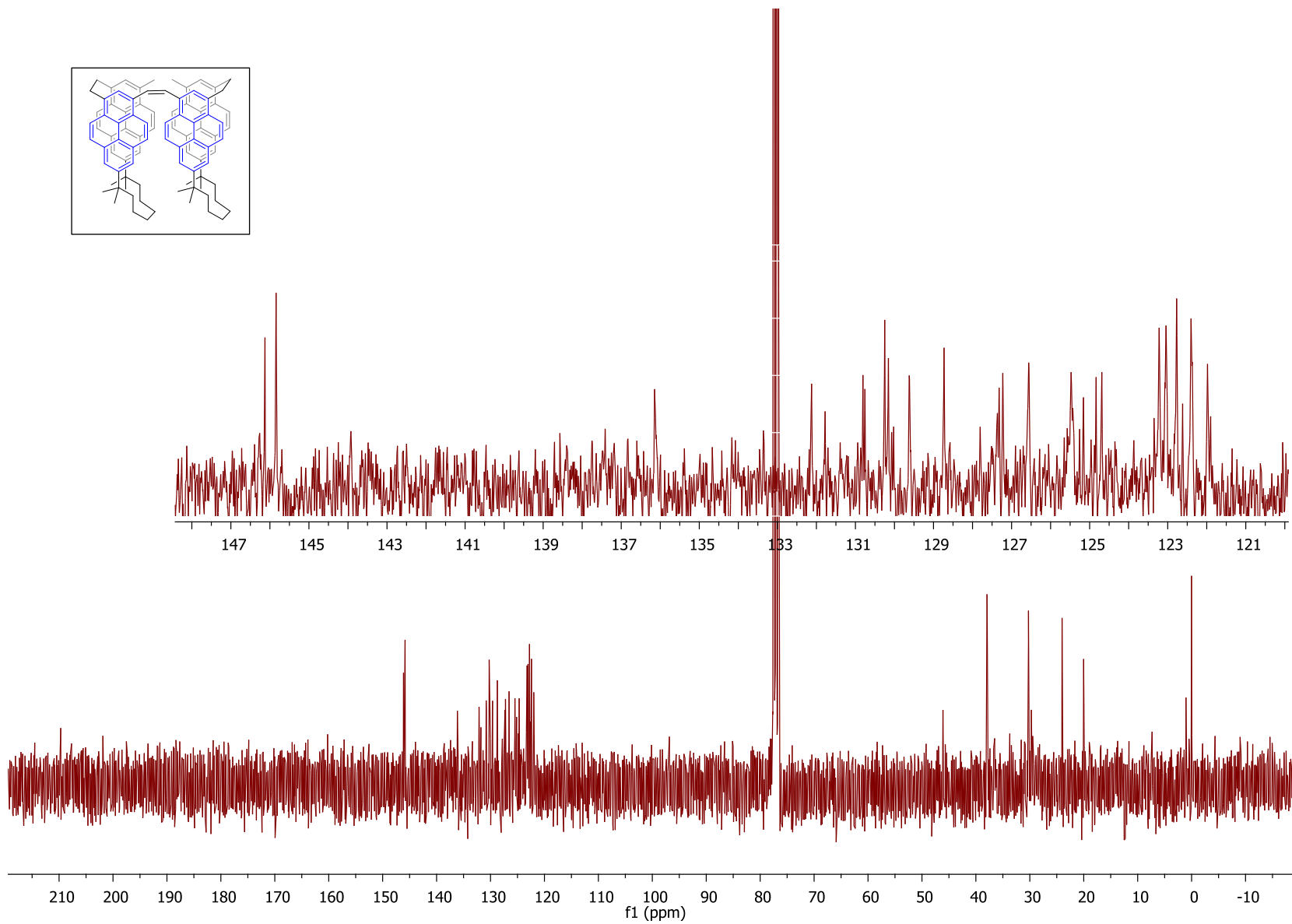
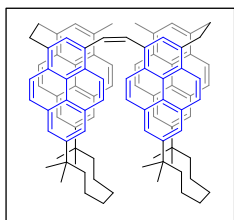


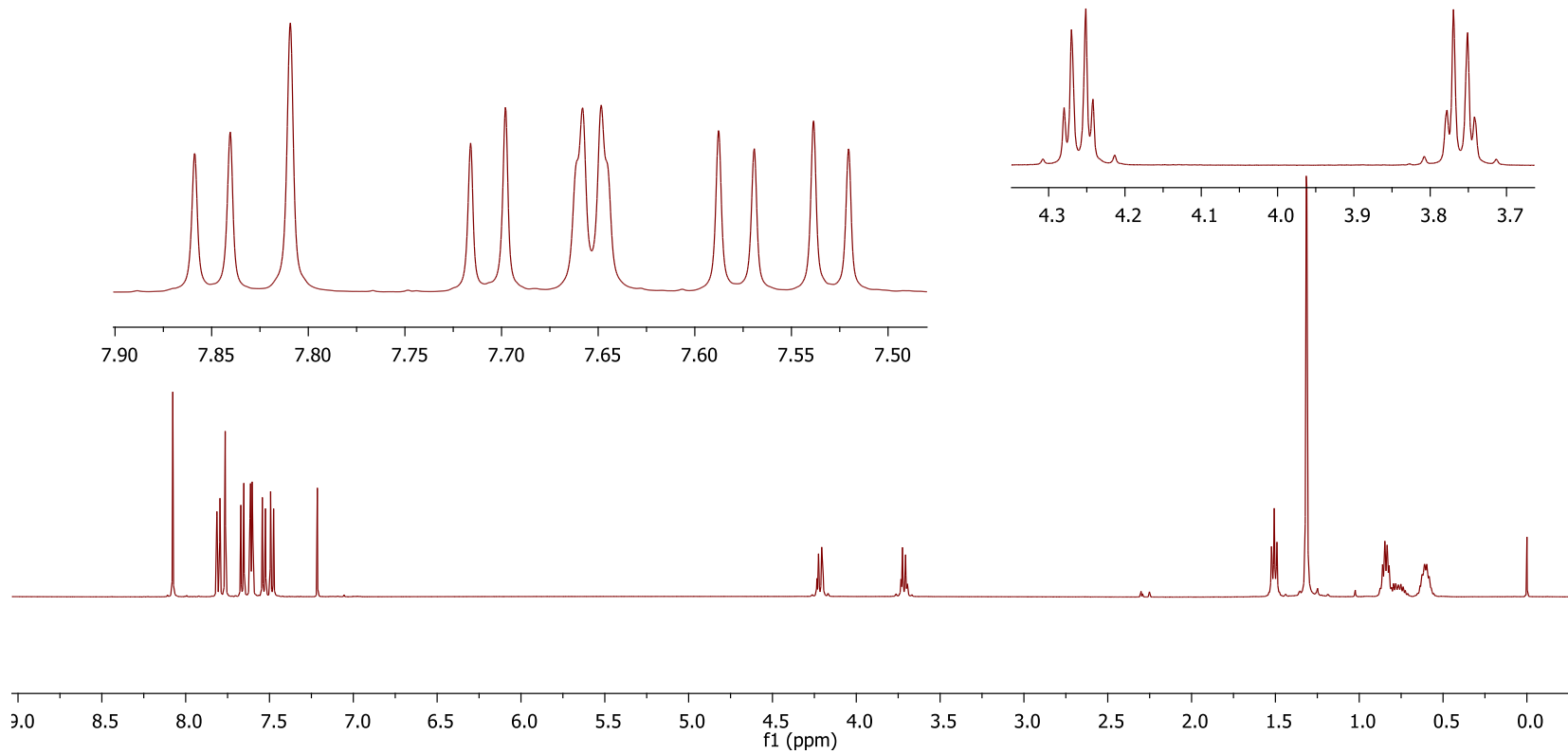
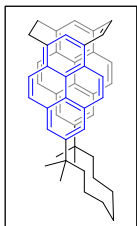


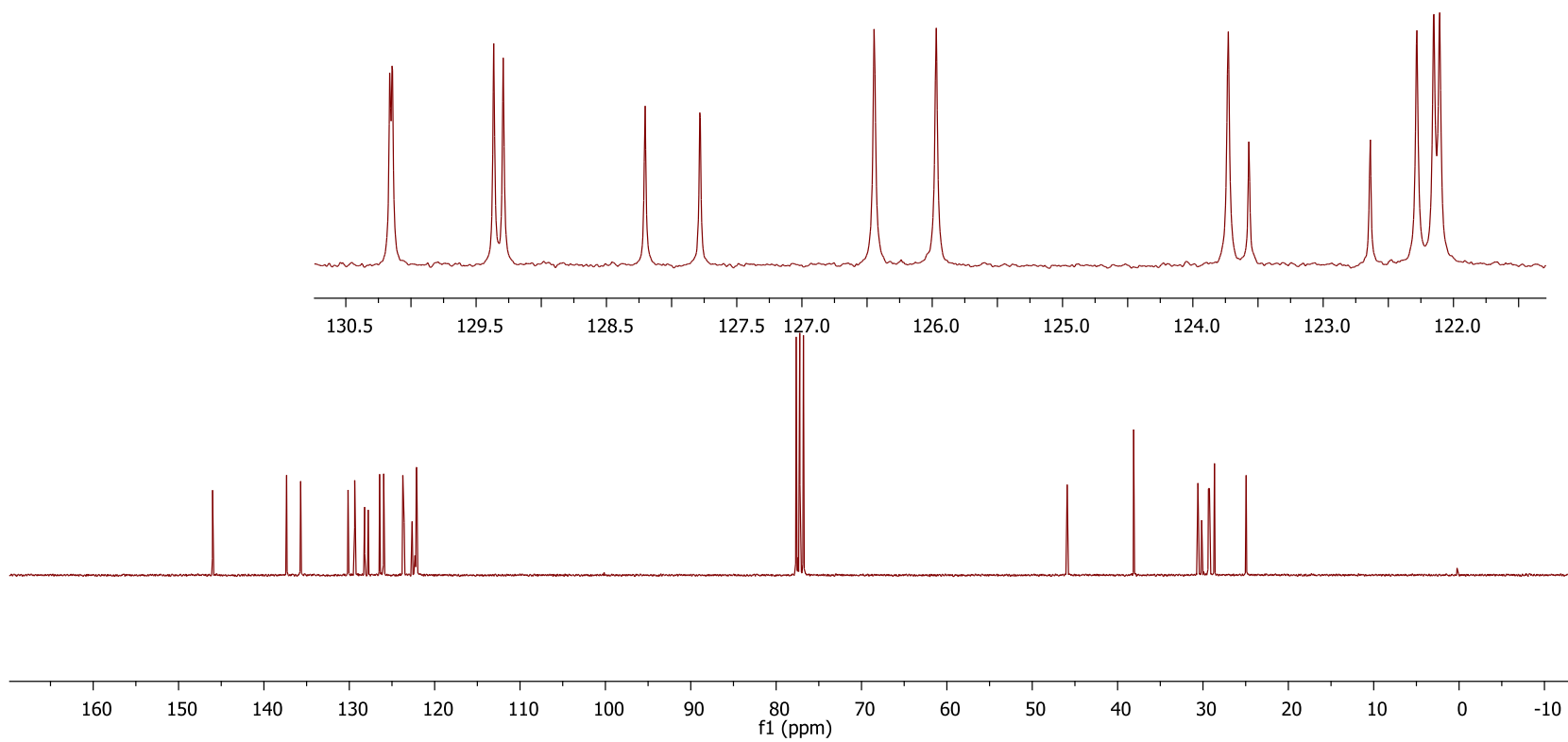
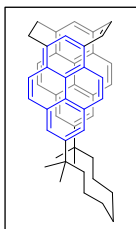


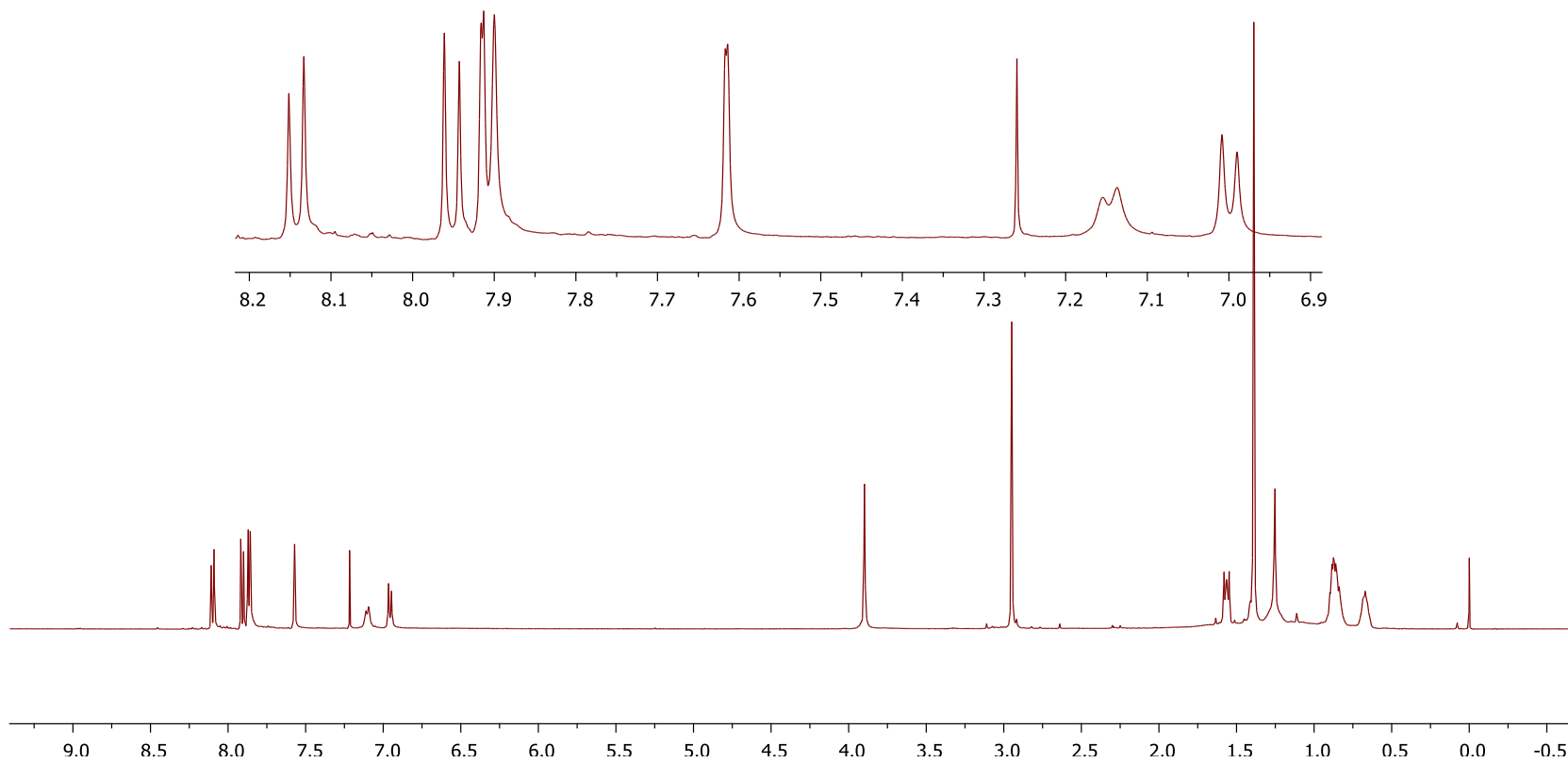
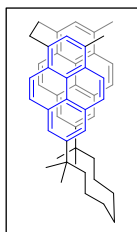


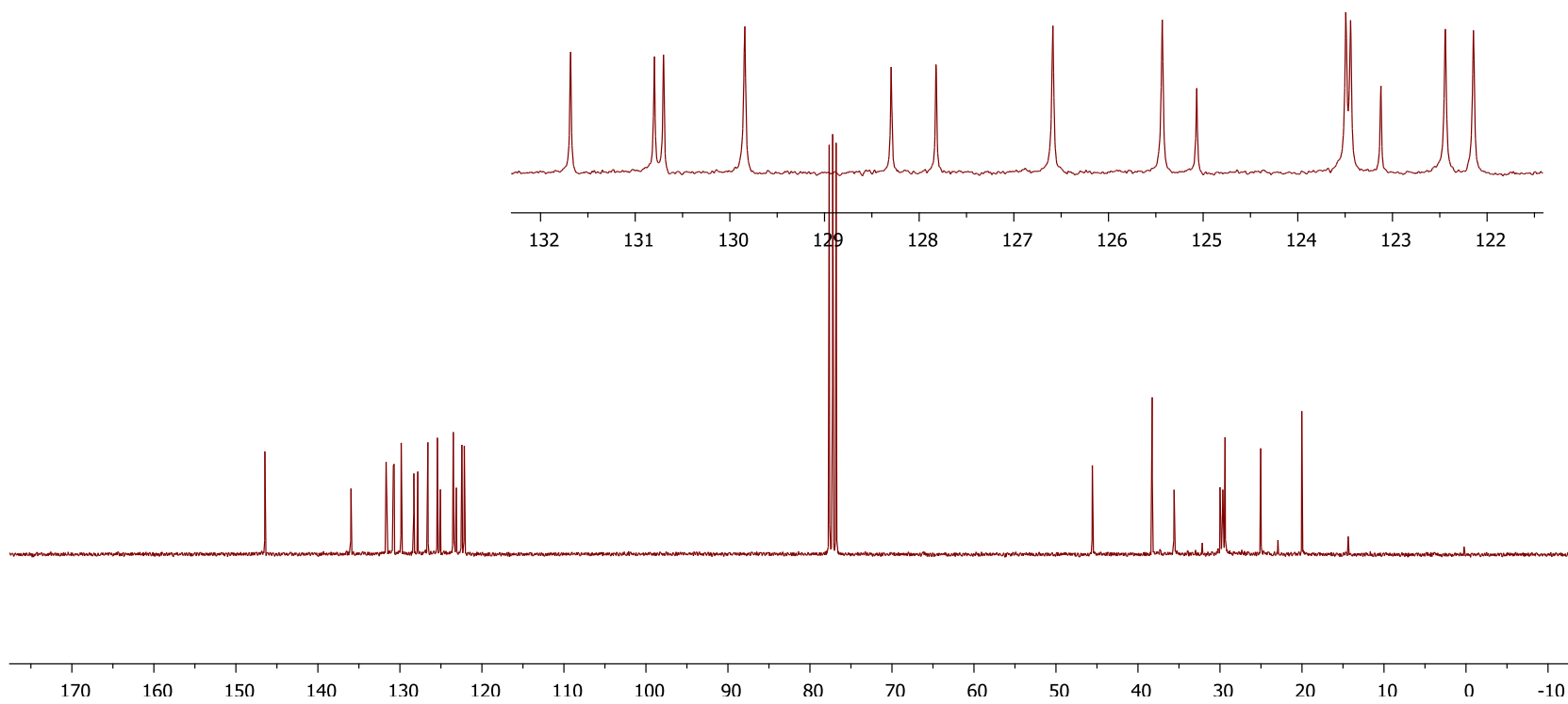
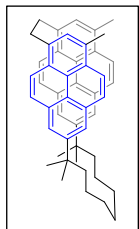




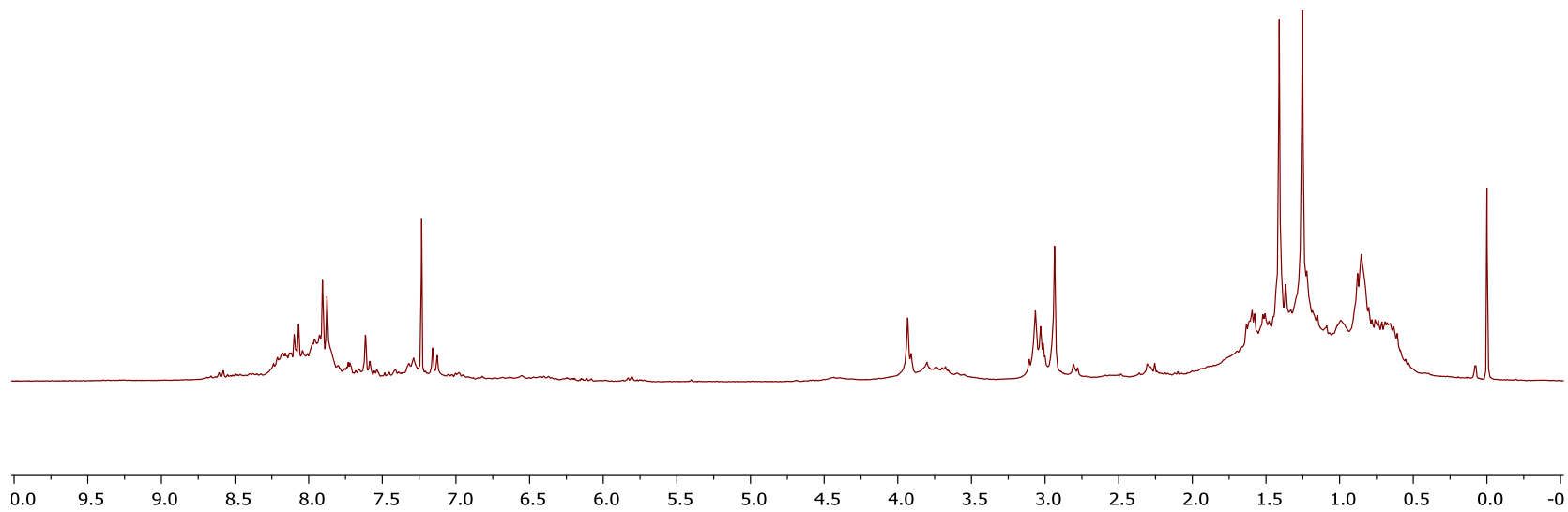
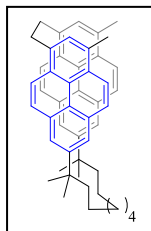


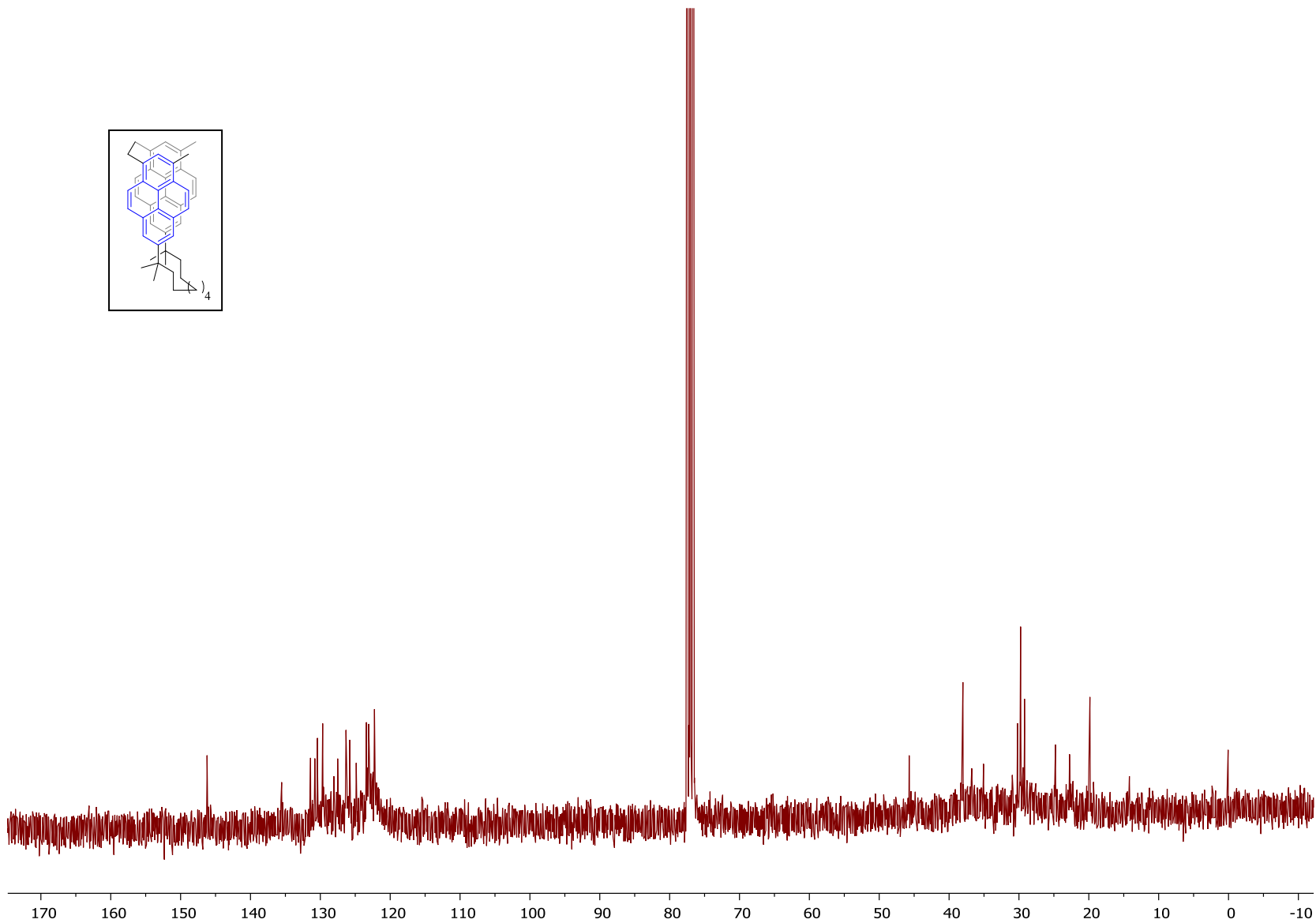
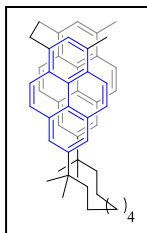


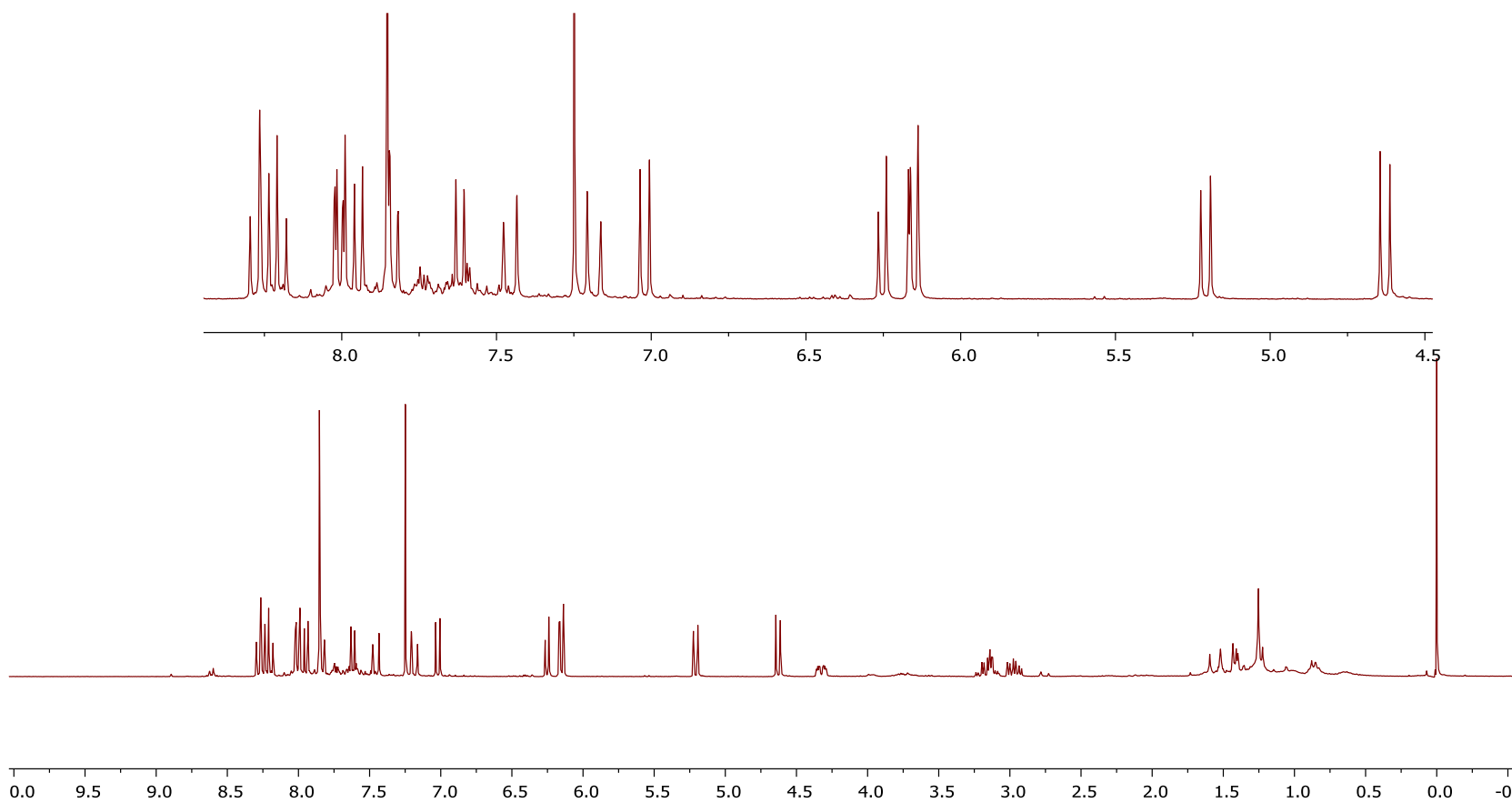
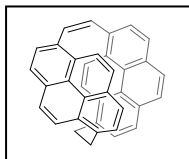


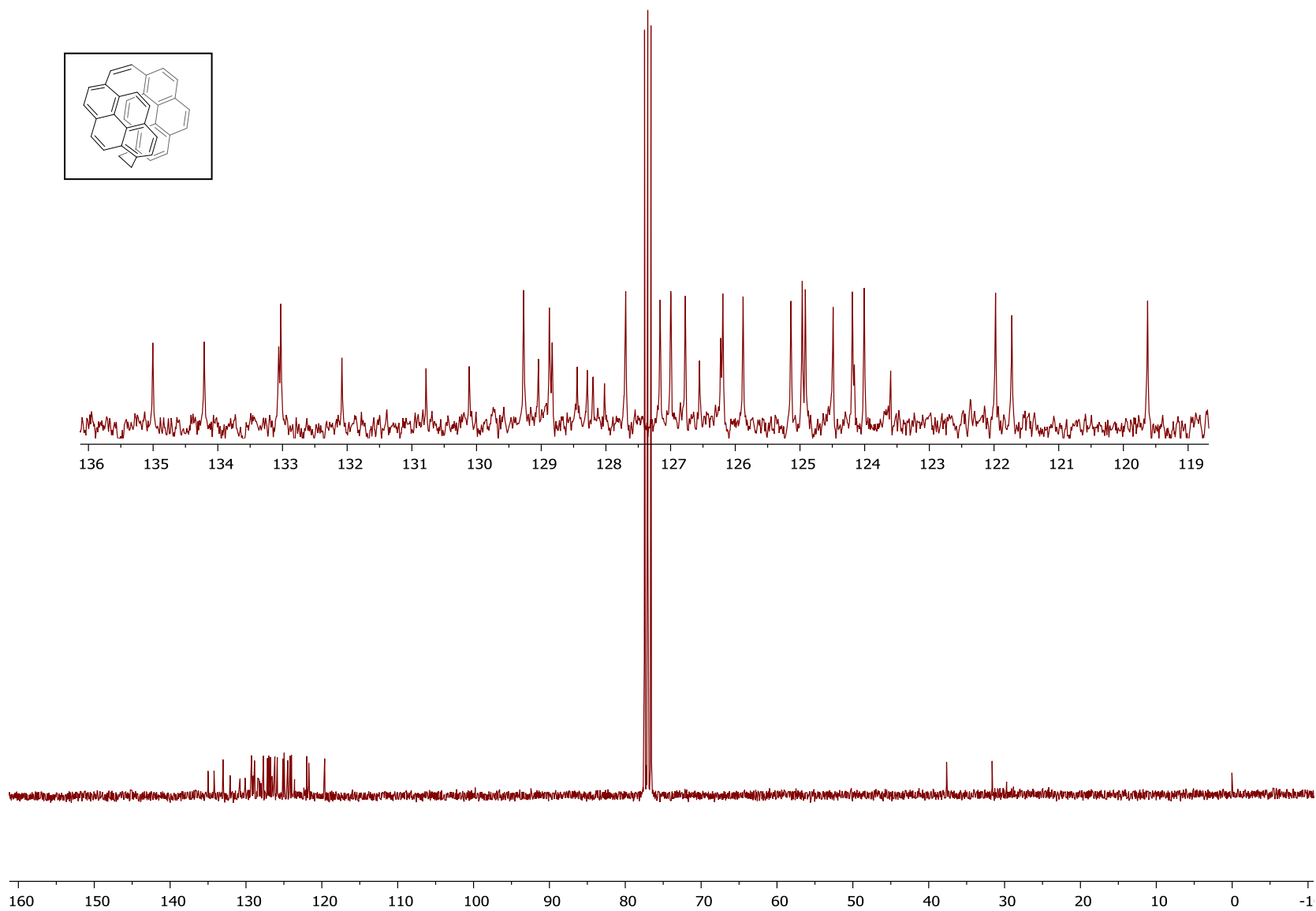
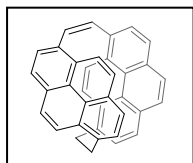




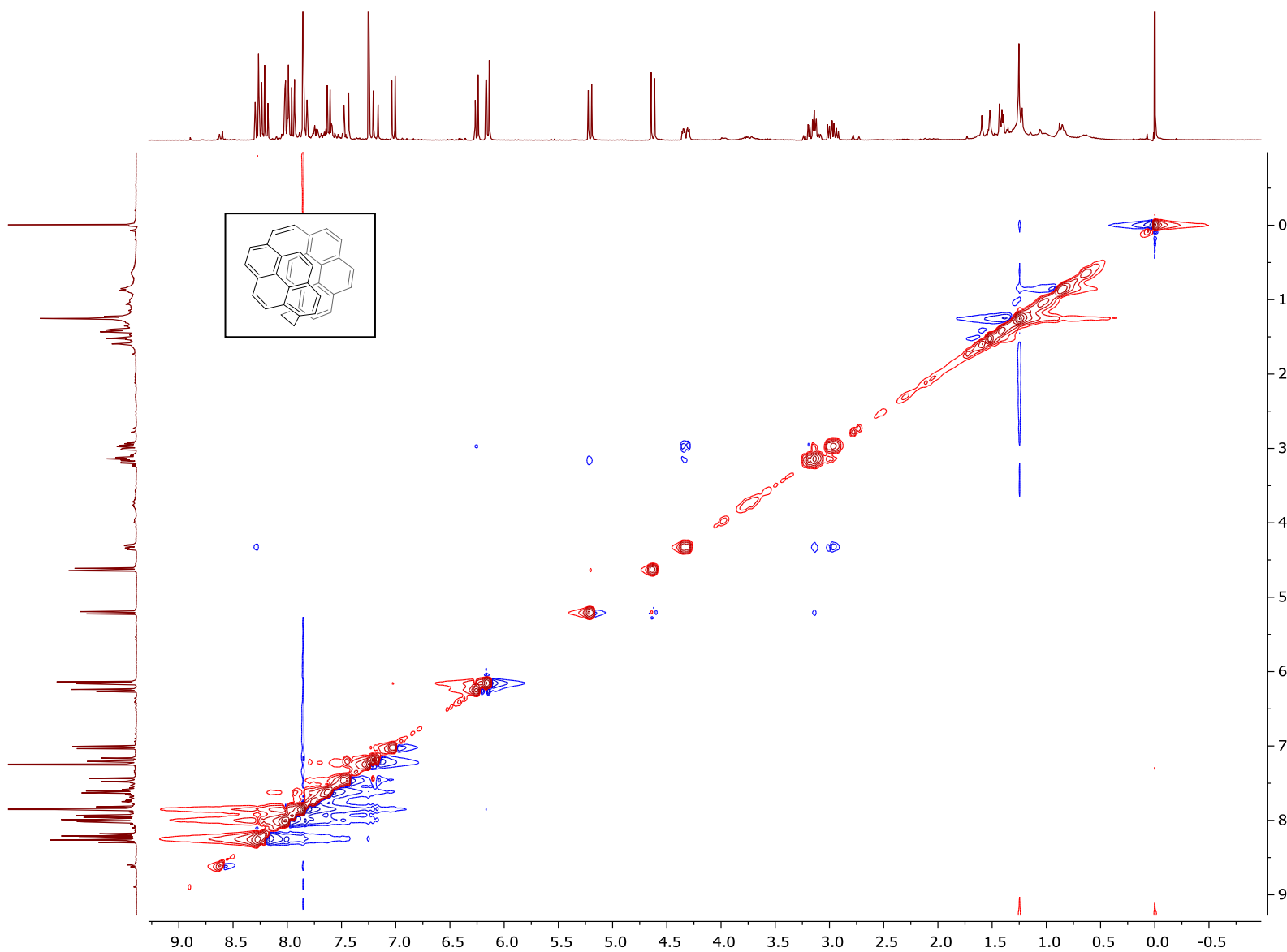


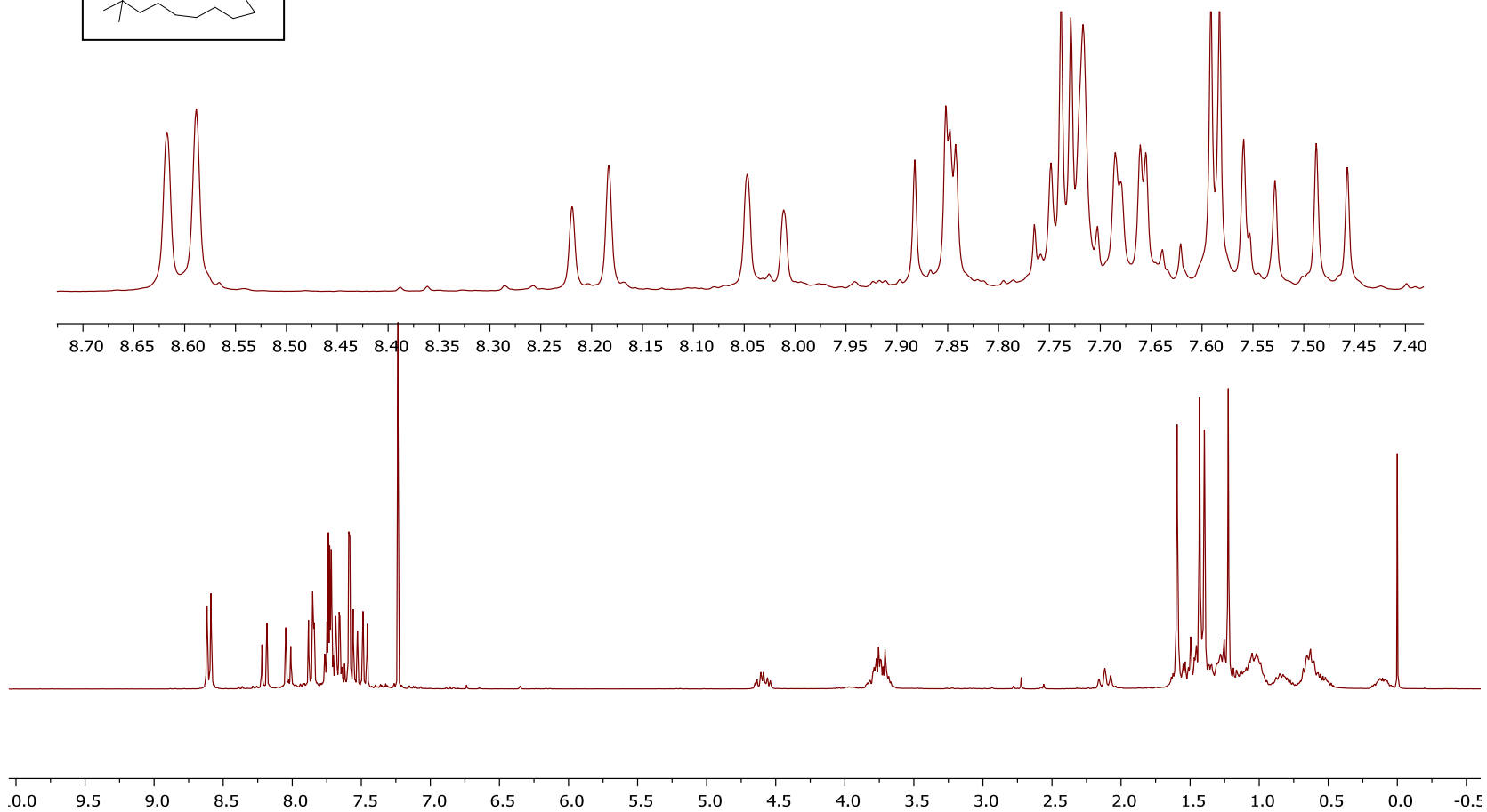
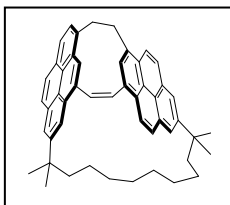


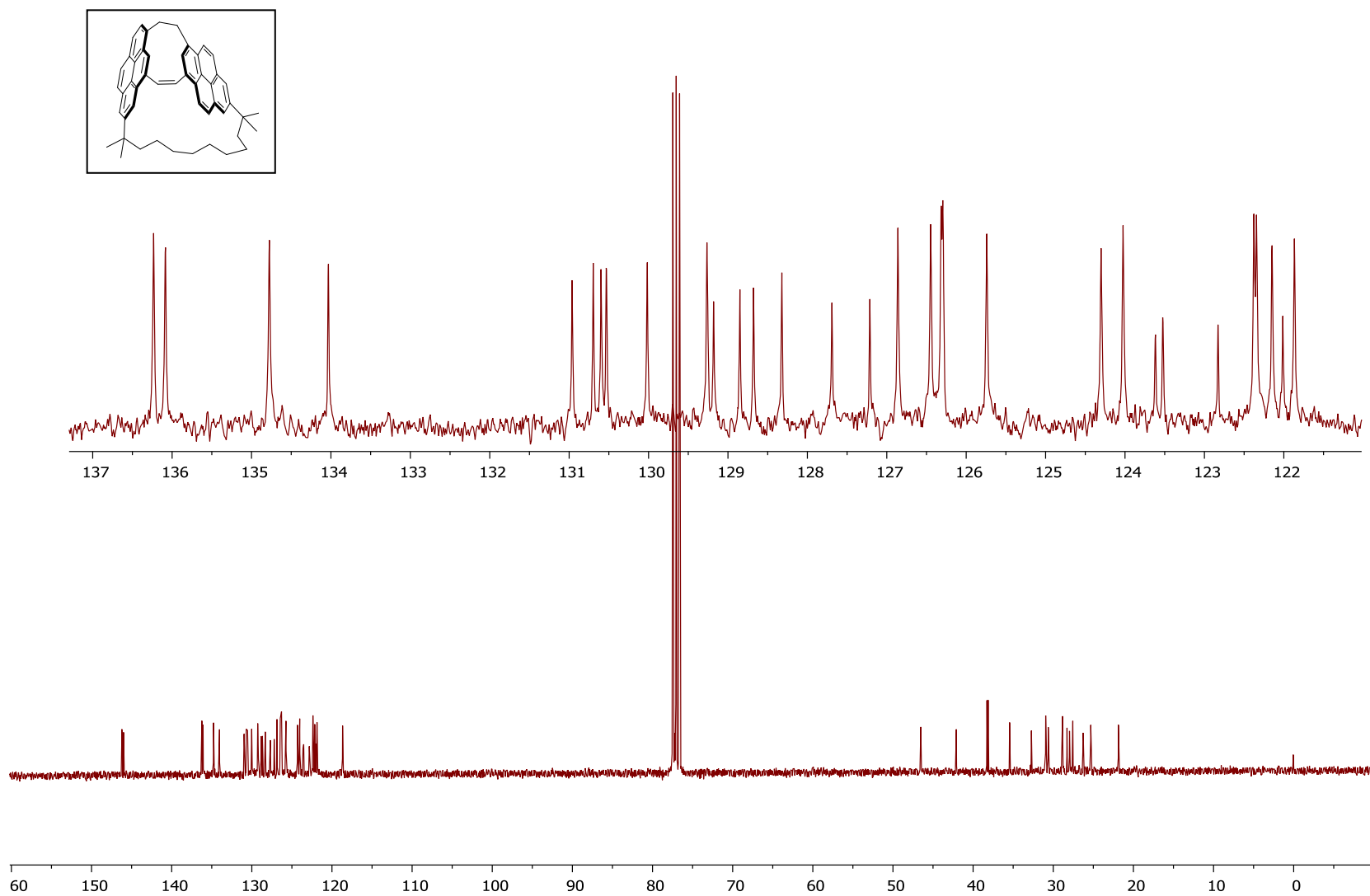




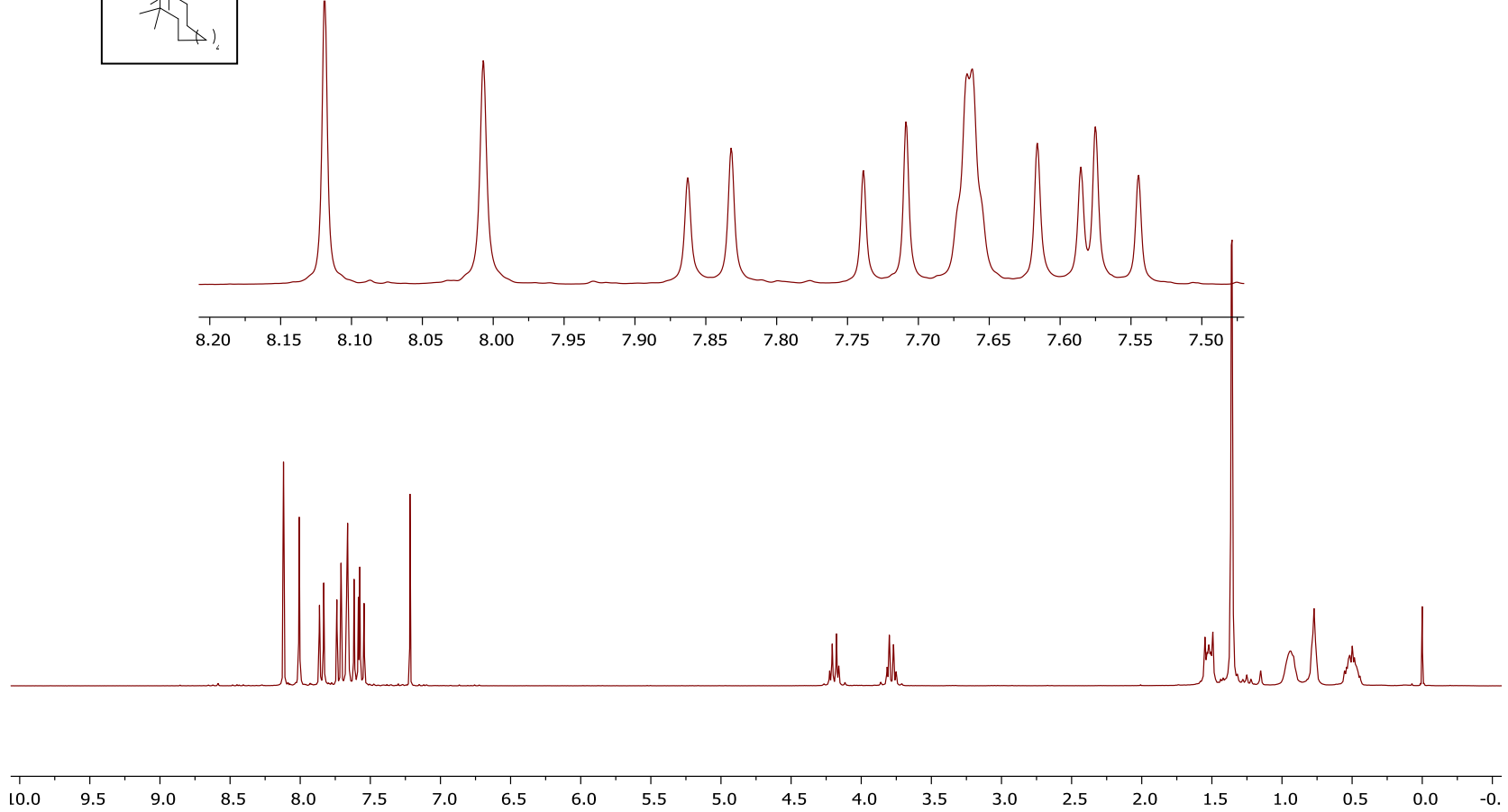
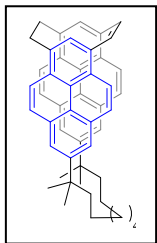


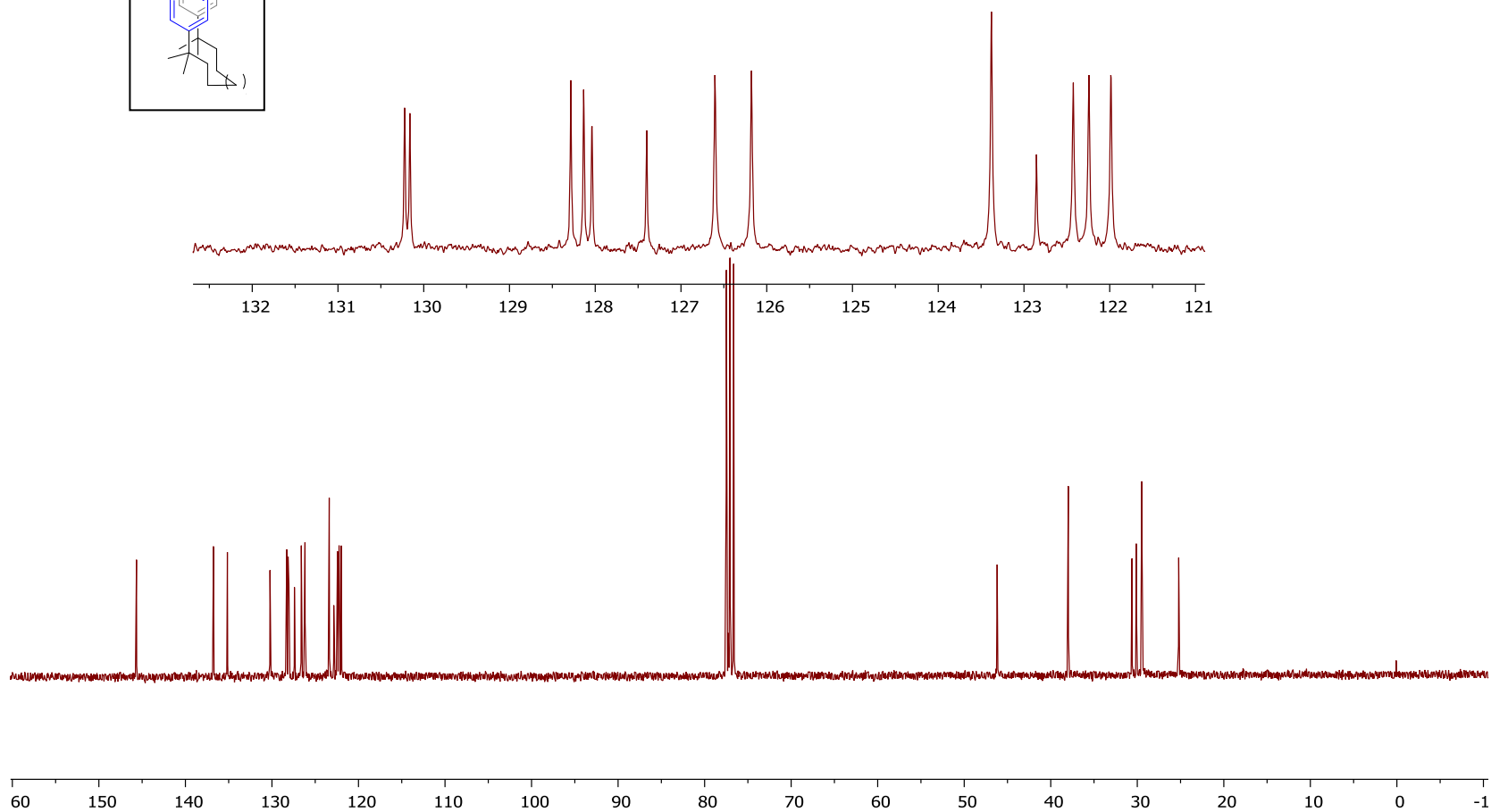
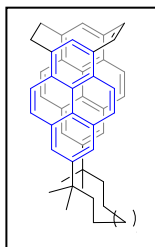


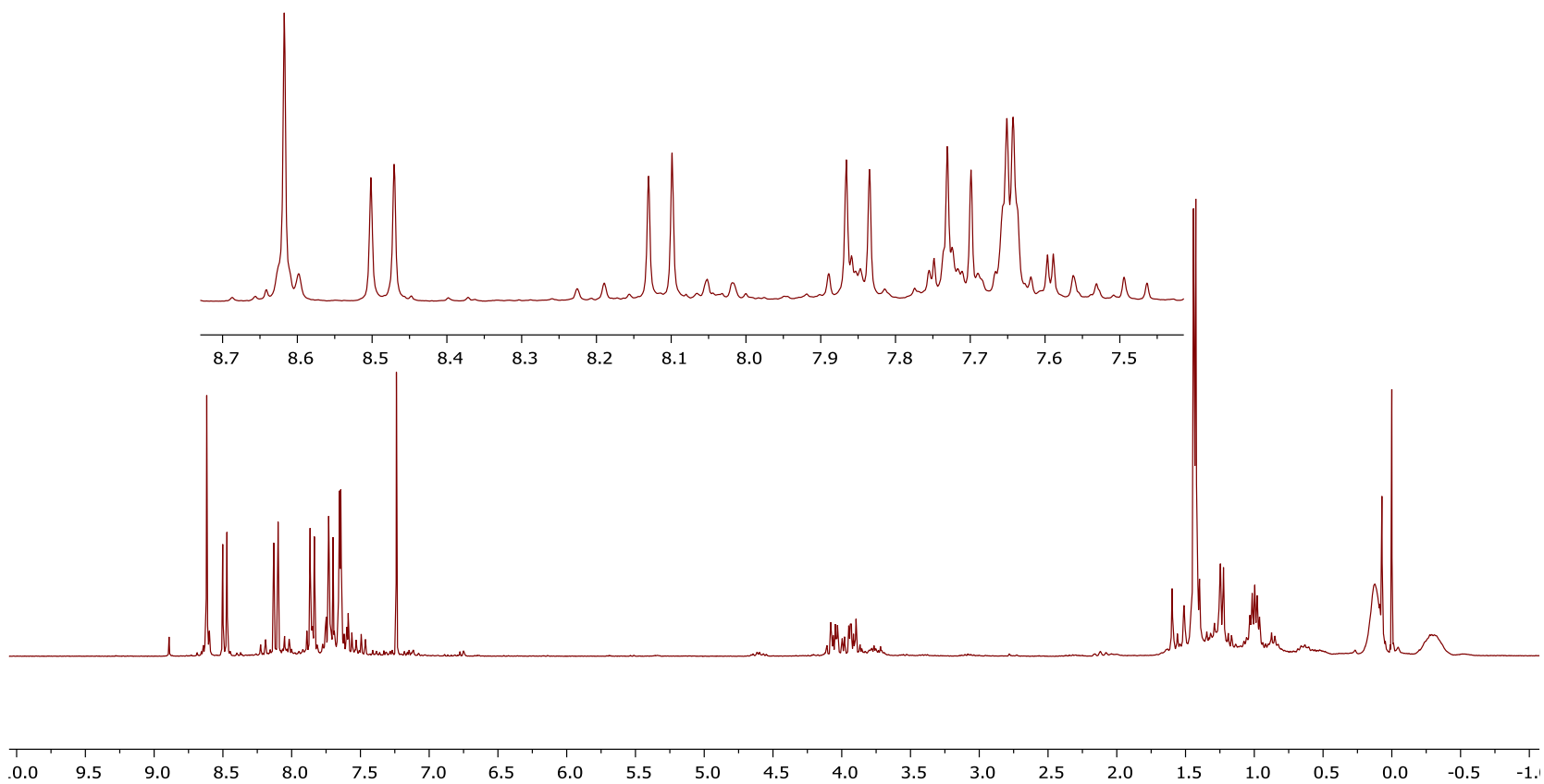
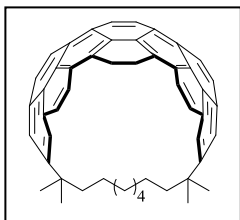


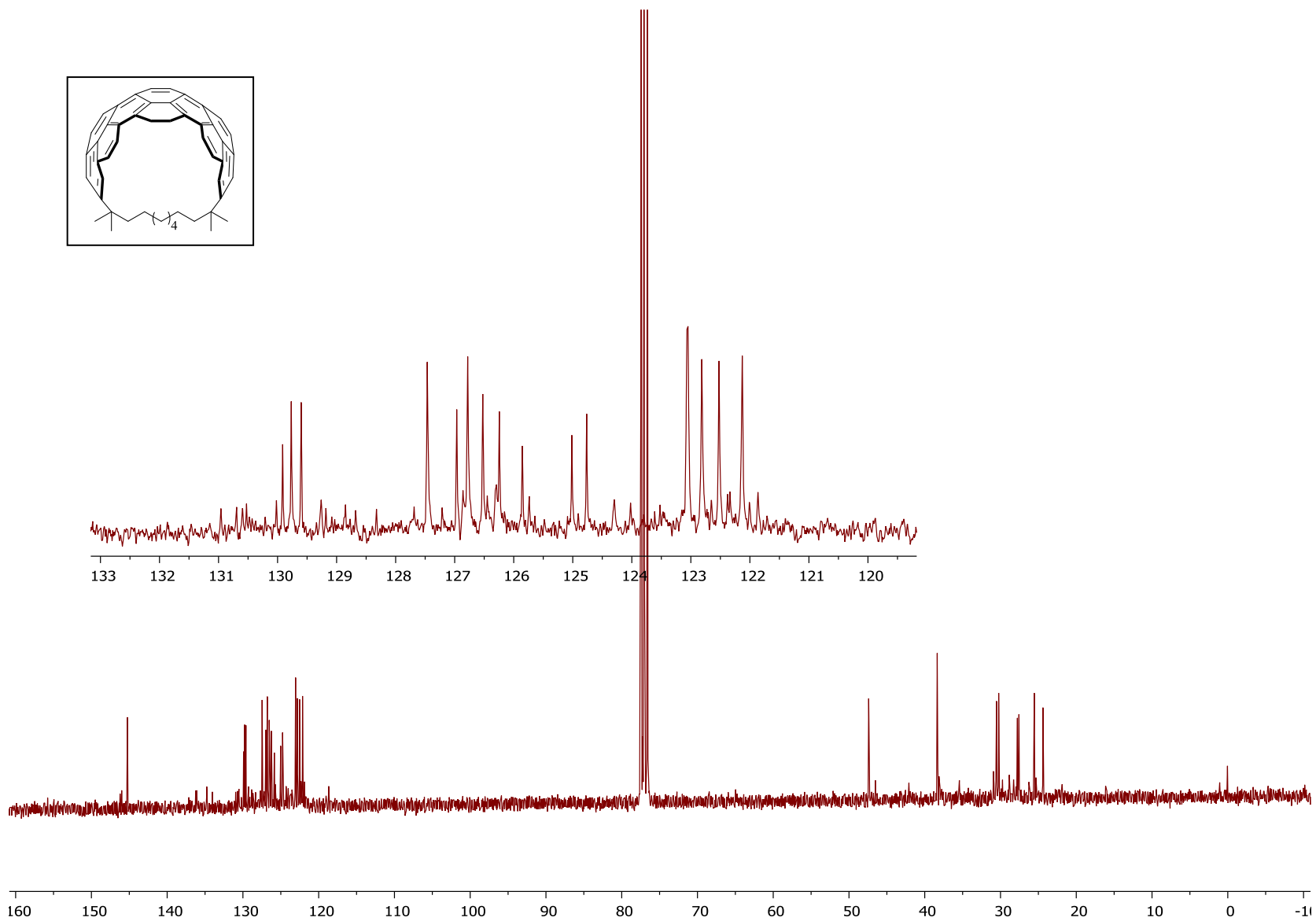
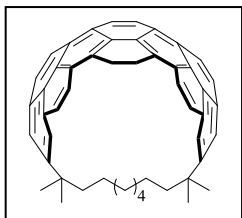


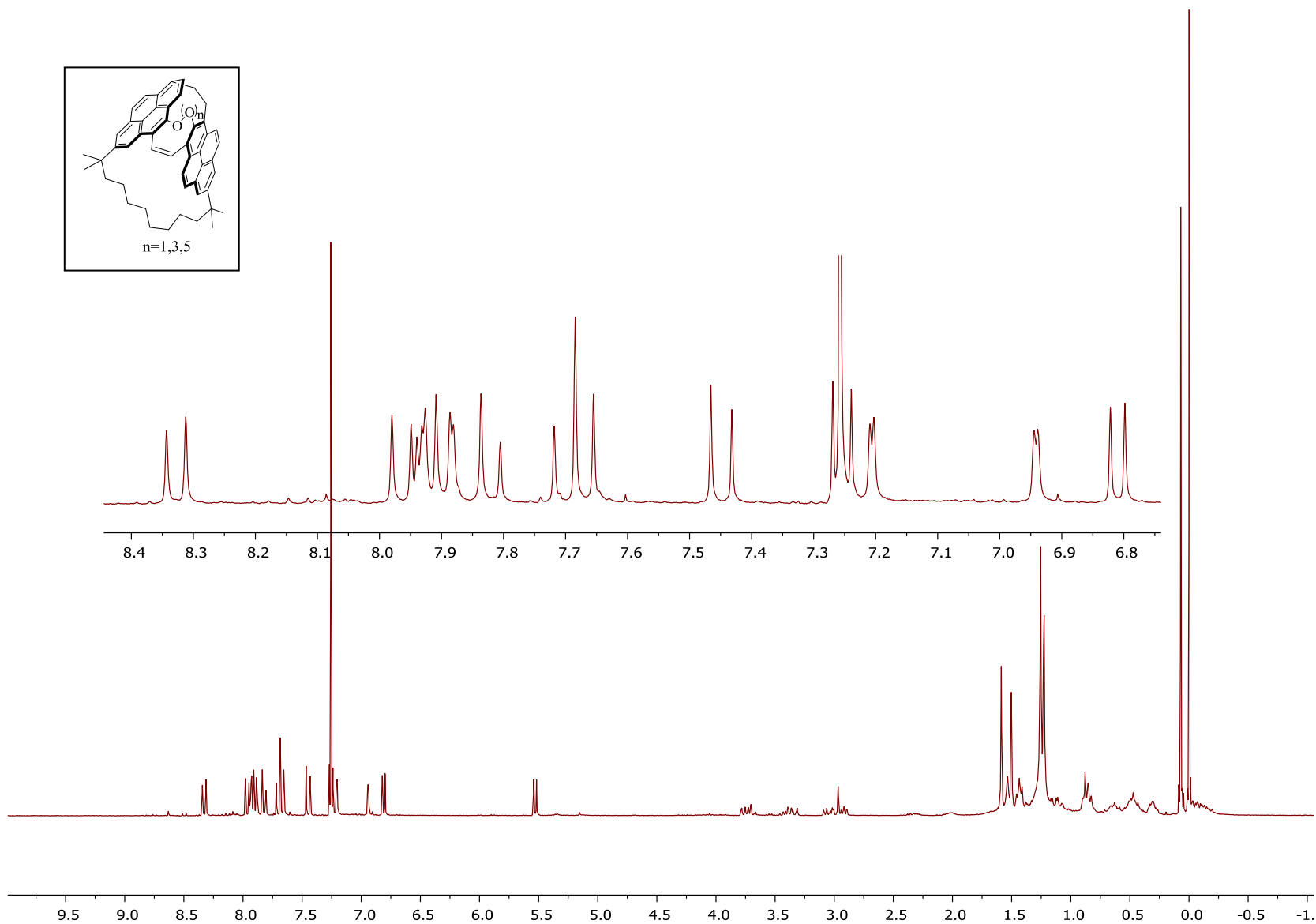
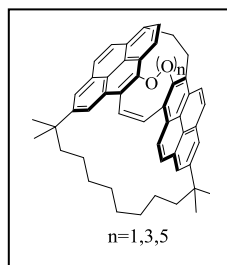


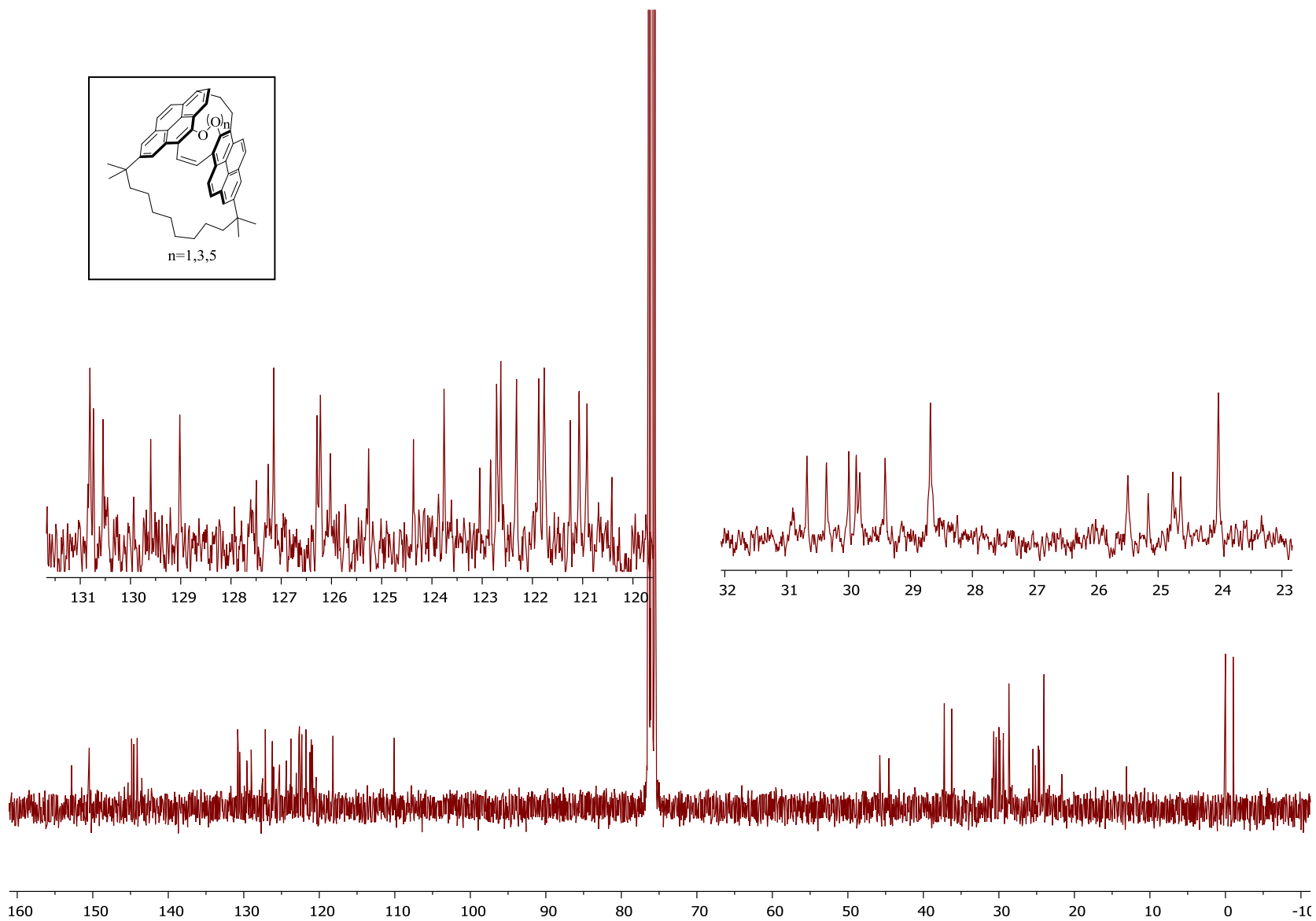
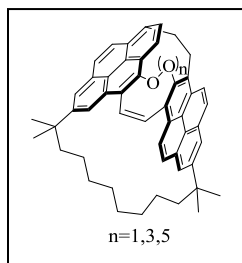


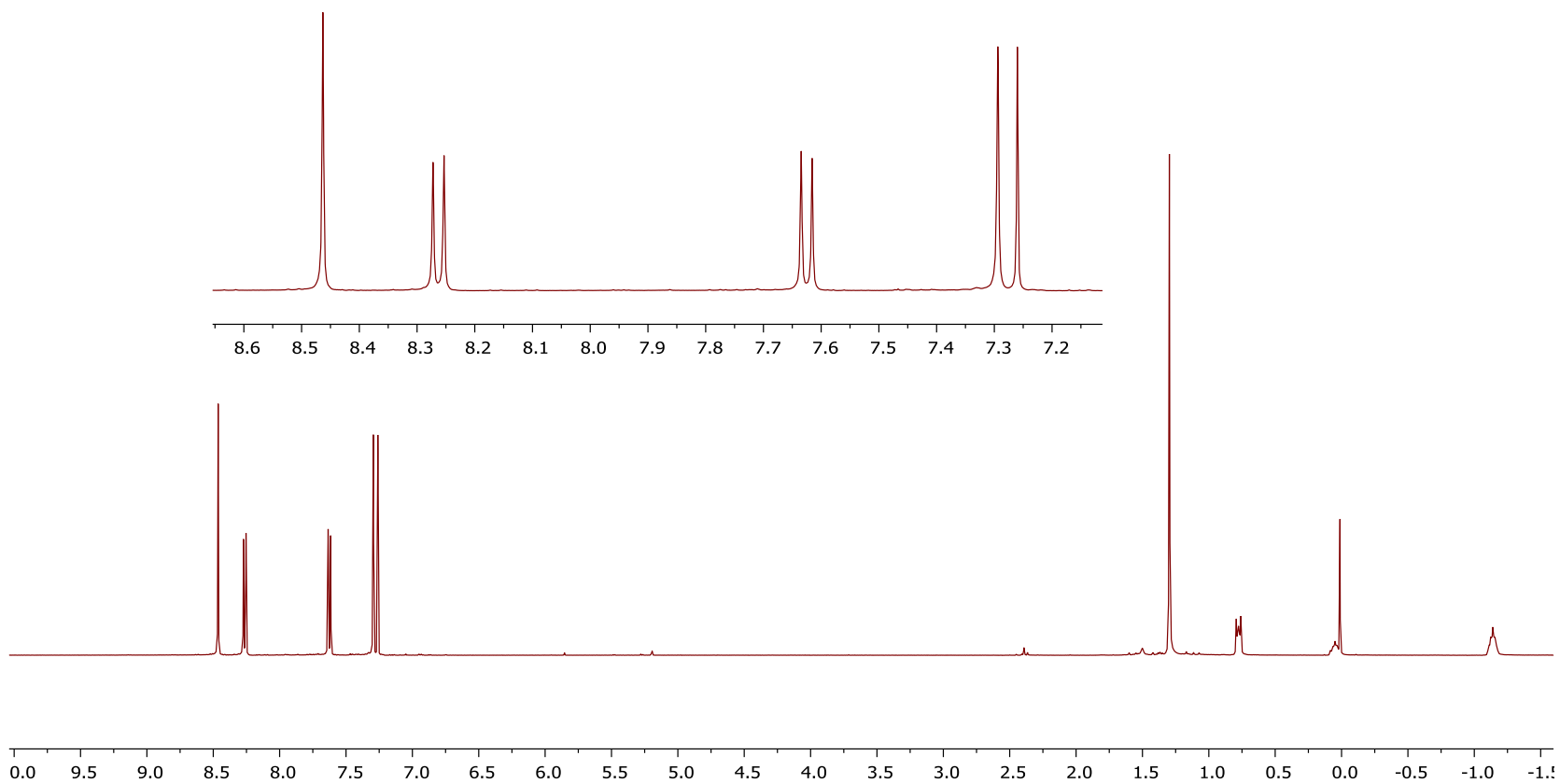
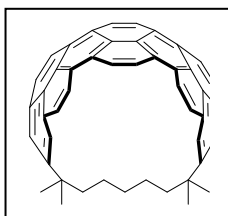


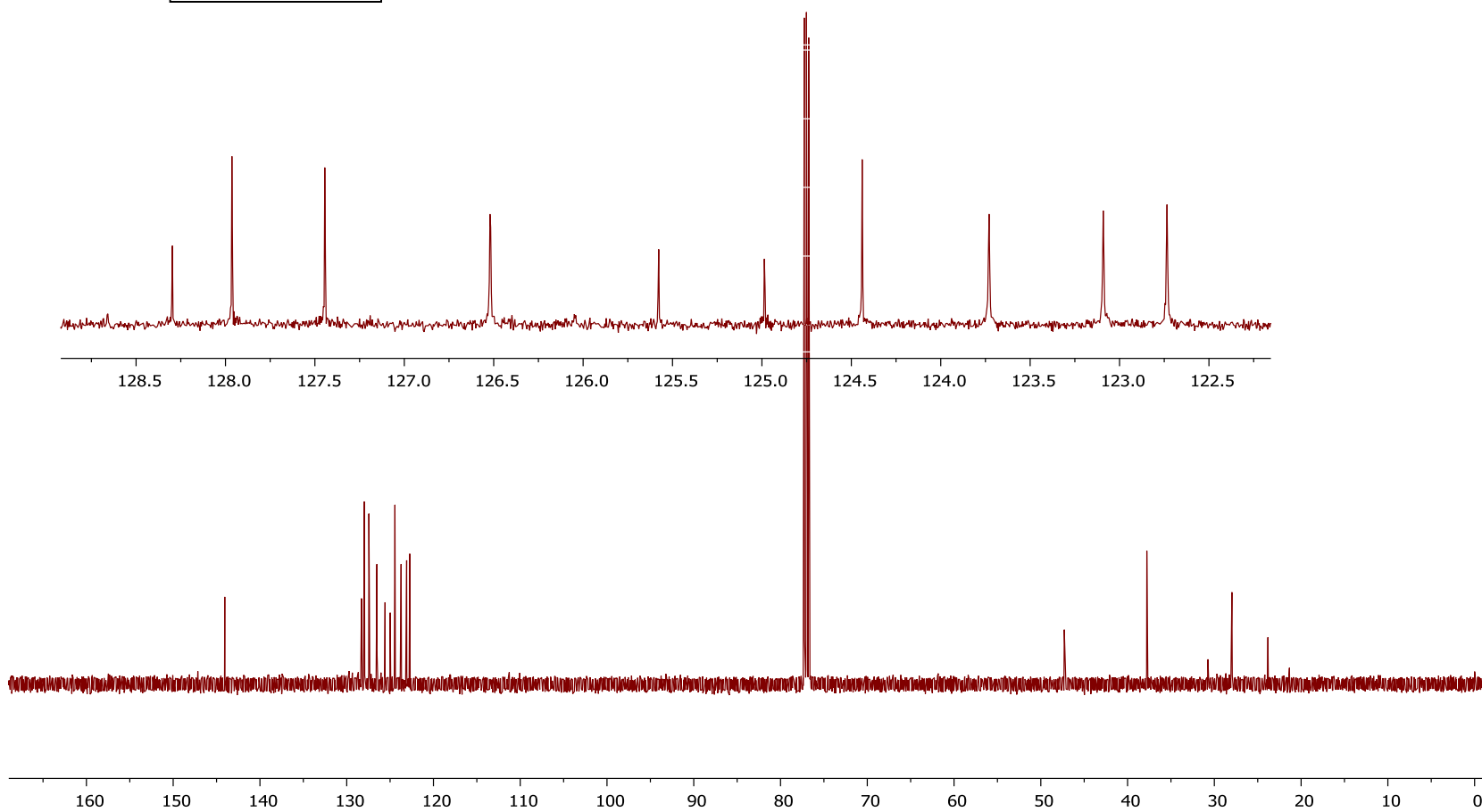
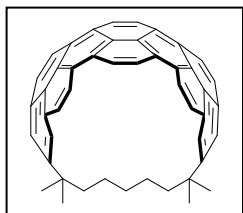




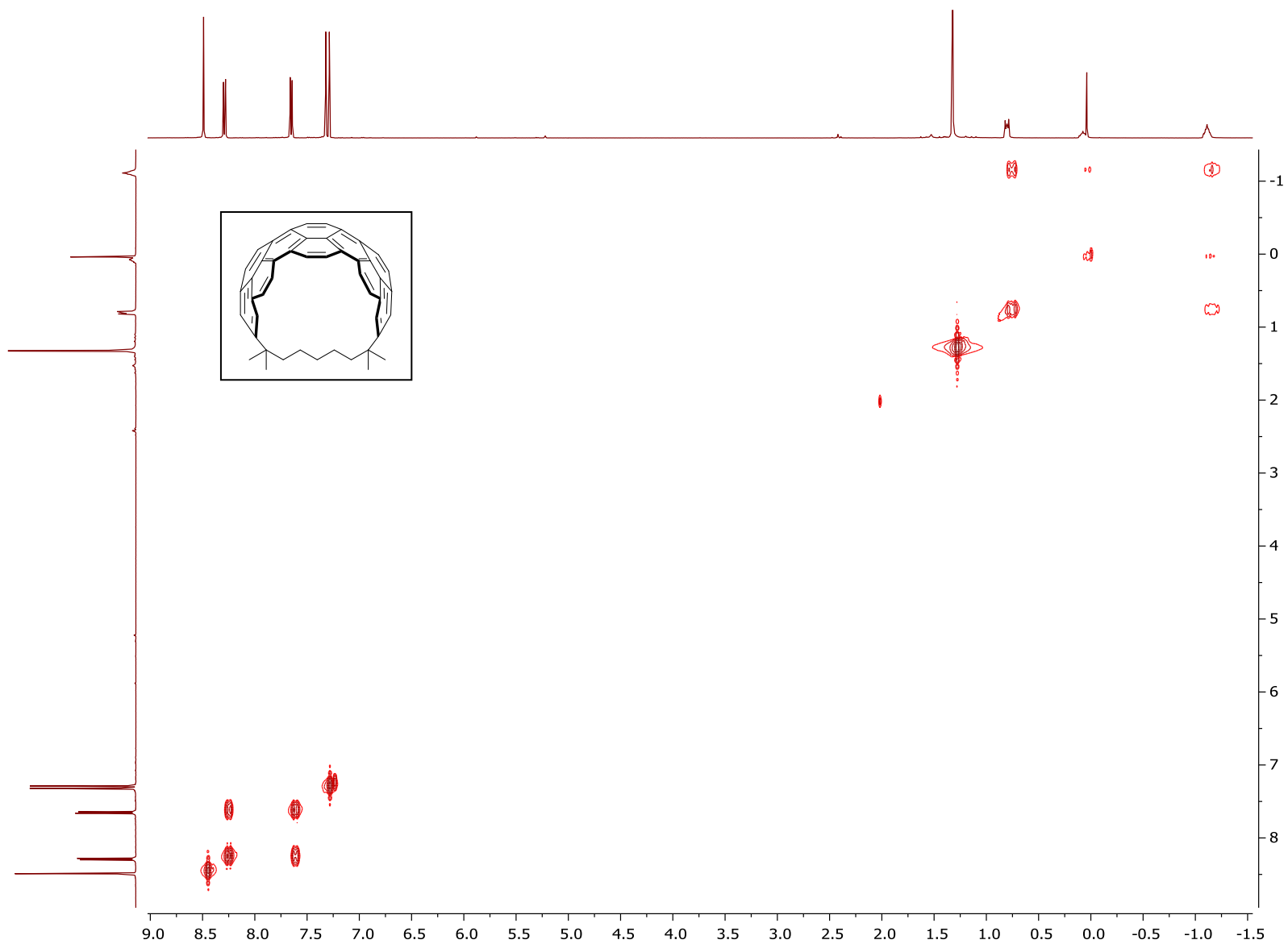


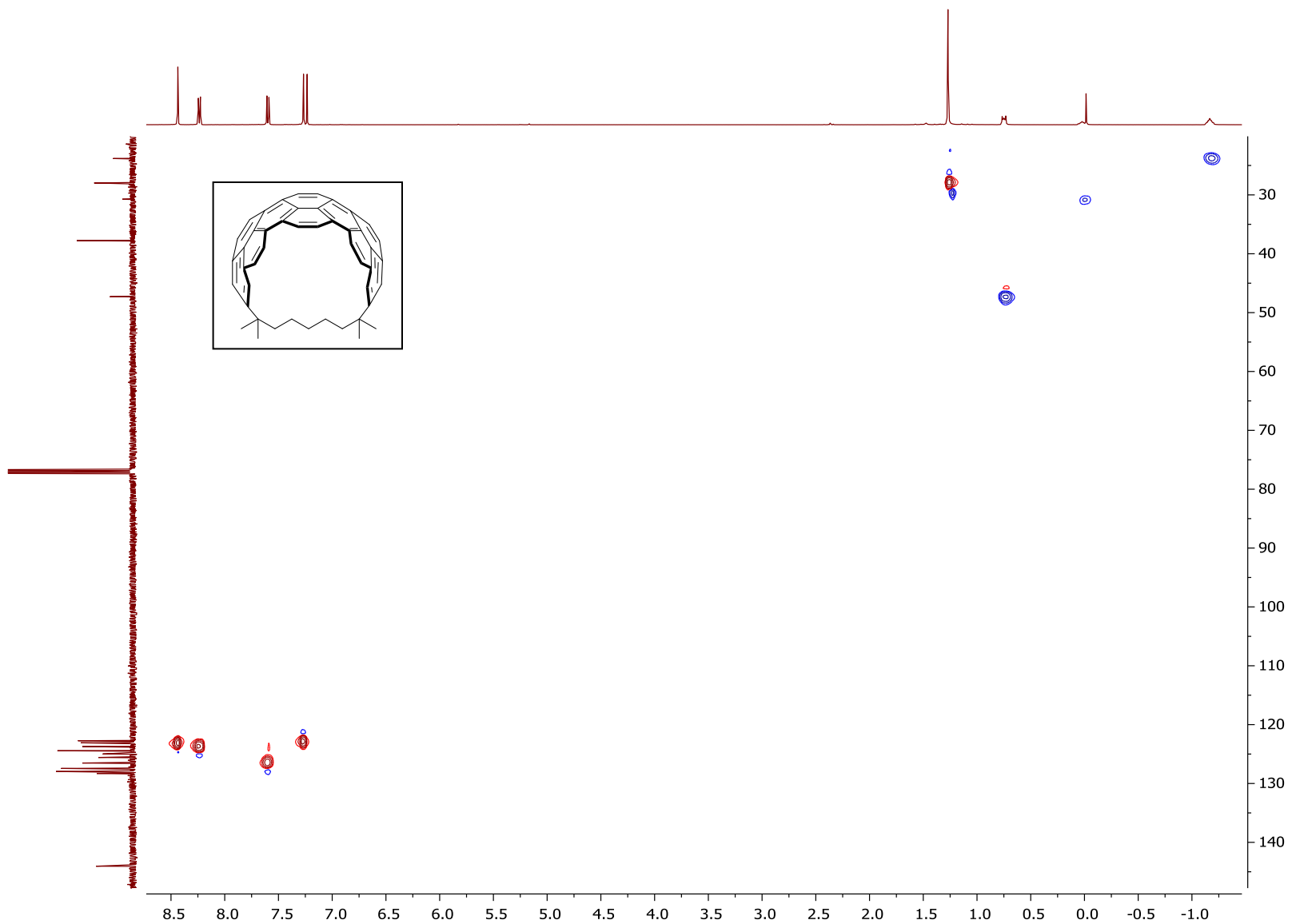


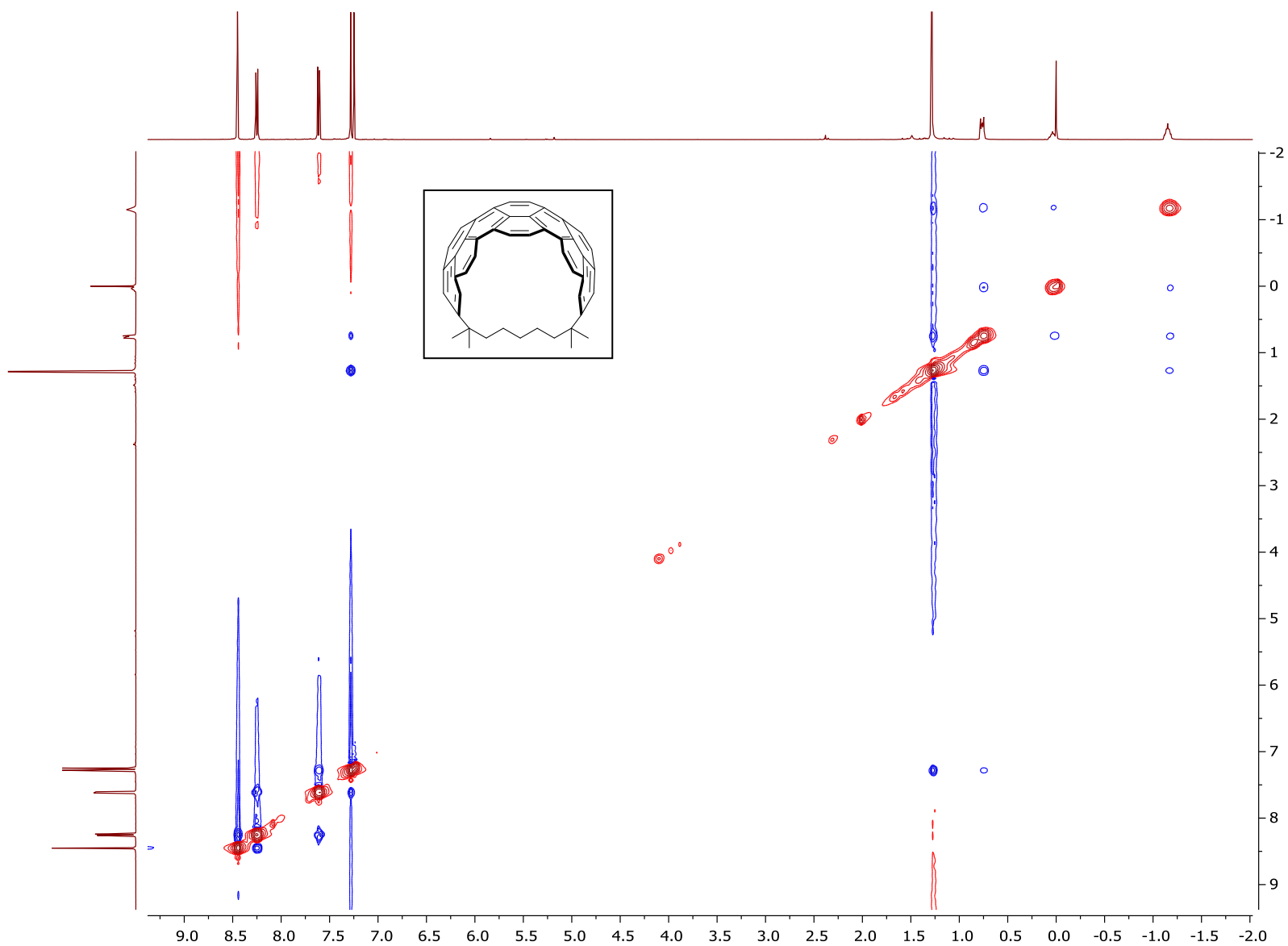


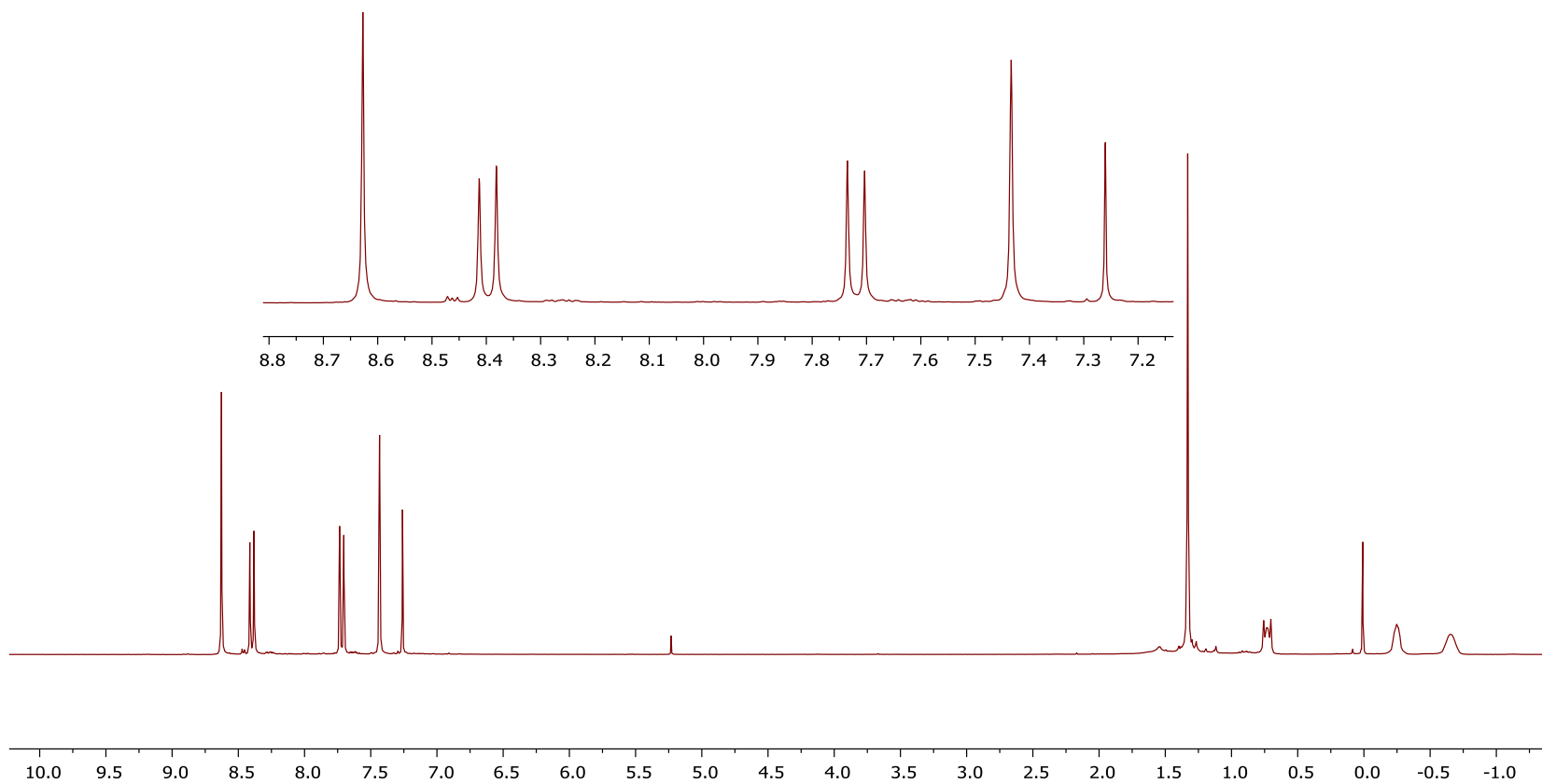
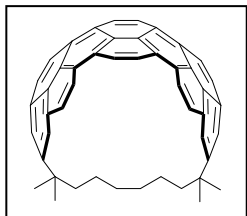


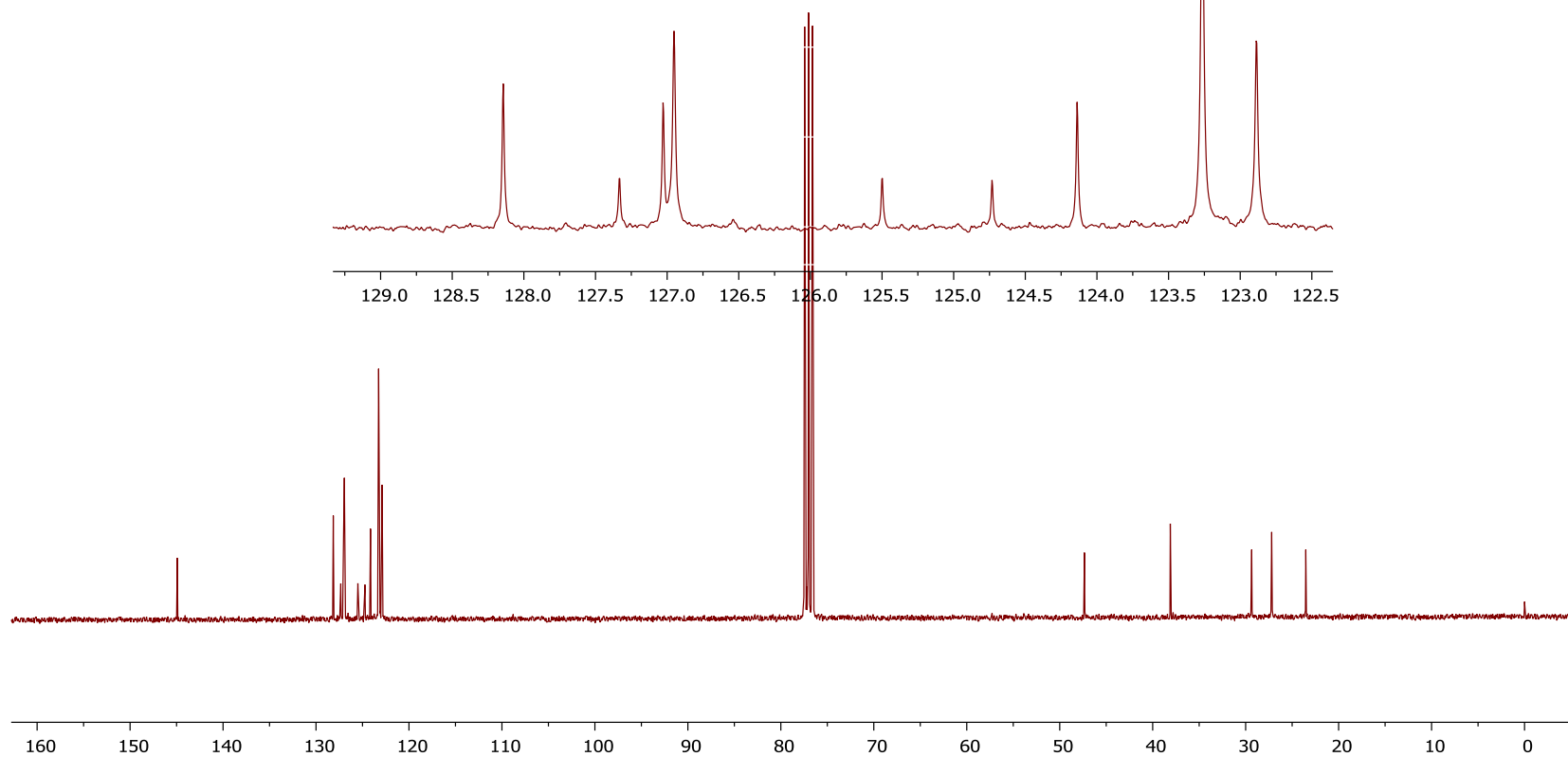
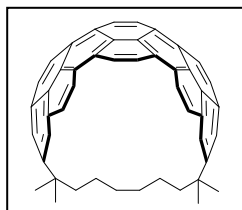


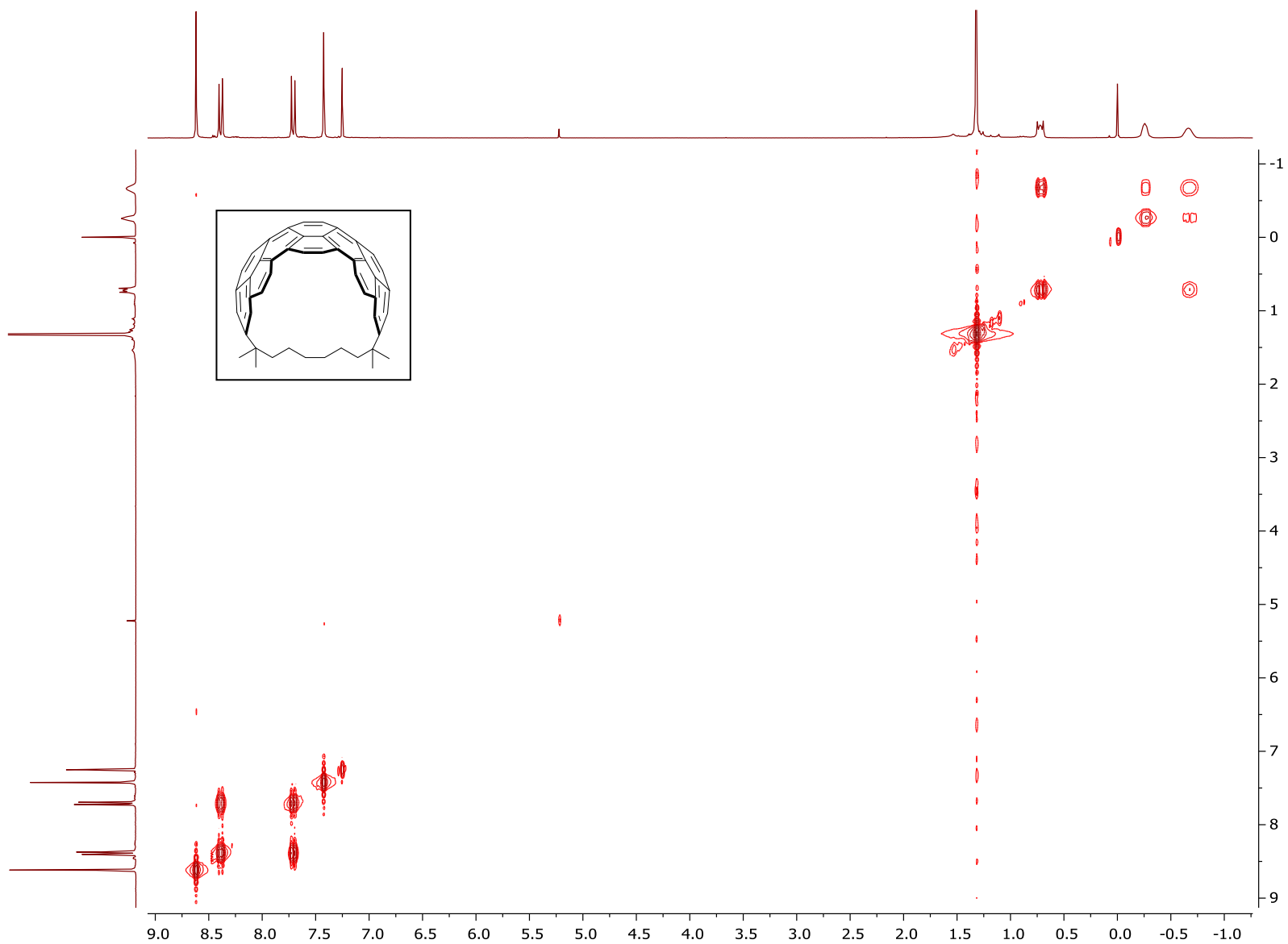


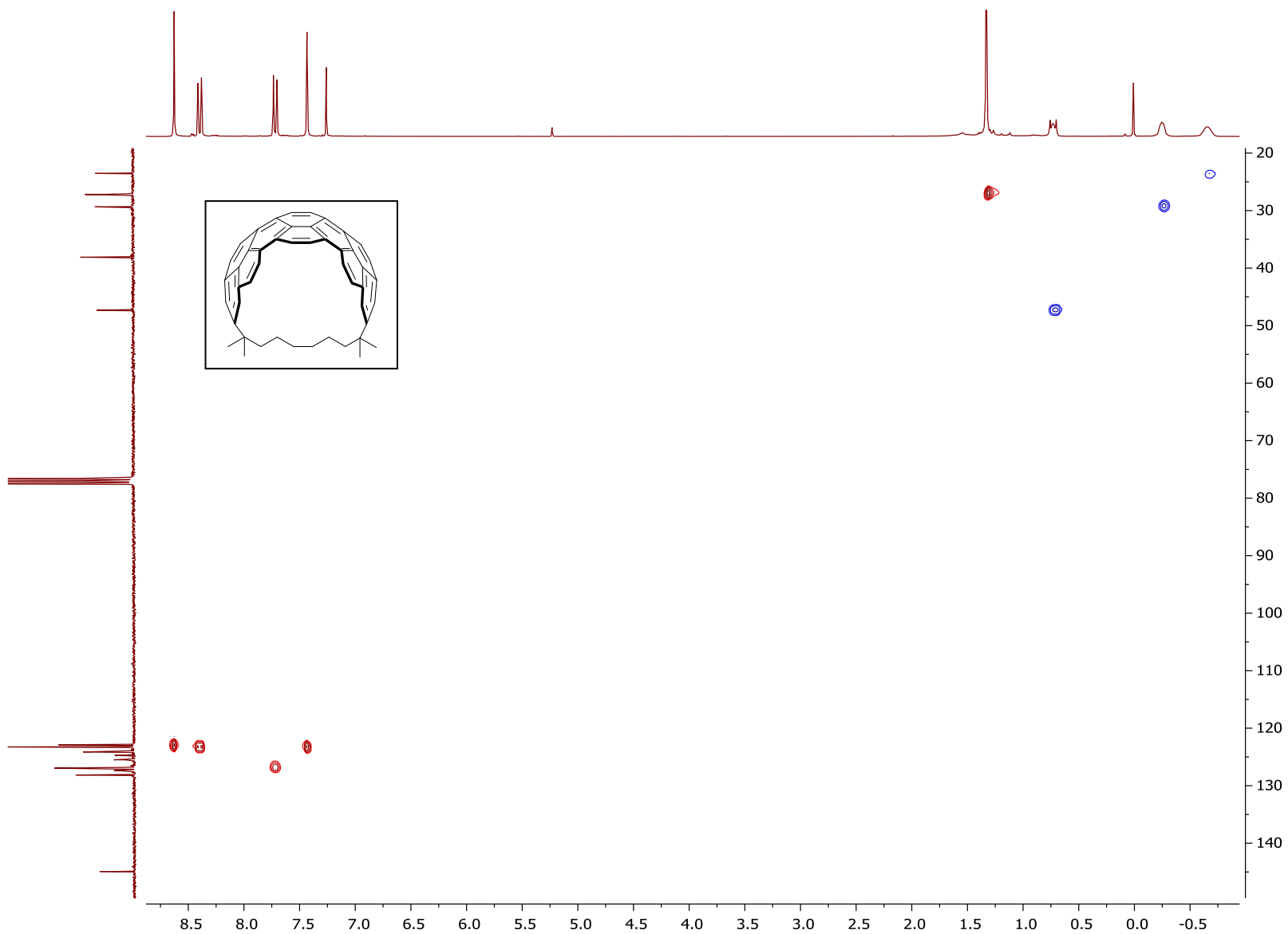


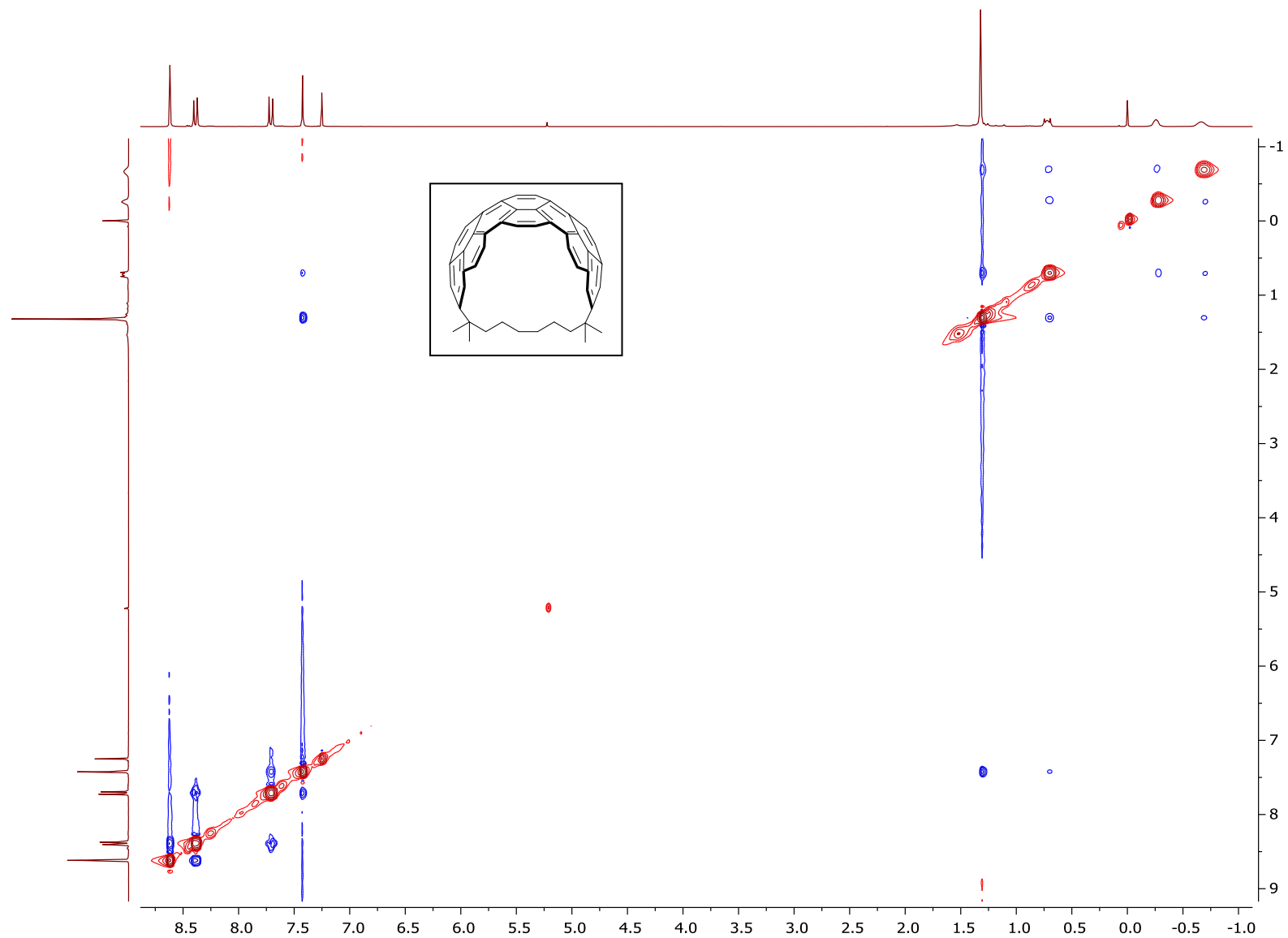




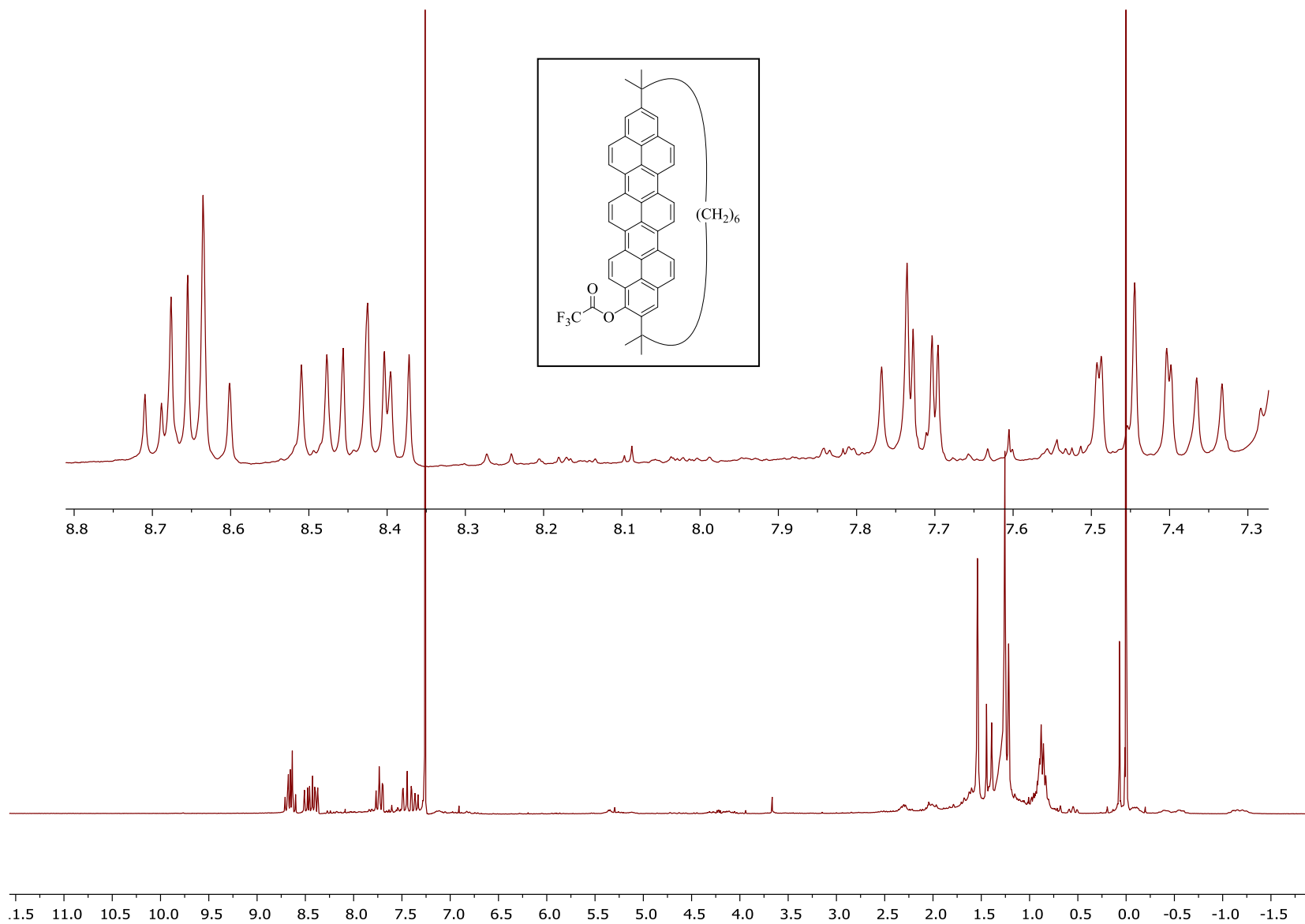


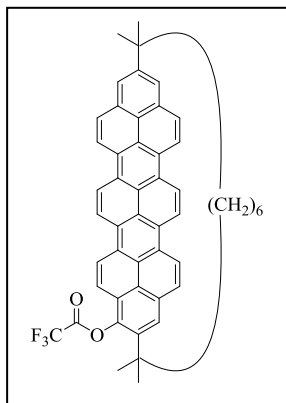




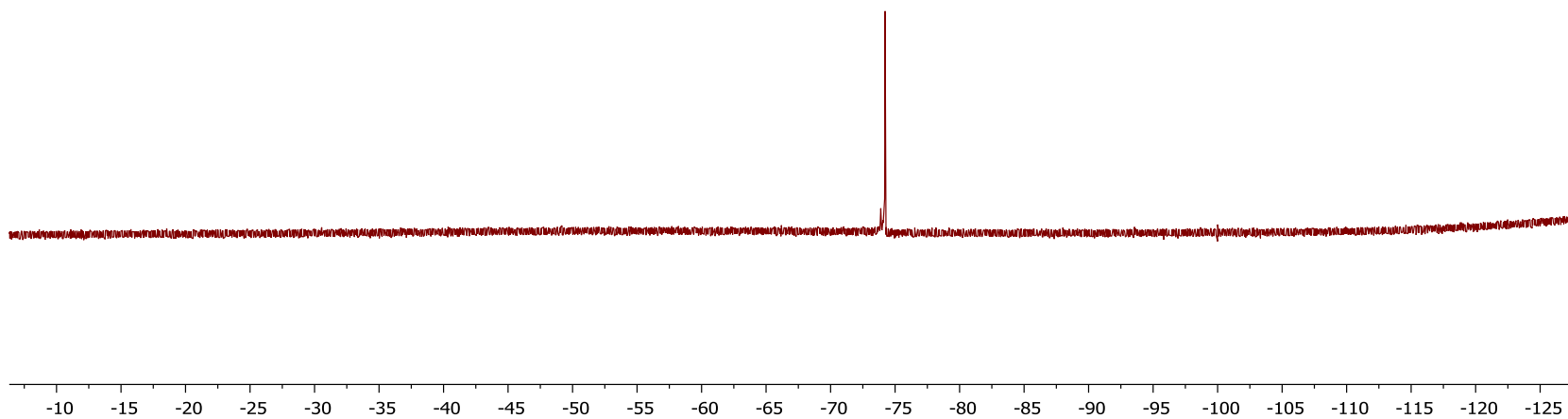


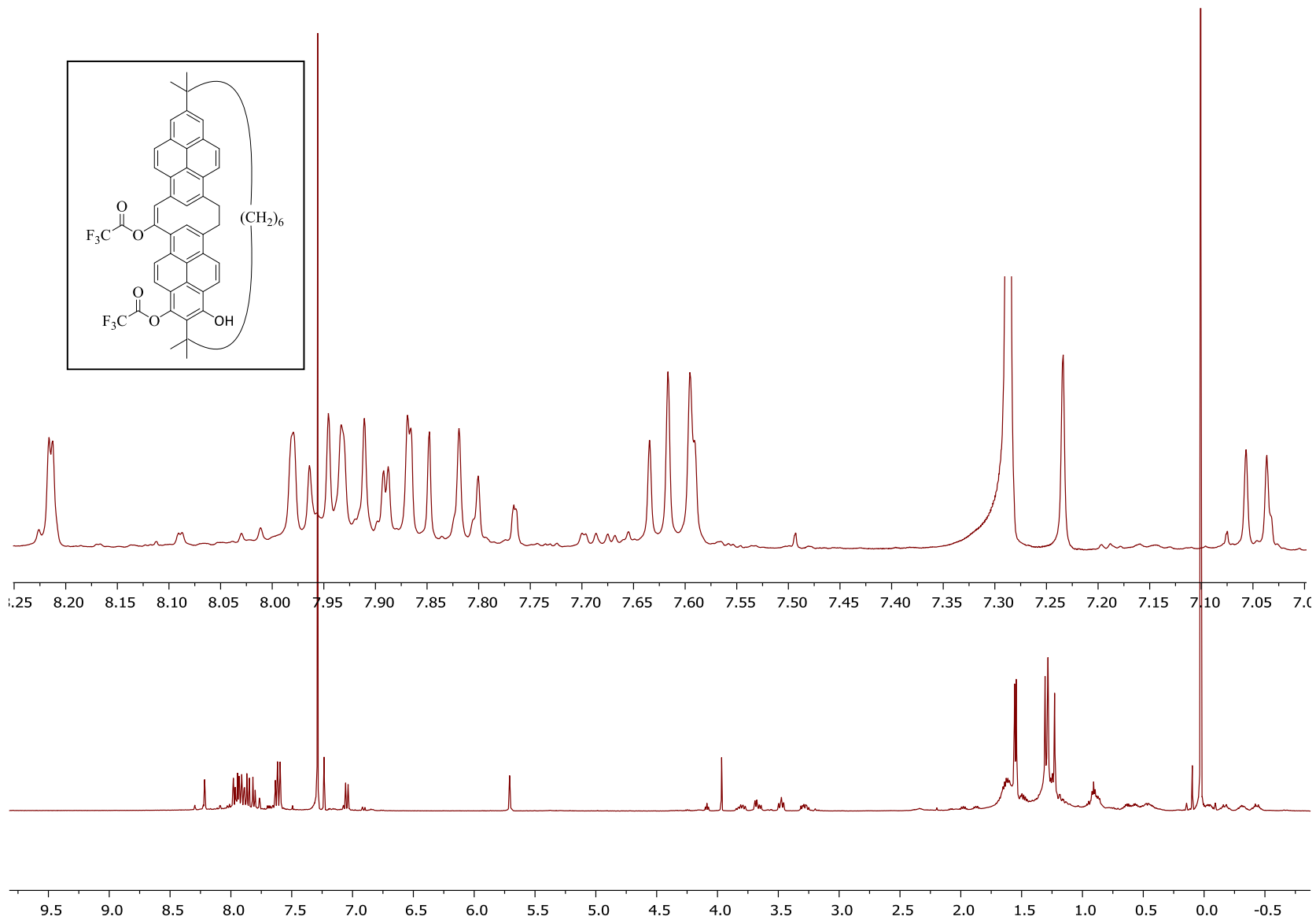




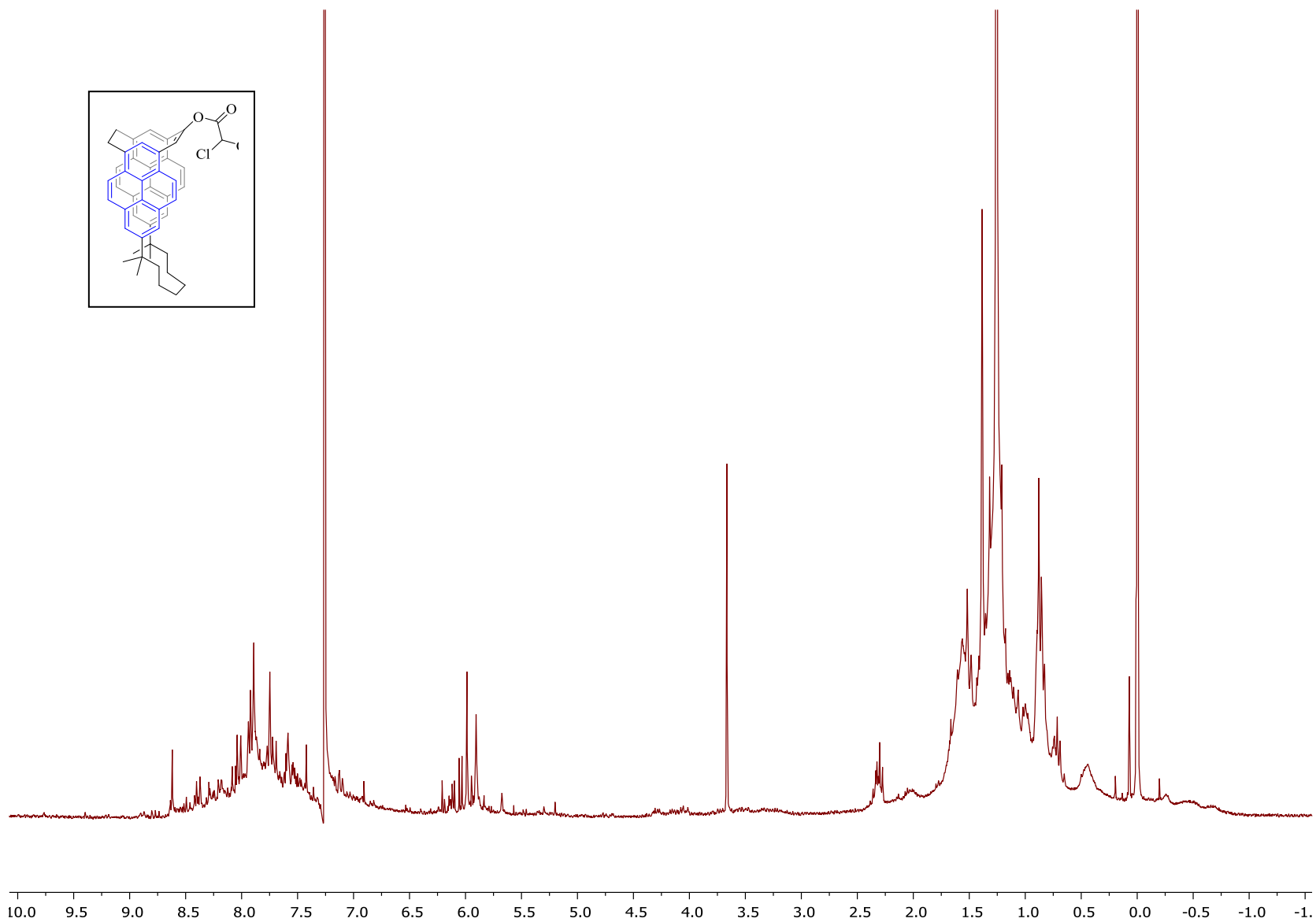
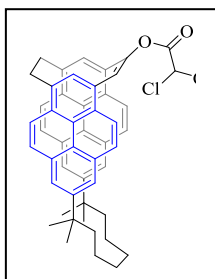


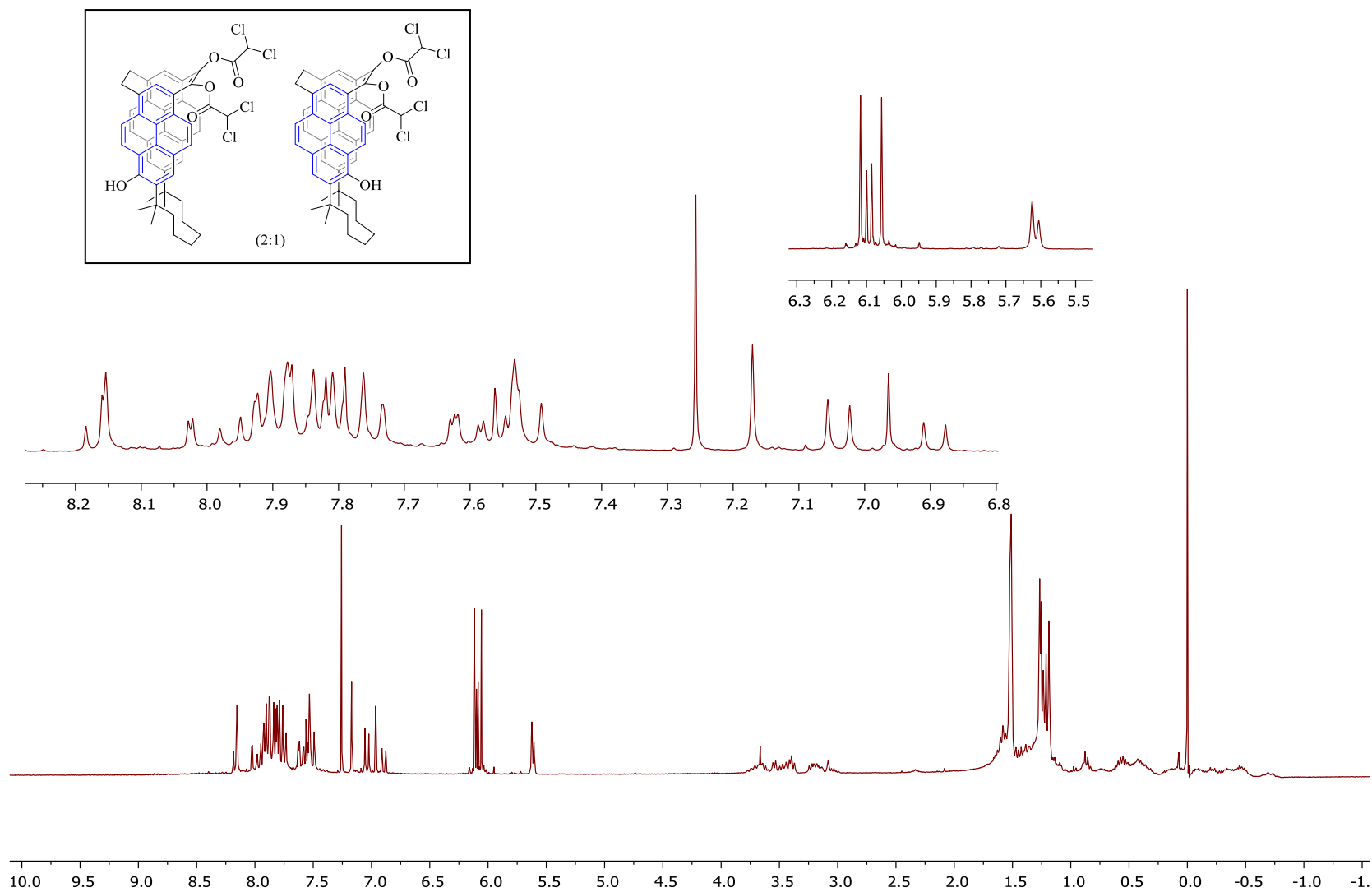
$^{19}\text{F}$  NMR

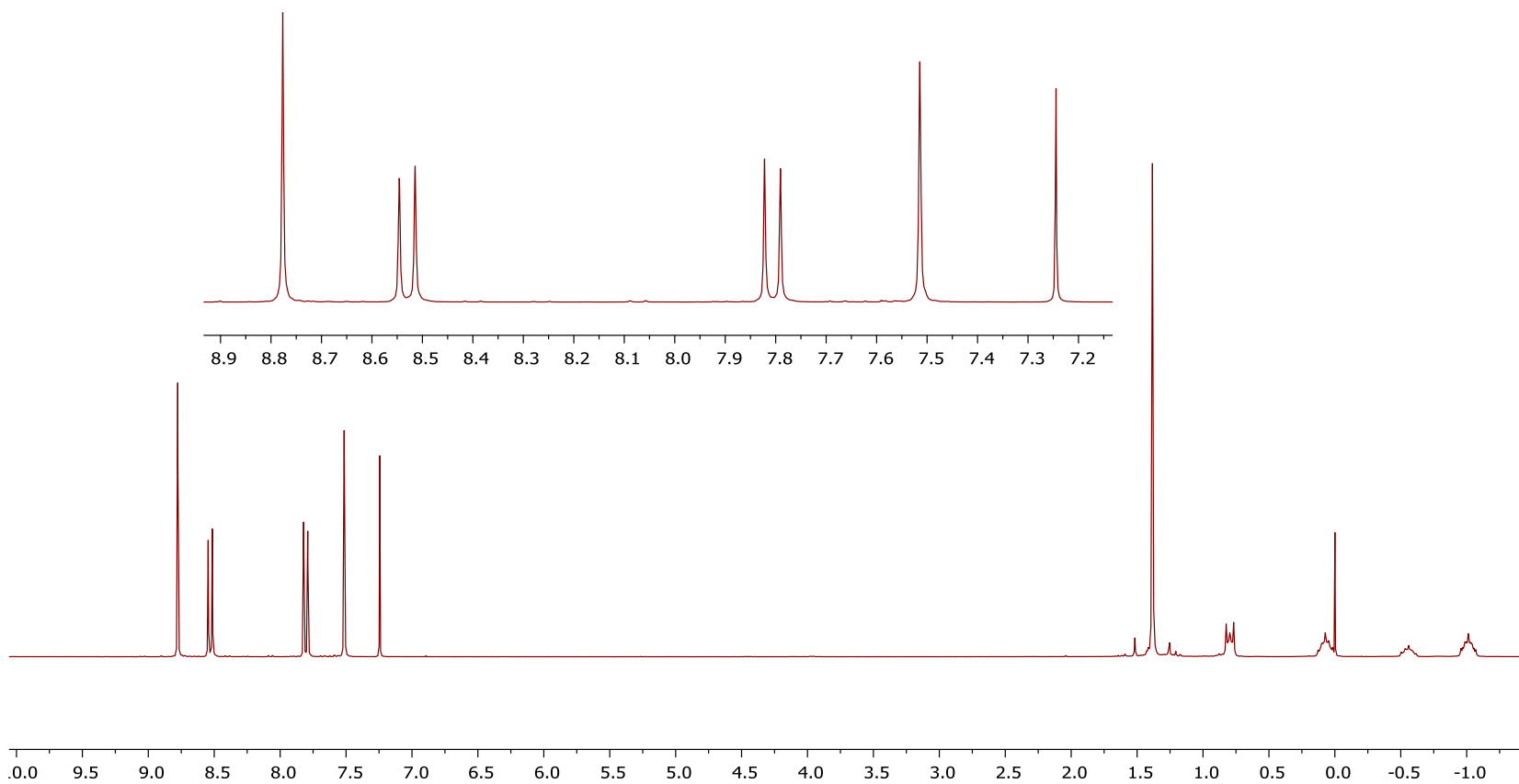
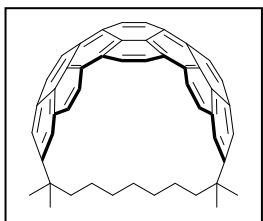


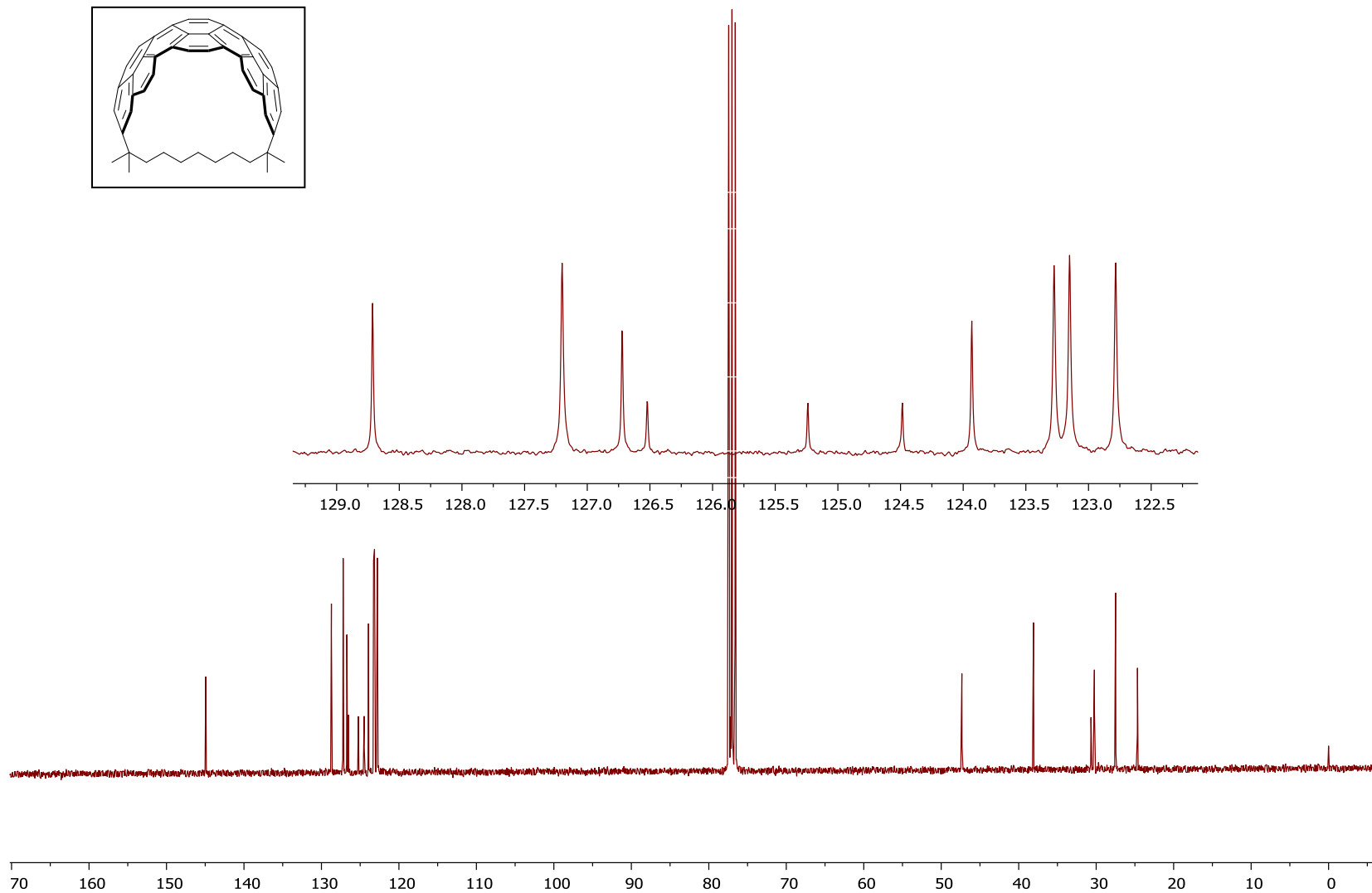
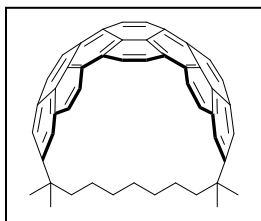




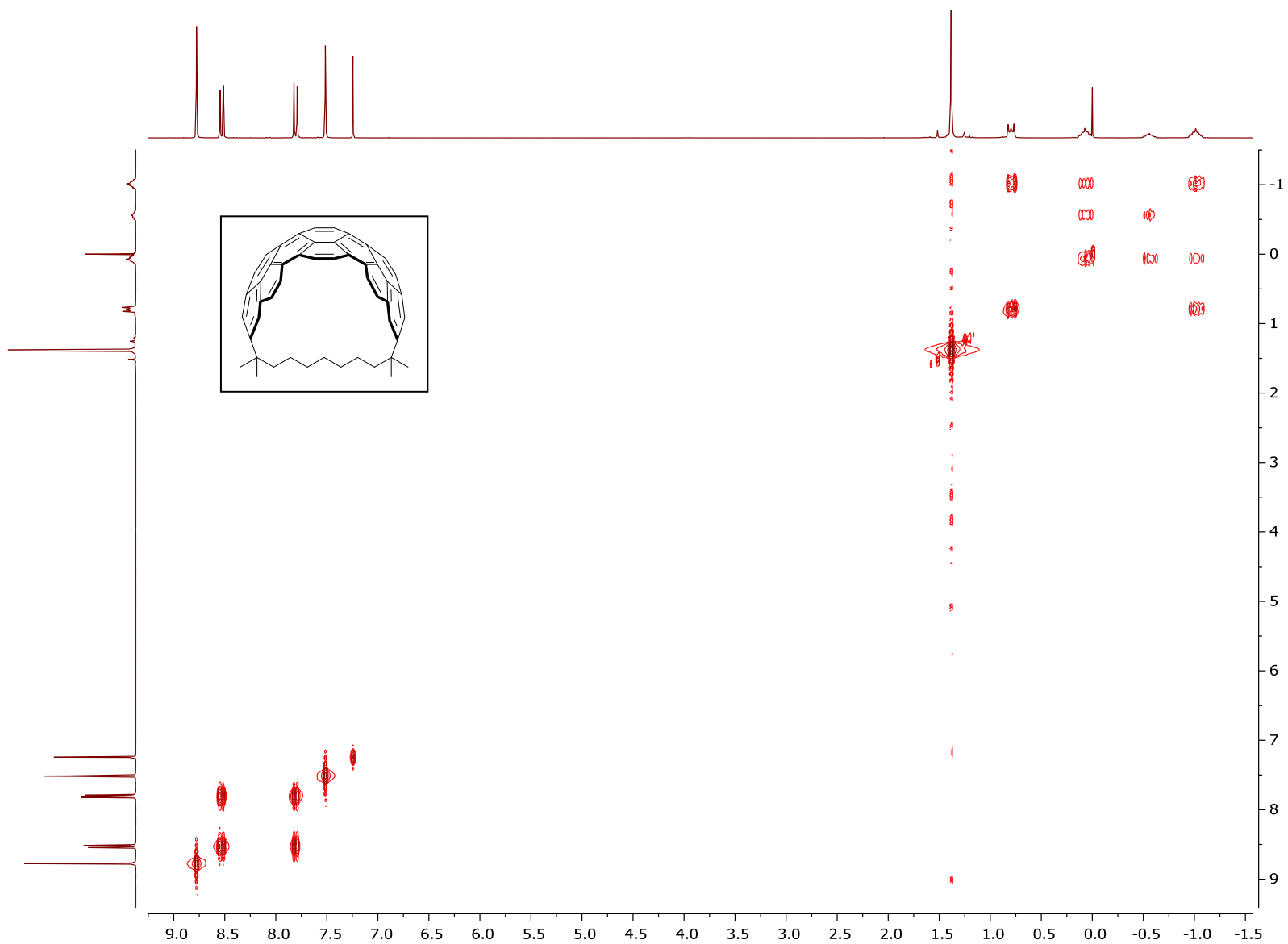


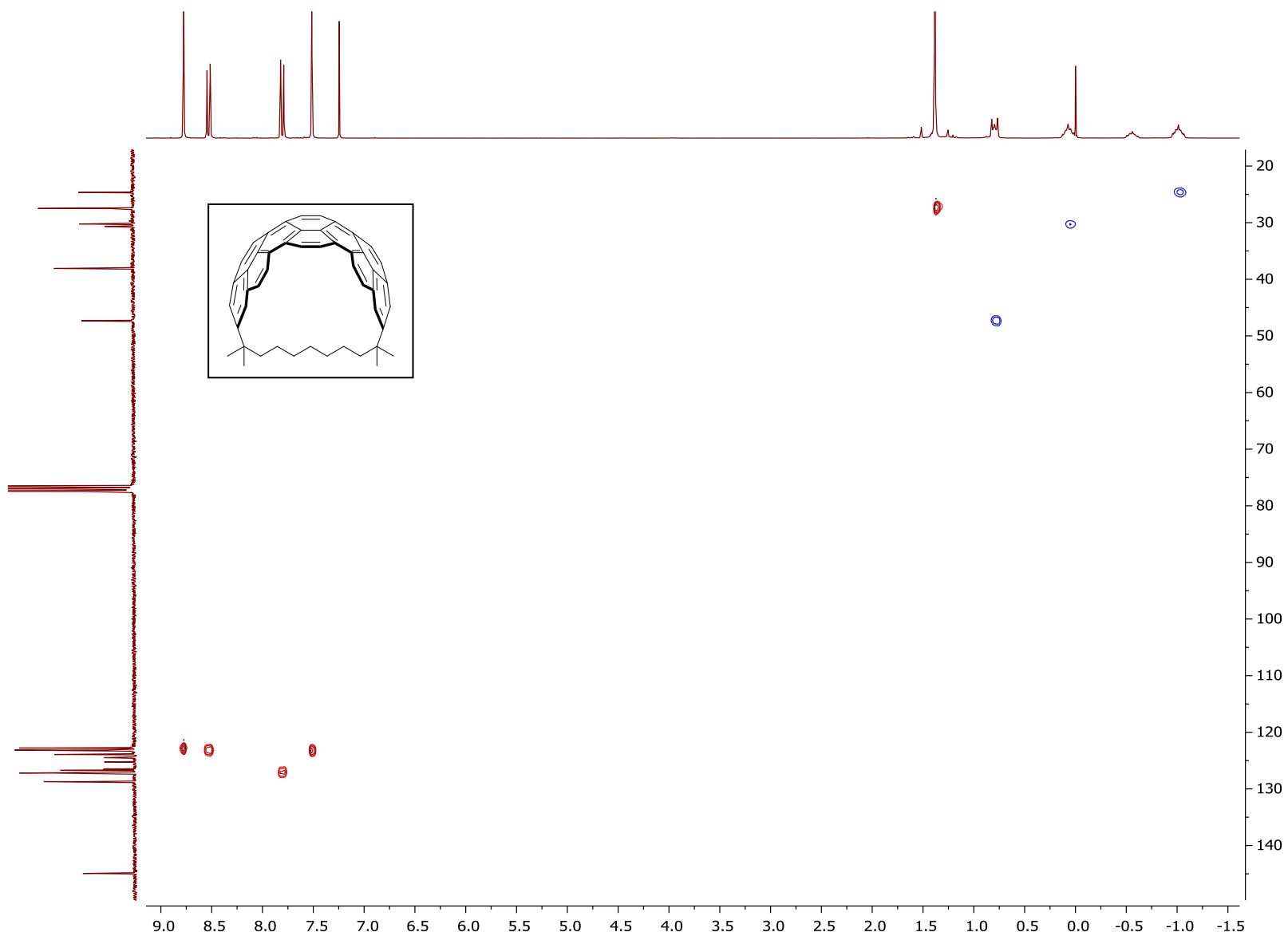


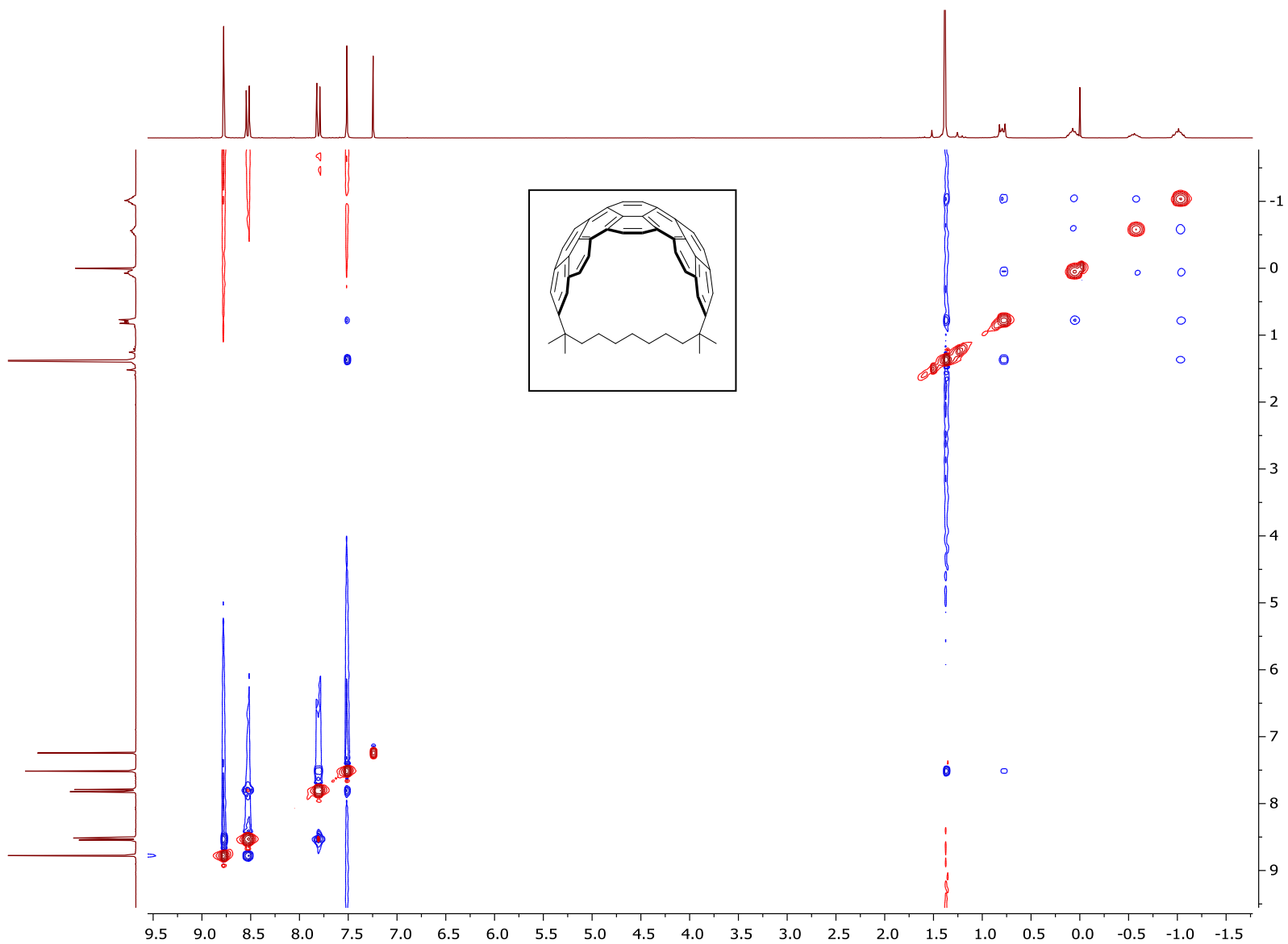


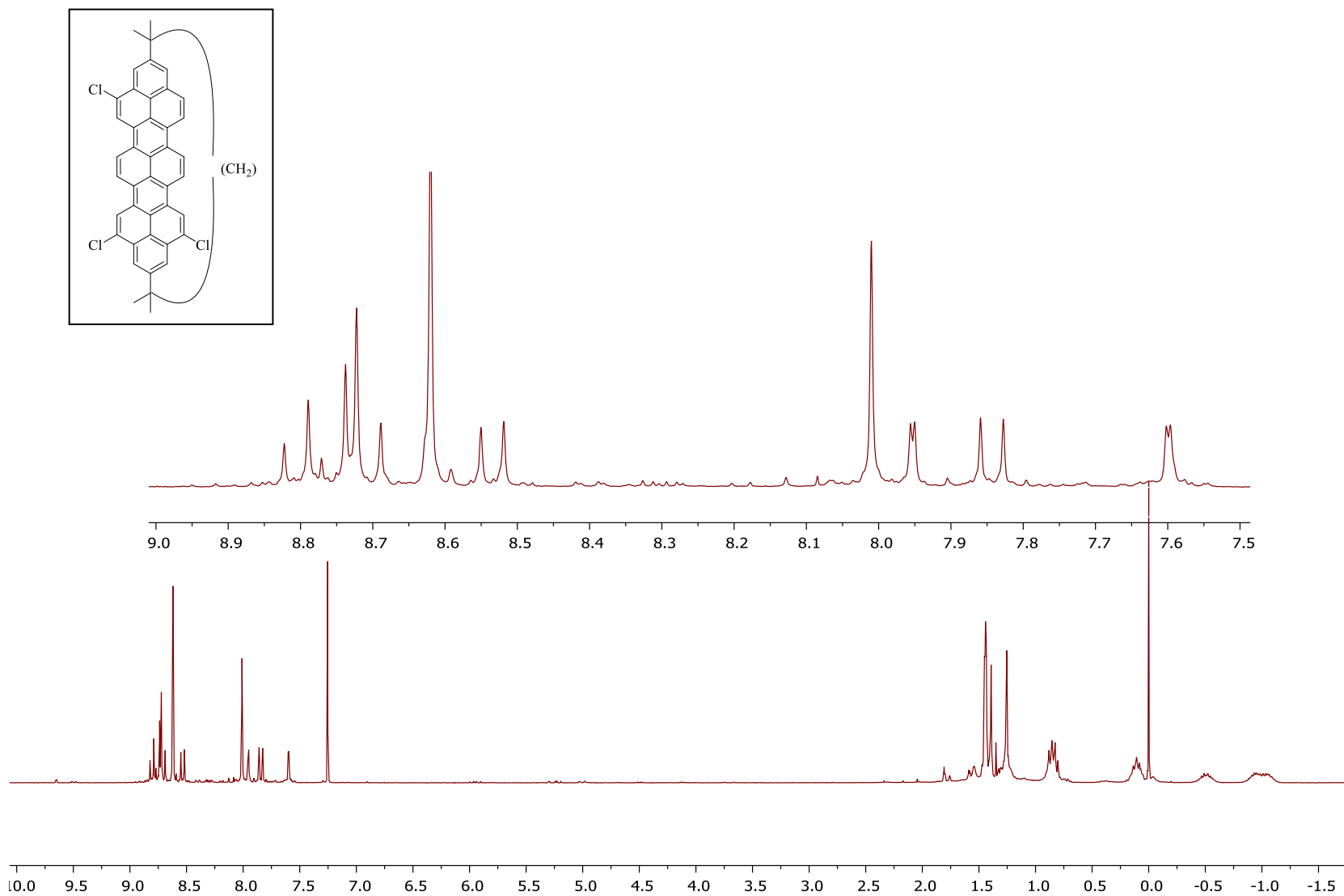


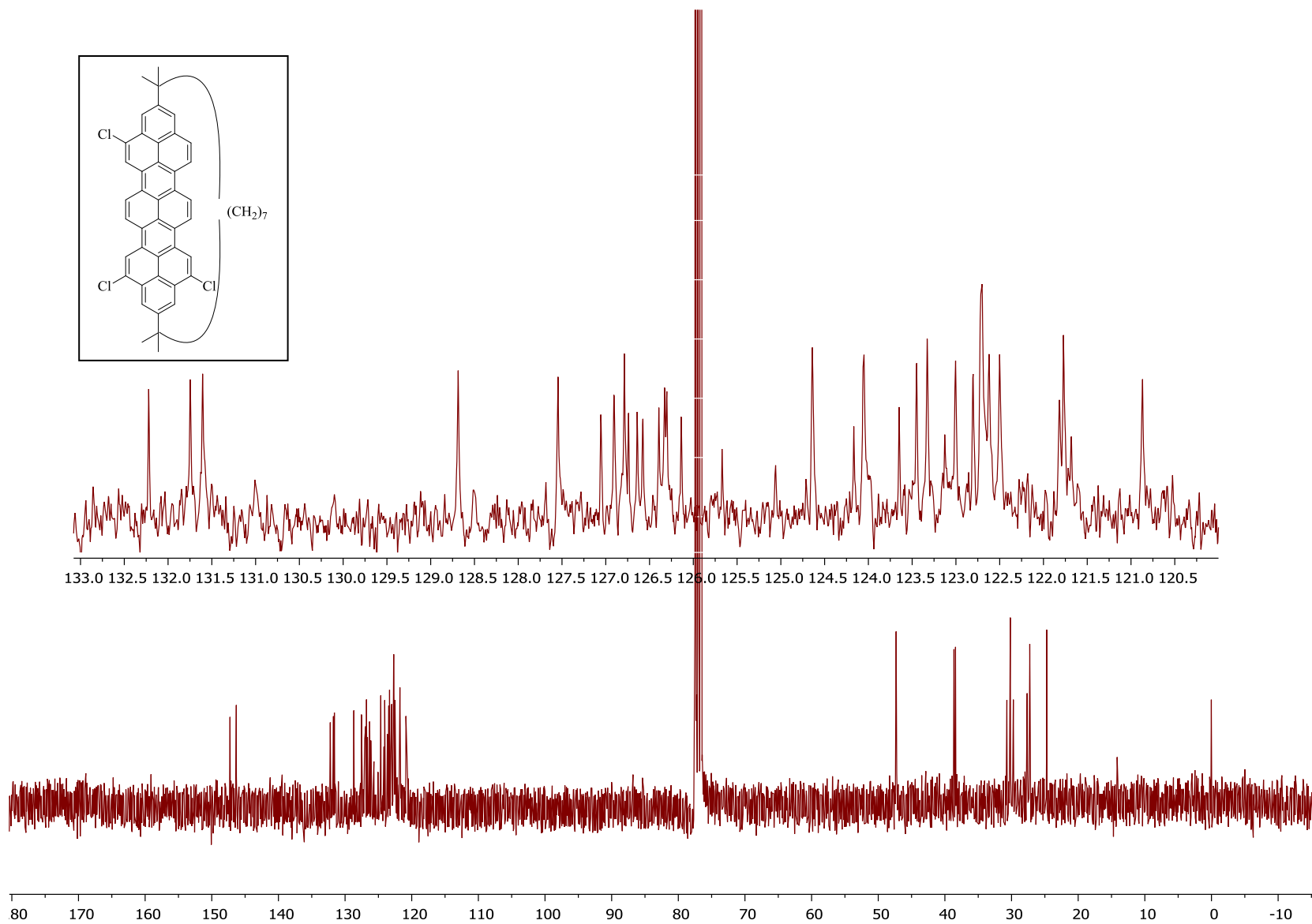




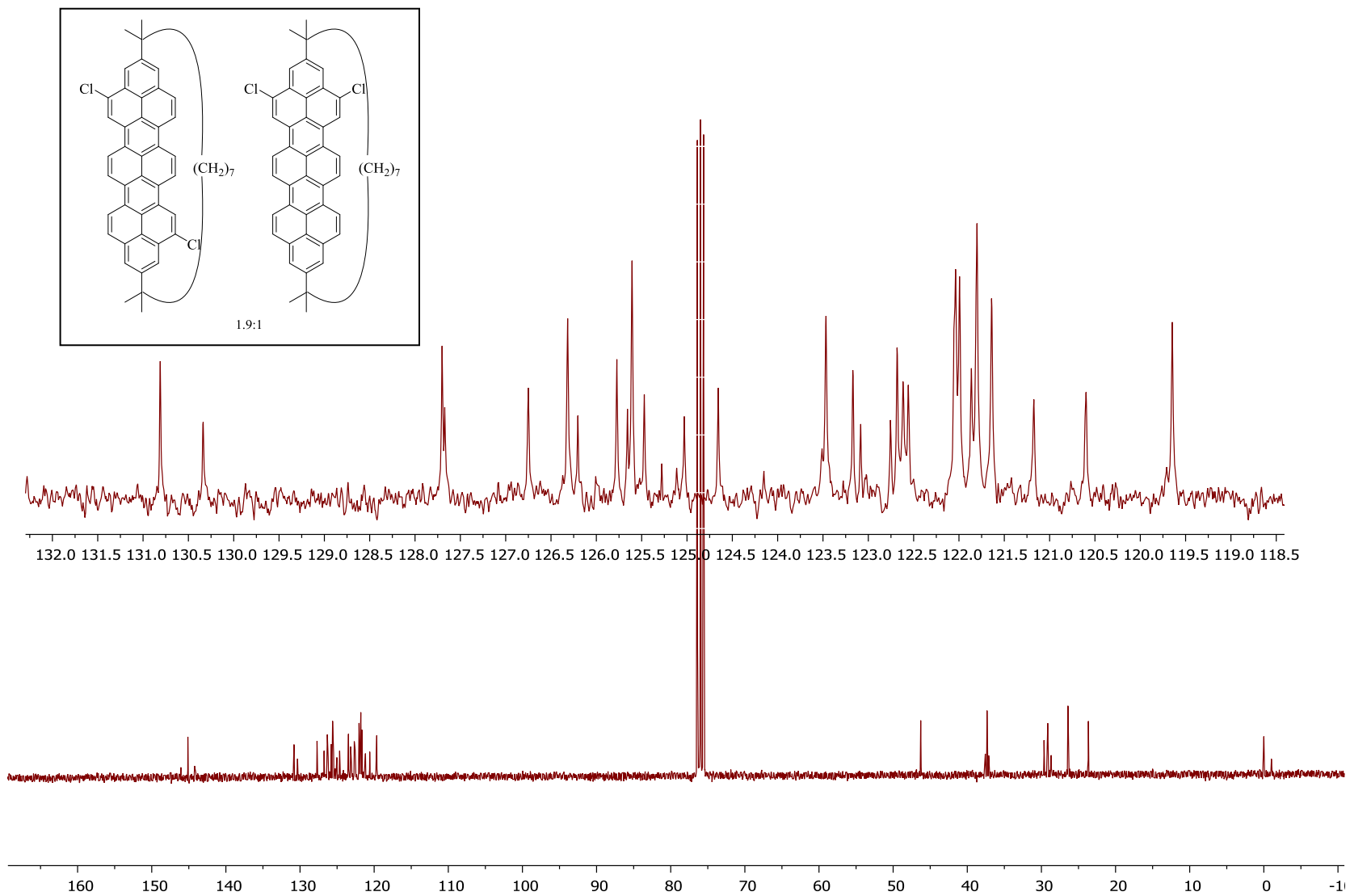


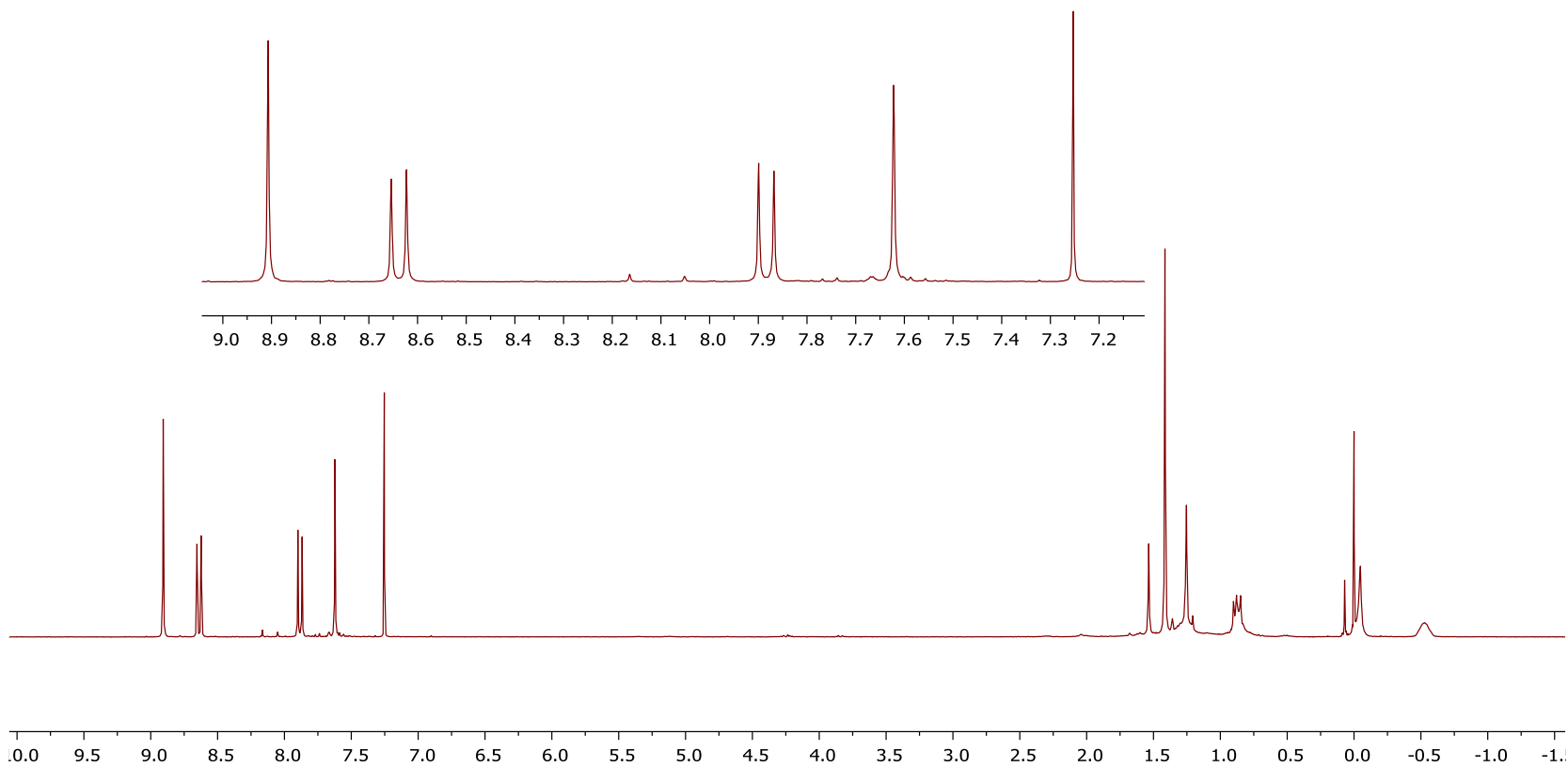
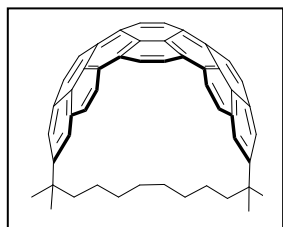




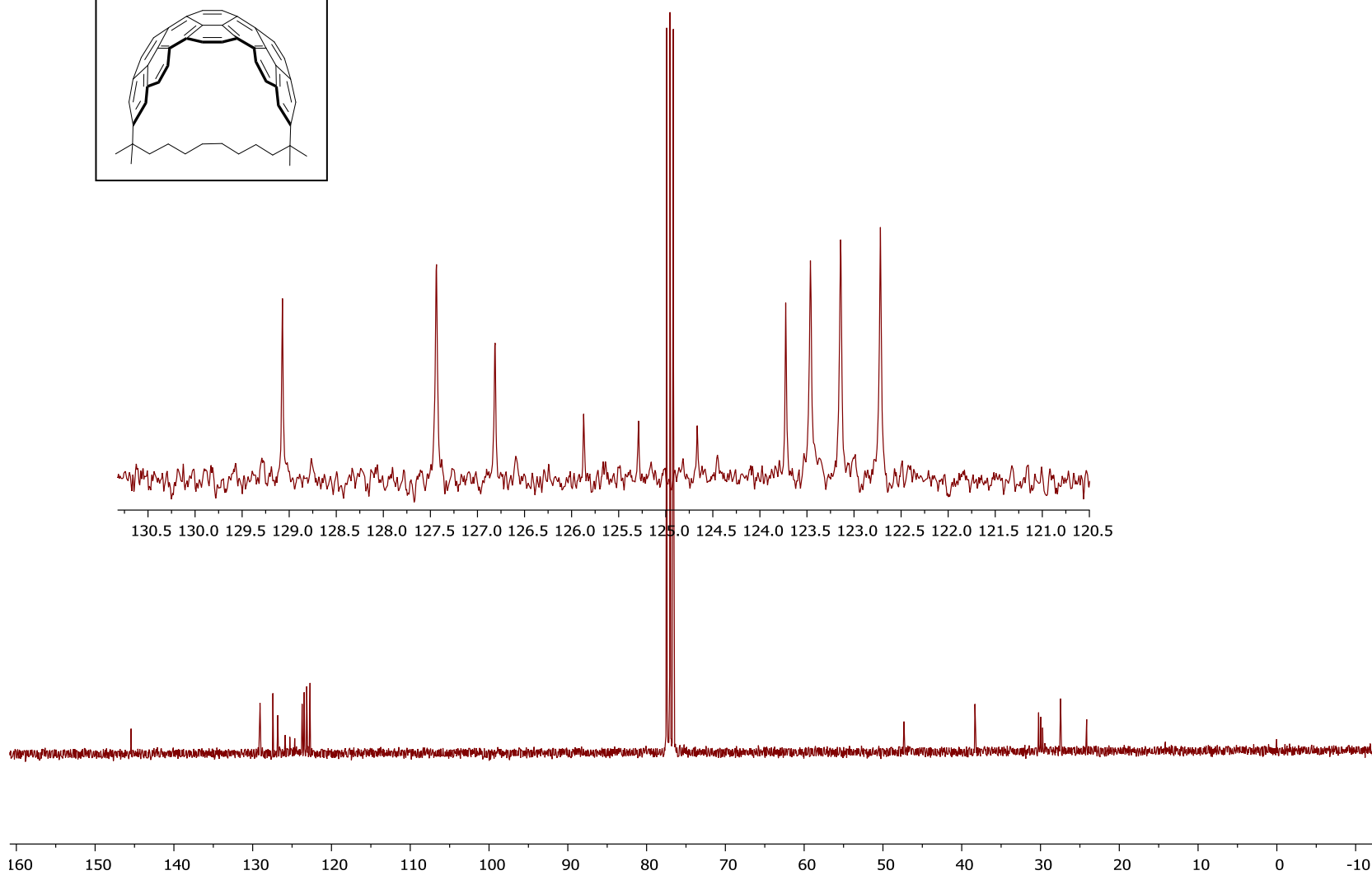
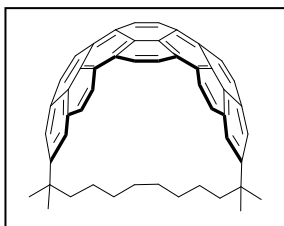


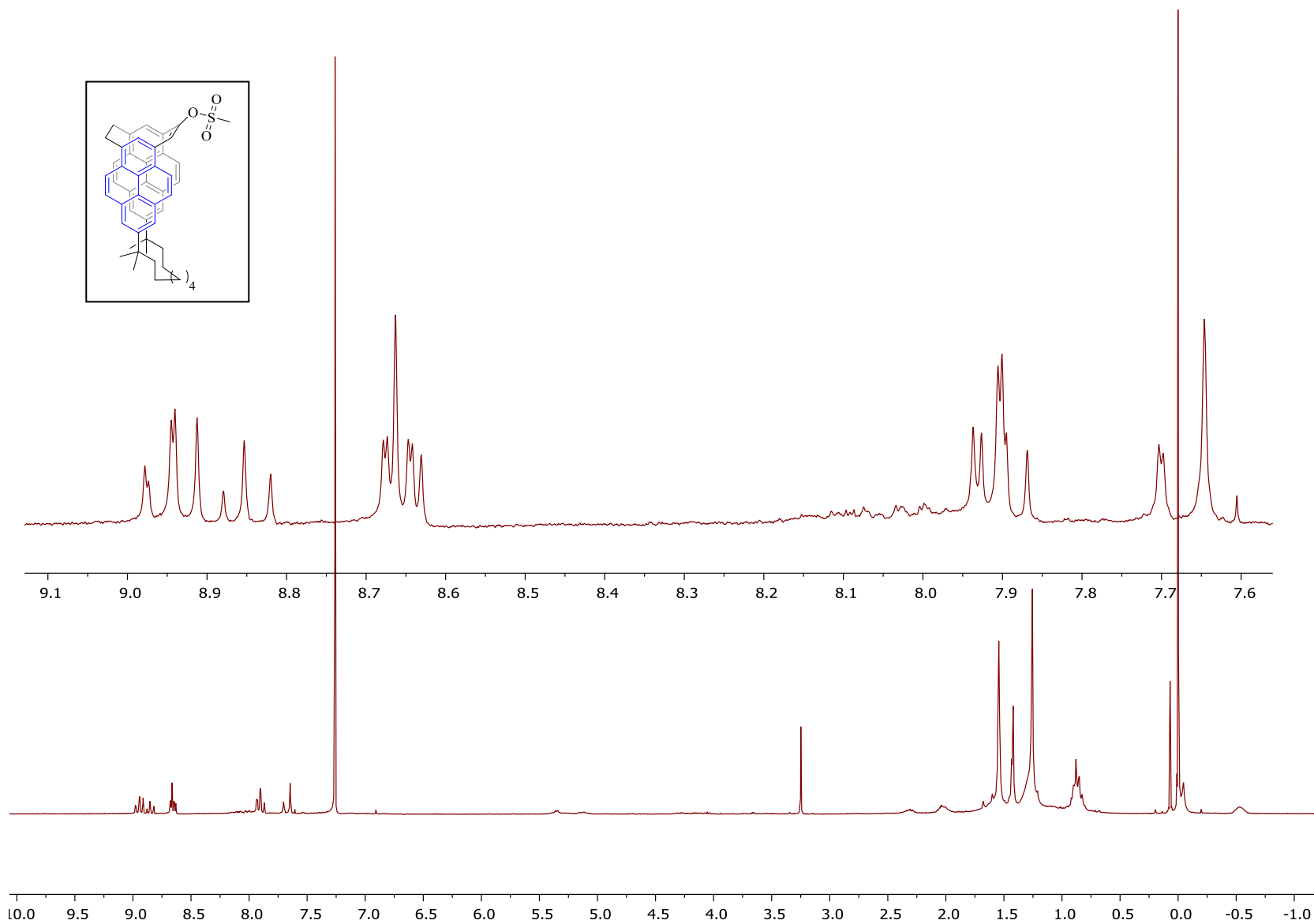


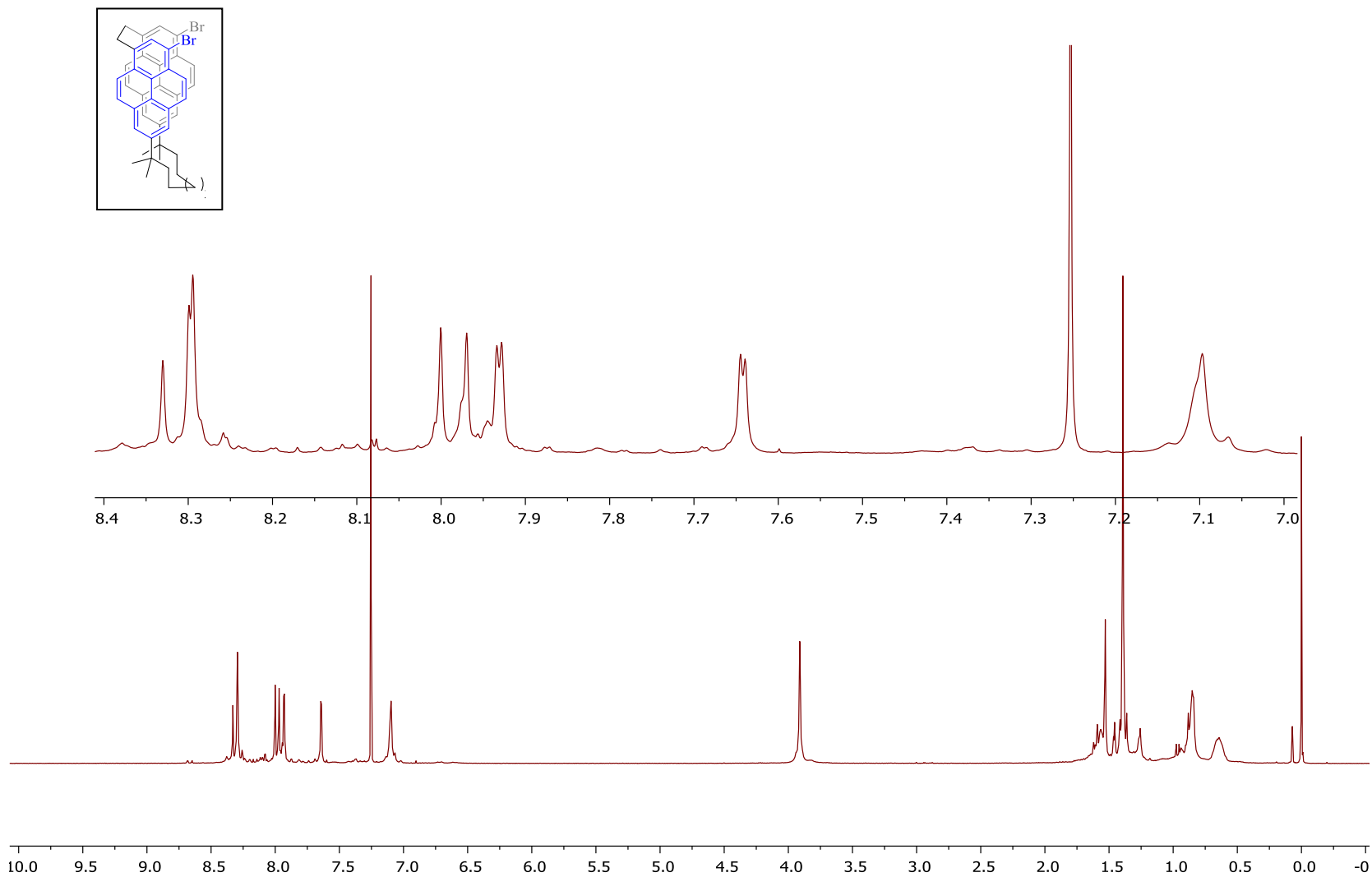
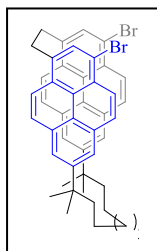


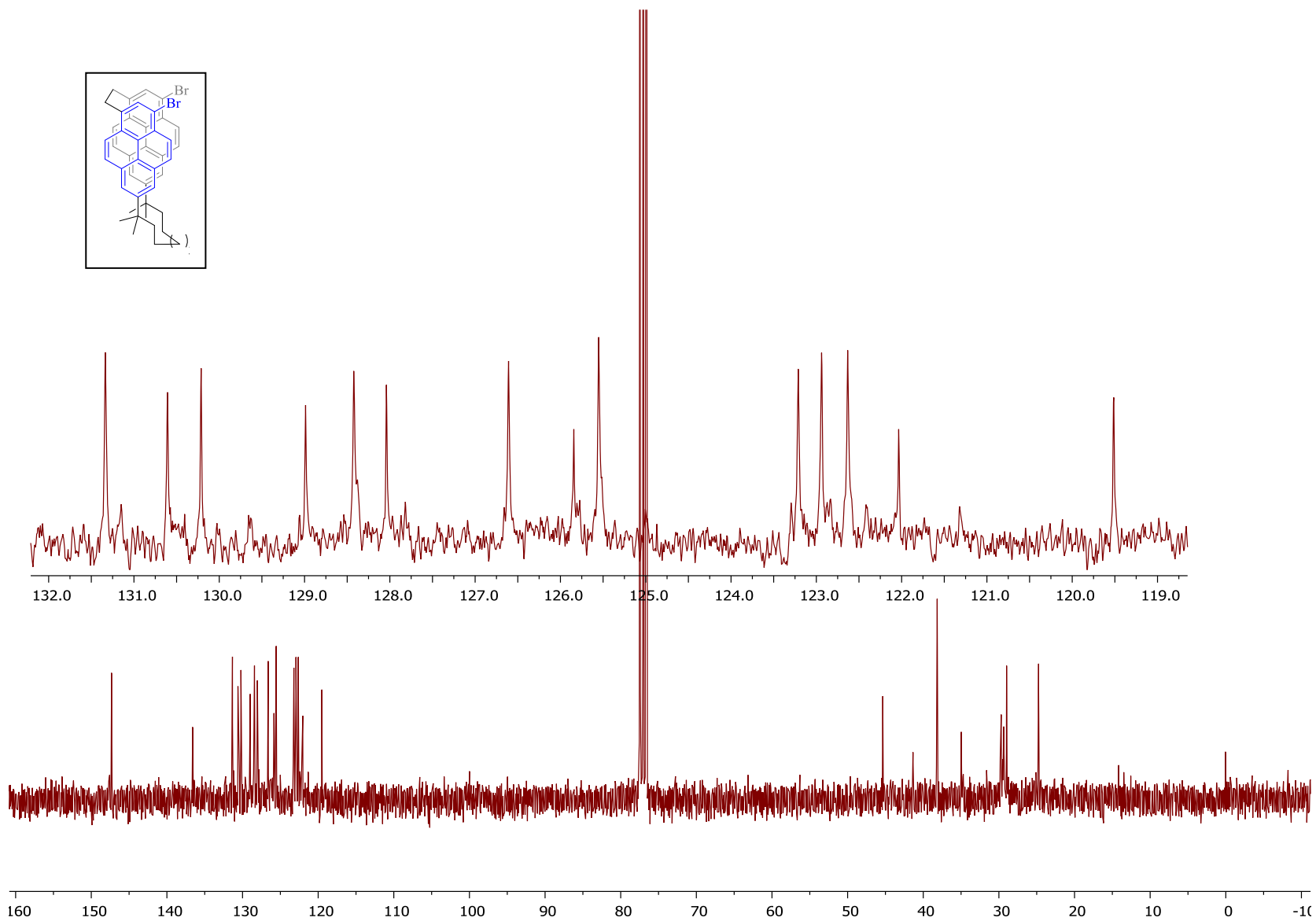
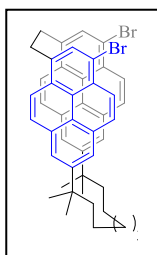


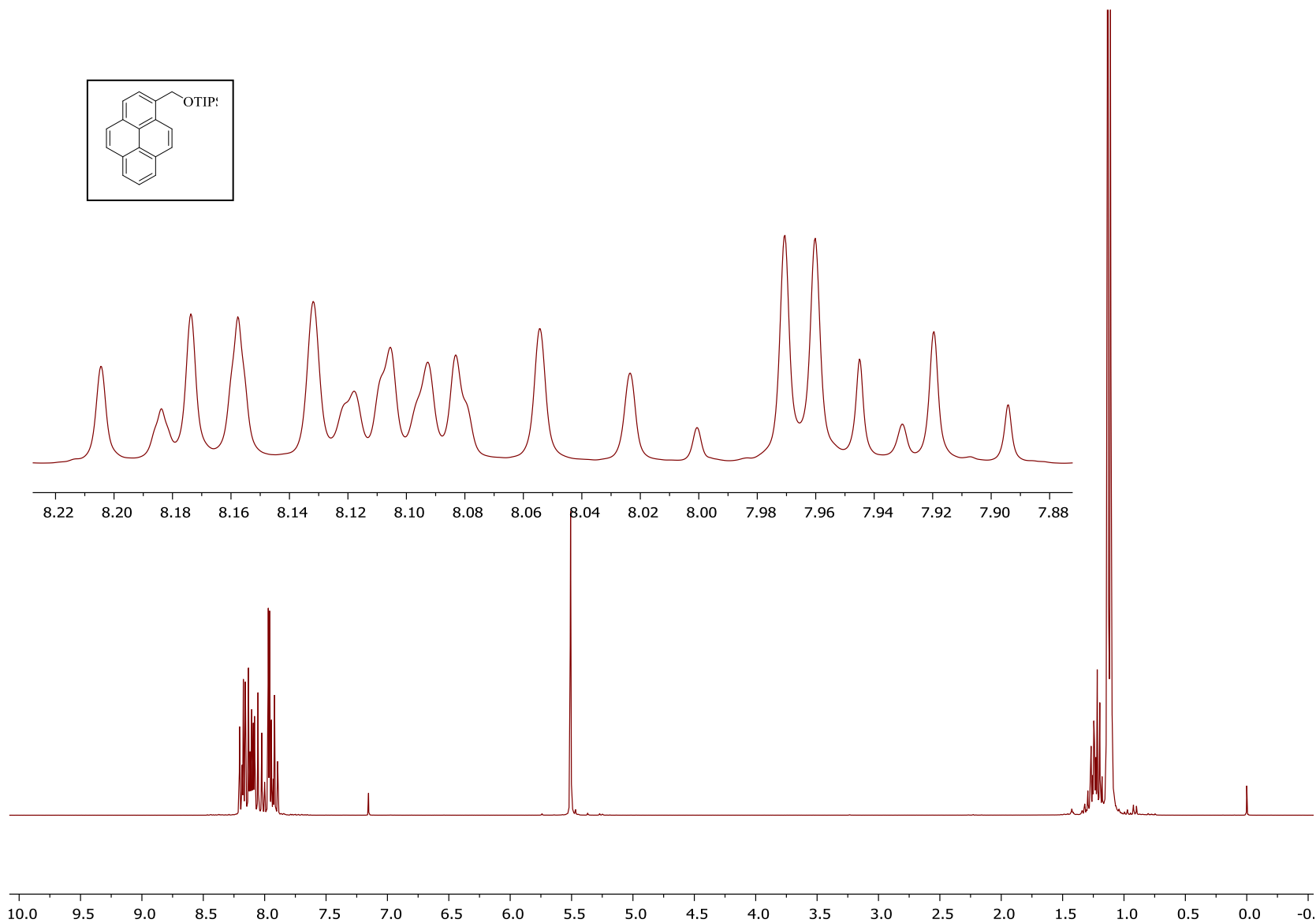
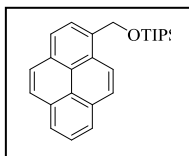


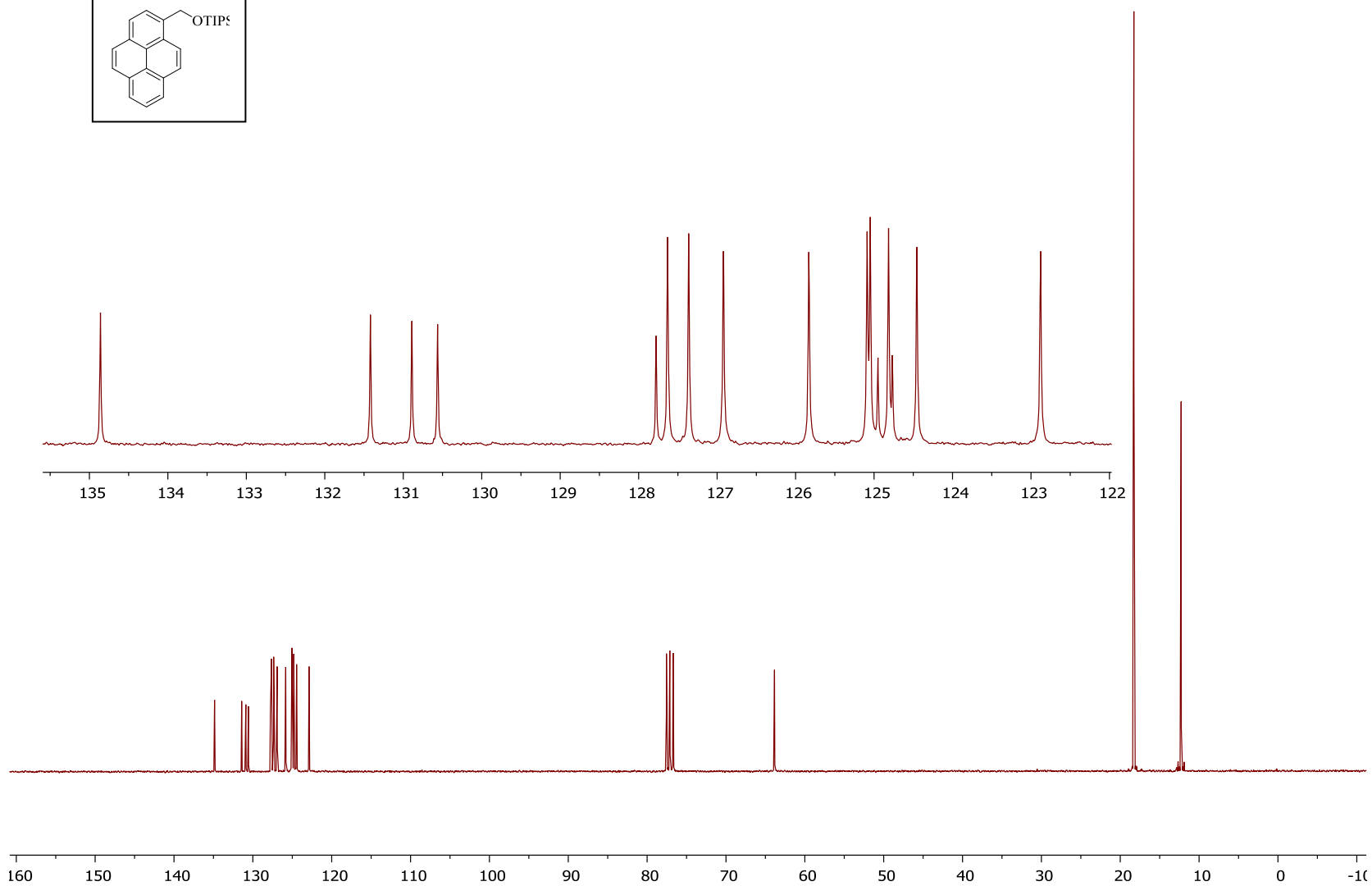
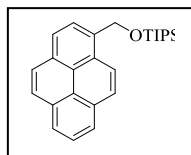


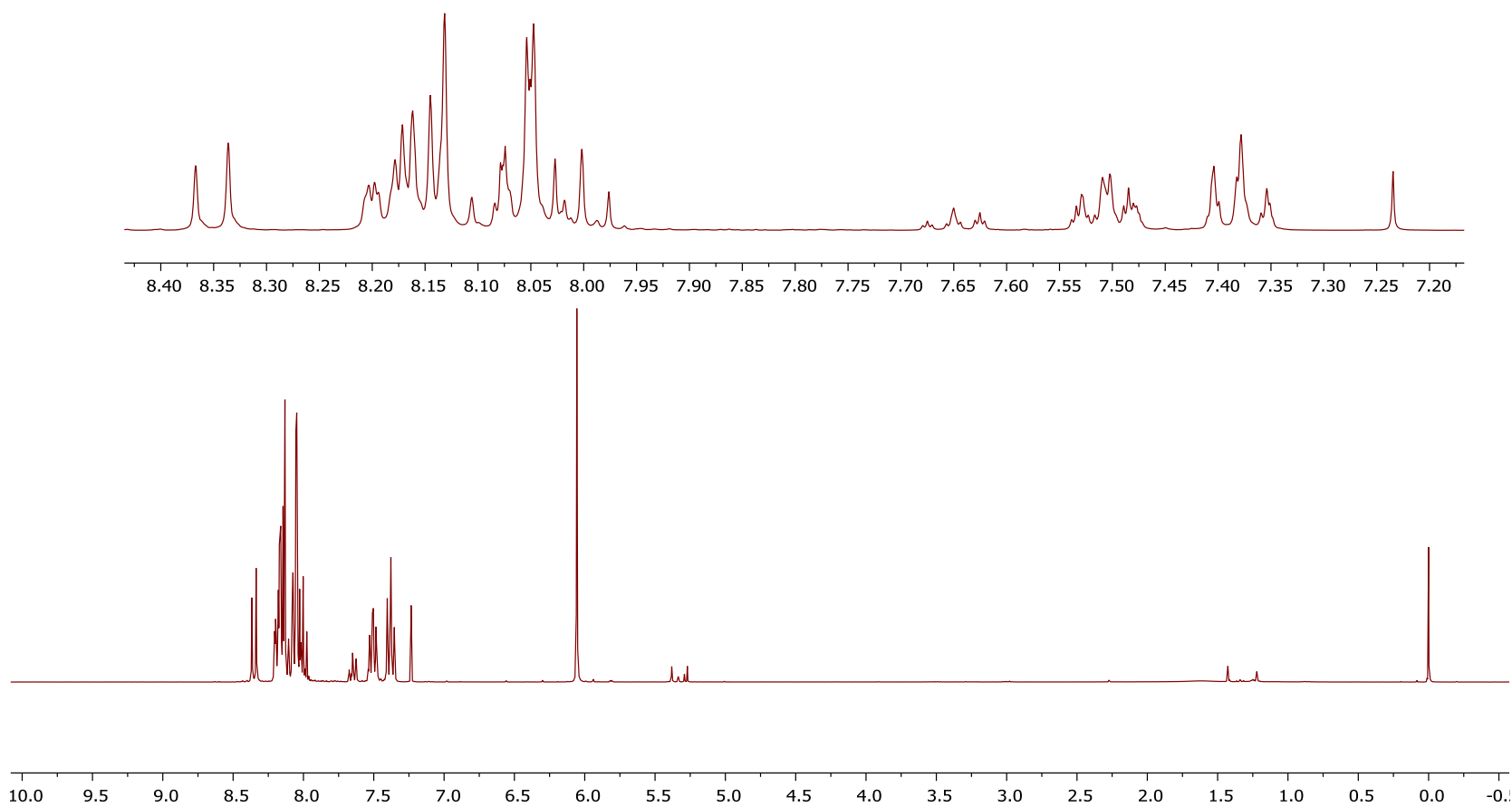
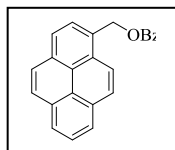


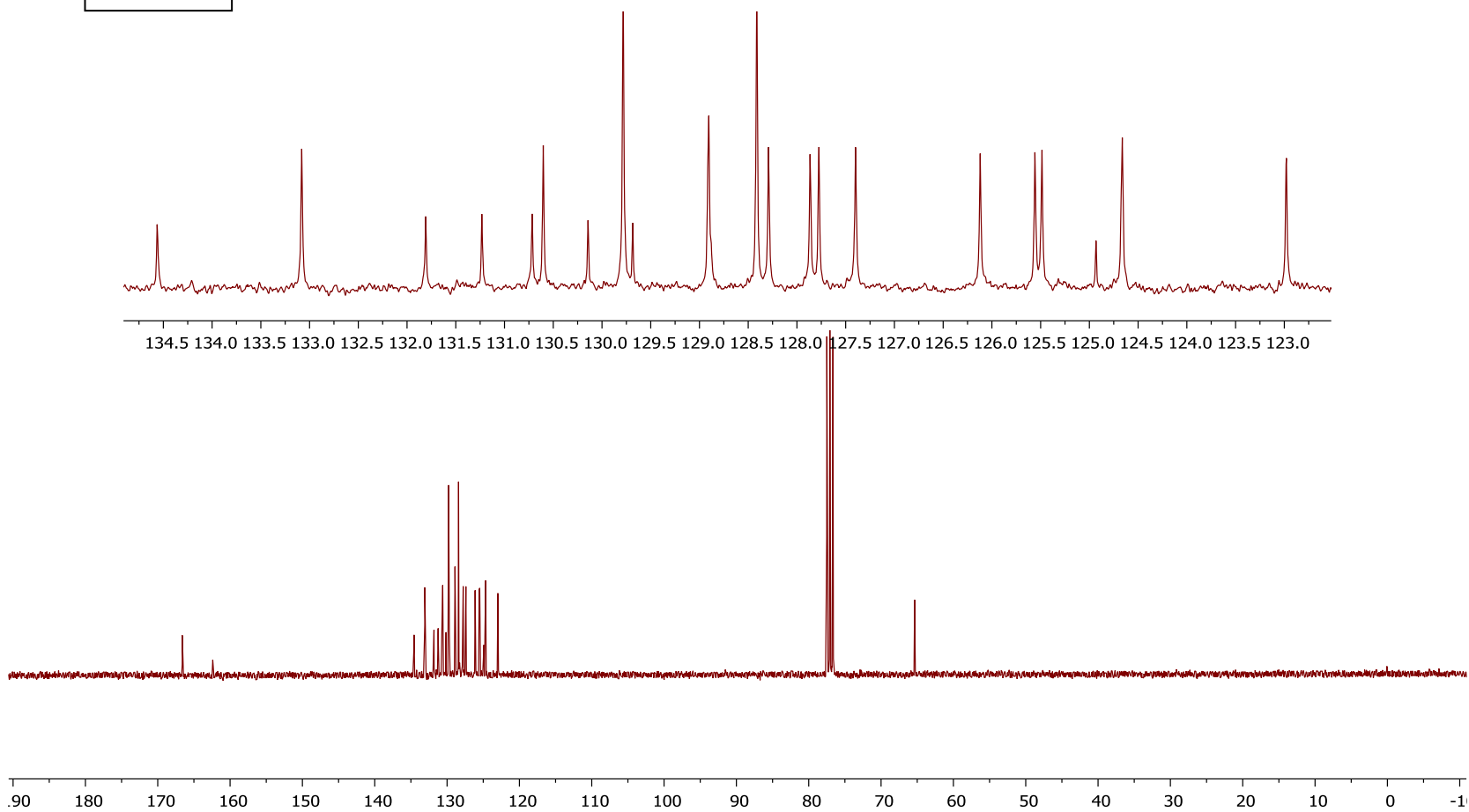
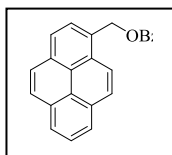














## Chapter 5: Bromination of the 1,1,*n,n*-Tetramethyl[*n*](2,11)teropyrenophanes

### 5.1 Introduction

The discovery of carbon nanotubes (CNT) as a mixture of multi-walled CNTs in 1991 by Iijima<sup>1</sup> marked the beginning of widespread interest in these new forms of carbon, which have remarkable mechanical (strongest known materials),<sup>2</sup> photophysical,<sup>3</sup> electrical,<sup>4</sup> photoelectrical<sup>5</sup> and guest encapsulating<sup>6</sup> properties. Methods for the production of single-walled carbon nanotubes (SWCNT) were developed soon thereafter.<sup>7</sup> The electronic properties (metallic or semiconducting) of SWCNTs depend on their structure, which is described by their (*n,m*) indices (often referred to as their “chirality”). When *n=m*, the structure is of the “armchair” type and when *m=0*, the structure is of the zig-zag type (Figure 5.01). Both of these types of nanotubes are achiral (in the classic organic sense). All other SWCNTs are chiral and are accordingly referred to as chiral SWCNTs. Current production methods such as chemical vapour deposition and arc discharge, which utilize metals as surfaces for nanotube growth and very high temperatures (> 500 °C), provide complex mixtures of SWCNTs that differ in their length, diameter and structure. Tedious, expensive and imperfect purification methods are required to separate them from multi-walled CNTs, metal particles and amorphous carbon to afford metal-free, SWCNTs. The production or separation of specific SWCNTs is still an unsolved problem. As an alternative to these top-down approaches, a bottom-up approach to the production of single-chirality SWCNTs is to synthesize well-defined segments of SWCNTs and use them as seeds for nanotube growth, either using existing

production methods or synthetic organic methods.

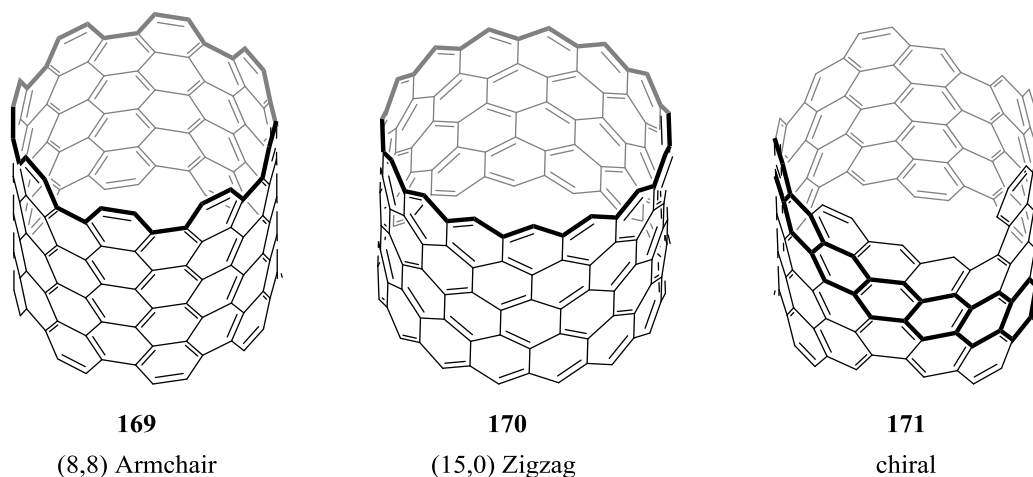


**Figure 5.01** Arm-chair, zig-zag and chiral CNTs.

Aromatic belts such as the Vögtle belts (**171**)<sup>8</sup> and cycloparaphenylenes (CPP) (**113**)<sup>9</sup> correspond to small segments of armchair SWCNT sidewalls, whereas the cyclacenes (**172**) correspond to small segments of zig-zag SWCNT sidewalls. On the other hand, corannulene (**112**)<sup>10</sup> and related buckybowls **111** correspond to end-cap segments (Figure 5.02). All of these compounds could conceivably function as seeds for single-chirality SWCNT growth. Some progress toward the achievement of these goals has been made using both CPPs<sup>11</sup> and buckybowls,<sup>12</sup> but the control of the nanotube structure has not been complete. This is presumably due to isomerization of the nanotubes at the high temperatures used for growth or, in the case of CPPs, rupture of the seeds (heterolytic cleavage of a biaryl bond) prior to growth.

Edge functionalization of the seeds followed by growing them chemically in a stepwise and controlled manner at lower temperatures may prove to be a more

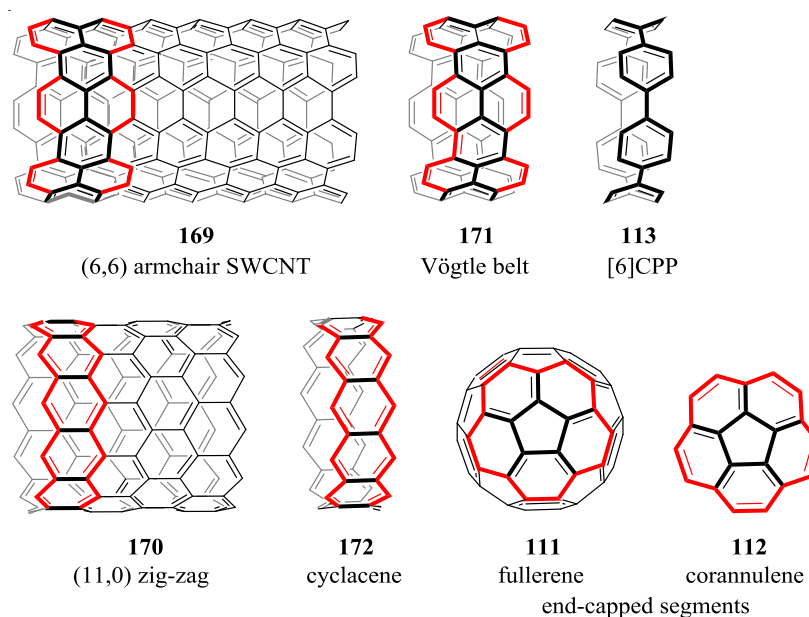


**Figure 5.02** Segments of armchair and zig-zag CNTs and fullerenes.

effective approach. Unfortunately, despite access to synthetically useful amounts of materials, controlled direct functionalization of buckybowls and CPPs is problematic. Recently, penta, and deca-halogenation on the side rim of corannulene was reported,<sup>13</sup> which ultimately allowed the introduction of various other substituents on the rim. One of these compounds, 1,3,5,7,9-pentachlorocorannulene, was converted into a short end-capped (5,5) SWCNT segment.<sup>14</sup> For the CPPs, direct functionalization suffers from a lack of regioselectivity and separation issues, which means that substituents have had to be carried through from the beginning of the synthesis. This brings with it limitations to the nature, number and positions of the substituents.<sup>11b</sup>

Aromatic belts such as the Vögtle belts (**171**) would be expected to avoid the problem of CPP rupture, but nanotube isomerization (*e.g.* by Stone-Wales rearrangement) at high temperature may still be a problem. In any event, free-standing belts have not yet

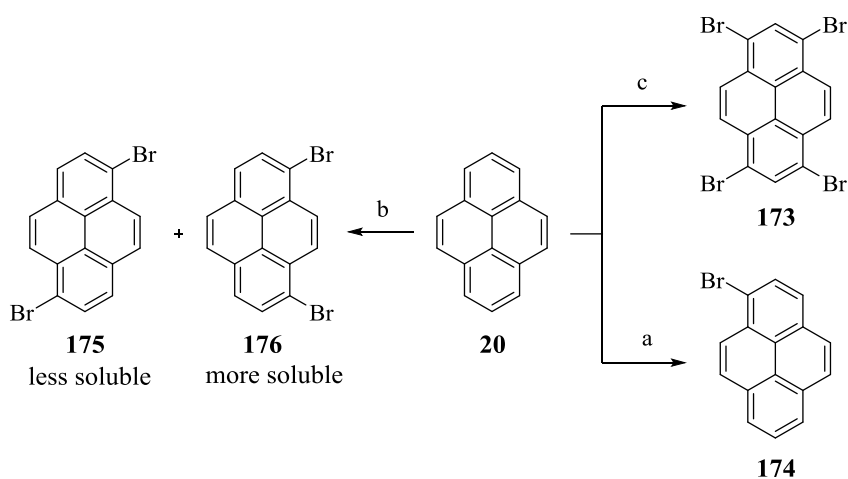
been synthesized. Despite several concerted efforts, the same is true for the cyclacenes (**172**), which are predicted to have rather low stability.<sup>15</sup>

The aromatic systems in the 1,1,*n,n*-tetramethyl[*n*](2,11)teropyrenophanes (*n* = 7-10) **103b-e** described in Chapters 2-4 structurally resemble about half of a Vögtle belt and one of them, 1,1,9,9-tetramethyl[9](2,11)teropyrenophane (**103d**), was synthesized on a multi-gram scale.<sup>16</sup> Having access to synthetically useful amount of this nicely soluble compound provided the opportunity to study the chemistry of the teropyrene system. Since the parent (planar) teropyrene is vanishingly soluble, nothing is known about its chemistry. Lessons learned from this work may be prove to be valuable when aromatic belts eventually become available. Bromination was chosen as the first reaction to study because of the variety of subsequent reactions that aryl bromides can participate in. Since teropyrene **21** is a higher homologue of pyrene (**20**) in the capped rylene series, it would be instructive to first review the bromination chemistry of pyrene.

### 5.1.1 Bromination chemistry of pyrene

Pyrene (**20**) undergoes electrophilic aromatic substitution reactions with very high selectivity for the 1, 3, 6 and 8 positions as preceded by numerous experimental and theoretical studies.<sup>17</sup> The only exception is Friedel-Crafts *tert*-alkylation, which is completely selective for the 2 and 7 positions due to steric effects. The bromination of pyrene occurs with the normal 1,3,6,8 regioselectivity and, depending upon the conditions, can be use to introduce anywhere from one to four bromine atoms. Since Br is a deactivating substituent, each successive bromination becomes slower, so good

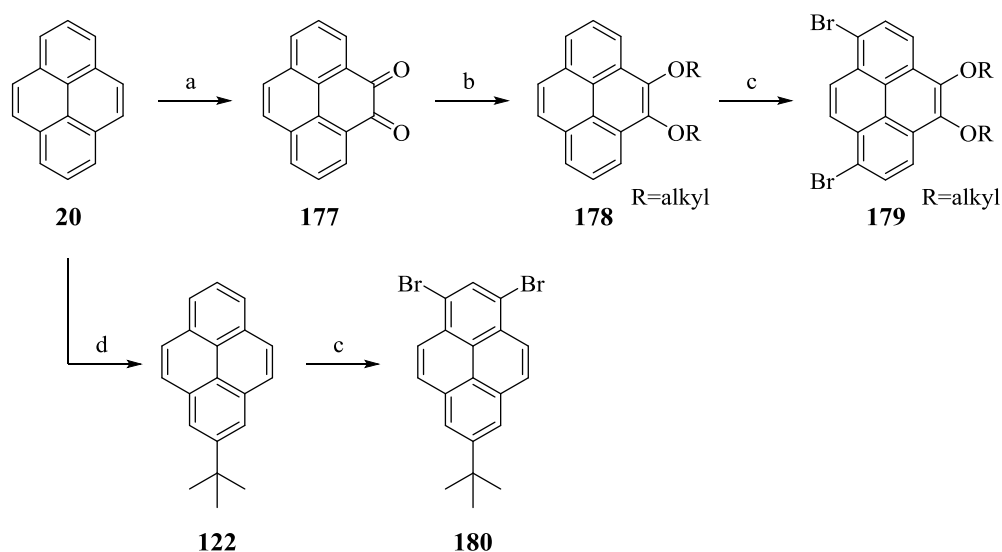
selectivity for the number of Br atoms can be achieved by controlling the number of equiv. of brominating agent. Monobromination to afford **173** occurs under mild conditions, whereas the synthesis of 1,3,6,8-tetrabromopyrene (**174**) requires quite forcing conditions (Scheme 5.01). For the dibromination of pyrene, a regioselectivity issue arises. Of the three dibromides that could potentially form (1,3-, 1,6- and 1,8), the latter two form in roughly equal amounts and make up the majority (> 90%) of the product mixture. This is in line with expectations based on the inductive electron withdrawing and *ortho/para*-directing nature of Br as a substituent, both of which would be expected to disfavour formation of the 1,3-isomer. Of the two major isomers, 1,6-dibromopyrene (**175**) is less soluble and it can be obtained in pure form by repeated fractional crystallization. The more soluble 1,8-isomer **176** can be purified through further crystallizations, but the process can be troublesome.<sup>18</sup>



**Scheme 5.01** Reagents and conditions: a) HBr (1.1 eq), H<sub>2</sub>O<sub>2</sub> (1.0 eq), CH<sub>3</sub>OH/Et<sub>2</sub>O (1:1), rt, 12 h, 95%; b) Br<sub>2</sub>, CCl<sub>4</sub>, 17 h; c) PhNO<sub>2</sub>, Br<sub>2</sub>, 120 °C, 100%.

Introducing alkoxy groups at the 4,5-positions (*via* diketone **177**) results in

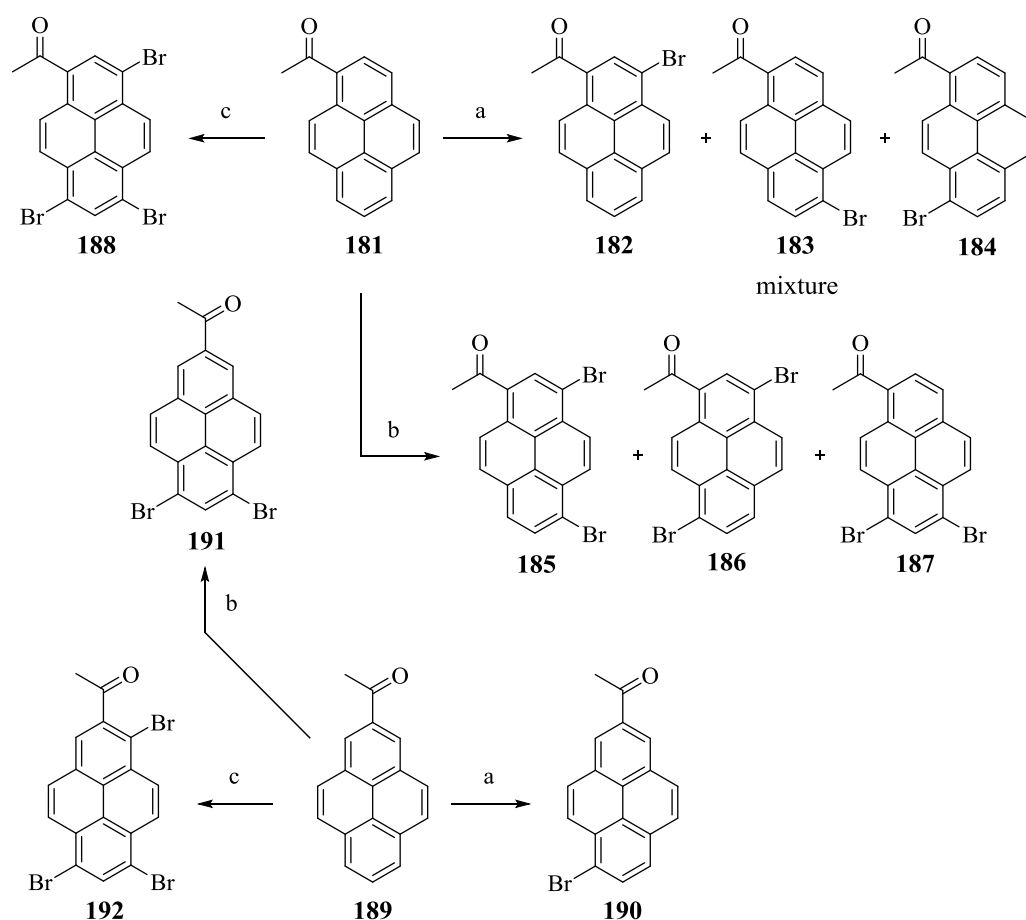
complete regioselectivity for 1,8-dibromo-4,5-dialkoxypyrene (**179**) (Scheme 5.02).<sup>19</sup> Access to the 1,3 substitution pattern can also be achieved through the introduction of a substituent. In this case, the presence of a bulky *t*-butyl group at the 2 position of pyrene hinders bromination at the sites *ortho* to it. As a result, completely selective bromination takes place at the other end of the molecule to afford 1,3-dibromo-7-*t*-butylpyrene (**180**).<sup>20</sup>



**Scheme 5.02** Reagents and conditions: a)  $\text{RuCl}_3 \cdot 3\text{H}_2\text{O}$ ,  $\text{NaIO}_4$ , THF,  $\text{CHCl}_3$ ,  $\text{H}_2\text{O}$ , 2.5 h, 45%; b) 1.  $\text{Na}_2\text{S}_2\text{O}_4$ ,  $n\text{-Bu}_4\text{NBr}$ , THF,  $\text{H}_2\text{O}$  2.  $\text{KOH}$ ,  $\text{RX}$ ,  $100^\circ\text{C}$ , 6 h, 86-92%; c)  $\text{Br}_2$ ,  $\text{CH}_2\text{Cl}_2$ , rt, 5 min, **179** (95%), **180** (90%); d) *t*-BuCl,  $\text{AlCl}_3$ ,  $0^\circ\text{C}$ , 30 min, 65%.

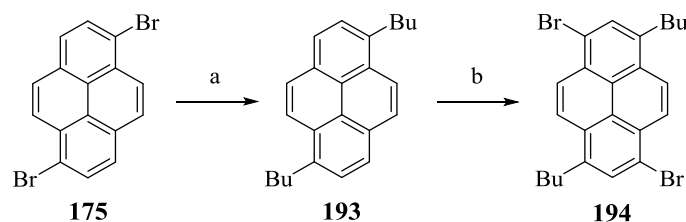
As expected for an electron deficient system, monobromination of 1-acetylpyrene (**181**) with  $\text{Br}_2$  (1.5 equiv.) requires heating at  $60^\circ\text{C}$  and generates a mixture of 3-, 6- and 8-bromides **182-184** (Scheme 5.03). The product distribution was not reported. Likewise, dibromination under the same conditions, but using 2.5 equiv. of  $\text{Br}_2$  gave a mixture of the 3,6-, 3,8- and 6,8-dibromides **185-187** in unspecified proportions.

Tribromide **188** could be obtained in high yield upon heating **181** at 120 °C with three equiv. of bromine. Bromination of 2-acetylpyrene (**189**) under the same sets of reaction conditions proceeds much more selectively to afford mono-, di- and tribromides **190-192** in 90%, 90% and 78% yield, respectively (Scheme 5.03).<sup>21</sup> The observation that bromination can occur *ortho* to the acetyl group highlights pyrene's very strong electronic preference for reaction at the 1, 3, 6 and 8 positions.



**Scheme 5.03** Reagents and conditions: a)  $\text{Br}_2$  (1.50 equiv.),  $\text{CCl}_4$ , 60 °C, **182-184** (95%), **190** (90%); b)  $\text{Br}_2$  (2.50 equiv.),  $\text{CCl}_4$ , 60 °C, **191** (90%); c)  $\text{Br}_2$  (3.00 equiv.),  $\text{PhNO}_2$ , 120 °C, **188** (92%), **192** (78%).

1,6-Dibutylpyrene (**193**) can be synthesized easily from 1,6-dibromopyrene (**175**) by lithium-halogen exchange followed by alkylation. With two of the reactive sites occupied by alkyl groups, the remaining two sites can be brominated with complete regioselectivity to afford dibromide **194** (Scheme 5.04).<sup>22</sup>

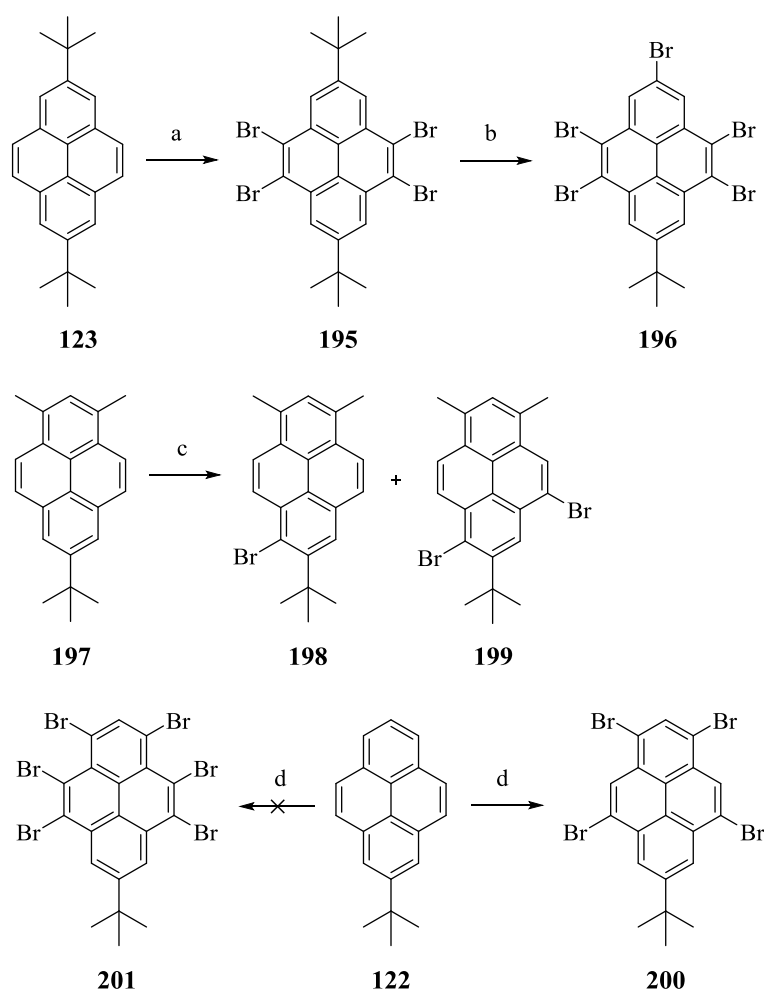


**Scheme 5.04** Reagents and conditions: a) (i) *n*-BuLi, THF,  $-78\text{ }^{\circ}\text{C}$ , (ii) 1-bromobutane; b)  $\text{Br}_2$ ,  $\text{CCl}_4$ , rt, 30 min (65% over 2 steps).

When all of the reactive sites (1, 3, 6 and 8) are either occupied or sterically hindered, bromination can occur at the *K*-region (4, 5, 9 and 10 positions). (Scheme 5.05). For example, when 2,7-di-*t*-butylpyrene (**123**) is reacted with bromine in the presence of Fe powder for 4 h, 4,5,9,10-tetrabromopyrene (**195**) is obtained in very high yield. Extending the reaction for longer periods results in *ipso*-substitution of one of the *t*-butyl groups by a bromine atom to afford pentabromide **196** in high yield.<sup>23</sup> In compound **197**, the 1 and 3 positions are occupied by methyl groups and the 6 and 8 positions are hindered by the 7-*t*-butyl group. Bromination of **197** using NBS gives bromide **198** as the major product, in which the substitution contains a bromine substituent *ortho* to the bulky *t*-butyl group of **197** along with a minor product **199**.<sup>24</sup> It is quite surprising to see that *K*-region bromination appears to be the slower process. In **199**, where some *K*-region bromination has occurred, the regioselectivity is what one would expect based on



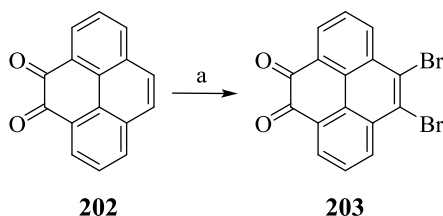
*ortho/para* directing effects of the two methyl groups and the *t*-butyl group. *t*-Butylpyrene (**112**) undergoes bromination with Br<sub>2</sub>/Fe to afford 1,3,5,9-tetrabromopyrene (**200**) instead of 1,3,4,5,9,10-hexabromopyrene (**201**) which was the product expected by the authors.<sup>25</sup> It seems that the initial bromination takes place at 1,3-positions, which then prevents bromination at the 4 and 10 positions (probably due to *peri* interactions). Therefore, the next brominations occur at the 5 and 9 positions. This regiochemistry is



**Scheme 5.05** Reagents and conditions: a) Br<sub>2</sub>, Fe powder, CH<sub>2</sub>Cl<sub>2</sub>, rt, 4 h, 90%; b) Br<sub>2</sub>, Fe powder, CH<sub>2</sub>Cl<sub>2</sub>, rt, 8 h, 85%; c) NBS, CCl<sub>4</sub>, rt, 2 h, **198** (83%), **199** (8%); d) Br<sub>2</sub>, Fe powder, CH<sub>2</sub>Cl<sub>2</sub>, rt, 4 h, 84%.

also in accord with the combined *ortho/para* directing effects of the first two bromine atoms and the *t*-butyl group.

In considering the previous examples, it seems that the nature of the brominating agent has some influence on the regiochemistry. NBS is the reagent of choice if selectivity for a hindered 1, 3, 6 or 8 position over a K-region is required. On the other hand, Br<sub>2</sub>/Fe appears to be the reagent of choice if the opposite selectivity is required. This may have its origin in the size and/or reactivity of the active brominating agents. *K*-region bromination can also be achieved indirectly, *i.e.* by brominating diketone **202** with NBS/H<sub>2</sub>SO<sub>4</sub> to afford 9,10-dibromopyrene-4,5-dione (**203**) in quantitative yield (Scheme 5.06).<sup>26</sup> Reductive alkylation of the diketone regenerates the pyrene system (*cf.* **177** to **178**).



**Scheme 5.06** Reagents and conditions: a) NBS, H<sub>2</sub>SO<sub>4</sub>, rt, 4 h, 100%.

In looking to the next higher homologue of the capped rylene series, peropyrene, very little work appears to have been done on its bromination. A SciFinder search found no hits for 1-, 2-, 4, or 5-bromoperopyrene (**204-207**) and only one Japanese patent for 1,3,8,10-tetrabromoperopyrene (**208**) (Figure 5.03). The poor solubility of peropyrene (**21**) is presumably why so little work has been done with the chemistry of this class of PAHs. As stated earlier, nothing is known about the chemistry of teropyrene (**22**).

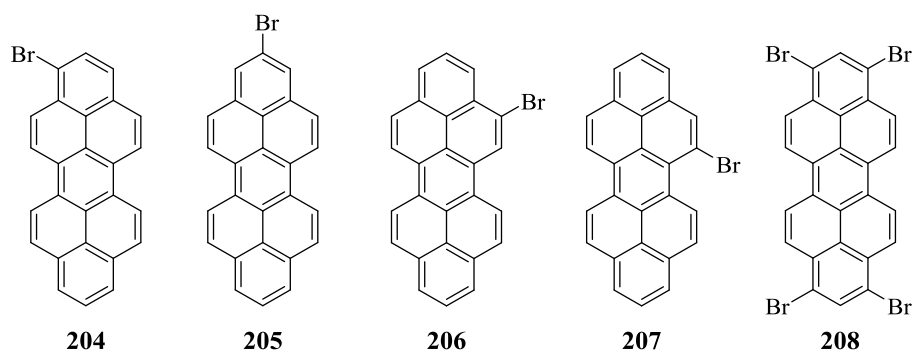


**Figure 5.03** Various brominated teropyrenes.

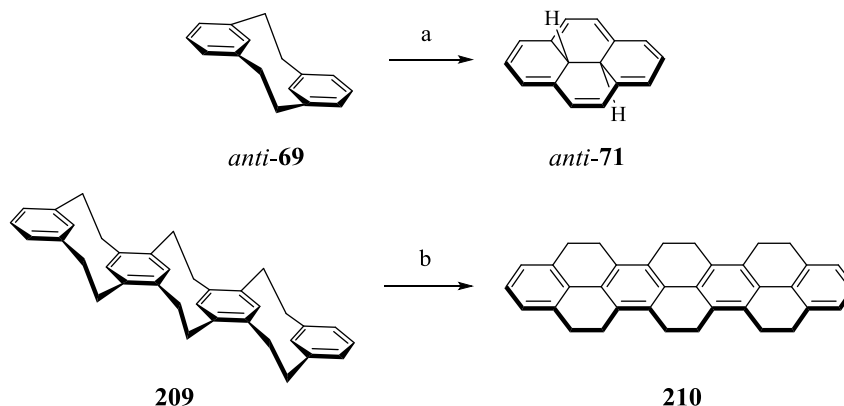
## 5.2 Results and discussion

Before addressing the bromination reactions of the teropyrenophanes **103b-e**, it is necessary to first shift the focus back one step in their syntheses. During the work aimed at the large scale synthesis of the teropyrenophanes **103b-e**, the difficulties encountered during the key teropyrene-forming reaction prompted consideration of the use of oxidants other than DDQ. It had long been known that *anti*-[2.2]metacyclophanes (**69**) undergoes transannular bond formation to afford 4,5,9,10-tetrahydropyrenes (**71**) under the conditions of electrophilic aromatic substitution reactions such as bromination (Scheme 5.07). In fact, this chemistry was used in Misumi's<sup>27</sup> synthesis of teropyrene (**22**). Quadruple-layered metacyclophane **209** was treated with pyridinium perbromide (PyHBr<sub>3</sub>) to generate dodecahydroteropyrene **210**, which was then dehydrogenated using DDQ (Scheme 5.07).

### 5.2.1 Bromination of Cyclophanemonoene 109d

Initial work was done with cyclophanemonoene **109d**, which has a 9-membered

bridge, because this was the most well-behaved member of the series. Since the starting material had one unsaturated bridge, the product of the reaction would be

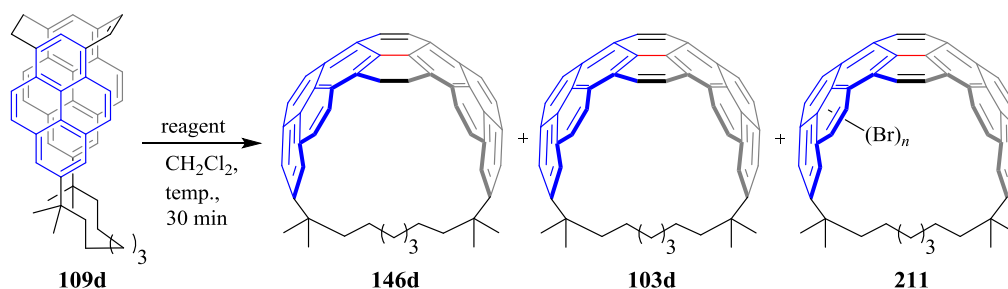


**Scheme 5.07** Bromination of layered metacyclophanes; *Reagents and conditions*: a)  $\text{Br}_2$ , Fe,  $\text{CCl}_4$ ; b)  $3\text{Py}\cdot\text{HBr}_3$ ,  $\text{CH}_2\text{Cl}_2$ ,  $0\text{ }^\circ\text{C}$ , 1 h, 55%.

dihydroteropyrenophane **146d** if it proceeded in an analogous fashion to the conversion of *anti-69* to *anti-71*. It was envisaged that excess oxidant might bring about *in situ* conversion of **146d** to the desired teropyrenophane **103d**, so the first experiment involved treatment of compound **109d** with 2.1 equiv. of  $\text{PyHBr}_3$  (Table 1, Entry 1). No reaction was observed. Instead, when 2.1 equiv. of  $\text{Br}_2$  was used the starting material (10 mg) was fully consumed in 30 minutes and a mixture of products consisting of teropyrenophane **103d** and brominated teropyrenophanes was produced (Table 1, Entry 2). The presence of mono- and dibrominated products was indicated by LC-MS analysis of the crude reaction mixture. The  $^1\text{H}$  NMR spectrum of the crude reaction mixture was difficult to interpret due to overlap of the signals of the different products, so only a very rough estimate of product ratios could be made. One of the brominated products was isolated by column chromatography and analysis of its  $^1\text{H}$  NMR spectrum revealed that it

contained two bromine atoms. The structure assignment of this compound is discussed later. Cutting the number of equiv. of Br<sub>2</sub> by half produced an inseparable *ca.* 2.2:1 mixture (<sup>1</sup>H NMR and LC-MS analysis) of dihydroteropyrenophane **146d** and teropyrenophane **103d** with no brominated products (Table 1, Entry 3). This implies that **146d** is indeed an intermediate during the formation of **103d**. To find out whether teropyrenophane could be produced exclusively (*i.e.* without any brominated products or dihydroteropyrenophane **146d**), a series of reactions was performed in which the number of equiv. of Br<sub>2</sub> was varied.

**Table 5.01** Reactions of cyclophanemonoene **109d** with bromine.



entry	reagent	equiv.	temp (°C)	ratio <sup>a</sup>		monobromo compound	dibromo compound
				<b>146d</b>	<b>103d</b>		
1	PyHBr <sub>3</sub>	2.1	0	-	-	-	-
2	Br <sub>2</sub>	2.1	0	4	1	1	1
3	Br <sub>2</sub>	1.0	0	2.2	1	-	-
4	Br <sub>2</sub>	1.1	0	1.8	1	-	-
5	Br <sub>2</sub>	1.2	0	1.6	1	-	-
6	Br <sub>2</sub>	1.3	0	1.9	1	0.3	trace
7	Br <sub>2</sub>	1.4	0	1.2	1	1.5	0.8
8	Br <sub>2</sub>	1.4	35	1.2	1	1.5	0.8
9	Br <sub>2</sub>	1.4	-40	1.2	1	1.5	0.8
10	Br <sub>2</sub>	1.4	-80	1.4	1	1.7	0.6
11 <sup>b</sup>	I <sub>2</sub>	2.2	rt	2	1	-	-

a. determined by NMR

b. starting material was recovered after two days along with **146d** and **103d**

Reactions were performed on a 10 mg scale and product ratios were assessed by analysis of the  $^1\text{H}$  NMR spectrum of the crude reaction mixture. As before, the product ratios are quite rough due to peak overlap. With 1.1 equiv. of  $\text{Br}_2$ , a *ca.* 1.8:1 mixture of **146d**:**103d** was observed (Table 1, Entry 4) and with 1.2 equiv. of  $\text{Br}_2$  the ratio increased to *ca.* 1.6:1 (Table 1, Entry 5). When 1.3 equiv. of  $\text{Br}_2$  were used, the ratio of **146d**:**103d** remained at about 1.9:1 and the first traces of brominated products were observed (Table 1, Entry 6). Upon moving to 1.4 equiv. of  $\text{Br}_2$ , more extensive bromination had occurred and the ratio of **146d**:**103d** decreased slightly to *ca.* 1.2:1 (Table 1, Entry 7). Therefore, 1.3 equiv. of  $\text{Br}_2$  is the limit where bromination started to interfere. By fixing the amount of  $\text{Br}_2$  at 1.4 equiv. (where significant bromination was observed), the reaction temperature was varied to see if the extent of bromination was affected. However, performing the reaction at 35 °C, -40 °C and -80 °C (Table 1, Entries 8-10) did not result in any significant change in the product distribution. Only the time required for the reaction to go to completion was affected. Therefore, it appeared as though selective oxidation of **109d** to either **146d** or **103d** using bromine was not viable. All of the reactions described above were also performed using NBS as the oxidant, both with and without irradiation with visible light. Essentially identical results were obtained. The use of  $\text{I}_2$  (2.2 equiv.) as the oxidant resulted in no observable reaction at room temperature even after two days (Table 1, Entry 11). In the experiments described above, no evidence ( $^1\text{H}$  NMR, LC-MS) for the formation of brominated versions of **109d** or **146d** were observed, which indicated that **103d** is the most reactive of these species with respect to electrophilic aromatic bromination.

### 5.2.2 Structure determination of dibromoteropyrenophane **212**

As mentioned earlier, a dibromoteropyrenophane was isolated from one of the bromination reactions of cyclophanemonoene **109d**. Its structure was determined by detailed analysis of its  $^1\text{H}$  NMR spectrum. The starting point of this analysis was the spectrum of teropyrenophane **103d**, which has just four 4H signal for the 16 aromatic protons due to the presence of two mirror planes (vertical and horizontal dashed blue lines in Figure 5.05a). The  $^1\text{H}$  NMR spectrum of the dibromoteropyrenophane contains seven 2H signals (six doublets and a singlet), which not only indicated that two bromine atoms were present (also indicated by LC-MS) and that the molecule had some sort of symmetry. The dibromination of teropyrenophane **103d** can conceivably produce 54 positional isomers, 4 of which are *meso* compounds are due to the vertical plane of symmetry, 4 of which are *meso* compounds are due to the horizontal plane of symmetry and 4 of which have  $C_2$  symmetry (Figure 5.04). The remaining 42 were excluded

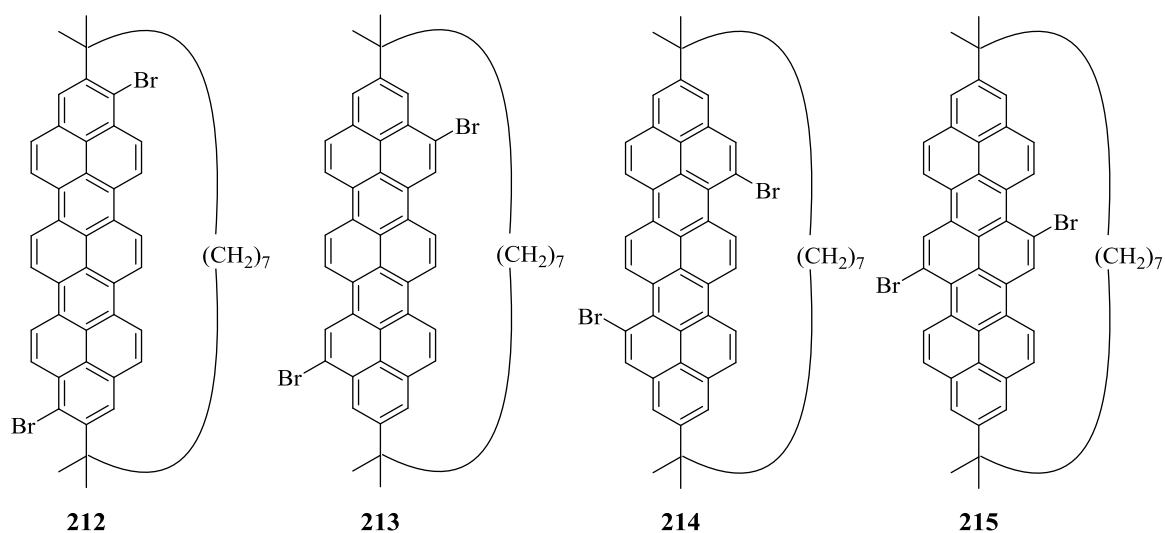


**Figure 5.04** Four possible  $C_2$ -symmetric isomers of dibromo compound.

because they are unsymmetrical ( $C_1$  symmetric) and would exhibit too many signals. The presence of two 2H doublets at  $\delta$  7.58 and 7.91 with a small coupling constant ( $J = 1.6$  Hz) was indicative of *meta*-coupled protons, which could only be possible if the two protons on either side of the bridgehead were different. This ruled out all the 4 *meso* isomers resulted due to horizontal mirror plane. The presence of only one singlet in the  $^1\text{H}$  NMR spectrum eliminates the 4 *meso* isomers due to the vertical mirror plane and left out with only the four  $C_2$ -symmetric isomers **212-215**. In fact, **212** was also ruled out at this stage because it would not have *meta*-coupled protons.

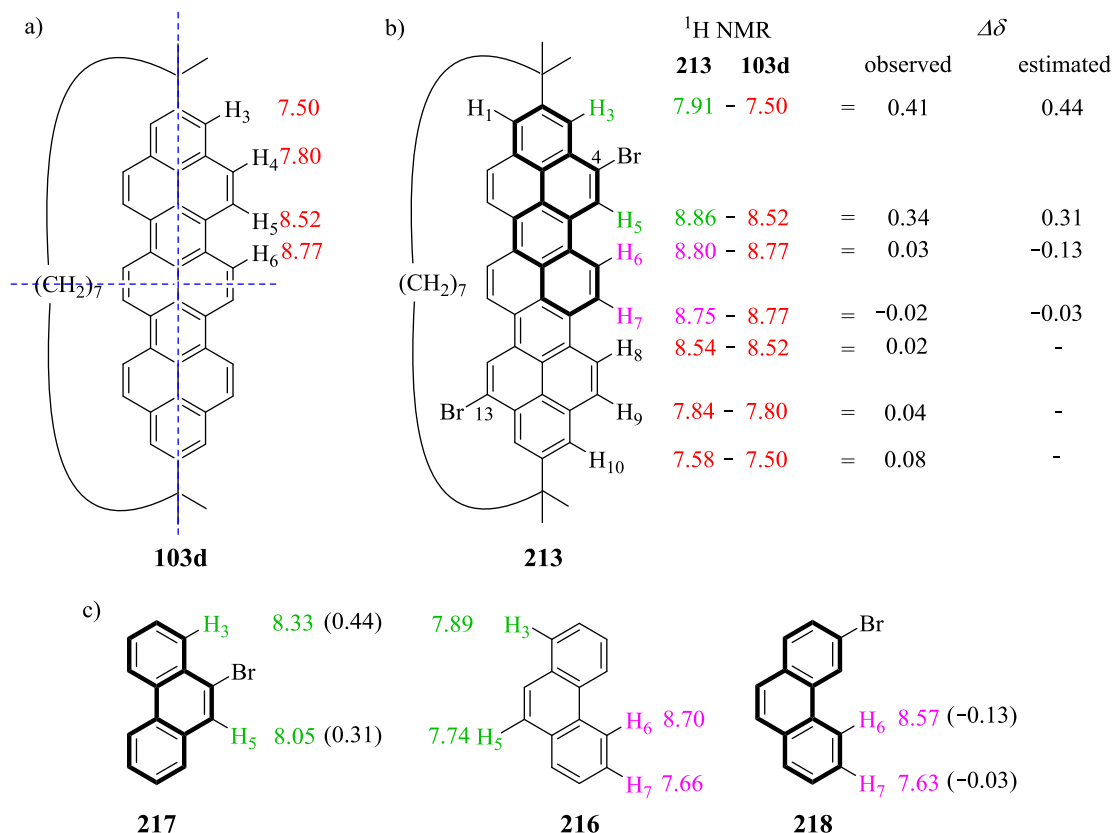


**Figure 5.05** Structure determination of 12,21-dibromo-1,1,9,9-tetramethylterpyrenophane.



To decide between the remaining three isomers **213-215**, published spectra of phenanthrene (**216**)<sup>28</sup> and bromophenanthrenes **217**,<sup>29</sup> **218**<sup>28</sup> were considered to gauge how bromination affects the chemical shifts of protons close to the site of bromination (Figure 5.05c). The  $\Delta\delta$  values that were obtained from this analysis were then used in conjunction with the known spectrum of teropyrenophane **103d** to predict the spectra of isomers **213-215**. Only the predicted spectrum of isomer **213** came close to matching the NMR data of the unknown dibromide (Figure 5.05b), so bromination very likely occurred at the 4 and 13 positions of the teropyrene system. Therefore, the dibromide was assigned as 12,21-dibromo-1,1,9,9-tetramethyl[9](2,11)teroprenophane (**213**) with reasonable confidence.<sup>#</sup>

### 5.2.3 Interesting points about dibromoteropyrenophane 213

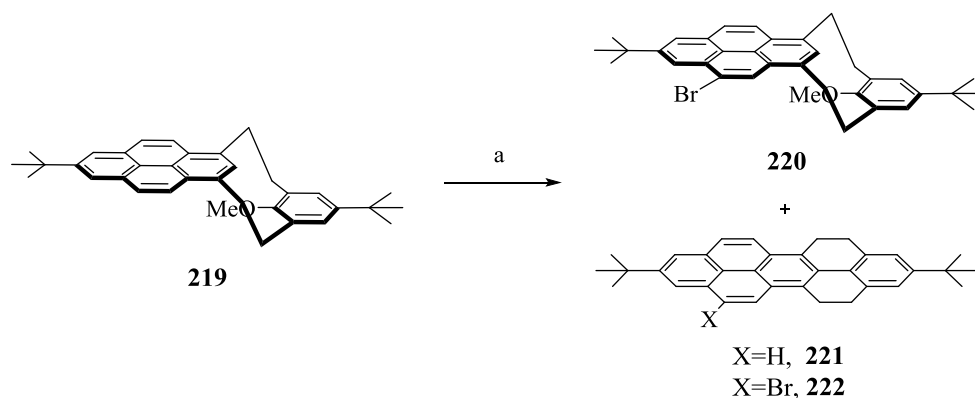
Several points regarding the formation of **213** are worth making. First, it is interesting to note that compound **197** (Scheme 5.05), which has the same substitution pattern as the pyrene systems in **109d**, undergoes bromination at the position *ortho* to the bulky *t*-butyl group under similar reaction conditions. It thus appears that the reaction leading to **40** (by whatever mechanism) is a much faster process than bromination of the pyrene system. Second, the bromination of two symmetry-related sites of teropyrenophane **103d** points toward greater reactivity of the 4, 9, 13 and 18 positions of teropyrene than elsewhere, with the possible exception of the sterically hindered 1, 3, 10 and 12

---

<sup>#</sup> Note that the sites of bromination according to cyclophane nomenclature are 12 and 21. The 4 and 13 numbering that is being used in the discussion comes from numbering of free teropyrene. The latter numbering is being used because it does not vary from cyclophane to cyclophane, as it does when the cyclophane numbering is used.

positions. If this is the case, one would expect two other dibromides to form, *i.e.* those resulting from bromination of the 4 and 9 positions and the 4 and 18 positions (*cf.* dibromination of pyrene to give the 1,3, 1,6 and 1,8 dibromopyrenes). Neither of these compounds were isolated, but this does not mean that they were not formed, so it was not possible to state with any confidence that the dibromination of **103d** was completely regioselective. It would certainly be remarkable if first bromine atom directed the regioselectivity of second bromination reaction completely. In this regard, it is worth noting that a hint about regioselectivity in electrophilic aromatic substitutions of the teropyrenophanes was obtained earlier – a dichloro[9]teropyrenophane (compound **157d** in Chapter 4, section 4.2.10.2) was formed as a mixture of two regioisomers in a *ca.* 1:1 ratio. At this stage, monobromide, presumably the one resulting from bromination at the 4 position of the teropyrene system, was not isolated either (Table 5.01). One would certainly expect the rate of the second bromination to be slower than that of the first one.

Work published by Yamato *et al.* provided some possible precedent for the site of bromination.<sup>22</sup> Under very similar reaction conditions, *anti*-8-methoxy[2]metacyclo[2]-

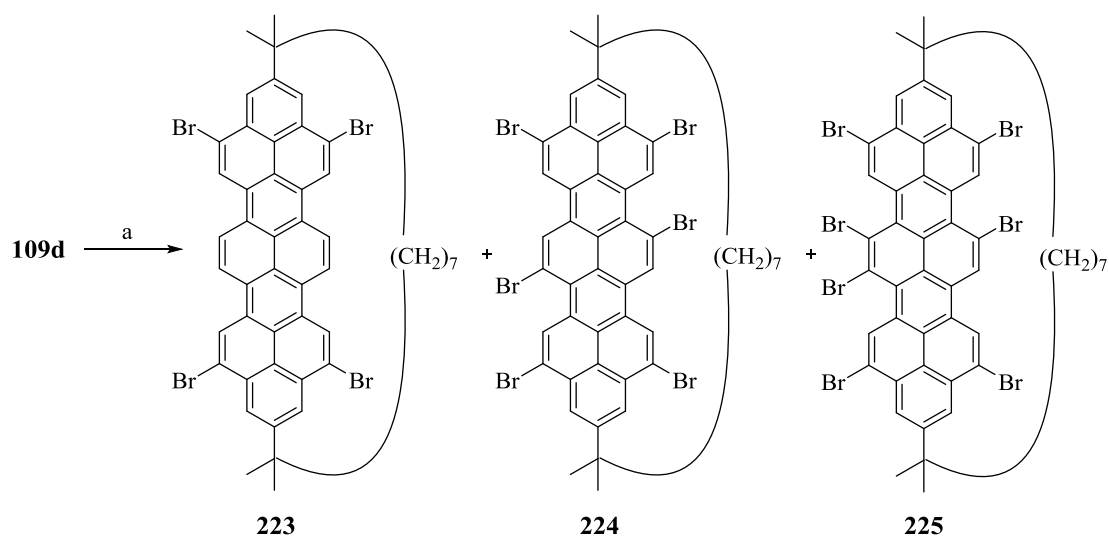


**Scheme 5.08** Bromination of *anti*-8-methoxy[2]metacyclo[2]-(1,3)pyrenophane **219**; *Reagents and conditions:* a) Br<sub>2</sub>, CH<sub>2</sub>Cl<sub>2</sub>, rt.

(1,3)pyrenophane **219** underwent ring closure and bromination to afford 13-brominated compound **222** when 2.2 equiv. of Br<sub>2</sub> were used (Scheme 5.08). The use of 1.1 equiv. of Br<sub>2</sub> afforded a mixture of compounds **220** and **221**. Treatment of this mixture with another 1.1 equiv. of Br<sub>2</sub> converted them to **222**, which suggests that both **220** and **221** are intermediates during the formation of **222**.

#### 5.2.4 Treatment of 109d with excess Br<sub>2</sub>

With dibromination already in the mix, questions arose as to how many bromines could be introduced into the teropyrene system and which sites would brominate once all of the 4, 9, 13 and 18 positions were brominated. To probe these questions, compound **39** was reacted with 10.0 equiv. of Br<sub>2</sub> and this resulted in the formation of three major product spots (tlc analysis) (Scheme 5.09). All three newly-formed products were isolated by column chromatography (hexanes). The <sup>1</sup>H NMR spectrum of the spot with



**Scheme 5.09** Reaction of 109d with excess bromine; *Reagents and conditions*: a) Br<sub>2</sub> (10 eq.), CH<sub>2</sub>Cl<sub>2</sub>, rt, 30 min.

$R_f = 0.54$  (10% dichloromethane / hexanes) was very clean and contained only three 4H singlets in the aromatic region, which indicated the presence of four bromine atoms. Since the position of two of the bromines in **213** was already known, the structure of this compound could be easily deduced as 12,17,21,27-tetrabromoteropyrenophane **223** (bromination of the 4, 9, 13 and 18 positions of the teropyrene system). This was later confirmed by a single crystal X-ray structure determination, the details of which are discussed later.

The  $^1\text{H}$  NMR spectrum of the spot with  $R_f = 0.75$  was not as clean as that of tetrabromide **213** (*ca.* 85% purity), and the major component exhibited three 2H singlets and two narrow 2H doublets ( $J = 1.6$  Hz), which points to the presence of six bromine atoms on the teropyrene system. There are three ways in which the fifth and sixth bromine atoms could add to give the observed set of signals, *i.e.* **224**, **224A** and **224B** (Figure 5.06). At the time, the assignment of the structure could not be made with any

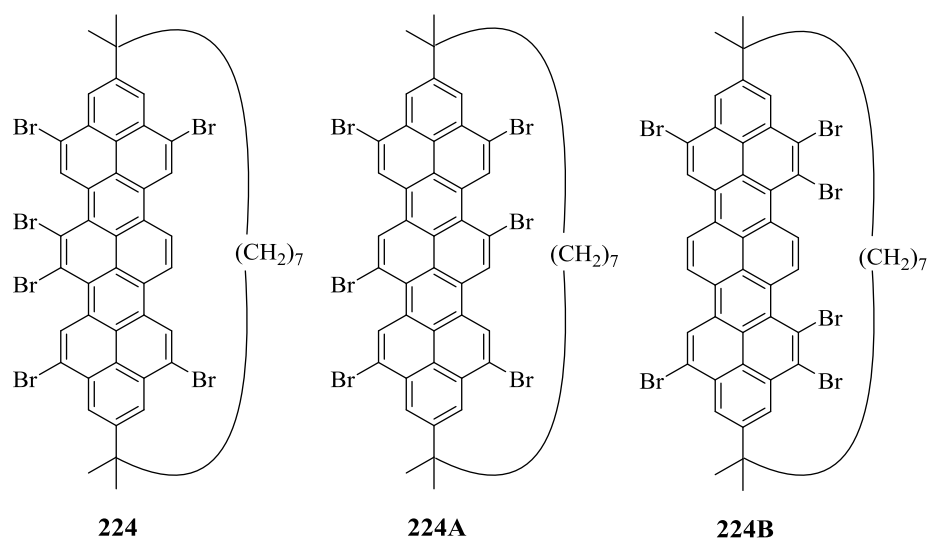


**Figure 5.06** Possible structures for the hexabrominated product.

confidence, but structure **224A** was identified as a “best guess” because it is the only one in which no *K*-region bears two bromine atoms. The structural assignment of this compound is discussed later in this Chapter.

The  $^1\text{H}$  NMR spectrum of the spot with  $R_f = 0.80$  was also not completely pure (*ca.* 90% purity). The major component exhibited five  $^1\text{H}$  singlets as well as four narrow  $^1\text{H}$  doublets ( $J = 1.6$  Hz), which corresponds to the presence of seven bromine atoms on the teropyrene system. If this compound arises from the bromination of the major hexabromide, then **224B** cannot be the major hexabromide because all heptabromides derived from **224B** would exhibit at least one AB or AX system with  $J \approx 10$  Hz. Starting from **240** and **240A**, there are only three possible structures for the heptabromide, namely **225**, **225A** and **225B** (Figure 5.07). The structural assignment of the heptabromide was determined later using X-ray crystallographic methods and the details of this work are discussed later in this Chapter. In any event, it seemed likely at this point that the 6, 7,

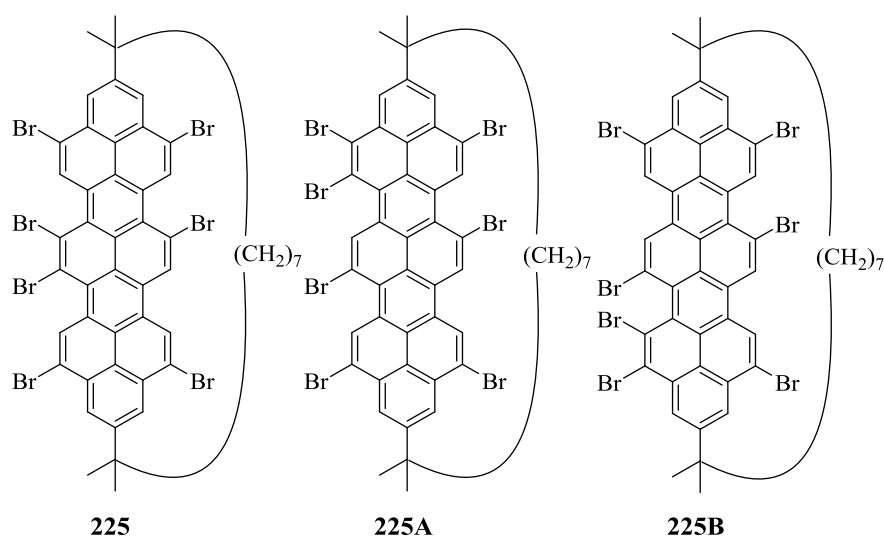


**Figure 5.07** Possible structures for the heptabromo compound.

15 and 16 positions of the teropyrene system (central *K*-regions) were the next most reactive positions after the 4, 9, 13 and 18 positions.

### 5.3 Bromination chemistry of teropyrenophane **103d**

Although the initial idea of cleanly producing teropyrenophane **103d** from cyclophanemonoene **109d** using bromine was unsuccessful, the observation that teropyrenophane **103d** underwent bromination readily and with some degree of selectivity was a very promising development. With access to gram quantities of teropyrenophane **103d** (Chapter 4), it was therefore decided to conduct a more careful study of the bromination reactions of **103d**.

To begin with, 21 vials were each charged with a solution of teropyrenophane **103d** (3.0 mg) in dichloromethane. A stock solution of Br<sub>2</sub> in dichloromethane was (experimental section) then used to add Br<sub>2</sub><sup>§</sup> to the first 20 vials in 0.5 equiv. increments. Thus, the first 20 vials spanned a range of 0.5 to 10 equiv. of Br<sub>2</sub>. In the 21<sup>st</sup> vial, 20 equiv. of Br<sub>2</sub> were added. In a 22<sup>nd</sup> vial, neat Br<sub>2</sub> (0.1 mL) was added to solid teropyrenophane **103d** (3.0 mg). Subsequently, 10 more reactions were performed at 35 °C using 6.0-10.0 equiv. of Br<sub>2</sub> (0.5 equiv. increments) and 20 eq of Br<sub>2</sub> (Table 5.02). An additional reaction at this temperature was performed using neat Br<sub>2</sub> (0.1 mL). The first 22 reactions were stirred at room temperature whereas, the later 11 reactions were stirred at 35 °C for 30 minutes before being passed through a plug of silica gel and evaporated to

---

<sup>§</sup> The overall concentration of dichloromethane was maintained as 4.0 mL and the capped vials were closed tightly during the progress of the reaction.

dryness. It is worth noting that rapid discharge of the colour of Br<sub>2</sub> was observed<sup>‡</sup> in the reactions with up to 4 equiv. of Br<sub>2</sub>, but the Br<sub>2</sub> colour persisted thereafter. <sup>1</sup>H NMR spectra were recorded for the crude products and the product ratios were estimated using integration values of characteristic signals. As discussed later, most of the brominated compounds could be separated chromatographically and characterized. As such, it was (for the most part) clear which signals in a mixture corresponded to which compound.

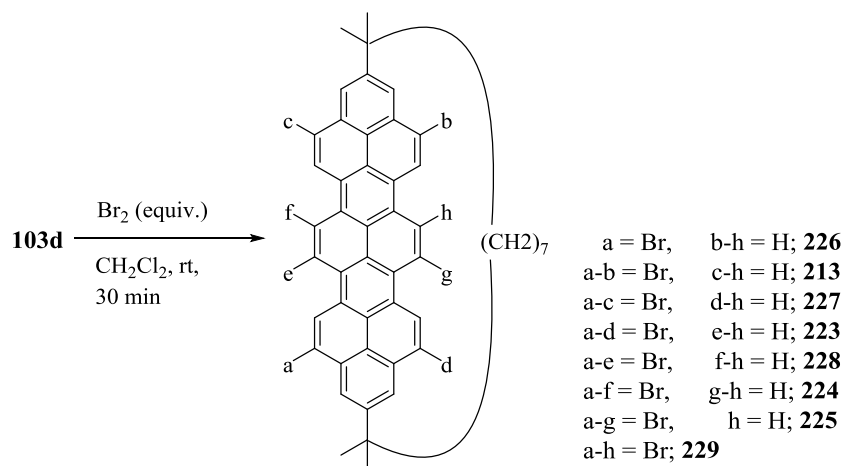
An attempt to determine product ratios using LCMS provided data that was inconsistent with the NMR data. In particular, the more heavily brominated the teropyrenophanes became, the more their proportions tended to be underestimated, presumably due to fragmentation (loss of bromine) and/or issues with volatilization (e.g. hexabromides have a molar mass of 1097.79 g/mol).

As mentioned earlier, the symmetry-related 4, 9, 13 and 18 positions of the teropyrene system in **103d** are the most reactive sites. From the <sup>1</sup>H NMR data (Table 5.02, Figures 5.08 and 5.09, left), it can be clearly seen that the mono-, di-, tri- and tetrabromoteropyrenophanes **226** ( $\delta$  7.89 ppm, 1H, d ( $J$ =1.6 Hz), C(3)-H), **213** ( $\delta$  7.91 ppm, 2H, d ( $J$ =1.6 Hz), C(3,12)-Hs), **227** ( $\delta$  7.93 ppm, 1H, d ( $J$ =1.6 Hz), C(3)-H) and **223** ( $\delta$  7.99 ppm, 4H, s, C(1,3,10,12)-Hs) successively become the major components (*ca.* 70%, 80%, 75% and 100%, respectively) at 1.0, 2.0 3.0 and 4.0 equiv. of Br<sub>2</sub>. Reminiscent of what is observed for pyrene (**20**), this is consistent with a reduction in the

---

<sup>‡</sup> Initially, the discolouration of Br<sub>2</sub> occurred very instantaneously, as soon as it was added to the pale green dichloromethane solutions of teropyrenophane **103d** and the speed of discolouration was slightly and gradually decreased with the increase in the equivalents of bromine until 4.0.

**Table 5.02** Distribution of the product mixture (in terms of mole fractions) during the reaction of teropyrenophane **103d** with varying equiv. of Br<sub>2</sub>.



equiv. (Br <sub>2</sub> )	<b>103d</b>	<b>226</b>	<b>213</b>	<b>227</b>	<b>223</b>	<b>228</b>	<b>224</b>	<b>225</b>	<b>229</b>
0.5*	0.65	0.35	-	-	-	-	-	-	-
1.0*	0.20	0.70	0.10	-	-	-	-	-	-
1.5*	0.05	0.60	0.30	0.05	-	-	-	-	-
2.0*	-	0.05	0.80	0.15	-	-	-	-	-
2.5*	-	-	0.45	0.50	0.05	-	-	-	-
3.0*	-	-	0.05	0.75	0.15	-	-	-	-
3.5*	-	-	-	0.60	0.40	-	-	-	-
4.0*	-	-	-	-	1.00	-	-	-	-
4.5*	-	-	-	-	0.85	0.15	-	-	-
5.0*	-	-	-	-	0.60	0.40	-	-	-
5.5*	-	-	-	-	0.50	0.50	-	-	-
6.0*	-	-	-	-	0.40	0.50	0.10	-	-
6.5*	-	-	-	-	0.30	0.50	0.15	0.05	-
7.0*	-	-	-	-	0.20	0.50	0.15	0.15	-
7.5*	-	-	-	-	0.10	0.50	0.20	0.20	-
8.0*	-	-	-	-	0.05	0.50	0.25	0.20	-
8.5*	-	-	-	-	0.05	0.40	0.30	0.25	-
9.0*	-	-	-	-	0.05	0.40	0.40	0.35	-
9.5*	-	-	-	-	0.05	0.35	0.30	0.30	-



**Table 5.02** contd.

equiv. (Br <sub>2</sub> )	<b>103d</b>	<b>226</b>	<b>213</b>	<b>227</b>	<b>223</b>	<b>228</b>	<b>224</b>	<b>225</b>	<b>229</b>
10.0*	-	-	-	-	0.02	0.30	0.30	0.38	-
20.0*	-	-	-	-	0.02	0.15	0.25	0.58	-
neat*	-	-	-	-	0.10	0.30	0.10	0.45	0.05
6.0**	-	-	-	-	0.50	0.40	0.05	0.05	-
6.5**	-	-	-	-	0.5	0.40	0.05	0.05	-
7.0**	-	-	-	-	0.25	0.55	0.10	0.10	-
7.5**	-	-	-	-	0.25	0.55	0.10	0.10	-
8.0**	-	-	-	-	0.1	0.50	0.20	0.20	-
8.5**	-	-	-	-	0.05	0.45	0.25	0.25	-
9.0**	-	-	-	-	0.05	0.45	0.25	0.25	-
9.5**	-	-	-	-	0.05	0.45	0.25	0.25	-
10.0**	-	-	-	-	0.10	0.45	0.20	0.25	-
20.0**	-	-	-	-	0.10	0.25	0.20	0.45	-

\* at room temperature

\*\* at 35 °C

rate of bromination with the introduction of each successive bromine atom. On the other hand, in contrast to how pyrene behaves, the second bromination of the teropyrene system appears to be very regioselective for the 4,13-dibromo isomer (12,21-dibromo-1,1,9,9-tetramethyl[9](2,11)teropyrenophane (**213**)). The origin of this remarkable regioselectivity is unclear and warrants further investigation.

A notable feature of dibromoteropyrenophane **213** is that it has  $C_2$  symmetry and is therefore a chiral molecule. The conformational behaviour of the bridge is not an issue in this case because it has an odd number of atoms, which means that the flipping of the

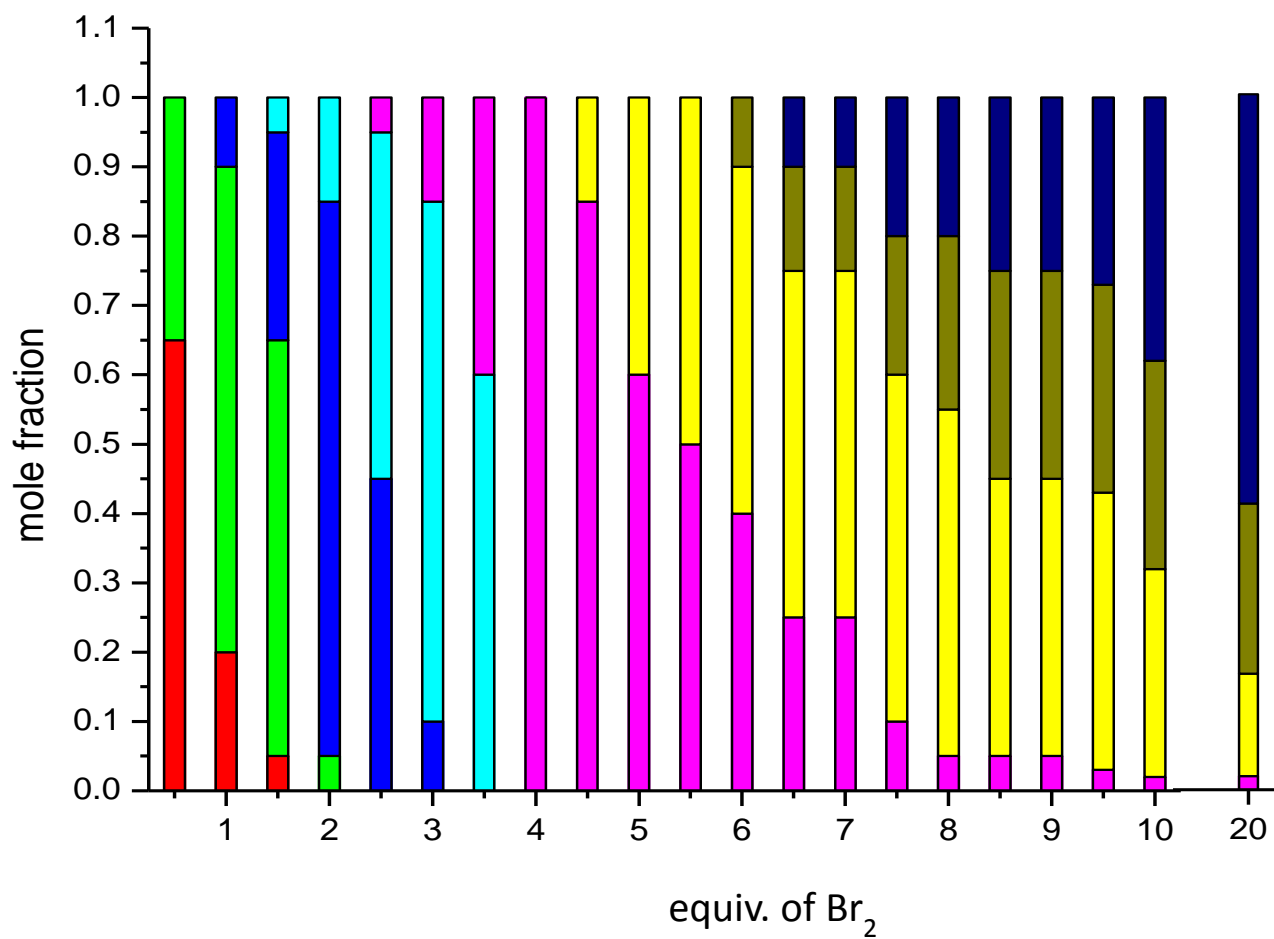


**Figure 5.08** Left) Bar chart showing the results of the bromination of **103d** at rt. Right) Bar chart showing the results of the bromination of **103d** at 35 °C; ■ - 0 bromine, ■ - 1 bromine, ■ - 2 bromines, ■ - 3 bromines, ■ - 4 bromines, ■ - 5 bromines, ■ - 6 bromines, ■ - 7 bromines.

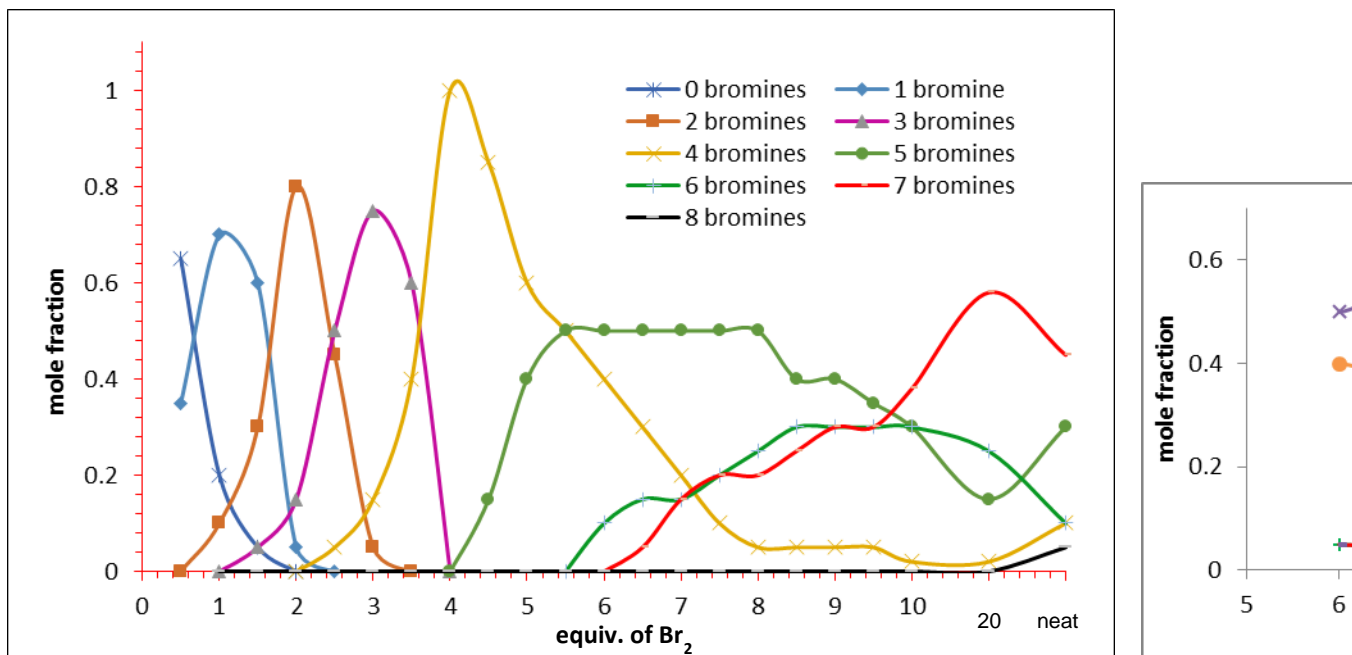


**Figure 5.09** Left) distribution of various brominated products at rt using 0.0–10.0 equiv., 20.0 equiv. of bromine (in dichloromethane) and neat bromine. Right) at 35 °C using 6.0–10.0 equiv. and 20.0 equiv. of bromine (in dichloromethane).

bridge interconverts identical species, *i.e.* it is a degenerate process.<sup>†</sup> This means dibromoteropyrenophane **213** holds great promise as a starting material for the synthesis

<sup>†</sup> With an even number of atoms in the bridge, the bridge flip would interconvert two diastereomers and would therefore be nondegenerate.

of large, chiral nonplanar PAHs.

Beyond 4.0 equiv. of Br<sub>2</sub>, the situation becomes less cut-and-dried. The four most reactive sites are all brominated, which means that the remaining sites on the teropyrene system are not only innately less reactive, but also deactivated. Nevertheless, further bromination still occurs and it appears to be favoured at the 6, 7, 15 and 16 positions of the teropyrene system. Starting from 4.5 equiv. of Br<sub>2</sub>, pentabromide compound **228** started to be observed ( $\delta$  9.98, 1H, s, C(7)-H) and it became the major component (50%) at 6.0 equiv. of Br<sub>2</sub>. A smaller singlet at  $\delta$  9.97 also emerged as of 4.5 equiv. of Br<sub>2</sub>, but this compound was never isolated and its structure has not been determined.

The hexabromide obtained from the bromination of teropyrenophane **103d** (see above) appeared as of 6.0 equiv. Br<sub>2</sub> ( $\delta$  9.60, 1H, s, C(15)-H). At the same time, a singlet at  $\delta$  9.56 was also observed from 6.0 equiv. Br<sub>2</sub>. It is uncertain what compound it corresponds to, but it may well be a regioisomeric hexabromide. The two hexabromides could be **224** (the previous best guess) and **224A**. A signal for the previously observed heptabromide ( $\delta$  10.03, 1H, s, C(16)-H) was first observed at 6.5 equiv. Br<sub>2</sub>. A second signal ( $\delta$  10.04, 1H, s, C(6)-H) that was attributed to a regioisomeric heptabromide was also observed. Initially, the signal at  $\delta$  10.03 was the major signal (3:1), but the ratio changed steadily in favour of the signal at  $\delta$  10.04 until it had become the major signal (1:5) at 20 equiv. of Br<sub>2</sub>. The two regioisomers could be bridge conformers **225** and **225'** (Figure 5.10), although it is hard to explain why the ratio would change according to the number of equiv. of Br<sub>2</sub>. It may also be that the minor signal observed for the pentabromide was also a bridge conformer **228'** (Figure 5.10).

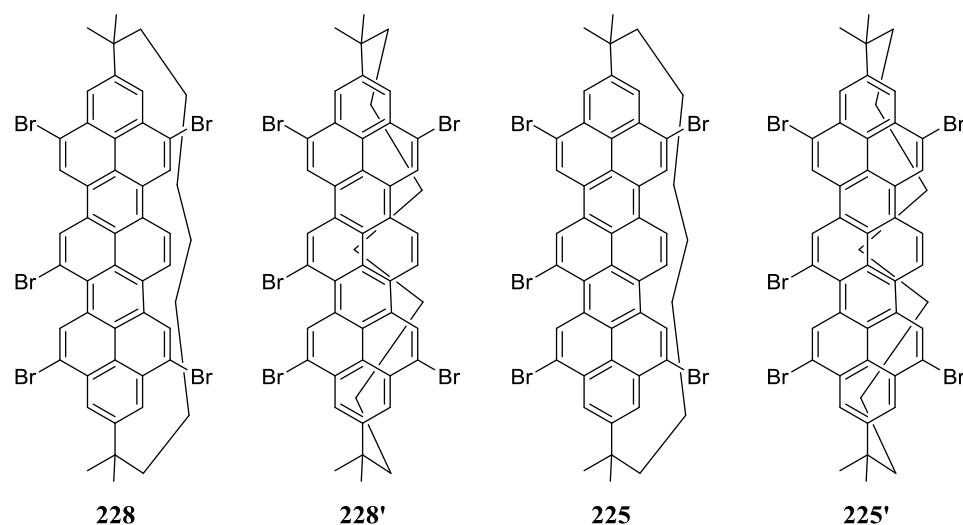


**Figure 5.10.** Two possible heptabromo isomers **225** and **225A**.

Up to this point, the introduction of seven bromine atoms to the teropyrene system had been observed. In an attempt to force an eight substitution to occur (to hopefully afford symmetrical octabromide **229**), a bromination reaction was performed using neat bromine. This gave rise to the formation of a mixture of tetrabromide **223**, pentabromide **228**, hexabromide **224** or **224A**, heptabromide **225** or **225A**, and a small amount (5%) of octabromide **229** ( $\delta$  9.70, 4H, s, C(5)-H, C(8)-H, C(14)-H, C(17)-H). Four very small singlets below  $\delta$  10.05 ppm ( $\delta$  10.08 – 10.30) were also observed, which may suggest that further bromination is occurring.

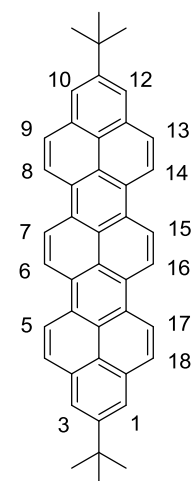
To further pursue octabromination, a set of reactions of teropyrenophane **8** with Br<sub>2</sub> (6.0–10.0 equiv.) in dichloromethane was conducted at 35 °C (Table 5.02; Figure 5.08, right; Figure 5.09, right). The product distributions were determined using <sup>1</sup>H NMR analysis as before. The results are not substantially different from those obtained from

the reactions performed at room temperature, so gentle heating did not prove to be useful. When a bromination reaction of **8** in neat Br<sub>2</sub> was heated at 35 °C, insoluble purple products were generated. Planar teropyrene (**22**) is known to be dark purple colour and very poorly soluble,<sup>25</sup> so it would appear that bridge cleavage occurs under these conditions. HBr is generated during the bromination reaction, so bridge cleavage could conceivably occur by retro-Friedel-Crafts reaction.

Tlc analysis of the brominated teropyrenophanes **226**, **213**, **227**, **223**, **228**, **224** and **225** revealed that they have *R<sub>f</sub>* values (10% CH<sub>2</sub>Cl<sub>2</sub>:hexanes) of 0.36, 0.41, 0.46, 0.54, 0.61, 0.75 and 0.80, respectively. As such, they could be separated using column chromatography to afford reasonably pure samples (70-95% by <sup>1</sup>H NMR; Table 5.03 and Figure 5.11). Interestingly, **228** which appeared as two different isomers (<sup>1</sup>H NMR spectrum of the crude reaction mixture), appeared as a single isomer after its subjection to column chromatography. <sup>1</sup>H NMR analysis showed that this isomer is the one that is thermodynamically more stable. The same is observed in the case of heptabromo compound **225**. A comparison of the <sup>1</sup>H NMR data for all brominated compounds revealed that, the most deshielded proton of the compounds with an odd number of bromine atoms (**228**, five Br atoms,  $\delta$  9.98; **225**, seven Br atoms,  $\delta$  10.04) appeared further downfield than those of the compounds with even number of bromines (**224**, six Br atoms,  $\delta$  9.60; **229**, eight Br atoms,  $\delta$  9.70). This rather low chemical shift in the penta and hepta systems is due to the reason that the respective Hs are present on the central pyrene unit (which is the most deshielded H in the parent teropyrenophane) and also lies *ortho*- to the 5th and 7th bromines in compounds **228** and **225**. On the other hand, in

**Table 5.03**  $^1\text{H}$  NMR data of bromocompounds **226-225**.

$\delta$ (ppm)	compound						
	<b>226</b>	<b>213</b>	<b>227</b>	<b>223</b>	<b>228</b>	<b>224</b>	<b>225</b>
H <sub>1</sub>	7.56	7.58	7.59	7.99	8.05-8.01	8.08	8.22-8.14
H <sub>3</sub>	7.89	7.91	7.92	7.99	8.05-8.01	8.12	8.22-8.14
H <sub>5</sub>	8.85	8.85	8.74	8.86	8.93	9.60	9.63/9.57
H <sub>6</sub>	8.83-8.70	8.80	8.83	8.76	—	—	—
H <sub>7</sub>	8.83-8.70	8.74	8.72/8.80	8.76	9.98	—	—
H <sub>8</sub>	8.54	8.54	8.85	8.86	8.85	9.60	9.63/9.57
H <sub>9</sub>	7.83	7.84	—	—	—	—	—
H <sub>10</sub>	7.53	7.58	7.97	7.99	8.05-8.01	8.12	8.22-8.14
H <sub>12</sub>	7.53	7.91	7.97	7.99	8.05-8.01	8.08	8.22-8.14
H <sub>13</sub>	7.81	—	—	—	—	—	—
H <sub>14</sub>	8.54	8.85	8.85	8.86	8.82/8.69	8.82	8.82/8.66
H <sub>15</sub>	8.83-8.70	8.80	8.72/8.80	8.76	8.69/8.71	8.62	—
H <sub>16</sub>	8.83-8.70	8.74	8.75	8.76	8.69/8.71	8.62	10.04
H <sub>17</sub>	8.54	8.54	8.54	8.86	8.82/8.69	8.82	8.82/8.66
H <sub>18</sub>	7.83	7.84	7.85	—	—	—	—



hexabromo compound **224** the Hs lie on the opposite side of the middle naphthalene unit whereas, in the octabromo compound **229** the Hs correspond to  $\delta$  8.80 present on the terminal *K*-regions. On the other hand, in mono-, di-, tri- and tetrabromo compounds the most deshielded Hs appeared at nearly the same region (**226**, one Br atom,  $\delta$  8.80; **213**, two Br atoms,  $\delta$  8.85; **227**, three Br atoms,  $\delta$  8.86; **223**, four Br atoms,  $\delta$  8.86). Tetrabromide **223** was observed to be the least soluble of the brominated teropyrenophanes,

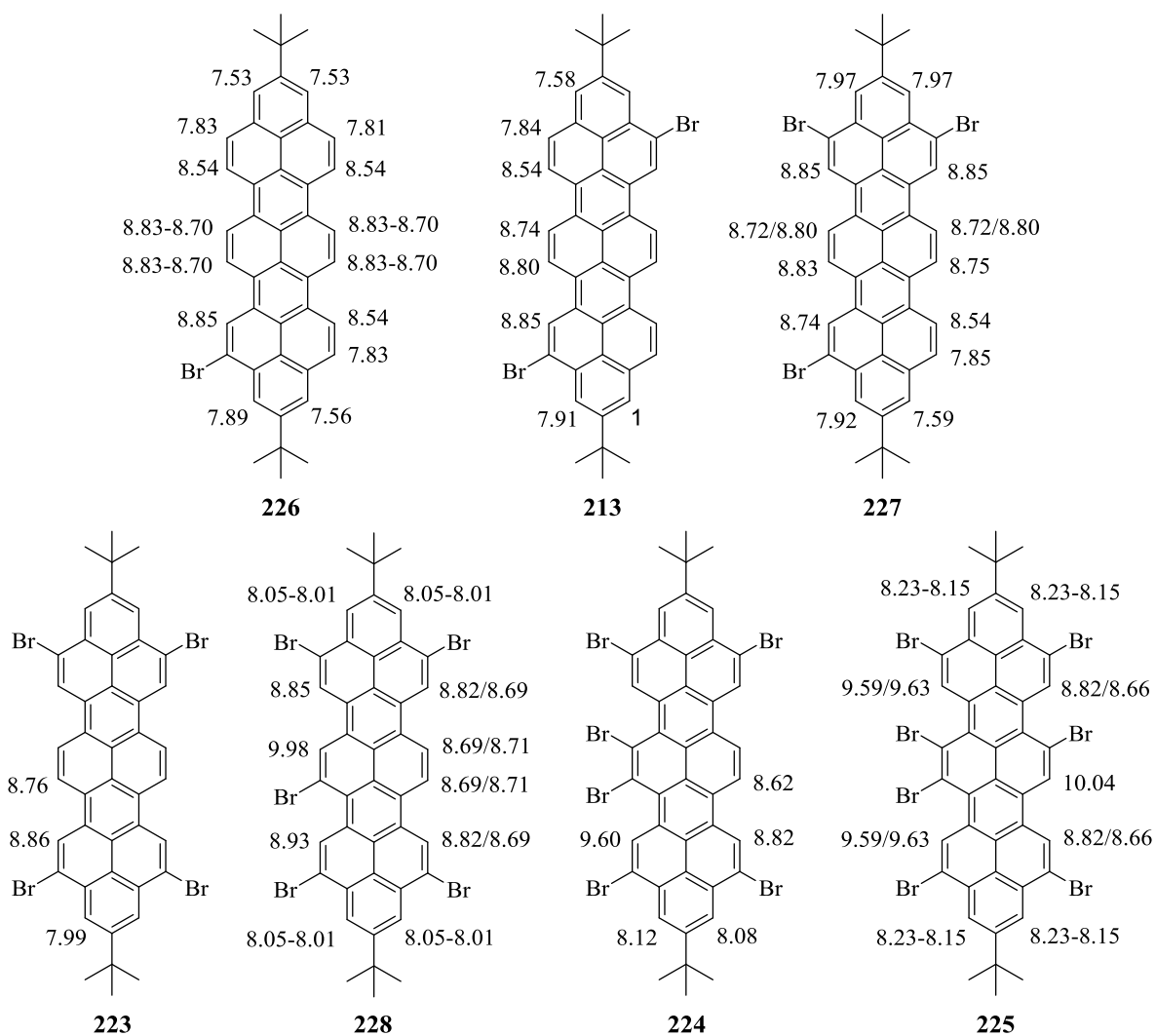


**Figure 5.11**  $^1\text{H}$  NMR chemical shifts of brominated teropyrenophanes.

presumably because it has the highest symmetry. (The same is expected for octabromo compound (some insoluble compound was observed in the bottom of the NMR tube when the crude reaction mixture corresponding to the 20 equiv. of  $\text{Br}_2$  reaction was dissolved in  $\text{CDCl}_3$ ) and this may be the reason why this compound could not be isolated).



### 5.3.1 Crystal structures of **223**, **224** and **225**.

With reasonably pure sample of most of the brominated teropyrenophanes in hand, attempts were made to grow crystals of all of them to confirm the NMR-based structural assignments. Good quality crystals were obtained for **223**, **224** and **225**. X-ray data were collected on Bruker APEX-II CCD diffractometer by Dr. Paul Boyle at Western University. Structures were solved by Dr. Louise Dawe at Wilfrid Laurier University.

#### 5.3.1.1 X-Ray structure of tetrabromo[9](2,11)teropyrenophane (**223**)

The asymmetric unit of tetrabromide **223** contains one primary molecule and half of a hexane molecule in close proximity, but not engaged in any supramolecular contacts, with the pore of the main molecule (Figure 5.12 shows the full symmetry-expanded hexane molecule). The overall bend of the teropyrene system ( $\theta_{\text{tot}}$ ) is  $157.4^\circ$ , which is slightly larger than that of the parent teropyrenophane **103d** ( $154.3^\circ$ ). Examination of the packing for **223** revealed close contacts between the  $\pi$ -systems for adjacent molecules. The centroid-to-centroid separations for the plane defined by the six carbon atoms of the terminal benzene ring in the teropyrene system in one molecule and its symmetry related ( $-x, 1-y, 1-z$ ) equivalent is  $3.68 \text{ \AA}$  (Figure 5.13). There are also close methyl  $\text{C}_{\text{sp}^3}\text{-H}\cdots\pi$  contacts ( $3.01$  and  $3.21 \text{ \AA}$ ) leading to a chain-like arrangement parallel to the  $b$ -axis (Figure 5.14).

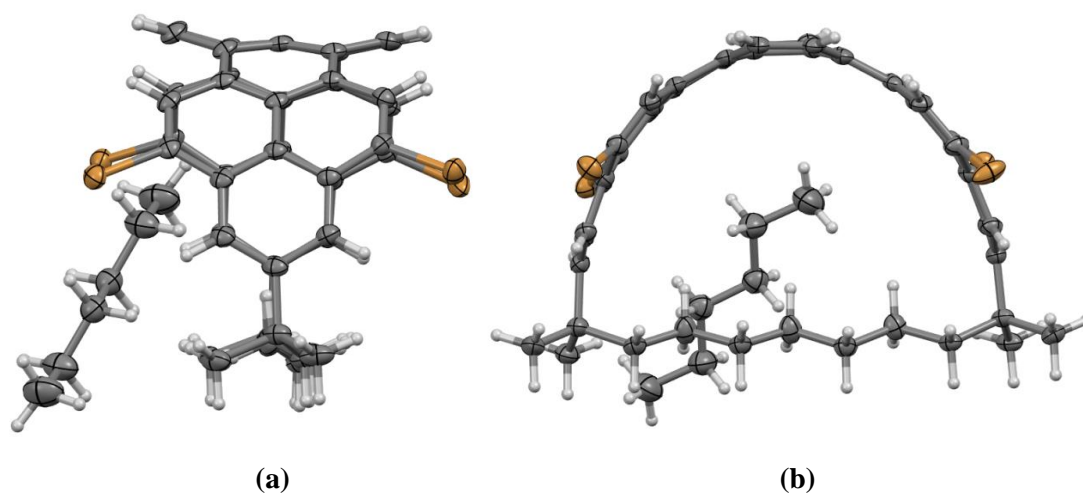


**Figure 5.12** Asymmetric unit of **223** with the symmetry expanded hexane molecule, represented with 50% probability ellipsoids. (a) and (b) are rotated by  $90^\circ$  to each other.

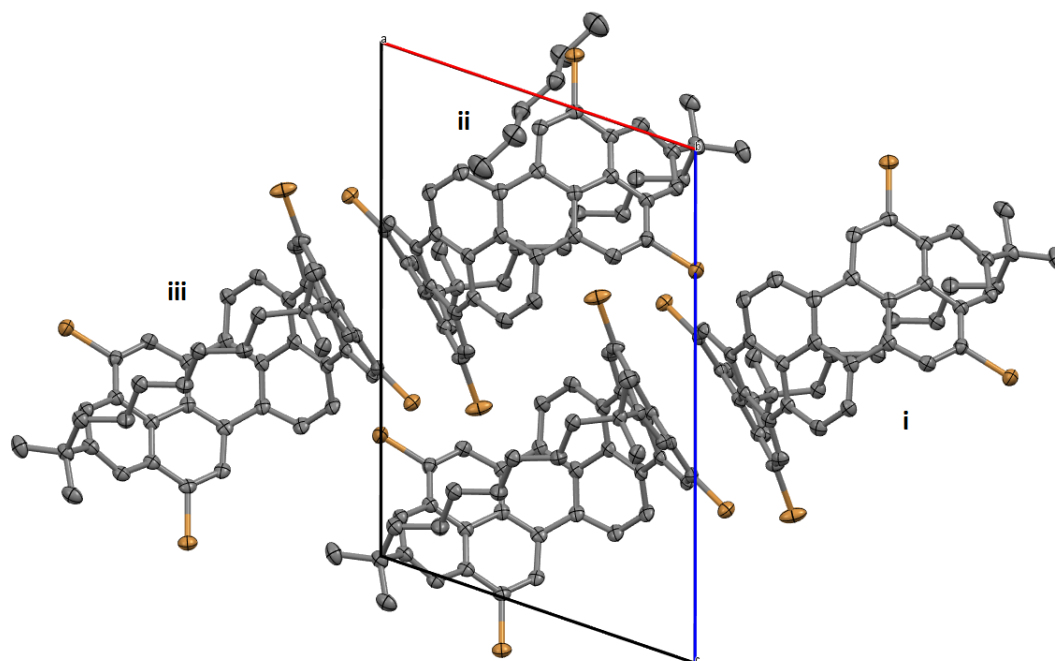


**Figure 5.13** Close  $\pi$ - $\pi$  contacts in **223**. H-atoms omitted for clarity. Symmetry operations  $i = -x, 1-y, 1-z$ ;  $ii = 1-x, 1-y, 1-z$ ;  $iii = 1+x, y, z$ .

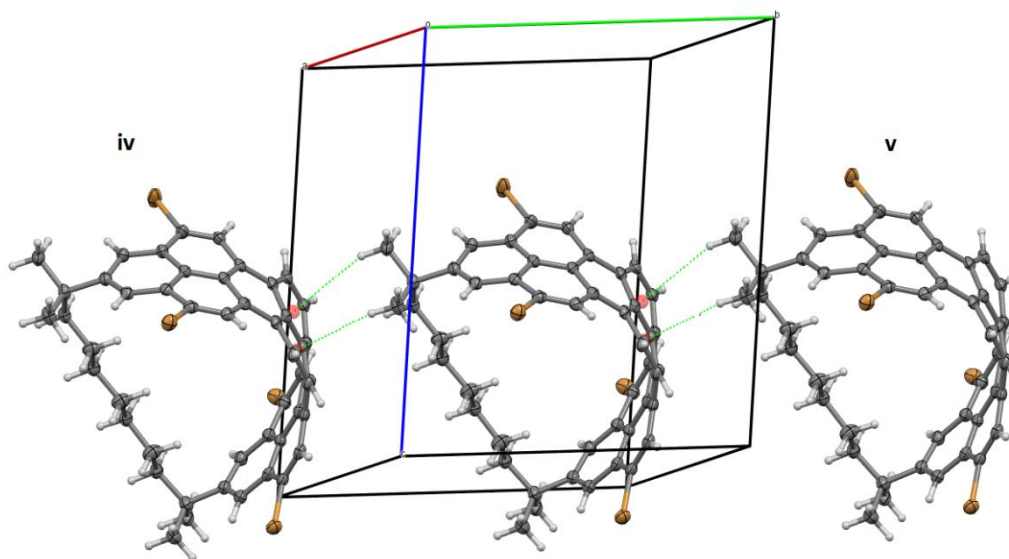


**Figure 5.14** Close methyl  $C_{sp3}\text{-H}\cdots\pi$  contacts in **223**. H-atoms omitted for clarity. Symmetry operations  $iv = x, -1-y, z$ ;  $v = x, 1+y, z$ .

### 5.3.1.2 X-Ray structure of hexabromo[9](2,11)teropyrenophane **224A**

The crystal structure of the hexabromoteropyrenophane immediately revealed that the structure was not **50** (the best guess from earlier), but rather **224A**, in which one of the two central *K*-regions bears two bromine atoms. The asymmetric unit of **224A** contains three independent primary moieties (A, B, and C, Figure 5.15). One of the molecules (Figure 5.15, molecule C) exhibited clear disorder in the Br atom positions with atoms Br(3), Br(4), Br(7) and Br(8) having refined occupancies of 0.945(3), 0.901(3), 0.060(3) and 0.091(3) respectively (Figure 5.16). The overall bend ( $\theta_{\text{tot}}$ ) for the teropyrene system in molecules A, B and C was found to be  $154.7^\circ$ ,  $154.6^\circ$  and  $154.4^\circ$ , respectively.

The selectivity in the sixth bromination event for the 4,6,7,9,13,18 isomer may have its origin in strain. Unlike the first four brominations, which place bromine atoms in

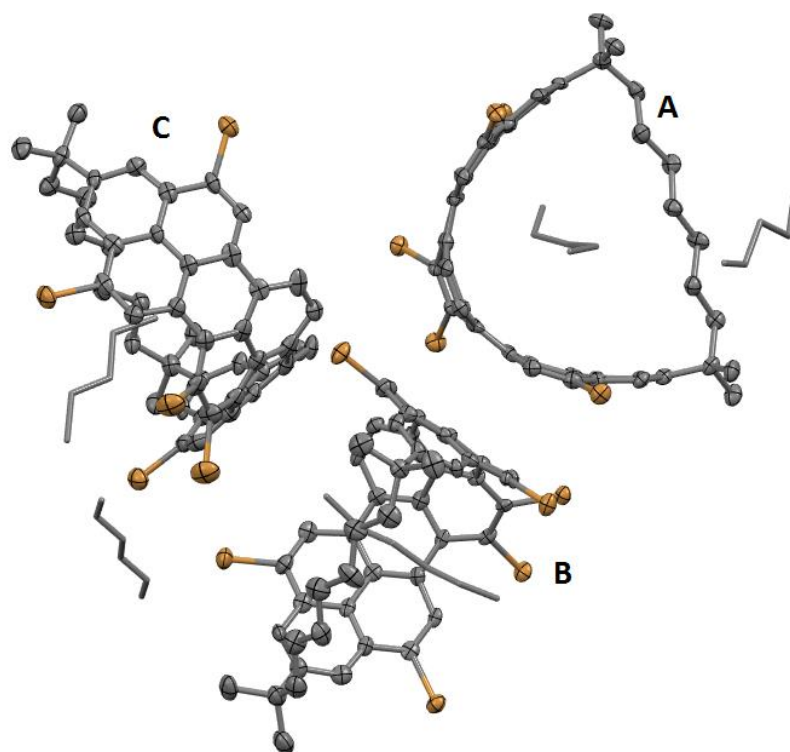


**Figure 5.15** The asymmetric unit of **224A**. H-atoms and minor Br disorder components omitted for clarity. Solvent molecules represented as capped sticks. All other atoms represented as 50% probability ellipsoids.

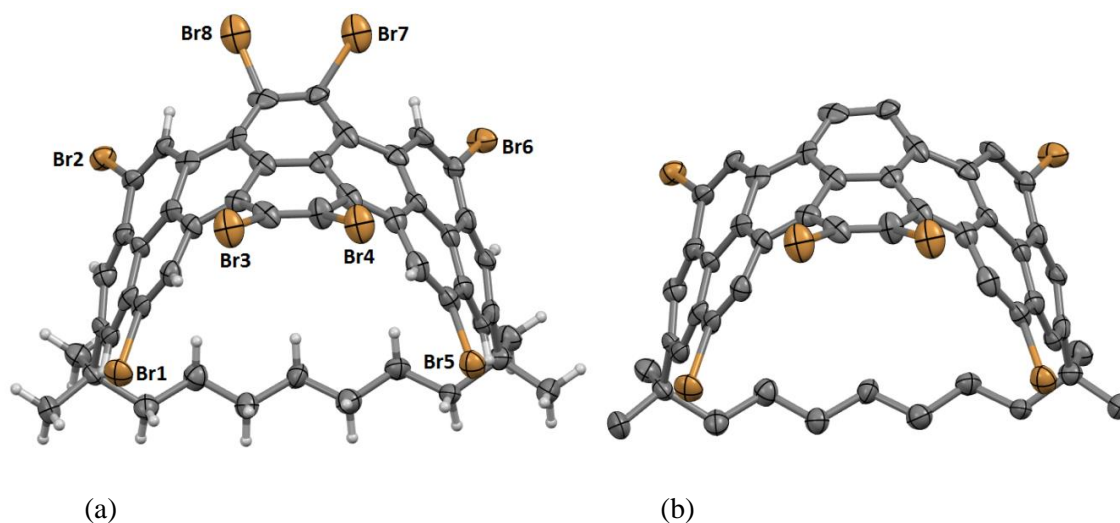


**Figure 5.16** Molecule **C** from **224A**; (a) includes both major and minor occupancy Br atoms while (b) has omitted both the minor occupancy Br(7) and Br(8) as well as the H-atoms.

*peri* positions, the fifth bromination places a bromine atom in a bay region (6 position of the teropyrene system). This causes local strain (*cf.* 1-bromophenanthrene), which pushes the bromine atom *and the C=C unit it is bonded to* up from the C–H unit on the other side of the bay. If the sixth bromination occurs at the 15 position (as originally guessed), then a similar amount of local strain would be expected to accrue. On the other hand, bromination at the 7 positions (as observed) would not be expected to result in much of an increase in strain because the C=C unit is already distorted as a result of the fifth bromination.

### 5.3.1.3 X-Ray structure of heptabromo[9](2,11)teropyrenophane **225**

The asymmetric unit of **225** contains one primary molecule, and both a full and half-occupancy *n*-hexane molecule in close proximity, but not engaged in any supramolecular contacts with the pore of the main molecule (Figure 5.17a shows the full symmetry-expanded hexane molecule). Disorder is present in the position of the bromine atoms, with Br1, Br2, Br7 and Br8 present at full occupancy and Br3, Br4, Br5 and Br6 present at 0.757(3), 0.834(3), 0.817(3) and 0.819(3) occupancy respectively (Figure 5.17b). These partial occupancy Br atoms sum to approximately 3.2, which is close to three, in agreement with the  $^1\text{H}$  NMR and mass spectrometry results. The overall bend ( $\theta_{\text{tot}}$ ) of the teropyrene system ( $\theta_{\text{tot}}$ ) is  $146.8^\circ$ . Examination of the packing for **225** reveals the inversion relationship (space group P-1) between the half-occupancy *n*-hexane molecule and close packing of two primary molecules (Figure 5.18). Close contacts (3.56–3.96 Å) between benzene ring centroids in adjacent molecules are also present

(Figure 5.19).

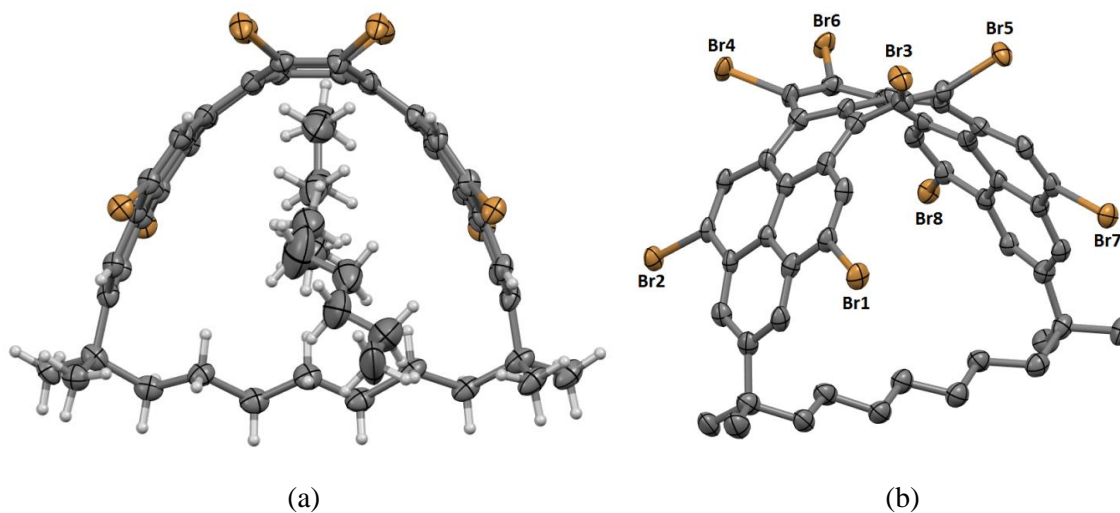


**Figure 5.17** 50% probability ellipsoids showing (a) the asymmetric unit of **225**, including the symmetry expanded half-occupancy *n*-hexane molecule and (b) the bromine atom labelling to show the location of the partial occupancy Br(3), Br(4), Br(5) and Br(6) atoms, with H atoms omitted for clarity.

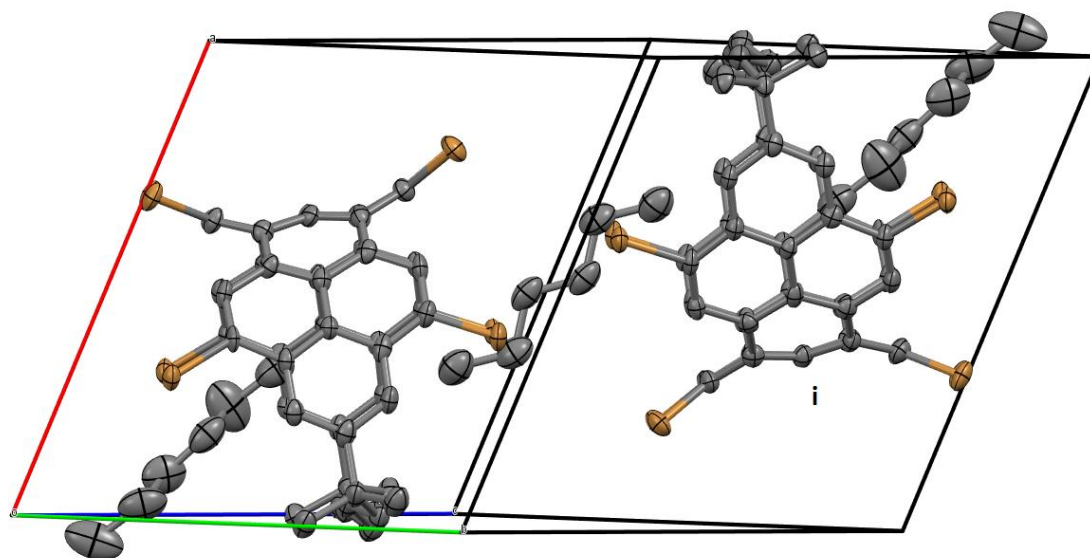


**Figure 5.18** Packed unit cell showing the inversion relationship and close contacts between **225** and the *n*-hexane molecules present in the lattice. H atoms omitted for clarity.  $i = 1-x, 1-y, 1-z$ .

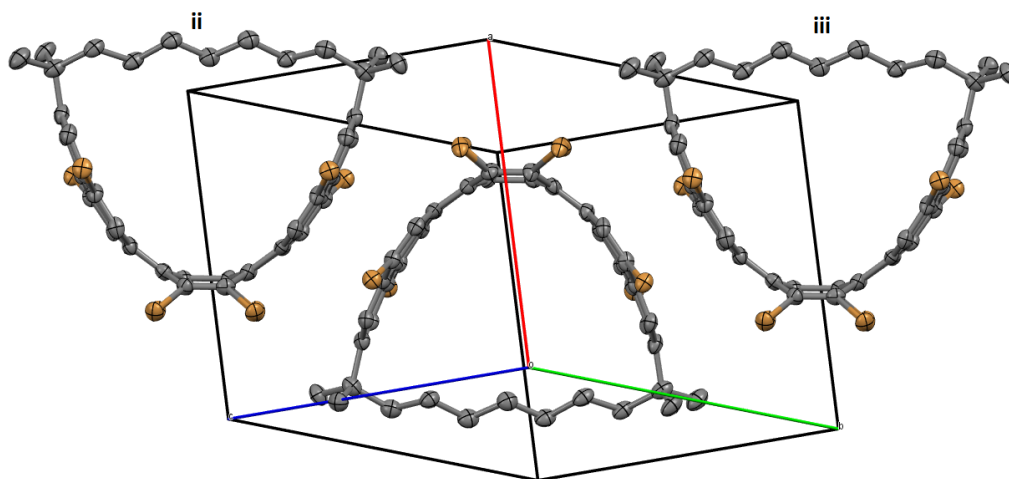


**Figure 5.19** Packing diagram showing close  $\pi$ - $\pi$  contacts in **225**. H atoms omitted for clarity. ii =  $1-x, -y, 1-z$ ; iii =  $1-x, 1-y, -z$ .

#### 5.4 Bromination of 1,1,7,7-tetramethyl[7](2,11)teropyrenophane (**103b**), 1,1,8,8-tetramethyl[8](2,11)teropyrenophane (**103c**) and 1,1,10,10-tetramethyl[10](2,11)teropyrenophane (**103e**)

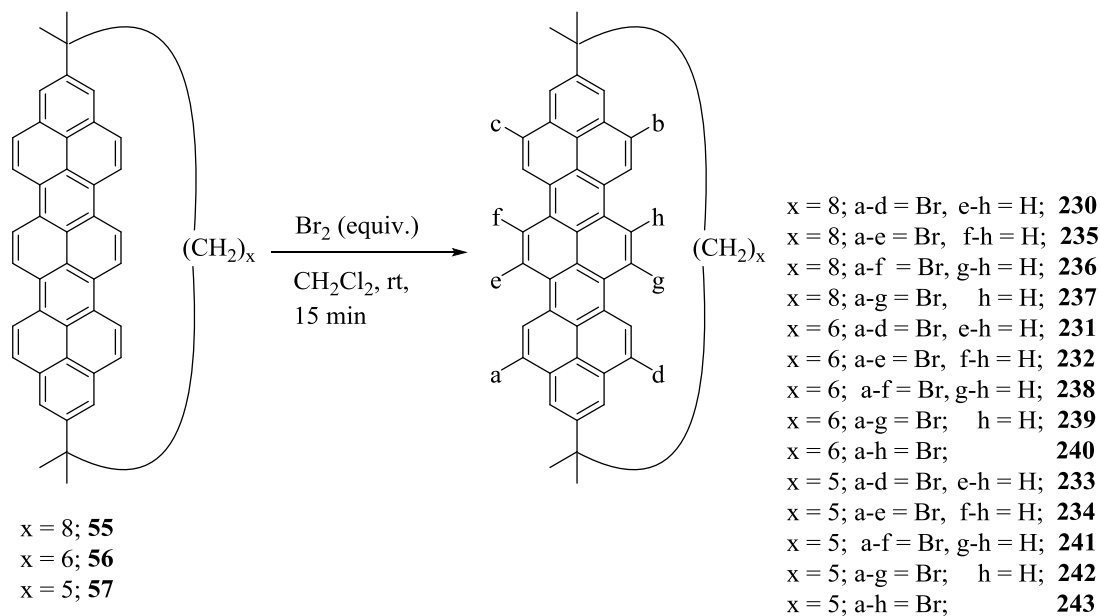
The excellent selectivity observed for the bromination of **103d** to afford tetrabromide **223** exclusively prompted an investigation of whether the other teropyrenophanes (**103b-c**, and **103e**) could be tetrabrominated in the same way. When the less strained 1,1,10,10-tetramethyl[10](2,11)teropyrenophane (**103e**) was treated with 4.0 equiv. of  $\text{Br}_2$ , bromination proceeded smoothly and tetrabromide **230** was obtained as the only product (Table 5.04). Upon moving to the more strained 1,1,8,8-tetramethyl[8](2,11)teropyrenophane (**103c**), its reaction with 4.0 equiv. of  $\text{Br}_2$  afforded a 70:30 mixture of tetrabromide **231** and pentabromide **232** ( $^1\text{H}$  NMR analysis). Similarly, the most strained teropyrenophane **103b**, reacted to afford a 60:40 mixture of

tetrabromide **233** and pentabromide **234** ( $^1\text{H}$  NMR analysis). The latter two results imply not only that the teropyrene systems becomes more reactive as it becomes more bent (at least as far as the fifth bromination is concerned), but also that at least 4.4 equiv. of  $\text{Br}_2$  must have been present in the solution of  $\text{Br}_2$  that was added to the starting materials. The *ca.* 10% error in the amount of  $\text{Br}_2$  that was added is likely a consequence of the small scale that the bromination reactions were performed on (3.0 mg).

Teropyrenophanes **103b-c** and **103e** were then brominated using 20 equiv. of  $\text{Br}_2$ . The least strained member of the series **103e** afforded a mixture of tetrabromide **230**, pentabromide **235**, hexabromide **236** and heptabromide **237** in a 0.30:0.40:0.15:0.15 mole ratio ( $^1\text{H}$  NMR analysis). This reaction clearly did not progress as far as the analogous reaction of [9]teropyrenophane **103d**, which afforded only traces amounts of tetrabromide **223** along with penta-, hexa- and heptabromides **228**, **224A** and **225** in a 0.15:0.25:0.58 ratio. The reaction of [8]teropyrenophane **103c** resulted in the formation of a 0.20:0.70:0.10 mixture of hexabromide **238**, heptabromide **239** and octabromide **240**, the latter of which exhibited two singlets at  $\delta$  9.51 ppm and  $\delta$  8.16 ppm in its  $^1\text{H}$  NMR spectrum. Although the observation of a significant amount of an octabromide was a gratifying result, this more highly symmetrical compound was found to have rather low solubility. The crude product of the reaction could not be completely dissolved for analysis by  $^1\text{H}$  NMR, which may mean that the proportion of octabromide **240** is actually underestimated. The most strained teropyrenophane **103b** reacted to afford hexabromide **241**, heptabromide **242** and octabromide **243** in a ratio of 0.20:0.50:0.30. The increase in the mole fraction of the octabromide ( $\delta$  9.39, s, 4H;  $\delta$  8.02, s, 4H) again indicates an



**Table 5.04** Bromination of teropyrenophanes **103b**, **103c** and **103d**.



bromo compound	4.0 equiv. Br <sub>2</sub>			20.0 equiv. Br <sub>2</sub>		
	103e	103c	103b	103e	103c	103b
<b>230</b>	1.00	-	-	0.30	-	-
<b>235</b>	-	-	-	0.40	-	-
<b>236</b>	-	-	-	0.15	-	-
<b>237</b>	-	-	-	0.15	-	-
<b>231</b>	-	0.70	-	-	-	-
<b>232</b>	-	0.30	-	-	-	-
<b>238</b>	-	-	-	-	0.20	-
<b>239</b>	-	-	-	-	0.70	-
<b>240</b>	-	-	-	-	0.10	-
<b>233</b>	-	-	0.60	-	-	-
<b>234</b>	-	-	0.40	-	-	-
<b>241</b>	-	-	-	-	-	0.20
<b>242</b>	-	-	-	-	-	0.50
<b>243</b>	-	-	-	-	-	0.30

increase in reactivity with an increase in the bend in the teropyrene system. This behaviour may be related to the fact that the fifth to eight brominations occur in bay regions. As the teropyrene system becomes more bent, the four bay regions become more distorted. In so doing, the introduction of a bromine atom requires less and less additional distortion of the bay region.

#### 5.4.1 X-Ray structure of octabromo[8](2,11)teropyrenophane **241**

The asymmetric unit of **241** contains one primary molecule, and two half-occupancy *n*-hexane molecules in close proximity, but not engaged in any supramolecular contacts, with the pore of the main molecule (Figure 5.20b shows the full symmetry-expanded hexane molecules). Disorder is present in the position of the bromine atoms Br5 and Br6 (their minor components are named Br5a and Br6a). Br5 and Br6 are present at 0.924(2) and 0.960(2)-occupancy, respectively, while the minor components are present at 0.076(2) and 0.040(2)-occupancy. This suggests that there is a small amount (*ca.* 10%) of isomeric octabromide **242** present in the sample. The alkyl chain also exhibited positional disorder with occupancy that was not tied to the bromine atoms (respective occupancy of the major and minor chain were 0.779(14):0.221(14); Figure 20a). The overall bend of the main molecule sums to 162.3°, which is a little smaller than that observed for the parent teropyrenophane **103c** ( $\theta_{\text{tot}} = 167.0^\circ$ ). Examination of the packing for **241** reveals the 45° rotation relationship between the half-occupancy *n*-hexane molecule and close packing with two primary molecules (Figure 5.21). The molecules further exhibit inverse pairwise association *via*  $\pi$ - $\pi$  interactions on one side

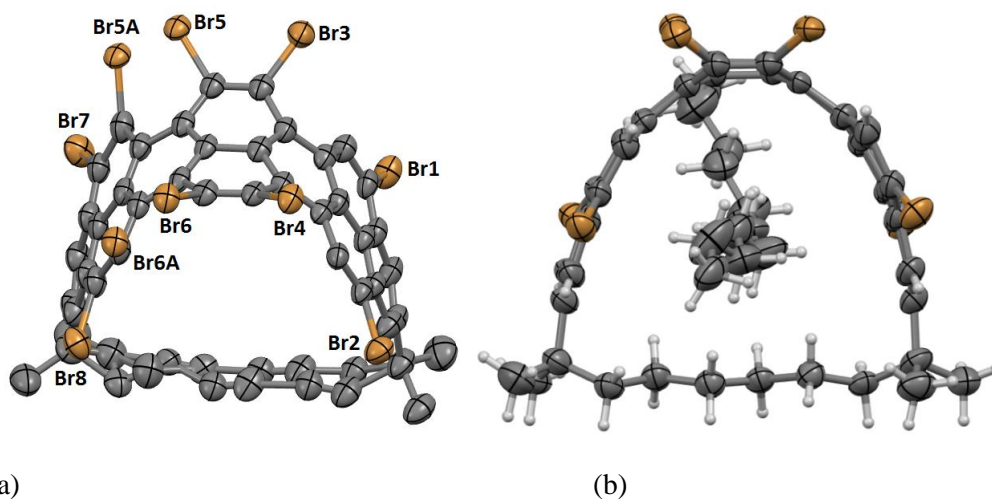


**Figure 5.20** 50% probability displacement ellipsoids for **241** showing (a) the minor disorder components for both bromine atoms and the alkyl chain (with H-atoms and lattice solvent omitted for clarity) and (b) the asymmetric unit of **241** with minor disorder components omitted for clarity, and lattice solvent included to show close association with the main molecule.

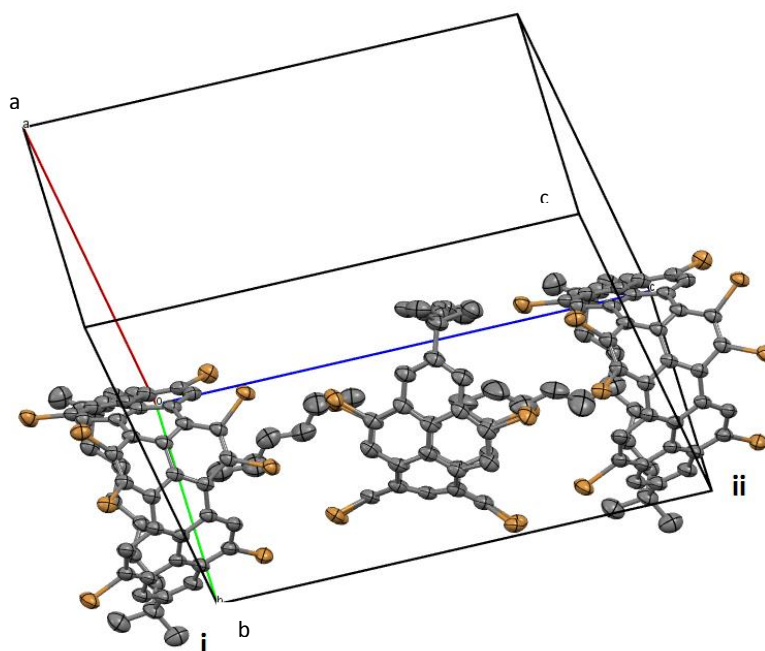


**Figure 5.21** Partially packed unit cell showing the rotation by  $45^\circ$  and close contacts between **241** and the *n*-hexane molecules present in the lattice, running parallel to the *c*-axis. H-atoms omitted for clarity.  $i = \frac{1}{2}-x, y, \frac{1}{2}-z$ ;  $ii = \frac{1}{2}-x, y, \frac{3}{2}-z$ .

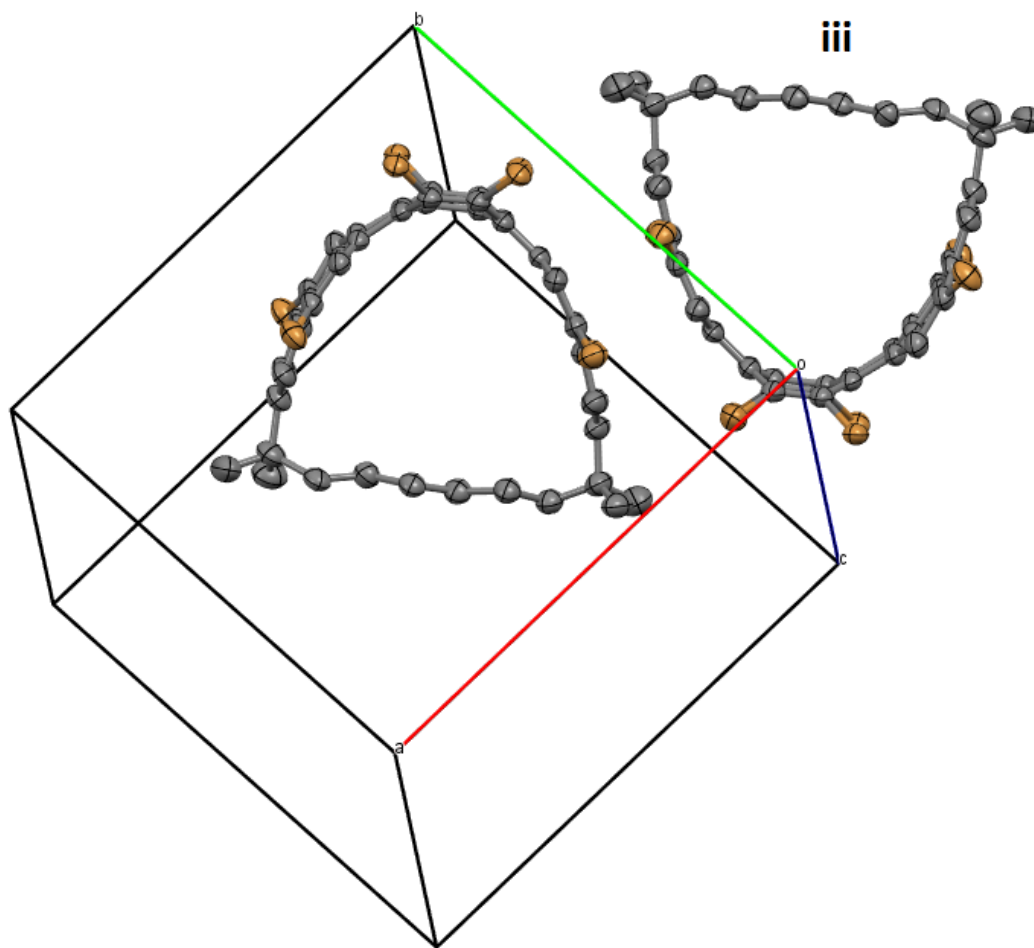


**Figure 5.22** The inverse pairwise association of molecules in **241** *via*  $\pi$ - $\pi$  interactions. H-atoms, lattice solvent and minor disorder components omitted for clarity.  $\text{iii} = -x, 1-y, 1-z$ .

only (Figure 5.22), with closest contacts between the planes formed by a six-membered ring in the teropyrene system to its symmetry related centroid of 3.24 Å, and centroid-to-centroid separations of 3.38 Å off-set by 0.97 Å.

## 5.5 Conclusion

The bromination of cyclophanemoene **109d** suggested the more reactivity of teropyrenophane **103d** when compared to the intermediate dihydroteropyrenophane **146d** and ends up delivering the brominated teropyrenophanes. Therefore, the bromination chemistry of teropyrenophanes has been explored on a series of teropyrenophanes **103b-e**. Series of bromination experiments on **103d** by varying the equiv. of bromine proved the most reactive sites for the bromination are 4, 9, 13 and 18 positions, followed by 6, 7, 15 and 16 positions. Mono-, di- and tribromo compounds **226**, **213** and **227** are formed in 65%, 80% and 70% at 1.0, 2.0 and 3.0 equiv. of bromine respectively. On the other hand, the tetrabromo compound **223** showed excellent selectivity and is formed as the only product when 4.0 equiv. of bromine was used. Thereon, the bromination became sluggish and the next higher brominated products were formed as a mixture.

The regioselectivity of the dibromo compound is very interesting in which the two bromines occupied 4 and 13 positions. No other regio-isomers were observed by <sup>1</sup>H-NMR spectroscopy. The origin of this particular selectivity is not clear. This ultimately directed the next two bromines to 9 and 18 to obtain the 4,9,13,18-tetrabromo compound as the only isomer. Also, the selectivity for hexa bromination was observed at 4,6,7,9,13,18 positions and this is possibly due to minimization of strain in the molecule.

The teropyrene system appears to become more reactive toward bromination as it becomes more distorted and this is clearly seen in the case of octabromination. The ratio of occurrence of octabromination increased from **103e** to **103b** (trace to 30%). This may

also have its roots in strain: the more strained teropyrene systems become, the less that bromination in the central *K*-region causes an increase in strain.

## 5.6 Experimental section

### General procedure for bromination of teropyrenophanes

[*n*](2,11)teropyrenophane (3.0 mg, 0.005 mmol) was dissolved in dichloromethane (*x* mL) and bromine (*x* mL, *x* mmol in dichloromethane (*x* mL)) (Table 5.04) was added to the teropyrenophane solution in a 10 mL vial. The vial was tightly sealed with cap and the reaction mixture was stirred at room temperature or 35 °C (Table 5.04) for a period of 30 min. The reaction mixture was then suction filtered through a plug of silica gel. The plug of silica was washed with excess chloroform and the solvents were removed under reduced pressure. The crude solid obtained was characterized by <sup>1</sup>H NMR spectroscopy.

#### *Preparation of the stock solution of bromine in dichloromethane:*

0.3 mL of bromine was dissolved in 250 mL of dichloromethane (freshly prepared) of which 0.1 mL solution contains 0.0023 mol bromine (0.5 equiv.). 0.1 mL increments of this solution was used for the higher equiv. of bromine. For 20 equiv. of bromine a total amount of 4.0 mL of stock solution is required (see Table 5.04). The total volume of dichloromethane for all the reactions were maintained as 4.0 mL.

In order to purify the product mixture, the combined crude products were subjected to Column chromatography as described below. The crude products resulted from 0.5-3.5 equiv. bromine were combined and subjected to column chromatography (8.0 cm × 2.5

**Table 5.04** List of the experiments performed by increasing 0.5 equiv. of Br<sub>2</sub>.

Exp No.	stock solution (mL)	Br <sub>2</sub> , mmol (equiv.)	CH <sub>2</sub> Cl <sub>2</sub> (x mL)
1 <sup>a</sup>	0.1	0.0023 (0.5)	3.9
2	0.2	0.0047 (1.0)	3.8
3	0.3	0.0070 (1.5)	3.7
4	0.4	0.0094 (2.0)	3.6
5	0.5	0.0117 (2.5)	3.5
6	0.6	0.0141 (3.0)	3.4
7	0.7	0.0164 (3.5)	3.3
8	0.8	0.0188 (4.0)	3.2
9	0.9	0.0211 (4.5)	3.1
10	1.0	0.0235 (5.0)	3.0
11	1.1	0.0258 (5.5)	2.9
12 <sup>b</sup>	1.2	0.0281 (6.0)	2.8
13	1.3	0.0304 (6.5)	2.7
14	1.4	0.0327 (7.0)	2.6
15	1.5	0.0350 (7.5)	2.5
16	1.6	0.0373 (8.0)	2.4
17	1.7	0.0603 (8.5)	2.3
18	1.8	0.0833 (9.0)	2.2
19	1.9	0.1063 (9.5)	2.1
20	2.0	0.1293 (10.0)	2.0
21	4.0	0.3450 (20.0)	–
22	neat	–	–

<sup>a</sup>experiments 1-22 were conducted at room temperature<sup>b</sup>experiments 12-22 were conducted at 35 °C.

cm, 5% dichloromethane:hexanes). The monobromo product **226** was unable to obtain in pure form (*ca.* 70% purity by  $^1\text{H}$  NMR). The dibromo product **213** was isolated in about 85% purity and the tribromo compound **227** was obtained in about 85% purity. The crude products resulted from 5.0-10 equiv. of bromination reaction were combined and then subjected to a second column chromatography (8.0 cm  $\times$  2.5 cm, 100% hexanes) to obtain penta, hexa and heptabromo compounds **228**, **224** and **225** in *ca.* 90%, 85% and 90% respectively ( $^1\text{H}$  NMR).

4-Bromo-1,1,9,9-tetramethyl[9](2,11)teropyrenophane **226**:  $R_f$  = 0.36 (10% dichloromethane / hexanes);  $^1\text{H}$  NMR (300 MHz,  $\text{CDCl}_3$ )  $\delta$  8.85 (s, 1H), 8.83–8.70 (m, 4H), 8.54 (d,  $J=9.4$  Hz, 3H), 7.89 (d,  $J=1.7$  Hz, 1H), 7.83 (d,  $J=9.4$  Hz, 2H), 7.81 (d,  $J=9.4$  Hz, 1H), 7.56 (d,  $J=1.7$  Hz, 1H), 7.53 (s, 2H), 1.44 (s, 3H), 1.40 (s, 3H), 1.38 (s, 3H), 1.38 (s, 3H), 0.93–0.71 (m, 4H), 0.18–0.03 (m, 4H), –0.38–(–0.65) (m, 2H), –0.83–(–1.18) (m, 4H); LCMS (APCI-positive)  $m/z$  (rel. int.) 713 (9), 712 (5), 711 ( $[\text{M}+\text{H}]^+$ , 100), 710 (61), 709 (99), 708 (13); APPI calculated for  $\text{C}_{49}\text{H}_{41}\text{Br}$  ( $[\text{M}+\text{H}]^+$ ) 708.2368, found 708.2368.

4,13-Dibromo-1,1,9,9-tetramethyl[9](2,11)teropyrenophane **213**:  $R_f$  = 0.41 (10% dichloromethane/hexanes);  $^1\text{H}$  NMR (300 MHz,  $\text{CDCl}_3$ )  $\delta$  8.58 (s, 2H), 8.80 (d,  $J=10.0$  Hz, 2H), 8.74 (d,  $J=10.0$  Hz, 2H), 8.54 (d,  $J=9.5$  Hz, 2H), 7.90 (d,  $J=1.6$  Hz, 2H), 7.83 (d,  $J=9.5$  Hz, 2H), 7.58 (d,  $J=1.6$  Hz, 2H), 1.43 (s, 6H), 1.40 (s, 6H), 0.97–0.76 (m, 4H), 0.15–0.03 (m, 4H), –0.43–(–0.60) (m, 2H), –0.91–(–1.10) (m, 4H); LCMS (APCI-positive)  $m/z$  (rel. int.) 793 (6), 792 (26), 791 (60), 790 (49), 789 (100), 788 (36), 787 ( $[\text{M}+\text{H}]^+$ , 46); APPI calculated for  $\text{C}_{49}\text{H}_{40}\text{Br}_2$  ( $[\text{M}+\text{H}]^+$ ) 786.1497, found 786.1407.



4,9,13-Tribromo-1,1,9,9-tetramethyl[9](2,11)teropyrenophane **227**;  $R_f$  = 0.46 (10% dichloromethane/hexanes);  $^1\text{H}$  NMR (300 MHz,  $\text{CDCl}_3$ )  $\delta$  8.56 (s, 2H), 8.82 (d,  $J=10.0$  Hz, 1H), 8.78 (d,  $J=10.0$  Hz, 1H), 8.76–8.70 (m, 3H), 8.54 (d,  $J=9.5$  Hz, 1H), 7.97 (s, 2H), 7.92 (d,  $J=1.6$  Hz, 1H), 7.86 (d,  $J=9.5$  Hz, 1H), 7.59 (d,  $J=1.6$  Hz, 1H), 1.45 (s, 6H), 1.43 (s, 3H), 1.39 (s, 3H), 0.93–0.80 (m, 4H), 0.23–0.03 (m, 4H), –0.36–(–0.65) (m, 2H), –0.80–(–1.15) (m, 4H); LCMS (APCI-positive)  $m/z$  (rel. int.) 951 (23), 950 (24), 949 (59), 948 (65), 947 (100), 946 (32), 945 (32), 944 (74), 943 (15), 942 ( $[\text{M}+\text{H}]^+$ , 15), 941 (15); APPI calculated for  $\text{C}_{49}\text{H}_{40}\text{Br}_2$  ( $[\text{M}+\text{H}]^+$ ) 941.9707, found 941.8865.

4,9,13,18-Tetrabromo-1,1,9,9-tetramethyl[9](2,11)teropyrenophane **223**;  $R_f$  = 0.54 (10% dichloromethane/hexanes);  $^1\text{H}$  NMR (300 MHz,  $\text{CDCl}_3$ )  $\delta$  8.86 (s, 4H), 8.76 (s, 4H), 7.99 (s, 4H), 1.45 (s, 12H), 0.91–0.80 (m, 4H), 0.25–0.03 (m, 4H), –0.36–(–0.59) (m, 2H), –0.82–(–1.07) (m, 4H);  $^{13}\text{C}$  NMR (75 MHz,  $\text{CDCl}_3$ )  $\delta$  147.56, 127.49, 126.80, 126.39, 126.29, 125.94, 124.43, 123.89, 123.15, 122.87, 122.29, 47.30, 38.59, 37.13, 31.96, 30.18, 29.74.

4,6,9,13,18-Pentabromo-1,1,9,9-tetramethyl[9](2,11)teropyrenophane **228**;  $R_f$  = 0.61 (10% dichloromethane/hexanes);  $^1\text{H}$  NMR (300 MHz,  $\text{CDCl}_3$ )  $\delta$  9.98 (s, 1H), 8.92 (s, 1H), 8.85 (s, 1H), 8.82 (s, 1H), 8.73–8.67 (m, 3H), 8.07–8.00 (m, 4H), 1.46 (s, 9H), 1.45 (s, 3H), 0.80–0.70 (m, 4H), 0.21–0.04 (m, 4H), –0.37–(–0.59) (m, 2H), –0.82–(–1.12) (m, 4H).

4,6,7,9,13,18-Hexabromo-1,1,9,9-tetramethyl[9](2,11)teropyrenophane **224**;  $R_f$  = 0.75 (10% dichloromethane/hexanes);  $^1\text{H}$  NMR (500 MHz,  $\text{CDCl}_3$ )  $\delta$  9.60 (s, 1H), 8.82 (s,

1H), 8.62 (s, 1H), 8.12 (d,  $J=1.6$  Hz, 2H), 8.08 (d,  $J=1.6$  Hz, 2H), 1.49 (s, 6H), 1.46 (s, 6H), 1.00–0.84 (m, 4H), 0.22–0.10 (m, 4H), –0.37–(–0.55) (m, 2H), –0.78–(–1.04) (m, 4H).

4,6,7,9,13,15,18-Heptabromo-1,1,9,9-tetramethyl[9](2,11)teropyrenophane **225**;  $R_f = 0.80$  (10% dichloromethane/hexanes);  $^1\text{H}$  NMR (300 MHz,  $\text{CDCl}_3$ )  $\delta$  10.04 (s, 1H), 9.63 (s, 1H), 9.57 (s, 1H), 8.82 (s, 1H), 8.67 (s, 1H), 8.20–8.12 (m, 4H), 1.51 (s, 3H), 1.50 (s, 3H), 1.47 (s, 6H), 1.00–0.84 (m, 4H), 0.07–0.01 (m, 4H), –0.59–(–0.68) (m, 2H), –0.69–(–1.08) (m, 4H).

## 5.7 References

1. S. Iijima, *Nature*, 1991, **354**, 56–58.
2. a) B. Lassagne, Y. Tarakanov, J. Kinaret, D. Garcia-Sanchez, A. Bachtold, *Science*, 2009, **325**, 1007–1110. b) M. Aykol, B. Hou, R. Dhall, S.-W. Chang, W. Branham, J. Qiu, S. B. Cronin, *Nano Lett.*, 2014, **14**, 2426–430.
3. a) M. Freitag, M. Steiner, A. Naumov, J. P. Small, A. A. Bol, V. Perebeinos, P. Avouris, *ACS Nano*, 2009, **3**, 3744–3748. b) Y. Yamaguchi, S. Haraguchi, N. Nakashima, *Chem. Lett.*, 2008, **37**, 546–547.
4. a) P. Avouris, G. Dresselhaus, M. S. Dresselhaus, *Carbon Nanotubes: Synthesis, Structure, Properties and Applications*, Springer-Verlag: Berlin, 2000. b) M. Meyyappan, *Carbon Nanotubes-Science and Applications*, CRC Press: New York,

2005. c) Z. Liu, J. Zhao, W. Xu, L. Qian, S. Nei, Z. Cui, *Appl. Mater. Interfaces*, 2014, **6**, 9997–10004.
5. a) D. Wei, Y. Liu, L. Cao, H. Zhang, L. Huang, G. Yu, *Chem. Mater.*, 2010, **22**, 288–293. b) L. Jia, H. Kou, Y. Jiang, S. Yu, J. Li, C. Wang, *Electrochimica Acta*, 2013, **107**, 71–77.
6. M. del C. Giménez-López, F. Moro, A. L. Torre, C. J. Gómez-García, P. D. Brown, J. van Slageren, A. N. Khlobystov, *Nat. Commun.*, 2011, **2**, 1415.
7. a) P. M. Ajayan, *Chem. Rev.*, 1999, **99**, 1787–1800; b) M. M. A. Rafique, J. Iqbal, *J. Encapsulation adsorp. Sci.*, 2011, **1**, 29–34; c) C. Journet, W. K. Maser, P. Bernier, A. Loiseau, M. L. de la Chapelle, S. Lefrant, P. Deniard, R. Lee and J. E. Fischer, *Nature*, 1997, **388**, 756–758.
8. a) E. Heilbronner, *Helv. Chim. Acta*, 1954, **37**, 921–935. K. Tahara, Y. Tobe, *Chem. Rev.*, 2006, **106**, 5274–5290. b) T. Yao, H. Yu, R. J. Vermeij, G. J. Bodwell, *Pure Appl. Chem.*, 2008, **80**, 533–546.
9. a) F. Sibbel, K. Matsui, Y. Segawa, A. Studer, K. Itami, *Chem. Commun.*, 2014, **50**, 954–956. b) H. Omachi, S. Matsuura, Y. Segawa, K. Itami, *Angew. Chem. Int. Ed.*, 2010, **49**, 10202–10205. c) Y. Ishii, Y. Nakanishi, H. Omachi, S. Matsuura, K. Matsui, H. Shinohara, Y. Segawa, K. Itami, *Chem. Sci.*, 2012, **3**, 2340–2345. d) H. Omachi, Y. Segawa, K. Itami, *Acc. Chem. Res.*, 2012, **45**, 1378–1389. e) K. Matsui, Y. Segawa, K. Itami, *J. Am. Chem. Soc.*, 2014, **136**, 16452–16458. f) T. J. Sisto, M. R. Golder, E. S. Hirst, R. Jasti, *J. Am. Chem. Soc.*, 2011, **133**, 15800–15802. g) E. R. Darzi, T. J. Sisto, R. Jasti, *J. Org. Chem.*, 2012, **77**,

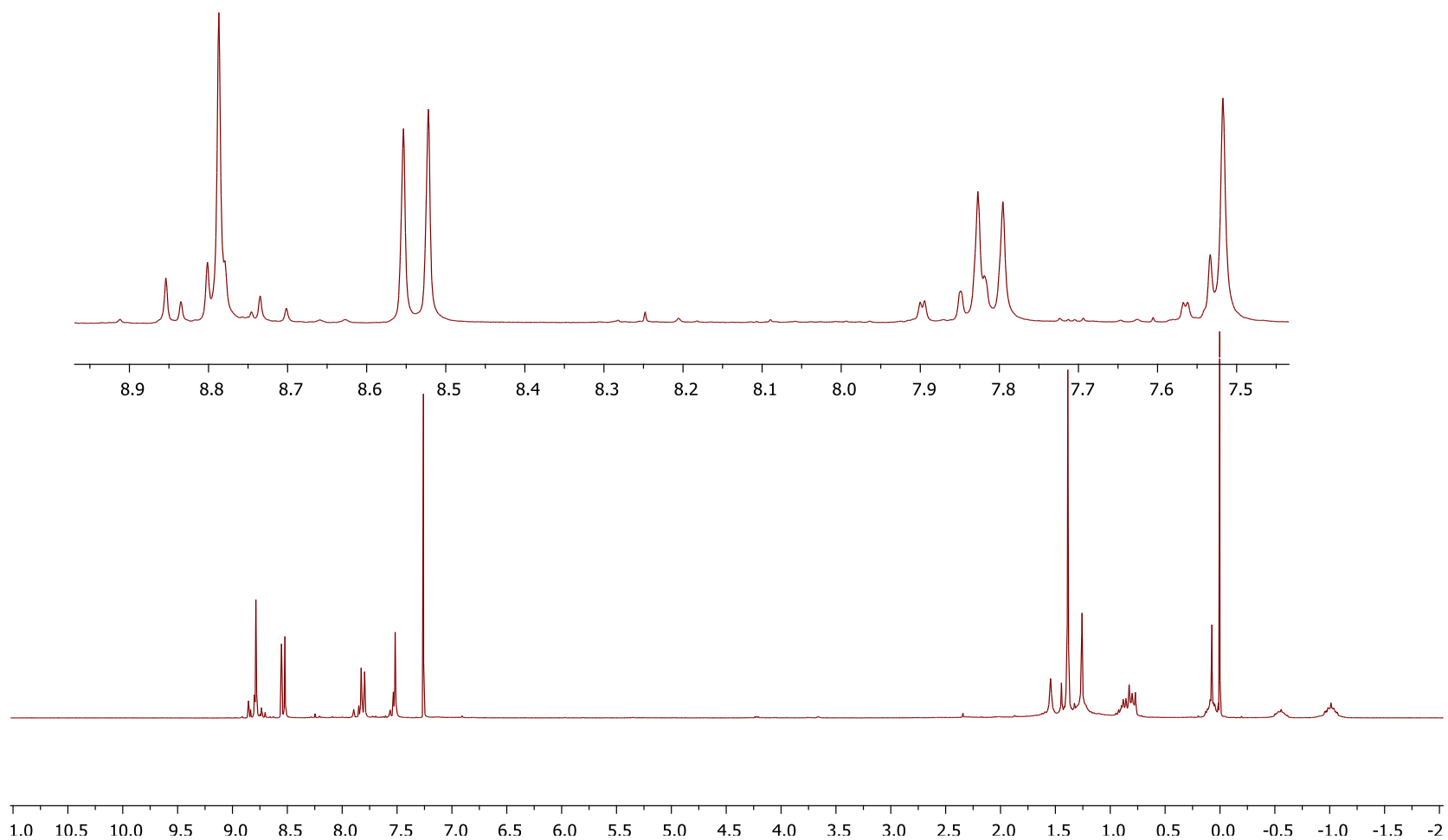
- 6624–6628. h) J. Xia, R. Jasti, *Angew. Chem. Int. Ed.*, 2012, **51**, 2474–2476. i) P. J. Evans, E. R. Darzi, R. Jasti, *Nat. Chem.*, 2014, **6**, 404–408. j) T. Iwamoto, Y. Watanabe, Y. Sakamoto, T. Suzuki, S. Yamago, *J. Am. Chem. Soc.*, 2011, **133**, 8354–8361. k) E. Kayahara, Y. Sakamoto, T. Suzuki, S. Yamago, *Org. Lett.*, 2012, **14**, 3284–3287. l) E. Kayahara, V. K. Patel, S. Yamago, *J. Am. Chem. Soc.*, 2014, **136**, 2284–2287. m) T. Iwamoto, E. Kayahara, N. Yasuda, T. Suzuki, S. Yamago, *Angew. Chem. Int. Ed.*, 2014, **53**, 6430–6434.
10. a) L. T. Scott, *Pure Appl. Chem.*, 1996, **68**, 291–300. b) Y. -T. Wu, J. S. Siegel, *Chem. Rev.*, 2006, **106**, 4843–4867. c) B. Liu, J. Liu, H. -B. Li, R. Bhola, E. A. Jackson, L. T. Scott, A. Page, S. Irle, K. Morokuma, C. Zhou, *Nano Lett.* 2015, **15**, 586–595.
11. a) H. Omachi, T. Nakayama, E. Takahashi, Y. Segawa and K. Itami, *Nature Chem.*, 2013, **5**, 572–576; b) A.- F. Tran-Van and H. A. Wegner, *Beilstein J. Nanotechnol.*, 2014, **5**, 1320–1333 and the references therein; c) M. Quernheim, F. E. Golling, W. Zhang, M. Wagner, H.- J. Räder, T. Nishiuchi and K. Müllen, *Angew. Chem. Int. Ed.*, 2015, **54**, 10341–10346; d) S. E. Lewis, *Chem. Soc. Rev.* 2015, **44**, 2221–2304.
12. a) X. Yu, J. Zhang, W. Choi, J.- Y. Choi, J. M. Kim, L. Gan and Z. Liu, *Nano Lett.*, 2010, **10**, 3343–3349; b) T. Fujita, Y. Matsuo and E. Nakamura, *Chem. Mater.*, 2012, **24**, 3972–3980; c) B. Lui, J. Liu, H.- B. Li, R. Bhola, E. A. Jackson, L. T. Scott, A. Page, S. Irle, K. Morokuma and C. Zhou, *Nano Lett.*, 2015, **15**, 586–595.

13. A. Pogoreltsev, E. Solel, D. Pappo, E. Keinan, *Chem. Commun.*, 2012, **48**, 5425–5427.
14. L. T. Scott, E. A. Jackson, Q. Zhang, B. D. Steinberg, M. Bancu, B. Li, *J. Am. Chem. Soc.*, 2012, **134**, 107–110.
15. a) b) E. S. Hirst, F. Wang and R. Jasti, *Org. Lett.*, 2011, **13**, 6220–6223; R. Gleiter, B. Esser and S. T. Kornmayer, *Acc. Chem. Res.*, 2009, **42**, 1108–1116; c) R. Gleiter, B. Hellbach, S. Gath and R. J. Schaller, *Pure Appl. Chem.*, 2006, **78**, 699–706.
16. a) B. L. Merner, L. N. Dawe, G. J. Bodwell, *Angew. Chem. Int. Ed.*, 2009, **48**, 5487–5491. b) B. L. Merner, K. S. Unikela, L. N. Dawe, D. W. Thompson, G. J. Bodwell, *Chem. Commun.*, 2013, **49**, 5930.
17. a) M. J. S. Dewar, R. D. Dennington, *J. Am. Chem. Soc.*, 1989, **111**, 3804–3808. b) K. Ogino, S. Iwashima, H. Inokuchi, Y. Harada, *Bull. Chem. Soc. Jpn.*, 1965, **38**, 473–477. c) J. M. Casas-Solvas, J. D. Howgego, A. P. Davis, *Org. Biomol. Chem.*, 2014, **12**, 212–232.
18. J. Grimshaw, J. Trocha-Grimshaw, *J. Chem. Soc., Perkin Trans. 1*, 1972, 1622–1623.
19. G. Venkataramana, P. Dongare, L. N. Dawe, D. W. Thompson, Y. Zhao, G. J. Bodwell, *Org. Lett.*, 2011, **13**, 2240–2243.
20. T. M. Figueira-Duarte, P. G. D. Rosso, R. Trattnig, S. Sax, E. J. W. List, K. Müllen, *Adv. Mater.*, 2010, **22**, 990–993.

21. I. V. Astakhova, V. A. Korshun, J. Wengel, *Chem. Eur. J.*, 2008, **14**, 11010–11026.
22. Y. Niko, S. Kawauchi, S. Otsu, K. Tokumaru, G. Konishi, *J. Org. Chem.*, 2013, **78**, 3196–3207.
23. J. -Y. Hu, X. -L. Ni, X. Feng, M. Era, M. R. J. Elsegood, S. J. Teat, T. Yamato, *Org. Biomol. Chem.*, 2012, **10**, 2255–2262.
24. T. Yamato, A. Miyazawa, M. Tashiro, *J. Chem. Soc. Perkin Trans.* 1993, **1**, 3127–3137.
25. X. Feng, J. -Y. Hu, F. Iwanaga, N. Seto, C. Redshaw, M. R. J. Elsegood, T. Yamato, *Org. Lett.*, 2013, **15**, 1318–1321.
26. L. Zöphel, D. Beckmann, V. Enkelmann, D. chercka, R. Reiger, K. Müllen, *Chem. Commun.* 2011, **47**, 6960–6962.
27. T. Umemoto, T. Kawashima, Y. Sakata and S. Musumi, *Tetrahedron Lett.*, 1975, 1005–1006.
28. A. J. Murphy, *Angew. Chem. Int. Ed.*, 2007, **46**, 5178–5183.
29. A. N. Nesmeyanov, T. P. Tolstaya, L. N. Vanchikova, A. V. Patrakov, *Izv. Akad. Nauk, SSSR, Ser. Khim.*, 1980, 2530–2534.

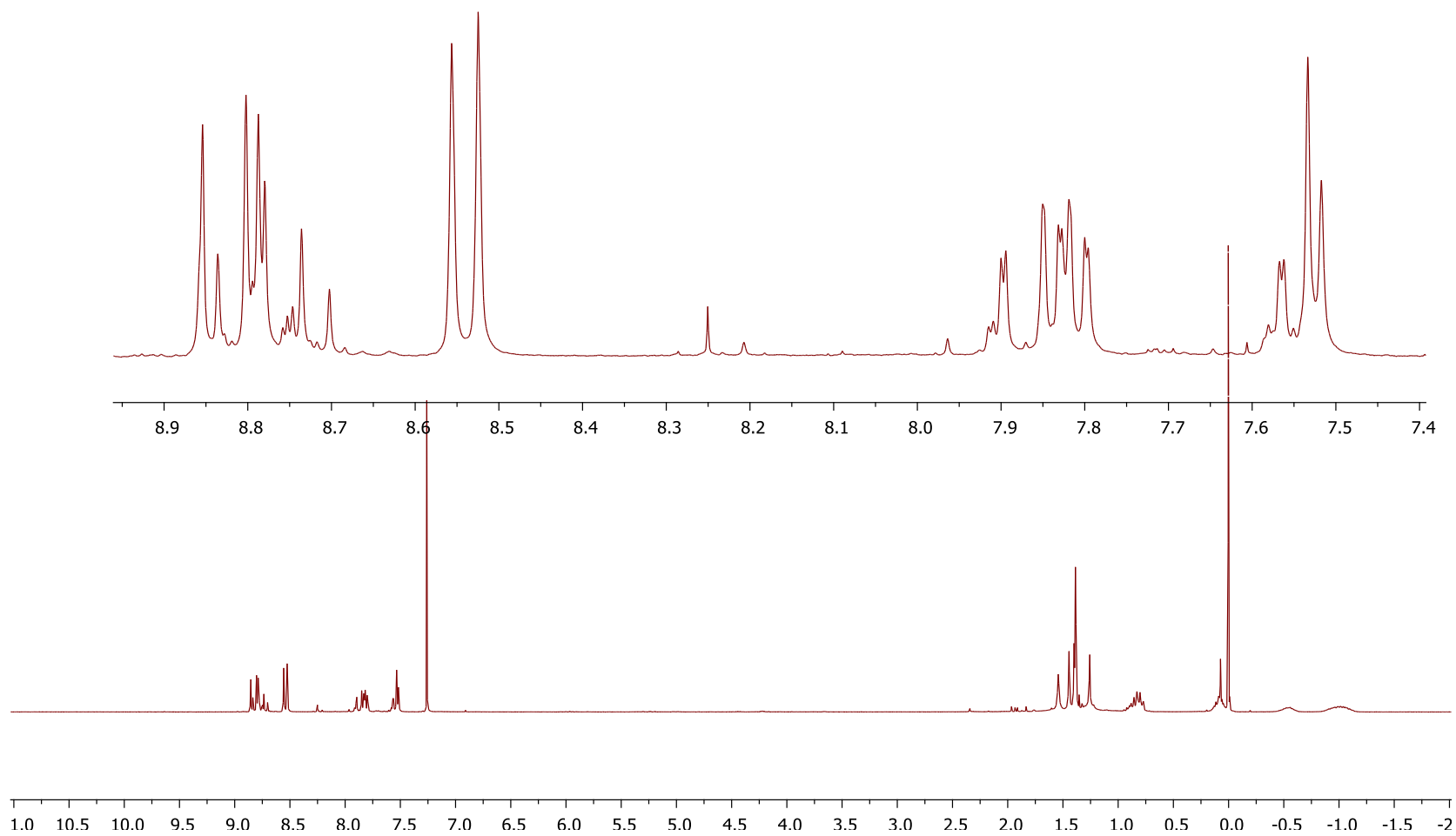
# APPENDIX 3

0.5 equiv. Br<sub>2</sub> with **103d** at rt

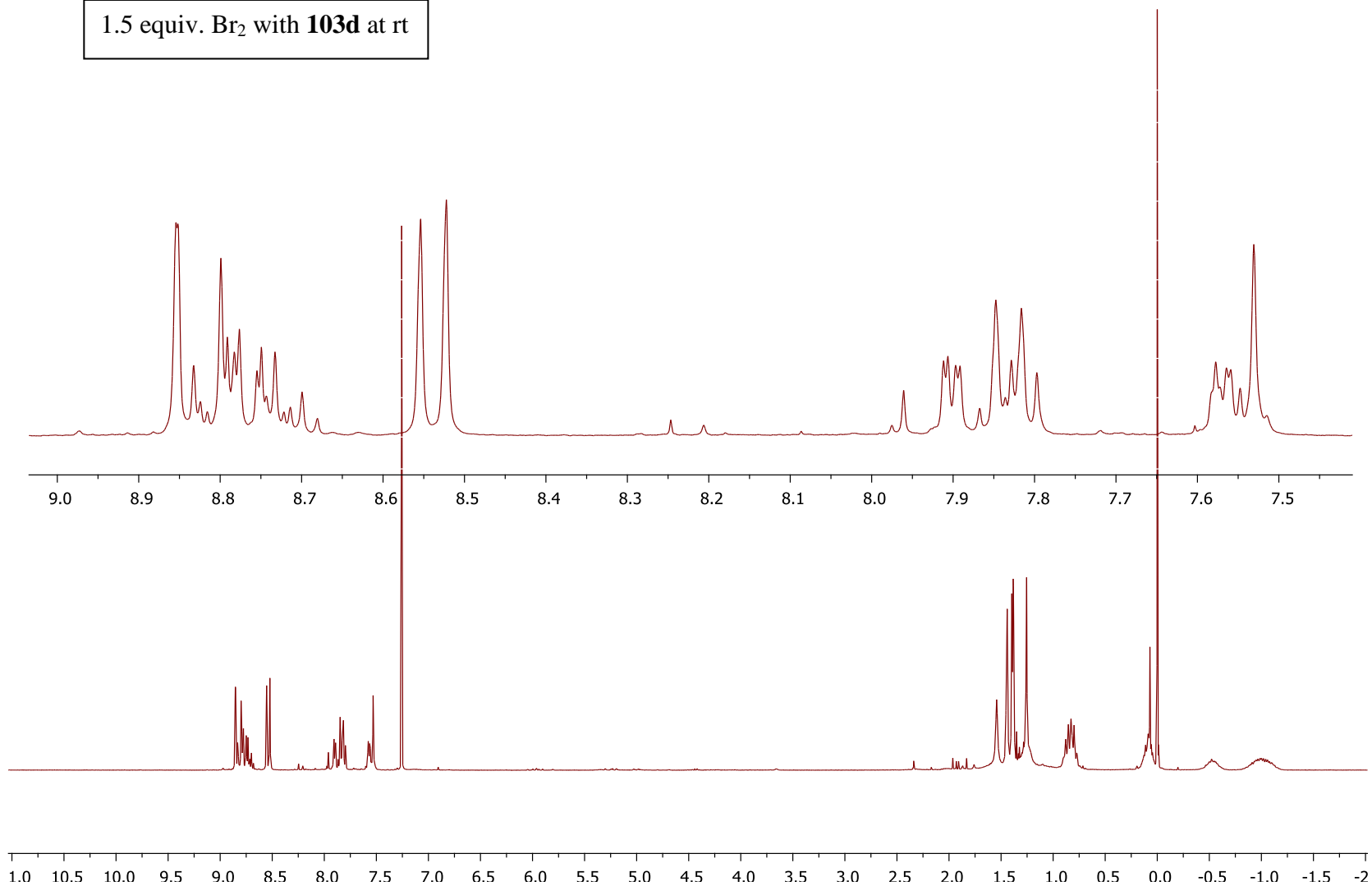


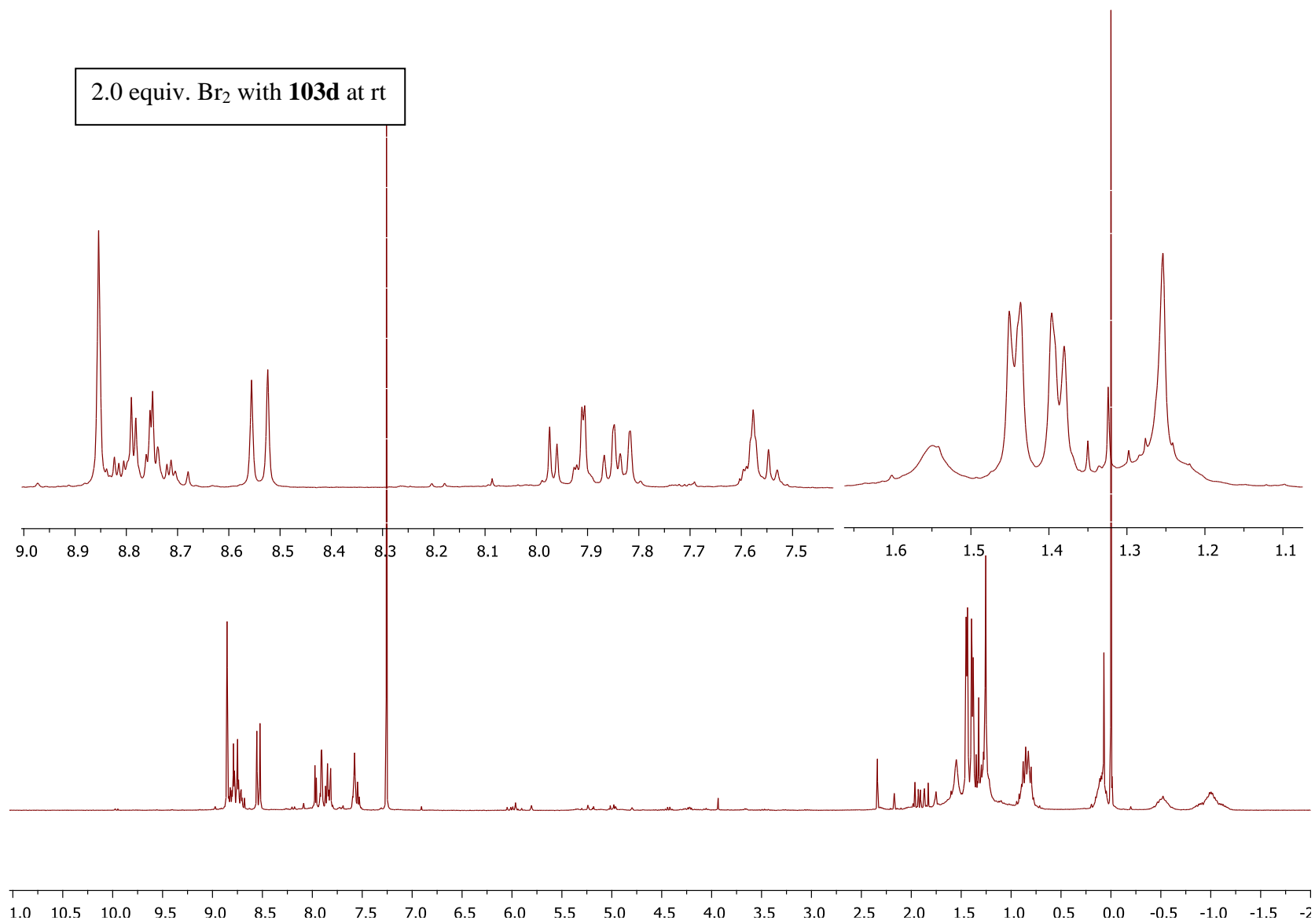


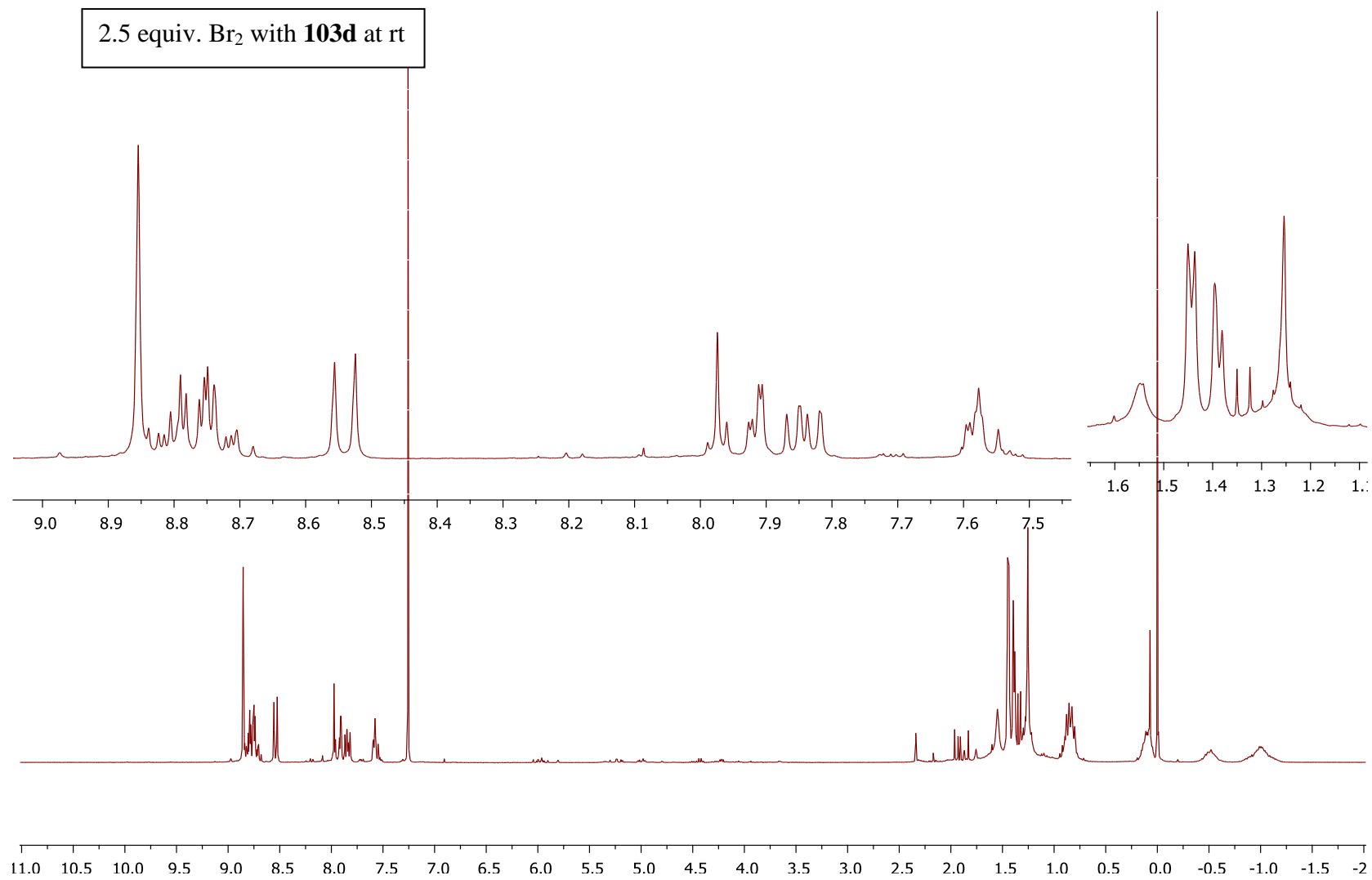
1.0 equiv. Br<sub>2</sub> with **103d** at rt



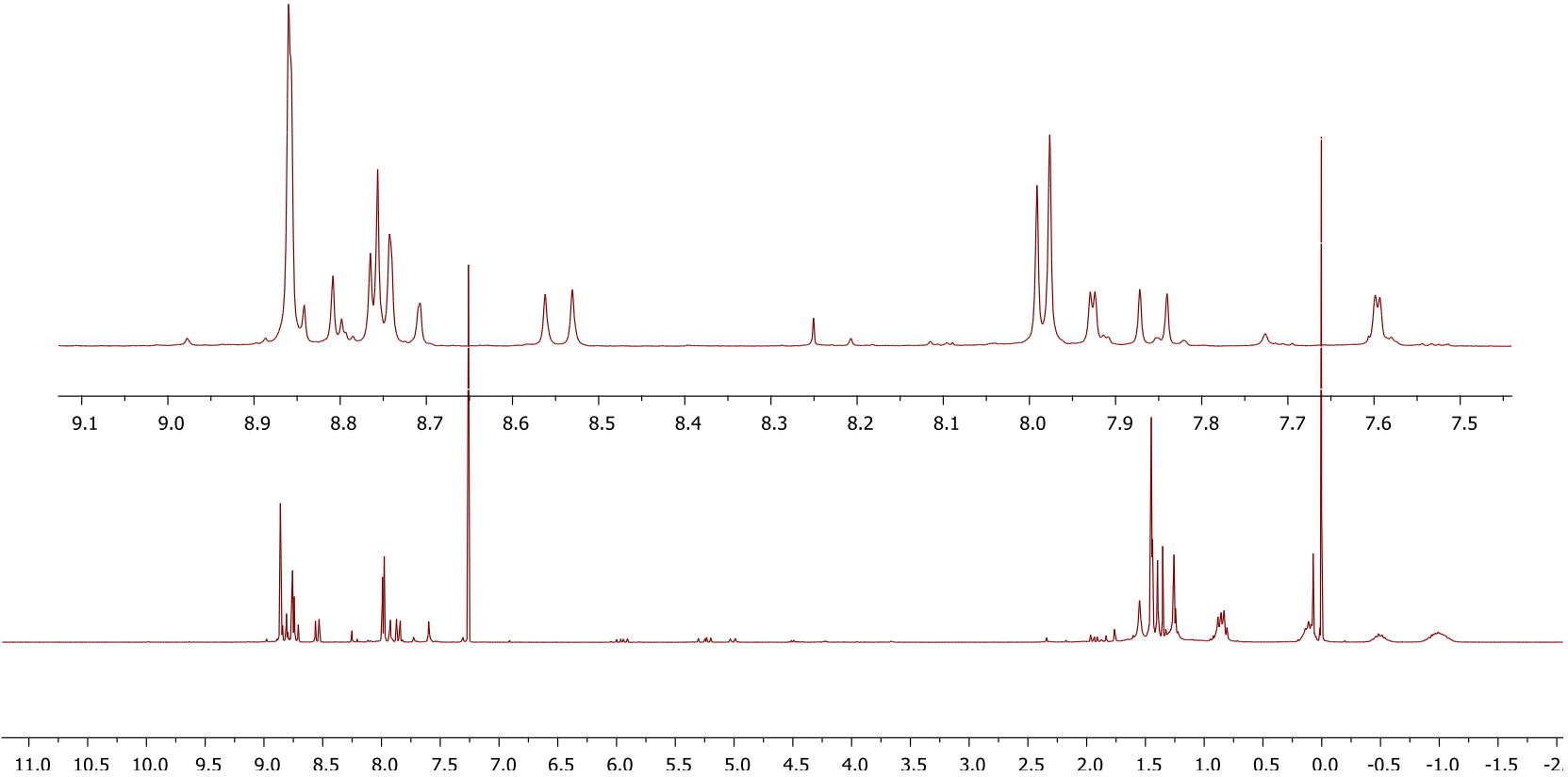
1.5 equiv. Br<sub>2</sub> with **103d** at rt

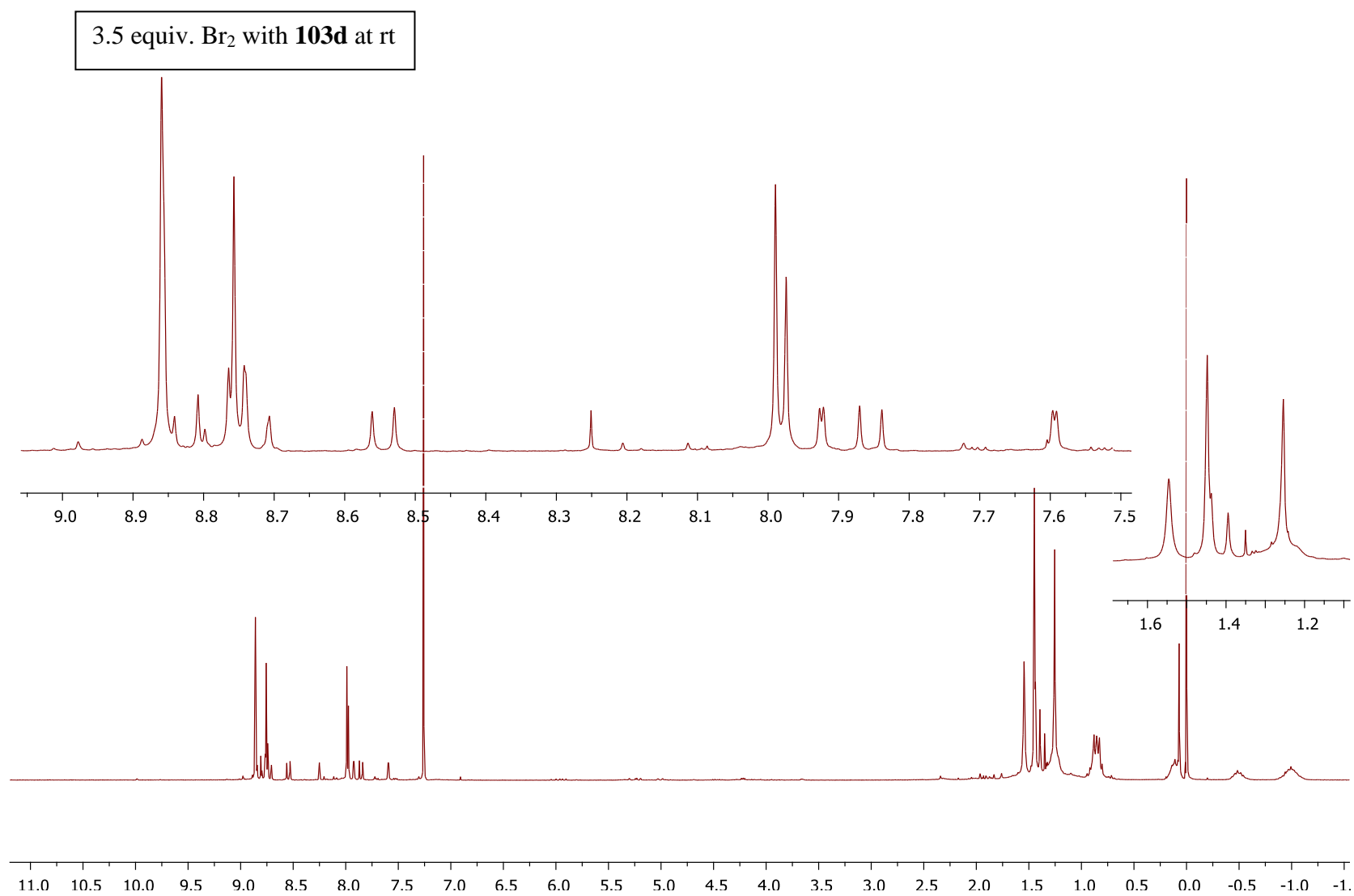




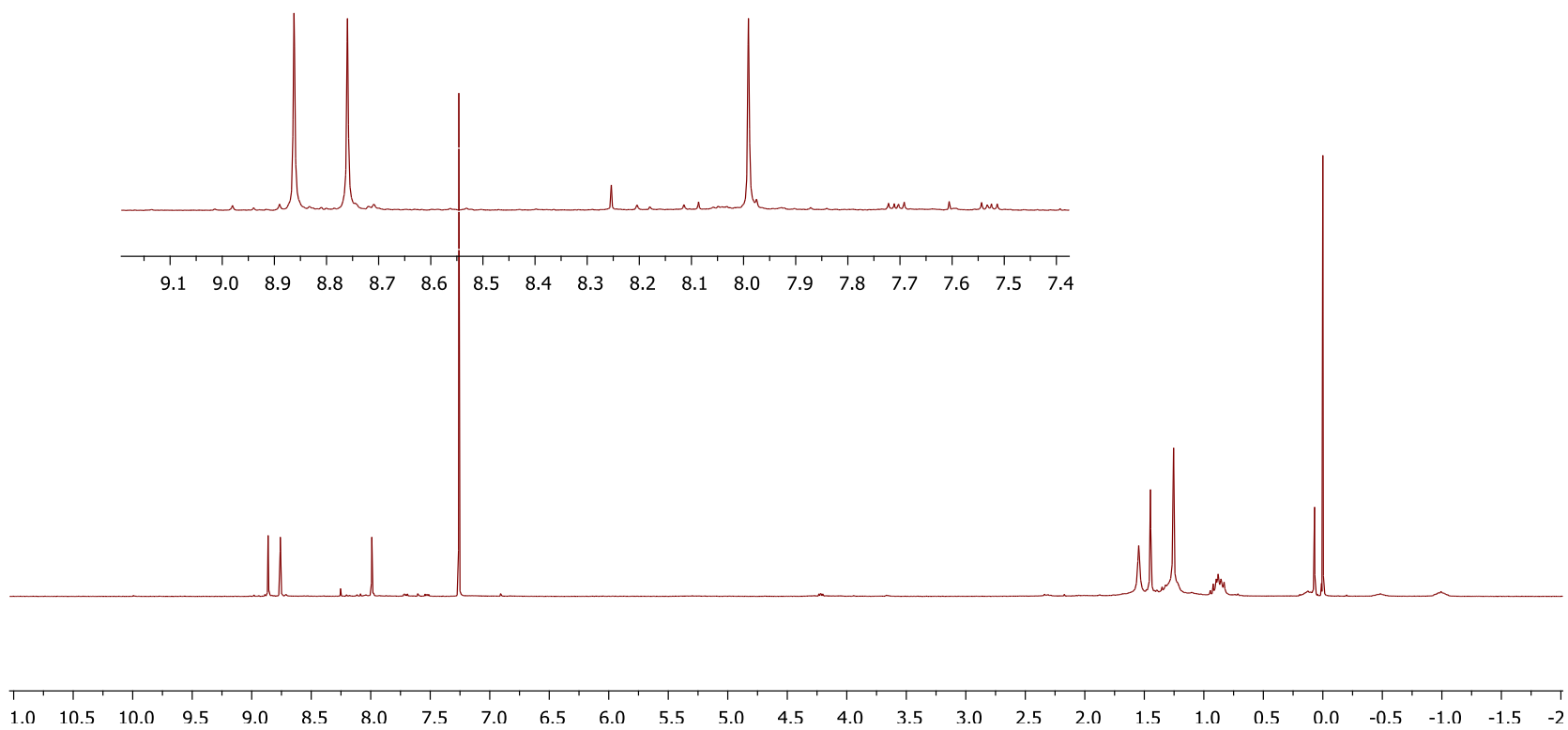


3.0 equiv. Br<sub>2</sub> with **103d** at rt

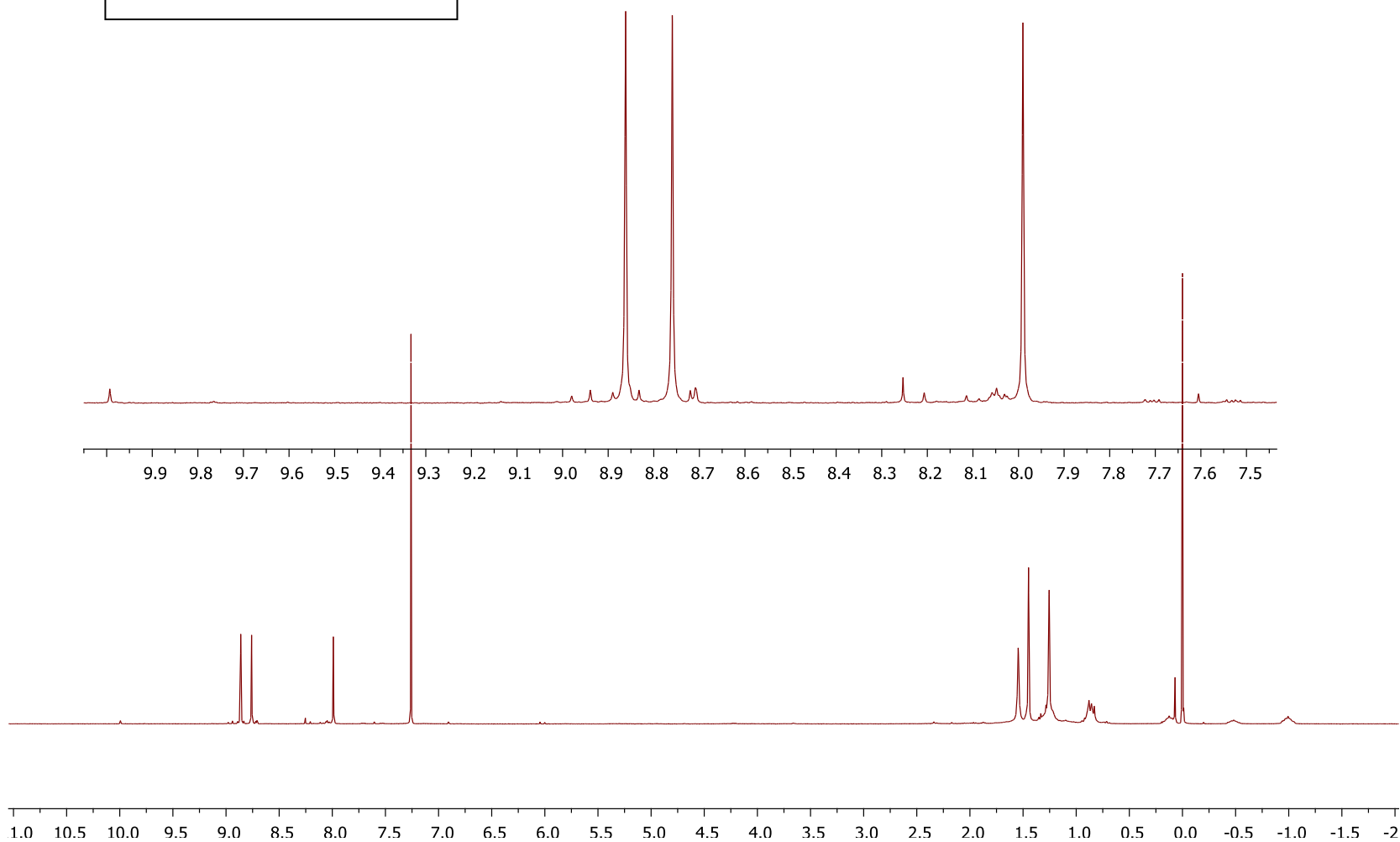




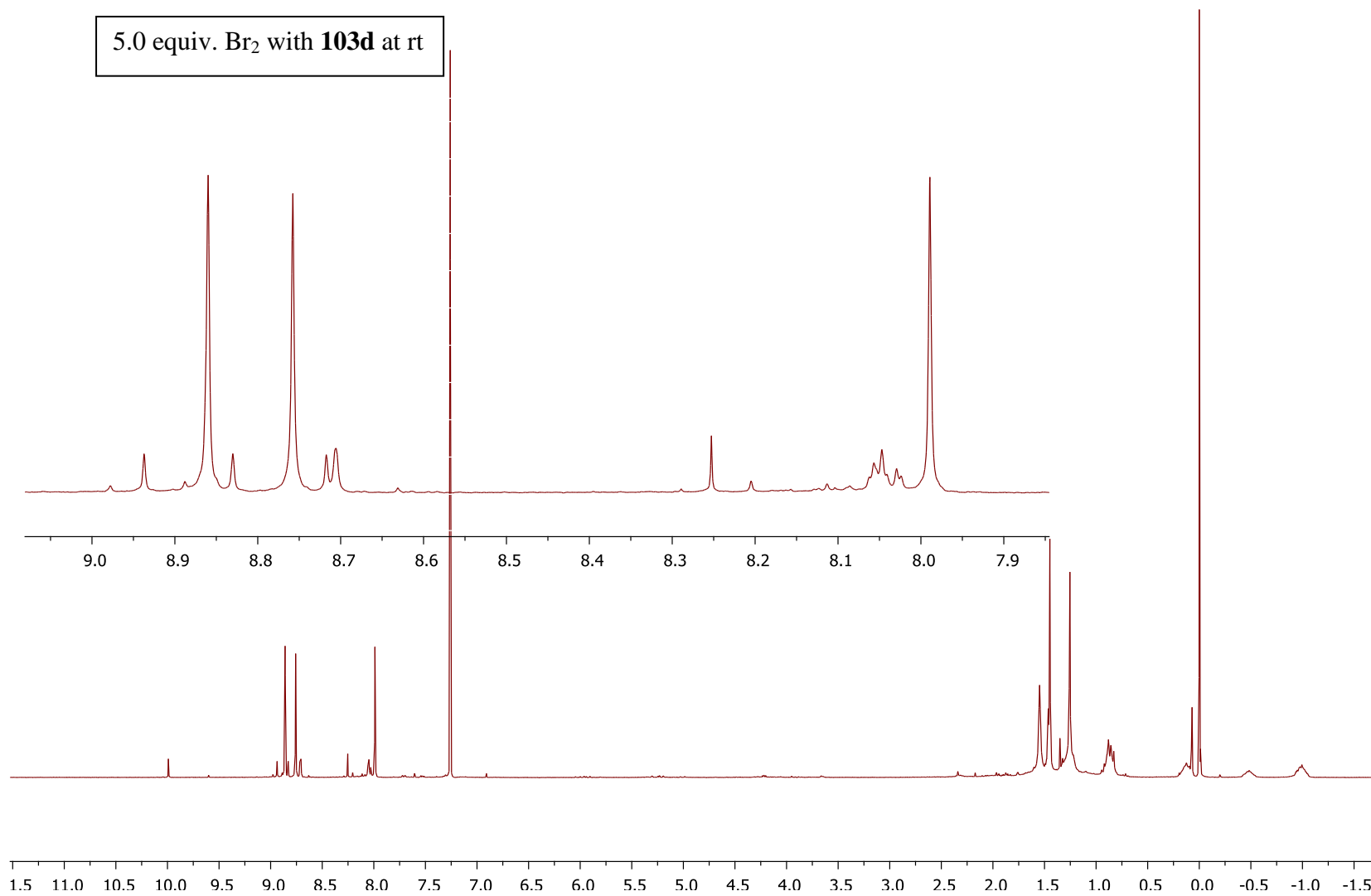
4.0 equiv. Br<sub>2</sub> with **103d** at rt



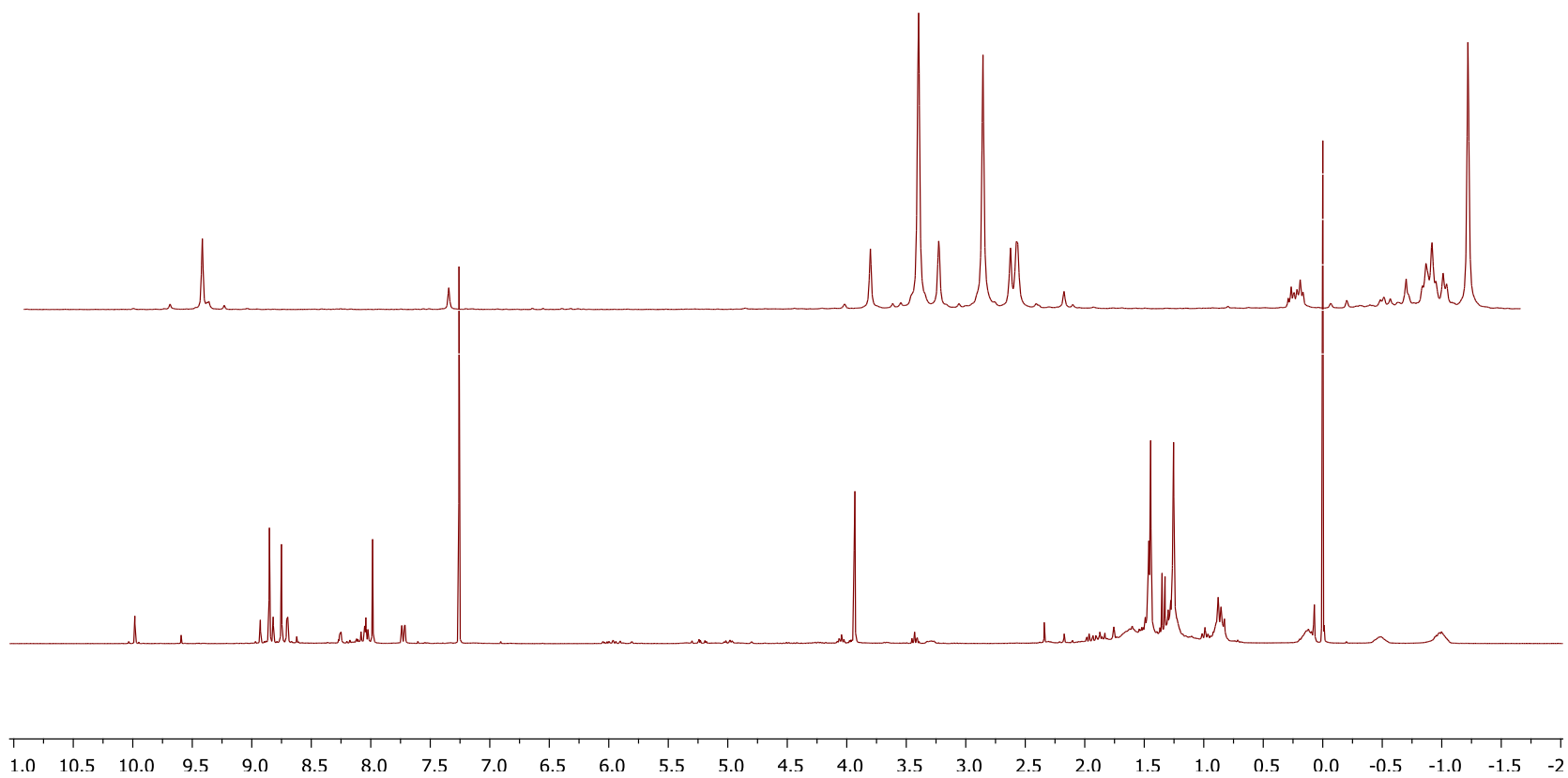
4.5 equiv. Br<sub>2</sub> with **103d** at rt



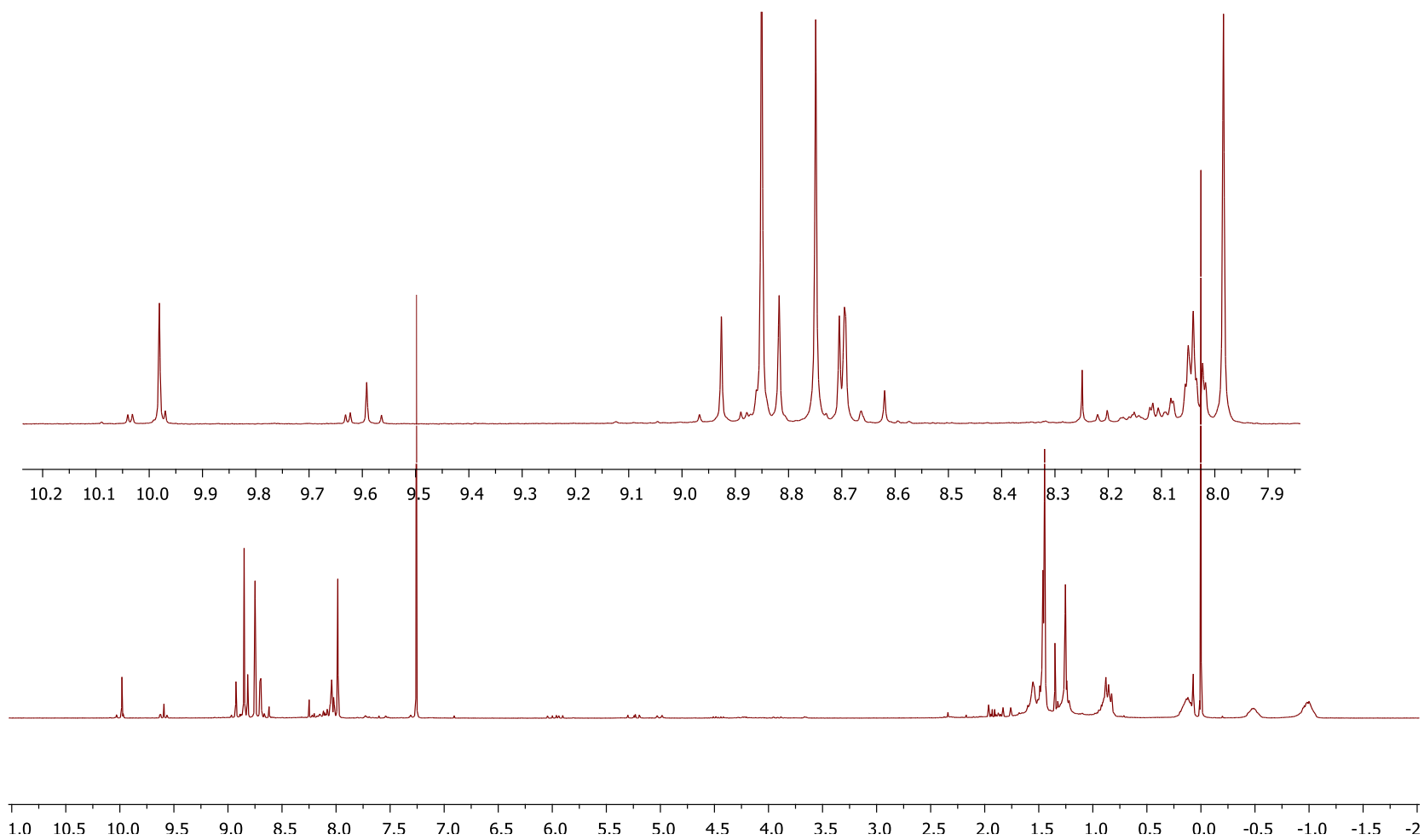


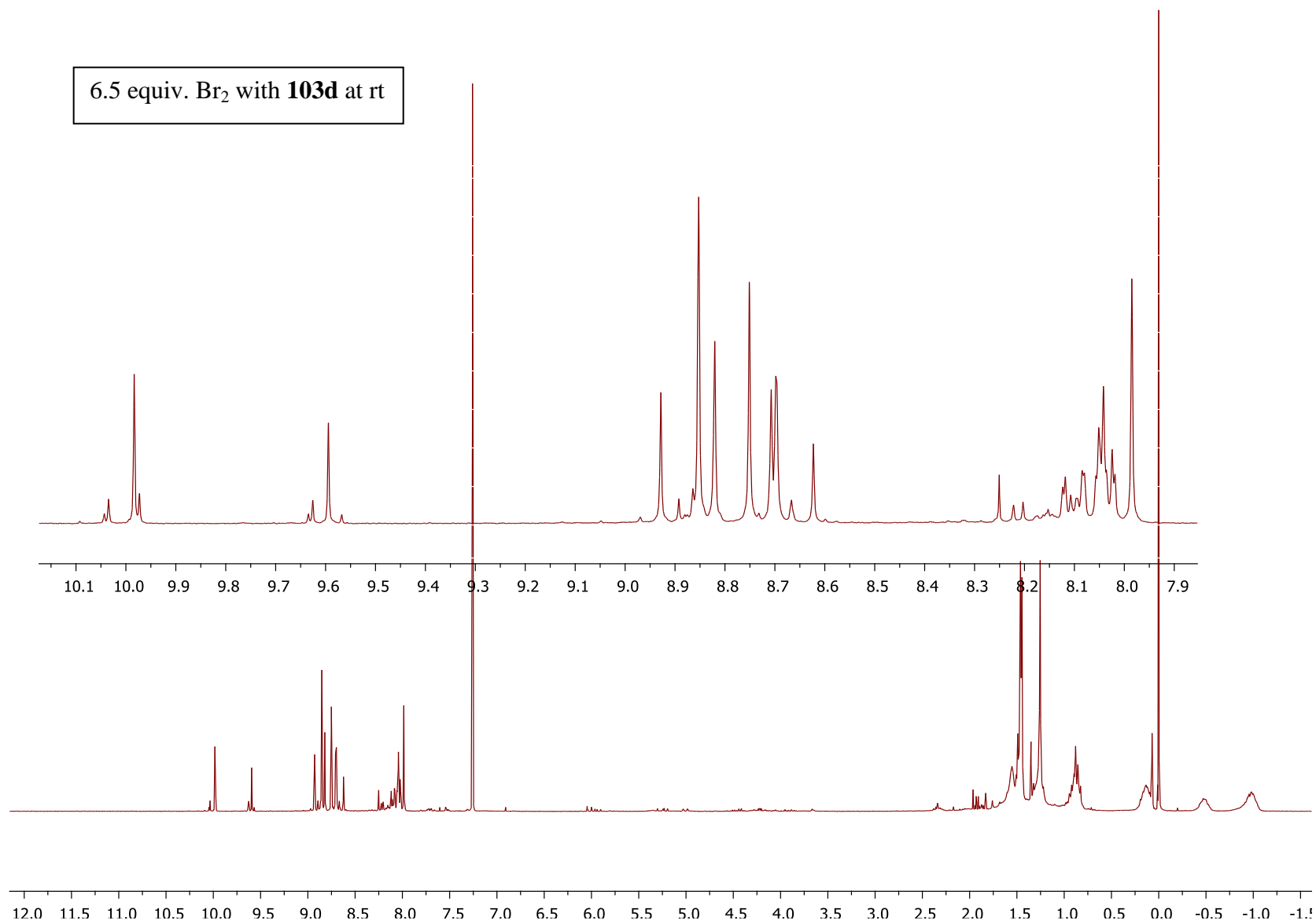


5.5 equiv. Br<sub>2</sub> with **103d** at rt

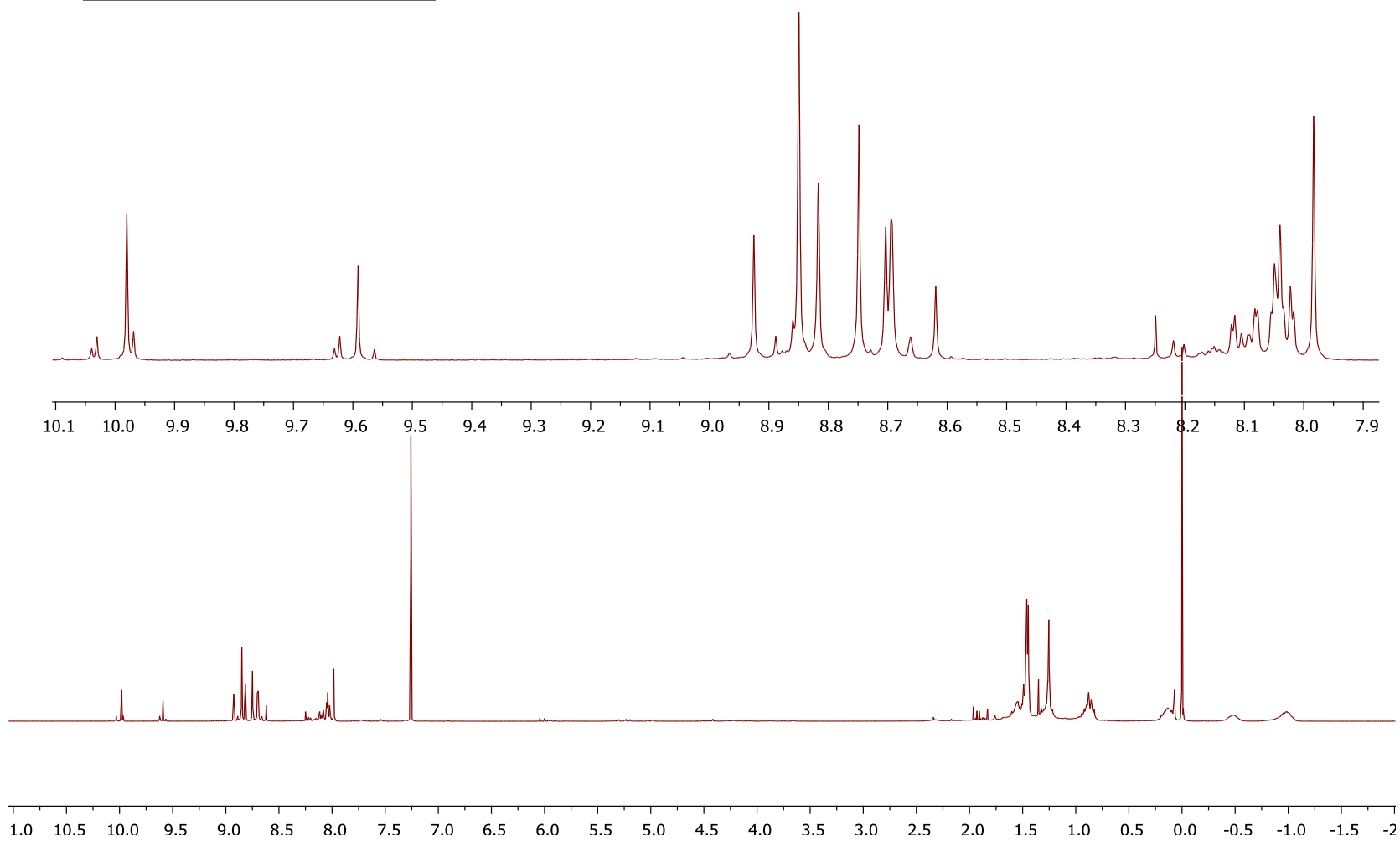


6.0 equiv. Br<sub>2</sub> with **103d** at rt

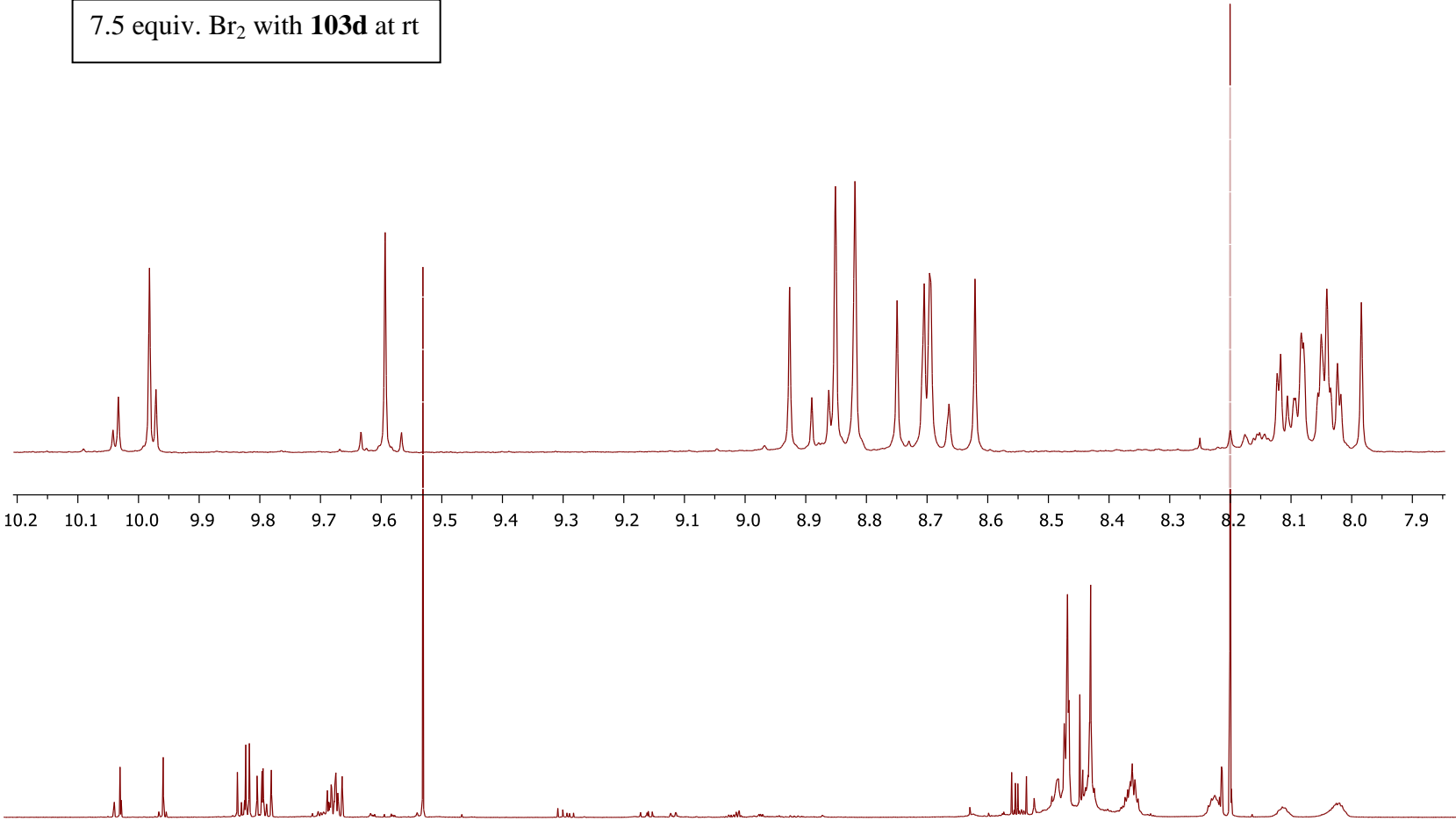


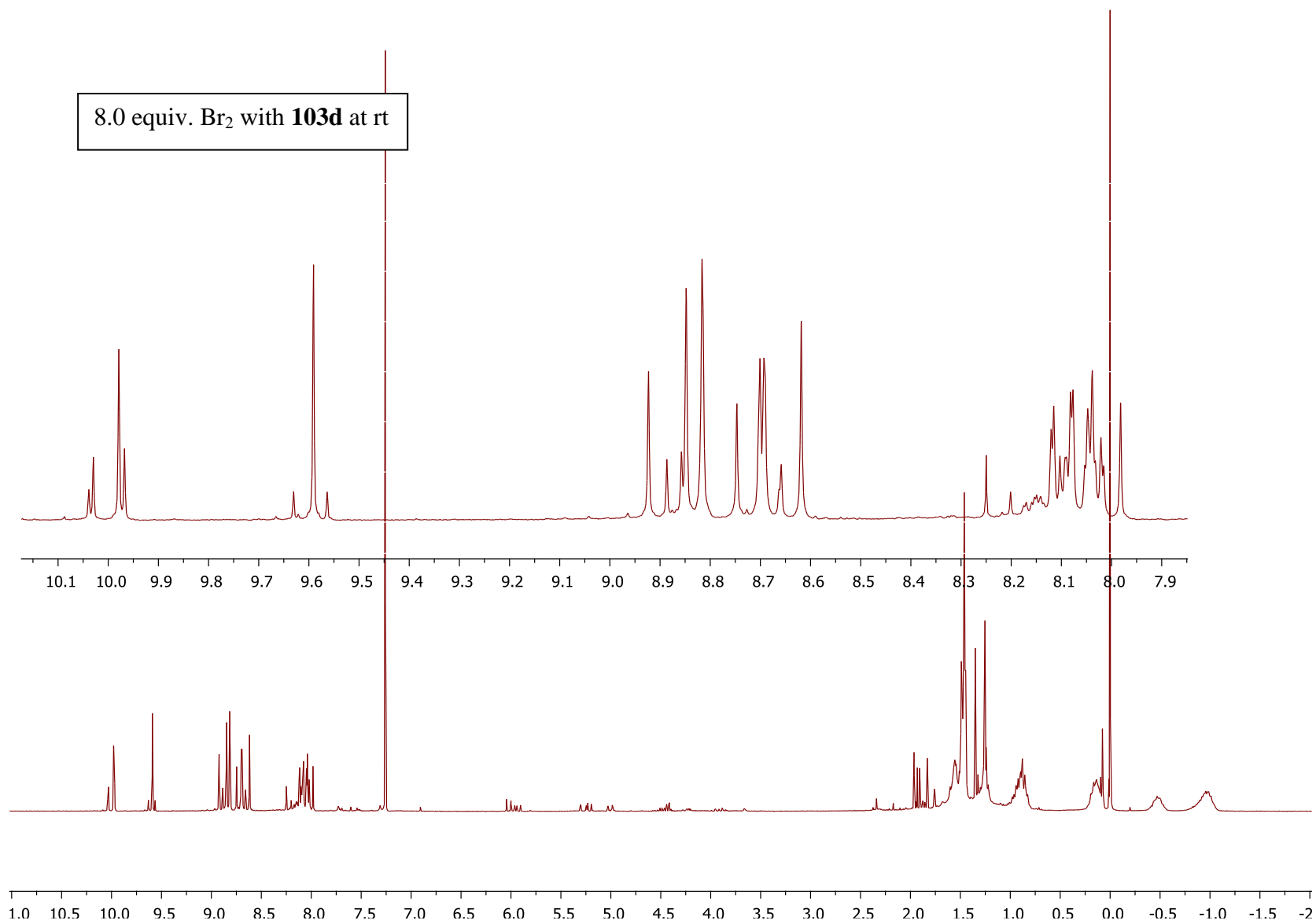


7.0 equiv. Br<sub>2</sub> with **103d** at rt

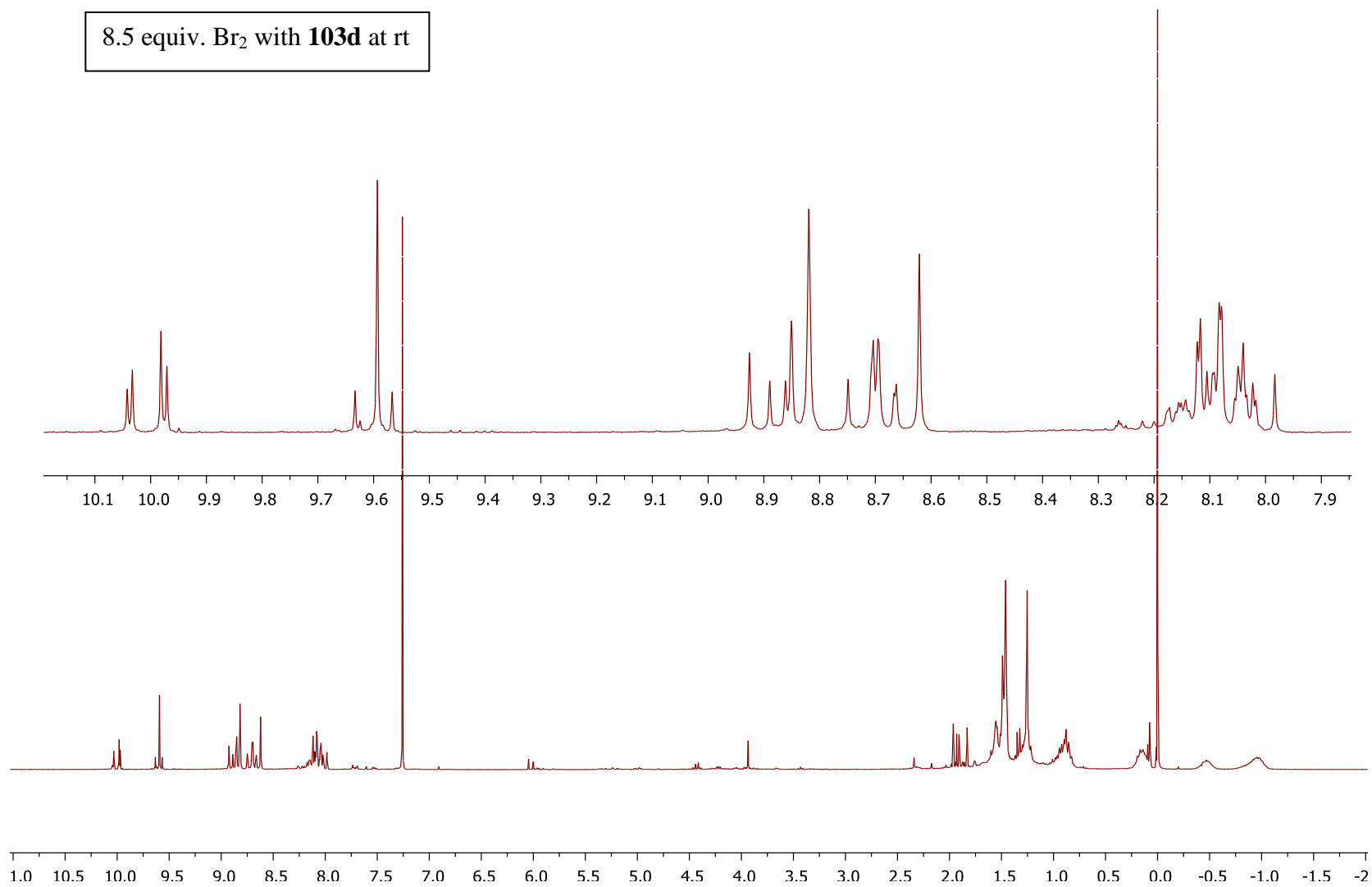


7.5 equiv. Br<sub>2</sub> with **103d** at rt



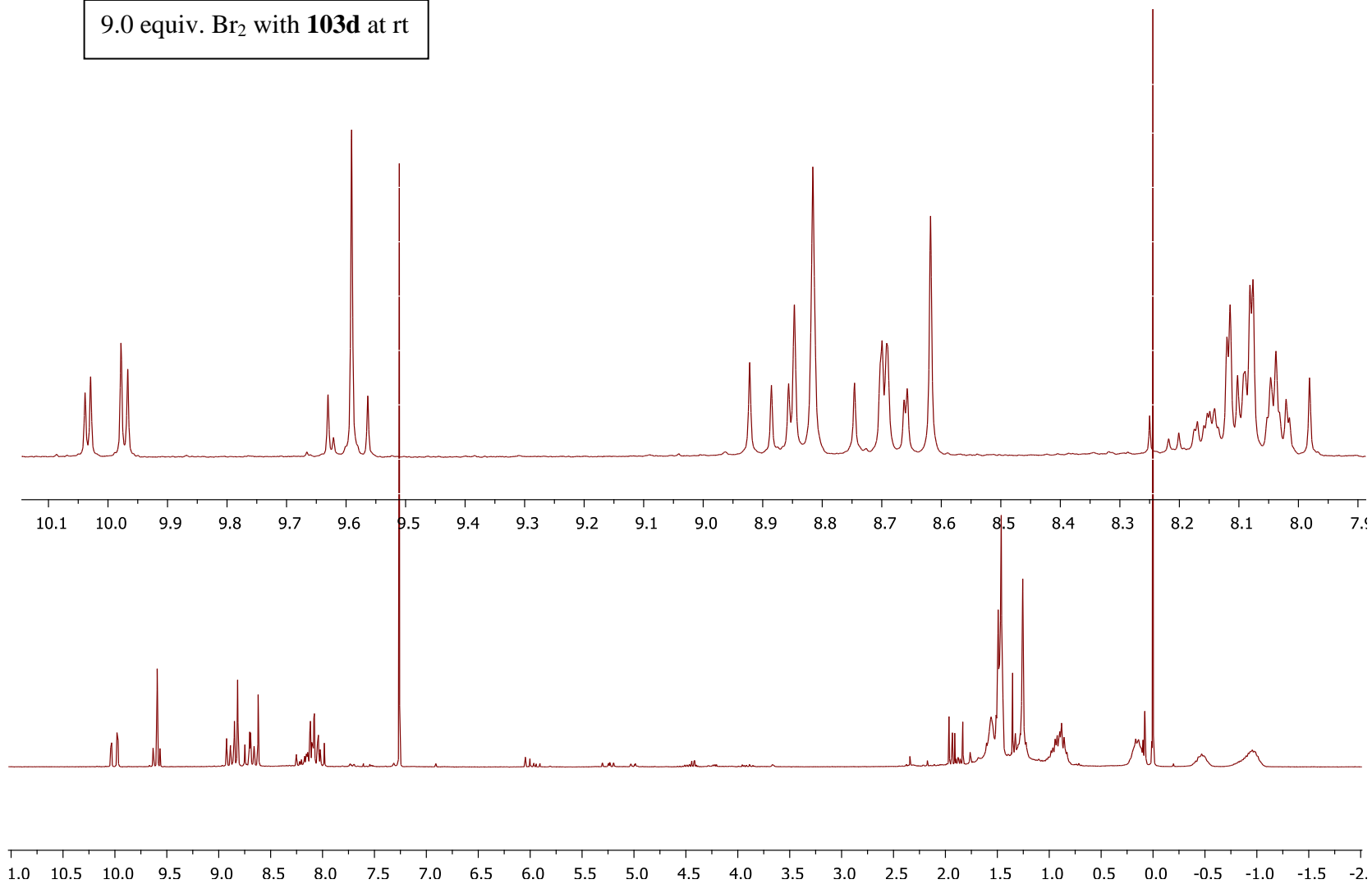


8.5 equiv. Br<sub>2</sub> with **103d** at rt

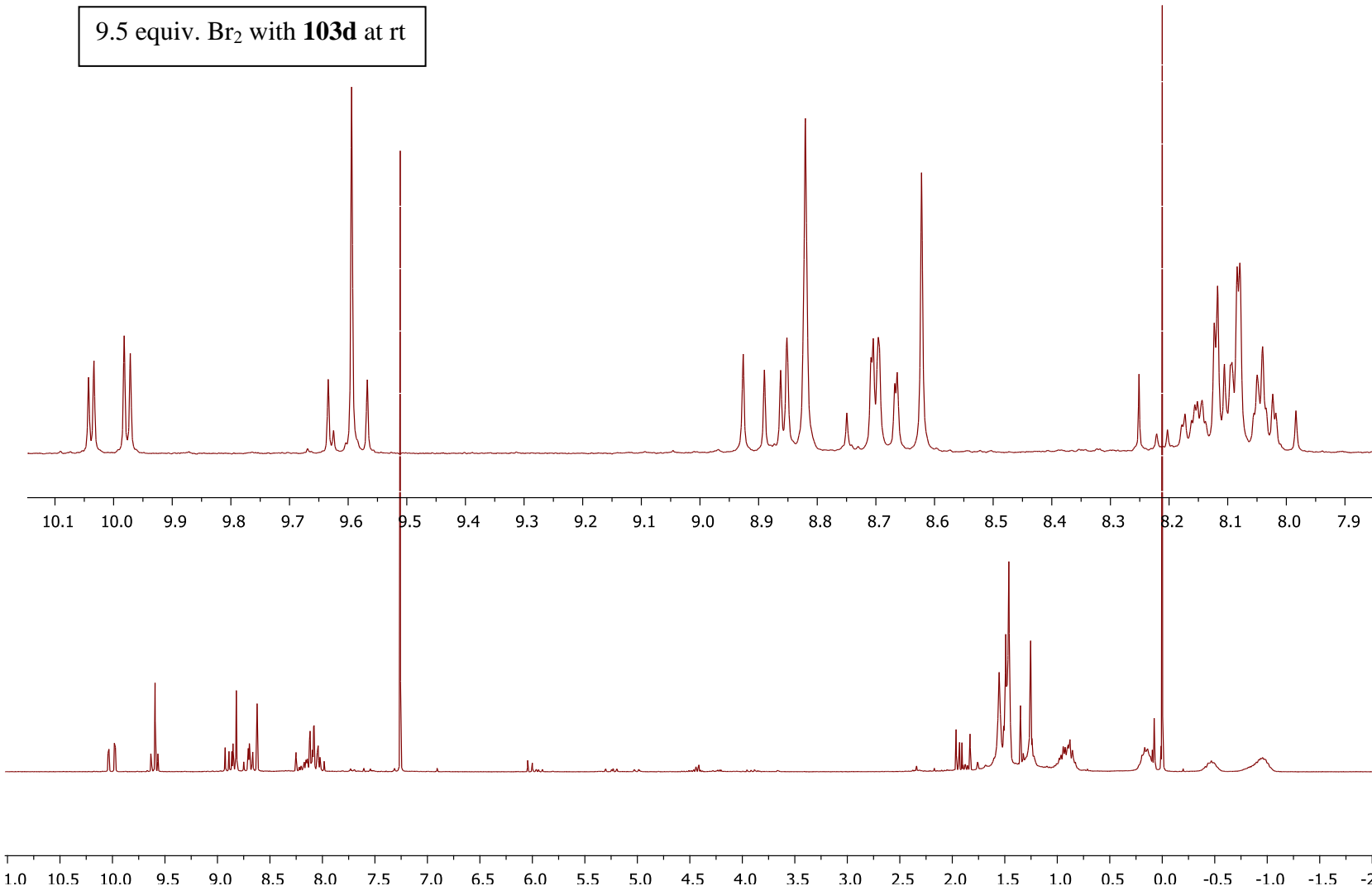




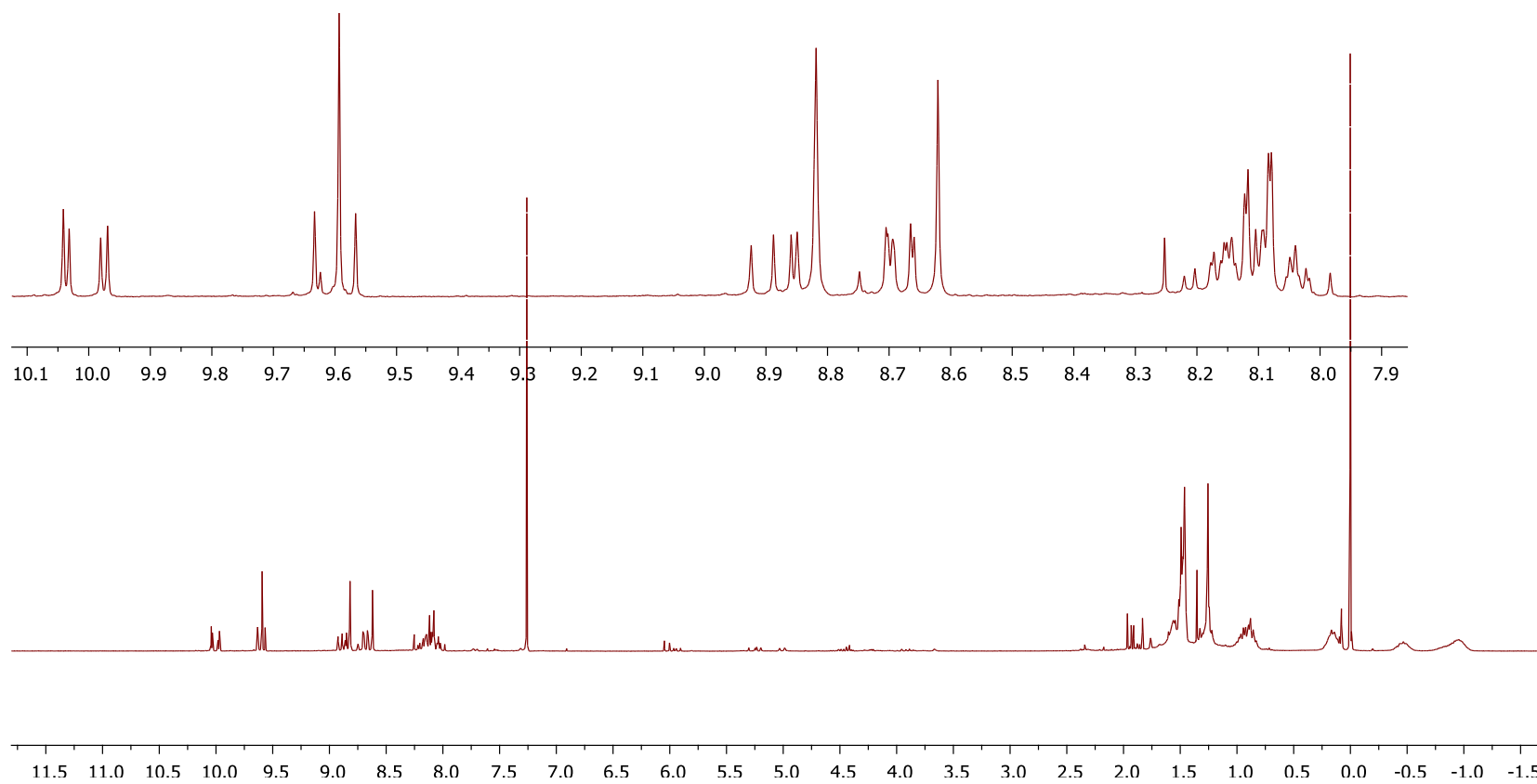
9.0 equiv. Br<sub>2</sub> with **103d** at rt

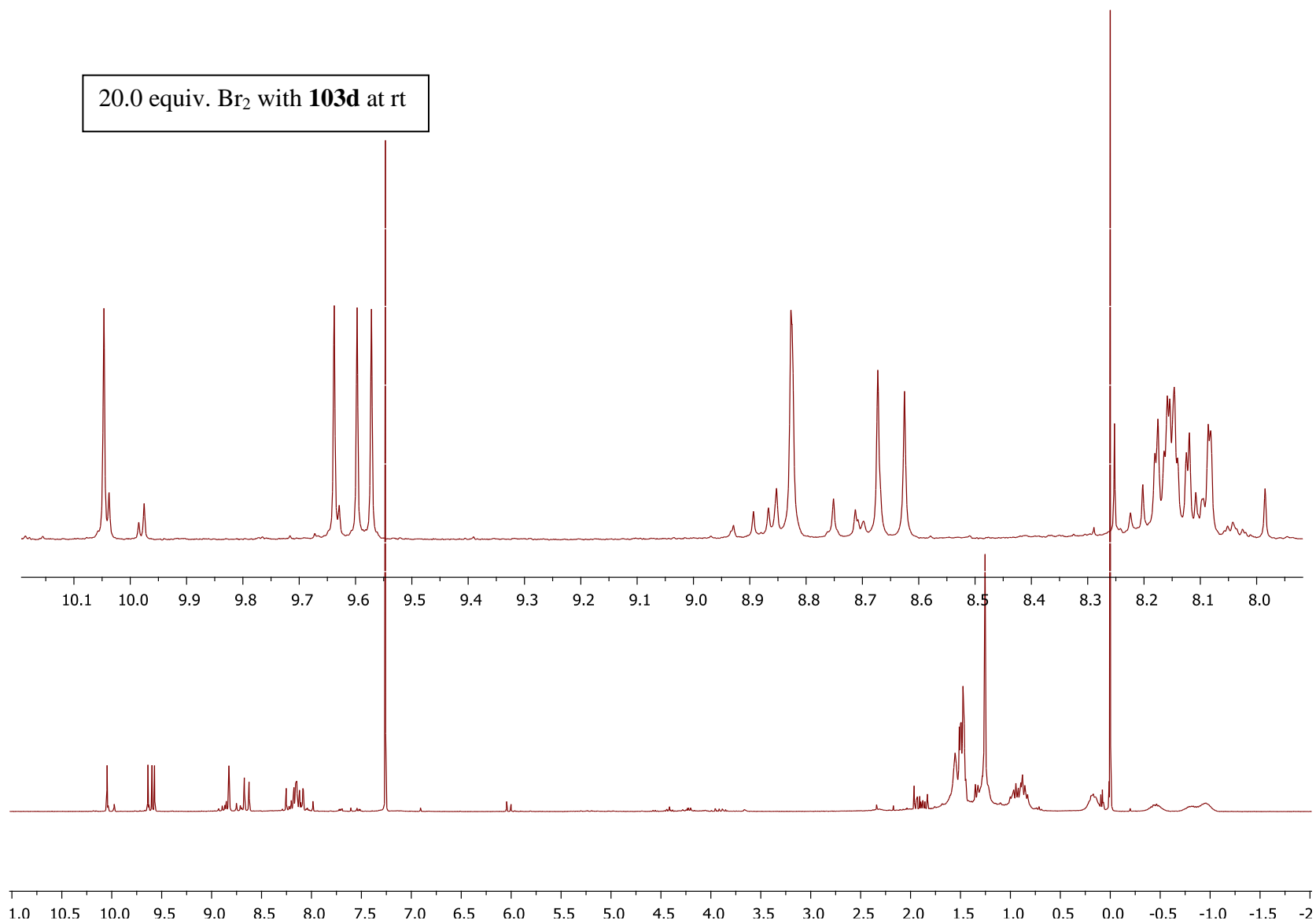


9.5 equiv. Br<sub>2</sub> with **103d** at rt

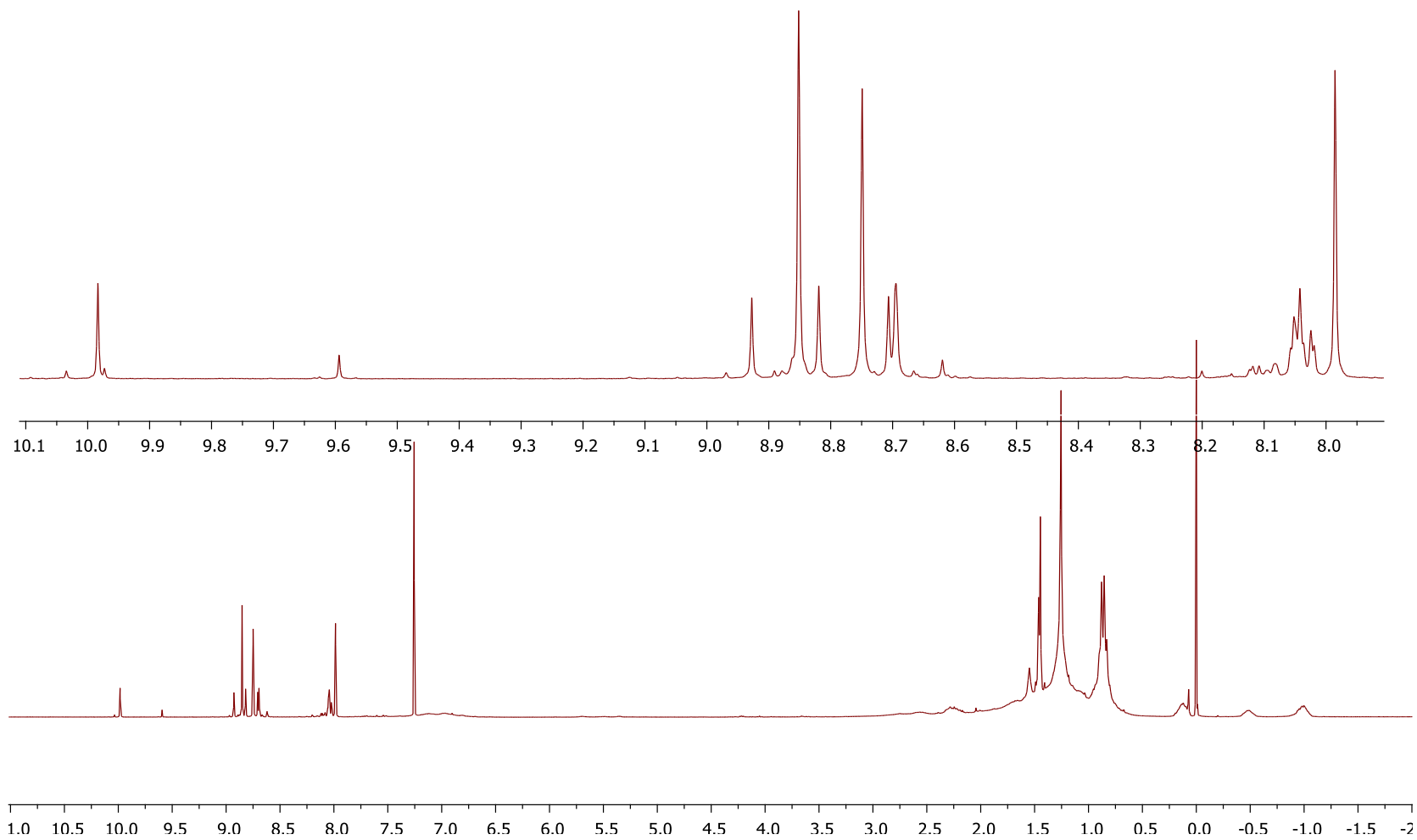


10.0 equiv. Br<sub>2</sub> with **103d** at rt

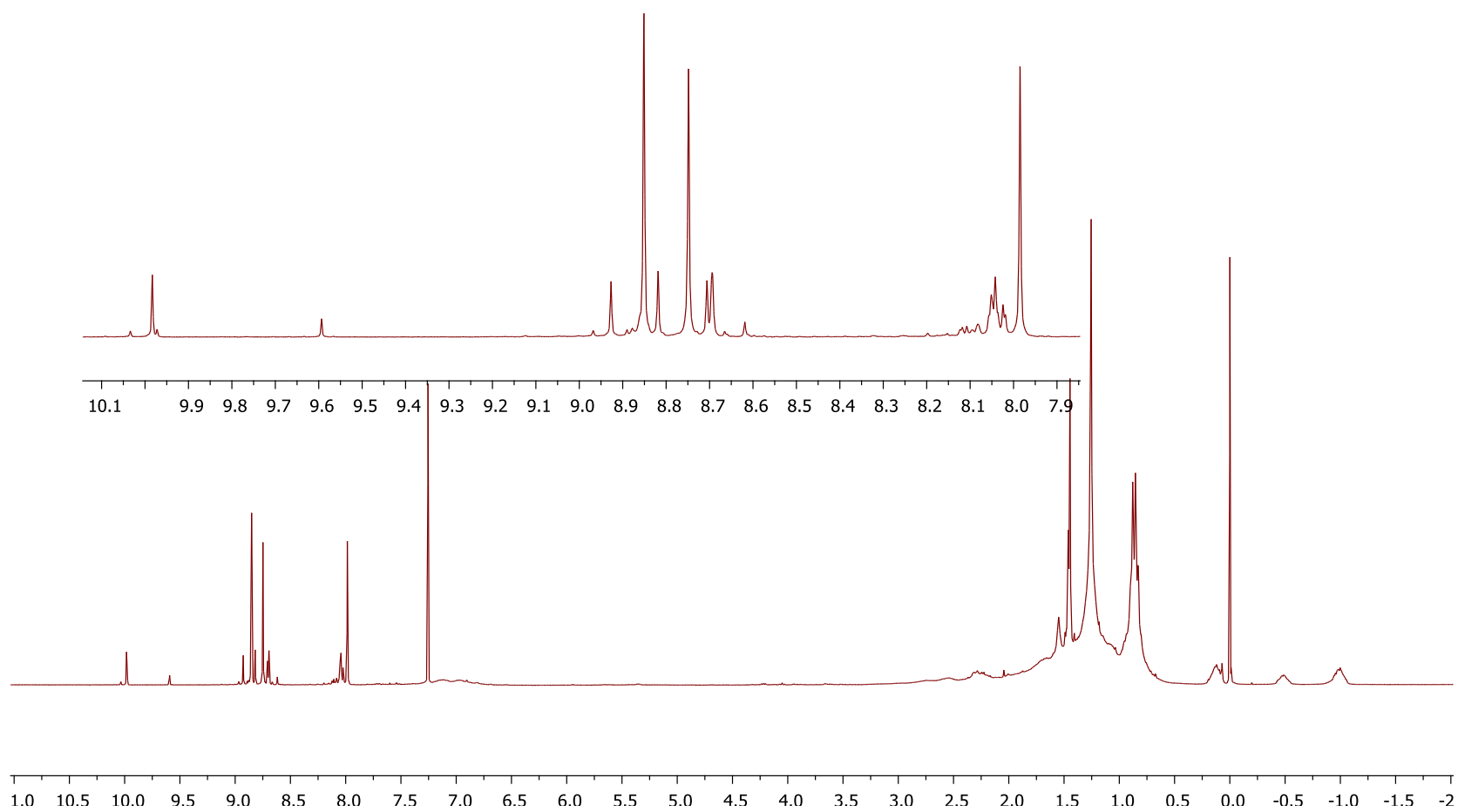




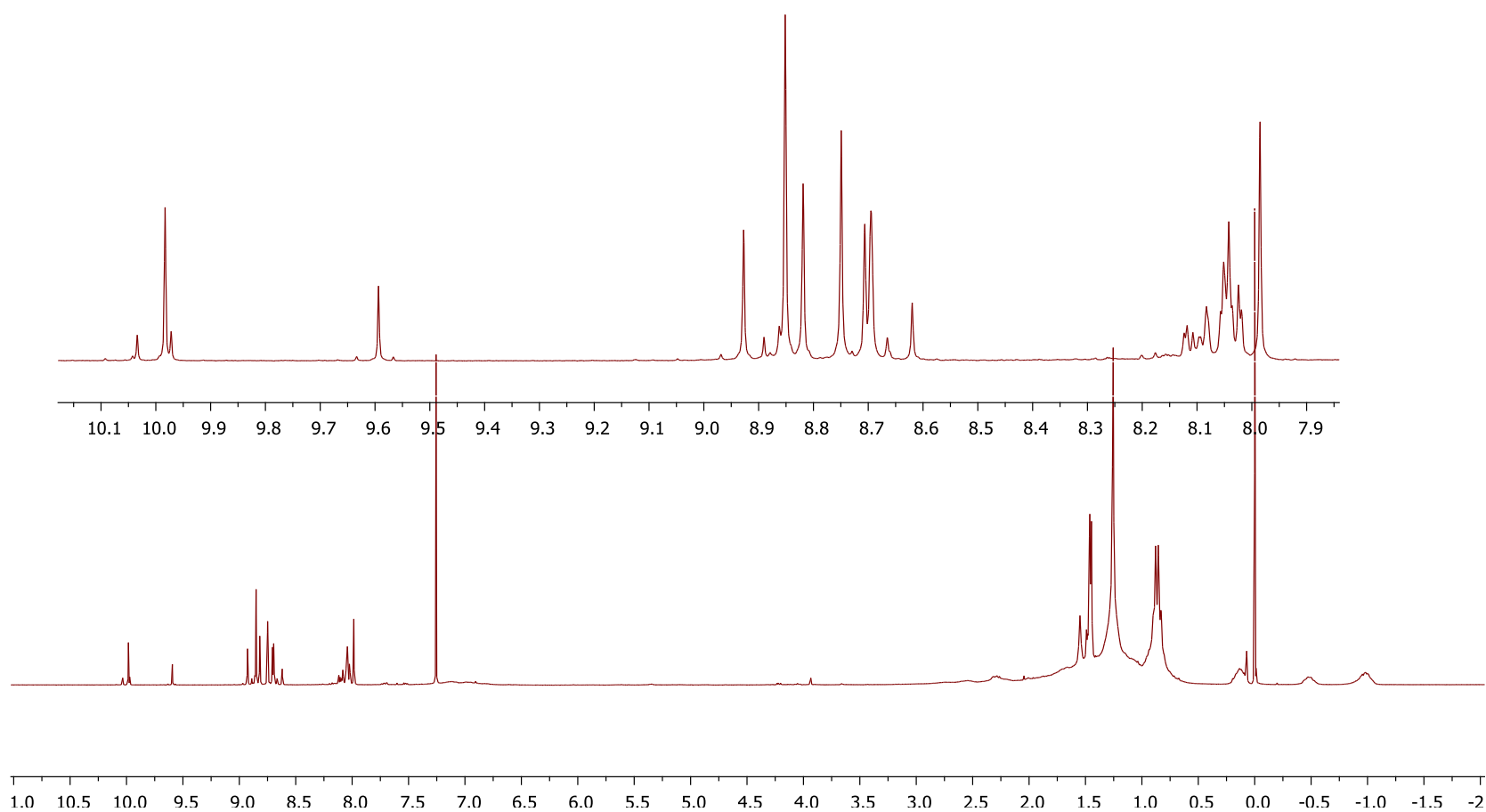
6.0 equiv. Br<sub>2</sub> with **103d** at 35 °C



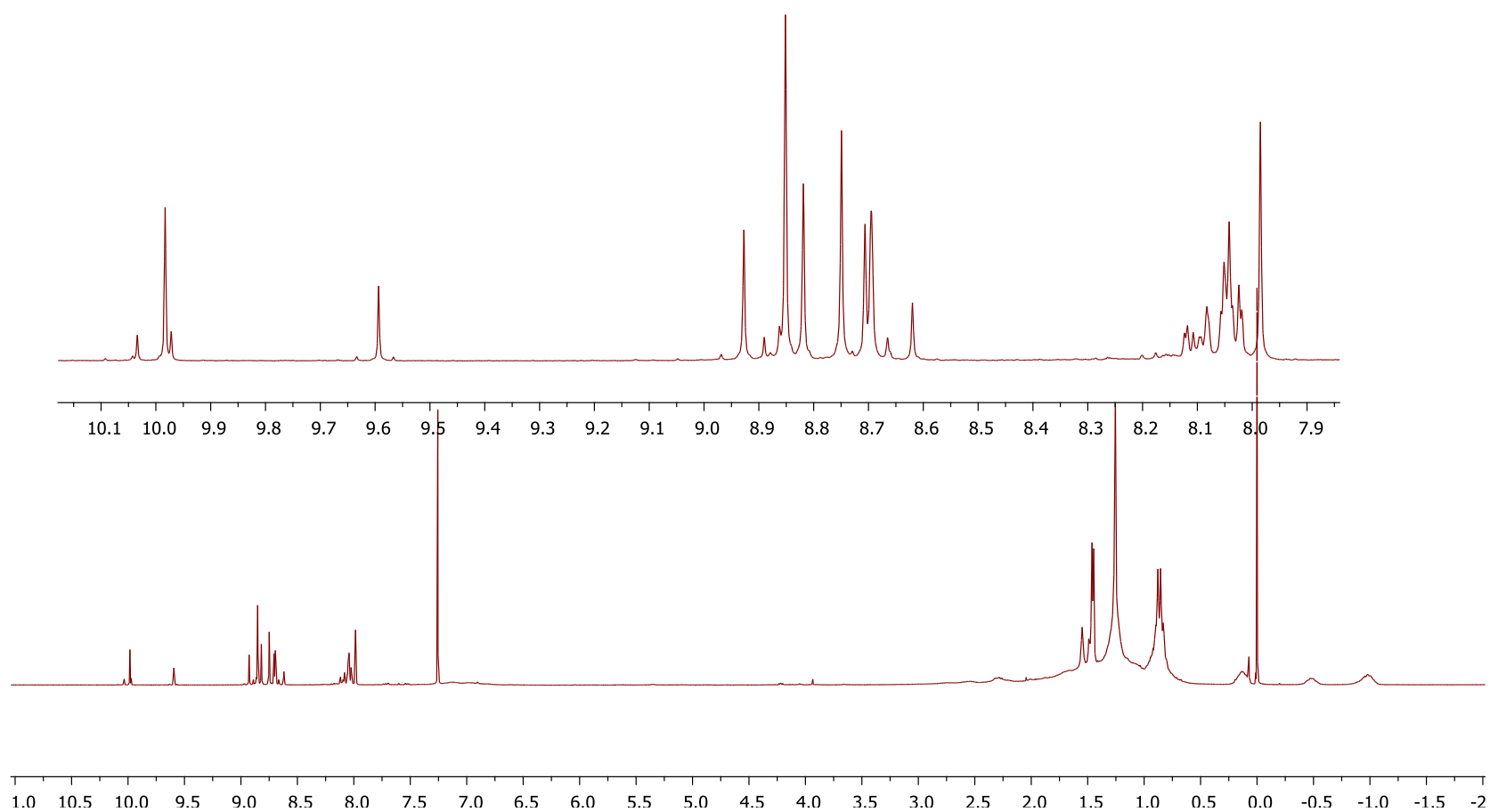
6.5 equiv. Br<sub>2</sub> with **103d** at 35 °C



7.0 equiv. Br<sub>2</sub> with **103d** at 35 °C

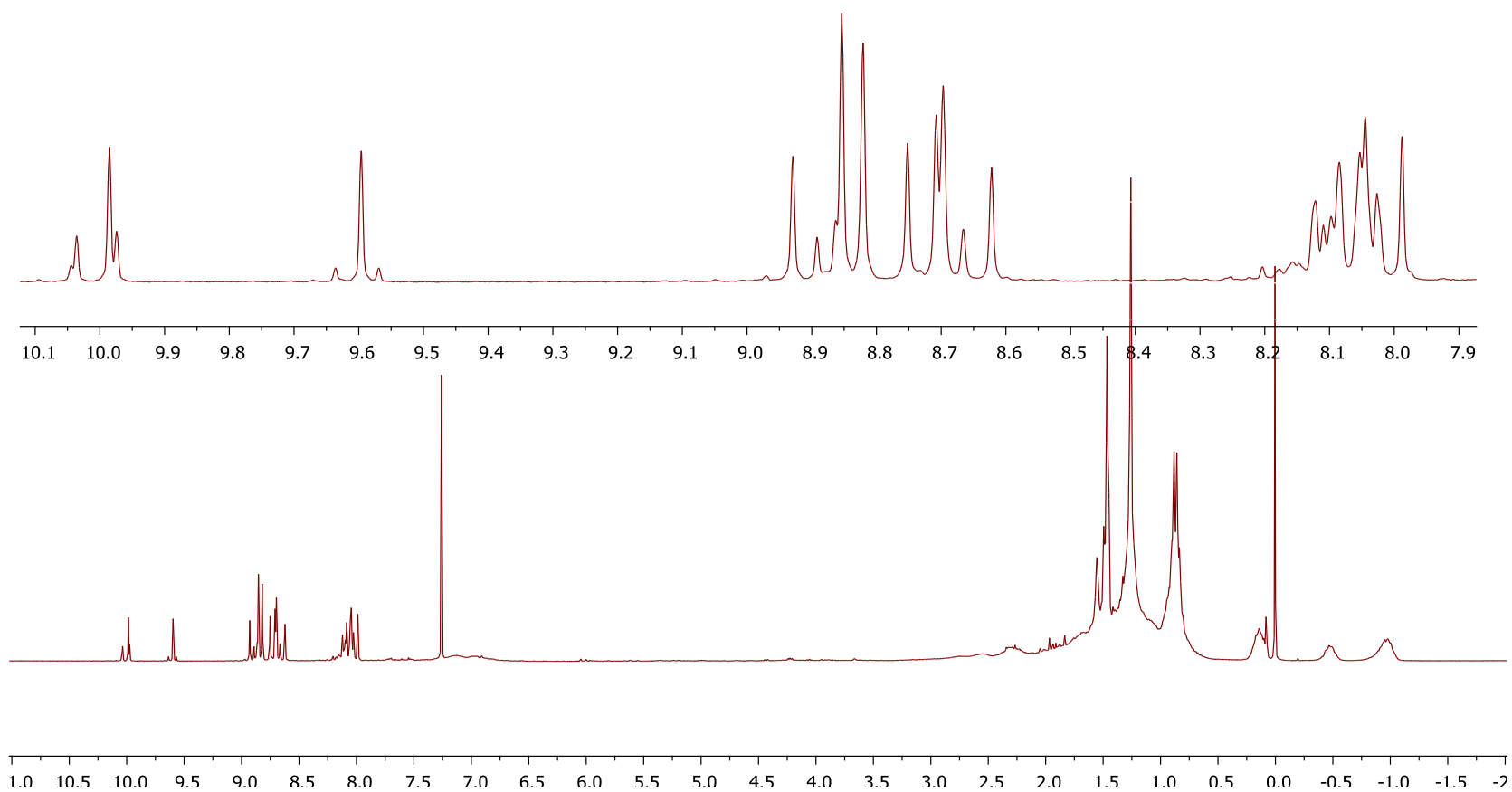


7.5 equiv. Br<sub>2</sub> with **103d** at 35 °C

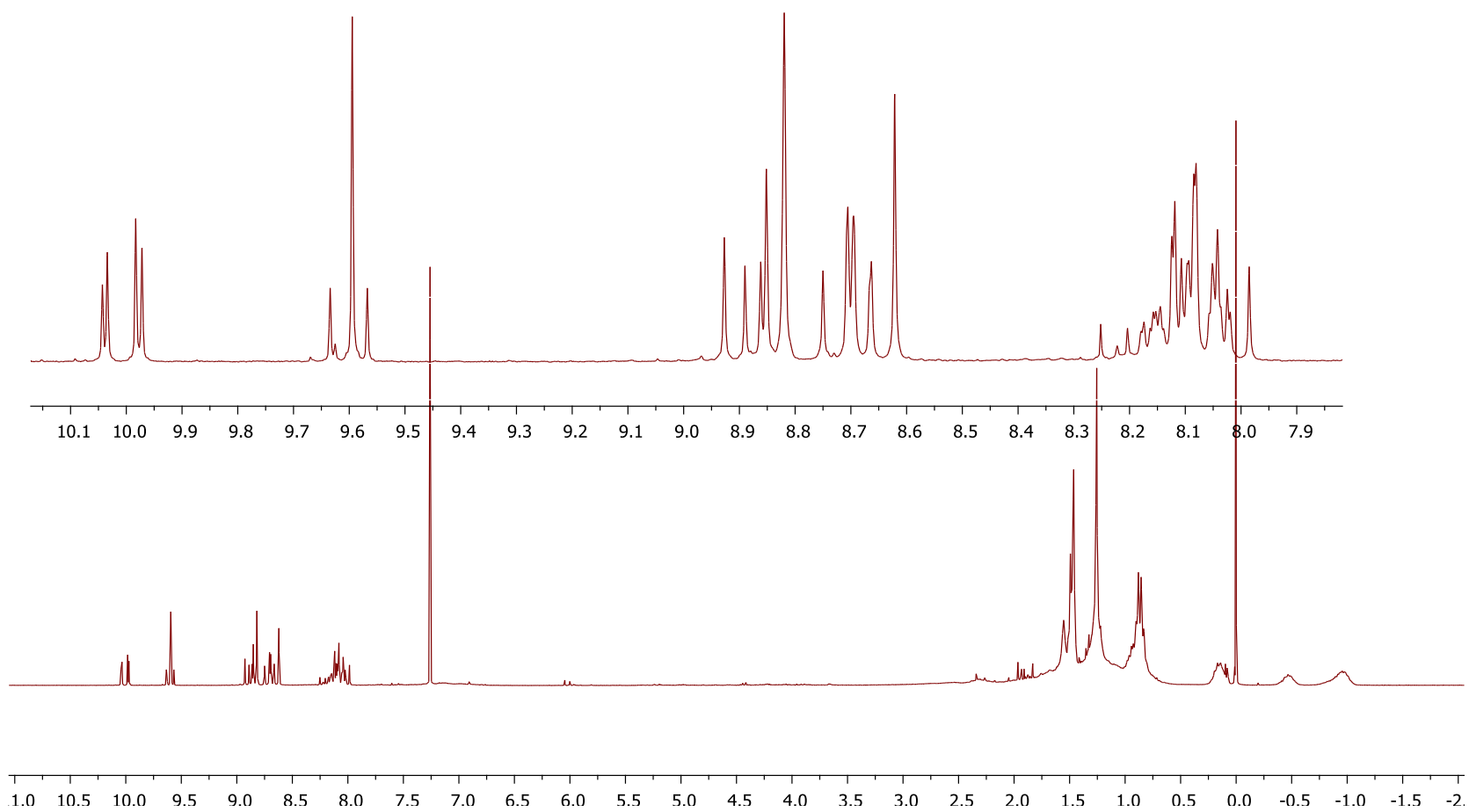




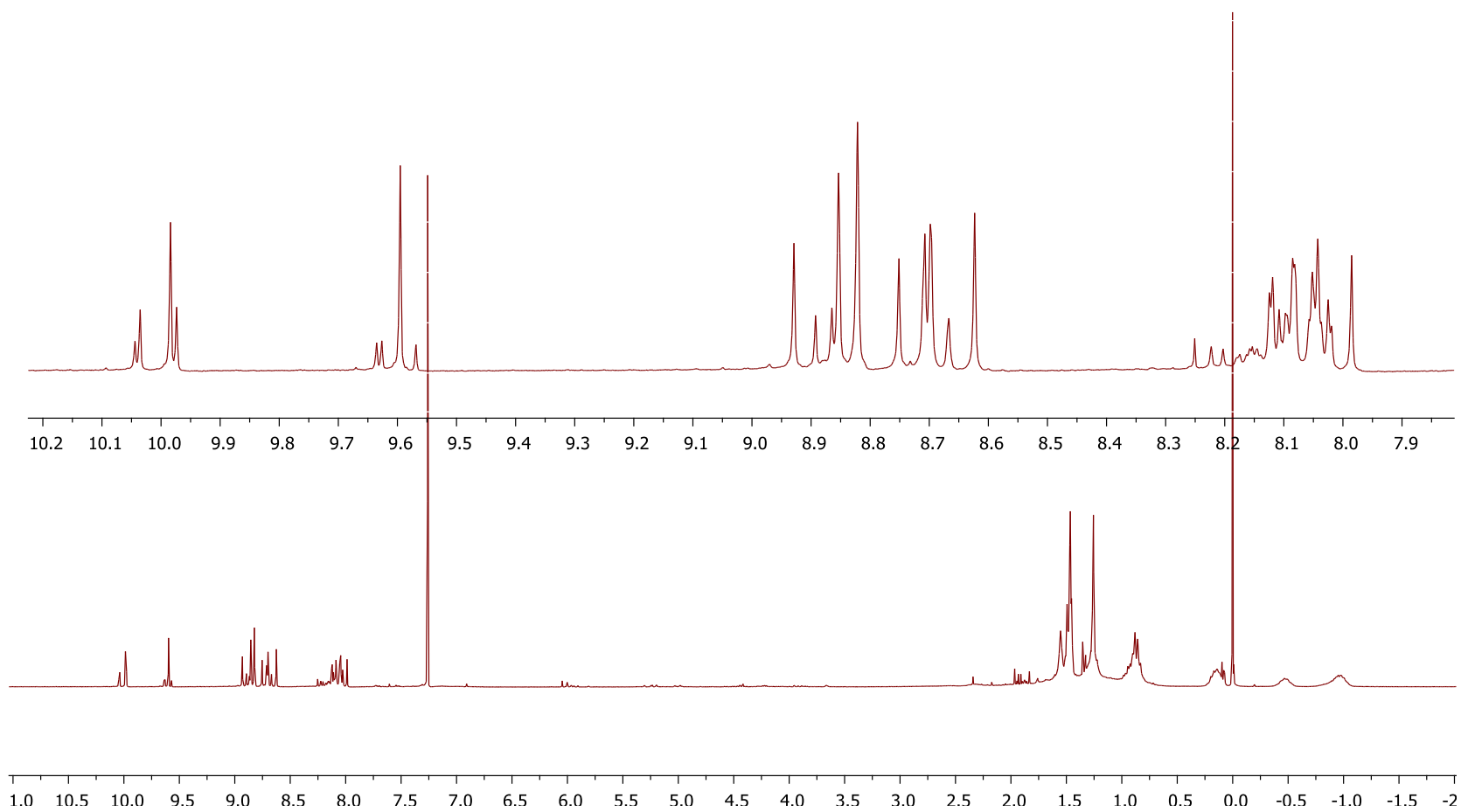
8.0 equiv. Br<sub>2</sub> with **103d** at 35 °C



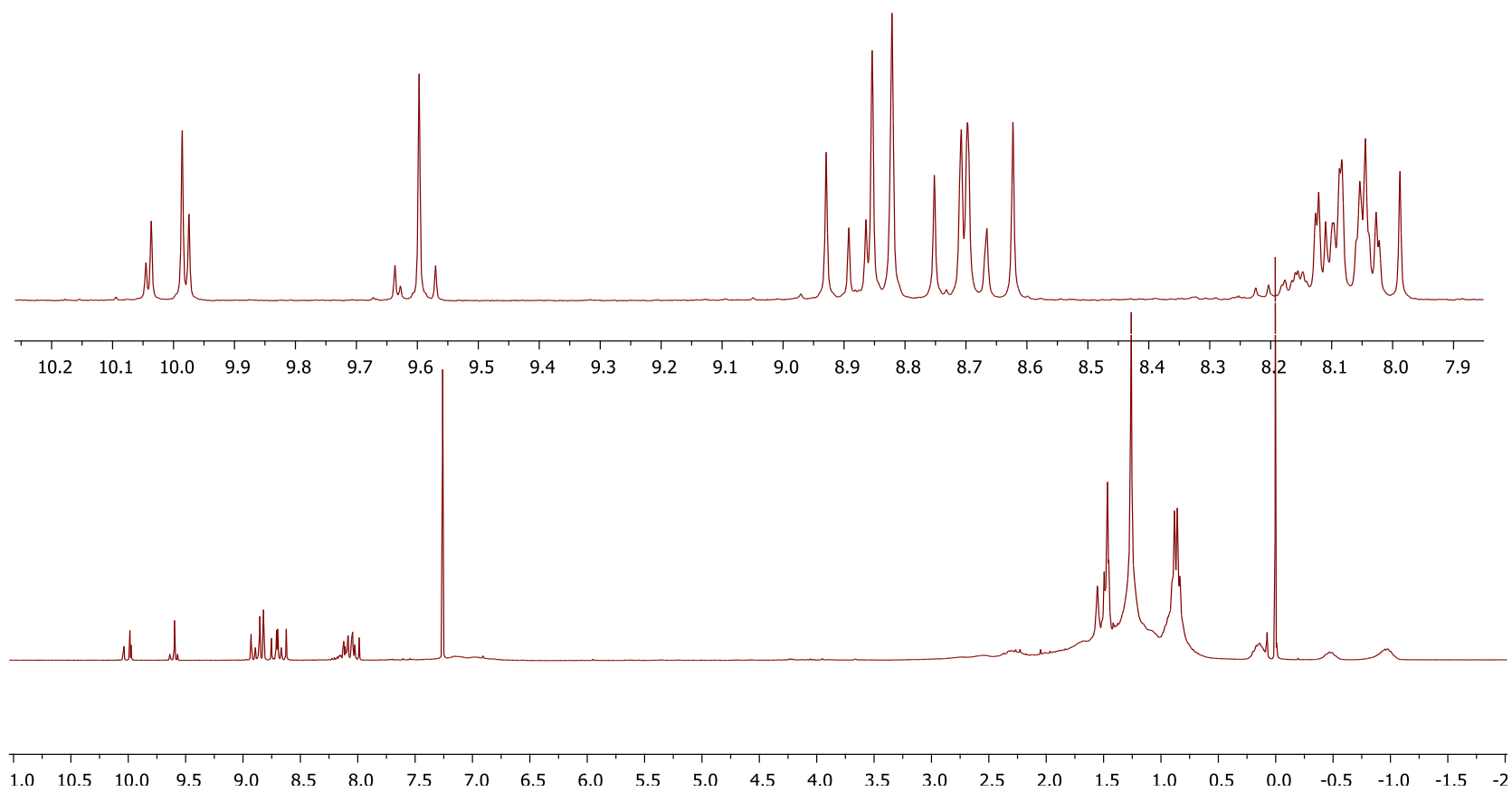
8.5 equiv. Br<sub>2</sub> with **103d** at 35 °C



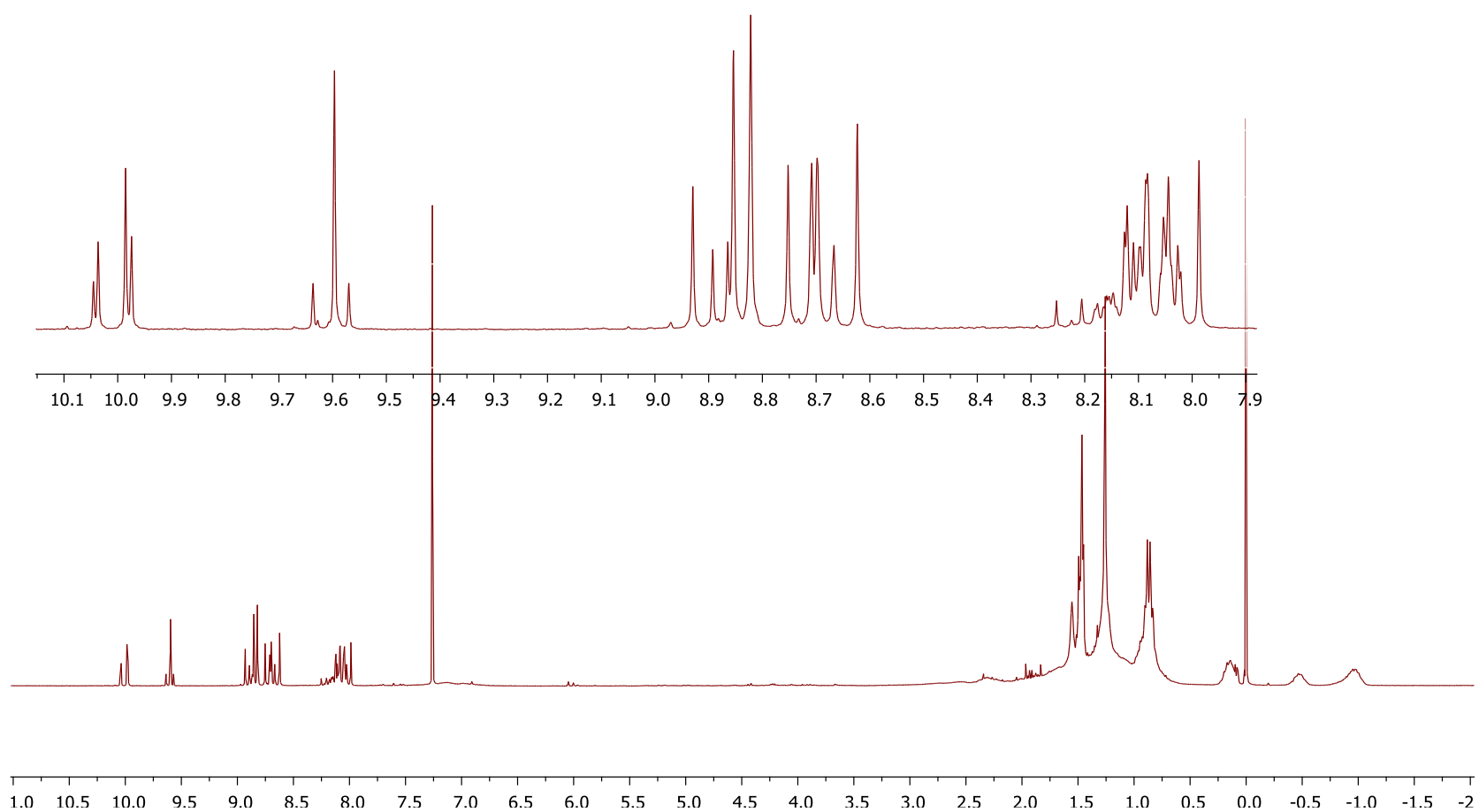
9.0 equiv. Br<sub>2</sub> with **103d** at 35 °C



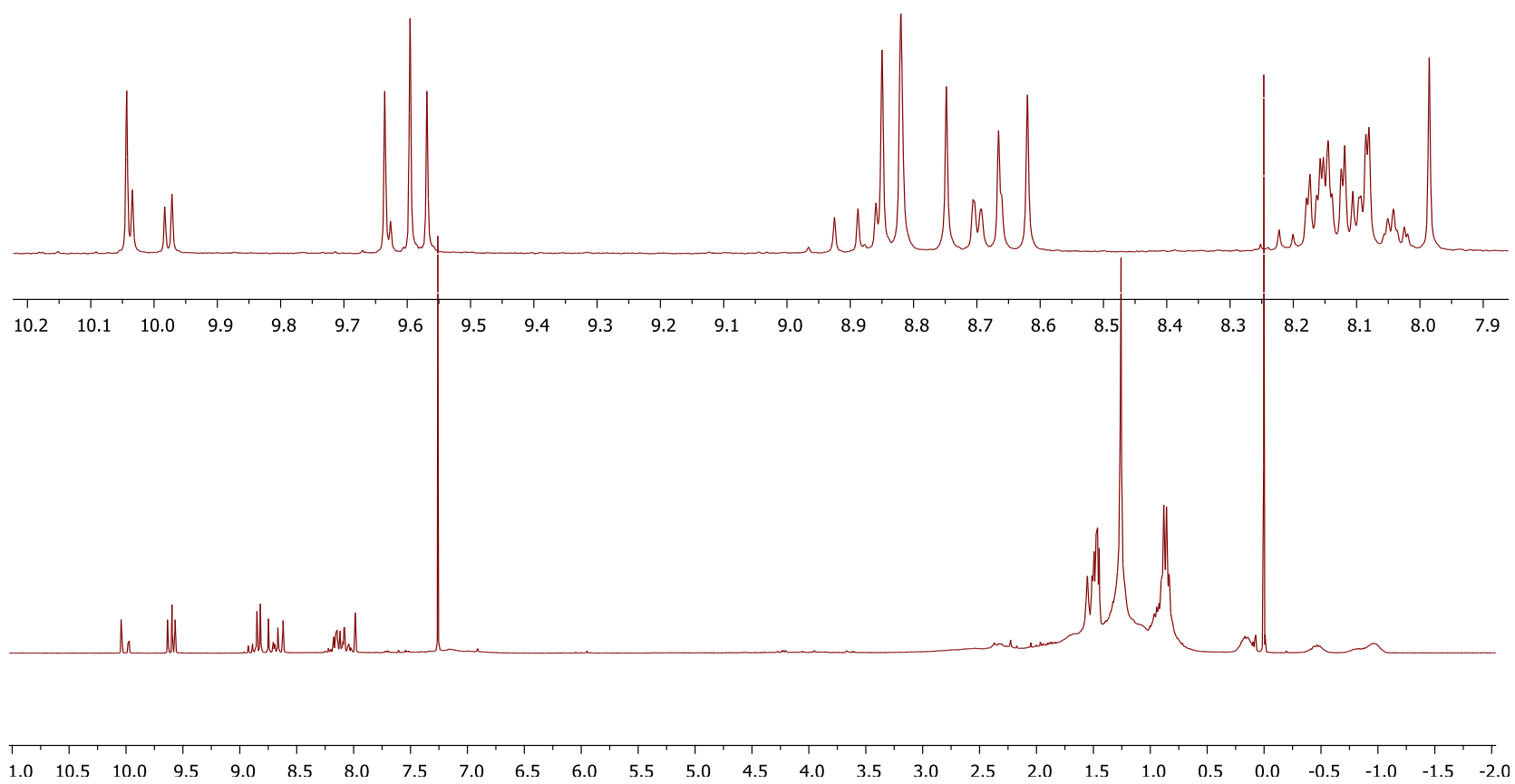
9.5 equiv. Br<sub>2</sub> with **103d** at 35 °C

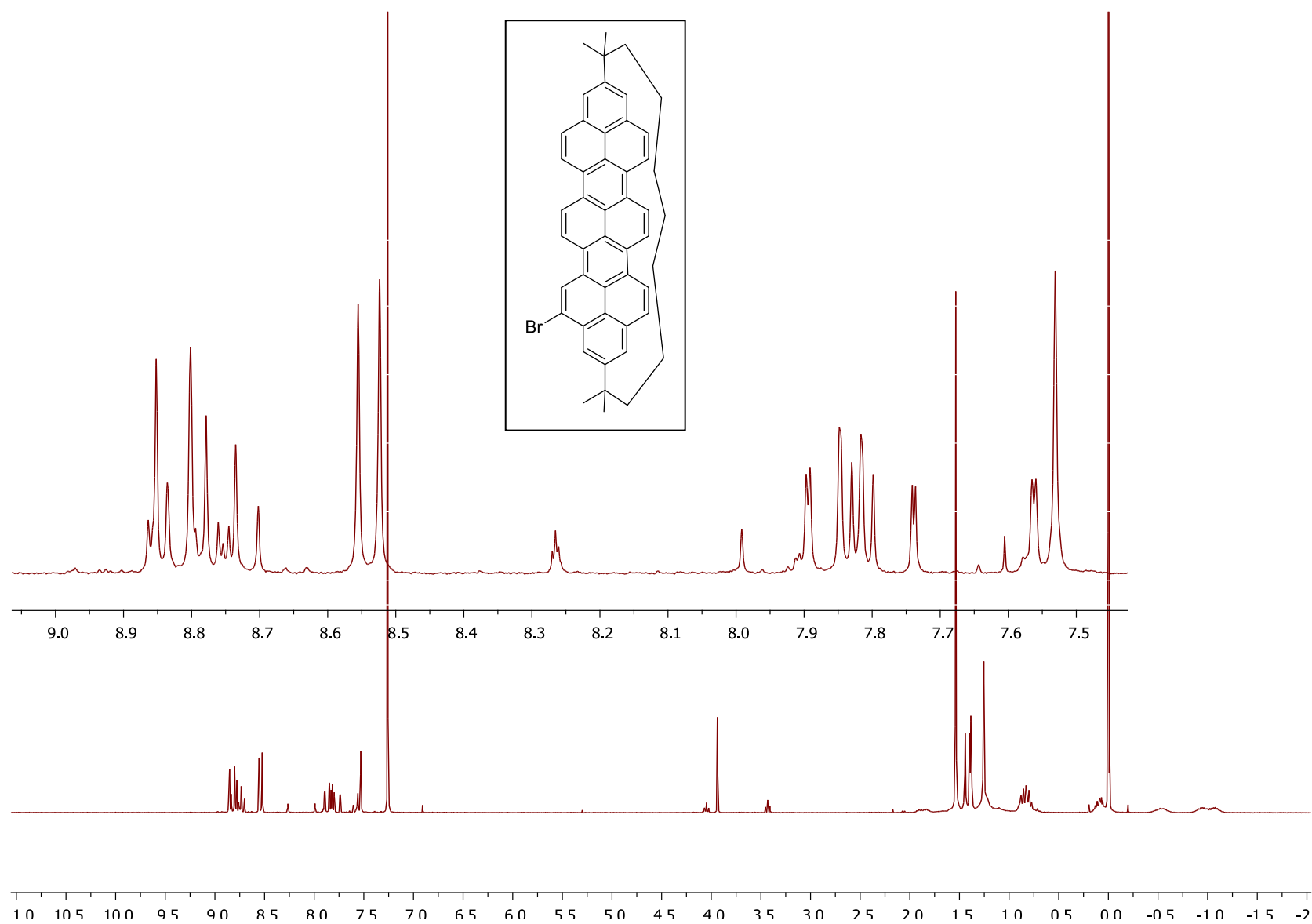


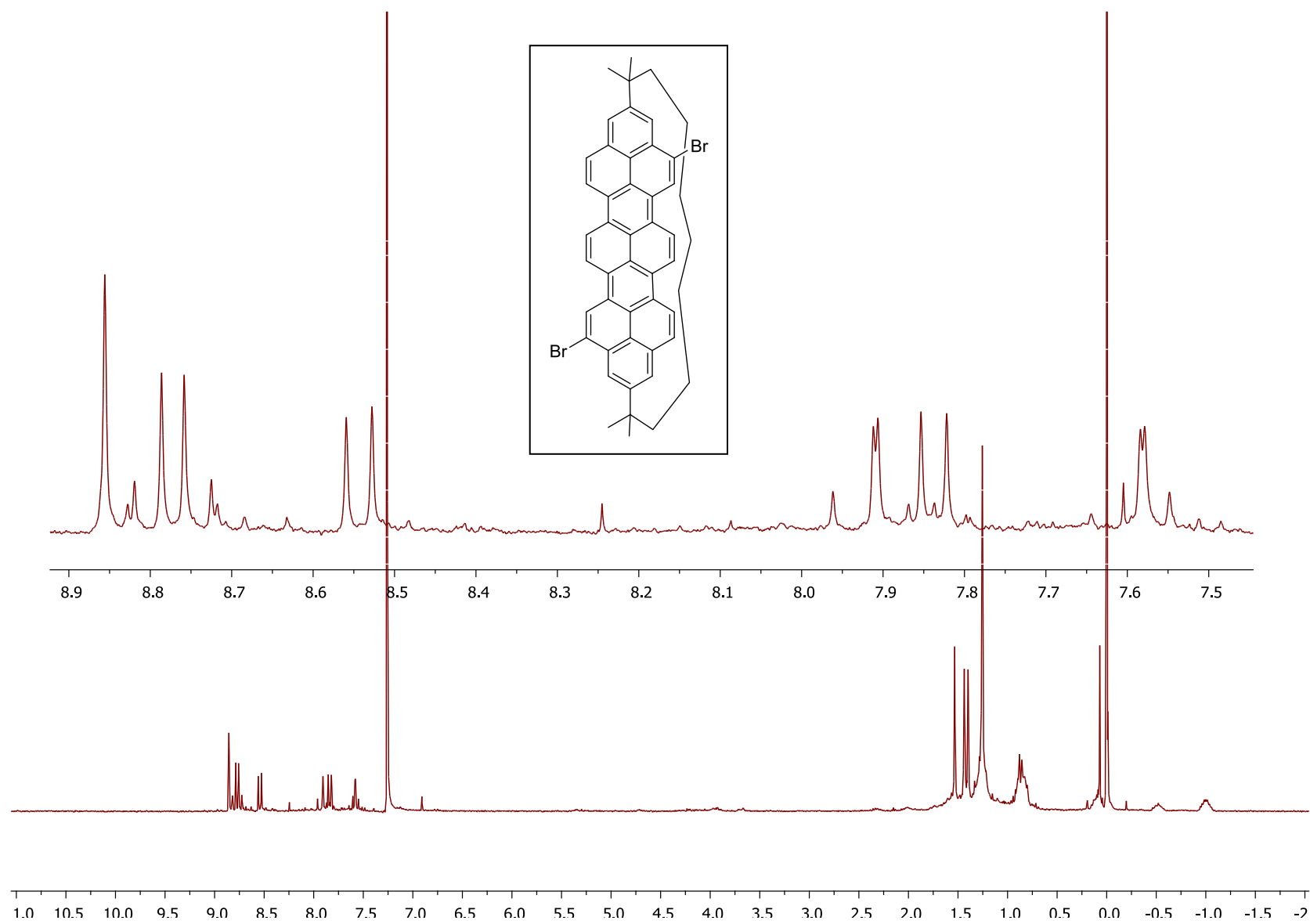
10.0 equiv. Br<sub>2</sub> with **103d** at 35 °C



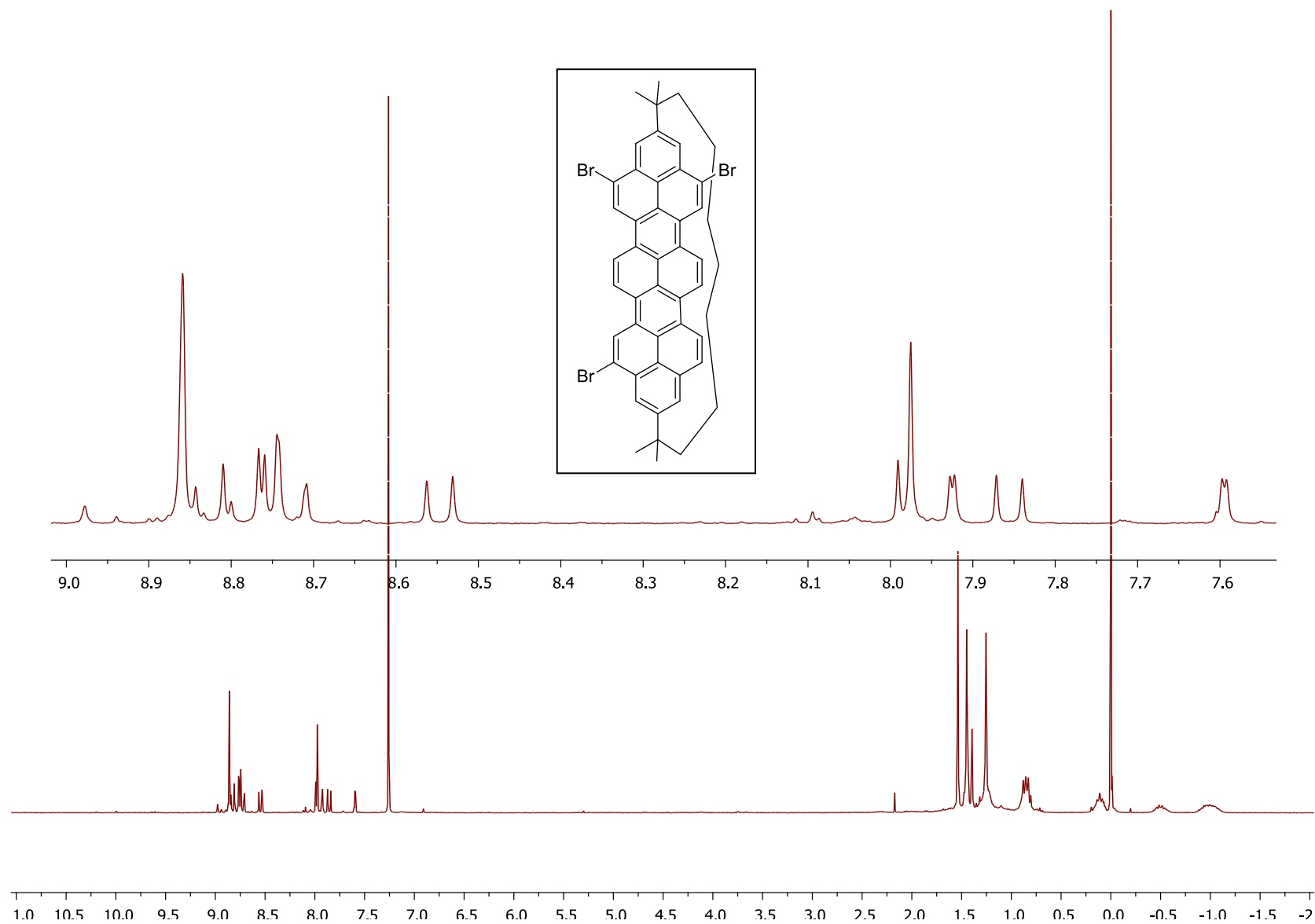
20.0 equiv. Br<sub>2</sub> with **103d** at 35 °C

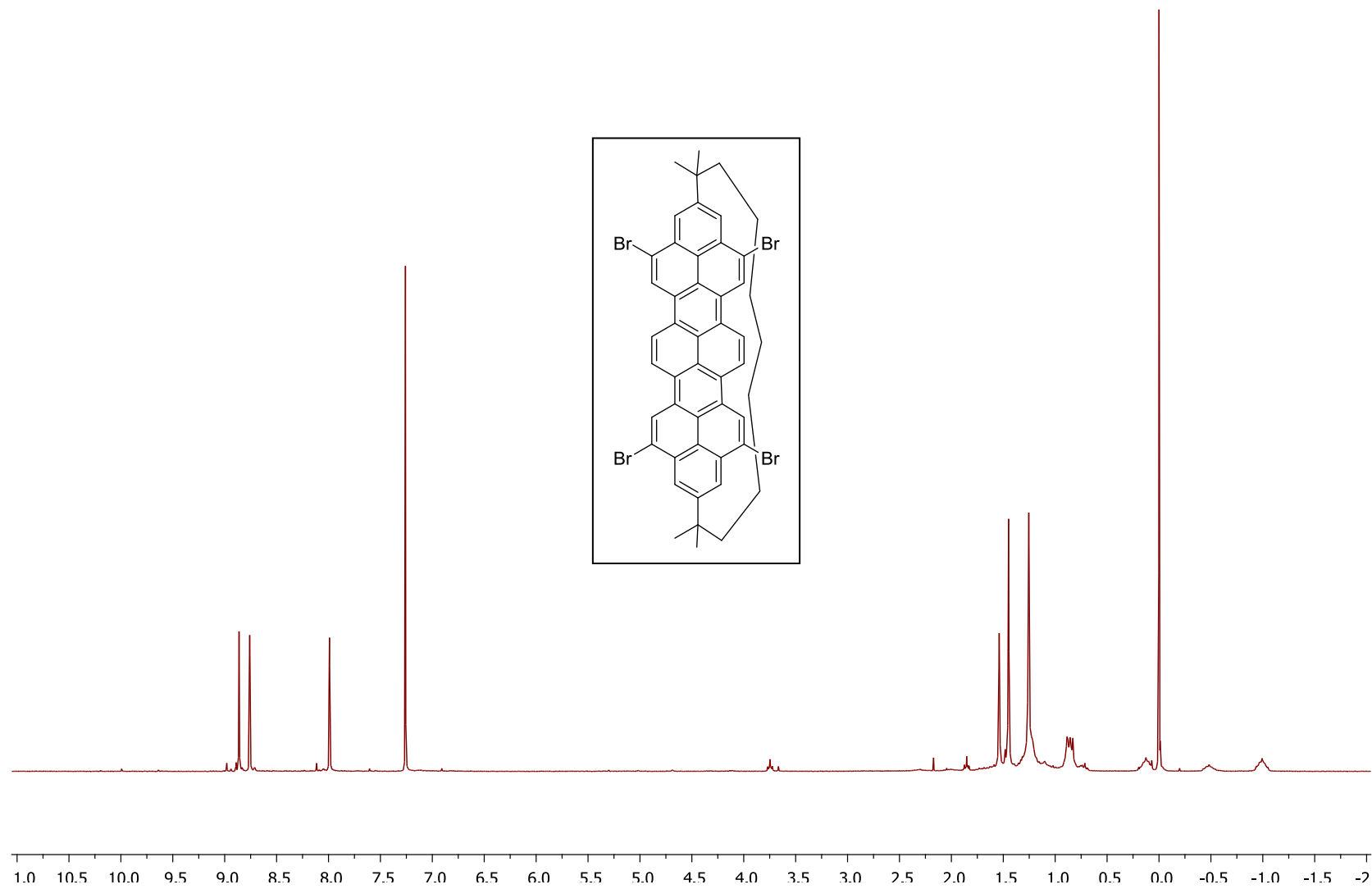


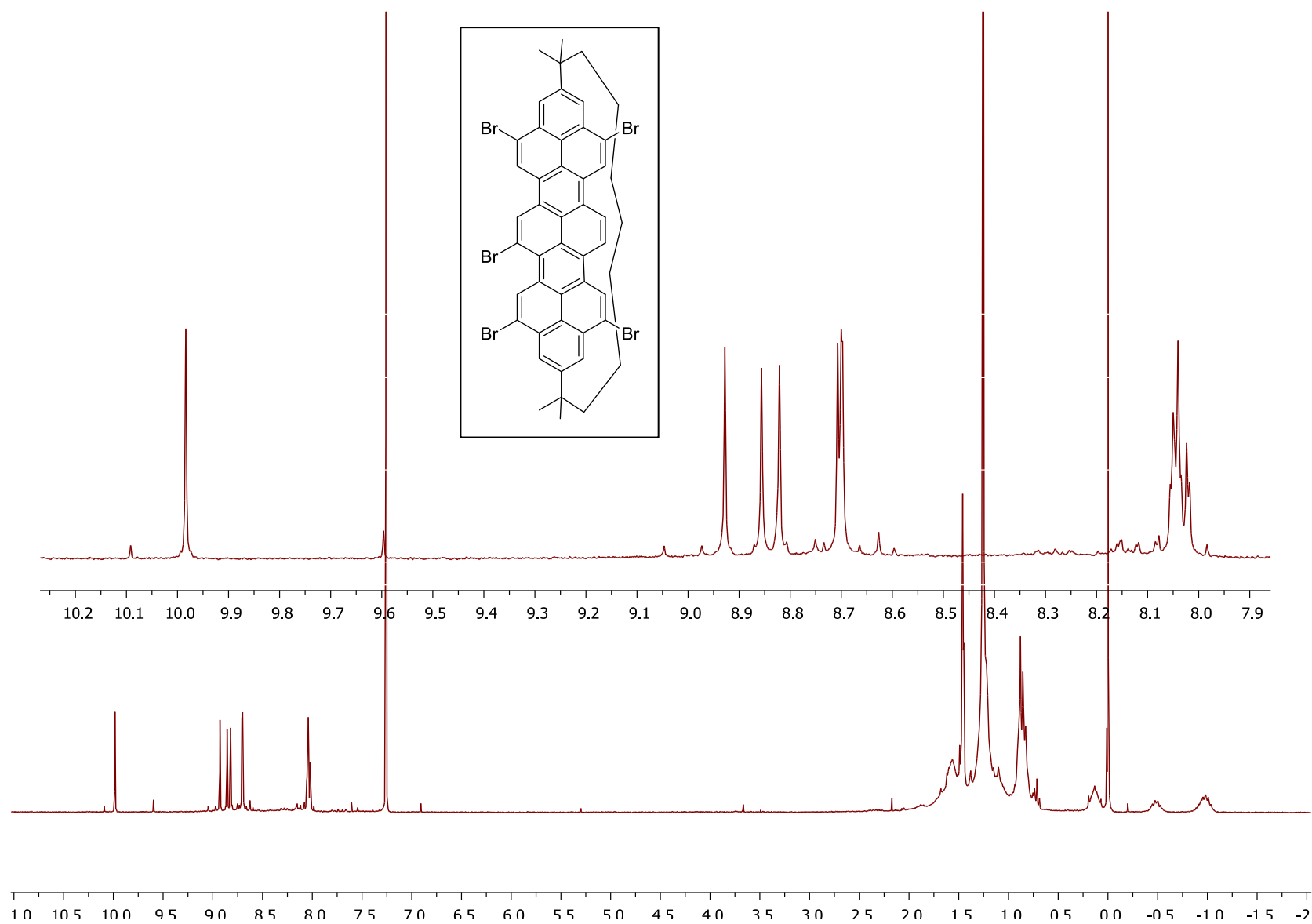


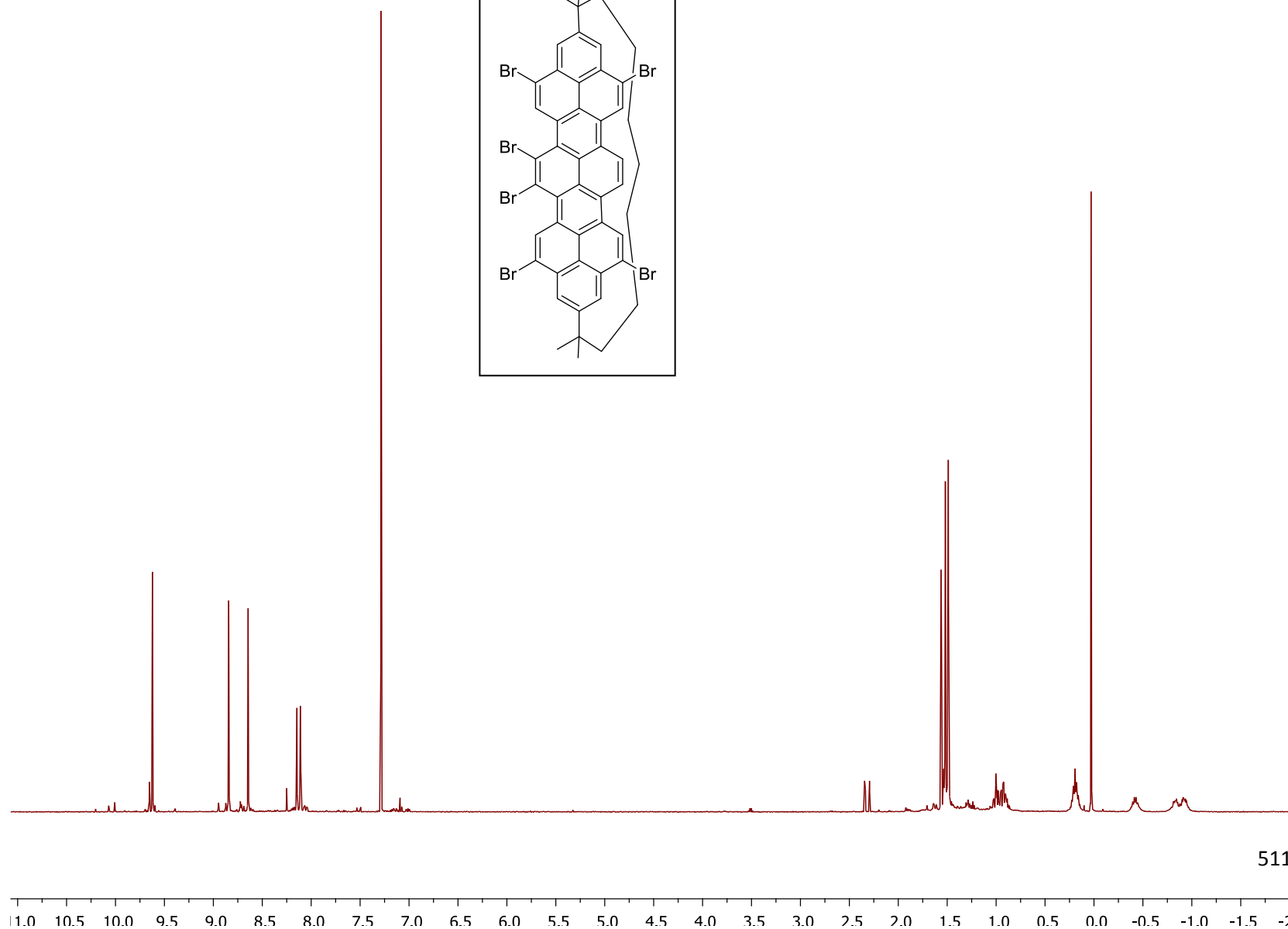
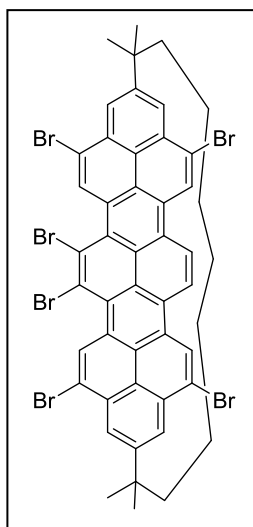


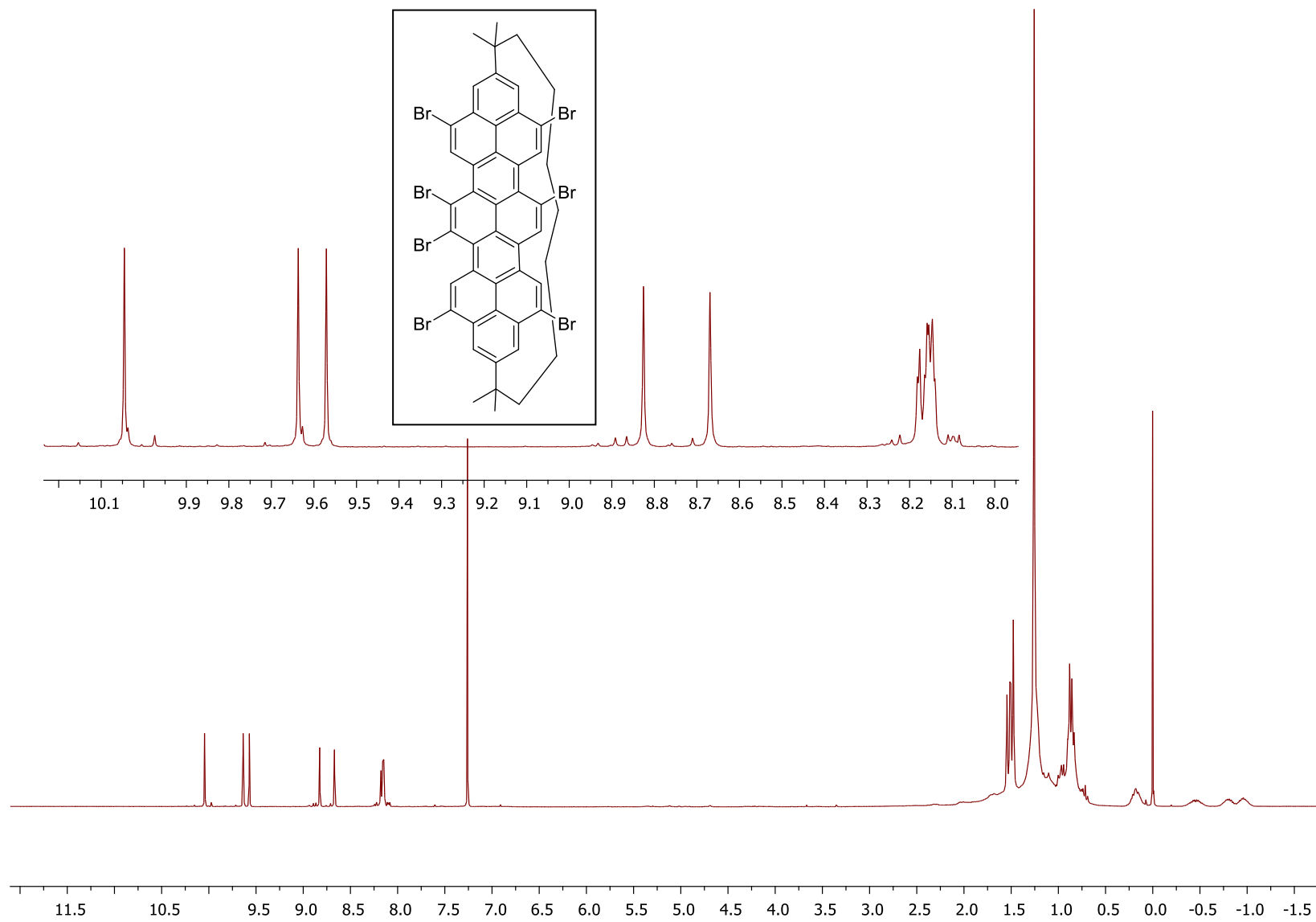




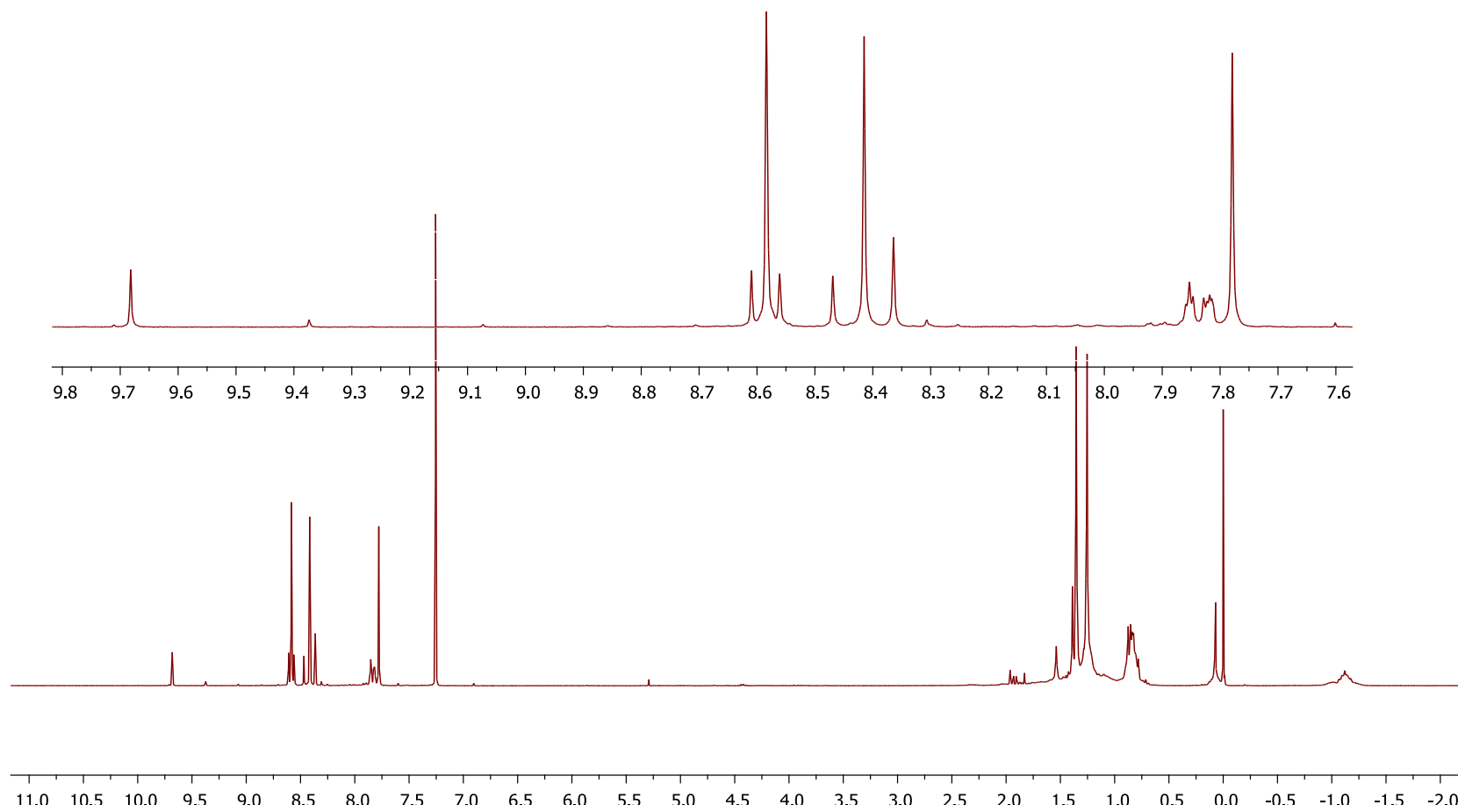




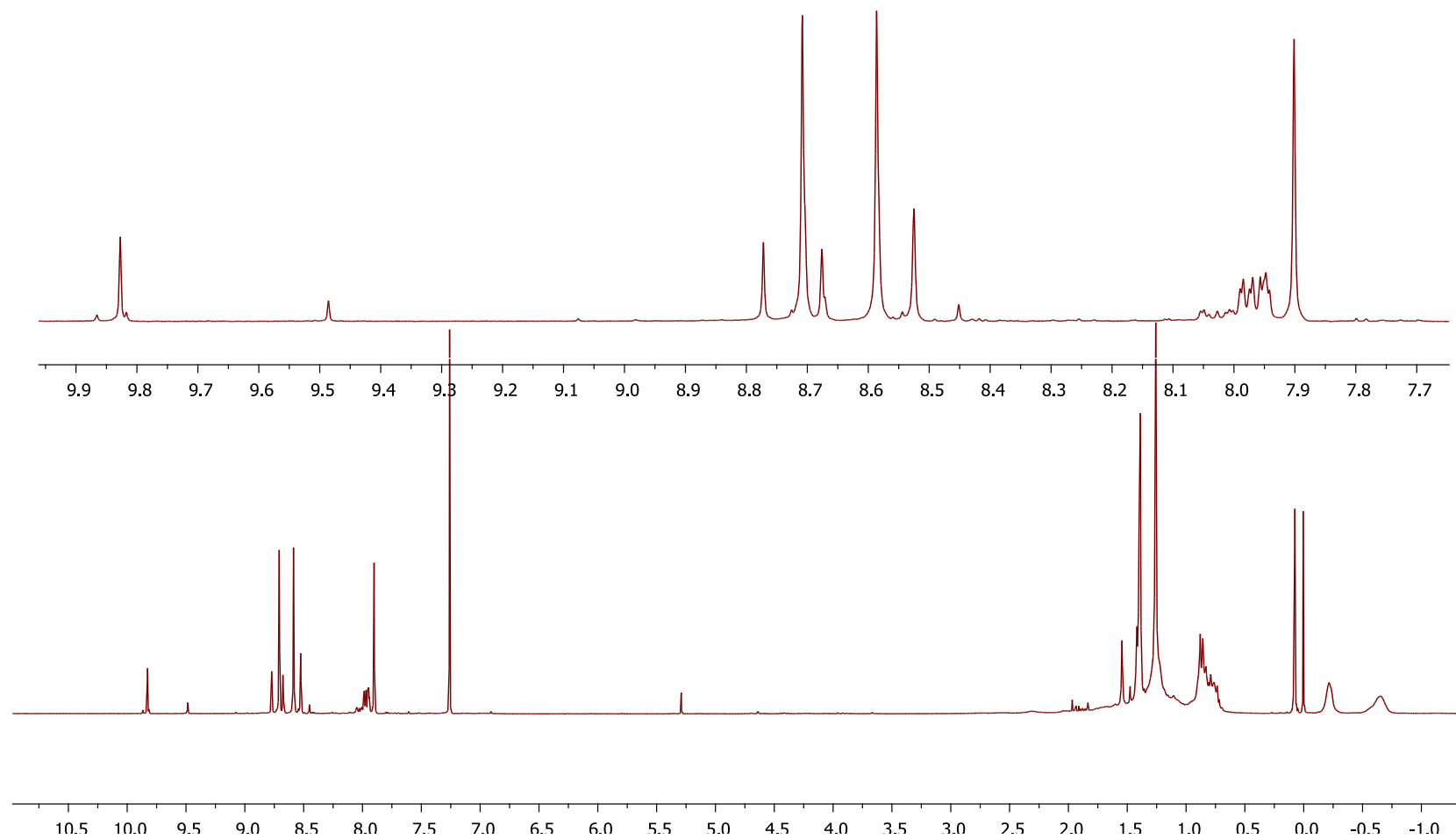




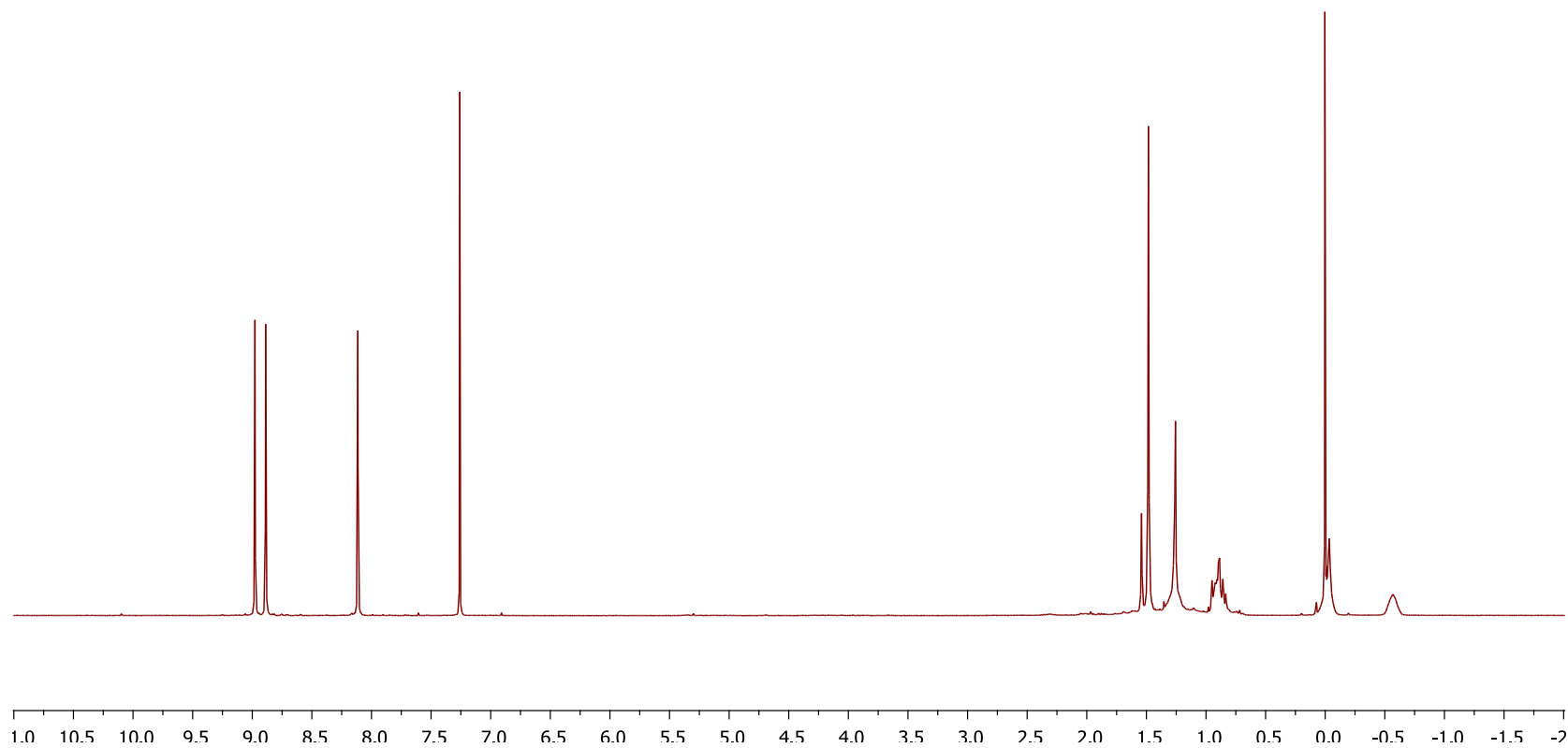
4.0 equiv. Br<sub>2</sub> with **103b** at rt



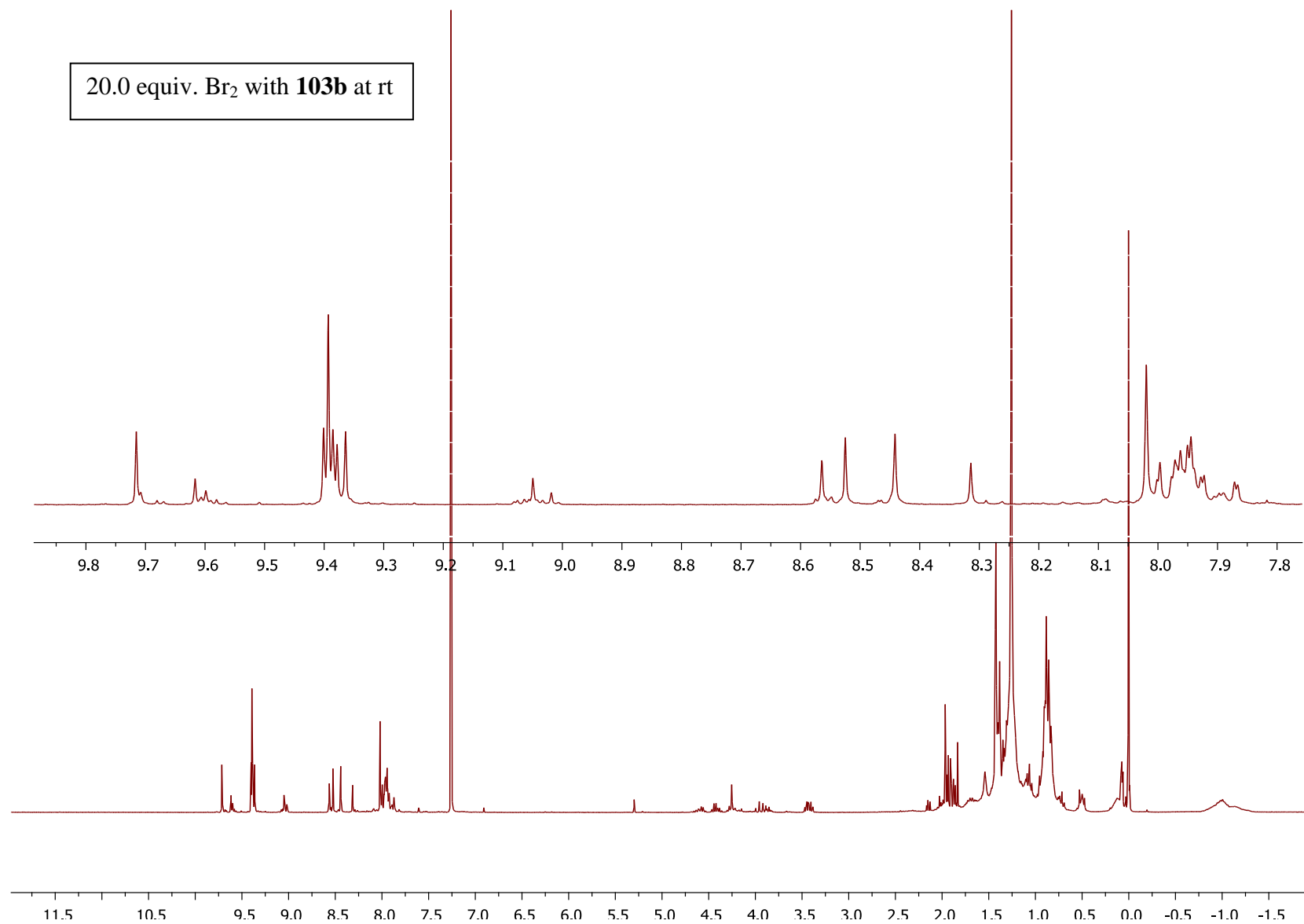
4.0 equiv. Br<sub>2</sub> with **103c** at rt

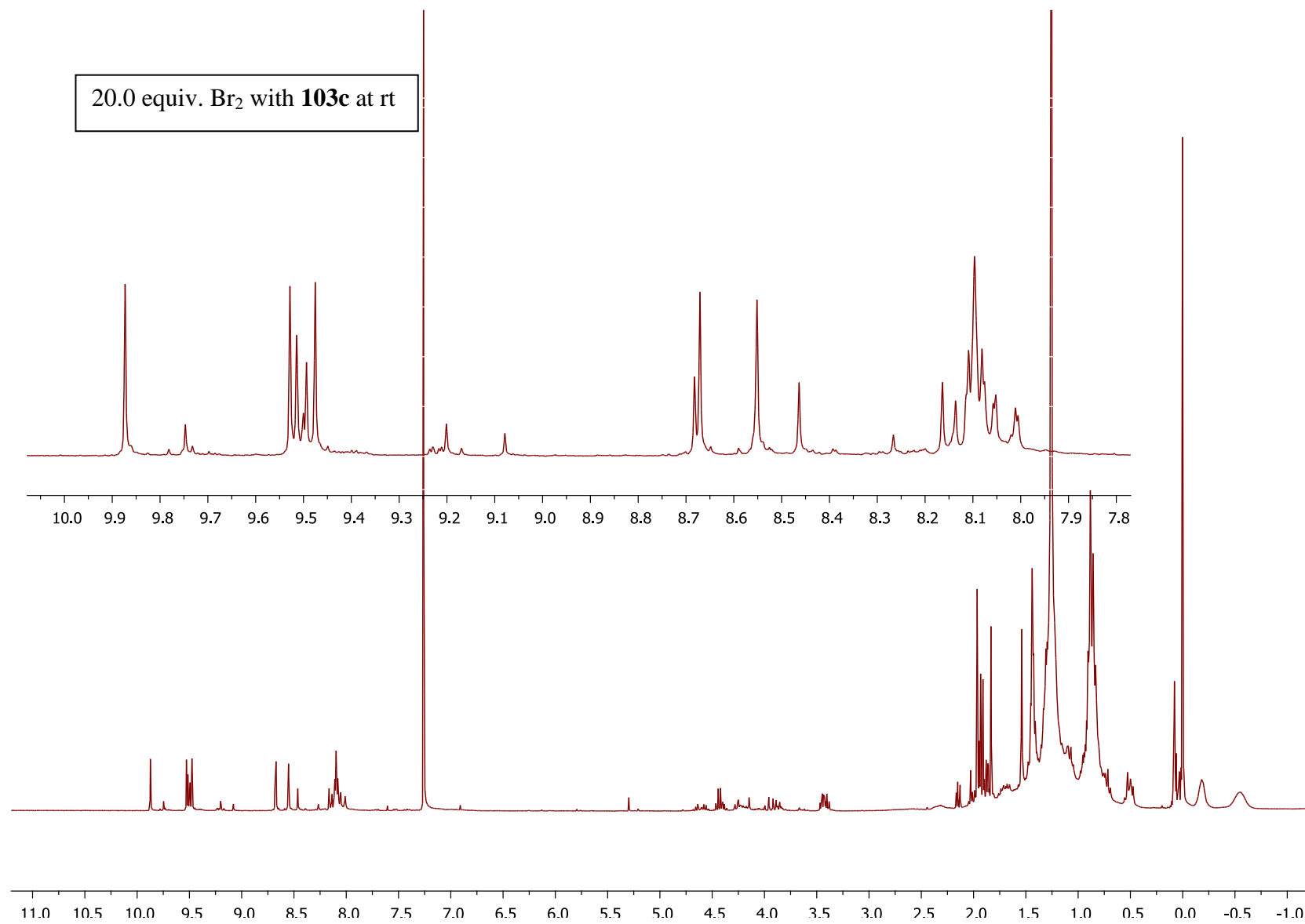


4.0 equiv. Br<sub>2</sub> with **103e** at rt

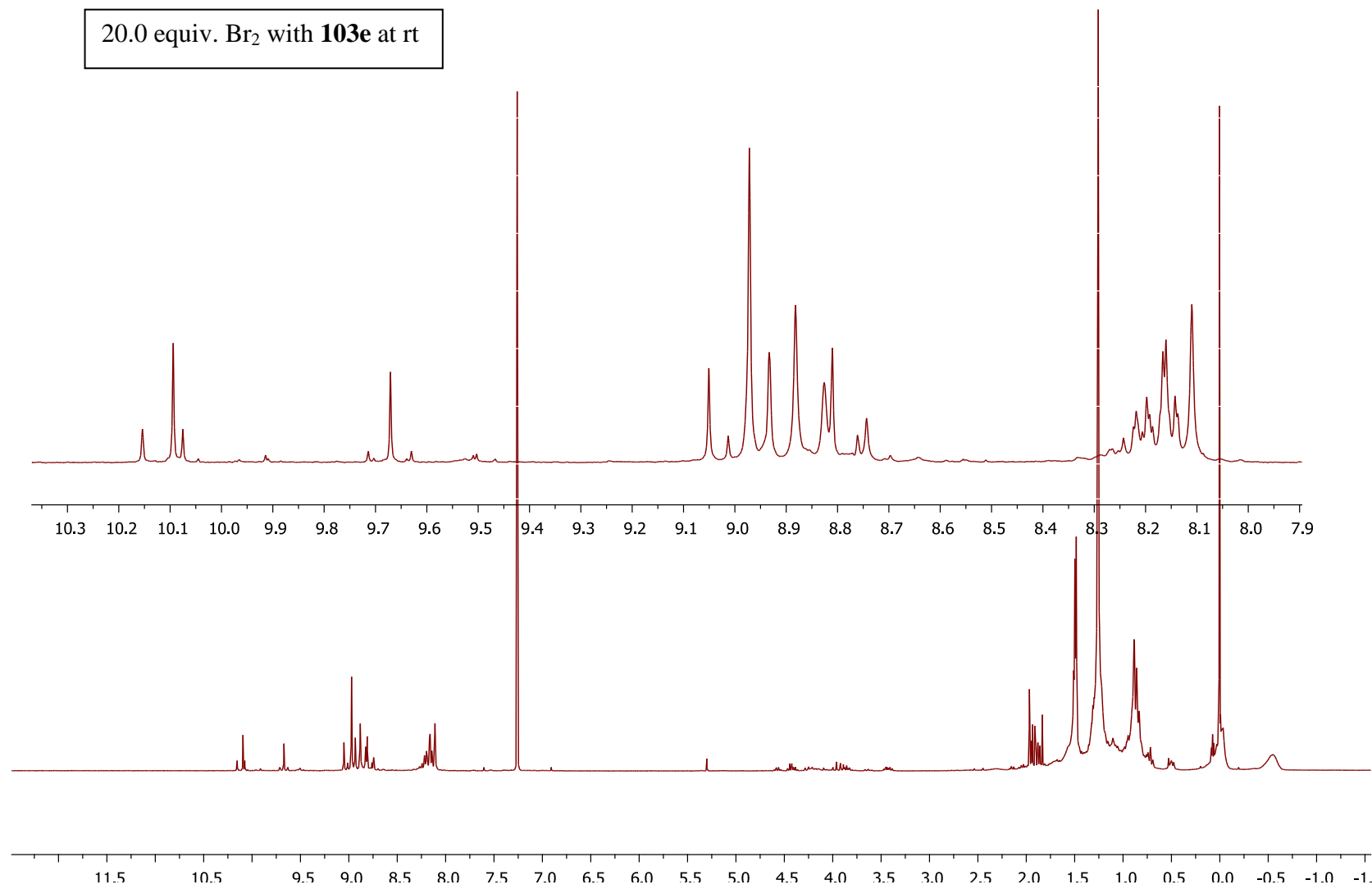








20.0 equiv. Br<sub>2</sub> with **103e** at rt

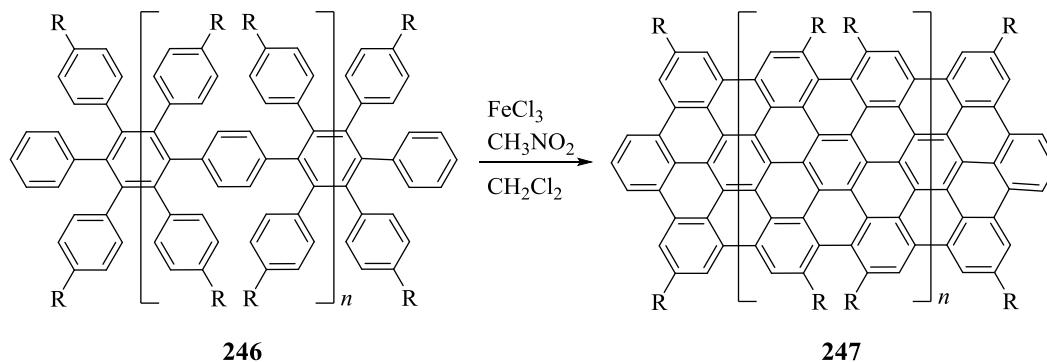


## Chapter 6: Chemistry of 1,1,*n,n*,-Tetramethyl[*n*](2,11)teropyrenophanes

### 6.1 Introduction

Having few hundred milligrams to gram quantities of teropyrenophanes **103b-e** in hand (Chapters 2-4), the opportunity to investigate the chemical reactivity of these severely distorted large cyclophane molecules arose. In this regard, it was of special interest to study how systematic changes in the structure of the teropyrene system affected the chemical reactivity of these bent systems. The first step in this direction was an investigation of the electrophilic bromination reactions teropyrenophanes **103b-c** (Chapter 5). From this work it was found that bromination occurs most rapidly at the 3, 9, 13 and 18 positions of the teropyrene system, which allows for the selective formation of symmetrical tetrabromides. Subsequent bromination occurs more slowly at the 6, 7, 15 and 16 positions of the teropyrene system. The reactivity of the teropyrene system increases with increasing bend such that octabromination becomes increasingly viable from **103e** to **103b**.

It is well known in the literature that halogenated aromatic systems are versatile substrates for a range of cross-coupling reactions. In general, these reactions are normally performed on relatively small aromatic systems. Indeed, not many large aromatic systems have been subjected to a halogenation reaction followed by extending their  $\pi$ -structure using coupling reactions. A major problem is often the solubility of large aromatic systems (and more so with halogenated version), which obstructs the exploration of their chemical reactivity. Large solubilising groups are often required in

segments (nanographenes).<sup>1</sup>

**Scheme 6.01** A strategy for the synthesis of a nanographene sheet.

## 6.2 Results and discussion

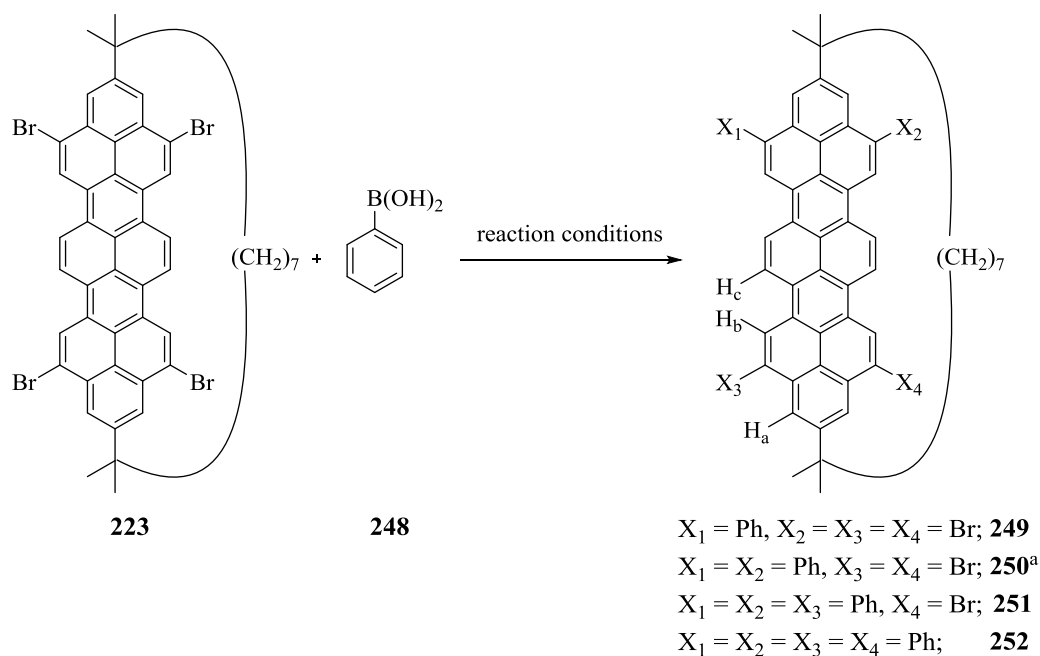
Being the most well-behaved and abundantly available system of all the teropyrenophanes, tetrabromo[9](2,11)teropyrenophane **223** was used for initial studies aimed at the construction of larger PAH-based cyclophanes. The very reliable Suzuki-Miyaura reaction was chosen for initial studies.

### 6.2.1 Suzuki coupling of tetrabromo[9](2,11)teropyrenophane **223**

When **223** was reacted with phenylboronic acid (**248**) in dioxane at 80 °C in the presence of Pd(PPh<sub>3</sub>)<sub>4</sub>, the majority of the starting material was still present after 12 h of reaction. Only traces amounts of new products were observed (tlc analysis) (Table 6.01, Entry 1). LCMS analysis of the crude product indicated that no species with a mass correspond to the desired product **252** was present. The sluggishness of this reaction is not surprising considering that the sites of reaction are *peri* positions and thus somewhat hindered. Extending the reaction time to 36 h or increasing the reaction temperatures had no significant effect on the outcome of the reaction. Upon conducting the reaction for 1 h at 120 °C in a microwave reactor, three new (minor) spots ( $R_f$  = 0.56, 0.33 and 0.32; 40% chloroform / hexanes) were observed and these correspond to the mono-, di- and tri-coupled products **249**, **250** and **251**, respectively (LCMS analysis;  $m/z$  = 941, 939, 937). No peak for the desired tetra-coupled product **252** was observed (Table 6.01, Entry 2). Increasing the reaction time or temperatures did not lead to any significant improvement in the outcome of the reaction (tlc analysis). Instead, when Aliquat<sup>®</sup> 336 (a phase transfer catalyst) was used in conjunction with K<sub>2</sub>CO<sub>3</sub> as a base and toluene/H<sub>2</sub>O as the solvent, a 1 h reaction at 120 °C under microwave irradiation resulted in the formation of a fourth

new spot ( $R_f = 0.30$ ; 40% chloroform / hexanes) along with the three other previously observed spots and only a trace quantity of starting material was remained (Table 6.01, Entry 3). The crude reaction mixture containing all these four products is nicely soluble in chlorinated solvents, but poorly soluble in hydrocarbon solvents. For this reason,

**Table 6.01** Attempted Suzuki coupling reactions.



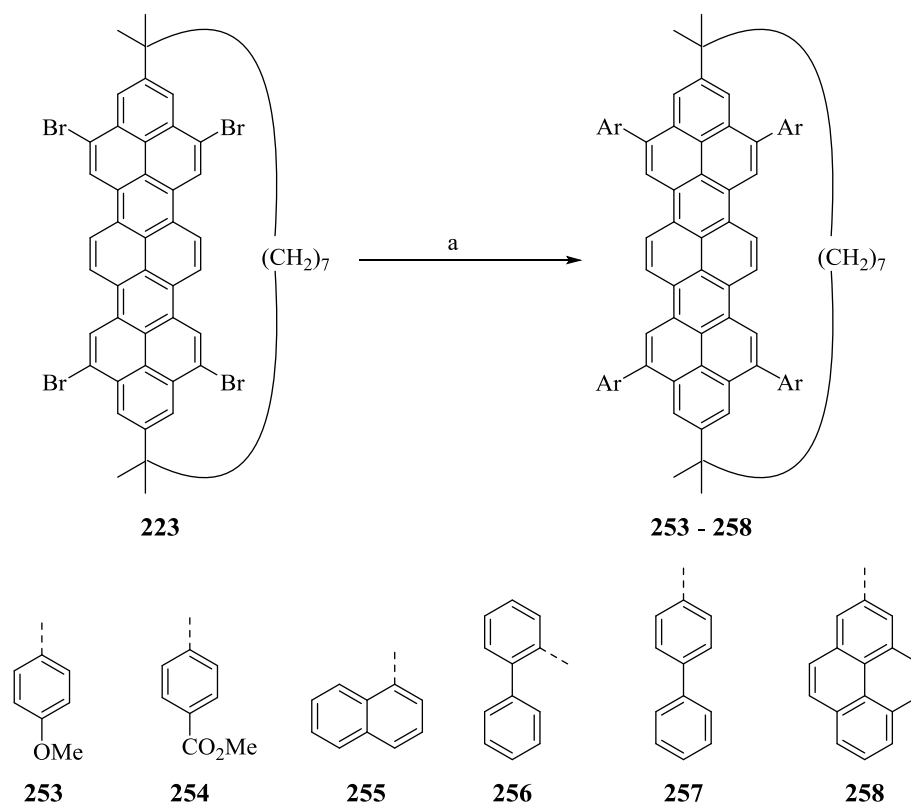
entry	reaction conditions	observation
1	$\text{Pd(PPh}_3)_4$ , 1,4-dioxane, 80-120 °C, 12-36 h	SM + traces amounts of unknown products
2	$\text{Pd(PPh}_3)_4$ , 1,4-dioxane, MW, 120-150 °C, 1-3 h	SM (major) + ( <b>249</b> + <b>250</b> + <b>251</b> ) (minor)
3	$\text{Pd(PPh}_3)_4$ , $\text{K}_2\text{CO}_3$ , aliquat® 336, toluene / $\text{H}_2\text{O}$ , MW, 120 °C, 1 h	SM (minor) + <b>252</b> (33%) + ( <b>249</b> + <b>250</b> + <b>251</b> ) (major)

<sup>a</sup>regioselectivity is tentatively assigned

column chromatographic separation of the product mixture (which requires 20-40% dichloromethane / hexanes) became problematic and no product separation was achieved. However, in only one instance, the product **252** could be obtained in about 85% pure form (APPI-HRMS [M+1] = 935.4520; found) using preparative tlc. The mass of product obtained would correspond to a 33% yield if it were pure **252**. The  $^1\text{H}$  NMR spectrum of tetraphenylteropyrenophane **252** contains three singlets at  $\delta$  8.98, 8.71 and 7.58, which corresponds to  $\text{H}_c$ ,  $\text{H}_b$  and  $\text{H}_a$  of compound **252**, respectively (Table 6.01). The phenyl protons appear further upfield ( $\delta$  7.94-7.55) as two broad multiplets in a 2:3 ratio.

Using these reaction conditions, a set of other aryl systems such as (4-methoxyphenyl (**253**), 4-(methoxycarbonyl)phenyl (**254**), 1-naphthyl (**255**), 2-biphenyl (**256**), 4-biphenyl (**257**) and 2-pyrenyl (**258**)), were screened (Scheme 6.02) using corresponding boronic acids. All of these reactions proceeded in a similar way to the phenylboronic acid and showed good product conversions (tlc analysis). Unfortunately, purification issues persisted with all these compounds except for the tetrakis(2-biphenyl)-substituted compound **256** (33%), which was eluted through a column without any difficulties. The use of other purification methods is currently under investigation by another student. The aromatic region of the  $^1\text{H}$ -NMR spectrum of compound **256** contains only very broad peaks in the range of  $\delta$  9.07–6.09. This is most likely due to the presence of multiple atropisomers and/or the conformational processes that interconvert them being near coalescence. Most of the peaks in the  $^{13}\text{C}$  NMR spectrum are also broadened. Further optimization work for the Suzuki-Miyaura coupling chemistry is currently underway by another student.



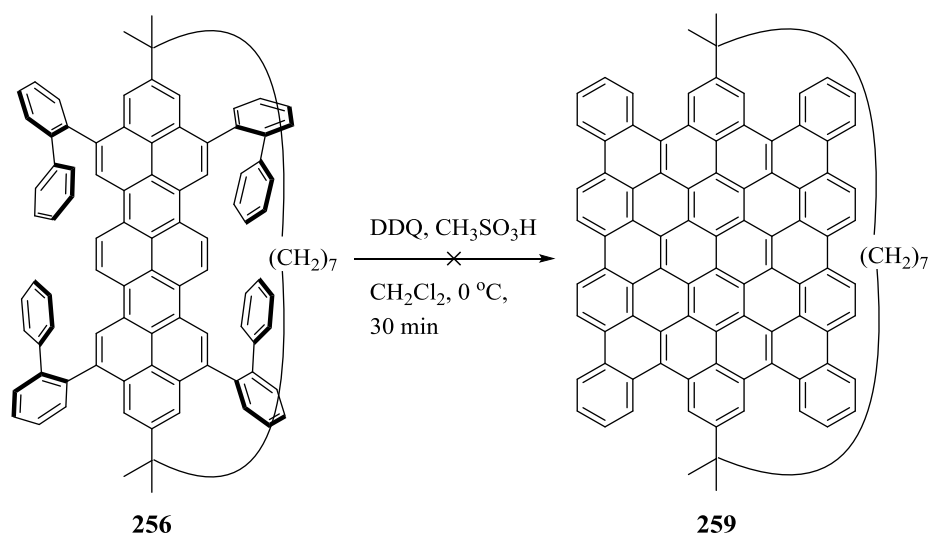


**Scheme 6.02** Suzuki coupling of tetrabromoteropyrenophane **223**; *Reaction conditions*: a)  $Pd(PPh_3)_4$ , arylboronic acid,  $K_2CO_3$ , Aliquat<sup>®</sup> 336, toluene /  $H_2O$ , MW, 120 °C, 1 h. Compound **256** (33%).

### 6.2.2 Attempted cyclodehydrogenation reaction of compound **256**

Compound **256** is especially interesting because the four biphenyl units provides an opportunity to perform a ten-fold cyclodehydrogenation reaction (Scholl reaction), which could conceivably provide access to  $C_{84}$ -PAH-based cyclophane **259**, which can certainly be viewed as a warped nanographene. Subjecting **256** to Rathore's Scholl reaction conditions ( $DDQ$  in  $CH_3SO_3H$ )<sup>2</sup> resulted in no new product formation and the starting material was recovered (Scheme 6.03). Further investigation of this transformation using

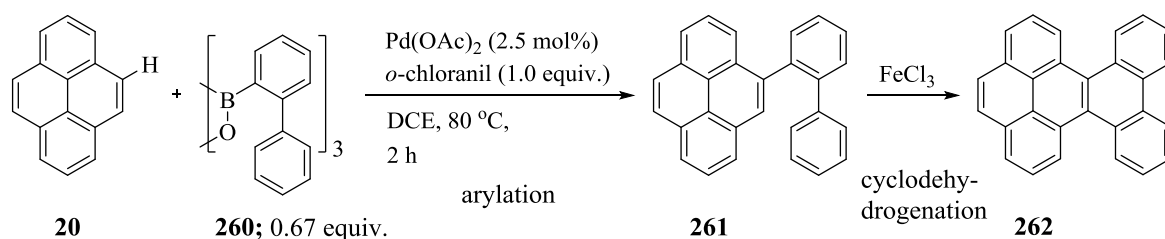
classical Scholl reaction conditions is currently under investigation by another student.



**Scheme 6.03** An unsuccessful attempt to achieve a ten-fold cyclodehydrogenation reaction.

### 6.2.3 Coupling chemistry by C-H activation of aryl systems

The Itami group at the University of Nagoya recently developed methodology for the direct C–H activation of polyfused aromatic systems.<sup>3</sup> It involves the coupling of arylboroxines with aromatic systems in the presence of palladium catalysts and leads to the generation of arylated arenes. For example, pyrene (**20**) reacts with 2-biphenylboroxine trimer **260** at 80 °C in the presence of Pd(OAc)<sub>2</sub> and *o*-chloranil in DCE to afford the 4-substituted pyrene derivative **261** (Scheme 6.04). The great advantages of this particular methodology are that the bromination of the corresponding aromatic system is not required and that it is selective for the *K*-region of PAHs.



**Scheme 6.04** Coupling of pyrene **20** and phenylboraxine **260** using direct C-H activation.

Using this C-H activation / coupling methodology, the syntheses of penta-(2-biphenyl)corannulene (**263**) and deca-(4-*t*-butylphenyl)corannulene (**264**) were achieved directly from corannulene (**112**), albeit in low yields (Figure 6.01).<sup>4</sup> Like corannulene (**112**), the teropyrene system in teropyrenophane **103d** is nonplanar and has multiple *K*-regions. As such, it was of interest to see whether **103d** would be a viable substrate for the Itami methodology and, if so, to determine how many arylations could be achieved and whether any regioselectivity would be observed. Work on this and related chemistry (see below) was performed during a two month stay in the Itami laboratory.

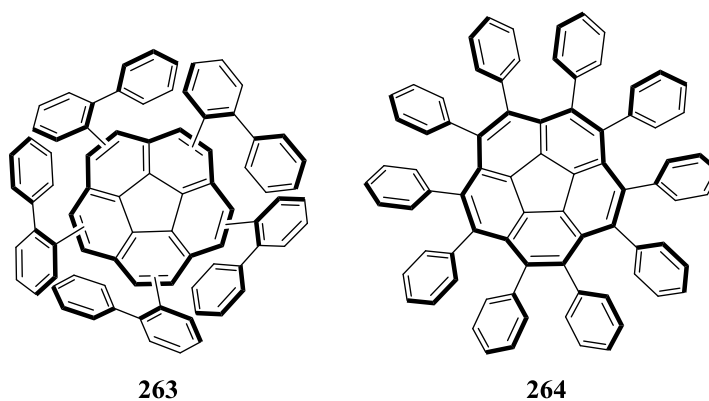
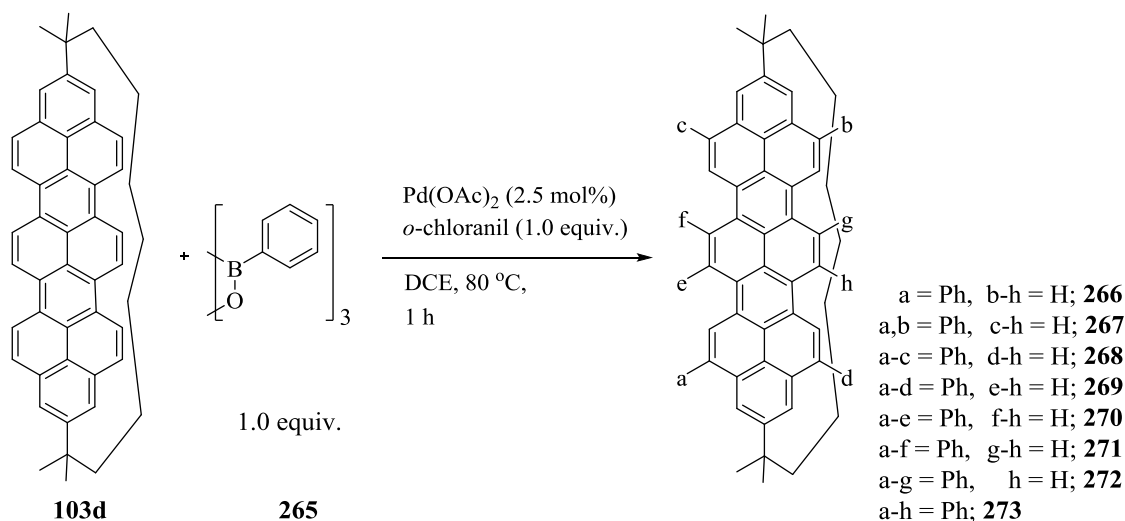


**Figure 6.01** penta-(*o*-biphenyl)corannulene (**263**) and deca-(*p*-*t*-butylphenyl)corannulene (**264**).

### 6.2.3.1 Attempted coupling chemistry by C-H activation of **103d**

[9](2,11)Teropyrenophane **103d** was first treated with 1.0 equiv. of phenylboroxine trimer **265**. Each phenylboroxine molecule can supply three phenyl units, so the 1.0 equiv. of **265** was equal to 3.0 equiv. of phenyl units. After 1 h, the starting material was completely consumed and MALDI-TOF MS analysis of the crude reaction mixture indicated that products containing two (**267**), three (**268**) and four (**269**) phenyl units had formed in a *ca.* 0.3:0.5:0.2 ratio (Scheme 6.05). This is consistent with almost complete uptake of the phenyl units from the boroxine trimer **265**. In comparison, the reaction of pyrene (**20**) with boroxine **265** was incomplete after 2 h.<sup>3</sup> The observation of a faster reaction may indicate that the bent teropyrene system is more reactive than pyrene, but this may also be due to the use of a less hindered aryl group in the boroxine. With just MALDI-TOF MS analysis, it was not possible to determine which positions of

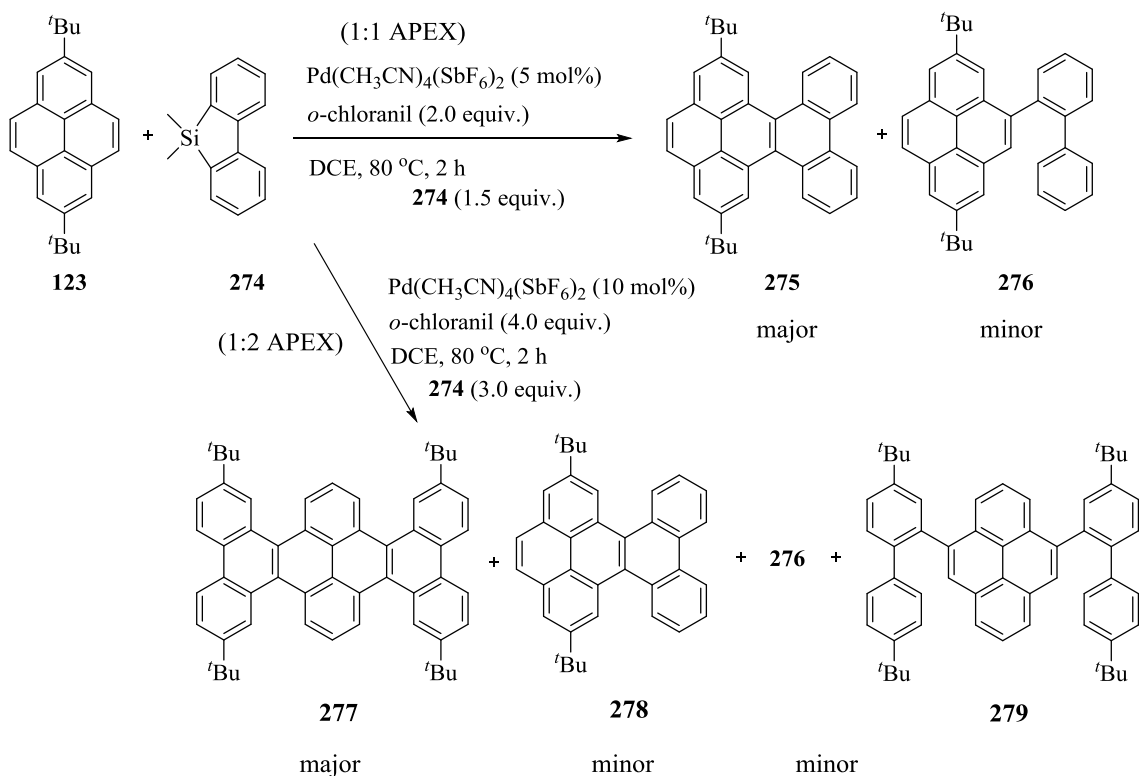


**Scheme 6.05** Direct C-H arylation of [9](2,11)teropyrenophane **103d**. The regio-chemistry of the products **266-273** was assigned based the bromination reaction and is purely tentative. Each of these compounds could be a mix of regio-isomers.

the teropyrene system had been arylated or whether there was any regioselectivity at all in the arylation reaction, as there was for bromination (Chapter 5). Similar to the bromination of **103d** with 3.0 equiv. of Br<sub>2</sub>, which gave a mixture with the tribromide **227** as the major component (75%), the arylation reaction gave a product mixture in which triarylated product(s) was(were) the major component(s) (50%). In addition to being slower than bromination, it would seem that each successive arylation has less of a detrimental effect on the rate of the subsequent reaction than bromination. Upon moving to 1.4 equiv. of boraxine trimer **265** (4.2 equiv. of phenyl units), products containing three (**268**), four (**269**), five (**270**) and six (**271**) were observed in a *ca.* 0.2:0.5:0.1:trace ratio. With 5.0 equiv. of phenylboraxine trimer **265**, (15 equivalent of phenyl units) a *ca.* trace:0.40:0.50:0.08 mixture of products containing four (**269**), five (**270**), six (**271**) and seven (**272**) phenyl units were observed (MALDI-TOF MS analysis). Again, it appears as though each successive arylation leads to a reduction in the rate of the subsequent reaction and, reminiscent of the bromination of **103d**, the maximum number of substituents that can be easily introduced to the [9](2,11)teropyrenophane system is seven. Using AgOTf as an additive resulted in the formation of no tlc-mobile products. Even though, the starting material was consumed in 30 min no significant product spots were seen on the tlc plate. Replacing *o*-chloranil with *p*-chloranil, *p*-benzoquinone, 9,10-phenanthrenequinone, 2,5-di-*t*-butyl-1,4-benzoquinone or 3,5-di-*t*-butyl-1,2-benzoquinone significantly reduced the reactivity and starting material was mainly recovered in all the cases.

#### 6.2.4 One-shot *K*-region-selective annulative $\pi$ -extension (APEX) reaction

The oligoarylene products obtained using the two previously-described methods (bromination followed by Suzuki-Miyaura reaction, and direct arylation) require an additional dehydrogenation step in order to achieve much larger polyfused aromatic systems. An example of this cyclodehydrogenation is the reaction of 4-(2-biphenyl)pyrene (**261**) with FeCl<sub>3</sub>, which resulted in the formation fused product **262** (Scheme 6.04).<sup>3</sup> The main problems with these two-to-three-step approaches for extending PAH frameworks are that (1) bromination of an arene may be difficult to achieve regioselectively, (2) bromination often leads to a decrease in solubility and (3) the intramolecular cyclodehydrogenation step typically has low functional group compatibility and can cause skeletal rearrangement.<sup>5</sup> The Itami group recently reported the development of a one-shot, *K*-region-selective annulative  $\pi$ -extension (APEX) reaction,<sup>6</sup> which enables direct the conversion of a *K*-region-containing PAH into a larger one. For example, 2,7-di-*t*-butylpyrene (**123**) was treated with dimethyldibenzosilol<sup>7</sup> (**274**) in the presence of Pd(CH<sub>3</sub>CN)<sub>4</sub>(SbF<sub>6</sub>)<sub>2</sub> and *o*-chloranil at 80 °C for 2 h in DCE to afford annulated product in one shot (Scheme 6.06). The outcome of the reaction depends on the ratio of **123** and **274**. When a 1:1 ratio of **123**:**274** was employed, the main product is mono-fused system **275** (1:1 APEX reaction). On the other hand, with a 1:2 ratio of **123**:**274**, di-fused product **277** (1:2 APEX reaction) was obtained as the major product. Minor products were the arylated, but non-cyclodehydrogenated compounds **276** and **279**. The overall reaction results in the annulation of three new fused rings (a phenanthrene unit) per equivalent of silyl reagent that is used.



**Scheme 6.06** 1:1 APEX and 1:2 APEX reactions.

The APEX reaction is still at a relatively early stage of development and has so far been tested only on planar systems such as pyrene (**20**). It has yet to be applied on curved aromatic systems, especially segments of CNTs that could be grown using APEX methodology. As such, it was of considerable interest to apply the APEX methodology to teropyrenophanes **103b-e**, which feature severely distorted teropyrene systems and contains six *K*-regions (two central and four flanking) as potential reaction sites. As with the arylation reaction discussed above, the immediate questions were whether the APEX reaction would be successful on the *K*-regions of **103b-e** and, if so, whether there would be any selectivity for one type of *K*-region over the other (central *vs* flanking *K*-regions) and how many  $\pi$  extensions could be achieved (1:4 APEX for the flanking *K*-regions *vs*

1:2 APEX for the central *K*-regions). The teropyrene system contains 36 carbon atoms and each APEX reaction adds three rings and 12 carbon atoms, so there was great potential for very rapidly growing the PAH.

#### 6.2.4.1 1:4 APEX reaction of teropyrenophane **103d**

Again, owing to its abundance, [9](2,11)teropyrenophane **103d**<sup>§§</sup> was used for exploration of the APEX methodology. Initially, **103d** was subjected to the originally reported APEX reaction conditions, *i.e.* silyl reagent **274** (6.0 equiv.), *o*-chloranil (9.6 equiv.), Pd[(MeCN)<sub>4</sub>(BF<sub>4</sub>)<sub>2</sub>] (20 mol%) in DCE at 80 °C for 2 h. Tlc analysis revealed that starting material was completely consumed and that a streak of faint new spots appeared, (*R*<sub>f</sub> = 0.45-0.12; 40% CHCl<sub>3</sub> / hexanes), within which two spots were most prominent (Table 6.02, Entry 1). It was subsequently established that these two spots corresponded to hexa- and hepta-fused systems of unknown structures, but the very messy TLC plate was already an indication of an unsatisfactory result. Filtration of the reaction mixture resulted in the isolation of a small quantity of black insoluble material. Heating the reaction at 80 °C for 1 h also resulted in the formation of black insoluble material, although the starting material was not fully consumed (Table 6.02, Entry 2). Upon reducing the amount of silyl reagent **274** to 4.0 equiv. and heating the reaction for 1.5 h, several new product spots were observed by TLC, three of which were isolated using preparative TLC.<sup>\*\*\*</sup> MALDI-TOF MS<sup>†††</sup> analysis showed signals at *m/z* = 1382, 1526 and

---

<sup>§§</sup> This work was conducted at Nagoya University, Japan in the laboratory of Prof. Itami group. All reactions were performed on a 3-5 mg scale unless otherwise stated.

<sup>\*\*\*</sup> Preparative TLC was used to separate reaction products.



1680, respectively, which correspond to a penta-fused product, a hexa-fused product with three extra dehydrogenations ( $-6\text{H}$ ) and a hepta-fused product with one extra dehydrogenation ( $-2\text{H}$ ) (Table 6.02, Entry 3). It was surprising to see evidence of a hepta-substitution product, as there are only six *K*-regions available in the teropyrene system. At the same time, the examination of molecular models very clearly suggested that if the first four  $\pi$  extensions (phenanthrannulations) occur at the four flanking *K*-regions, then the central *K*-regions are too sterically crowded to accommodate annulations at the central *K*-regions. The converse is also true. Wherever the first  $\pi$  extensions took place, it appeared as though subsequent  $\pi$  extensions must have taken place on the non-*K*-regions of the newly-extended  $\pi$ -system. In order to prevent such overreaction (the formation of penta- and more highly substituted products), the proportion of the silyl reagent was further reduced to 3.0 equiv. (Table 6.02, Entry 4). This resulted in the formation of a di-fused product ( $m/z = 930$ , one possible structure is **281**), along with the starting material **103d** ( $m/z = 630$ ). In addition, some products resulting from reaction of **103d** with 2-4 molecules of silyl reagent **274** were isolated, but that were one or two cyclodehydrogenations short of complete  $\pi$  extension:  $m/z = 930$  (one possible structure is **281**),  $m/z = 1082$  (one possible structure is **284**),  $m/z = 1086$  (one possible structure is **286**) and  $m/z = 1234$  (one possible structure is **289**) (Figure 6.02).

Clearly, 3.0 equiv. of silyl reagent **274** was not sufficient (for tetra- $\pi$  extension), so the number of equiv. was raised to 4.0. At the same time, the temperature of the reaction was reduced to 60 °C in an attempt to disfavour overreaction. Reduction of

---

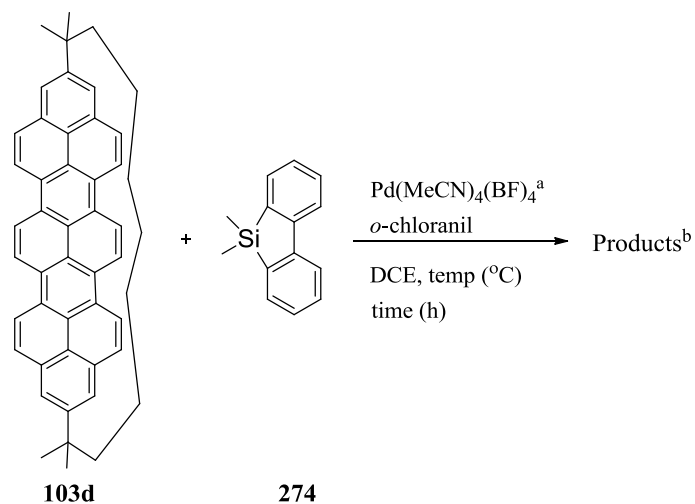
<sup>†††</sup> Purified products or crude reaction mixtures were analysed by MALDI-TOF MS unless otherwise stated.

temperature has no significant effect on the reaction time and the starting material was completed within 1.5 h and it gave rise mainly to di- and tri-reacted products with incomplete  $\pi$  extension (Table 6.02, Entry 5). When the temperature was reduced to 40 °C, the reaction was incomplete even after 6 h. However, masses corresponding to tetra-reacted products ( $m/z = 1232, 1238$ ) were observed (Table 6.02, Entry 6). The observation of signals corresponding to tetra-reacted compounds was very encouraging. It also provided some indication that a 1:4 APEX product arising from selective reaction at the flanking *K*-regions was more likely to be within reach than a 1:2 APEX product arising from selective reaction at the central *K*-regions. Hence, subsequent work was aimed at finding conditions that would maximize the signal for required mass ( $m/z = 1230$ ) for the tetrafused system **287**.

Up to this point, all the products were characterized after their partial purification *via* preparative tlc. It was quite laborious to purify each reaction, which may have led to the loss of some valuable information. This is because some amount of product mixture always remained at the baseline during the preparative tlc. Therefore, it was decided to quickly pass the reaction mixture through a plug of Celite and analyse the obtained crude product mixture by MALDI-TOF MS.

The proportion of the oxidant was then varied. Increasing the number of equiv. of *o*-chloranil from 9.6 to 12.0 reduced the reactivity of the system, giving just mono- and di-reacted products (Table 6.02, Entry 7). Upon reducing the number of equiv. to 8.0, the tlc spot corresponding to tetra-reacted products returned to the intensity it showed when 9.6 equiv. were used (Table 6.02, Entry 8). At the same

**Table 6.02** Optimization of the 1:4 APEX reaction conditions.



entry	temp (°C)	time (h)	silyl reagent (equiv.)	<i>o</i> -chloranil (equiv.)	products, (m/z)
1	80	2.0	6.0	9.6	black insoluble material
2	80	1.0	6.0	9.6	black insoluble material + SM
3	80	1.5	4.0	9.6	1526, 1680
4	80	1.5	3.0	9.6	630, 930, 934, 1082, 1086, 1234
5	60	1.5	4.0	9.6	932, 934, 1084
6	40	6.0	4.0	9.6	1232, 1238 (mainly)
7	40	6.0	4.0	12.0	780, 934,
8	40	6.0	4.0	8.0	780, 934, 1084, 1232
9	40	6.0	4.0	6.0	780, 934, 1086, 1232

<sup>a</sup>20 mol% catalyst loading was used

<sup>b</sup>See Figure 6.01 for few of the observed products

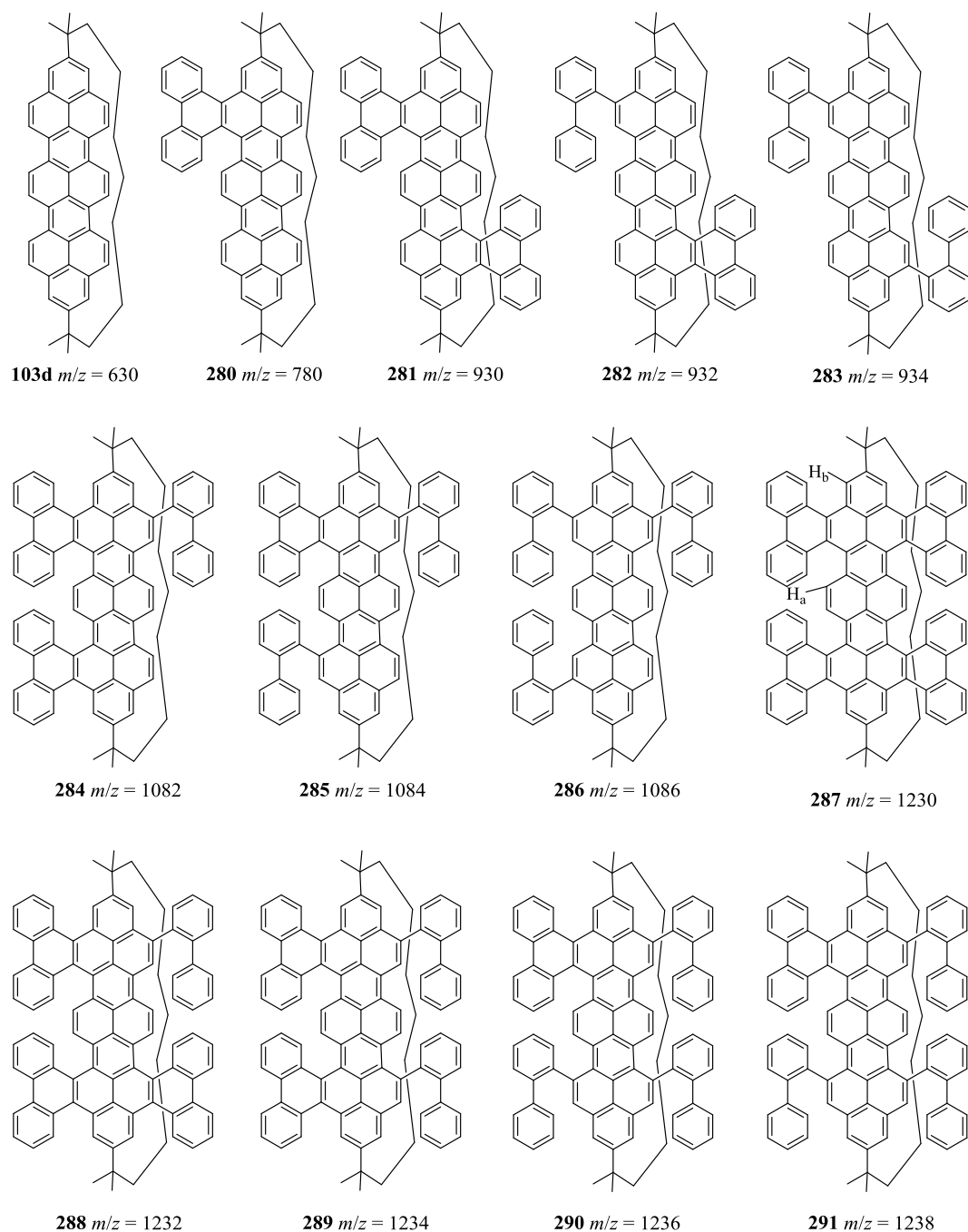


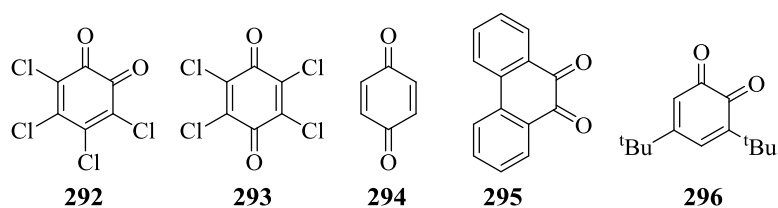
**Figure 6.02** A few possible products of the 1:4 APEX reaction of **103d** with **274**.

time, the MS signal with  $m/z = 1232$  became dominant. Further reducing the number of equiv. to 6.0 resulted in a decrease in intensity of the tlc spot and MS signal of interest

(Table 6.02, Entry 9). Therefore, 8.0-9.6 equiv. of *o*-chloranil appeared to be the optimal range for the oxidant.

The reaction temperature was then fixed at 60 °C and *o*-chloranil was replaced with a series of other oxidizing agents, namely *p*-chloranil (**293**), *p*-benzoquinone (**294**), 9,10-phenanthrenequinone (**295**) and 3,5-di-*t*-butylbenzoquinone (**296**). No reactivity was observed with the first three of these oxidants, even after conducting the reaction for 6 h. Only slight decomposition of the starting material was observed (Table 6.03, Entries 2-4). With 3,5-di-*t*-butylbenzoquinone (**296**), a little progress was observed, giving fused mono-, di- and tri-reacted products along with trace quantities of products with  $m/z$  = 1504, 1716 and 1809 (Table 6.03, Entry 5). The latter number suggests that octa-reaction had occurred. Whatever the case, *o*-chloranil was still easily the most effective of the oxidizing agents screened for the APEX reaction of **103d**.

**Table 6.03** Other oxidizing agents screened for the 1:4 APEX.



oxidizing agent	equiv.	time (h)	products
<b>292</b>	9.6	1.5	932, 934, 1084
<b>293</b>	9.6	6.0	SM + unidentified products
<b>294</b>	9.6	6.0	SM
<b>295</b>	9.6	6.0	SM
<b>296</b>	9.6	6.0	SM, 782, 934, 1564, 1716, 1868

Having had little success working with the silyl reagent and the oxidant, attention was turned to the Pd catalyst. In order to do this, the equiv. of silyl reagent and *o*-chloranil were fixed at 6.0 and 12.0, respectively, and the temperature at 80 °C (according to the original reaction conditions; Scheme 6.06). Accordingly, various palladium catalysts were screened and the results are shown in Table 6.04.

The use of a 1:2 ratio of Pd(CF<sub>3</sub>CO<sub>2</sub>)<sub>2</sub>/AgOTf resulted in the formation of small quantities of a compound with a mass corresponding to that of the desired 1:4 APEX product **287** ( $m/z = 1230$ ) along with what appeared to be a penta-fused product and another intermediate with  $m/z = 1642$  (Table 6.04, Entry 1). The use of Pd(CF<sub>3</sub>CO<sub>2</sub>)<sub>2</sub> alone gave only products with masses above  $m/z = 1376$  (Table 6.04, Entry 2). Therefore, it appeared as though AgOTf attenuates the catalytic activity of Pd(CF<sub>3</sub>CO<sub>2</sub>)<sub>2</sub> in some way. Meanwhile, various other Pd catalysts were also tested for this reaction. The combination of Pd(OAc)<sub>2</sub> / AgSbF<sub>6</sub> afforded none of the desired product, but rather a partially-fused species, such as **290** ( $m/z = 1236$ ). In the absence of the silver salt Pd(OAc)<sub>2</sub> behaved similarly to Pd(CF<sub>3</sub>CO<sub>2</sub>)<sub>2</sub> (Table 6.04, Entries 3,4). On the other hand, palladium halides (PdX<sub>2</sub>) showed poor catalytic activity in the APEX reaction (Table 6.04, Entries 5-7). In contrast, Pd(allyl)Cl showed over-reactivity (Table 6.04, Entry 8). Reactions using catalysts Pd[(*o*-tol)<sub>3</sub>P]<sub>2</sub> and Pd[(phen)<sub>2</sub>(PF)<sub>6</sub>]<sub>2</sub> showed little or no progress after heating for 12 h (Table 6.04, Entries 9,10).

Although Pd(OAc)<sub>2</sub> and Pd(allyl)Cl showed some promise as catalysts for the APEX reaction, it was still only Pd(CF<sub>3</sub>CO<sub>2</sub>)<sub>2</sub> that resulted in the formation of observable

quantities of a compound with the mass of the desired product ( $m/z = 1230$ ). Consequently, further work was concentrated on this particular palladium species. From Table 6.04, Entry 1, it can be seen that products arising from five or more reactions are forming along with **287**. In order to avoid this over-reactivity, the reaction time was reduced to 50 min, but still the product was formed in small quantities (tlc analysis) (Table 6.04, Entry 11). Reducing the time of the reaction to 20 min resulted in incomplete reaction: **103d** and

**Table 6.04** Optimization of the 1:4 APEX reaction conditions.

<p style="text-align: center;"> <b>274</b> (6.0 equiv.)  catalyst (20 mol%)  <i>o</i>-chloranil (12.0 equiv.)  <b>103d</b> <math>\xrightarrow{\text{DCE, 80 } ^\circ\text{C, time (h)}}</math> Products<sup>a</sup> </p>			
entry	time (h)	catalyst	products
1	1.5	Pd(TFA) <sub>2</sub> , AgOTf <sup>b</sup>	<b>1230</b> , 1380, 1642
2	1.5	Pd(TFA) <sub>2</sub>	1376, 1528, 1588, 1774
3	1.5	Pd(OAc) <sub>2</sub> , AgSbF <sub>6</sub> <sup>b</sup>	1084, 1236, 1422, 1610
4	50 min	Pd(OAc) <sub>2</sub>	1376, 1528, 1588, 1774
5	12.0	PdCl <sub>2</sub>	630 (major), 1080 (minor)
6	12.0	PdBr <sub>2</sub>	1034, 1079
7	12.0	PdI <sub>2</sub>	630 (major), 1036 (minor)
8	50 min	Pd(allyl)Cl	1378, 1528, 1588
9	12.0	Pd[( <i>o</i> -tol) <sub>3</sub> P] <sub>2</sub>	630
10	12.0	Pd[(phen) <sub>2</sub> (PF) <sub>6</sub> ] <sub>2</sub>	630, 912
11	50 min	Pd(TFA) <sub>2</sub> , AgOTf <sup>b</sup>	<b>1230</b> , 1376, 1530, 1588
12	20 min	Pd(TFA) <sub>2</sub> , AgOTf <sup>b</sup>	630, 780, 930

<sup>a</sup>See Figure 6.01 for the observed products; <sup>b</sup>40 mol%

mono-fused product were present in nearly equal quantities in the reaction mixture, while the di-fused system was just starting to grow in (Table 6.04, Entry 12). It thus seemed that a reaction time between 20 and 50 minutes would be best for the formation of the desired 1:4 APEX product.

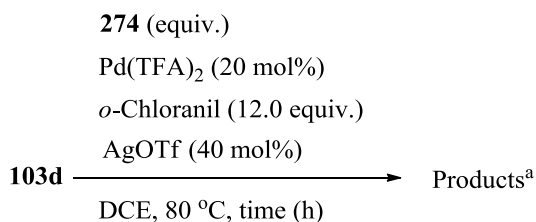
To determine how the product distribution changed with time, a reaction using the conditions from Table 6.04, Entry 12 was monitored by MALTI-TOF MS at regular intervals of 10 minutes. Another reaction, which differed only in the number of equiv. of silyl reagent **274** (4.0 instead of 6.0), was performed simultaneously and monitored in the same way and the results are presented in Table 6.05. For clarity, only the peaks corresponding to the masses of mono- ( $m/z = 780$ ), di- ( $m/z = 930$ ), tri- ( $m/z = 1080$ ) and tetra- $\pi$ -extended ( $m/z = 1230$ ) are included in Table 6.05, even though a few other products were always present in significant amounts.

After the addition of the reagents had been completed and before the reaction mixture was heated to 80 °C, only the starting material was present in both reactions. After 10 minutes, the reaction with 6.0 equiv. of silyl reagent **274** had progressed to the point where the ratio of starting material **103d** to mono- $\pi$ -extended product **280** to di- $\pi$ -extended product(s) **281** was 1.00:0.91:0.23 (Table 6.05, Entry 1). After 20 minutes, the ratio had changed in favour of di- $\pi$ -extended product(s) **281** to 0.95:1.00:0.85 (Table 6.05, Entry 2). The signal corresponding to the tri- $\pi$ -extended product **283** was first observed after 30 minutes (Table 6.05, Entry 3). The starting material was completely consumed after 40 minutes and, at the same time, the signal for the tetra- $\pi$ -extended product **287** had grown rapidly to become the most prominent one (Table 6.05, Entry 5).



After 50 minutes, the ratio of **280:281:283:287** had not changed significantly, but the relative intensities of other peaks present had increased and new peaks with higher mass ( $m/z > 1230$ ) had appeared. Clearly, the bent teropyrene system is more reactive than the planar pyrene system in the APEX reaction. Moreover, the reaction does not stop at **287**,

**Table 6.05** Optimization of 1:4 APEX reaction.



entry	time (min)	<b>274</b> (equiv.)	key MALDI-MS signals ( $m/z$ )	ratio (MALDI TOF)			
				<b>103d</b>	mono	di	tri
1	0	6.0	630	1.00			
2	10	6.0	630, 780, 930	1.00	0.91	0.23	
3	20	6.0	630, 780, 930	0.95	1.00	0.85	
4	30	6.0	630, 780, 930, 1080	0.50	0.62	1.00	0.79
<b>5</b>	<b>40</b>	<b>6.0</b>	<b>780, 930, 1080, 1230</b>		<b>0.11</b>	<b>0.21</b>	<b>0.30</b>
<b>6</b>	<b>50</b>	<b>6.0</b>	<b>780, 930, 1080, 1230</b>		<b>0.09</b>	<b>0.18</b>	<b>0.35</b>
7	0	4.0	630	1.00			
8	10	4.0	630, 780, 930	0.62	1.00	0.25	
9	20	4.0	630, 780, 930	1.00	1.00	1.00	
10	30	4.0	630, 780, 930, 1080	0.15	0.26	1.00	0.37
<b>11</b>	<b>40</b>	<b>4.0</b>	<b>780, 930, 1080, 1230</b>		<b>0.20</b>	<b>0.20</b>	<b>0.23</b>
<b>12</b>	<b>50</b>	<b>4.0</b>	<b>780, 930, 1080, 1230</b>		<b>0.23</b>	<b>0.25</b>	<b>0.20</b>

<sup>a</sup>See Figure 6.01 for the observed products

which explains why it was not observed when longer reaction times were employed. Indeed, **287** does not appear to have significantly different reactivity than any of the compounds leading up to it.

The parallel reaction involving 4.0 equiv. of silyl reagent **274** proceeded in a similar fashion, but with slightly different product ratios. As before, the tetra- $\pi$ -extended product **287** appeared between 30 and 40 minutes and the intensity of the MS signal and tlc spot that correspond to it dropped off significantly at 50 minutes. Therefore, it was concluded that it was optimal to stop the reaction between 40 and 45 minutes. Performing a reaction under these conditions allow tetra- $\pi$ -extended product **287** to be isolated by preparative tlc in 20% yield (3.0 mg of **103d**). Increasing the scale of the reaction to 20 mg still afforded **287** in 15% yield. The rather low yield should be weighed against what is accomplished in going from **103d** to **287**. Eight new bonds are formed and the PAH grows in size from ten rings and 36 carbon atoms to 22 rings and 84 carbon atoms. Another key point is that the APEX reaction was successfully applied to a nonplanar PAH, which means that it holds promise for the synthesis of even larger curved PAHs.

The  $^1\text{H}$  NMR spectrum of **287** contains singlets at  $\delta$  8.30 and 8.20 due to  $\text{H}_a$  and  $\text{H}_b$  (Figure 6.02). It has not yet been determined which signal corresponds to which proton, but it is clear that  $\text{H}_a$  resonates at significantly higher field ( $\Delta\delta = -0.47$  or  $-0.57$  ppm) than the corresponding proton in **103d** ( $\delta$  8.77 ppm), whereas  $\text{H}_b$  resonates at significantly lower field ( $\Delta\delta = 0.70$  or  $0.80$  ppm) than the corresponding proton in **103d** ( $\delta$  7.50). The introduction of the four new phenanthrene units means that  $\text{H}_a$  is situated at

the end of a local [5]helicene (fjord region). As such, H<sub>a</sub> would be expected to be in the shielding zone of the benzene ring at the opposite end of the [5]helicene system. On the other hand, H<sub>b</sub> is on the end ring of a local [4]helicene (cove region), which means that there will be steric interactions between H<sub>b</sub> and a proton on the benzene ring at the other end of the [4]helicene system. Steric interactions are known to cause deshielding.<sup>refs</sup>

#### 6.2.4.2 Structural characteristics of the cyclophane **287**

Cyclophane **287** is very interesting for several reasons. First, the PAH (tetraphenanthro[9,10-*e*;9,10-*i*;9,10-*t*;9,10-*b'*]teropyrene) contains 84 carbon atoms, which makes it largest PAH to have ever been incorporated into a cyclophane. The previous record-holder was hexabenz[*bc,ef,hi,kl,no,qr*]coronene (HBC), which has exactly half the number of carbon atoms (42).<sup>8</sup> The structure of **287** was calculated at the DFT calculations (Figure 6.03).<sup>†††</sup> The fusion of four phenanthrene systems to the teropyrene system resulted in the generation of four [5]helicene systems, which all spiral away from the cavity of the cyclophane. There are also four [4]helicene system, which are less helical, but also all spiral away from the cavity of the cyclophane. There is approximate C<sub>2v</sub> symmetry in the PAH and the calculated bend angle ( $\theta_{\text{tot}} = 169.4^\circ$ ) is close to that of **103d** ( $\theta_{\text{tot}} = 156.6^\circ$ ). The PAH formally maps onto the surface of armchair SWCNTs, but the structural resemblance to a side wall segment is not close due to the twist in the helicene units. It is striking that **287** is readily soluble in common organic solvents such as dichloromethane, chloroform, THF, ethyl acetate and

---

<sup>†††</sup> Calculations were performed by Dr. Hideto Ito of the Itami Group, University of Nagoya, Japan.

acetonitrile. The nonplanarity that is enforced by the 9-membered bridge and the helicene units is presumably prevents effective packing in the solid state.

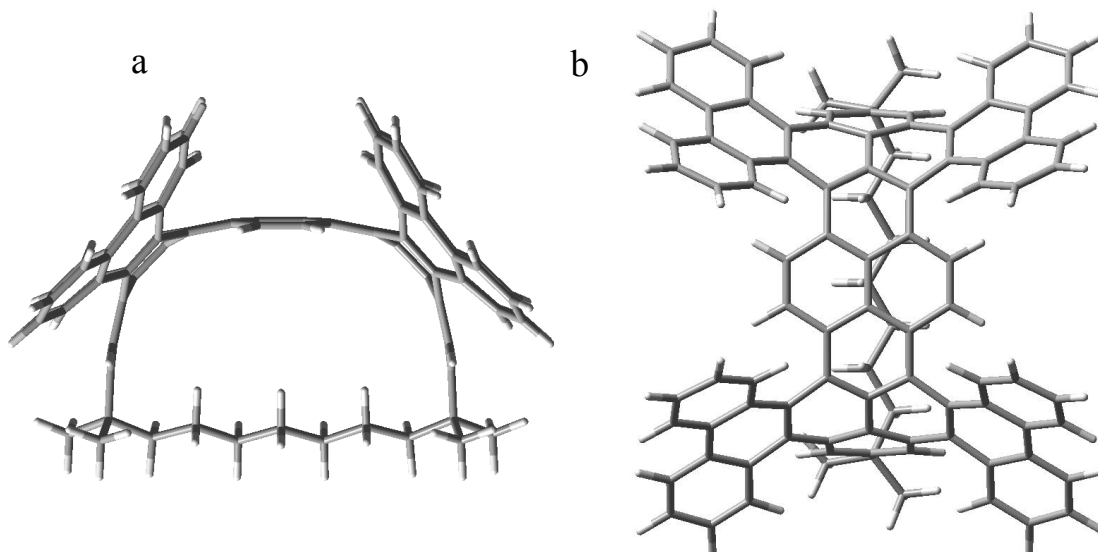


**Figure 6.03** Calculated structure of cyclophane **287**. a) side view and b) top view

#### 6.2.4.3 Absorption and emission properties of cyclophane **287**

The absorption spectrum of cyclophane **287** was measured in acetonitrile solution (Figure 6.04). Like **103d**, the spectrum of **287** contains three band envelopes that become less intense with decreasing energy. However, they are now broad and almost structureless. The longest wavelength absorption maximum is observed at  $\lambda_{\text{max}} = 510$  nm, which is only 14 nm red-shifted from that of teropyrenophane **103d** ( $\lambda_{\text{max}} = 496$  nm).

The emission spectrum of cyclophane **287** (acetonitrile,  $\lambda_{\text{exc}} = 350$  nm) is also very broad and lacks structure. There appear to be three overlapping bands with  $\lambda_{\text{max}}$  566, 529 and 468 nm. Interestingly, the highest energy band ( $\lambda_{\text{max}} = 468$  nm) is clearly

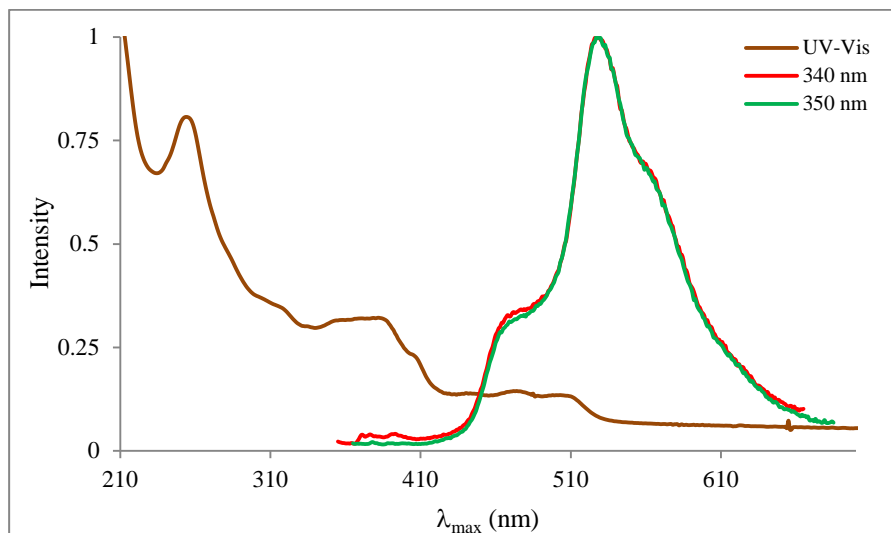


**Figure 6.04** Normalized absorption and emission spectra ( $\lambda_{\text{ex}} = 350 \text{ nm}$ ) of cyclophane **287**; recorded in ( $6.5 \times 10^{-5} \text{ M}$ ) acetonitrile solutions.

underneath the absorption spectrum, which immediately suggested that Kasha's rule is also being violated in this system. Upon excitation at 340 nm, some additional weak bands in the region of 370-410 nm also appeared, which may be the beginnings of some very interesting and unusual photophysical behaviour. More detailed investigation of **287** is currently underway in collaboration with the Thompson group at Memorial University.

### 6.2.5 Bay region Diels-Alder chemistry of [9](2,11)teropyrenophane **287**

In addition to six *K*-regions, teropyrene has four bay regions (Scheme 6.07). It has long been known that certain bay regions can act as dienophiles in the Diels-Alder reaction.<sup>9</sup> Recently, the Scott group demonstrated that benzannulation of bay regions could be achieved using Diels-Alder reactions with nitroethene (an acetylene equivalent) and even acetylene itself, followed by *in situ* dehydrogenation. The impetus behind developing this chemistry was to eventually apply it to bay region-containing SWCNT

segments (e.g. Vögtle belts **171**, Figure 6.05) to grow single-chirality SWCNTs.

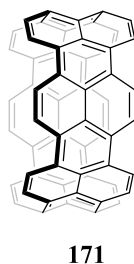
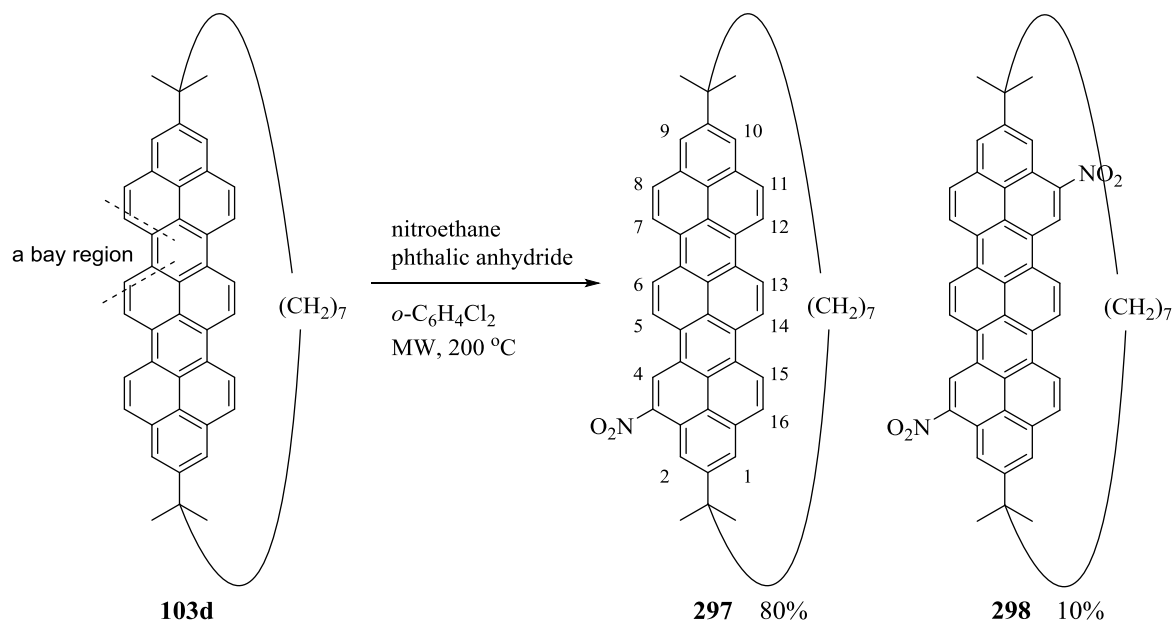


**Figure 6.05** A Vögtle belt **171**.

To date, there has been no example of a Diels-Alder-based benzannulation of a bay region of a nonplanar PAH. Thus, the teropyrene unit in the  $[n](2,11)$ teropyrenophanes, which structurally resembles about half of a Vögtle belt, presented itself as an interesting system on which to investigate the bay region Diels-Alder chemistry. Accordingly,  $[9](2,11)$ teropyrenophane **103d** (3 mg) was reacted with phthalic anhydride and nitroethanol (*in-situ* generation of nitroethylene)<sup>9a</sup> in *o*-dichlorobenzene under microwave irradiation at 200 °C (Scheme 6.07). After 1 h, the solution had become dark purple in colour and tlc analysis showed a major new spot ( $R_f = 0.28$ ; 10% ethyl acetate / hexanes) along with a minor spot ( $R_f = 0.36$ ). Column chromatography and afforded two compounds, HRMS analysis of which indicated that they were mono- (80%) and dinitro-teropyrenophanes (8%), respectively. The aromatic region of the  $^1\text{H}$  NMR spectrum of the mononitroteropyrenophane contained two narrow doublets ( $J = 1.7$  Hz) at  $\delta$  8.30 and 7.62, ten *K*-region doublets ( $J = 9.5$ -10.0 Hz) in the range of  $\delta$  8.97–7.80, a 1H singlet at  $\delta$  9.64 and a 2H singlet at  $\delta$  7.57, which is like due to two overlapping narrow doublets. This data fits very well with nitration at the 4 position of the teropyrene system, *i.e.* **297**,

which is consistent with the bromination chemistry of **103d** (Chapter 5). Not enough of the dinitroteropyrenophane was obtained to obtain a  $^1\text{H}$  NMR spectrum, so it was not possible to determine whether or not there was selectivity for the product arising from nitration of the 4 and 13 positions of the teropyrene system, *i.e.* **298** (*cf.* dibromide **213**, Chapter 5).

The failure of **103d** to undergo Diels-Alder reaction was not surprising. Clar analysis<sup>10</sup> of teropyrene leads to the prediction that the  $\pi$ -electronic structure in compound **103d** with four aromatic sextets (Scheme 6.06) will most accurately reflect its nature. As such, the bay regions have very little diene character and will be highly unreactive in the Diels-Alder reaction. Alternatively, Diels-Alder reaction (through a less favourable resonance structure) would result in the destruction of all but one of the aromatic sextets



**Scheme 6.07** Attempted Diels-Alder reaction on the bay regions.

in the teropyrene system. This means that the transition state of the Diels-Alder reaction would be very high in energy. Either way, the prospects for successful Diels-Alder-based benzannulation of **103d** are poor. On the other hand, the cyclophane **259** (the cyclodehydrogenation product **259** (Scheme 6.03) of tetra- $\pi$ -extended cyclophane **287**) does have diene character in the bay regions and would therefore be expected to be a much better candidate for Diels-Alder-based benzannulation.

### 6.2.6 Host guest chemistry of $[n](2,11)$ teropyrenophanes

Many of the larger cyclophanes have cavities and can participate in host-guest chemistry.<sup>11</sup> In this regard, the shape of the cavity and various weak interactions ( $\pi$ - $\pi$ , C-H $\cdots\pi$ , hydrogen bonding, *etc.*) between the cyclophane host and a guest molecule or ion can work together to afford very strong host-guest complexes. In the case of the  $[n](2,11)$ teropyrenophanes **103b-e**, the large curved  $\pi$ -surface and the reasonably large cavity would be expected to provide a suitable environment for certain small molecules. In the series, from **103b-e** the distance across the cavity (distance between the bridgehead carbon atoms) increases from 8.08 Å to 10.59 (Chapter 3) and hence it would be interesting to observe how the host-guest chemistry changes along the series.

Preliminary work in this area was conducted with **103b-d** as the host and 7,7,8,8-tetracyano-1,4-quinodimethane (TCNQ, **299**) as the guest. TCNQ was selected because it looked to be an appropriate size for the cavities of **103b-d** and because of its excellent electron accepting character. As such, host-guest charge transfer complexes **103b-d** were envisioned (Figure 6.06). A series of solutions of **299:103b-d** (2:1) in CDCl<sub>3</sub> and



DMSO- $d_6$  were prepared solutions and their  $^1\text{H}$  NMR spectra were recorded after 2 h (Figures 6.07 and 6.08). The colour of the  $\text{CDCl}_3$  solution of **103d** remained unchanged for several days, but that of **103c** had turned dark after about 2 h. On the other hand, the solution containing **103b** had turned dark in few minutes, which may be an indication that TCNQ forms increasingly strong complexes as the cavity of the teropyrenophane becomes smaller. The  $^1\text{H}$  NMR of **103d** was unchanged in the presence TCNQ (**299**),

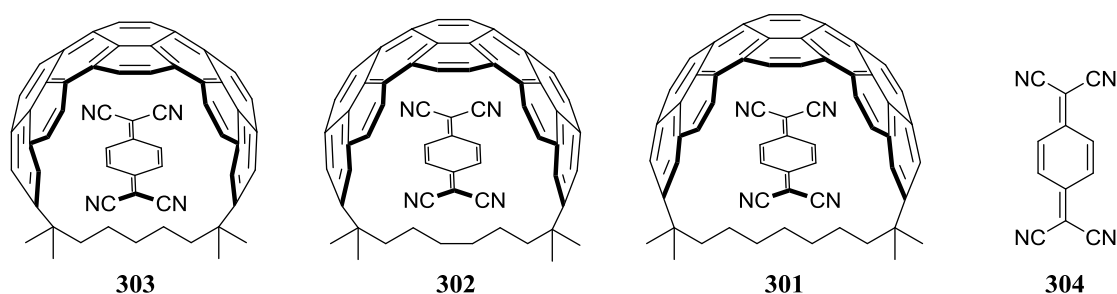


**Figure 6.06** Inclusion complexes of **103b-d** with TCNQ, **304**.

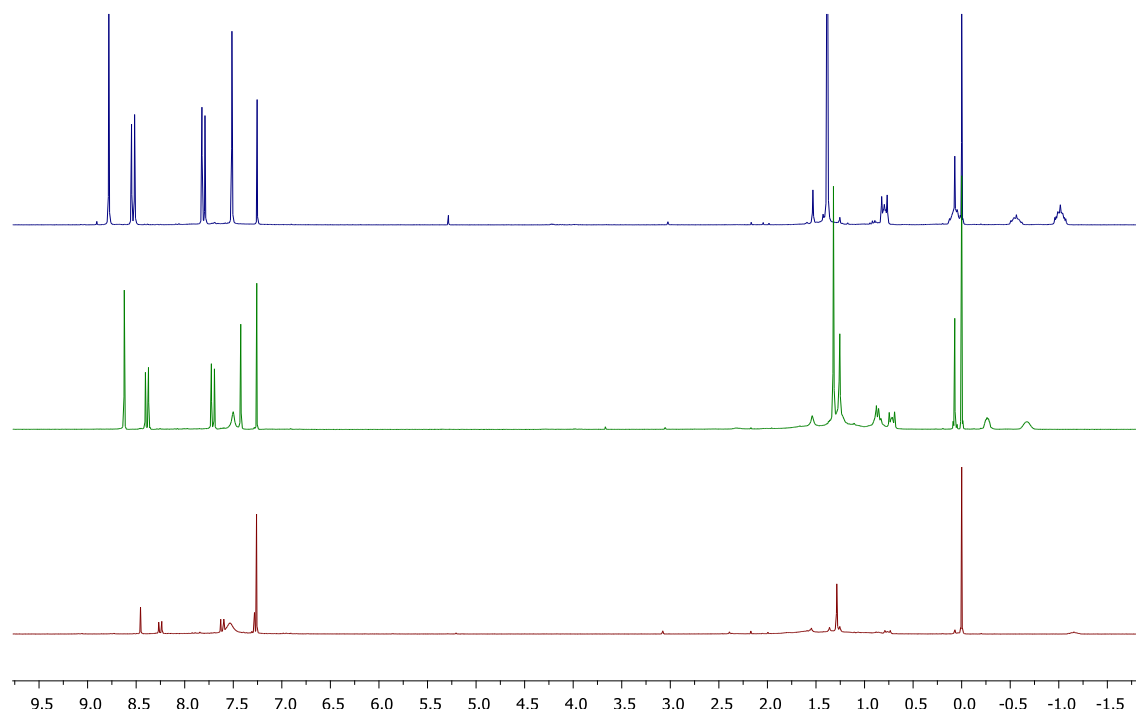


**Figure 6.07**  $^1\text{H}$  NMR spectra of 2:1 solutions of **304** : **103b-d** in  $\text{CDCl}_3$ .

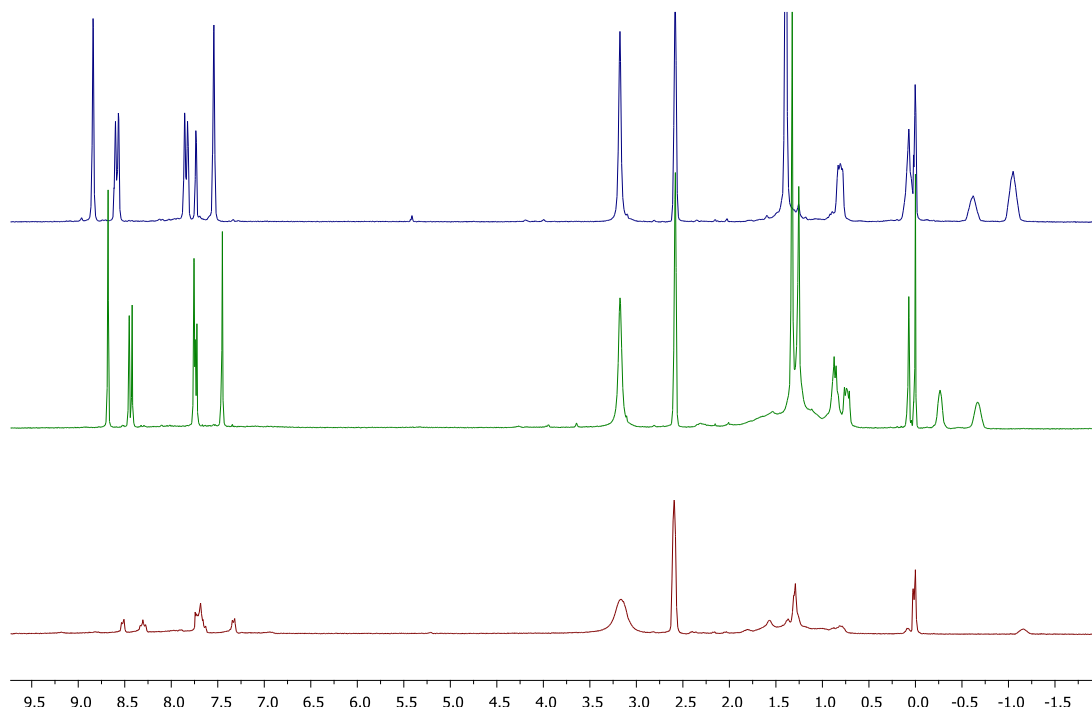


**Figure 6.08**  $^1\text{H}$  NMR spectra of 2:1 ratio of **304** : **103b-d** in  $\text{DMSO}-d_6$ .

those of **103c** and **103b** contained a new broad signal at  $\delta$  7.50 that correspond to TCNQ. This evidence merely is not sufficient to comment that TCNQ is forming inclusion complex with **103c** or **103b**. Unfortunately, none of the solutions yielded crystals as they slowly evaporated to dryness upon standing for several weeks.

The DMSO solution of **103d** and TCNQ eventually turned dark after several days. By the same token, the solution of **103c** took only 10-15 minutes to turn dark and that of **103b** turned dark almost instantaneously. Whatever process is responsible for the formation of the dark colour, *e.g.* host-guest charge transfer complex formation, it occurs more rapidly in  $\text{DMSO}-d_6$  (more polar) than it does  $\text{CDCl}_3$  (less polar). The  $^1\text{H}$  NMR spectrum of the dark solution of **299** and **103b** had broad peaks, which would not be inconsistent with a host-guest charge transfer complex. Of course, it would also be

consistent with a charge transfer complex in which the TCNQ is not inside the cyclophane cavity. Much more detailed studies would be required to clearly demonstrate the formation of host-guest charge transfer complexes. Work aimed in this direction is currently underway in collaboration with Prof. Brian Wagner, University of Prince Edward Island. As before, none of the solutions yielded crystals upon standing for several weeks.

## 6.5 Conclusions

Work directed toward using the bent aromatic system in the teropyrenophanes as starting points for the synthesis of larger bent PAHs were conducted using to three different strategies. In the first strategy, tetrabromoteropyrenophane **223** was subjected to a microwave-assisted Suzuki-Miyaura coupling reaction with various arylboronic acids to afford tetraarylated systems **253-258**. Both the tetraphenylteropyrenophane **252** and tetra-2-biphenyl analogue **256** were obtained in 33% yield. Further optimization of this work is currently under investigation. An attempted ten-fold cyclodehydrogenation reaction to afford cyclophane **259** was unsuccessful. In the second strategy, the parent teropyrenophane **103d** was subjected to direct C-H arylation using a Pd-mediated coupling reaction. Disappointingly, the excellent selectivity observed during the bromination reactions was not present. In the third strategy, teropyrenophane **103d** was subjected to a recently developed one-shot *K*-region-selective annulative  $\pi$ -extension (APEX) reaction. After a considerable amount of optimization, conditions were found under which **103d** underwent a four-fold APEX reaction to afford the tetra- $\pi$ -extended

system **287**. Cyclophane **287** contains 84 carbon atoms in its aromatic system, which makes it by far the largest PAH to have been incorporated into a cyclophane. The absorption and emission spectra of **287** suggest a violation of Kasha's rule, but this needs to be established rigorously through more detailed investigation.

The attempted microwave-assisted bay-region Diels-Alder chemistry of **103d** was unsuccessful. While the failure of the reaction was not surprising, the formation of nitrated products **297** and **298** was observed. The formation of host-guest charge transfer complexes of teropyrenophanes **103b-d** with TCNQ was also attempted. Colour changes became more rapid as the teropyrenophane became smaller and as the solvent became more polar. In the case of **103b** in DMSO-*d*<sub>6</sub>, wholesale broadening of the signals in the <sup>1</sup>H NMR spectrum was observed. No crystals were obtained, so no firm conclusions could be drawn about the formation of host-guest charge transfer complexes.

## 6.6 Experimental Section

### 4,9,13,18-Tetraphenyl[9](2,11)teropyrenophane **252**

Teropyrenophane **103d** (3.0 mg, 0.0032 mmol), phenylboronic acid (12.0 mg, 0.096 mmol) and K<sub>2</sub>CO<sub>3</sub> (5.3 mg, 0.038 mmol) were placed in a 10 mL CEM reaction vial and Aliquat<sup>®</sup>336 (1 drop) was added. Pd(PPh<sub>3</sub>)<sub>4</sub> (0.4 mg, 0.0003 mmol) was then added and toluene (1.0 mL), deionized water (0.5 mL) were subsequently added to the reaction mixture and the resulting mixture was heated in a CEM microwave reactor at 120 °C for 1 h. The reaction mixture was then quenched with deionized water (5 mL) and the layers

were separated. The aqueous layer was extracted with dichloromethane ( $2 \times 5$  mL) and the combined organic layers were washed with brine (10 mL). The solvent was removed under reduced pressure and the residue was purified using preparative tlc (20% ethyl acetate / hexanes) to afford the **252** (1.0 mg, 33%) as a dark reddish purple solid:  $R_f$  = 0.31 (20% ethyl acetate / hexanes);  $^1\text{H}$  NMR (300 MHz,  $\text{CDCl}_3$ )  $\delta$  8.98 (s, 4H), 8.70 (s, 4H), 7.94–7.87 (m, 8H), 8.98 (s, 4H), 7.65–7.45 (m, 16 H), 0.66–0.52 (m, 4H), 0.44–0.64 (br m, 4H), 0.98–0.17 (br m, 6H); LCMS (APCI positive)  $m/z$  (rel. int.) 938 (1), 937 (7), 936 (30), 935 ( $[\text{M}+\text{H}]^+$ , 100); HRMS (APPI) calculated for  $\text{C}_{73}\text{H}_{58}$  ( $[\text{M}]^+$ ) 935.4619, found 935.4622.

#### **4,9,13,18-Tetrakis-(2-biphenyl)[9](2,11)teropyrenophane 256**

Teropyrenophane **103d** (25.0 mg, 0.026 mmol), 2-biphenylboronic acid (154.0 mg, 0.780 mmol) and  $\text{K}_2\text{CO}_3$  (43.0 mg, 0.31 mmol) were placed in a 10 mL CEM reaction vial and Aliquat<sup>®</sup> 336 (6 drops) was added.  $\text{Pd}(\text{PPh}_3)_4$  (3.0 mg, 0.0026 mmol) was then added and toluene (1 mL), deionised water (0.5 mL) were subsequently added to the reaction mixture and the resulting mixture was heated in a CEM microwave reactor at 120 °C for 1 h. The reaction mixture was then quenched with deionised water (5 mL) and the layers were separated. The aqueous layer was extracted with dichloromethane ( $2 \times 5$  mL) and the combined organic layers were washed with brine (10 mL). The solvents was removed under reduced pressure and the residue was purified using preparative tlc (20% ethyl

acetate / hexanes) to afford the **256** (10.6 mg, 33%) as a dark reddish purple solid:  $R_f$  = 0.33 (20% ethyl acetate / hexanes);  $^1\text{H}$  NMR (300 MHz,  $\text{CDCl}_3$ )  $\delta$  9.07–6.08, numerous broad peaks,  $\delta$  1.25–(–1.86), numerous broad peaks;  $^{13}\text{C}$  NMR (75 MHz,  $\text{CDCl}_3$ )  $\delta$  142.5, 141.59 (br), 138.90 (br), 133.49, 132.34, 132.20, 131.90 (br), 131.51, 131.51, 130.58 (br), 129.19 (br), 128.53, 128.42, 128.17 (br), 127.43 (br), 126.35 (br), 125.90 (br), 123.40 (br), 122.38 (br), 47.29, 37.93, 30.36, 29.70, 24.22; LCMS (APCI positive)  $m/z$  (rel. int.) 1244 (4), 1243 (11), 1243 (6), 124 (41), 1242 (11), 1241 ( $[\text{M}+\text{H}]^+$ , 100); HRMS (APPI) calculated for  $\text{C}_{97}\text{H}_{74}$  ( $[\text{M}+\text{H}]^+$ ) 1239.5871, found 1239.5872.

**1,1,9,9-Tetramethyl-tetraphenanthro[9,10-*e*;9,10-*i*;9,10-*t*;9,10-*b'*][9](2,11)teropyrenophane **287****

Teropyrenophane **103d** (20.0 mg, 0.032 mmol), silyl reagent **274** (30 mg, 0.144 mmol), *o*-chloranil (47 mg, 0.192 mmol) were placed in a 10 mL CEM reaction vial.  $\text{Pd}(\text{TFA})_2$  (0.2 mg, 0.006 mmol) and  $\text{Ag}(\text{OTf})$  (0.3 mg, 0.0013 mmol) were quickly added to the reaction vial containing above mixture and the vial was sealed with a rubber septum. The reaction vessel was evacuated at 0.01 mmHg for 5 min and was filled with dry nitrogen gas and (2 times). Dry 1,2-dichloroethane (4 mL) was added under nitrogen atmosphere and the reaction mixture was heated at 80 °C for 40 min. The reaction mixture was then quenched with deionised water (5 mL) and the layers were separated. The aqueous layer was extracted with dichloromethane (3 × 5 mL) and the combined organic layers were washed with brine (15 mL). The solvent was removed under reduced pressure and the residue was subjected to column chromatography (8.0 × 3.0 cm; 7% ethyl acetate / hexanes) to afford compound **287** as a reddish brown solid (5.9 mg, 15%):  $R_f$  = 0.25 (10%

ethyl acetate); m.p. > 300 °C;  $^1\text{H}$  NMR (300 MHz,  $\text{CDCl}_3$ )  $\delta$  9.11–9.03 (m, 8H), 8.93–8.84 (m, 8H), 8.30 (s, 4H), 8.20 (s, 4H), 7.85–7.67 (m, 16H), 1.25 (s, 12 H), 0.78–0.70 (br m, 4H), 0.24–0.09 (br m, 4H), 0.32–0.61 (br m, 6H);  $^{13}\text{C}$  NMR (75 MHz,  $\text{CDCl}_3$ )  $\delta$  130.39, 130.10, 129.74, 129.11, 129.08, 128.81, 127.39, 127.16, 126.69, 126.40, 125.82, 125.67, 125.61, 125.20, 124.79, 124.60, 123.86, 123.39, 122.15, 122.04, 121.03, 44.54, 37.03, 30.86, 29.53, 27.87, 23.98; LCMS (APCI-positive)  $m/z$  (rel. int.) 1234 (4), 1233 (17), 1232 (41), 1232 (11), 1231 ( $[\text{M}+\text{H}]^+$ , 100), 1230 (95); APPI calculated for  $\text{C}_{97}\text{H}_{66}$  ( $[\text{M}+\text{H}]^+$ ) 1231.5245, found 1231.5188.

#### 4-Nitro-1,1,9,9-tetramethyl-[9](2,11)teropyrenophane **297**

Teropyrenophane **103d** (3.0 mg, 0.0047 mmol), nitroethanol (0.03 mL, 0.47 mmol) and phthalic anhydride (77 mg, 0.52 mmol) were placed in a 10 mL CEM reaction vial. *o*-Dichlorobenzene (2 mL) was added and the reaction mixture was heated in a CEM microwave reactor at 120 °C for 1 h. The reaction mixture was then quenched with deionized water (5 mL) and the layers were separated. The aqueous layer was extracted with dichloromethane (2  $\times$  5 mL) and the combined organic layers were washed with brine (10 mL). The solvent was removed under reduced pressure and the resulting residue was subjected to column chromatography (6.0  $\times$  3.0 cm; 7% ethyl acetate / hexanes) to afford compound **297** as a reddish brown solid (2.8 mg, 80%):  $R_f$  = 0.20 (30% ethyl acetate / hexanes);  $^1\text{H}$  NMR (300 MHz,  $\text{CDCl}_3$ )  $\delta$  9.64 (s, 1H), 8.93 (d,  $J$ =10.0 Hz, 1H), 8.93 (d,  $J$ =10.0 Hz, 1H), 8.92 (d,  $J$ =10.0 Hz, 1H), 8.85 (d,  $J$ =10.0 Hz, 1H), 8.79 (d,  $J$ =10.0 Hz, 1H), 8.59–8.51 (m, 3H), 8.30 (d,  $J$ =1.7 Hz, 1H), 7.89–7.82 (m, 3H), 7.62 (d,  $J$ =1.7 Hz, 1H), 7.57 (s, 2H), 1.76–1.47 (m, 4H), 1.42 (s, 3H), 1.40 (s, 3H), 1.39 (s, 6H), 0.40–0.08 (br m, 4H),

−0.41−(−0.66) (br m, 2H), −0.85−(−1.00) (br m, 2H), −1.00−(−1.20) (br m, 2H); LCMS (APCI-positive)  $m/z$  (rel. int.) 678 (1), 677 (14), 676 (53), 675 ( $[M+H]^+$ , 100); APPI calculated for  $C_{49}H_{41}NO_2$  ( $[M+H]^+$ ) 672.3217, found 672.3201.

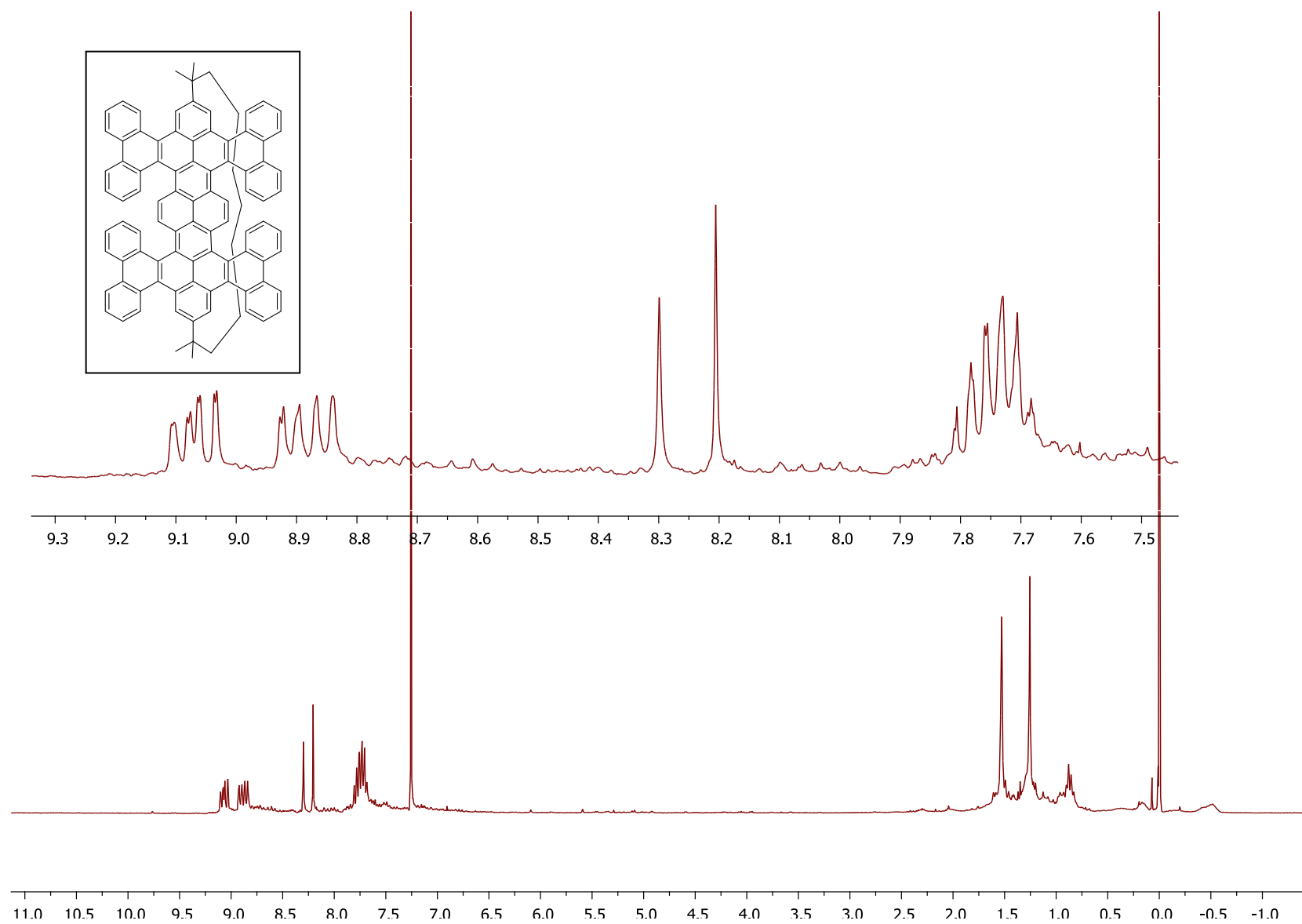
## 6.7 References

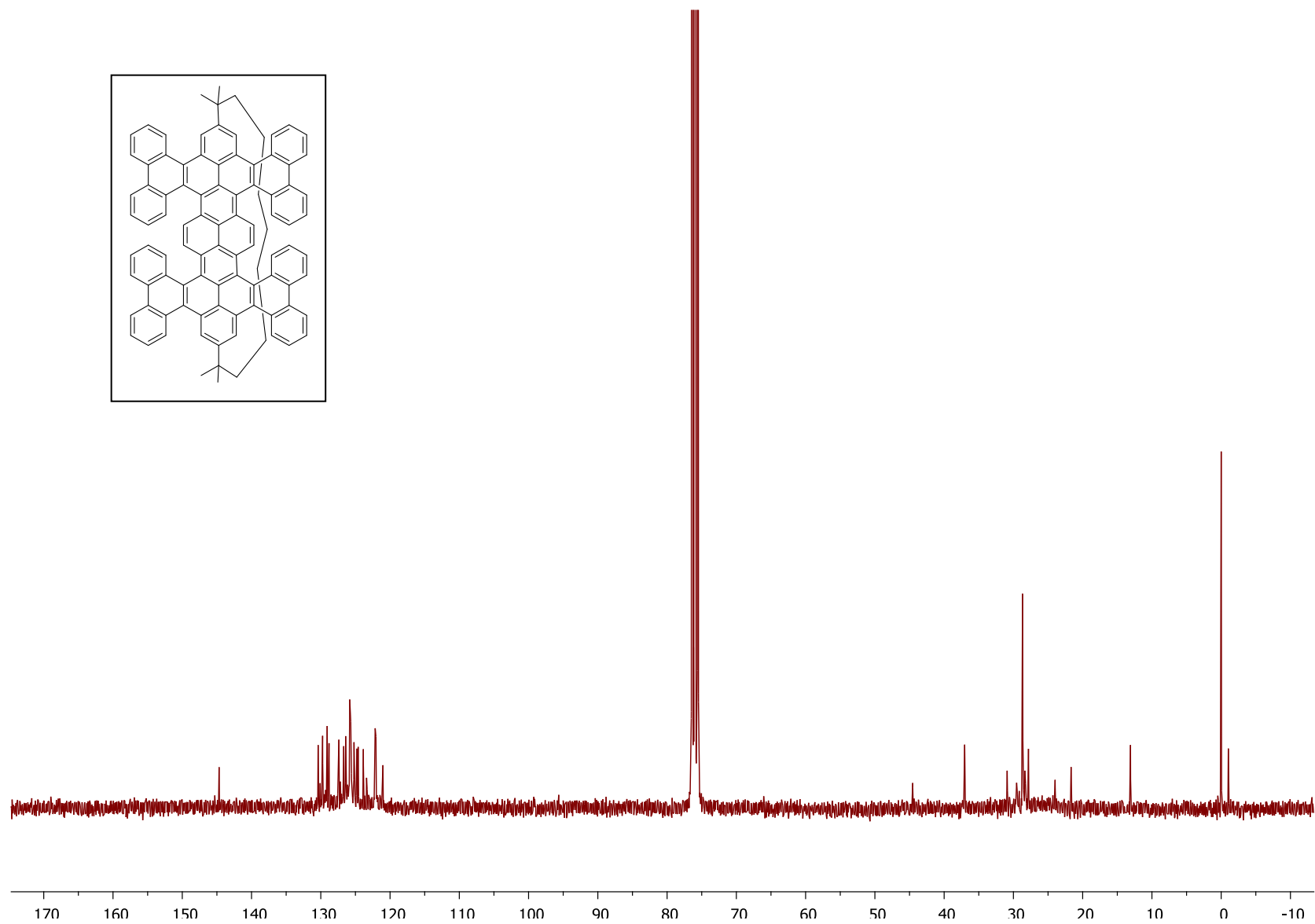
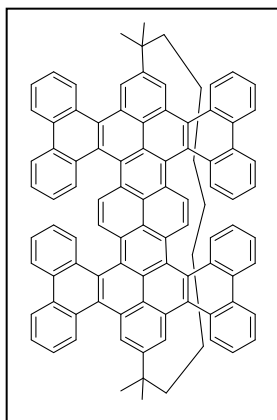
1. a) M. D. Watson, A. Fechtenkötter and K. Müllen, *Chem. Rev.* 2001, **101**, 1267–1300; b) K. Kawasumi, Q. Zhang, Y. Segawa, L. T. Scott and K. Itami, *Nature Chem.*, 2013, **5**, 739–744.
2. L. Zhai, R. Shukla and R. Rathore, *Org. Lett.*, 2009, **11**, 3474–3477.
3. a) H. Kawai, Y. Kobayashi, S. Oi and Y. Inoue, *Chem. Commun.*, 2008, 1464–1466; b) K. Mochida, K. Kawasumi, Y. Segawa and K. Itami, *J. Am. chem. Soc.*, 2011, **133**, 10716–10719.
4. K. Kawasumi, Q. Zhang, Y. Segawa, L. T. Scott and K. Itami, *Nature Chem.* 2013, **5**, 739–744.
5. a) X. Dou, X. Yang, G. J. Bodwell, M. Wagner, V. Enkelmann and K. Müllen, *Org. Lett.*, 2007, **9**, 2485–2488; b) M. Müller, V. S. Iyer, C. Kübel, V. Enkelmann and K. Müllen, *Angew. Chem. Int. Ed.*, 1997, **36**, 1607–1610 c) A. Pradhan, P. Dechambenoit, H. Bock and F. Durola, *J. Org. Chem.*, 2013, **78**, 2266–2274.
6. K. Ozaki, K. Kawasumi, M. Shibata, H. Ito and K. Itami, *Nature*, 2015, **6**, 1–7.

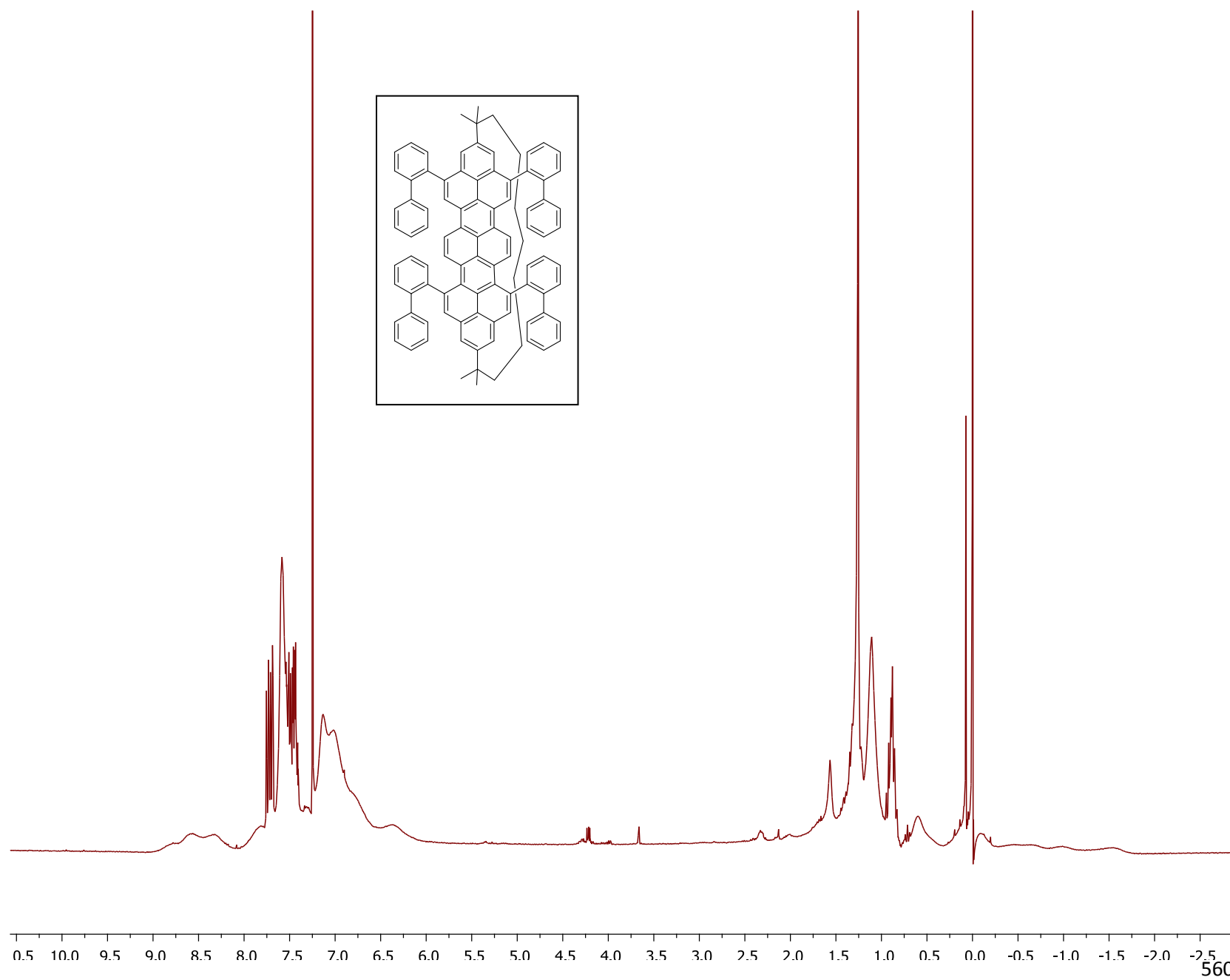
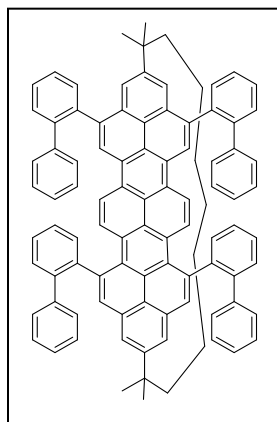


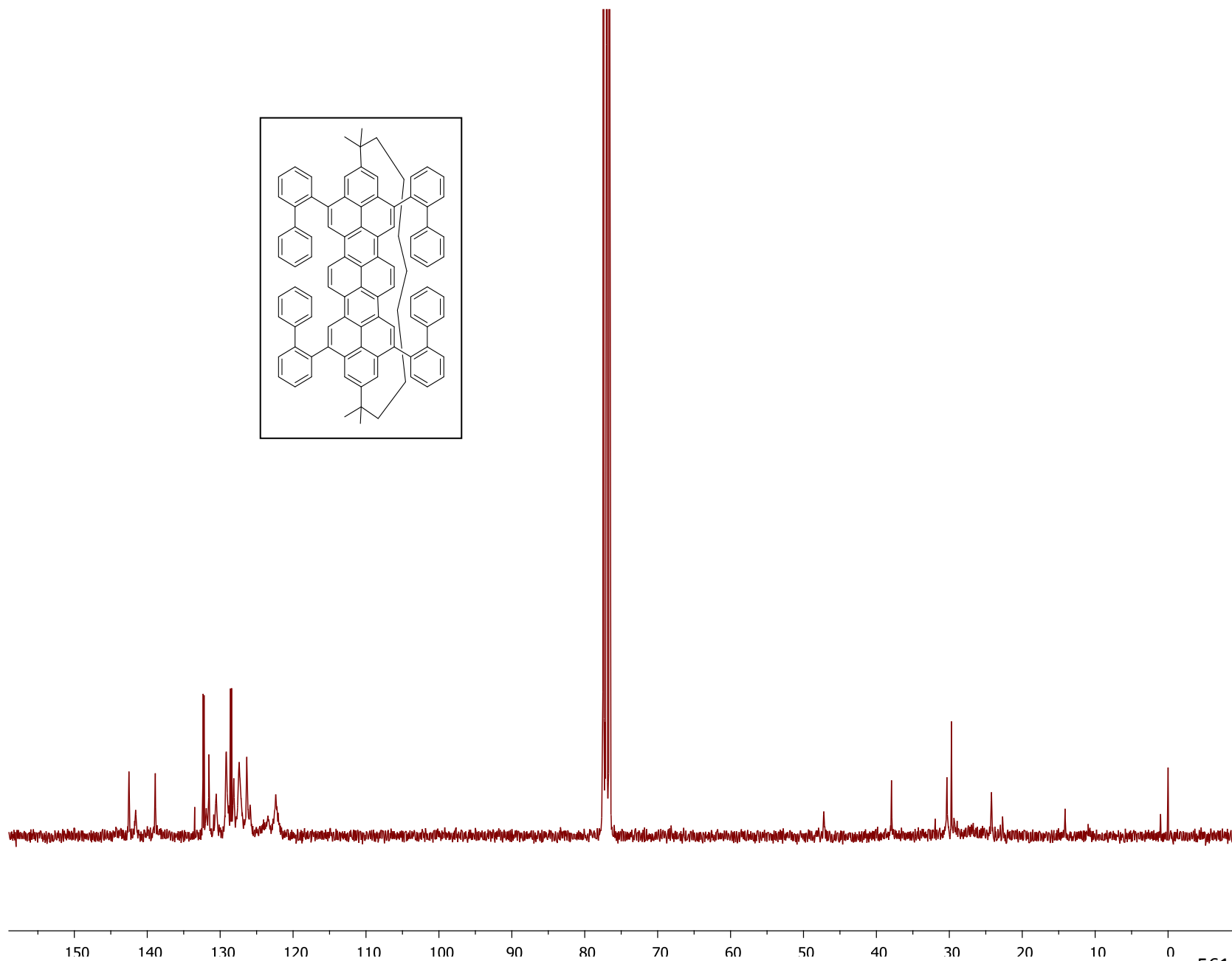
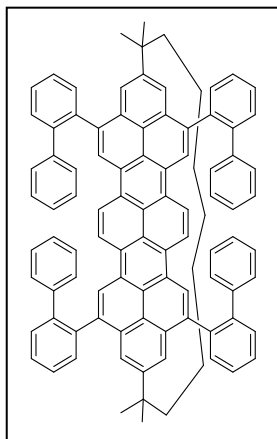
7. W. Neugebauer, A. J. Kos and P. v. R. Schleyer, *J. Organomet. Chem.*, 1982, **228**, 107–118.
8. a) M. D. Watson, F. Jäkei, N. Severin, J. P. Rabe and K. Müllen, *J. Am. Chem. Soc.*, 2004, **126**, 1402–1407; b) J. Wu, W. Pisula and K. Müllen, *Chem. Rev.*, 2007, **107**, 718–747.
9. a) E. H. Fort and L. T. Scott, *Angew. Chem., Int. Ed.*, 2010, 49, 6626–6628; b) E. H. Fort, M. S. Jeffreys and L. T. Scott, *Chem. Commun.*, 2012, **48**, 8102–8104.
10. a) E. Clar, *The Aromatic Sextet*, Wiley-VCH: New York, 1972; b) J. Zhu, C. Dahlstrand, J. R. Smith, S. Villaume and H. Ottosson, *Symmetry*, 2010, **2**, 1653–1682; c) I. Gutman, *Match*, 1985, 75–90; d) M. Solà, *Front. Chem.*, 2013, **1**, 1–8.
11. a) C. Seel and F. Vögtle, *Angew. Chem. Int. Ed.*, 1992, **31**, 528–549; b) F. Diederich, *Angew. Chem. Int. Ed.*, 1988, **27**, 362–386; c) B. P. Czech, P. Kus, C. M. Stetson, N. K. Dalley and R. A. Bartsch, *Tetrahedron*, 2007, **63**, 1360–1365 d) O. Tomomi and H. Nakashima, *Chem. Lett.* 2011, **40**, 134–135 e) N. K. Dalley, X. Kou, R. A. Bartsch, P. Bronislaw and P. Kus, *J. Incl. Phenom. Mol. Recognit. Chem.* 1997, **29**, 323–334; f) R. A. Bartsch, P. Kus, N. K. Dalley and X. Kou, *Tetrahedron Lett.*, 2002, 43, 5017–5019; g) C. Virués, E. F. Velázquez, M. B. Inoue and M. Inoue, *J. Incl. Phenom. Macrocyc. Recognit. Chem.* 2004, **48**, 141–146; h) C. Virués, R. Navarro, E. F. Velázquez, and M. Inoue, *Supramol. Chem.*, 2008, **20**, 301–307.

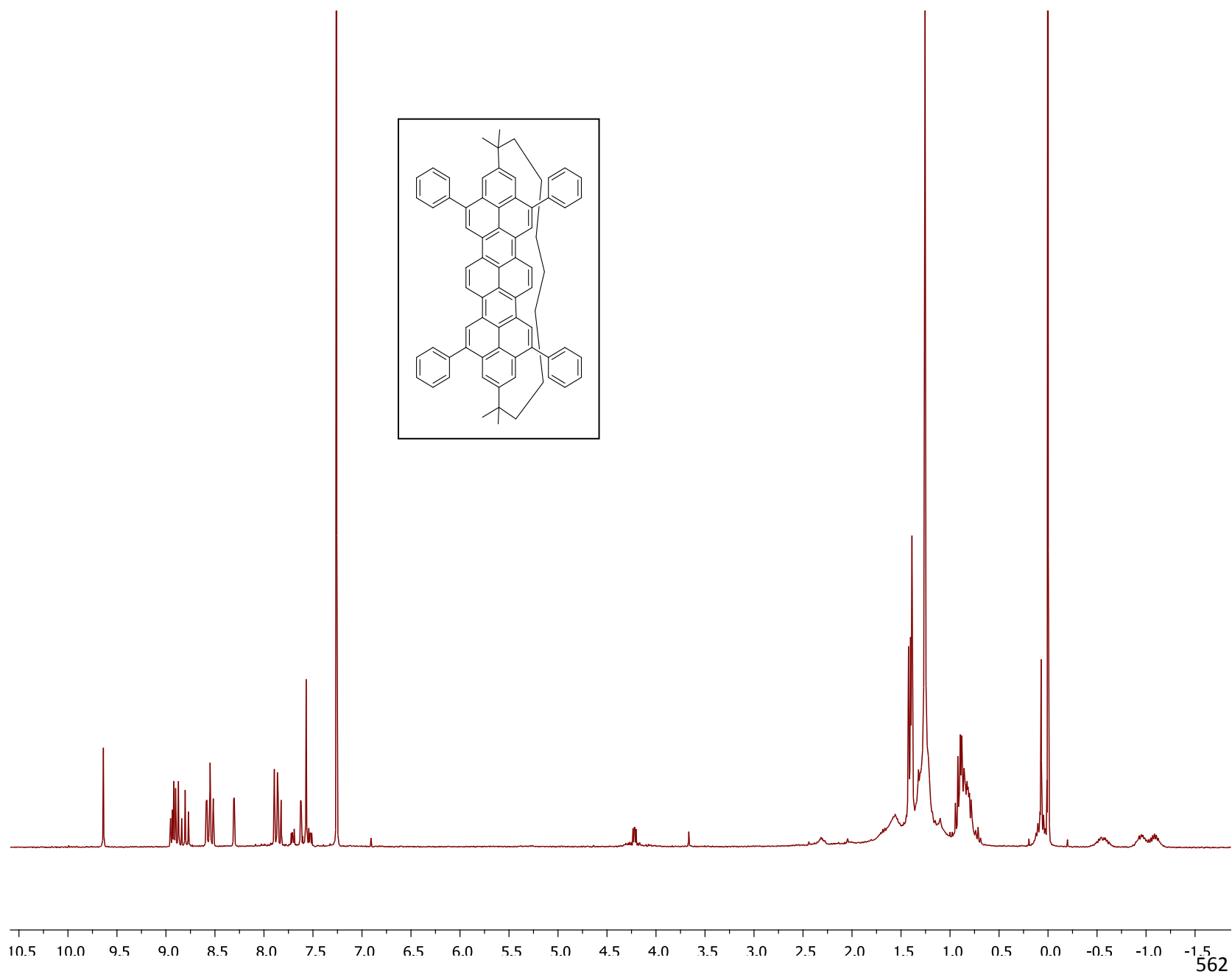
# APPENDIX 4

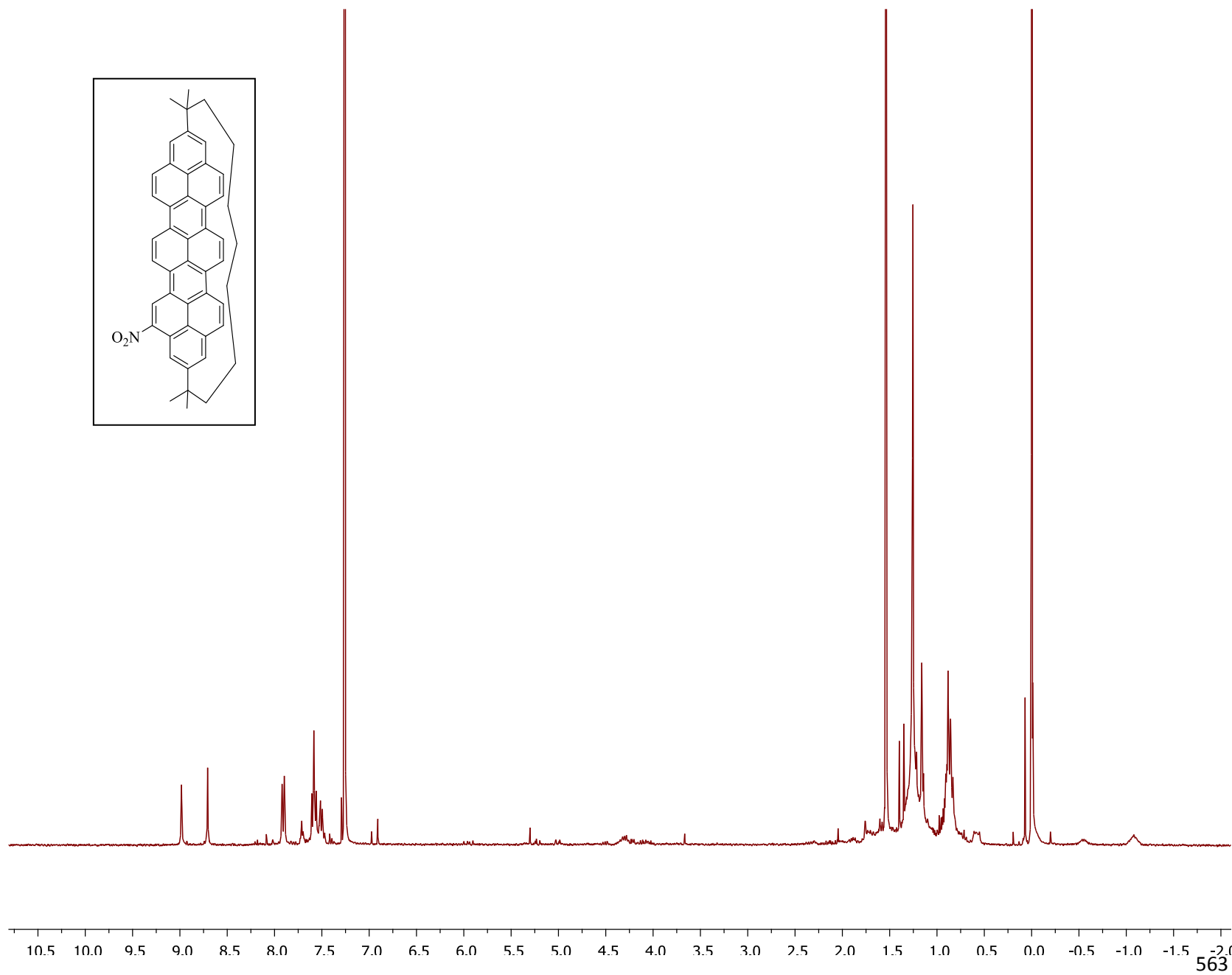
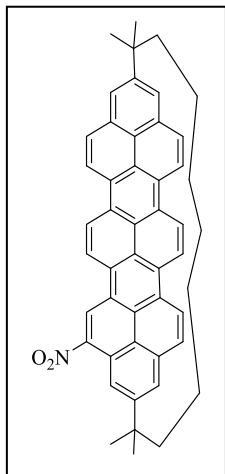














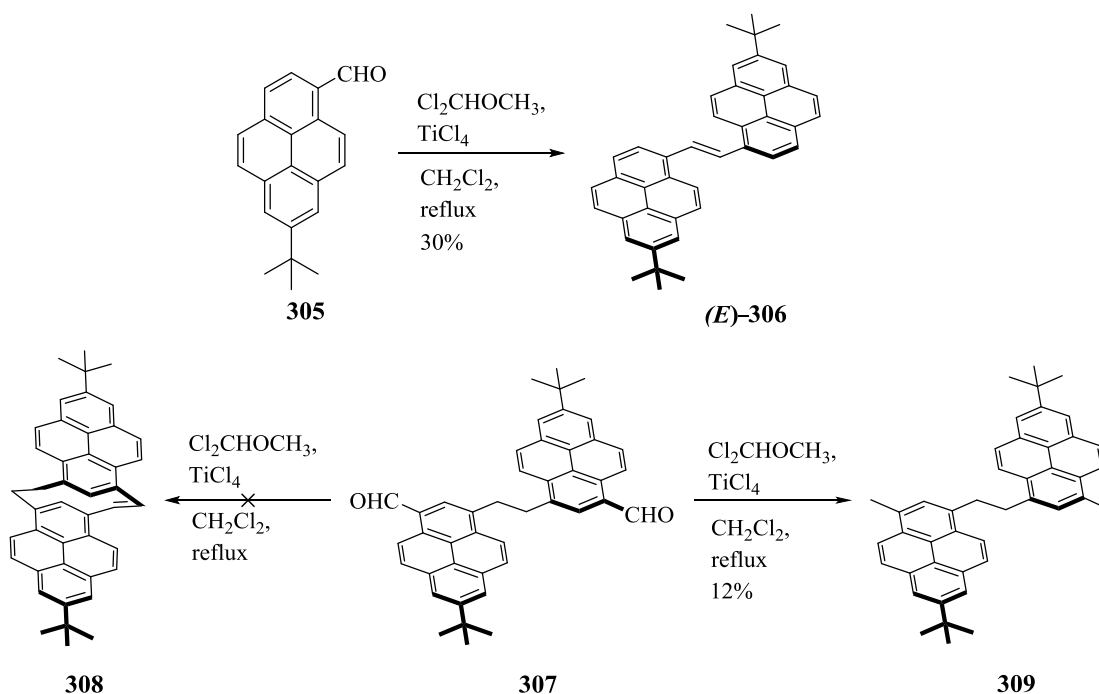
## Chapter 7: Attempted synthesis of the model compound (2,7-di-*t*-butylteropyrene)

### 7.1 Introduction

Having a series of  $[n](2,11)$ teropyrenophanes ( $n = 7-10$ ) that contain an increasingly distorted teropyrene system allowed for the exploration of how incremental changes in structure affect the chemical and physical properties. Although several interesting trends were observed over the range of bend that was available ( $\theta = 145.2^\circ-177.9^\circ$ ), the absence of a planar teropyrene system means that there is no baseline against which changes associated with distortion from planarity can be assessed. As discussed in Chapter 1, the only known teropyrene prior to the Bodwell group's contributions was the parent hydrocarbon **22** (Chapter 1) and it was found to have very low solubility in organic solvents.<sup>1</sup> In fact, the only characterization reported was a UV-vis spectrum. On the other hand, the teropyrenophanes exhibited good solubility in common organic solvents. This is presumably due to the nonplanar nature of the teropyrene systems and the presence of the aliphatic bridge, both of which prevent long range  $\pi$ - $\pi$  stacking in the solid state. Based on these consideration, 2,11-di-*t*-butylteropyrene (**318**) (Scheme 7.02) was identified as an appropriate model compound. The bulky *t*-butyl groups at the 2 and 11 positions of teropyrene system were expected to improve the solubility and effectively mimic the nature of the substitution in the  $[n](2,11)$ teropyrenophanes.

The plans for the synthesis of the model compound **318** relied on the same strategies that were developed for the syntheses of the  $[n](2,11)$ teropyrenophanes (Chapters 2-4). Initial work on this target was performed by a previous group member<sup>2</sup>

and this involved both the double-McMurry and Wurtz / McMurry approaches. The former approach failed to produce required Z-isomer when aldehyde **305** was subjected to an intermolecular McMurry reaction and the latter approach failed at the stage of the intramolecular McMurry reaction. Dialdehyde **307** gave only complete reduction of the aldehyde groups (**308**) instead of the desired [2.2](1,3)pyrenophane **309** (Scheme 7.01).



**Scheme 7.01** Two previously explored and failed approaches to model compound **318**; top) a double-McMurry strategy; bottom) a Wurtz / McMurry strategy.

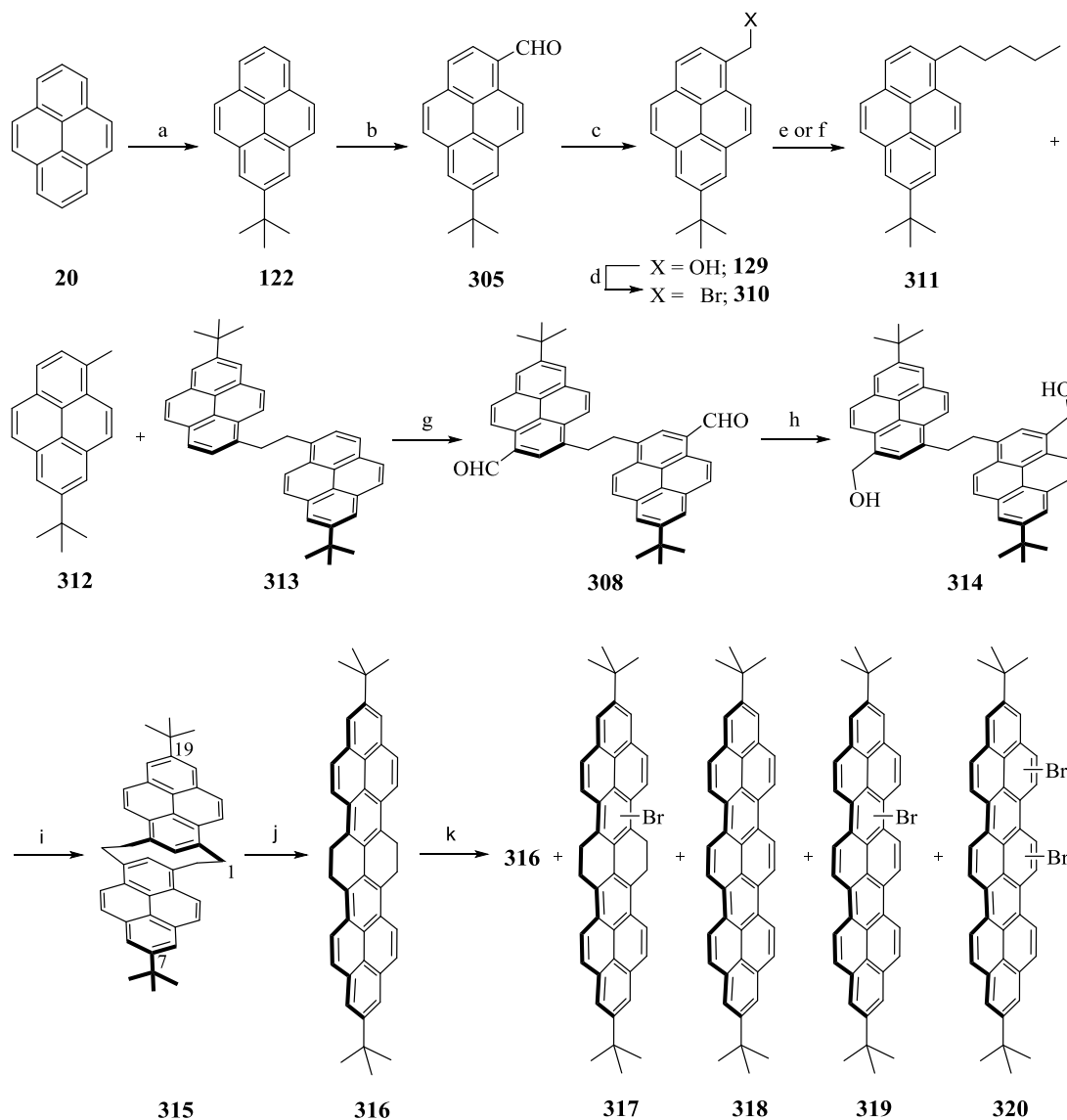
## 7.2 Attempted synthesis of compound **318** using a double-Wurtz coupling strategy

The failure of the double-McMurry and Wurtz / McMurry approaches is not surprising considering the very poor track record of the McMurry reaction for the formation of [2.2]metacyclophanes.<sup>3</sup> By comparison, the Wurtz coupling generally performs better when called upon to generate such strained systems.<sup>4</sup> This prompted the

investigation of whether a double-Wurtz route could provide access to **318**. Pyrene **20** was subjected to Friedel-Crafts alkylation with *t*-butyl chloride to form *t*-butyl pyrene **122** (63%),<sup>5</sup> which was formylated under Rieche conditions to give aldehyde **305** (81%) (Scheme 7.02). Aldehyde **305** was reduced to alcohol **129** using sodium borohydride and the crude product obtained was brominated to yield bromide **310**. Immediate treatment of the unchromatographed bromide **310** with *n*-BuLi brought about intermolecular Wurtz coupling to obtain compound **313** (73%, over 3 steps), in which two pyrene systems are connected by a two carbon alkane chain. When using chromatographed bromide **310**, the Wurtz coupling reaction proceeded in 86% yield on an 800 mg scale. Unfortunately, the yield dropped off dramatically as the scale increased. When the reaction was performed on a 4 g scale, the yield was only 10% (3 steps).

To avoid this problem, the *in-situ* iodination / Wurtz coupling protocol described in Chapter 4 was applied to alcohol **129**. This proved to be a superior method as it produced the required product **313** in 70% yield (3 steps) when the reaction was performed on an 8.9 g scale. Rieche formylation of **313** proceeded smoothly to produce the dialdehyde **308** in 72% yield. In contrast to what was observed in the formylations of **108c-e** (Chapter 4), no regioisomeric dialdehydes were obtained. The quite poorly soluble dialdehyde **308** was reduced using NaBH<sub>4</sub> to produce diol **314**, which was subjected without purification to the *in-situ* iodination / Wurtz coupling protocol to form the *anti*-7,19-di-*t*-butyl[2.2](1.3)-pyrenophane **315** in 73% yield (100 mg scale of diol **314**). The product was purified by subjecting it to column chromatography. Upon increasing the reaction scale to 3.4 g the product precipitated from the reaction as it formed and was

isolated in 60% yield by filtration. In contrast to dialdehyde **308**, compound **315** is nicely soluble in dichloromethane and it could be characterized without any difficulty.



**Scheme 7.02** Reagents and conditions: a) *t*-Butyl chloride, pyrene (**20**),  $\text{AlCl}_3$ ,  $\text{CH}_2\text{Cl}_2$ ,  $0^\circ\text{C}$  to rt, 2.5 h, 63%; b)  $\text{Cl}_2\text{CHOCH}_3$ ,  $\text{TiCl}_4$ ,  $\text{CH}_2\text{Cl}_2$ , rt, 2 h, 81%; c)  $\text{NaBH}_4$ , THF, rt, 1 h; d)  $\text{PBr}_3$ ,  $\text{CH}_2\text{Cl}_2$ ,  $0^\circ\text{C}$  to rt, 1 h; e) **310**, *n*-BuLi, THF,  $0^\circ\text{C}$ , 10 min, 10–86%; f) 1. **129**, PMHS,  $\text{I}_2$ , THF, rt, 20 min 2. *n*-BuLi, THF,  $0^\circ\text{C}$ , 10 min, 70%; g)  $\text{Cl}_2\text{CHOCH}_3$ ,  $\text{TiCl}_4$ ,  $\text{CH}_2\text{Cl}_2$ ,  $0^\circ\text{C}$  to rt, 2 h, 72%; h)  $\text{NaBH}_4$ , THF, rt, 1 h; i) 1. PMHS,  $\text{I}_2$ , THF, rt, 20 min 2. *n*-BuLi, THF,  $0^\circ\text{C}$ , 10 min, 60%; j)  $\text{Br}_2$ ,  $\text{CH}_2\text{Cl}_2$ , rt, 30 min, 95%; k)  $\text{Br}_2/\text{NBS}$ , hv,  $\text{CHCl}_3$ , reflux, 1.0 h, 96%.

### 7.2.1 Absorption and emission spectra of compound **315**

The absorption spectrum of compound **315** recorded in chloroform is very similar to that of the parent *anti*-[2.2](1,3)pyrenophane<sup>6</sup> (with no *tert*-butyl groups at the 7 and 19 positions) (Figure 7.01). The spectrum is composed of two absorption envelopes, ( $\beta/\beta'$  bands and  $p$  bands), which are red-shifted (10-25 nm) and broadened compared to those of pyrene.<sup>6a</sup> The longest wavelength absorption envelope consists of three closely overlapping bands ( $p$  bands) at  $\lambda_{\text{max}} = 363, 343$  and  $325$  nm. The higher energy envelope contains four poorly-resolved bands ( $\beta$  and  $\beta'$  bands) at  $\lambda_{\text{max}} = 285, 273, 263$  and  $252$  nm.

The emission spectrum of compound **315** when irradiating at 285 nm showed three closely overlapping bands at  $\lambda_{\text{max}} = 394, 400$  and  $409$  nm that are reminiscent of the monomer emission of pyrene also present (Figure 7.01). An additional structureless broad shoulder at  $\lambda_{\text{max}} = 470$  nm was also present. A similar band was observed previously in case of the parent *anti*-[2.2](1,3) pyrenophane, but only in the case of the polar solvents such as acetonitrile.<sup>6b</sup> The band was attributed to intramolecular excimer formation via intramolecular charge transfer. Curiously, irradiation of **314** at 250 nm gave rise to an additional broad and very weak fluorescence band at  $\lambda_{\text{max}} = 310$  nm which may be due to emission from  $S_2$  (Violation of Kasha's rule). Further examination of the photochemistry of this compound would be required to confirm this.

In the  $^1\text{H}$  NMR spectrum the singlet corresponding to the internal protons of the pyrene systems (H-12 and H-24) of **14**, appeared at a significantly high field  $\delta = 4.43$  ppm, as would be expected for and *anti*-[2.2]metacyclophane.<sup>6c</sup>

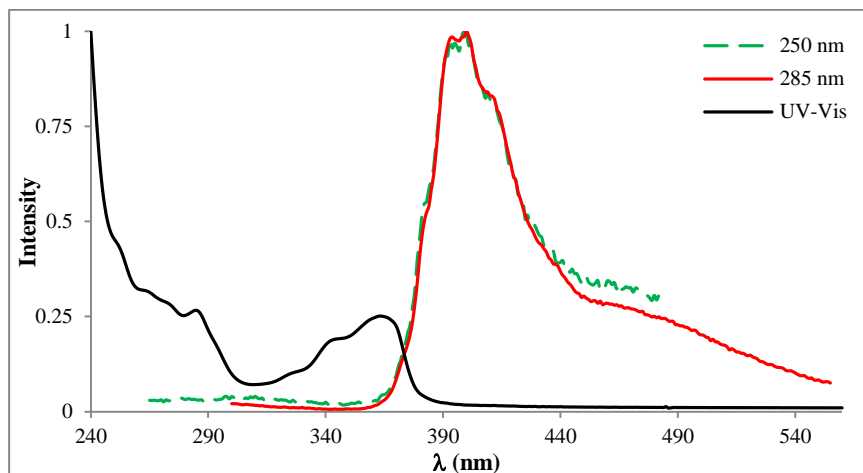
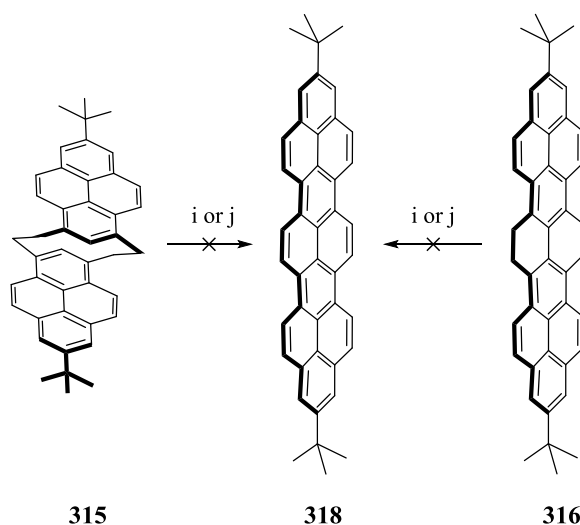


**Figure 7.01** Absorption and emission spectra of compound **315**.

Unlike the teropyrenophane precursors **109b-e** and **102b-d**, which contain at least one unsaturated two-carbon bridge, the cyclophane **315** obtained using the double-Wurtz route has two saturated two-carbon bridges. The absence of unsaturation in the bridges of **315** meant that a VID reaction is not possible. Indeed, when cyclophane **315** was refluxed in benzene or *m*-xylene in the presence of DDQ, no reaction was observed and only the starting material was recovered (Scheme 7.03). Applying the reaction conditions used for the synthesis of [9](2,11)teropyrenophane **103d**, (DDQ (2.5 equiv.), CH<sub>2</sub>Cl<sub>2</sub>:CH<sub>3</sub>SO<sub>3</sub>H) were also resulted in no product formation and only the starting material was recovered.

It is well known that the transannular reaction of [2.2]metacyclophanes to give 4,5,9,10-tetrahydropyrenes can occur under the conditions of various electrophilic aromatic substitution reactions. In fact, Misumi *et al.* used PyHBr·Br<sub>2</sub> extensively as a reagent to convert metacyclophanes to tetrahydropyrenes in their work on layered



**Scheme 7.03** *Reagents and conditions:* i) DDQ (10 equiv.), benzene or m-xylene, reflux, 24 h; j) DDQ (2.5 equiv.), CH<sub>2</sub>Cl<sub>2</sub>:CH<sub>3</sub>SO<sub>3</sub>H (9:1), rt, 2 h.

metacyclophanes<sup>1</sup> including their synthesis of teropyrene (**22**). Somewhat surprisingly, when **315** was treated with 3.0 equiv. of PyHBr·Br<sub>2</sub> in dichloromethane at 0 °C as described by Misumi, no reaction occurred (tlc analysis). In contrast, when compound **315** (50 mg scale) was treated with 1.0 equiv. of molecular bromine in dichloromethane, tetrahydroteropyrene **316** precipitated from the reaction and was isolated in 95% yield by filtration. No dihydroteropyrene, teropyrene or corresponding brominated products were observed in this reaction (LC-MS analysis), even when 3.0 equiv. of Br<sub>2</sub> were employed. Thus the planar tetrahydroteropyrene system appears to be reluctant to undergo further dehydrogenation or electrophilic bromination, like the bent teropyrene precursors do (Chapter 5). Increasing the scale of the reaction to 1 g had no effect on the yield of the product. In order to obtain the required 2,11-di-*t*-butylteropyrene (**318**), the solvent for the bromination reaction of compound **315** was changed to THF. Unfortunately, no

product formation was observed due to the relatively low solubility of starting material in THF.

### 7.2.2 Absorption and emission spectra of compound **316**

Tetrahydroteropyrene **316** is deep purple in colour and is poorly soluble in dichloromethane. The absorption spectrum of compound **316** was recorded as a chloroform solution (Figure 7.02). As with compound **315**, the spectrum of **316** consists of two absorption envelopes, but the bands are better resolved and significantly red-shifted. The lowest energy absorption envelope consists at least four bands at  $\lambda_{\text{max}} = 547, 507, 472$  and  $444$  nm and the intensity of these bands decreases gradually with increasing energy. Absorption in this region is probably responsible for the dark purple colour of the compound. The higher energy absorption envelope also contains at least 5 closely overlapping bands at  $\lambda_{\text{max}} = 361, 334, 317, 302$  and  $289$  nm.

The emission spectrum of compound **316** was obtained in chloroform solution (Figure 7.02). The spectrum contains two emission envelopes in the range  $375\text{-}510$  nm and  $510\text{-}700$  nm. The first envelop consists of two equally intense bands at  $\lambda_{\text{max}} = 415$  and  $437$  nm along with a third band at  $462$  nm which is nearly one third of the intensity of the other two bands and a very weak band at  $495$  nm. The second emission envelope contains bands at  $\lambda_{\text{max}} = 539, 555$  and  $593$  nm. A weak band at  $645$  nm is also noted. Interestingly, these longest wavelength absorption bands are nearly overlapping with the longest wavelength emission bands. Both these longest wavelength absorption and emission bands in the region  $470\text{-}670$  nm are assigned as the charge transfer bands in the



excited state. More detailed studies are currently underway in collaboration with Dr. David Thompson group at Memorial University of Newfoundland in order to elucidate the situation.

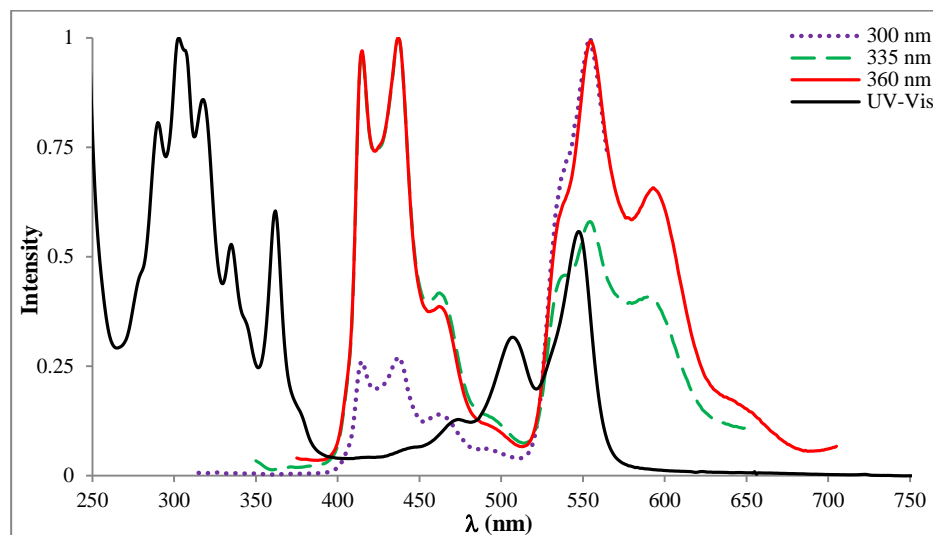


**Figure 7.02** Absorption and emission spectra of compound **316**.

Returning to the attempted synthesis of teropyrene **318**, a suspension of compound **15** in dichloromethane was irradiated at reflux in the presence of bromine. A deep purple solid was obtained, which had a shinier appearance than the deep purple starting material. The very poor solubility of this solid did not allow its characterization by solution phase NMR. On the other hand, a solid state  $^{13}\text{C}$  NMR spectrum could be obtained (Figure 7.03). The spectrum was very similar to that of its precursor, tetrahydroteropyrene **316**, except that the tetrahydroteropyrene spectrum contains an additional prominent peak at 22 ppm, which corresponds to the carbons of saturated two-carbon units. The absence of this peak indicates the solid obtained from the reaction must be either teropyrene **318** or some mixture of **318** and brominated teropyrenes.

This notion was supported by the APPI-HRMS analysis of the product mixture. The APPI-HRMS analysis showed the presence of four new products along with majority of unreacted tetrahydroteropyrene **316** (Scheme 7.02). The masses of the products suggested that these are the intermediate bromo compound **317** ( $[M+H] = 645.2133$ ; found), teropyrene **318** ( $[M+H] = 563.2737$ ; found), bromoteropyrene **319** ( $[M+H] =$

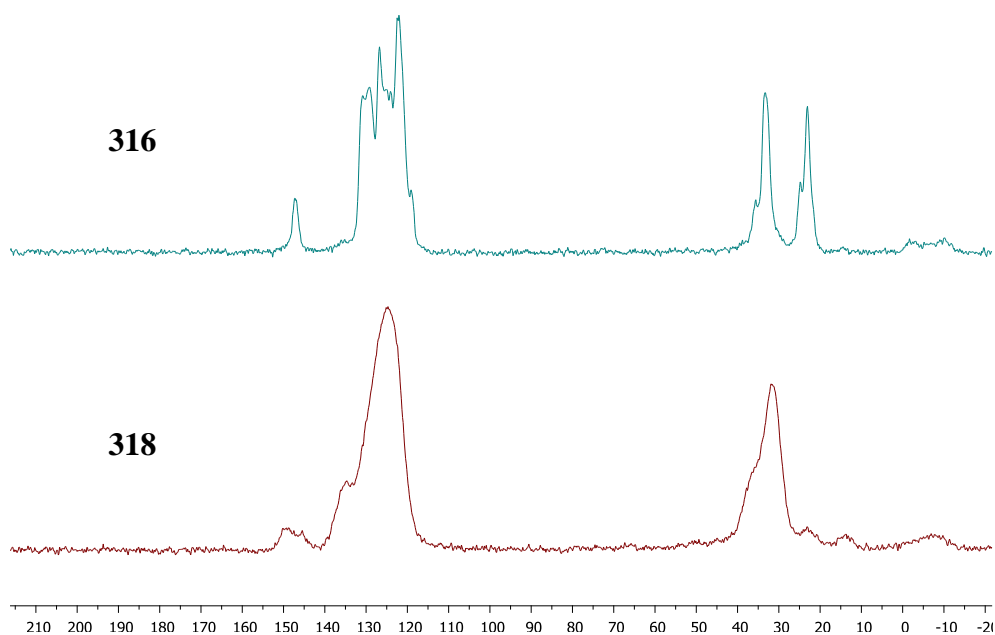
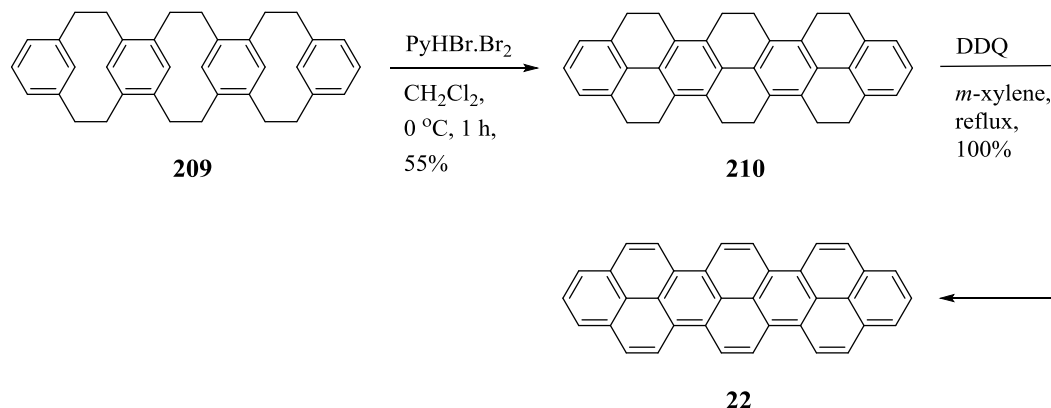


**Figure 7.03** Solid state  $^{13}\text{C}$  NMR spectra of compounds **316** and **318**.

641.1838; found) and dibromoteropyrene **320** ( $[M+H] = 719.094$ ; found). The presence of dihydroteropyrene or its corresponding brominated compounds were not observed. Low solubility of these products remained as the major obstacle for the purification of these products as well as for further screening of the reaction conditions.

In Misumi's report, the teropyrene **22** was obtained by oxidizing dodecahydroteropyrene **210** using *m*-xylene as solvent and in the presence of DDQ (equiv. were not

mentioned) (Scheme 7.04). Attempted conversion of **316** to **318** using DDQ (10 equiv.) in benzene or *m*-xylene at reflux was not successful (Scheme 7.03). Rathor's Scholl reaction conditions (DDQ (2.5 equiv.), CH<sub>2</sub>Cl<sub>2</sub>:CH<sub>3</sub>SO<sub>3</sub>H (9:1)) were also resulted in no product formation and only the starting material was recovered (Scheme 7.03).

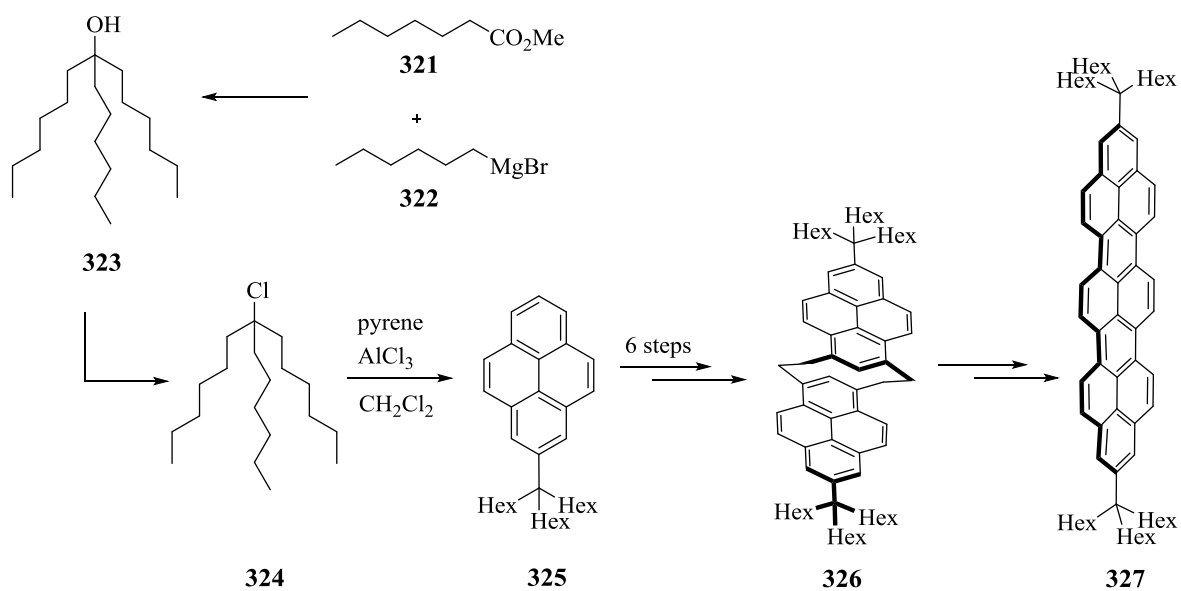


**Scheme 7.04** Misumi's synthesis of teropyrene **22**.

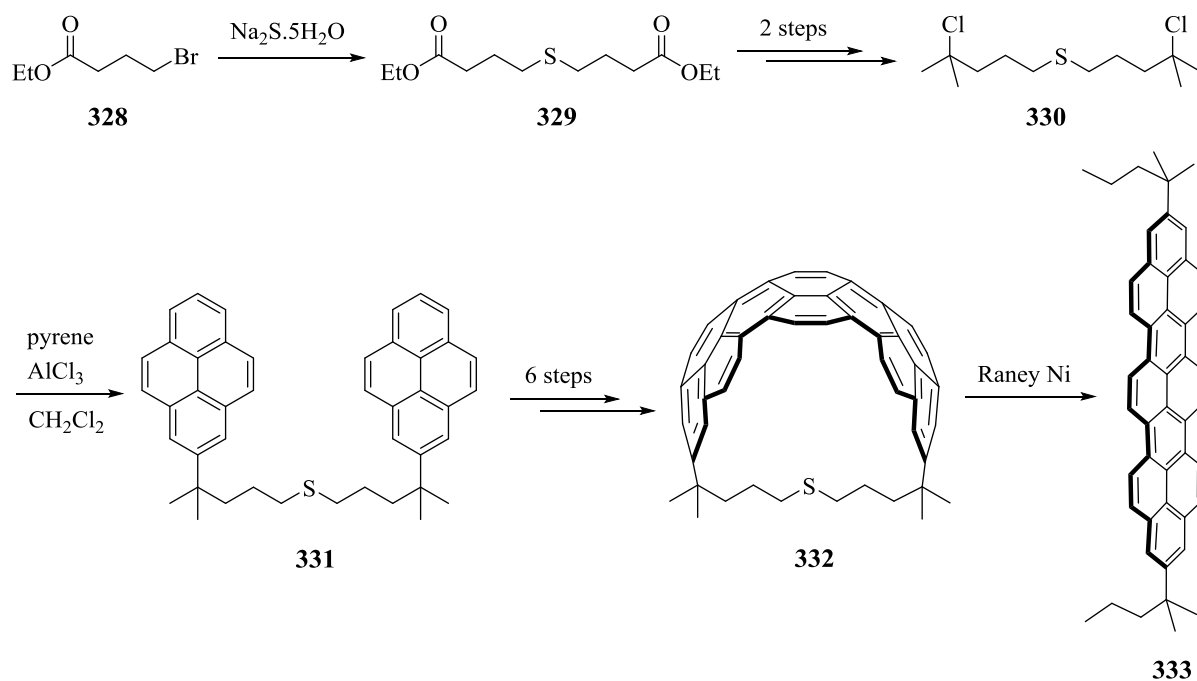
### 7.03 Plausible alternatives of synthesizing a teropyrene system

Even after introducing *t*-butyl groups to the teropyrene precursors solubility issues still persisted. One option for the future investigation would be to include even larger solubilizing groups. For example, tertiary alkyl chloride **324** could conceivably be synthesized the reaction between methyl heptanoate (**321**) and *n*-hexylmagnesium bromide (**322**) followed by chlorination of *tert*-alcohol **323**. Friedel-Crafts alkylation of pyrene with **20** should afford **325**, which would be expected to lead to cyclophane **326** and then teropyrene **327** (Scheme 7.05). Alternatively, the good solubility of the teropyrenophanes, 4-thia[9]teropyrenophane **332** should be accessible using the approach shown in Scheme 7.06. This approach guarantees the formation of an intact teropyrene

system.



**Scheme 7.05** Introduction of large alkyl group to improve the solubility of teropyrene system.



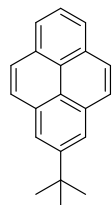
**Scheme 7.06** A plausible strategy for generating the teropyrene system.

## 7.04 Conclusions

A double-Wurtz route for the synthesis of a planar 2,11-di-*t*-butylteropyrene **318** was been explored. Gram scale synthesis of metacyclophane **315** and tetrahydroteropyrene **316** were achieved and their UV-Vis and fluorescence spectra were recorded. The later shows exceptional behaviour in its photophysical properties and extensive studies are required at this stage to elucidate the scenario. Poor solubility of the planar systems **315** and **316** caused problems in exploring the reaction conditions to achieve the planar teropyrene system.

## 7.05 Experimental Section

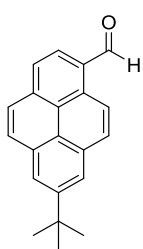
### 2-*t*-Butylpyrene (122)<sup>7</sup>



*t*-Butyl chloride (15.24 mL, 135.7 mmol) was dissolved in dichloromethane (200 mL) and pyrene (**20**) (25.03 g, 123.4 mmol) was added. The resulting solution was cooled to 0 °C followed by the addition of AlCl<sub>3</sub> (19.74 g, 148.1 mmol). The resulting dark brown mixture was stirred at room temperature for a period of 2.5 h. The reaction was then poured into ice-cold water (400 mL) and the layers were separated. The aqueous layer was extracted with dichloromethane (2 × 100 mL) and the combined organic layers were washed with brine (300 mL), dried over Na<sub>2</sub>SO<sub>4</sub>, filtered and concentrated under reduced pressure. The yellow residue was suspended in methanol (400 mL) and the suspension was heated at reflux for 30 min. The insoluble material was removed by suction filtration while the solution was still hot and the filtrate was cooled to 0 °C. The crystals that formed were collected by suction filtration and were

recrystallized from hexanes to afford 2-*t*-butylpyrene (**122**) as an off-white solid (20.10 g, 63%):  $R_f = 0.57$  (10% dichloromethane / hexanes); m.p. 107–108 °C (lit. m.p. 110–112 °C);  $^1\text{H}$  NMR (300 MHz,  $\text{CDCl}_3$ )  $\delta$  8.24 (d,  $J=1.0$  Hz, 2H), 8.17 (d,  $J=7.6$  Hz, 2H), 8.07 (s, 4H), 8.00–7.95 (s, 1H), 1.62 (s, 9H);  $^{13}\text{C}$  NMR (75 MHz,  $\text{CDCl}_3$ )  $\delta$  147.55, 130.94, 130.85, 127.58, 127.12, 125.45, 124.67, 124.58, 122.81, 122.76, 45.14, 38.18, 29.46, 25.60; LCMS (APCI-positive)  $m/z$  (rel. int.) 261 (5), 260 (28), 260 ( $[\text{M}+\text{H}]^+$ , 100); APPI calculated for  $\text{C}_{20}\text{H}_{18}$  ( $[\text{M}+\text{H}]^+$ ) 259.1489, found 259.1497.

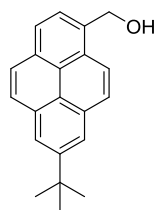
### 7-*t*-Butyl-1-formylpyrene (**305**)



2-*t*-Butylpyrene (**122**) (10.02 g, 38.8 mmol) was dissolved in dichloromethane (700 mL) and the solution was cooled to 0 °C. Dichloromethyl methyl ether (10.32 mL, 116.2 mmol), titanium(IV) chloride (12.81 mL, 116.2 mmol) were then added. The reaction mixture was stirred at room temperature for 2 h. The reaction was then cooled to 0 °C and quenched with ice-cold water (1 L). The layers were separated and the aqueous layer was extracted with dichloromethane (2 × 200 mL). The combined organic layers were washed with brine (500 mL) and the solvents were concentrated under reduced pressure to afford a yellow residue. The crude residue was subjected to column chromatography (4.5 cm × 10 cm; dichloromethane) to afford 7-*t*-butyl-1-formylpyrene (**305**) as a yellow solid (9.00 g, 81%):  $R_f = 0.30$  (dichloromethane); m.p. 136–137 °C;  $^1\text{H}$  NMR (300 MHz,  $\text{CDCl}_3$ )  $\delta$  10.75 (s, 1H), 9.37 (d,  $J=9.3$  Hz, 1H), 8.37 (d,  $J=8.0$  Hz, 1H), 8.34 (d,  $J=1.8$  Hz, 1H), 8.32 (d,  $J=1.8$  Hz, 1H), 8.28 (d,  $J=9.3$  Hz, 1H), 8.19 (d,  $J=8.9$  Hz, 1H), 8.19 (d,  $J=7.9$  Hz, 1H), 8.04 (d,  $J=8.9$  Hz, 2H), 1.61 (s, 9H);  $^{13}\text{C}$  NMR (75 MHz,  $\text{CDCl}_3$ )  $\delta$  192.90, 149.71,

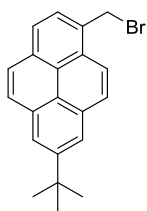
135.10, 130.77, 130.71, 130.61, 130.17, 127.05, 126.89, 124.32, 124.25, 124.12, 123.97, 122.68, 122.09, 35.31, 31.95; LC-MSD-Trap (CI-positive)  $m/z$  (rel. int.) 289 (2), 288 (22), 287 ( $[M+H]^+$ , 100); APPI calculated for  $C_{21}H_{18}O$  ( $[M+H]^+$ ) 287.1438, found 287.1416.

### 7-*t*-Butyl-(1-hydroxymethyl)pyrene (**129**)



7-*t*-Butyl-1-formylpyrene (**305**) (8.90 g, 31.1 mmol) was dissolved in THF (300 mL). To this solution, sodium borohydride (3.53 g, 93.3 mmol) was added and the reaction was stirred at room temperature for a period of 1 h. The reaction mixture was cooled to 0 °C and was neutralized using a 5.0 M aqueous HCl solution. As much THF as possible was removed under reduced pressure and the solid residue was dissolved in dichloromethane (250 mL). The organic layer was subsequently washed with water (2 × 200 mL), washed with brine (200 mL), dried over  $Na_2SO_4$ , filtered and concentrated to afford 7-*t*-butyl-(1-hydroxymethyl)pyrene (**129**) as a fluffy light brown solid (9.00 g, 99%):  $R_f$  = 0.28 (50% ethyl acetate / hexanes); m.p. 156–157 °C;  $^1H$  NMR (500 MHz,  $CDCl_3$ )  $\delta$  8.35 (d,  $J$ =9.2 Hz, 1H), 8.24 (d,  $J$ =1.8 Hz, 1H), 8.23 (d,  $J$ =1.8 Hz, 1H), 8.13 (d,  $J$ =9.2 Hz, 1H), 8.12 (d,  $J$ =7.8 Hz, 1H), 8.03 (dd,  $J$ =13.7, 9.0 Hz, 2H), 8.01 (d,  $J$ =7.8 Hz, 1H), 5.40 (s, 2H), 1.59 (s, 12H);  $^{13}C$  NMR (75 MHz,  $CDCl_3$ )  $\delta$  149.11, 133.59, 131.15, 130.97, 130.68, 128.45, 127.99, 127.57, 127.27, 125.54, 124.80, 124.48, 123.03, 122.83, 122.60, 122.46, 63.59, 35.30, 32.04; LCMS (APCI-positive)  $m/z$  (rel. int.) 273 (3), 272 (23), 271 ( $[M-OH]^+$ , 100); HRMS (EI-(+)) calculated for  $C_{21}H_{20}O$  ( $[M]^+$ ) 288.1514, found 288.1509. The product obtained was used in the next step without further purification.

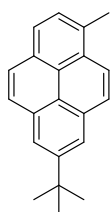
### (1-Bromomethyl)-7-*t*-butyl-pyrene (310)



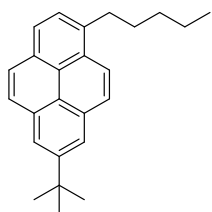
7-*t*-Butyl-(1-hydroxymethyl)pyrene (**129**) (3.36 g, 11.7 mmol) was dissolved in dichloromethane (150 mL) and the solution was cooled to 0 °C.

PBr<sub>3</sub> (0.82 mL, 8.8 mmol) was added and the reaction mixture was stirred at room temperature for 1 h. The reaction mixture was then quenched with ice-cold water (200 mL) and the layers were separated. The aqueous layer was extracted with dichloromethane (2 × 40 mL) and the combined organic layers were washed with brine (150 mL), dried over Na<sub>2</sub>SO<sub>4</sub>, filtered and concentrated to afford (1-bromomethyl)-7-*t*-butylpyrene (**310**) (3.71 g, 91%) as a pale yellow solid: *R*<sub>f</sub> = 0.60 (10% ethyl acetate / hexanes); m.p. 195–197 °C; <sup>1</sup>H NMR (500 MHz, CDCl<sub>3</sub>) δ 8.35 (d, *J*=9.2 Hz, 1H), 8.28 (d, *J*=1.8 Hz, 1H), 8.25 (d, *J*=1.8 Hz, 1H), 8.21 (d, *J*=9.2 Hz, 1H), 8.08 (d, *J*=7.9 Hz, 1H), 8.07 (d, *J*=8.9 Hz, 1H), 8.01 (d, *J*=8.9 Hz, 1H), 7.98 (d, *J*=7.8 Hz, 1H), 5.29 (s, 2H), 1.59 (s, 9H); <sup>13</sup>C NMR (75 MHz, CDCl<sub>3</sub>) δ 147.50, 131.81, 131.12, 130.69, 130.38, 128.92, 128.45, 128.26, 127.38, 127.22, 125.07, 124.67, 122.97, 122.92, 122.75, 35.30, 32.36, 31.98; LCMS (APCI-positive) *m/z* (rel. int.) 273 (3), 272 (21), 271 ([M(<sup>81</sup>Br)–Br, 100]; HRMS data could not be obtained.

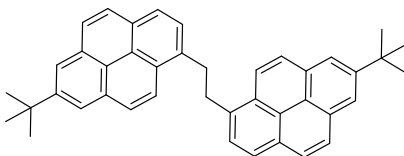
### 7-*t*-Butyl-1-methylpyrene (**312**), 7-*t*-Butyl-1-pentylpyrene (**311**) and 1,2-Bis(7-*t*-butylpyren-1-yl)ethane (**313**)



**311**



**312**



**313**

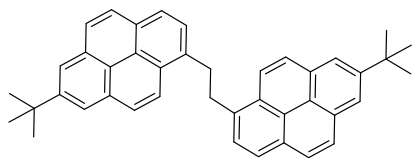
(1-Bromomethyl)-7-*t*-butylpyrene (**310**) (800 mg, 2.26 mmol) was dissolved in dry



THF (60 mL) and the solution was cooled to 0 °C. To this solution, *n*-BuLi (1.50 M, 0.45 mL, 1.13 mmol) was added dropwise through a septum, under nitrogen atmosphere over a period of 20 min. The reaction mixture was then quenched with water (50 mL) and as much THF as possible was removed under the reduced pressure. Dichloromethane (50 mL) was added to the resulting turbid aqueous layer and the layers were separated. The aqueous layer was extracted with dichloromethane (2 × 20 mL) and the combined organic layers were washed with brine (40 mL), dried over Na<sub>2</sub>SO<sub>4</sub>, filtered and concentrated under reduced pressure. The light yellow residue was subjected to column chromatography (3.5 × 20 cm; 17% chloroform / hexanes) to first afford 7-*t*-butyl-1-methylpyrene (**312**) as a white solid; (10 mg, 1%): m.p. 97–99 °C (lit. m.p. 99-100 °C), *R*<sub>f</sub> = 0.56 (20% chloroform / hexanes); <sup>1</sup>H NMR (500 MHz, CDCl<sub>3</sub>) δ 8.28–8.25 (m, 3H), 8.12 (d, *J*=9.2 Hz, 1H), 8.07 (d, *J*=7.8 Hz, 1H), 8.05–8.00 (m, 2H), 7.85 (d, *J*=7.7 Hz, 1H), 3.00 (s, 3H), 1.65 (s, 9H); <sup>13</sup>C NMR (75 MHz, CDCl<sub>3</sub>) δ 149.04, 132.19, 131.49, 131.04, 129.76, 129.21, 127.68, 127.60, 127.48, 126.79, 124.97, 124.64, 123.77, 123.31, 122.31, 122.14, 35.40, 32.17; LCMS and HRMS data could not be obtained; 7-*t*-butyl-1-pentylpyrene (**311**) as a colourless liquid; (55 mg, 7%): *R*<sub>f</sub> = 0.53 (20% chloroform / hexanes); <sup>1</sup>H NMR (500 MHz, CDCl<sub>3</sub>) δ 8.30 (d, *J*=9.2 Hz, 1H), 8.25 (d, *J*=1.9 Hz, 2H), 8.24 (d, *J*=1.9 Hz, 2H), 8.12 (d, *J*=9.2 Hz, 1H), 8.10 (d, *J*=7.8 Hz, 1H), 8.03 (dd, *J*=9.7, 9.0 Hz, 2H), 7.86 (d, *J*=7.8 Hz, 1H), 3.38–3.34 (m, 2H), 1.94–1.87 (m, 2H), 1.64 (s, 9H), 1.55–1.41 (m, 4H), 1.00–0.96 (m, 3H); <sup>13</sup>C NMR (75 MHz, CDCl<sub>3</sub>) δ 149.24, 137.56, 131.74, 131.23, 129.94, 128.86, 127.83, 127.67, 127.27, 127.07, 125.46, 124.98, 123.86, 123.76, 122.47, 122.26, 35.61, 33.96, 32.45, 32.38, 32.06, 23.11, 14.55; LCMS (APCI-

positive)  $m/z$  (rel. int.) 331 (6), 330 (26), 329 ( $[M+H]^+$ , 100); HRMS (EI-(+)) calculated for  $C_{25}H_{28}$  ( $[M]^+$ ) 328.2191, found 328.2201; 1,2-bis(7-*t*-butylpyren-1-yl)ethane (**313**) (535 mg, 86%) as a fluffy white solid:  $R_f$  = 0.31 (20% chloroform / hexanes); m.p. 283–285 °C;  $^1H$  NMR (500 MHz,  $CDCl_3$ )  $\delta$  8.37 (d,  $J$ =9.2 Hz, 2H), 8.23 (d,  $J$ =1.9 Hz, 4H), 8.23 (d,  $J$ =1.9 Hz, 4H), 8.12 (d,  $J$ =9.2 Hz, 2H), 8.02 (dd,  $J$ =10.8, 9.0 Hz, 4H), 8.03 (d,  $J$ =7.7 Hz, 2H), 7.76 (d,  $J$ =7.7 Hz, 2H), 3.88 (s, 4H), 1.61 (s, 18H);  $^{13}C$  NMR (75 MHz,  $CDCl_3$ )  $\delta$  149.16, 136.02, 131.51, 130.99, 130.02, 128.72, 127.86, 127.64, 127.17, 127.08, 125.29, 124.87, 123.54, 123.35, 122.45, 122.23, 35.77, 35.43, 32.17; LCMS (APCI-positive)  $m/z$  (rel. int.) 546 (1), 545 (12), 544 (48), 543 ( $[M+H]^+$ , 100); HRMS (EI-(+)) calculated for  $C_{42}H_{38}$  ( $[M]^+$ ) 542.2974, found 542.2970.

#### 1,2-Bis(7-*t*-butylpyren-1-yl)ethane (**313**) (*in-situ* Wurtz coupling reaction)

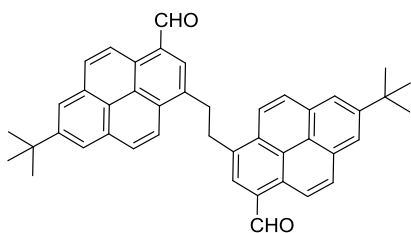


(1-Hydroxymethyl)-2-*t*-butyl-pyrene (**129**) (8.90 g, 30.7 mmol) was dissolved in THF (100 mL) and polymethylhydrosiloxane (2.75 mL, 50.1 mmol),

iodine (7.94 g, 31.3 mmol) were subsequently added. The resulting brown solution was stirred at room temperature under nitrogen atmosphere until the starting material was completely consumed (~1 h) (observed by TLC). Then, the reaction mixture was further diluted with THF (150 mL) and was cooled to 0 °C. To the cooled solution *n*-BuLi (1.60 M, 82 mL, 92.6 mmol) was added through cannula over a period of 1 h, during which the brown colour solution turned pale yellow. As much of the THF as possible was then removed under reduced pressure and the resulting solid residue was dissolved in dichloromethane (300 mL). The solution was cooled to 0 °C followed by quenching with

ice-cold water (300 mL) and the organic layer was separated. The aqueous layer was extracted with dichloromethane ( $2 \times 100$  mL) and the combined organic layers were washed with brine (300 mL), dried over  $\text{Na}_2\text{SO}_4$ , filtered and concentrated under reduced pressure. The obtained yellow residue was subjected to column chromatography ( $5.5 \times 20$  cm; 8% chloroform / hexanes) to afford 1,2-bis(7-*t*-butylpyren-1-yl)ethane (**313**) as a fluffy white solid (5.90 g, 70%). See previous experiment for the characterization data.

### 1,2-Bis(7-*t*-butyl-3-formylpyren-1-yl)ethane (**308**)

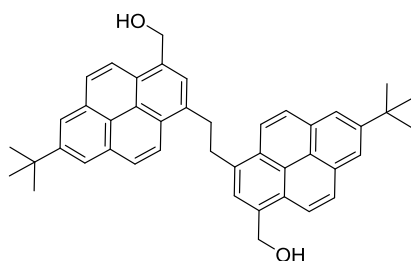


1,2-Bis(7-*t*-butylpyren-1-yl)ethane (**313**) (4.70 g, 8.6 mmol) was dissolved in dichloromethane (470 mL) and the solution was cooled at 0 °C. Titanium(IV) chloride (14.30 mL, 129.9 mmol) and dichloromethyl methyl

ether (11.51 mL, 129.9 mmol) were subsequently added and the resulting dark purple reaction mixture was stirred at room temperature, under nitrogen atmosphere over a period of 2 h. The reaction mixture was poured into ice-cold water (500 mL) and the organic layer was separated. The aqueous layer was extracted with dichloromethane ( $2 \times 100$  mL) and the combined organic layers were washed with brine (300 mL), dried over  $\text{Na}_2\text{SO}_4$ , filtered and concentrated under reduced pressure. The yellow residue was subjected to column chromatography ( $5.5 \times 8$  cm; dichloromethane) to afford 1,2-bis(7-*t*-butyl-3-formylpyren-1-yl)ethane (**308**) as a yellow solid (3.68 g, 72%):  $R_f = 0.20$  (dichloromethane); m.p. 232–236 °C;  $^1\text{H}$  NMR (300 MHz,  $\text{CDCl}_3$ )  $\delta$  10.75 (s, 2H), 9.37 (d,  $J=9.3$  Hz, 2H), 8.40–8.21 (m, 12H), 3.95 (s, 4H), 1.61 (s, 18H); a  $^{13}\text{C}$  NMR spectrum could not be obtained due to low solubility; LCMS (APCI positive)  $m/z$  (rel. int.) 602 (3),

601 (12), 600 (50), 599 ( $[M+H]^+$ , 100); HRMS (EI-(+)) calculated for  $C_{44}H_{38}O_2$  ( $[M]^+$ ) 598.2872, found 598.2874.

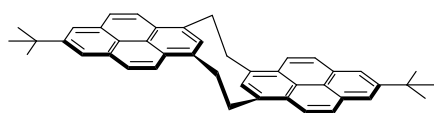
**1,2-Bis(7-*t*-butyl-3-hydroxymethylpyren-1-yl)ethane (314)**



**1,2-Bis(7-*t*-butyl-3-formylpyren-1-yl)ethane (308)**

(3.68 g, 6.1 mmol) was dissolved in THF (150 mL), sodium borohydride (1.39 g, 36.9 mmol) was added and the reaction mixture was stirred at room temperature for a period of 1 h. The reaction mixture was then cooled to 0 °C and neutralized using a 5.0 M aqueous HCl solution. As much of the THF as possible was removed under reduced pressure. The resulting residue was dissolved in dichloromethane (100 mL) and subsequently washed with water (2 × 50 mL), washed with brine (100 mL), dried over  $Na_2SO_4$ , filtered and concentrated to afford 1,2-bis(7-*t*-butyl-3-hydroxymethylpyren-1-yl)ethane (**314**) as a fluffy off-white solid (3.68 g, 99%):  $R_f$  = 0.20 (50% ethyl acetate / hexanes); m.p. 252–254 °C;  $^1H$  NMR (500 MHz,  $CDCl_3$ )  $\delta$  8.37 (d,  $J$ =9.2 Hz, 2H), 8.28 (d,  $J$ =9.2 Hz, 2H), 8.25–8.22 (m, 4H), 8.11 (d,  $J$ =9.2 Hz, 2H), 8.07 (d,  $J$ =9.2 Hz, 2H), 7.31 (s, 2H), 5.11–5.00 (m, 4H), 3.82 (s, 4H), 1.60 (s, 18H);  $^{13}C$  NMR (75 MHz,  $CDCl_3$ )  $\delta$  149.12, 135.09, 132.88, 130.97, 128.55, 128.22, 127.81, 127.52, 127.45, 125.43, 124.00, 123.06, 123.00, 122.83, 122.58, 122.45, 67.98, 35.21, 321.92; LCMS (APCI-positive)  $m/z$  (rel. int.) 588 (2), 587 (12), 586 (49), 585 ( $[M-OH]^+$ , 100); HRMS data could not be obtained. The product obtained was used in the next step without further purification.

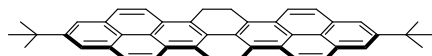
***Anti*-7,19-di-*t*-butyl][2.2](1,3)pyrenophane (**315**) (*in-situ* Wurtz coupling reaction)**



1,2-Bis(7-*t*-butyl-3-hydroxymethylpyren-1-yl)ethane

(**314**) (3.40 g, 5.6 mmol) was dissolved in THF (60 mL) and polymethylhydrosiloxane (1.00 mL, 16.8 mmol), iodine (2.97 g, 11.8 mmol) were subsequently added. The reaction mixture was stirred at room temperature under nitrogen atmosphere until the starting material was completely consumed (observed by TLC). The reaction mixture was then further diluted with THF (300 mL) and cooled to 0 °C. To the cooled solution, *n*-BuLi (1.60 M, 22.7 mL, 36.4 mmol) was added through cannula over a period of 0.5 h during which the brown colour solution turned pale yellow. As much of the THF as possible was removed under reduced pressure and the resulting residue was dissolved in dichloromethane (200 mL), cooled to 0 °C and quenched with ice-cold water (200 mL). The organic layer was separated and the aqueous layer was extracted with dichloromethane (2 × 50 mL). The combined organic layers were washed with brine (200 mL), dried over Na<sub>2</sub>SO<sub>4</sub>, filtered and concentrated under reduced pressure to afford a yellow residue which was washed with hexanes to afford *anti*-7,19-di-*t*-butyl][2.2](1,3)pyrenophane (**315**) (1.90 g, 60%) as an off-white solid: *R*<sub>f</sub> = 0.28 (20% chloroform / hexanes); m.p. >300 °C; <sup>1</sup>H NMR (500 MHz, CDCl<sub>3</sub>) δ 8.49 (d, *J*=9.2 Hz, 4H), 8.24 (s, 4H), 8.13 (d, *J*=9.2 Hz, 4H), 4.43 (s, 2H), 4.41 (m, 4H), 2.34 (m, 4H) 1.61 (s, 18H); <sup>13</sup>C NMR (75 MHz, CDCl<sub>3</sub>) δ 148.83, 134.72, 132.82, 131.26, 127.05, 126.92, 126.06, 124.13, 123.17, 121.88, 36.26, 35.18, 31.95; LCMS (APCI-positive) *m/z* (rel. int.) 572 (2), 571 (11), 570 (46), 559 ([M+H]<sup>+</sup>, 100); APPI calculated for C<sub>44</sub>H<sub>40</sub> ([M+H]<sup>+</sup>) 569.3210, found 569.3187.

### 2,11-Di-*t*-butyl-6,7,15,16-tetrahydroteropyrene (316)



Anti-7,19-di-*t*-butyl[2.2](1,3)pyrenophane (315)

(1.02 g, 1.8 mmol) was dissolved in dichloromethane (40 mL) and bromine (0.16 mL in 10 mL dichloromethane) was added. The reaction mixture was stirred at room temperature for a period of 30 min. The reaction mixture was then neutralized using saturated sodium thiosulphate solution and the organic layer was separated. The aqueous layer was extracted with dichloromethane (2 × 50 mL) and the combined organic layers were washed with brine (150 mL). The organic layer was dried over Na<sub>2</sub>SO<sub>4</sub>, filtered and concentrated under reduced pressure to obtain a dark purple powder which was washed with hexanes to obtain 2,11-di-*t*-butyl-6,7,15,16-tetrahydroteropyrene (316) (950 mg, 95%) as a dark purple solid: m.p. >300 °C; <sup>1</sup>H NMR (300 MHz, CDCl<sub>3</sub>) δ 8.43 (d, *J*=9.3 Hz, 4H), 8.19 (s, 4H), 8.08 (d, *J*=9.3 Hz, 4H), 3.78 (s, 8H), 1.60 (s, 18H); <sup>13</sup>C NMR data could not be obtained; LC-MSD-Trap (CI-positive) *m/z* (rel. int.) 569 (9), 568 (49), 567 ([M+H]<sup>+</sup>, 100); APPI calculated for C<sub>44</sub>H<sub>38</sub> ([M+H]<sup>+</sup>) 567.3054, found 567.3025.

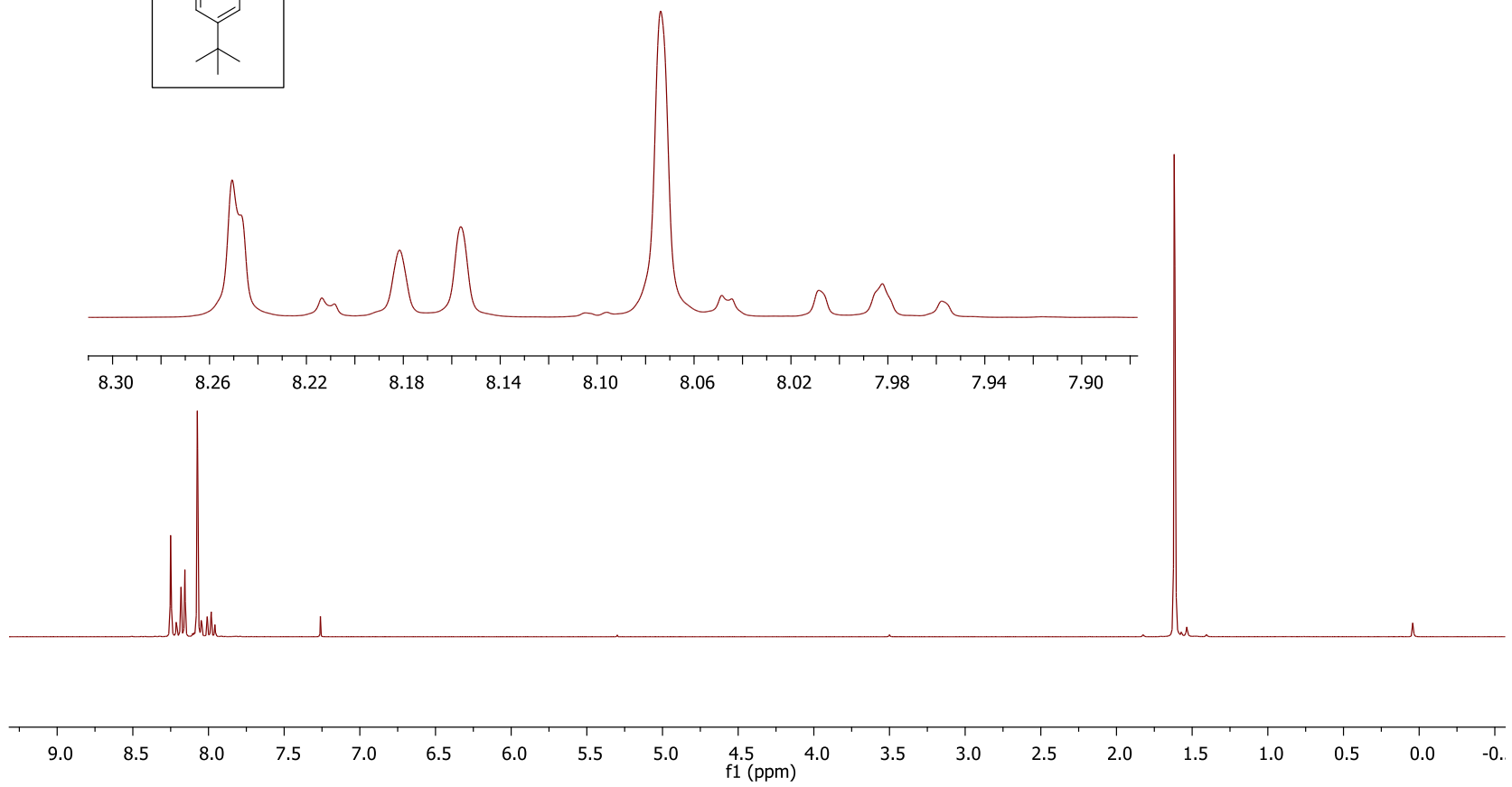
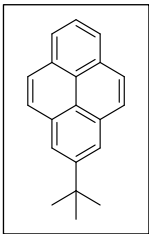
### 7.06 References

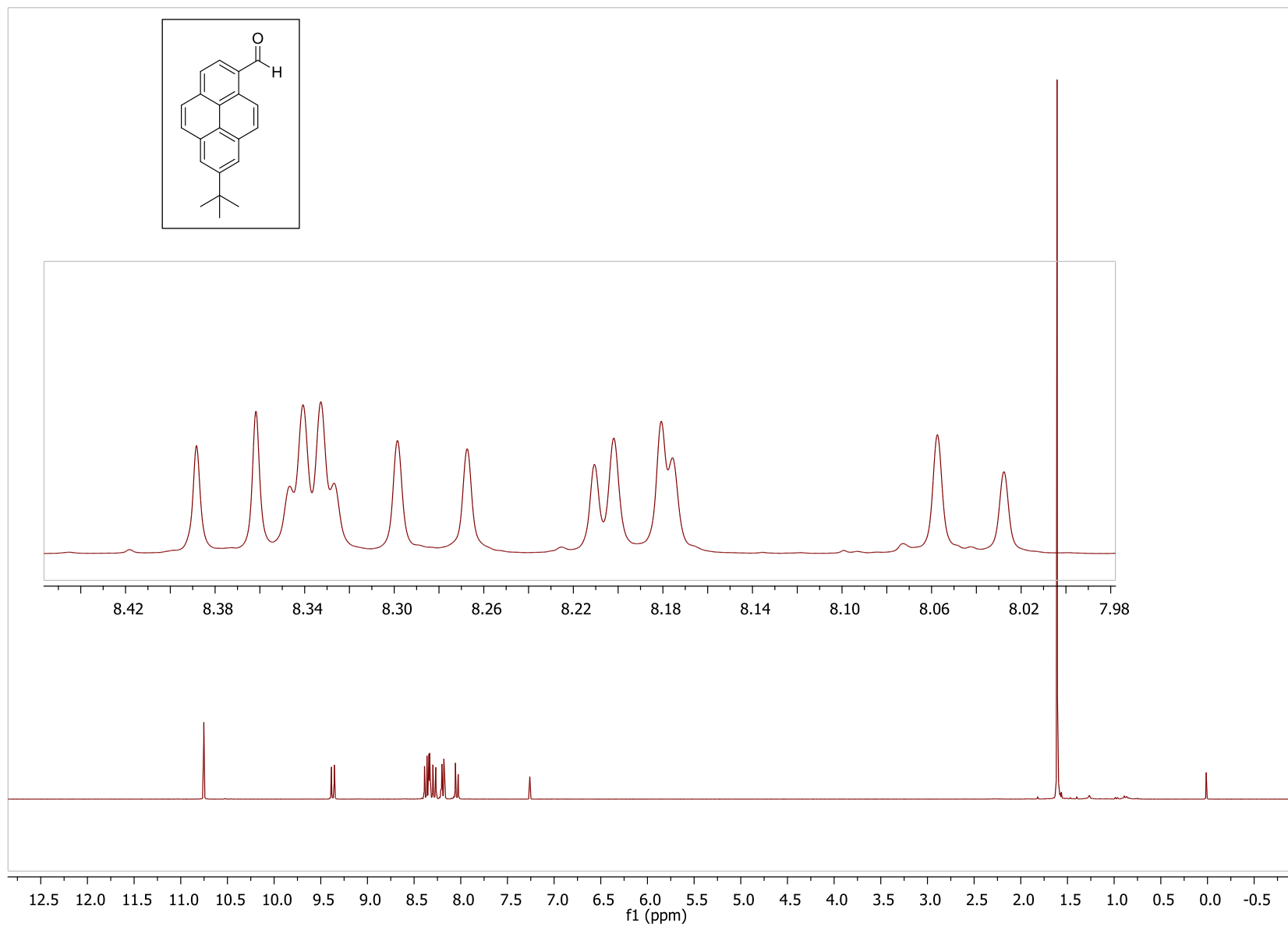
1. T. Umemoto, T. Kawashima, Y. Sakata and S. Misumi, *Tetrahedron Lett.*, 1975, **16**, 1005–1006.
2. B. L. Merner and Bodwell G. J., unpublished results.
3. G. J. Bodwell and P. R. Nandaluru, *Isr. J. Chem.*, 2012, **52**, 105–138.

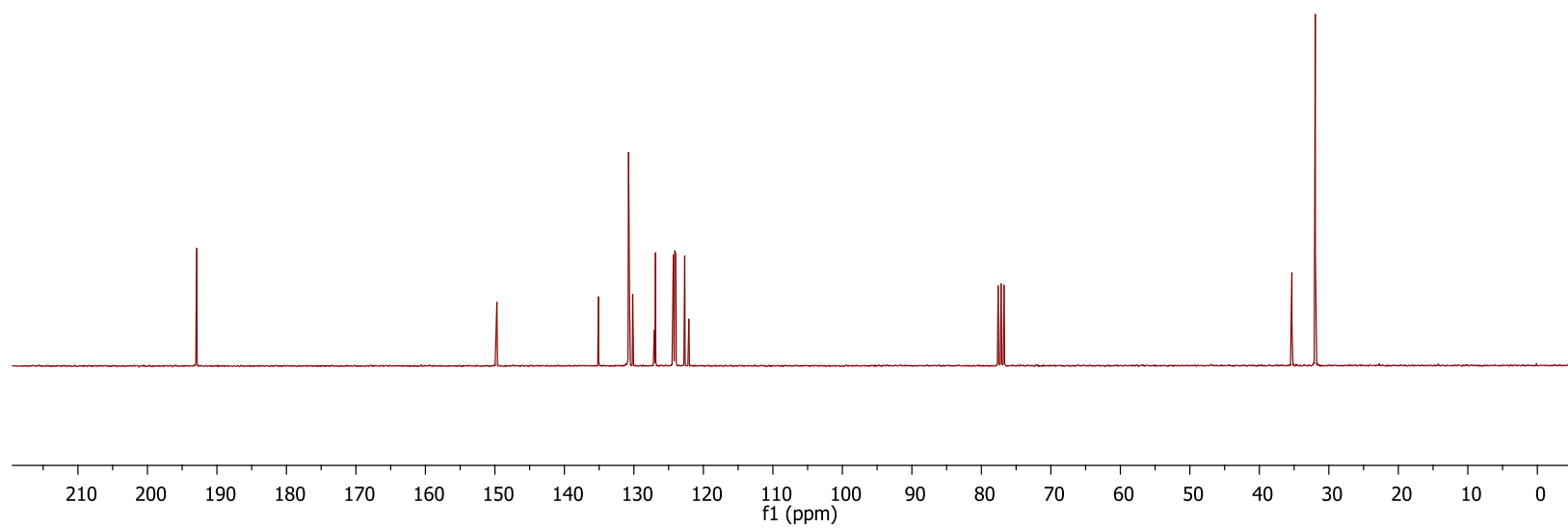
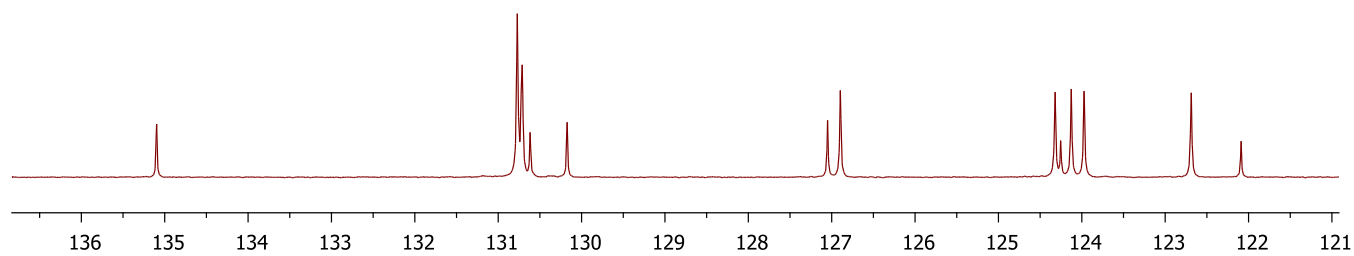
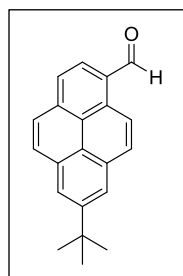
4. a) A. Tsuge, H. Nago, S. Mataka and M. Tashiro, *J. Chem. Soc. Perkin Trans. 1*, 1992, 1179–1185; b) H. Hopf, *In Cyclophanes*, P. M. Keehn and S. M. Rosenfeld (Eds.), *Academic Press*: New York, 1983, vol. 2.
5. T. M. F. Duarte, S. C. Simon, M. Wagner, S. I. Durzhinin, K. A. Zachariasse and K. Müllen, *Angew. Chem. Int. Ed.* 2008, **47**, 10175–10178.
6. a) T. Hayashi, N. Mataga, T. Umemoto, Y. Sakata and S. Misumi, *J. Phys. Chem.*, 1977, 81, 424–429; b) T. Hayashi, N. Mataga, Y. Sakata and S. Misumi, *Chem. Phys. Lett.*, 1976, **41**, 325–328; c) T. Umemoto, T. Kawashima, Y. Sakata and S. Misumi, *Chem. Lett.*, 1975, 837–840.
7. M. Tashiro, T. Yamato, K. Kobayashi and T. Arimura; *J. Org. Chem.*, 1987, 15, 3196–3199.

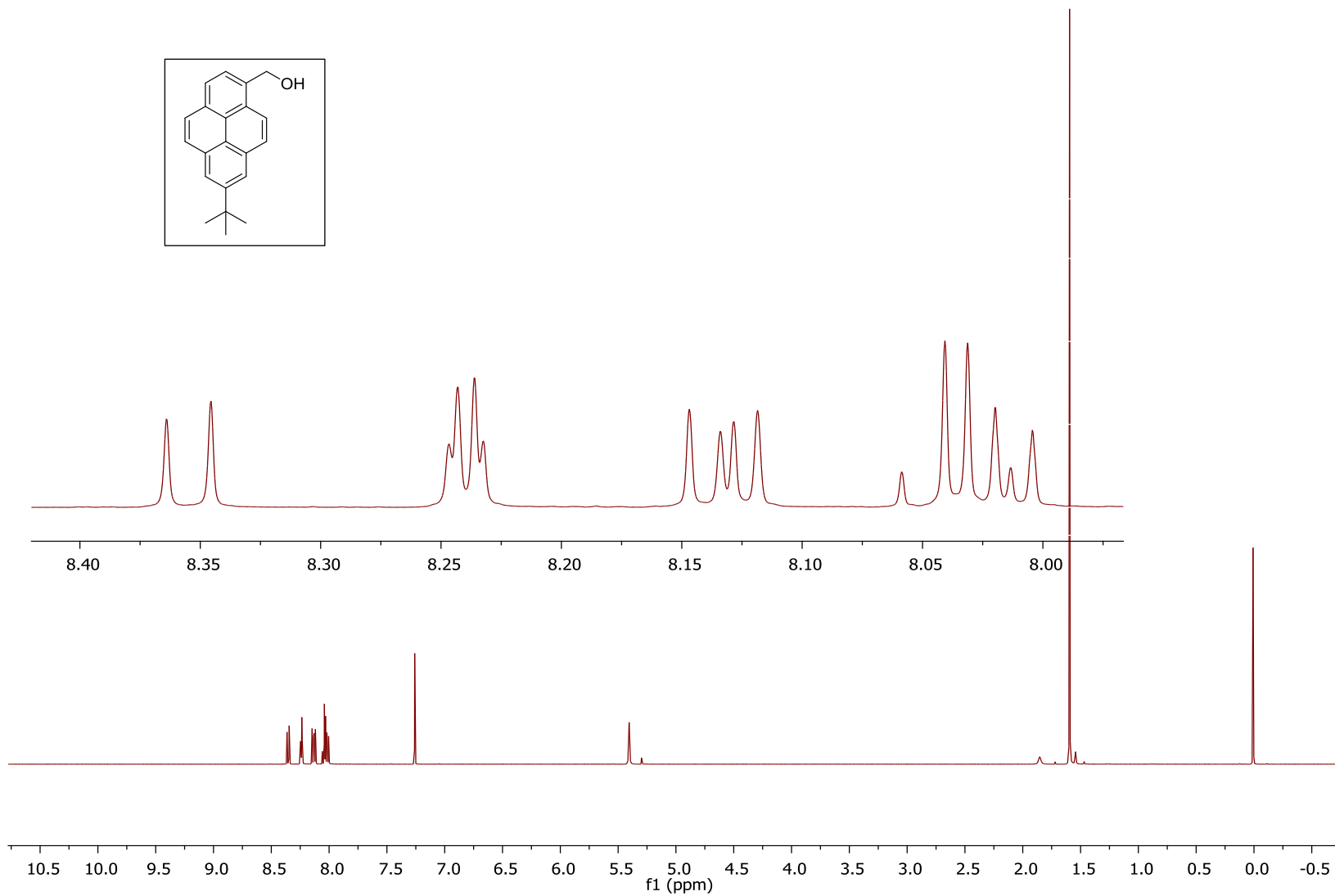
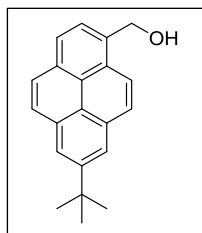
# APPENDIX 5

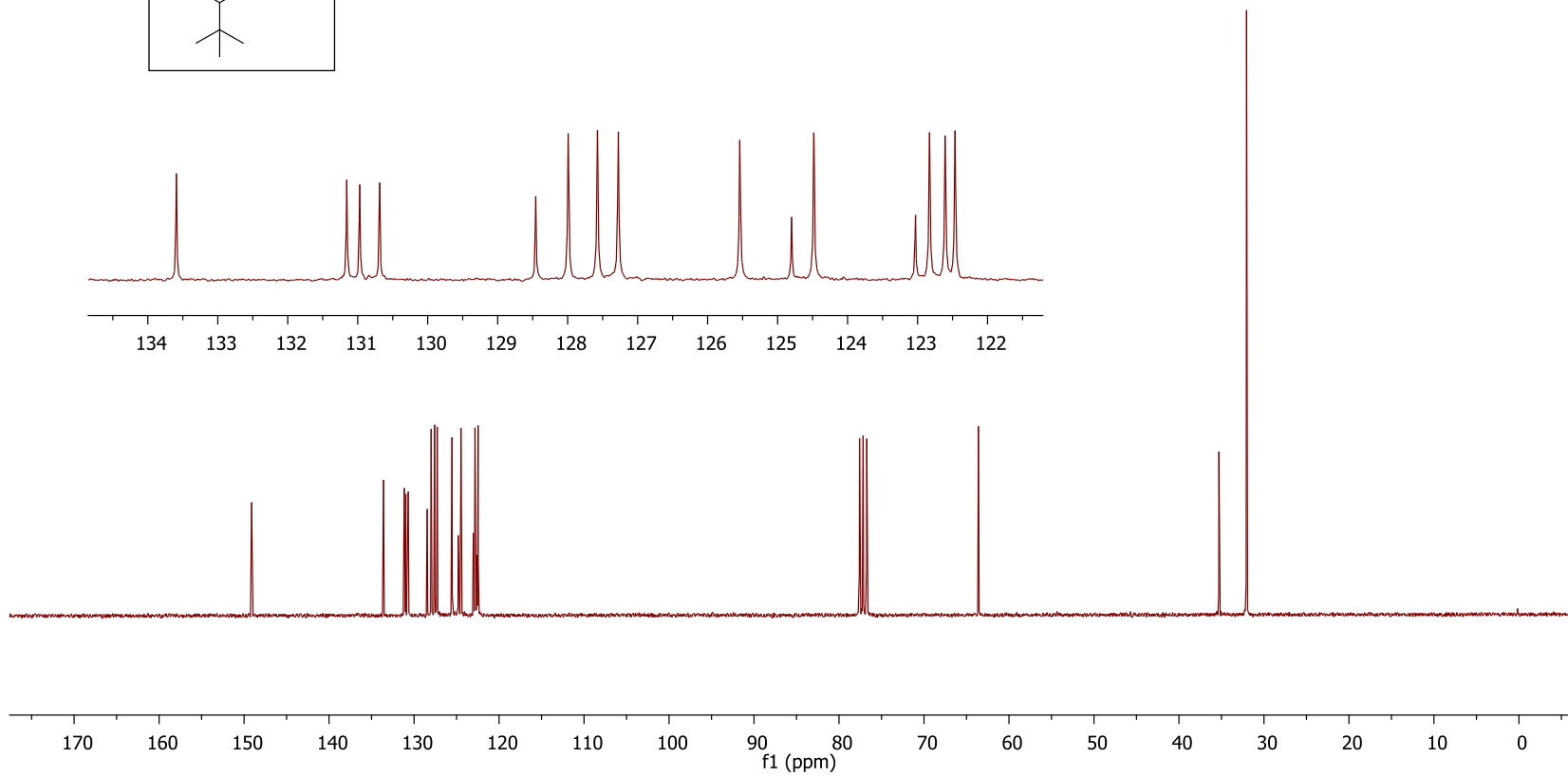
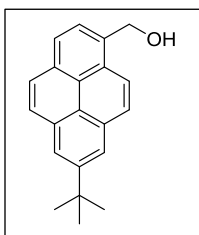


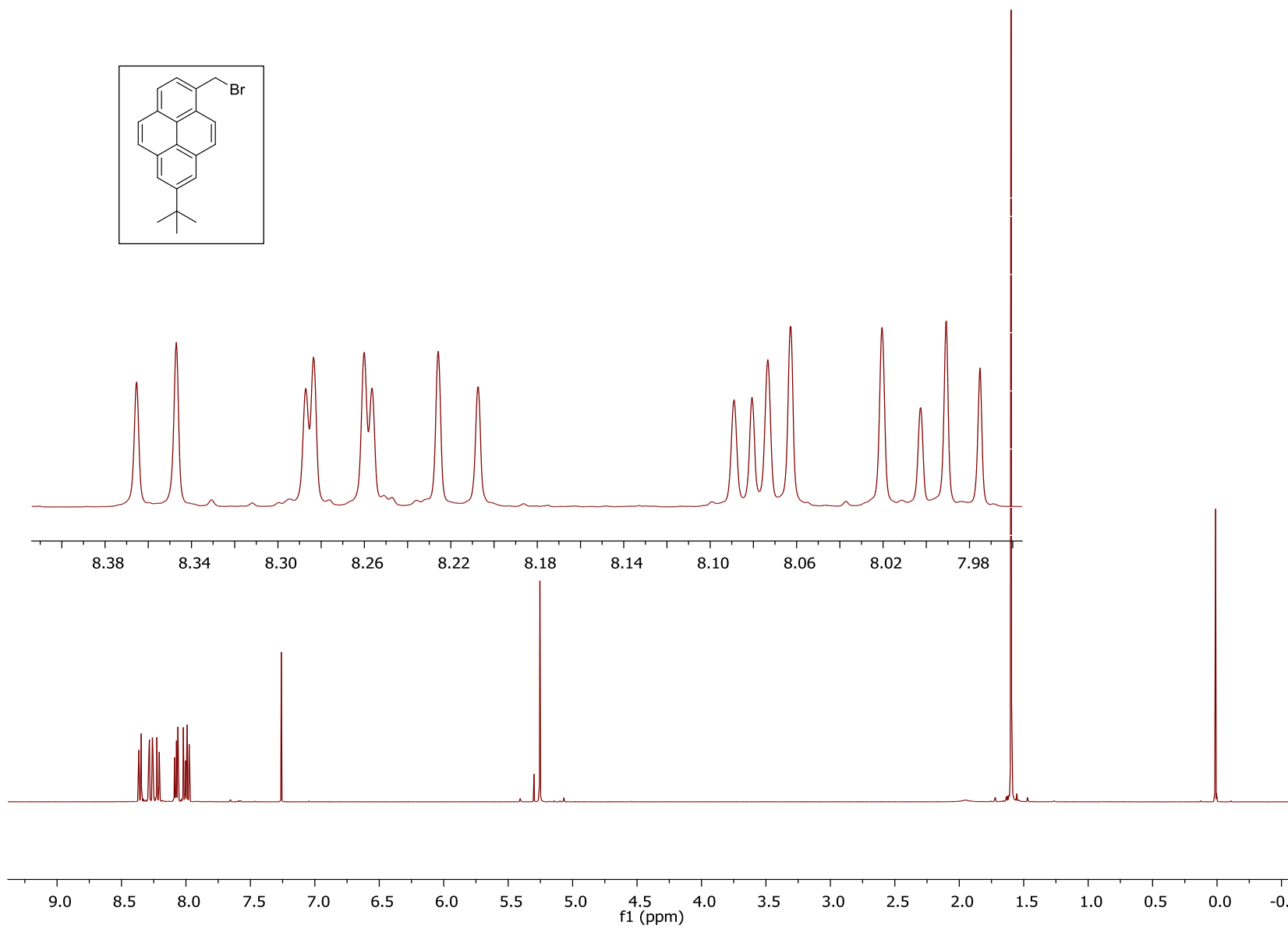
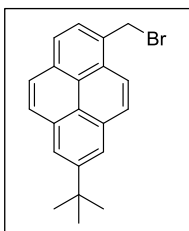


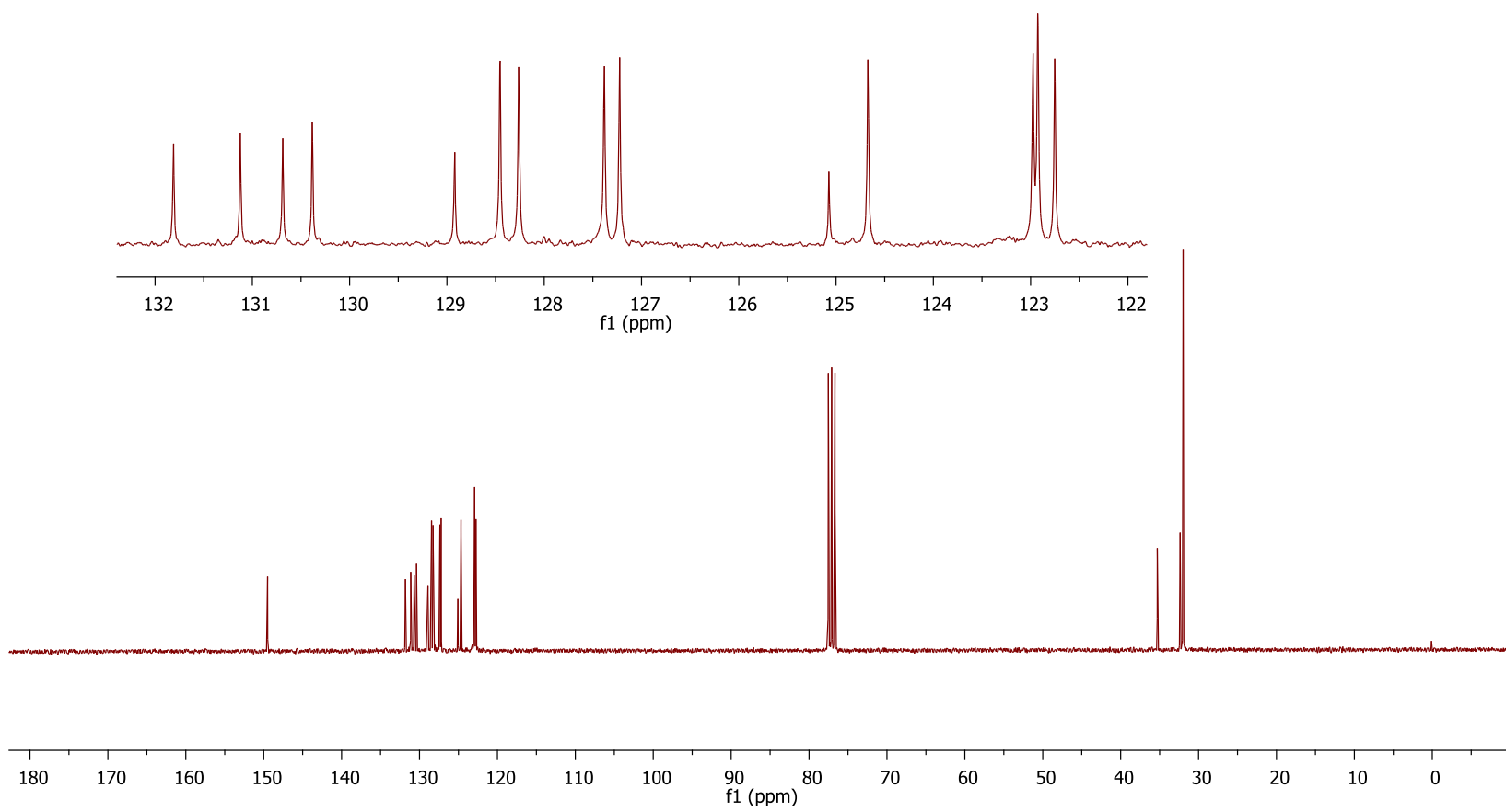
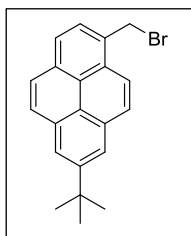


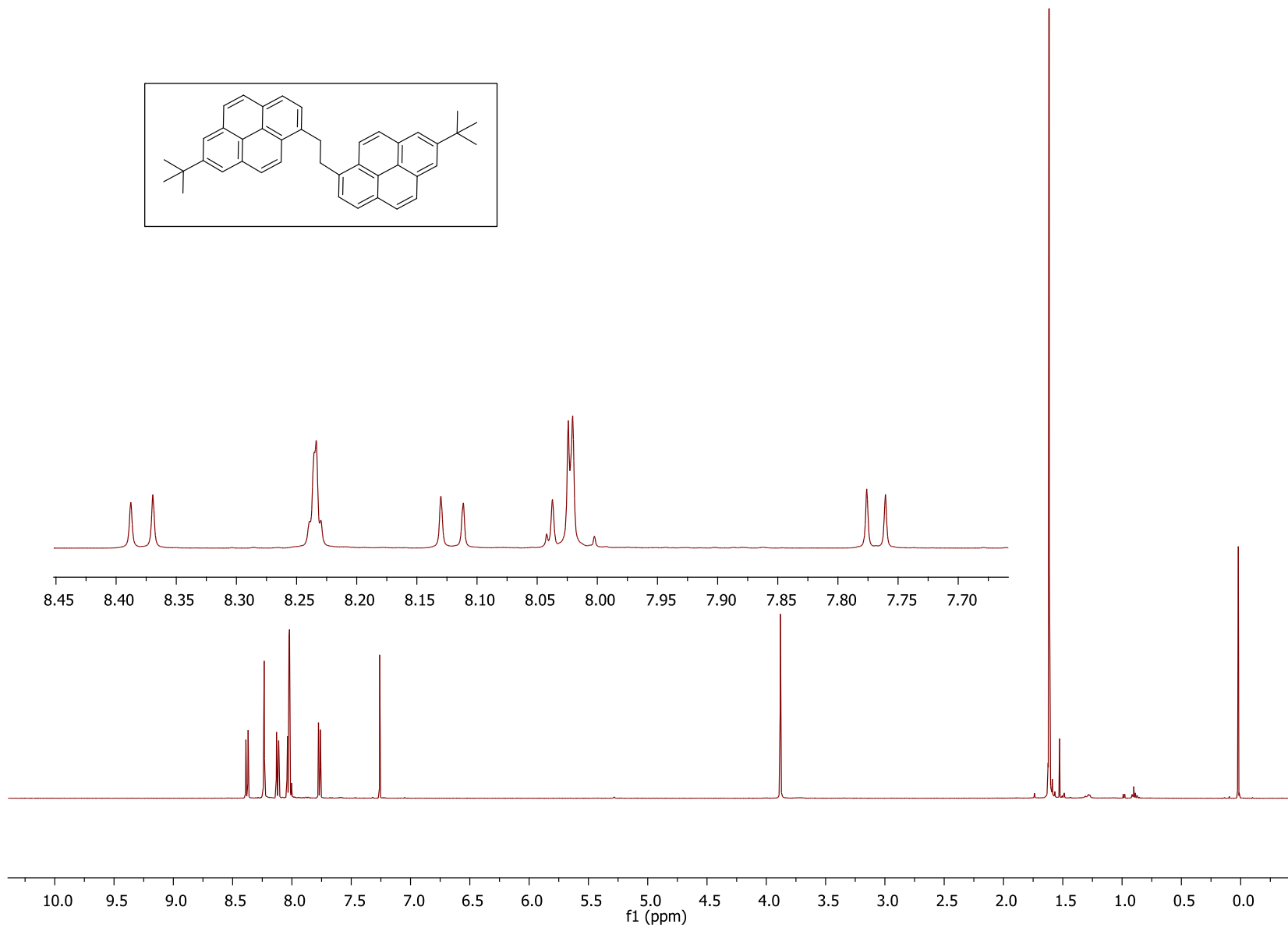
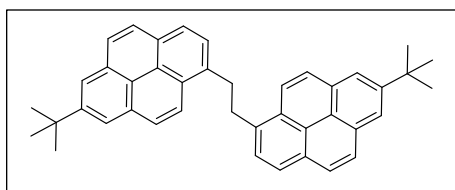




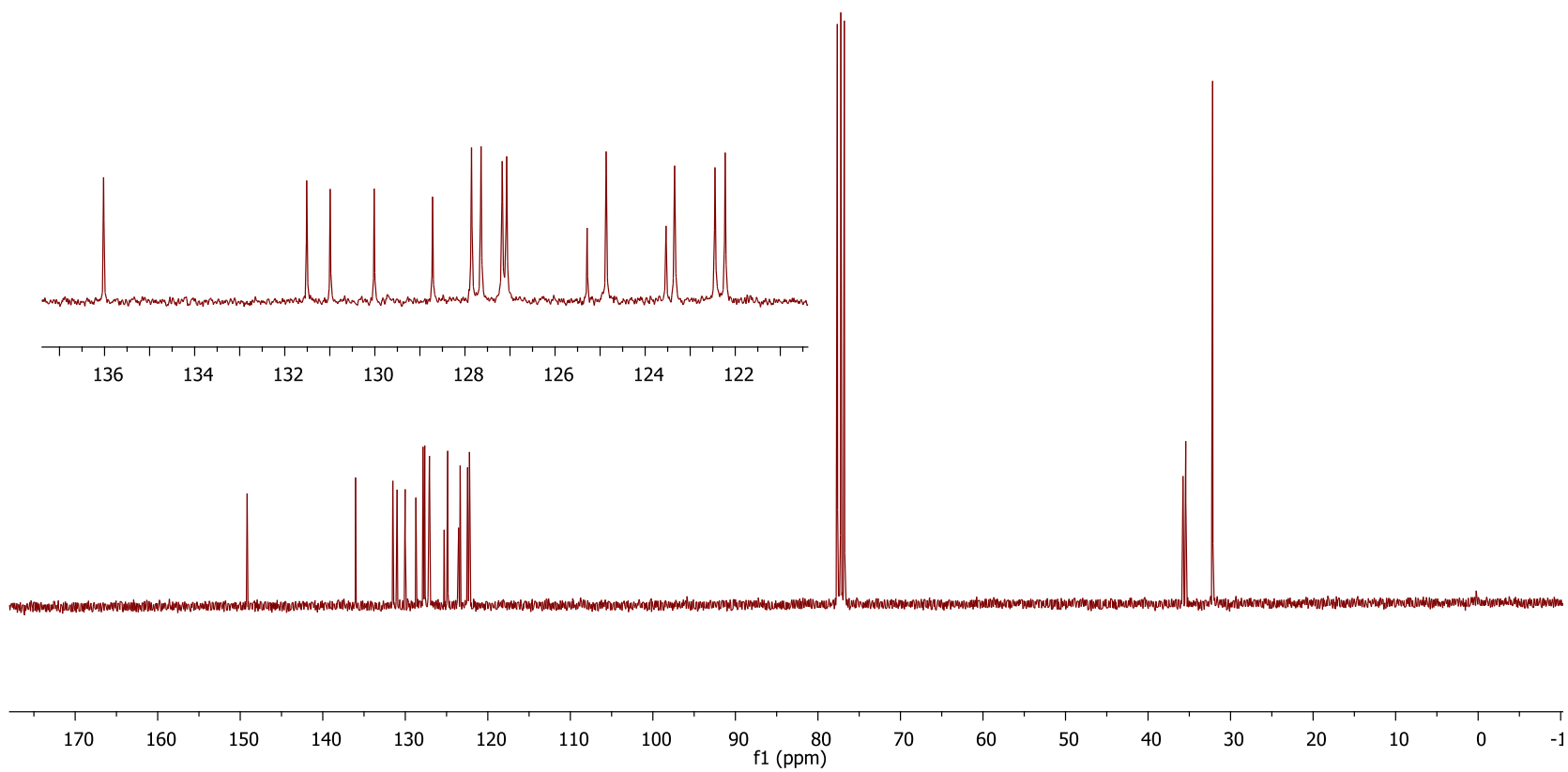
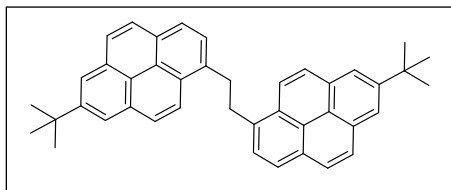


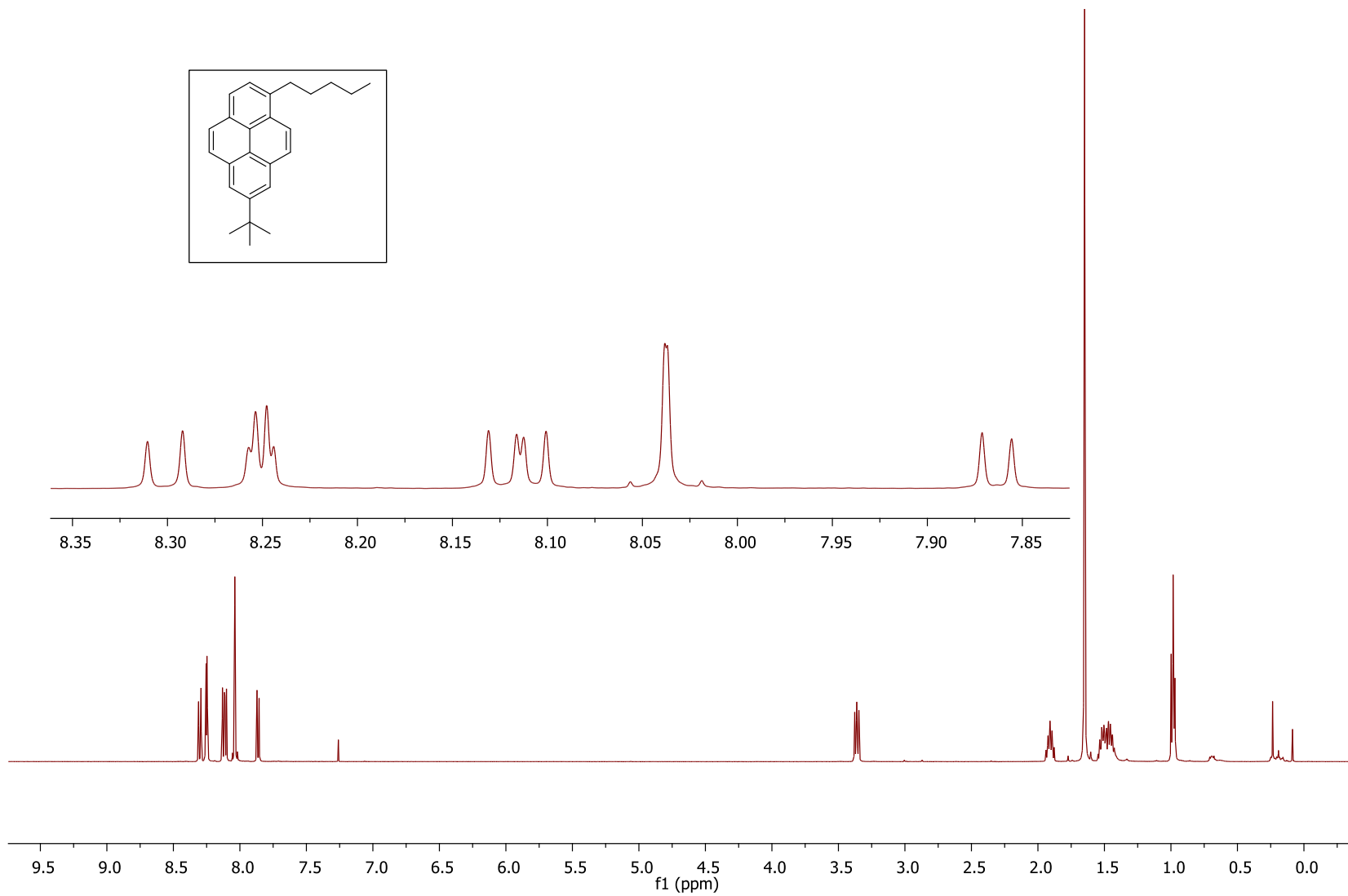
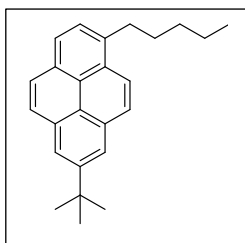


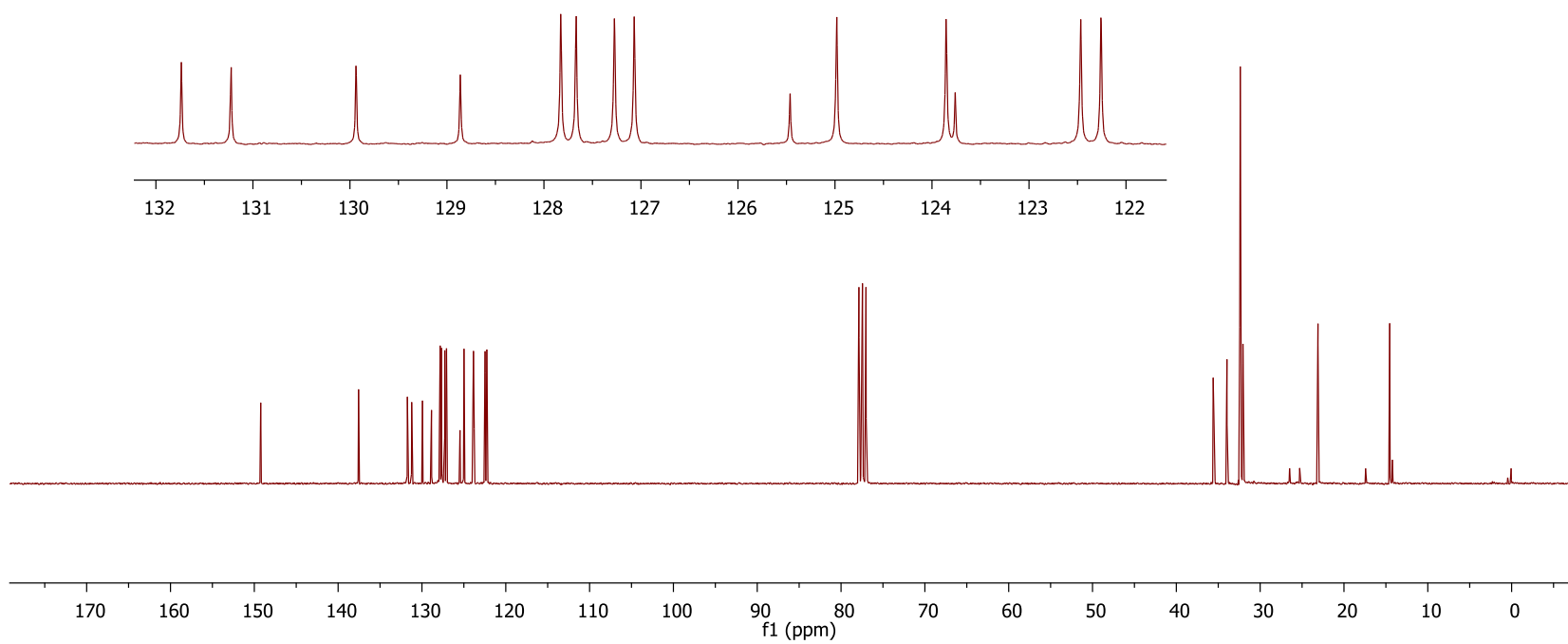
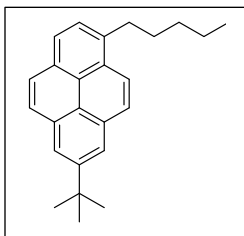


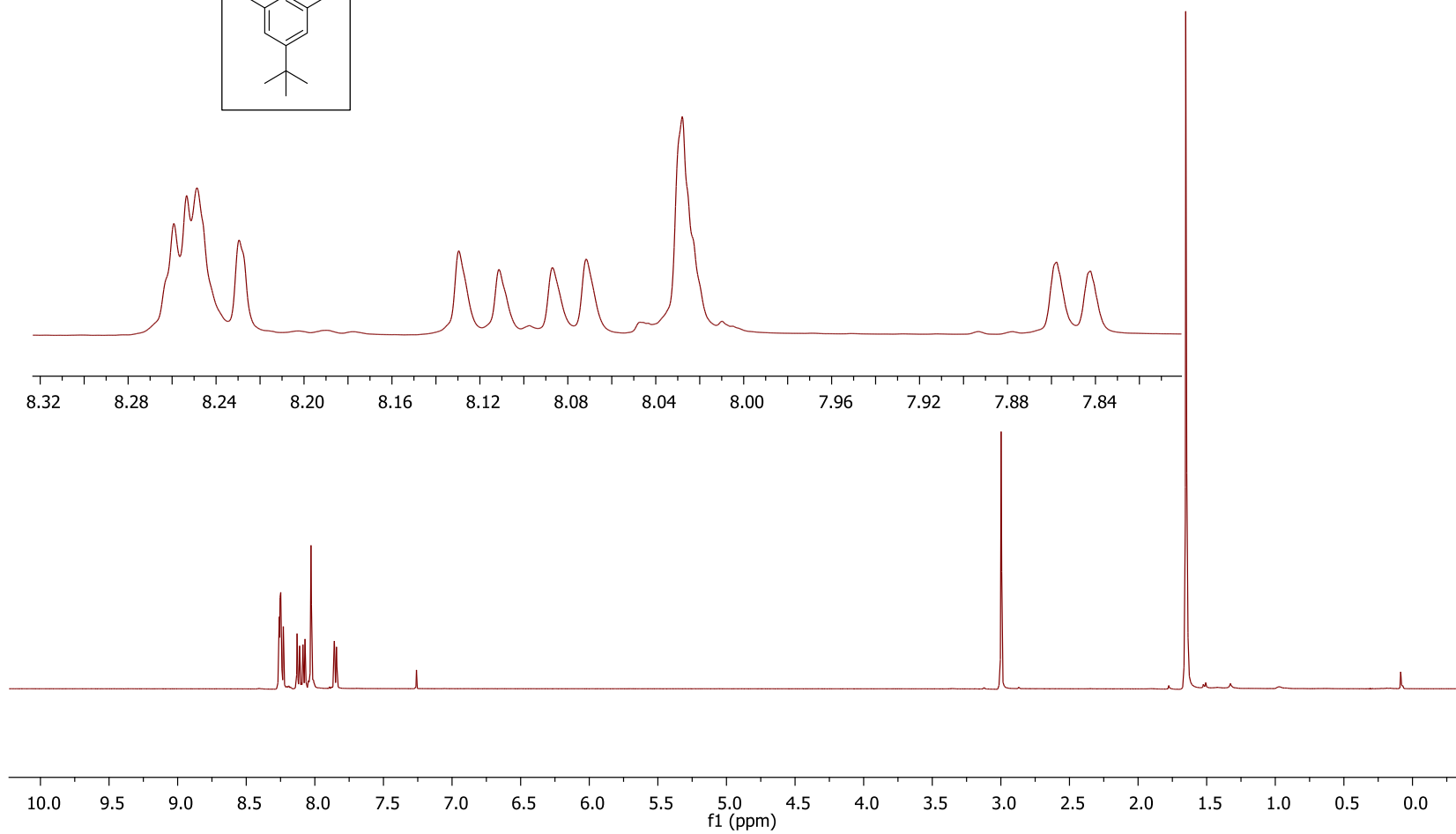
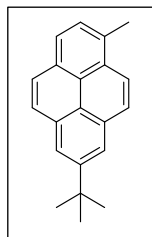


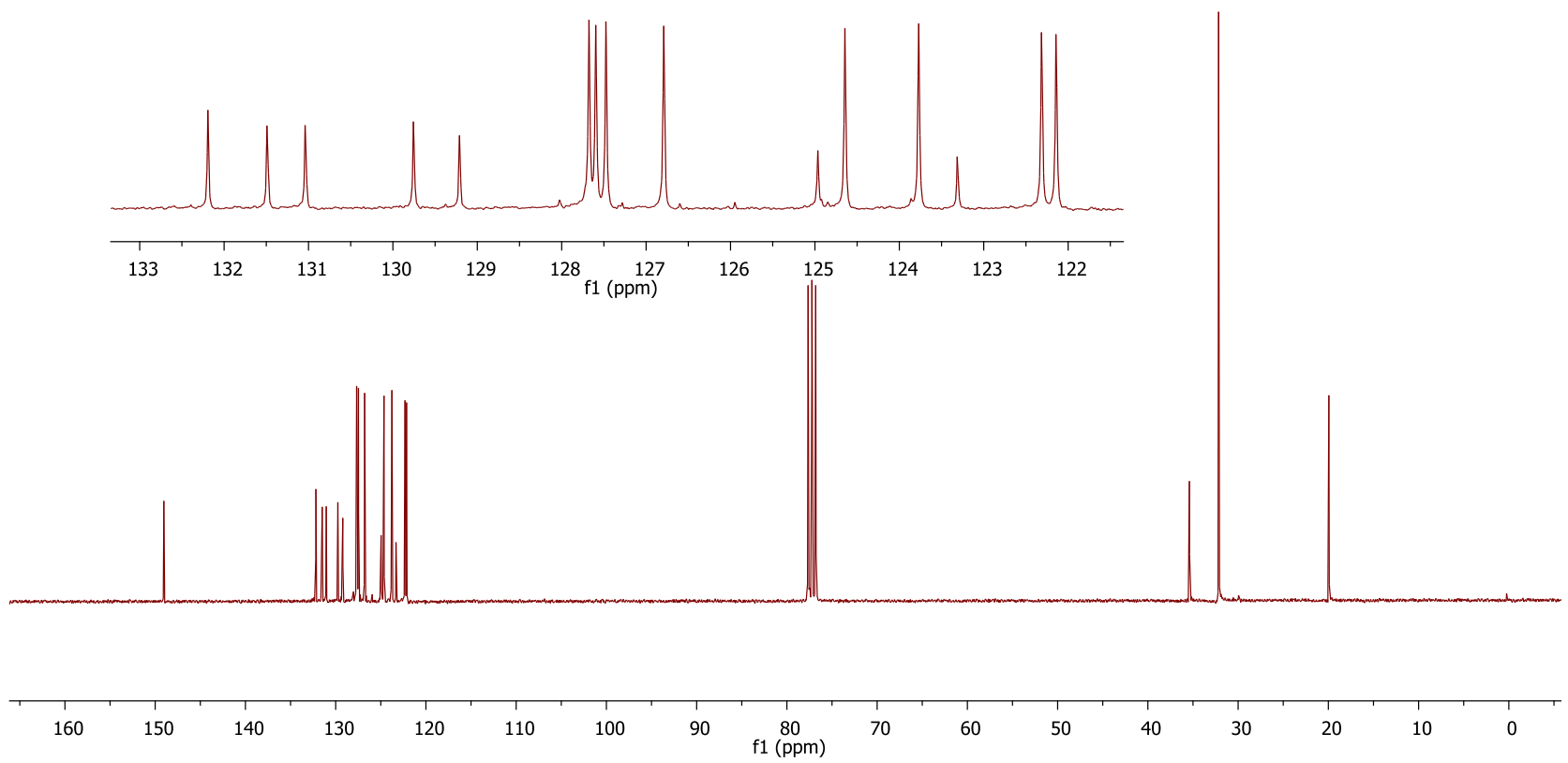
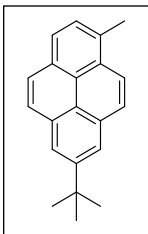


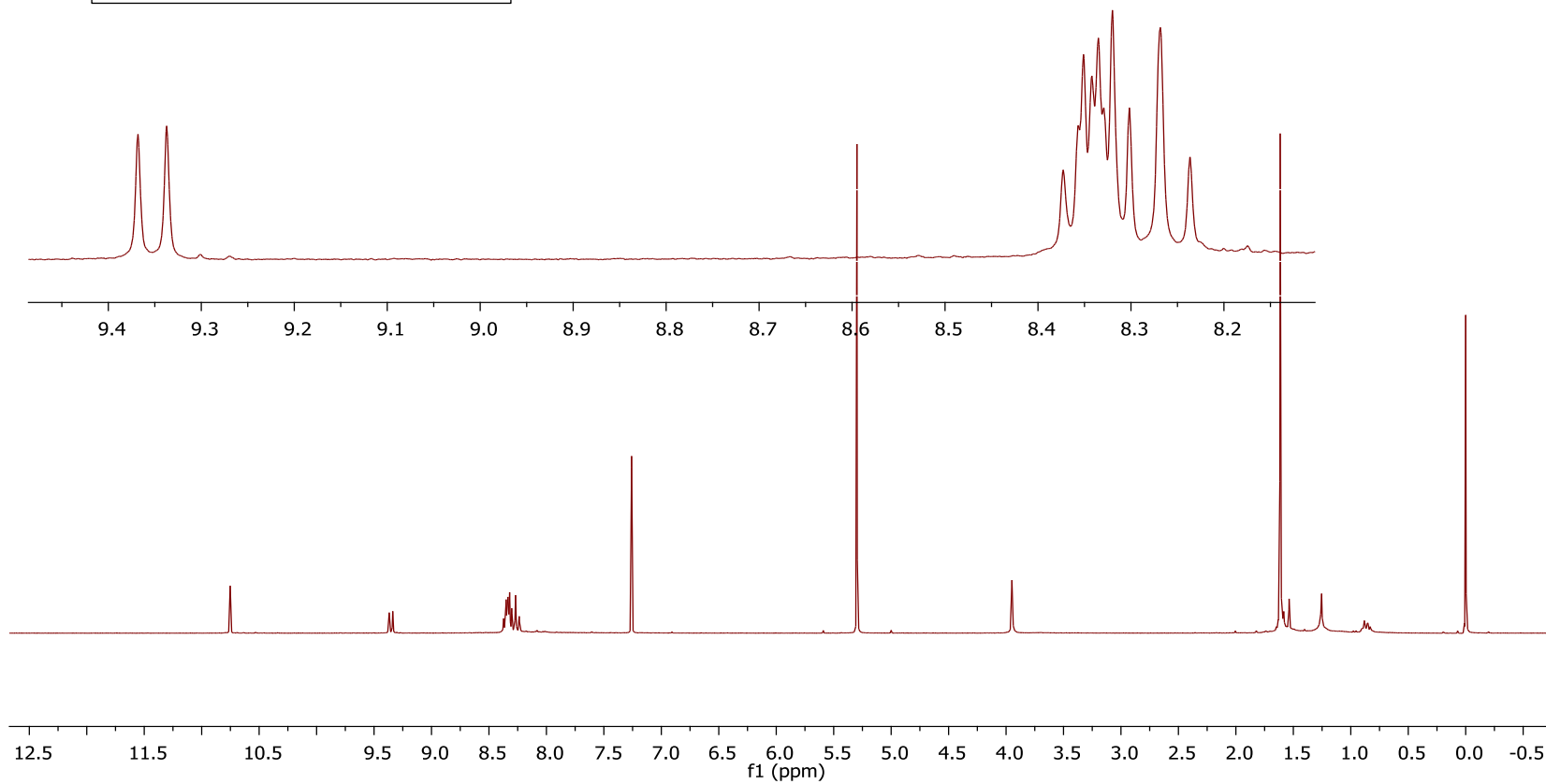
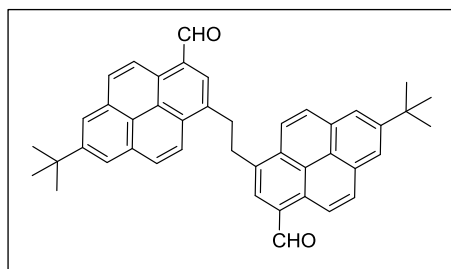


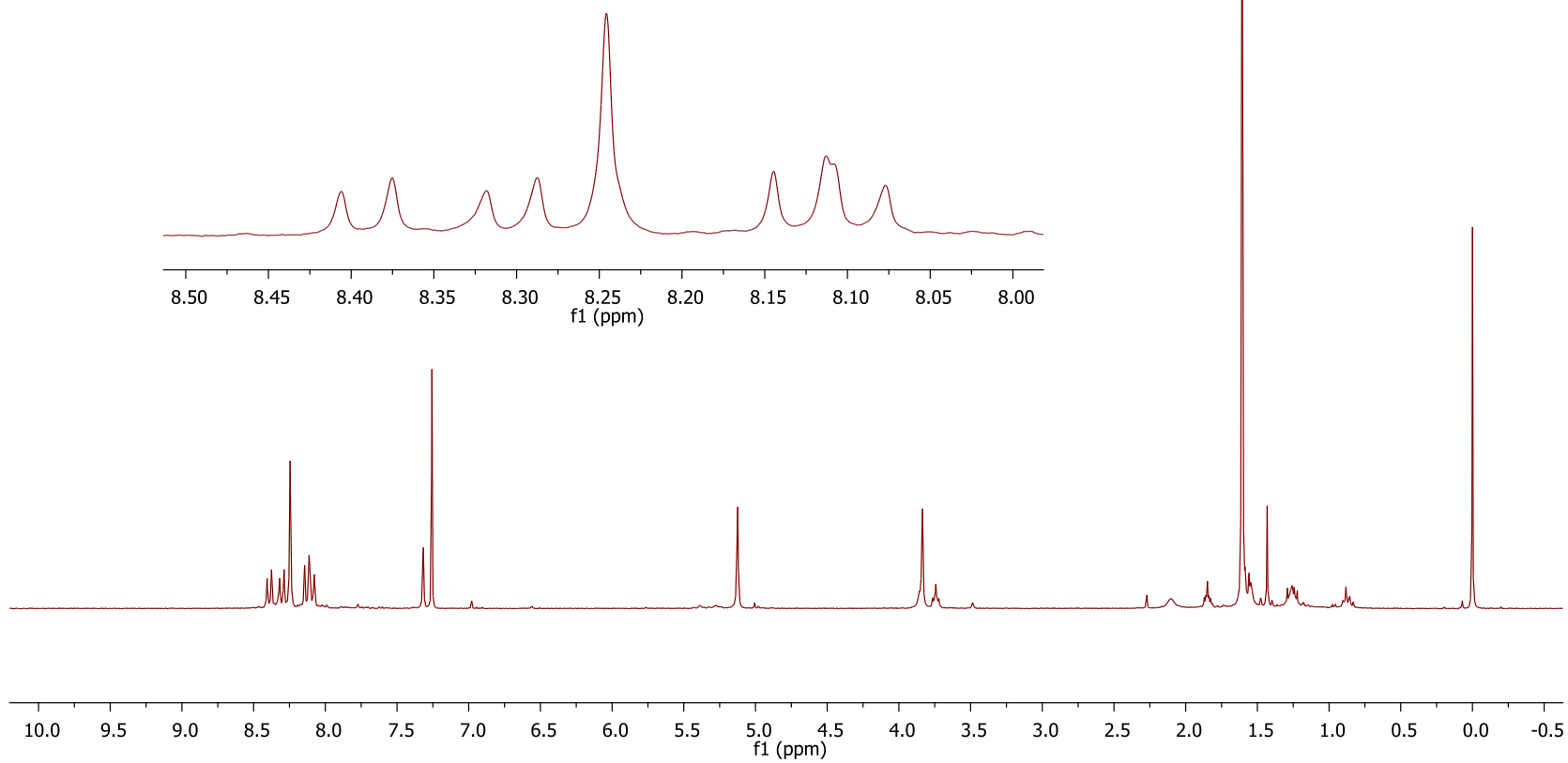
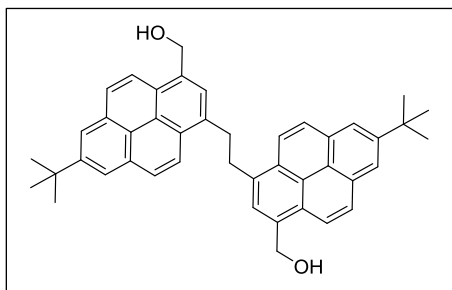


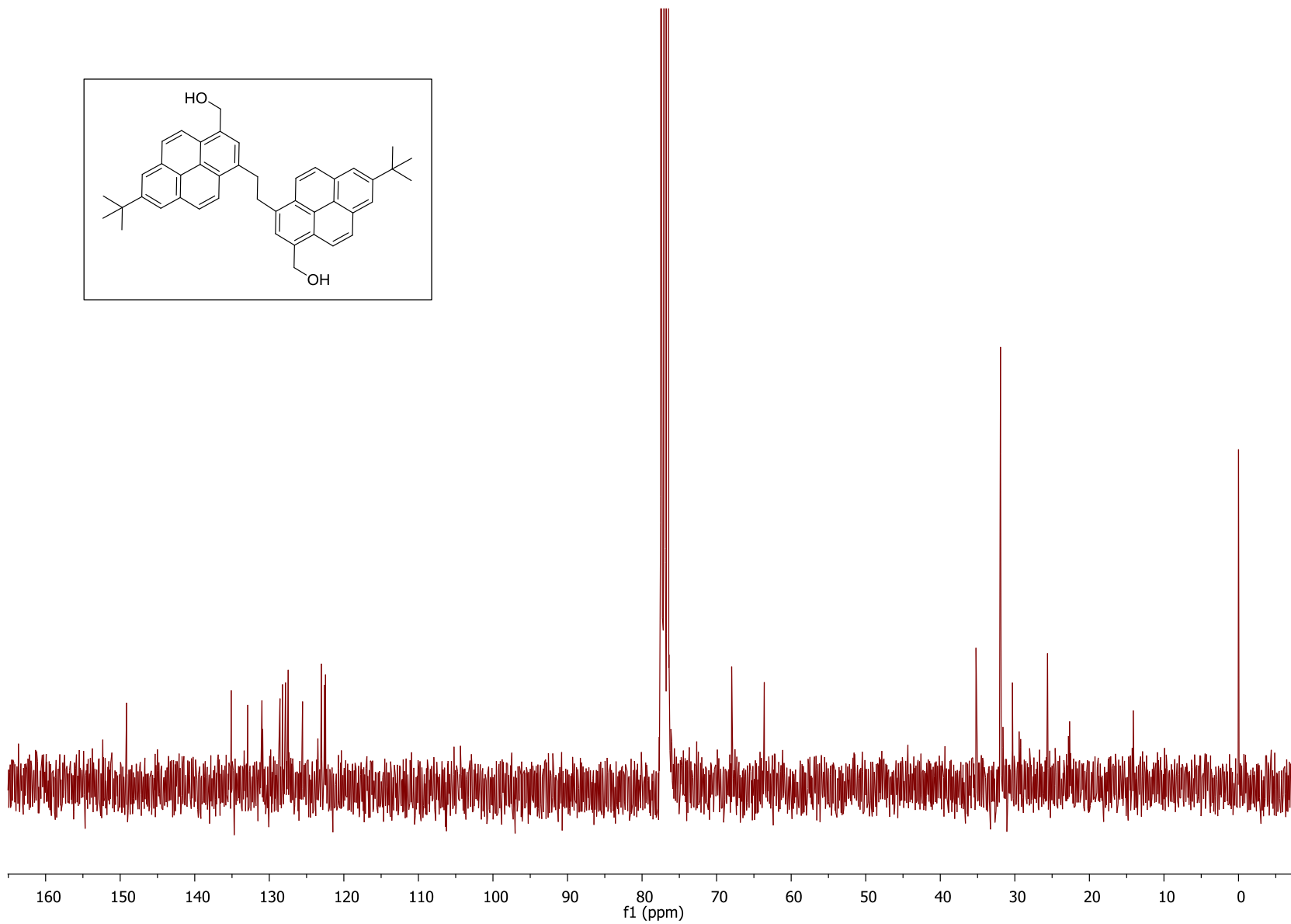
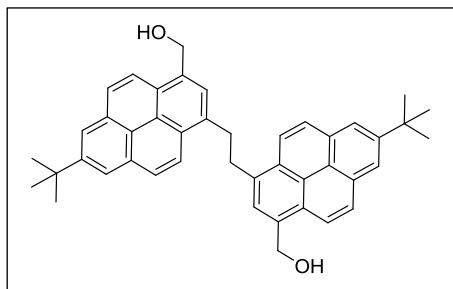












603



